Maria-Elisabeth Krautwald-Junghanns · Michael Pees · Sven Reese · Thomas Tully

Diagnostic Imaging of Exotic Pets

Birds · Small Mammals · Reptiles

vet

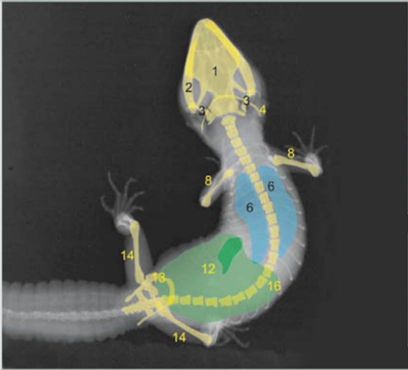

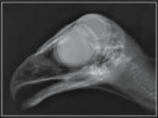

schlütersche

vet

Maria-Elisabeth Krautwald-Junghanns · Michael Pees · Sven Reese · Thomas Tully

Diagnostic Imaging of Exotic Pets

Birds · Small Mammals · Reptiles

This page intentionally left blank

Maria-Elisabeth Krautwald-Junghanns · Michael Pees ·
Sven Reese · Thomas Tully

Diagnostic Imaging of Exotic Pets

Birds · Small Mammals · Reptiles

With the cooperation of

Thomas Bartels, Michael Fehr, Michaela Gumpenberger, Jutta Hein, Ingo Hoffmann, Ingmar Kiefer, Veit Kostka, Jan-Gerd Kresken, Eberhard Ludewig, Cordula Poulsen Nautrup, Susanne Schlieter, Volker Schmidt, Sandra Schroff, Jochen Spennes

English translation

Teresa J. Gatesman

schlütersche

Original edition: Atlas der bildgebenden Diagnostik bei Heimtieren. Vögel, Kleinsäuger, Reptilien. © 2009,
Schlütersche Verlagsgesellschaft mbH & Co. KG, Hans-Böckler-Allee 7, 30173 Hannover
E-mail: info@schluetersche.de

Printed in Germany

ISBN 978-3-89993-049-8

Bibliographic information published by Die Deutsche Nationalbibliothek
Die Deutsche Nationalbibliothek lists this publication in the Deutsche Nationalbibliografie; detailed bibliographic data are available in the Internet at http://dnb.ddb.de.

The authors assume no responsibility and make no guarantee for the use of drugs listed in this book. The authors / publisher shall not be held responsible for any damages that might be incurred by the recommended use of drugs or dosages contained within this textbook. In many cases controlled research concerning the use of a given drug in animals is lacking. This book makes no attempt to validate claims made by authors of reports for off-label use of drugs. Practitioners are urged to follow manufacturers' recommendations for the use of any drug.

Typesetting: Dörlemann Satz, Lemförde, Germany
Printing: Werbedruck Aug. Lönneker GmbH & Co. KG, Stadtoldendorf, Germany

Contents

2 Small Mammals

General principles

Special diagnostics, pathological findings

3 Reptiles

General principles

Special diagnostics, pathological findings

Authors

Thomas Bartels PD, Dr. rer. nat.
Clinic for Birds and Reptiles
University of Leipzig
An den Tierkliniken 17
04103 Leipzig
Germany

Michael Fehr Prof. Dr. med. vet. Dipl ECZM (small mammal),
Specialist in small animal medicine
Clinic for pets, reptiles, pet and wild birds
University of Veterinary Medicine Hanover
Bischofsholer Damm 15
30173 Hanover
Germany

Michaela Gumpenberger Dr. med. vet.
Assistant professor
Clinic of Diagnostic Imaging
University of Veterinary Medicine Vienna
Veterinärplatz 1
1210 Vienna
Austria

Jutta Hein Dr. med. vet.
Senior veterinarian for health care and small pets
Small Animal Medical Clinic
Faculty of Veterinary Medicine
Ludwig-Maximilian University Munich
Veterinärstrasse 13
80539 Munich
Germany

Ingo Hoffmann Dr. med. vet.
Additional qualifications in ophthalmology
Veterinary Ophthalmology Practice
Breslauer Str. 366
90471 Nuremberg
Germany

Ingmar Kiefer Dr. med. vet.
Specialist in small and pet animals, specialist in radiology
Department of Small Animal Medicine
University of Leipzig
An den Tierkliniken 23
04103 Leipzig
Germany

Veit Kostka Dr. med. vet.
Specialist in poultry, wild and pet birds,
Specialist in microbiology, additional qualifications in reptiles
Leegmoor 30
22417 Hamburg
Germany

Maria-Elisabeth Krautwald-Junghanns
Prof. Dr. med. vet., Dipl ECZM (avian)
Poultry specialist; additional qualifications in pet, zoo
and wild birds; additional qualifications in reptiles
Clinic for Birds and Reptiles
University of Leipzig
An den Tierkliniken 17
04103 Leipzig
Germany

Jan-Gerd Kresken Dr. med. vet.
Small mammal specialist, additional qualifications in cardiology
Small Animal Clinic am Kaiserberg
Wintgensstraße 81–83
47058 Duisburg
Germany

Eberhard Ludewig Dr. med. vet., Dipl ECVDI
Specialist in small and pet animals, radiology specialist
Department of Small Animal Medicine
University of Leipzig
An den Tierkliniken 23
04103 Leipzig
Germany

Michael Pees Dr. med. vet., Dipl ECZM (avian)
Poultry specialist; additional qualifications in pet, zoo, and
wild birds; additional qualifications in reptiles
Clinic for Birds and Reptiles
University of Leipzig
An den Tierkliniken 17
04103 Leipzig
Germany

Cordula Poulsen Nautrup Prof. Dr. med. vet.
Anatomy specialist, additional qualifications in cardiology
Institute of Animal Anatomy, Faculty of Veterinary Medicine
Ludwig-Maximilian University Munich
Veterinärstrasse 13
80539 Munich
Germany

Sven Reese PD, Dr. med. vet.
Anatomy specialist, specialist in information technology
Institute of Animal Anatomy, Faculty of Veterinary Medicine,
Ludwig-Maximilian University Munich
Veterinärstrasse 13
80539 Munich
Germany

Susanne Schlieter Dr. med. vet.
Practical veterinarian
Veterinary practice for cardiology and ultrasound diagnostics
Glümerstrasse 17
79102 Freiburg im Breisgau
Germany

Volker Schmidt Dr. med. vet., Dipl ECZM (avian)
Clinic for Birds and Reptiles
University of Leipzig
An den Tierkliniken 17
04103 Leipzig
Germany

Sandra Schroff veterinarian
Clinic for Birds and Reptiles
University of Leipzig
An den Tierkliniken 17
04103 Leipzig
Germany

Jochen Spennes
Practical veterinarian
Small Animal Clinic am Kaiserberg
Wintgensstrasse 81–83
47058 Duisburg
Germany

Thomas Tully DVM, Dipl ABCP, Dipl ECZM (avian)
Professor of Zoological Medicine
Veterinary Teaching Hospital and Clinics
Louisiana State University
Baton Rouge
Louisiana 70802
USA

English translation

Teresa J. Gatesman BVSc
Striet 9
37083 Göttingen
Germany

Abbreviations

µCT	micro-computed tomography
µm	micrometer
2D	two-dimensional
2DE	two-dimensional echocardiography
3D	three-dimensional
A	ampere
AO	aorta
ASD	atrial septal defect
AV valve	atrioventricular valve
A wave	late diastolic inflow during atrial contraction
$BaSO^4$	barium sulphate
bwt	body weight
CaCr	caudocranial
CFM	color flow mode
Chap.	Chapter
cm	centimeter
CNS	central nervous system
CrCa	craniocaudal
CSF	cerebrospinal fluid
CT	computed tomography
CW	continuous wave
d	diastolic
DCM	dilatative cardiomyopathy
DP	dorsopalmar
DV	dorsoventral
E wave	early diastolic passive inflow in the ventricle
E. coli	*Escherichia coli*
EA wave	fused E and A waves
ECG	electrocardiogram
EF	ejection fraction
EPSS	E-point to septal separation
FFD	film-focus distance
Fig.	Figure
FS	fractional shortening
FSH	follicle stimulating hormone
G	gauge
g	gram
GnRH	gonadotropin releasing hormone
h	hour
HCM	hypertrophic cardiomyopathy
HU	Hounsfield unit
Hz	Hertz
IV	intravenous
ICS	intercostal space
IVS	systolic thickness of the interventricular septum
kg	kilogram
kV	kilovolt
kW	kilowatt
L	level (CT)
LA	left atrium
LH	luteinizing hormone
LVD	diameter of the left ventricle
LVM	left ventricular myocardium
LVV	left ventricular volume
m	meter
mA	milliampere
mAs	milliampere second
MBD	Metabolic Bone Disease
mg	milligram
MHz	Megahertz
min	minute
ml	milliliter
mm	millimeter
mmHg	millimeter mercury
MRI	magnetic resonance imaging
n. k.	not known
n. s.	not specified
NAD	nothing abnormal diagnosed
PD	penetration depth
PDD	proventricular dilatation disease
PDW	proton-density weighted
PHT	pressure half time
PRT	pulse repitition time
PW	pulsed wave
ROI	region of interest
s	second
s	systolic
s.c.	subcutaneous
SD	slice density
sp./spp.	species (singular/plural)
V	volt
Vao	aortic valve
VD	ventrodorsal
VHS	vertebral heart score
VM	mitral valve
V_{max}	maximum velocity
VP	pulmonary valve
VSD	ventricular septal defect
VT	tricuspid valve
W	width (CT)

This page intentionally left blank

Preface

The idea to compile an atlas for imaging techniques that includes diagnostic information for birds, small pet mammals and reptiles requests by colleagues for a complete reference text on this subject. The proposed book was to include companion extotic animal species that are most often treated in veterinary practices with an emphasis on common presented problems.

In the last 20 years arguably no other area of veterinary medicine has evolved as much as exotic pet medicine and surgery. Many diagnostic tests that, until recently, were not considered for these animals are now available and routinely used. In particular diagnostic imaging methods have achieved a pivotal significance for companion exotic animal patients. Despite the advantages and the availability of improved diagnostic imaging techniques they are still not being used or rarely accessed in many veterinary practices. The various reasons for why veterinarians under utilize the available diagnostic imaging technologies include the uncertainty in handling companion exotic animals (i.e. beginning with capture and suitable fixation) and the uncertainties associated with performing the proper investigations and the interpretation of those images.

With this atlas, the practicing veterinarian is provided information regarding the most important investigation techniques and interpretation aids, so that these valuable diagnostic methods can be used on a daily basis. Two diagnostic imaging modalities (computed tomography [CT] and magnetic resonance imaging [MRI]) are also described which, in most cases, are only available in specialized clinics. The respective indications for the use of CT and MRI on companion exotic animals are explained so that an attending clinician can determine if one of thes advanced imaging tests is required for thier patient.

The production of such a comprehensive book on imaging diagnostics for companion avian and exotic animals would not have been possible without the competent support of the coauthors. Our heartfelt thanks are therefore extended to our colleagues T. Bartels (Leipzig), M. Fehr (Hanover), M. Gumpenberger (Vienna), J. Hein (Munich), I. Hoffmann (Nuremberg). I. Kiefer (Leipzig), V. Kostka (Hamburg), J. G. Kresken (Duisburg), E. Ludewig (Leipzig), C. Poulsen Nautrup (Munich), S. Schlieter (Freiburg in Breisgau), V. Schmidt (Leipzig), S. Schroff (Leipzig) and J. Spennes (Duisburg). In addition, we wish to thank all our colleagues who provided us with visual materials for the book.

The German-US American cooperation in the compilation of the visual materials and the composition of the chapters has ensured the depiction of a broad spectrum of species that play a special role in both the North American and European regions. The publication of the book in both German and English is welcomed by the publisher as is enables a transfer and understanding of knowledge between colleagues throughout the world.

The authors have tried to ensure that the text, pictures, and drawings are correct and didactically suitable. For their valuable aid in the production of the positioning photographs in the bird radiography section, we wish to especially thank Ms. Festerra from the Institute of Veterinary Anatomy, Leipzig, and Ms. Merseburger from the Small Animal Clinic, Leipzig, for their support in the undertaking of the CT and MRI investigations. Many former and current PhD students and veterinarians working at the Institute of Animal Anatomy in Munich and the clinics in both Leipzig and Munich have participated in obtaining the images published in this text. In addition, many unnamed helpers have contributed by voluntarily undertaking additional work, thereby enabling the authors to carry out the time-consuming and often difficult work involving the texts and visual materials. We wish to thank everyone who participated in the development of this book, especially the coworkers at the Clinic for Birds and Reptiles in Leipzig and all the coworkers in the Department of Small Pets in the Small Animal Medical Clinic in Munich.

The work on such a comprehensive book requires many years of planning and coordination therefore places great challenges on both the publisher and the authors. Due to the opportunity of simultaneously publishing this book in English-speaking countries, the necessary resources were made available. We would like to particularly thank Dr. Oslage and Ms. Sodemann for their engagement and their professional supervision during both the book's planning and execution phases.

The authors wish to request that all readers of this book inform them of any suggestions, desired corrections or revisions. Thank you.

Leipzig, Munich and Baton Rouge

Summer 2010

Maria-Elisabeth Krautwald-Junghanns
Michael Pees
Sven Reese
Thomas Tully

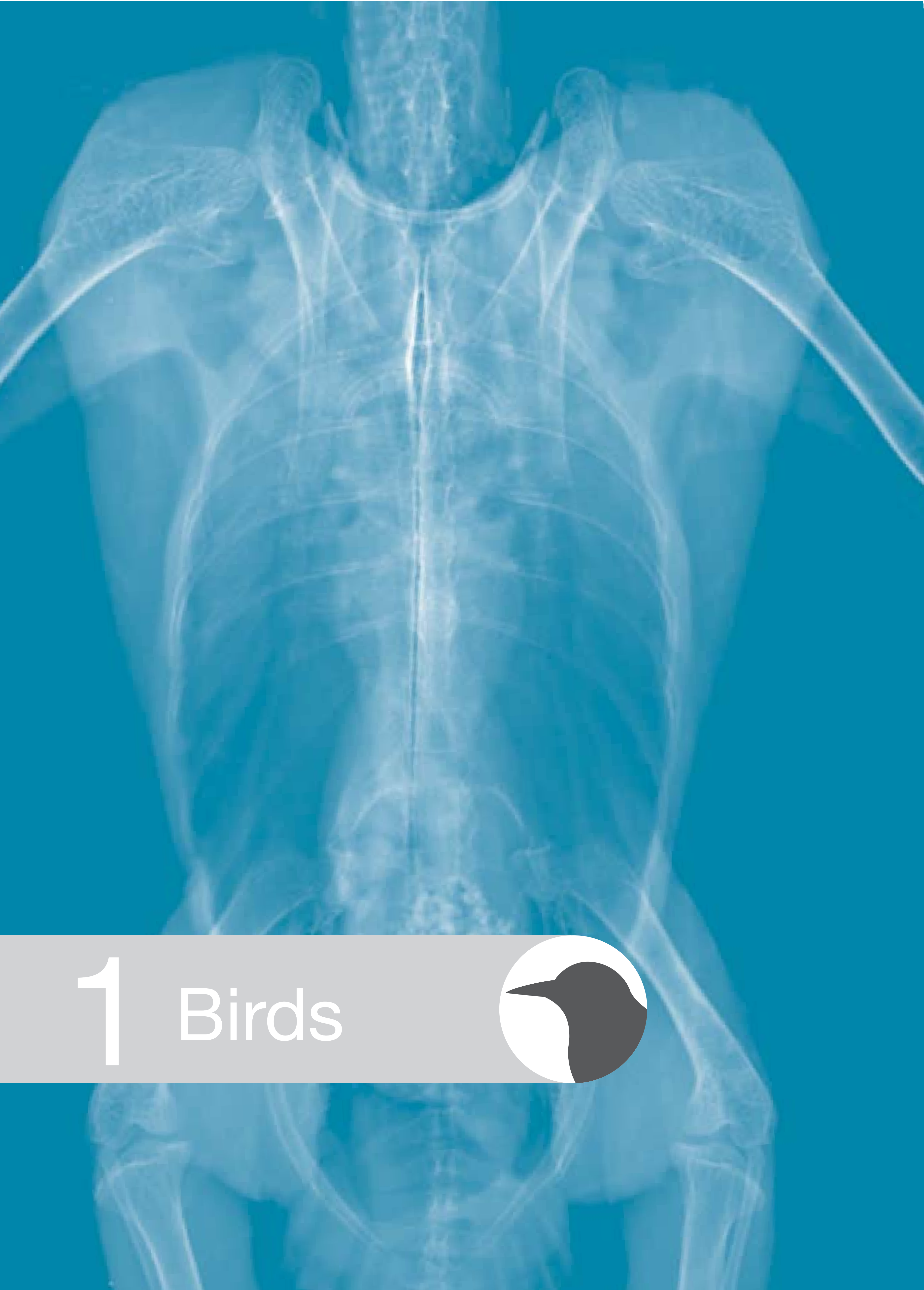

1 Birds

Introduction

Maria-Elisabeth Krautwald-Junghanns

The role of imaging techniques is becoming increasingly important in pet, zoo and wild birds medicine. While conventional radiography has been established as an important veterinary diagnostic test for many years, an increasing number of scientific studies on the routine use of ultrasonographic and computed tomographic methods have become available in recent years. As a result these newer imaging modalities, especially ultrasonography, has found its place in veterinary practices and is predominantly used to diagnose internal disorders of companion avian species maintained indoors. Conversely in wild and free-flying pet birds, imaging diagnostics are used frequently in the surgical/orthopedic fields.

Radiography is being used with increasing frequency to obtain a diagnosis in avian medicine. Many diagnostic test results have limited interpretive value in avian patients (e.g., percussion, body temperature, the collection of adequate amounts of blood from birds with a body weight under 40 g, etc.) and avian patients can often hide their clinical disease signs for a long period of time. Therefore when many birds first present to a veterinary hospital they are severely ill and require a rapid health assessment to determine an underlying disease etiology. Using different imaging modalities can often aid in rapidly determining an underlying disease etiology for the presenting avian patient that requires life saving treatment.

While the size of many birds with a body weight of under 40 g may be a limiting factor (especially with digital radiography systems due to the current limited detail rendition of this method), the cost of this method has decreased for small inexpensive birds. On the other hand undertaking a radiographic investigation is often easy due to the small size of the bird: a bird's whole body can generally be imaged using one exposure. In addition, the danger of personnel being exposed to radiation is not a problem when conventional radiography or CT investigation performed using published health and safety guidelines and the patient is restrained with a Plexiglas plate. Moreover, the interpretation of a radiograph of a bird is easy for an experienced radiologist as the avian air sac system acts as a negative contrast to the organs. However, the air sac system makes an ultrasonographic investigation more difficult. Despite the adverse effect of the air sac system on the interpretation of ultrasonographic images, ultrasonographic investigation in unsedated birds is an easy noninvasive diagnostic method, especially when examining the heart, liver and urogenital tract. Ultrasonography often provides important supplementary information about disease subsequent to an unclear radiographic result. Advanced imaging modalities (CT, MRI) are increasingly being used to achieve more precise imaging detail, especially in larger avian patients. Currently CT is preferred over MRI due to the shorter time period required to perform the examination.

General principles

1.1 Radiographic investigation

Maria-Elisabeth Krautwald-Junghanns, Sandra Schroff, Thomas Bartels

1.1.1 Equipment

1.1.1.1 Radiography unit

Highly detailed radiographic images are a basic requirement to successfully achieve a radiographic diagnosis on an avian patient. Highly detailed radiographs are advantageous because the anatomic details are superior, allowing for expert interpretation and recognition of pathological changes. Moreover, the anatomical differences between avian groups are also enhanced by detailed radiographic images, which is of greater importance in birds because of the relatively small size of many avian patients. To obtain high, quality images, it is not only necessary to have the proper radiographic equipment (e.g. x-ray apparatus, film-screen combination, developing system), but the technical support staff performing the procedure must be experienced handling avian patients. A comprehensive discussion regarding basic radiology technical parameters and a full explanation of the radiation protection requirements would exceed the scope of this book. As a consequence, only the technical aspects that have a particular importance for avian radiography will be described

Basically, the radiographic interpretation of a bird requires similar equipment to that used in small animal radiography. Although, or especially because, such interpretations usually involve relatively small patients, high-power X-ray machines are particularly useful. In addition to the anatomical differences in avian patients, motion blur due to the high respiratory rate, even in anesthetized birds, adversely affects image quality. As a consequence, short exposure times (maximal 0.015–0.05 s, if possible even lower) should be used. Increasing the anode voltage enables the exposure time to be reduced; however, this can lead to an extreme reduction in contrast. The anode voltage should be maintained as low as possible (45–55 kV) to achieve radiographic images with a high degree of contrast and a wide grey scale range.

To decrease the dose of radiation, the film-focus distance can be reduced by placing the patient as close to the film as possible. The radiation dose that a particular area of the body receives can be reduced by 25% if the distance between the radiation source and the object is doubled (Inverse square law). Accordingly, by halving the film-focus distance, the amount of radiation needed to produce a radiograph can be reduced by a quarter. However, in practice, certain minimum values must be taken into consideration; otherwise the image quality is reduced. This is especially true to the body areas located further away from the film, which may appear larger and out of focus. In addition, low-power machines have a larger focal spot (ca. 2 mm × 2 mm) than units that are highly powered (focal spot 0.6 mm × 0.6 mm to 1.2 mm × 1.2 mm), which causes a reduction in image sharpness when low-powered machines are used. This effect is intensified if the film-focus distance is increased. A reduction of the film-focus distance to 60–70 cm is acceptable as long as a fine film-screen combination is used.

1.1.1.2 Screens and films

In order to achieve diagnostic radiographs of birds, fine film-screen combinations should be used. With fine film-screen combinations, the film must correspond to the screen with respect to both its sensitivity and degree of fineness. The use of more highly intensifying screens is not beneficial because with increasing intensification there is an associated loss of image sharpness and consequently, detail. An optimal system for the radiographic investigation of the internal organs of birds is the combination of rare earth screens and suitable films. Mammography screens are used for the radiographic investigation of the avian skeleton, although the usual increase in exposure time is not implemented. The radiographic images reproduced in this chapter were principally taken with the following screens and films:

Screens

- ☐ Kodak Lanex Medium Screens, Kodak X-OMAT cassette (soft tissues)
- ☐ Kodak MIN-R 2000 screen/windowless, Kodak MIN-R 2 cassette (bones)

Films

- ☐ Kodak T-MAT PLUS DG Film (soft tissues)
- ☐ Kodak MIN-R L Film (bones)

1.1.1.3 Radiation safety

Avian radiodiagnostics often involves positioning small patients that are difficult or impossible to manipulate when wearing protective clothing. Despite this, the basic principles of radiation safety may not be ignored **(Fig. 1-1)**. Protective clothing should be worn to protect technical personnel from scatter radiation produced while the radiographic images are being taken. The primary radiation beam will even penetrate the material incorporated in lead gloves. As a consequence, the avian patient should be positioned so they do not have to be held by hand when the images are taken. The bird should be sedated/anesthetized then placed in the appropriate position by taping or using a restraint board (see Chap. 1.1.2). The radiographic format should be adapted to the size of the patient or the area of the body being investigated by using a suitable cassette or by having the beam adequately collimated. If a bird has to be held when the radiographic images are taken, the person(s) holding the bird should hold their hands outside of the primary beam and have them covered with radiopaque material (e.g. lead gloves) to protect them from the scatter radiation.

1.1.2 Positioning and projections

1.1.2.1 Introduction

The radiographic anatomy of healthy birds often displays a certain degree of variability depending on the bird's age, gender, reproductive status, and environmental conditions in which they live. Therefore, for one to correctly assess a radiographic image, it is necessary to have a thorough knowledge of avian anatomy and physiology.

Each radiographic interpretation should always involve images taken in at least two projections **(Fig. 1-2)**. In general, both VD and lateral projections are taken for imaging the body. Correct positioning is imperative for the radiographic results to be properly assessed. However, this is often not considered in practice due to the clinician's uncertainty in positioning the avian patient (see **Fig. 1-1**).

For the lateral projection, the bird is placed in standard right lateral recumbency. Special care should be taken when positioning birds in lateral recumbency if they are suffering from respiratory depression. The extension of the patient's wing(s), as required when a bird is placed in lateral recumbency, often results in respiratory compromise.

Due to the relatively small body size of many birds, a whole body radiograph, which includes proximal regions of the fore and hindlimbs, can be taken.

Under normal conditions, the following structures are observed in the lateral projection:

- ☐ spine
- ☐ heart/major blood vessels
- ☐ lung structure/main bronchus
- ☐ caudal walls of the air sacs (if pathologically changed)
- ☐ spleen
- ☐ kidneys/gonads
- ☐ crop/esophagus, proventriculus and gizzard
- ☐ intestines and cloaca.

In comparison, VD radiographs are suitable for assessing the following:

- ☐ variations in symmetry of the relative positions of the organs
- ☐ pectoral girdle/pelvis
- ☐ hip and femur
- ☐ heart and liver shadows
- ☐ axillary diverticula/caudal air sacs

Since the wing is depicted in the mediolateral plane of both the ventrodorsal and lateral positions, a caudocranial radiograph is needed for another plane of assessment of the forelimbs (= second projection; see **Figs. 1-2** and **1-18**).

In weak or fractious birds, the clinician can attempt to take an exploratory radiographic image(s) of an unsecured patient. For example, if it is suspected that the bird has ingested heavy metal particles, a survey radiographic image will identify the toxic material thereby allowing for immediate initiation of a proper treatment protocol. To take exploratory radiographic images on an unsecured patient, 2 views may be taken, 1) (using a vertical beam) DV projection, with the bird being placed in a radiolucent container on the x-ray cassette; 2) (using a horizontal beam) bird held as perpendicular as possible, on the x-ray table and as close to the cassette as possible **(Fig. 1-3)**.

The latter position is also useful for the diagnosis of ascites as the level of fluid can be identified in the standing animal.

In most cases, avian patients require fixed positioning to produce diagnostic radiographic images. Various methods can be used, but the method of choice is the use of restraint board fixation. The bird is tethered to a Plexiglas® avian restraint board **(Figs. 1-4A, B, 1-5 and 1-6)** in the positions desired for imaging. With many avian patients sedation is not necessary. The board should not be thicker than 5 mm, as the sharpness of the radiographic image is adversely affected as the board's thickness increases. To secure the head, exchangeable neck pieces are needed, adapted to the size of the patient's cervical area. The limbs should be tied with laces or leather bands that are at least 3–5 mm wide, as narrower bands can lead to cutting injuries. With board fixation, the bird has a greater chance of moving which will lead to motion blur thereby causing a greater loss in detail than that noted with handheld patients. While the bird may move while in the restraint board, the personnel involved with obtaining the images are not exposed to radiation and the board method does not appear to have any disadvantages for the patient. To help sedate the restrained bird, especially parrots, it is useful to offer them a piece of wood to bite on or to cover their heads with a light cloth.

Board restraint is contraindicated in critically ill birds or those suffering from circulatory and/or respiratory depression. Board restraint is contraindicated in critically ill birds because the clinicians do not have any direct contact with the bird during the procedure, therefore they are unlikely to recognize deterioration in the patient's condition at that time. In addition, with manual restraint a bird can be brought quickly into an upright position if needed, whereas with board fixation the bird will have to be released first. High-risk patients should be manually retrained for a radiographic investigation. Manual restraint is also suitable for raptors with a body weight of more than 1000 g as these birds can be held with lead gloves without difficulty.

It is very hard to properly hold small birds (i.e. with a body weight of less than 40 g) in a desired position when one is wearing lead gloves. Only in extreme circumstances should manual restraint be used by placing the bird in the correct position with unprotected hands. An assistant must then cover the investigator's hands completely with either lead gloves or lead plates **(Figs. 1-7** and **1-8)**.

Positioning small birds with adhesive tape is only applicable in relatively few cases. The bird must be sedated because only then can the patient be positioned tautly enough to the cassette to prevent motion artifact. Adhesive tape (e.g. adhesive film, crepe) can be used to position birds for taking radiographs of the head or an individual toe. The influence of the tape on the radiographic quality is generally minimal. It is important that the brand of tape is not too sticky so that it does not cause any large-scale damage to the bird's skin or feathers when removed. For feathered parts of the body, adhesive crepe tape is more suitable, while products with a stronger degree of tackiness have been used successfully for the horny parts of the body (e.g. beak, leg, foot; **Figs. 1-9A–C, 1-13, 1-14)**. The horny tissue can be cleansed using soapy water before being taped to ensure that the adhesive adheres better

1.1.2.2 Positioning for imaging the body

Ventrodorsal radiographs

If the patient needs to be held manually, then the bird's head should be caught from behind with the thumb and index finger of one hand holding the jaws together. The bird's legs are then stretched away from the body and held by the other hand. In this position, the bird is placed on its back on the x-ray table. One should make sure that the bird is in the correct position (i.e. the bird must be positioned so that the ridge of the breast bone and the spine are superimposed on the radiograph). The wings are stretched outwards and held in position with weighted material to prevent superimposition of the limbs in the region of the shoulder joint **(Figs. 1-5** and **1-7A)**. The hand fixing the head should be slightly bent so that the bird gets enough air and is able to breathe properly.

Allthough larger birds can be placed in a proper position manually while using lead gloves, this is not possible in birds with a body weight of less than 40 g. If small birds (i.e. < 40 g) have to be manually positioned, this should initially be performed as described above with unprotected hands. Once the beam has been focused properly, the hands holding the bird should be covered with radiopaque material (e.g. lead gloves, lead plates). The assistant's hands must be kept out of the primary beam at all times **(Fig. 1-7)**!

In extremely rare cases, sedated small birds can be fixed to the x-ray table using adhesive tape. The neck, the wings at the level of the primary feathers, and the legs in the region of the intertarsal joints are fixed into position with tape. If necessary, additional tape can be placed over the chest to minimize motion blur. Loss of feathers from such regions due to the tape removal cannot be avoided.

If an avian restraint board is available, the bird should be positioned to the board as described above. Care should always be taken in patients with long tail feathers (macaws, pheasants, etc.) so that the tail lies in a straight line to the spine ensuring that a symmetrical image can be taken.

The central beam should be directed vertically to the cassette targeting the bird medially, roughly at the level of the caudal costal arch.

Lateral radiographs

For a lateral projection, the patient must be placed on its right side. With manual restraint, the head of the bird is held with the thumb and index finger of one hand holding the jaws together and the other hand should hold the feet stretched of the caudally as much as possible. This is important to prevent superimposition on the radiograph by the legs, which would make interpretation images difficult at best **(Fig. 1-10)**. The wings should be pulled over the back of the bird and kept in place by the forearm of the person holding the bird **(Fig. 1-8)**. To prevent superimposition, the right wing should be positioned slightly lower and in front of the left wing and the right leg in front of the left leg. To prevent the bird's body from being twisted, a radiolucent object (e.g. cellulose wadding, pillows) with a suitable width should be placed between the wings. This enables a torsion-free radiograph to be made of a hand-held patient **(Fig. 1-6)**.

If due to the size of the bird (i.e. but < 40 g), positioning of the patient is not feasible when wearing lead gloves, then the bird should be put into position using bare hands which are then covered with radiopaque material **(Fig. 1-8)**.

Small birds with a body weight of less than 40 g should only be fixed with adhesive tape in rare cases for a lateral radiograph and only after being sedated. The bird should be placed on its right side on the x-ray table and placed into position using adhesive tape over the neck, the dorsally stretched wings, and the caudally stretched legs. An additional piece of tape can be placed over the breast to help reduce motion artifact with unsettled birds.

The method of choice for proper positioning is an avian restraint board, whereby the bird is placed in the lateral position as described above. Once the head has been secured by a suitably sized neck piece **(Figs. 1-4A, B, 1-6)**, the wings are placed in their proper position. To ensure that there is no twisting, a radiolucent spacer of suitable width should be situated between the wings. The legs should be stretched out as far as possible then secured using the ties attached to the board **(Fig. 1-6)**. The position of the bird can be additionally stabilized by placing weights on the feet. Transferring the bird from supine to lateral recumbency can be done without releasing the bird's head from the board – the neck pieces used to secure the head usually provide enough room for the bird to be able to turn its head.

The central beam is directed vertically to the table and should be aimed at the longitudinal axis of the body, roughly at the caudal part of the costal arch. If the body has been positioned correctly, the hips are superimposed in the lateral projection.

1.1.2.3 Positioning for imaging the head

For radiologic images of the head, the standard projections are DV, VD and lateral. With these views, it is possible to diagnose the radiographically depicted anomalies with a satisfactory degree of confidence. In addition, further images can be obtained from the rostrocaudal projection at angles of 30° or 75° **(Fig. 1-9)**.

Principally, radiography of the head can be performed with either manual positioning of the patient or by using an avian restraint board. However, as exact positioning is a prerequisite for diagnosis of diseases involving the head, sedation of the bird is required. Without the use of a board to restrain the bird, it is usually necessary, in the majority of cases, to heavily sedate the patient to prevent the occurrence of motion artifact. If an avian restraint board is available, then light sedation is usually all that is needed. One disadvantage of the avian restraint board is the neck piece, which causes a reduction in image quality by attenuating the beam as its radiographic shadow superimposes on the back of the head and/or the cranial cervical vertebra **(Fig. 1-17)**. As a consequence, one should consider the benefits of leaving the neck piece off versus the risk of placing the patient under a deeper level of sedation.

Fig. 1-1: Radiograph referred for assessment of a beak fracture (and subsequent repair with a cerclage wire) in a small parakeet. The image quality, aiming of the central beam, correct positioning of the patient, and radiation protection measures are often neglected in small avian patients, often resulting in the radiographic image being uninterpretable.

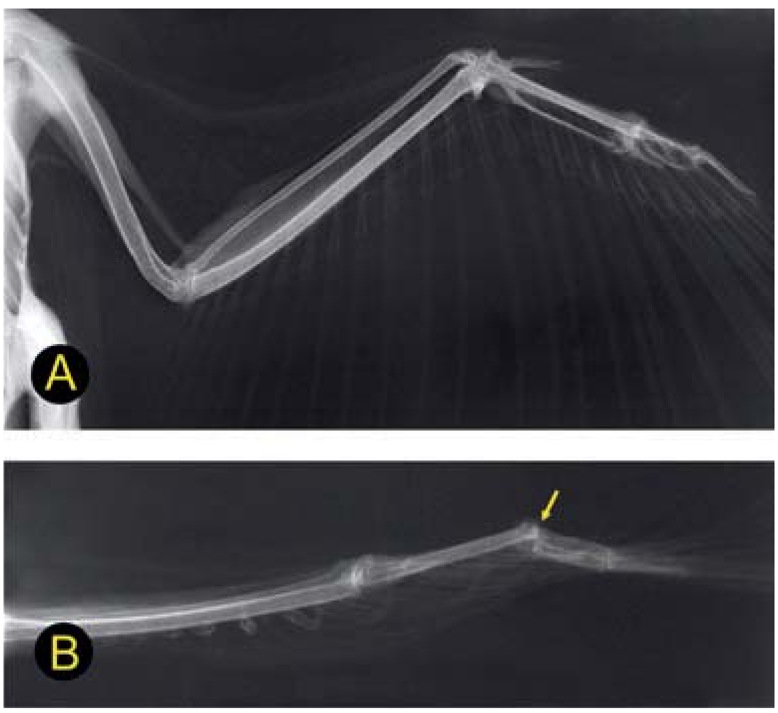

Fig. 1-2: Radiographic images of a barn owl (*Tyto alba*) wing showing the ventrodorsal (A) and caudocranial (B) projections. The luxation of the metacarpal joint is only visible in the caudocranial projection (arrow) due to the different planes of the skeletal structures in the two projections. This underlines the need to always take radiographs in at least two planes.

Fig. 1-3: Radiographic examination of a canary placed in a radiolucent container (behind the box is the cassette) to rule out the ingestion of heavy metal particles. The x-ray tube is to the right of the picture.

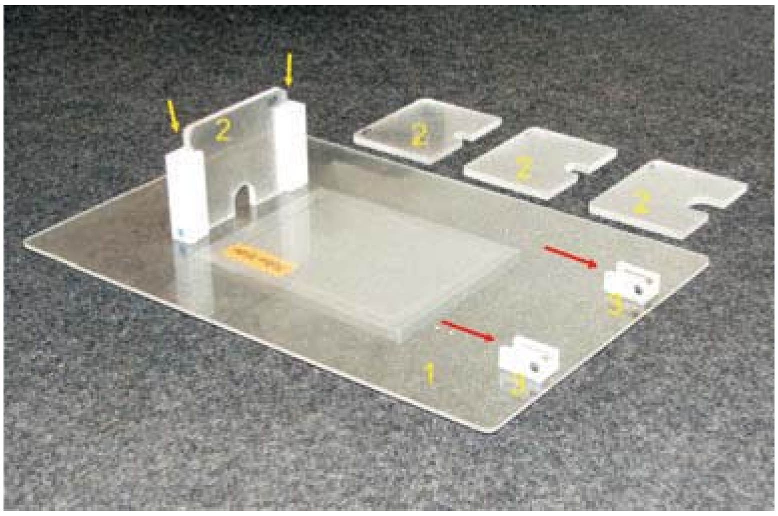

Fig. 1-4A: Plexiglas® avian restraint board (1) with various head pieces (2) used for the fixation of birds. The head piece needs to be locked into the fastener (yellow arrows). Additional device (3) for the fixation of the hindlegs with shoe laces or similar cord (red arrows: direction of tightening). The film cassette is lying under the restraint board.

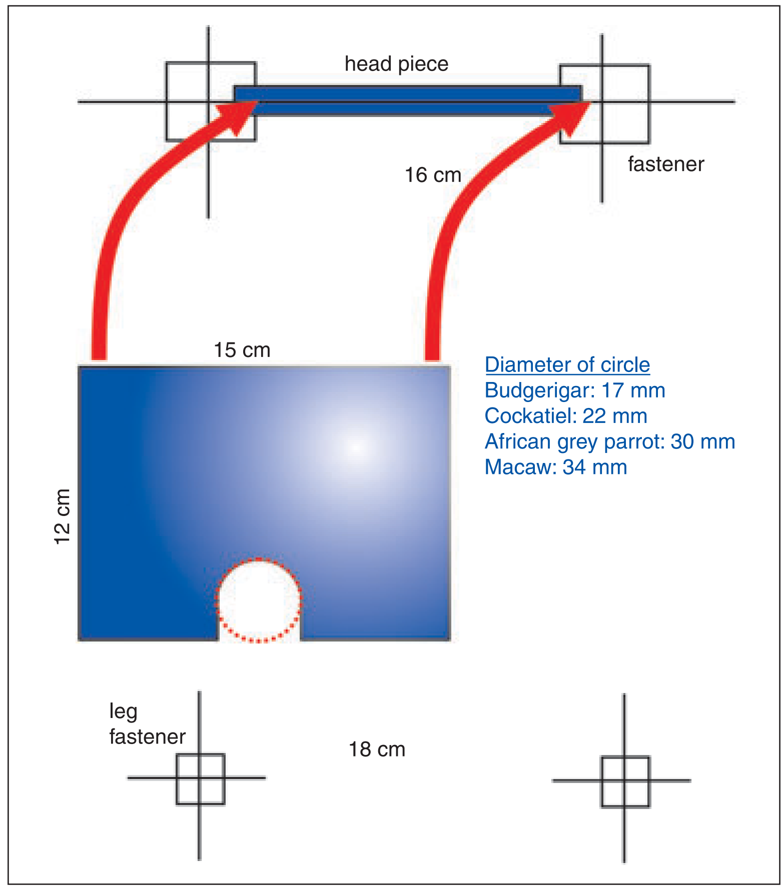

Fig. 1-4B: Schematic drawing and dimensions of the plexiglas® avian restraint board from Fig. 1-4A.

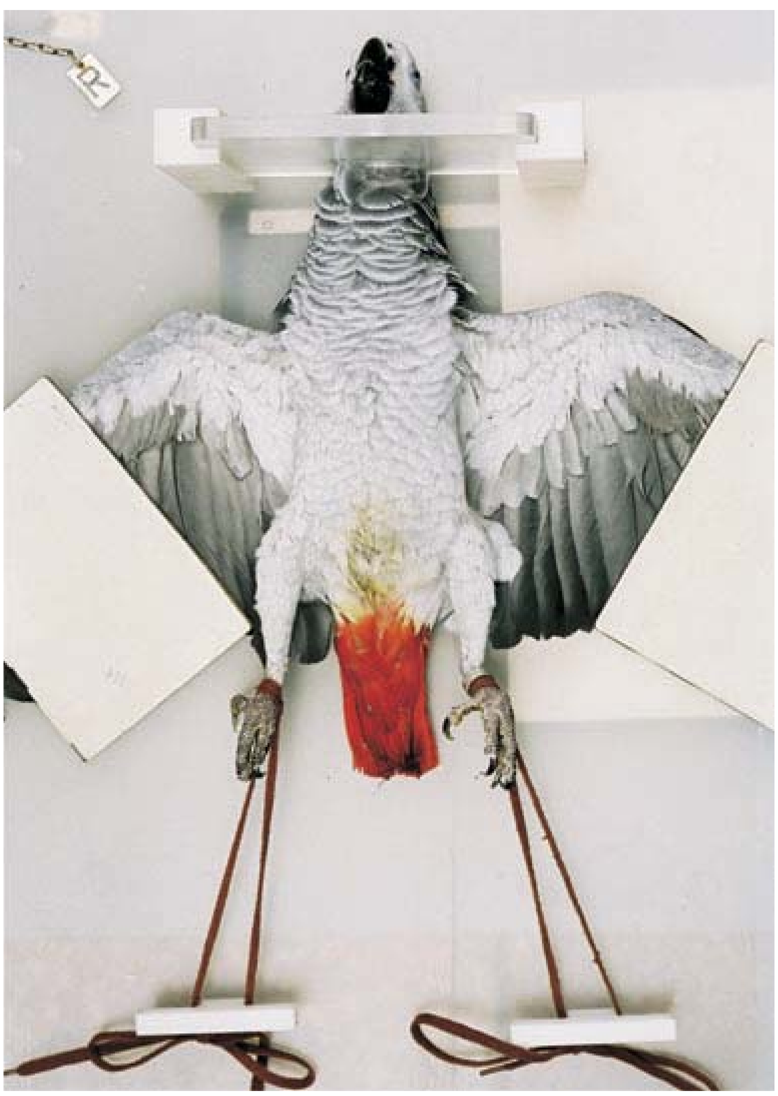

Fig. 1-5: African grey parrot (*Psittacus erithacus*): Board fixation for a ventrodorsal radiograph.

Fig. 1-6: African grey parrot (*Psittacus erithacus*): Board fixation for a lateral radiograph.

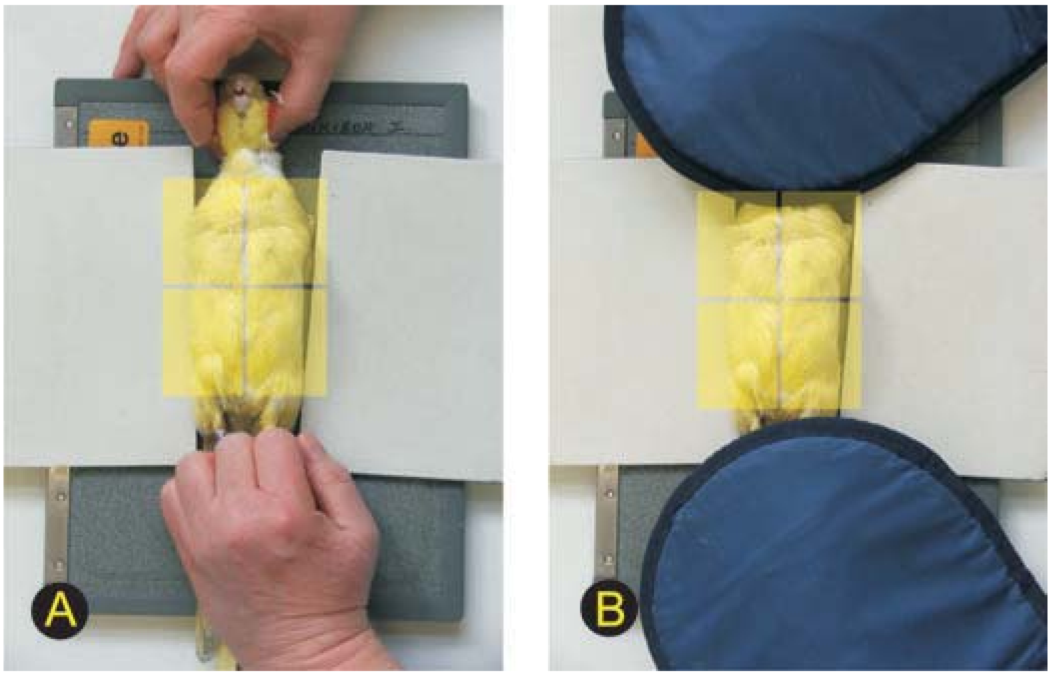

Fig. 1-7: Cockatiel (*Nymphicus hollandicus*): Manual fixation for a ventrodorsal radiograph.

A: Without any radiation protection.

B: With radiopaque shielding of the hands.

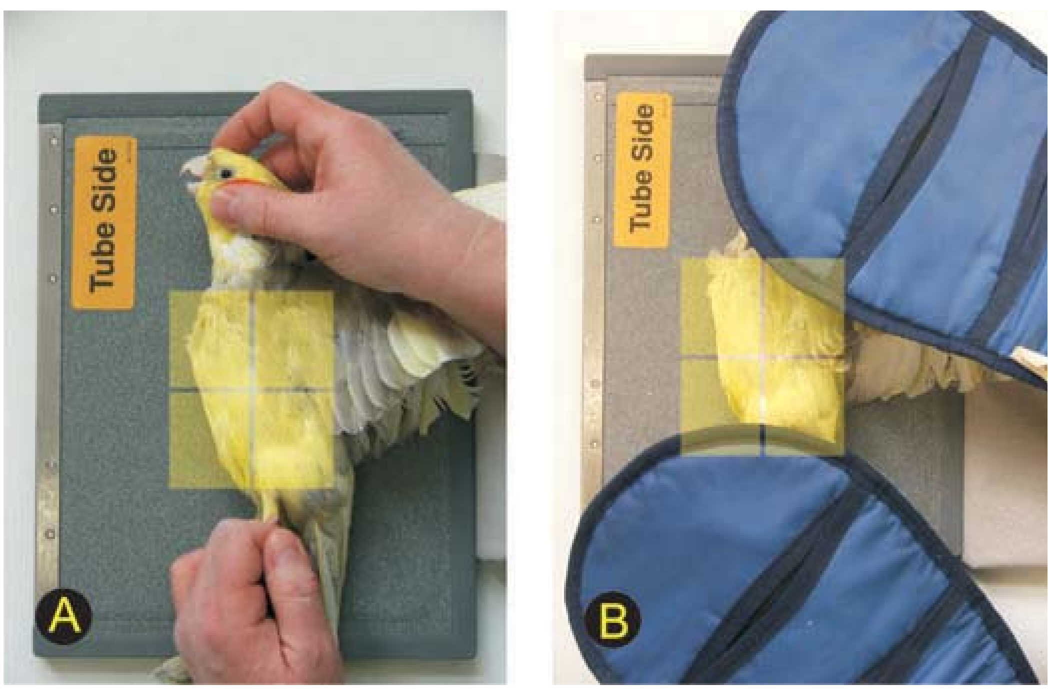

Fig. 1-8: Cockatiel (*Nymphicus hollandicus*): Manual fixation for a lateral radiograph.

A: Without any radiation protection.

B: With radiopaque shielding of the hands.

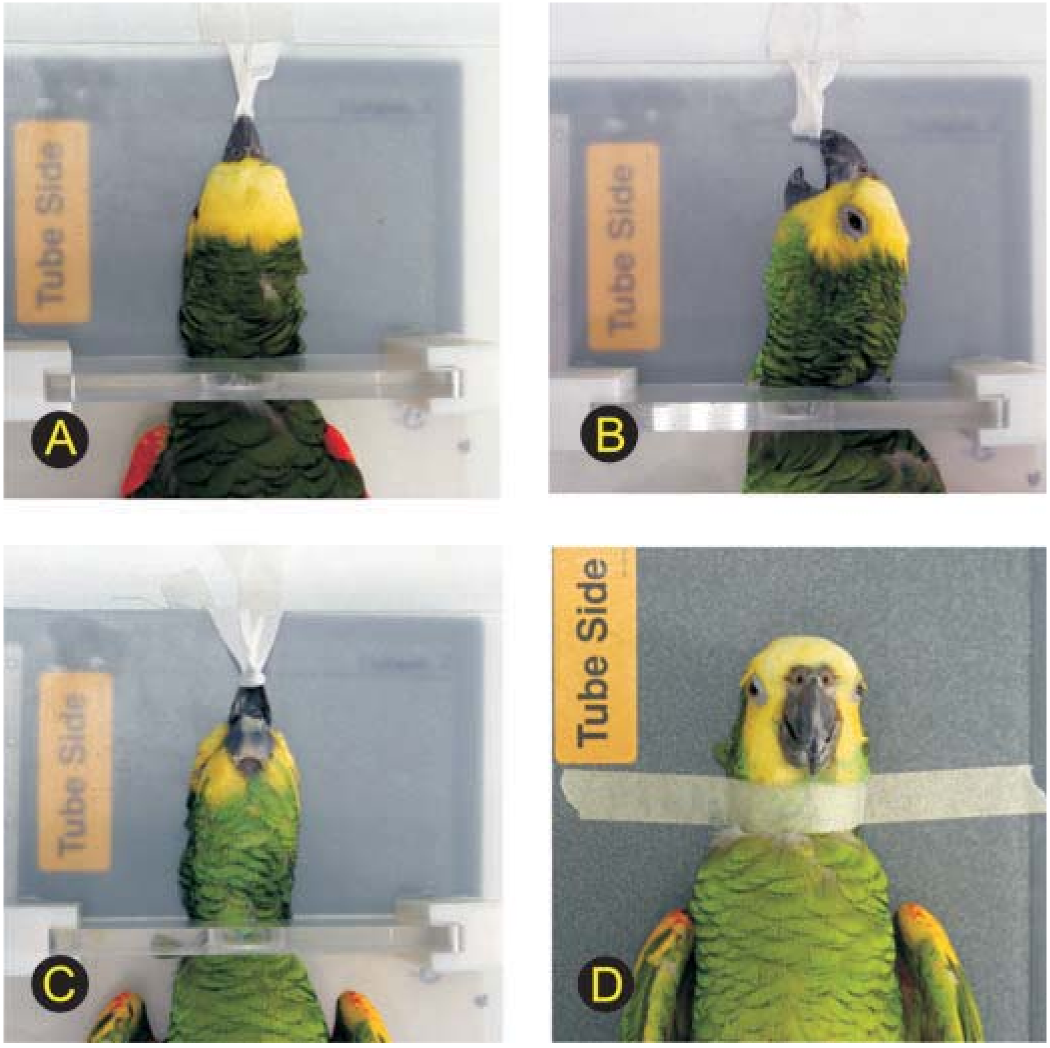

Fig. 1-9: Blue-fronted Amazon (*Amazona aestiva*): Positioning of the head for (A) dorsoventral, (B) lateral, (C) ventrodorsal, and (D) rostrocaudal radiographs following isoflurane induction for short-term sedation.

Fig. 1-10: Radiographic image of a common buzzard's (*Buteo buteo*) body using a lateral projection. The internal organs cannot be assessed because the legs have not been completely extended in a caudal position.

Dorsoventral radiographs

For a DV radiograph, the sedated bird is placed in ventral recumbancy (prone). The tip of the upper beak is cleansed and secured with extremely tacky adhesive tape. The extremities of the patient can be held either manually or with an avian restraint board using ties and adhesive tape. The neck of the bird is stretched and held in position using the tape on its beak. When done correctly, the head now lies symmetrically with both lower jaws flat on the cassette or restraint board **(Fig. 1-9A)**.

Ventrodorsal radiographs

A VD radiograph can be taken in a similar manner. The sedated patient is placed in dorsal recumbancy and fixed. It is important to ensure that the positioning is symmetrical. By pulling on the adhesive tape attached to the bird's beak, the neck is stretched and fixed without twisting. With exact positioning, both the lower jaws lie parallel to the cassette **(Fig. 1-9C)**.

Lateral radiographs

If the head needs to be radiographed on its side, the patient is placed in right lateral recumbency and restrained either manually or using an avian restraint board. The neck of the bird is stretched as far as possible and secured in this position using a tape attached to its upper beak. It is important when interpreting the radiographic images that the positioning is exactly symmetrical, especially in this projection, since assessment of the radiographs can be adversely affected by asymmetry **(Fig. 1-9B)**.

Rostrocaudal, caudorostral, and oblique radiographs

For rostrocaudal radiographs, the bird is laid on its back with its body and limbs secured. The head of the bird is laid at an angle of 90° to the cassette with its beak closed or slightly opened. The head is held in this position by a piece of adhesive tape placed on the base of its neck. For this projection, the central beam is directed vertically towards the cassette and is aimed at the tip of the beak **(Fig. 1-9D)**.

If the head needs to be radiographed in the caudorostral projection, the bird is placed and secured in a similar position but this time in ventral recumbency.

For oblique radiographs, the head of the x-ray machine is placed at the required angle (i.e. 30° or 75° are most often used) and the central beam is aimed at the middle of the parietal bone (back of the head).

1.1.2.4 Positioning for imaging the wing

When the bird is positioned for radiographs of the body in dorsal or lateral recumbency, the wings are always viewed in the mediolateral plane. For radiographic images of the wing, the patient is usually positioned in dorsal recumbency and secured as described above. The wing is stretched as far as possible before being held in place **(Fig. 1-11)**.

To position the bird for the second projection of the wing (caudocranial), it is necessary to place the bird on the edge of the table with its head lying down (the cassette is placed on the edge of the table). The feet and tail are held with one hand, while the head is held at the base of the beak with the thumb and index finger of the other hand. A second person should stretch the wing to be radiographed as far as possible away from the bird's body, with the front of the wing lying on the cassette parallel to the edge of the cassette **(Fig. 1-12)**. The central beam is aimed at a 90° angle to the cassette, focusing on the elbow joint.

1.1.2.5 Positioning for imaging the hindlimb

A dorsoplantar radiograph of the hindlimbs is performed with the bird positioned in dorsal recumbency as described above for the VD radiograph of the body **(Fig. 1-13)**.

The patient is radiographed in lateral recumbency for mediolateral radiographs. Depending on the disease condition being evaluated, the animal is placed on its right or left side, so that the extremity to be radiographed is placed as close to the cassette as possible. The central beam is aimed vertically at the cassette and focused on the intertarsal joint. If the toes need to be radiographed, it is recommended to position each individually to the table or cassette using adhesive tape **(Fig. 1-14)**.

Fig. 1-11: Common buzzard (*Buteo buteo*): Positioning of the wing for a mediolateral radiograph. The bird has been fixed on a plexiglas® avian restraint board.

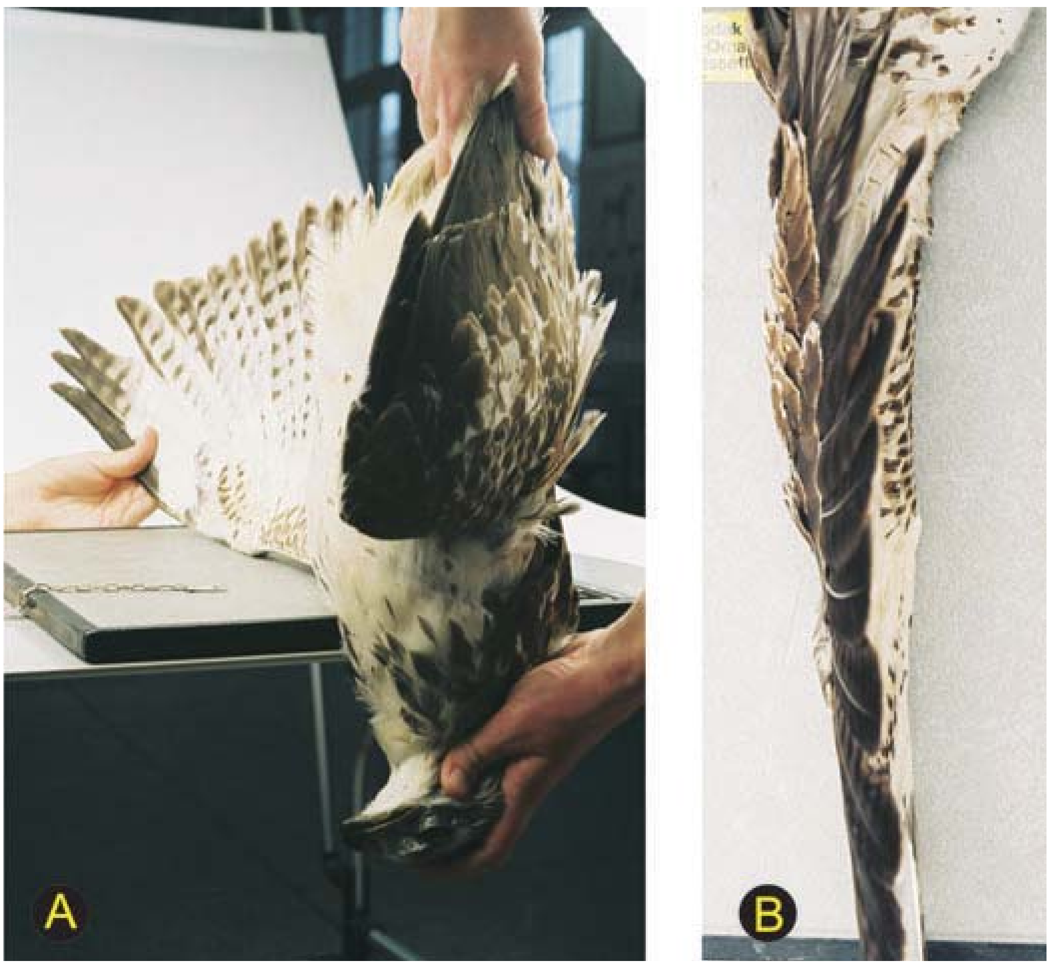

A: side projection.

B: projection from above.

Fig. 1-12: Common buzzard (*Buteo buteo*): Positioning and fixation of the wing for a caudocranial radiograph.

Fig. 1-13: Blue-fronted Amazon (*Amazona aestiva*): Positioning of the legs for a dorsoplantar radiograph.

Fig. 1-14: Blue-fronted Amazon (*Amazona aestiva*): Positioning of the legs for a mediolateral radiograph.

1.1.3 Anatomical-physiological representation

1.1.3.1 Skeletal system

Cranium and axial skeleton

There is significant anatomic variation of the beak between avian species along with breed-specific differences within a species (e.g. domestic pigeons). The owls (strigiforms), primarily a nocturnal avian group, have voluminous eyeballs set in large orbits. The two eyes are only separated by a thin, slightly radiopaque wall. A radiopaque structure that is distinctive to the avian eye is the ossified scleral ring. The bones of the cranium are pneumatic (filled with air), with the extent of air within this area dependent on the species examined **(Figs. 1-15** and **1-16)**. The air spaces within the cranial bones are in direct contact to the infraorbital sinus through connections called diverticula.

The cervical and parts of the thoracic vertebral bones are also pneumatized. In contrast to mammals, the number of vertebrae within the class Aves is not constant but is variable depending on the species (e.g. domestic chicken 16, mute swan 25). In many avian species, there is a fusion of the free thoracic vertebrae forming the notarium. When the caudal thoracic vertebra, lumbar vertebrae, and sacrum, as well as, some of the cranial coccygeal vertebrae fuse, this forms a structure called the synsacrum (the dorsal wall of the pelvic girdle) **(Fig. 1-22)**. The last free thoracic vertebra before the synsacrum is often movable and this area of the spine is predisposed to fractures.

Indications

- ☐ trauma, beak injuries, fractures of the jaw or hyoid apparatus, suspicion of spinal fracture
- ☐ swelling or increased size of the head (e.g. chronic sinusitis)
- ☐ suspicion of tumor formation (e.g. retrobulbar tumors)
- ☐ injuries of the cervical air sac

Possible clinical signs

- ☐ external injuries, hemorrhages
- ☐ paralysis, with injuries of the spine often in combination with difficulties in defecation
- ☐ CNS abnormalities
- ☐ abnormal stance, torticollis
- ☐ swellings
- ☐ chronic respiratory problems, nasal discharge
- ☐ therapy-resistant subcutaneous emphysema
- ☐ problems with food uptake, weight loss of unknown cause

Trunk and limb skeleton

To aid in the reduction of their body weight, the skeletal system of flighted birds is characterized by a high degree of pneumatization, primarily involving bones of the proximal skeleton. Bones within the proximal skeleton that contain air include the humerus and coracoid, but also the thorax (i.e. parts of the ribs and especially the sternum, including the sternal ridge), the pelvic girdle, and femur. Typical radiographic images of pneumatized bones show thin radiopaque cortices surrounding a loose system of fine three-dimensionally connected bony trabeculae. In contrast, the distal parts of the wing and leg skeleton do not have any air-filled spaces.

The ulna appears more prominent in the avian forewing skeleton **(Fig. 1-18)** than the radius. Both the wing and foot skeletal structures are characterized by reductions and fusions of the bones. The distal carpal and metacarpal bones fuse to form the carpometacarpus, while the tibia and proximal parts of the tarsus form the tibiotarsus. In the foot, the tarsal bones are fused with the metatarsal bones forming the tarsometatarsus **(Fig. 1-19)**.

The increase of circulating blood estrogen when female birds are reproductively active leads to an increased radiopacity of the medullary cavity within the long bones of female birds. This increase in radiopacity within the long bones is due to an increased thickness of the compact bone and the laying down of calcium deposits in the form of so-called medullary bone tissue within the medullary cavity **(Fig. 1-21)**.

The radiographic assessment of the pectoral girdle and the pelvic region is hindered by the superimposition of the well-formed wing and leg musculature. There is superimposition of the coracoid and scapula in the VD projection of the pectoral girdle **(Fig. 1-23)**. If there is suspicion of changes in this area, then asymmetrical positioning is needed; by slightly tilting the patient off center, both parts of the pectoral girdle can be assessed. In addition, the imaging of the cranial air sac system can also be impaired due to the superimposition of the well-developed pectoral musculature.

Indications

- ☐ fractures, fissures, investigations to control the course of healing
- ☐ malpositioning of the extremities, luxations
- ☐ infections that also involves the skeletal structures (e.g. pododermatitis [Bumblefoot], tuberculosis, etc.)
- ☐ metabolic disturbances, nutritional deficiency (e.g. rickets in young birds)
- ☐ suspicion of a foreign body (e.g. gunshot in wild or imported birds)

Possible clinical signs

- ☐ reduced resistance of the hindlimbs
- ☐ reduction or loss of ability to fly, abnormal posture of one or both wings
- ☐ abnormal posture, skeletal deformation
- ☐ neoplasia or osteophyte production on the skeleton
- ☐ swellings, inflammation
- ☐ cachexia of unknown etiology
- ☐ abdominal hernia (in connection with bony changes associated with pathological hyperostosis)

Normal variations

The diagnostic capability of radiographic imaging of young birds is poor due to the lack of radiodense skeletal structures **(Fig. 1-20)**. Only with increasing calcification can the bones be adequately radiodense for optimum evaluation.

In contrast to mammals, the epiphyses of growing birds exhibit no epiphyseal zones of ossification, with one exception, the intertarsal joint. During the maturation of the intertarsal joint, each of the tarsal bones develops separately. In birds the proximal row of the tarsal bones fuse with the tibia to form the tibiotarsus, while the tarsometatarsus develops from the fusion of the distal tarsal bones with the metatarsus.

The air sac diverticuli that grow into the humerus are at first not very large and attain their final size by successive pneumatization of the medullary cavity. Due to the lack of age-related scientific investigations, neither the degree of humeral pneumatization nor the state of calcification of the skeleton can be used for age determination in pet birds.

During reproductive activity, female birds have a higher degree of bone density due to their hormonal status. This increased bone density affects the femurs and other long bones and should be considered as being normal. Starting in the endosteum, medullary bony tissue is formed in reproductively active females thereby acting as a calcium reserve for producing egg shells **(Fig. 1-21)**.

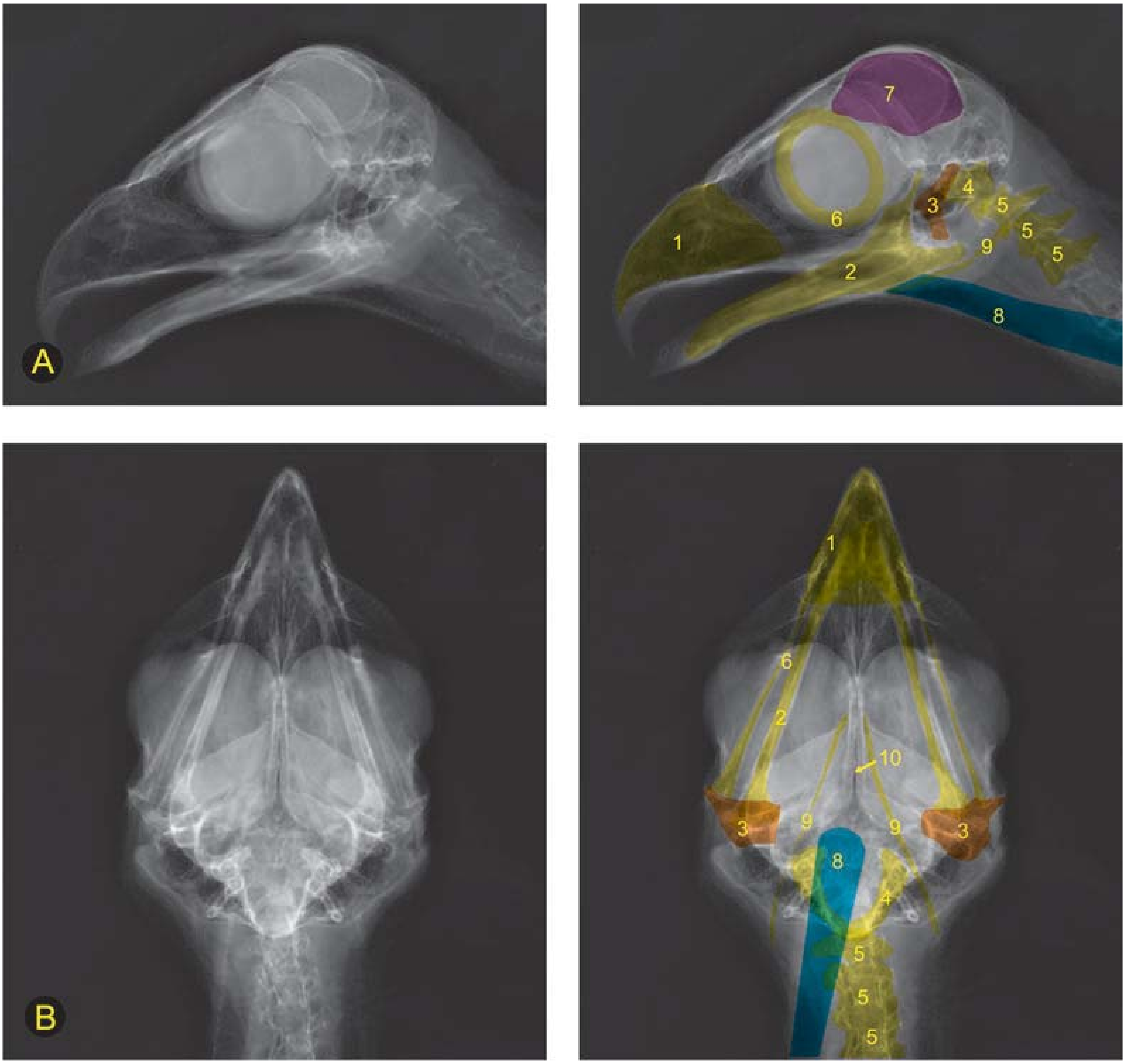

Fig. 1-15: Radiographic images of a goshawk's (*Accipiter gentilis*) head showing the (A) lateral and (B) ventrodorsal projections.

1: upper beak
2: lower beak
3: quadrate bone
4: dorsal arch of the atlas
5: cervical vertebrae
6: scleral ring
7: brain
8: trachea
9: hyoid bone
10: vomer

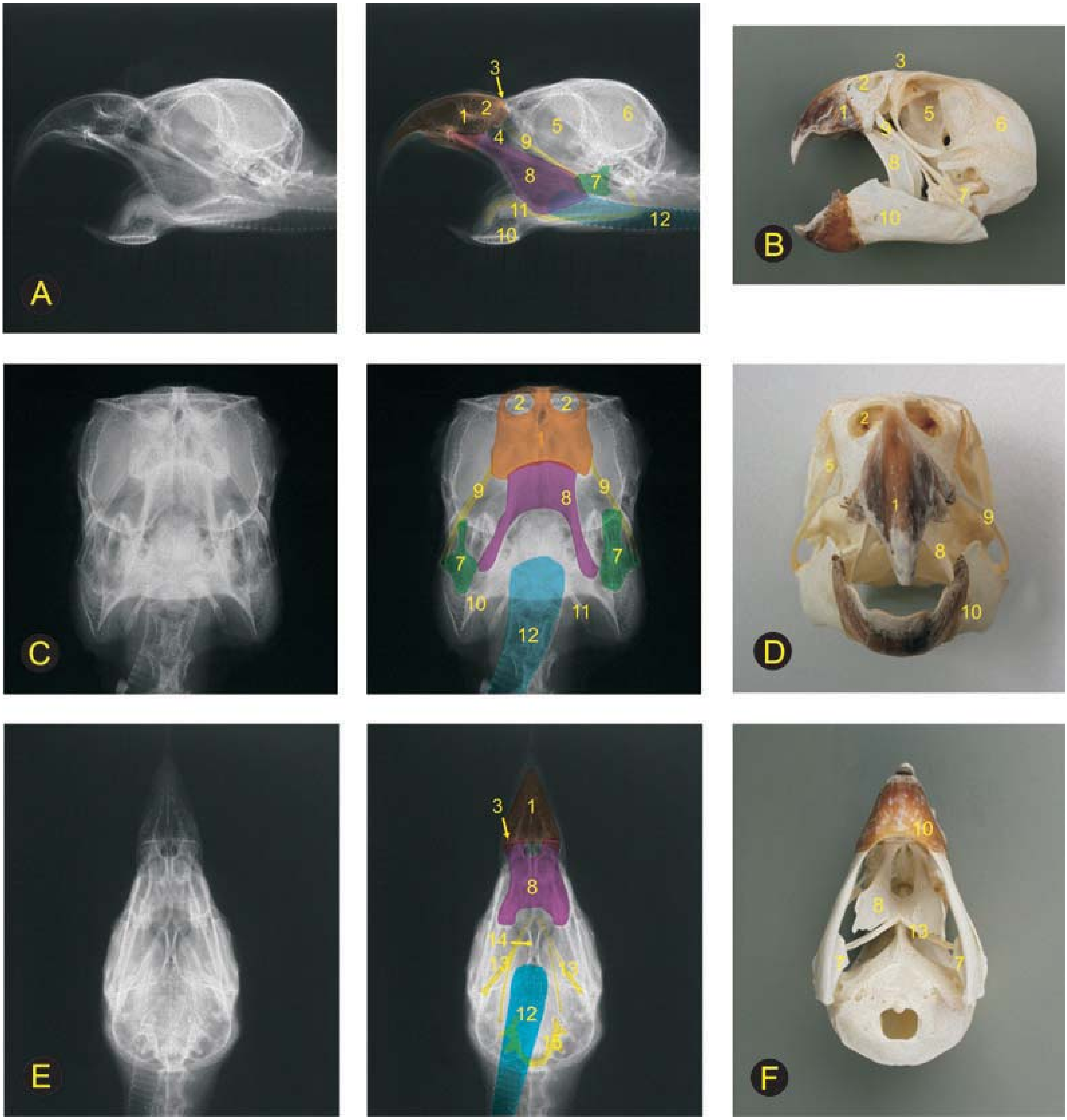

Fig. 1-16: Radiograph images of a blue-fronted Amazon parrot's (*Amazona aestiva*) head showing the (A) lateral, (C) rostrocaudal, (E) ventrodorsal projections, each with the respective projection of the cranium (B, D, F).

1: horny sheath of the upper beak
2: bony nares
3: craniofacial fissure
4: parts of the infraorbital sinus
5: orbit
6: parietal bone
7: quadrate bone
8: palatine bone
9: jugal bar
10: horny sheath of the lower beak
11: hyoid bone
12: trachea
13: pterygoid process of sphenoid bone
14: vomer
15: dorsal arch of the atlas

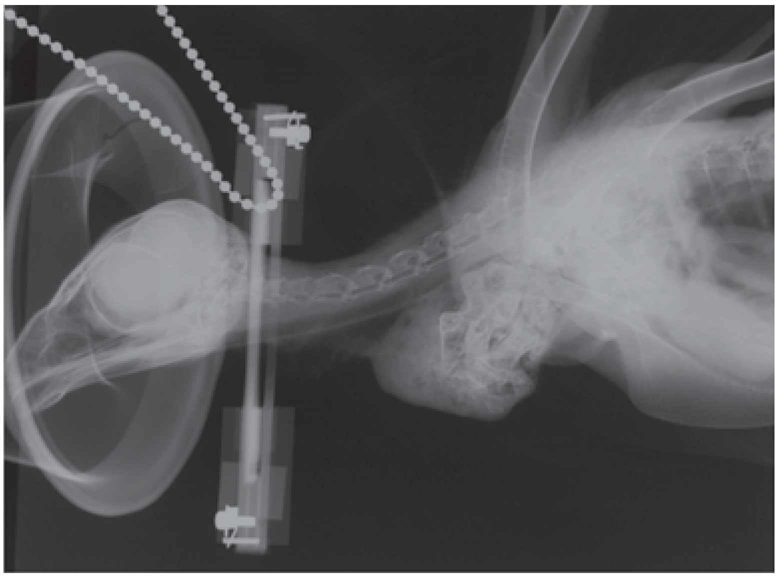

Fig. 1-17: Radiographic image of the craniocervical region of a gyrfalcon (*Falco rusticolus*) showing a lateral projection. A bone is lying in the esophagus. The bird was sedated using an inhalational anesthetic administered with a face mask and positioned on a plexiglas® avian restraint board.

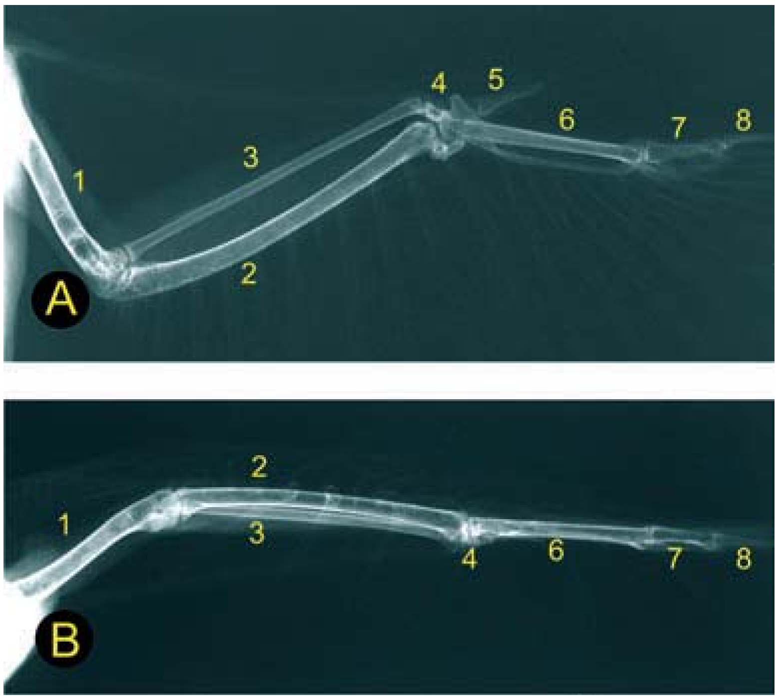

1: humerus
2: ulna
3: radius
4: carpometacarpus
5: alula (thumb)
6: metacarpal bone
7: proximal phalanx
8: distal phalanx

Fig. 1-18: Radiographic images of a blue-fronted Amazon's (*Amazona aestiva*) wing showing the (A) ventrodorsal and (B) caudocranial projections.

1: femur
2: tibiotarsus
3: tarsometatarsus
4: metatarsus
5, 6, 7: digit with phalanges

Fig. 1-19: Radiographic images of a blue-fronted Amazon parrot's (*Amazona aestiva*) leg showing the (A) mediolateral and (B) dorsoplantar projections.

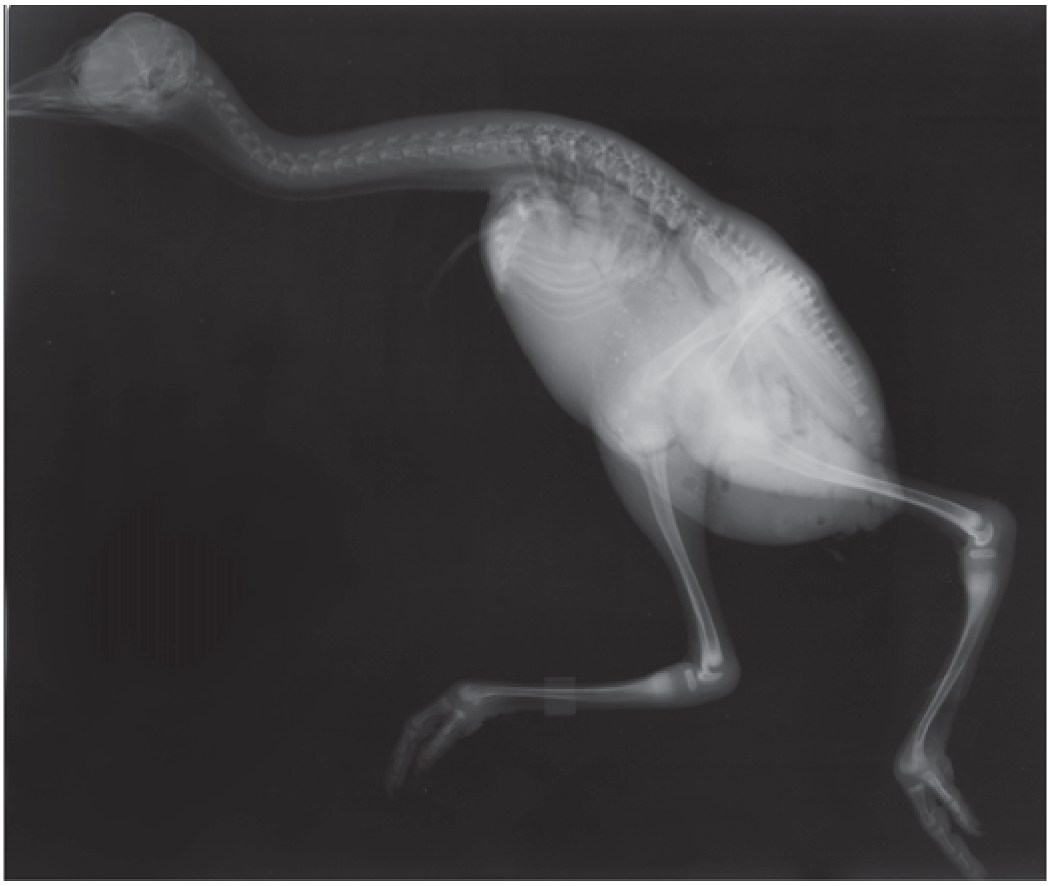

Fig. 1-20: Total body radiographic image of an emu (*Dromaius novaehollandiae*) showing the lateral projection. Young birds, such as this, have wide joint cavities because their bones lack ossification; this condition is especially prominent in the ankle. The emu's stomach and intestines have a voluminous silhouette, which is typical for young birds.

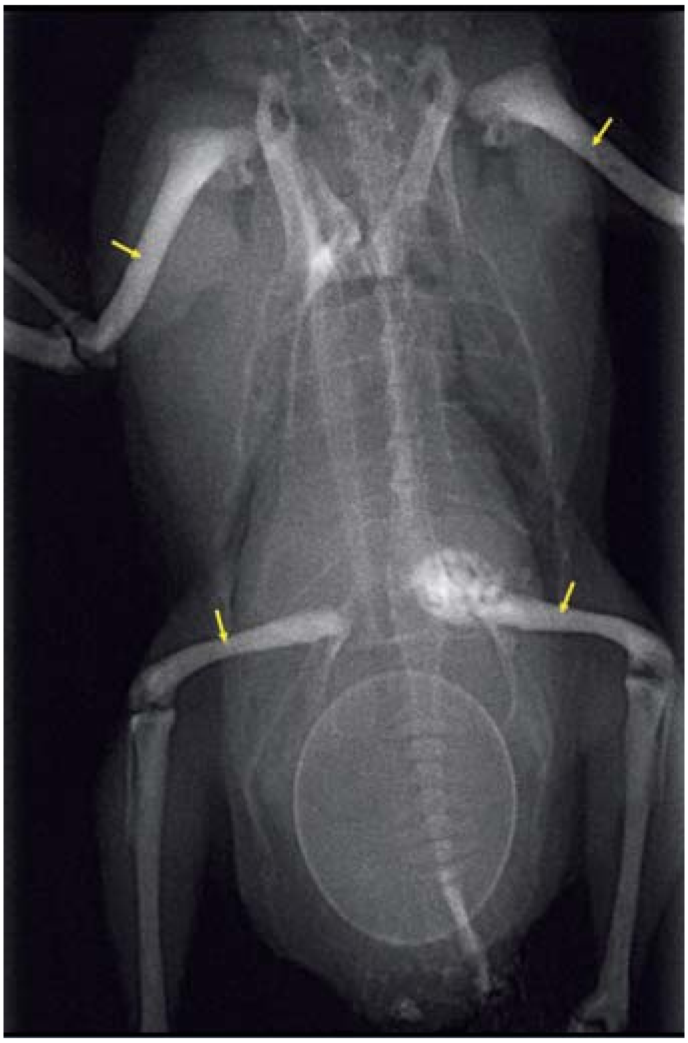

Fig. 1-21: Total body radiographic image of a budgerigar (*Melopsittacus undulatus*) showing the ventrodorsal projection. Formation of medullary bone can be observed in the pectoral girdle, humerus (arrows), femur (arrows), and tibiotarsus. Egg formation in the abdomen has led to the compression of the air sacs, displacement of the gizzard and changes in the silhouette of the heart and liver.

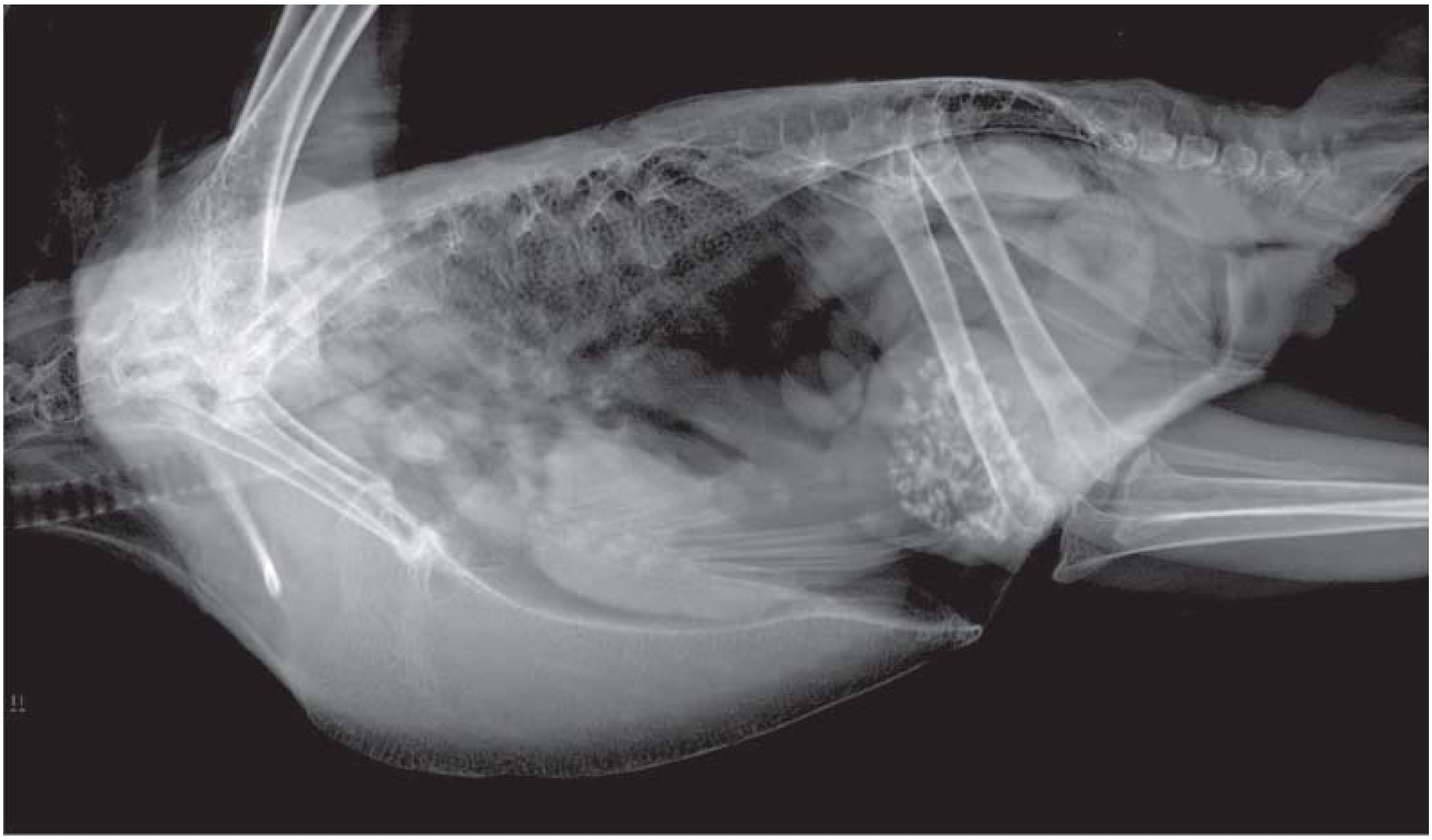

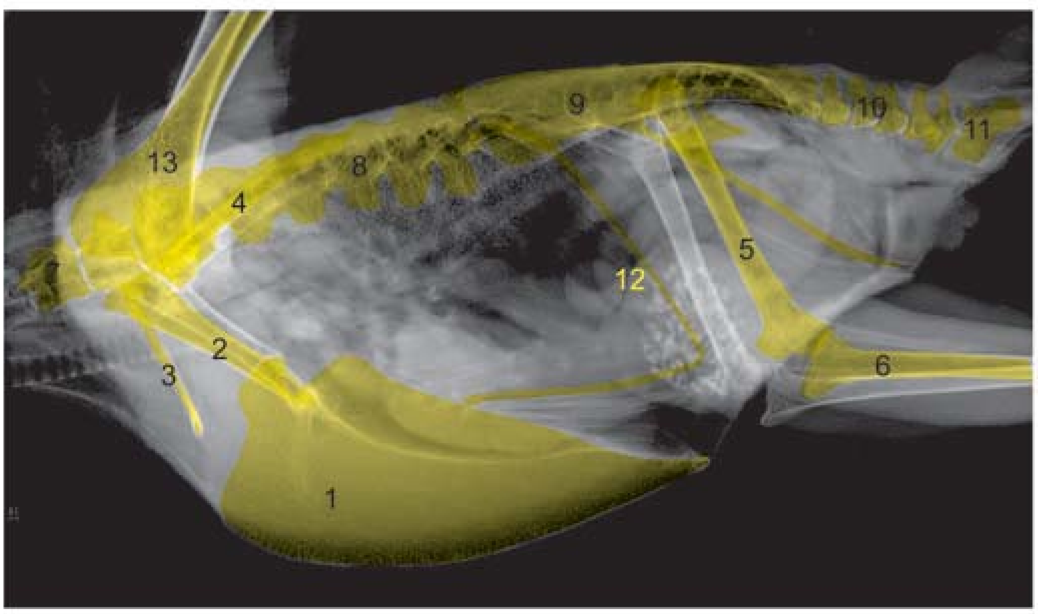

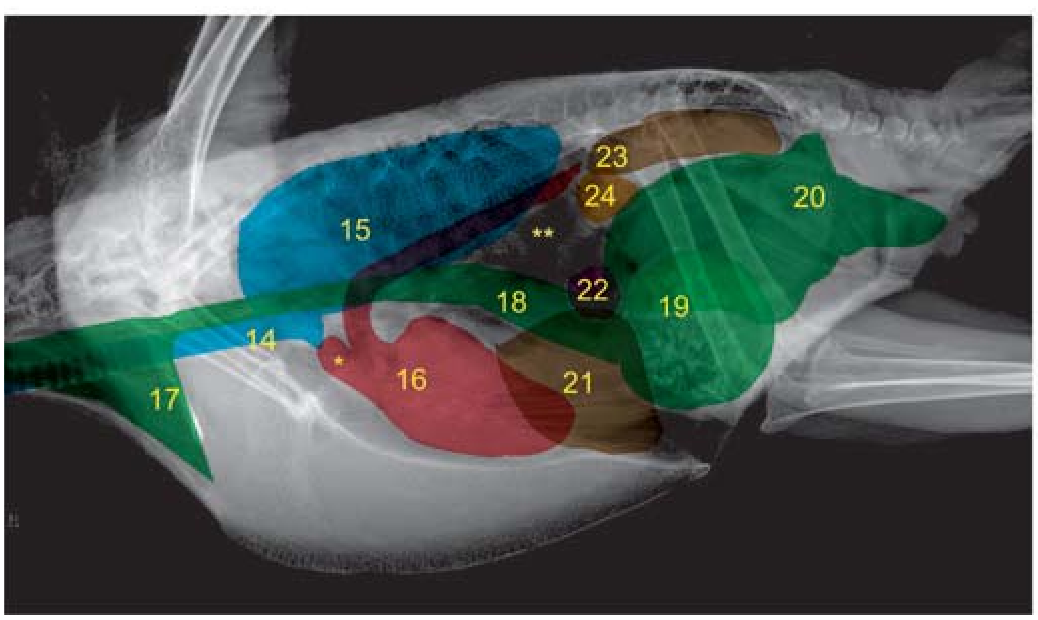

1: sternum
2: coracoid
3: clavicle
4: scapula
5: femur
6: tibiotarsus
7: cervical vertebrae
8: thoracic vertebrae, notarium
9: synsacrum
10, 11: tail vertebrae, pygostyle
12: rib
13: humerus
14: trachea with syrinx
15: lung with the thoracic and abdominal air sacs (**)
16: heart with the brachiocephalic trunk (*)
17: crop
18: proventriculus
19: ventriculus with grit
20: loop of intestine
21: liver
22: spleen
23: kidney
24: gonad

Fig. 1-22: Total body radiographic images of a blue-and-yellow macaw (*Ara ararauna*) showing the lateral projection.

Fig. 1-23: Total body radiographic images of a blue-and-yellow macaw (*Ara ararauna*) showing the ventrodorsal projection.

1: humerus
2: coracoid
3: clavicle
4: scapula
5: sternal carina, superimposed by the spine
6: femur
7: tibiotarsus
8: fibula
9: rib
10: pelvis
11: tail vertebrae, pygostyle
12: trachea with syrinx
13: lung
14: thoracic and abdominal air sacs
15: diverticuli of the clavicular air sacs
16: heart with major blood vessels
17: liver
18: ventriculus with grit
19: loop of intestine
20: cloaca

1.1.3.2 Cardiovascular system

The heart is situated in the VD projection roughly between the 2nd and 5th–6th ribs. The base of the heart is directed craniodorsally, while the apex lies close to the sternum in the radiographic shadow of the liver. Typically in granivores, an hourglass shape is formed by the shadows of the heart and liver **(Figs. 1-23** and **1-25)**. Only in cockatoos can the apex of the normal heart be differentiated when viewing the lateral projection due to the position of the air sacs.

A slight dorsal bending over of the left atrium may be observed radiographically in a number of avian species. In macaws, there is a characteristically obvious ventrally directed bend between the heart and liver shadows in the lateral projection.

Both in the DV and lateral radiographic views, the major blood vessels can be identified as round or cord-like structures. These circulatory structures are readily apparent in many older avian patients because of increased calcification of the major blood vessel walls (**Figs. 1-22** to **1-24,** and **1-37**).

Indications

- ☐ diseases characterized by changes in the position, size, and form of the heart
- ☐ infectious processes that may lead to secondary changes in the heart (e.g. pericarditis after generalized infection)
- ☐ non-infectious disease (e.g. space-occupying lesions, rare genetic defects, neoplasia)

Possible clinical signs

- ☐ numerous clinical signs are possible as the changes in the heart observed radiographically are often secondary and the clinical signs are influenced by the primary disease
- ☐ cardiovascular insufficiency, bluish discoloration of the skin (especially around the eyes) and mucous membranes, incoordination, disequilibrium, tendency to develop shock, etc.
- ☐ depression
- ☐ respiratory distress
- ☐ reduced ability to fly
- ☐ seizure activity

Normal variations

The large blood vessels in older birds can be clearly observed on radiographs due to the higher degree of calcification of the vessel walls **(Fig. 1-37)**. It is not always possible to make a clear distinction between a physiological and pathological (arteriosclerosis) degree of calcification.

1.1.3.3 Respiratory tract

The avian respiratory tract exhibits only a few radiographic variations. The trachea can be easily observed on a radiographic image due to its cartilaginous or bony supporting rings. The syrinx (voice organ in birds) lies in the area where the trachea branches into the two main bronchi. The syrinx is not clearly visible due to superimposition of other anatomic structures in the area and is best observed on lateral radiographic images. The lungs are relatively nonelastic structures embedded within the ribs and are evident in lateral radiographs due to their honeycomb-like shadowing.

In contrast to other animals, the lung volume is constant in birds because they lack a diaphragm. With avian patients, taking radiographic images during maximum inspiration is not usually possible due to their high respiratory rate. Characteristic of all birds is their extensive, radiographically variable, but easily observed air sac system. The avian air sac system usually consists of nine air sacs, whose diverticuli extend, in part, into individual bones. Normal air sac walls cannot be imaged using standard radiographic techniques. There are group-specific differences (e.g. raptors) with respect to the extent of the air sac system and the dimensions of the different air sacs **(Figs. 1-22** to **1-25, 1-28, 1-29)**. An example of these group-specific differences involves accipitriforms and falconiforms which have extensive clavicular air sacs.

Indications

- ☐ suspicion of infections, especially mycoses (e.g. aspergillosis), bacterial infections
- ☐ air sac rupture, chronic overextension of an air sac
- ☐ suspicion of a foreign body in the upper respiratory tract, other types of stenosis
- ☐ suspicion of aspiration pneumonia

Possible clinical signs

- ☐ respiratory sounds
- ☐ cardiovascular insufficiency, seizure activity, ataxia
- ☐ »cheek blowing«
- ☐ tail bobbing
- ☐ loss of voice
- ☐ nasal discharge, conjunctivitis, coating in the throat
- ☐ apathy, increased »yawning«
- ☐ reduced flight ability, lack of endurance
- ☐ chronic subcutaneous emphysema
- ☐ nonspecific symptoms such as diarrhea, cachexia, anorexia, retching, vomiting (especially associated with mycoses)

Normal variations

The tracheal rings are, at first, laid down as cartilage in young birds and become ossifed with age. The length of the trachea varies greatly according to the avian species being examined. In cranes, swans, and flamingos, the trachea can be longer than the body length. In some birds the trachea can even lie in loops underneath the sternum **(Fig. 1-30)**, while in other birds the trachea lies in a special cavity within the sternum. Mynas have a typical bend in the trachea that occurs proximal to the thoracic inlet. In penguins, the trachea appears to be divided due to a bifurcation of the structure located in cervical area.

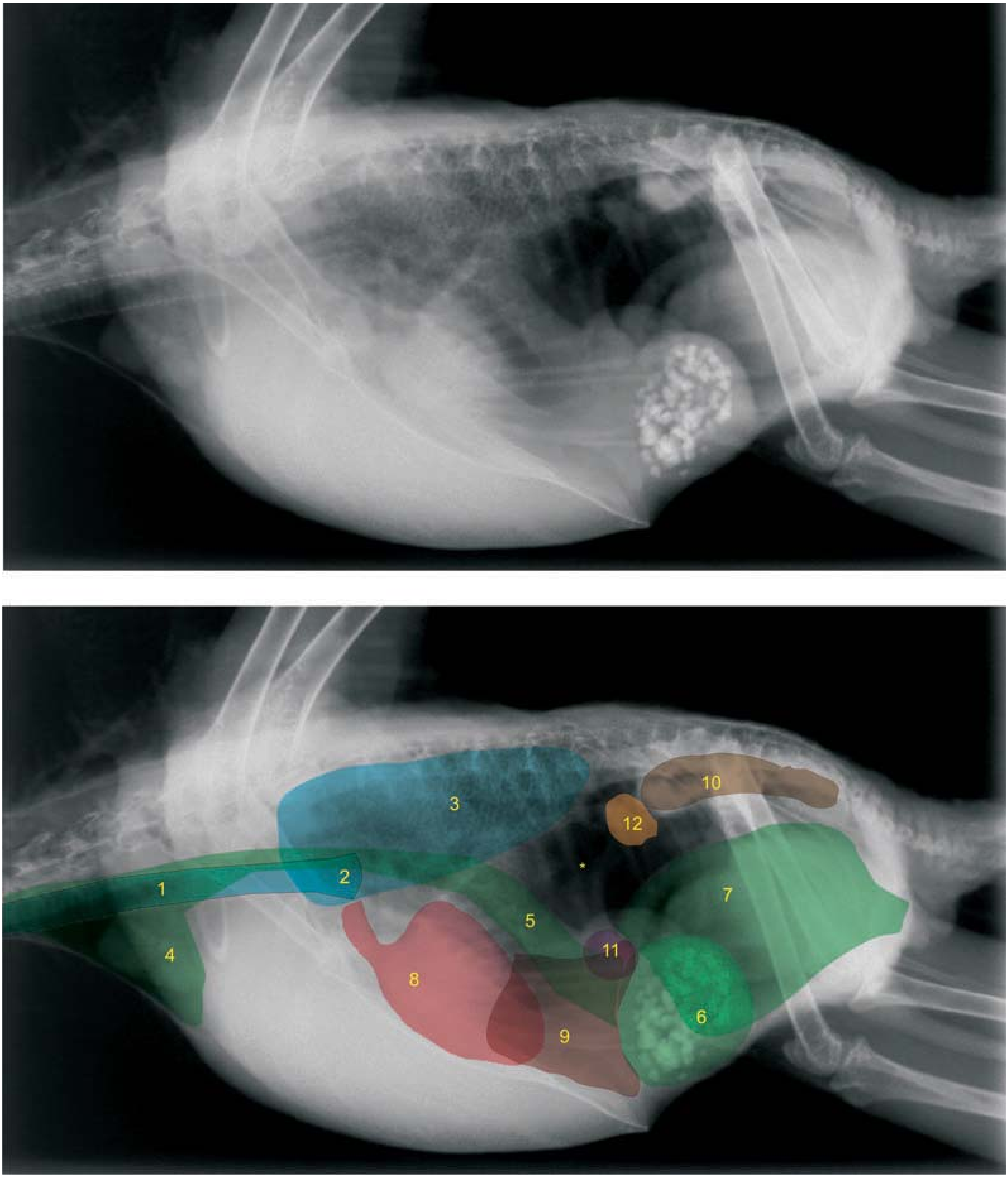

Fig. 1-24: Total body radiographic image of an orange-winged Amazon (*Amazona amazonica*) showing the lateral projection.

1: trachea
2: syrinx
3: lung with connecting thoracic and abdominal air sacs (*)
4: crop
5: proventriculus
6: ventriculus with grit
7: loop of intestine
8: heart
9: liver
10: kidney
11: spleen
12: gonad

The bronchi are highly ossified in older great crested grebe males **(Fig. 1-31)**. An ossified protrusion of the trachea lying close to the syrinx is typically found in drakes of many duck species, the so-called bulla (tympaniformis) syringealis **(Fig. 1-27)**.

The diverticuli of the clavicular air sac which penetrate into the humerus are at first small and reach their final size as the bird ages **(Fig. 1-23)**.

1.1.3.4 Liver

The radiographic shadow of the liver can vary greatly with respect to its form and size. The differences in the radiographic shadow are partly species specific, but also depend on the nutritional status of the bird (compare **Figs. 1-22** and **1-23** with **Fig. 1-26**). Under physiological conditions, the outlines of the liver on a VD radiograph do not extend beyond a line formed between the coracoid and acetabulum. In parrots and other granivores, the typical hourglass shape formed by the soft-tissue shadows of the heart and liver is influenced on the left side by the degree of filling of the proventriculus **(Figs. 1-23** and **1-25)**. In the lateral projection, the liver cannot be differentiated from the gastrointestinal tract without the use of a contrast agent.

The gallbladder cannot be radiographically differentiated and is often not present many species of pigeons or parrots.

Indications

- ☐ neoplasia (especially in budgerigars)
- ☐ metabolic disturbances (e.g. hemosiderosis in mynas, fatty liver degeneration in obese birds)
- ☐ infectious processes (liver swelling in many virus infections, e.g. Pacheco's disease [parrot herpesvirus], leucosis, PMV-1 infection; in psittacosis often in association with swelling of the spleen)

Possible clinical signs

- ☐ abdominal swelling
- ☐ icterus (rare)
- ☐ diarrhea with a yellowish discoloration of the urates
- ☐ abnormal feathering with discoloration of the feathers (chronic hepatitis) and pruritis
- ☐ nonspecific symptoms such as cachexia, anorexia, apathy, general malaise
- ☐ vomiting
- ☐ obesity, respiratory distress (e.g. with fatty liver)
- ☐ paralysis of the hindlimbs (e.g. liver tumor in budgerigars)

Normal variations

The size of the liver can vary considerably depending on the avian species being examined. The size of the liver also depends on the nutritional status of the bird as hepatomegaly or fatty liver is often observed in obese birds **(Fig. 1-26)**.

1.1.3.5 Spleen

A normal spleen is observed on lateral radiographs as a spherical, at times egg or bean-shaped, soft-tissue shadow dorsal to the proventriculus **(Figs. 1-22** and **1-24)**. The splenic shadow cannot be differentiated from the surrounding tissues on VD radiographs in birds. The size of the spleen in budgerigars is ca. 1 mm and in the larger parrots (e.g. grey parrots or Amazons), ca. 6 mm. The spleen can only be seen satisfactorily in roughly 30% of radiographic images taken of large parrots. In pigeons the spleen cannot be clearly differentiated from the surounding tissue because it is usually embedded in fat.

Indications

- ☐ infectious processes (swelling of the spleen, tuberculosis, psittacosis [with massive swelling of the spleen in connection with the clinical disease signs it is possible to make a quick tentative diagnosis of this disease])
- ☐ neoplasia (especially in budgerigars, tends to be rare in other avian species)

Possible clinical signs

- ☐ nonspecific clinical signs (e.g. cachexia, anorexia, apathy)
- ☐ changes in the feces (diarrhea, black-green inanition feces, etc.)
- ☐ conjunctivitis, rhinitis (psittacosis)
- ☐ rare signs of paralysis of the hindlimbs (splenic tumor)

Normal variations

The size of the spleen may vary considerably depending on the avian species being examined.

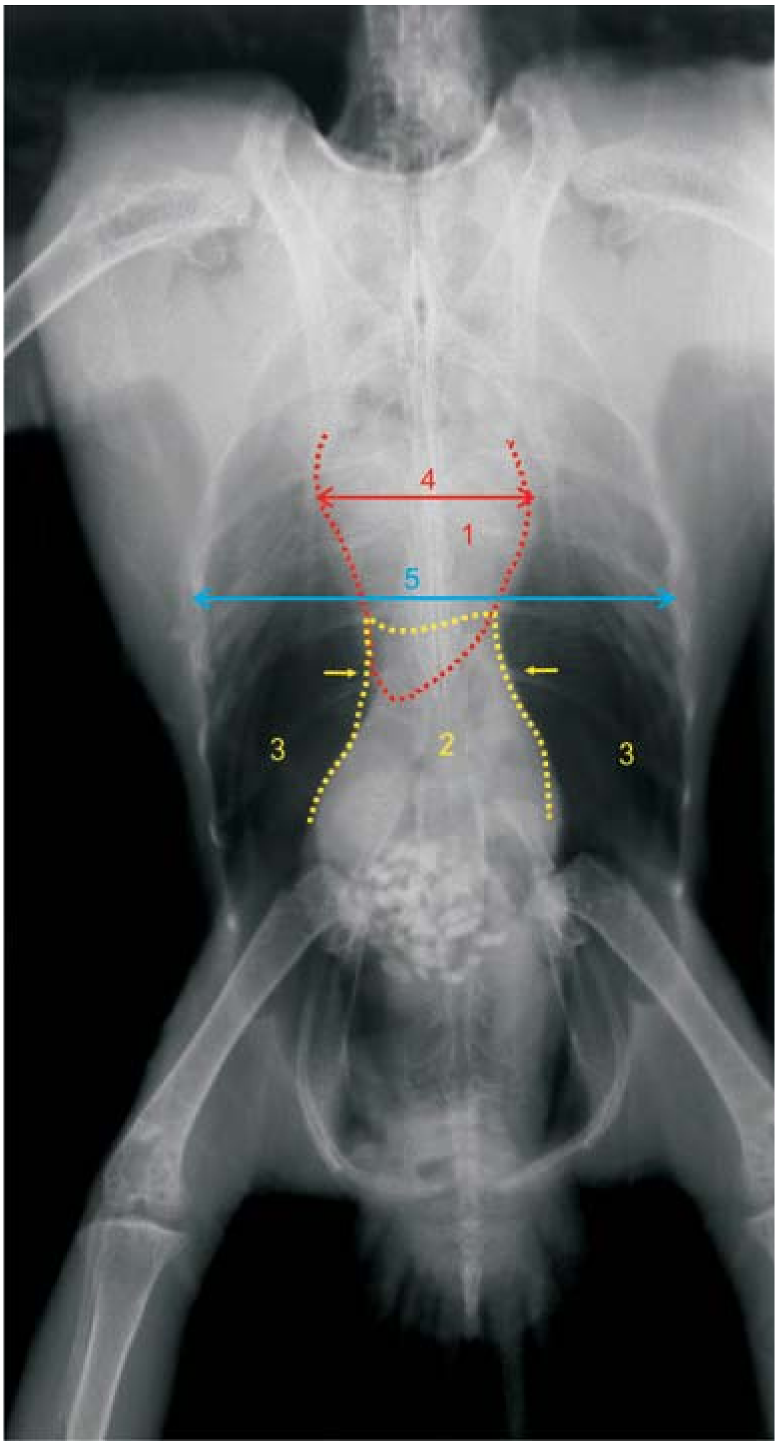

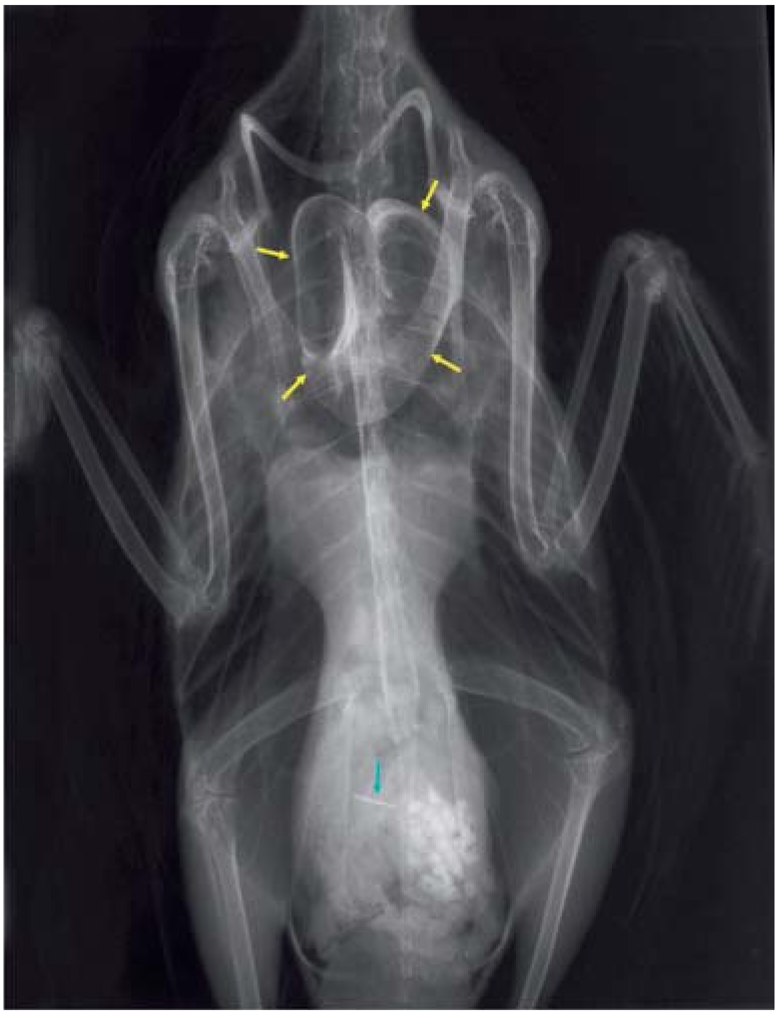

Fig. 1-27: Total body radiographic image of a red-breasted merganser (*Mergus serrator*) showing the ventrodorsal projection: Bulla syringealis (arrows).

◀ 1: heart
2: liver
3: thoracic and abdominal air sacs
4: measurement line for the heart shadow width
5: measurement line for the thoracic width

Fig. 1-25: Total body radiographic image of an orange-winged Amazon (*Amazona amazonica*) showing the ventrodorsal projection. The same bird as in Fig. 1-24. Representation of an unchanged heart (1) and liver (2) silhouette. Measurement of the cardiac shadow width (4) should be undertaken on a ventrodorsal radiograph with complete symmetrical positioning. It should be compared to the maximal width of the thorax (5). In medium-sized parrots (body weight 200–500 g), the width of the heart on a radiograph should be ca. 51–61% of the maximal width of the thorax.

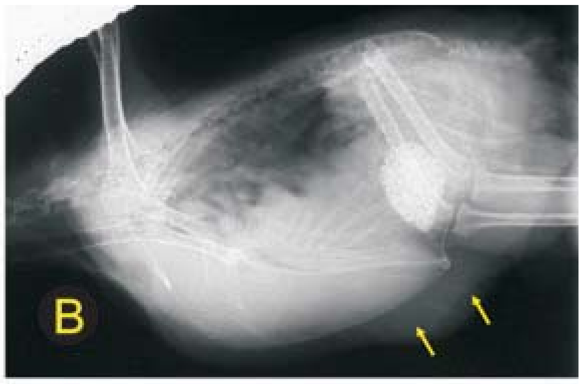

Fig. 1-26: Total body radiographic images of a blue-fronted Amazon (*Amazona aestiva*) showing the (A) ventrodorsal and (B) lateral projections: Obesity (arrows: fat deposits). The heart-liver silhouette is enlarged.

1.1.3.6 Gastrointestinal tract

In many birds, the cervical part of the esophagus widens to form a crop. Particularly voluminous crops or esophageal diverticuli can be found in granivorous, carnivorous, and carrion-feeding birds **(Fig. 1-17)**. In pigeons the crop divides into two lateral sacs. With granivorous species, the caudal esophagus, proventriculus, and ventriculus can be well differentiated on a lateral radiographic image. Additionally, radiopaque particles, which may be noted as a »normal finding,« can be identified in the ventriculus due to the presence of grit. In fructivorous, nectarivorous, and carnivorous species, the proventriculus and ventriculus cannot be differentiated from each other radiographically, especially after the patient has ingested a large meal. With fructivorous, nectarivorous, and carnivorous birds the ventriculus is more distendable than in granivorous species. In raptors, owls, and other avian carnivorous, piscivorous, or molluscivorous species, calcified parts of the diet (e.g. bone or even complete prey, mollusk, or snail shells) can be seen as radiopaque structures in the gastrointestinal tract **(Figs. 1-17, 1-29)**.

The gastrointestinal tract can only be radiographically examined through the administration of a suitable contrast agent **(Figs. 1-36 A–F)**. Without any contrast agent and only on rare occasions is it possible to observe a loop of intestine on the right side of the abdomen and the cloacal region.

The cecum is often observed as a double organ that can achieve a rather a large size in game birds (grouse), ducks, geese, and owls. In some species (e.g. herons, loons), the ceca is reduced. In many avian species maintained as pets (e.g. parrots, pigeons, mynas), the two ceca are only rudimentary or are completely absent.

Indications

- ☐ suspicion of a foreign body (primarily heavy metals which can be diagnosed radiographically)
- ☐ mechanical or paralytic ileus (e.g. neoplasia, engorgement with food)
- ☐ abdominal hernia
- ☐ cloacal prolapse
- ☐ infectious gastrointestinal disease (e.g. parasitic infections: tentative diagnosis in the prepatent period is possible; viral infections: e.g. proventriculus dilatation disease – important possibility of confirming a tentative diagnosis in the live bird)

In order to properly differentiate the gastrointestinal tract, after taking a survey radiographic image, gastrography using a contrast agent is indicated **(Fig. 1-36)**.

Possible clinical signs

- ☐ vomiting, retching
- ☐ cachexia, anorexia
- ☐ swelling of the abdomen
- ☐ cloacal prolapse
- ☐ adhesions in the cloaca, changes in the cloacal mucosa
- ☐ no defecation or difficulties in defecation, changes in the feces (e.g. undigested grain in candidiasis, proventriculus dilatation disease, etc.; hematochezia with heavy metal poisoning)
- ☐ polydipsia, polyuria
- ☐ discoloration of the feces and/or urates
- ☐ changes in the amount of feces (e.g. pancreatic insufficiency)
- ☐ CNS disturbances with cachexia and a negative parasitological investigation

Normal variations

The gastrointestinal tract can differ radiographically according to the nutritional requirements and normal diet of the bird. In granivorous birds, radiopaque particles (grit) are normally identified in the ventriculus. In pigeon chicks or nestlings of granivorous species, the gastrointestinal tract appears to be very voluminous in the first few weeks of life due to the consistency of the food fed to the young by adults (e.g. crop milk, food mash). Parts of prey skeleton (bone, mollusk shells) can be found in the radiographic images of carnivorous birds (e.g. **Fig. 1-17**).

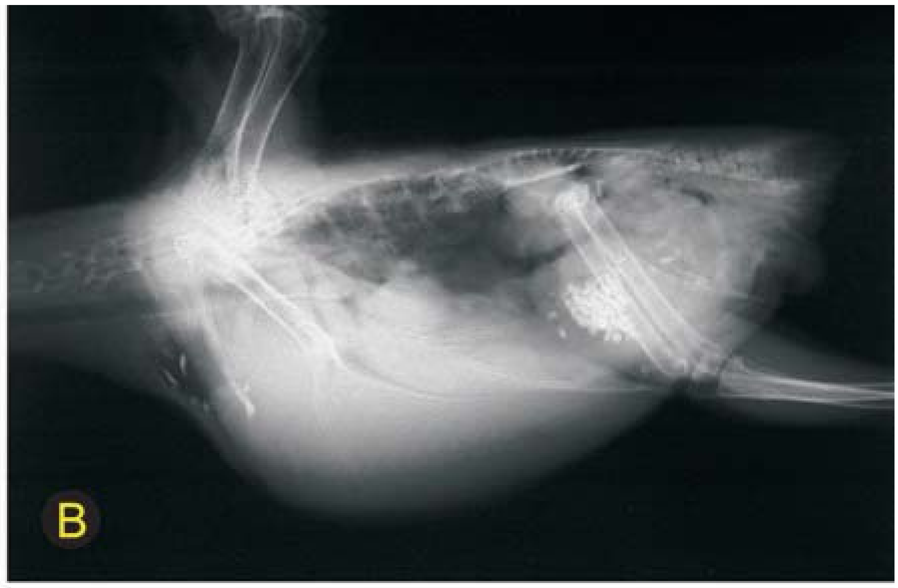

Fig. 1-28: Total body radiographic image of a pigeon (*Columba livia* f. *domestica*) showing the (A) ventrodorsal and (B) lateral projections. Grit is not only present in the ventriculus, but also in the crop, just cranial to the thoracic inlet, and within the intestinal lumen.

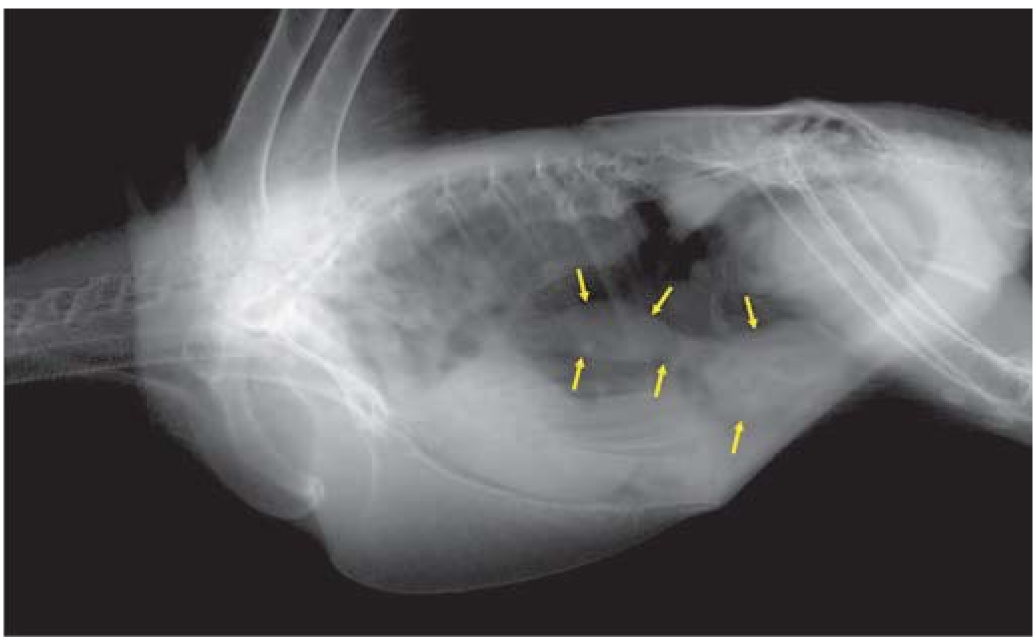

Fig. 1-29: Total body radiographic image of a gyrfalcon (*Falco rusticolus*) showing the lateral projection: Tube-like proventriculus and gizzard (arrows). There are bones from prey the bird ate in the ventriculus.

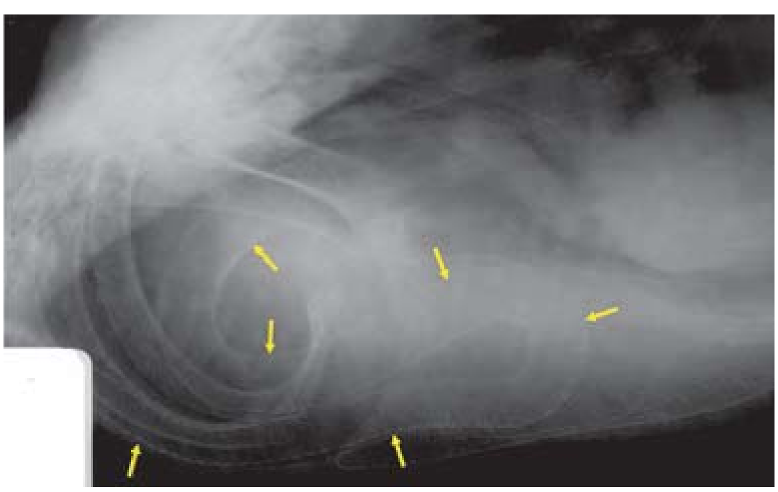

Fig. 1-30: Total body radiographic image of a mute swan (*Cygnus olor*) showing the lateral projection: Long convoluted trachea (arrows).

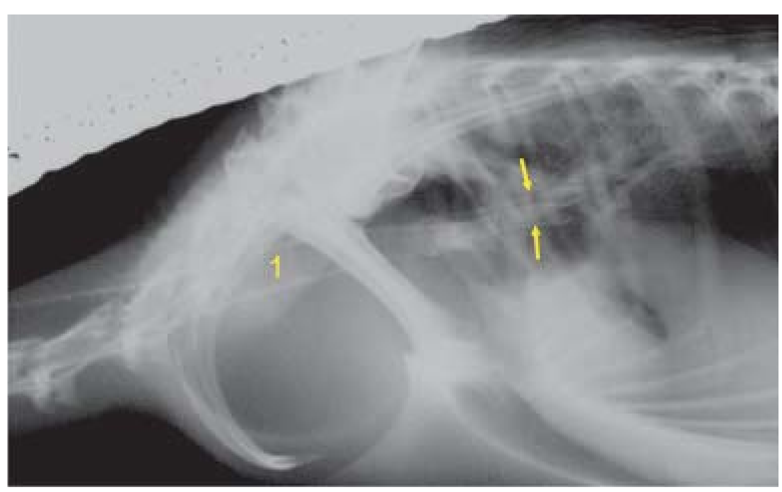

Fig. 1-31: Total body radiographic image of a great crested grebe (*Podiceps cristatus*) showing the lateral projection: Calcified main bronchi (arrows).

1: trachea

arrows: main bronchi

1.1.3.7 Urinary tract

Birds have a pair of kidneys that are embedded retroperitoneally on either side of the vertebral column in a depression in the ventral surface of the synsacrum. Each one of the kidneys has a three-part structure. In lateral radiographs, the cranial end of the kidney is superimposed by the gonad, although the degree of superimposition depends on the bird's reproductive status as the genital tract can be very enlarged during the breeding season **(Figs. 1-22, 1-24, 1-32, 1-33A, B)**. In VD radiographs, the kidneys are often not visible or are indistinct. The kidney of the domestic chicken is ca. 7–9 cm long, whereas in the African grey parrot it is ca. 3 cm. The typical structural and functional divisions (i.e. external renal cortex and internal renal medulla with a renal pelvis) found in mammalian kidney are missing in the avian renal organs. The most significant radiographic feature is the renal portal vein system, as this allows for a rapid excretion of contrast during urographic investigations. Neither a urinary bladder nor a urethra is present in birds. The excrement is discharged directly from the ureters into the cloaca via the urodeum. Both these structures can become radiopaque under certain disease conditions (e.g. urate congestion, nephrolithiasis; see Chap. 1.10).

Indications

- ☐ infectious processes (renal swelling e.g. psittacosis, nephrocalcinosis often associated with bacterial nephritis)
- ☐ suspicion of renal cysts
- ☐ neoplasia (especially in budgerigars)
- ☐ metabolic disturbances (e.g. vitamin A deficiency, nephrocalcinosis)
- ☐ other noninfectious processes which affect the kidney (e.g. chronic lead poisoning – with respect to the prognosis, severe dehydration)

Possible clinical signs

- ☐ polydipsia
- ☐ polyuria, discoloration of the urates
- ☐ vomiting
- ☐ dehydration
- ☐ crooked posture, severe general malaise
- ☐ paralysis of the hindlimbs
- ☐ disturbances in feather growth and skin changes without pruritis, hyperkeratosis
- ☐ abnormal blood values, e.g. increased urate concentration

1.1.3.8 Genital tract

The pair of testicles in male birds lies cranioventral to the cranial aspect of the kidneys. The size of the avian testicle depends on the reproductive status of the bird. The testicles of sexually active males in passeriform species can be up to 500 times larger than those in the same birds when not reproductively active. Testicles enlarged due to reproductively active males should not be confused with renal tumors **(Figs. 1-32** and **1-33A)**.

In female birds, only the left ovary is functional in most cases. The right ovary is formed during the embryonic stage but does not really grow and usually degenerates. In raptors, such as the goshawk (*Accipter gentilis*) and sparrow hawk (various *Accipter* spp.), the right ovary can undergo cystic development, which in rare cases is completely functional. When the female is sexually active, the ovary appears as a structured soft-tissue shadow with different degrees of radiodensity **(Fig. 1-33B)**. The oviduct is visible in the abdomen as a soft-tissue shadow

Indications

- ☐ egg binding
- ☐ formation of a laminated egg, changes in the form and/or surface of the egg
- ☐ suspicion of ovarian cysts
- ☐ abdominal hernia (often in female birds in association with increased bone density)
- ☐ neoplasia (testicular tumors, especially in budgerigars)
- ☐ infectious processes (e.g. salpingitis)

Possible clinical signs

- ☐ difficulties in defecation
- ☐ increased amount of urates in the feces
- ☐ sitting with legs far apart, pressing on the cloaca
- ☐ soft or hard palpable masses in the abdomen with swelling of the abdomen
- ☐ infertility
- ☐ cachexia, changes in cere coloration, varying degrees of lameness of the hindlimbs (neoplasia, budgerigars)

Normal variations

The functional left ovary may be observed as an irregularly radiopaque, furrowed soft-tissue shadow at the cranial pole of the kidney in the female bird when she is reproductively active **(Fig. 1-33B)**.

Due to its position between the liver, kidneys, and intestines, the oviduct should not be misinterpreted as radiographic evidence of hepatomegly. Normal eggs that are fully developed can be easily identified due to their radiopaque shell. Radiographically, eggs that are fully developed may displace the gastrointestinal tract **(Fig. 1-21)**.

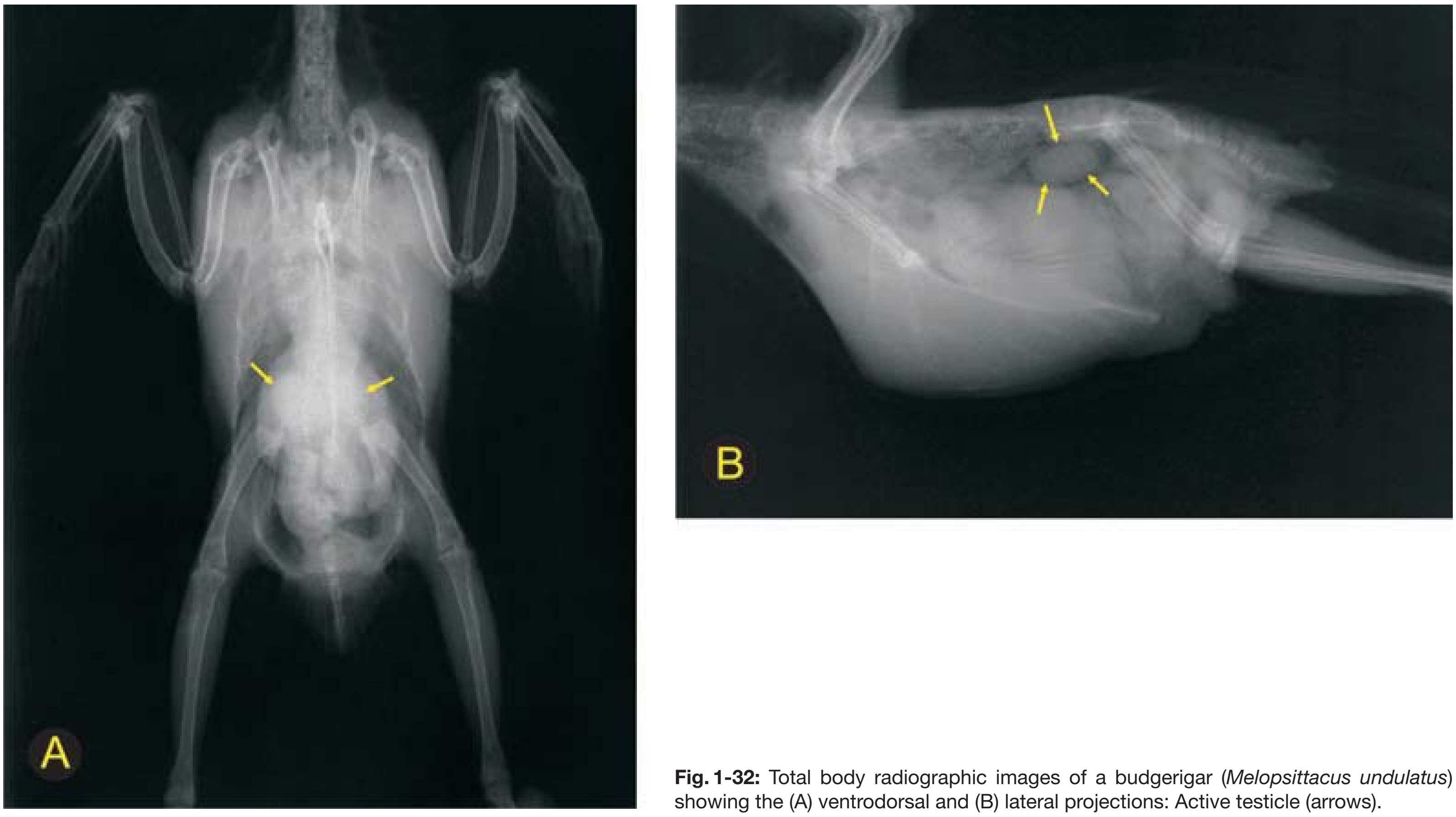

Fig. 1-32: Total body radiographic images of a budgerigar (*Melopsittacus undulatus*) showing the (A) ventrodorsal and (B) lateral projections: Active testicle (arrows).

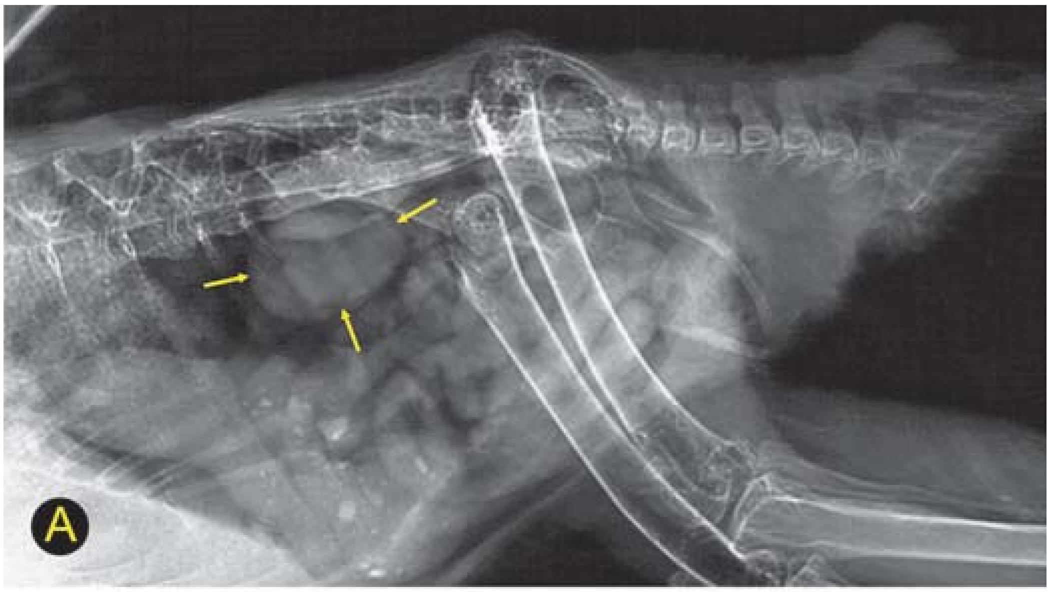

Fig. 1-33A: Total body radiographic image of a red kite (*Milvus milvus*) showing a lateral projection: Active testicle (arrows).

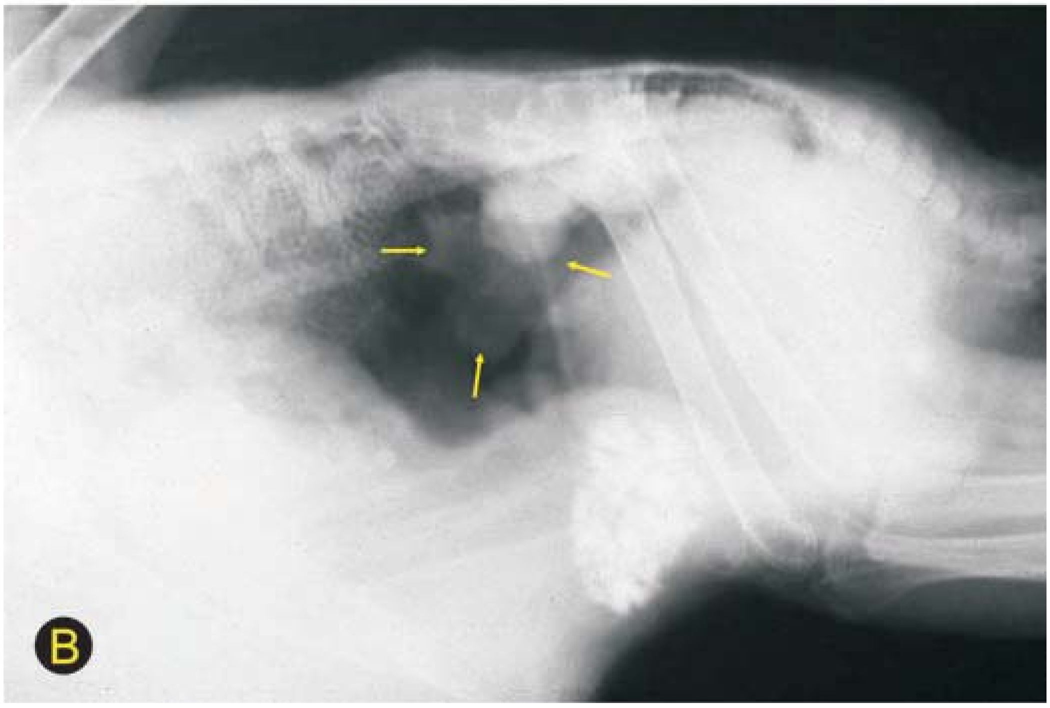

Fig. 1-33B: Caudal body (section) radiographic image of a blue-fronted Amazon (*Amazona aestiva*) showing the lateral projection: Active ovary (arrows).

1.1.4 Contrast studies

1.1.4.1 Introduction

Principally, contrast agents are differentiated into positive and negative forms, whereby the latter only plays a minor role in avian radiodiagnostics. The more clinically relevant contrast agents are those which increase the radiopacity of organs or blood vessels. To achieve this, substances are used whose radiopacity is increased due to their content of elements with a high atomic number, in particular barium and iodine.

Barium sulfate can only be used for investigations of the gastrointestinal tract. With the synthesis of tri-iodinated benzoic acid, it was possible to design radiopaque substances that could be used within the blood vessels. As a rule, water-soluble iodine compounds are utilized. Generally, in radiography, there is a differentiation between ionic and non-ionic iodine compounds, whereby the non-ionic compounds, such as iodixanol and iotrolan, are preferred due to their better tolerance by the patient and less toxic side effects. Organic iodine compounds are primarily given intravenously, in rare cases orally, or in sinography studies, locally administered. However, iodine-based contrast agents are hypertonic and should only be used intravenously in dehydrated patients after adequate rehydration.

1.1.4.2 Contrast studies of the gastrointestinal tract

The indications for a contrast study of the gastrointestinal tract are varied. They include all of the pathological conditions which are characterized by morphological changes in the gastrointestinal tract as a whole (e.g. dilatation of the proventriculus in proventriculus dilatation disease, displacement of intestinal loops in abdominal hernia) or of its walls (e.g. thickening in vitamin A deficiency, chronic candidiasis). In addition, the administration of a contrast agent can be used to differentiate the gastrointestinal tract from its neighboring organs (e.g. liver, spleen, gonads, kidney) which may be affected by neoplastic **(Fig. 1-34)** or inflammatory processes. The administration of a contrast agent in food also allows the functionality of the gastrointestinal tract to be assessed, as the transit of the intestinal contents in ileus is extremely slow or even nonexistent, while accelerated intestinal transit times can be identified when the patient is suffering from an acute gastrointestinal infection. If there is suspicion that the bird has ingested a foreign body, a contrast study enables one to determine the position of the foreign body after a survey radiograph is of no diagnostic aid because the foreign body is radiolucent.

A survey radiograph should always be taken prior to the administration of contrast material. If there is a suspected perforation of the proventriculus, ventriculus, or intestine only those contrast agents which will not induce tissue damage may be used. Only contrast agents that do not contain barium sulfate, can be resorbed by the body.

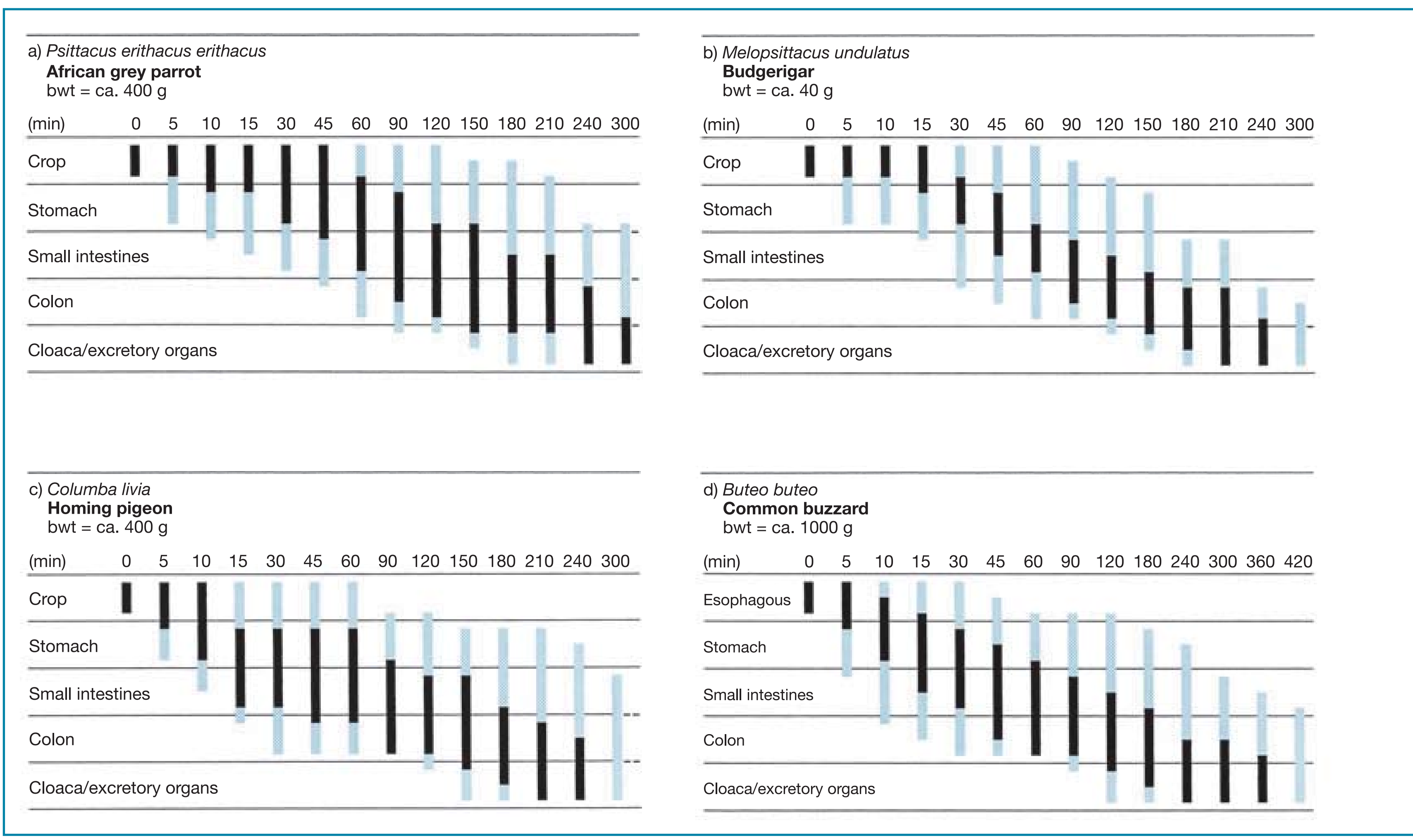

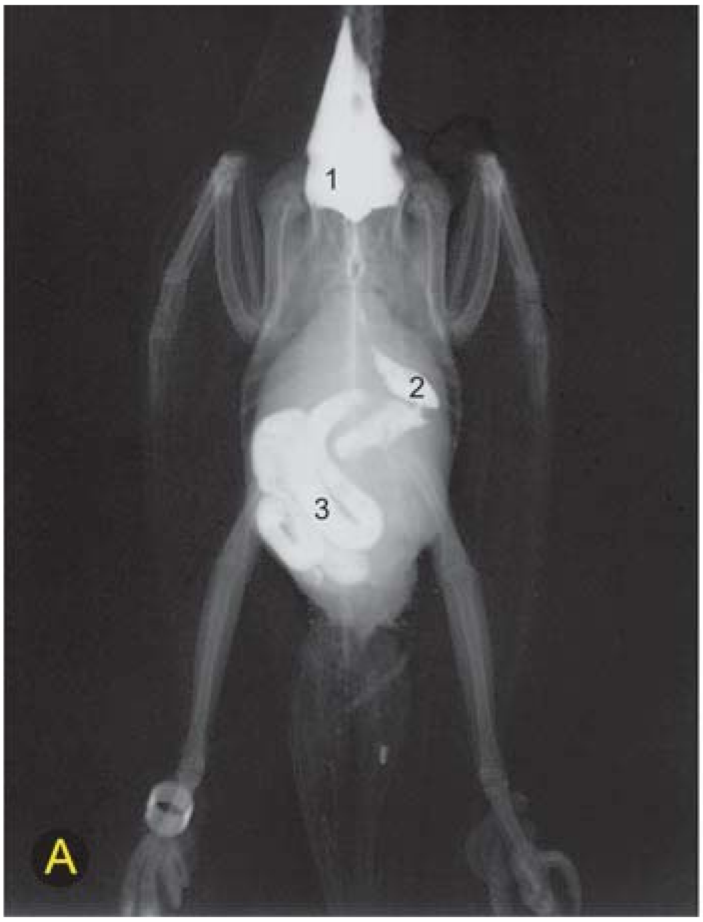

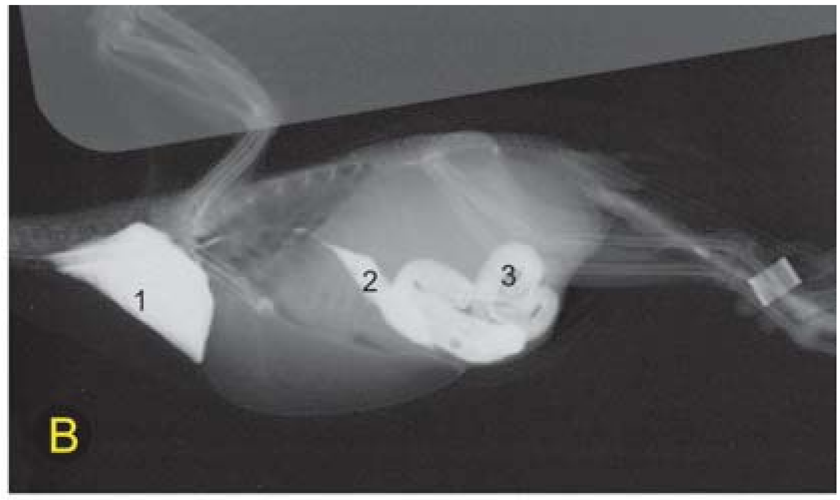

1: crop
2: proventriculus
3: loop of intestine

Fig. 1-34: Total body radiographic images of a budgerigar (*Melopsittacus undulatus*) 45 min after the administration of 1 ml barium sulfate in the crop showing the (A) ventrodorsal and (B) lateral projections. A renal tumor is ventrally displacing the intestines.

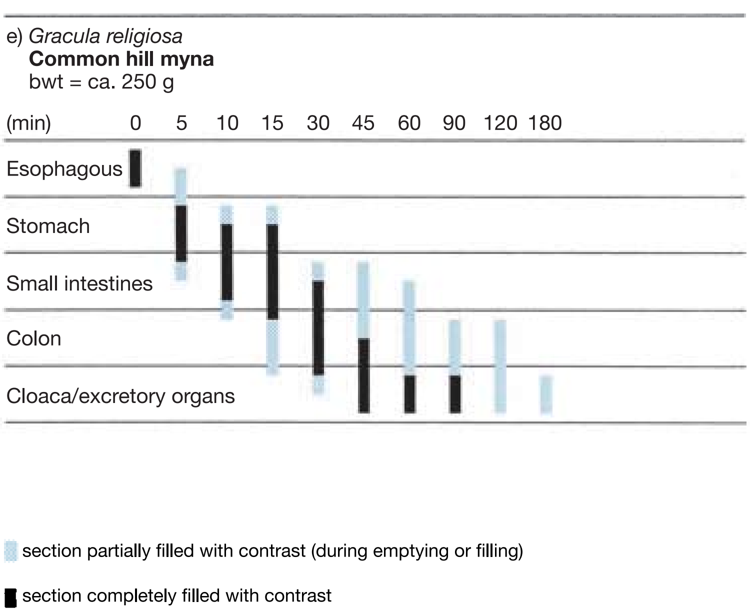

Fig. 1-35a–e: Sequence showing the passage of a barium-based contrast agent in a bird with an empty crop after the administration of 20 ml/kg body weight of a 25% barium sulfate suspension.
Figure reproduced from Krautwald-Junghanns et al. 1992 with kind permission.

Standard barium sulfate suspensions are often used as contrast agents when doing contrast studies of the gastrointestinal tract. Organic iodine compounds are only used for gastrography in rare cases, because they usually do not have good image quality and have a much faster transit time.

Barium-based contrast agents are always administered as a suspension using a tube or a ball-tipped gavage needle. A 25–45% barium sulfate suspension (ca. 20 ml/kg body weight) is the recommend concentration and dose for avian contrast studies of the gastrointestinal tract.

The quantity of barium sulfate in the suspension should be adjusted to the patient's condition and clinical signs associated with the presenting complaint. A weaker suspension should be administered to differentiate the gastrointestinal tract from its neighboring tissues, while a more viscous suspension is better suited for diagnosing changes in the gastrointestinal tract itself. Alternatively, when there is suspicion of perforation, non-ionic iodine-based contrast agents should be administered orally at a dosage of 10 ml/kg body weight (iodine content of the suspension: 250 mg iodine/ml).

To prevent regurgitation of the contrast material and to reduce the possibility of aspiration pneumonia, the bird should be held for a short time in the upright position after orally administering the contrast agent. Gastrography should not be performed on anesthetized or sedated birds, as intestinal function can be reduced by the effects of the narcotics or sedatives used.

Only approximate values can be given for the transit time of contrast agents in the avian gastrointestinal tract, because these factors vary greatly between species and individuals **(Figs. 1-34 to 1-36)**. The transit time depends not only on the bird's required diet (e.g. granivore, fructivore, carnivore) which may reflect an associated variability in gut length, but also the size, nutritional condition, and age of the patient, as well as the consistency of the contrast suspension. There can be a relatively rapid transit time observed in birds that eat soft foods and in cachexic or stressed birds, whereas the contrast agent tends to have a longer passage time in the gastrointestinal tract of large granivores. The transit time is also slower in young, obese, or richly fed birds, as well as in patients that have been anesthetized or sedated. If the bird has been subjected to a prolonged period of fasting before the administration of the contrast material, then initially the barium sulfate suspension is transported rapidly to the ventriculus; thereafter it only leaves the ventriculus after a delay.

There is always a danger with ingluvial (crop) administration of a contrast suspension of aspiration after regurgitation of the contrast agent. For this reason, it is recommended that the bird should be fasted prior to the contrast procedure. If the crop is filled with food, then one should wait until the crop has emptied before administering the contrast agent because it is nearly impossible to prevent regurgitation in these patients. The oral or cloacal administration of paraffin oil to increase the emptying of the gut should only be done in rare cases.

If a bird regurgitates the contrast material, the patient should immediately be held with its head in a downward position. Afterwards, the bird should be returned to its accustomed surroundings to reduce stress. If the patient aspirates a large amount of barium suspension, in rare cases, respiratory problems can occur due to the resulting cellular damage to the lung parenchyma. However, birds appear to be less sensitive to aspiration of barium suspension due to the anatomical differences of their lower respiratory tract when compared to mammals (i.e. no blind-ending alveoli as in mammals).

The danger of an ileus developing after the administration of a contrast suspension is particularly great in dehydrated birds due to the excessive dissicating properties of the contrast agent. Therefore, it is imperative that an adequate fluid supply (20 ml/kg body weight s.c.) is provided prior to the administration of the contrast agent and until it is evacuated from the gastrointestinal tract.

Due to their hygroscopic effects, ionic iodine-based contrast agents (e.g. Gastrographin®) should not be used. These ionic iodine-based contrast agents can cause the loss of body fluid into the lumen of the intestines thus diluting the contrast suspension, and thereby greatly reducing the diagnostic value of the gastrography. Newer non-ionic substances (e.g. Omnipaque®) are much better suited for gastrography as they are not hygroscopic. The transit time of these contrast agents is usually twice as fast as with barium sulfate **(Fig. 1-37)**.

A form of gastrography which is relatively rarely used in avian medicine is the double-contrast method in which both a positive and negative contrast agent (i.e. usually barium sulfate and air) are administered to the patient at the same time **(Fig. 1-38)**. With this method, a fine layer of positive contrast material covers the walls of the gastrointestinal tract, whereby lesions or other anomalies in the intestinal wall (e.g. neoplasia, papillomatous changes in the rectum) can be identified. The gastrointestinal tract should be evaluated for contents that may affect the radiographic quality of the contrast study by taking a survey radiograph prior to administering the two contrast agents. The patient is prepared for the investigation as described above.

For double-contrast studies, the bird is given **10 ml/kg body weight of a 25 % barium sulfate suspension** orally or via the cloaca. Immediately after administration of the barium sulfate suspension, the bird is given air orally or via the cloaca as the negative contrast agent. The volume of air given should be roughly twice as much as the volume of positive contrast material (i.e. ca. **20 ml/kg body weight**). Adequate distribution of the contrast agents can be achieved by the careful (**!**) back and forth movement of the bird.

Further reading

KRAUTWALD-JUNGHANNS, M.-E., TELLHELM, B., HUMMEL, G., KOSTKA, V., KALETA, E. F.: Atlas zur Röntgenanatomie und Röntgendiagnostik des Ziervogels. Paul Parey Verlag, Berlin 1992.

1: crop
2: proventriculus
3: gizzard
4: loop of intestine
5: cloaca

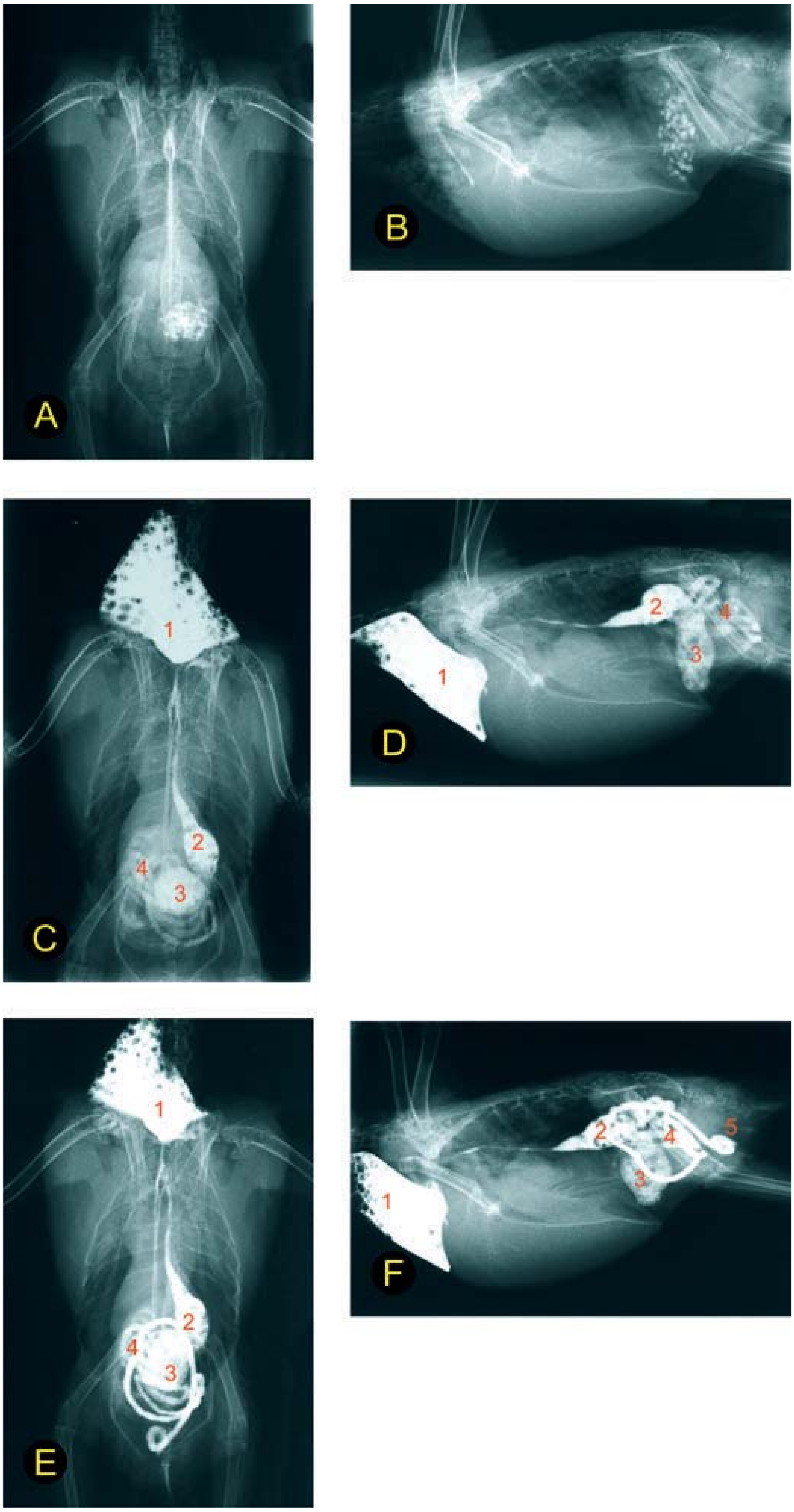

Fig. 1-36A–F: Total body radiographic images of a cockatiel (*Nymphicus hollandicus*) showing ventrodorsal and lateral projections, before (A and B), 30 min (C and D) and 120 min (E and F) after the administration of 2 ml barium sulfate into the crop. It should be noted that the transit time through a full crop is longer than with an empty crop (Fig. 1-35a–e).

1.1.4.3 Contrast investigation of the excretory organs (urography)

Urographic investigations have only a limited diagnostic value in the bird due to the anatomic and functional differences between that of the avian and mammalian excretory system (e.g. lack of a clear differentiation between renal medulla and cortex, lack of a renal pelvis, loss of bladder and urethra).

The indications for urography include dysfunction of the urinary tract (e.g. polyuria, polydipsia) or changes in the size and form of the kidneys (e.g. acute nephritis) where survey radiographs or ultrasonographic investigations have not provided a definite diagnosis. The administration of a contrast agent is also indicated to differentiate the kidney from the surrounding tissues or organs (e.g. ovarian cysts, tumors of the gonads), which is not possible when viewing a nonenhanced radiographic image.

If the kidney and/or ureter is only vaguely depicted or not observable, this is an indication that tumors or cysts may be present within the urinary tract. Normally, there is a rapid excretion of the contrast material due to the efficiency of the renal portal venous system in birds, whereas delayed contrast excretion occurs when the patient is suffering from renal insufficiency.

In addition, urography is also suitable for controlling the function of the ureters (i.e. after the surgical removal of uroliths). Urography is also indicated in special cases to help detect disease in other parenchymal organs through the concentration of contrast material in these structures.

The contrast agent (an organic iodine compound with an iodine content of **300–400 mg iodine/ml**) must be warmed to body temperature for urography. It is then slowly administered intravenously (usually in the ulnar vein) to the sedated or anesthetized patient at a dosage of **2 ml/kg bwt**. It is important that only highly concentrated compounds which are registered for use in urography are utilized for an avian urography procedure otherwise the results of the study will be nondiagnostic due to inadequate contrast of the desired anatomic structures.

The quality of the radiographic contrast is affected by both the iodine content of the contrast agent and the ability of the kidney to concentrate the preparation used. The heart, aorta, and lung arteries are already depicted 10 seconds after injection. After 30–60 seconds, the contrast reaches the kidneys and ureters **(Fig. 1-39)**, and after 2–5 minutes, the rectum and cloaca.

A urographic investigation is, however, contraindicated in dehydrated birds unless the patient has been sufficiently rehydrated before the contrast agent is administered.

1.1.4.4 Contrast investigation of the infraorbital sinus and diverticula (sinography, rhinosinography)

To depict the nasal passages and sinuses, resorbable contrast agents (non-ionic iodine compounds) can be administered directly into the region of the head that is being investigated. However, the interpretation of sinographic radiographs is difficult due to the extensiveness and superimposition of the nasal (infraorbital) sinus. In the majority of cases, a CT investigation would provide a better diagnostic result (also at times with the administration of a contrast agent). If CT imaging cannot be used because it is either not available or is too expensive for the client's budget, then disease diagnosis using contrast radiography of the infraorbital sinus and diverticula can be attempted using a conventional radiographic investigation. Sinography or rhinosinography can depict the presence of a blockage of the airways, especially when the disease condition is associated with chronic rhinitis and/or sinusitis, or if there is suspicion of an intranasal tumor or head trauma.

Delineation of the sinuses can be achieved by injecting **0.1–1 ml** (dosage relative to the size of the bird) of an iodine-based preparation (iodine content of **200–250 mg iodine/ml**) directly into the paranasal sinus. A standardized method for avian sinography/rhinosinography has not been published at the present time. The contrast agent should be immediately flushed out of the sinus with sterile saline solution once the investigation has been completed. Flushing of the contrast material from the upper respiratory system helps minimize the effects and reduce the potential of local tissue irritation, edema, and periorbital swelling **(Fig. 1-40)**.

1.1.4.5 Contrast studies of the cardiovascular system (angiocardiography)

Angiography is the method of choice for investigating the avian cardiovascular system. Angiography is especially useful for the assessment of heart size and function in those cases which cannot be adequately diagnosed using echocardiography (e.g. congenital diseases of the vascular system, morphological changes of the heart). Aneurysms of the right avian coronary artery can also be depicted using angiography. Angiographic investigations are not considered a substitute for echocardiography, but they can have additional diagnostic value that the ultrasound evaluation does not provide (i.e. when details are unsatisfactorily depicted in a B-mode echocardiogram). Conversely, for practical reasons, angiography is indicated when no suitable coupling sites are available for the ultrasonographic transducer (i.e. in aquatic birds where it is difficult to pluck enough feathers from the area of the coupling site).

Angiography should always be done under general anesthesia. The iodine-based contrast agent (e.g. iopamidol: 380 mg iodine/ml) used at a dose of 2–4 mg/kg body weight should be slowly injected intravenously through a catheter which has been placed in either the jugular or basilic vein.

Fig. 1-37: Total body radiographic image of a peregrine falcon (*Falco peregrinus*) during a gastrography examination in the ventrodorsal projection, 30 min after the oral administration of 10 ml/kg bwt iohexol (250 mg iodine/ml solution). The tube-like proventriculus (1) can be clearly identified in the image. Cross-sections of the cardiac blood vessels can be clearly seen (arrows).

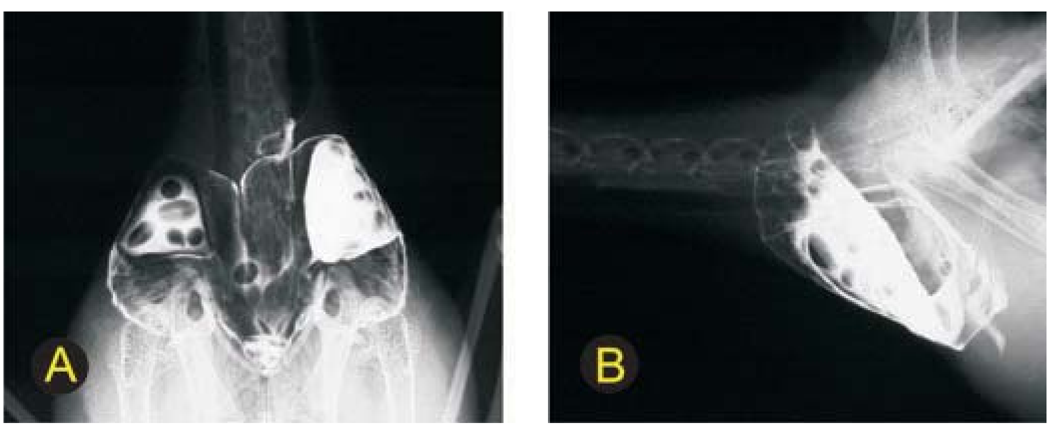

Fig. 1-38: Radiographic images of a pigeon's (*Columba livia* f. *domestica*) crop showing ventrodorsal (A) and lateral (B) projections, after the administration of 10 ml/kg bwt barium sulfate and 20 ml/kg bwt air into the crop. The double-contrast method enables the depiction of the crop mucosa as well as the particles of grain within the organ.

1: kidney
2: cloaca

arrow: ureters

Fig. 1-39: Total body radiographic image of a pigeon (*Columba livia* f. *domestica*) during a urography procedure in the lateral projection, approximately 1 min after the intravenous administration of 2 ml/kg bwt iomeprol (300 mg iodine/ml solution).

The avian dose, 2–4 mg/kg body weight is roughly twice the published amount for mammals. Subsequently, a series of radiographs are taken at a rate of several **pictures per second** either in the VD or lateral projection. Due to the rapid beating of the avian heart, an assessment of cardiac contractility is difficult; however, hypertrophy (ventricle), dilatation (ventricle, atria), stenosis (blood vessels, heart valves) and aneurysms (blood vessels) can be diagnosed with angiography **(Fig. 1-41)**.

1.1.4.6 Myelography

Myelographic studies are indicated when there is suspicion of congenital vertebral deformation or a spinal injury that results in a narrowing of the spinal canal. However, at the present time, there has been only two scientific study, which was performed on chickens and pigeons (HARR et al. 1997, NAEINI et al. 2006). In practice, myelographic investigations are rarely attempted because of the high degree of risk associated with the procedure for the avian patient. Currently there is a better diagnostic method available to diagnose spinal injuries, MRI. Also, with many avian species, the spinal cord caudal to the lumbar glycogen body cannot be well imaged using myelography as the subarachnoid space is narrowed by the glycogen body which hinders the flow of contrast. Experience has shown that myelography in raptors and pigeons due to the better anatomical conditions in these species (i.e. injection cranial to the synsacrum is possible) are more diagnostic than in woodpeckers and aquatic birds.

The volume of contrast agent needed is **0.5–1 ml/kg, which should be injected slowly with a small-calibre needle (23–26 gauge)**. Iodine compounds of a low concentration (200–250 mg iodine/ml) should be used for all avian patients on whom the procedure is to take place. Immediately after the injection, the patient should be held in the upright position for five minutes. Following the injection, the myelogram can be performed on the patient.

There are two injection sites that are commonly used in avian patients: 1) an injection in the thoracolumbar region at the level of the first palpable dip cranial to the synsacrum or 2) an injection in the atlanto-occipital space lying over the cerebromedullary cistern **(Fig. 1-42)**. The latter site is, however, risky as it is very small and is covered by a large plexus of veins. Furthermore, pressure necrosis can occur due to the injection of an excessive volume leading to myelography-induced trauma. Another risk in small birds is the inadvertent injection into the spinal cord instead of the subarachnoid space, which will result in life-threatening consequences (e.g. cardiac arrest, CNS disease).

Further reading

HARR, K., KOLLIAS, V., RENDANO, V., DELAHUNTA, A. (1997): A myelographic technique for avian species. Veterinary Radiology & Ultrasound **38**: 187–192.

NAEINI, A., DADRAS, H., NAEINI, B. (2006): Myelography in the Pigeon (*Columba livia*). Journal of Avian Medicine and Surgery **20**: 27–30.

Fig. 1-40: Radiographic image of a blue-fronted Amazon's (*Amazona aestiva*) head during a sinography procedure in the rostrocaudal projection, approximately 1 min after the injection of 0.5 ml iopamidol (250 mg iodine/ml solution) into the right infraorbital sinus,: The contrast has reached the contralateral side due to a communication between the two sinuses (arrow: nares, part of the infraorbital sinus).

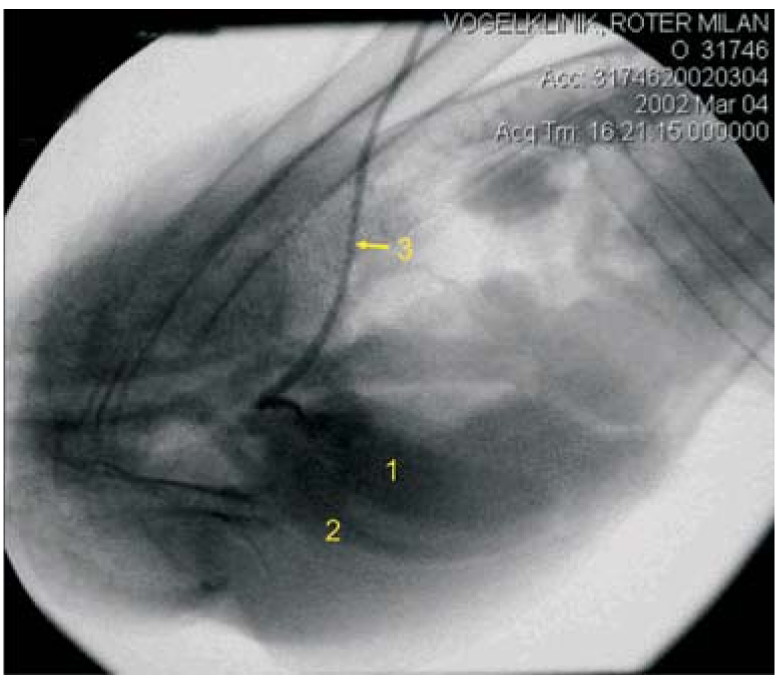

1: left ventricle
2: right ventricle
3: ulnar vein

Fig. 1-41: Radiographic image of a red kite's (*Milvus milvus*) body during an angiocardiographic procedure in the lateral projection, immediately after the intravenous administration of 2 ml/kg bwt iopamidol (250 mg iodine/ml solution) into the cutaneous ulnar vein.

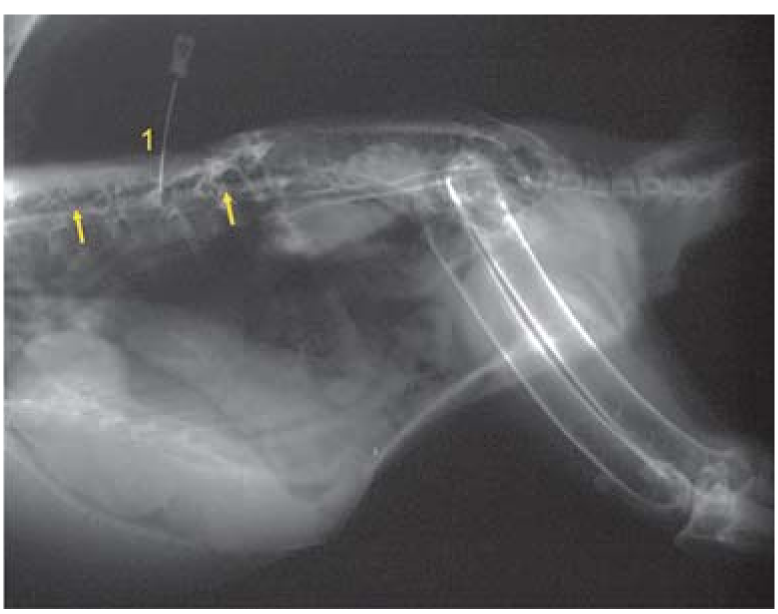

Fig. 1-42: Total body radiographic image of a common buzzard (*Buteo buteo*) during a myelography procedure in the lateral projection, immediately after a subarachnoidal injection cranial to the synsacrum of 1 ml/kg bwt iopamidol (200 mg iodine/ml solution). The radiographic image clearly shows both the (1) cannula and spinal cord stained with contrast (arrows).

1.2 Ultrasonographic examination

Maria-Elisabeth Krautwald-Junghanns, Michael Pees

Although the use of ultrasonography in birds is restricted [due to the small size of many of the patients, the restricted number of coupling sites, and some anatomical differences (e.g. air sacs)], it has become an important and useful diagnostic tool due to the recent development of technical advances. Often ultrasonography is used after a radiographic investigation has been completed (e.g. to assess the type of a soft-tissue shadow or to visualize the internal structure within an organ).

Avian ultrasonographic investigations are of primary importance when investigating the cardiovascular and urogenital systems as well as the liver parenchyma. Typical indications for examining these areas of the body are the differentiation of hydropericardium from cardiomegaly, assessment of parenchymal changes (e.g. differentiation between neoplasia, cysts, or inflammatory changes) and investigating radiolucent masses in the reproductive tract of female birds (e.g. the formation of a laminated egg). Furthermore, this imaging method is the only one that can be used in the living bird to diagnose certain disease processes (e.g. pericardial effusion). In addition, sonographically guided biopsy collection is becoming more important in avian medicine.

Although the ultrasonographic imaging of internal organs in healthy birds may be difficult, this is not the case in avian patients with disease conditions. Organ enlargement, displacement of the air sacs, and fluid accumulation facilitates the coupling of the transducer therefore improving image quality.

1.2.1 Technical requirements

In general, scanners used in small animal veterinary practice (e.g. cats, dogs) can be used on avian patients. The small size of avian organs and – with respect to echocardiography – the high heart rate requires specific technical parameters of the equipment thereby limiting the use of older ultrasound scanners in avian medicine.

The following requirements are mandatory for the ultrasonographic investigation of a bird with a body weight of up to ca. 2 kg:

- ☐ transducers with a small coupling surface [micro-convex transducers **(Fig. 1-43)** are preferable; phased-array transducers are less suitable]
- ☐ transducers with a frequency of between 7 MHz and 12 MHz
- ☐ internal hard disk for the storing of images and movement sequences, or video recording

The size of the transducer is of paramount importance in small birds. The best results are achieved with scanners that have been developed for pediatric medicine, operative, or gynecological use. A spacer is sometimes useful for investigations in small birds to obtain a optimum viewing field.

A scanner frequency of 7.5 MHz is recommended for birds with a body weight of up to 2 kg, so that the anatomic structures can be effectively imaged. Higher frequencies may provide an image with better resolution, but these frequencies will cause a reduction in the frame rate and maximum depth of penetration of the ultrasound waves. The recording of ultrasonographic images on digital video clips or video tape is recommended as the anatomic assessment and evaluation can be performed after the investigation of the patient has been completed. The video image allows the veterinarian to evaluate the ultrasonographic examination without any additional stress to the patient.

The following points are important for doing ultrasonography in birds:

- ☐ refresh rate of at least 100 frames per second
- ☐ Doppler function (color, power, and spectral Doppler, are all useful)
- ☐ electrocardiography with trigger function

A high frame rate is necessary to acquire images of certain cardiac phases (e.g. systole, diastole). In birds with heart rates of up to 600 beats per minute (i.e. 10 beats per second), a frame rate of 100 frames per second produces 10 images per cardiac cycle. Although there has been only limited information published regarding the use of the Doppler function on birds, the ultrasonography scanner should be able to perform both the spectral and color Doppler functions for cardiological investigations. The trigger function is helpful when using the Doppler functions as it enables the heart images and measurements to be correlated to particular phases of the ECG (i.e. it is possible to identify certain cardiac phases – end-diastole and end-systole).

Fig. 1-43: Transducers used on birds for ultrasonography examinations should have a small coupling surface. This micro-curved probe with a frequency of 7.5 MHz is ideal for the examination of birds up to a body weight of 2 kg.

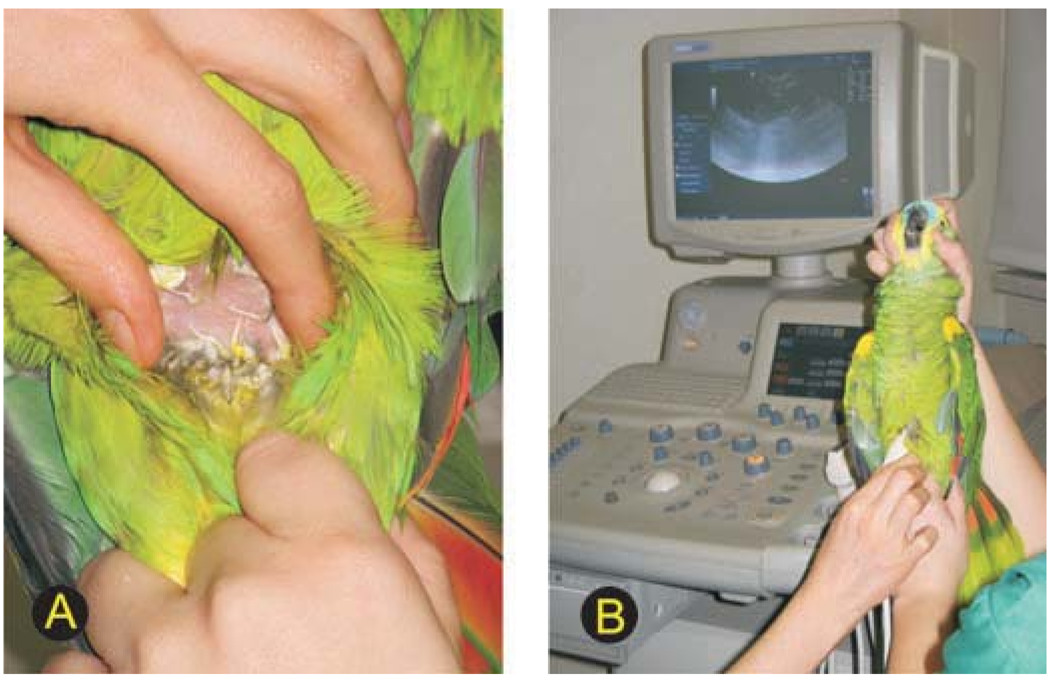

Fig. 1-44: Ventromedian approach of a ultrasonographic examination on a blue-fronted Amazon (*Amazona aestiva*). The transducer is placed on the midline behind the sternum. There is a naturally feather-free region – the brood patch – at this site, which prevents one from having to pull out feathers.

1.2.2 Preparation of the patient, coupling sites

Ideally birds should be fasted before the ultrasonographic examination as an ingesta-filled gastrointestinal tract can disturb the penetration of the ultrasound waves, thereby reducing one's ability to image organs outside of the GI tract (i.e. especially when a ventromedial coupling site is used; see below). In the clinically ill bird that has had a reduced appetite over a prolonged period, fasting is often neither necessary nor possible. The fasting time for psittacines before an ultrasonographic examination is generally acknowledged as 1 to 2 hours. Pigeons with an extremely full gastrointestinal tract may need to be fasted for up to 12 hours and raptor species up to 48 hours.

Usually, anesthesia is not required for ultrasonographic examinations, however the stress involved in handling the bird to be evaluated can lead to problems in interpreting images of the cardiovascular system. Anesthesia can also affect the patient's heart rate and contractility. In their experience, the authors of this text recommend generalized anesthesia for only avian patients sensitive to stress when using B-mode for imaging pathological changes in the heart. In contrast, when using the spectral Doppler function, these ultrasonographic examinations should be done under a full anesthesia to minimize the effects of handling on the patient and fixation on the rate of blood flow.

The patient can be held by an assistant or the owner in dorsal or lateral recumbency or even in an almost upright position for the ultrasonographic examination **(Figs. 1-44 and 1-49)**. In patients with clinical signs of heart disease or respiratory depression, lying in dorsal rumbancy can lead to circulatory problems; therefore this position should be avoided. In general, it is advisable to hold the birds as upright as possible for the ultrasonographic procedure.

Due to their anatomy, the number of locations where one can bring a transducer in close contact to the skin of avian patients is limited. Since close contact between the transducer and the skin is necessary to achieve optimal imaging quality, only two coupling sites are particularly suitable in birds: the ventromedial site (cranial and caudal) behind the sternum and the parasternal site behind the last rib (Table 1-1). The ventromedial coupling site is the one most frequently used. The transducer is placed on the ventromedial aspect of the body wall directly behind the caudal end of the sternum **(Fig. 1-44)**. The parasternal coupling site can be particularly used in birds with enough space between the last rib and the pelvis (e.g. pigeons and some raptor species). The transducer is generally placed on the right side of the bird, as the ventriculus, located on the left side, can disturb the penetration of ultrasound waves. The leg is drawn either forwards or backwards, and the transducer is pressed lightly on the body wall in order to compress the air sacs lying below it **(Fig. 1-49)**.

Feathers hamper the contact between the transducer and the skin, adversely affecting image quality. Whether the feathers need to be plucked or whether it is enough just to part them for better transducer contact is dependent on the species. Usually in pigeons, chickens, and raptors some feathers need to be plucked to obtain a better contact for the transducer to the skin. In comparison, parting of the feathers is often enough for the majority of psittacine species examined in veterinary hospitals. In psittacine species, a featherless site behind the sternum (brood patch, **Fig. 1-44**) can be used for the ventromedial coupling site. If the coupling site is difficult to access in aquatic birds, plucking should performed as judiciously as possible because in this type of bird excess feather loss can lead to a hypothermic condition and they may lose their ability to swim.

An adequate amount of a commercial water-soluble ultrasonography gel should be used to ensure adequate contact between the transducer and skin. The water-soluble gels that are currently available are, in general, well tolerated by birds and can be easily removed from the feathers and skin once the examination is complete.

Table 1-1: Coupling sites used for ultrasonographic investigations in birds

order	body weight	ventro-median (cranial)	ventro-median (caudal)	parasternal
Psittaciformes	150–1500 g	yes	yes	no
Accipitriformes	100–1500 g	yes	yes	yes/no
Falconiformes	100–1000 g	yes	yes	yes/no
Strigiformes	100–2000 g	yes	yes	yes
Galliformes	75–250 g	yes	nein	yes
Galliformes	250–2000 g	yes	yes	yes
Columbiformes	150–500 g	yes	yes	yes
Passeriformes	< 75 g	yes	no	no
Passeriformes	> 150 g	yes	yes	no

1.2.3 Procedure

In ultrasonographic diagnostic examinations, the assessment of results is more subjective and more dependent on the individual technique being used and experience of the investigator than with radiodiagnostics. As a consequence, a hard-and-fast examination procedure should be used for routine ultrasonographic assessment. The authors recommend the following for the ultrasonographic examination of birds:

- ☐ liver **(Fig. 1-45)**
- ☐ heart **(Fig. 1-46)**
- ☐ gastrointestinal tract **(Fig. 1-47)**
- ☐ urogenital tract **(Fig. 1-47)**.

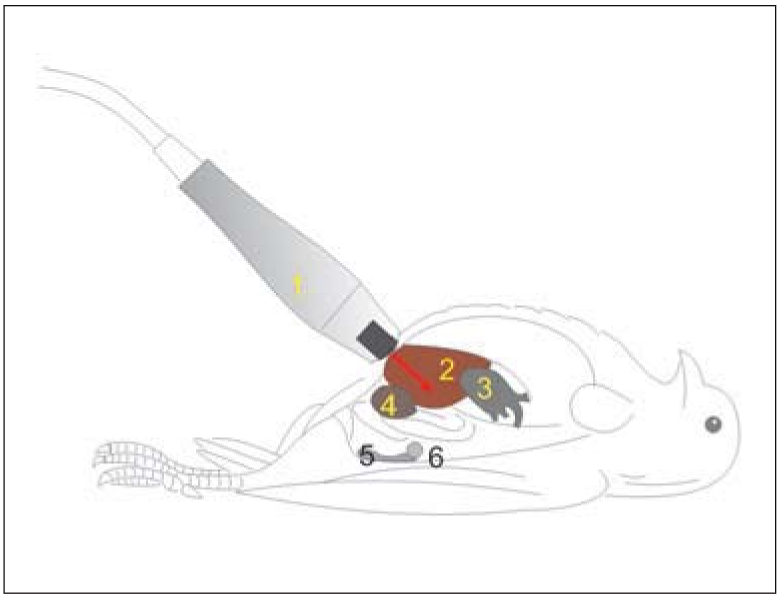

1: transducer
2: liver
3: heart
4: ventriculus
5: kidney
6: gonad

Fig. 1-45: Schematic representation of a liver examination using a ventromedian coupling site.

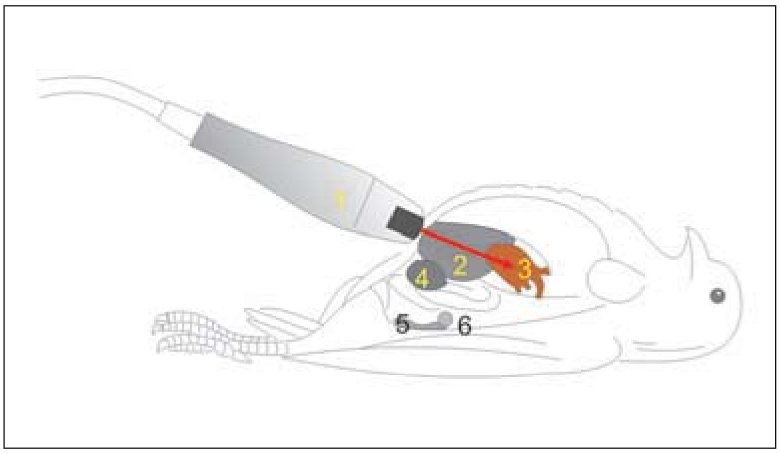

1: transducer
2: liver
3: heart
4: ventriculus
5: kidney
6: gonad

Fig. 1-46: Schematic representation of a heart examination using a ventromedian coupling site.

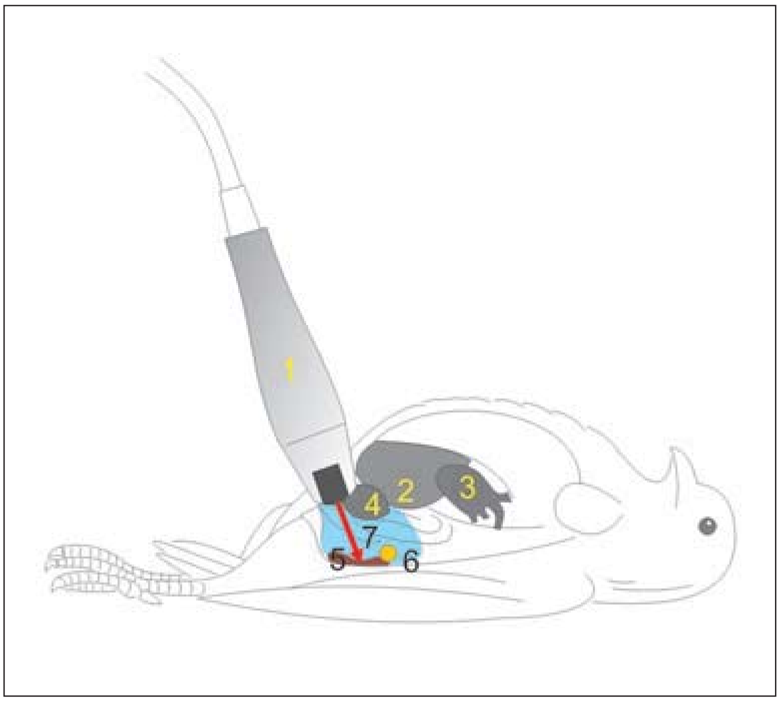

1: transducer
2: liver
3: heart
4: ventriculus
5: kidney
6: gonad
7: air sac

Fig. 1-47: Schematic representation of the kidney, gonads and gastrointestinal tract examination using a ventromedian coupling site.

Using the ventromedial coupling site, the transducer is aimed cranially to image the liver **(Fig. 1-45)**. Once the liver has been identified, the transducer is swiveled from the lateral to the medial until the whole liver has been visualized. If indicated, a biopsy can be taken under ultrasonographic control (see below).

To investigate the heart, the transducer is aimed craniodorsally until the heart is identified – the liver acts as an acoustic window due to its homogenous structure and the lack of a diaphragm **(Fig. 1-46)**. Once the heart has been visualized, the transducer is swung laterally to investigate the heart section by section **(Fig. 1-48)**. Then the vertical plane is investigated (vertical to the sternum) which allows the imaging of the left ventricle and atrium. This projection is equivalent to the two-chamber projection in mammals. Subsequently, the transducer is turned through 90° to show the second, horizontal plane. In this projection the ventricles, atria, and aorta can be observed (see **Fig. 1-52**). Before measurements can be determined, the transducer must be so adjusted that the maximum width of the chambers is shown.

Using the parasternal coupling site, additional transverse scans of the heart can be visualized **(Fig. 1-48)**.

The transducer is then swung towards the left to start investigating the gastrointestinal tract **(Fig. 1-47)**. The ventriculus is easy to identify in carnivorous birds due to its thick musculature and the large amount of grit that may be present in its lumen. At suitable frequencies (>12 MHz), the koilin layer can be imaged. The proventriculus is occasionally observed lying on the left side. The small intestines are best imaged with higher frequencies (from 10 MHz) and even the layers of the intestinal wall can be assessed. Furthermore, the peristalsis of the small intestines can be observed. The cloaca is situated in the caudal part of the body cavity.

The last part of the ultrasonographic examination involves the urogenital tract which lies behind the intestines **(Fig. 1-47)**. The examination of the urogenital tract begins with imaging the kidneys, which under normal conditions are not commonly observed due to being surrounded by air sacs. Only with an enlargement of the kidneys and an associated displacement of the air sacs is it possible to view these organs. To identify renal tissues, the kidney should be assessed in cross-section (see below). Once it has been identified, the size of the organ can be imaged using a longitudinal projection.

The depiction of the testicles and the ovaries depends on the bird's sexual status. Juvenile and inactive gonads are as a rule not visible with a transcutaneous coupling site due to interference by the surrounding air sacs. Putting a light degree of pressure on the transducer can aid in the imaging of the urogenital tract as this will compress the air sacs, thereby reducing the interference of the sound waves by these structures.

1.2.4 Additional coupling sites

Another coupling site used especially for imaging the crop, lies to the left and right of the thoracic inlet. As plucking of feathers is usually required for an improved transducer contact to the skin and these feathers are difficult to remove, this structure and location should be the last examined sonographically in an avian patient. Many birds react to feather plucking with signs of stress and defensive movements, as a result it is advisable to only use this coupling site with the patient under general anesthesia. A spacer is usually needed because the crop lies directly under the skin.

In larger birds with a body weight of more than 2 kg, an intracloacal ultrasonographic examination can be achieved. With this coupling site, the normal kidney and gonads are well visualized **(Figs. 1-66** and **1-67)**. So far, this coupling site has been mainly used for experimental purposes as the bird needs to be anesthetized, a large patient, and indications for examining this area are rare.

When sonographically examining ratites, transcutaneous coupling sites are generally used in conjuction with the right type of transducer (linear transducer, 3.5 MHz) on unsedated birds.

1.2.5 Biopsy

To achieve a definitive etiological diagnosis, it may be necessary to take a biopsy of an organ for a histological and/or microbiological diagnostic interpretation.

The most common indications for a sonographically controlled biopsy are changes in the liver parenchyma **(Fig. 1-50)**. In addition, tumors of unknown origin in the body cavity can also be biopsied. Biopsies of the kidney are not recommended by the authors as they are associated with a high risk of hemorrhage in the bird. Sonographically controlled aspiration for therapeutic use (i.e. drainage of fluid accumulations) in ascites, cysts, and pericardial effusion is easily performed on avian patients.

The preparation of both the aspiration site and of the coupling site is achieved as described above for the ultrasonographic procedure. Instead of contact gel, coupling can be carried out using a mild disinfectant suitable for mucous membranes (e.g. Octenisept®). The organ of interest (often the liver) is visualized on the screen and the larger blood vessels and neighbouring organs should be localized and assessed. The color or power Doppler function is of great use when visualizing and identifying the larger blood vessels around the heart. If there is an increased risk of hemorrhage from the organ to be biopsied, the potential diagnostic results of a biopsy sample(s) must be carefully weighed against the danger of performing the procedure.

With liver biopsies, once the needle has penetrated the skin it must be pushed quickly into the liver to minimize damage to the liver capsule. Once the desired position has been reached in the liver by the needle, the tissue sample(s) is retrieved using standard biopsy instruments. The internal diameter of the True-cut® needles (COOK Company, Queensland, Australia) used in our clinic is 20 G with a length of 15 cm. With this type of needle, a 10 mm long biopsy sample can be collected **(Fig. 1-51)**.

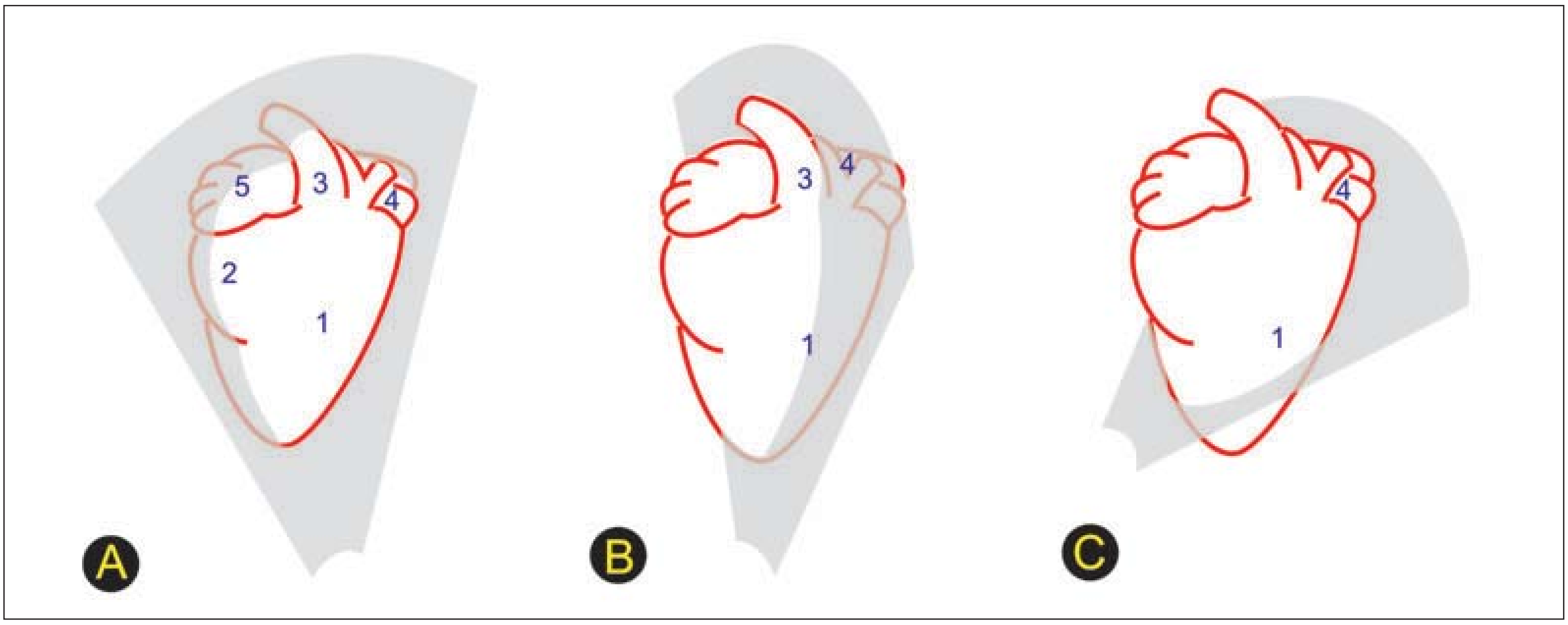

Fig. 1-48: Schematic representation of the sectional planes through the heart using a ventromedian coupling site (A: horizontal four-chamber projection, B: vertical two-chamber projection) and a parasternal coupling site (C: short-axis slice).

1: left ventricle
2: right ventricle
3: aorta
4: left atrium
5: right atrium

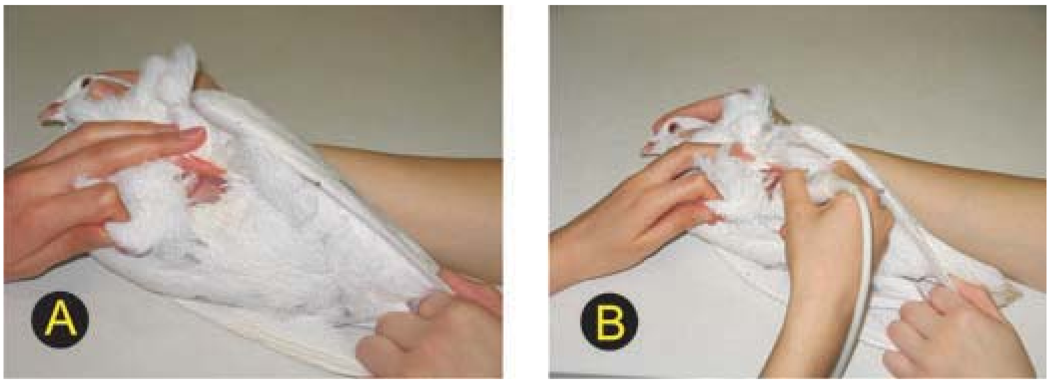

Fig. 1-49: Parasternal approach of a ultrasonographic examination on a homing pigeon (*Columba livia* f. *domestica*): For this approach, the bird's leg is pulled either in a cranial or caudal position. This approach is only possible in birds where there is enough room between the final rib and the pelvis to properly position the transducer (see Table 1-1).

Fig. 1-50: Ultrasonographically guided liver biopsy in a galah cockatoo (*Eolophus roseicapilla*). The biopsy needle is pushed under ultrasonographic guidance into the liver tissue which lies immediately under the skin.

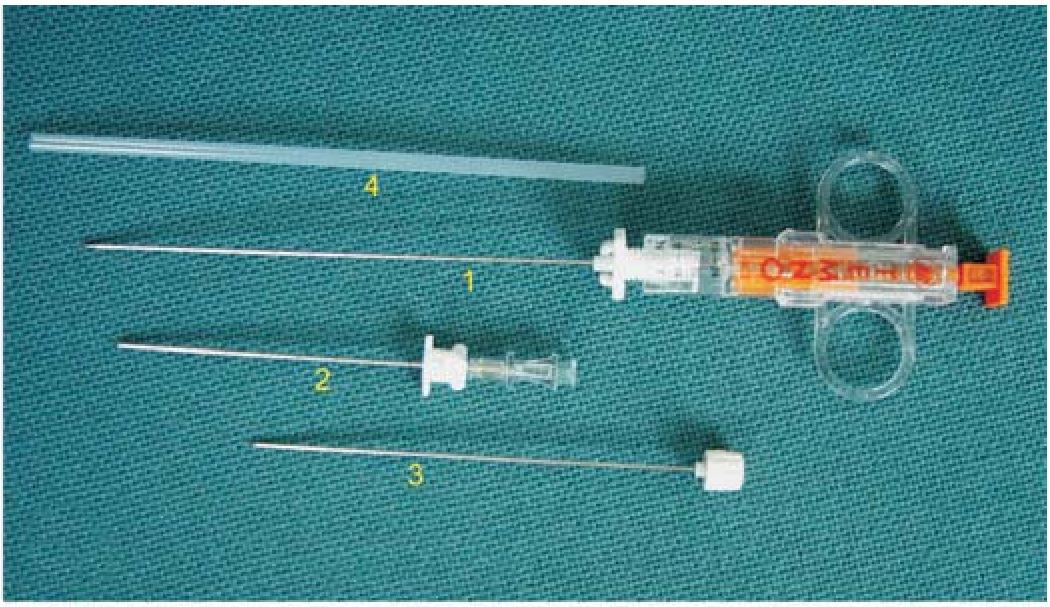

Fig. 1-51: Biopsy instruments, COOK Company, Queensland, Australia.

1: biopsy needle
2: trocar
3: guide sleeve
4: protective sleeve

Complications and tolerance

The undertaking of a sonographically controlled fine needle biopsy should in general be carefully considered in patients with cardiovascular disease, prolonged coagulation times, or a general tendency to hemorrhage.

Although the relevant scientific literature does not consider it necessary, it may be prudent to give sick birds vitamin K in their drinking water for 24 to 48 h before the procedure to provide prophylaxis against hemorrhaging. The patient's platelet count should be obtained in order to determine the avian patient's coagulation status. Currently, determination of the coagulation time cannot be used in practice because at this time there is no suitable method available to determine an avian patient's coagulation status.

The problems associated with a full gallbladder that occur in mammalian medicine are of little significance in avian medicine as the majority of parrot species do not have this anatomic structure. In species which have a gallbladder and if the gallbladder appears in the ultrasonographic images, this could be a possible source of sonographic wave interference. In such cases, edible oil can be given as in small animal medicine to facilitate the emptying of the gallbladder.

To prevent defensive reactions, it is advisable to anesthetize the patient when performing a fine needle biopsy of the liver.

Hemorrhages in the liver can occur but have no clinical relevance in the experience of the authors. This biopsy method has proven to have a great deal of safety in clinical studies, even in patients with coagulation disorders. When the body cavity remains closed, the pressure in the individual sections ensures a rapid cessation of any possible hemorrhaging. Reports from human and small animal medicine have shown that since using ultrasonographic imaging with this biopsy procedure there has been a significant reduction of complications associated with compromising liver tissue; this can also be confirmed in birds.

1.2.6 Contrast studies

Contrast studies are used in ultrasonographic examinations to image the gastrointestinal tract. Once the water or an ultrasonographic contrast agent has been placed in the crop or esophagus (up to 20 ml/kg body weight orally), the contrast material is transported distally within an extremely short period of time – depending on the species – and greatly improves the image quality of the gastrointestinal tract. Intracloacal placement of a contrast agent is also achieved with few complications and improves the diagnostic quality of the ultrasonographic examination **(Figs. 1-62** and **1-65A, B)**.

In addition to water, which is used at the body temperature of the avian patient, other types of contrast agents are available for ultrasonographic examinations. Contrast agents, other than water, recommended for ultrasonographic examinations develop air-filled microparticles (microbubbles) in the suspension. After being given orally, such suspensions (e.g. Levovist®, Schering) produce a strong ultrasound scattering pattern, which gives the appearance of a snowstorm in the gastrointestinal tract.

The use of such microbubble contrast agents provides a better image of intestinal peristalsis than that of water. As the intestinal walls appear relatively hyperechoic, they are not usually differentiated from the lumen due to the »snowstorm« effect of the contrast agent. Consequently, warmed water is the preferred contrast material when the intestinal walls need to be examined.

1.2.7 Ultrasonographic imaging of normal structures

1.2.7.1 Skeletal system

As yet there are no known indications for sonographically examining the skeletal system.

1.2.7.2 Cardiovascular system

Imaging of the heart in psittacine, raptor, and corvidae species can only be performed using the coupling site situated caudal to the sternum (ventromedial). The ventromedial coupling site limits the available scanning planes for visualizing the heart in the species listed above to just the apical two- and four-chamber projections **(Figs. 1-48, 1-52** and **1-53)**.

In other avian species (e.g. pigeons, chickens) the parasternal coupling site is also usable (Table 1-1) and is situated in the fenestra medialis or lateral trabeculae of the sternum. For these investigations, only the right coupling site is used as the ventriculus lies on the left (a very reflex-rich organ) and hides the heart lying behind it. In these birds, the heart can be observed in four different planes (apical two- and four-chamber, right parasternal long axis and short axis views; **Figs. 1-48** and **1-55**).

The significant advantage of ultrasonography when examining the avian heart is being able to image its internal structure. By examining the internal structure of the heart one has an improved ability to determine its anatomic and functional status. However, due to the anatomical peculiarities of the avian heart, the protocol recommended for performing echocardiography in mammals (standardized scanning planes) cannot be used in birds. M-mode, a useful aid for the assessment of wall thickness and contractility in mammals, is not really useful in birds as the avian heart can only be imaged in the longitudinal and semitransverse planes. The established method of choice in birds is the B-mode method (2D echocardiography) and reference values are already available for various species (Table 1-2). Doppler echocardiography has been successfully tested in birds **(Figs. 1-53** and **1-56)**.

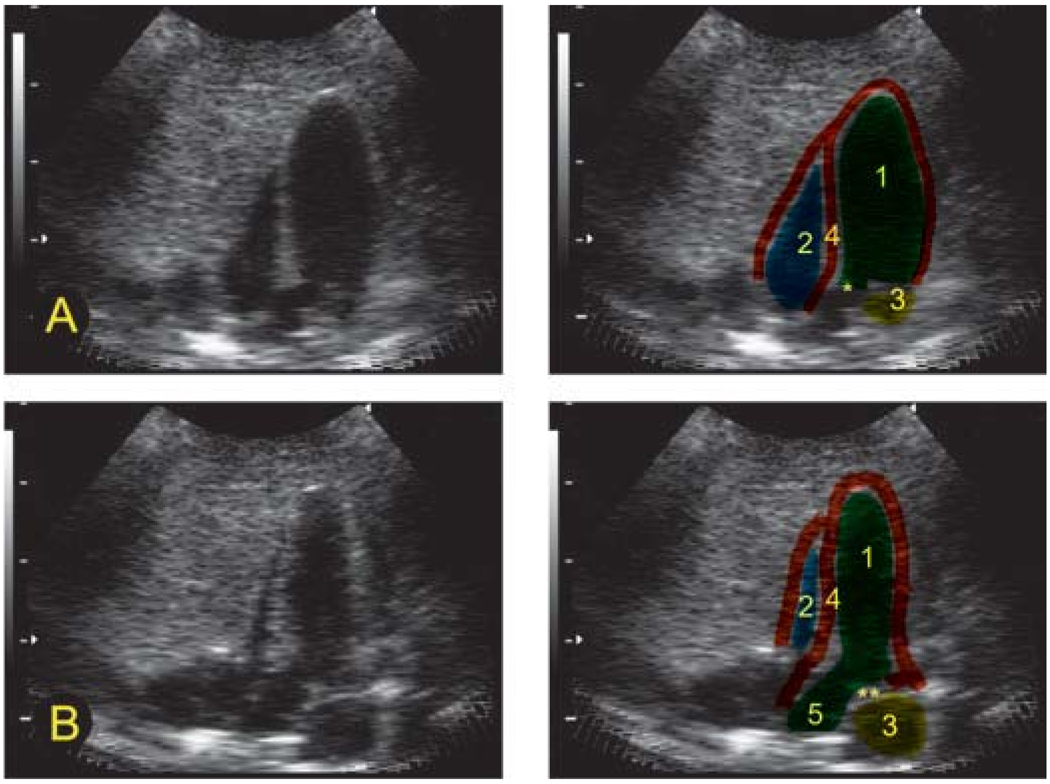

1: left ventricle
2: right ventricle
3: right atrium
4: intraventricular septum
5: aorta,
*: aortic valve
**: atrioventricular valve

Fig. 1-52: Sonographic images of an African grey parrot's (*Psittacus erithacus*) heart using the ventromedian coupling site, 7.5 MHz, PD 4.5 cm: Horizontal section of the heart (four-chamber projection) in (A) diastole and (B) systole.

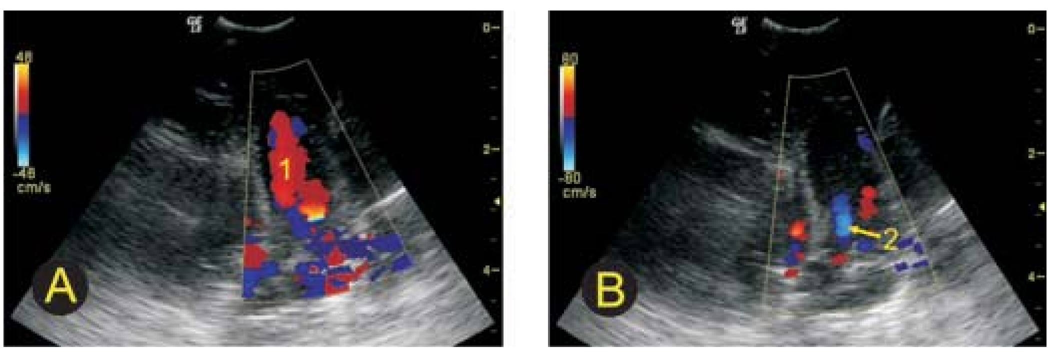

Fig. 1-53: Color Doppler ultrasonographic images of an African grey parrot's (*Psittacus erithacus*) heart using the ventromedian coupling site, 10 MHz, PD 5 cm, horizontal section.

A: Filling of the left ventricles (1) during diastole.

B: Outflow from the left ventricle through the aorta (2) during systole.

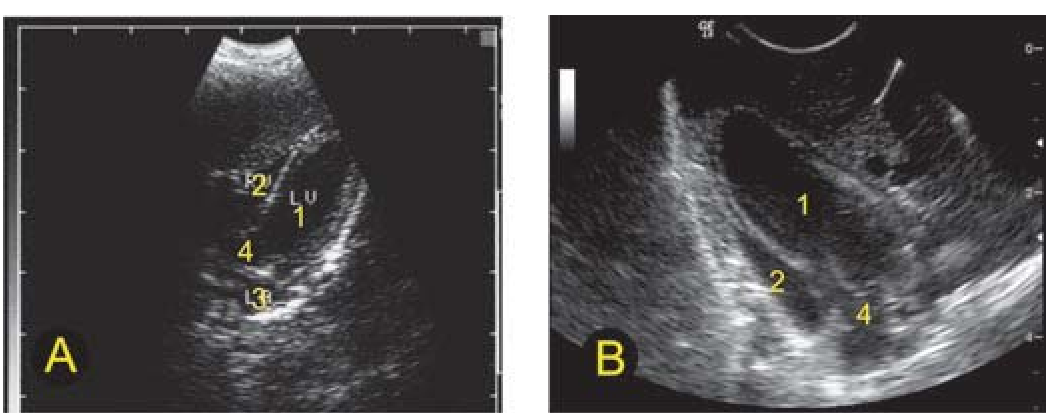

1: left ventricle
2: right ventricle
3: left atrium
4: aorta

Fig. 1-54: Ultrasonographic images of the avian heart using the parasternal coupling site.

A: 7.5 MHz, PD 6 cm, dove (*Columba livia* f. *domestica*).

B: 10 MHz, PD 4.5 cm, Eurasian eagle owl (*Bubo bubo*): Longitudinal image of the heart using a lateral coupling site.

Blood flow patterns can be depicted in the color mode and blood flow rates are measured in the region of the atrioventricular opening and the root of the aorta. Systematic investigations and reference values using pulsed-wave spectral Doppler function are available for some species (Table 1-3), whereas the use of the color Doppler function has only been reported in a few case studies.

The body weight and external palpable length of the sternum are useful parameters for relating the measurements to the size of the bird. It is sensible to perform an electrocardiogram (ECG) at the same time as the ultrasonographic examination so that heart images can be investigated in the end-systolic or end-diastolic phase.

Indications

- ☐ all clinical (see Chap. 1.1) and radiographic indications of heart disease, as well as enlarged or diminished (rare) heart shadows, changes in heart form
- ☐ noninfectious (e.g. space-occupying disease conditions, hypocalcemia) and infectious diseases that cause secondary changes to the heart (e.g. pericardial effusion due to congestion in the pulmonary or systemic circulation, often as a consequence of liver or lung disease).

Table 1-2: 2D echocardiography, important parameters measured and calculated in birds (mean ± standard deviation, n/k: not known).

Parameter		***Psittacus e. erithacus*** **(PEES et al. 2004)**	***Amazona* spp. (PEES et al. 2004)**	***Cacatua* spp. (PEES et al. 2004)**	**Diurnal birds of prey* (BOSKOVIC et al. 1999)**	**Pigeons (SCHULZ 1995)**
		ventromedial approach				**parasternal approach**
Body weight [g]		493 ± 55	353 ± 42	426 ± 162	720 ± 197	434 ± 52
left ventricle	Systolic length [mm]	22.5 ± 1.9	21.1 ± 2.3	19.0 ± 1.3	14.7 ± 2.8	17.9 ± 1.0
	Diastolic length [mm]	24.0 ± 1.9	22.1 ± 2.2	19.9 ± 1.6	16.4 ± 2.7	20.1 ± 1.4
	Systolic width [mm]	6.8 ± 1.0	6.7 ± 1.2	6.4 ± 1.7	6.3 ± 1.1	5.2 ± 0.4
	Diastolic width [mm]	8.6 ± 1.0	8.4 ± 1.0	8.3 ± 1.5	7.7 ± 1.2	7.4 ± 0.6
	Fractional shortening [%]	22.6 ± 4.4	22.8 ± 4.2	25.6 ± 7.0	n/k	27.2 ± 4.5
right ventricle	Systolic length [mm]	9.2 ± 1.4	9.4 ± 1.8	10.3 ± 1.2	12.7 ± 2.7	n/k
	Diastolic length [mm]	11.5 ± 1.9	10.3 ± 1.3	11.3 ± 2.3	13.9 ± 2.5	9.9 ± 0.8
	Systolic width [mm]	2.8 ± 0.9	3.1 ± 0.7	2.3 ± 0.0	2.1 ± 0.6	n/k
	Diastolic width [mm]	4.8 ± 1.1	5.2 ± 1.3	3.5 ± 0.5	2.5 ± 0.8	4.0 ± 0.5
	Fractional shortening [%]	40.8 ± 11.9	34.1 ± 3.7	33.3 ± 10.3	n/k	n/k
interventricular septum	Systolic thickness [mm]	2.9 ± 0.5	2.2 ± 0.1	1.9 ± 0.3	1.9 ± 0.6	3.8 ± 0.1
	Diastolic thickness [mm]	2.5 ± 0.3	2.1 ± 0.4	1.7 ± 0.4	1.9 ± 0.5	3.3 ± 0.2

* *Buteo buteo, Accipiter nisus, Accipiter gentilis, Milvus milvus*

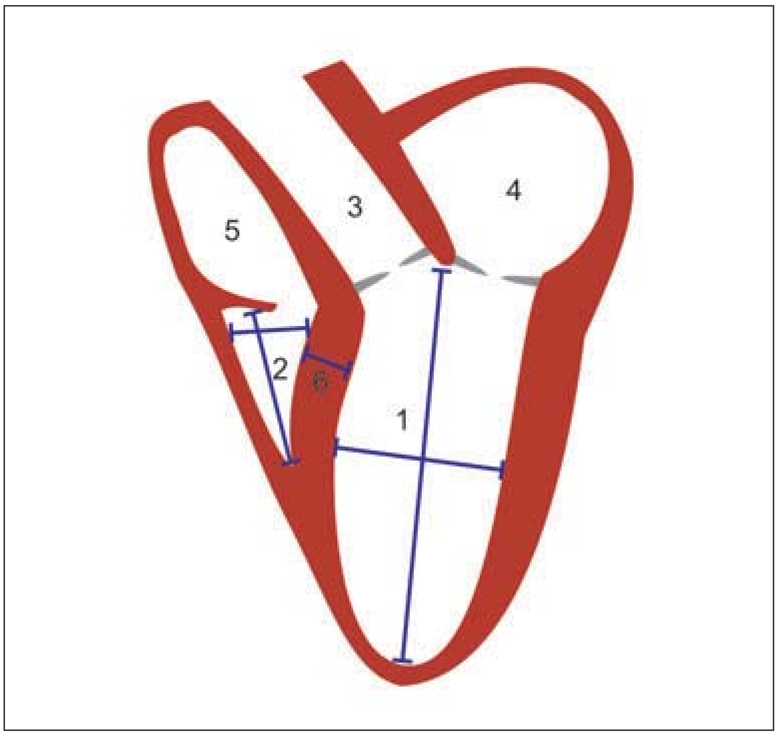

1: left ventricle, length and width
2: right ventricle, length and width
3: aorta, diameter
4: left atrium (there is no reason to measure this chamber)
5: right atrium (there is no reason to measure this chamber)
6: intraventricular septum, thickness

Fig. 1-55: Schematic representation of the measuring points in the avian heart, four-chamber projection.

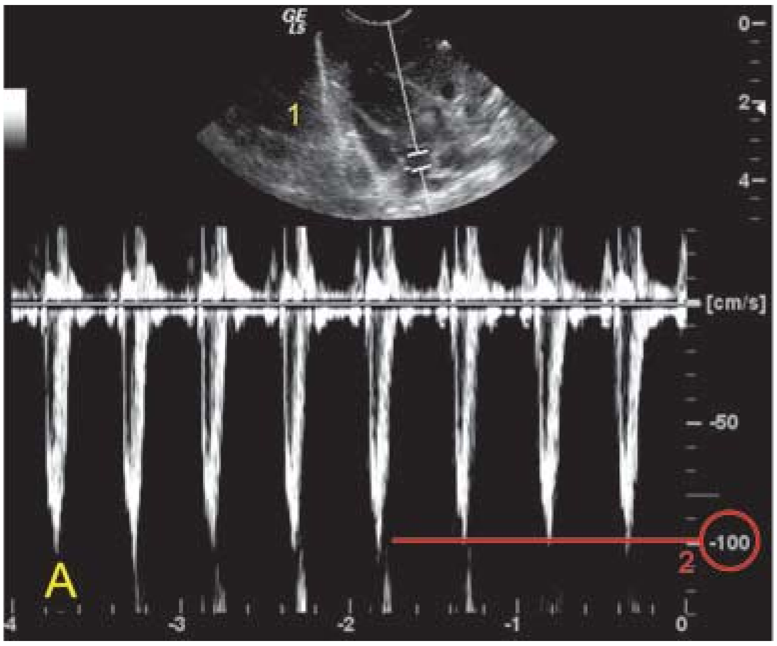

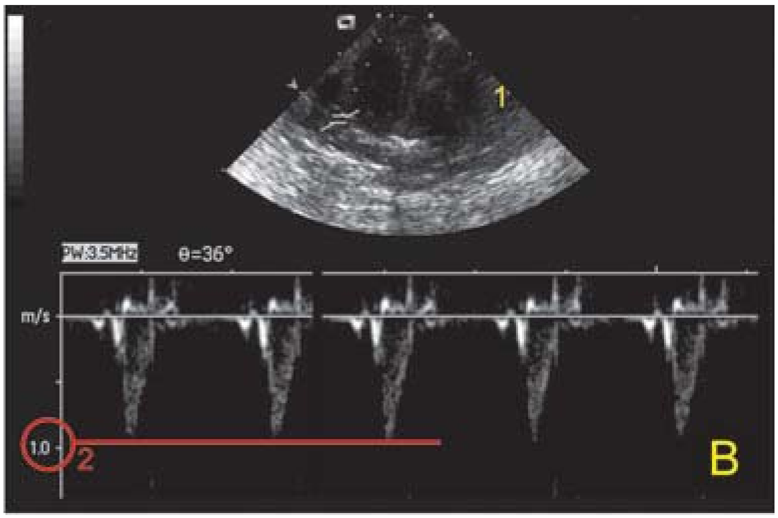

Fig. 1-56: Spectral Doppler ultrasonography examination of avian hearts using a ventromedian coupling site.

A: 10 MHz, PD 4.5 cm, Eurasian eagle owl (*Bubo bubo*).

B: 7 MHz, PD 4.5 cm, carrion crow (*Corvus corone*):

Blood flow through the aorta during systole (1: Doppler gate). The maximum value (2) is approximately 1 m/s in each bird.

Table 1-3: Intracardial blood flow velocities in some avian species (anesthetized; n.k.: not known).

Parameter	*Amazona* spp. (PEES et al. 2005)	*Ara* spp. (CARRANI et al. 2003)	*Cacatua galerita* (CARRANI et al. 2003)	*Psittacus erithacus* (CARRANI et al. 2003)	*Falco* spp. (STRAUB et al. 2001)	*Buteo buteo* (STRAUB et al. 2001)
Diastolic flow into the left ventricle [m/s]	0.18 ± 0.03	0.54 ± 0.07	0.32 ± 0.15	0.39 ± 0.06	0.21 ± 0.03	0.14 ± 0.01
Diastolic flow into the right ventricle [m/s]	0.22 ± 0.05	n.k.	n.k.	n.k.	0.21 ± 0.04	0.14 ± 0.02
Systolic flow out of the aortic root [m/s]	0.83 ± 0.08	0.81 ± 0.16	0.78 ± 0.19	0.89 ± 0.13	0.95 ± 0.07	1.18 ± 0.05

B-mode (2D echocardiography)

With 2D echocardiography, the structures within the heart can be assessed subjectively by the examiner or through measurement **(Fig. 1-52)**. The size of the ventricles, the thickness of the intraventricular septum and the contractility of the ventricles are important parameters for judging the heart's morphology and function. In addition, the left atrioventricular (AV) valves, the aortic valves and the muscular right AV valve can be assessed independent of the image quality. Measurements in the 2D pictures are performed using the inner edge method. In addition to size, the ventricular contractility (fractional shortening; FS) is especially important and is calculated using the following formula:

$$FS\ [\%] = \frac{(\text{diastolic value} - \text{systolic value}) \times 100}{\text{diastolic value}}$$

Due to the crescent-moon shape of the right ventricle in the avian heart, the contractility of this chamber is much higher than that of the left.

Doppler ultrasonography

The spectral Doppler function is used in birds to determine the rate of blood flow (inflow, outflow), which is shown in a 2D curve against time **(Fig. 1-56)**. Reference values are available for the diastolic inflow in the right and left ventricles as well as the systolic outflow in the aorta (Table 1-3).

Color Doppler images of the heart are primarily used to set a frame rate for the spectral Doppler echocardiography, although it is also used in the diagnosis of valvular insufficiency and aneurysms. As the frame rate is significantly reduced when the color Doppler function is used, its applicability in avian echocardiography is currently limited.

1.2.7.3 Respiratory tract

Currently, there are no indications for the use of ultrasonographic examination of the avian espiratory tract.

1.2.7.4 Liver

The avian liver is, in general, easily visualized using ultrasonography; although the patient should have a relatively clear gastrointestinal tract (i.e. the superimposition of the gastrointestinal tract can make it difficult or near to impossible to image the liver). The imaging of the liver can be difficult if the surrounding organs are severely altered (e.g. enlarged).

For the investigation of the liver, the transducer is placed on the midline, caudal to the xiphoid, and aimed in the craniodorsal direction (see **Fig. 1-46)**. The liver tissue is assessed both longitudinally and in the cross-section. Sonographically, the normal texture of avian liver tissue has a medium degree of echogenicity and is finely granulated to homogenous. The internal structure of the liver is interrupted by cross-sectional or longitudinal hepatic blood vessels **(Figs. 1-57** and **1-58)**, with the edges of the liver appearing sharp. Since the liver can only be evaluated in sections at any one time, taking measurements of its size is difficult.

To visualize the gallbladder, one to two days of fasting are required, depending on the avian species being sonographically examined. In birds that have a gallbladder, it can be easily observed when full, lying on top of the liver. The gall bladder images as a hypoechoic oval to roundish structure with a narrow hyperechoic rim situated caudal to the right lobe of the liver **(Fig. 1-59)**. On occasion, large blood vessels are noted over the dorsal surface of the gallbladder.

Indications

- ☐ often: clinical (see Chap. 1.1.3.4), blood biochemical and radiographic indications of liver disease such as enlargement (more rarely reduced in size, changes in form) of the liver silhouette in the radiographic investigation; especially differentiation of neoplasia, inflammation and fatty degeneration by assessing the liver parenchyma
- ☐ suspicion of ascites during palpation

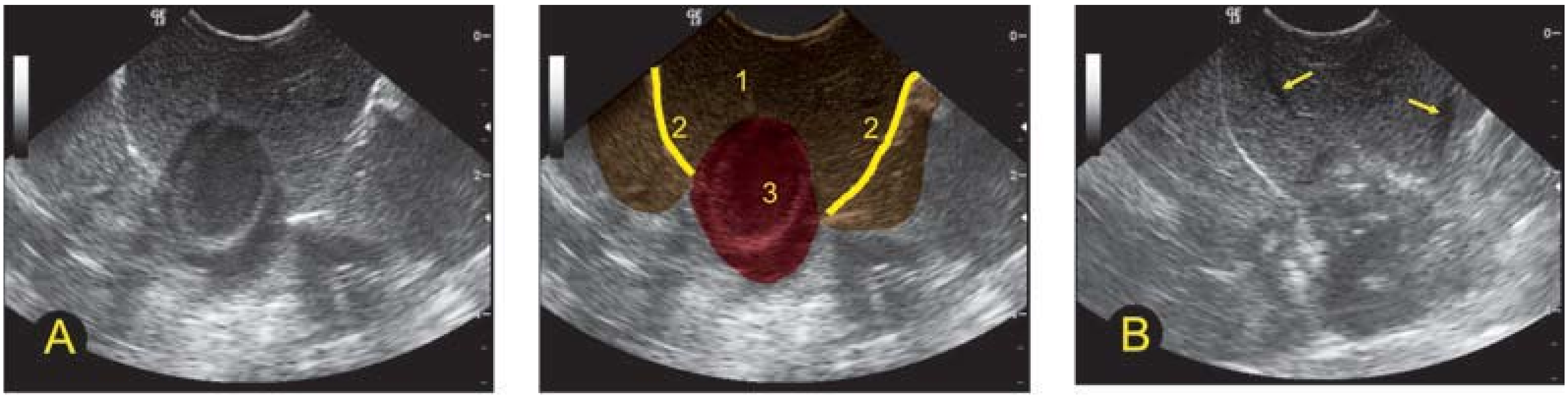

Fig. 1-57: Liver and heart ultrasonographic images of an Eurasian eagle owl (*Bubo bubo*) using a ventromedian coupling site, 10 MHz, PD 4.5 cm: (A) The liver (1) is lying around the apex of the heart (3). The boundary between the hepatic lobes (2) can be observed as an echogenic zone. Individual blood vessels are differentiated as hypoechoic areas (B: arrows).

1: liver
2: boundary between the hepatic lobes
3: heart

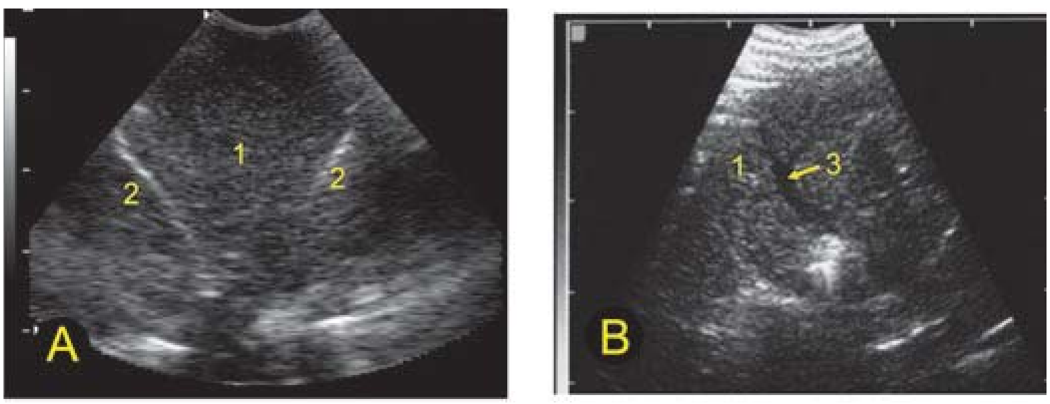

1: liver
2: boundary between the hepatic lobes
3: caudal vena cava

Fig. 1-58: Ultrasonographic images of avian livers using a ventromedian coupling site.

A: 7.5 MHz, PD 4.5 cm, African grey parrot (*Psittacus erithacus*).

B: 7.5 MHz, PD 6 cm, common buzzard (*Buteo buteo*).

The hepatic tissue (1) appears homogenous apart from areas between the hepatic lobes (2). The course of the hepatic blood vessels (3) can be visualized with suitable adjustment of the beam.

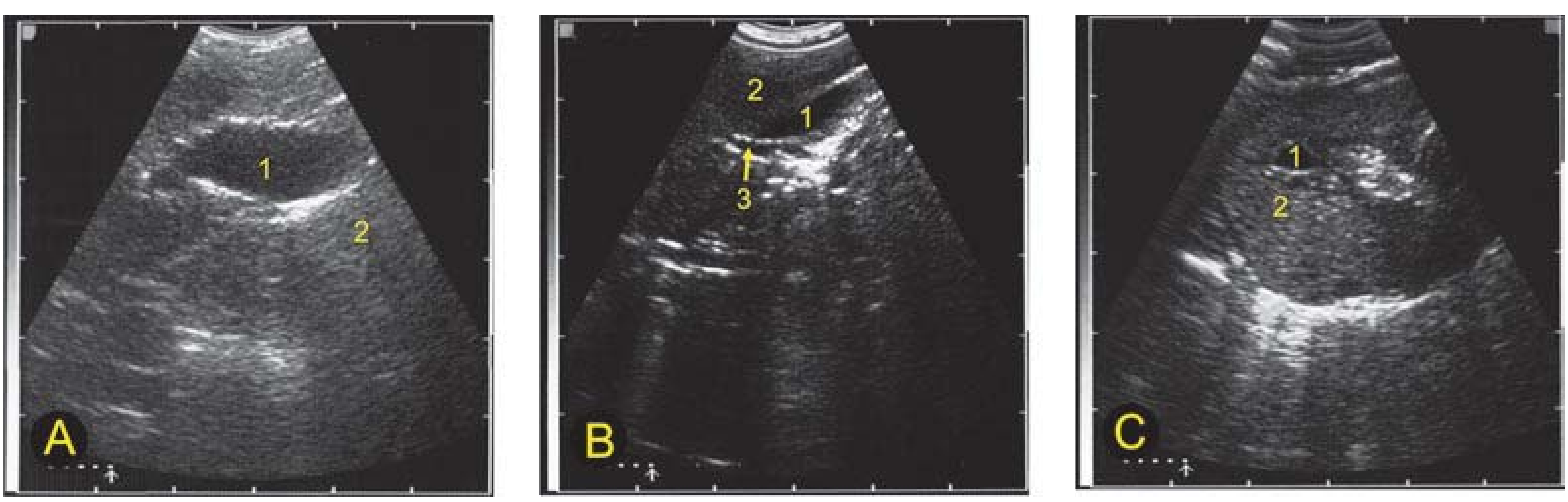

Fig. 1-59: Ultrasonographic images of the avian liver and gallbladder using a ventromedian coupling site, 7.5 MHz, PD 6 cm.

A: Saker falcon (*Falco cherug*).

B: Carrion crow (*Corvus corone*).

C: Indian hill myna (*Gracula religiosa*).
The gallbladder (1) appears as a hypoechoic fluid-filled structure. The liver parenchyma (2) and caudal vena cava (3) have the same appearance as shown in Fig. 1-58B.

1: gallbladder
2: liver parenchyma
3: caudal vena cava

1.2.7.5 Spleen

The spleen appears to be slightly less echogenic than the liver in a ultrasonographic image. The ultrasonographic form of the spleen depends on the avian species being examined. The lateral coupling site must be used to investigate a normal spleen, though it is often difficult or virtually impossible to image because, when normal, it is hidden by the ventriculus and duodenum.

In birds with splenomegaly (see Chap. 1.9.4), the spleen can be identified as a round or oval structure with a medium degree of echogenicity. However, differentiation between inflammatory and neoplastic changes is often difficult to determine.

Indications

- ☐ rare: enlargement of the spleen in radiographic studies, especially for the differentiation between neoplasia and inflammation.

1.2.7.6 Gastrointestinal tract and pancreas

The gastrointestinal tract should be as empty as possible for the examination or, under ideal conditions, contain fluid. Neither food (i.e. such as solid particles or bone [in carnivorous species]) nor gas can be penetrated by sound waves due to interference from acoustic reflection and absorption. While imaging of the crop and esophagus in the majority of avian patients is not possible due to the lack of an adequate coupling site (see Chap. 1.2.4), the ventriculus can be easily visualized from the median and lateral coupling sites, especially in granivorous species due to its grit content. Grit in the ventriculus is often observed as hyperechoic particles with a distal shadow. The grit particles are mainly surrounded by an hypoechoic region which is dependent on the amount of food present. The muscle layer is depicted as a round to oval, hypoechoic zone. An acoustic shadow can be seen behind the ventriculus due to the total reflection of the sound waves (see **Fig. 1-60**). With transducer frequencies of above 12 MHz, the koilin layer of the ventriculus can be depicted and assessed.

The cranially situated proventriculus can be initially identified by locating the ventriculus then cranially angling the transducer. The proventriculus is usually round in cross-section, has a medium degree of echogenicity and hyperechoic contents (food particles), some of which have distal acoustic shadows (**Figs. 1-61** and **1-62**). However, often with smaller granivores, the proventriculus can only be imaged if it is enlarged. Identification of a normal-sized proventriculus is difficult in granivorous species.

The intestines can be identified from their peristaltic movements and ingesta within the lumen. Both longitudinal and cross-sectional views of the intestinal loops may be observed (**Figs. 1-63** and **1-64**). Layers within the intestinal walls can be recognized, but the classical five layers noted in routine investigations of mammals are discernable only to a certain degree. The intestinal loops in birds with a body weight up to 1 kg can only be assessed with transducers that have a frequency of at least 10 MHz. With such transducers, the intestinal wall layers and the luminal contents can be depicted (**Fig. 1-64**). Intestinal peristalsis, as stated above, can be recognized but with lower frequencies. The duodenum is easily recognized by its U-shaped form in cross-section (**Fig. 1-63**).

A spacer is useful for the imaging of the pancreas due to its position immediately under the skin. However, even when using a spacer, attempts at visualizing this organ often remain unsuccessful. The pancreas is observed as a hyperechoic structure lying between the loops of the duodenum (**Fig. 1-63**). This organ contains a blood vessel through the center of its structure.

The cloaca can be imaged using the ventrocaudal coupling site by caudally tipping the transducer. Depending on the consistency of the feces, the contents of the cloaca can have differing degrees of echogenicity. The wall of the cloaca can be observed by the retrograde administration of fluid after the organ has been cleared of fecal material by flushing with a warmed saline solution. The cloaca has a narrow, hypoechoic oval form with a regular edge (see **Fig. 1-65**).

Indications

- ☐ assessment of intestinal peristalsis
- ☐ assessment of the intestinal loops in an abdominal hernia or a diverticulum
- ☐ suspicion of tumors in the intestinal wall (contrast necessary)
- ☐ suspicion of a radiolucent foreign body

1.2.7.7 Urinary tract

Kidneys of normal size and shape are not visible with a transcutaneous coupling site because of intestinal interference when using a ventral coupling site and the air sacs prevent a lateral projection due to a total reflection of the sound waves. When enlarged, however, the kidneys can be clearly identified when performing an ultrasonographic examination. When one is able to examine kidneys sonographically, both organ size and renal parenchyma can be easily assessed without difficulty in both large and small birds (e.g. budgerigars) (see Chap. 1.10.1).

Indications

- ☐ clinical (see Chap. 1.1.3.7), blood biochemical and radiographic indications of renal disease such as enlargement (rare: changes in form) of the renal silhouette in the radiographic investigation; especially differentiation between neoplasia, inflammation and cysts by assessing the renal parenchyma.

Fig. 1-60: Ultrasonographic images of an African grey parrot's (*Psittacus erithacus*) ventriculus using the ventromedian coupling site.

A: 10 MHz, PD 3 cm.

B: 12 MHz, PD 4 cm.

The ventriculus is characterized by a slightly hyperechoic muscle layer (1) and strongly hyperechoic contents (2). Higher frequencies enable the imaging and assessment of the koilin layer (3). The contents of the ventriculus cause an acoustic shadow (4) due to sound extinction.

1: ventriculus: muscle layer
2: ventriculus: contents
3: ventriculus: koilin layer
4: acoustic shadow

Fig. 1-61: Ultrasonographic images of a sulphur-crested cockatoo's (*Cacatua galerita*) proventriculus using the ventromedian coupling site, 10 MHz, PD 3 cm. The contents of the proventriculus (1) can be either fluid or solid, therefore the echogenicity within this organ is variable. The proventricular wall (2) is usually very thin and often not identified; consequently, the identification of the proventriculus is very difficult in most avian patients.

1: proventriculus: contents
2: proventriculus: wall

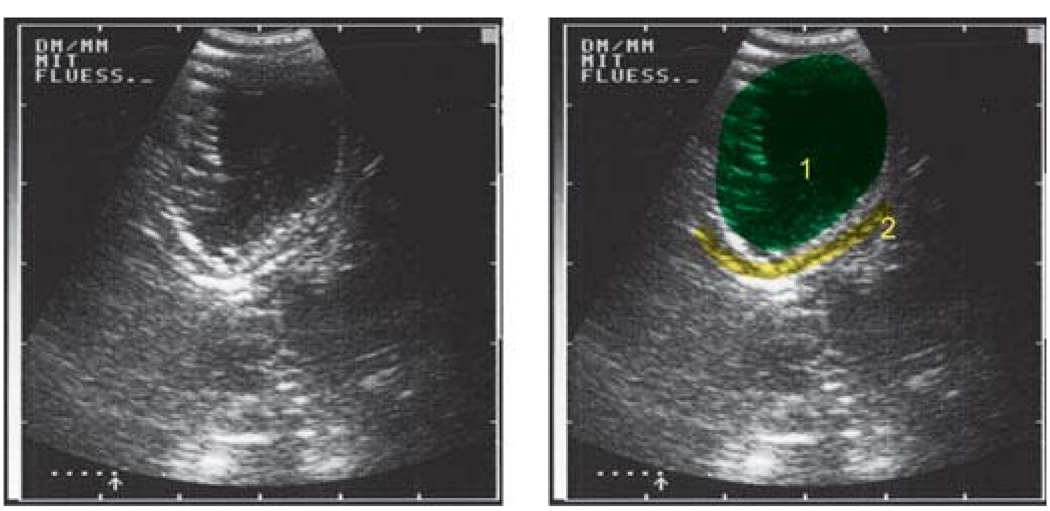

Fig. 1-62: Ultrasonographic images of a common buzzard (*Buteo buteo*) using a ventromedian coupling site, 7.5 MHz, PD 6 cm, 10 minutes after the administration of 20 ml/kg water into the crop. Proventriculus and ventriculus.

1: proventriculus/ventriculus: contents
2: proventriculus/ventriculus: wall

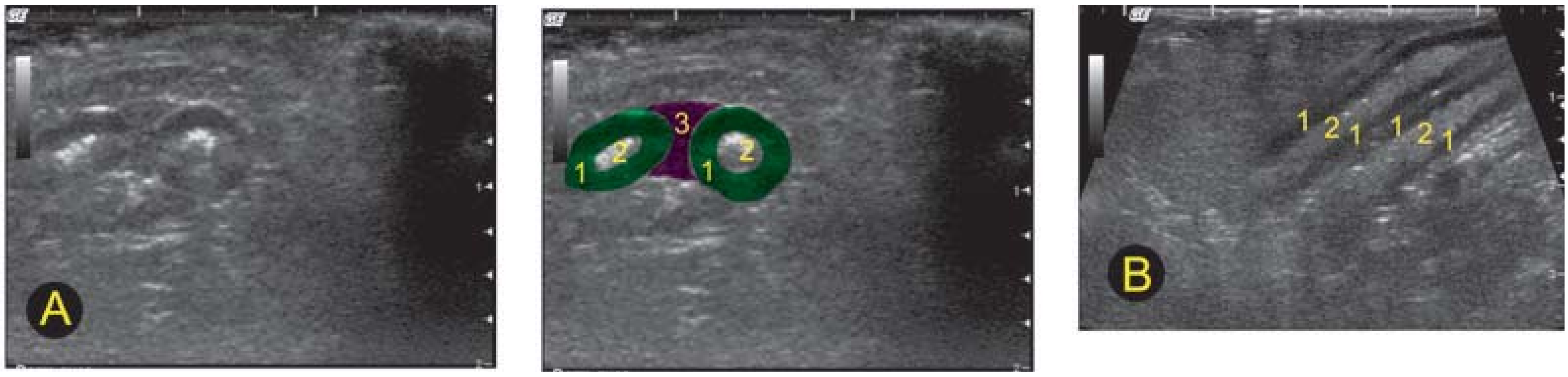

Fig. 1-63: Ultrasonographic images of the duodenum using a ventromedian coupling site.

A: 12 MHz, PD 4 cm, dove (*Columba livia* f. *domestica*): Both the duodenal flexure with its contents (1) and wall (2) as well as the pancreas (3) lying within the flexure can be observed on this image.

B: 14 MHz, PD 2 cm, channel-billed toucan (*Ramphastos vittelinus*): longitudinal image of a duodenal loop.

1: duodenum with contents
2: wall of duodenum
3: pancreas

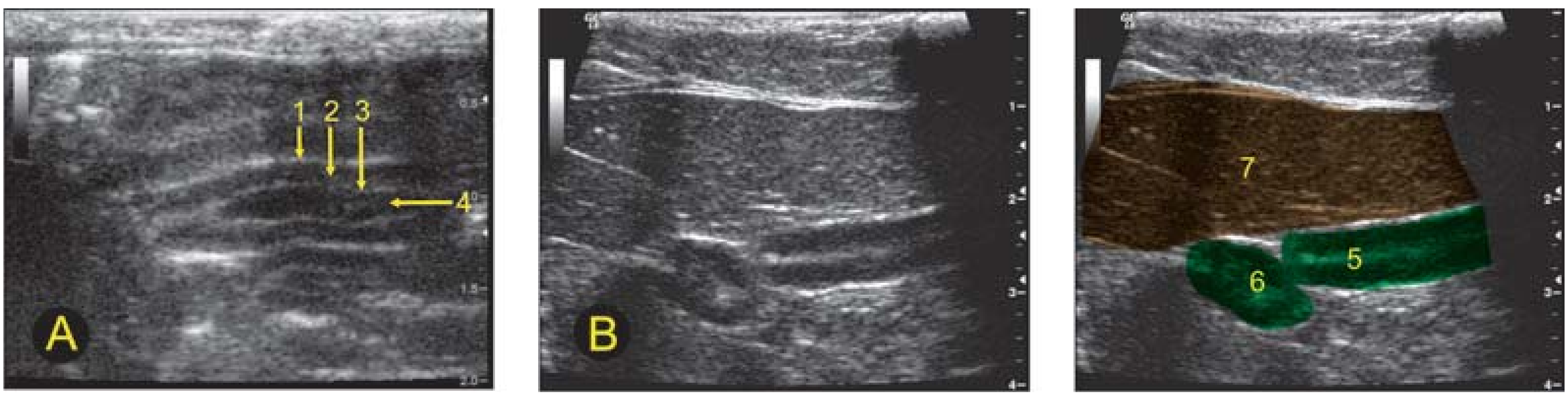

Fig. 1-64: Ultrasonographic images of the intestines using the ventromedian coupling site.

A: 12 MHz, PD 2 cm, African grey parrot (*Psittacus erithacus*): The different layers of the intestinal wall can be clearly observed in this sonogram.

B: 12 MHz, PD 4 cm, golden eagle (*Aquila chrysaetos*): Sonogram showing both longitudinal (5) and cross-sectional (6) images of intestinal loops.

1: serosa
2: muscularis
3: mucosa
4: contents
5: longitudinal section of an intestinal loops
6: of an intestinal loop in cross-section
7: fat

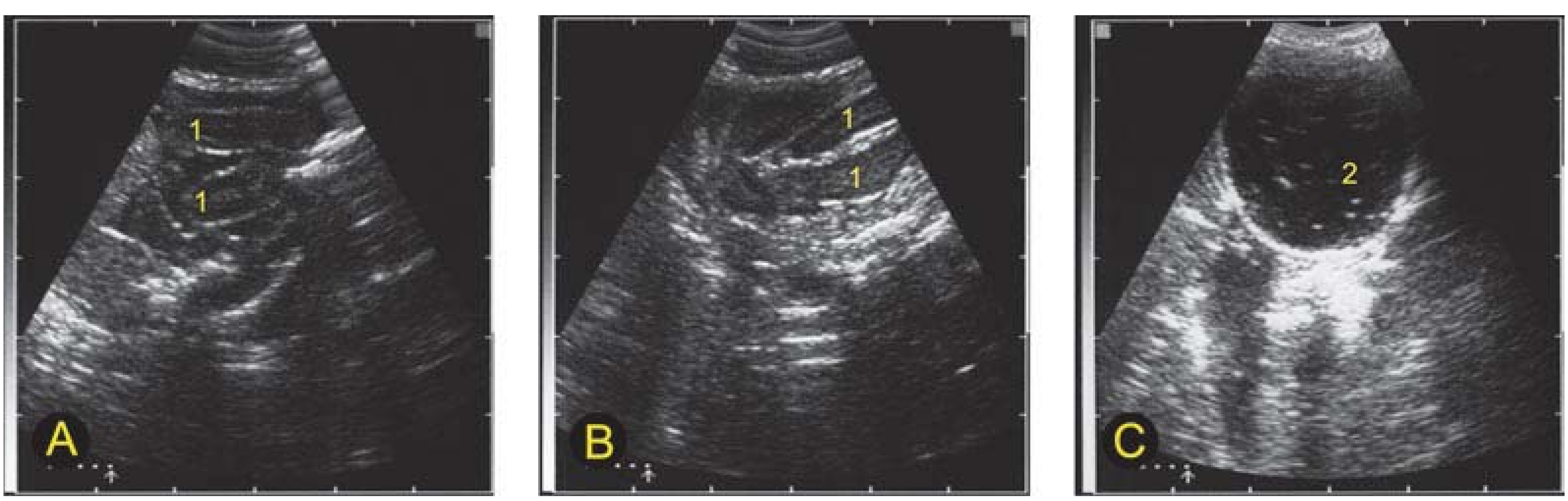

Fig. 1-65: Ultrasonographic images of a peregrine falcon (*Falco peregrinus*) using a ventromedian coupling site, 7.5 MHz, PD 4.5 cm.

A and B: Intestinal tract and cloaca.: Sonogram showing the intestinal loops (1) after the oral instillation of 20 ml/kg bwt water as contrast.

C: Sonogram of the cloaca after retrograde instillation of lukewarm water into the cloaca.

1: loops of intestines
2: cloaca

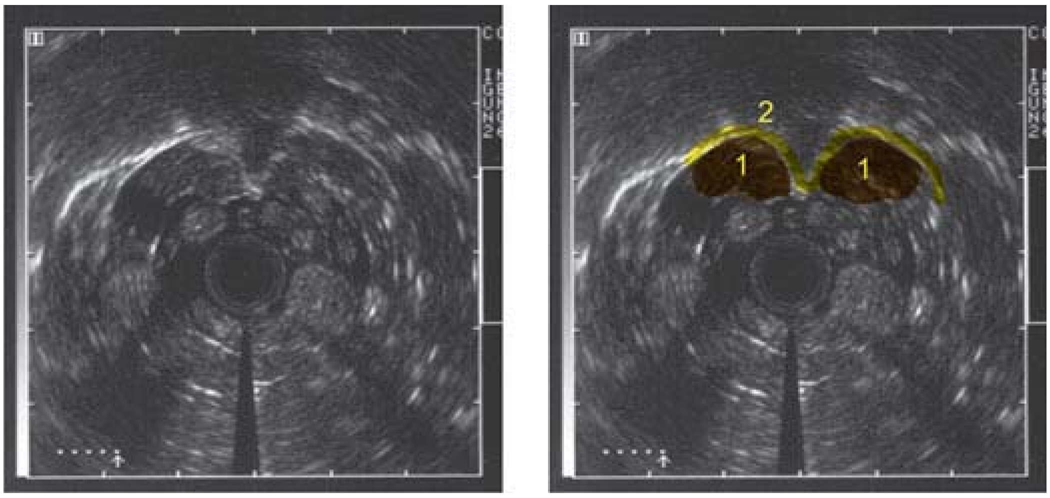

1: kidneys
2: vertebral column

Fig. 1-66: Ultrasonographic images of a barnacle goose (*Branta leucopsis*) using the intracloacal coupling site, PD 6 cm.

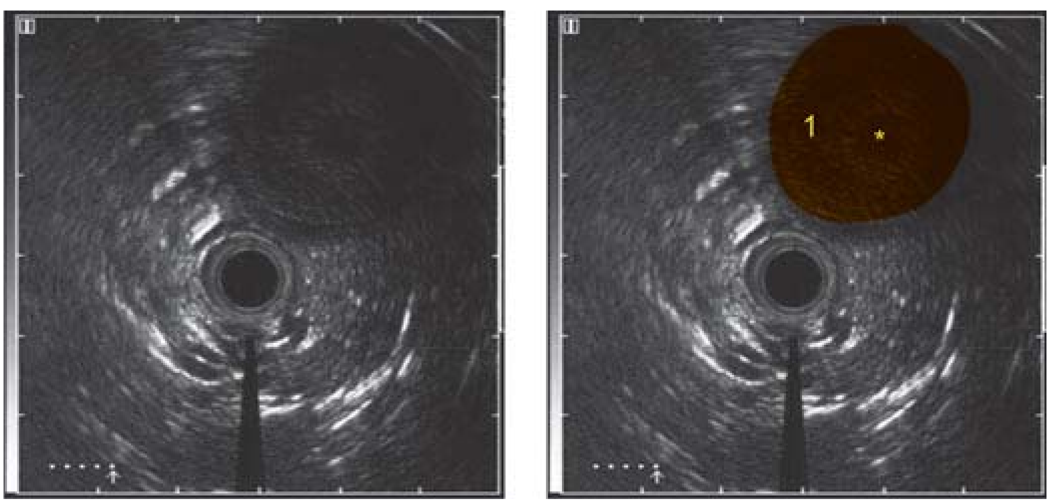

1: follicle
*: echogenic center of the follicle

Fig. 1-67: Ultrasonographic images of a red-and-green macaw (*Ara chloroptera*) using the intracloacal coupling site, 10 MHz, PD 6 cm: (1) Follicle with an echogenic area in its centre (*).

1.2.7.8 Genital tract

Due to its anatomy, the avian reproductive tract is not as difficult to image as in mammals. Currently, sex determination of avian patients can only be performed in female birds with large follicles or eggs, or in large birds, such as ratites, by using intracloacal transducers **(Fig. 1-67)**.

Inactive testicles and ovaries are not visible with transcutaneous coupling sites **(Fig. 1-47)**. The intestines cover the gonads with a ventral coupling site, while laterally the abdominal air sac prevents the identification of these organs as it causes a total reflection of the sound waves.

If the gonads are enlarged, they can often be visualized during an ultrasonographic examination. The ultrasonographic imaging of the active ovaries is possible in the majority of female birds with a body weight of more than 70 g; also in much smaller birds such as canaries **(Fig. 1-68B)**. Depending on the species, both the ventral and lateral coupling sites can be used when viewing the enlarged active gonads. The image of the active ovaries is characterized by the presence of follicles with differing sizes, which represent different stages of development. Developing follicles initially appear as round areas with an echo-free or hypoechoic internal structure **(Fig. 1-68)**. At an advanced stage of follicle development, the hyperechoic yolk can be visualized.

Distally, in the magnum section of the oviduct, the egg is observed with a clear division between the hyperechoic yolk and the surrounding hypoechoic vitreous **(Fig. 1-69A)**. The mineralized shell, which is formed later in the uterus, can be easily differentiated due to its high degree of echogenicity. The yolk is either slightly or no longer visible, due to the absorption or reflection of the sound waves by the shell **(Fig. 1-69B)**.

The normal oviduct is not clearly evident during a ultrasonographic examination. Depending on the functional status of the oviduct, it is difficult to differentiate the female reproductive tract from other abdominal structures (intestines). The active oviduct can be identified due to the presence of eggs and the lack of contractions (in comparison to the intestines).

The ultrasonographic imaging of the testicle is only successful in reproductively active birds. The testicular parenchyma has a finely grained structure with a medicum degree of echogenicity.

Indications

- ☐ often: clinical (see Chap. 1.1.3.8), anamnesic and radiographic indications of disease in the genital tract, with soft-tissue swelling in the abdomen in the radiographic investigation, with or without formation of medullary bone; especially differentiation between neoplasia, cysts and egg binding due to laminated or wind eggs
- ☐ suspicion of salpingitis

1.2.7.9 Eye

The use of ultrasonography on the avian eye is useful in the diagnosis of ocular changes, especially when the interior of the eye cannot be visualized through other means (e.g. when the lens is cloudy). A-mode ultrasonography is mainly used for the biometry of the globe, while 2D B-mode ultrasonography provides more information about the individual ocular structures and pathological changes within the eyes.

After the topical application of a local anesthetic agent on the eye, the transducer can be placed directly on the cornea. Ultrasonographic gels are only necessary when the transducer is placed on the closed eyelid. The anterior chamber of the eye and the vitreous body are normally free of echogenic structures **(Fig. 1-70)**. For more detailed information about the ultrasonographic investigation of the avian eye see the relevant literature (e.g. GUMPENBERGER and KORBEL 2001).

Further reading

BOSKOVIC, M., KRAUTWALD-JUNGHANNS, M.-E., FAILING, K. (1999): Möglichkeiten und Grenzen echokardiographischer Untersuchungen bei Tag- und Nachtgreifvögeln (Accipitriformes, Falconiformes, Strigiformes). Tieraerztliche Praxis **27**: 334–341.

CARRANI, F., GELLI, D., SALVADORI, M. (2003): A preliminary echocardiographic initial approach to diastolic and systolic function in medium and large parrots. European Association of Avian Veterinarians, Proc., 145–149.

GUMPENBERGER, M., KORBEL, R. T. (2001): Comparative aspects of diagnostic imaging in avian ophthalmology using sonography and computed tomography. European Association of Avian Veterinarians, Proc., 99–102.

PEES, M., STRAUB, J., KRAUTWALD-JUNGHANNS, M.-E. (2004): Echocardiographic examinations of 60 African grey parrots and 30 other psittacine birds. Veterinary Record **155**: 73–76.

PEES, M., STRAUB, J., SCHUMACHER, J., GOMPF, R., KRAUTWALD-JUNGHANNS, M.-E. (2005): Pilotstudie zu echokardiographischen Untersuchungen mittels Farb- und pulsed-wave-Spektraldoppler an Blaukronenamazonen (*Amazona ventralis*) und Blaustirnamazonen (*Amazona a. aestiva*). Deutsche Tierärztliche Wochenschrift **112**: 39–43.

SCHULZ, M. (1995): Morphologische und funktionelle Messungen am Herzen von Brieftauben (*Columba livia* forma *domestica*) mit Hilfe der Schnittbildechokardiographie. Vet. Med. Dissertation.

STRAUB, J., PEES, M., SCHUMACHER, J., KRAUTWALD-JUNGHANNS, M.-E. (2001): Doppler-echocardiography in birds. European Association of Avian Veterinarians, Proc., 92–94.

Fig. 1-68: Ultrasonographic images of the ovary using a ventromedian coupling site.

A: 12 MHz, PD 4 cm, African grey parrot (*Psittacus erithacus*): Follicles (1) on an active ovary.

B: 10 MHz, PD 3 cm, canary (*Serinus canaria*): Individual follicle (arrows).

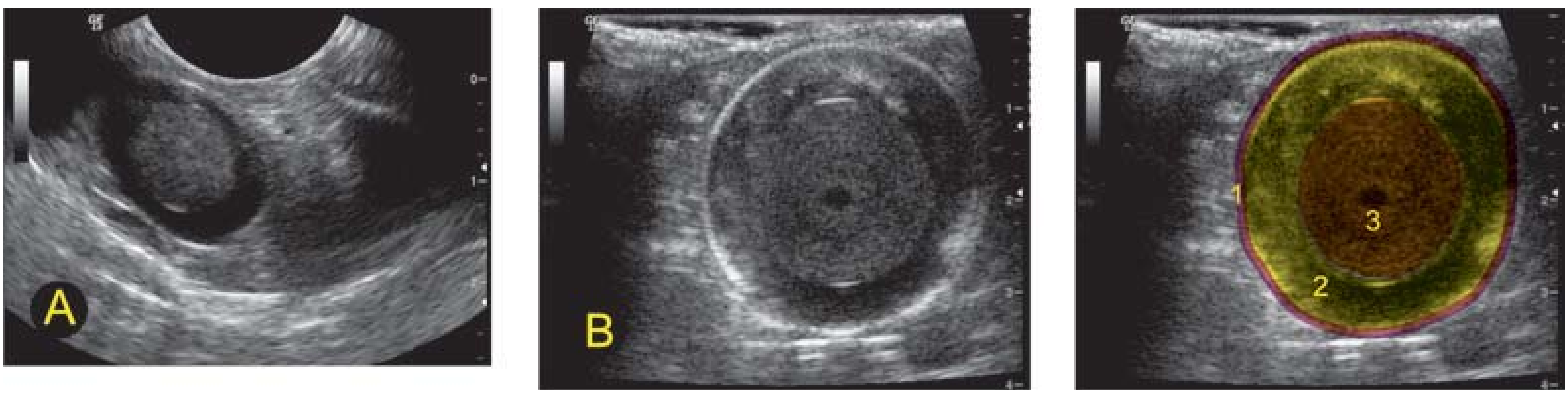

Fig. 1-69: Ultrasonographic images of the oviduct using a ventromedian coupling site.

A: 10 MHz, PD 3 cm, budgerigar (*Melopsittacus undulatus*): Longitudinal section of an egg which has not yet received its calcified shell.

B: 7 MHz, PD 4 cm, African grey parrot (*Psittacus erithacus*): Egg with calcified shell. A low transducer frequency was chosen so that the contents of the egg could be imaged through the calcified shell.

1: shell
2: albumen
3: yolk

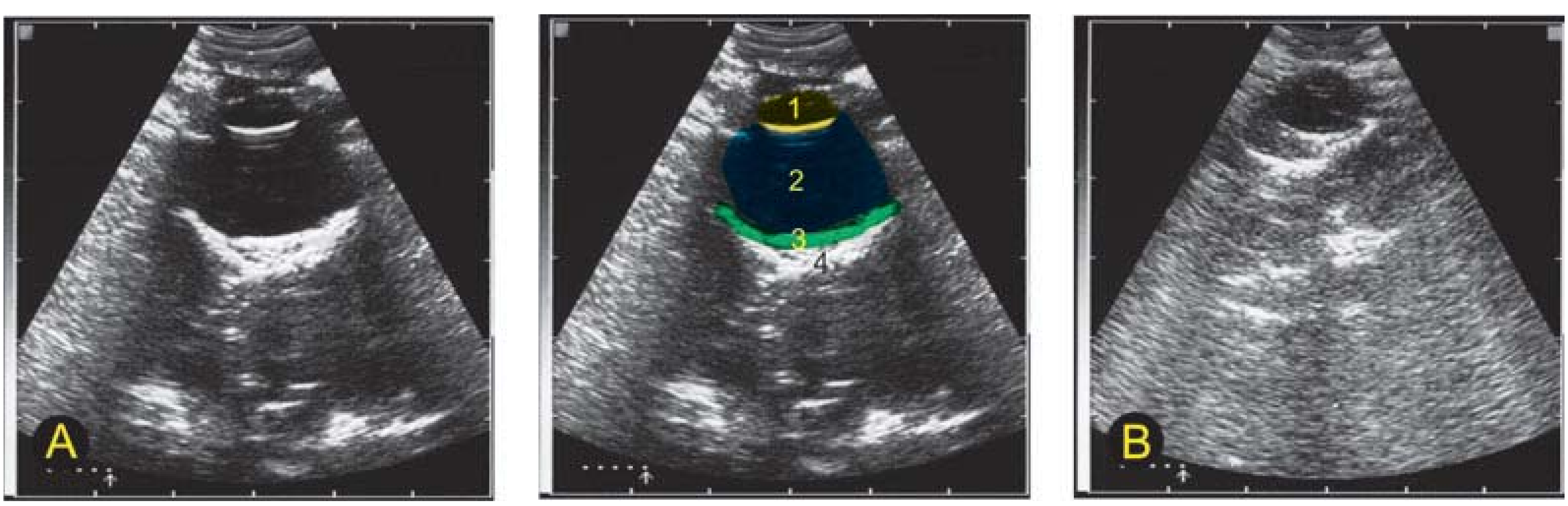

Fig. 1-70: Transcorneal ultrasonographic images of the eye.

A: 7.5 MHz, PD 6 cm, common buzzard (*Buteo buteo*): Ultrasonographic examination of the eye showing the lens (1), vitreous body (2), ocular fundus (3) and orbit (4) with distal sound reinforcement.

B: 7.5 MHz, PD 6 cm, Timneh African grey parrot (*Psittacus erithacus timneh*): Eye with lens and vitreous body.

1: lens
2: vitreous body
3: ocular fundus
4: orbit

1.3 Computed tomography (CT)

Maria-Elisabeth Krautwald-Junghanns, Michael Pees

1.3.1 Equipment

Computed tomographic examinations have a great diagnostic value in avian patients and are indicated more often than those using MRI. An important advantage with respect to the CT examination's effects on the avian patient is the very short investigation time of 1 or 2 minutes needed with today's modern scanners. In comparison to humans, dogs, and cats, birds can also be placed transverse to the gantry opening due to their usually short body length; therefore, avian patients can be examined in longitudinal slices **(Fig. 1-71A)**. This reduces the number of scans which have to be made during a CT examination (body width is shorter than body length). However, with older CT scanners, the identification of internal organs is easier as the very informative sagittal scan does not need to be reconstructed which would leading to a loss in quality. The higher radiation dose associated with CT in comparison to a conventional radiographic investigation does not have any significance in birds due to the small size of the patients and the relative insensitivity of the class Aves to x-rays.

One great advantage of CT in comparison to radiodiagnostics is the imaging of the avian patient's anatomy in individual scanning planes without superimposition of other anatomical structures. As birds are small in size, relatively thin slices should be used for the CT examination. Depending on the goal of the study, slices with a thickness of 0.6–1 mm are preferable for parrots.

1.3.2 Preparation, positioning and planes

Special preparation of the avian patient is usually not necessary; however, it is recommended that the bird should be fasted (food and water) immediately prior to the examination. As the time needed to do the CT exam is very short, general anesthesia is not always required. The decision regarding the use of general anesthesia should depend on the goal of the study and sensitivity of the patient to stress.

Birds can be fixed on a Plexiglas® avian restraint board as described for conventional radiography **(Fig. 1-71A)**. Such boards should not contain any metallic components (e.g. screws) to prevent artifacts from interfering with the interpretation of the images. To minimize movement artifacts, it may be necessary in individual cases to quieten the patient by placing a light cloth over its head or by giving it a sedative. Birds under general anesthesia can be positioned without an avian restraint board **(Fig. 1-71B)**.

Placing the patient in dorsal recumbency is preferable and symmetrical positioning is a prerequisite for a reliable interpretation of the CT images. Depending on the goal of the study or in birds with cardiovascular insufficiency, a tilted position can be used **(Fig. 1-71B)** or the bird is placed in ventral recumbency while making sure there is no interference with the mechanical ability of the patient to breathe. The bird is usually placed across the gantry mouth (sagittal scanning, **Fig. 1-71A**) or longitudinally to the machine as in humans (transverse scanning, **Fig. 1-71B**). The advantage of sagittal scanning enables one to examine the whole body thereby achieving a better degree of orientation of the anatomical structures, as observed in the lateral projection in radiography. In comparison to transverse scanning, as described earlier, relatively fewer sections are needed to complete the examination, thereby reducing the rework time in the computer for the investigator.

1.3.3 Assessment of the organs

After the CT examination, reliable – usually corresponding to the anatomical conditions – reconstructions of the patient's organs and structures in different planes, measurements in the computer **(Figs. 1-73** and **1-81)** and also 3D models **(Fig. 1-72)** can be produced and assessed. By determining the radiodensity of the anatomical structures imaged, more valuable information about the type and extent of the pathological processes can be attained. The radiodensity (Hounsfield units, HU) of the bones, fat, and parenchymatous organs is generally the same as that for humans. However, the tissue windows, as well as the W and L values for the optimal imaging of individual organs must be defined for each species.

The limits to imaging structures are, as in mammals, dependent on the spatial resolution of the CT scanners, differences in density between the object of interest, surrounding structures, and size of the object. This is especially true of the air sac walls, which due to their thinness cannot be observed over the whole of their surface **(Figs. 1-79** and **1-80)**. However, most of the larger internal organs can be imaged and assessed in their entirety. Other diagnostic options provided by CT imaging are the use of virtual endoscopy and contrast studies for imaging the vascular system or cavernous structures **(Figs. 1-84** and **1-85)**.

The main indications for performing a CT examination on an avian patient are currently; abnormalities in the skeletal system (cranium, spine) and respiratory tract (sinus, lung); *q.v.* Chaps. 1.5 and 1.7, respectively).

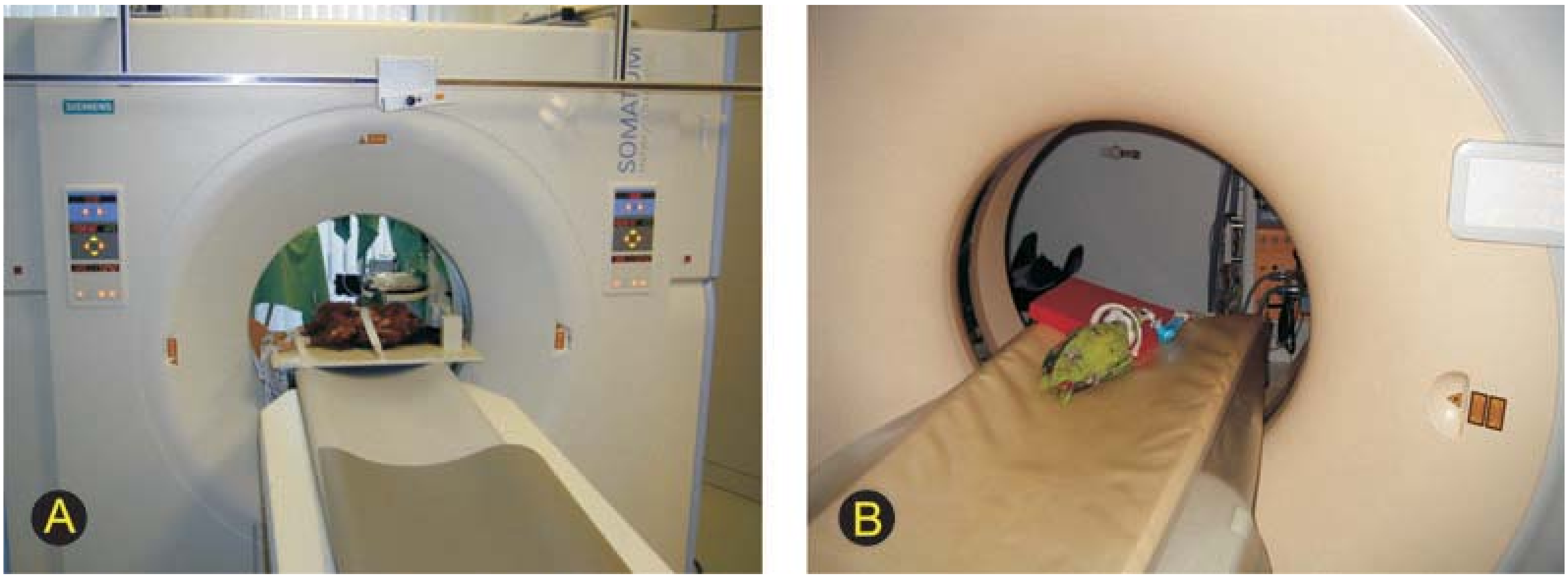

Fig. 1-71:

A: Positioning of a chicken (*Gallus gallus*) on a plexiglas® avian restraint board for a sagittal CT scan. This scanning plane is very useful in birds. It can also be produced from transverse scanning data using reformation.

B: Positioning of a blue-fronted Amazon parrot (*Amazona aestiva*) for a transverse CT scan under isoflurane general anesthesia. The positioning can be selected according to need; however, freedom of movement of the sternum should always be ensured to prevent respiratory comprise in the patient.

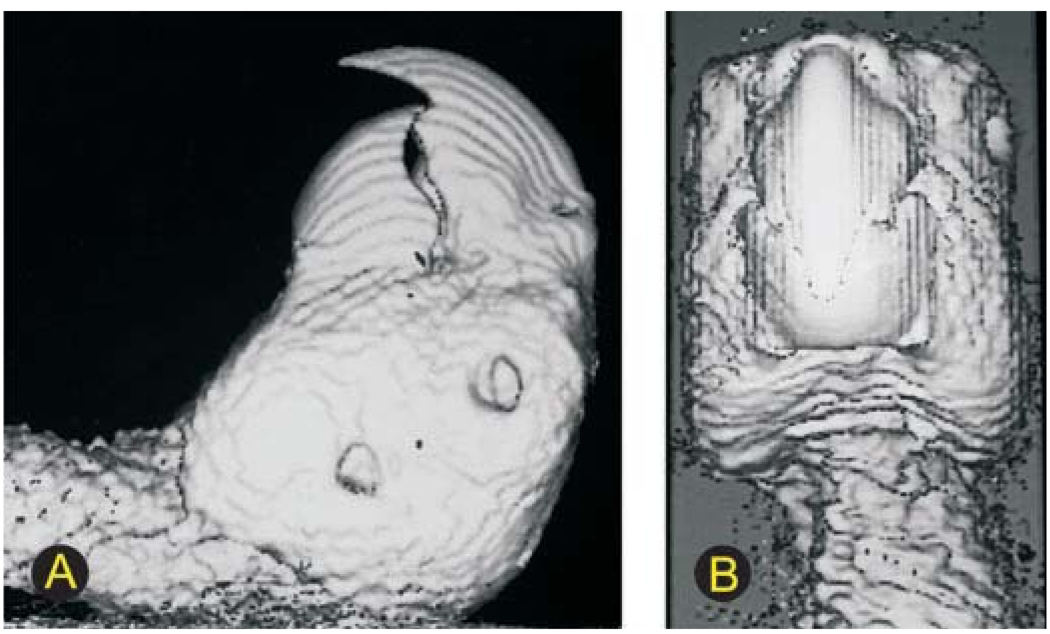

Fig. 1-72: Three-dimensional (3D) reconstruction of CT head images of a blue-fronted Amazon (*Amazona aestiva*), (120 kV, 165 mA).

1.3.3.1 Skeletal system

Computed tomography is a valuable aid for the investigation of the skeletal system. Conventional radiography is adequate when used as the only imaging modality to examine the majority of routine cases that affect the skeletal structure (e.g. fractures); however, other disease presentations, especially of the surrounding soft tissues, often cannot be imaged with any degree of certainty using traditional radiography. For this purpose, CT is gaining a much greater degree of importance as image assessment can be performed using a number of planes and 3D reconstruction **(Figs. 1-72** and **1-85)**.

The main indications for a CT examination of skeletal structures are disease presentations involving the areas of the head **(Figs. 1-73** and **1-74)** and spine **(Figs. 1-75, 1-76** and **1-78)**. In these areas, disease conditions can only be identified with great difficulty using conventional radiographic techniques due to significant superimpositions of the surrounding structures. When using CT, not only the extent of such changes can be visualized but also density measurements which delineate the type of change are possible. In addition, with the so-called highlighting method (the measurement of air-filled spaces after the previous determination of the region of interest or ROI), the volume of the aerated spaces in the cranium can be determined **(Fig. 1-73)**. In Amazons and African grey parrots, this value is 5–6% of the total cranial volume (KRAUTWALD-JUNGHANNS et al. 1998).

The measurement of the air-filled spaces in the cranium is useful in follow-up examinations to evaluate the treatment success in a patient suffering from upper respiratory disease. In such cases, conventional as well as reconstructive radiological methods can be combined with the use of contrast (e.g. to assess the flow of contrast through the nose and infraorbital sinus).

Avian bone can be judged, as in mammals, with respect to its radiodensity and the thickness of the cortex (STREUBEL et al. 2005). Bird joints are anatomically much simpler than in mammals. The bones' congruence and the presence of tumors are the main features evaluated in CT images, whereby the effectiveness of interpreting the image is directly correlated to the size of the bird being examined. Luxations and bony changes (e.g. infections, lysis) can be visualized and assessed with respect to the degree of change in the skeletal structures imaged. When the spine needs to be examined **(Figs. 1-75, 1-76** and **1-78)**, vertebral fissures or fractures, luxations of the vertebral body, and narrowing of the vertebral canal can be imaged using CT.

Indications

- ☐ clinical and radiographic indications of a spinal fracture or other changes in this region
- ☐ ambiguous increases in size in the musculoskeletal system
- ☐ suspicion of fractures in the cranium, especially of the hyoid bone and beak apparatus
- ☐ vague soft-tissue anomalies in the head; especially for the assessment of the extent of an upper respiratory infection or of the effects of treatment in a bird diagnosed with an upper respiratory infection.

1.3.3.2 Respiratory tract

Computed tomography is currently the most reliable and sensitive method for the diagnosis of lung disease in birds. In addition to the imaging of abnormalities affecting lung parenchyma, the large pulmonary blood vessels and the primary and secondary bronchi in the individual scanning planes **(Figs. 1-76, 1-77, 1-79** and **1-80)**, measurements of the lung field **(Fig. 1-81)** and subsequent determination of the lung density enable the diagnosis of problematic lung conditions in the early stages of a disease process. Furthermore, follow-up investigations using CT provide a quick and reliable method for a patient under treatment that does not excessively stress the animal (KRAUTWALD-JUNGHANNS 1997).

The lungs appear as homogenous »honey-comb-like« radiopaque structures, each of which has a central blood vessel and a number of craniocaudal secondary bronchi **(Figs. 1-76, 1-77, 1-79, 1-80** and **1-82)**. The normal lung density values show – in comparison to humans with a mean density of between –300 HU and –800 HU – only a slight degree of variation and lie, for example, in Amazon and African grey parrots between –600 HU and –650 HU (total lung density). The total lung density value is not enough information for one to determine a diagnosis of »healthy lungs«. Therefore other criteria, such as the depiction of unchanged lung tissue, main bronchi, and pulmonary blood vessels in all scanning planes, as well as the density of individual or suspicious areas of lung must also be included when assessing the health of the lungs (KRAUTWALD-JUNGHANNS 1997).

In comparison to mammals, the determination of the lung volume **(Fig. 1-81A)** has no diagnostic relevance as there is little change due to the physiological differences of the avian lung. As a consequence, the determination of the expiratory and inspiratory phases does not have any significance in the bird.

The extent of the avian air sac system provides less diagnostic information than the lungs from a CT examination due to the problems described above (resolution dependent on the difference in density between the object, surrounding structures, and the size of the object of interest). A complete image of the individual air sac wall is not possible with either sagittal or transverse scanning. The more cranial air sacs in the craniocervical region have little diagnostic value as they do not play a significant role in gaseous exchange. The more important air sacs lie within the body cavity (e.g. thoracic and, abdominal air sacs) and appear as thin radiopaque lines when the boundary of the air sac is scanned obliquely **(Figs. 1-79** and **1-80)** and do not lie against organs or other structures with a similar density (especially in the gastrointestinal tract region). The imaging limits for the air sacs are also dependent on the spatial resolution of the scanner.

Using highlighting (see above) a rough determination of the total volume of all the air sacs in the body cavity can be achieved **(Fig. 1-81)**. The results of air sac volume interpretation should be interpreted carefully due to the varying degrees of physiological variation between patients and species (e.g. egg formation).

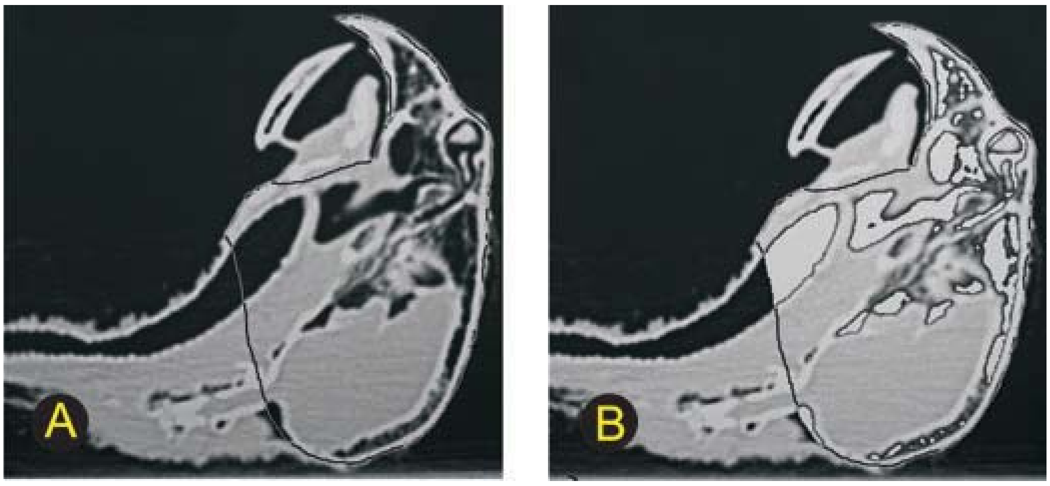

Fig. 1-73: CT images of an orange-winged Amazon parrot's (*Amazona amazonica*) head in a sagittal plane (120 kV, 165 mA, 1 mm SD, W: 2000, L: –800).

A: Scan showing the structures in the cranium and upper respiratory tract. By tracing the outline of the cranium, the surface area can be measured and with the assessment of each slice the total volume of the region of interest (ROI) can be determined. The measurement of the volume of the cranium is important as a reference parameter for determining the proportion of air-containing regions (see B).

B: In a subsequent step, the volume of all air-containing structures (as the density of air is known) in the ROI, measured as in A, can be determined by using highlighting. This may be used in follow-up investigations or for determining the prognosis of chronic sinusitis cases. The volume of all air-containing structures in Amazon and African grey parrots is approximately 5–6% of the cranial volume.

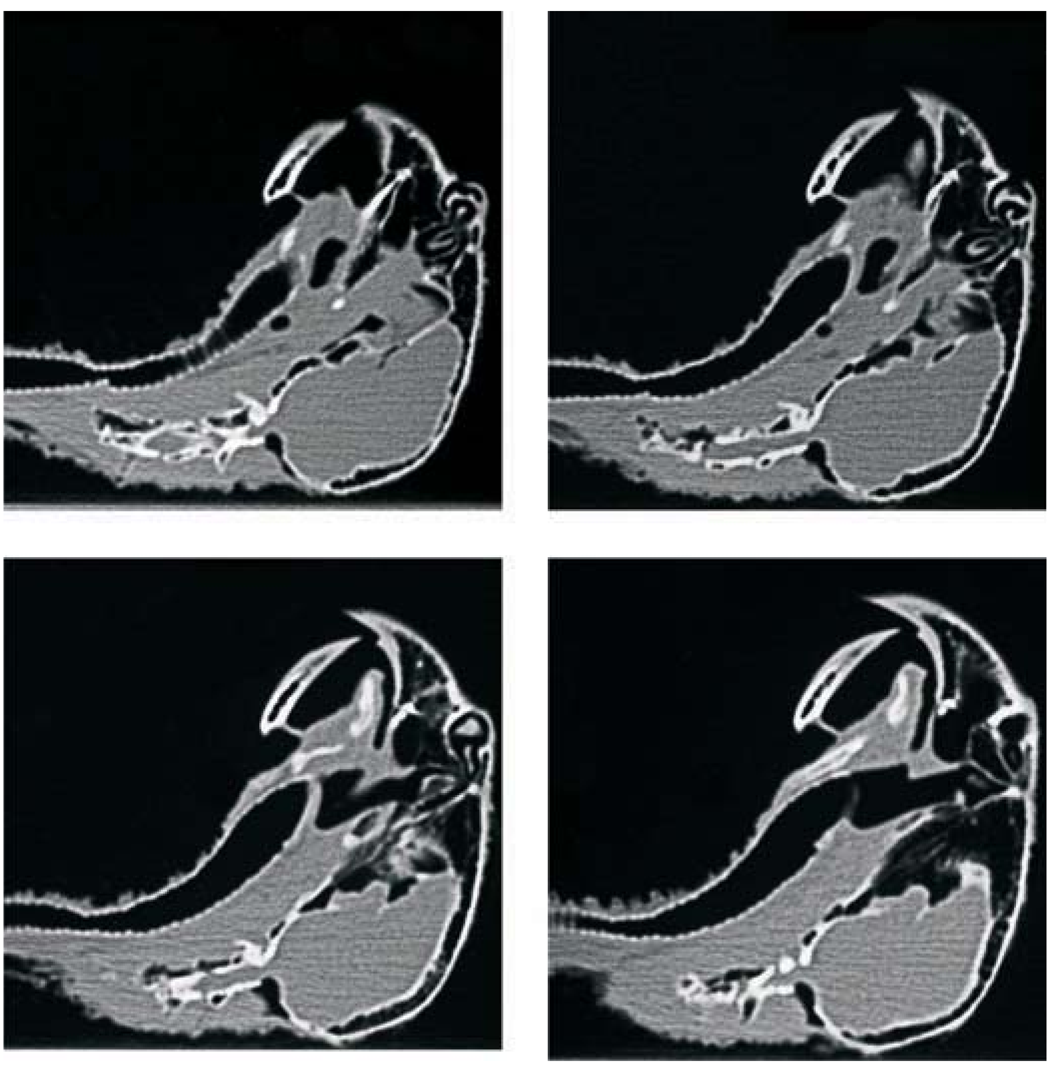

Fig. 1-74: CT: Different sagittal slices (120 kV, 165 mA, 2 mm SD, W: 2000, L: –800) of CT images taken of a blue-fronted Amazon parrot's (*Amazona aestiva*): head. The scan shows the structures in the cranium and the upper respiratory tract. The nasal conchae and part of the infraorbital sinus (black air-filled regions) can be observed lying behind the air-filled upper beak.

Computed tomography is often not necessary for imaging the trachea and syrinx. However, since both structures are present in the individual CT scanning planes **(Fig. 1-78)**, they should be always assessed so that any possible subclinical abnormalities may be identified. A respiratory-related dilatation of the trachea is not possible in the bird due to the bony tracheal rings, and so measurements in this area are not pertinent.

Horizontal and oblique septae can be observed in individual slices of the lungs; in older birds, it is normal to find calcification (increased radiodensity).

Indications

- all clinical and radiographic indications of changes in the lungs, prognosis, diagnosis of early stages of diseases with unclear or negative radiographic results

1.3.3.3 Other organs

Specific indications for CT imaging of the **gastrointestinal tract** are rare; however, this structure can be well assessed throughout its course using this diagnostic modality **(Figs. 1-75, 1-77, 1-78, 1-82** and **1-83)**. A well-defined differentiation of the intestinal wall from the surrounding soft tissues is possible using contrast (as in radiodiagnostics, see Chap. 1.1.3.6). Placing the bird in dorsal recumbancy can cause organ position to change, in particular that of the gastrointestinal tract.

The **heart** and the blood vessels close to the heart can also be visualized with respect to their size and structure **(Figs. 1-77** and **1-78)**. As echocardiography has a much greater diagnostic value in the bird and is easier to do, indications for imaging the heart with CT tend to be rare. There is currently a lack of assessment values available for the proper evaluation of blood vessel walls with respect to arteriosclerotic changes. Angiocardiographic investigations using iodine-based contrast agents in combination with CT are also possible and provide reliable diagnostic results **(Figs. 1-84** and **1-85)**.

The **liver** can be well assessed with CT – especially in combination with contrast **(Figs. 1-77, 1-82** and **1-84)**. The radiodensity of the liver is equivalent to that in mammals. The organ should be homogenous with sharp edges. The gallbladder, if present, is situated on the left caudal surface of the liver.

In the **urogenital tract (Figs. 1-77** and **1-83)**, a (tentative) diagnosis arising from radiographic and ultrasonographic investigations can be verified. Lesions of the urogenital tract can be optimally localized or judged with respect to their size, shape, and location within or attached to the structures that comprise this system. Contrast studies are useful in combination with CT for imaging renal function **(Figs. 1-84** and **1-85)**.

Various indications regarding the need to perform a CT examination on a patient arise in individual cases as in mammalian medicine (i.e. after trauma or when there is an unclear space-occupying lesions present).

Further reading

GUMPENBERGER, M., HENNINGER, W. (2001): The use of computed tomography in avian and reptile medicine. Sem Avian Exot Pet Med **10**: 174–180.

KRAUTWALD-JUNGHANNS, M.-E.: Computertomographie des aviären Respirationstraktes. Reihe: Akademisches Forum, Blackwell Wissenschafts-Verlag, Berlin 1997.

KRAUTWALD-JUNGHANNS, M.-E., KOSTKA, V., DÖRSCH, B. (1998): Comparative studies on the diagnostic value of conventional radiography and computed tomography in evaluating the heads of psittacine and raptorial birds. J Avian Med Surg **12**: 149–157.

STREUBEL, R., BARTELS, T., KRAUTWALD-JUNGHANNS, M.-E. (2005): Computertomographische, chemische und biomechanische Untersuchungen zur Knochendichte und Knochenbruchfestigkeit von Legehennen. Archiv für Geflügelkunde **69**: 206–212.

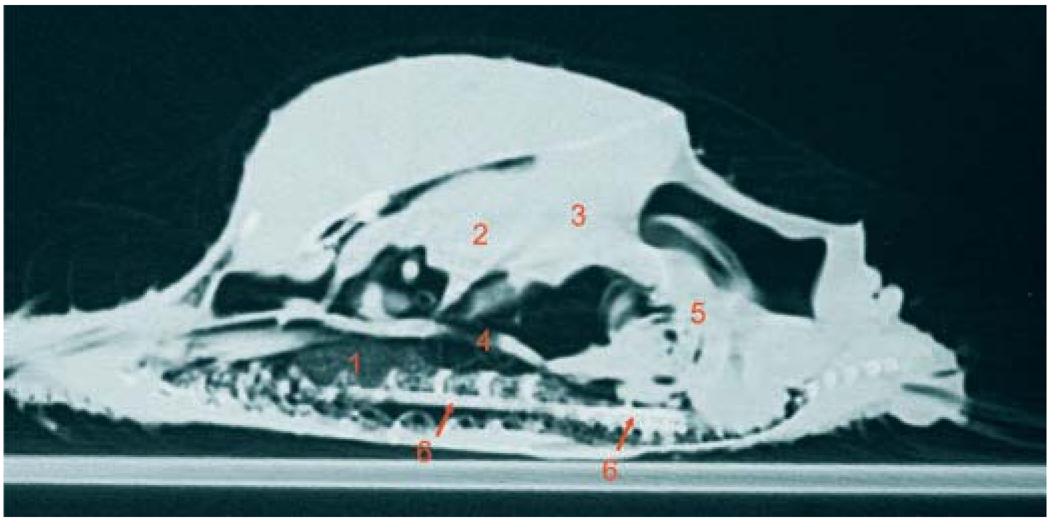

1: lung
2: heart
3: liver
4: proventriculus (only partly)
5: intestines
6: spinal cord

Fig. 1-75: CT image of an African grey parrot (*Psittacus erithacus*) showing a sagittal plane in the middle of the body (120 kV, 165 mA, 2 mm SD, W: 2802, L: –300): The spinal cord (6) is obviously thicker in the region of the synsacrum. Immediately in front of the synsacrum is a site where vertebral fractures often occur.

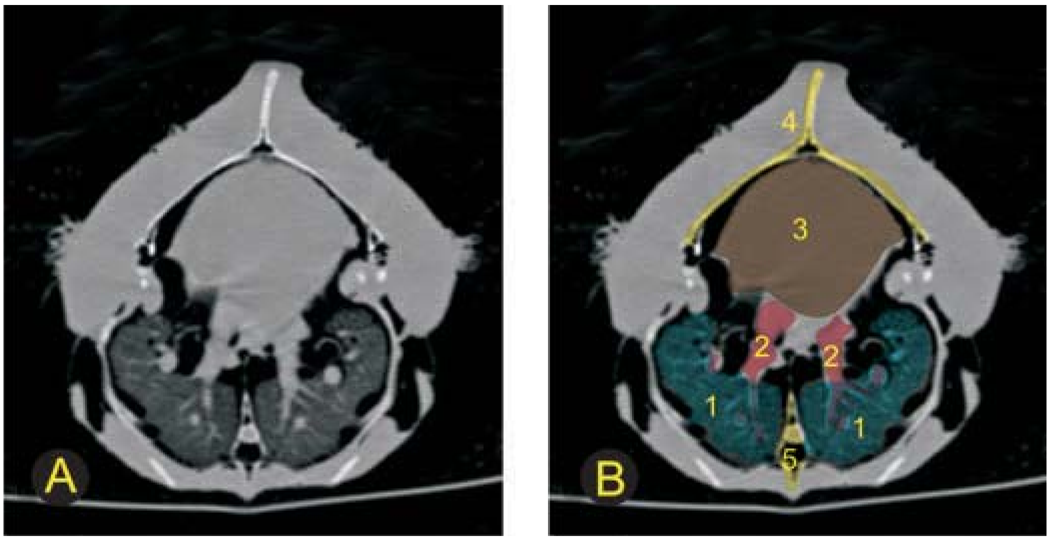

1: lungs
2: large blood vessels
3: liver
4: thoracic musculature
5: vertebral canal with spinal cord

Fig. 1-76: CT images of a gyrfalcon's (*Falco rusticolus*) body in a transverse plane (120 kV, 120 mA, 1.0 mm SD, W: 1977, L: 38): Scan showing the lungs (1) and the large blood vessels (2). The branching of the vascular tree can be assessed. The lung tissue is homogenous. There is a small rim of air between the lung and body wall.

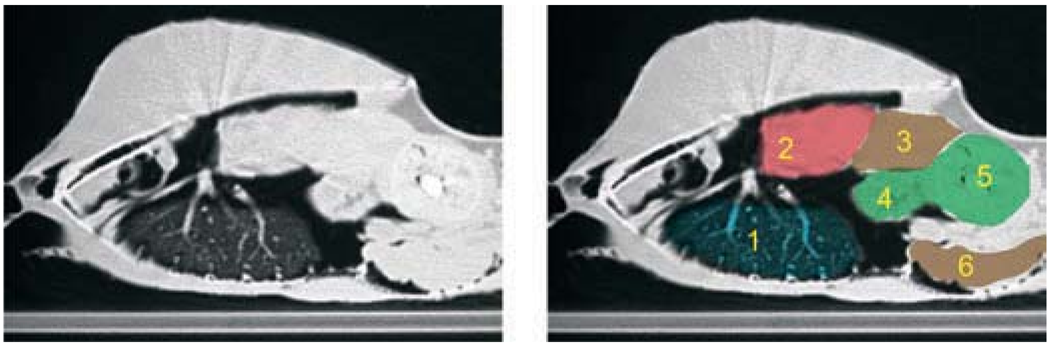

1: left lung
2: heart
3: liver
4: proventriculus
5: ventriculus
6: kidney

Fig. 1-77: CT images of a blue-fronted Amazon parrot's (*Amazona aestiva*) body in a sagittal plane (120 kV, 165 mA, 2 mm SD, W: 2000, L: –200) scanned at the level of the left lung (1) and the ventriculus (5). At this level, the lungs and the blood vessels can be evaluated longitudinally.

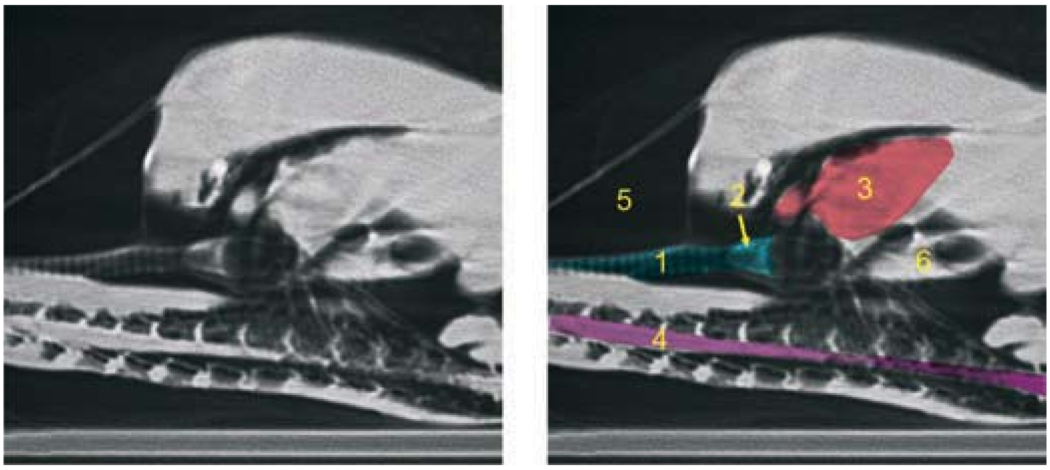

1: trachea
2: syrinx
3: heart
4: spinal cord
5: crop
6: proventriculus

Fig. 1-78: CT images of an African grey parrot's (*Psittacus erithacus*) body in a sagittal plane (120 kV, 165 mA, 2 mm SD, W: 2800, L: –200) scanned at the level of the trachea (1) and syrinx (2).

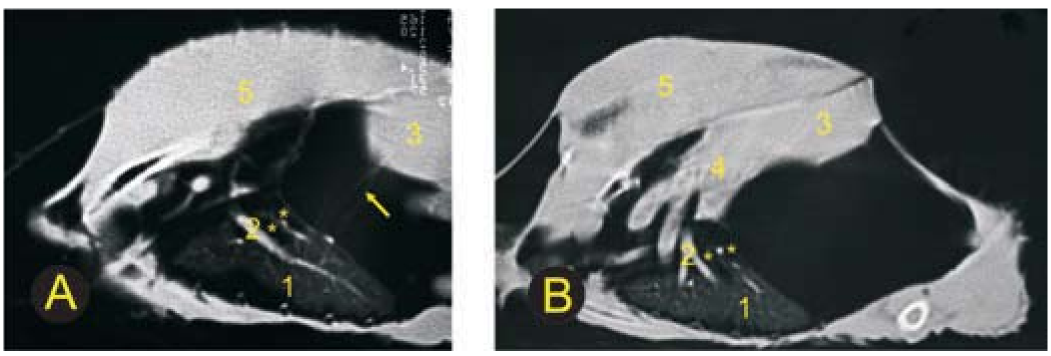

1: lungs
2: pulmonary blood vessels
3: liver
4: heart
5: thoracic musculature
*: large bronchi

arrow: wall of the thoracic air sacs

Fig. 1-79: Body CT images of a blue-fronted Amazon (*Amazona aestiva*) in a sagittal plane.

A: (120 kV, 165 mA, 2 mm SD, W: 2800, L: 80): Scan showing the lungs (1), vascular supply (2) and secondary bronchi (*). The walls of the thoracic air sacs are recognisable (arrow) (3: liver, 5: thoracic musculature).

B: (120 kV, 165 mA, 2 mm SD, W: 2800, L: 80) blue-fronted Amazon (*Amazona aestiva*): Scan showing the lungs (1) with the large bronchi (*). The heart (4) can be seen with its major blood vessels (aorta, brachiocephalic trunk).

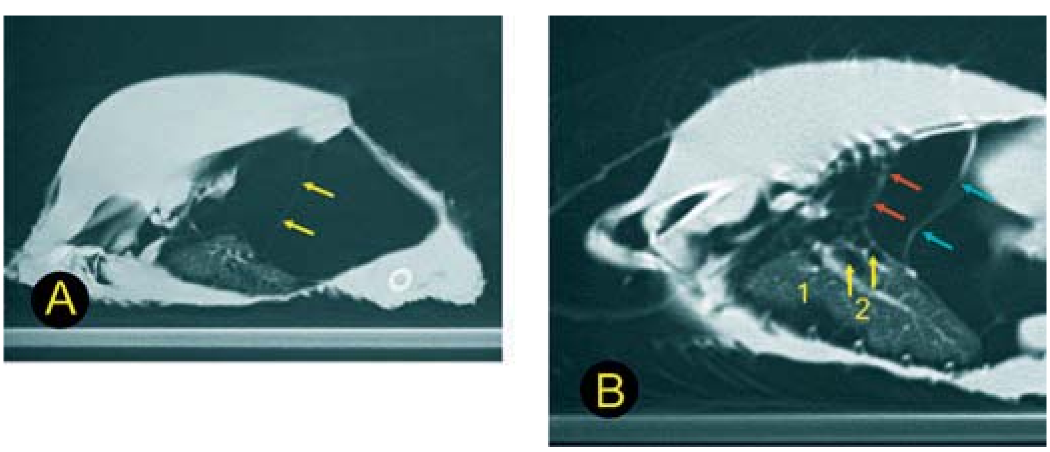

1: lungs
2: blood vessels

yellow arrows: secondary bronchi
red and blue arrows: air sac walls

Fig. 1-80: Body CT images of a blue-fronted Amazon (*Amazona aestiva*) in a sagittal plane.
A: (120 kV, 165 mA, 2 mm SD, W: 2802, L: –300): Air sac wall between the caudal thoracic air sac and abdominal air sac.
B: (120 kV, 165 mA, 2 mm SD, W: 2800, L: 80) blue-fronted Amazon (*Amazona aestiva*): Scan showing the lungs (1), nutrient arteries (2), secondary bronchi (yellow arrows) and air sac walls (red and blue arrows).

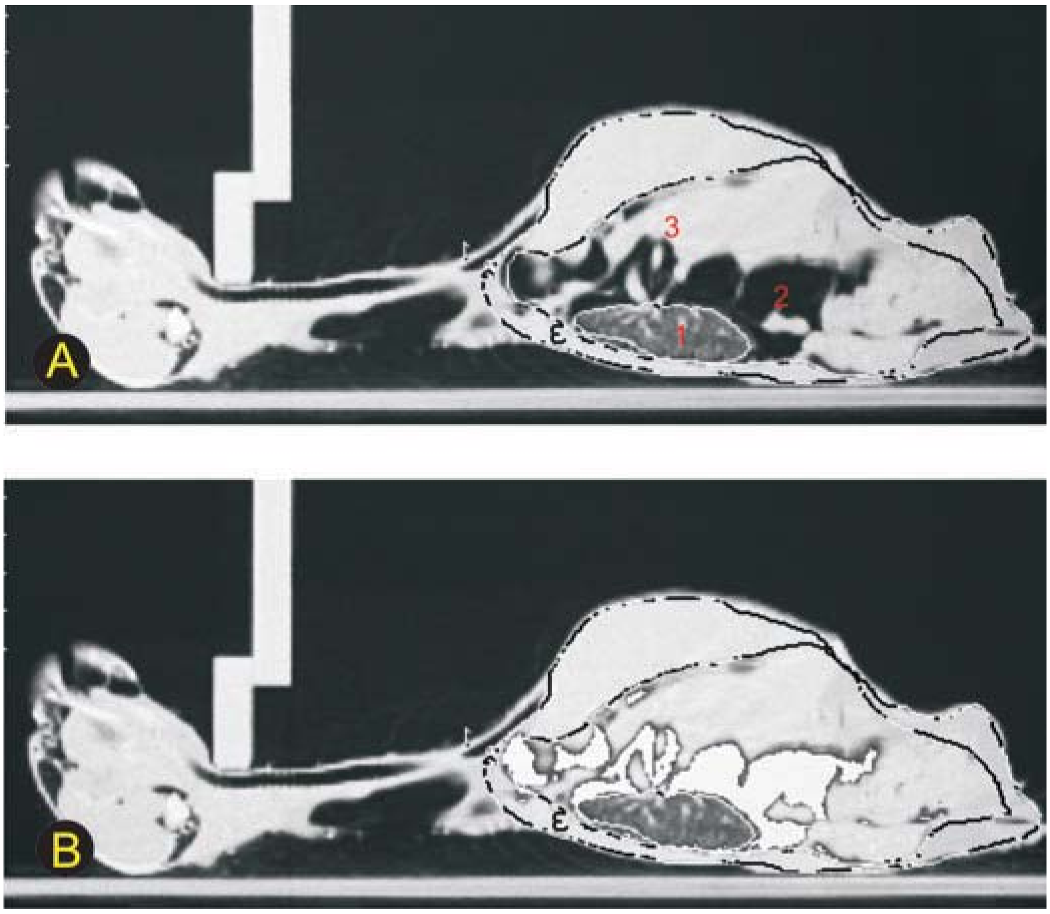

1: lung
2: air sacs
3: heart

Fig. 1-81: Whole body CT images of an African grey parrot (*Psittacus erithacus*) in a sagittal plane (120 kV, 165 mA, 2 mm SD, W: 2800, L: 80).

A: Scan showing the lungs (1), air sacs (2) and heart (3). By tracing the outline of the trunk, body cavities, and lungs, the areas of these structures can be measured. By assessing each slice, the volume of the region of interest (ROI) can be determined. The measurement of the lung volume does not have any diagnostic significance in birds; however, the lung density, which has a large diagnostic significance, can be determined with CT imaging.

B: In a further step, the volume of all the air-filled structures in the ROIs measured in A can be determined using highlighting (as the density of air is known).

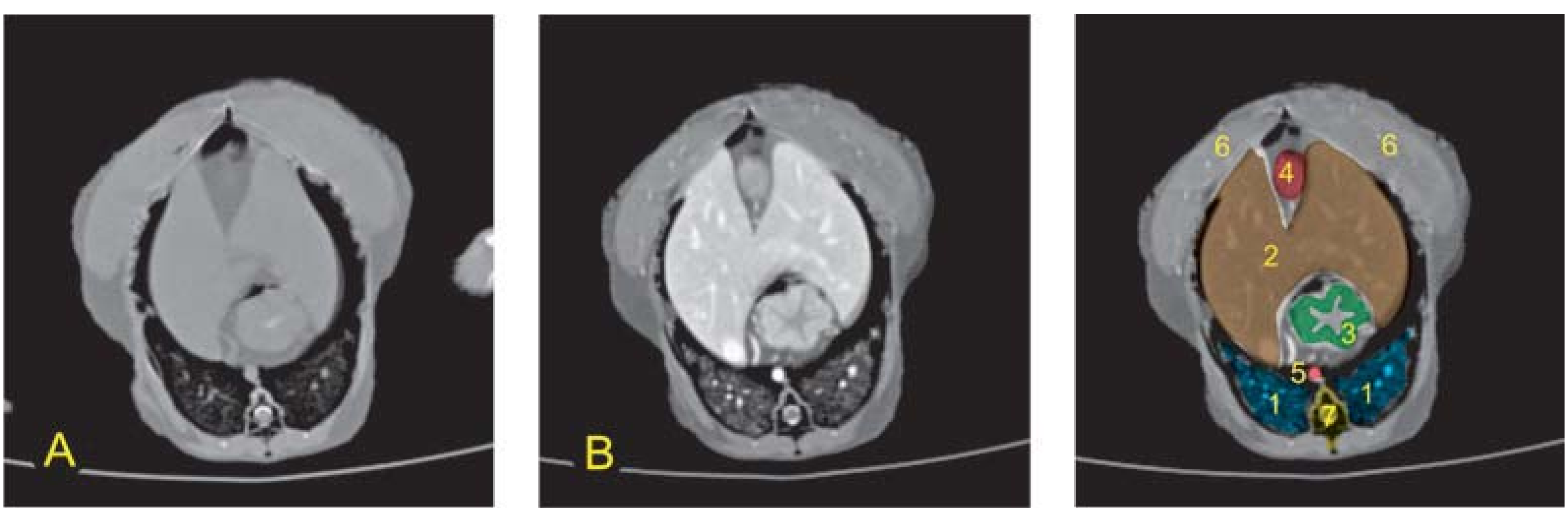

Fig. 1-82: CT images of a common buzzard's (*Buteo buteo*) body in a transverse plane (120 kV, 120 mA, 1.0 mm SD, W: 1500, L: 350). The scanned images show the liver, lung, and proventriculus before (A) and approximately 1 minute after (B) the intravenous administration of an iodine-based contrast agent (iomeprol 300 mg/ml, 3 ml/kg bwt). In addition to showing the perfusion of the lungs (1) and liver (2), the wall of the proventriculus (3), and the blood flow in the aorta (5) can be depicted using this method.

1: lungs
2: liver
3: wall of the proventriculus
4: heart
5: aorta
6: thoracic musculature
7: vertebral canal with spinal cord

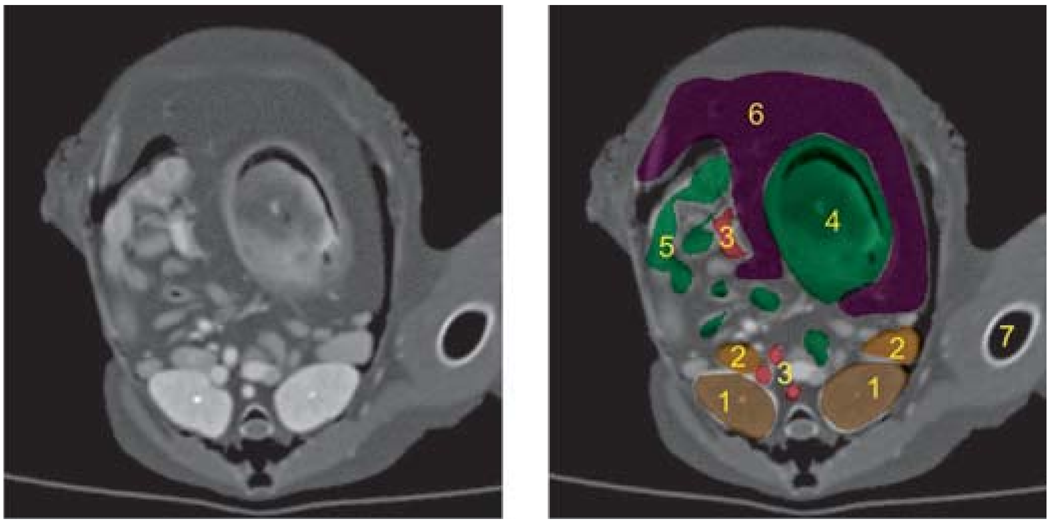

1: kidneys
2: testicles
3: blood vessels
4: gizzard
5: loop of intestine
6: fat
7: femur

Fig. 1-83: CT images of a common buzzard's (*Buteo buteo*) body in a transverse plane (120 kV, 120 mA, 1.0 mm SD, W: 1900, L: 490). The scanned images show the internal organs approximately 1 minute after the intravenous administration of an iodine-based contrast agent (iomeprol 300 mg/ml, 3 ml/kg bwt). Both the kidneys (1) and the nutrient arteries (3) of the loops of intestines (5) can be clearly seen.

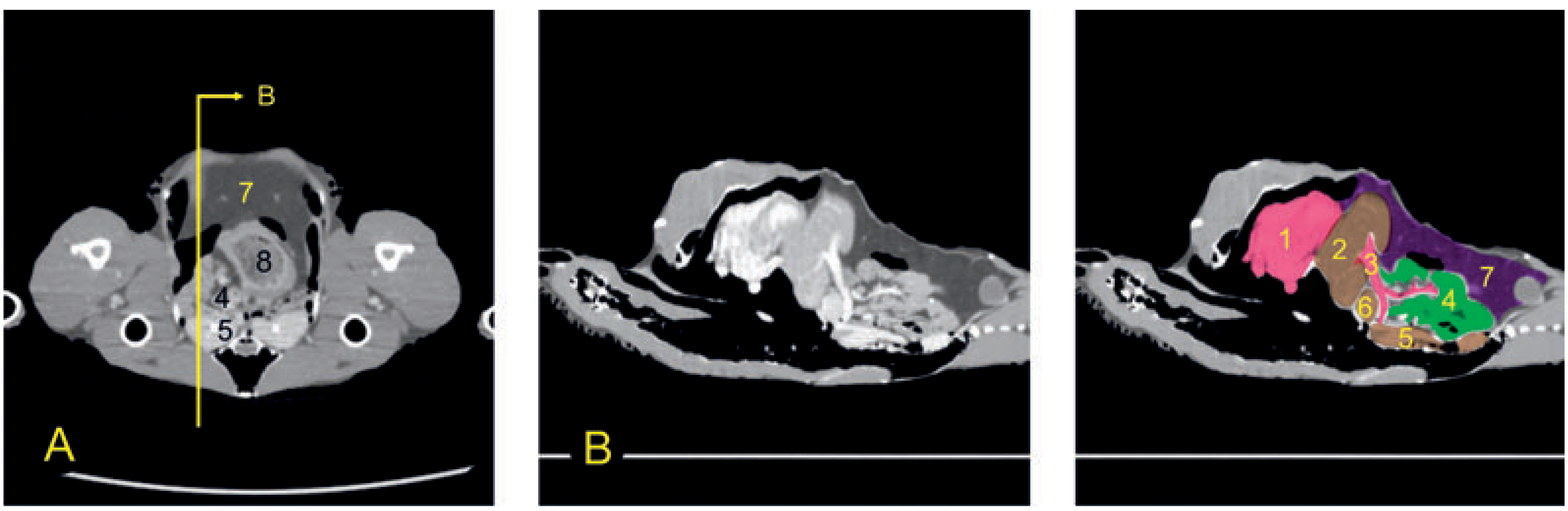

Fig. 1-84: Body CT images of a steppe eagle (*Aquila nipalensis*) in (A) transverse and (B) sagittal planes (120 kV, 151 mA, 1.0 mm SD, W: 649, L: 45). Scan showing the internal organs approximately 1 min after the intravenous administration of an iodine-based contrast agent (iomeprol 300 mg/ml, 3 ml/kg bwt). In addition to the kidneys (5), the nutrient arteries (3) of the loops of intestines (5) and the blood flow to the liver (2) can be seen. The filling of the heart (1) with blood is also visible.

1: heart
2: liver
3: right hepatic portal vein
4: loop of intestine
5: kidney
6: testicle
7: fat
8: gizzard)

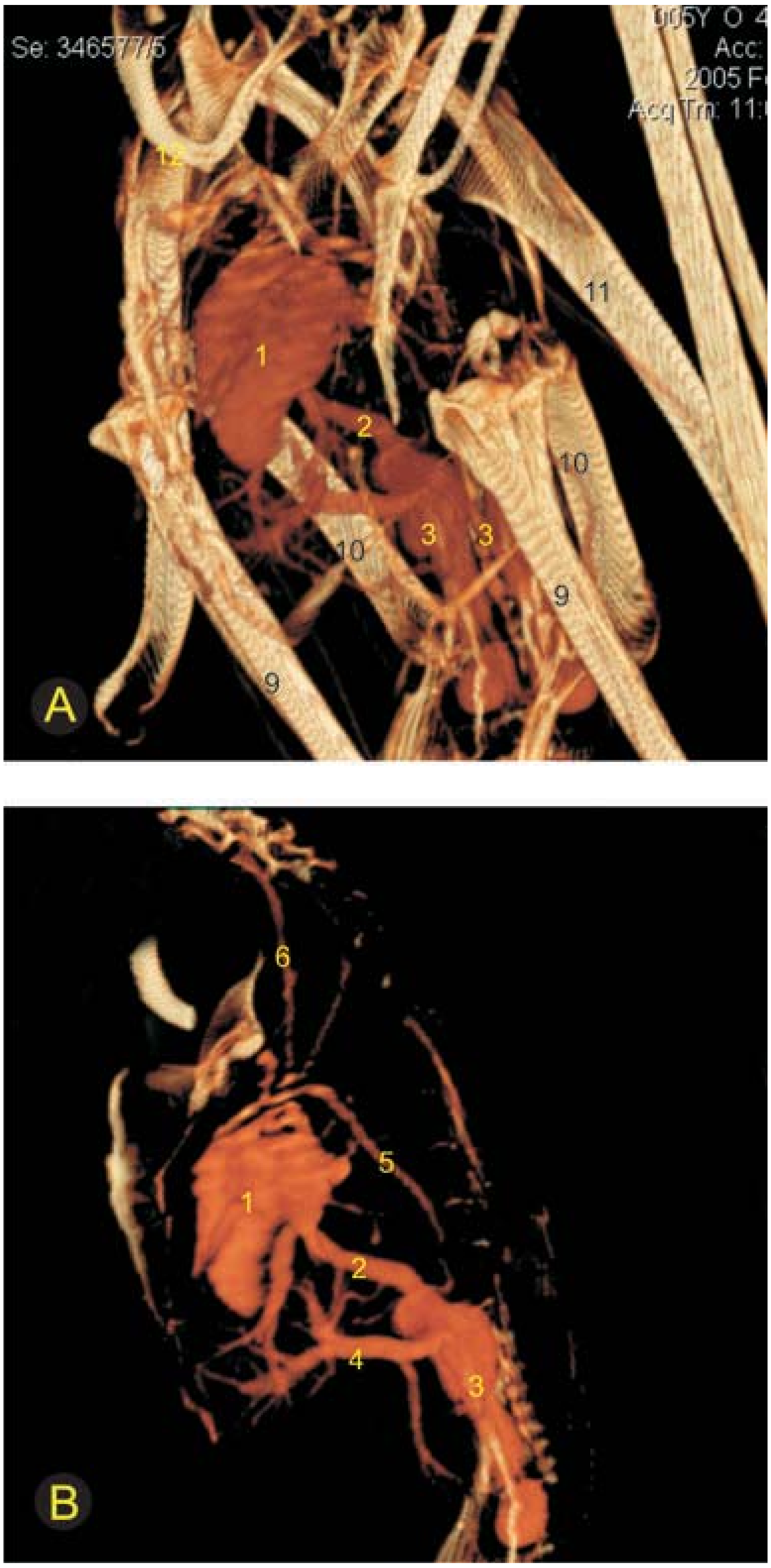

1: heart
2: vena cava
3: kidney
4: mesenterial blood vessels
5: aorta
6: carotid artery
9: tibiotarsus
10: femur
11: humerus
12: clavicula

Fig. 1-85: Three-dimensional reconstruction of CT body images of a steppe eagle (*Aquila nipalensis*) (120 kV, 151 mA, 1.0 mm SD, W: 649, L: 45): Reconstruction showing the blood vessel system approximately 1 min after the intravenous administration of an iodine-based contrast agent (iomeprol 300 mg/ml, 3 ml/kg bwt) (A) with and (B) without imaging of the skeletal system.

1.4 Magnetic resonance imaging (MRI)

Eberhard Ludewig, Maria-Elisabeth Krautwald-Junghanns

1.4.1 Equipment and uses

At the moment, MRI is rarely used in avian medicine. The main reason for the relatively little use of MRI imaging is the long periods of time needed to perform the examination, which is a significant concern for the anesthesiologist who has limited access to the patient in dorsal recumbency **(Fig. 1-86)**. The other reasons why MRI is rarely used to image avian patients are the small size of the structures to be imaged and the high respiratory and heart rates in avian patients, which make it difficult to achieve images of diagnostic quality. Especially low-field MRI machines (field strength < 0.5 Tesla) are of limited use in the investigation of small birds. However, one may assume that with the increase in number of high-field systems (> 1.5 Tesla) in veterinary institutes, the number of MRI examinations on avian patients will increase. High-field scanners provide a much better spatial and temporal resolution.

With MRI, the signaling relies on the interaction of protons (nuclei of hydrogen atoms) with a strong static magnetic field and high frequency impulses.

The contrast of the MRI image provides information about the hydrogen content of the tissue (»proton imaging«). By changing the scanner's parameters (pulse repetition time [PRT], echo time), different tissue weightings (whereby variations in the contrast) can be achieved. By using this technique, a step progression examination of the tissue composition can take place.

Three types of weighting are used:
- ☐ T1-weighted images (T1)
- ☐ T2-weighted images (T2)
- ☐ proton-density-weighted images (PDW)

With the aid of different types of sequences, the signal of certain tissues (e.g fat) can be selectively reduced.

A paramagnetic intravenous contrast agent (gadolinium) changes the local magnet field in tissues that concentrate the material (e.g. tumors) which allows their delineation from surrounding structures. Gadolinium atoms have their own magnetic field which allows the protons in the immediate surrounding area to give off a higher signal (positive contrast). Currently, information regarding the use of gadolinium in diseased avian patients is not available.

Due to its imaging characteristics, MRI is primarily advantageous in the diagnosis of soft-tissue changes. In avian medicine, the indications for MRI are therefore mainly associated with neurological disease (CNS, eye) and internal medicine (soft-tissue changes) (see Chaps. 1.5.1, 1.6, 1.10 and 1.11).

The indications for MRI arise from the analysis of its advantages and disadvantages.

Advantages:
- ☐ exceptionally good for soft-tissue contrast (see **Figs. 1-88** to **1-91)**, especially to diagnose (pathological) changes in tissue composition
- ☐ multiplanar reconstruction method for primary interpretation, with no need for changes in the position of the patient
- ☐ no artifacts due to bone
- ☐ no exposure to radiation

Disadvantages:
- ☐ only limited imaging of compact bone, mineralization, and gases
- ☐ low spatial resolution (compared to CT)
- ☐ long investigation times
- ☐ difficulties in patient monitoring
- ☐ expensive
- ☐ high artifact potential (movement, metal **[Fig. 1-87]**, picture reconstruction)

1.4.2 Preparation

At the beginning of the investigation, it should be noted that metal implants (e.g. microchips) cause large-scale signal extinction, therefore the affected region cannot be evaluated **(Fig. 1-87)**.

MRI investigations require the patient to be placed under general anesthesia. In order to facilitate respiration, the bird should be placed in a semi-upright position. Positioning aids made of MRI-compatible materials (pillows, sand bags, special devices) should be used **(Figs. 1-86 A** and **C)**.

The choice of coils has a significant impact on MRI image quality. Coils are used to induce a local change in the magnet field and to measure the resulting signal. Superficial coils are suitable for use in birds, though it is important to choose the smallest coil possible **(Fig. 1-86)**.

To achieve the image quality necessary for clinical diagnosis, it is important to develop investigation protocols – a »film script«. The machine settings in the protocol take into account the imaging characteristics of the region (e.g. size, movement characteristics) being investigated and the performance characteristics of the machine (e.g. field strength, gradients, slew rate).

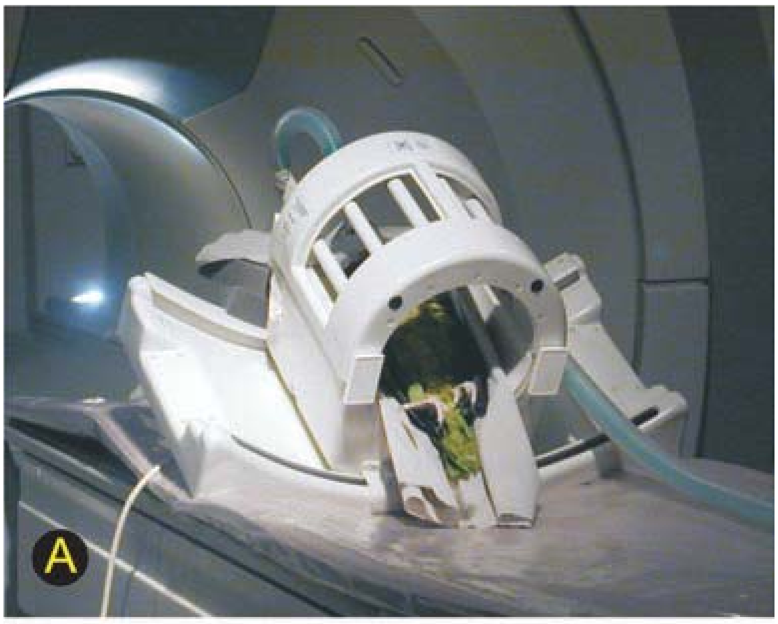

Fig. 1-86: MRI.

A: Examination of a blue-fronted Amazon (*Amazona aestiva*) under general isoflurane anesthesia using a quadrature knee coil. The bird is held in a semi-upright position to reduce respiratory compromise.

B: Examination of a Humboldt penguin (*Spheniscus humboldti*) in dorsal recumbancy under isoflurane general anesthesia using a quadrature knee coil.

C: Examination of a blue-fronted Amazon (*Amazona aestiva*) under isoflurane general anesthesia using a flexible ring-shaped surface coil. The bird is being held in a semi-upright position to reduce respiratory compromise.

1.4.3 Investigatory procedure

The actual MRI investigation consists of a sequence of pulses. This serves to characterize and identify changed tissues (e.g. hemorrhage, inflammation, neoplasia).

Principally with MRI, it is possible to arbitrarily orientate the scanning planes without changing the position of the patient. For the identification of pathological changes, it is necessary to compare an image to a known imaging protocol with a similarly orientated engram of the normal image. For this reason, the scanning planes used in birds are orientated on the standards used for MRI investigations in mammals (e.g. transverse, dorsal, sagittal). Depending on the image results, other planes can be selected in order to aid in the diagnosis.

To achieve a usable signal-to-noise ratio, it is difficult to use a slice thickness of less than 1–3 mm, especially with machines with low field strengths. In addition, when low-field systems are used, the different sequences required must be done in order, which is very time-consuming. The time needed per sequence is, on average, two to five minutes; therefore a full investigation may take as long as 45 minutes. A subsequent and time-saving reconstruction of further planes from the primary data can only be performed when all the edges of the voxel are of an equally small size (< 1 mm).

1.4.4 Imaging of the organs

The imageability of the organs is more or less like that found in mammals **(Figs. 1-88** to **1-91)**. Till now, MRI has been used in birds for the anatomical examination of different organ systems in connection with scientific investigations of domestic poultry (e.g. JANZEN et al. 1989), pigeons (e.g. ROMAGNANO et al. 1996), and pet birds. The use of MRI in clinically ill birds is relatively uncommon at the moment, when compared to other imaging modalities (e.g. ENDERS et al. 2001, FLEMING et al. 2003, STAUBER et al. 2007). Some experience has been attained in larger birds for diagnosing changes in the brain and spinal cord (*q.v.* Chap. 1.11; **Figs. 1-114** and **1-205**).

Previous investigations have illustrated the value of MRI for imaging hepatic structures (e.g. amount of fat, intrahepatic blood vessels, gallbladder [if present]), the gastrointestinal tract (walls and contents) and the urogenital tract (especially the kidneys). In addition, MRI has been used to analyze growth processes in young birds and to investigate production quality by determining the amount of abdominal body fat in domestic poultry. MRI investigations on the passeriform brain have been performed to determine the topographical relationship between brain structures and singing ability (e.g. DE GROOF et al. 2006, VAN MEIR et al. 2006).

Further reading

DE GROOF, G., VERHOYE, M., VAN MEIR, V., TINDEMANS, I., LEEMANS, A., VAN DER LINDEN, A. (2006): In vivo diffusion tensor imaging (DTI) of brain subdivisions and vocal pathways in songbirds. Neuroimage **29**: 754–763.

ENDERS, F., JURINA, K., STRAUB, J., KRAUTWALD-JUNGHANNS, M.-E. (2001): Magnetic resonance imaging in birds. Proc. EAAV Conf, Munich, pp. 87–91.

FLEMING, G. J., LESTER, N. V., STEVENSON, R., SILVER, X. S. (2003): High field strength (4.7 T) magnetic resonance imaging of hydrocephalus in an African Grey parrot (*Psittacus erithacus*). Vet Radiol Ultrasound **44**: 542–545.

JANZEN, E. G., LEESON, S., PARTLOW, G. D., OEHLER, U. M., TOWNER, R. A. (1989): Cross-sectional anatomy of the chicken: An atlas for magnetic resonance imaging. University of Guelph.

ROMAGNANO, A., SHIROMA, J. T., HEARD, D. J., JOHNSON, R. D., SCHIERING, M. R., MLADINICH, C. R. J. (1996): Magnetic resonance imaging of thebrain and coelomic cavity of the Domestic Pigeon (*Columba livia* f. *domestica*). Vet Radiol Ultrasound **37**: 431–440.

STAUBER, E., HOLMES, S., DEGHETTO, D. L., FINCH, N. (2007): Magnetic resonance imaging is superior to radiography in evaluating spinal cord trauma in three Bald eagles (*Haliaeetus leucocephalus*). J Avian Med Surg **21**: 196–200.

VAN MEIR, V., PAVLOVA, D., VERHOYE, M., PINXTEN, R., BALTHAZART, J., EENS, M., VAN DER LINDEN, A. (2006): In vivo MR imaging of the seasonal volumetric and functional plasticity of song control nuclei in relation to song output in a female songbird. Neuroimage **31**: 981–992.

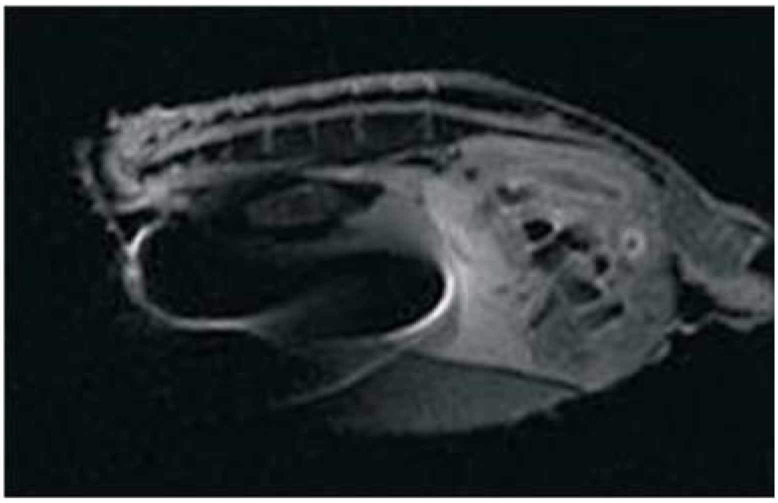

Fig. 1-87: MRI sagittal slice of a blue-fronted Amazon parrot's (*Amazona aestiva*) trunk. There is a disturbance of the magnetic field due to the presence of a microchip in the bird's thoracic muscles leading to the formation of an artifact in the cranial body cavity. The images from this MRI examination are nondiagnostic.

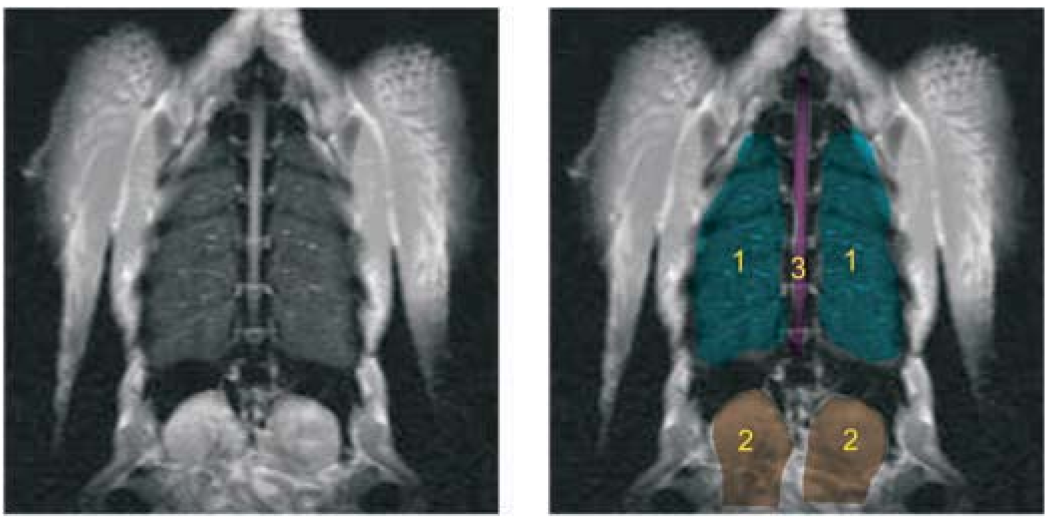

1: lungs
2: kidney (only partly)
3: spinal cord

Fig. 1-88: MRI images of a white-tailed eagle's (*Haliaeetus albicilla*) trunk in a dorsal plane, T1-weighted: The scanned images show the lungs (1), parts of the kidneys (2), and the spinal cord (3).

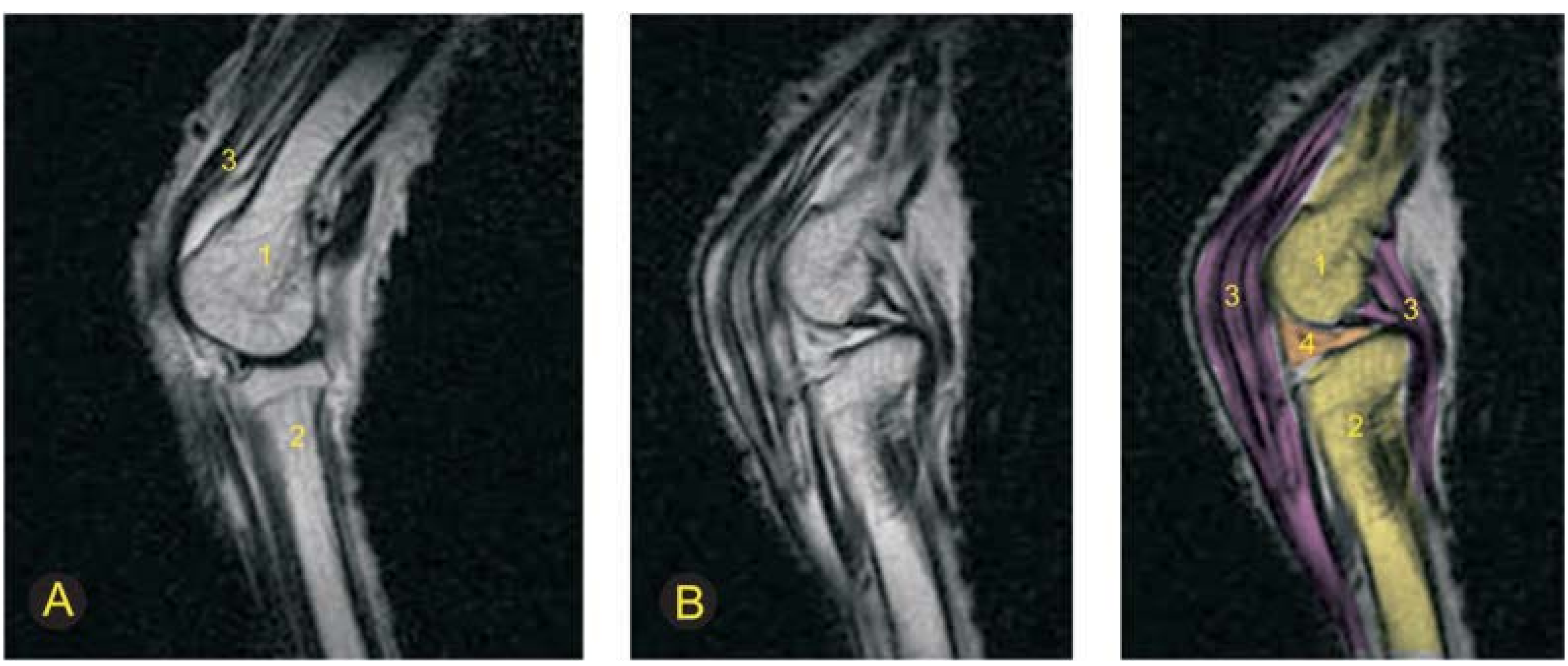

Fig. 1-89: MRI images of a turkey's (*Melleagris gallopavo*) knee joint in different sagittal planes, T2-weighted: The scanned images show the distal femur (1), proximal tibiotarsus (2), tendons (3), and patella (4).

1: distal femur
2: proximal tibiotarsus
3: tendons
4: patella

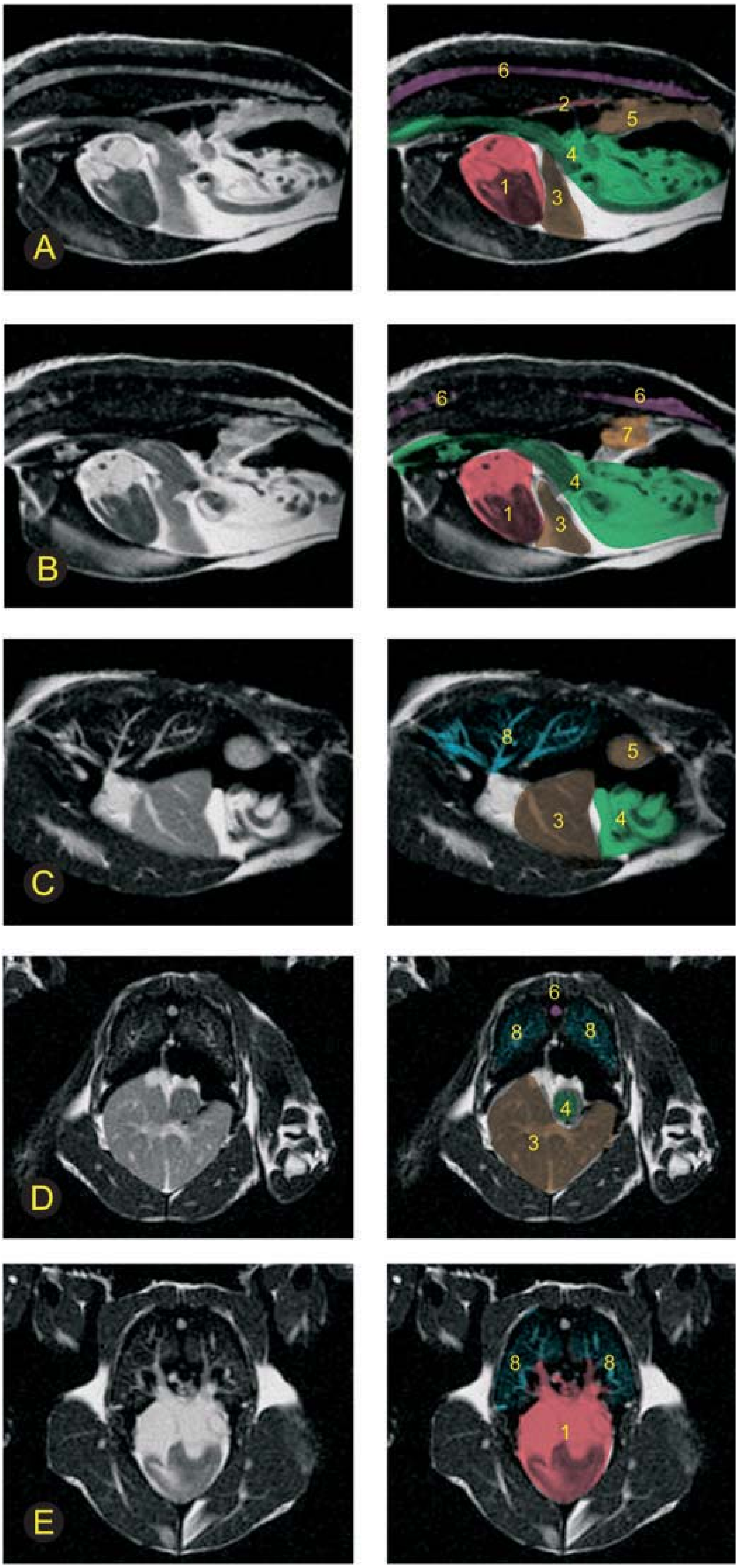

1: heart
2: aorta
3: liver
4: gastrointestinal tract
5: kidney
6: spinal cord
7: gonad
8: pulmonary blood vessels

Fig. 1-90: MRI images of a goshawk's (*Accipter gentilis*) trunk; T2-weighted.

A, B, C: Different sagittal planes.

D, E: Different transverse planes.

1: loop of intestine
2: stomach
3: spinal cord
4: kidney
5: liver
6: testicle
7: spleen
8: hindlegs

Fig. 1-91: MRI images of a Humboldt penguin's (*Spheniscus humboldti*) trunk; T2-weighted.

A, B, C: Different transverse slices.

D, E: Different dorsal slices.

Special diagnostics, pathological findings

1.5 Skeletal system

Maria-Elisabeth Krautwald-Junghanns, Volker Schmidt

In many cases that involve fractured bones, conventional radiography is often the only suitable imaging modality. When using conventional radiological techniques other abnormal presentations, especially when the surrounding soft tissues are involved, should be assessed within the context of the patient's clinical examination as well as their laboratory diagnostic test results. Little is known about the utilization of ultrasonography for assessing pathological changes that occur in the avian skeletal system. Even iodine-containing contrast agents have been rarely used on avian patients apart from rhinosinography studies. Computer tomography is quickly gaining acceptance as an imaging modality for birds because it allows for the acquisition of more detailed images without superimposition. The lack of tissue summation provides the examiner more precise information about the anatomical relationships within the structures being imaged.

To assess the age of a **fracture** **(Figs. 1-92** to **1-94)** and the degree of healing **(Fig. 1-95)**, the extent of the endosteal callus formation should be evaluated as there is often much less periosteal bone formation in avian bones than observed in mammalian fracture repair. However, survey radiographs should be performed at regular intervals to exclude osteomyelitis **(Fig. 1-96)** and other complications that can occur during the healing process. The time required for avian fracture repair is variable and depends on the size of the bird and type of fracture. The formation of a stable bone callus can take 7–21 days, or even a number of months (e.g. fractures of the humerus). In avian medicine, joint luxations are rarely diagnosed relative to fractures, but as with fracture assessment, two projections are required for the diagnosis of joint luxations **(Fig. 1-97)**.

Primary malignant **bone tumors** are characterized in birds by extreme osteolysis, pathological fractures, and pronounced soft tissue swelling with no periosteal or sclerotic processes involved **(Fig. 1-98)**. Other forms of neoplasia, such as squamous cell carcinomas and fibrosarcomas, can also become clinically evident due to massive soft-tissue swelling and the potential occurrence of pathological fractures; however, there is little osteolytic reaction observed **(Fig. 1-99)**. The presence of a periosteal reaction is often interpreted as being characteristic of a malignant bone tumor, especially when the periosteal reaction with non-neoplastic new bone is viewed in the radiographic image. The radiographic images of a malignant bone tumor in birds are similar to that found with mammalian species diagnosed with the same disease. In the bird, however, these changes are mainly associated with infectious changes **(Figs. 1-100** and **1-101)**. Extreme periosteal reactions **(Fig. 1-102)** are rarely associated with inflammation of avian bones. In addition, the characteristic tissue hardening which is used to differentiate these lesions is less pronounced in the bird.

Individual bones and even large areas of the avian skeleton can be affected by generalized **infections** (e.g. *Salmonella* spp.) **(Figs. 1-101)**. Generally, one should remember that infectious agents can enter the body via the vascular, gastrointestinal, and respiratory systems. Although infections with *Mycobacteria* spp. are characterized by the formation of granulomas in various parenchymatous organs (e.g. lungs, liver), this disease can also affect the skeleton **(Fig. 1-100)** by forming typical multiple, focal osteolytic and sclerotic lesions in the medullary cavities of the long bones. Lytic processes around the joints often indicate the presence of a septic arthritis **(Fig. 1-103)**.

Narrowing of the joint cavity, subchondral sclerosis, periosteal changes, and massive swelling of the soft tissue layers are characteristic radiographic signs of **primary arthritis**. In pigeons, arthritic changes are frequently diagnosed in the wing and leg joints as a consequence of *Salmonella typhimurium* infections **(Fig. 1-101)**.

Nutritional deficiencies are often associated with **metabolic skeletal changes**. Poor diets that contain an inadequate vitamin, mineral, and/or protein content may result in young birds having curvature and folding fractures of the long bones and pathological stress fractures in the region of the metaphysis. The radius, ulna, femur, and tibiotarsus are most frequently affected **(Figs. 1-104** and **1-105)**. Deformation of the sternal ridge can also be observed. In older birds secondary hyperparathyroidism **(Fig. 1-106)** and osteomalacia can occur as a result of nutritional deficiencies.

While excessive calcification is easy to diagnose, reduced bone density on a radiograph is not enough to make a definitive diagnosis as this is influenced by the quality of the image and its development. Definite signs of metabolic bone changes are not only a reduction in bone density but also the characteristic bending of long bones and/or fractures in the region of the metaphyses **(Figs. 1-104** and **1-105)**.

Polyostotic hyperostosis (Fig. 1-107) should not be confused with the formation of medullary bone as a physiological calcium store. In contrast to medullary bone, polyostotic hyperostosis is not found in the long bones but in the axial skeleton and the thorax. Such pathological calcification of the skeleton is not infrequent in budgerigars and is often diagnosed in combination with disease changes affecting the gonads (e.g. ovarian tumors, ovarian cysts) or with abdominal hernias. Occasionally, polyostotic hyperostosis within the medullary cavity appears mottled due to the varying degrees of calcification observed on the radiograph and therefore it may resemble granuloma formation. However, the radiodensity of the excessively calcified bone, in contrast to granulomas, is that of cortical bone thus making the diagnosis easier.

1.5.1 Cranium

In the region of the head, not only the cranium but also its cavities (e.g. nasal passages and sinuses, air sac diverticula) and its soft tissue layers may be affected by changes that can be diagnosed using standard radiographic techniques. **Fractures** of the cranial capsule are relatively easy to identify **(Fig. 1-108)**, while fractures in the region of the beak apparatus **(Fig. 1-109)** and the hyoid bone are much more difficult to recognize due to the summation of many anatomic structures. It is important therefore to ensure that the patient is symmetrically positioned to reduce the summation effect within the head region. In addition, as required to properly assess all patients, at least two radiographic projections must be taken.

Cranial deformation indicates the presence of disturbances in bone formation and/or mineral metabolism (e.g. osteomalacia, osteoporosis) especially in young birds **(Figs. 1-110** and **1-111)**. **Increased radiopacity** of the cranial bones **(Fig. 1-106)** is a rare consequence of disturbances in calcium uptake and deposition (e.g. secondary hyperparathyroidism).

Increased radiopacity of the cavities within the head may occur due to the presence of large amounts of secretions or granuloma formation (e.g. mycotic infections) and/or infections of the upper respiratory tract (e.g. rhinitis, sinusitis; see Chap. 1.7). In chronic cases that involve inflammatory/infectious disease, the neighboring bones can also be infected **(Fig. 1-112A, B)**. The soft-tissue changes associated with inflammatory/infectious disease are often difficult to identify in radiographic images **(Fig. 1-204**; *q.v.* Chaps. 1.7 and 1.11). Exceptions to this inability to view soft tissue disease in radiographic images of the head are various tumor growths (e.g. retrobulbar tumors, osteomas, carcinomas), which due to their large size and their increased radiopacity are generally easy to identify.

1.5.2 Axial skeleton

The spinal region that is most predisposed to **fractures** has proven to be the junction of the caudal thoracic vertebrae and synsacrum **(Fig. 1-113)**. This region is often difficult to diagnose in the VD projection because of summation, therefore myelography may be required to make a definitive diagnosis. Due to the anatomical differences of a bird's spinal structure (see Chap. 1.1.4.6), myelography is associated with a great deal of patient risk. A CT or MRI examination would provide better diagnostic results and are currently the methods of choice for the diagnosis of spinal fractures **(Fig. 1-114)**. **Deformation** of the spine (e.g. kyphosis, **Fig. 1-115**), and more rarely scoliosis **(Fig. 1-116)** occur due to malnutrition (e.g. rickets, osteoporosis) or injury (trauma) and can be easily observed radiographic images.

1.5.3 Forelimbs

Fractures of the shoulder girdle are often diagnosed in wild birds. The diagnosis of fractures of the shoulder girdle is difficult when viewed from the VD projection due to the almost complete summation of the scapula and coracoid **(Figs. 1-92** and **1-93)**. The shoulder region cannot be adequately assessed from the lateral projection. As a consequence, fractures of the shoulder blade, coracoid, and furcula are often underdiagnosed.

1.5.4 Hindlimbs

Both **metabolic** and **infectious skeletal changes** will often affect the skeleton because of the added stress of the bird's body weight. Areas of the skeleton frequently affected by metabolic and infectious disease are the toe joints and tarsometatarsus, intertarsal joint, tibiotarsus, knee, and femur.

Pathological changes occurring on the phalanges and the tarsometatarsus due to varying degrees arthritis or osteolysis **(Fig. 1-117)** are often the consequence of septic **pododermatitis**. Generally, poor husbandry techniques (e.g. unsuitable perches, inadequate hygiene, lack of exercise) are responsible for this disease condition known commonly as bumblefoot. Essential for making a realistic prognosis in cases of septic pododermatitis is the proper assessment of periosteal changes affecting the bones of the foot: the more the diaphysis is affected, the less chance there is of recovery.

Fig. 1-92: Cranial body radiographic image of a great spotted woodpecker (*Dendrocopos major*), ventrodorsal projection, showing an old coracoid fracture (arrows) with obvious callus formation and rounding of the bone fragments.

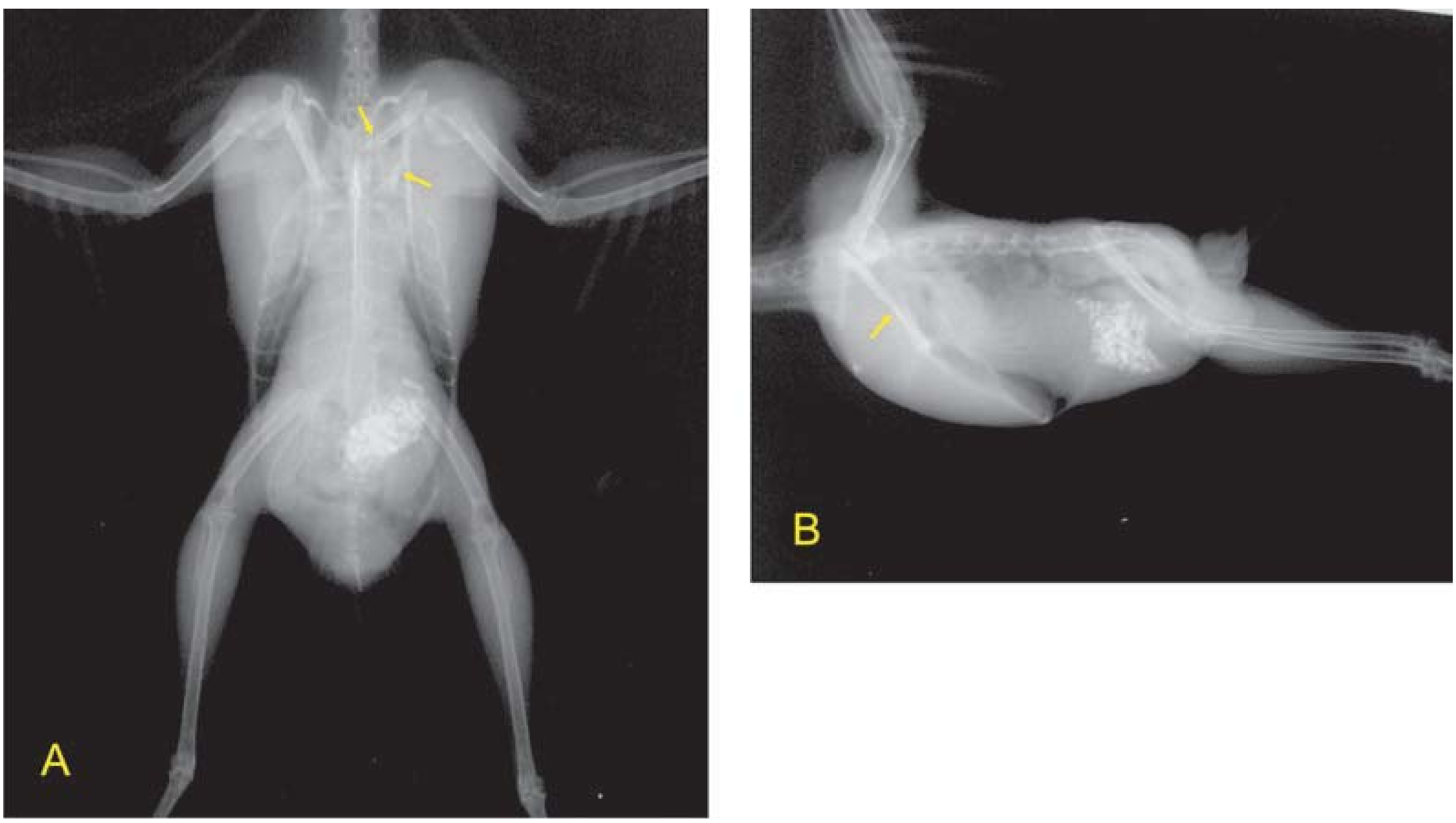

Fig. 1-93: Total body radiographic images of a house sparrow (*Passer domesticus*), ventrodorsal (A) and lateral (B) projections, recent coracoid fracture with sharp edges to the bone fragments. The sharp bone edges are barely recognized in the lateral projection due to summation (arrows).

Fig. 1-94: Radiographic images of a mallard's (*Anas platyrhynchos* f. *domestica*) leg showing a tarsometatarsal fracture, anterior-posterior (A) and mediolateral (B) projections. The edges of the fracture are sharply demarcated in this recent fracture. Due to their brittleness, bird bones often splinter as one can observe in these images.

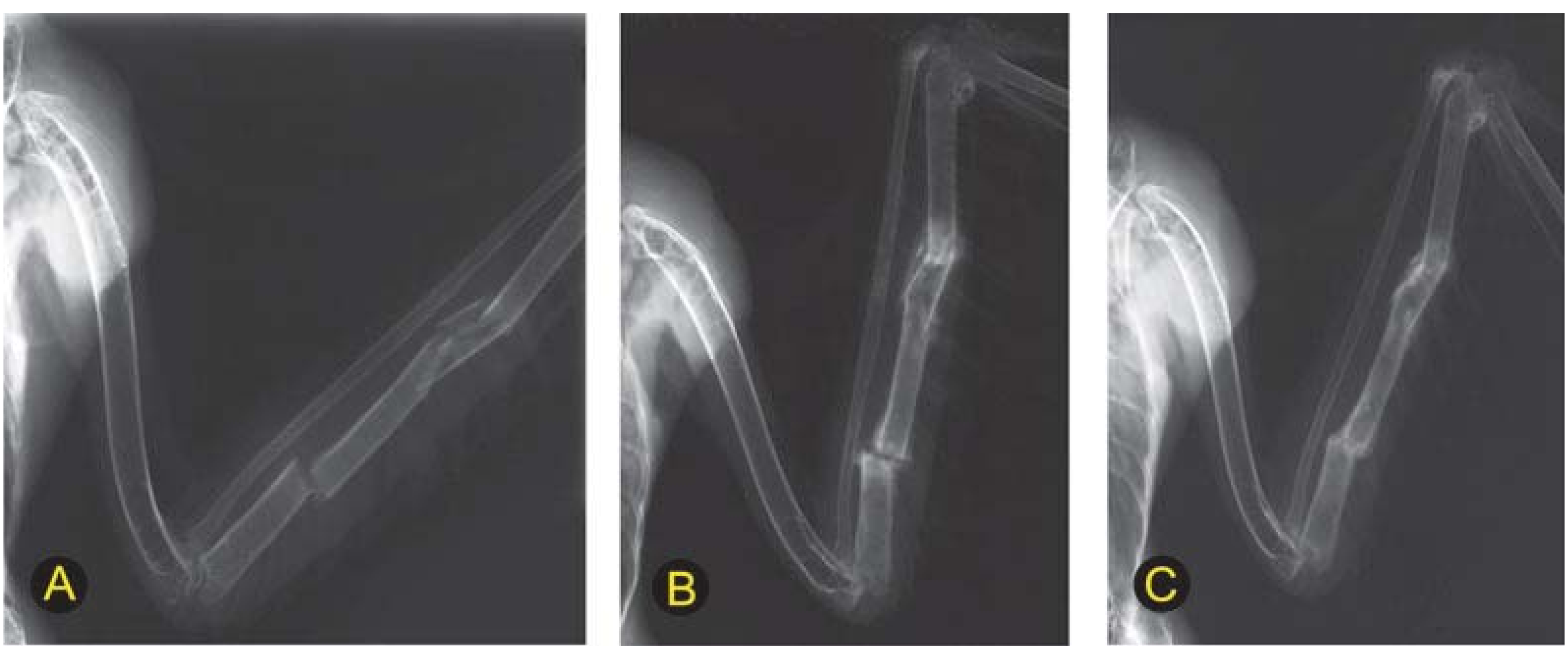

Fig. 1-95: Radiographic images of a common buzzard's (*Buteo buteo*), wing showing a splintered fracture of the ulna, mediolateral projection. There were no complications noted when conservative therapy was used to treat this fracture.

A: Day 0 (presentation).

B: Day 10.

C: Day 21.

Fig. 1-97: Radiographic image of an Eurasian widgeon's (*Anas penelope*) wing, mediolateral projection, luxation of the elbow joint.

Fig. 1-96: Radiographic image of a common buzzard's (*Buteo buteo*) wing, mediolateral projection. This bird developed osteomyelitis as a result of an ulna fracture that occurred close to the elbow joint. The characteristic radiographic evidence used to diagnose osteomyelitis is the hazy apparence to the cortices (arrows) and increased radiodencity within the medullary cavity.

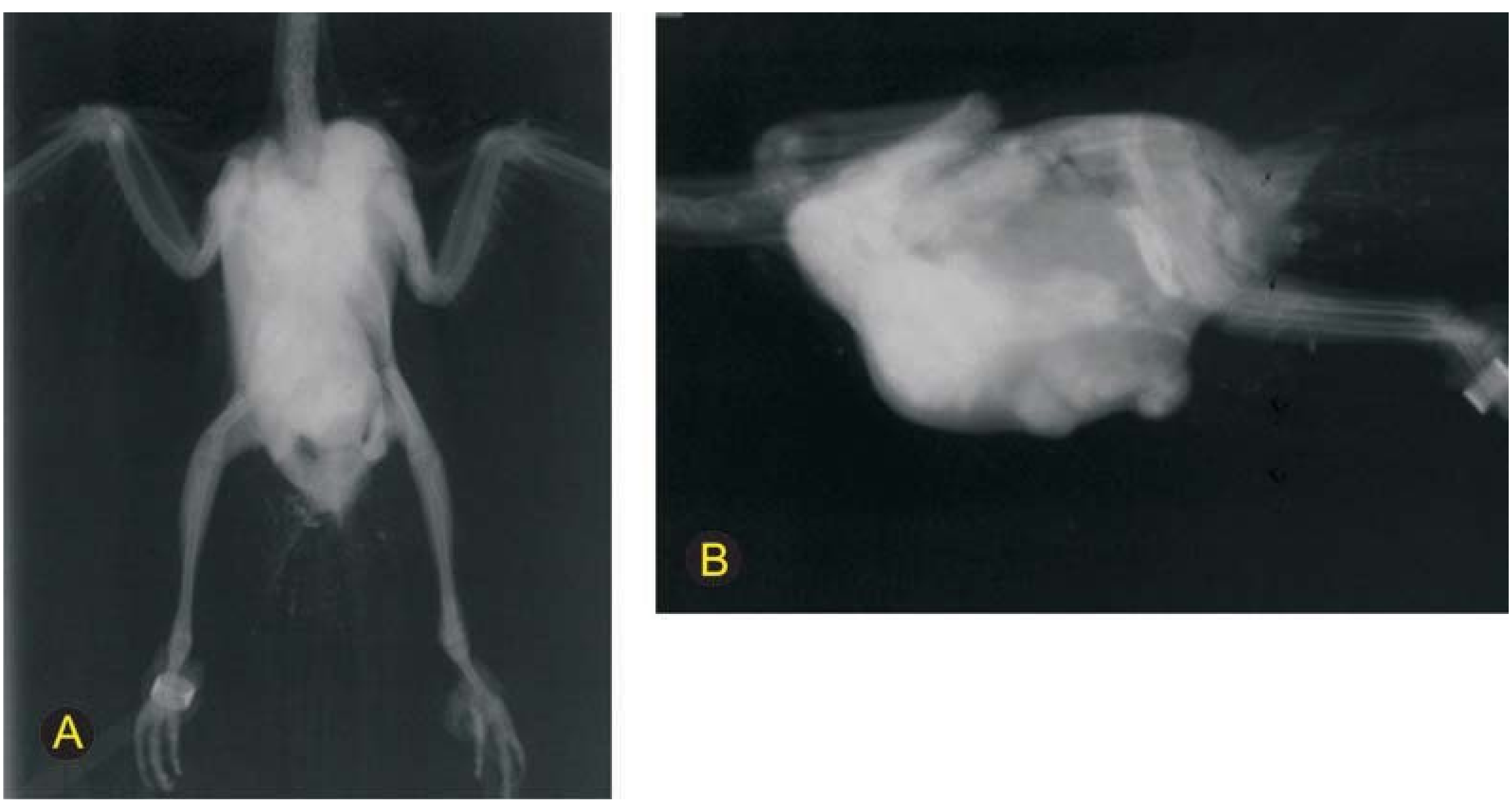

Fig. 1-98: Full body radiographic images of a red-rumped parrot (*Psephotus haematonotus*), (A) ventrodorsal and (B) lateral projections, osteoma.

Fig. 1-99: Radiographic image of an Eurasian eagle owl's (*Bubo bubo*), wing, caudocranial projection, squamous cell carcinoma.

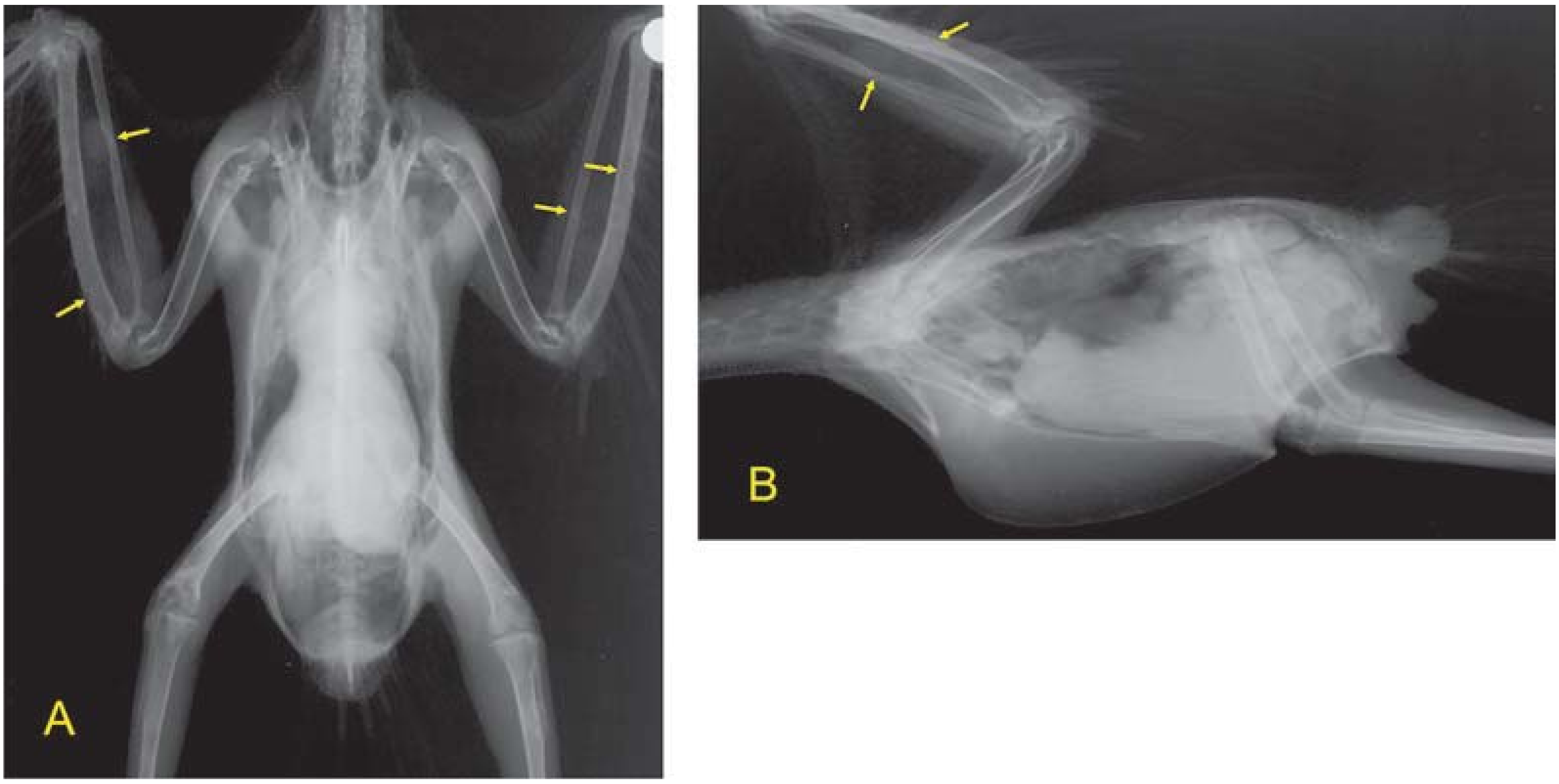

Fig. 1-100: Total body radiographic images of an African grey parrot (*Psittacus erithacus*) diagnosed with tuberculosis, (A) ventrodorsal and (B) lateral projections. A slight osteolysis is observed in the area of the radius and ulna (arrows) along with an overexpansion of the intraclavicular air sacs and loss of the hour-glass shape between the heart and liver (hepatic swelling) in the ventrodorsal projection. Additionally, an enlarged convoluted loop of intestine is visible in the lateral projection.

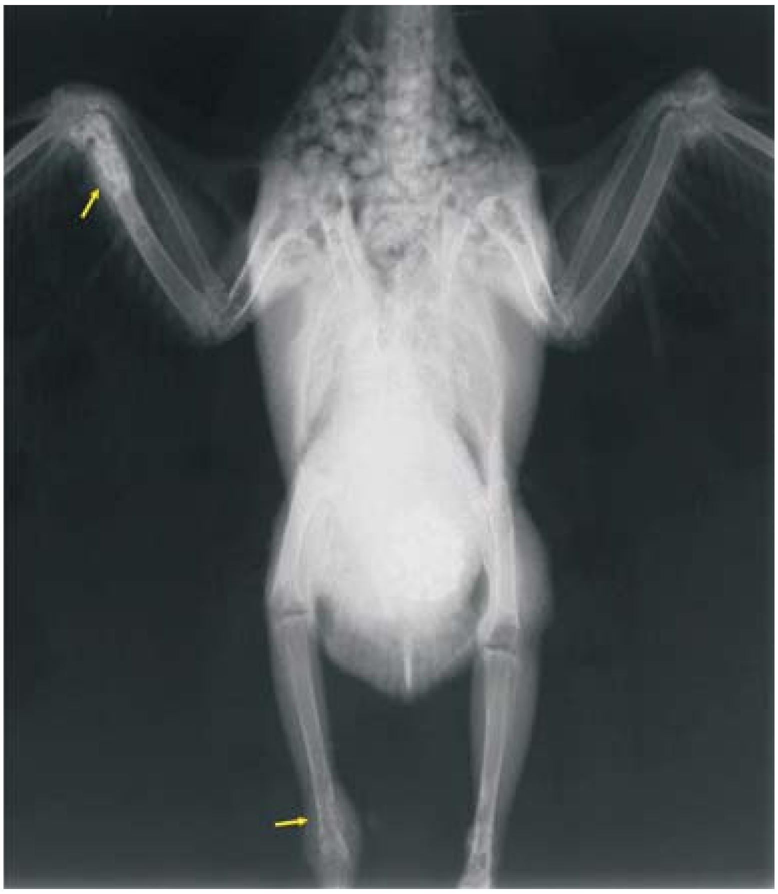

Fig. 1-101: Total body radiographic image of a pigeon (*Columba livia* f. *domestica*) diagnosed with salmonellosis, ventrodorsal projection. Numerous areas of osteolysis are visable in the distal tibiotarsus and the right distal ulna (arrows).

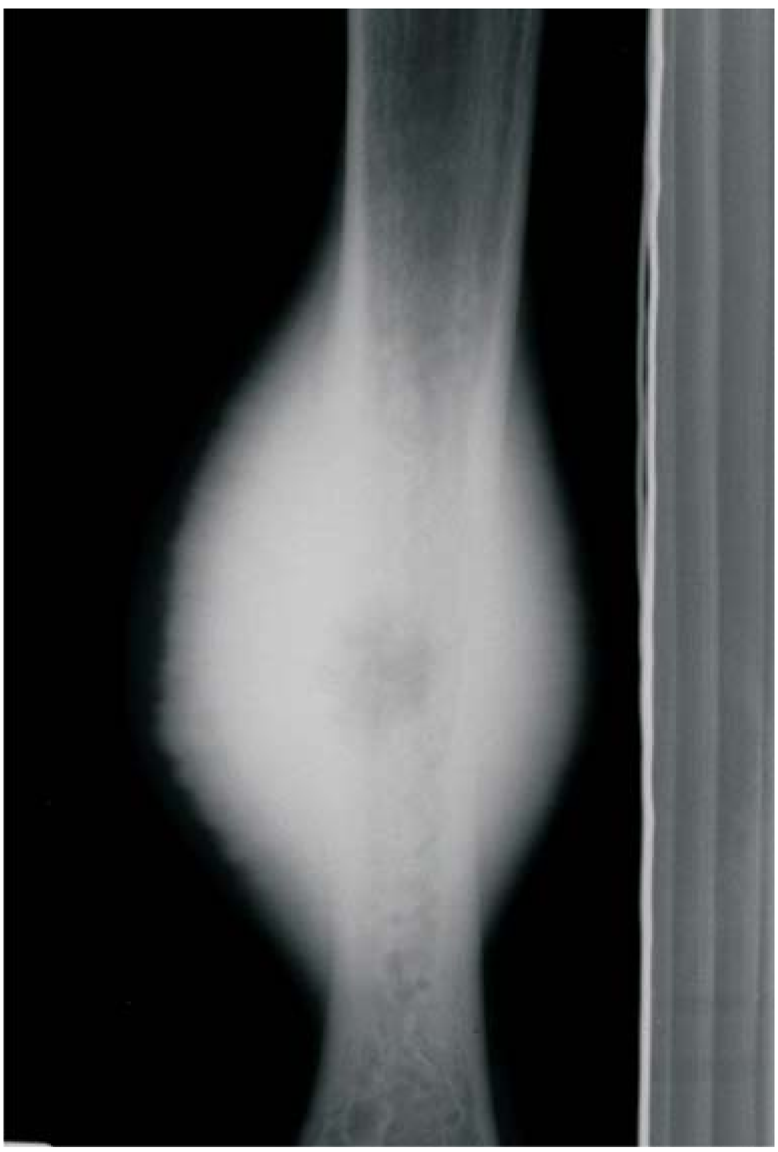

Fig. 1-102: Radiographic image of an emu's (*Dromaius novaehollandiae*) tarsometatarsus diagnosed with bacterial infection, anterior-posterior projection. Significant soft tissue swelling with osteolysis is clearly visible in this image.

Fig. 1-103: Radiographic image of a white-tailed eagle's (*Haliaeetus albicilla*) wing, mediolateral projection. This image shows the development of arthritis in the carpometacarpal joint with narrowing of the joint cavity.

Fig. 1-104: Total body radiographic images of an African grey parrot (*Psittacus erithacus*) (1.5 years old) with severe metabolic disturbance of the skeleton (rickets), (A) ventrodorsal and (B) lateral projections, Bending and deformation of the long bones, vertebrae, ribs, and pelvis are often observed in patients diagnosed with rickets.

Fig. 1-105: Radiographic images of a young domestic goose's (*Anser anser*) leg diagnosed with metabolic disease, (A) anterior-posterior and (B) lateral projections. Bending of the tibiotarsus is an indication that the bird is suffering from a metabolic disease.

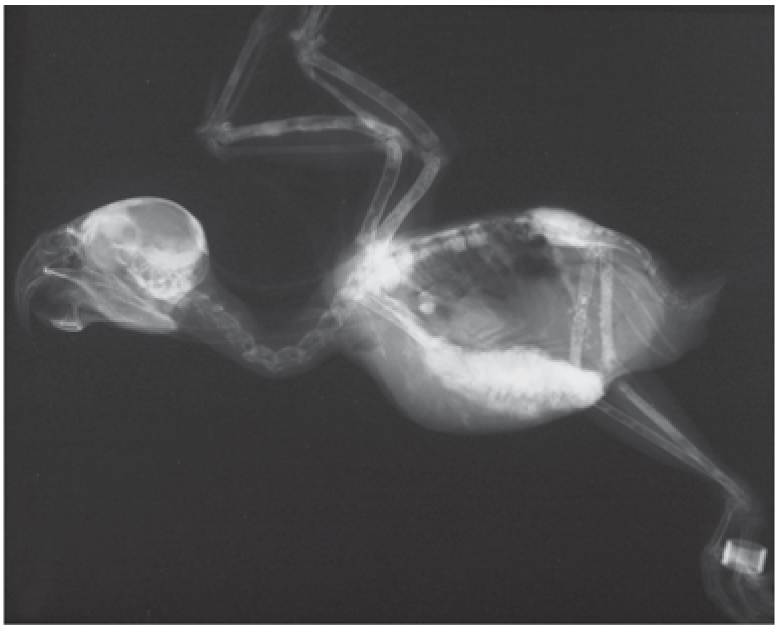

Fig. 1-106: Total body radiographic image of a plum-headed parakeet (*Psittacula cyanocephala*), lateral projection, secondary hyperparathyroidism with hypercalcification of the bone.

Fig. 1-107: Total body radiographic images of a canary (*Serinus canaria* f. *domestica*) diagnosed with polyostitic hyperostosis (arrows), (A) ventrodorsal and (B) lateral projections. The formation of medullary bone and the presence of an abdominal hernia are clearly visible in these images.

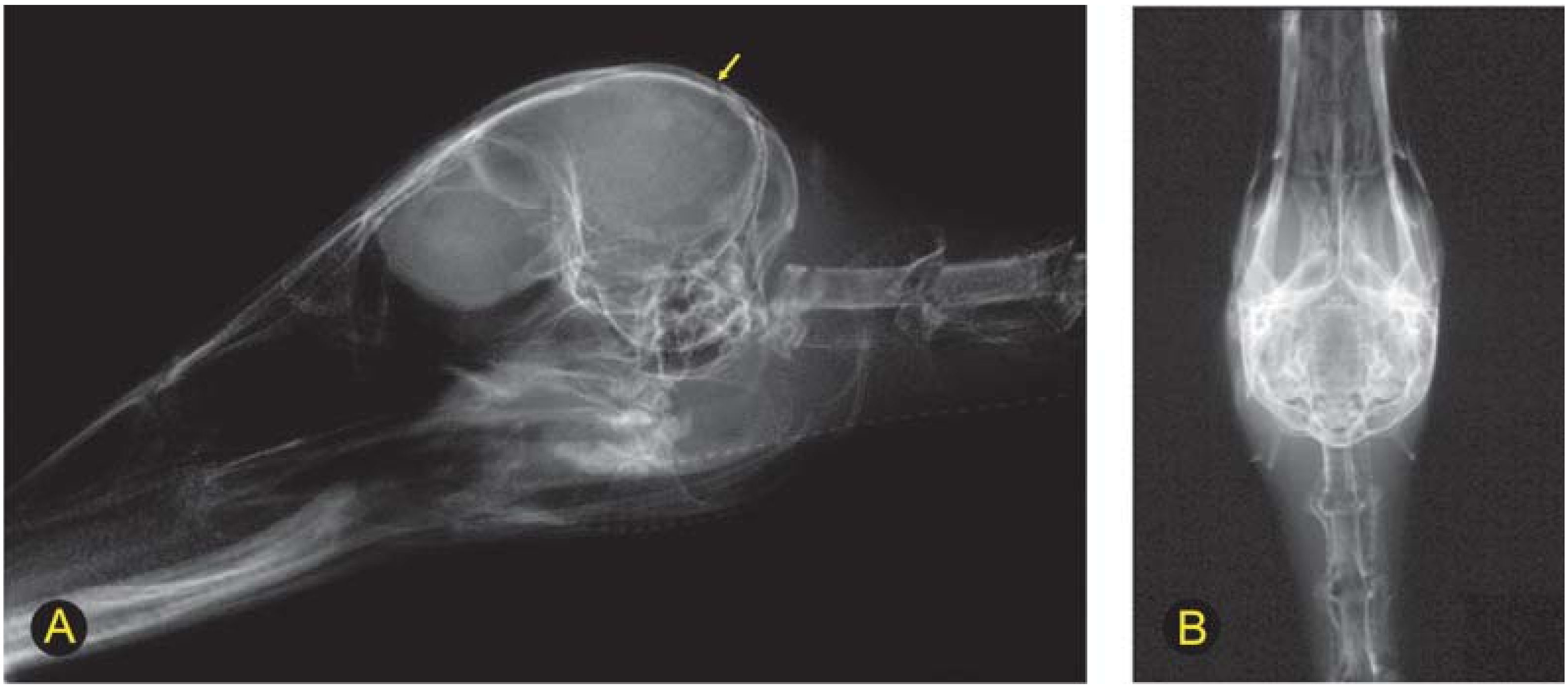

Fig. 1-108: Radiographic images of a mallard's (*Anas platyrhynchos*) head showing a cranial fissure, (A) lateral and (B) ventrodorsal projections. In contrast to the ventrodorsal projection, the fissure (arrow) in the neurocranium is easily observed in the lateral projection.

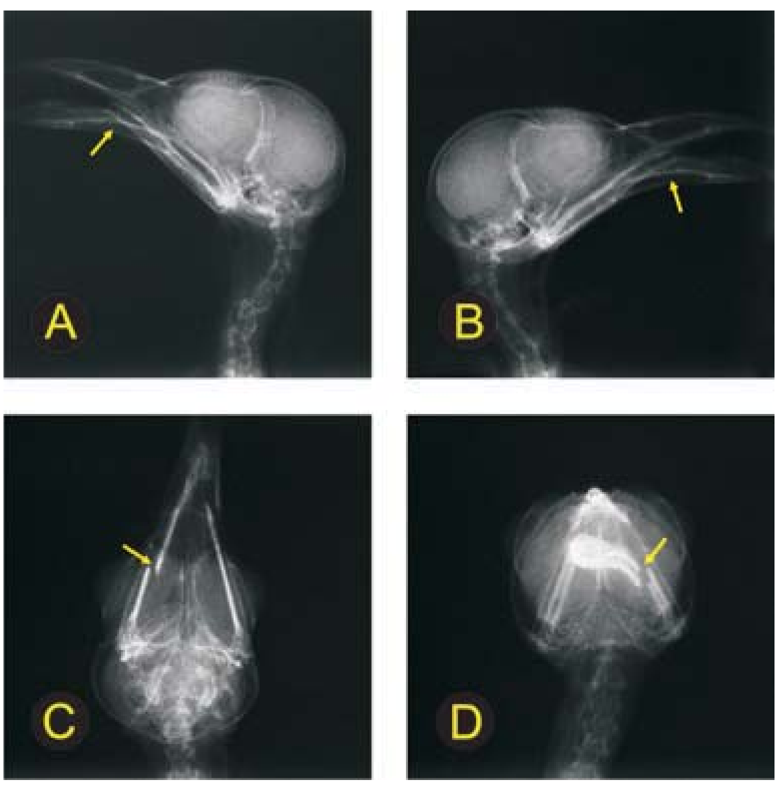

Fig. 1-109: Radiographic images of a red-billed leiothrix's (*Leiothrix lutea*) head with a fracture of the lower jaw, (A) right lateral, (B) left lateral, (C) ventrodorsal, and (D) rostrocaudal projections. The fracture (arrows) in the lower jaw appears different when viewed from different angles.

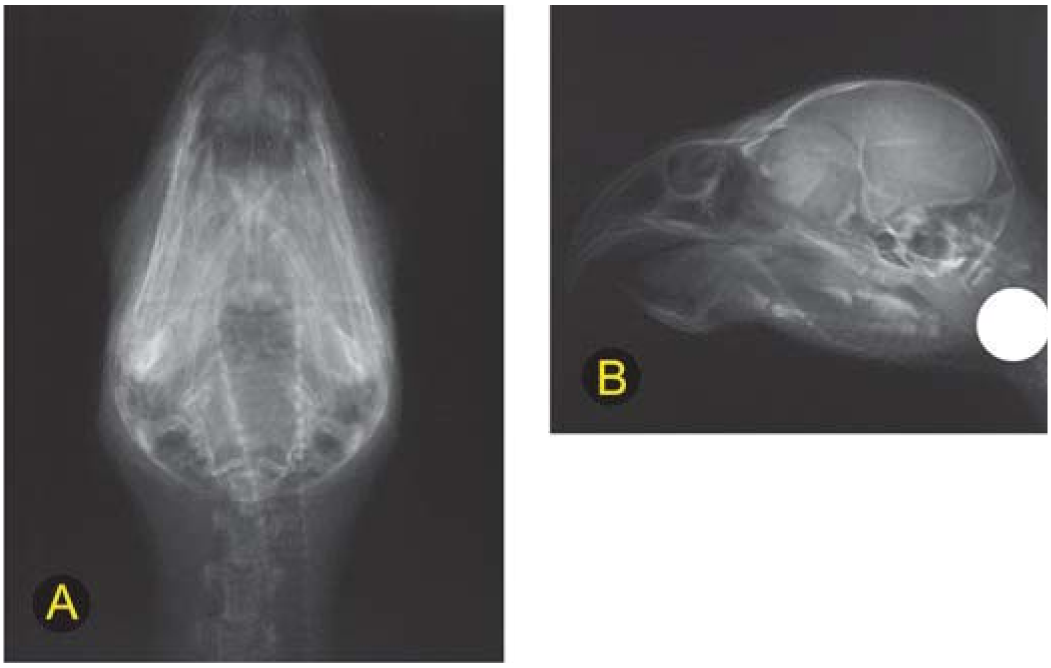

Fig. 1-110: Radiographic images of a young African grey parrot's (*Psittacus erithacus*) head diagnosed with rickets, (A) lateral and (B) ventrodorsal projections. The bones of the head show obvious changes of bending, thickening, and inadequate calcification due to a metabolic disturbance.

Fig. 1-111: Radiography, head, lateral projection, Hyacinth Macaw (*Anodorhynchus hyacinthinus*): osteomalacia. Deformation and osteolytic changes of the upper beak can be seen (bird is narcotized, endotracheal tube is also visible).

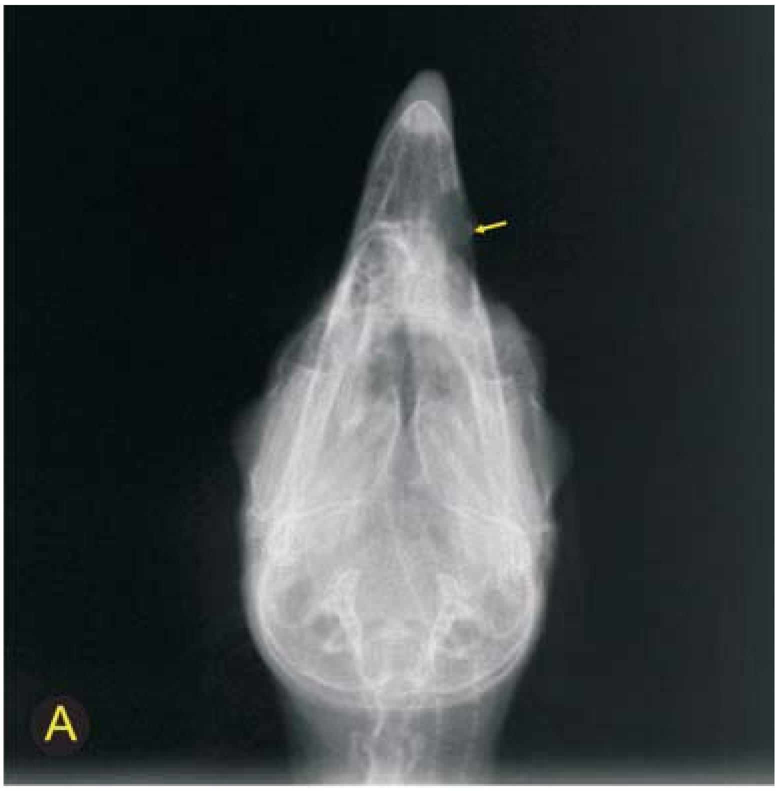

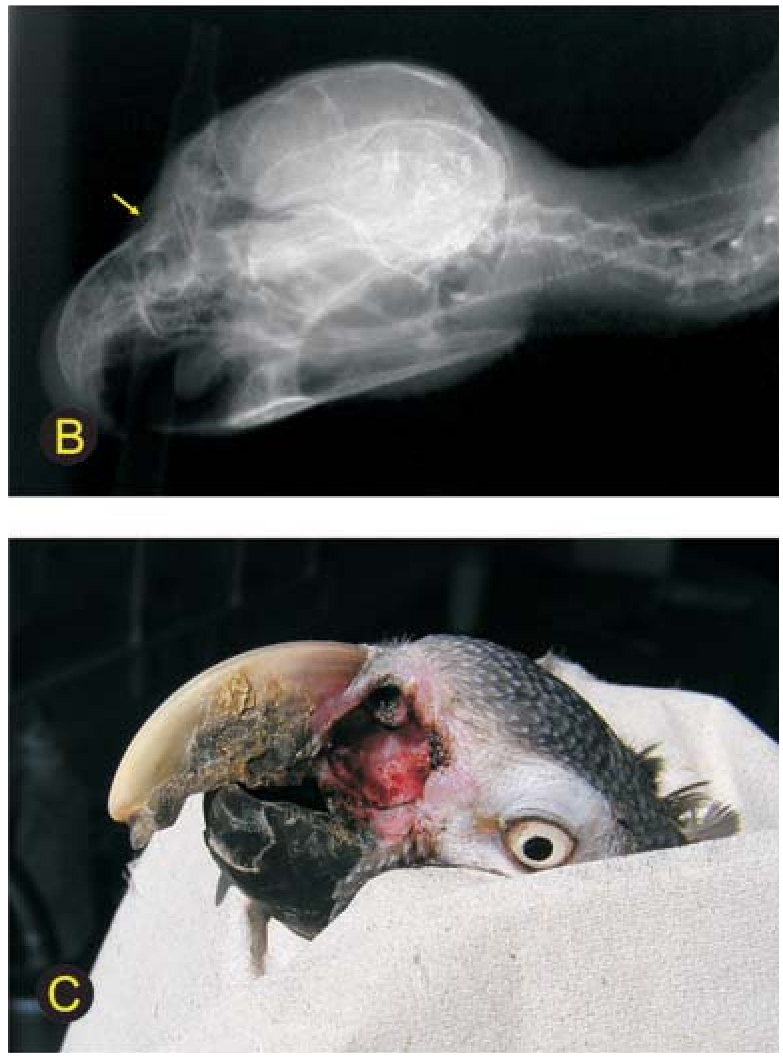

Fig. 1-112: Radiographic images of a Timneh African grey parrot's (*Psitticus erithacus timneh*) head, (A) ventrodorsal and (B) lateral projections. A rhinolith has caused partial destruction of the bones in the surrounding area of the cranium (arrows).

C: Image of bird after removal of the rhinolith.

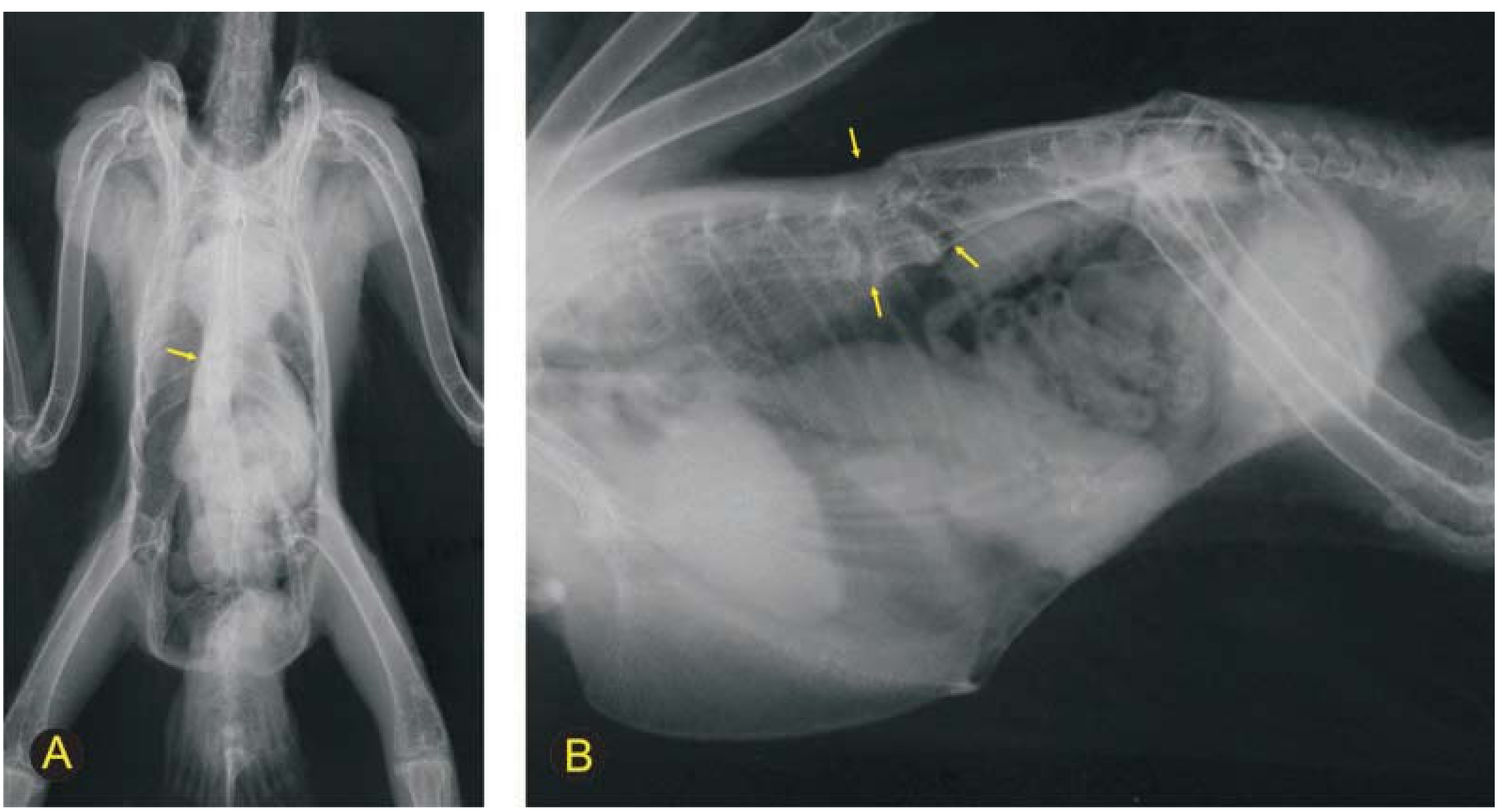

Fig. 1-113: Total body radiographic images of a common kestrel (*Falco tinnunculus*) showing a fracture of the spine (arrows), (A) ventrodorsal and (B) lateral projections. Distended intestinal loops and the heart malpositioned above the sternum due to traumatic rupture of an air sac can be observed in the lateral projection.

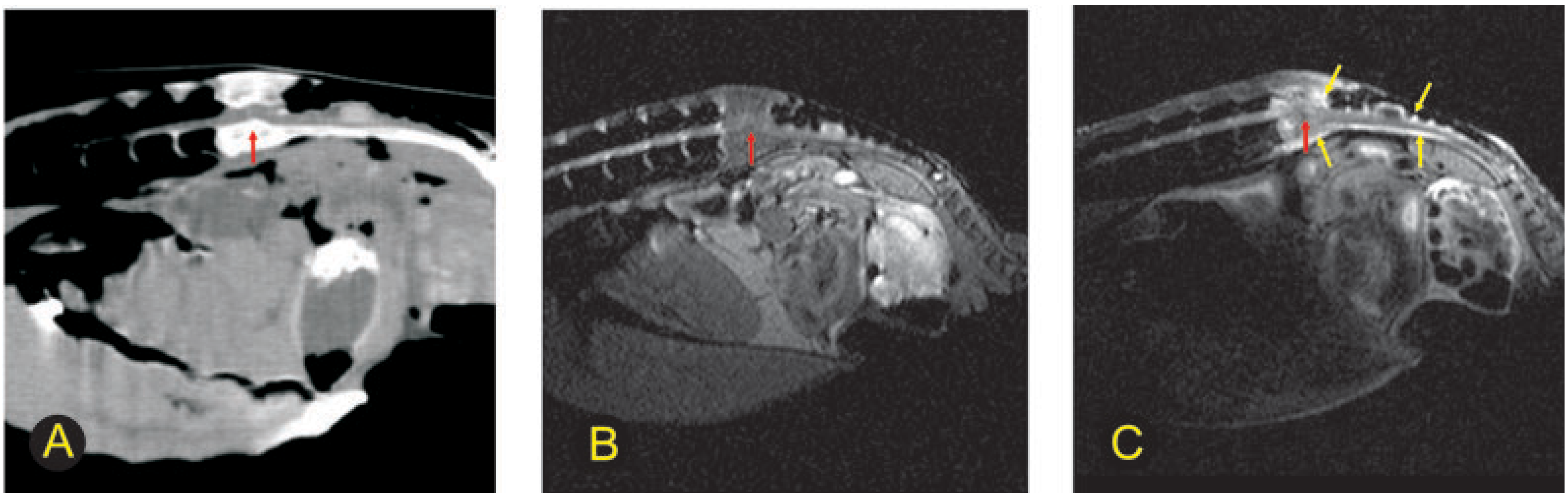

Fig. 1-114:

A: Total body CT image of an African grey parrot (*Psittacus erithacus*) with spinal trauma, sagittal reformation (120 kV, 222 mA, 1.0 mm SD, W: 529, L: 9). The CT image shows a narrowing of the spinal canal due to displaced bone (red arrow). This was not observed in the conventional radiograph.

B, C: Total body MRI image of the same bird, sagittal plane, (B) T1-weighted and (C) T2-weighted images. The spinal cord can be assessed in the MRI image. Using these, one can see the compression of spinal cord tissue (red arrow) due to the narrowing of the spinal canal. In the T2-weighted image, edema, resulting from trauma, can be visualized in the spinal canal (yellow arrows).

D: Clinical presentation of the African grey parrot from A–C.

Fig. 1-115: Total body radiographic image of a Cuban Amazon (*Amazona leucocephala*) diagnosed with rickets, lateral projection. There is a kyphosis of the caudal spine present in this approximately 4-year-old bird, caused by an earlier metabolic disturbance when young. Problems often arise in birds with skeletal abnormalities similar to this patient when the female becomes reproductively active as they may result in egg binding due to the deformed vertebral column. The clearly visible kyphosis of the caudal vertebral column apparent on the lateral projection, was only evident by a relatively short body silhouette on the ventrodorsal projection.

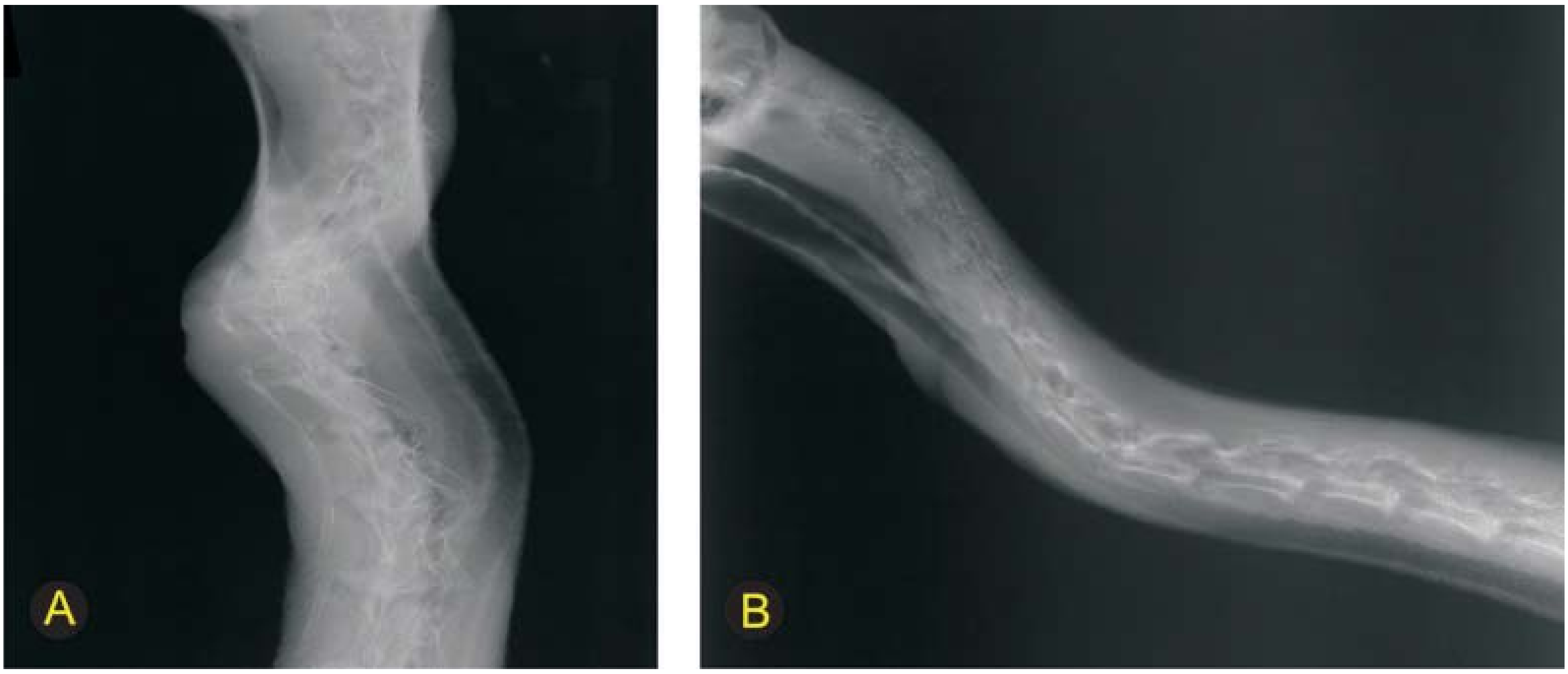

Fig. 1-116: Radiographic images of an emu's (*Dromaius novaehollandiae*) neck, (A) ventrodorsal and (B) lateral projections, showing scoliosis in the region of the cranial and central cervical vertebrae arising from unprofessional capture and fixation of the head.

Fig. 1-117: Radiographic image of a gyrfalcon's (*Falco rusticolus*) foot with a padded bandage diagnosed with pododermatitis (bumblefoot), dorsoplantar projection. Soft tissue swelling and in places osteolysis of the phalanges (arrows) are visible in this image.

1.6 Cardiovascular system

Maria-Elisabeth Krautwald-Junghanns, Michael Pees, Sandra Schroff

For imaging the heart, ultrasonography is a better diagnostic imaging modality than radiography. In general, the clinical signs of cardiovascular insufficiency in birds are often nonspecific. Usually an echocardiographic investigation is performed after a radiographic examination has revealed a suspicion of heart disease. Echocardiography allows for the depiction of individual cardiac structures in motion, thereby enabling the examination to assess changes in cardiac morphology and function. Both CT and MRI examinations play a secondary diagnostic role when examining the heart, especially as an MRI scan is not without risk due to the time needed to obtain the images and the required patient positioning. In addition, there is little empirical data available for avian MRI cardiac image assessment. Birds that present with a suspicion of cardiovascular disease should be handled carefully and maintained in an upright position as much as possible, especially when the clinical picture indicates that the patient has a weak circulation. A further advantage of echocardiography in comparison to the other imaging methods is the ability to hold the patient in an upright position during the examination. Currently, the descriptions of the *in vivo* diagnosis of heart disease consist of case studies; systematic studies have not been published.

1.6.1 Heart

A clear radiographic depiction of the apex of the heart is normal in some bird species (e.g. cockatoos) **(Fig. 1-118)**. In other species, a clear view of the apex of the heart indicates the presence of an air sac rupture as a result of **trauma**, as the air surrounding the heart works as a contrast medium **(Fig. 1-119**; see also **Figs. 1-113, 1-141** and **1-147)**. In such cases, echocardiographic imaging is limited.

In the conventional radiographic examinations, other asymmetrical changes in the form of the heart shadow due to **neoplasia, congenital malformation of the heart,** or **soft-tissue tumors** are rather rare in birds **(Fig. 1-120)**. As a rule, the morphological changes affecting the heart must be substantial to be radiographically evident. Increased radiopacity is sometimes seen with inflammatory changes; however, this is often difficult to definitively assess. In comparison, enlargement of the heart shadow is frequently observed on radiographic images **(Figs. 1-121** and **1-122)**, which may be the expression of cardiac **hypertrophy** or **dilatation.** Cardiac hypertrophy may develop as the consequence of chronic respiratory tract infection, and is considered a secondary disease sign. An enlargement of the heart shadow and/or an increase radiopacity of the heart shadow can also be caused by **pericardial effusion, pericarditis,** or **epicarditis**, or even extensive fatty deposits. A differentiation between hypertrophy, dilatation, and pericardial effusion is not possible using traditional radiographic imaging, therefore an echocardiographic examination should be performed after the intial radiographic assessment. With echocardiography, morphological changes of the epi-, myo-, endo-, and pericardium can be imaged along with **valvular dysfunctions**. Reference values of the size and contractility of the heart are available for a relatively few avian species (Table 1-2).

The most frequently diagnosed pathological findings involving the avian heart through echocardiography are hydropericardium and hypertrophy or dilatation of the right ventricle. The latter two changes are often caused by a **right-sided cardiac insufficiency (Figs. 1-123B, C)**. In such cases, the right ventricle can appear almost as large as the left, with the ventricular walls being thickened. Hypertrophy of the right ventricle is usually associated with hypertrophy of the right muscular AV-valve. **Changes in the left ventricle** are, in comparison to the right ventricle, rarely diagnosed. Left ventricular abnormalities are normally associated with changes to the right side of the heart and congestion in the pulmonary circulation. It is not uncommon that the underlying etiology of left ventricular disease is valvular insufficiency. The valves are echogenic and easily differentiated, therefore valvular disease is relatively easy to diagnose. The use of Doppler for assessing blood flow in the region of the heart valves is possible; however, the ability to effectively utilize this echogenic function depends on the experience of the examiner.

Microcardia (Fig. 1-118) is usually associated with severe dehydration of the patient. The heart appears greatly diminished in size and is often separated from the sternum. In cases involving **pericarditis** (e.g. infections, gout), the pericardium can be readily observed because it will be hyperechoic; the assessment is, however, difficult. In birds with **hydropericardium**, there is an anechogenic region around the heart clearly visible on the sonogram. Usually, the pericardium itself is visible as an outer boundary; especially if ascites is also present **(Figs. 1-122C, D, 1-123A, B** and **1-124C)**. The apex of the heart is movable due to the surrounding fluid, and this can be assessed during the examination. In individual cases, it may be necessary to perform a needle aspirate of the pericardium under ultrasonographic guidance. Furthermore, echocardiography is well suited for determining the degree of success in treating hydropericardium or controlling the contractility of the ventricle once the patient has been administered medication.

1.6.2 Blood vessels

Due to the **calcification** of their **blood vessel walls**, the vessels of older birds may be observed on radiographic images as radiopaque structures (see **Figs. 1-130B, 1-142** and **1-144**). The transition to arteriosclerosis is seamless. Typical radiographic presentation for avian **arteriosclerosis** is, in addition to an increased density of the heart shadow, an increased radiopacity of the caudal lungs due to congestion. Only in the final stages of arteriosclerosis is there an obviously increased radiopacity of parts of the calcified blood vessel – mainly the aorta and/or the pulmonary artery **(Fig. 1-125)**. Furthermore, congested large cardiac vessels can be easily differentiated in the lateral projection, which is often the result of congestion in the pulmonary or systemic circulation (see **Fig. 1-134)**. The lack of such radiopacity does not mean that arteriosclerosis as a disease diagnosis can be dismissed.

At the use of echocardiography to image blood vessel walls has not been scientifically investigated. Clinical examination of blood vessel walls has shown that the assessment of the aorta close to the heart is possible and that hyperechoic areas indicate the presence of calcification within the vessel wall. However, the diagnosis present, of vascular disease using echocardiography is very subjective and requires an experienced examiner. Therefore the evaluation of vascular **congestion** using this diagnostic modality is significantly more important than diagnosing vascular disease. Such congestion can be particulary obvious in the liver **(Fig. 1-126** and **1-174)**. The congested blood vessels can also be imaged using Doppler **(Fig. 122E;** see also **Figs. 1-167B, C).** Dilated blood vessels may be found in CT images, too **(Fig. 1-134)**.

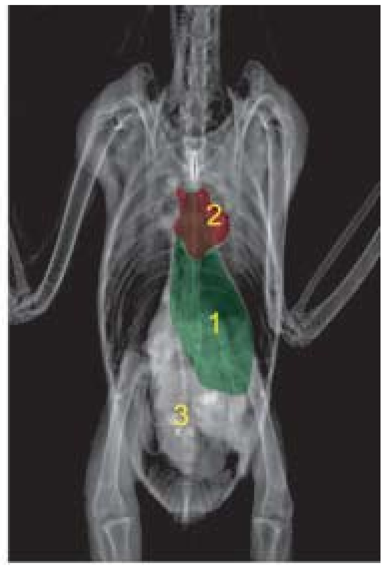

1: proventriculus
2: heart
3: loop of intestine

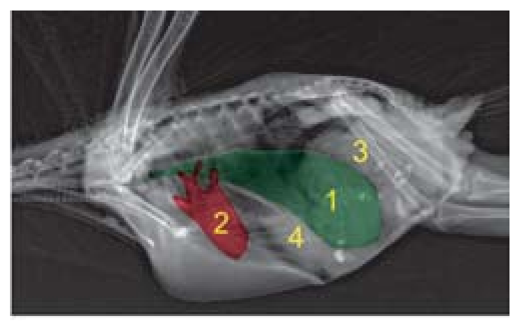

1: proventriculus
2: heart
3: loop of intestine
4: liver

Fig. 1-118: Total body radiographic images of an umbrella cockatoo (*Cacatua alba*) diagnosed with microcardia caused by fluid loss via the gastrointestinal tract, (A) ventrodorsal and (B) lateral projections. The proventriculus (1) is severly enlarged (neurogenic proventriculus dilatation disease):

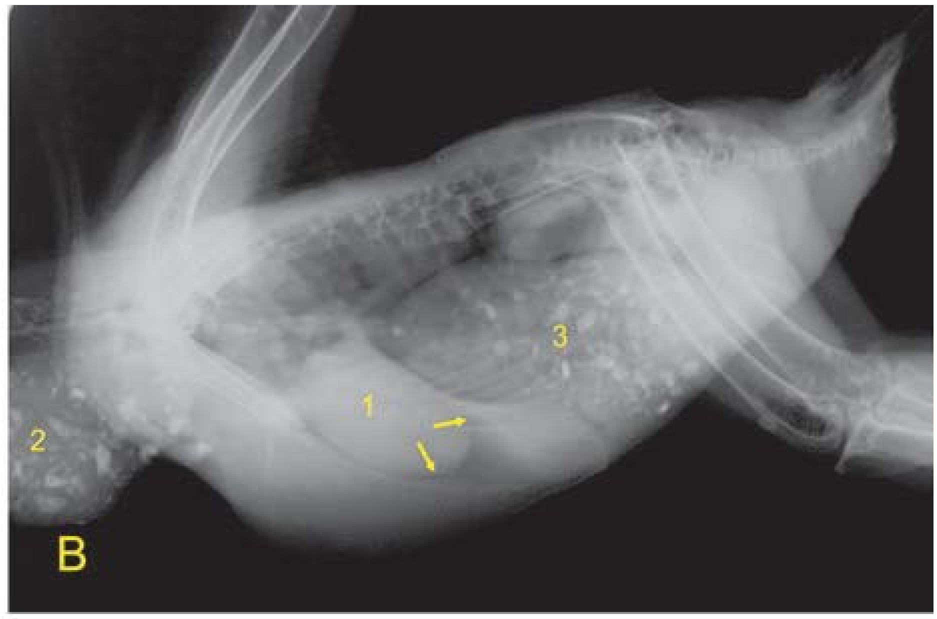

1: heart
2: crop-like dilatation
3: stomach

arrows: heart apex

Fig. 1-119: Total body radiographic images of a common buzzard (*Buteo buteo*) with air sac rupture due to landing trauma, (A) ventrodorsal and (B) lateral projections. A rim of air has formed around the apex of the heart (arrows) as a result of the air sac rupture, causing this area to be well demarcated.

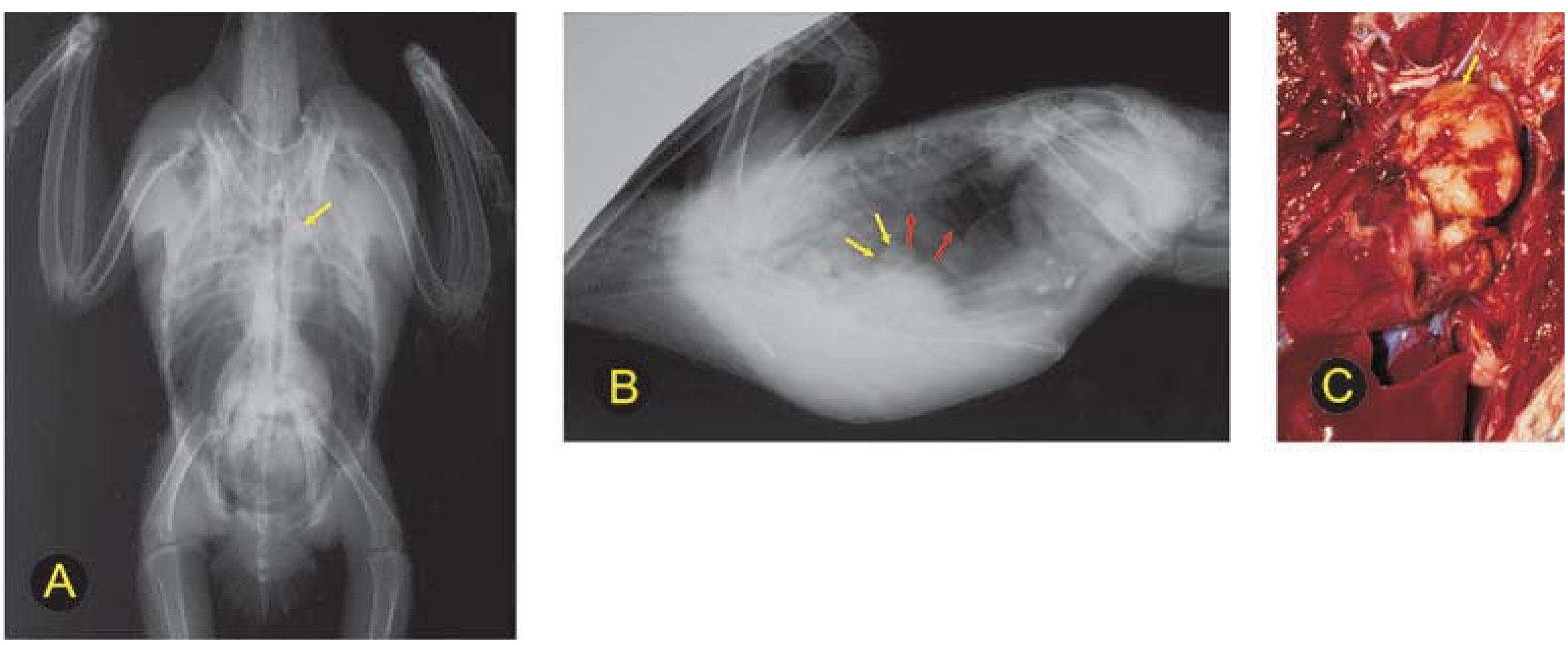

Fig. 1-120: Total body radiographic images of an African grey parrot (*Psittacus erithacus*) diagnosed with mycotic granuloma on the base of the heart, (A) ventrodorsal and (B) lateral projections. A radiodense tumor (yellow arrows) is present on the base of the heart. In the lateral projection, it is evident that the tumor has caused a dorsal displacement of the caudal esophagus (red arrows).

C: Obduction site, same bird: granuloma on the base of the heart (arrow).

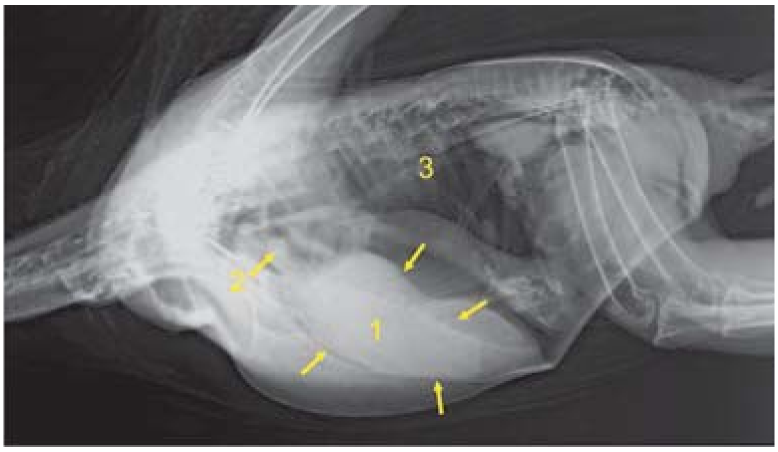

1, arrows: heart
2: brachiocephalic trunk
3: aorta

Fig. 1-121: Total body radiographic image of a white-tailed eagle (*Haliaeetus albicilla*) diagnosed with cardiomegaly of an unknown etiology, lateral projection. The heart (1, arrows) is generally enlarged and radiopaque. The vessels are unremarkable in this image.

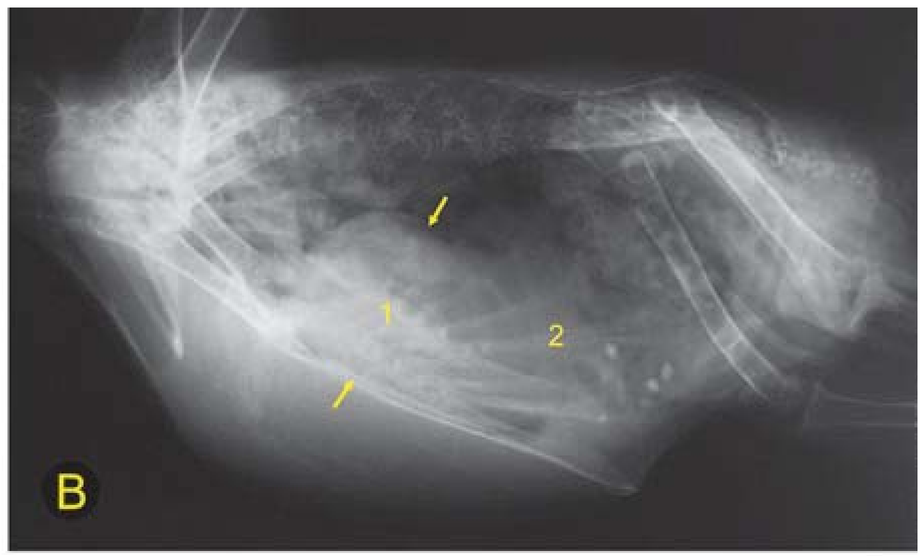

1, arrows: heart
2: liver
3: left ventricle
4: left atrium
5: right ventricle
6: ascites
7: liver
8: pericardium

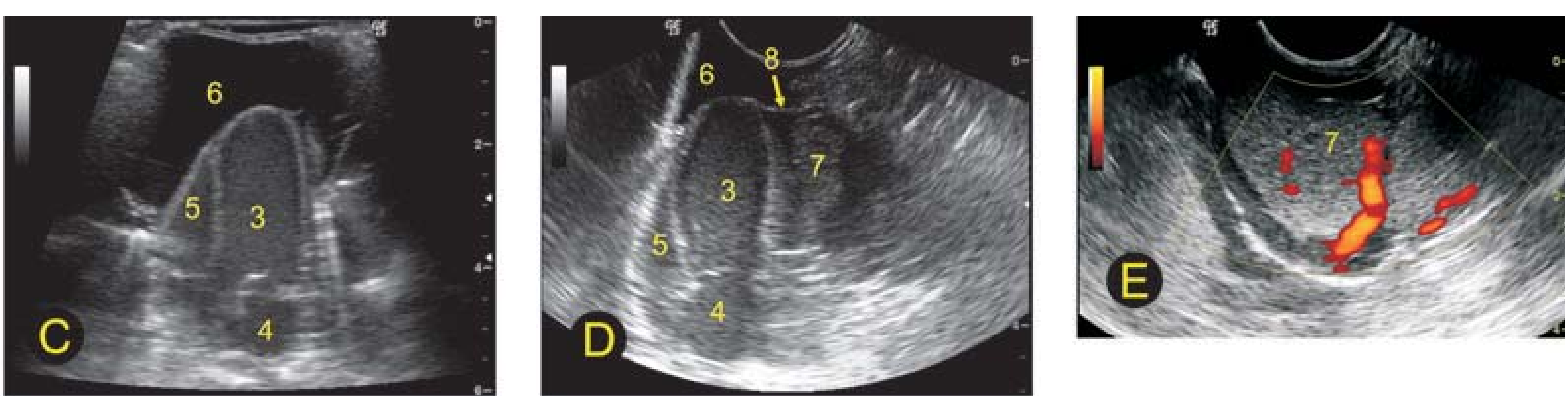

Fig. 1-122:

A, B: Total body radiographic images of an African grey parrot (*Psittacus erithacus*) diagnosed with cardiac insufficiency, (A) ventrodorsal and (B) lateral projections. The heart (1, arrows) is clearly enlarged. The liver shadow (2) is difficult to differentiate and is enlarged; the typical hour-glass shape is no longer present.

C–E: Ultrasonographic images of the same bird, ventromedian coupling site, 7 MHz (C) or 10 MHz (D, E): PD 6 cm (C) or 4 cm (D, E), which is confirmed in the color Doppler (E). Enlarged chambers of the heart (3, 4, 5) with collection of fluid in the body cavity (6). The liver (7, D) appears congested. The pericardium (8) is separated from the heart.

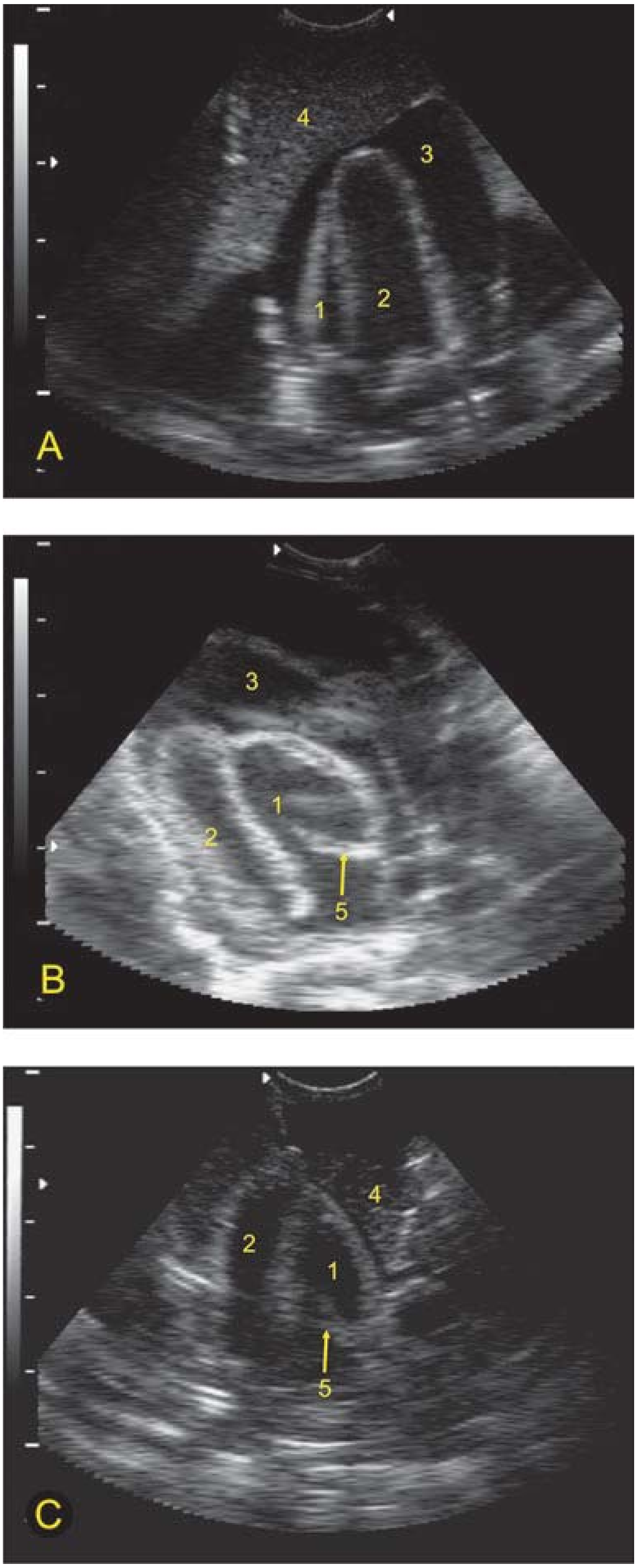

1: right ventricle
2: left ventricle
3: ascites
4: liver
5: muscular AV valve

Fig. 1-123:

A: Ultrasonographic image of an African grey parrot (*Psittacus erithacus*) diagnosed with avian chlamydiosis and hydropericardium, ventromedian coupling site, 7.5 MHz, PD 6 cm. The heart's size and function are unremarkable in this image

B: Ultrasonographic image of an African grey parrot (*Psittacus erithacus*) diagnosed with right-sided cardiac insufficiency, hypertrophy, and dilatation, ventromedian coupling site, 7.5 MHz, PD 6 cm. The right ventricle (1) is almost as large as the left ventricle (2). The muscular AV valve (5) is severly hypertrophied (3: ascites).

C: Ultrasonographic image of a blue-fronted Amazon (*Amazona aestiva*) diagnosed with right-sided cardiac insufficiency, hypertrophy, and dilatation, ventromedian coupling site, 7.5 MHz, PD 6 cm. The heart disease observed in this patient, in addition to hydropericardium, is among the most common sonographically diagnosed heart abnormalities.

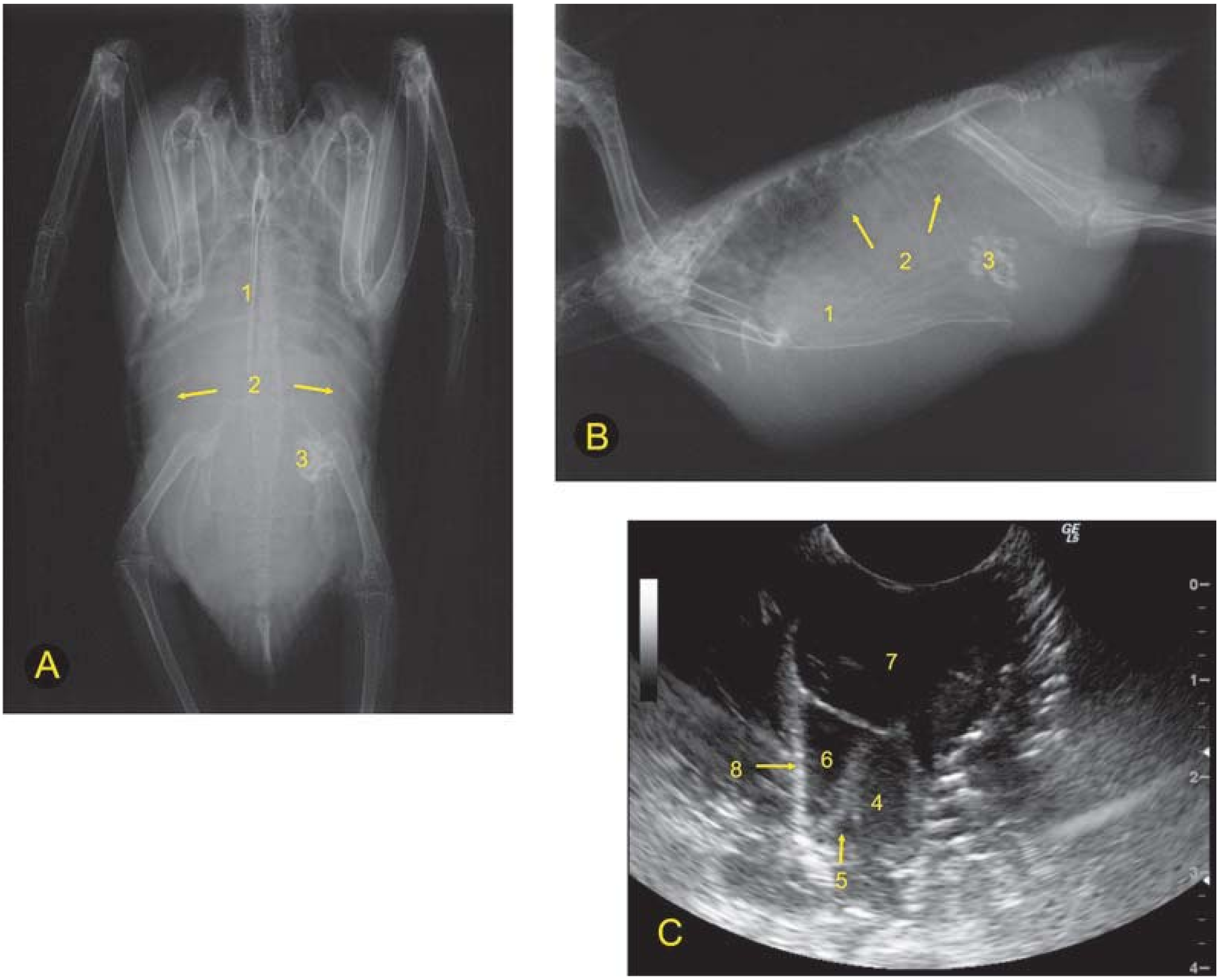

Fig. 1-124:

A, B: Total body radiographic images of a cockatiel (*Nymphicus hollandicus*) diagnosed with cardiomegaly, liver congestion, and ascites, (A) ventrodorsal and (B) lateral projections. Both the heart (1) and liver (2) are obviously enlarged. The ventriculus (3) has been displaced caudally.

C: Ultrasonographic image of the same bird, 10 MHz, PD 4 cm: the heart (4: left ventricle, 5: right ventricle) is surrounded by fluid lying in the pericardium (6).

1: heart
2: liver
3: ventriculus
4: left ventricle
5: right ventricle
6: pericardium
7: ascites
8: sternum

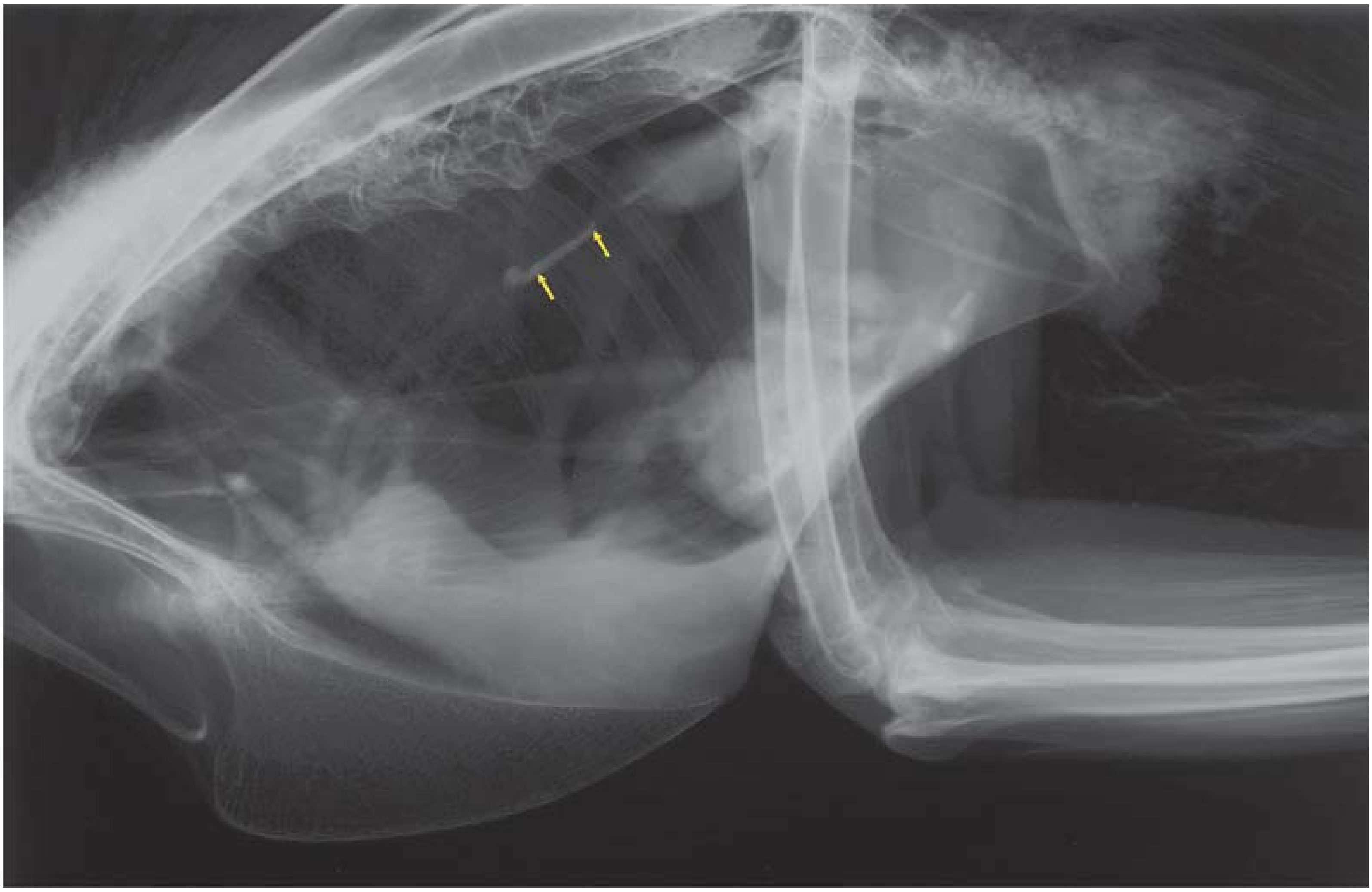

Fig. 1-125: Total body radiographic image of an Eurasian eagle owl (*Bubo bubo*) diagnosed with arteriosclerosis and aortic calcification, lateral projection. The radiodense abdominal aorta (arrows) can be clearly observed in the lateral projection; this finding was not visible in the ventrodorsal projection.

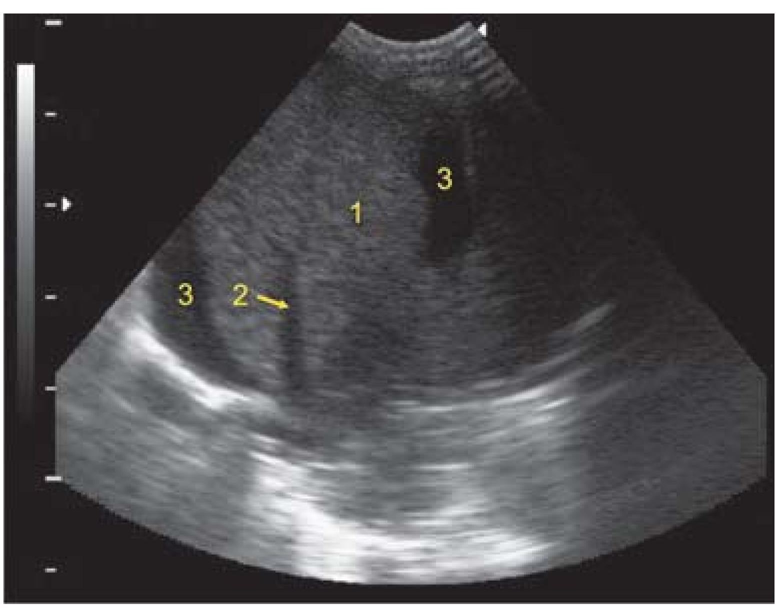

1: liver
2: blood vessel
3: ascites

Fig. 1-126: Ultrasonographic image of an African grey parrot (*Psittacus erithacus*) diagnosed with ascites and liver congestion due to cardiac insufficiency, ventromedian coupling site, 7.5 MHz, PD 6 cm.

1.7 Respiratory tract

Maria-Elisabeth Krautwald-Junghanns

Diseases of the lung and air sac system frequently occur in birds and when diagnosed are indications for diagnostic imaging examinations. Inspiration and expiration are not required to assess lung images due to the anatomy of the avian lung. The avian lung volume remains more or less constant and therefore is not a significant criterion for disease diagnosis. Conventional radiodiagnostic techniques are the most important diagnostic measures to assess tissue abnormalities resulting from respiratory disease. However, in most cases, only advanced or severe disease conditions can be observed affecting the respiratory tract of birds. Mild changes or changes in an early stage of a disease are better diagnosed using a reconstructive method (e.g. CT). Owners usually recognize clinical signs of respiratory illness only after the disease processes have reached an advanced stage. This allows for a greater degree of success in revealing clear signs of disease involving the patient's respiratory system using traditional radiographic imaging techniques. Currently, no information has been published regarding the use of ultrasonography for examining the avian respiratory system.

A radiographic examination of the bird is particularly indicated in cases where respiratory mycotic disease is a top differential diagnosis. Respiratory mycotic disease is one of the commonly diagnosed diseases in tropical avian species (e.g. parrots, mynas), raptors, and waterfowl **(Figs. 1-127** to **1-130)**. Radiographs in combination with laboratory diagnostic testing (e.g. tracheal swab, serological detection of antibodies) are still the most important techniques for determining both a diagnosis and prognosis of respiratory disease affecting an avian patient. A prerequisite to maximizing the radiographic diagnosis of pathological changes of the lung and air-sac system is symmetrical positioning of the bird. With improper positioning of the patient, the asymmetrical changes of the respiratory system cannot be adequately assessed. In addition, muscle summation over parts of the respiratory tract can be misinterpreted as shadows or radiopaque areas **(Fig. 1-131B)**.

With CT, it is possible to recognize changes in the respiratory tract earlier and with more precision – especially changes that occur in the lung – due to the lack of summation in the individual slices **(Figs. 1-132** to **1-135)**. With various post-processing methods (density measurement, highlighting and volume determination, **Figs. 1-133A, B;** *q.v.* Chap. 1.3.3) pathological changes are easier to define and follow-up investigations can provide information about the course of the disease or healing. The measurement of lung density has proven to be an important parameter in assessing pathological changes to this tissue. Computed tomographic imaging is, therefore, primarily used for investigating valuable birds after purchase, when the patient has nonspecific clinical or radiographic test results regarding the health of its lungs, or for follow-up examinations.

1.7.1 Nasal passages and sinuses

Infections of the upper respiratory tract (e.g. rhinitis, **sinusitis**), appear on radiographic images as radiopacities within the region of the affected cavities **(Figs. 1-136** to **1-140)** due to a large accumulation of cellular secretions or the formation of granulomas (e.g. mycotic infections). In chronic cases, even the surrounding bones of the nasal passages and sinuses can be infected (see **Fig. 1-112A, B)**. In many cases of soft-tissue swelling, the use of contrast media or CT will provide more definitive results for determining the extent of disease involvement. With a CT examination, not only can the extent of the disease changes be imaged but also the nature of the tissue abnormalities can be determined using density measurements. In addition, highlighting may be used to determine the volume of air-filled spaces within the cranium (see **Fig. 1-138**, and Chap. 1.3.3). Follow-up CT examinations will allow for a more precise prognosis of a diagnosed sinusitis case and treatment response. Both traditional and reconstructive radiological methods can be combined with the use of contrast media **(Fig. 1-140)**. The flow of contrast material through the nasal passage and infraorbital sinus will provide information regarding the presence of an obstruction in the upper respiratory system due to sinusitis and aid in the diagnosis of **choanal atresia**

1.7.2 Trachea and syrinx

The trachea can be palpated and inspected endoscopically so that radiographic investigations are only indicated with specific case presentations (e.g. suspicion of foreign body, traumatic injuries). Allthough the syrinx can be seen on radiographs **(Figs. 1-130, 1-131B, 1-141** and **1-142B)**, it frequently may not be adequately observed because of summation by the coracoid, cranial heart, and flight muscles. The presence of **syrinx stenosis** can be diagnosed indirectly on radiograph images when overextension of the abdominal air sacs (air trapping) is noted **(Figs. 1-127, 1-143** and **1-144B)**. Due to the valve-like effects of syringeal narrowing, expiration is hindered resulting in the air sac congestion.

Both the trachea and the syrinx are readily identified on CT images and can be measured. However, there are few indications for the use of CT diagnostic imaging of the trachea and syrinx.

1.7.3 Lungs

Radiographic imaging of lung abnormalities is best performed via the lateral projection (see **Figs. 1-128** and **1-131)** as this projection provides the best view of a normal lung tissue's honeycomb pattern. By comparison, the VD projection provides useful information regarding symmetrical changes in the lung tissue **(Fig. 1-130)**. The comparison to a normal radiographic image from the same avian species can be helpful in the assessment of a **homogenously dense lung shadow (Fig. 1-142).** If on first observation, there are only unremarkable changes in the lung field then the radiographs should be more closely assessed using a lens, especially in small birds. With CT imaging, it is possible to assess lung abnormalities more precisely using lung density measurements. **Dilatation of the large bronchi (Fig. 1-128)** or **rounding of the caudal edge of the lungs (Fig. 1-129)** are two other nonspecific radiographic signs of lung disease, which are easier to recognize using CT imaging. A diffuse lung tissue radiopacity or thickening of the bronchial walls can be frequently identified after infiltration or as a consequence of exudative processes. As a result of granuloma formation, mycotic lesions often appear as **irregular patches in the lung field (Figs. 1-127** to **1-130)** of varying sizes on traditional radiographic images. Conversely, bacterial infections of lung tissue appear as a homogenous density within the lung field **(Fig. 1-142)** with the exception of tuberculosis, in which radiopaque foci are formed **(Fig. 1-145)**. Compared to mammalian species, the differentiation from lung neoplasms is not significant in birds as such neoplasms are extremely rare and focal tumors **(Fig. 1-145)**, in general, result from infectious disease (e.g. fungal disease). With CT imaging, pathological changes of the pulmonary vessels and the secondary bronchi can also be observed. Anatomically, **increased lung density** is often related to reduced imaging of the bronchi or blood vessels. A lack or inadequate visualization of the main bronchus may be observed in avian patients diagnosed with severe mycotic infection causing a compensatory dilatation of the secondary bronchi **(Fig. 1-133)**. Diagnosis of dilated pulmonary vessels is often associated with an increased radiopacity of the vascular walls (e.g. arteriosclerotic processes; **Figs. 1-130** and **1-142**) or due to congestion of the pulmonary circulation **(Fig. 1-134)**. Lung tissue in which there are focal areas of calcification are nonspecific signs of chronic, usually infectious disease that can be observed using both radiographic and CT imaging modalities.

1.7.4 Air sacs

The anatomic assessment of the air sacs is difficult with both traditional and CT radiographic imaging modalities. Using CT imaging, it is not always possible to differentiate the air sacs from the surrounding soft tissues due to the thin walls of the sacs. As a rule, air sac abnormalities observed on traditional radiographic imaging (see below: thickening, calcification) are better visualized without summation utilizing CT **(Fig. 1-132)**. **Changes in air sac volume** (e.g. narrowing) are often noted on traditional radiographic images; however, the extent of the affected tissue can only be determined by CT **(Fig. 1-133B)**. Diagnostically and prognostically, air sac volume changes are not of any great importance when determining a diagnosis and prognosis of a case in contrast to the lung density, as the air sac volume can undergo large physiological variation in birds (e.g. during egg production).

In a traditional radiographic examination of an avian air sac system, two projections should be taken, VD and lateral. While the symmetry of the air sac changes can be assessed in the VD projection **(Figs. 1-127A, 1-130A** and **1-145A)**, **thickening of the air sac walls** (»cavern« formation) is better visualized in the lateral projection **(Figs. 1-127B** and **1-129)**. Only with extreme tissue changes are thickened air sac walls visible on the VD projection (**Fig. 1-127A)**. Stenosis of the upper respiratory tract can be diagnosed by an overdilatation of the abdominal air sacs (air trapping; **Figs. 1-143** and **1-144**) which can be observed on both the VD and lateral projections. In severe disease conditions or more rarely after exhaustion, an adverse affect on the patient's respiration will result in a **dilatation of the axillary diverticulum** which may be noted in the VD projection **(Fig. 1-131A)**. Overdilatation of the cervical air sacs **(Fig. 1-146)** is frequent observed in homing pigeons after an exhausting race. Injuries affecting the cervical air sacs will often result in the formation of extensive subcutaneous emphysema. If such cases of subcutaneous emphysema are refractory to treatment, the possible cause of the **air sac injury** (e.g. foreign body) should be identified through the use of radiographic imaging. Rupture of the cranial air sac walls can also occur due to trauma (e.g. collisions). Radiographically, rupture of the cranial air sac is characterized by improved imaging of the internal organs, especially the heart and liver **(Figs. 1-141** and **1-147)** as the air surrounding the organs acts as a negative contrast medium. With increased resorption of air and recovery of the traumatized avian patient, imaging of the internal organs becomes less of a useful diagnostic tool. The air sacs are also often affected by infectious diseases within the lungs. The air sacs are frequently altered bilaterally to the same degree in a response to **air sac inflammation** caused by bacterial infections, **(Fig. 1-142A)**. In the lateral projection **»cavern« formation (Fig. 1-129)**, asymmetrical air sac changes together with thickened walls and in the later disease stages, focal areas of shadowing **(Fig. 1-128B)**, are often characteristic of mycotic air sacculitis.

When using the VD projection in obese birds a homogenous shadowing of the air sacs may be apparent (this superimposition arises because the x-ray beam has to pass through the fat; **Fig. 1-148)**. However, no thickened air sac walls can be seen when using the lateral projection.

Calcification of the air sac walls can be clearly recognized and are a nonspecific sign for chronic infectious disease.

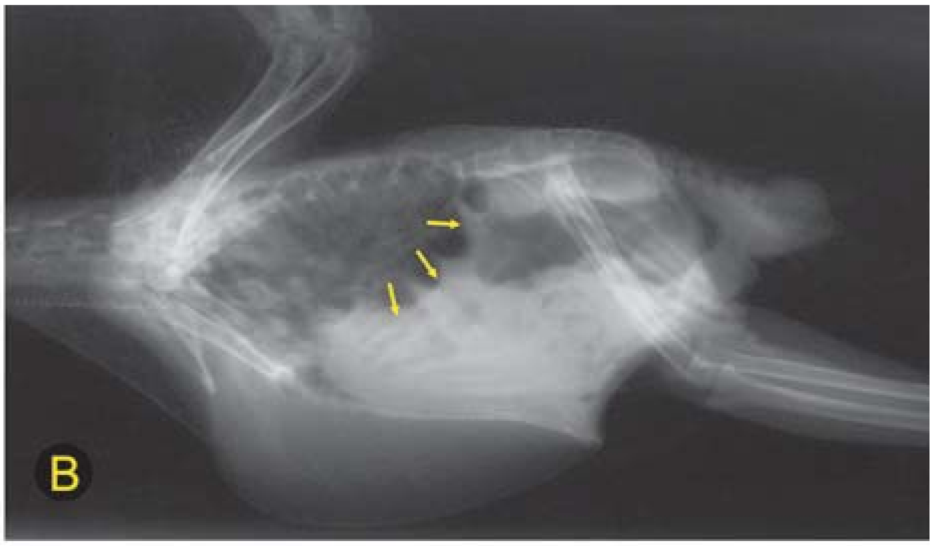

Fig. 1-127: Total body radiographic images of a Jardine's parrot (*Poicephalus gulielmi*) diagnosed with severe advanced mycosis of the respiratory tract, (A) ventrodorsal and (B) lateral projections.

A: The internal organs cannot be differentiated from each other due to the presence of nonhomogenous concretions throughout the body cavity. In some areas, thickened edges of the air sacs (arrows) can be seen. Air trapping is present in the abdominal air sac.

B: Nonhomogeneous compacted lung field. Cavern formation (arrows) makes it almost impossible to discern the individual internal organs.

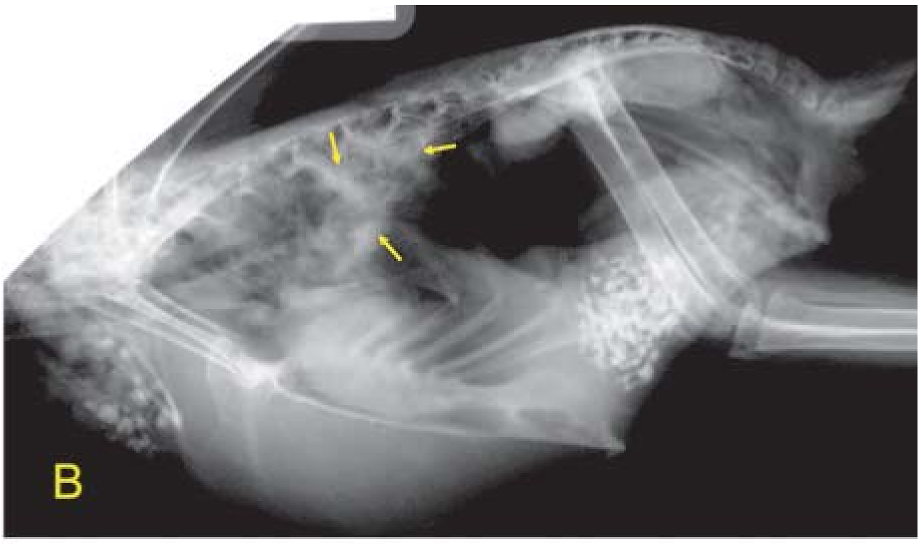

Fig. 1-128: Total body radiographic images of a blue-fronted Amazon (*Amazona aestiva*) diagnosed with pulmonary mycosis, (A) ventrodorsal and (B) lateral projections.

A: When compared to the lateral projection (B), the changes in the lung are barely visible due to summation in the ventrodorsal view, especially with the wings lying too close to the body.

B: Radiodense nonhomogeneous concretions in the caudoventral area of the lungs (arrows). A dilated bronchus is visualized lying over the trachea.

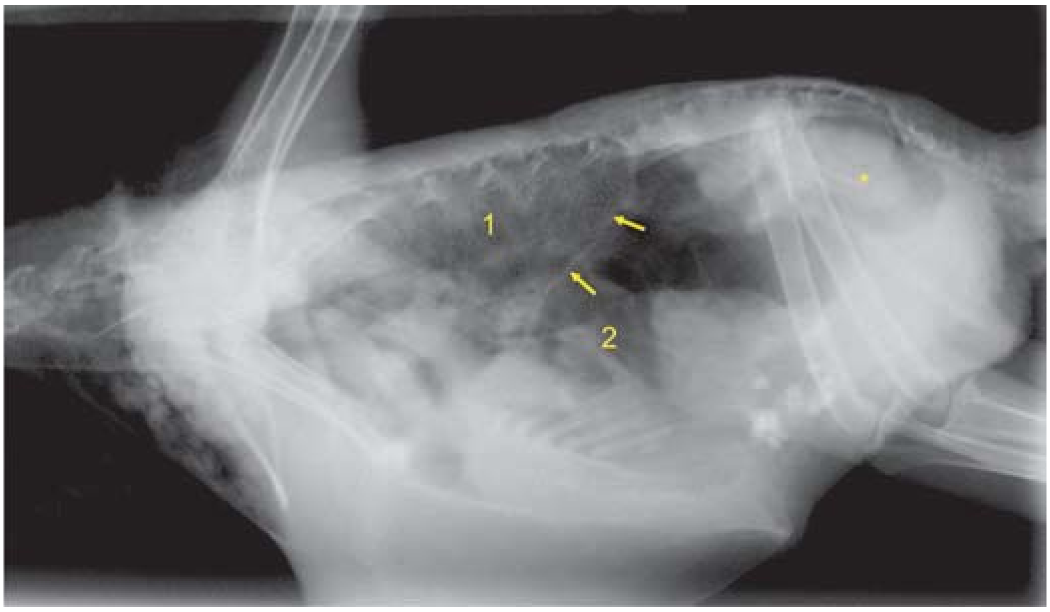

1: lung
2: cavern formation
*: air trapping
arrows: rounded caudal lung edge

Fig. 1-129: Total body radiographic image of an African grey parrot (*Psittacus erithacus*) diagnosed with advanced mycosis of the respiratory tract, lateral projection. Rounding of the caudal edge of the lungs (arrows), compaction in the ventral area of the lungs, (2) cavern formation, and air trapping (*) are all evident in this image.

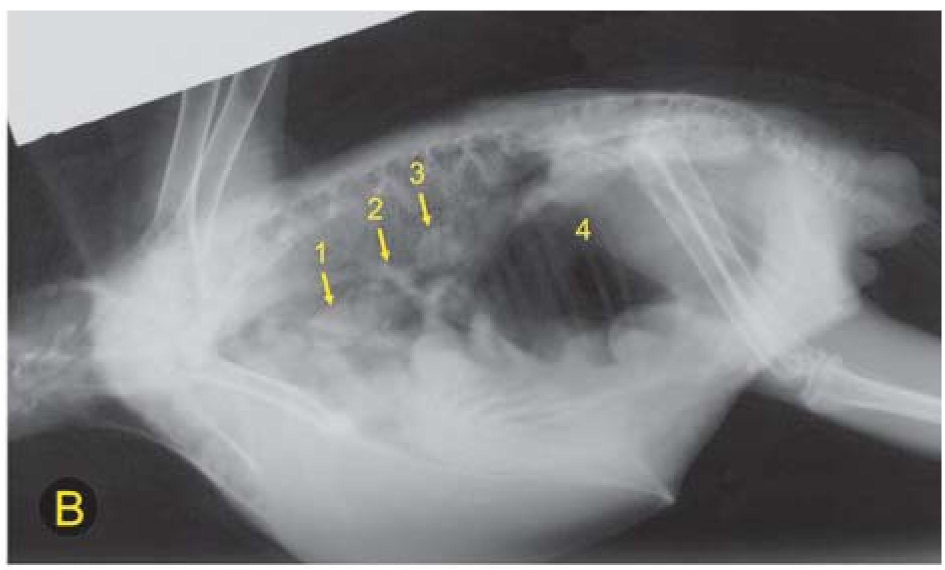

1: syrinx
2: large heart vessels
3: granuloma
4: air sacs

Fig. 1-130: Total body radiographic images of an African grey parrot (*Psittacus erithacus*) diagnosed with mycosis of the respiratory tract, (A) ventrodorsal and (B) lateral projections.

A: nonhomogeneous, compacted lungs and (4) air sacs. The granuloma (3) in the left lung field is more difficult to see in the lateral projection.

B: syrinx region (1), compact radiopaque large heart vessels (2). A region of compaction (3) is present in the ventral area of the lungs. The caudal air sacs (4) are compacted.

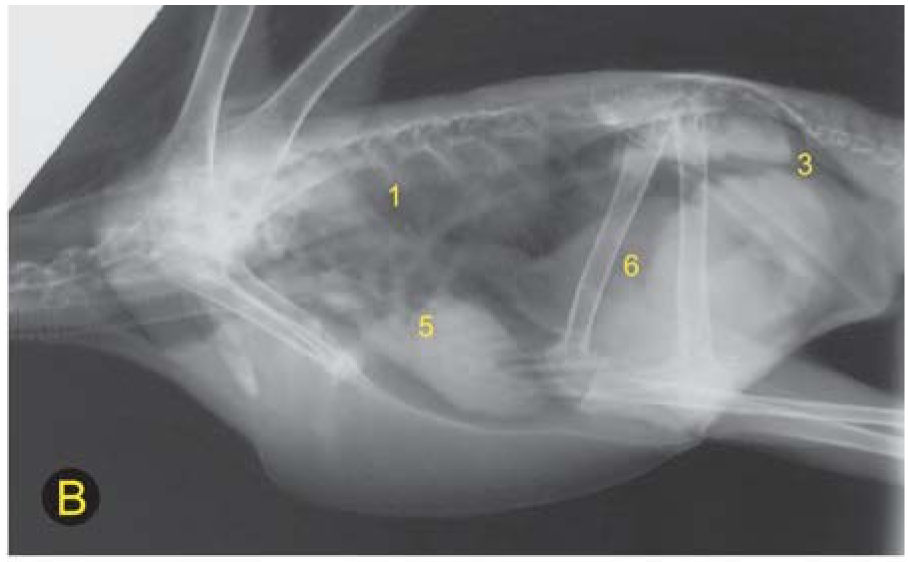

1: lung
2: axillary air sacs
3: abdominal air sacs
4: subcutaneous emphysema
5: heart
6: proventriculus

Fig. 1-131: Total body radiographic images of a red-and-green macaw (*Ara chloroptera*) that was exhausted after escaping, (A) ventrodorsal and (B) lateral projections.

A: Homogenous compaction of the thoracic and abdominal air sacs and the lungs (1); overexpansion of the axillary air sacs (2) and of the abdominal air sacs (3); subcutaneous emphysema (4) due to exertion.

B: Due to overexpansion of the anterior air sacs, the heart, blood vessels and syrinx region (5) are clearly visible. The walls of the posterior air sacs cannot be visualized due to the legs not being pulled far enough back, leading to summation. The assessment of the enlarged proventriculus (6) must also be done with reservation because the bird was incorrectly positioned.

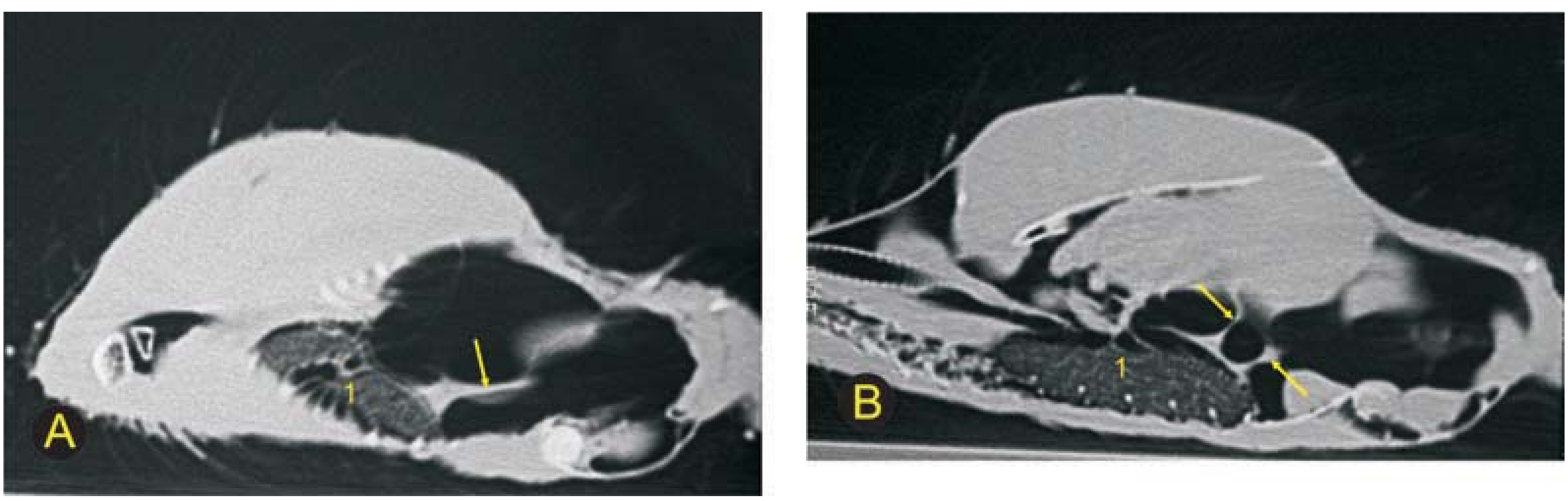

Fig. 1-132: Total body CT images of a blue-fronted Amazon (*Amazona aestiva*) diagnosed with mycosis of the respiratory tract, sagittal plane, (A) lateral slice through the right half of the body, (B) paramedian slice on the right, close to the middle of the body (120 kV, 85 mA, SD 2 mm, W: 2800, L: –300).

A: Caudal wall of the thoracic air sac is thickened (arrow).

B: Cranial and caudal thoracic air sac walls are thickened (arrows).

1: lung

arrows: wall of thoracic air sac

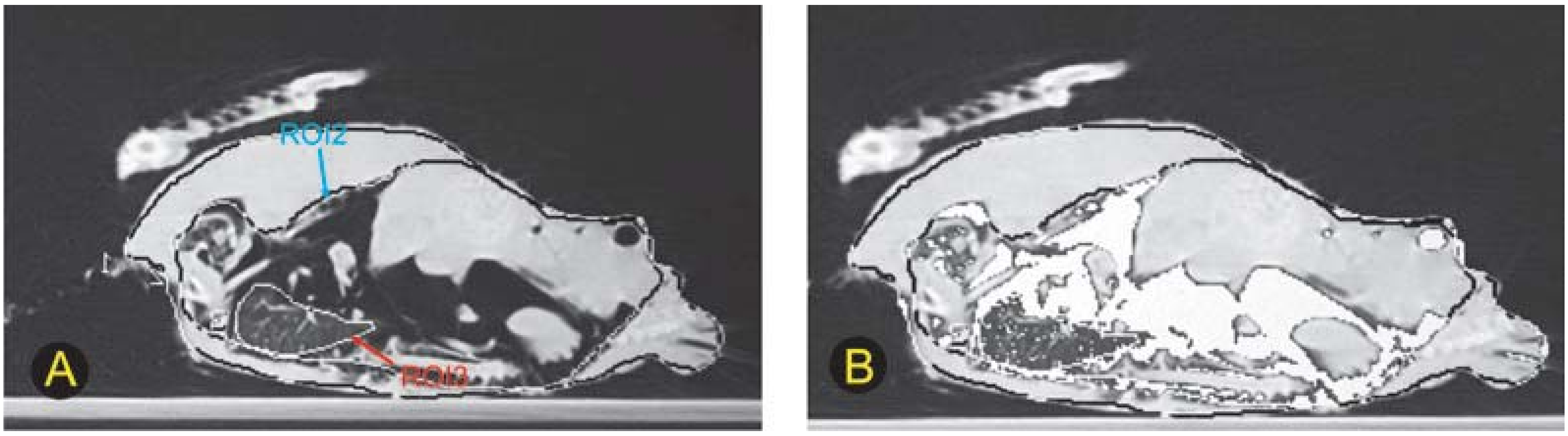

Fig. 1-133: Total body CT images of an African grey parrot (*Psittacus erithacus*) diagnosed with over-expanded secondary bronchi due to displacement of the main bronchus, body, sagittal plane (120 kV, 165 mA, SD 2 mm, W: 2800, L: –300).

A: Measurement of different areas: ROI 3: lung, ROI 2: body cavity; these measurements are the preparation for B and can be used to determine the lung density of the bird.

B: Image highlighting the aerated spaces of the lung measured in A (ROI 3) and the body cavity (ROI 2). This enables the overexpansion of the secondary bronchi and the area of the air sac to be determined in these slices. A total assessment can be achieved by measuring, determing the density and highlighting in every plane.

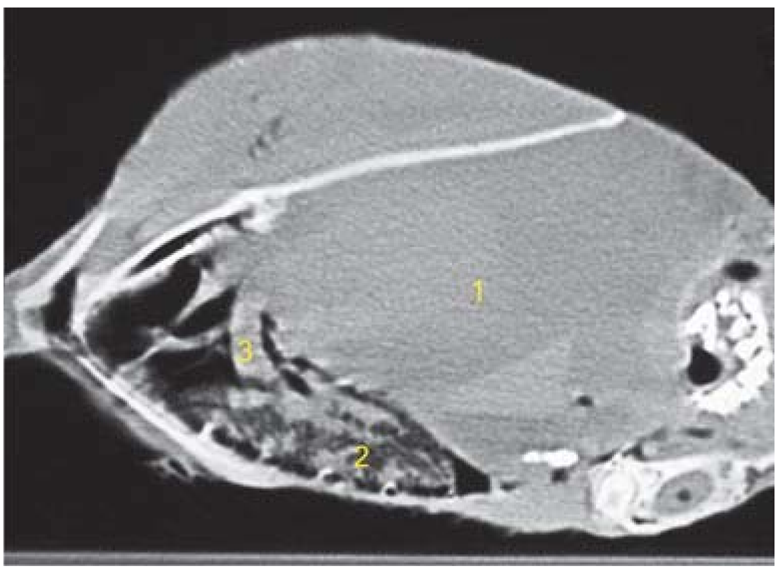

1: ascites
2: lung
3: dilated blood vessels

Fig. 1-134: Total body CT image of an orange-winged Amazon (*Amazona Amazonica*) diagnosed with ascites (1) of unkown etiology, sagittal plane (120 kV, 165 mA, SD 2 mm, W: 2800, L: –300). Foam cell granuloma in the lung (2), and dilated blood vessels (3) can be viewed in this image.

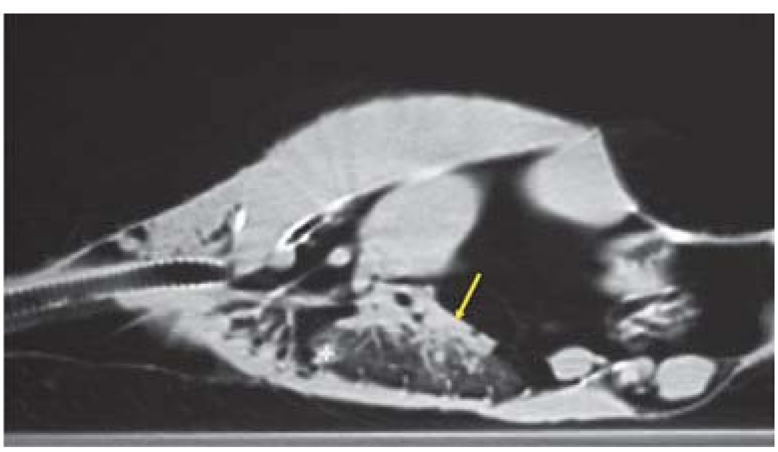

Fig. 1-135: Total body CT image of an African grey parrot (*Psittacus erithacus*) diagnosed with mycosis of the lungs, sagittal plane, right paramedian (120 kV, 85 mA, 2 mm SD, W: 1552, L: –67). The ventral area of the lungs is compacted (*, arrow). The density measurements of the right lung revealed a significantly increased density value for this area.

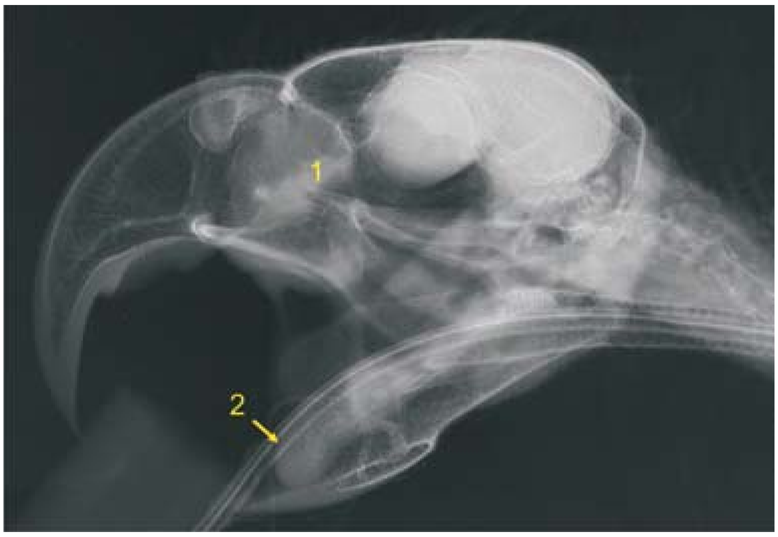

1: soft-tissue swelling
2: endotracheal tube

Fig. 1-136: Radiographic image of a hyacinth macaw's (*Anodorhynchus hyacinthinus*) head diagnosed with chronic sinusitis due to mycosis, lateral projection.

A: radiopaque soft-tissue swelling (1) in the area of the infraorbital sinus can be visualized in this image. Bird under general anesthesia.

Fig. 1-137: Red-lored Amazon (*Amazona autumnalis*): chronic sinusitis. Patient in Figs. 1-139 and 1-140.

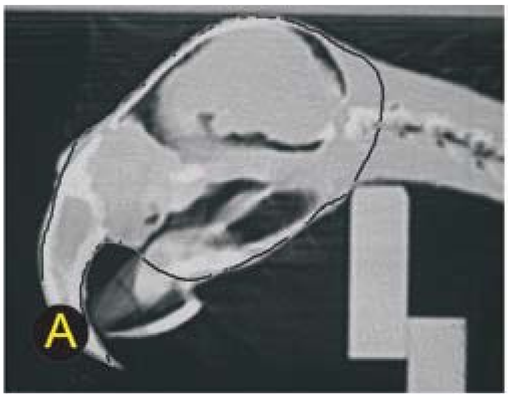

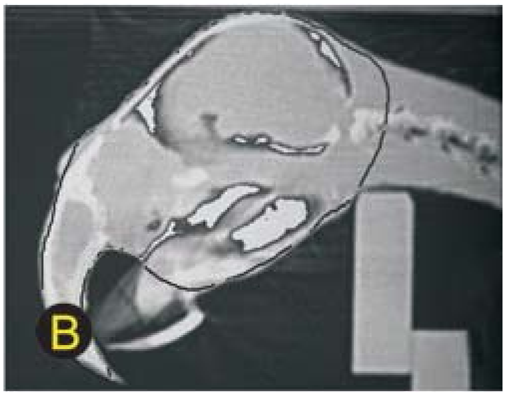

Fig. 1-138: CT images of an African grey parrot's (*Psittacus erithacus*) head diagnosed with chronic sinusitis, sagittal plane (165 kV, 120 mA, SD 2 mm W: 2800, L: –300).

A: In these slices, the extent of the inflammatory changes can be observed. Preparation of the highlighting and measurement of a defined area of the head.

B: Highlighting with imaging of the aerated area measured in A allows one to determine the degree of sinusitis and reduction of aerated spaces in the patient.

A total assessment of a patient's condition can be achieved by measuring or highlighting in each plane. An objective appraisal of the effectiveness of a therapeutic protocol can be achieved by looking at the calculated values (see Chap. 1.3.3).

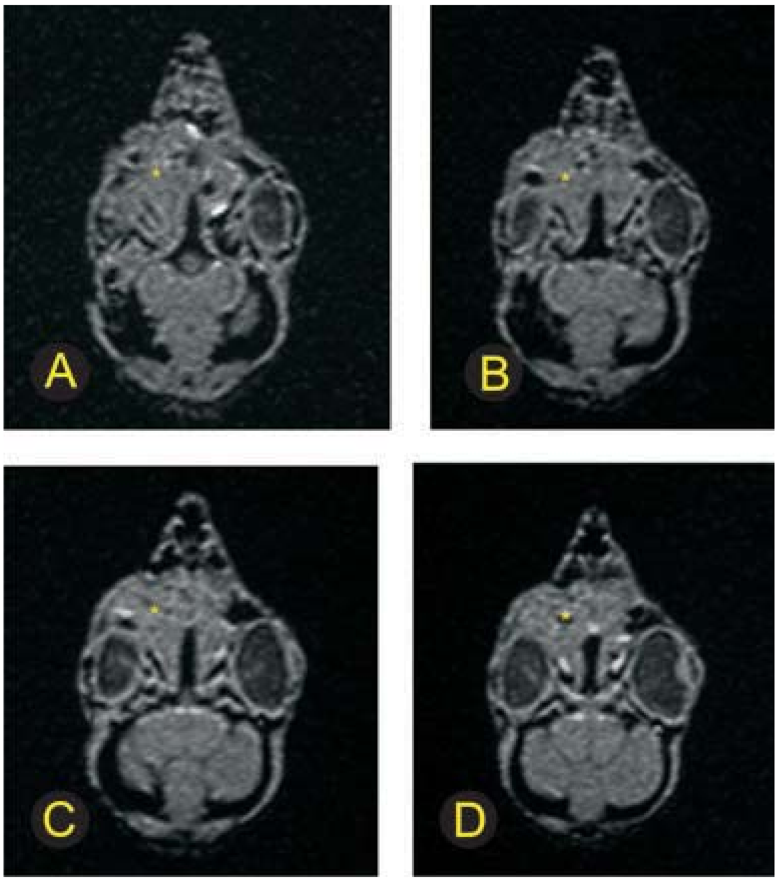

Fig. 1-139: MRI images of a red-lored Amazon's (*Amazona autumnalis*) head diagnosed with chronic sinusitis, transverse scan, surface coil, T1-weighted. The extent of the inflammatory changes (*) can be followed in these slices by comparing the symmetry of the structures imaged.

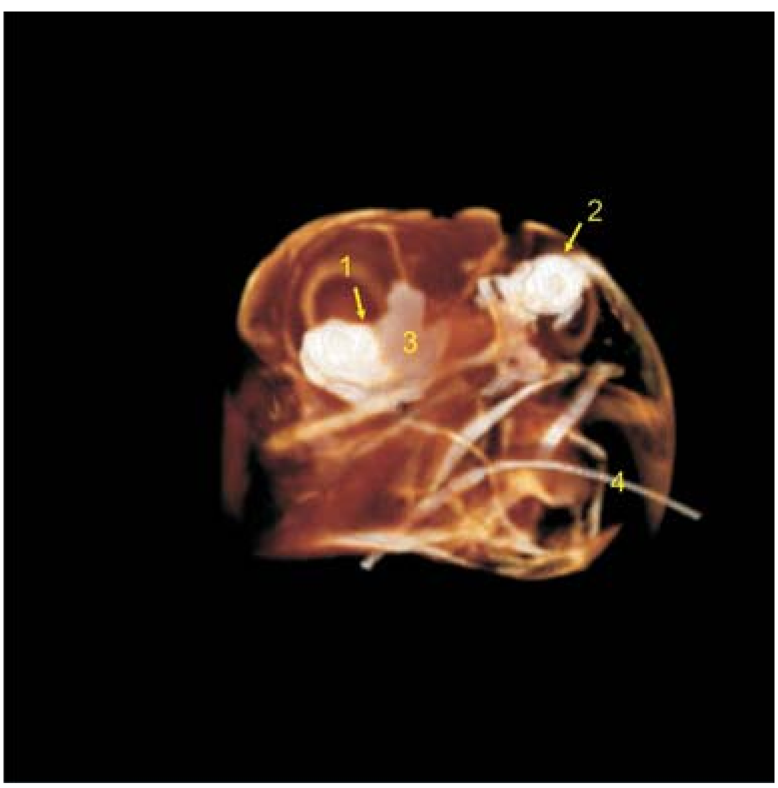

1: sinus
2: nares
3: barrier to the flow of contrast
4: endotracheal tube

Fig. 1-140: CT, 3D reconstruction image of a red-lored Amazon's (*Amazona autumnalis*) head diagnosed with chronic sinusitis after instillation of iopamidol (Solutrast® 250 mg iodine/ml; 1 ml in the sinus for a sinus contrast study) (140 kV, 150 mA). By administering a nonionic iodine-containing contrast medium in the sinus (1) or the nares (2), barriers (3) to the flow of contrast can be depicted; investigation under general anesthesia.

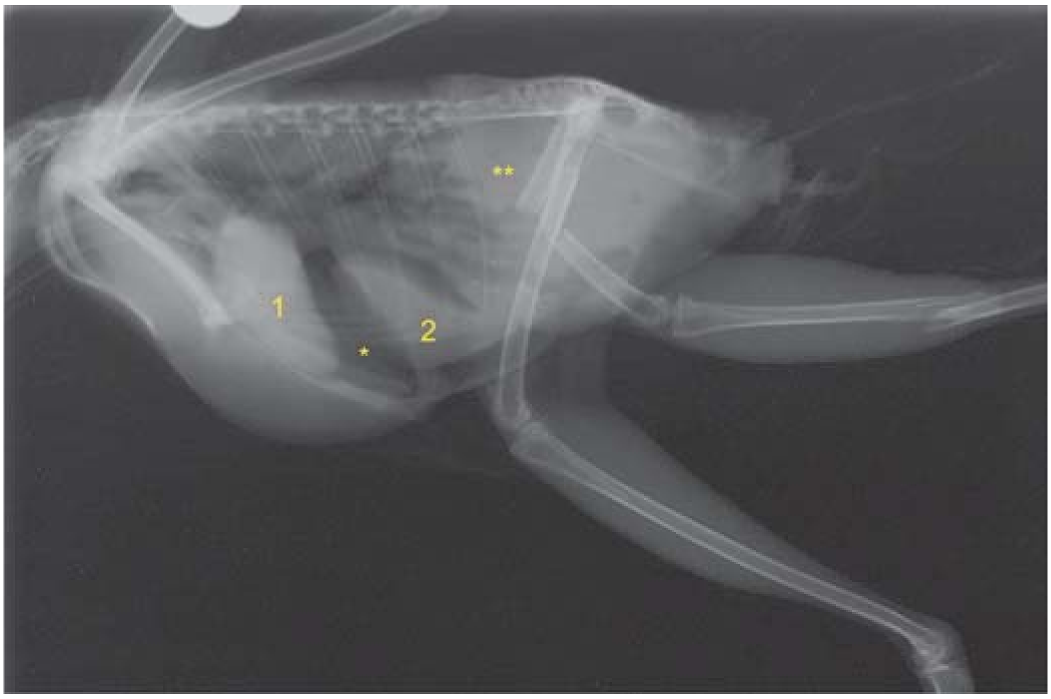

1: heart
2: liver

*: air between liver and heart
**: hemorrhage in caudal body cavity

Fig. 1-141: Total body radiographic image of a great bittern (*Botaurus stellaris*) diagnosed with trauma, lateral projection. The heart shadow (1) is obviously raised by air that has escaped from a ruptured air sac. Air is also lying between parts of the cranial gastrointestinal tract and between the liver (2) and heart (*). The bird also has fractures of the tibiotarsus and femur. There is a hemorrhage (**) in the caudal body cavity, which makes the individual organ identification difficult. The physiologically normal, large syrinx is easy to see in this image.

1: syrinx
2: large heart vessels

Fig. 1-142: Total body radiographic images of an African grey parrot (*Psittacus erithacus*) diagnosed with mycosis and secondary bacterial infection of the respiratory tract, (A) ventrodorsal and (B) lateral projections.

A: Within this image, one can see homogenous shadowing of the lungs and air sacs; (1) thickened syrinx, (2) radiopaque large heart vessels (often noted in older birds). Note the lack of grit.

B: (1) Thickened syrinx, (2) radiopaque large heart vessels. Note the lack of grit.

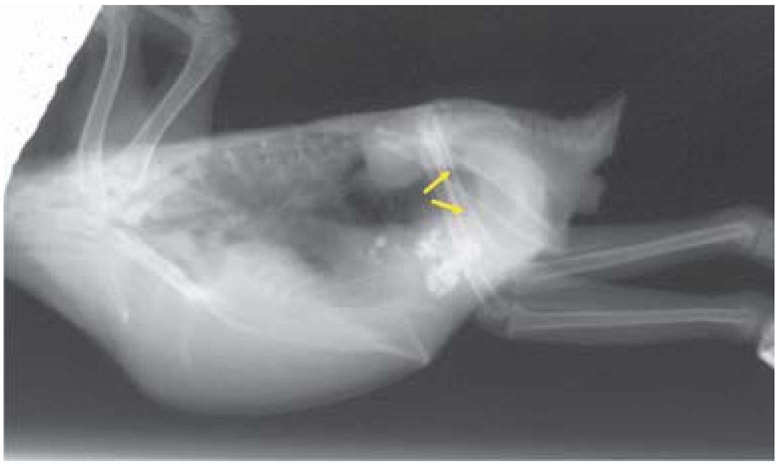

Fig. 1-143: Total body radiographic image of a budgerigar (*Melopsittacus undulatus*) diagnosed with a bacterial Infection involving the upper respiratory tract, lateral projection. Air trapping (arrows) due to a stenosis in the upper region of the respiratory tract is evident in this image.

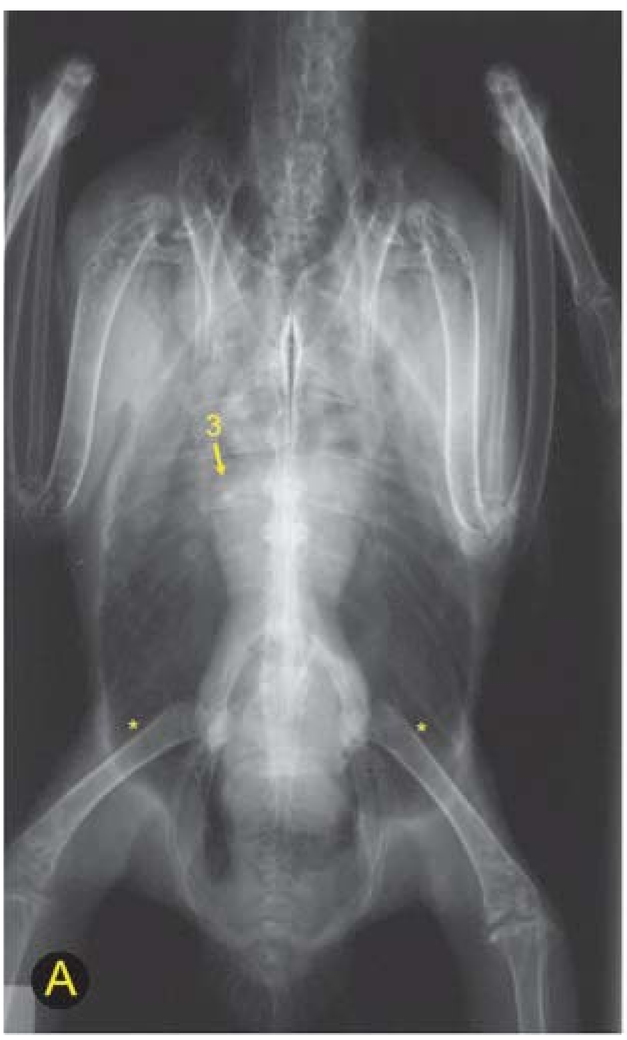

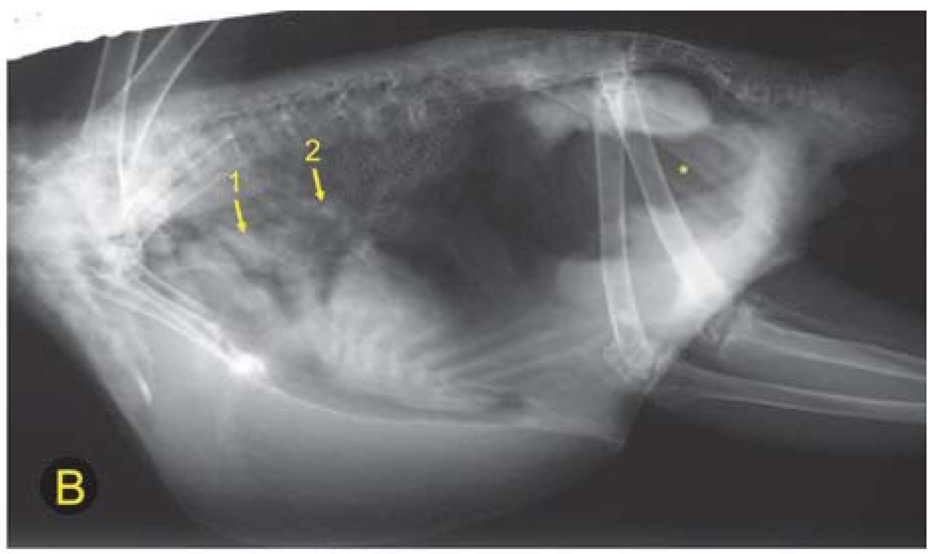

1: syrinx
2: calcifications
3: calcified vessels

*: air trapping

Fig. 1-144: Total body radiographic images of an eclectus parrot (*Eclectus roratus*) diagnosed with a mycotic granuloma in the upper respiratory tract, (A) ventrodorsal and (B) lateral projections.

A: Enlargement of the air sac region was initially interpreted as being caused by the »inspiratory phase« but the overexpansion of the caudal air sacs was actually caused by a stenosis (*) in the cranial region; rounding of the caudal air sacs, punctate radiodense tumors in the area at the base of the heart (3: calcified vessels).

B: Thickened syrinx region (1) with punctate radiopaque areas in the ventral region of the lungs (2, calcifications); (*) air trapping.

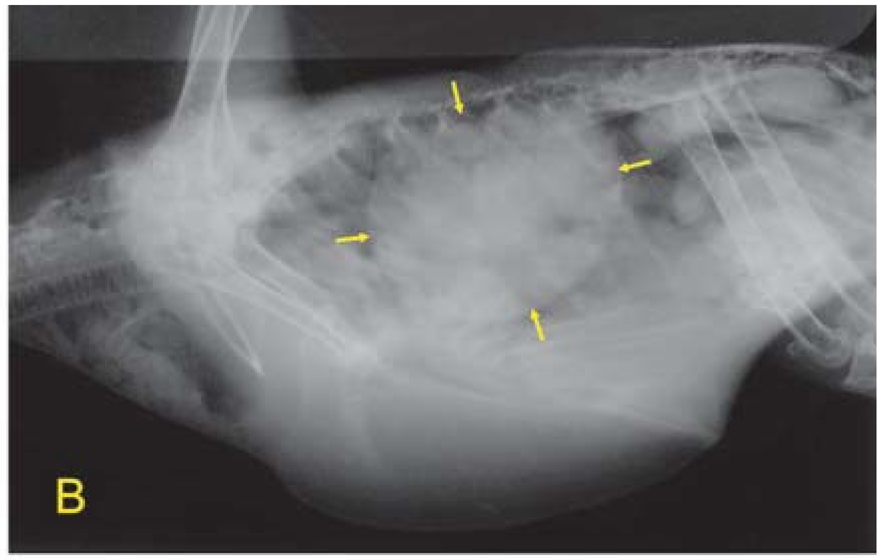

Fig. 1-145: Total body radiographic images of a blue-fronted Amazon (*Amazona aestiva*) diagnosed with tuberculosis, (A) ventrodorsal and (B) lateral projections. Radiopaque circumscribed areas of nonhomogeneous soft-tissue swelling (arrows) in the anterior body cavity with compression of the caudal air sacs and overshadowing of the lung field can be observed in these images.

1: cervical air sacs
2: crop

Fig. 1-146: Radiographic image of an Edwards's fig-parrot (*Psittaculirostris edwardsii*) head and neck region, rostrocaudal projection: Overexpansion of the (1) cervical air sacs after exhaustion; in addition, the bird has an air-filled crop (2).

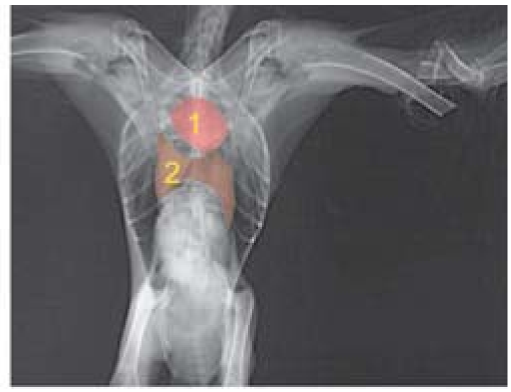

1: heart
2: liver

Fig. 1-147: Total body radiographic image of a long-eared owl (*Asio otus*) diagnosed with an air sac rupture due to trauma, ventrodorsal projection. As a result of the air sac rupture the apex of the heart (1) and the edges of the liver (2) are clearly visualized (air as negative contrast medium). A comminuted fracture of the humerus is also shown in the image.

Fig. 1-148: Total body radiographic image of an obese double yellow-headed Amazon (*Amazona ochrocephala oratix*), ventrodorsal projection. Homogenous symmetrical shadowing of the lungs and caudal air sacs due to overlapping by fat is evident in this radiograph. There is no hour-glass shape between the heart and liver because of summation of the over-expanded air sacs on the right.

1.8 Gastrointestinal tract

Maria-Elisabeth Krautwald-Junghanns, Michael Pees

With respect to the gastrointestinal tract, in the majority of avian patients, traditional radiography which includes the use of contrast media provides the veterinarian with an adequate degree of diagnostic information such as that found with other imaging modalities. Consequently, the other diagnostic imaging modalities are rarely used for gastrointestinal examination on avian patients. As scientific investigations into the use of ultrasonography for the examination of the gastrointestinal tract in sick birds are rare, the image assessment of such examinations is correlated to the subjective experience of the sonographer. Therefore, the use of ultrasonography for the examination of an avian gastrointestinal tract, in comparison to the other imaging methods, is limited. However, pathological findings in the gastrointestinal tract are often discovered by chance in routine ultrasonographic investigations. The most frequent avian gastrointestinal findings are increased or reduced peristalsis, enlarged or diminished organ size, or increased thickness of the intestinal wall (e.g. inflammation). Oral or cloacal administration of water will aid in the ultrasonographic diagnosis of increased intestinal wall thickness. Another indication for using ultrasonography to assess the gastrointestinal tract is for »abdominal« herniation and a verification of intestinal loops outside the coelomic cavity.

Frequently diagnosed changes in the gastrointestinal tract are abnormal contents (for example foreign body, gas, grit, polyphagia; e.g. **Figs. 1-149** to **1-153**), displacement of all parts of the gastrointestinal tract, changes in its form or size (e.g. **Figs. 1-154** to **1-159**) and hypo- or hyperperistalsis. A survey radiograph provides a reliable diagnosis if there is suspicion of a **foreign body** containing heavy metal (e.g. lead, zinc) in the gastrointestinal tract **(Figs. 1-149** and **1-150)**. Parrots and ostriches regularly ingest foreign bodies containing heavy metal **(Figs. 1-149** and **1-150)** or other substances **(Figs. 1-151** and **1-152)** from their surrounding environment. It is not uncommon to find fish hooks in waterfowl or lead shot being ingested when birds (e.g. ducks) dabble on the bottom of lakes and ponds where hunting has occurred. Foreign bodies within a fluid-filled (e.g. water) gastrointestinal tract are also visualized using ultrasonographic imaging, particularly when the examination takes place on large birds **(Fig. 1-160B)**. After lightly swinging the avian patient from side to side, upon reexamination, one can determine if the foreign body is movable or stationary within the gastrointestinal tract.

Bloat of the gastrointestinal tract is rare in birds, but when identified this condition is usually associated with an advanced, inflammatory bacterial infection of the gastrointestinal mucosa or with neurogenic proventricular dilatation disease **(Figs. 1-153, 1-154** and **1-158)**. Both excessive food distension and large quantities of grit, of and in the gastrointestinal tract are highly visible on radiographic images. Contrast examinations, using either barium sulfate alone or when required a double-contrast technique using both barium sulfate and air, are important procedures for the radiographic assessment and differentiation of the gastrointestinal tract from surrounding tissues. A survey radiographic image should always be obtained before every gastric examination to rule out excessive food distention and severe bloat. Food distention and severe bloat may circumvent the need to administer contrast material. Additionally, perforation of the gastrointestinal wall (i.e. due to a foreign body) can be identified on a survey image. Both gas and barium sulfate in the intestinal tract prevent ultrasonographic imaging of this body system, however, abnormal presentation of the cloaca due to food distention or urate concentration **(Fig. 1-161B)** can be identified.

By determining the rate of passage of the contrast material through the gastrointestinal tract **(Fig. 1-35)**, allows for multiple diagnostic assessments including the size, form, and site of the tract but also its ability to function. Dilatation in any part of the gastrointestinal tract often leads to a reduced movement of the contrast material through the tract **(Figs. 1-150C, D** and **1-151)**.

1.8.1 Esophagus and crop

Chronic trichomoniasis in domestic pigeons often causes a thickening and **ulceration** of the crop mucosa. After being administered contrast material, the ulcerated sections of the ingluvial wall are clearly visible due to the deposition of barium sulfate. **Thickening** of the esophageal wall can also occur in association with ingluvitis (e.g. with candidiasis) or it may be associated with vitamin A deficiency and concurrent renal swelling. Pathological dilatation of the esophagus and/or crop can be identified on a radiographic image as this condition will cause a delay in the passage of the contrast material from these areas **(Figs. 1-150C, D** and **1-151)**. The causes of esophageal and/or ingluvial dilatation with an associated delay in normal peristaltic movement are manifold. In addition to neurogenic infections (e.g. neurogenic proventriculus dilatation) and toxicity related to neurotoxin exposure, both food distention and/or ileus of the caudal intestines (e.g. parasitic infestations) can affect the function of the esophagus and crop.

Ultrasonography of the crop and esophagus is rarely performed due to the difficulty in locating a suitable coupling site (the feathers may only be removed in this region under general anesthesia). Ultrasonographic examination may be possible by dilating the esophagus and crop with water. A spacer is always needed in this region.

1.8.2 Proventriculus

The radiographic characteristics of neurogenic proventricular dilatation disease (PDD) include a massive **dilatation** of the proventriculus **(Fig. 1-154)** and an atrophic and deformed ventriculus, especially in large parrot species (e.g. macaws). Pathological dilatation of the proventriculus can also occur with a *Macrorhabdus ornithogaster* infection (i.e. going-light syndrome) in budgerigars, with severe ascarid infections, with food distention due to reduced peristaltic function and, infrequently, with bacterial or mycotic **(Fig. 1-155)** induced inflammation of the gastrointestinal mucosa. A **thickening** of the proventricular mucosal wall can be identified with vitamin A deficiency. **Changes in position** occur less commonly with the proventriculus than the ventriculus and are usually associated with the enlargement of neighboring organs, especially the liver (see Chap. 1.9). The proventriculus can contain **abnormal substances**, such as foreign bodies or an excessively large amount of grit **(Fig. 1-159)**. Gas can form in the proventriculus with neurogenic PDD **(Fig. 1-154)**, bacterial infections (especially *Streptococcus* spp. or *Escherichia coli*) and the inflammation associated with these diseases. The ultrasonographic diagnostic capabilities regarding the examination of an enlarged proventriculus are limited. **Dilatation (Fig. 1-161A)** of the proventriculus and pathological changes to the mucosal walls of this structure can be demonstrated in large birds as long as no gas is present.

1.8.3 Ventriculus

Changes to the size and form of the ventriculus are rarely observed in granivorous birds **(Fig. 1-159)**, as the ventriculus in these species has a well-developed musculature and therefore a stable form. **Ventricular atrophy and dilatation,** however, occur in association with neurogenic PDD. A chronic lack of grit can also result in atrophy of the ventricular wall. A **high proportion of grit** in the ventriculus should be considered as a sign of inadequate food intake in many bird species (i.e. diseases of the gastrointestinal tract) **(Figs. 1-156** and **1-157)**. However, in some avian species (e.g. the electus parrot) a large amount of grit in the ventriculus is normal. When there is a deficiency of suitable stones in the ventriculus, a bird may ingest foreign bodies of a suitable size, which ultimately collect in this organ **(Figs. 1-149** and **1-150)**.

Displacement of the ventriculus indicates an increase in volume of the neighboring gastrointestinal structures (e.g. proventriculus, duodenum). This condition is easily identified in granivorous species as the position of the ventriculus is easily recognizable due to the radiopaque grit particles in its lumen. With hepatomegaly, the ventriculus is displaced dorsocranially or dorsocaudally (see Chap. 1.9.1), whereas with enlargement of the kidneys or spleen it is displaced ventrocranially or ventrocaudally with the intestines (see **Fig. 1-34)**. The ventriculus is also displaced ventrocaudally with dilatation of the proventriculus, while dilated intestines or an enlarged oviduct (normal during the breeding season) results in a ventrocranial relocation.

Ventricular ultrasonographic examinations on granivorous species is not rewarding due to its thick muscle layer and grit within the lumen. Rarely, abnormal ventricular contents can be well visualized in carnivorous and fructivorous birds (and those that eat other soft foods).

1.8.4 Intestines

Usually the intestinal tract is not very well differentiated on a survey radiographic image **(Fig. 1-157)** and only in individual cases can the intestines be satisfactorily imaged without using contrast material. **Dilatation (Figs. 1-153** and **1-156)** of the intestines can be diagnosed in birds with substantial ascarid infestations, food or fecal distention (e.g. ileus), toxicity due to neurotoxins, infections, and enteritis. **Thickening** of the intestinal wall can be an indication of a chronic infection or ascarid infestation. Papilloma-like **tumors** can be identified within the cloacal lumen of large parrots **(Fig. 1-161). Concretions** within the cloacal lumen appear as irregular radiopaque densities and dilate the cloaca similar to a bloat presentation **(Figs. 1-158, 1-159** and **1-161B, C). Displacement** of the intestines occurs as a consequence of a ventricular position change, enlargement of the kidneys or genital tract (see Chap. 1.10).

Changes in the radiographic appearance of the intestinal wall primarily appear as nonspecific enlarged intestinal shadows. The double-contrast method is particularly suitable for the imaging of the intestinal wall (i.e. to determine the extent of papilloma-like changes in the rectum after prolapse of the cloaca). The degree of changes to the intestinal mucosa associated with chronic inflammation provides important information for determining a prognosis. Thickening of the intestinal mucosa may indicate the presence of a significant ascarid infection, a chronic infectious **(Fig. 1-160C)** or neoplastic disease. Other granulomatous changes in the intestinal wall, as found with tuberculosis or leucosis **(Fig. 1-160A)**, are difficult to differentiate. Granulomatous changes can be identified sonographically in larger birds after oral or cloacal administration of water. **Invagination** of intestinal loops is rarely diagnosed in birds using traditional radiographic imaging techniques but can be observed in an ultrasonographic examination. With a complete ileus, there is a cessation of intestinal content movement. Reduction in volume, paralysis, or dilatation of all or parts of the gastrointestinal tract will lead to an increased **contrast transit** time through the intestinal tract **(Figs. 1-150C, D** and **1-151)**. Conversely, with acute inflammation of the gastrointestinal mucosa, there is often a decreased contrast transit time through the intestinal tract. Although subjective and depending on the experience of the examiner, ultrasonographic investigation can obtain excellent images of intestinal **peristalsis** and the transit of food particles through the tract.

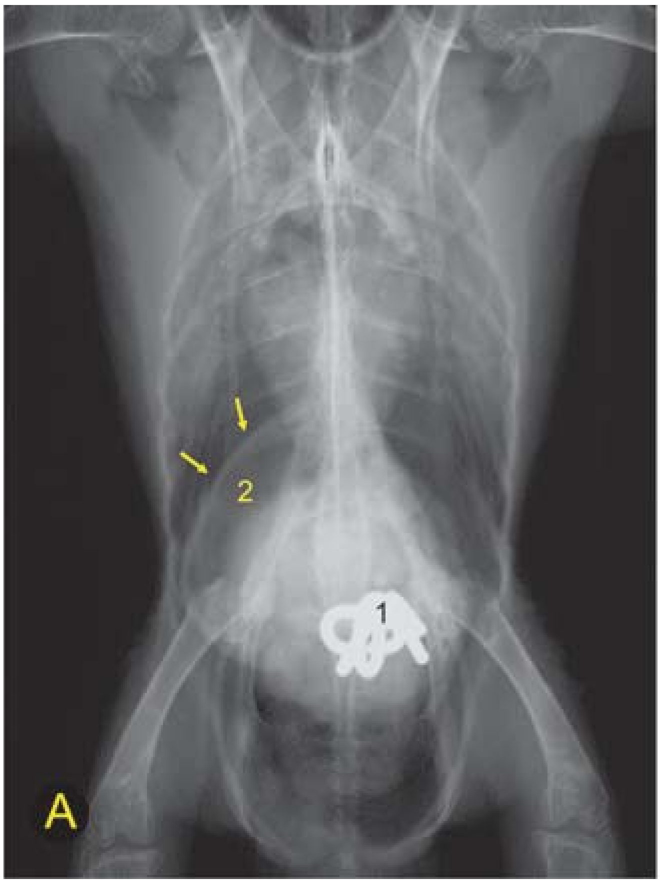

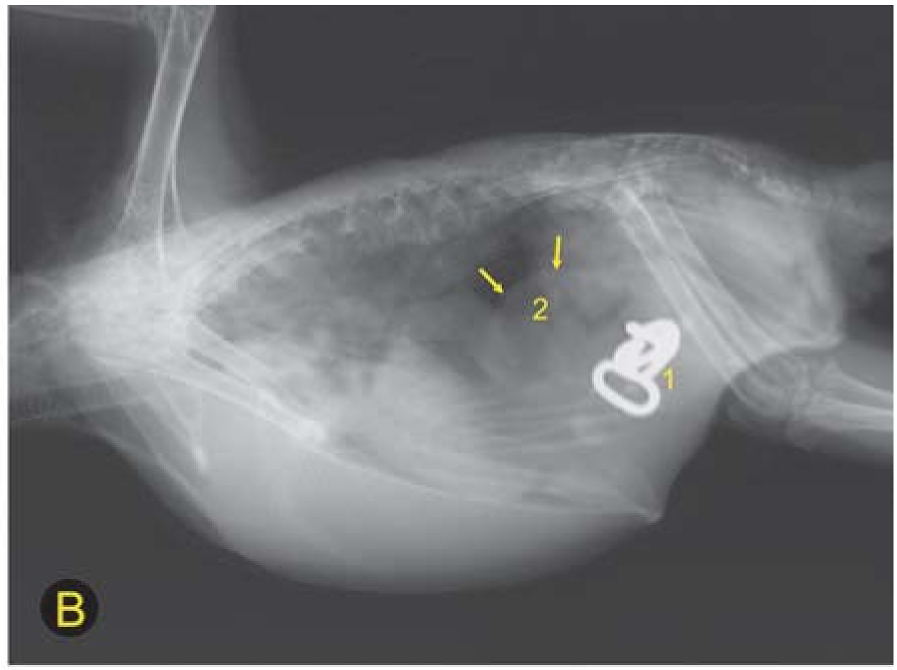

1: ventriculus
2: proventriculus

arrows: contour of the proventriculus

Fig. 1-149: Total body radiographic images of an African grey parrot (*Psittacus erithacus*) that has ingested a foreign body, (A) ventrodorsal and (B) lateral projections. The proventriculus (2) is dilated due to a disturbance in the peristaltic activity of the gastrointestinal tract. There are chain links in the ventriculus (1); the number of chain links cannot be determined due to summation of the objects.

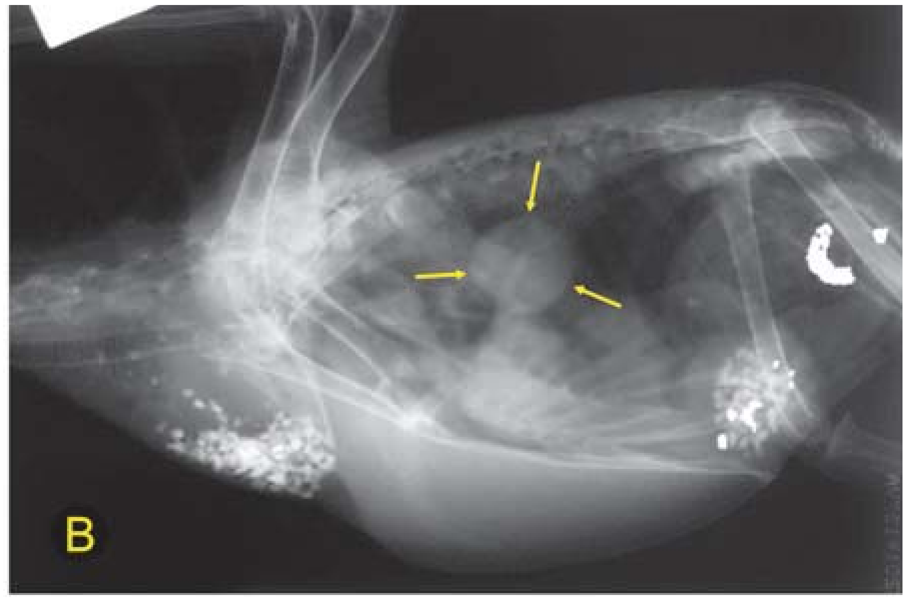

Fig. 1-150:

A, B: Total body radiographic images of an African grey parrot (*Psittacus erithacus*), (A) ventrodorsal and (B) lateral projections, with heavy metal poisoning. Radiopaque particles can be seen in the ventriculus and caudal intestines. The metallic particles are easily differentiated from grit. There is an excessive amount of grit in the crop and the soft-tissue swelling (arrows) in the lateral projection is a mycotic granuloma. In comparison, this tumor is barely visible in the dorsoventral projection.

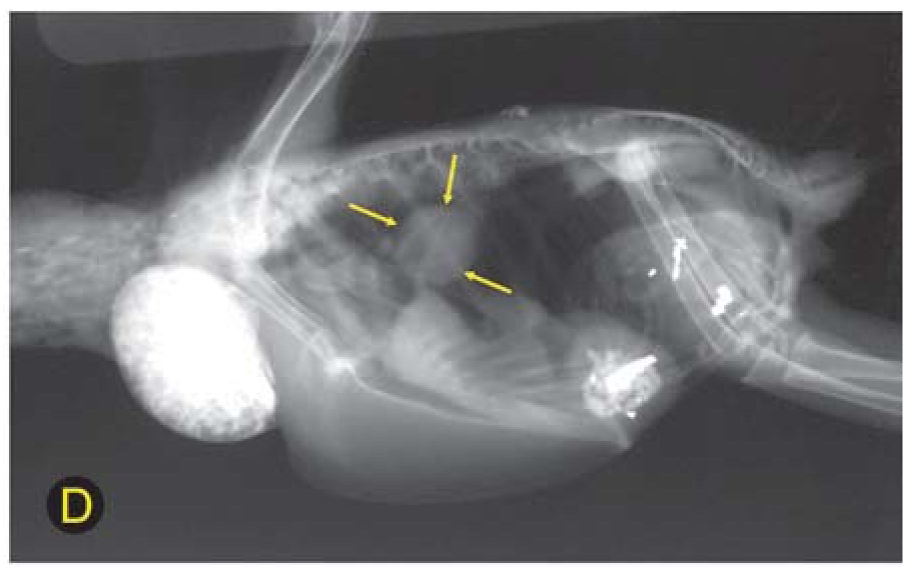

C, D: Total body radiographic images of the same bird, (C) ventrodorsal and (D) lateral projections, 30 min after the administration of barium sulfate (350 mg/ml, 20 ml/kg, in the crop): delayed passage of the contrast material due to the intestinal disturbance is apparent. The crop is dilated and still excessively filled with food and contrast material (Arrows: mycotic granuloma.

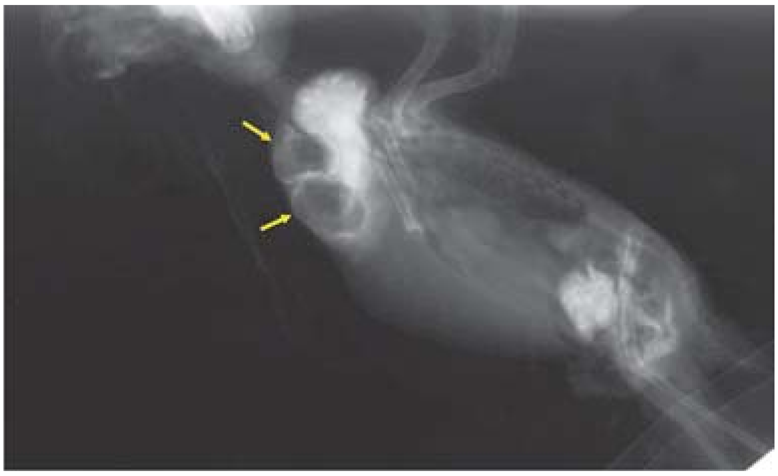

Fig. 1-151: Total body radiographic image of a budgerigar (*Melopsittacus undulates*), lateral projection, 45 min after the administration of barium sulphate (350 mg/ml, 20 ml/kg bwt, in the crop): crop bezoar (arrows). The passage through the crop is delayed due to the presence of the foreign body.

1, arrows: bezoar
2: femur

Fig. 1-152: Radiographic image of the caudal half of an emu's (*Dromaius novaehollandiae*) body, ventrodorsal projection: a bezoar (1, arrows) is lying in the gastrointestinal tract.

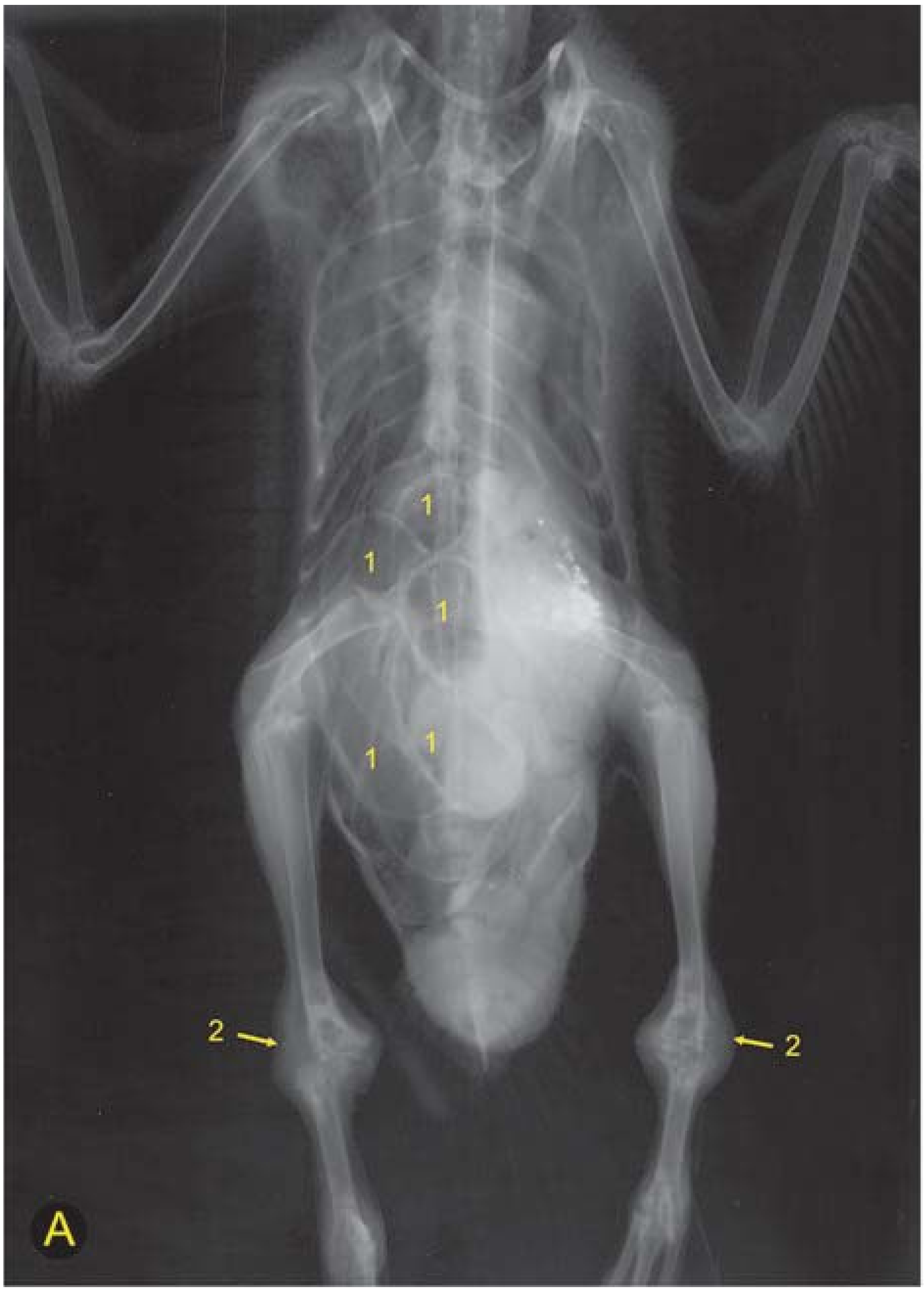

1: loop of intestine
2: osteolysis in tibiotarsal joint

Fig. 1-153:

A: Total body radiographic image of muscovy duck (*Cairina moschata*), diagnosed with tuberculosis, ventrodorsal projection. The intestinal loops (1) are severely distended. There are areas of osteolysis (2) in the region of both tibiotarsal/tarsometatarsal joints.

B: Radiographic image of the muscoy duck's leg, lateral projection, showing the area of osteolysis (2) involving the tibiotarsal/tarsometatarsal joint.

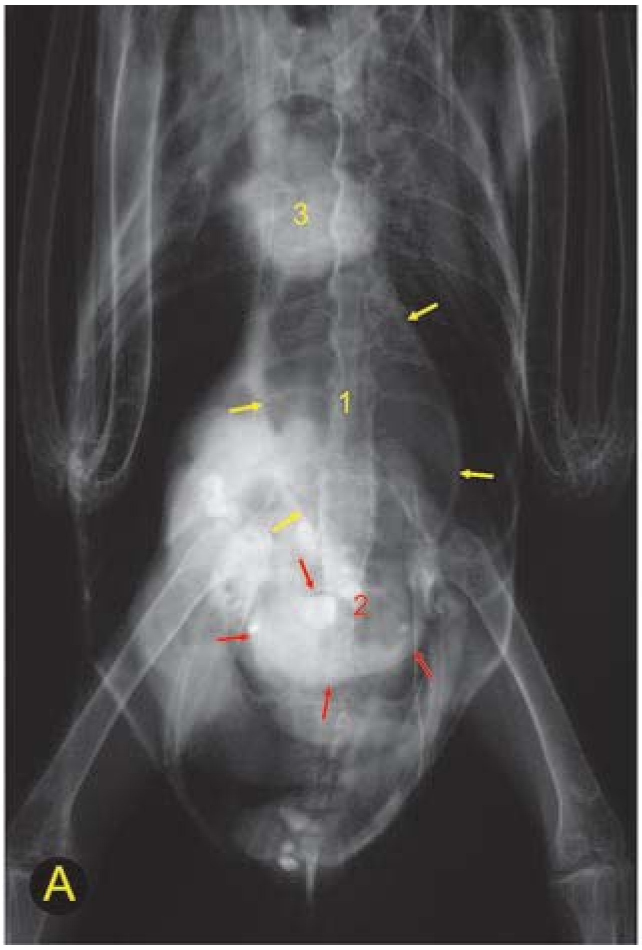

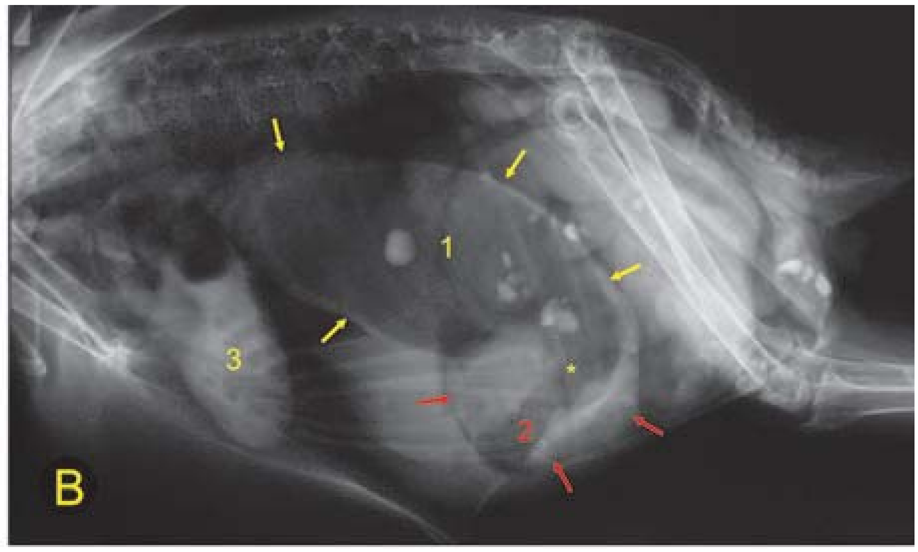

1, yellow arrows: proventriculus
2, red arrows: ventriculus
3: heart

*: isthmus

Fig. 1-154: Total body radiographic images of an umbrella cockatoo (*Cacatua alba*), diagnosed with neuropathic proventriculus dilatation (proventricular dilatation disease or PDD, (A) ventrodorsal and (B) lateral projections. The proventriculus (1) is severely dilated (yellow arrows). The isthmus, which forms the boundary to the ventriculus (2), is also dilated (red arrows). The wall of the ventriculus is already atropic and its lumen is dilated. Grit is distributed throughout the intestines.

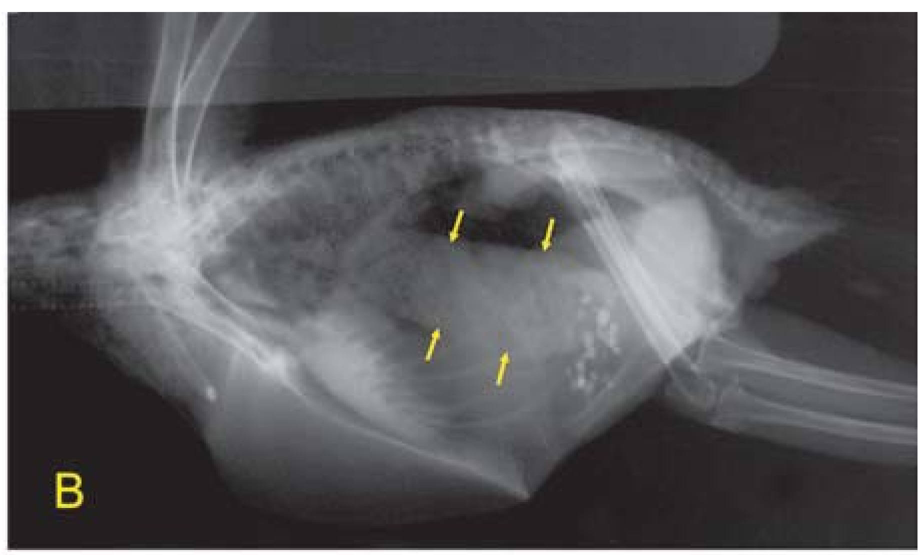

Fig. 1-155: Total body radiographic images of a sulfur-crested cockatoo (*Cacatua galerita*), with a yeast infection, (A) ventrodorsal and (B) lateral projections. The proventriculus (arrows) is dilated and filled with food. PDD must be considered as a differential diagnosis (see Fig. 1-154).

Fig. 1-156: Total body radiographic images of an African grey parrot (*Psittacus erithacus*), with a bacterial gastroenteritis and septicemia, (A) ventrodorsal and (B) lateral projections. There is an excessive amount of grit distributed throughout the gastrointestinal tract. The intestinal loops are severely engorged; one intestinal loop is enlarged (arrows).

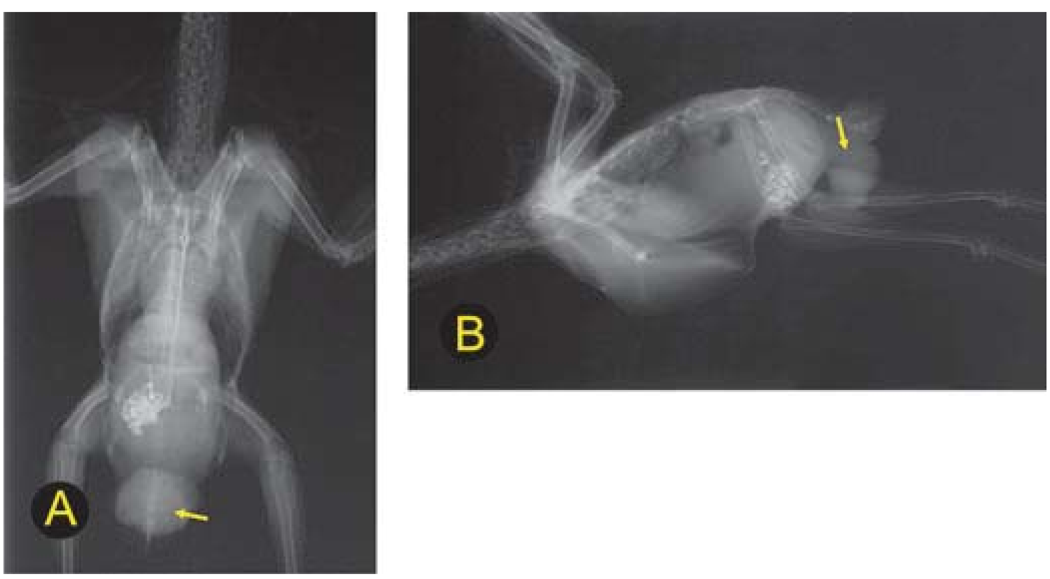

Fig. 1-157: Total body radiographic images of a canary (*Serinus canaria* f. *domestica*), diagnosed with coccidiosis, (A) ventrodorsal and (B) lateral projections. The cloaca is filled with feces and prolapsed (arrow). Due to the enlargement of the gastrointestinal tract, the normal hour-glass shape of the heart and liver silhouette is no longer present. There are radiopaque soft-tissue swellings in the caudal coelom. In addition, there is an excessive amount of grit present within the gastrointestinal tract.

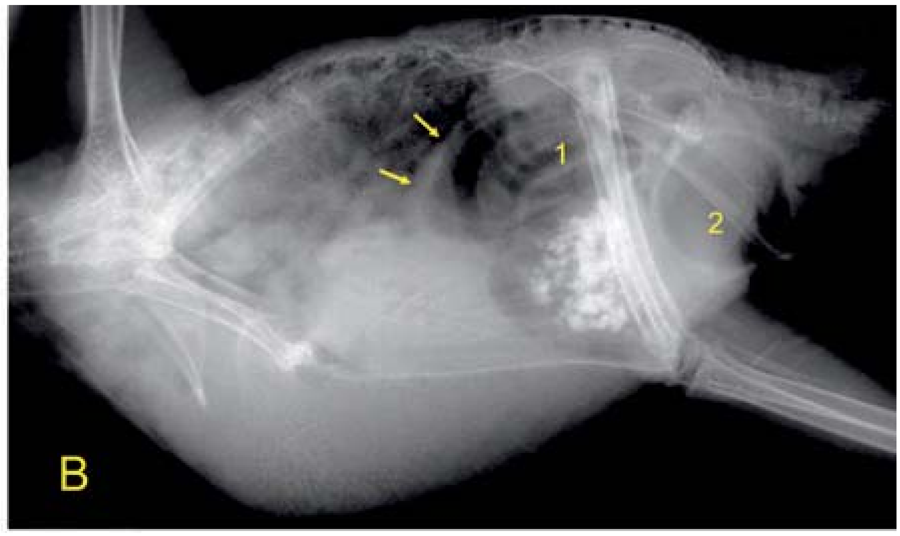

1: gastrointestinal tract
2: cloaca

arrows: caudal wall of the thoracic air sac

Fig. 1-158: Total body radiographic images of a Jardine's parrot (*Poicephalus gulielmi*), diagnosed with a yeast infection and aspergillosis, (A) ventrodorsal and (B) lateral projections. The gastrointestinal tract (1) is filled with gas and the normal hour-glass shape of the heart and liver silhouette is no longer present. The cloaca (2) is also filled with gas. In addition, the air sacs are cloudy, while the caudal wall of the thoracic air sac is thickened (arrows).

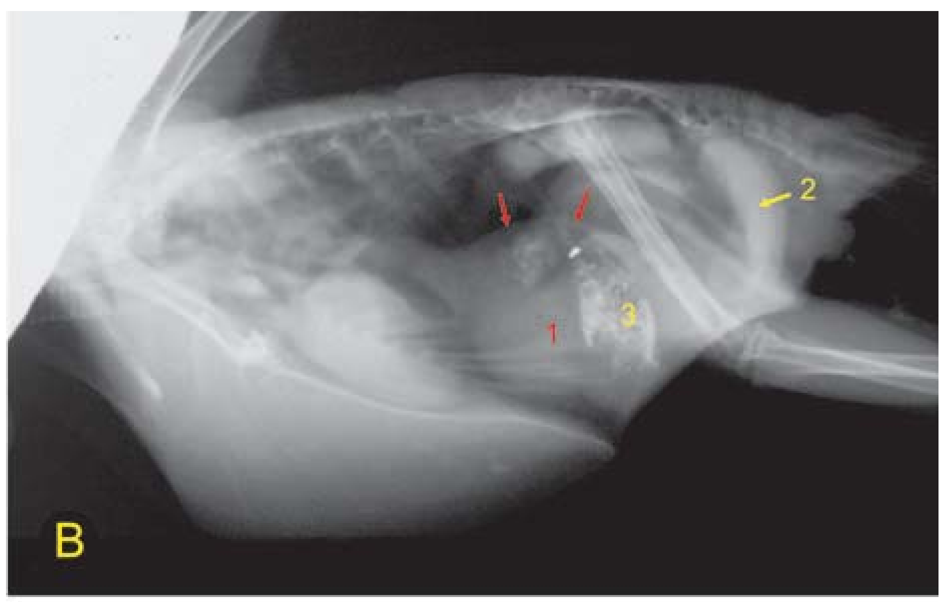

1, red arrows: proventriculus
2: cloaca
3: ventriculus with grit

Fig. 1-159: Total body radiographic images of a galah cockatoo (*Eolophus roseicapilla*), diagnosed with gastrointestinal parasitism, (A) ventrodorsal and (B) lateral projections. The proventriculus (1, red arrows) is dilated and filled with an excessive amount of grit. A large quantity of grit is also present in the ventriculus (3) and its normal shape has been changed. The cloaca (2) shows radiopaque changes (cloacitis with accumulation of feces). In the ventrodorsal projection, the apex of the heart is visible due to the gas-filled proventriculus, which acts as contrast material.

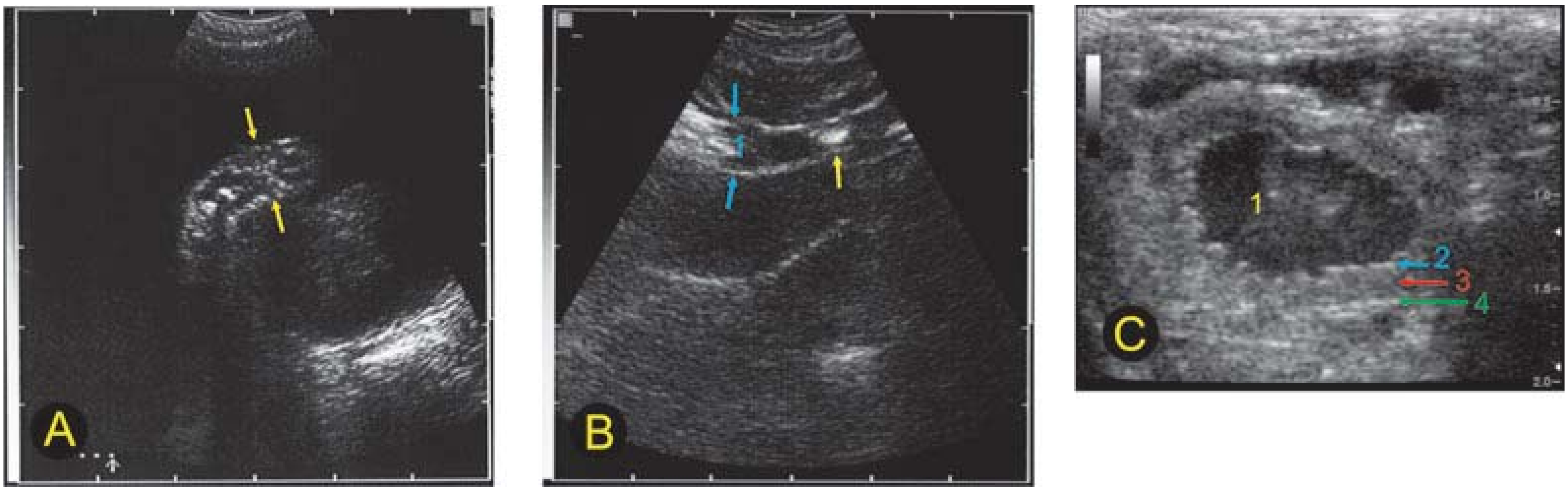

Fig. 1-160:

A: Ultrasonographic image of a chicken (*Gallus gallus*) with leukosis, ventromedian coupling site, oblique, 7.5 MHz, PD 6 cm. There are tumors (arrows) on one of the intestinal loops.

B: Ultrasonographic image of a honey buzzard (*Pernis apivorus*) with a foreign body, ventromedian coupling site, 7.5 MHz, PD 6 cm. Image of the hyperechoic roundish foreign body (yellow arrow) can be observed in the longitudinal section of intestine (1, blue arrows).

C: Ultrasonographic image of a rainbow lorikeet (*Trichoglossus haematodus*) diagnosed with bacterial enteritis, ventromedian coupling site, oblique, 12 MHz, PD 2.0 cm. The intestinal lumen (1) is filled with fluid; the intestinal wall is thickened.

1: intestinal lumen
2: mucosa
3: muscularis
4: serosa

Fig. 1-161:

A: Ultrasonographic image of a military macaw (*Ara militaris*) diagnosed with proventriculus dilatation and compaction, ventromedian coupling site, oblique, 7.5 MHz, PD 2 cm. Image of dilated thin-walled cross-section of the proventriculus (arrows); food has accumulated in the lumen.

B: Ultrasonographic image of a red kite (*Milvus milvus*) that has a distended cloaca (1) with hyperechoic urate deposits (2), ventromedian coupling site, longitudinal, 7.5 MHz, PD 2 cm.

C: Ultrasonographic image of a blue-fronted Amazon a (*Amazona aestiva*) diagnosed with intracloacal »papillomatosis,« ventromedian coupling site, oblique, 7.5 MHz, PD 2 cm. The typical cauliflower-like growths can be seen as echogenic structures (arrow) in the wall of the lumen of the oblique section of the (1) cloaca.

1: cloaca
2: urate deposits

arrows: growths in the wall of the cloaca

1.9 Liver and spleen

Maria-Elisabeth Krautwald-Junghanns, Michael Pees

To properly assess the liver using imaging methods, traditional radiodiagnostics are important in providing the first indications of liver abnormalities followed by ultrasonography to examine the liver parenchyma. Although the echogenicity of liver tissue affected by inflammation, neoplasia, calcification, and granulomas are different, one can only gain a tentative diagnosis of a lesion from its ultrasonographic image. For a definitive diagnosis, a fine needle aspirate or tissue biopsy is required. As with mammalian patients, sonographically-controlled biopsies are easily collected from the liver parenchyma at predetermined sites (see Chap. 1.2.5). There is little information gained by examining the avian gallbladder that one can use for diagnostic purposes, since many pet birds do not have a gallbladder and as few pathological gallbladder changes have been described in the literature. Splenomegaly is often diagnosed in combination with enlargement of the liver and/or kidneys, and is usually considered an indication of infectious disease. Sonographically, the spleen should be assessed and evaluated on a case-by-case basis.

1.9.1 Liver

The most common anatomic change observed on radiographic images is an enlargement of the liver shadow. However, the size of the liver is variable within an avian species and between species, therefore establishing diagnostic measures is unrealistic. Determination of the liver's exact size is nearly impossible sonographically since it is only partially observed and due to summation of the gastrointestinal tract. In contrast, a more exact assessment of liver mass can be determined radiographically, as its comparative size (i.e. usually with respect to the length of individual vertebrae) can be established **(Fig. 1-162A)**.

If liver tissue is observed extending caudal of the xiphoid, then it can be assumed that the bird has **hepatomegaly (Fig. 1-162C)**. The underlying etiological causes of hepatomegaly can be infectious (e.g. herpesviruses, other viruses, psittacosis, tuberculosis), neoplasia, metabolic disease (e.g. hemochromatosis in Mynas!), and obesity. In granivorous species (e.g. parrots), the soft-tissue shadow of the heart and liver in the VD projection loses its typical hourglass shape **(Figs. 1-162A** and **1-163A)**. In infections with *Chlamydophila psittaci*, often swelling of other organs is observed, especially the spleen **(Figs. 1-162** and **1-163)** and kidneys. If one has determined that heptomegaly is present, then further radiographic images can be taken after the administration of barium sulfate to differentiate the liver from any other enlarged organs.

Liver tumors, commonly diagnosed in budgerigars, are also characterized on radiographic images by an enlarged liver shadow. Liver tumors also cause a dorsal displacement of the proventriculus. Gastrographic imaging is also necessary for cases involving liver tumors to provide an exact differentiation of the surrounding tissue **(Fig. 1-164)**. However, a ultrasonographic examination provides significantly better delineation of surrounding tissue structures, therefore the use of a radiographic contrast medium is usually not required. One of the most common indications for an ultrasonographic examination in birds is enlargement of the liver silhouette in radiographic images. The **change in the liver parenchyma** can be determined sonographically and a distinction made between neoplasia **(Figs. 1-164** and **166B, C)**, cyst, inflammation **(Fig. 1-167B)**, congestion **(Fig. 1-174)** or fatty degeneration **(Fig. 1-168)**. Basically, ultrasonography can differentiate not only the changes within the liver parenchyma (e.g. diffuse, focal) and thier size, but also **changes in form (Figs. 1-168A** to **1-169)** and changes to the **hepatic vessels (Fig. 1-174)**. As with mammalian species, ultrasonographic image of a **fatty liver** in birds is characterized by increased echogenicity (i.e. diffuse changes in the liver parenchyma) and hepatomegaly **(Figs. 1-168** and **1-169)**. Disturbances in blood vessel architecture are not observed.

The most common cause of focal changes within the liver parenchyma is **neoplasia (Figs. 1-164** to **1-166)**. Liver tumors are characterized by a variable echogenicity of the liver tissue in the ultrasonography image. In addition to the liver tumors diagnosed in budgerigars, bile duct carcinomas have been anecdotally associated with psittacine papillomatosis disease. Bile duct carcinomas can also appear as focal changes within the liver parenchyma **(Fig. 1-171)**. These focal changes can be diffusely distributed throughout the liver tissue. Both **acute** and **chronic hepatitis** have an unspecific ultrasonographic appearance **(Fig. 1-167B)**. In comparison, infectious **granulomatous processes**, including leukosis **(Fig. 1-172)**, tuberculosis, or *E. coli* granulomatosis have been identified. In the ultrasonographic image, individual liver abscesses, granulomas, and necrotic areas are usually observed as being well demarcated from the normal liver tissue **(Fig. 1-170)**. Depending on the cellular structure of these foci, the images can be hypoechoic with corpuscular constituents or have a variable hyperechoic pattern due to the presence of numerous chambers.

Comparatively diffuse **liver necrosis** has a patchy nonhomogeneous pattern within the ultrasonographic image **(Fig. 1-174A)**. These tissue changes can become calcified over time in avian patients suffering from diffuse liver necrosis. There is large variation to the size of cirrhotic livers in birds. However, the majority of birds usually present in advanced stages of liver disease and therefore exhibit only a mild hepatomegaly **(Fig. 1-173)**. The sonomorphology is not uniform, although an increased echogenicity of the liver's interior indicates the presence of **liver cirrhosis**.

Cardiovascular insufficiency (e.g. shock) can result in acute and chronic **liver congestion,** which presents sonographically as hepatomegaly with an increased echogenicity (see Chap. 1.2; **Fig. 1-126**).

Liver cysts are structures with hyperechoic walls and anechogenic contents, and are characterized by a distal artifact due to sound reinforcement (this means that the distal area under the cyst appears more hyperechoic than the surrounding tissue because of the reduction of the ultrasound waves in the cyst fluid). **Liver hematomas** appear as hypoechoic areas in the liver tissue. In follow-up ultrasonographic examinations, these areas tend to become organized, characterized by an ice-flow-like increase in the echogenicity of the affected area. **Displacement of the liver** is rare and occurs only in cases of massive soft-tissue tumors situated in the abdomen. Additionally, a reduction in the liver shadow can occur after long periods of fasting, especially in raptors; this should not be misinterpreted as a pathological change. The **form of the liver** can only be assessed with reservation in birds due to the incomplete ultrasonographic visualization of the organ. Parts of the liver can be well differentiated, especially in the presence of ascites **(Fig. 1-174B)**. In small birds, a partial differentiation of the liver can be achieved, especially the caudal edge near to the transducer, with the use of a spacer.

1.9.2 Gallbladder

The gallbladder cannot be radiologically identified; however, on rare occasions, **gallstones** can be observed sonographically as an obvious hyperechoic concentration of particles within the appropriate area of the liver. In addition to the anechogenic bile inside the lumen of the gallbladder, there are hyperechoic particles which in contrast to connective tissue deposits can be made to swirl around. It is also possible to sonographically identify enlargement of the gallbladder **(Fig. 1-167A)**.

1.9.3 Ascites

A diffuse soft-tissue shadowing of a bird's celoemic cavity apart from the lung field is indicative of ascites (see **Figs. 1-122** to **1-124** and **1-126**). Ascites is often associated with severe inflammation of the liver and liver tumors. Ascites occurring within the framework of a hepatopathy is often associated with hemochromatosis in the myna bird **(Fig. 1-175)**. Due to fluid accumulation within the celoemic cavity, internal organs cannot be differentiated radiographically apart from the air-filled lungs. However, free fluid is a good contrast medium for ultrasonography and the liver can be easily imaged and pathological changes recognized **(Figs. 1-167B, C** and **1-174B)**. Furthermore, ultrasonography can be used without difficulty to monitor the patient's response to ascites treatment.

1.9.4 Spleen

Splenomegaly is often considered as the organ's reaction to an infectious disease process **(Figs. 1-162** and **1-163)**. Depending on the clinical history and individual case, splenomegaly may be a response to avian chlamydiosis or mycobacteriosis infections. If avian chlamydiosis is on the differential diagnosis list and severe splenomegaly is observed radiologically, then diagnostic samples should be submitted specifically for *Chlamydophila psittaci* testing. After the collected samples have been submitted, appropriate treatment for avian chlamydiosis should be initiated and continued until the diagnostic test results are received. At this time, the treatment protocol can be reassessed utilizing the information provided by the diagnostic laboratory. Splenic tumors which are rarely diagnosed and primarily found in budgerigars can cause a dorsocranial displacement of the gastrointestinal tract in a radiographic image. When sonographically imaging an avian patient's enlarged spleen, the organ can occasionally be identified as a round or oval structure exhibiting a medium echogenic return. A differentiation between inflammatory and neoplastic changes is difficult to determine in the spleen, although at times hemorrhages can be identified due to their variable echogenicity **(Fig. 1-176A)**. If the spleen significantly increases in size, it can be sonographically identified by using the median coupling site. In addition to the homogenous **changes in the splenic parenchyma** observed in association with infectious disease **(Fig. 1-176B)** and trauma **(Fig. 1-176A)**, tumor-like changes (e.g. leukosis) can be depicted sonographically as focal nonhomogeneous changes within the splenic parenchyma.

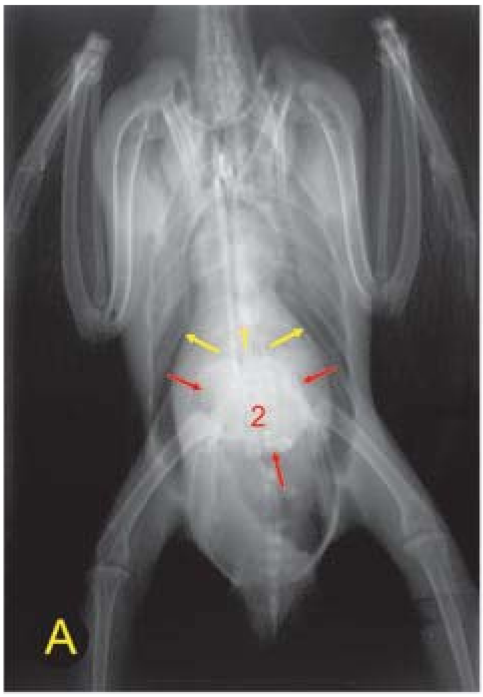

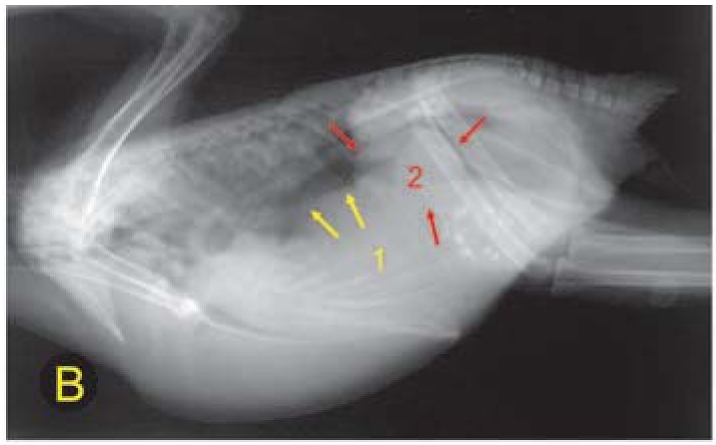

1, yellow arrows: liver
2, red arrows: spleen

Fig. 1-162:

A, B: Total body radiographic images of a blue-fronted Amazon (*Amazona aestiva*) diagnosed with psittacosis, (A) dorsoventral and (B) lateral views. The liver (1, yellow arrows) is obviously enlarged and the typical »hour-glass shape«is no longer present. The spleen (2, red arrows) can also be seen in both views and is greatly enlarged.

C: Gross pathological image of a Blue-fronted Amazon (*Amazona aestiva*) with clinically manifested psittacosis. The liver (1) extends well over the caudal edge of the keel and has rounded edges. The hemorrhage noted in the region of the thoracic musculature is the site of an intramuscular injection.

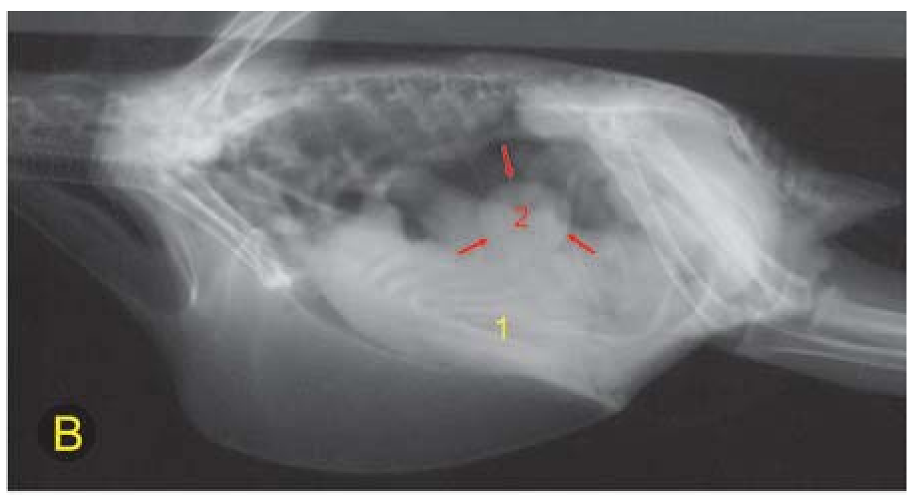

1, yellow arrows: liver
2, red arrows: spleen

Fig. 1-163: Total body radiographic image of a white-fronted Amazon (*Amazona albifrons*) diagnosed with psittacosis, (A) dorsoventral and (B) lateral projections. The liver enlargement (yellow arrows) has resulted in the loss of the »hour-glass« shape of the cardiohepatic shadow (yellow lines). The spleen (2) is also clearly visible, while the intestines appear distended in the lateral projection. There is also addition a lack of grit in the gastrointestinal tract.

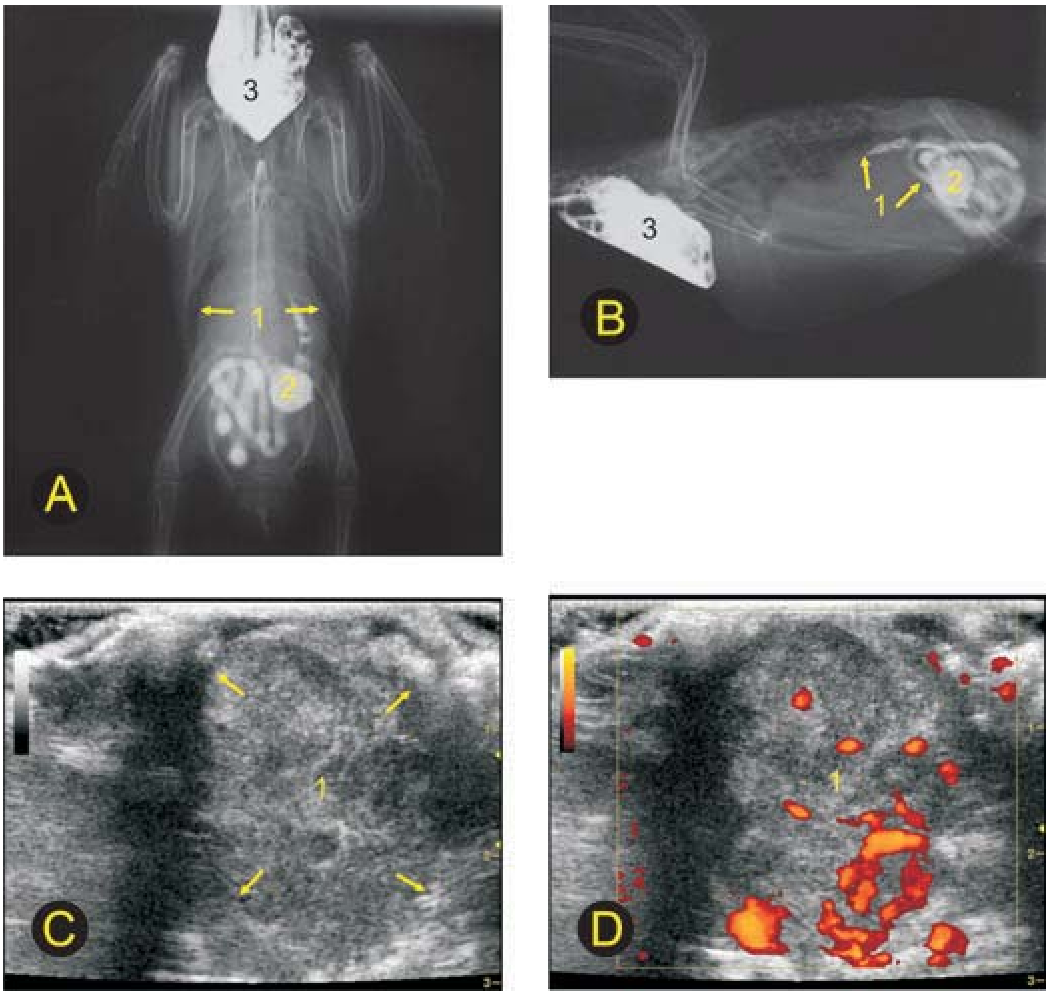

1: liver
2: gastrointestinal tract
3: crop

Fig. 1-164:

A, B: Total body radiographic images of a budgerigar (*Melopsittacus undulatus*) diagnosed with a hepatic tumor, (A) dorsoventral and (B) lateral projections, 1 h after the administration of barium sulphate [350 mg/ml, 20 ml/kg bwt, in the crop (3)]. The enlarged liver (1) and the caudodorsally displaced gastrointestinal tract (2) can be seen in the radiograph. Further differentiation is not possible.

C,D: Ultrasonographic images of the same bird, ventromedian coupling site, oblique, 12 MHz, PD 3 cm, Power-Doppler method (D). The liver (1) appears sonographically hyperechoic with a nonhomogeneous increase in size. The perfusion is diffuse (D).

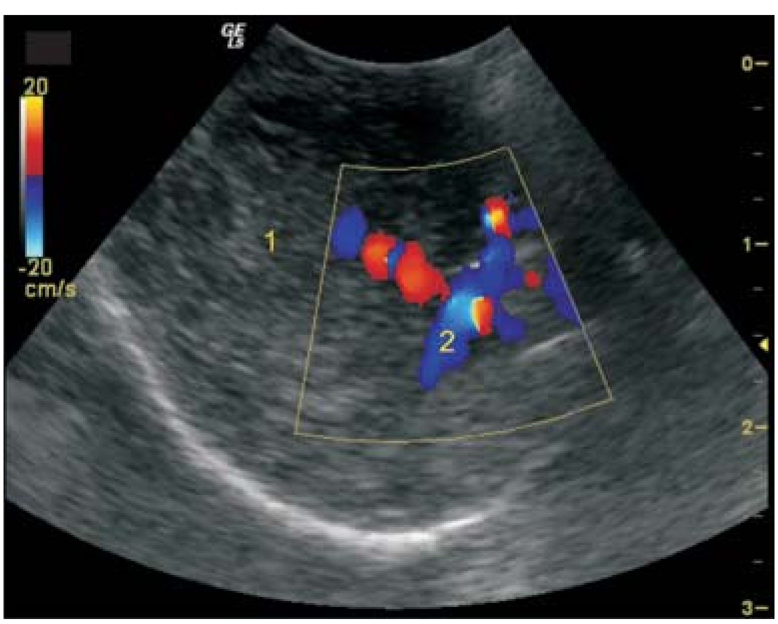

1: liver
2: focal areas of increased liver perfusion

Fig. 1-165: Ultrasonographic image of a budgerigar (*Melopsittacus undulatus*) with a hepatic tumor, ventromedian coupling site, longitudinal, 10 MHz, PD 3 cm, color-Doppler method. The liver (1) is homogenously enlarged, whereby there are focal areas of increased perfusion (2).

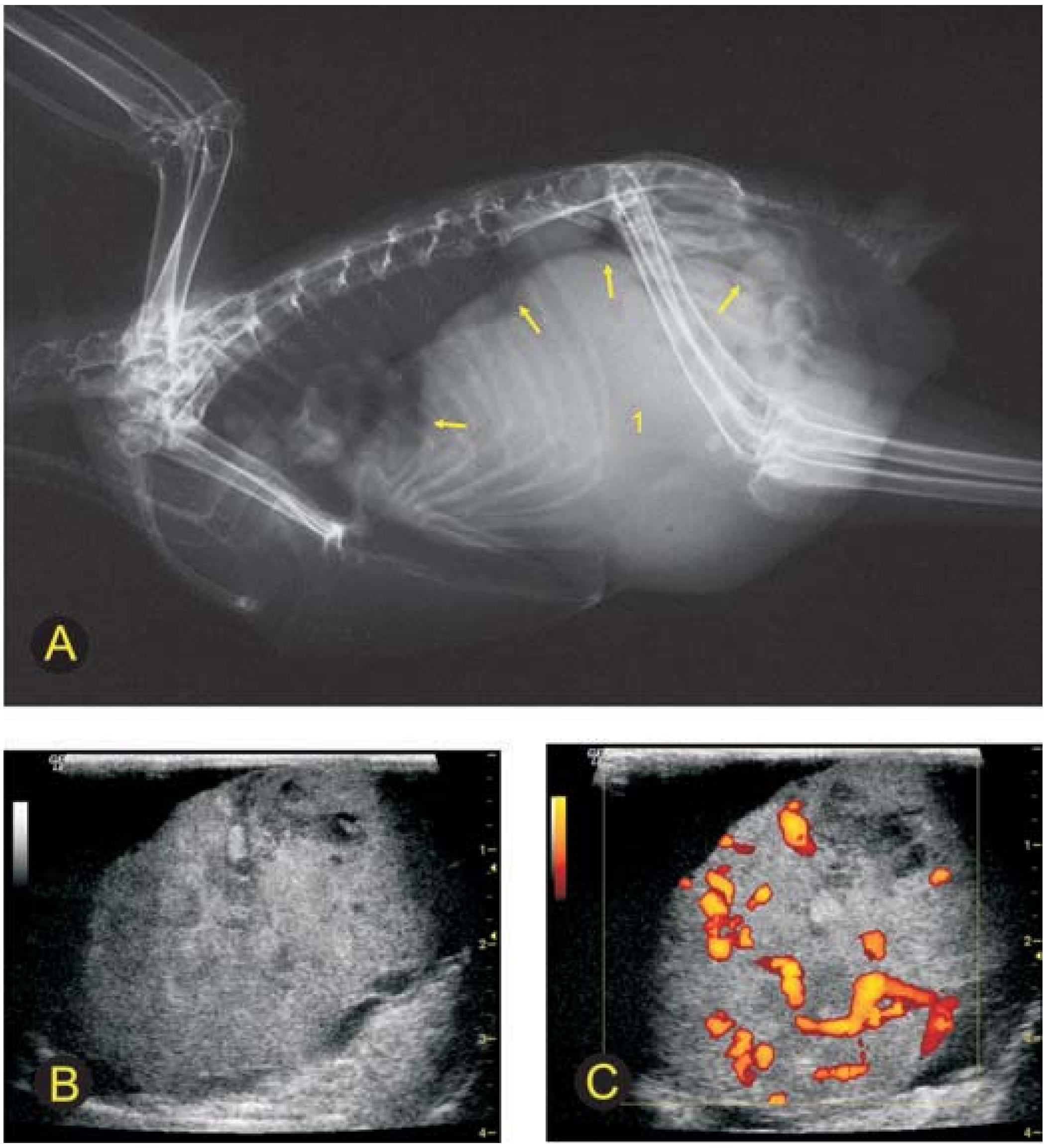

1: liver

Fig. 1-166:

A: Total body radiographic image of an Indian hill myna (*Gracula religiosa*) diagnosed with lymphosarcoma, lateral projection. The air sacs have been significantly displaced by the liver (1). The details within the body cavity are difficult to identify. The radiograph also shows signs of hemochromatosis, which is often found in Hill Mynas (see Fig. 1-175).

B: Ultrasonographic image of the same bird, ventromedian coupling site, oblique, 12 MHz, PD 4 cm.

C: Power-Doppler method of the same bird with the liver appearing hyperechoic and heterogenous. The perfusion is diffuse and there are areas of focal necrosis present.

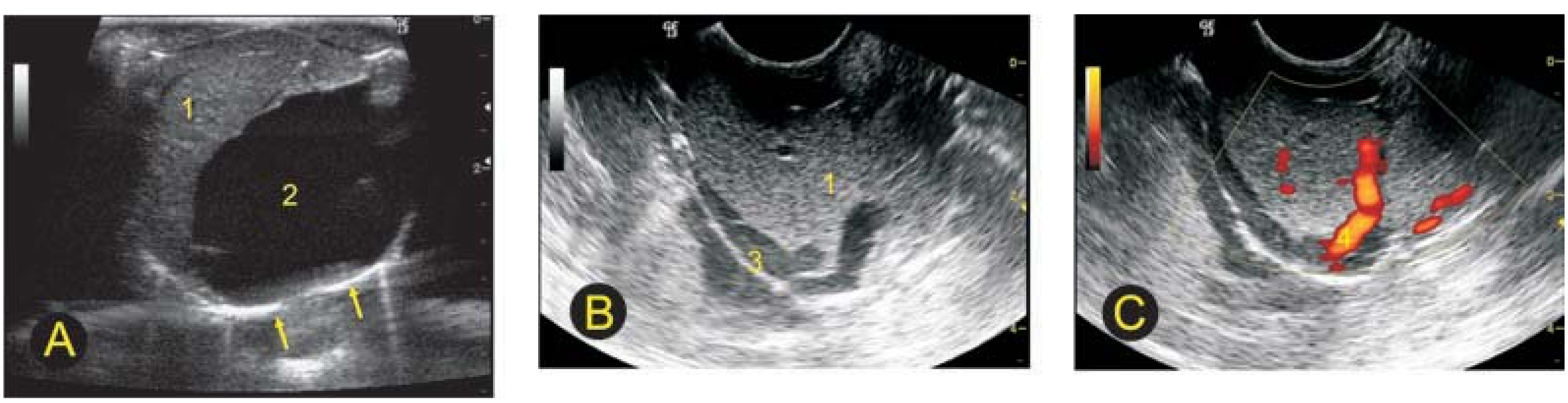

Fig. 1-167:

A: Ultrasonographic image of a Moluccan cockatoo (*Cacatua moluccensis*) with a congested gallbladder, ventromedian coupling site, longitudinal, 12 MHz, PD 5 cm. The gallbladder (2) appears as an echo-free region with distal sound reinforcement (arrows) in the unremarkable hepatic tissue (1). As a gallbladder occurs in numerous cockatoo species, it must be differentiated from cystic changes in the liver by considering its position, form, and size.

B, C: Ultrasonographic images of an African grey parrot (*Psittacus erithacus*) diagnosed with bacterial hepatitis, ventromedian coupling site, longitudinal, 10 MHz, PD 5 cm, Power-Doppler method. The liver (1) is enlarged and in some areas there is fluid (3) within the hepatic tissue. The hepatic vessels (4) are dilated.

1: liver
2: gallbladder
3: fluid
4: hepatic vessels

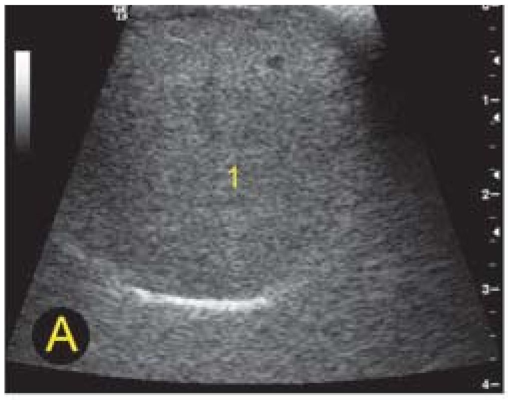

1: liver
2: heart
3: ventriculus

Fig. 1-168:

A: Ultrasonographic image of a galah cockatoo (*Eolophus roseicapillus*) with hepatic lipidosis, ventromedian coupling site, oblique, 10 MHz, PD 4 cm. The liver (1) is significantly enlarged, homogenous, and hyperechoic. The limits of the organs are barely visible. The intrahepatic vessels cannot be seen.

B: Gross pathological image of the same bird clearly showing the swollen edges and yellow discoloration of the liver due to fat deposition.

1: liver

arrows: limits of the liver lobes

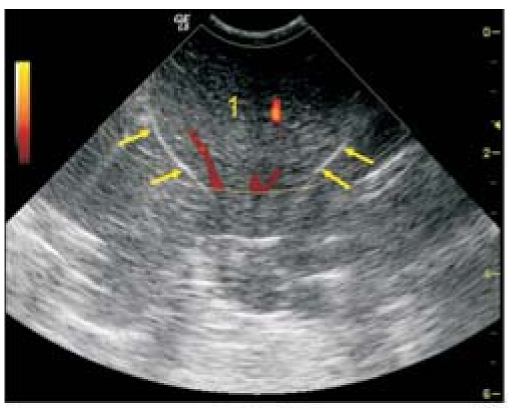

Fig. 1-169: Ultrasonographic image of an African grey parrot (*Psittacus erithacus*) with an idiopathic hepatomegaly, ventromedian coupling site, oblique, 10 MHz, PD 6 cm, Power-Doppler method. The size of the liver (1) can be sonographically evaluated by viewing the hyperechoic limits between the lobes (arrows). The liver lobes are displaced away from each other when there is an enlargement of the middle lobe.

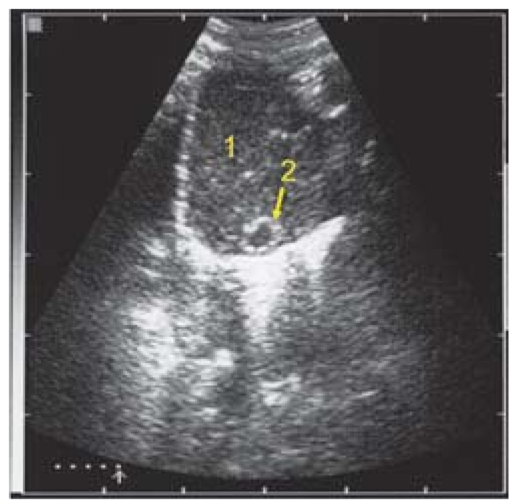

1: liver
2: area of calcification

Fig. 1-170: Ultrasonographic image of a budgerigar (*Melopsittacus undulatus*) with chronic hepatitis and small areas of calcification, ventromedian coupling site, longitudinal, 7.5 MHz, PD 6 cm. A well-defined hyperechoic structure (2) can be seen lying in the liver tissue (1). This area of calcification is a secondary tissue response to inflammation.

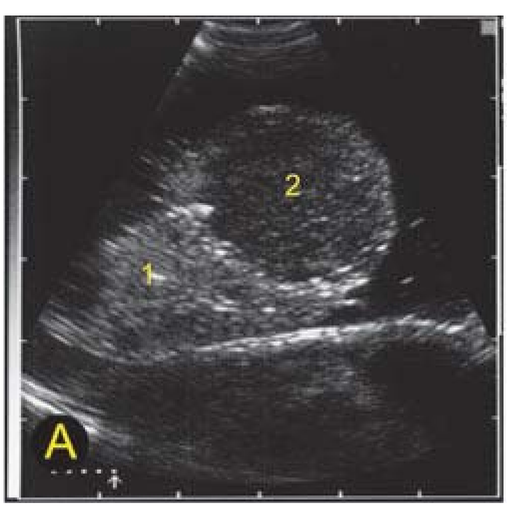

1: liver
2: tumor

Fig. 1-171:

A: Ultrasonographic image of a double yellow-headed Amazon parrot (*Amazona ochrocephala*) diagnosed with a bile duct carcinoma, ventromedian coupling site, longitudinal, 7.5 MHz, PD 6 cm. The well-defined structure (2) within the liver tissue (1) is a bile duct carcinoma, commonly believed to be associated with cloacal papillomatosis.

B: Gross pathological image of the same bird showing the tumor (2) lying within the hepatic tissue (1).

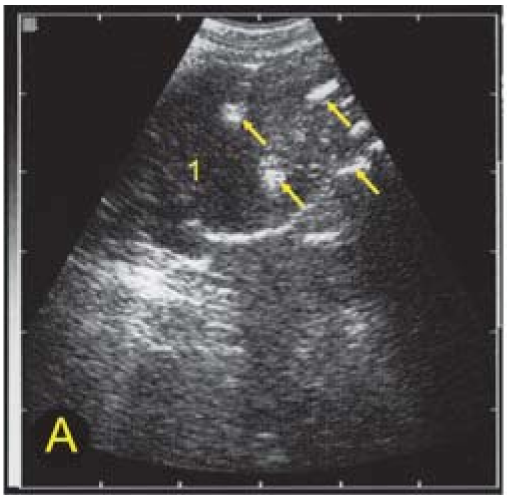

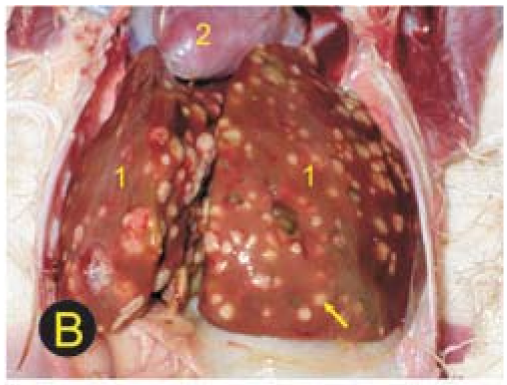

1: liver
2: spleen

arrows: leukemic changes

Fig. 1-172:

A: Ultrasonographic image of a red-crowned parakeet (*Cyanoramphus novaezelandiae*) diagnosed with leukosis, ventromedian coupling site, longitudinal, 7.5 MHz, PD 6 cm. The leukemic changes (arrows) appear as hyperechoic areas within the liver tissue (1).

B: Gross pathological image of the same bird showing the multifocal neoplastic changes (arrow) within the liver tissue (1).

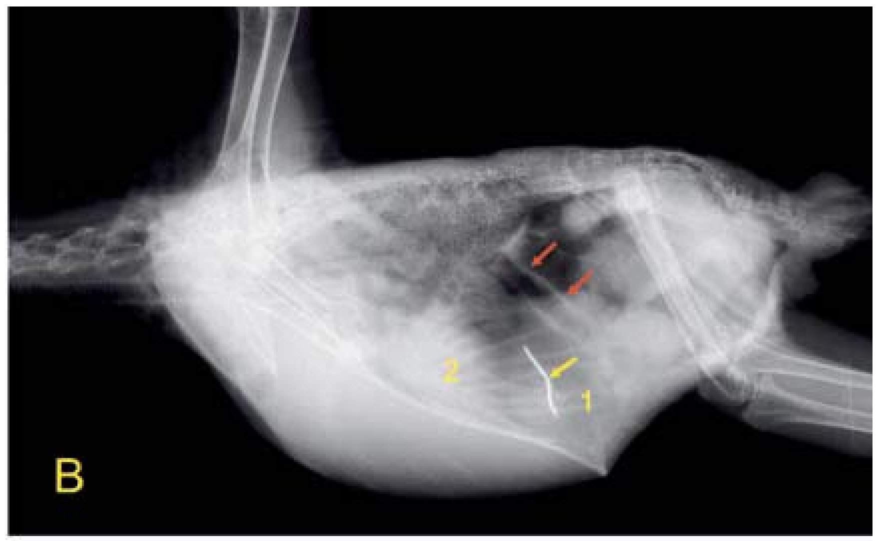

1: liver
2: heart

red arrows: edges of air sacs
yellow arrows: wire

Fig. 1-173: Total body radiographic images of an African grey parrot (*Psittacus erithacus*) with liver cirrhosis, inflammation of the caudal coelomic cavity, and a foreign body within the liver tissue, (A) ventrodorsal and (B) lateral projections. The assessment of cirrhotic liver changes is not easy. In this bird, a wire (yellow arrows) has migrated through the liver capsule (1) leading to a chronic inflammatory condition. The coelomic cavity is inflamed, and the edges of the air sacs are thickened (red arrows).

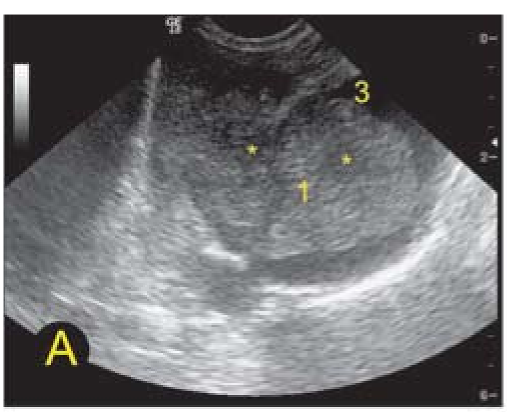

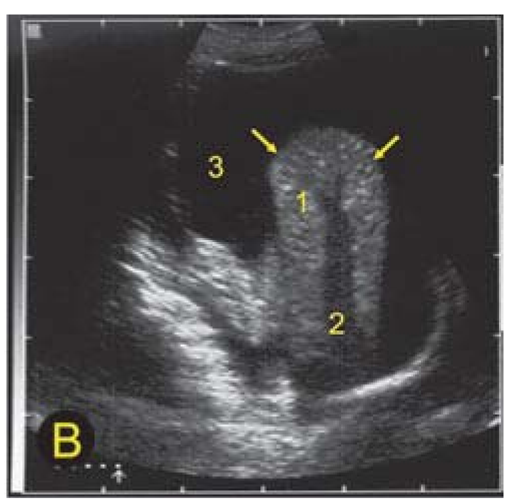

1: liver
2: hepatic vessels
3: ascites

*: necrotic foci

Fig. 1-174:

A: Ultrasonographic image of a blue-fronted Amazon (*Amazona aestiva*) with liver necrosis, ventromedian coupling site, longitudinal, 10 MHz, PD 6 cm. The hepatic tissue (1) appears nonhomogenous with hypoechoic necrotic foci (*). The hepatic vessels (3) appear to be congested.

B: Ultrasonographic image of an African grey parrot (*Psittacus erithacus*) with liver congestion and ascites, ventromedian coupling site, oblique, 7.5 MHz, PD 6 cm. In this case, the liver (1) is congested, the hepatic vessels (2) are clearly visible. The edge of the liver is rounded (arrows)

Fig. 1-175: Total body radiographic images of an Indian hill myna (*Gracula religiosa*) with hemochromatosis (iron storage disease), (A) ventrodorsal and (B) lateral projections. The liver is severly enlarged and is compressing the other organs in the coelomic cavity. The details of structures within the coelomic cavity are not easily identified due to the accumulation of fluid. (The bend of the trachea is physiologically normal in this species.)

C: Ultrasonographic image of the same bird, ventromedian coupling site, oblique, 12 MHz, PD 3.0 cm. The liver is also enlarged in the ultrasonographic image. It is hyperechoic and irregular in form.

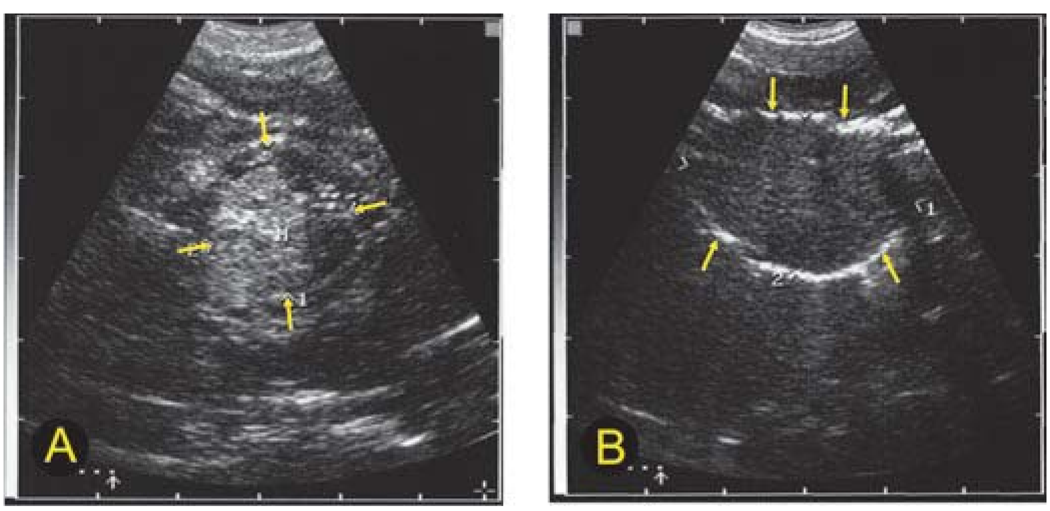

Fig. 1-176:

A: Ultrasonographic image of a blue-and-yellow macaw (*Ara ararauna*) with splenic rupture, ventromedian coupling site, oblique, 7.5 MHz, PD 6 cm. The spleen (yellow arrows) appears to be very nonhomogenous due to hemorrhaging.

B: Ultrasonographic image of a common buzzard (*Buteo buteo*) with splenomegly due to tuberculosis, ventromedian coupling site, oblique, 7.5 MHz, PD 6 cm. This is a rare example of the spleen (yellow arrows) being identified using ultrasonographic imaging.

1.10 Urogenital tract

Maria-Elisabeth Krautwald-Junghanns, Michael Pees

Renal disease often occurs in association with general systemic infections. The diagnostic imaging methods used to evaluate the kidneys are often limited to traditional radiography and – sometimes – ultrasonography, while CT and MRI imaging modalities are rather rarely used.

Renomegly, observed in radiographic images, is a nonspecific condition that may be a consequence of an infectious process **(Fig. 1-177)**, vitamin A deficiency, cyst formation, or, especially in budgerigars, neoplasia **(Fig. 1-178)**. A radiographic examination of the kidneys and ureters using organic iodine compounds as contrast material (see **Fig. 1-39)**,can provide additional information about the function and form of these organs **(Fig. 1-179)**. With disturbances in renal function or ureter blockage or displacement, the renal excretion of the contrast can be adversely affected and thus delayed.

The use of ultrasonographic diagnostic imaging is only recommended in cases of renal enlargement with displacement of the surrounding air sacs (*see* **Fig. 1-178)**, as this enables the kidneys to be imaged. The size and the parenchyma can be evaluated, both in small (e.g. budgerigars) and large birds without difficulty. In cross-section (i.e. scanning plane vertical to the spine), the kidneys are depicted in a W-shaped area of total reflection formed by the bones of the pelvis and spine **(Figs. 1-177** and **1-180A)**. In this projection, the two kidneys can be compared with each other. In cross-section, the kidneys appear round to oval and size measurements can be determined. By turning the transducer through 90°, the kidneys can be examined down their longitudinal axis (i.e. along the spine).

Diseases affecting the female genital organs occur in association with egg formation and/or laying problems. Male birds, in comparison, are mainly affected by gonadal tumors. For the latter, there is a definite species and age predisposition in middle-aged budgerigars (4–6 years old). Pathological changes of the gonads should never be confused with the extensive but normal physiological size increases of the testicles or ovaries and oviduct during reproductive activity. Imaging methods used for examining the genital tract are usually limited to traditional radiography and ultrasonography, whereby ultrasonographic imaging – as in renal diagnostics (see above) – can only be used in cases where there is enlargement of the genital tract and an associated displacement of the air sacs.

1.10.1 Kidneys

Inflammation of the kidneys can be observed as an enlarged renal shadow in radiographic images. Sonographically, the echogenicity of the enlarged, inflamed kidney is often hypoechoic with a reduced ability to image internal structures **(Figs. 1-177C** and **1-180A)**. Renal **neoplasia** is identified radiologically in the lateral projection as an obviously enlarged renal shadow or as a diffuse soft-tissue swelling in the caudodorsal abdomen **(Fig. 1-178)**. The enlarging cancerous mass will cause compression of primarily the caudal air sacs and a ventral displacement of the intestinal tract. The highly enlarged gonads found in both genders during the breeding season should not be interpreted as renal tumors (see Chap. 1.1.3.8). In order to verify the diagnosis of a renal tumor, it may be reasonable to utilize contrast investigations **(Figs. 1-178C, D** and **1-179)**, thereby localizing the affected organs. Gastrography can reveal the caudally displaced intestines thus providing information about the tumor location **(Figs. 1-178C, D)** and extent of renal enlargement. Neoplasia can lead to reduced urographic visualization of the kidney and ureters or there may be a lack of contrast flow through these structures **(Fig. 1-179)**. Sonographically, in comparison to inflamed kidneys, tumors can occasionally be observed as homogenously hyperechoic structures or as nonhomogeneous parenchyma with focal necrosis **(Fig. 1-180B)**.

By using the Doppler function, both the abdominal aorta lying between the two kidneys and extent of renal perfusion **(Fig. 1-181)** can be visualized. With the Doppler function, assumptions can be determined about the type and malignancy of the neoplastic mass. However, an exploratory laparotomy is necessary to obtain a definative diagnosis. Renal biopsies are associated with the risk of massive hemorrhaging in avian patients independent of whether ultrasonographic or endoscopic imaging is used to guide the tissue collection.

Cysts appear as a diffuse enlargement of the renal shadow on traditional radiographic images (analogous to the tumor in **Fig. 1-178)**. Sonographically, renal cysts have a typical appearance and can be easily differentiated from the renal parenchyma. On ultrasonographic images, renal cysts appear as structures with hyperechoic, smooth walls, hypoechoic contents and the phenomenon of distal sound reinforcement **(Fig. 1-182)**. If there is difficulty in differentiating a renal and ovarian cyst, then a sonographically controlled aspiration of the cyst cavity can be performed to evaluate the collected sample.

In addition to an enlargement of the renal shadow, specific case presentations will have an **increased radiopacity** of the kidney tissue, which may be caused by dehydration, vitamin A deficiency, or inflammatory processes. However, increased radiopacity of the renal tissue is difficult to assess due to the summation of the pelvic girdle in this region. A nonspecific sign of renal dysfunction is radiopaque particles observed in both standard radiographic projections within the renal shadow **(Figs. 1-183** and **1-184)**. The radiopaque particles are caused by **hypercalcification**, which often causes a parallel increase in blood calcium values of the patient.

A prolonged state of dehydration can lead to the crystallization of urates within the kidney. However, this crystallization or visceral gout is not visible on radiologic images. Urate deposits and/or calcification occasionally cause hyperechoic reflections in the ultrasonographic image with the renal tissue appearing nonhomogeneous. Sonographically, these structural abnormalities are not visible unless the kidneys are enlarged; therefore **renal gout** must be diagnosed using other methods (e.g. endoscopic biopsy, blood chemistry).

1.10.2 Gonads

Radiologically, **gonadal tumors** appear as diffuse soft-tissue swellings in the celoemic cavity compressing primarily the caudal air sacs and displacing the gastrointestinal tract **(Figs. 1-185** and **1-186)**. The gastrointestinal tract can be clearly depicted by using barium sulfate for contrast imaging. Particularly when viewing the lateral projection, the cranial gastrointestinal tract is displaced cranioventrally and on occasion in a caudoventral position **(Fig. 1-187)**. Sonographically, urogenital tumors are depicted with certainty and usually appear as enlarged organs with a nonhomogeneous, complex echo structure, often associated with a hypoechoic transition zone. Generally, the avian patient presents in an advanced stage of neoplastic disesae with a massive increase in size of the affected organs; consequently, classification of the tumor to the tissue of origin is very difficult when using ultrasonographic imaging **(Figs. 1-187** to **1-189)**. To obtain a definitive diagnosis, a biopsy of the affected tissue (N.B.: danger of internal hemorrhaging) and subsequent histological investigation of the collected sample are necessary.

Changes in the size and form of the gonads can be differentiated (e.g. ovarian cysts) **(Fig. 1-190)**, but they cannot be completely distinguished from each other when observed during the ultrasonographic examination. **Ovarian cysts,** due to their size, can lead to a severe swelling of the celoemic cavity while almost completely compressing the air sacs and surrounding organs. There is a species predisposition in budgerigars and canaries, however, other birds can develop these disease conditions. Radiologically, a severely enlarged soft-tissue shadow can be observed within the celoemic cavity. Often **medullary bone** has also been produced, which can be seen as a homogenous or nonhomogeneous radiopacity (e.g. calcium deposition) within the long bones **(Fig. 1-190A, B)**. Cysts are easily identified sonographically **(Fig. 1-190C)** and are characterized by their echogenic, smooth walls with hypoechoic contents and the phenomenon of distal sound reinforcement. Although oviductal cysts are uncommon presentations when compared to ovarian cysts, they can occur and have been diagnosed in avian patients.

1.10.3 Oviduct

An egg within the oviduct can be palpated as long as its shell has been mineralized and the egg is not too deep in the celoemic cavity. Radiography is indicated to diagnose **egg binding**, especially to determine the number, form, size, composition of the shell, and position of the egg(s). Once the above information has been obtained, a treatment decision is established on whether to use either a conservative or surgical method to treat the egg binding **(Figs. 1-191** to **1-193)**. Laminated eggs and eggs with very thin shells appear radiologically as diffuse soft-tissue swellings within the celoemic cavity, primarily compressing the caudal air sacs and displacing the gastrointestinal tract **(Fig. 1-194)** (i.e. similar to tumors, inflammation, and cysts found in this area). Mummified eggs, however, can be seen easily as radiodense objects **(Fig. 1-196)**. An additional radiographic sign that indicates the presence of an increased blood estrogen level is the development of medullary bone (see above). Sonographically, it is possible to differentiate between a tumor, cyst, and egg binding. Eggs with a mineralized shell can also be observed using ultrasonographic imaging (see Chap. 1.2.7.8 and **Fig. 1-69B**). As opposed to radiographic images, the strong sound reflections associated with an ultrasonographic examination will, only on rare occasions, identify shell abnormalities (e.g. roughness [see **Fig. 1-193**], deformation [see **Fig. 1-192**]). The advantage of ultrasonographic examination is the diagnosis of egg binding due to eggs with an unmineralized or only slightly mineralized shell (»wind eggs«) **(Fig. 1-197)** or egg concretions caused by inflammation and contain abnormal fibrinous egg components that often have a multilayered structure (e.g. laminated eggs) and lie either in the oviduct or celoemic cavity **(Figs. 1-194** and **1-198)**. Laminated eggs situated in the oviduct appear as onion-like, round to round/oval structures of varying echogenicity, surrounded by a hypoechoic layer of fluid.

Essentially, the assessment of an egg through diagnostic means aids in the decision-making process about whether or not surgery is required. The following radiographic or ultrasonographic criteria are important when formulating a treatment plan for this disease process:

- ☐ **Number:** As the transit of the egg through the avian oviduct takes approximately 24 hours after ovulation and for the majority of parrots and parakeets, ovulation takes place every second day, only one calcified egg is anticipated during an examination. However, in some avian species there can be two inconspicuous eggs of the same shape present, which do not therefore need to be surgically removed **(Fig. 1-191)**.
- ☐ **Form:** Deformed and collapsed eggs are frequently the cause of egg binding and these presentations are usually an indication for surgery **(Fig. 1-192)**.
- ☐ **Shell:** Egg binding, which is associated with shell abnormalities (e.g. unmineralized shell, laminated eggs, eggs with hypercalcified shells, broken shells) usually need to be treated surgically **(Figs. 1-192** to **1-194** and **1-198)**.
- ☐ **Egg size:** As birds do not have a bony pelvis base, egg size is rarely a problem in laying, though in some cases treatment may be necessary **(Fig. 1-191)**.

Indications of the **oviduct changes** found in association with egg binding, include inflammation of the oviduct (salpingitis) **(Fig. 1-195)**, and can only be identified radiographically in rare severe cases due to nonspecific findings like diffuse soft-tissue changes within the celoemic cavity. Often, eggs with abnormal shells are thought to be associated with salpingitis. With hernias involving the celoemic wall muscular **(Fig. 1-107)**, displacement of the gastrointestinal tract, and increased radiopacity in the long bones, the presence of egg concretions should be suspected, which can then be observed as extensive soft-tissue shadows in the celoemic cavity. Sonographically, salpingitis can be clearly identified in an advanced stage due to the increased wall thickness. In the lumen of the oviduct, physiological structures associated with inflammation can be identified with varying degrees of echogenicity. The variability of the echogenic response from structures within the lumen of the ovident is relative to their density and physiological integrity **(Figs. 1-195C** and **1-197)**. In contrast to the ingesta found in the intestines, whose active transport can be easily followed using ultrasonography, the inflammatory products within the salpinx can be moved passively by applying slight pressure on the ventral aspect of the caudal celoem or by moving the patient.

Egg-induced peritonitis can be identified radiologically as a diffuse overshadowing of the celoem. With severe ascites, there is a characteristic lack of definition of the internal organs apart from the air-filled lungs. Sonographically, ascites is clearly visible as the fluid acts as an ideal contrast medium. In some case, flakes of fibrin or fibrinous deposits can be identified on the surrounding organs **(Fig. 1-199)**. However, an advanced case of peritonitis cannot be definitively diagnosed using ultrasonography. Often a yellowish exudate can be collected via celoemocentesis, which may contain flakes of yolk or vitreous.

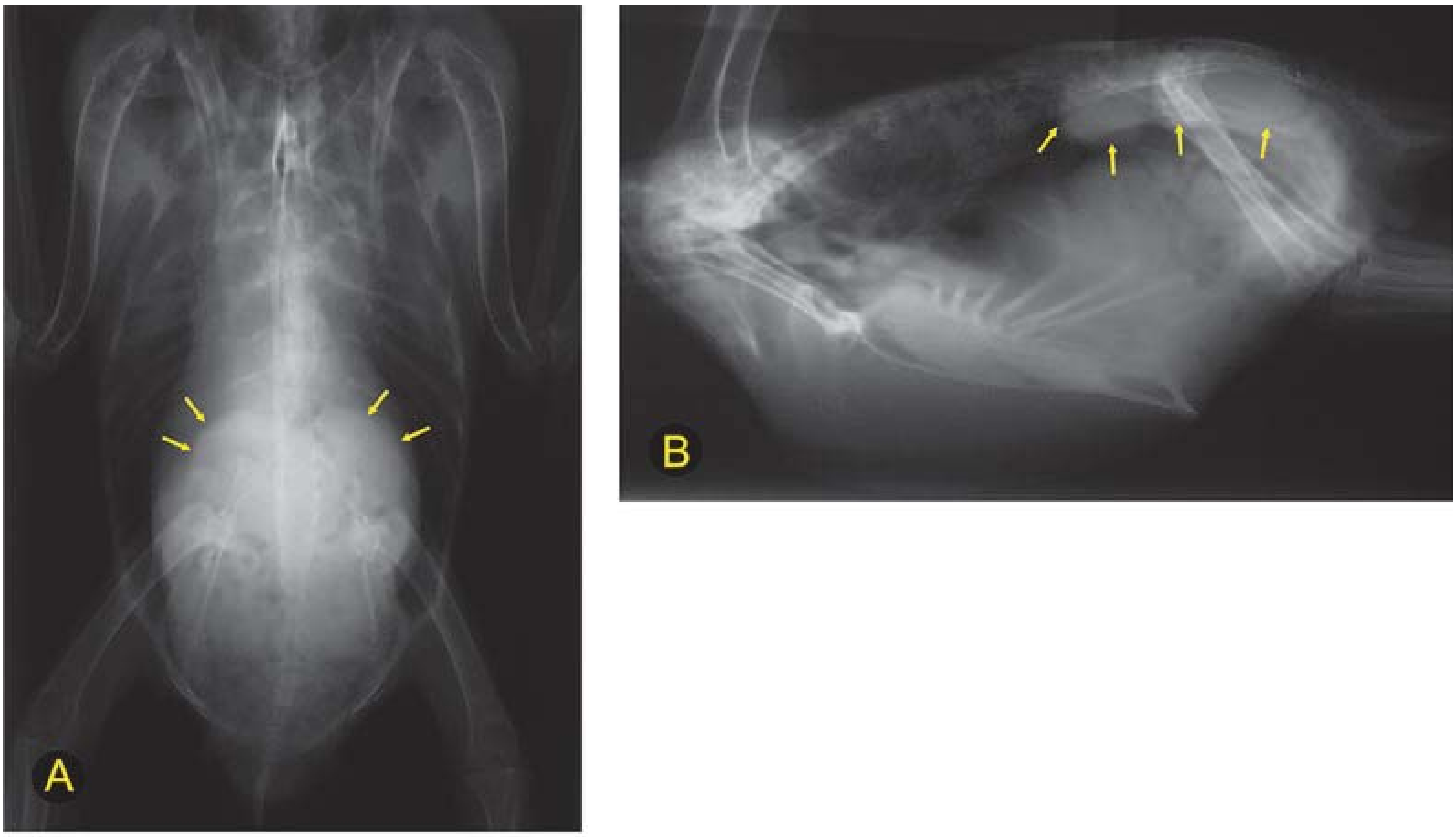

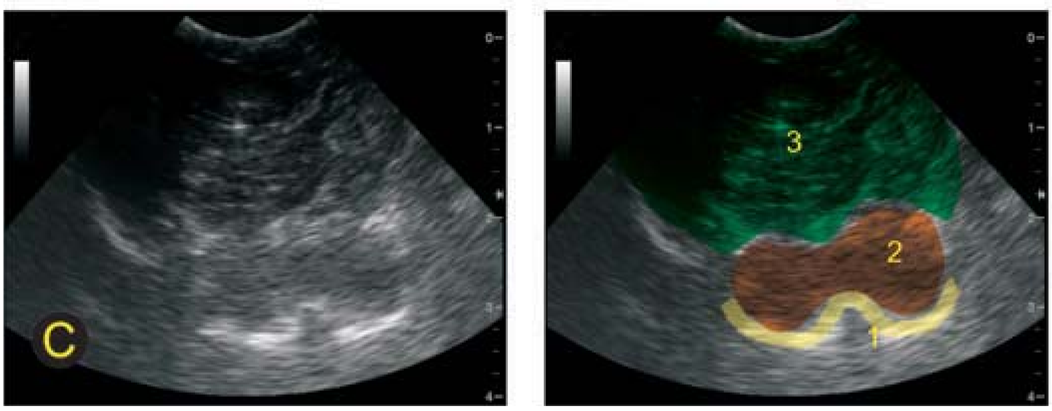

1: renal fossa
2: kidney
3: loop of intestine

arrows: swollen kidneys

Fig. 1-177:

A, B: Total body radiographic images of an orange-winged Amazon (*Amazona Amazonica*) with bacterial nephritis, (A) ventrodorsal and (B) lateral projections. The cardio hepatic silhouette's »hour-glass« shape (ventrodorsal projection) has been lost due to renal swelling (arrows). The gastrointestinal tract is distended and in places severely enlarged.

C: Ultrasonographic image of the same bird's kidney showing renomegly (2) with a homogenous parenchyma; ventromedian coupling site, transverse, 7.5 MHz, PD 4 cm. The W-shaped renal fossa (1) can also be seen.

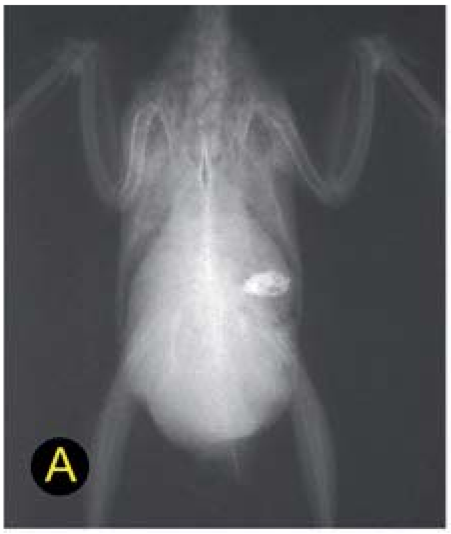

Fig. 1-178: A, B: Total body radiographic images of a budgerigar (*Melopsittacus undulatus*) with a renal tumor, (A) ventrodorsal and (B) lateral projections.

A: Loss of the cardiohepatic silhouette's »hour-glass« shape, displacement of the ventriculus, radiopaque soft-tissue swelling with compression of the caudal air sacs.

B: Radiopaque soft-tissue swelling with compression of the caudal air sacs and cranial compression of the ventriculus.

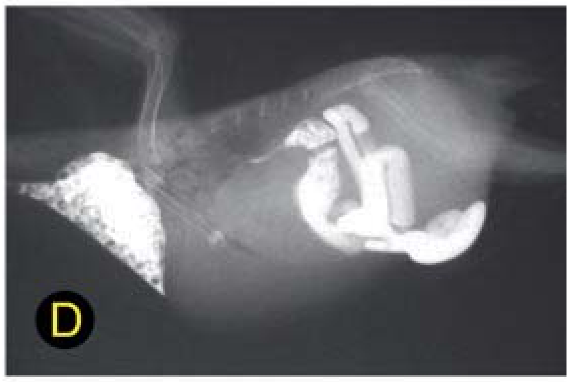

C, D: Total body radiographic images of the same bird, (C) ventrodorsal and (D) lateral projections, 1 hour after the administration of barium sulphate (350 mg/ml, 20 ml/kg bwt in the crop). There is cranial displacement of the stomach and the small intestines by the soft tissue tumor, along with a ventral compression of the caudal loop of intestines. These findings are especially pronounced in the lateral projection. The crop is filled with grain.

yellow arrows: kidneys
red arrow: intravenous catheter in the wing vein

Fig. 1-179: Radiographic image of the caudal coelom of a budgerigar (*Melopsittacus undulatus*) with a renal tumor, ventrodorsal projection, 1 minute after the administration of iomeprol (Imeron, 300 mg iodine/ml, 2 ml/kg bwt, i. v.). The kidneys are radiopaque and appear enlarged and changed in form (yellow arrows). The excretion of the contrast medium is delayed. The ureters are not radiopaque.

1: kidneys
2: loop of intestine

yellow arrows: renal fossa
red arrows: tumor

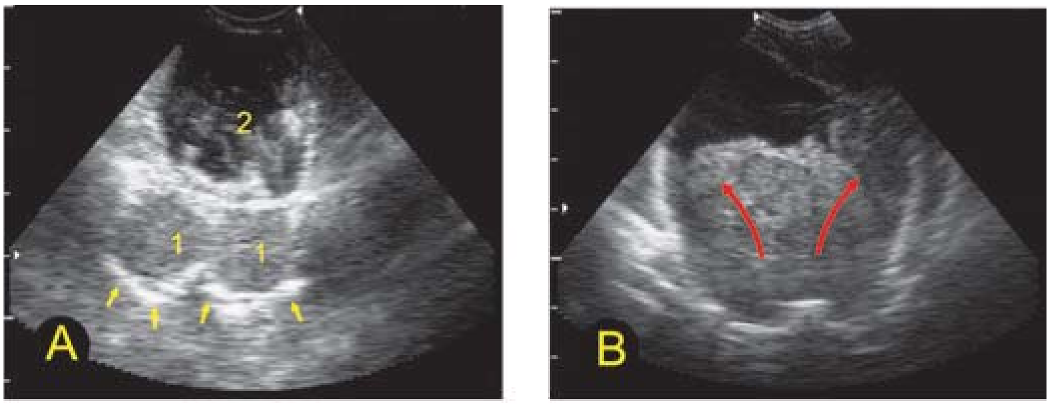

Fig. 1-180:

A: Ultrasonographic image of an African grey parrot (*Psittacus erithacus*) suffering from intoxication due to ingesting cigarette butts, ventromedian coupling site, oblique, 7.5 MHz, PD 6 cm. Swelling and increased density of the kidneys (1) in the renal fossa (yellow arrows).

B: Ultrasonographic image of a double yellow-headed Amazon parrot (*Amazona ochrocephala*) with a renal tumor, ventromedian coupling site, oblique, 7.5 MHz, PD 6 cm. An irregular echogenic tumor is visible originating from the renal fossa and extending into the coelomic cavity (red arrows).

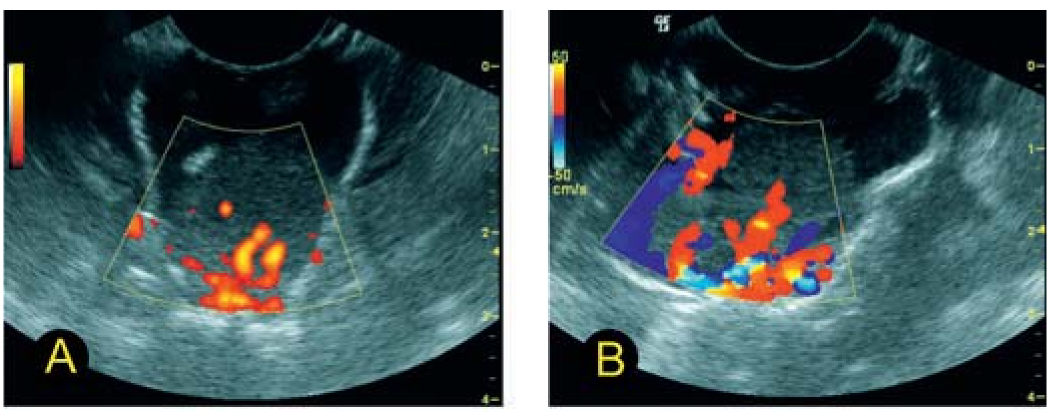

Fig. 1-181: A, B: Ultrasonographic images of a budgerigar (*Melopsittacus undulatus*) with a renal tumor, ventromedian coupling site, oblique, Color-Doppler method, 10 MHz, PD 4 cm. Image of the perfusion of a renal tumor using the (A) Power-Doppler method and (B) Color-Doppler method.

1: body wall or renal fossa
2: renal swelling
3: renal cysts
4: hemorrhage

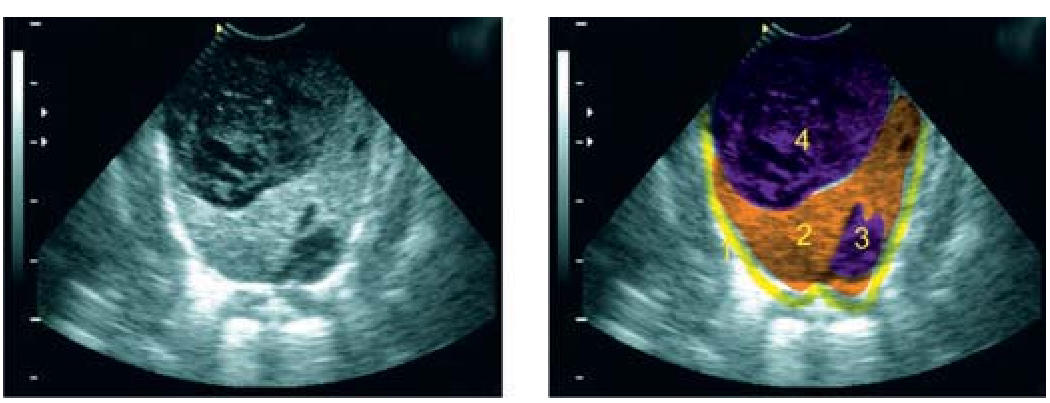

Fig. 1-182: Ultrasonographic images of a sulfur-crested cockatoo (*Cacatua galerita*) with renal swelling (2), hemorrhage (4), and idiopathic renal cysts (3), ventromedian coupling site, oblique, 7.5 MHz, PD 6 cm.

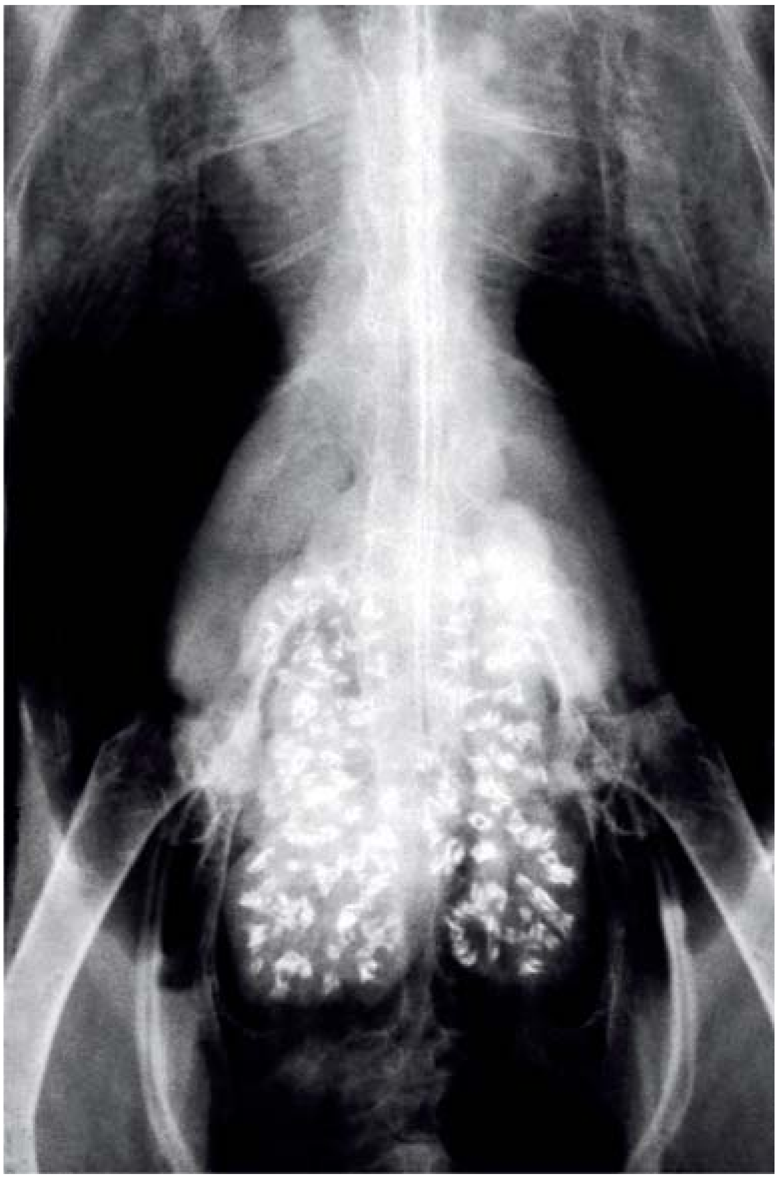

Fig. 1-183: Total body radiographic image of an African grey parrot (*Psittacus erithacus*) with renal hypercalcification, ventrodorsal projection. The foci of hypercalcification appear radiopaque.

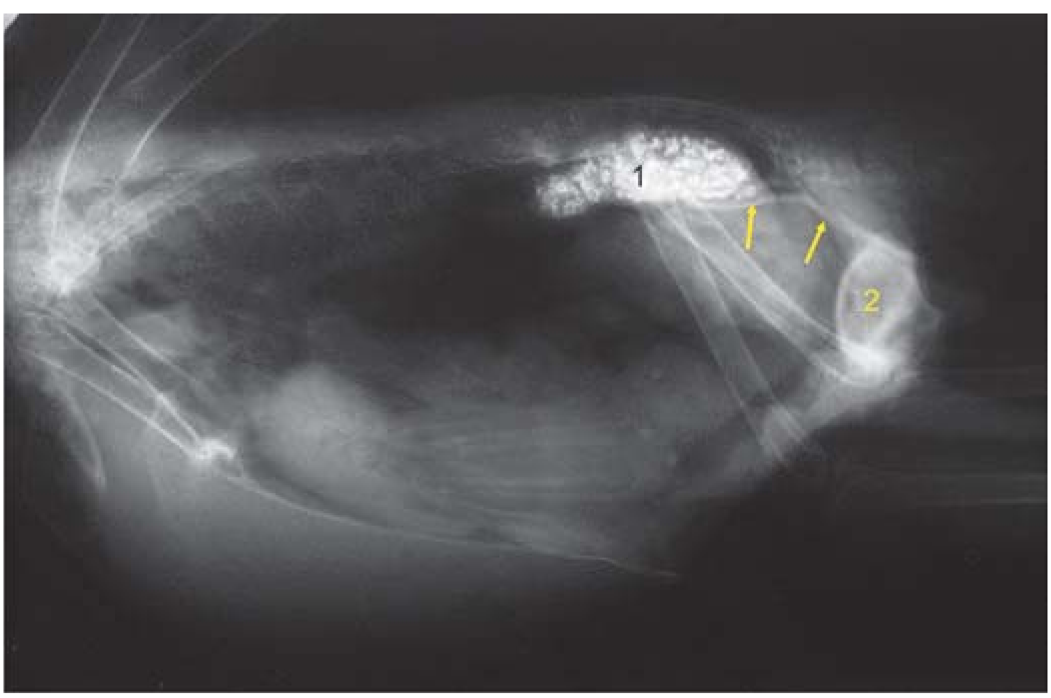

1: kidneys
2: cloaca

arrows: ureter

Fig. 1-184: Total body radiographic image of the same bird as in Fig. 1-183 with radiopaque homogenous dispersed foci of hypercalcification in the kidney, lateral projection, 30 s after the administration of amidotrizoate (Urografin 76%, 370 mg iodine/ml solution, 2 ml/kg bwt, i. v.). Urography revealed an unchanged excretion of the contrast medium.

Fig. 1-185: Total body radiographic images of a budgerigar (*Melopsittacus undulatus*) with a testicular tumor, (A) ventrodorsal and (B) lateral projections.

A: Loss of the cardiohepatic »hour-glass«-shaped silhouette due to soft-tissue swelling (arrows) with compression of the air sacs and displacement of the ventriculus.

B: Radiopaque soft-tissue swelling ventral to the kidneys with compression of the air sacs and ventriculus (arrows).

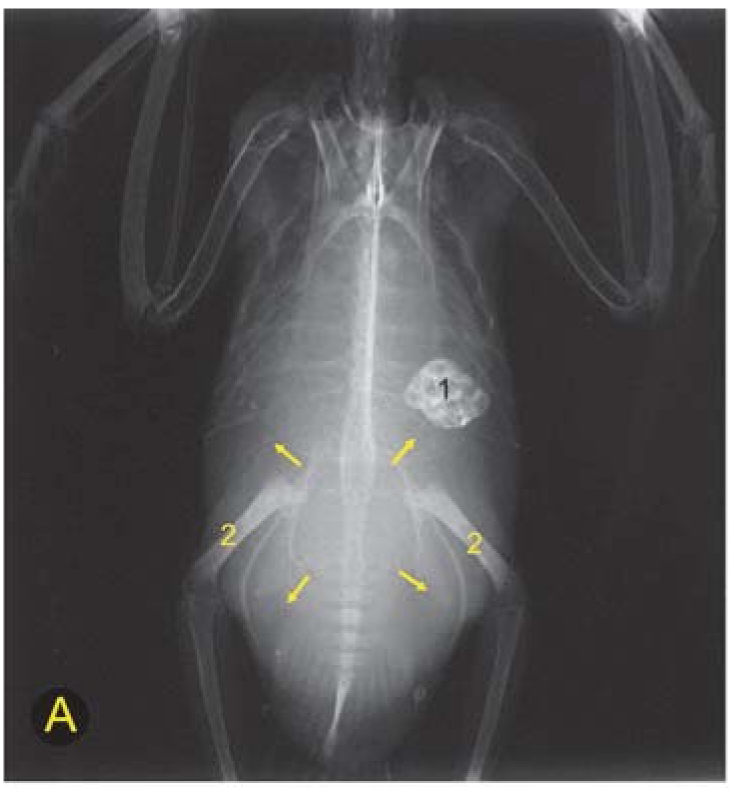

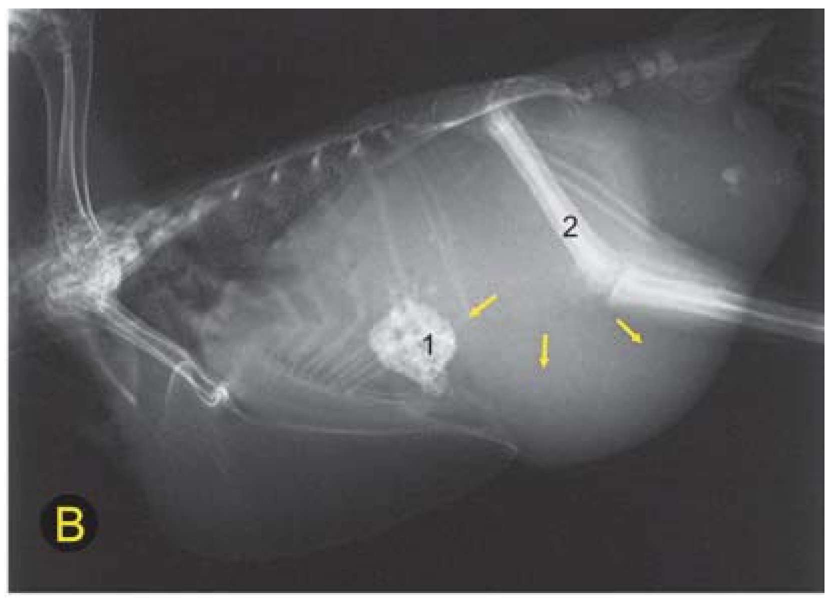

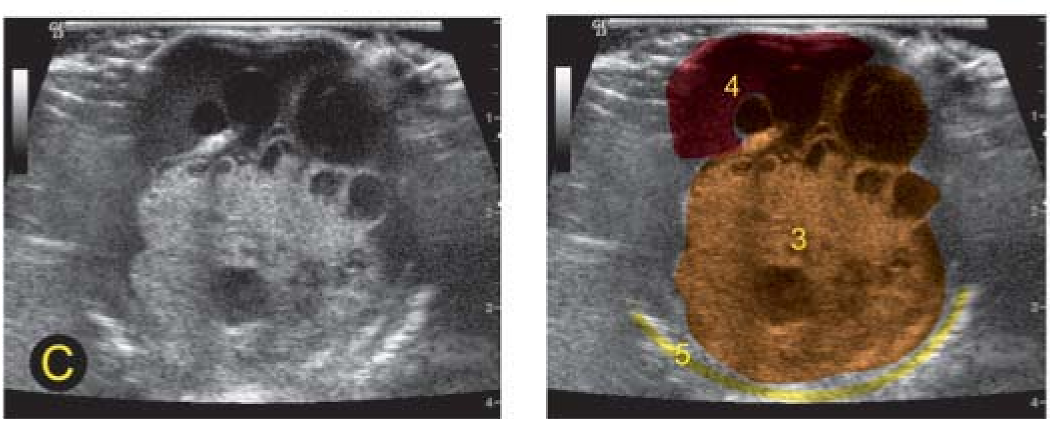

1: ventriculus
2: femur
3: ovary
4: hemorrhage
5: body wall

Fig. 1-186:

A, B: Total body radiographic images of a cockatiel (*Nymphicus hollandicus*) with an ovarian tumor, (A) ventrodorsal and (B) lateral projections. Medullary bone is particulary well developed in the femurs (2). There is a severe degree of soft-tissue swelling in the body cavity (arrows). The ventriculus (1) is displaced craniolaterally.

C: Ultrasonographic image of the same bird's caudal coelomic cavity, transverse, ventromedian coupling site, 12 MHz, PD 4 cm. The ovary (3) is hyperechoic, enlarged, and cystic. Hemorrhage (4) has already occurred within the coelomic cavity:.

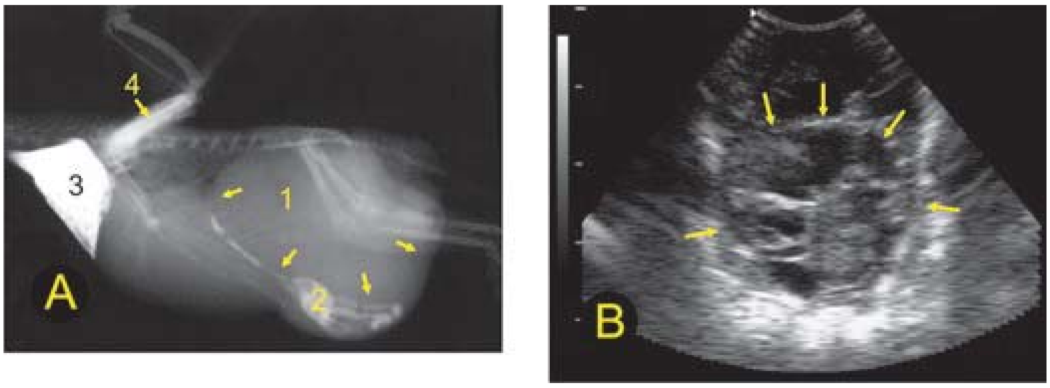

1, arrows: soft-tissue swelling
2: ventriculus
3: crop filled with barium sulfate
4: humerus

Fig. 1-187:

A: Total body radiographic image of a budgerigar (*Melopsittacus undulatus*) with an ovarian tumor, lateral projection, 30 min after the administration of barium sulphate (350 mg/ml, 20 ml/kg bwt, in the crop). The contrast medium has clearly revealed the extent of the ventral displacement of the caudal loop of intestines (arrows) by a radiodense soft-tissue swelling (1). Medullary bone is clearly recognizable in the ulna, however in this projection, it is not distinguishable with any great certainty within the humerus due to summation of both wings (4).

B: Ultrasonographic image of the same bird's ovary, ventromedian coupling site, transverse, 7.5 MHz, PD 4.5 cm. This image clearly shows the nonhomogeneous hyperechoic enlarged ovary.

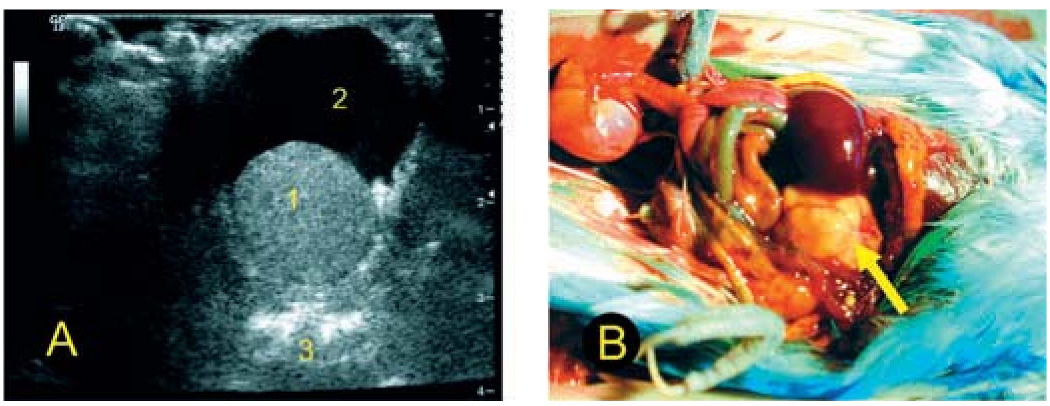

1, arrow: testicular tumor
2: ascites
3: spine

Fig. 1-188:

A: Ultrasonographic image of a budgerigar's (*Melopsittacus undulatus*) testicular tumor, ventromedian coupling site, oblique, 12 MHz, PD 4 cm. The tumor (1) is clearly defined against the surrounding tissue. Ascites (2) is present.

B: Gross pathological image of the testicular tumor (arrow).

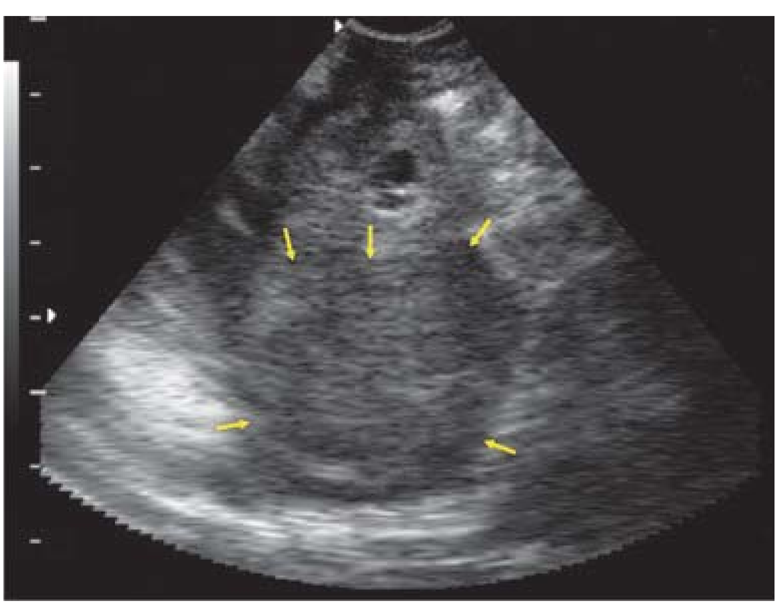

Fig. 1-189: Ultrasonographic image of a hyacinth macaw's (*Anodorhynchus hyacinthinus*) ovarian tumor, ventromedian coupling site, longitudinal, 7.5 MHz, PD 6 cm. The tumor is well defined (arrows), somewhat nonhomogeneous and fills most of the central body cavity.

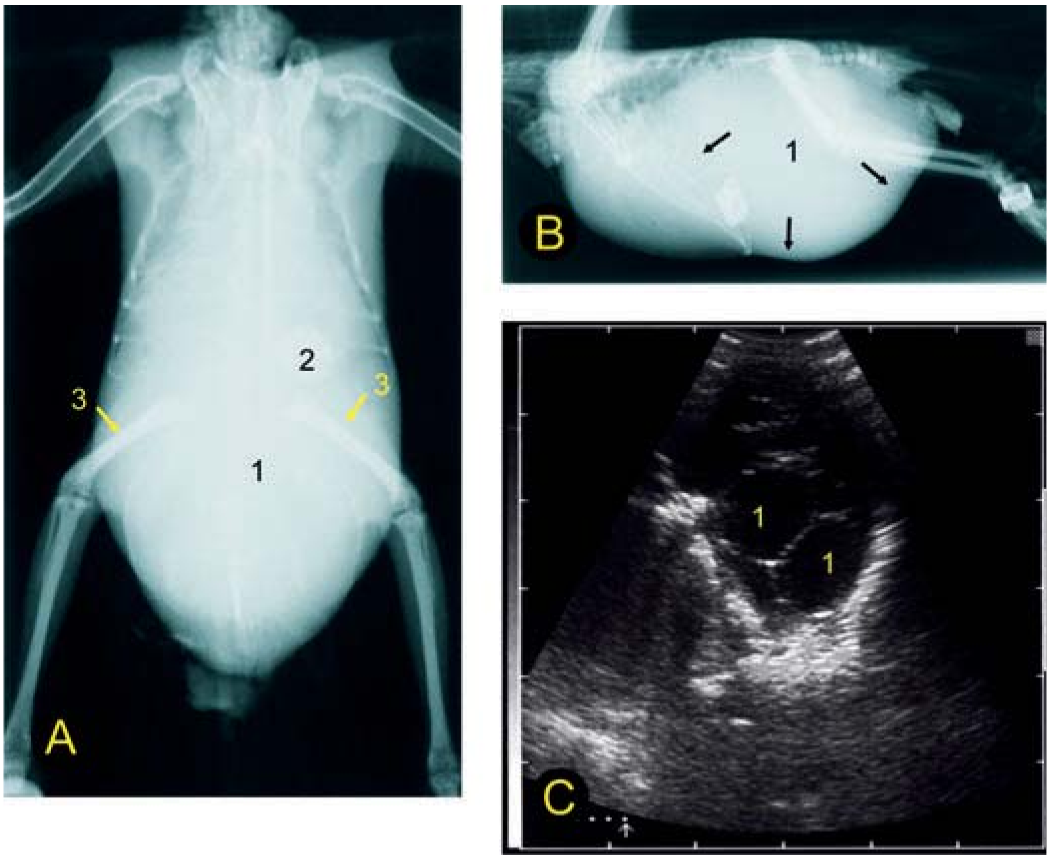

1: ovarian cysts
2: ventriculus
3: femur

Fig. 1-190:
A, B: Total body radiographic images of a cockatiel (*Nymphicus hollandicus*) with ovarian cysts, (A) ventrodorsal and (B) lateral projections. These images show an increase in the size of the coelomic cavity, loss of the cardioheptic silhoutte's »hour-glass« shape, compression of the air sacs, displacement of the ventriculus (2); nonhomogeneous medullary bone in the femur (3) and tibiotarsus.
C: Ultrasonographic image of the same bird, ventromedian coupling site, oblique, 7.5 MHz, PD 6 cm: image of the echo-free ovarian cyst (1).

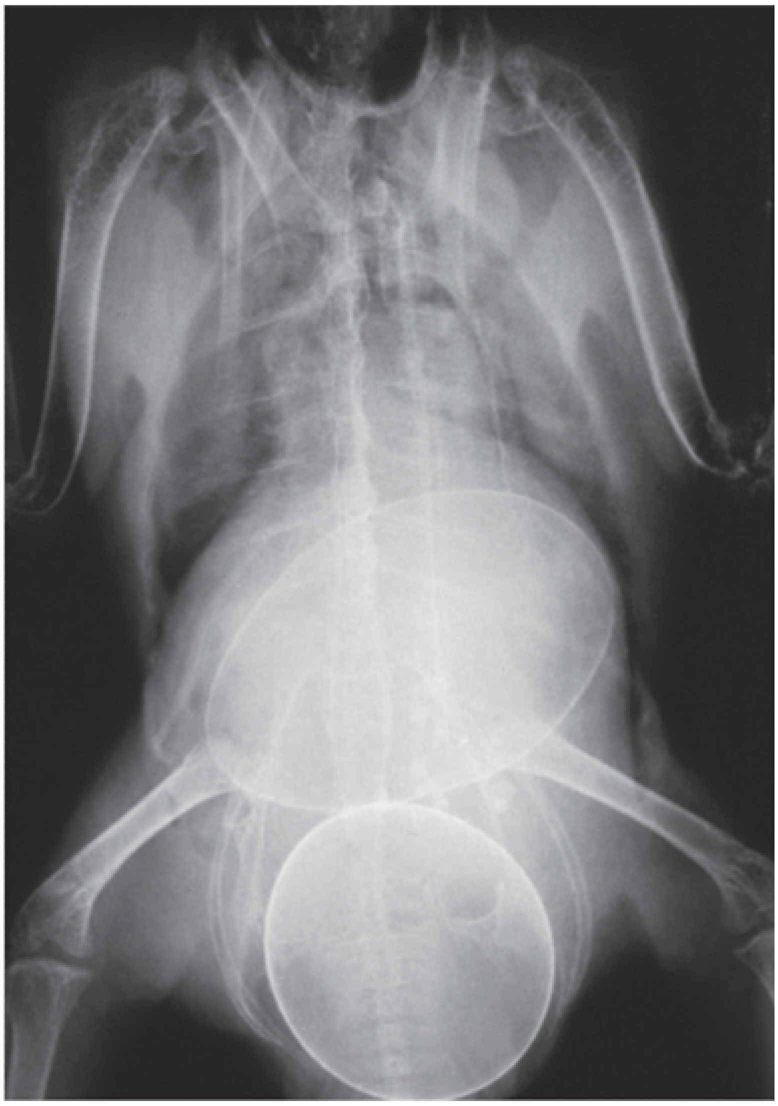

Fig. 1-191: Total body radiographic image of an egg-bound eclectus parrot (*Eclectus roratus*), ventrodorsal projection. Two eggs are present in the body cavity. Due to the interval between laying eggs in psittacines, it is normal to only identify one egg. The size and the position of the eggs in this case was not difficult to treat. A conservative treatment plan for egg binding presentations usually provides a successful resolution to such cases.

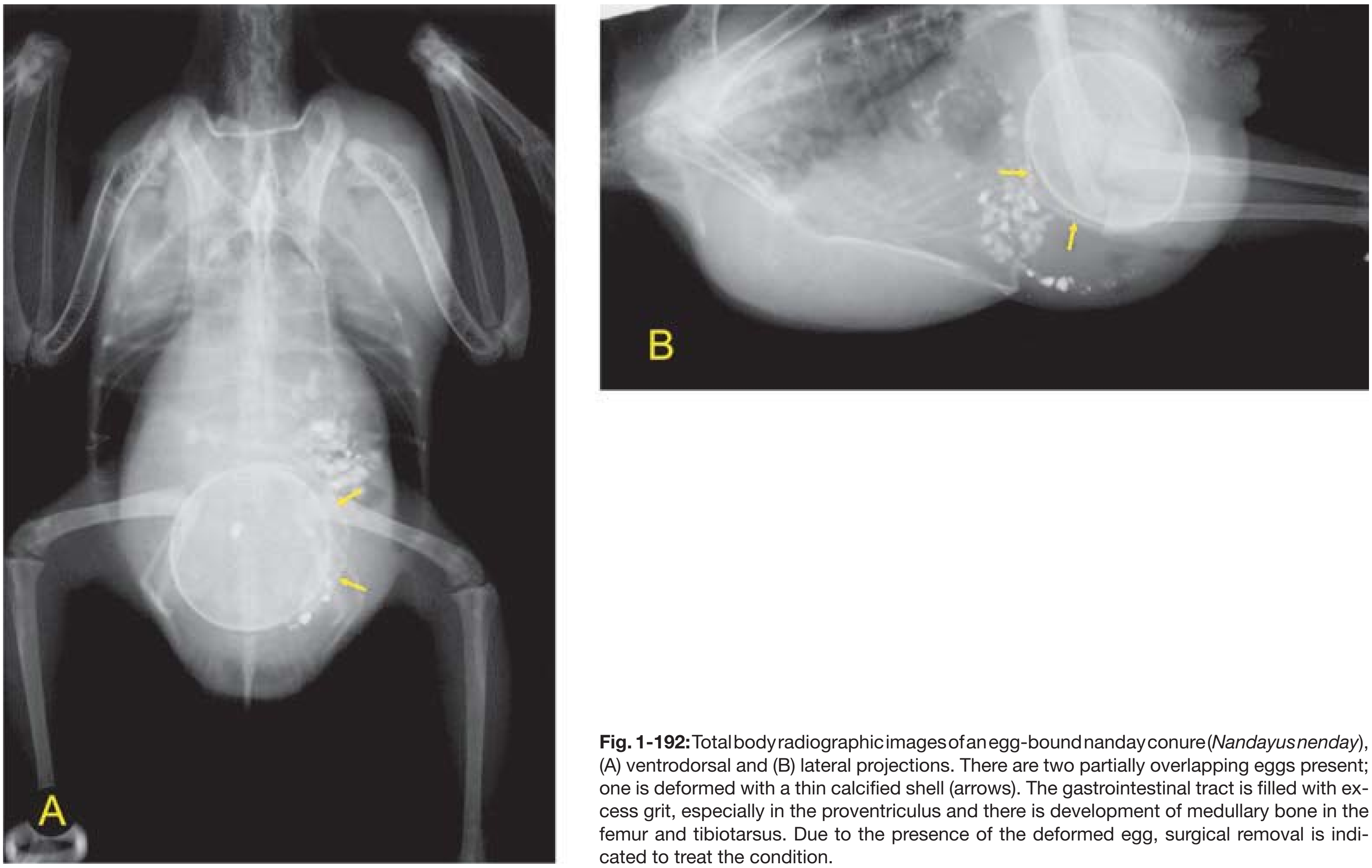

Fig. 1-192: Total body radiographic images of an egg-bound nanday conure (*Nandayus nenday*), (A) ventrodorsal and (B) lateral projections. There are two partially overlapping eggs present; one is deformed with a thin calcified shell (arrows). The gastrointestinal tract is filled with excess grit, especially in the proventriculus and there is development of medullary bone in the femur and tibiotarsus. Due to the presence of the deformed egg, surgical removal is indicated to treat the condition.

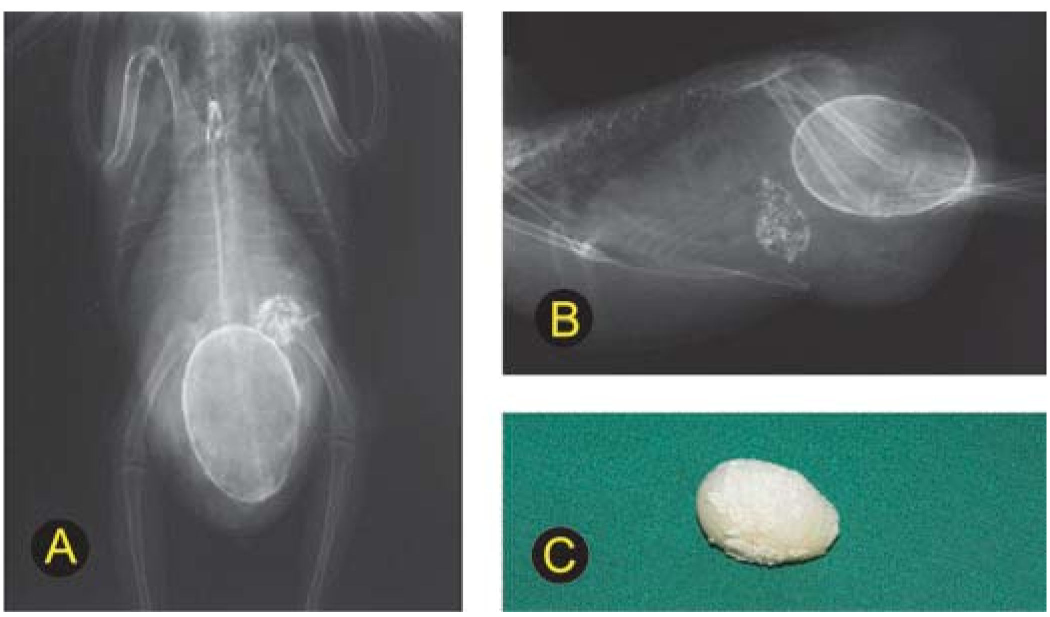

Fig. 1-193: Total body radiographic images of an egg-bound cockatiel (*Nymphicus hollandicus*), (A) ventrodorsal and (B) lateral projections. An egg with an excessively calcified shell is an indication that the egg has already been in the oviduct for a prolonged period of time. Often this condition is associated with adhesions being formed in the salpinx due to inflammation (salpingitis). Egg binding in association with salpingitis is usually an indication for a surgical intervention.

C: Irregularly calcified egg after surgical removal.

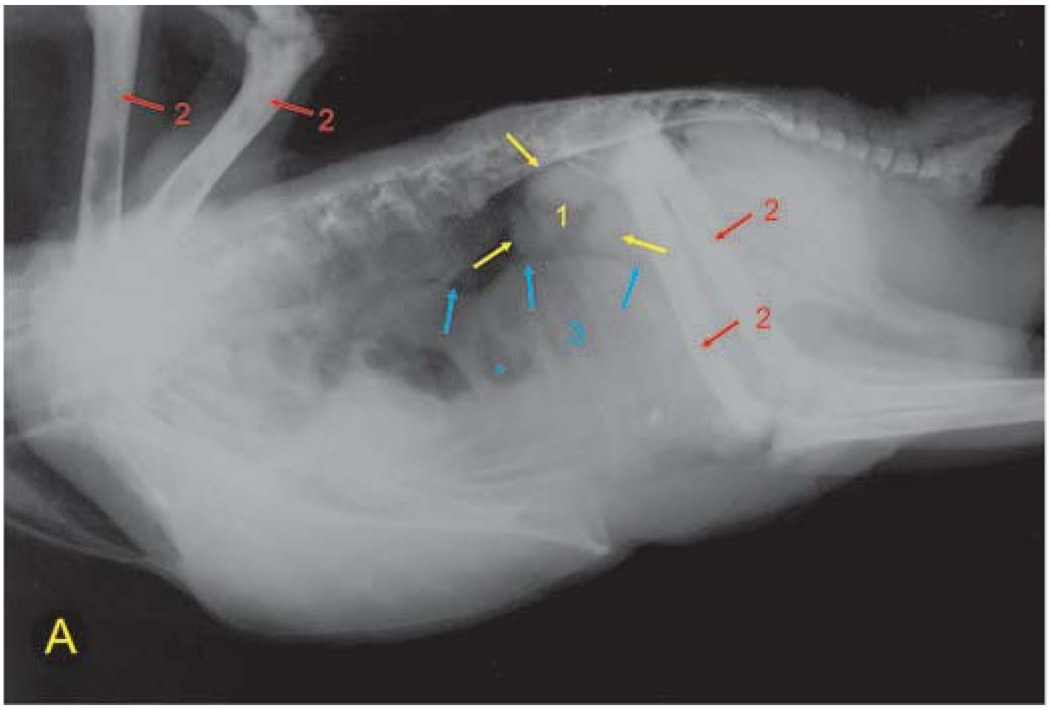

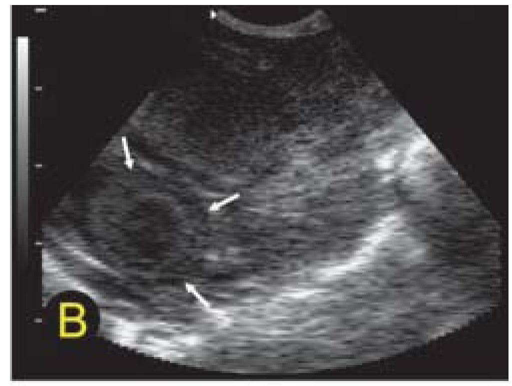

1, yellow arrows: ovary
2, red arrows: medullary bone
3, blue arrows: proventriculus

Fig. 1-194:

A: Total body radiographic image of an eclectus parrot (*Eclectus roratus*) with laminated eggs, lateral projection. A soft-tissue swelling can be seen in the caudal body cavity. The proventriculus (3) is distended (*) due to the passage of food being blocked by the pressure of the egg on the gastrointestinal tract. The active ovary (1) is visible. Partially nonhomogeneous medullary bone (2) has been formed in the humerus, femur and tibiotarsus.

B: Ultrasonographic image of the same bird, ventromedian coupling site, oblique, 7.5 MHz, PD 4.5 cm: the laminated eggs (white arrows) can be easily identified in this image.

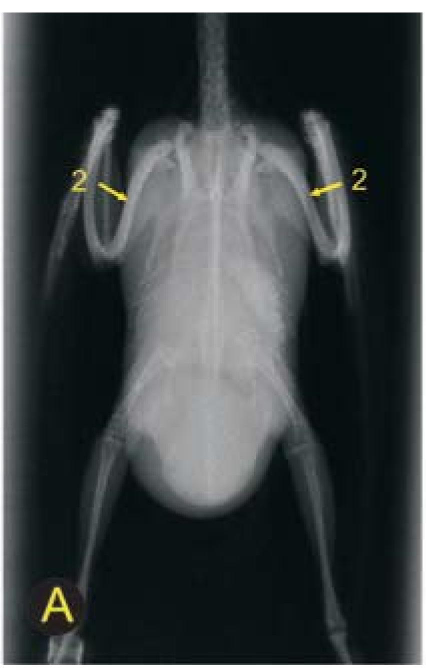

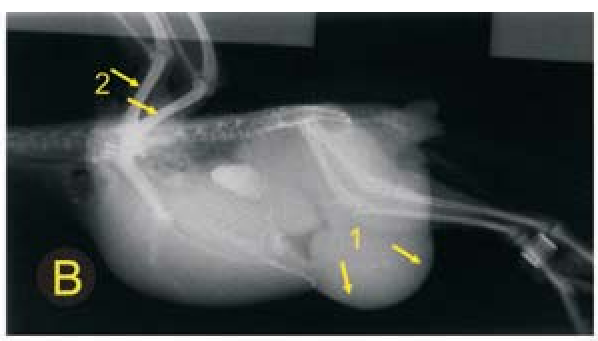

1: abdominal hernia
2: medullary bone (humerus)

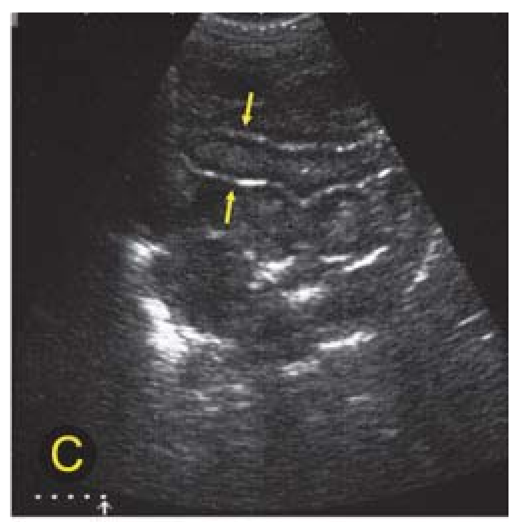

Fig. 1-195:

A, B: Total body radiographic images of a budgerigar (*Melopsittacus undulatus*) with salpingitis, (A) ventrodorsal and (B) lateral projections. Radiopaque soft-tissue swelling with compression of the grit-filled proventriculus and ventriculus as well as with compression of the air sacs (1, abdominal hernia [arrows] and development of medullary bone in the humerus (2) and ulna can be observed in these images.

C: Ultrasonographic image of a budgerigar (*Melopsittacus undulatus*) with salpingitis, ventromedian coupling site, oblique, 7.5 MHz, PD 6 cm. This image shows the oviduct filled with inflammatory material and its hyperechoic thickened wall (arrows) in both longitudinal and cross-sections.

Fig. 1-196: Total body radiographic images of an egg-bound budgerigar (*Melopsittacus undulatus*, (A) ventrodorsal and (B) lateral projections. Medullary bone has been formed in the long bones. There is a soft-tissue swelling in the caudal body cavity with a loss of the cardiohepatic »hour-glass«-shaped silhouette and compression of the air sacs. Two small mummified eggs (arrows) can be identified below the ventriculus. Food has collected in the crop (B).

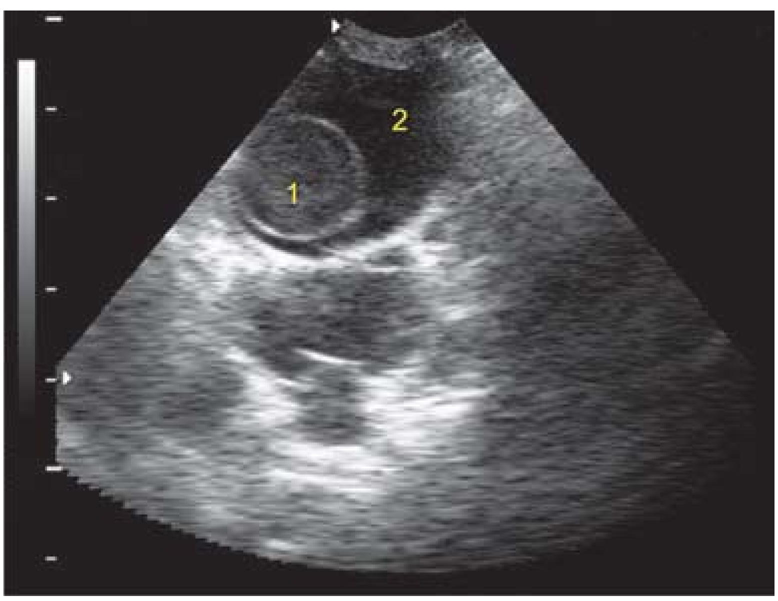

1: egg
2: oviduct

Fig. 1-197: Ultrasonographic image of a budgerigar (*Melopsittacus undulatus*) with an old egg, ventromedian coupling site, oblique, 7.5 MHz, PD 6 cm. The egg (1) is lying in the fluid-filled oviduct (2). The egg became mummified after progesterone was administered to the bird when it was actively laying eggs.

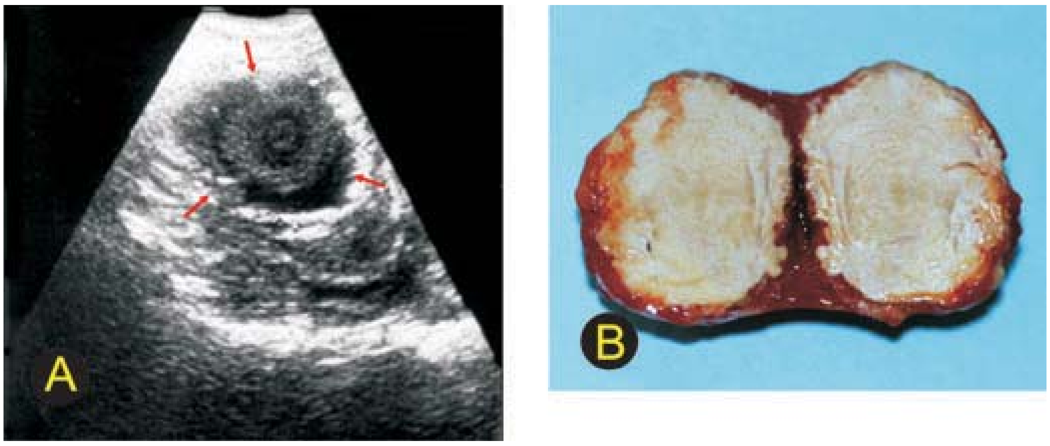

Fig. 1-198:

A: Ultrasonographic image of an African grey parrot (*Psittacus erithacus*) with laminated eggs, ventromedian coupling site, oblique, 7.5 MHz, PD 6 cm. The laminated eggs (arrows) have the typical concentric layers of differing echogenicity.

B: Photograph of a laminated egg in an opened oviduct. The concentric layers of paste-like concretions can be observed in this image.

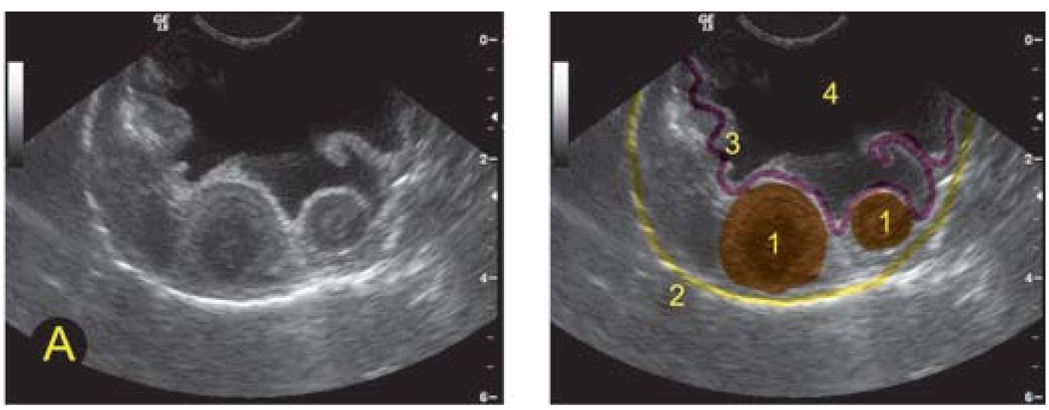

1: follicles
2: body wall
3: fibrinous material
4: ascites

Fig. 1-199: Ultrasonographic image of an African Grey Parrot (*Psittacus erithacus*) with egg yolk peritonitis, ventromedian coupling site, oblique, 8 MHz, PD 6 cm. The follicles (1) are covered with a fibrinous material (3). There is free fluid in the caudal coelomic cavity (4).

1.11 Miscellaneous

Maria-Elisabeth Krautwald-Junghanns, Michaela Gumpenberger

Diseases of the skin and subcutis can have an effect on radiographic imaging; for example, after the subcutaneous injection of large amounts of fluid or the placement of topical ointment on skin wounds **(Figs. 1-200** and **1-201)**. Feathers and skin can adversely affect the quality of the radiographic images through summation, which can occasionally lead to misdiagnosis. Tumors can develop into massive soft-tissue swellings within the affected area and incorporate neighboring musculature, skin, and subcutis into the disease process **(Figs. 1-202** and **1-203)**. Little is known regarding ultrasonographic diagnostics in such cases. However, it is possible to sonographically differentiate between a solid mass and a fluid-filled cyst.

Soft-tissue changes of the head cannot be diagnosed easily nor readily using traditional radiographic techniques **(Fig. 1-204)**. Exceptions to the above statement are tumors of different histogenesis (e.g. retrobulbar tumors in the budgerigar, osteomas, carcinomas). Due to their large size and increased radiopacity, tumors of the head can be easily identified.

In the majority of cases of soft-tissue swelling, more specific results can be obtained using contrast medium or a CT examination. A computed tomogram can not only demonstrate the extent of the changes, but also the type of change can be determined using density measurements and the administration of a contrast medium **(Figs. 1-138** and **1-140)**. MRI investigations are also suitable for the diagnosis of soft-tissue changes **(Fig. 1-139)**, especially **changes affecting the brain (Fig. 1-205C)**. However, the long period of time needed to examine the patient using this modality is a problem for the avian patient and needs to be weighed up against the advantages gained by using this diagnostic imaging modality.

The ultrasonographic diagnosis of **eye changes** is particularly helpful when a direct inspection of the inner eye is not possible (e.g. due to clouding of the lens or hemorrhage in the anterior chamber). Whereas earlier, A-mode ultrasonography was used for the biometry of the eye, currently the measurement of distances and the imaging of the ocular structures and associated pathological changes are done using 2D B-mode ultrasonography. The most frequent changes observed sonographically in the eye are lens opacity (i.e. noted as a hyperechoic densification with thickening of the lens capsule; **Fig. 1-206**), hemorrhages in the vitreous body (i.e. particles of differing echogenicity in an otherwise echo-free vitreous body; **Fig. 1-207**), retinal detachment (i.e. linear, V-shaped or bow-like echoes which are stuck to the ocular fundus; **Fig. 1-206**) or in rare cases lens luxation. Furthermore, injuries of the pecten oculi can be identified. In addition, inflammation within the eye can be depicted as echogenic changes **(Fig. 1-208)**.

Using CT imaging, the bony scleral rings and the core of the lens can be clearly observed, even though the pecten oculi cannot be distinguished from the rest of the vitreous body. Above all, the position of the lens can be established in order to verify suspected luxations of these structures **(Fig. 1-209)**.

When **spinal cord disease** is at or near the top of a differential diagnosis list, and the condition appears associated with a spinal fracture **(Fig. 1-113)**, in order to obtain a definitive diagnosis myelography is required. Due to a few anatomical perculiarities of the bird (see Chap. 1.1.4.6), this method is associated with a high degree of risk for the patient. Both CT and MRI investigations provide diagnostic information and are the methods of choice for diagnosing spinal fractures in avian patients **(Fig. 1-114)**.

The diagnosis of **pancreatic disease** using the different imaging modalities is generally unsuccessful. Only in individual cases can ultrasonography be used diagnostically with any success, [i.e. when examining an enlarged pancreas (e.g. with severe inflammation, neoplasia)] and this organ lies superficially within the duodenal loop.

Further Reading

GUMPENBERGER, M., KOLM, G. (2006): Ultrasonographic and computed tomographic examinations of the avian eye: physiological appearance, pathological findings and comparative biometric measurement. Vet Radiol & Ultrasound **47**: 492–502.

Fig. 1-200: Radiographic image of an eclectus parrot (*Eclectus roratus*), ventrodorsal projection. Radiographic appearance after a subcutaneous injection in the fold of the knee (arrow).

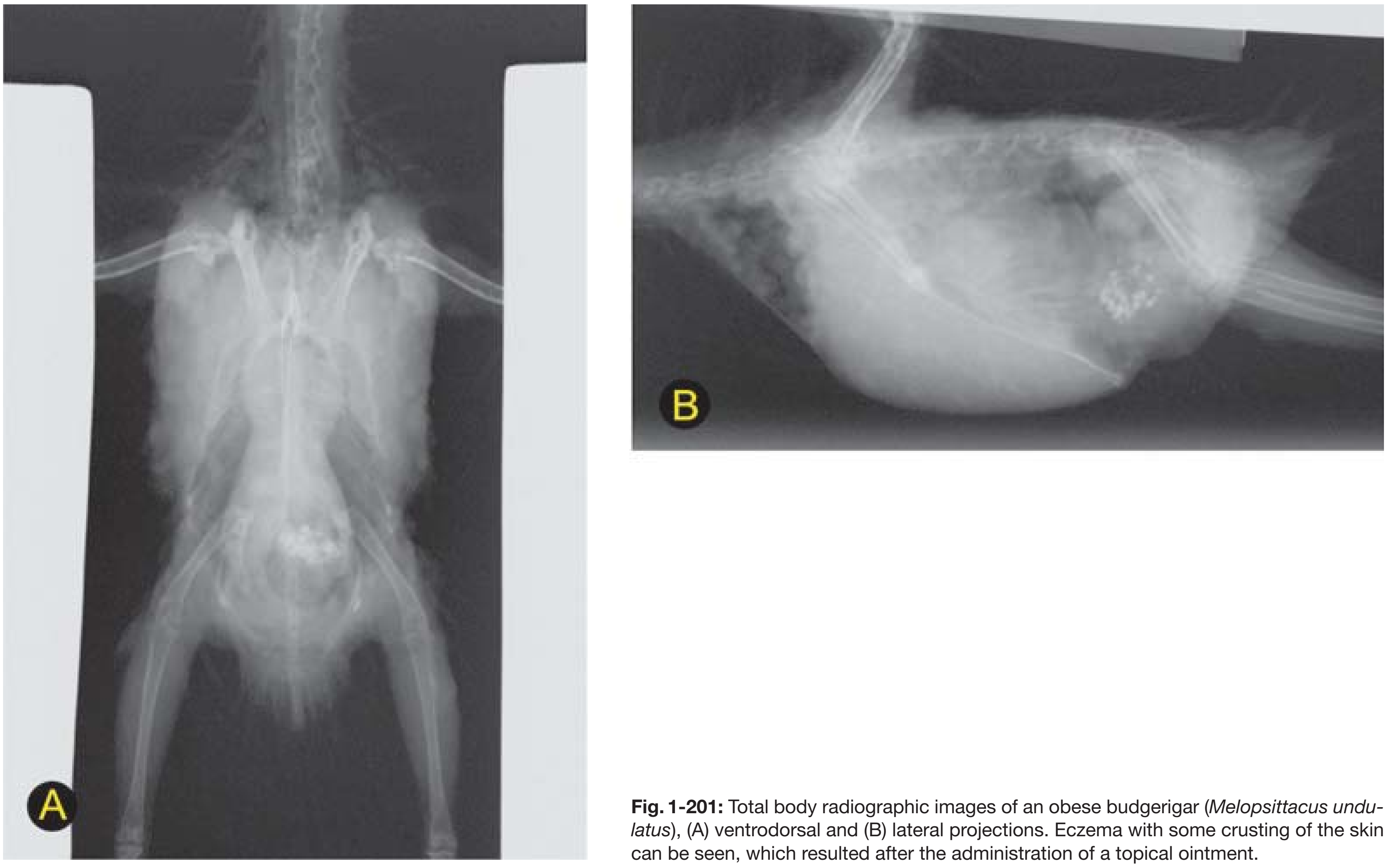

Fig. 1-201: Total body radiographic images of an obese budgerigar (*Melopsittacus undulatus*), (A) ventrodorsal and (B) lateral projections. Eczema with some crusting of the skin can be seen, which resulted after the administration of a topical ointment.

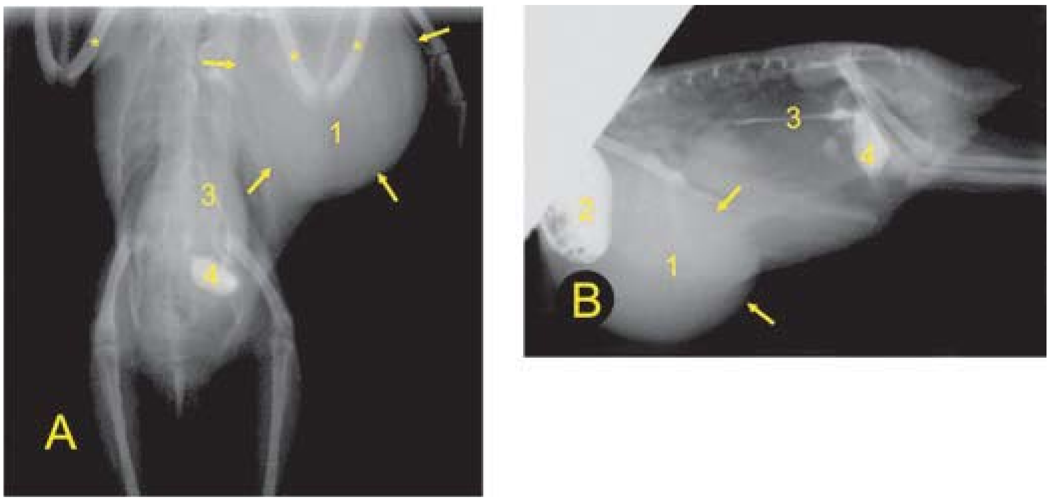

1, arrows: abscess
2: crop
3: proventriculus
4: ventriculus

*: medullary bone

Fig. 1-202: Total body radiographic images of a budgerigar (*Melopsittacus undulatus*) with an abscess (1, arrows) in the thoracic inlet, (A) ventrodorsal and (B) lateral projections, 45 min after the administration of barium sulfate (350 mg/ml, 20 ml/kg bwt, in the crop). Development of medullary bone (*) in the long bones.

1: tumor
2: crop
3: proventriculus
4: ventriculus

Fig. 1-203: Total body radiographic image of a crimson rosella (*Platycercus elegans*) with a fibrosarcoma of the esophageal wall, ventrodorsal projection, 1.5 hours after the administration of barium sulphate (350 mg/ml, 20 ml/kg bwt, in the crop). A massive tumor (1) is pressing on the crop (2), therefore only a small amount of food can pass through this part of the gastrointestinal tract.

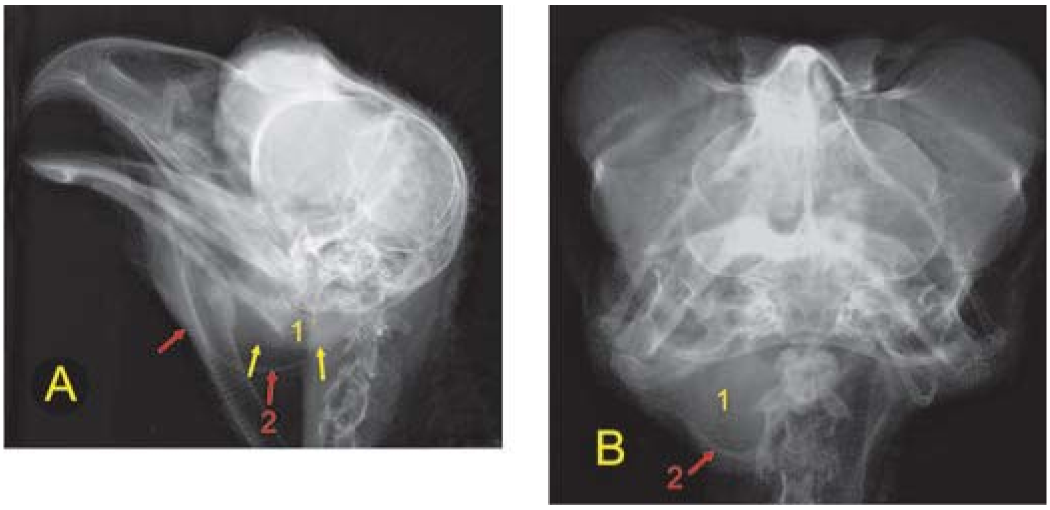

1: soft-tissue swelling
2: hyoid bone

Fig. 1-204: Radiographic image of a Eurasian eagle owl's (*Bubo bubo*) head diagnosed with trichomoniasis, (A) lateral and rostrocaudal (B) projections. Soft tissue swelling (1) of the upper gastrointestinal tract due to a massive infestation with trichomoniads. There is summation of the upper gastrointestinal tract with the frontal bone (only recognizable in the lateral projection) and the lower beak in the two images. The eyes appear to be asymmetrical in the lateral projection due to the slight oblique positioning of the bird's head. The hyoid bone (2) has been displaced ventrally by the swelling.

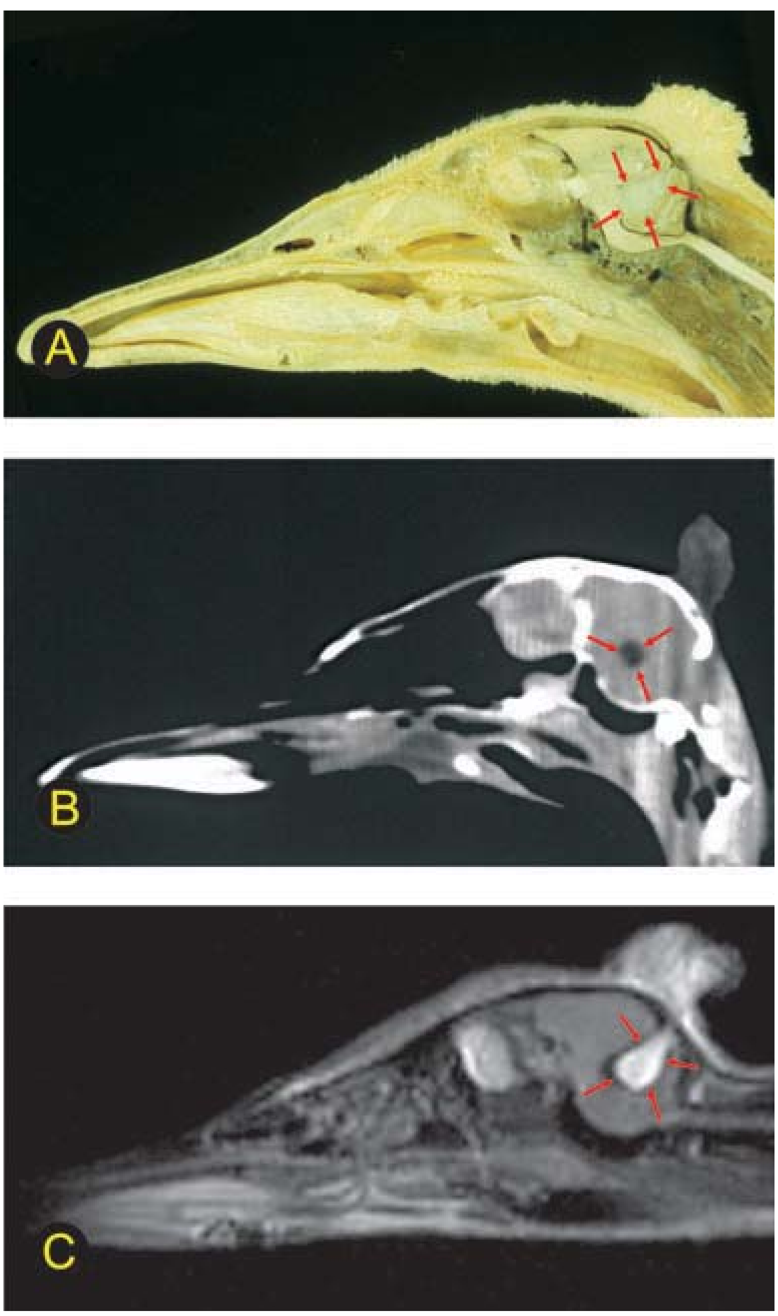

Fig. 1-205: Crested duck (*Anas platyrhynchos* f. *domestica*): lipoma in the tentorium cerebelli (arrows).

A: Longitudinal slice through the cranium.

B: CT, sagittal plane (120 kV, 170 mA, SD 1 mm, W: 250, L: 70). In this image the fat-rich contents of the tumor can be identified using the density detemination (HU).

C: MRI, head, sagittal plane, T1-weighted.

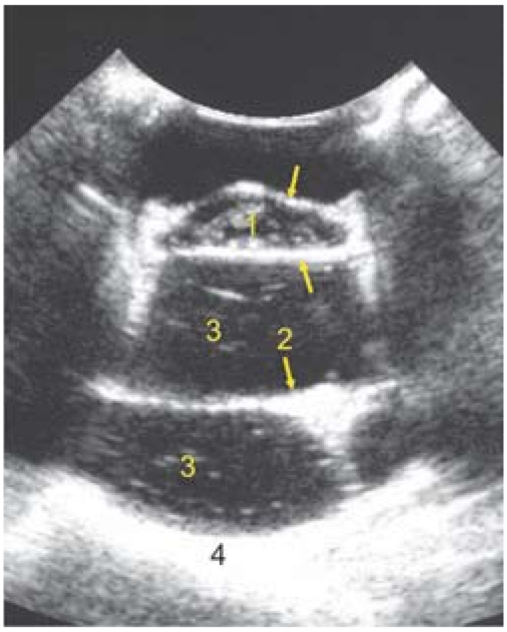

1: lens
2: vitreous body: retinal degeneration
3: vitreous body: hyperechoic particles
4: ocular fundus

arrows: lens capsule

Fig. 1-206: Ultrasonographic image of an Eurasian eagle owl (*Bubo bubo*) with a severe cataract and retinal degeneration, transcorneal coupling site, 7.5 MHz, PD 4 cm. The lens capsule (arrows) is thickened and the lens (1) is shrunken. A hyperechoic line (2) can be observed in the body humor, which runs in a T-form to the back of the eye (retinal degeneration). Individual hyperechoic particles (3), lying in the vitreous body, were diagnosed as fibrin or hemorrhages.

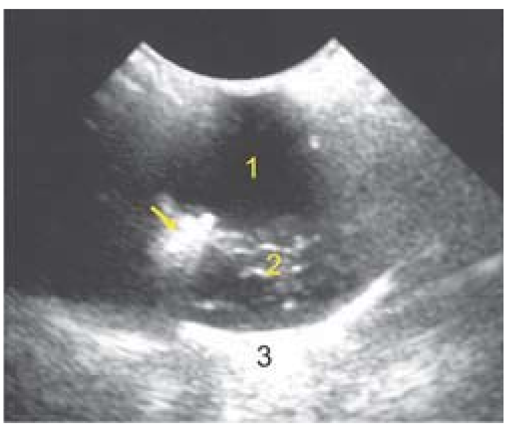

1: vitreous body
2, arrow: vitreous body: hyperechoic particles
3: ocular fundus

Fig. 1-207: Ultrasonographic image of a tawny owl (*Strix aluco*) whose lens is missing, transcorneal coupling site, 7.5 MHz, PD 4 cm. Numerous hyperechoic particles (2) can be observed within the vitreous body (1), some of which have clumped together (arrow) along with remnants of the degenerate lens and hemorrhages.

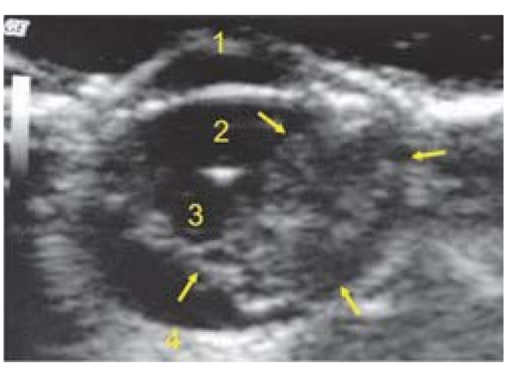

1: cornea
2: lens
3: vitreous body
4: ocular fundus

arrows: echogenic vitreous

Fig. 1-208: Ultrasonographic image of a blue-fronted Amazon (*Amazona aestiva*) with endophthalmitis, transcorneal coupling site, 10 MHz, PD 1.5 cm. There is an echogenic change (arrows) in the vitreous body.

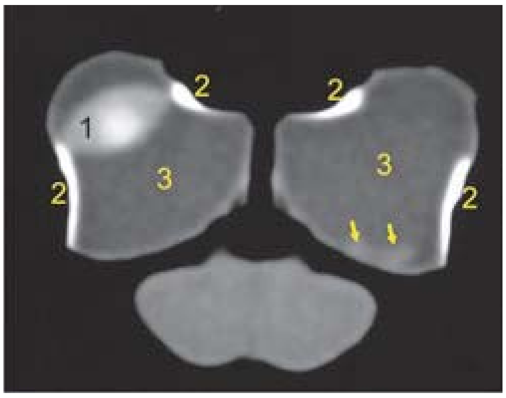

1: center of the lens
2: bony ocular ring
3: vitreous body

arrows: fragments of the lens

Fig. 1-209: CT image of a tawny owl's (*Strix aluco*) eye in which the right lens is missing, coronary plane (120 kV, 80 mA, SD 2 mm, W: 350, L: 40). Fragments of the right lens can be observed at the level of the ocular fundus (arrows). Typical for a CT image of the avian eye is the hyperdense center of the lens (1), while the individual compartments of the eye cannot be detected.

2 Small Mammals

Introduction

SVEN REESE

The importance of small exotic mammals as veterinary patients has continued to grow and in some practices these animals form a significant percentage of the clientele. At the same time, knowledge regarding the anatomical, physiological, and pathophysiological characteristics of these species has rapidly increased. In addition, the demands by many small exotic mammal owners for quality medical care for their animals has clearly continued to rise. The expectations of these pet owners have even progressed to specific requests for advanced radiographic and ultrasonographic imaging tests. Recent technical advances make it possible to routinely use these imaging modalities in small exotic mammals.

Radiographic investigations are routinely performed on rabbits, guinea pigs, and ferrets without complications. Not only do these radiographic images provide valuable information about the diverse areas of dental and skeletal disease, but also aid in the diagnosis of respiratory, gastrointestinal, and urinary diseases, thereby significantly impacting treatment decisions and prognosis determination.

Machines used for dog and cat **ultrasonographic examinations** have a high enough degree of resolution for use on small exotic mammals. Ultrasonography has developed into the imaging modality of choice for diagnosing diseases of the urogenital tract and often provides enough information for treatment decisions and prognosis determination. Both ultrasonography and echocardiography are recognized and established imaging methods for investigating other disease processes (e.g., imaging adrenal adenomas in the ferret or for the diagnosis of cardiac insufficiency).

The spectrum of small exotic mammalian species maintained as pets is continually increasing. However, many of these species are rarely presented to small animal veterinary hospitals. The emphasis in this book is placed on the nine species of small exotic mammals which are most frequently treated in small animal veterinary practices (Table 2-1). The anatomical and physiological similarities of zoologically related species enable the practitioner to use information in this text between species to evaluate diagnostic images.

Apart from short introductory chapters in standard companion animal veterinary textbooks, there is a paucity of relevant material available on the clinical and diagnostic use of imaging modalities in small exotic mammals – with the exception of echocardiography. Conversely, there are a significant number of individual publications regarding the use of imaging modalities on small exotic mammals in the specialized research literature. Since the specialized research information mentioned above has only limited use in the clinical veterinary setting, references for further reading have been largely omitted from this text.

Table 2-1: Small mammals kept as pets

Zoological classification	Species
Weasel family (Mustelidae)	Ferret (*Mustela putorius* f. *furo*)
Hares and rabbits (Lagomorpha)	Rabbit (*Oryctolagus cuniculus* f. *domestica*)
Guinea pigs and their relatives (Caviomorpha)	Guinea pig or cavy (*cavia aperea* f. *porcellus*) Chinchilla (*Chinchilla lanigera*) Degu (*Octogon degu*)
Hamsters and their relatives (Cricetidae) [Mouse-like rodents (Myomorpha)]	Golden hamster or Syrian hamster (*Mesocricetus auratus*) Mongolian gerbil, gerbil, or clawed jird (*Meriones unguiculatus*)
True mice, rats, etc. (Muridae) [Mouse-like rodents (Myomorpha)]	Rat (*Rattus norvegicus* f. *domestica*) Mouse (*Mus musculus* f. *domestica*)

General principles

2.1 Radiography

Sven Reese, Jutta Hein

2.1.1 Equipment

2.1.1.1 X-ray facilities

Due to their small body size, many of the small exotic mammal patients presented to a veterinary practice place extremely high demands on the available radiographic technology needed to obtain images of diagnostic quality. These demands involve not only the performance of the x-ray machine itself but also the film-screen combination, the development system, and the technical ability and experience of the investigator.

The x-ray machines normally used in small animal practices are, in most cases, suitable for the radiographic diagnostic imaging of small exotic mammals (**Fig. 2-1A**). This is particularly true for the larger small exotic mammals (e.g. rabbit, ferret, guinea pig) whose requirements, concerning the quality of the radiographic technology, are equivalent to that of cats and toy dog breeds. Higher powered machines are clearly advantageous for smaller rodents with a body weight of < 1000 g and extremely small animals (e.g. mouse). The most important parameter for x-ray machine performance is the **maximum output** (the product of the amperage [A] and the voltage [V]): the higher the maximum output, the higher the amperage with the same voltage, therefore the lower the exposure time. The stationary x-ray machines regularly used for small animal radiology examinations have a maximum output between 16 kW and 32 kW.

The respiratory rate of small mammals is much higher than in the dog and cat. In order to reduce motion artifact, the minimum adjustable **exposure time** should be 0.02 seconds or less.

The undersized tissue mass of the typical small exotic mammal patient results in a low degree of contrast in the radiographic image. To compensate for the low contrast observed in many small exotic mammal radiographs, relatively low **voltages** should be used. Values between 40 kV and 60 kV have proven to be suitable to obtain diagnostic images. The voltage should be adjusted in small increments on the x-ray machine to fulfill the requirements based on the varying sizes of individual patients.

The resolution detail is dependent on the size of the **focal spot:** the smaller the focal spot, the lower the geometric blur (= greater resolution). The main problem in generating a smaller focal spot also means a smaller energy throughput, which therefore must be compensated with a longer exposure time. The choice of focal spot size with conventional x-ray machines is, thus a trade-off between the desired degree of resolution and the maximum possible exposure time. Only with special high-resolution x-ray machines that have a very small focal spot (microfocus technique) and short exposure times are sharp radiographs with an extremely fine resolution possible. However, the relatively low diagnostic gain achieved with the extremely high resolution of the images obtained using this technique bears no correlation to the high acquisition costs. This technique has been unable to gain support in clinical veterinary medicine and is almost exclusively used in the testing of materials.

To cope with the broad spectrum of species and the various sizes of small exotic mammals treated at a small animal practice, preference should be given to powerful x-ray machines in which the size of the focal spot can be changed according to the size of the patient. The standard focal spot size is 0.6 mm × 0.6 mm (a very high degree of resolution can be reached using these dimensions), up to 2 mm × 2 mm, which is less suitable for use in small exotic mammals due to its low degree of resolution.

The amount of radiation needed for the exposure drops with a reduction in the film-focus distance (FFD). This occurrence can be exploited to compensate for the low performance of an x-ray machine. The geometric blur and the proportion of scatter radiation increases as the FFD is reduced, therefore a FFD of less than 70 cm should not be used.

2.1.1.2 Film cassettes and grids

The film **cassettes** should be chosen according to the size of the animal. For the examination of ferrets, the 18 cm × 43 cm cassette size has proven to be suitable. The low body weight of small exotic mammals means that a scattered radiation grid is not necessary. As a consequence, it is standard practice to lay small exotic mammalian patients directly on the cassette which provides the advantage of obtaining a sharper image using a smaller FFD. In addition, it is possible, especially in smaller animals, to utilize a film for more than one radiograph by covering parts of the cassette with radiopaque plates.

If the patient leaves material on the cassette, it should be cleaned off before being reused to prevent the production of artifacts (e.g. hair, mud), which can contaminate the film when being refilled. A recommended method to prevent damage or soiling the cassette is to lay a flat frame with a plexiglass cover over the device prior to positioning the animal (**Fig. 2-1B**).

Fig. 2-1A: Machines used to take radiographic images in the typical small animal practice (e.g. dogs, cats) are also appropriate for use in small exotic mammal patients.

2.1.1.3 Film-screen combinations, imaging plate systems, and direct digital radiography

The degree of detail observed on a radiographic image depends primarily on the **film-screen combination**. The use of fine film-screen combinations is particularly indicated for small rodents. It should be noted that the use of intensifying screens means a concomitant loss of resolution. Rare-earth screens have proven to be a suitable compromise between image intensification and the maintenance of an adequate degree of detail resolution when radiographing small exotic mammals. For the production of highly detailed images, especially of the skeleton of small rodents, mammography films are recommended. Dental films that can be placed in the oral cavity of a small exotic mammal patient are ideal for imaging individual teeth.

Fig. 2-1B: Plexiglas® cover for protecting x-ray film cassettes from debris and body fluids.

Imaging plate systems are being used more extensively as a replacement for conventional film-screen combinations. With these systems, an imaging plate is exposed, digitally read, and then cleared. The advantage of such systems is that they require approximately ⅓ of the radiation dose for the respective exposure factor than the film-screen combinations and they have a higher dynamic range, which makes it possible to correct exposure mistakes. Currently, the disadvantage of using imaging plate systems is that such systems have a slightly lower spatial resolution than conventional film-screen combinations.

In **direct digital radiography,** the radiographic images are detected by a sensor built into the examination table and can be visualized on a monitor without any appreciable time delay. Direct digital radiography produces images of a very high quality. Their essential disadvantage lies in their high acquisition costs as the x-ray machine forms a single technical unit with the electronic sensor, therefore in contrast to imaging plate systems the x-ray machine also needs to be renewed.

2.1.1.4 Exposure factors and development

The full performance of conventional film-screen combinations can only be completely implemented if optimal exposure factor values are selected. Developing an **exposure factor table** for each individual size of species of small exotic mammal specific for the respective x-ray machine and film-screen combination, is vital for maintaining good radiographic image quality.

It should be noted that not only the total radiation dose is decisive for image quality, but also the relationship of the voltage (kV) to the current-time product (mAs):

- high kV + low mAs = image without much contrast
- low kV + high mAs = image with a high degree of contrast

The correct use of exposure factor tables will not result in the ability to reproduce quality diagnostic radiographic images if the subsequent **film development** is not undertaken with care. Machine film development is definitely more preferable than manual development. However both of these film development systems are dependent on the regular regeneration and exchange of the solutions used.

2.1.1.5 Radiation safety

The apparently low dose of radiation and the difficult positioning and fixation of small exotic mammalian patients should not mislead one to disregard the general aspects of radiation safety. In addition to the self-evident wearing of lead-lined protective clothing (e.g. aprons, thyroid shield, gloves), one should always bear in mind the inverse square law. Veterinarians and veterinary nurses have a tendency to place their hands very close to the primary beam when positioning animals that are small. Consequently, the hands are subjected to a dose of radiation that is many times that to which their body is exposed. Basically, the following rules regarding radiation safety should always be followed:

- hands should never (not even with lead gloves) be placed in the primary beam
- the investigator's body should be kept as far away as possible from the primary beam (lean back)
- positioning the patient under sedation or general anesthesia is preferable to manual fixation.
- when using manual fixation, the holder's hands should be protected from scatter radiation (from above and below) by lead gloves.

Protective clothing is only capable of shielding against scatter radiation, not primary beam radiation. Creases in the protective clothing due to careless handling and improper storage (aprons should always be hung up without creases) lead to a breakdown in the shielding capabilities of the protective wear.

2.1.2 Positioning

2.1.2.1 General principles

A radiographic image is a two-dimensional summation of a three-dimensional body. A reliable evaluation and especially the topographical classification of the structures observed on radiograph images are only possible in small exotic mammals when the radiographic examination is performed in at least two planes (projections).

The methods of positioning and the projections used for the examination of small exotic mammals basically follow the same principles as those used in small animal radiology (e.g. dog, cat). Due to their physical dimensions, especially their small body size, small exotic mammals are far more difficult to position properly than dogs and cats.

With the exception of the rabbit and guinea pig, fully conscious small exotic mammals rarely allow themselves to be properly positioned for a radiographic examination. Defensive movements lead to images in which the patient is badly positioned and blurred due to motion artifacts. Poor patient positioning and motion artifact greatly reduces a radiographic image's informative value or even makes it worthless. It is, therefore, recommended to use sedation or short-term general anesthesia for small exotic mammals undergoing radiographic examination. One method that has proven its worth is the easily controlled inhalation general anesthesia using isoflurane or sevoflurane via a head mask (**Fig. 2-2**). In small rodents (e.g. golden hamster, gerbil, mouse), the induction of general anesthesia can be performed in an induction chamber that has already been filled with the anesthetic gas. The advantages of sedation or general anesthesia with regards to obtaining quality radiographic images far outweigh the disadvantages:

- less stress for the patient
- exactly positioned radiographic images that can be reliably evaluated
- fewer repeat radiographs are necessary (saves time and money; radiation safety!)
- manual fixation is not necessary (radiation safety!)

The general health of the patient is the primary consideration on whether to risk general anesthesia when trying to take radiographic images. In patients with critical health conditions, a poorly positioned radiograph may be able to provide enough information for the initial treatment. This is preferable to obtaining perfect radiographic images if performing such an examination would place the patient in a life-threatening situation.

The standard radiographic examinations of the head, thorax, abdomen, and pelvis are done in right-sided lateral recumbency, with the second plane being either the ventrodorsal (VD) or dorsoventral (DV) projection. Despite the small size of these animals, whole body radiographic examinations are generally not recommended. Radiographs of the thorax and abdomen should always be taken separately, especially in the larger small exotic mammal patients (e.g. chinchilla, ferret, guinea pig, rabbit).

There are a number of reasons for this recommendation:
- ☐ the exact positioning is easier when one only has to concentrate on a single section of the body.
- ☐ the image quality is better when the central beam is aimed at the middle of the region being investigated.
- ☐ radiographs of the abdomen should have a somewhat higher degree of contrast (lower kV) than those done of the thorax.
- ☐ a correct evaluation of the thorax is limited with survey radiographs.
- ☐ good radiographic images of the head, which allow an exact assessment of the teeth, are rarely achieved using whole body radiographs.

A radiographic image of a patient in right-sided recumbency and another in left-sided recumbency should always be performed to properly assess the lung field (i.e. looking for metastases) as only the lung further away from the plate can be properly judged. Additional oblique projections and radiographs taken with a horizontal beam should be obtained for additional information in individual cases. Oblique projections of the thorax can be advantageous for imaging proximal rib fractures. The use of a horizontal beam makes it easier to diagnose the presence of a mild pneumothorax.

Bilateral oblique projections with an opened mouth are a standard method for assessing individual rows of teeth.

Manual positioning of the patient is only recommended for larger, quieter animals (e.g. rabbit, guinea pig). In all cases, the primary beam should be collimated so that only the area being examined lies within the projection beam and not the holder's fingers. Animals under general anesthesia can be positioned on the cassette using small sandbags, bandages, or preferably adhesive tape (**Fig. 2-3**). When taking the radiographic images of a sedated/anesthetized patient, personnel can go behind a protective wall or to an adjoining room and thus are protected from radiation exposure.

The clinical signs with which small exotic mammals present to a veterinary practice are usually nonspecific, therefore the results of the routine clinical examination often provide the indications for radiographic examination of the cranium or teeth, thorax, abdomen, spine, or limbs.

Fig. 2-2: A guinea pig in which a plastic face mask has been used to induce and maintain the animal under general anesthesia. While anesthetized, the patient is easier to manipulate for proper radiographic positioning.

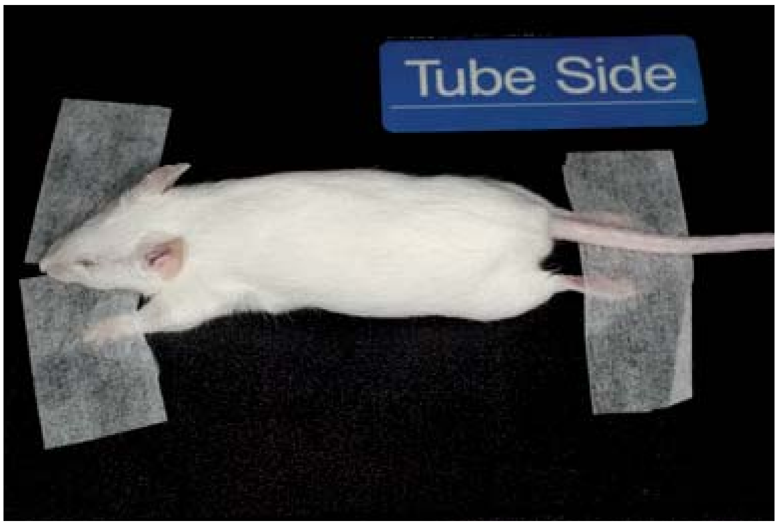

Fig. 2-3: Fixation of an anesthetized mouse with adhesive tape on the film cassette for a dorsoventral radiograph.

Indications for the radiographic investigation of the cranium

- ☐ anorexia without an underlying gastrointestinal etiology
- ☐ problems with gnawing, chewing, swallowing
- ☐ immovable space-occupying lesions
- ☐ swellings on the jaws
- ☐ malocclusion, overgrowth of individual teeth, variable tooth growth
- ☐ loose teeth
- ☐ abscess in the oral cavity
- ☐ epiphora and/or blockage of the nasolacrimal duct
- ☐ exophthalmos
- ☐ unilateral discharge from the nose or eyes
- ☐ chronic coryza
- ☐ hemorrhages from the mouth and/or nose
- ☐ torticollis
- ☐ severe purulent otitis externa (suspicion of otitis media/interna)
- ☐ bulging tympanic membrane

Indications for the radiographic investigation of the thorax

- ☐ dyspnea (mouth breathing, thoracic flank respiration)
- ☐ forced expiratory breathing
- ☐ paradoxical respiratory movements
- ☐ bloody-foamy nasal discharge
- ☐ severe serous or purulent nasal discharge (bilateral)
- ☐ slight nasal discharge with severe general malaise
- ☐ muffled heart or respiratory sounds
- ☐ heart murmurs
- ☐ suspicion of thoracic effusion
- ☐ gut sounds in the thorax
- ☐ reflux, regurgitation
- ☐ bilateral exophthalmos (rabbit)
- ☐ suspicion of metastases

Indications for the radiographic investigation of the abdomen

- ☐ swollen abdomen
- ☐ painful abdomen
- ☐ vomiting (ferret)
- ☐ palpable space-occupying lesion in the abdomen
- ☐ palpable hepatomegaly or splenomegaly
- ☐ over-distended, possibly painful urinary bladder
- ☐ suspicion of urolith formation in the urinary tract
- ☐ dysuria, hematuria, and polyuria
- ☐ vaginal discharges
- ☐ fur contaminated with urine in the perineum and inner thigh region
- ☐ swelling or cyanosis of the prepuce with dysuria
- ☐ swelling or cyanosis of the vulva with dysuria
- ☐ pregnancy diagnosis (e.g. guinea pig, chinchilla)
- ☐ parturition disturbances

Indications for the radiographic investigation of the spine

- ☐ ataxia
- ☐ paresis
- ☐ paralysis
- ☐ uncertain gait
- ☐ hindlimb muscle atrophy

Indications for the radiographic investigation of the limbs

- ☐ lameness in one limb
- ☐ lameness in alternating limbs
- ☐ suspicion of fracture or fissure
- ☐ pressure-sensitive space-occupying lesion on the limbs
- ☐ joint swelling
- ☐ ulcerative pododermatitis

2.1.2.2 Positioning for imaging the body

Lateral radiographs

Lateral projection radiographic images can be obtained either in right-sided or left-sided lateral recumbency. It is recommended to standardize the position of lateral recumbency (normally right-sided) in a practice, thereby increasing the ability to produce reproducible radiographic images. To obtain optimal radiographic images of the lungs (i.e. when looking for a tumor) variation from this method is acceptable as the lung lying next to the plate is compressed due to the pressure of the body weight and therefore cannot be properly evaluated. As a consequence, left lateral recumbency should be used when evaluating the right lung and right lateral recumbency for the left lung.

For a lateral radiograph, the fore- and hindlimbs of the patient are placed under slight traction without causing the trunk to be twisted, so that the sternum lies in the same horizontal plane as the spine. The animal can be supported in this position with small radiolucent foam wedges. For radiographic images of the thorax, the forelegs should be drawn as far cranially as possible to prevent summation into the cranial lung field. When taking radiographs of the thorax, care should be taken to prevent excessive cranial collimation: the first pair of ribs and if possible the caudal quarter of the neck should be included in the image so that the course of the trachea can be reliably evaluated. Caudally, the entire contour of the diaphragm must be visible on the radiograph.

The very short thoracic cage in rabbits and rodents often leads to a lack of sufficient cranial collimation on abdominal radiographic images. The entire diaphragm should form the cranial limit and be completely imaged on radiographs of the abdomen (**Fig. 2-4A**).

It should be noted that extension of the small exotic mammal patient and particularly the hindlimbs has an effect on the position of the internal organs. Excessive extension of the patient can lead to the stomach being pushed out of the thorax giving the impression of overfilling, especially in herbivorous species that normally have large stomachs. This should be taken into consideration when assessing radiographic images. It is very important that the entire pelvic anatomy (and especially the perineum) is included in radiographic images of the caudal abdomen. If the entire pelvic anatomy is not included in an abdominal radiograph, there is a danger that urethral stones (which occur relatively frequently in the rabbit, guinea pig, and chinchilla) will be overlooked.

Dorsoventral and ventrodorsal radiographs

In both these projections, the positioning of the patients should be such that the sternum is projected precisely over the spine. Only when the patient is positioned correctly is it possible to properly assess the heart silhouette. These positions are best attained when the spine is placed under slight traction by a gentle pulling of the fore- and hindlimbs. The hindlimbs should be held parallel with only the width of the trunk between them. As a rule, it is much easier to achieve this position with a supine placement of the patient (VD projection) (**Fig. 2-4B**) than prone (DV projection). The DV projection is primarily advantageous when radiographing the thorax as the bony ribs are less evident over the lungs and the heart does not tilt to the side to the same degree as in the VD projection.

With respect to the cranial and caudal collimation, the same rules described above for the lateral projection are applicable.

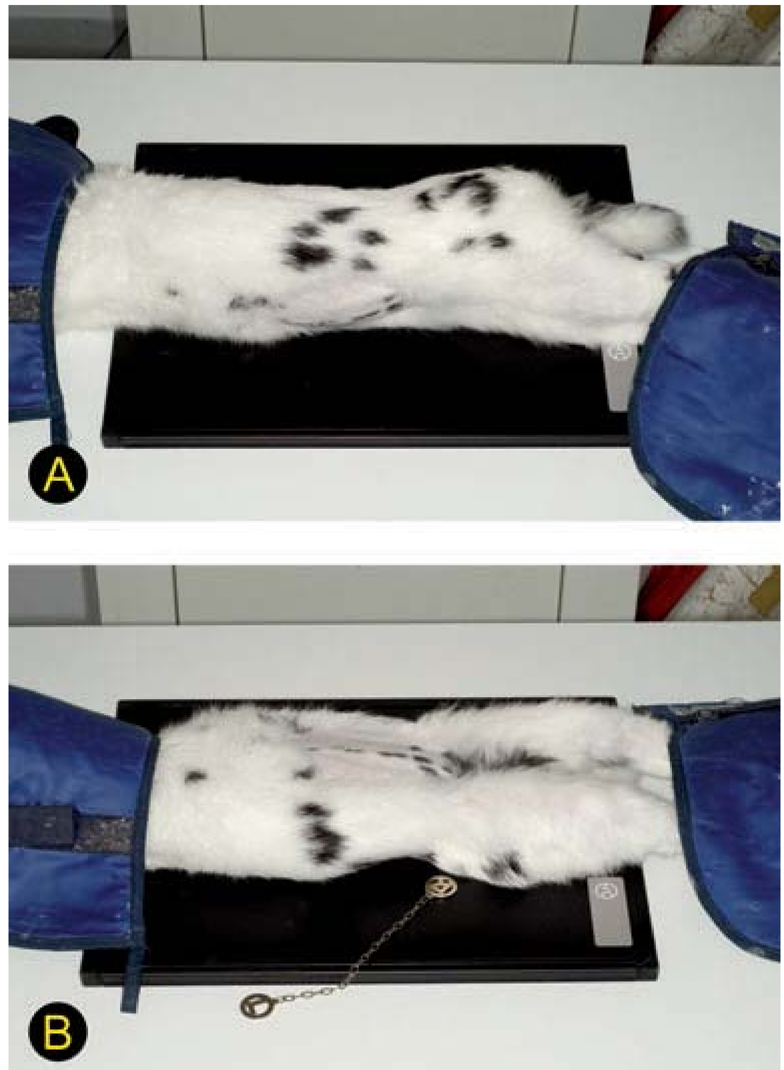

Fig. 2-4: Positioning of a rabbit for radiographs of the abdomen in a (A) lateral and a (B) ventrodorsal projection. When manually positioning a patient, the holder's hands must be protected from radiation, both above and below the animal.

2.1.2.3 Positioning for imaging the head and teeth

Michael Fehr

The standard radiographs in the lateral (forelimbs pulled backwards) and DV (positioning unproblematic) projections (**Fig. 2-5A**) are used for the diagnosis of diseases of the head or teeth in the rabbit and small rodents. Some authors recommend additional lateral projections with the head in a slightly tilted position or the use of the rostrocaudal projection for the imaging of dental disease or for the diagnosis of otitis media/interna (**Fig. 2-5B**). Similar to the recommendations for dog and cat patients, symmetrical positioning is important to obtain quality head and teeth radiographic images of lagomorphs and rodents.

Support of the rostral area of the cranium is required for a lateral radiograph of the head, especially in patients with a broad cranium or if they have space-occupying lesions in this region, otherwise the head tends to tilt rostrally with a slight rotation. If the head tilts rostrally with a slight rotation, this will lead to an incorrect projection of the zygomatic process (especially in the guinea pig), which may appear to be a tooth growing in a retrograde direction. The exact positioning of the head is achieved by using a cushion or by putting slight traction on the animal's pinna.

Positioning of anesthetized animals can be made easier by using a cut cardboard roll or something similar. If general anesthesia is not possible, a small exotic mammal can be placed in a tube bandage (e.g. sock) of a suitable size and brought into position by holding the tube at both ends.

In order to gain additional diagnostic information by using oblique radiographic images, the head should be tilted 25° for imaging the tooth root area (i.e. the upper incisors or rostral molars in rabbits) and 45° for imaging the jaws or the occlusal surface of the teeth. The area in question should always be placed next to the plate. Suitably angled foam cushions and adhesive tapes or holding bands attached to the upper jaw make positioning easier.

2.1.2.4 Positioning for imaging the forelimbs

Michael Fehr

The radiographic imaging of the pectoral limbs is performed in the same manner as in the dog and cat. The standard projections for radiographic imaging of the pectoral limbs are mediolateral (scapula: lateral) and craniocaudal (scapula: caudocranial). For the mediolateral image of individual limb segments, small mammals should be positioned in lateral recumbency with the limb to be radiographed lying adjacent to the plate. The end of the limb is fixed with a bandage or adhesive tape and the limb is pulled as far craniodistally as possible (the shoulder joint should lie ventral to the trachea). The upper contralateral foreleg is pulled in a caudal direction (**Fig. 2-6A**).

For the craniocaudal projection, the animal is placed in the prone position with the leg to be investigated pointing in a cranial direction. For the caudocranial projection, the animal is held in the supine position with the leg to be investigated pointing caudally.

When imaging diseased toes, it maybe advisable to pull the individual toes being examined cranially and position them in place with adhesive tape.

2.1.2.5 Positioning for imaging the hindlimbs

Michael Fehr

The radiographic imaging of the hindlimbs is performed similar to the dog or cat. The standard projections for the radiographic imaging of the hindlimbs are mediolateral (femur or pelvis: lateral) and craniocaudal. For the mediolateral projection of particular limb segments, small mammals should be placed in lateral recumbency with the limb to be radiographed lying next to the plate. The end of the limb is fixed with either a bandage or adhesive tape and pulled as far distal as possible (**Fig. 2-6B**).

For the craniocaudal projection, the animal is placed in the supine position with the limb to be examined pointing in a cranial direction. For the caudocranial projection, the animal is placed in the supine position with the limb being examined pulled in a caudal direction.

Fig. 2-5A: Positioning of a rabbit for a dorsoventral radiograph of the head. The head of the animal is maintained in position by a bandage placed over its dorsal cervical region.

Fig. 2-5B: Positioning of a guinea pig for a rostrocaudal radiograph of the head.

Fig. 2-6A: Radiographic examination of the right foreleg of a rabbit using a mediolateral projection. The right leg is pulled craniodistally with a bandage, while the contralateral limb is pulled caudally out of the x-ray beam.

Fig. 2-6B: Radiographic examination of the left hindleg of a rabbit using a mediolateral projection. The contralateral hindleg is pulled craniodorsally out of the x-ray beam.

2.1.3 Contrast studies

2.1.3.1 Introduction

Anatomical structures can only be distinguished from each other when they have differing radiodensities, which is not often the case with the soft tissues. Normally, only the presence of intra-abdominal fat enables a delineation of individual organs as it acts as a natural negative contrast. Young animals or cachexic animals do not have this fat; consequently, with most of these cases it is not possible to gain a clear radiographic differentiation of their abdominal organs. The soft tissue contrast can be improved by the administration of contrast agents with a low (negative contrast) or high (positive contrast) radiodensity in the different body cavities. A classical negative contrast agent is air, which can be administered directly in the body cavity/organ (e.g. stomach, urinary bladder) and possibly in combination with a positive contrast agent (double-contrast imaging). Rarely is air injected in the abdominal cavity (artificial pneumoperitoneum) to increase the contrast. Iodine and barium are the primary compounds used to produce a positive contrast in individual organs.

Barium sulfate is not resorbed into the body through the intestinal mucosa, none the less and despite its toxicity, it is the most commonly used positive contrast agent for the imaging the gastrointestinal tract. Water-soluble iodine compounds are not toxic and are used for a number of case presentations. The majority of the veterinary medical case presentations use water-soluble iodine compounds for established testing methods (e.g. angiography, lymphangiography (**Fig. 2-7**), portography and cholecystography), but are rarely used for clinical or diagnostic purposes in small mammals for various reasons (e.g. technical input, cost, lack of indications). In principle, these methods can be used and they have been established for small mammals in research. Contrast imaging of the urinary tract (urography) and of the spinal cord (myelography), in comparison, are more often used in the rabbit and ferret.

2.1.3.2 Contrast studies of the gastrointestinal tract

Negative contrast agents (e.g. air) are rarely used when imaging the gastrointestinal tract compared to positive contrast compounds (e.g. barium sulfate). One of the most common indications for a negative contrast study is the suspicion of a bezoar in the rabbit. Administering air through an esophageal tube directly in the stomach (5–10 ml/kg bwt), immediately before taking the radiographic images, will help push the gastric wall slightly away from the contents of the stomach, thereby revealing a bezoar in the majority of cases.

Through oral administration of positive contrast agents, the entire gastrointestinal tract can be investigated with respect to its position, width, patency, transit time, contents, and changes in the wall integrity. Although not always successful, an important indication for a positive contrast study is the imaging of bezoars. Other common indications include suspicion of radiolucent foreign bodies (e.g. ferret) and ileus (e.g. rabbit, guinea pig, chinchilla). As in these species, the aboral transport of food out of the stomach is dependent on the ingestion of new food, it is extremely important to ensure that the food can pass into the duodenum before forced feeding is performed, otherwise there is danger of a stomach rupture. To determine whether or not food can pass through the gastrointestinal tract, a small amount of barium sulfate (1–2 ml/kg bwt) should be administered to the animal at first and its transit into the duodenum radiographically confirmed.

Other indications for the use of positive contrast agents are the imaging of esophagus or intestinal displacement caused by intrathoracic or intra-abdominal space-occupying lesions, or even as a result of a diaphragmatic hernia. Dilatation of the esophagus (megaesophagus), which is rarely seen in small mammals, can only be diagnosed with a contrast study in the small exotic patient. As in the dog and cat, radiographic contrast studies can be used to diagnose changes in the gastrointestinal wall caused by neoplasia or chronic inflammation in small mammals; however, this method does not have any advantages in comparison to ultrasonography of the suspicious sections.

The positive contrast imaging of the gastrointestinal tract is performed primarily with the use of barium sulfate suspensions. Iodine-based contrast agents do not adequately cover the gastrointestinal mucosa; consequently, they are only indicated when there is suspicion of a perforation. Thus, the use of iodine-based contrast agents is of little importance in this application for small exotic mammals.

Imaging of the esophagus is done by administering a quantity of barium sulfate suspension with a syringe into the oral cavity and inducing the animal to swallow. Excessive extension of the head should be avoided at all costs because of the danger of aspirating the contrast material. In a healthy animal, the contrast bolus should be visible in the stomach within a few seconds after being swallowed, while the esophagus is only depicted by a thin line of the contrast agent (**Fig. 2-8**). If a gastrointestinal tract disease is considered, then it is advantageous to give the barium sulfate suspension directly into the stomach via an esophageal tube (**Fig. 2-9**). The distance of esophageal tube placement can be approximated by measuring the distance between the mouth and costal arch. The volume of barium sulfate suspension suggested in the literature varies up to 20 ml/kg bwt depending on species being examined. Our own experience has shown that the administration of 10–15 ml/kg bwt is adequate for the complete depiction of the gastrointestinal tract of most exotic small mammals. The dosage of the barium sulfate should be adjusted based on the degree of intestinal filling. In rabbits or rodents with severe gastric impaction or tympany, only 1–5 ml/kg bwt should be administered initially, to prevent possible stomach rupture. Only when this small amount has passed through the stomach should a larger dosage be given.

Fig. 2-7: Detailed radiographic examination. Rat: Lymphangiography (with contrast agent) of the popliteal lymph node showing the afferent and efferent lymph vessels.

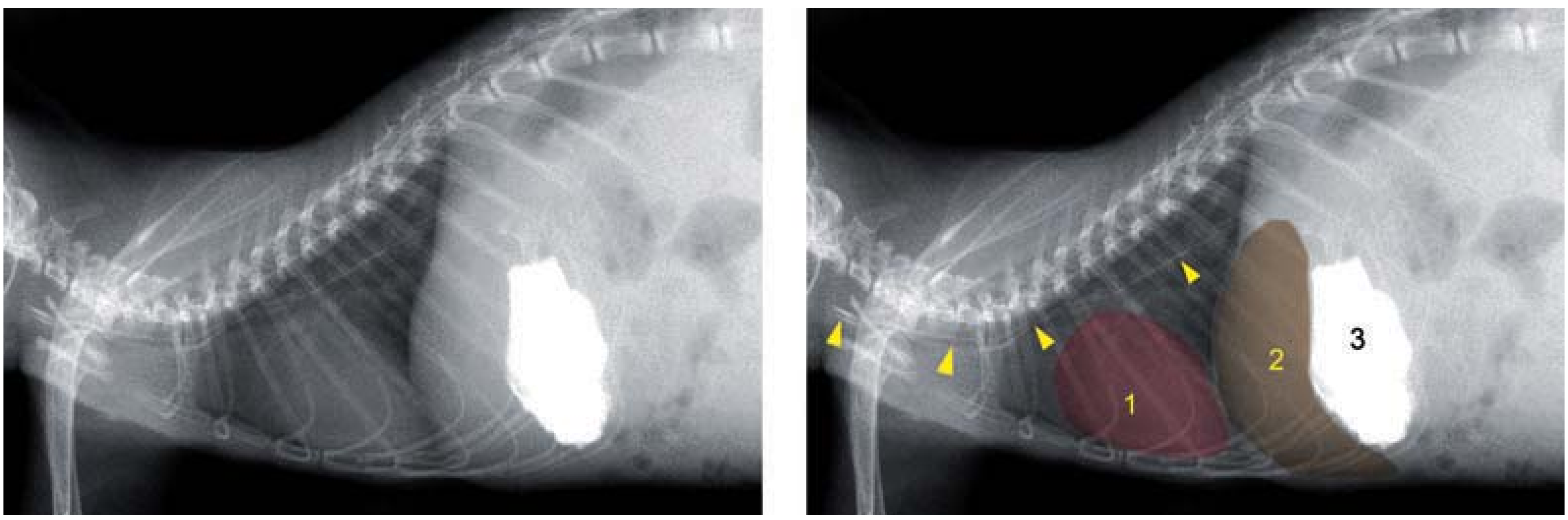

Fig. 2-8: Radiographic image of a chinchilla's thorax, lateral projection, 30 seconds after swallowing 1 ml barium sulfate suspension. There are fine traces of the contrast agent (arrowheads) in the folds of the esophageal mucosa.

Radiograph reproduced with kind permission from Jopp, I. P., Stengel, C., Kraft, W. (2004): Megaösophagus bei einem Chinchilla. Tierärztl Prax **32(K)**: 97 [98].

1: heart
2: liver
3: stomach

arrowheads: traces of contrast in the esophageal mucosa

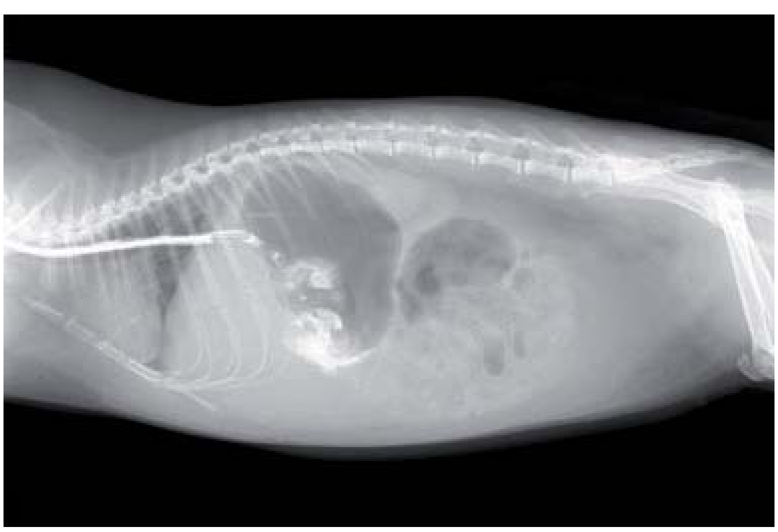

Fig. 2-9: Radiographic image of a guinea pig's thorax, lateral projection. This image shows the placement of a gastric tube that will allow administration of contrast suspension into the patient's stomach.

A contrast study not only provides the information, regarding the digestive system, mentioned above but also allows one to determine the transit time of the material through the gastrointestinal tract. Of clinical interest is the delay or even total cessation of the contrast agent's movement through the gastrointestinal tract. Coprophagia often leads to confusion when interpreting digestive system contrast studies in herbivorous small exotic mammals due to the apparent continued evidence of contrast material in the patient's stomach despite the appearance of movement and subsequent excretion in the feces.

Inadequate hydration of the patient is another reason for delayed intestinal passage and can lead to the solidification of barium sulfate suspension in the gastrointestinal tract (leading to the formation of cement). One should always watch out for signs of complications associated with a dehydrated patient that has been administered contrast material. The transit time of a contrast agent can be shortened in cases of diarrhea or gastrointestinal hypermotility, which are rarely an indication to perform a contrast study of the digestive system.

While assessing the passage of contrast through the digestive system, attention should be paid to the anatomical and physiological features of the particular species of small exotic mammal being examined.

Ferrets do not have an appendix, but have a very short digestive tract with a smooth transition between the small and large intestines. The passage of contrast material through the intestinal tract is similar to that observed in cats. In 30 minutes, the contrast material may be observed at the level of the rectum and roughly after 3 hours, all the contrast has been eliminated (**Fig. 2-10**).

It is important to acknowledge certain anatomical and physiological differences regarding the gastrointestinal tracts of **rabbits**, **guinea pigs**, and **chinchillas**. The food mass which is normally present in the stomach of these animals binds to a proportion of the administered contrast material (**Fig. 2-11A**). This food-contrast mixture has a lower degree of contrast than the original contrast bolus and may be observed for up to 24 hours or longer. The remainder of the contrast material moves through the stomach between the mucosa and the food bolus, and leaves the stomach relatively quickly, after 30–60 minutes. This rapid movement of contrast material results in an increased filling and imaging of the small intestines within 1–4 hours. The contrast material reaches the appendix after 1–2 hours (**Fig. 2-11B**) and in 2–4 hours, the colon. However, most of the contrast material collects in the appendix (**Fig. 2-11C**), in which the best degree of filling and imaging frequently occurs after 5–6 hours. During this time, the stomach and appendix are usually well imaged by the contrast agent, while it is no longer evident in the small intestines and only a minimal amount can be observed in the colon, although the contrast initially reaches the rectum approximately 5 hours after administration (**Fig. 2-11D**). Appropriate filling and imaging of the colon can be expected approximately 8–12 hours after administration of the contrast material.

It should be noted, that even in healthy animals, the contents of the animal's diet affects the transit time. Fiber-poor concentrated feed is associated with quicker transit times (8–10 hours), while fiber-rich feed with a low energy concentration has longer transit times (up to 30 hours).

It is possible that traces of contrast can be found up to 3 days after administration because some species re-ingest part of the excreted contrast through cecotrophy.

Despite the paucity of information regarding **degu** digestive physiology, it can be expected that there are similarities between this species and guinea pigs and chinchillas.

Although it is possible, a contrast study is rarely indicated in the small rodents (e.g. **golden hamster, gerbil, rat, mouse**). The time the contrast remains in the stomach and appendix of small rodents is shorter than in the guinea pig and chinchilla (which are adapted to a poor diet) and the contrast should be completely excreted after 24 hours.

The classical indication to perform a **double-contrast study** using barium sulfate and air is suspicion of pathological changes involving the gastric mucosa. The animals should be fasted prior to a double-contrast study, but this prerequisite is only applicable for ferret patients. In the rabbit, double-contrast imaging can be attempted when barium sulfate is in the stomach and there is an undetermined diagnosis of a trichobezoar despite the presence of positive contrast. In rodents, there are no indications for a double-contrast study.

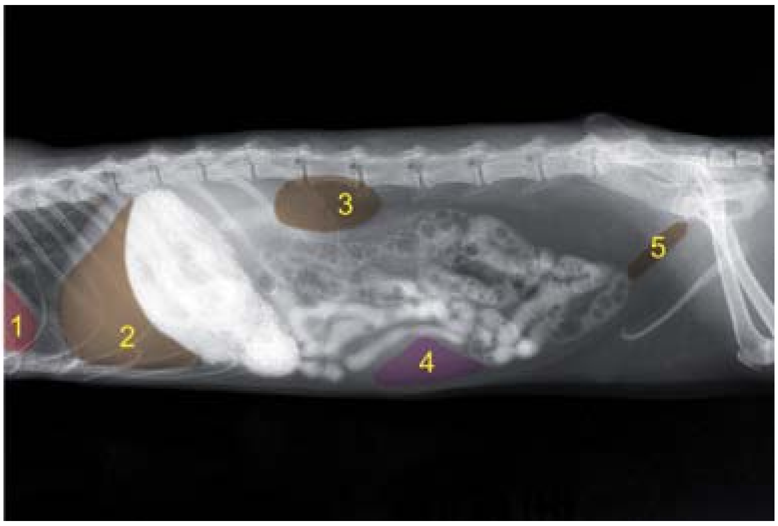

Fig. 2-10: Radiographic images of a ferret's abdomen, lateral projection, 20 minutes after administration of a barium sulfate suspension. The rapid rate of passage of the contrast suspension through the ferret's gastrointestinal system allows for a complete examination of this body system within 30 minutes.

1: heart
2: liver
3: kidney
4: spleen
5: urinary bladder

Fig. 2-11A: Radiographic image of a guinea pig's abdomen, lateral projection, 30 minutes after the administration of a barium sulfate suspension. The contrast agent has bound to food in the animal's stomach thus delaying its passage into the intestinal tract by approximately 30 minutes. The first trace of contrast material within the small intestine is evident in this radiographic image.

Fig. 2-11B: Radiographic image of a rabbit's abdomen, lateral projection, 60 minutes after administration of a barium sulfate suspension. The contrast agent defines the whole of the small intestine and is beginning to fill the cecum. A considerable proportion of the contrast material is still in the stomach.

Fig. 2-11C: Radiography image of a guinea pig's abdomen, lateral projection, 3 hours after the administration of a barium sulfate suspension. Contrast radiographic image of the cecum and the proximal colon. The small intestine is no longer visible. Contrast material bound to food is still faintly evident in the stomach.

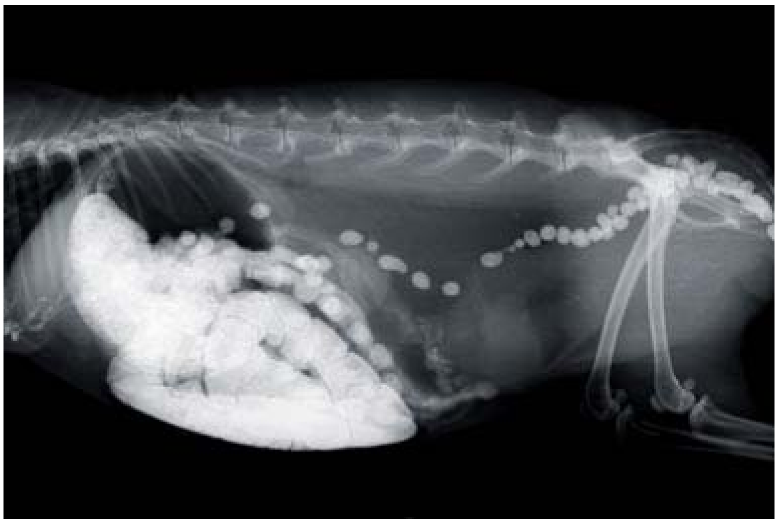

Fig. 2-11D: Radiographic image of a rabbit's abdomen, lateral projection, 6 hours after the administration of a barium sulfate suspension. After 5 hours, the cecum and colon are the principal structures visible and excretion of contrast agent via the rectum has started.

2.1.3.3 Contrast studies of the urinary tract (urography)

It is not possible to differentiate individual sections of the urinary tract using traditional radiographic techniques. Excretory urography not only improves renal imaging but also enables the remaining structures of the urinary tract to be visualized (e.g. collecting tubules, renal pelvis, ureters, urinary bladder, urethra). When examining the results of an excretory urogram an evaluation of renal function can be made. Alternatively, retrograde urography can be performed if pathological processes affecting the urinary bladder or urethra need to be investigated.

Recently, ultrasonography has become the preferred diagnostic method for many classical disease presentations in which urography was the procedure of choice. Therefore urography is rarely used at this time to diagnose renal disease in small exotic mammals. However, urography has not completely lost its value to diagnose ruptures of the ureter and urinary bladder or perforations of the urethra, which are only definitely identified and localized using this imaging technique. Moreover, the imaging of an ectopic ureter is most reliable with the aid of urography.

Intravenous access via a venous catheter should be established when performing **excretory urography**. An iodine-based ionic or non-ionic contrast agent at a dosage of 600–850 mg iodine/kg bwt is injected through this access port. The contrast distributes itself throughout the circulation and leads to a higher contrasting of all well-perfused organs such as the kidney (**vascular phase**, **parenchymal phase** or **nephrography**). To gain images during this phase, radiographs should be taken within the first 10 seconds after the injection. The contrast agent is excreted via the kidneys, but it is not reabsorbed in the tubuli, leading to a concentration of the contrast in the urine and an imaging of the remainder of the urinary tract. Optimum imaging of the renal pelvis (**pyelography phase**) occurs within the first few minutes after contrast administration to the patient (**Fig. 2-12**). Only a few minutes after the injection, the ureters are imaged as two fine white lines running parallel to the spine, which then terminate dorsally in the neck of the bladder (**Fig. 2-13**). There is then a concentration of contrast material in the urinary bladder. A delay in the movement of the contrast material into the bladder can be induced by a compression of the caudal abdomen with bandages, thus providing an enhanced diagnostic image of the renal pelvis and ureters. In comparison to the non-invasive alternative imagining modality of ultrasonography, excretory urography subjects the patient to a great deal of stress and with alternatives available, is rarely justified.

As an alternative route of administration in small rodents, the contrast agent can be injected subcutaneously. When injecting the contrast material in the subcutaneous space, the excretion is delayed; consequently, initial radiographic images should be taken 5 and 10 minutes after the introduction of contrast agent using this route.

2.1.3.4 Contrast studies of the spinal cord (myelography)

Sven Reese, Michael Fehr

If the results of a neurological investigation indicate that there is an obstruction or narrowing of the spinal cord, – and through the use of plain radiograph images no obvious diagnosis can be made – then a contrast study of the spinal cord contour is indicated (myelography).

The techniques for performing a myelography in small exotic mammals are similar to those well-established methods used in the dog and cat. Although the smaller size of these patients makes myelography technically more exacting, it is easily possible to achieve this diagnostic imaging technique in the ferret, rabbit, and guinea pig.

Myelography is done with the patient under general anesthesia – preferentially using an inhalation anesthetic gas. Water-soluble non-ionic iodine compounds are used as contrast at a concentration of 180–250 mg iodine/ml. The contrast solution should be warmed to body temperature before being injected. There are two sites that are preferred for injection of the contrast agent to obtain images for myelography: the atlanto-occipital space (injection into the cerebromedullary cistern) or between the 5th and 6th lumbar vertebrae. Spinal needles with a stylet in the size 22 G (0.73 mm × 40 mm) have proven to be suitable for rabbits.

Injection of the cerebromedullary cistern

The head of the patient is bent down as far as possible, after which the needle is inserted in the midline caudal to the occipital protuberance where it is crossed by an imaginary line between the wings of the atlas. The needle is pushed forwards at an angle of 90° to the vertebral canal until – if the positioning is correct – a small amount of CSF flows into the needle hub. Once the position of the needle is ascertained as being correct, the contrast agent is injected slowly to a maximum volume of 0.3 ml/kg bwt. The head must then be held upwards to ensure that the contrast flows caudally into the subarachnoid space of the spinal cord and not cranially into the ventricle.

Lumbar injection

For a lumbar injection, the patient is bent over as far as possible from the hips, with the hindlegs pulled cranially. The needle is inserted at an angle of 90° in the dorsal midline, centered between the relatively easily palpable L5 and L6 intervertebral space, and is pushed forward. The volume of injected contrast agent should not be any more than 0.5 ml/kg bwt (**Fig. 2-14**).

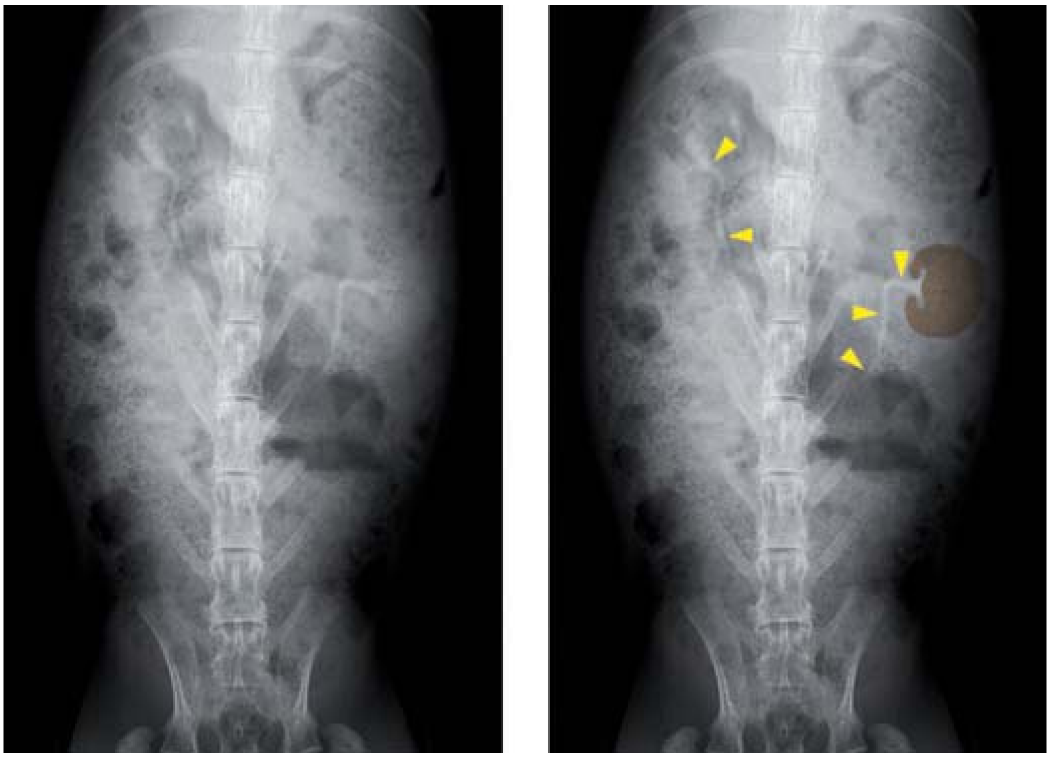

Abb. 2-12: Radiographic image of a rabbit's abdomen, ventrodorsal projection after the intravenous injection of an iodine-containing contrast agent. Image showing the renal pelvis (pylography) and the start of the ureter (arrowheads).

Abb. 2-13: Microfocus radiographic image of a rat's kidney, ventrodorsal projection (individual images from a radioscopy series). The ureter is transversed by peristaltic waves which transport the contrast-centraining urine in small portions.

A: Collection of urine in front of the ureter (arrowhead).

B: A wave of contraction (arrowhead) pushes the urine through the ureter.

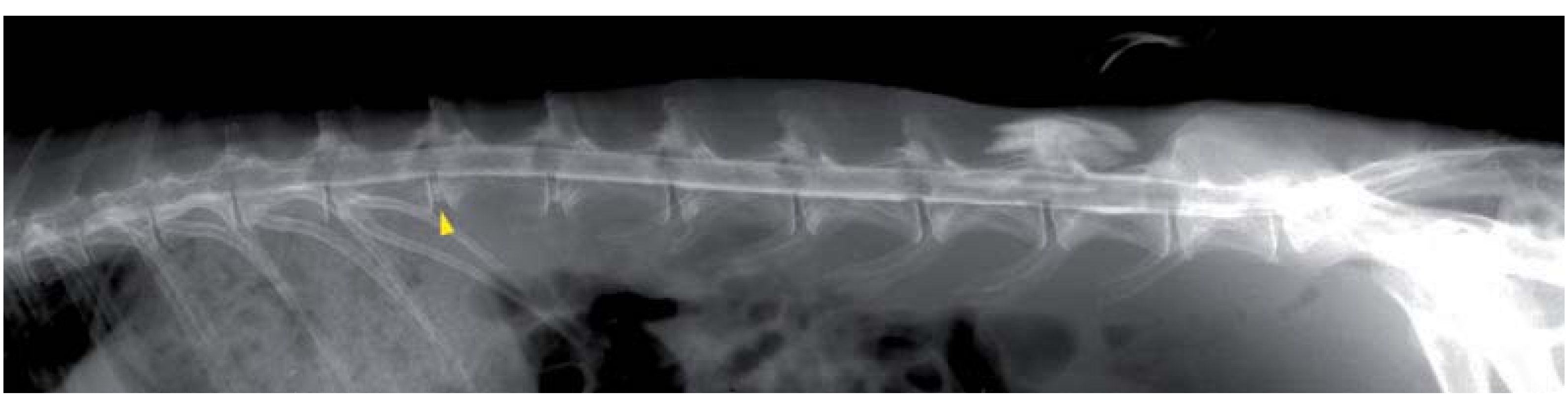

Fig. 2-14: Radiographic image of a rabbit's spine, lateral projection, myelography after lumbar punction between L5 and L6. Calcification of the vertebral disc between T13 and L1 (arrowhead).

2.2 Radioanatomy

2.2.1 Skeletal system

SVEN REESE, MICHAEL FEHR

The **rabbit** has the most fragile skeleton of all the small exotic mammals maintained as companion animals. During the course of domestication and breeding, the proportion of muscle has significantly increased in this species, with the skeleton forming only 6% of the total body weight in large rabbit breeds and 7–8% in dwarf rabbits. Wild rabbits have a much more balanced ratio of bone to muscle as the skeleton comprises 9% of their total body weight.

In the following, only the characteristics of the individual small exotic mammalian species are discussed, along with the clinically relevant radiographic structures of their skeletal system. For more details, please refer to more in-depth anatomy reference literature.

2.2.1.1 Cranium with teeth

The cranium of the **ferret** is elongated and flat. It has a characteristic narrow stricture in the upper cranium at the transition between the viscerocranium and the cranium. The very compact bones of the ferret's cranium are joined in such a way that no cranial sutures are formed (**Fig. 2-15**).

Ferrets have a typical secodont (cutting) carnivorous dentition with long carnassial teeth that are anchored in the jaw up to two-thirds of their length. The deciduous dentition erupts at 3–4 weeks after birth and consists of 30 teeth. The change to the permanent dentition, consisting of 34 teeth, begins in the 7th week of life and is complete by the 10th week.

The cranial bones in the **rabbit** are very thin when compared to the ferret. When prepared anatomically, a rabbit's cranial bones are partly translucent and therefore have a lower radiodensity. Typical for the rabbit is the large but very thin mandibular body, which forms the insertion surface for the strong masseter muscle. The lateral part of the nasal cavity is completely ossified as the maxilla in this region has sieve-like holes. In contrast to rodents, the flatter and broader jaws of rabbits are easier and best imaged radiographically in the rostrocaudal projection (**Figs. 2-16A** to **2-16C**).

Characteristic of **lagomorph** (e.g. rabbit) dentition are small rudimentary incisors (auxilary incisors or peg teeth) in a row lying directly behind the rodent front teeth in the upper jaw.

Fig. 2-15: Radiographic image of a ferret's head, dorsoventral projection. The narrow stricture between the facial and cranial parts (arrowheads) of the skull is a typical radiographic characteristic of a ferret head.

Dental formula of the ferret's deciduous dentition:

$$2 \times \frac{4dI\ 1dC\ 3dP\ 0M}{3dI\ 1dC\ 3dP\ 0M} = 30 \text{ milk teeth}$$

Dental formula of the ferret's permanent dentition:

$$2 \times \frac{3I\ 1C\ 3P\ 1M}{3I\ 1C\ 3P\ 2M} = 34 \text{ teeth}$$

Fig. 2-16A: Radiographic images of a rabbit's head, lateral projection. With optimal positioning, the ventral contours of both tympanic bullae (1) and the hemimandibles (2) are superimposed. The occlusal table of the molars is serrated in the rabbit (arrowheads). For assessing the length of the upper molars, a guide line is drawn from the rostral end of the nasal bone to the external occipital protuberance.

1: contours of both tympanic bullae
2: contours of the hemimandibles

arrowheads: serrated molars

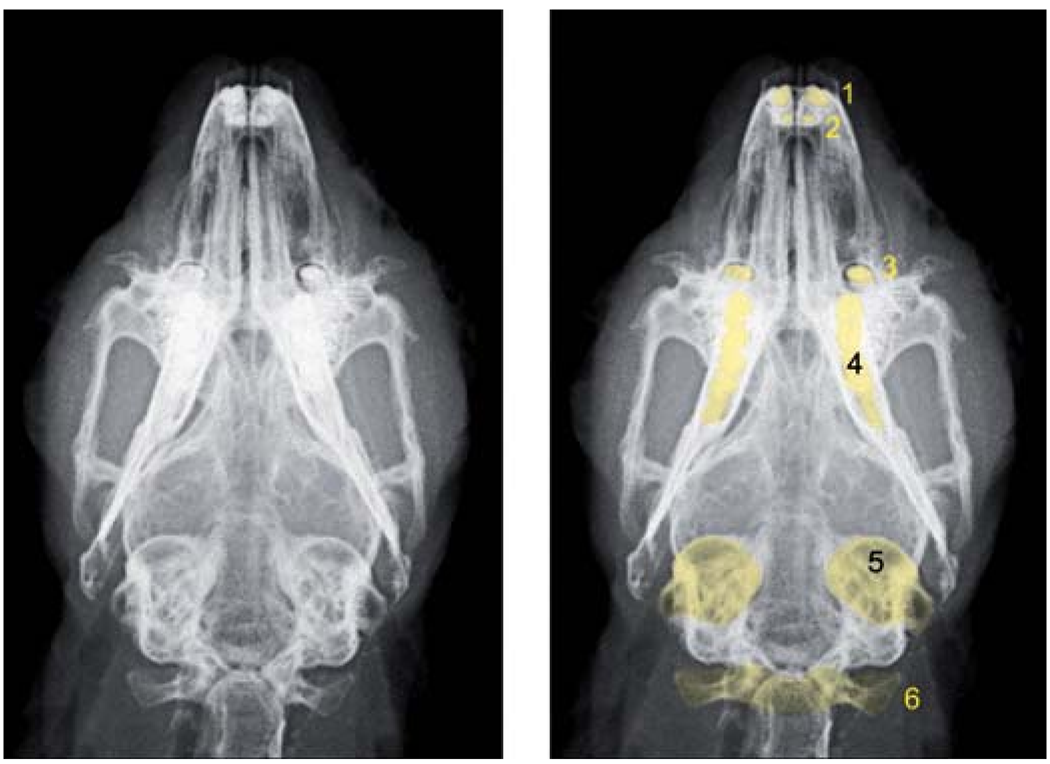

1: upper incisors
2: peg teeth
3: 1st premolar in the upper jaw (the only back tooth shown without any superimposition in this projection)
4: superimposed projections of the molars in the upper and lower jaws
5: tympanic bulla
6: atlas

Fig. 2-16B: Radiographic images of a rabbit's head, dorsoventral projection.

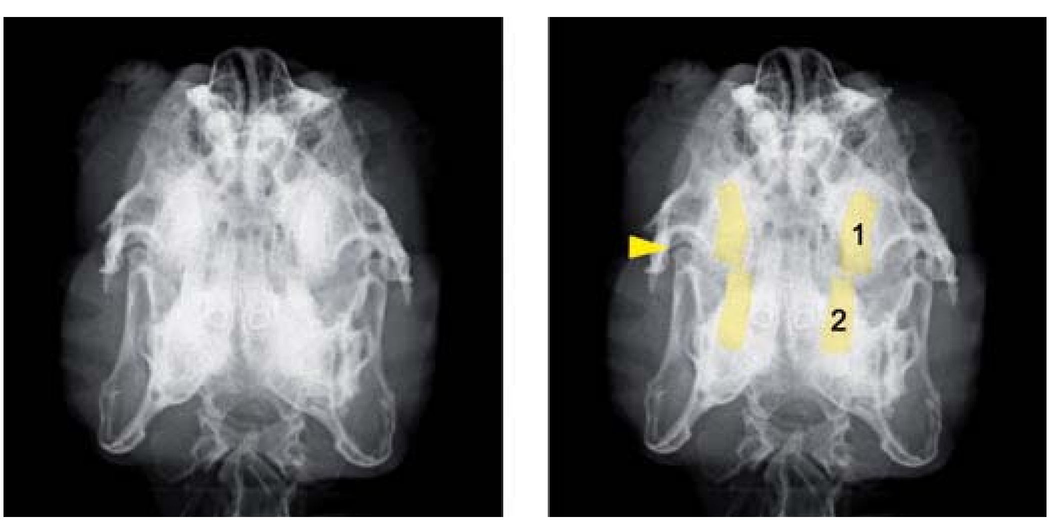

1: upper molars
2: lower molars

arrowhead: temporomandibular joint

Fig. 2-16C: Radiographic images of a rabbit's head, rostrocaudal projection. This projection emphasizes the wider spacing between the molars in the upper jaw (1) in comparison to that found between the molars in the lower jaw (2). This projection also provides a clean image of the temporomandibular joint (arrowhead).

Carnassial teeth are not formed. The transverse molars are situated in the depths of the oral cavity after the long diastema. The permanent dentition in the rabbit consists of 28 teeth, which are completely present from the 4th week of life onwards. The caudal molars may be so weak that they cannot be observed with certainty on a radiographic image. In contrast to many rodents species, the rabbit does have a deciduous dentition consisting of 12 teeth even though it is functionally insignificant.

In adaption to the high fiber, strongly abrasive diet of the rabbit, both incisors and molars grow continually throughout the animal's life. An anatomical characteristic of rabbit molars and incisors is the pulp cavity does not narrow apically but remains wide open. The periapical germinative tissue is seen radiographically as an area of low radiopacity in the incisors. In comparison, the periapical lucency is relatively very slight in the molars. On average, a rabbit's teeth grow 2 mm per week. In all likelihood, the tooth growth rate is controlled to some degree by normal wear, thus enabling an amount of adaption to the seasonal diet changes that occur in the wild. Malocclusion has a pathogenetic significance as it can lead to excessive strain on the teeth, whereby their growth in length is increased, thus exacerbating the problem.

In contrast to rodents, the outer surface of the rabbit's incisors completely consists of enamel. Consequently, these teeth will appear as being evenly radiopaque deep into the alveolus on a radiographic image. The position of the upper incisors, which can be observed on a lateral projection, forms an arch with a tight curve, while the incisors in the lower jaw form a weak arch and end behind the upper incisors, possibly abutting on the pivot teeth. The incisors extend far into the jaw bones, with the mandibular incisors ending just before the first premolars. In the upper jaw, the apical end of the incisor lies about halfway along the diastema.

The back teeth in the lower jaw lie closer together in the dental arch than those in the upper jaw. In the lateral projection, the back teeth have a longitudinal pattern that is an expression of the folded nature of their enamel. A rabbit's chewing movements are done primarily in the lateral direction, while the rostrocaudal movement of the lower jaw is very limited. These chewing movements lead to the formation of a regularly pointed occlusal surface on the back teeth in both the upper and lower jaws. In the rabbit, the dental arches do not touch each other when at rest; consequently, with optimal positioning the contour of the horizontal occlusal surfaces can be imaged with a lateral projection. The back teeth extend far into the jaw bones. They extend down to the ventral cortex in the lower jaw, whereas in the upper jaw, the apical ends lie under an imaginary line drawn between the rostral end of the nasal bone and the occipital protuberance.

The cranium in the **Caviomorpha**, which include the **guinea pig**, **chinchilla**, and **degu**, is elongated with an almost straight upper edge on the lateral view. Typical for these species are a strong broad zygomatic arch and a very long angular mandibular process, which extends to the level of the atlanto-occipital joint (**Fig. 2-17**). A species-specific characteristic of **chinchillas** are the gigantic tympanic bullae, which in the lateral projection appear as snail-like structures that superimpose on the cranium from an extreme caudal position to the ventral aspect of the cranium (**Fig. 2-18**).

The dentition of the Caviomorpha is adapted to ingesting a poor, fiber-rich diet with a high abrasive effect similar to the rabbit. Their incisors and back teeth are also elodont and grow throughout the animal's life. The number of permanent teeth in this species (20), which have all erupted and are in place at birth, is much lower than in the rabbit. It has been determined that with **chinchillas** the change from primary to permanent dentition occurs prenatally in the fetus. In the **guinea pig**, it appears that a complete deciduous dentition is no longer formed during prenatal development. Also regarding tooth development, only one primary molar is formed per quadrant between the 43^{rd} and 46^{th} day of pregnancy, which are then resorbed by the 55^{th} day.

The chisel-like incisors of the Caviomorpha do not touch each other when at rest, with the lower incisors lying in a more caudal direction than their upper counterparts. The higher mobility of the jaws in a rostrocaudal direction and the special ability of part of the masseter muscle enable the lower jaws to be pushed so far forward that the incisors come into an occlusal position that is suitable for gnawing. The apical end of the incisor in the upper jaw extends to over more than half of the diastema and in the guinea pig, it almost reaches the mesial surface of the first molar.

Dental formula of the rabbit's deciduous dentition:

$$2 \times \frac{1dI\ 0C\ 3dP\ 0M}{0I\ \ 0C\ 2dP\ 0M} = 12 \text{ milk teeth}$$

Dental formula of the rabbit's permanent dentition:

$$2 \times \frac{2I\ 0C\ 3P\ 3M}{1I\ 0C\ 2P\ 3M} = 28 \text{ teeth}$$

Dental formula of the Caviomorpha:

$$2 \times \frac{1I\ 0C\ 1P\ 3M}{1I\ 0C\ 1P\ 3M} = 20 \text{ teeth}$$

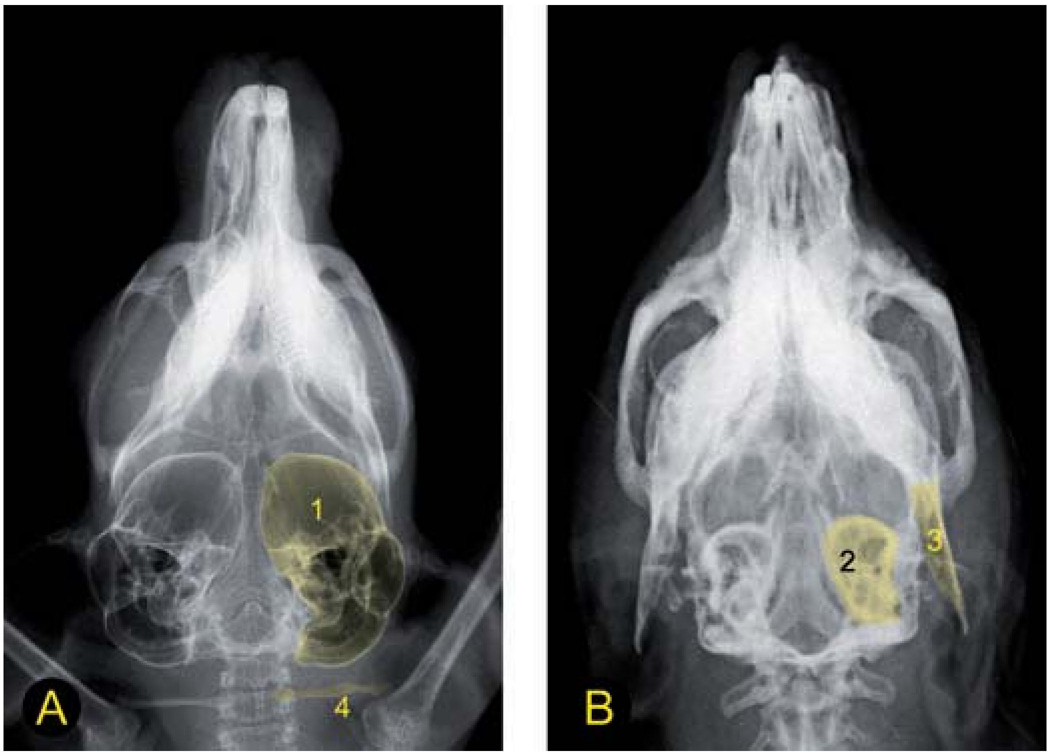

1, 2: tympanic bulla
3: angular mandibular process
4: clavicle

Fig. 2-17: Radiographic images of the head, dorsoventral projection. A: Chinchilla. B: Guinea pig.
The very large tympanic bulla (1) is characteristic of the chinchilla cranium. The guinea pig, in contrast to other Caviomorpha, has a relatively small tympanic bulla (2). The large caudal extension of the angular mandibular process (3) is typical of a guinea pig skull.

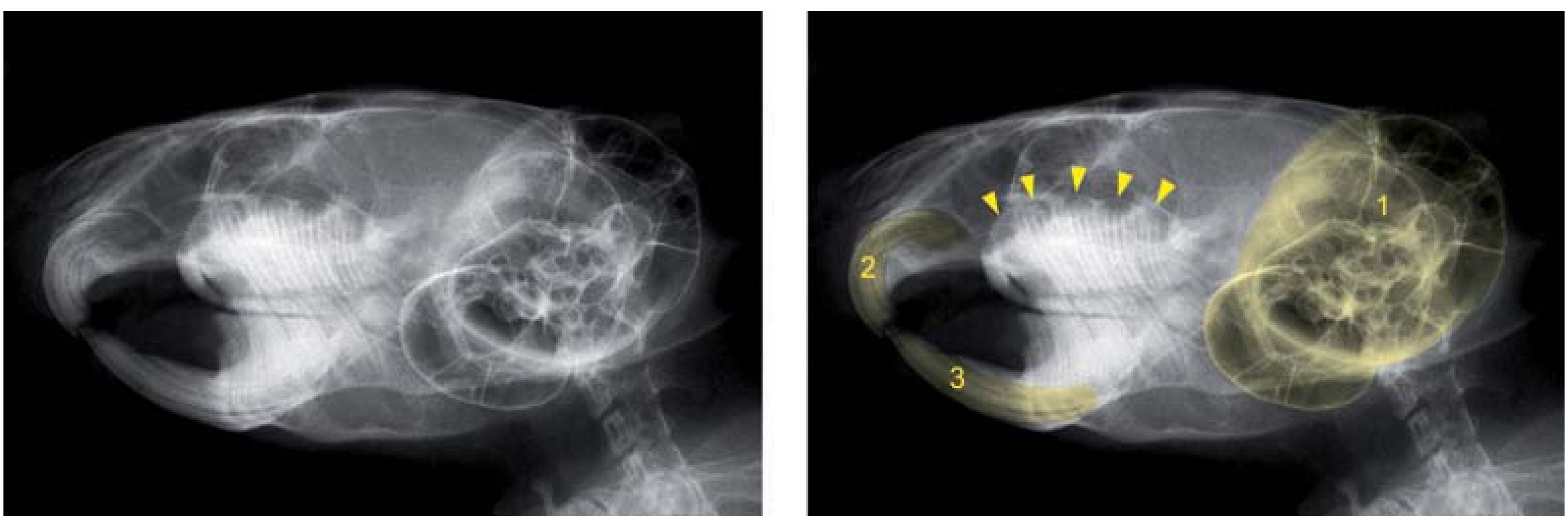

Fig. 2-18: Radiographic images of a chinchilla's head, lateral oblique projection, approximately 10°. The oblique projection allows a clear imaging of the upper molar roots without summation of surrounding structures. The arrowheads mark the periapical halo of radiolucency.

1: tympanic bulla
2: upper incisors
3: lower incisors.

arrowheads: periapical halo

Caviomorphic molars belong to the selenodont teeth, whereby they have a relatively simple anatomic design in the degu with only one crescent. The course of the crescent is reminiscent of an eight, from which the zoological name of the **degu**, *Octogon degu*, originates.

The dental arch of the back teeth stands further apart in the lower jaw than the upper. In the **guinea pig**, the occlusal surfaces are angled inward by 45°. This inward angle is caused by the molars in the upper jaw being curved in a slight buccal direction and those in the lower jaw having a small lingual curve and is depicted well in the rostrocaudal projection. In contrast, the occlusal surfaces of the **chinchilla** and **degu** back teeth are horizontal and can be observed in the lateral projection as fine black lines. In order to roughly judge the position of the occlusal surfaces of a **guinea pig** when viewed in a lateral projection, one should draw a line from the jaw to the apices of the incisors. The principle chewing movements in the Caviomorpha are rostrocaudal. This movement enables the teeth to wear evenly, therefore the occlusal surfaces of the back teeth are smooth, unlike those in the rabbit. In the DV projection, the rows of a Caviomorpha's back teeth diverge in a rostrocaudal direction. For the assessment of the peri- and retro-orbital bone boundaries, which should be sharp, the rostrocaudal projection is only suitable in the **chinchilla** and **degu** because the curved course of the back teeth in the guinea pig leads to severe summation. The position assessment of the apical ends of the molars in a **chinchilla's** upper jaw is clinically significant and is best performed using a lateral projection. With normal occlusion, the tooth roots may not extend any further than a line drawn from the middle of the tympanic bulla to the dorsal edge of the incisors.

The craniums of the **Myomorpha** (e.g. **golden hamster**, **gerbil**, **rat, mouse**) are shorter and more compact than the Caviomorpha. The upper edge of a myomorphic cranium is slightly convex. The elongated zygomatic arch is very thin and is superimposed medially by the coronoid process of the mandible and can be easily viewed radiographically in the **golden hamster**. The severely angled mandibular process is much shorter in myomorpha than that found in the Caviomorpha and ends at the level of the rostral half of the tympanic bulla (**Fig. 2-19**).

The dentition of the Myomorpha is adapted to a softer and less abrasive diet. In these species, only the incisors, which are subjected to strong use during gnawing, are elodont and grow throughout the animal's life. The molars are crowned teeth of the brachyodont type – premolars are not formed in Myomorpha. Although the dentition of the different Myomorpha species is basically very similar, the **Cricetidae** (e.g. **golden hamster**, **gerbil**) can be differentiated from the **Muridae** (e.g. **rat, mouse**) by the number of cusp rows on the molars: two rows in the Cricetidae, three rows in the Muridae. As a rule, Myomorpha have 16 permanent teeth. However individual golden hamsters may have only 12 teeth; which can also rarely occur in the rat and mouse.

The short gestation in the Myomorpha results in the first eruption of teeth *post partum*. In the **golden hamster**, tooth eruption occurs between the 3^{rd} and 21^{st} day of life. Young **rats** begin to »show« their incisors on the 8^{th}–10^{th} day of life and the three molars erupt in a rostrocaudal sequence on the 18^{th}, 21^{st}, and 35^{th} day after birth.

The extra-alveolar part of the incisors is two to three times longer in the lower than in the upper jaw. This apparent disparity may not be used as an excuse to shorten the incisors in the lower jaw. In addition, the lower incisors are anchored particularly deep in the jaw of the Myomorpha. The lower incisor reaches the level of the third molar in the **golden hamster** and **mouse**, and is even longer in the **rat**. In the upper jaw, the apical end of the incisor lies at roughly two-thirds of the length of the diastema. In contrast to the rabbit, the incisors only have enamel on their front surface. Due to the tooth enamel being on one tooth surface, the radiodensity of the incisors is not homogeneous in the lateral projection: the lingual side is less radiopaque than the labial aspect. As in the Caviomorpha, myomorphic incisors do not touch each other when in the resting position. The brachyodont molars only have enamel on their crowns. Similar to the ferret, their roots consist of only less radiopaque dentine and cement. In the DV projection, the relative molar position can be well visualized. Although the lower jaw is somewhat broader than the upper jaw, the dental arches of both jaws should be parallel to each other. The left and right dental arches diverge slightly in a rostrocaudal direction.

Dental formula of the Myomorpha:

$$2 \times \frac{1I\ 0C\ 0P\ 3M}{1I\ 0C\ 0P\ 3M} = 16 \text{ teeth}$$

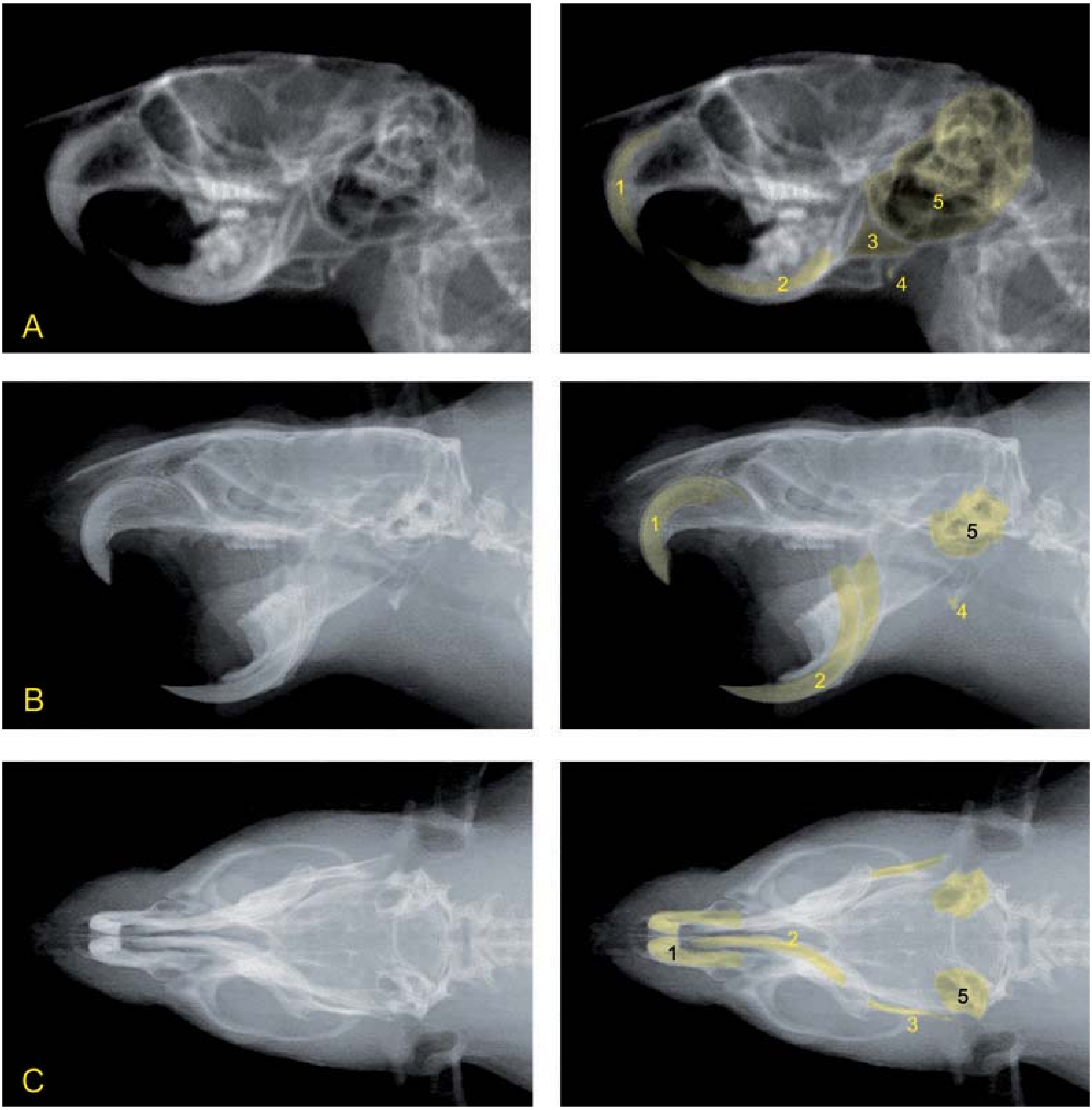

Fig. 2-19: Radiographic images of the head.

A: Lateral projection. Gerbil.

B: Lateral projection. Rat.

C: Dorsoventral projection. Rat.

In both these species, only the incisors grow throughout the animal's life and are anchored deep within the maxilla and mandible. This is particularly evident when viewing the lower jaw in the rat.

1: upper incisors
2: lower incisors
3: angular mandibular process
4: hyoid bone
5: tympanic bulla.

2.2.1.2 Spine, thorax

The construction of the spine in small exotic mammals is principally the same as in the dog and cat. In comparison to the dog and cat, the **rabbit** has clearly long and broad lateral processes on the caudal lumbar vertebrae (**Fig. 2-20**). An overview of the number of vertebrae for the differend species is given in Table 2-2

The **ferret's** thoracic cage is elongated, though the first pair of ribs is very short. As a result, the cranial thoracic inlet is rather narrow in the ferret, which is why space-occupying disease processes affecting this area can quickly cause a compression of the structures passing through the inlet (**Fig. 2-21**).

It should be noted that in the **rat**, the ribs are completely made of bone and do not have the usual composition of osseous and cartilaginous components. In older **guinea pigs**, the mineralization of the costal cartilage may lead to very prominent diffuse, cloud-like shadows on radiographic images that should not be confused with pathological processes affecting the lungs (**Fig. 2-22**).

2.2.1.3 Limbs

Pectoral girdle

In all small mammals, the bones of the pectoral girdle include not only the scapula but also a clavicle (**Fig. 2-23**), which is very small and inconspicuous in most of these species (e.g. **ferret**) and cannot be identified radiographically in every animal. In the **guinea pig**, the rudimentary clavicle lies very close to the cranial part of the shoulder joint and should not be confused with pathological changes affecting this joint. The clavicle of the **rat** and **mouse** continue to have a certain functional significance and articulate with both the scapula and the sternum. In these species, the clavicle is imaged without summation in the VD projection and can be always recognized without difficulty. A characteristic feature of **rabbit** and **rodent** scapulas is the obvious hamatus process that forms distally on the acromion, which is very elongated in the guinea pig, extending to the level of the shoulder joint. A special characteristic in the rabbit is the suprahamatus process which also projects a great distance in a caudoventral direction.

Upper and lower foreleg

The humerus, radius, and ulna are especially long and thin in the **rabbit** when compared to other small mammals. Fine linear shadows in the area of the epiphyses mark the closed epiphyseal plate or the transition from the epiphysis to the metaphysis. The closure of the epiphyseal plate on the distal end of the humerus starts in the 9th week and is completed by the 14th–15th week of life. In comparison, the closure of the epiphyseal plate of the humeral head begins in the 16th week and is completed around the 40th week of life.

The skeleton of the lower arm is complete in all small exotic mammals and allows them to have a high degree of supination. This helps small rodents grip and hold food with their fore-paws.

Forepaw

The skeleton of the forepaw has the classical five-digit construction in all small exotic mammals. Only in the **guinea pig** and **mouse** is the first toe not formed and in the **chinchilla** this digit is only rudimentary.

Pelvic girdle

The two hip bones (ossa coxarum) of the pelvic girdle consist of the ilium, ischium, and pubic bone (os pubis) as well as the small acetabulum, which can be easily observed in fetal **rabbits** and **rats**. The hip bones are joined ventrally by the pelvic symphysis.

The pelvic symphysis widens to a width of approximately 2 cm in the last 1–2 weeks of pregnancy in the **guinea pig** under the influence of relaxin to ensure a wide birth canal (**Fig. 2-24**). The separation of hip bones is supported by an increased laxity in the iliosacral joints. If a female guinea pig does not become pregnant within the first year of life, then the pelvic symphysis begins to ossify. Older primiparous guinea pigs can no longer completely widen their birth canal and thus tend to suffer from dystocia.

Upper and lower hindleg

The femur and tibia are particularly long and thin in the **rabbit** and **chinchilla**. The fibula is also present in all small exotic mammals, but can be fused with the tibia (e.g. rabbit) (**Fig. 2-25**). In the relatives of the guinea pig (**Caviomorpha**), the full length of the fibula is completely formed but it is very thin and lies very close to the lateral surface of the tibia. In contrast, the fibula in **Myomorpha** is curved and lies at a distance from the tibia. Distally, the fibula lies close or is fused (e.g. **rat**) to the tibia.

The closure of the epiphyseal plate in the proximal femur begins roughly from the 12th week and is completed by the 20th week, whereas in the distal femur closure of the epiphyseal plate initiates in the 18th week and is completed around the 36th week of life. The epiphyseal plate closure of the tibia begins in the proximal epiphysis in the 41st week and ends with the 101st week; in the distal epiphyseal plate, it begins with the 14th week and ends with the 30th week of life.

A species-specific radiographic peculiarity of the **guinea pig** stifle joint is the possible occurrence of up to five sesamoid bones, which lie cranially in the right and left meniscus.

Hindpaw

As the hind feet of the small exotic mammalian species discussed are not used for grasping objects but for walking, there is occasionally a reduction of the foot skeletal structures in some species (i.e. only four toes are present in the rabbit (**Fig. 2-25A**), chinchilla, and rat, while in the guinea pig there are three toes).

Table 2-2: Number of vertebra in small mammals

Species	Neck	Thorax	Lumbar	Sacrum	Tail
Chinchilla	7	14	6	4	21
Ferret	7	15	5 (6)	3	18)
Golden hamster	7	13	6	4	13 (14)
Guinea pig	7	13 (14)	6	3 (4)	4–7
Mouse	7	13	6	4	23–29
Rabbit	7	12 (13)	7	4	15 (16)
Rat	7	13	6	4	27

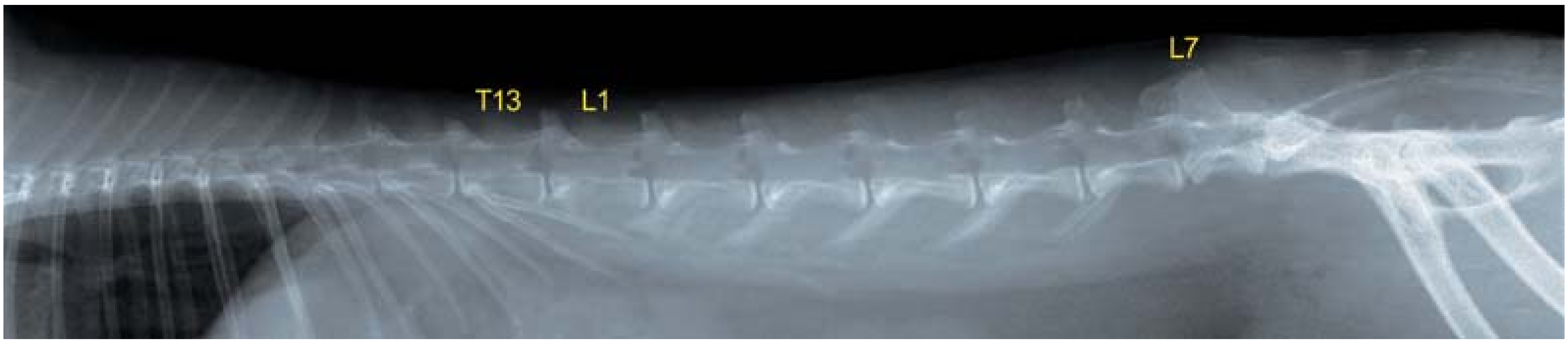

Fig. 2-20: Radiographic image of a rabbit's spine, lateral projection. The long lateral processes of the lumbar vertebra extend in a cranioventral direction and are characteristic of the rabbit spine.

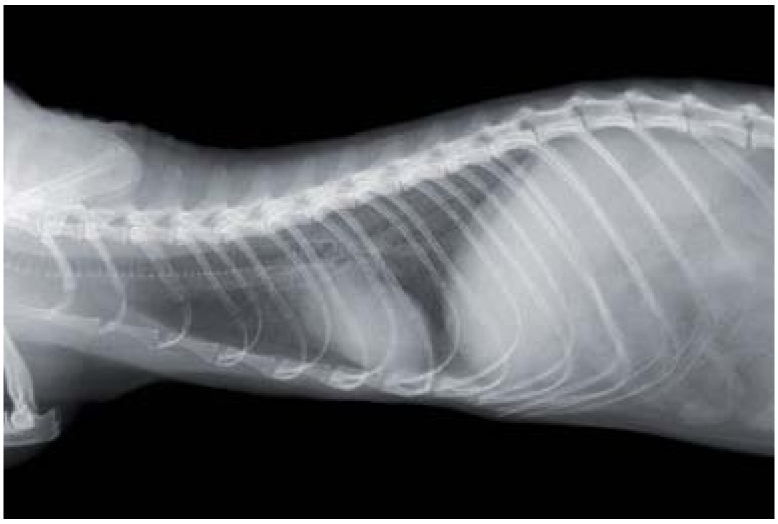

Fig. 2-21: Radiographic images of a ferret's, thorax, lateral projection. The ferret thorax is relatively long and has a narrow thoracic inlet.

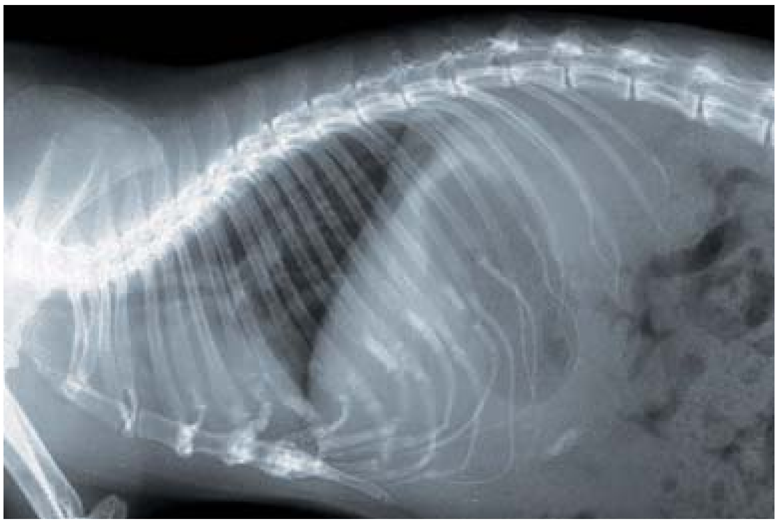

Fig. 2-22: Radiographic image of a guinea pig's thorax, lateral projection. Extensive cloud-like areas of mineralization can be identified in older guinea pigs' rib cartilage. These geriatric changes should not be confused with pathological changes to the lung tissue.

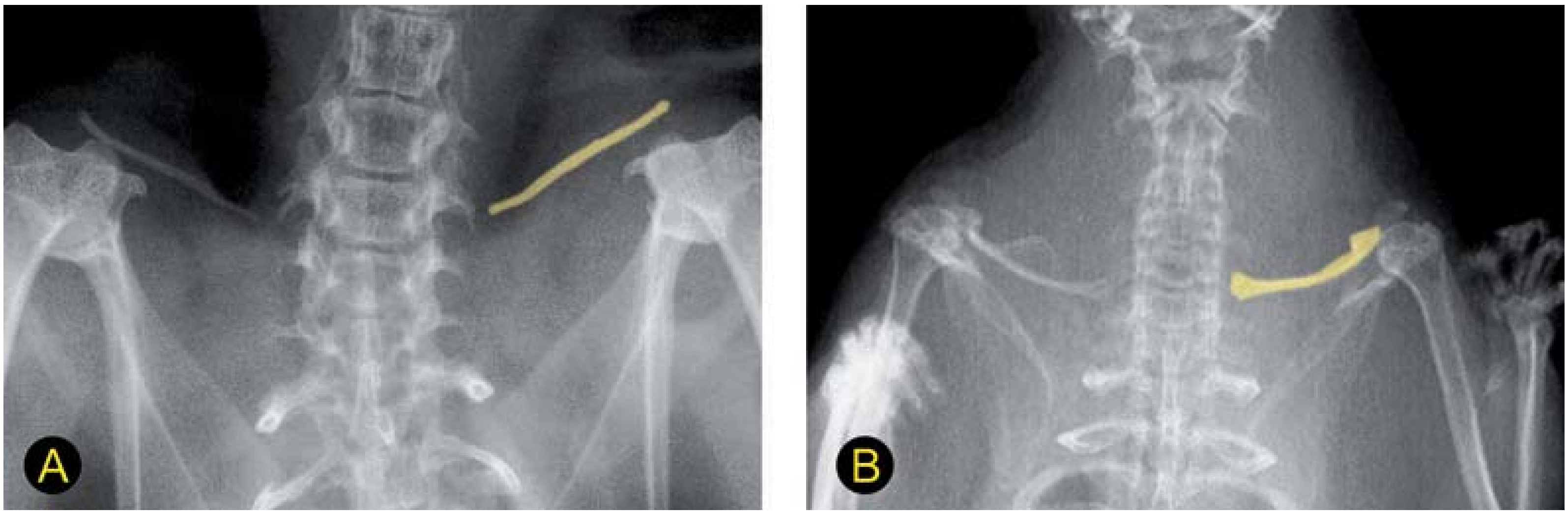

Fig. 2-23: Radiographic images of the clavicle, ventrodorsal projection.

A: Rabbit.

B: Rat.

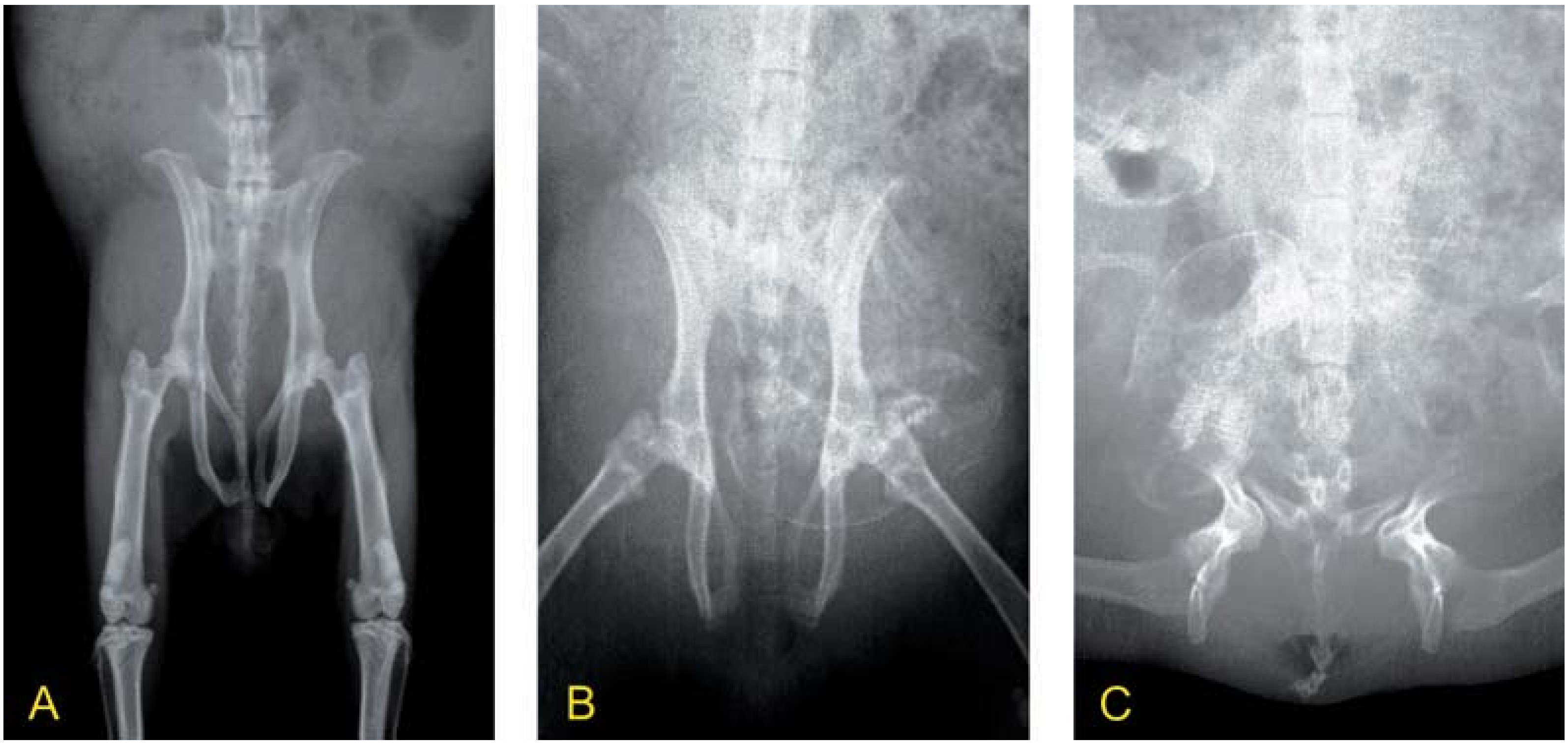

Fig. 2-24: Radiographic image of a guinea pig's pelvis, ventrodorsal projection.

A: Nonpregnant female with a narrow pelvic symphysis.

B: 50th day of pregnancy, slight distention of the pelvic symphysis.

C: Last day of pregnancy with widely opened pelvic symphysis.

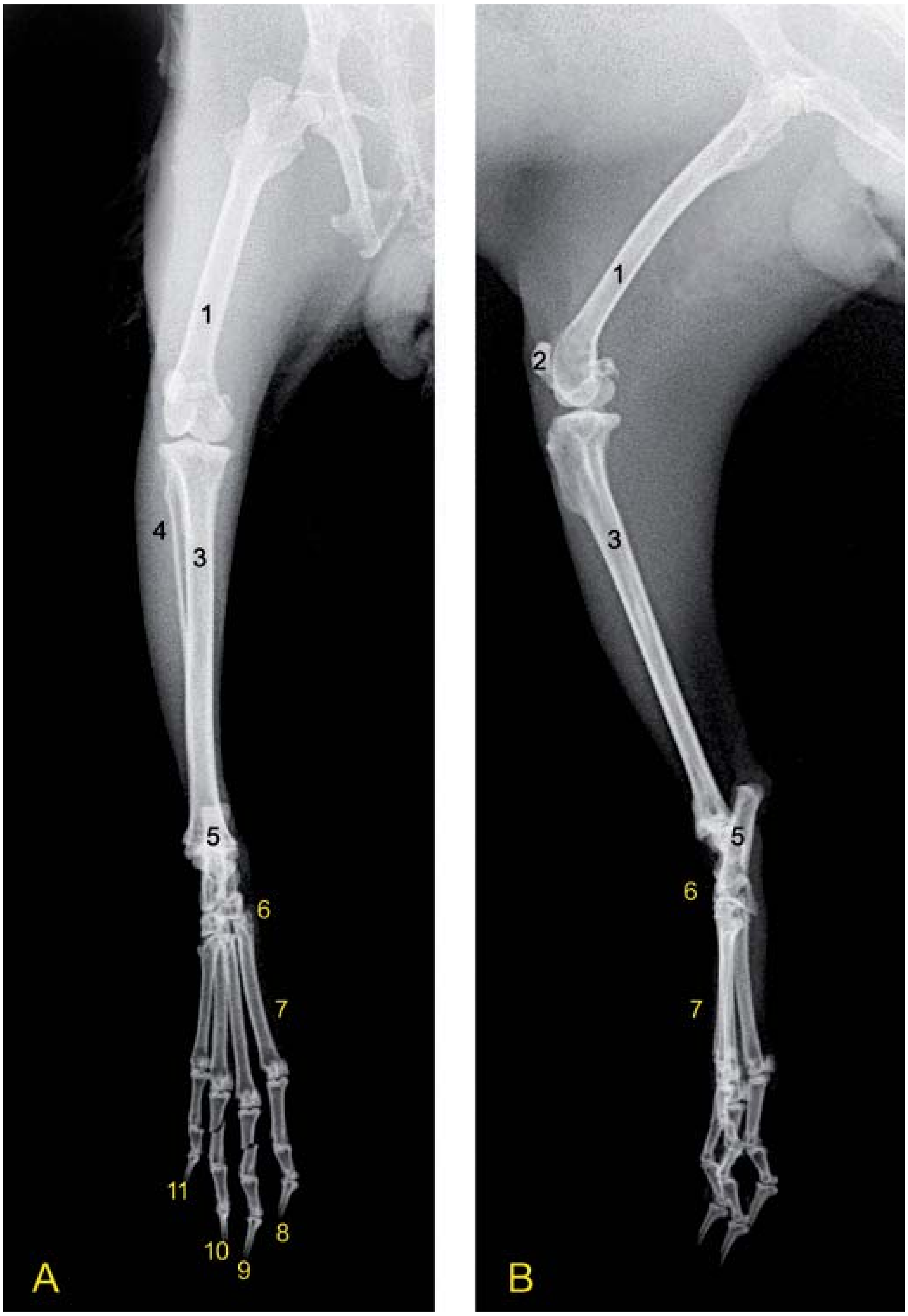

1: femur
2: patella
3: tibia
4: fibula (conjoined distally with the tibia)
5: calcaneus
6: tarsal bones
7: metatarsals
8–11: 2nd to 5th toes (the proximal phalanges of the 3rd and 4th toes are broken)

Fig. 2-25: Radiographic image of a rabbit's hindleg, (A) dorsoventral and (B) mediolateral projections.

2.2.2 Cervical soft tissues

Sven Reese, Jutta Hein

The greater part of the cervical soft tissue structures (e.g. **esophagus**, **thyroid**, **salivary glands**, **cervical milk gland complex**) in the rat and mouse cannot be differentiated radiographically from the surrounding muscles. However, it is possible to visualize the esophagus using a positive contrast agent so that its position, course, width, and patency can be examined. The **larynx** and **trachea** are differentiated in small rodents as less radiopaque shadowy structures. The trachea has a straight course through the cervical region, although at the level of the thoracic inlet it makes a sharp turn and runs close to the cervical vertebrae. Although the tracheal rings and laryngeal cartilage are easily identified in the ferret (**Fig. 2-26**), they can only be observed radiographically as shadows in the rabbit and are rarely imaged in small rodents.

2.2.3 Thorax

Sven Reese, Jutta Hein

The thorax of the **ferret** is extremely elongated. This principally affects the precardial region, which extends over the first five to six intercostal spaces in the ferret (**Fig. 2-21**) and includes the elongated cranial lobes of the lungs. In contrast, the thorax of the **rabbit** and **rodents** is very short and the precardial section is only the width of one to three intercostal spaces (**Fig. 2-27**).

When evaluating radiographic images of the thorax, special attention should be paid to the mediastinum, the intrathoracic organs (e.g. thymus, heart), conducting structures (e.g. esophagus, trachea, aorta, caudal vena cava), the lungs, and the surrounding pleural cavity.

2.2.3.1 Esophagus

The intrathoracic section of the esophagus is not discernable in standard radiographic images, although it can be identified using contrast imaging techniques (see Chap. 2.1.3.2).

2.2.3.2 Trachea

In the **ferret**, the trachea runs parallel to the thoracic vertebrae and divides into primary bronchi at the level of the 6th intercostal space (**Fig. 2-21**). In comparison, the **rabbit** trachea courses caudally in a slightly open angle to the thoracic vertebrae and ends in the 4th intercostal space (**Fig. 2-27**). A similar path is taken by the trachea in **rodents** where it divides into the main bronchi at the 3rd intercostal space (small rodents) or the level of the 4th rib (**guinea pig** [**Fig. 2-22**], **chinchilla** [**Fig. 2-8**]).

2.2.3.3 Thymus

The thymus remains present throughout a **rabbit's** and **rodent's** life. Only in the **guinea pig** is the thymus largely replaced by fat. The thymus cannot be radiographically differentiated, but due to its position in the cranial mediastinum it is responsible for the higher degree of radiopacity found in the precardial lung field in these species (**Figs. 2-8, 2-22**, and **2-27**).

2.2.3.4 Lungs

Since the lung parenchyma is filled with air it is the internal, more radiopaque structures of the lungs (the blood vessels and the walls of the bronchi) that can be imaged. It should be noted that the radiopacity of the lungs can differ significantly between the inspiratory and expiratory radiographs. It is recommended that radiographic images acquired for a lung examination be taken when the patient is in full inspiration. However, it is often not possible to take radiographic images in a predetermined respiratory phase, especially rodent patients that have a rapid respiratory rate.

The lungs in a correctly exposed radiographic image should exhibit a light pattern in addition to the blood vessel tree arising from the base of the heart and the bronchial tree. If the radiograph is completely black, then the radiographic image should be checked for a true reduced radiodensity of the lung tissue (e.g. pulmonary emphysema, hypovolemia, right-left shunt) or to determine if the radiograph is just overexposed.

Only **ferrets** have a large cranial lung field, which has a radiopacity equivalent to that of the caudal lung lobes (**Fig. 2-21**). In the **rabbit** (**Fig. 2-27**), **guinea pig** (**Fig. 2-22**), and **chinchilla** (Fig. **2-8**), the small precardial lung field is consistently somewhat more radiopaque than the caudal lung field. In small rodents with their tiny cranial lung lobes, there is no aerated lung tissue in the precardial region in a radiographic image taken from the lateral projection. In the VD projection, there is an obvious difference between the two anatomical areas the lungs occupy, especially in the **mouse** and **rat.** The right lung extends cranially into the 2nd intercostal space, while the left lung often ends in the 3rd intercostal space (**Fig. 2-28**).

In older **guinea pigs**, calcification of the costal cartilage is normal. The calcification of costal cartilage can be optimally viewed on DV radiographs as cloud-like shadows lying over the caudal lung field and should not be confused with pathological changes affecting the lung tissue (see Chap. 2.2.1.2).

The aortic arch and caudal vena cava can be observed without difficulty in all the small mammalian species as radiopaque structures using the lateral projection. The caudal vena cava of **rabbits** often has a slightly caudal narrowing in the direction of the diaphragm.

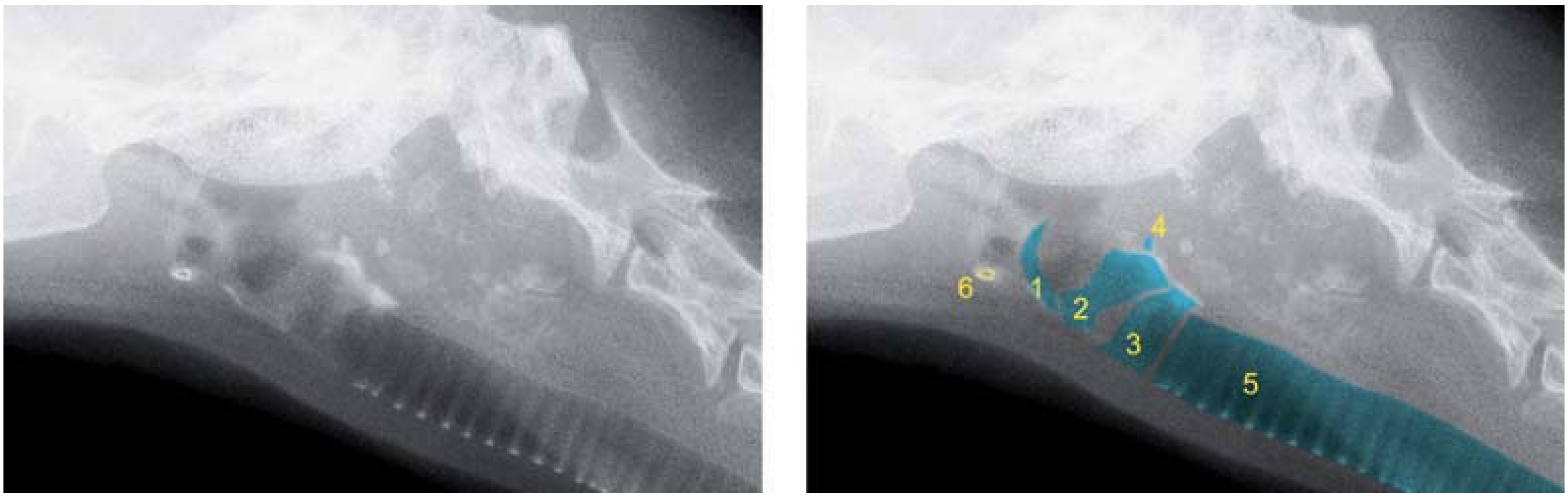

Fig. 2-26: Radiographic images of a ferret's larynx, lateral projection.

1: epiglottis
2: thyroid cartilage
3: cricoid cartilage
4: arytenoid cartilage
5: trachea
6: basihyoid

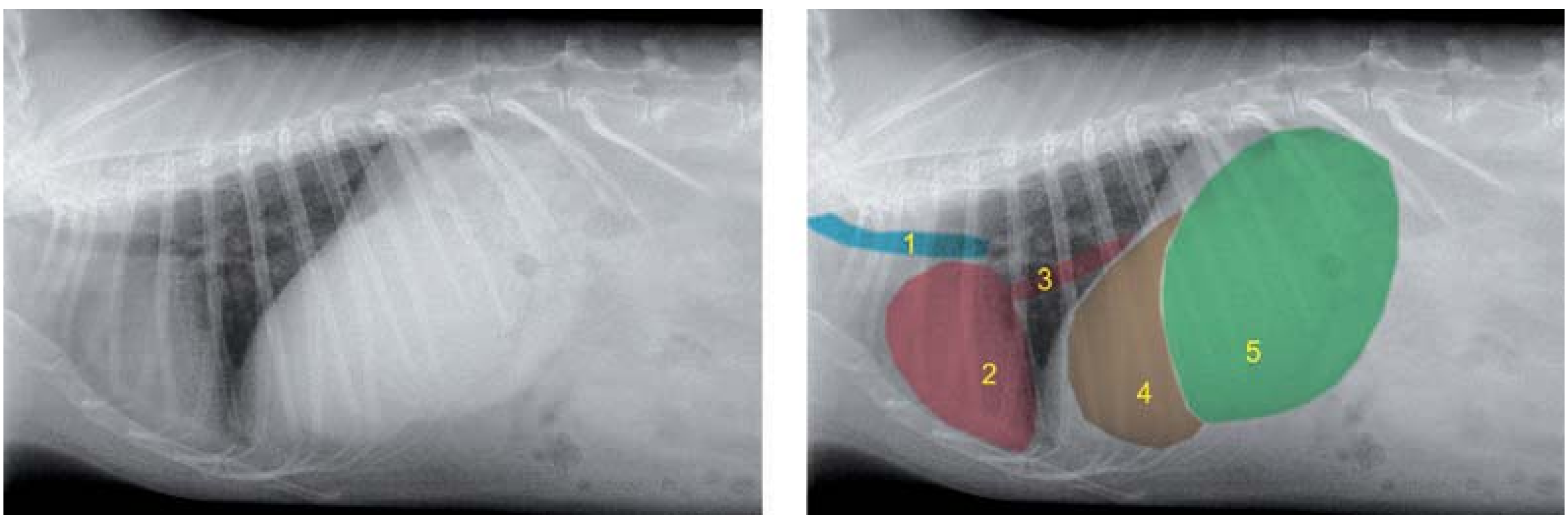

Fig. 2-27: Radiographic images of a rabbit's thorax, lateral projection.

1: trachea
2: heart
3: caudal vena cava
4: liver
5: stomach

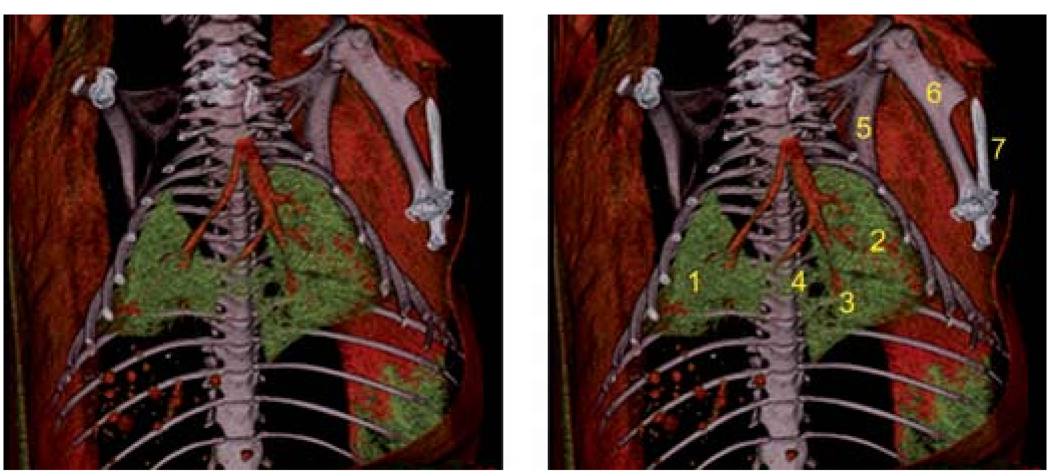

1: left lung
2: right lung, cranial lobe
3: right lung, caudal lobe
4: accessory lobe
5: scapula
6: humerus
7: ulna

Fig. 2-28: *In-vivo* µCT images of a mouse thorax, 3D reconstruction. The undivided left lobe of the lung (1) is much smaller than the right lobe in the mouse.

CT scan courtesy of S. J. Schambach and M. A. Brockmann, Neuroradiology Department, Medical Faculty Mannheim, University of Heidelberg, Germany.

2.2.3.5 Heart

Cordula Poulsen Nautrup

Standard radiographic images are an indispensable diagnostic aid in the cardiological evaluation of small exotic mammals. This imaging modality not only allows for visualization of heart size and changes in the size of the heart chambers and large blood vessels, but it also enables the evaluation of the trachea, lung parenchyma, bronchi, and pulmonary blood vessels. The imaging of the air-filled tissues is the domain of the radiographic examination, while ultrasonography is the clinical method of choice for the assessment of the cardiac structures, function, and their size.

The disease conditions, necessary radiographic quality, and the interpretation of thoracic radiographic images of small exotic mammals are equivalent to the standards set for dogs and cats (SCHWARZ and JOHNSON 2008).

Indications

Important disease conditions for which a radiographic examination of the heart is recommended are dyspnea and/or coughing. The results of the radiographic examination of these patients may be the first indication that their health issues are due to either respiratory or cardiac disease. Furthermore, these images may afford an evaluation of the extent of secondary congestion or reduced perfusion due to cardiac disease (i.e. there is a reduction in lung perfusion with either a severe pulmonary stenosis or lung edema due to advanced left-sided cardiac insufficiency). With the aid of radiographic images, a suitable treatment protocol can be determined and treatment success can be monitored by using control radiographic images.

Image quality

A prerequisite for optimal assessment of thoracic radiographs is good image quality.

Low-contrast radiographic images without motion blurring

With good radiographic images, the heart contours are clear and sharp. The aorta, or at least the base of the aorta, and the caudal vena cava appear to be overshadowed in the lateral projection. The pattern of the lung blood vessels can be observed extending from the hilus to the periphery (**Fig. 2-29**). To ensure that the latter situation is the case, the radiographic images must be low in contrast (i.e., taken with a relatively high voltage [kV] and a low current-time product [mAs]). All of the principles mentioned for acquiring good radiographic images of the thorax, which were originally established for the dog, also apply to small exotic mammals. Frequently, in small exotic mammals (e.g. golden hamster, gerbil, mouse, rat), the contrast appears too low or obvious picture noise occurs, especially when using digital radiographic techniques. In addition, with normal radiographic images, the spatial resolution is so low that the pixels cause a disturbance when there is a need to improve detail resolution through image enlargement (**Fig. 2-30**). In such cases, special methods such as direct mammography, microfocus x-ray technology, or micro-computed tomography (µCT) may be used (**Fig. 2-31**).

Minimizing motion blurring is achieved by using short exposure times of under 0.02 seconds. However, positioning and completely immobilizing conscious small exotic pet mammals while considering radiation safety guidelines is difficult, therefore motion blurring can occasionally occur despite the use of short exposure times. Only the rabbit can be positioned satisfactorily when awake.

Other factors that have a significant influence on the assessment and quality of radiographic images are projections, positioning of the animal, and time when the image was taken (e.g. inspiration, expiration).

Projections

Standard thoracic radiographs are taken in the lateral projection, in either right- or left-lateral recumbency, and in the DV or VD projections (**Figs. 2-32** and **2-33**).

Positioning

The positioning of the animal and the exposure of the film should be performed according to the following criteria:

- ☐ Imaging of the whole thorax including the diaphragm and, when possible, also the caudal neck. The apex of the diaphragm must be clear and easily recognizable.
- ☐ The pectoral limbs should be pulled forwards so that summation of scapulas onto the lung field does not occur. This is especially important when taking lateral radiographs. This prerequisite is difficult to fulfill in some fully conscious small exotic pet mammals.
- ☐ Detailed imaging of the bony structures such as ribs, vertebra, and sternum under the consideration of the following principles:
  - Lateral projections: exact summation of the dorsal extent of the ribs on both sides of the patient. Tilting of the animal makes the heart appear larger, covering a wide area of the sternum.
  - Dorsoventral and ventrodorsal projections: summation of the thoracic spinous processes in the middle of the vertebral bodies and the sternum, which itself should lie centralized under the vertebral bodies. For example, a tilting of the sternum towards the right mimics a displacement of the heart to the right.

The previously mentioned difficulty of adequately restraining and positioning of small exotic mammals correctly when they are awake, frequently leads to the procurement of nondiagnostic radiographic images. As a consequence, especially for reasons of radiation safety, general anesthesia is a recommended measure when performing radiographic examinations on small exotic pet mammals, apart from in the rabbit. Animals that are induced and maintained on general anesthesia can be restrained and positioned without difficulty.

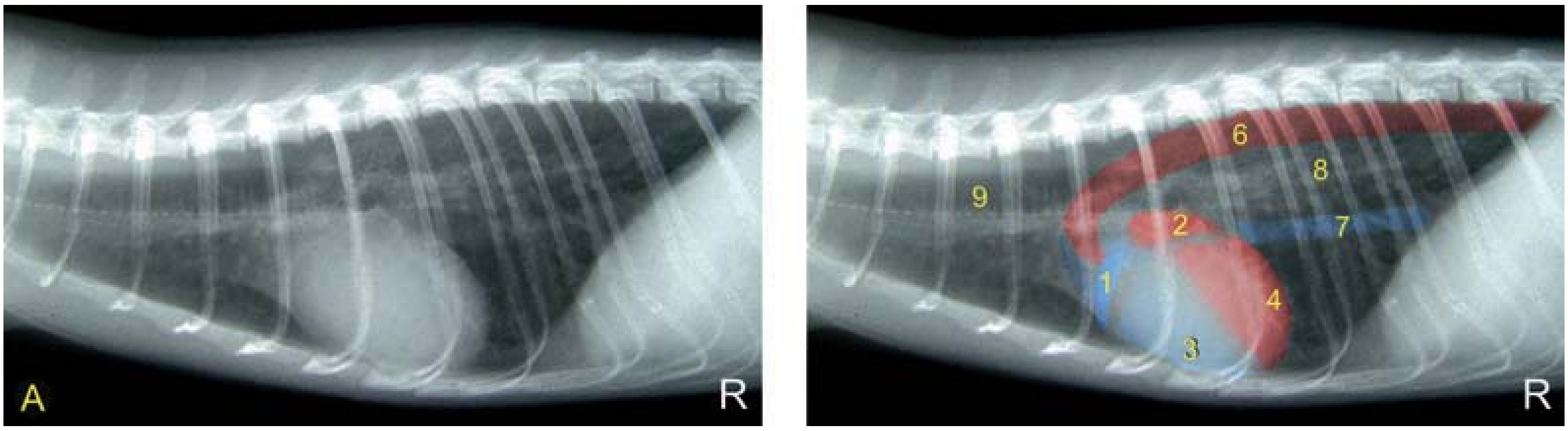

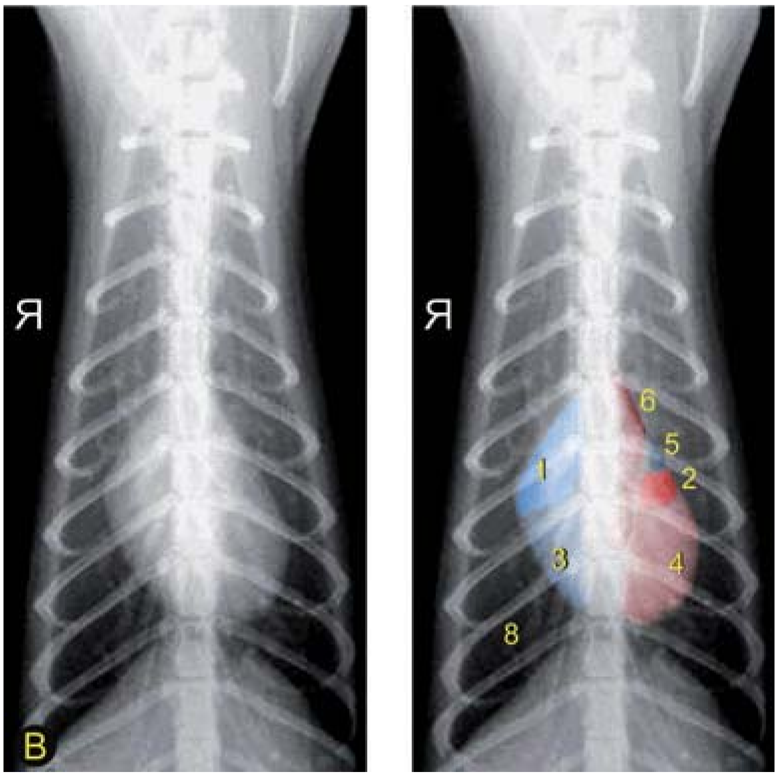

1: right atrium
2: left atrium
3: right ventricle
4: left ventricle
5: pulmonary trunk
6: thoracic aorta
7: caudal vena cava
8: lung with blood vessels
9: trachea

Fig. 2-29: Radiographic image of a ferret's thorax, lateral projection with patient in (A) right lateral recumbency and (B) dorsoventral projections.

Radiographs courtesy of C. Boonyapakorn, M. Skrodzki, E. Trautvetter, Berlin, Germany.

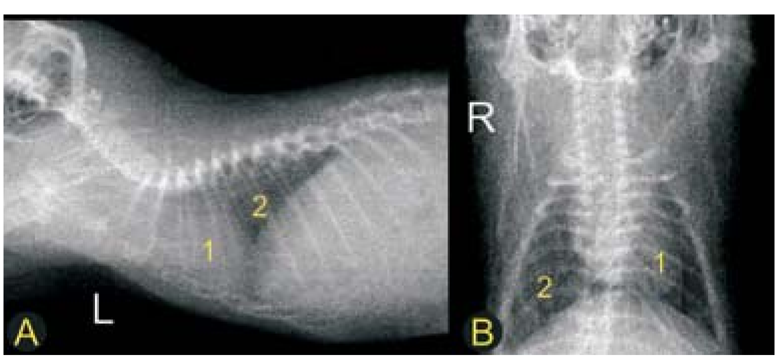

1: heart
2: lung with vessels

Fig. 2-30: Radiographic images of a gerbil's thorax, lateral projection with patient in (A) right lateral recumbency and (B) ventrodorsal projections. Both of these digital radiographs show a lack of detail and are pixilated due to the small size of the animal and necessary reduction in the mAs. This phenomenon is rare with conventional analogue radiographic machines that use high definition film-screen systems.

Timing of the exposure

Preferably, radiographic images of the thorax should be taken during full inspiration. However, this cannot always be achieved even in the dog and cat. In small exotic pet mammals with their rapid respiratory rates, the respiratory phase at the time of obtaining the radiographic image is accidental. One should also consider that small lung fields diagnosed during expiration can mimic displacement of the heart.

Interpretation of the radiographic images

Due to the extreme species variation found in the anatomy of small exotic pet mammals and the large variation within a species, general statements about »normal« radiographic images can only be provided with a great deal of reservation. This is especially true since publications regarding thoracic radiographic examinations of various small exotic mammalian species are rare or nonexistent. Investigations on age-related radiographically recognizable changes are completely lacking. In many cases, the preparation of comparative radiographic studies using another animal is helpful. The control animal, where and when possible, should be of the same sex, similar body shape, and age as the patient.

Normal results in lateral projections

In all adult small exotic pet mammals, apart from the rabbit, the angle between the longitudinal axis of the heart and the sternum is much smaller than in the dog (in which it is 45° in the middle); therefore, the heart usually appears to lie over a large area of the sternum.

The anatomic shape of the heart is extremely variable from species to species of small exotic mammal. The heart appears relatively large in the ferret, guinea pig, and the smaller small pet mammals. In healthy ferrets, the heart is described as being slim to round, but in rare individual cases, sternal contact of the heart is lacking. The phrenopericardial ligament, which is exclusively found in the ferret, can contain large amounts of fat and its radiographic image may appear similar to that of the heart silhouette. The normal width of the ferret's heart is 2.28 ± 0.3 intercostal spaces (range: 2–3 spaces) (**Fig. 2-34**).

In small exotic mammals, the cranial section of the cardiac silhouette is formed by the right side of the heart (dorsal: right atrium, ventral: right ventricle); the caudal section by the left side (dorsal: left atrium, ventral: left ventricle). The ascending aorta is partially visible, dorsal to the right atrium. The width of the thoracic aorta and the caudal vena cava are similar.

Caudally, the trachea in healthy, well-positioned ferrets, rabbits, and guinea pigs has an open angle to the spine. However, the angle can be much smaller in a few ferrets, rabbits, and guinea pigs as well as in the other small exotic mammal species or the trachea runs almost parallel to the vertebral bodies (**Figs. 2-35** and **2-36**, respectively).

Normal results in the dorsoventral and ventrodorsal projections

On all DV and VD radiographic images, the apex of the heart is positioned on the left side of the animal. This means that normally, as with dogs and cats, the DV radiograph is looked at from the back of the film (i.e. against the course of the projection). Accordingly, the right side of the heart lies more to the right in the thorax (**Figs. 2.29B, 2-30B** and **2-32C, D**).

Heart size assessment

The most frequently used method to determine heart size is by formulating a subjective estimate from a lateral radiographic image. The width of the heart is roughly assessed by counting the number of intercostal spaces that it spans. The normal width in a healthy ferret has been given as 2.28 + 0.3 intercostal spaces (range: 2–3) (BOONYAPAKORN 2007).

A more objective assessment of the heart size can be done using the so-called vertebral heart score (VHS), which is normally accomplished using a lateral radiographic image. The VHS has proven to be particularly useful for assessing the size of the dog heart.

A modified form of the VHS measurement has only been attempted for the ferret heart. The height of the heart is measured on a lateral radiographic image from the ventral edge of the left main bronchus to the extreme point of the heart apex. The width of the heart is defined as a perpendicular line formed at the widest section of the middle third of the heart's long axis, roughly at the level of the caudal vena cava. The sum of the so-measured heart length and width is transferred to the cranial edge of the 5th thoracic vertebral body and the VHS is the number of vertebral bodies covered. The measurement should be exact to a fourth of a vertebral body. The VHS in healthy ferrets varies slightly according to sex and positioning (right or left lateral recumbency) and the mean VHS lies between 5.25 ± 0.25 [STEPIEN et al. 1999] and 5.57 ± 0.57 (range: 4.75–6.75 [BOONYAPAKORN 2007]). However, the difference between the cardiac measurement between ferrets with healthy and diseased hearts is not always obvious (mean: 5.79 ± 0.37, range: 5.25–6.5 [BOONYAPAKORN 2007]).

Further reading

BOONYAPAKORN, C. (2007): Cardiologic examinations in ferrets with and without heart disease. Diss. med. vet. Berlin.

SCHWARZ, T., JOHNSON, V. (Eds.): BSAVA Manual of canine and feline thoracic imaging. British Small Animal Veterinary Association, Gloucester 2008.

STEPIEN, R. L., BENSON, K. G., FORREST, L. J. (1999): Radiographic measurement of cardiac size in normal ferrets. Vet Radiol Ultrasound, **40**: 606–610.

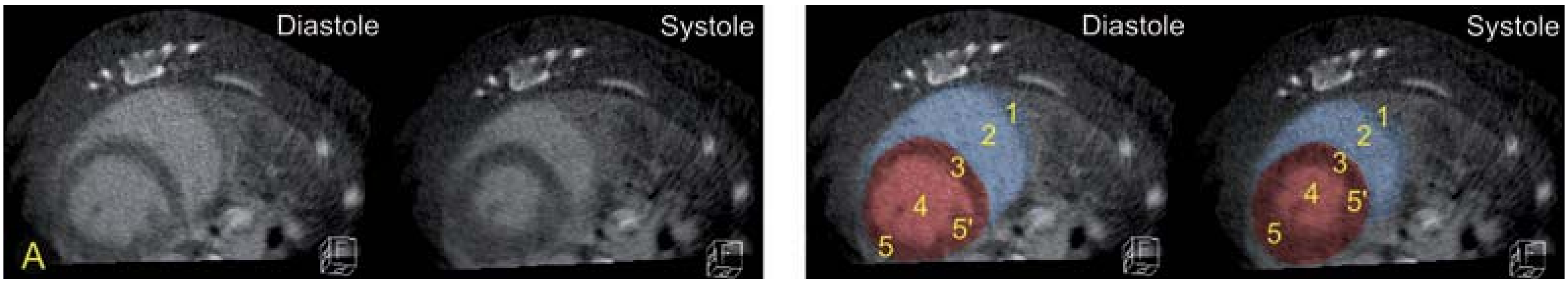

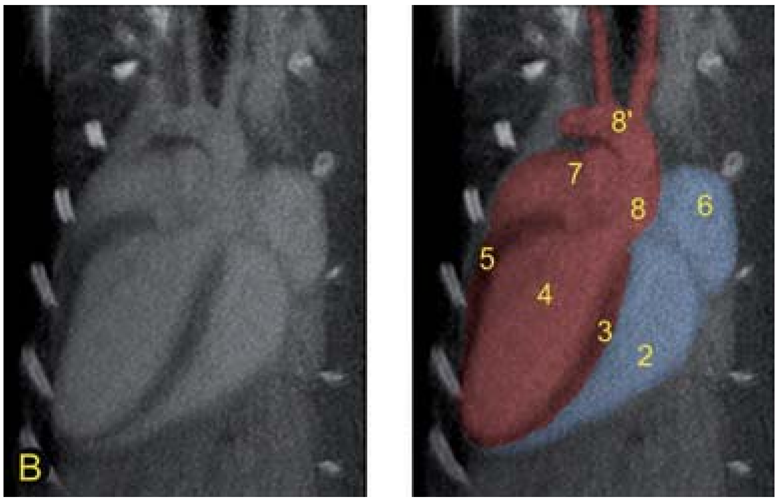

1: right myocardium
2: right ventricle
3: interventricular septum
4: left ventricle
5: left myocardium
5': papillary muscle
6: right atrium
7: left atrium
8: ascending aorta
8': aortic arch

Fig. 2-31: Three-dimensional µCT of a mouse thorax, (A) end-diastolic and end-systolic short-axis projection at the level of the ventricles and (B) end-diastolic long-axis four-chamber view of the heart.

CT scan: courtesy of S. J. Schambach, M. A. Brockmann, Neuroradiology Department, Medical Faculty Mannheim, University of Heidelberg, Germany.

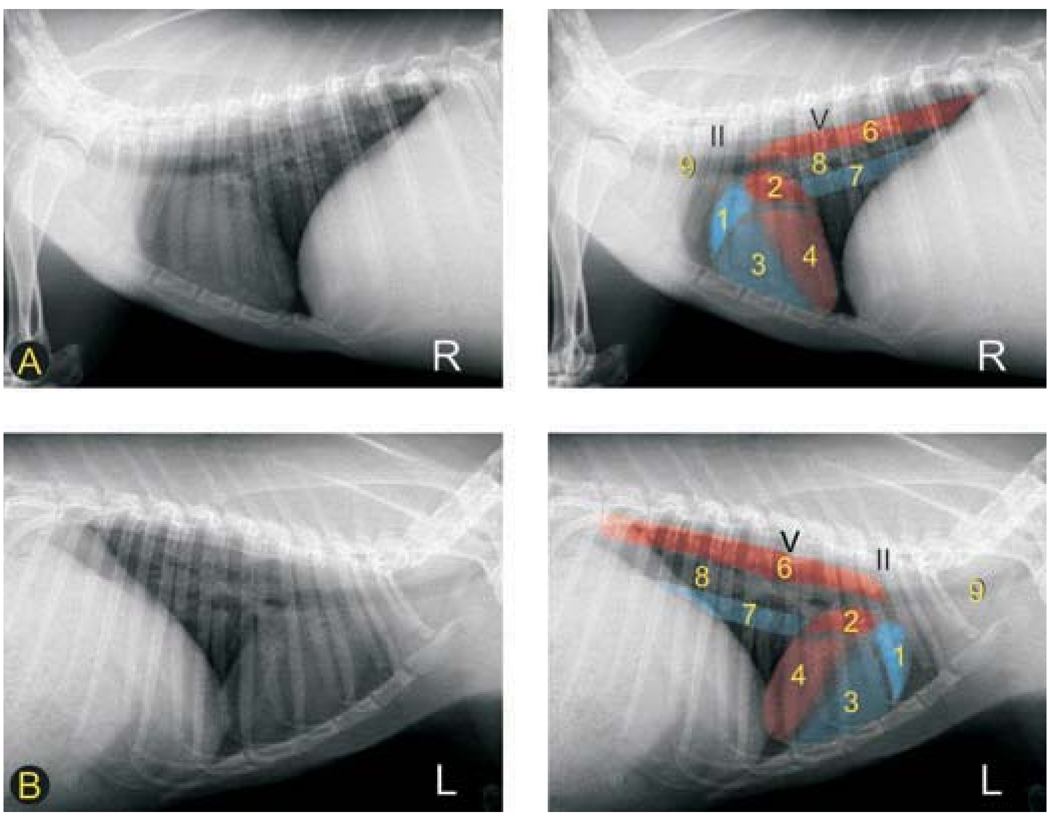

1: right atrium
2: left atrium
3: right ventricle
4: left ventricle
5: pulmonary trunk
6: thoracic aorta
7: caudal vena cava
8: lung with blood vessels
9: trachea

Fig. 2-32: Radiographic images of a rabbit's thorax, lateral projections with patient in (A) right lateral recumbency and (B) left lateral recumbency; (C) dorsoventral, and (D) ventrodorsal projections.

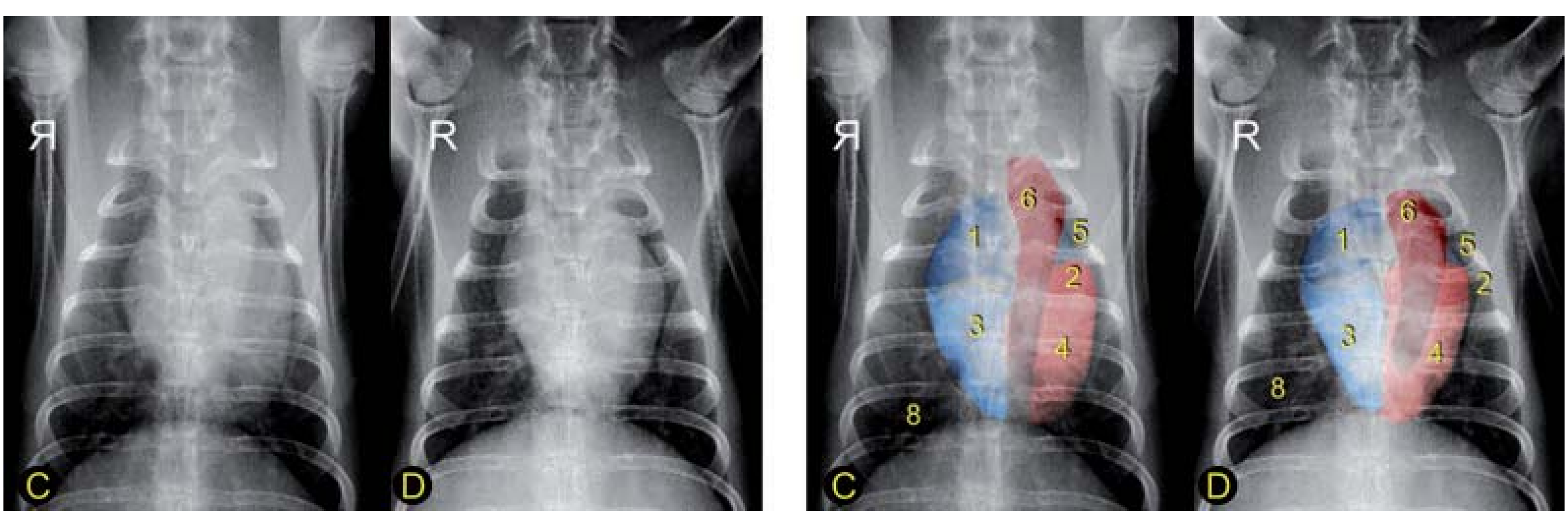

1: right atrium
2: left atrium
3: right ventricle
4: left ventricle
5: pulmonary trunk
6: thoracic aorta
7: caudal vena cava
8: lung with blood vessels

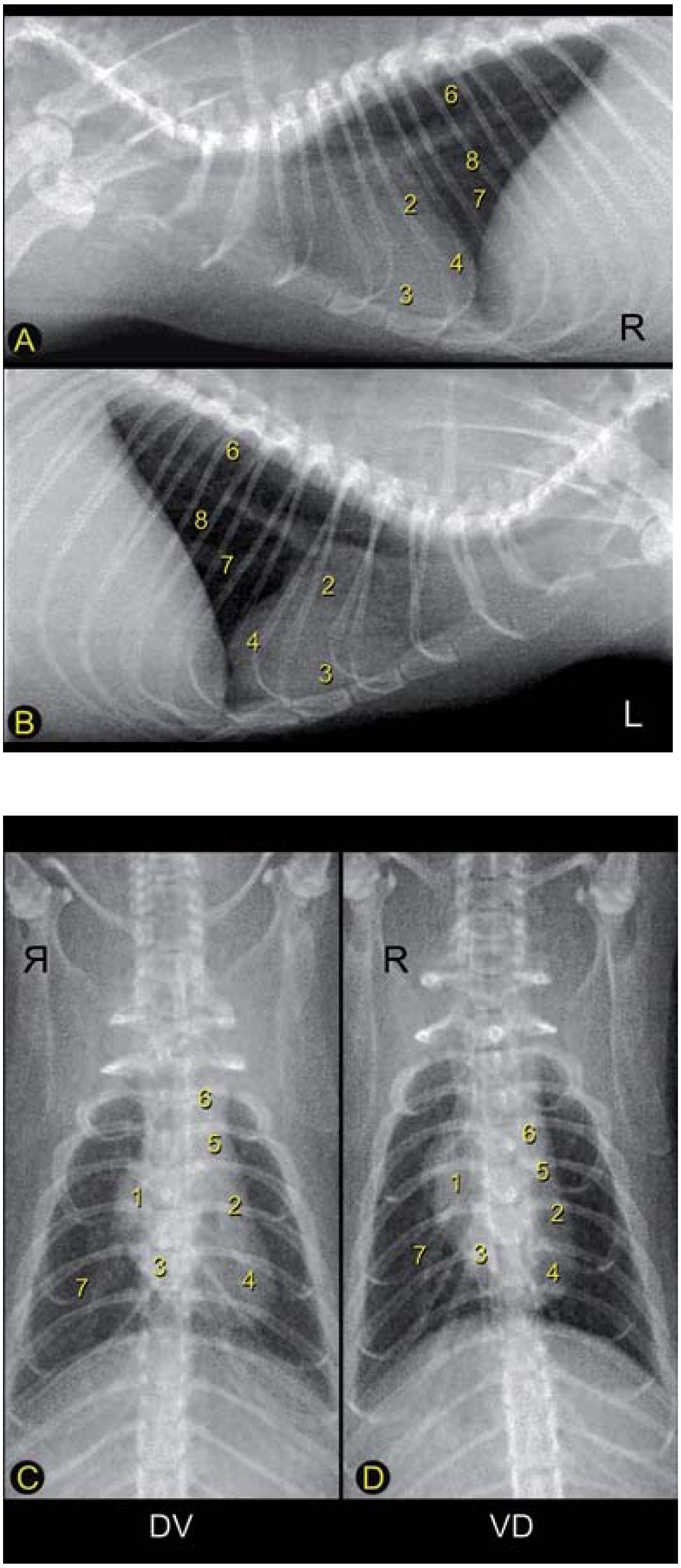

Fig. 2-33: Radiographic image of a rat's thorax, lateral projections with patient in (A) right lateral recumbency and (B) left lateral recumbency; (C) dorsoventral, and (D) ventrodorsal projections.

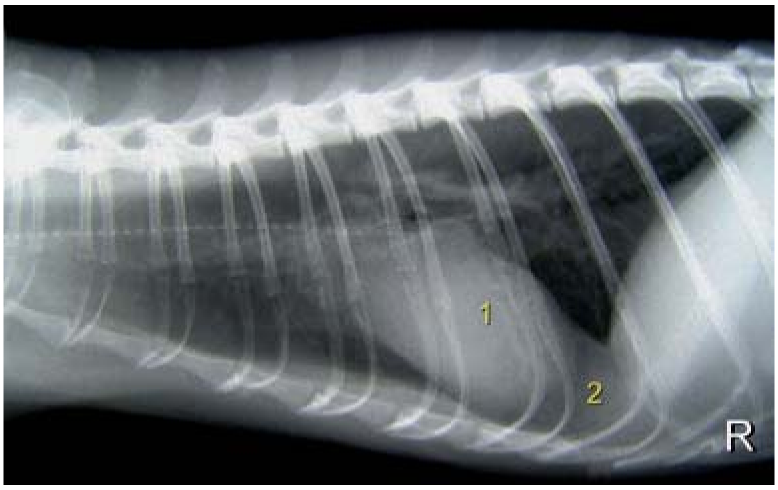

1: heart
2: fat in the phrenopericardial ligament

Fig. 2-34: Radiographic image of a ferret's thorax, lateral projection with patient in right lateral recumbency. The size of this animal's heart is 2.5 intercostal spaces, which is within the normal range provided for ferrets. The fat in the phrenopericardial ligament appears to be an obvious shadow; however, it has, at least in this case, a different radiodensity than the heart.

Radiograph courtesy of C. Boonyapakorn, M. Skrodzki, E. Trautvetter, Berlin, Germany.

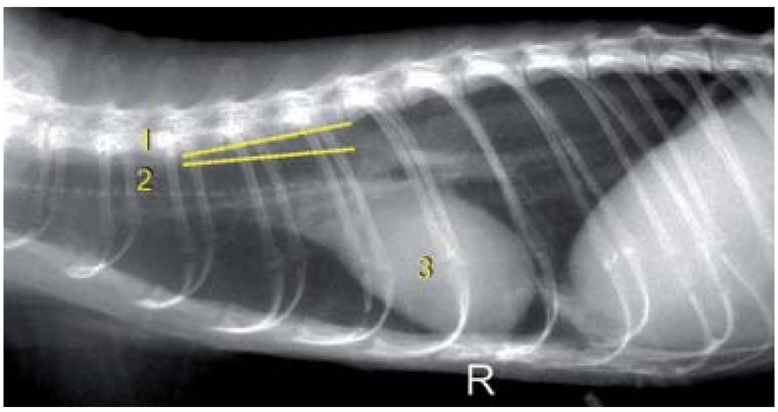

1: spine
2: trachea
3: heart

Fig. 2-35: Radiographic image of a ferret's thorax, lateral projection with the patient in right lateral recumbency. The trachea forms a narrow angle of approximately 10° with the spine, which is open caudally.

Radiograph courtesy of C. Boonyapakorn, M. Skrodzki, E. Trautvetter, Berlin, Germany.

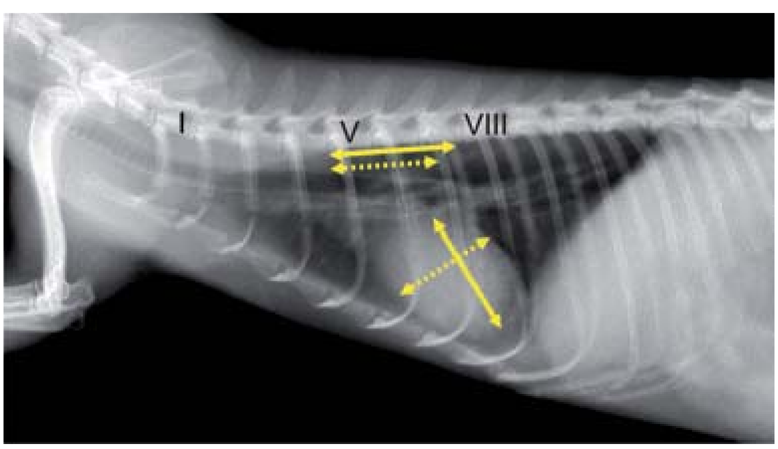

I: 1st thoracic vertebra
V: 5th thoracic vertebra
VIII: 8th thoracic vertebra.

Fig. 2-36: Radiographic image of a ferret's thorax, lateral projection with the patient in right lateral recumbency. Modified determination of the vertebral heart score (VHS) according to STEPIEN et al. 1999.

Radiograph courtesy of J.-G. Kresken, J. Spennes, Duisburg, Germany.

2.2.4 Abdomen

Sven Reese, Jutta Hein

All abdominal organs have a similar degree of radiopacity. However, since fat has a lower radiodensity than parenchyma and there are fat deposits in the mesentery and in the retroperitoneal space, differentiation of various organs within the abdominal space is possible. In young and cachexic animals, which have little intra-abdominal fat, radiographic images of the abdomen are low in contrast. A reliable differentiation and assessment of the individual abdominal organs in patients with little intra-abdominal fat is extremely difficult. Pet rabbits are frequently obese and have extensive sublumbar fat bodies, which in severe cases can incorporate the greater part of the abdomen, causing a cranioventral displacement of the internal organs (**Fig. 2-37**).

The abdomen of small exotic mammals can be divided into three approximate sections into which certain organs can be classified. The liver and stomach lie in the cranial abdomen. The middle section contains the pancreas, kidney, adrenals, ovaries, small and large intestines, and cecum. The caudal section includes the urinary bladder and uterus in the female or the urinary bladder, prostate, and seminal vesicle in male animals.

2.2.4.1 Gastrointestinal tract

The ability to radiographically image the gastrointestinal tract with its individual sections is primarily dependent on its contents. In the **ferret**, the gastrointestinal contents are frequently homogeneous and have a midrange radiodensity with only a few areas of gas (**Fig. 2-38A**). The characteristics of the ferret's gastrointestinal radiographic image described above makes it difficult to differentiate individual sections of the gut in this species. The gut contents are also relatively homogeneous in small rodent species; however, small air bubbles are often dispersed throughout this body system. The gastrointestinal tract in the **rabbit**, **guinea pig**, **chinchilla**, and **degu** should be evenly filled. The texture of the gastrointestinal contents in these species is often nonhomogeneous (»food structure« in the stomach), especially in the rabbit, and is interspersed with small bubbles of gas (**Fig. 2-38B**). These gas bubbles are especially pronounced in the guinea pig cecum. The balls of fecal material (which are round in the **rabbit** and bean-shaped in **rodents**), situated in the descending colon can be well differentiated from the sublumbar fat bodies as the latter have a lower radiodensity. These sublumbar fat bodies may be relatively voluminous in many pet rabbits, guinea pigs, chinchillas and degus; they are not present in small rodent species.

Stomach

The stomach lies on the left of the intrathoracic abdominal area in the **ferret** and **rodents**, with the pylorus extending just over the midline on to the right side of the body (**Fig. 2-39A**). In comparison, the stomach in the **rabbit** extends far over the midline and the pylorus almost touches the right abdominal wall. On lateral and VD radiographic images, the stomach's contour is oval to pear-shaped in the **rabbit** and **rodent** (**Fig. 2-38B**). Only in the **ferret** does the stomach have a u-shaped form on VD radiographs with a cranial facing deeply indented small curvature. How far the caudal edge of the stomach extends beyond the costal arch depends on its degree of filling and also the positioning technique used. If the hindlimbs are pulled back in a caudal direction, there is an elongation of the stomach in the **rabbit** and two-thirds of this organ appears to extend beyond the costal arch. At the same time, the **rabbit** stomach fills only a third of the height of the thoracic cavity and therefore lies at a distance from the ventral abdominal wall. In the rabbit, it may be considered as being normal if roughly a third of the stomach lies outside of the thorax and covers more than two-thirds of the thoracic cavity height. In comparison, the stomach and intestines occasionally lie next to each other in the **guinea pig** with the stomach lying to the left of the more right-sided liver and extending to the right (**Fig. 2-39B**).

Small intestines

The small intestines cannot be reliably identified radiographically in either the **rabbit** or **rodents**. For the assessment of pathological conditions affecting the small intestine, it is helpful to know the normal species-specific position of this structure. In the **rabbit**, the small intestines lie mainly on the left, caudal to the stomach, while in the **guinea pig** and **chinchilla** they are primarily observed in the right cranial abdomen. The small intestines also lie mainly on the right side of the abdomen in **small rodents**. The small intestines in the **ferret** form the major part of the gut length and approximately two-thirds of their length are situated in the right half of the abdomen and a third in the left caudal abdomen caudal to the stomach.

Cecum

The cecum takes up a large part of the abdomen (approx. ⅓) in the **rabbit**, **guinea pig**, **chinchilla**, and **degu**. There are also species-specific differences to be noted with this organ. The **rabbit** cecum lies mainly on the right of the ventral abdominal wall and extends caudally over to the left side. In the lateral projection, the cecum is typically situated in the middle of the ventral abdomen. There is frequently a conspicuous cranial displacement of the cecum in the rabbit. The cause of this cranial displacement is intra-abdominal fat. The intra-abdominal fat of rabbits extends, as a compact homogeneous mass, running caudodorsally to caudoventrally. It is frequently confused on a sonogram with a space-occupying lesion. In contrast to a true space-occupying lesion, morbid obesity also causes a significant (centimeters) ventral displacement of the kidneys and colon (**Fig. 2-37**). The fat deposits compress and push the entire gastrointestinal tract in a cranial direction. As a result of this compression, filling of the intestines in obese rabbits is reduced, which should be taken into consideration when force-feeding the patient. In the **guinea pig**, **chinchilla** and **degu**, the cecum lies equally in both halves of the abdomen and extends in a more dorsal direction. The cecum of small rodents (**golden hamster, gerbil** and especially that of the **rat** and **mouse**), is obviously smaller and a more simple structure. The cecum courses in a species-specific bow or hook-like path from the right side of the body to the left. Despite its size, the cecum is usually difficult to differentiate on radiographs without the administration of contrast agents. The texture of the cecal contents is similar to that of the stomach, though there is often more gas observed in guinea pig patients (**Fig. 2-39B**).

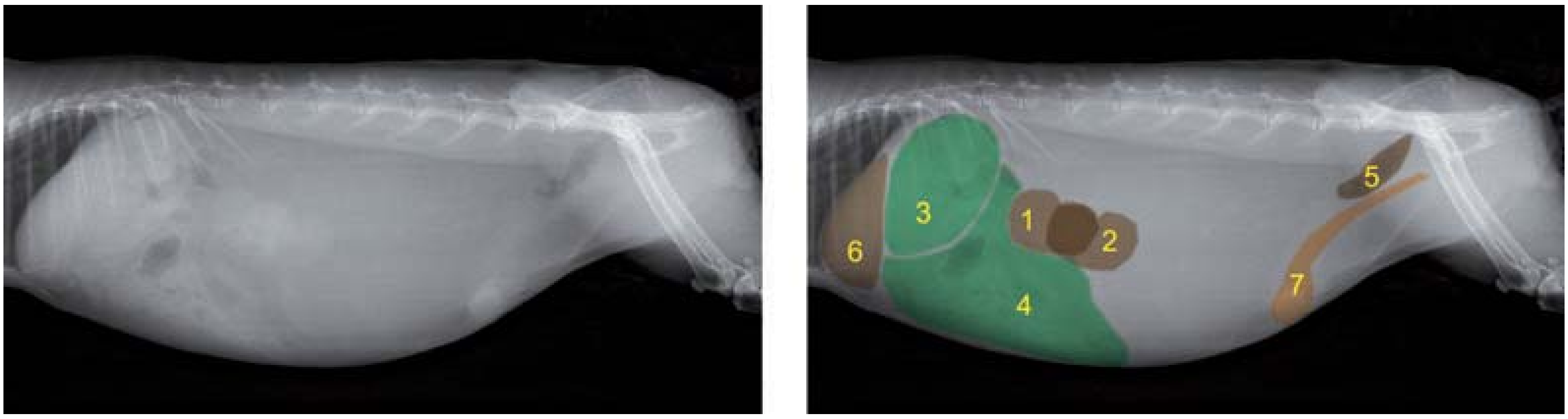

Fig. 2-37: Radiographic images of a rabbit's abdomen, lateral projection. This animal has an extensive sublumbar fat body that extends into the gastrointestinal tract located in the cranial part of the abdomen. This fat body can lead to problems with gastrointestinal function.

1: right kidney
2: left kidney
3: stomach
4: cecum and intestines
5: rectum
6: liver
7: uterus

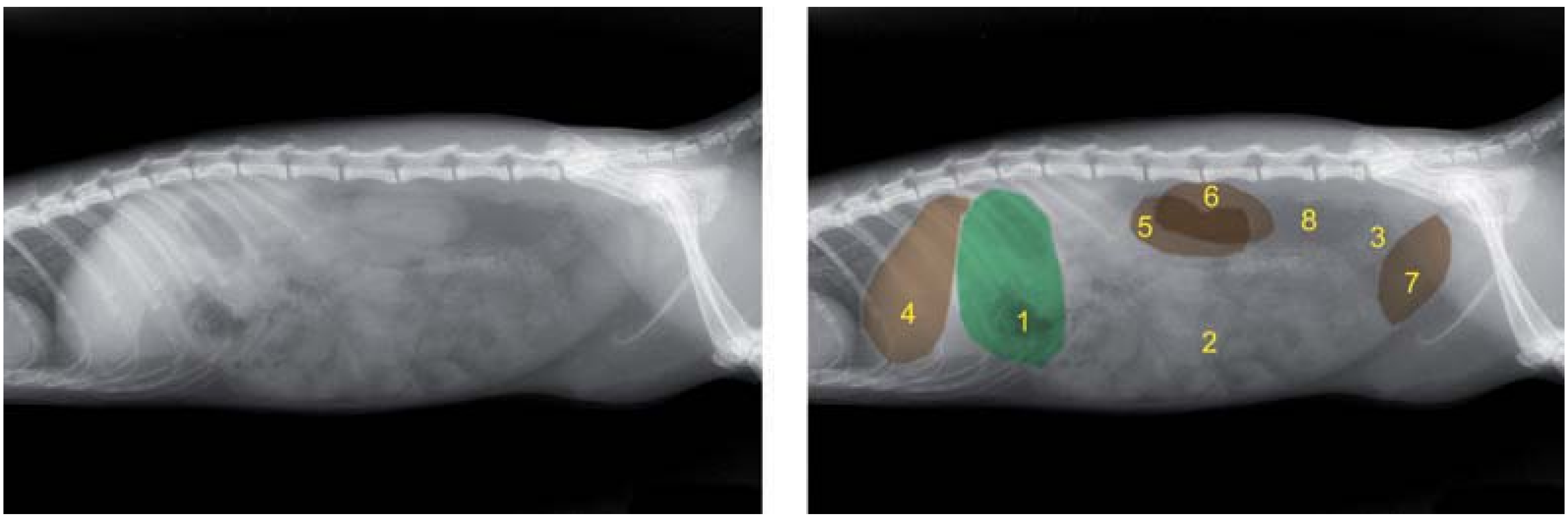

Fig. 2-38A: Radiographic images of a ferret's abdomen, lateral projection. The different sections of the ferret's gastrointestinal tract are difficult to delineate radiographically.

1: stomach
2: loop of intestines
3: rectum
4: liver
5: right kidney
6: left kidney
7: urinary bladder
8: sublumbar fat

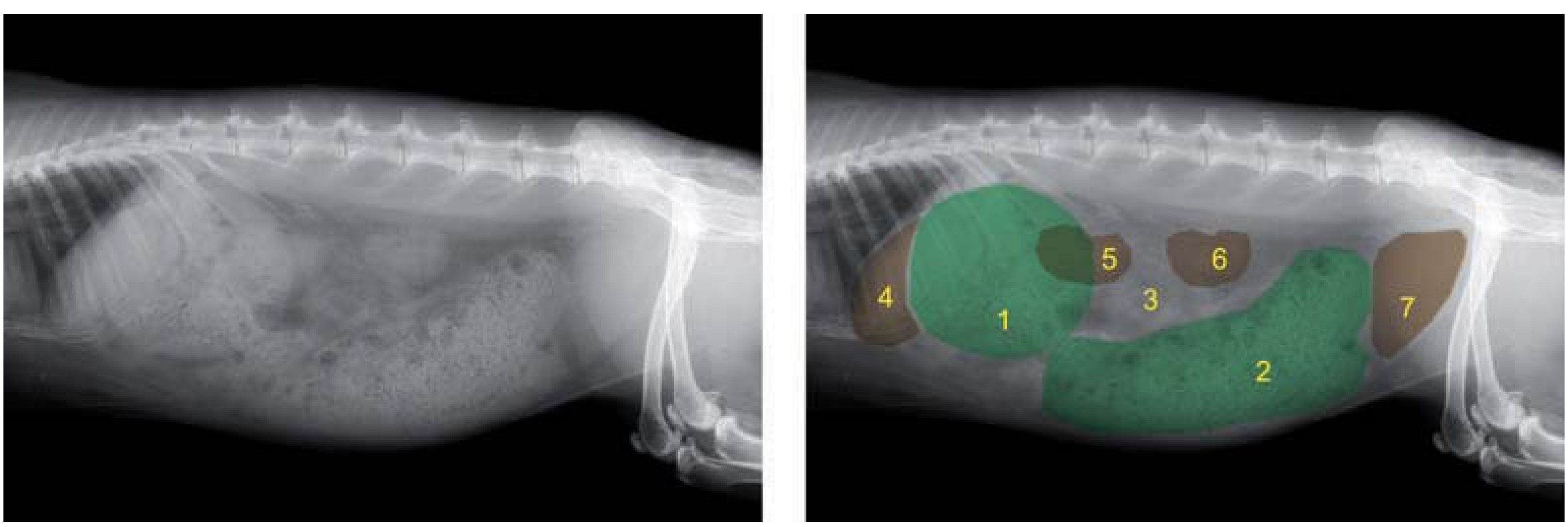

Fig. 2-38B: Radiographic images of a rabbit's abdomen, lateral projection. The stomach (1) and cecum (2) in the rabbit are usually well defined radiographically due to their nonhomogeneous ingesta intermingled with small gas bubbles.

1: stomach
2: cecum
3: loop of intestine
4: liver
5: right kidney
6: left kidney
7: urinary bladder

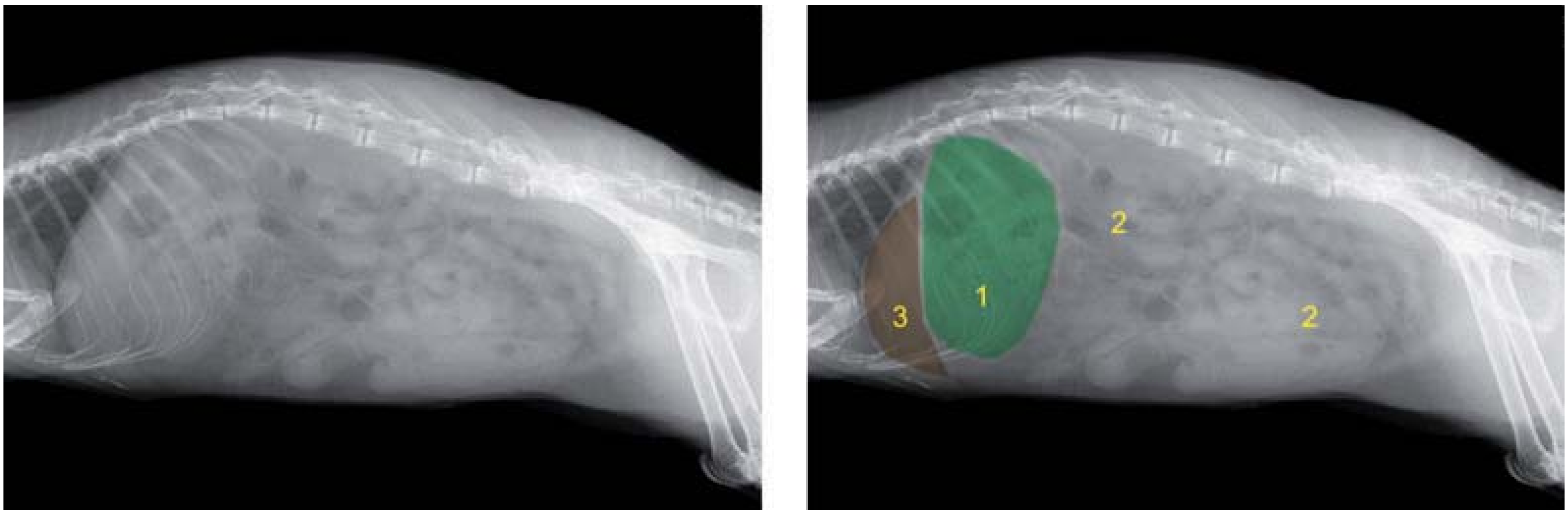

Fig. 2-38C: Radiographic images of a chinchilla's abdomen, lateral projection. The voluminous cecum in Caviomorpha is not usually distinguishable from the adjacent intestinal tract. The stomach is partially superimposed by loops of intestines on the right and cannot be differentiated with any certainty.

1: stomach
2: intestines
3: liver

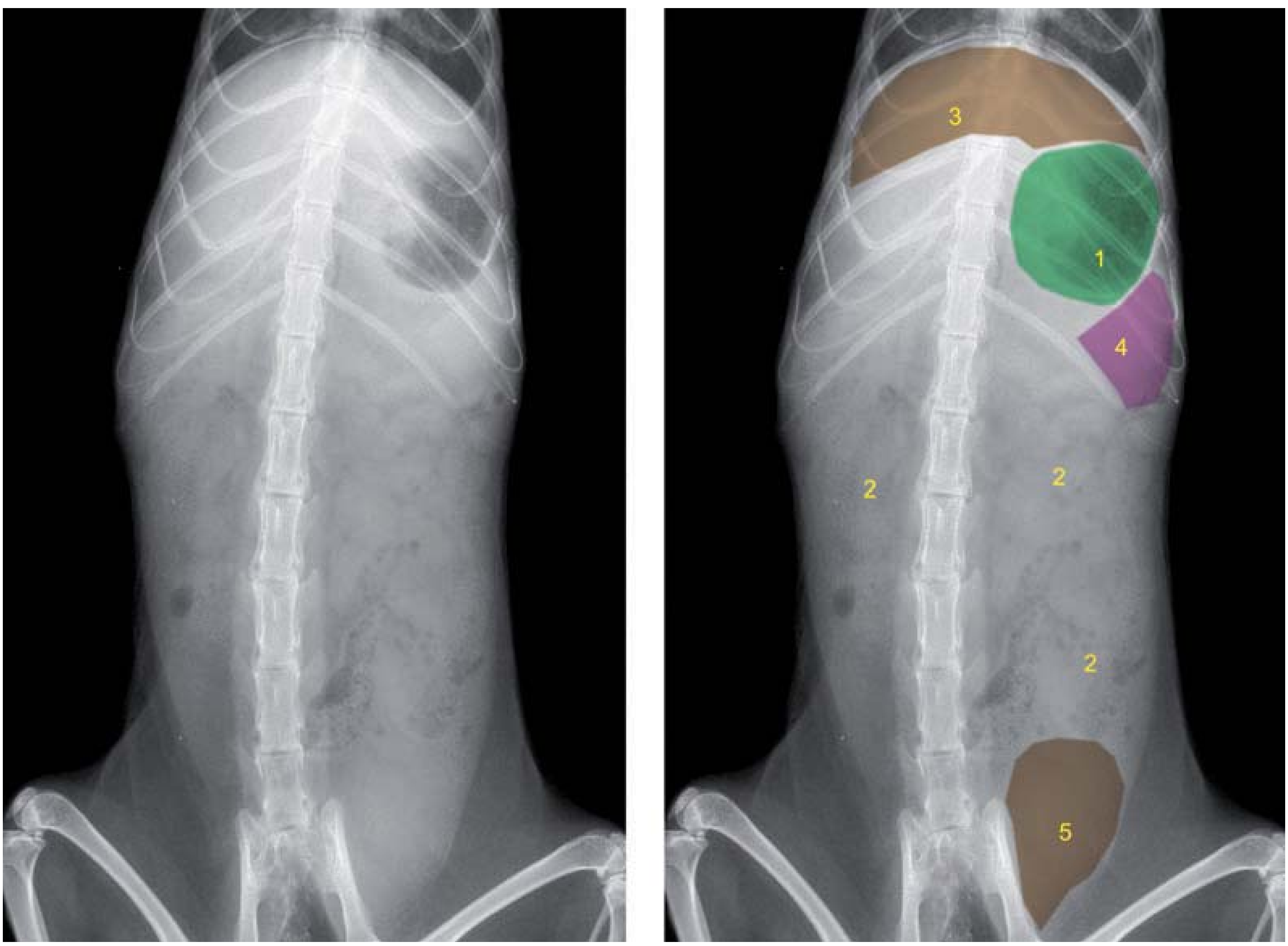

Fig. 2-39A: Radiographic images of a ferret's abdomen, ventrodorsal projection. The stomach (1) always lies to the left of center in the intrathoracic part of the abdomen. It can usually be identified by the gas bubble in its fundus.

1: stomach
2: intestines
3: liver
4: spleen
5: urinary bladder

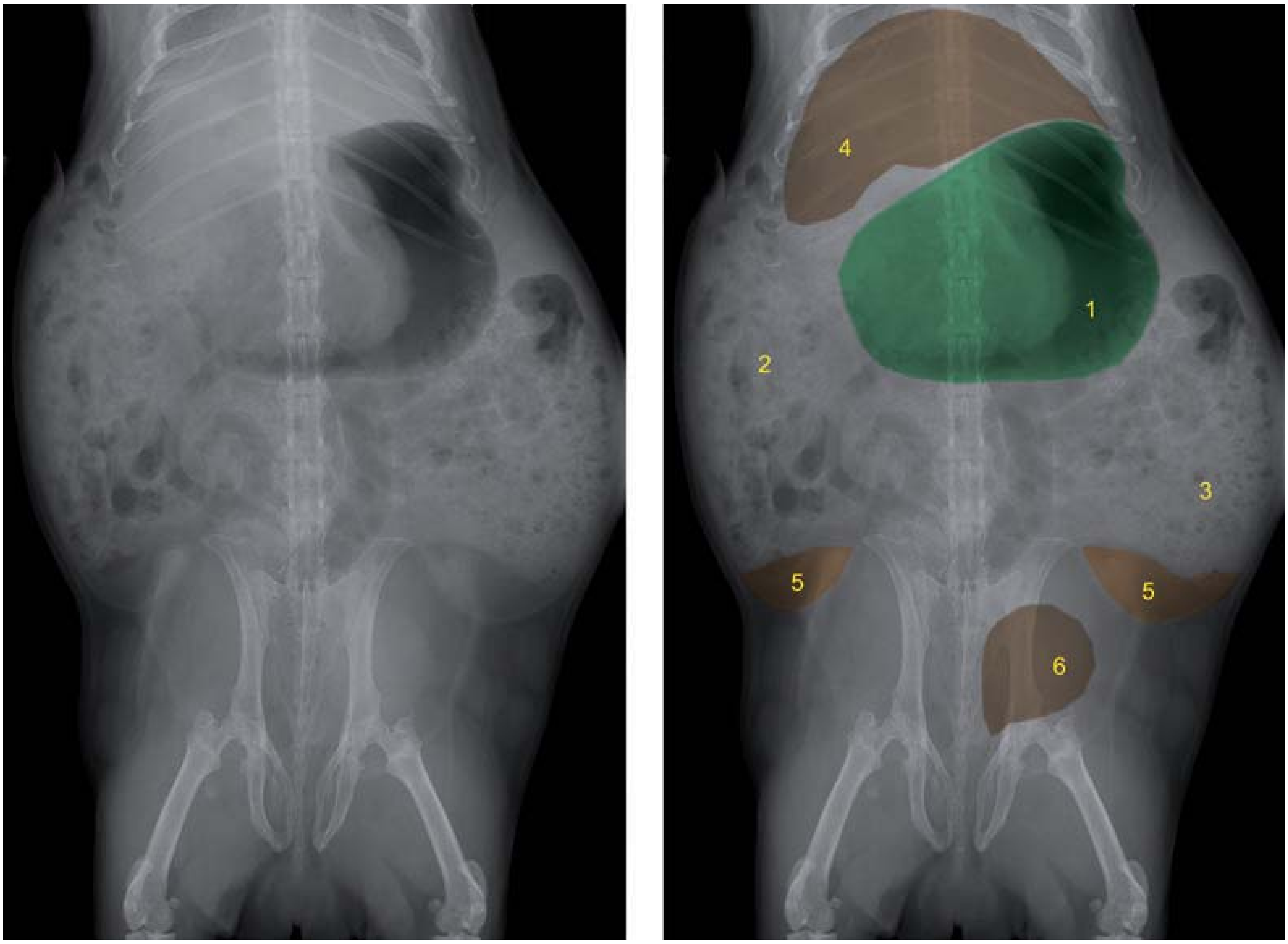

Fig. 2-39B: Radiographic images of a guinea pig's abdomen, ventrodorsal projection. Typical of the guinea pig is its asymmetrical liver (4) that lies more to the right, while its stomach (1) lies mainly to the left. Nearly all of the intestinal tract (2) is situated on the right side of the abdomen. The voluminous ovarian cysts (5) are almost completely superimposed by the gastrointestinal tract. These cysts have caused the right and left abdominal walls to obviously protrude.

1: stomach
2: small intestines
3: cecum
4: liver
5: ovarian cysts
6: urinary bladder

Only in the rat can the cecum be relatively well visualized as a radiopaque structure without the use of contrast material (compare **Fig. 2-38C** with **Figs. 2-40** and **2-42**). The ferret does not have a cecum.

Large intestines

The large intestines in the **ferret** are very short and can be compared to the cat with respect to its path. Radiographically, the large intestines are rarely differentiated with the exception of the feces-filled rectum. This radiographic observation is similar in the small rodents. By comparison, the ascending colon is elongated in the **rabbit**, **guinea pig**, **chinchilla** and **degu**. In addition, the ascending colon is rolled into a spiral (*ansa spiralis coli*) in the **rabbit** and **guinea pig**, and inconsistently rolled to various degrees in the **degu**. In the **chinchilla**, the colon courses in a wide curve through the abdomen. The superimposition of the colon with the cecum makes a radiographic differentiation of these two organs impossible without contrast. Only in the rabbit can the ascending colon be imaged in the VD projection when gas is present in the haustra. The descending colon is occasionally easy to recognize in the rabbit and guinea pig. Especially in obese rabbits, the sublumbar fat can cause a significant (centimeters) caudoventral displacement of the descending colon. The descending colon can be identified as structure with a caudal path that can be differentiated from the homogeneous fat due to its lower radiodensity.

2.2.4.2 Liver

The liver forms a homogeneous soft-tissue shadow in the intrathoracic part of the abdomen and its caudoventral edge should not extend outside of the costal arch (**Figs. 2-27** and **2-38A-C**). One exception to the location of the liver described above is the **rat**, as its liver extends beyond the costal arch even in the normal animal (**Figs. 2-40** and **2-42**). On occasion, the liver can extend beyond the costal arch, especially on the right, in clinically healthy **guinea pigs**. However, unusual positioning of the liver can be an indication of hepatic lipidosis, which is frequently diagnosed in pet guinea pigs.

2.2.4.3 Pancreas

The pancreas cannot be radiographically visualized in small exotic mammals.

2.2.4.4 Spleen

The spleen of the **rabbit** and **rodents** is relatively small and normally cannot be identified on a radiographic image. However, the **ferret** has a relatively large spleen, which is frequently enlarged in adult animals (**Fig. 2-41**). In ferrets, the spleen is imaged well radiographically both in the lateral and VD projections. On a lateral radiograph, the spleen can be observed as a homogeneous oval to triangular area with soft-tissue radiopacity, lying caudal to the liver and in contact with the ventral abdominal wall. In the VD projection, the spleen also forms a triangular to oval soft-tissue shadow situated caudal to the stomach on the left abdominal wall.

2.2.4.5 Urinary tract

Kidneys

The kidneys lie retroperitoneally on the dorsal abdominal wall with the left kidney usually positioned slightly more caudal than the right. The exact position of the kidneys is species-specific (Table 2-3).

All small exotic mammalian species discussed in this book have bean-shaped kidneys, which are smooth and have a single renal pelvis. Radiographically, the kidneys may be easily observed or not depending on the extent of the retroperitoneal fat deposits. The retroperitoneal fat deposits are variable depending on the individual patient and species being examined. The kidneys are usually easily identified radiographically in **ferrets** with a good nutritional status (**Fig. 2-38A**). This is also true in morbidly obese pet **dwarf rabbits**, due to the kidneys being surrounded by thick layers of fat. In these obese dwarf rabbits, the left kidney, in particular, may be displaced a significant distance ventrally into the abdomen by the fat (**Fig. 2-37**). The voluminous cecum in the **guinea pig**, **chinchilla**, and **degu** is usually superimposed on the kidneys, making identification of these organs difficult. Summation usually hinders a reliable identification of the kidneys in **small rodents**, but in these cases it is due to the gastrointestinal tract. The kidneys are best identified in very obese **rats** (**Fig. 2-42**).

Ureter

The ureters cannot be observed on a radiographic image without contrast. Sometimes ureters may become visible due to the deposition of calculi (see Chap. 2.9.7.2).

Urinary bladder

The appearance of the urinary bladder varies between an elongated pear to a round ball and lies on the ventral abdominal wall. In **rabbit** patients, the urinary bladder is easily recognized as an elongated fluid-filled structure that extends as far as the navel (**Fig. 2-38B**). In the **guinea pig**, **chinchilla**, and **degu**, the small urinary bladder lies in front of the pelvic inlet and in many cases is cranially superimposed by the appendix. The urinary bladder can be well differentiated in **small mammals**, especially when lateral projections of high-contrast radiographic images of are taken (**Fig. 2-42**).

Urethra

The course of the urethra through the pelvis and penis is not radiographically evident in most cases.

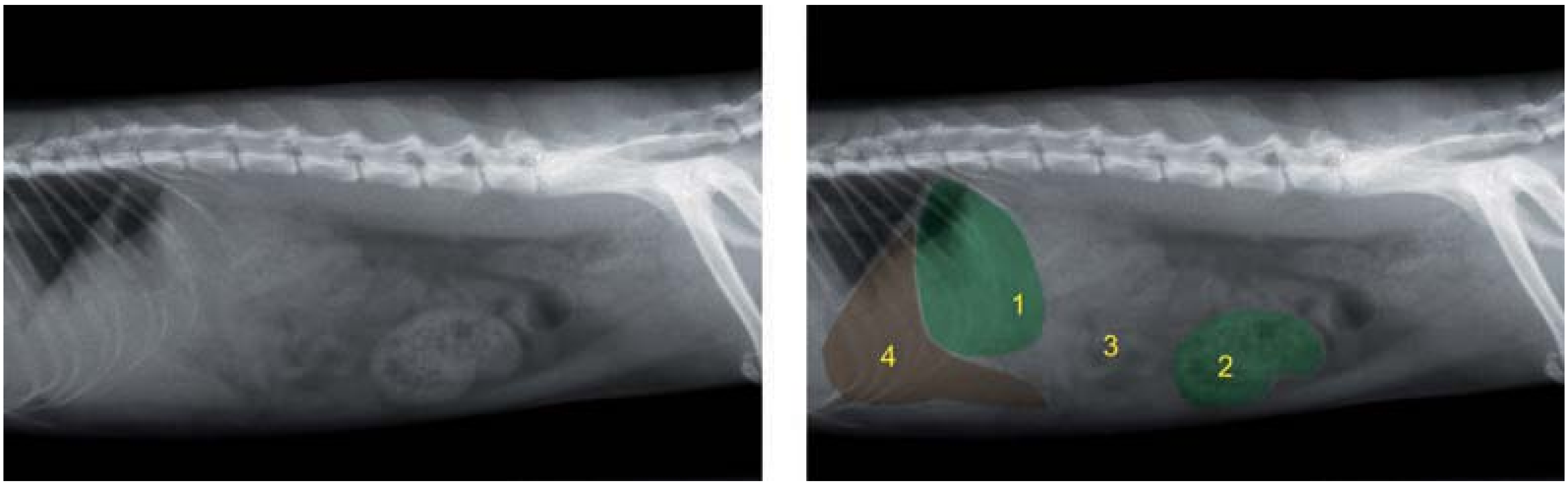

Fig. 2-40: Radiographic images of a rat's abdomen, lateral projection. The liver (4) of the rat extends beyond the costal arch in the normal animal.

1: stomach
2: cecum
3: intestines
4: liver

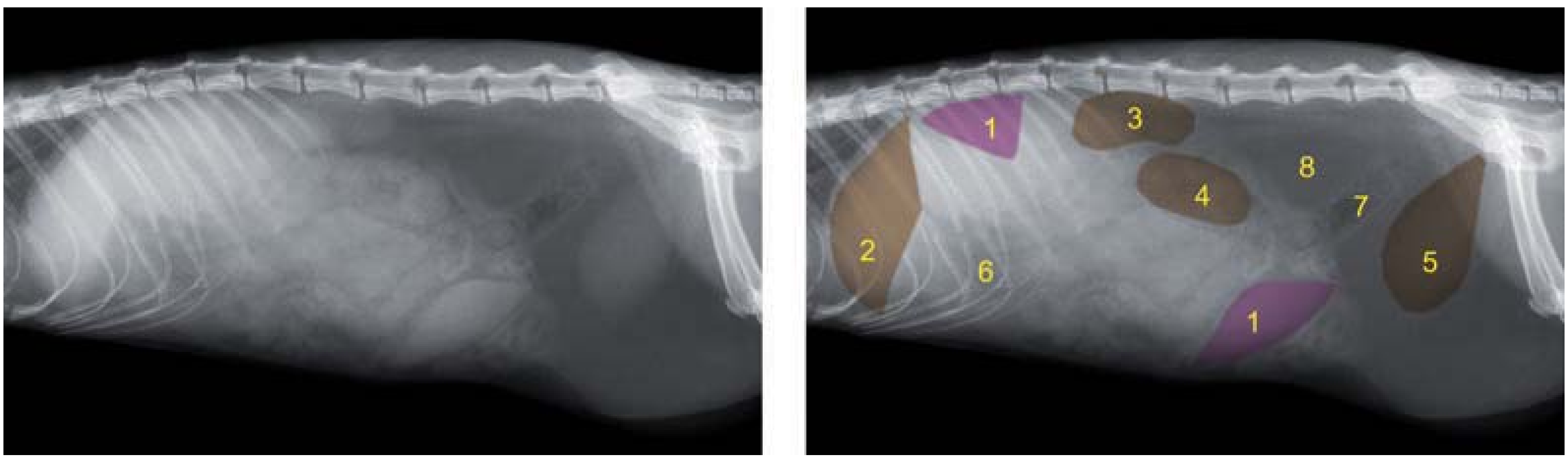

Fig. 2-41: Radiographic images of a ferret's abdomen, lateral projection. The spleen (1) in the ferret is usually very prominent. The differentiation from clinically relevant splenomegaly cannot be determined with any certainty.

1: spleen
2: liver
3: right kidney
4: left kidney
5: urinary bladder
6: stomach
7: rectum
8: sublumbar fat pad

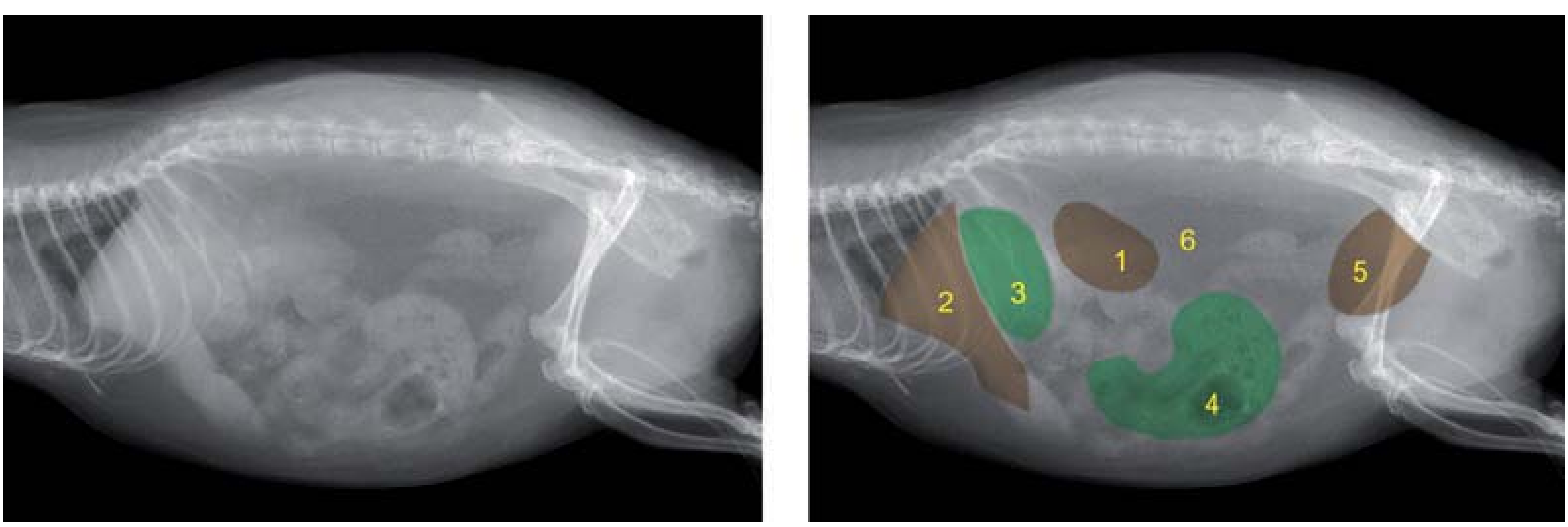

Fig. 2-42: Radiographic images of a rat's abdomen, lateral projection. The kidneys (1) can only be differentiated in obese rats with sublumbar fat pads (6).

1: kidneys
2: liver
3: stomach
4: cecum
5: urinary bladder
6: sublumbar fat pad

2.2.4.6 Genital organs

The majority of the intra-abdominal sections of the unchanged genital organs (e.g. uterus, ovaries, prostate, seminal vesicle) cannot be differentiated on a radiograph. Only in very obese **rabbits** can the uterus be identified in the lateral projection as a contrasting radiopaque cord against the surrounding fat, running dorsally to the urinary bladder until it reaches the ventral abdominal wall (**Fig. 2-37**). However, as a rule, such uteri are found to have a hyperplastic thickening during ultrasonographic examination (see Chap. 2.9.8.3). The ovaries in the **guinea pig** may grow to several centimeters in size and are visible in radiographic images as roundish radiopaque structures lying latero-caudally to the kidneys (see Chap. 2.9.8.4).

A **radiographic pregnancy investigation** is only practical for female **guinea pigs** and **chinchillas**. Due to the mineralization of their skeletons, the fetuses of these species can be easily imaged radiographically during the last trimester of pregnancy (**Fig. 2-43A**). The poor skeletal mineralization of rabbit fetuses allows for radiographic imaging only during the last few days of pregnancy (**Fig. 2-43B**). A typical physiological occurrence in female **guinea pigs** is that two weeks before the end of pregnancy the pelvic symphysis widens to form a sufficiently wide birth canal for the very large fetuses. This pelvic widening can be clearly observed in radiographic images (**Fig. 2-24**). The pelvic symphysis returns to its normal anatomical position within one day *post partum*.

2.2.4.7 Adrenals

The adrenal glands cannot be observed in radiographic images of small exotic mammals.

Table 2-3: Species-specific positioning of the kidneys

Species	Right kidney	Left kidney
Ferret	L2–L3	L3–L4
Golden hamster/Gerbil/Mouse	L2–L4	L3–L5
Guinea pig/Chinchilla	T12/13–L1	T13/14–L2
Rabbit	T13–L1	L3–L5
Rat	T12/T13–L1	T13–L2

Fig. 2-43A: Radiographic image of a guinea pig's abdomen, lateral projection. Fetuses can be observed radiographically in the last third of pregnancy in Caviomorpha due to their long gestation period and associated mineralization of the fetal skeleton.

Radiograph courtesy of the Veterinary Clinic Oberhaching, Munich, Germany.

Fig. 2-43B: Radiographic image of a rabbit's abdomen, lateral projection. Due to their short gestation period, the fetuses in the rabbit are only observed radiographically at the end of pregnancy.

Radiograph courtesy of the Veterinary Clinic Oberhaching, Munich, Germany.

2.3 Ultrasonography

SVEN REESE

2.3.1 Equipment

The resolution of the scanner is very important when sonographically examining small exotic mammals due to their small body size. Technological advancements in ultrasonography systems in recent years have enabled systems which can be used for producing good quality domestic cat images to be used in small exotic mammals. The limiting factor for producing good quality images from small exotic animals is the transducer used. For abdominal ultrasonographic examinations, a high-resolution linear probe is required. Even high-resolution microconvex probes are less suitable due to their narrow imaging range in the near field. Only when imaging the liver in the sagittal plane is the use of a microconvex probe occasionally easier than a linear probe. Otherwise the use of microconvex probes is reserved for unusual diagnostic needs (e.g. imaging of the cranial mediastinum through the cranial thoracic inlet).

With respect to linear probes, the so-called T-probes are most often used. In addition to T-probes, there are specialized shapes (e.g. intraoperative probes, fingertip probes). The T-probes usually ensure that one can obtain a higher degree of image quality. However, the small intraoperative probes with their lateral cables are definitely more versatile and flexible when used on small rodents. The width of a linear probe should not be more than 4 cm. If linear probes are more than 4 cm in width coupling will not be possible in all planes when examining small patients. Moreover, the majority of ultrasound units with broad linear probes do not allow a penetration depth of less than 4 cm, which in smaller exotic mammals is too deep since penetration depths of only 2 cm are required for these species.

The sonographic frequencies needed to examine small exotic mammals depend on the size of the species being investigated. Ultrasound units with a good resolution and a frequency of 7.5 MHz are quite suitable for diagnostic purposes in the larger exotic mammal species (e.g. rabbit, ferret, guinea pig, chinchilla). However, even with these species it is recommended to use medium frequencies of 10–12 MHz, which are also suitable for the rat. The 12-MHz probes commonly used on smaller rodents (e.g. golden hamster, gerbil, mouse) quickly reach their limits and high-resolution units with 15–20 MHz are much better suited to sonographically examine these species.

The special requirements placed by echocardiography and ophthalmosonography on the ultrasound units and probes are discussed in the respective chapters (see Chaps. 2.4.2.1 *f.f.* and 2.4.4.1).

In addition to using conventional ultrasonography in the B-mode, the use of Doppler techniques is also possible in small mammals. The use of Doppler techniques is of particular importance in echocardiography which is discussed at length below (see Chap. 2.4.2.6).

When performing a ultrasonographic examination of the abdomen, only the color Doppler and the more sensitive omnidirectional power Doppler are used for clinical or diagnostic purposes (e.g. to image the vascularization of tissues and organs). The small diameter of the blood vessels in small exotic mammals requires that the system being used has a high degree of sensitivity. Concurrently, there is the problem of the relatively rapid respiratory rate in these animals that leads to the formation of artifacts, which cannot be prevented by the use of wall filters. Such artifacts may even render the use of Doppler techniques in the cranial abdomen worthless.

Indications for the use of ultrasonography

The diagnostic use of ultrasonography should not compete with radiographic imaging. Depending on the case presentation, both imaging modalities should complement each other or one should be considered the method of choice.

Typical indications for performing abdominal ultrasonographic examinations are:

- palpable space-occupying lesions in the abdomen
- palpable enlargement of the liver, kidneys, and spleen
- pain on palpating the kidneys
- distended, possibly painful urinary bladder
- dysuria and hematuria
- vaginal discharge
- fur contaminated with urine in the perineum and inner thigh region
- pregnancy diagnosis

2.3.2 Positioning and fixation

Today, the majority of small exotic mammals maintained as pets are very tame and can usually be examined, if they are handled with patience and confidence, without the use of sedation. Before an attempt is made to remove the animal from its cage any structures in which the animal can hide should be taken out, if possible. To chase the animal(s) from hiding place to hiding place through their cage is usually counterproductive for the subsequent examination and does not engender owner confidence in the veterinarian's clinical skills.

Ferrets, **rabbits**, **guinea pigs**, and **chinchillas** allow themselves to be easily examined while lying on their backs. A positioning device made of foam plastic is a useful tool when sonographically examining these animals. One or two assistants should hold the animal in place by the pectoral girdle and the hindlimbs (**Fig. 2-44A**). Holding **ferrets** by the scruff of its neck may be necessary in very nervous or vicious animals (**Fig. 2-44B**). If

Fig. 2-44A: Manual positioning and restraint of a guinea pig for an abdominal ultrasonographic examination.

Fig. 2-44B: Restraint of a ferret by holding the scruff of its neck during a ultrasonographic examination is rarely used, but it may be necessary in excitable and aggressive animals.

Picture reproduced with kind permission from Reese, S., Frings, B. (2004): Die abdominale Ultraschalluntersuchung beim Frettchen. Tierärztl Prax **32(K)**: 182–189.

rabbits are placed symmetrically on their backs with an inability to move their heads sideways, they will become motionless with their hindlimbs slightly pulled towards the body and may slightly shake. In this position, it is not required to restrain the hindlimbs. Rabbits which attempt to turn themselves during the examination should be allowed to do so and after a short pause be replaced in the dorsal recumbent position. Not under any circumstances should a rabbit be maintained in dorsal recumbancy by force as the danger of the patient injuring itself by its strong defensive movements (e.g. strong leg kicks) is too high. For echocardiography (see Chap. 2.4.2.2), the animals should be held in lateral recumbency on an examination table with a cutout section similar to those used for dog and cat patients. Alternatively, ultrasonographic examinations in all small exotic animal species can be performed with the animal sitting on the lap of an assistant or the investigator. In such a position, the animals are usually less excitable. A food distraction using a supplement paste has proven to work very well in ferrets (**Fig. 2-51C**).

Small rodents do not tolerate the dorsal recumbent position very well. Depending on the patient's general disposition, **rats** and **degus** can be positioned by grasping their shoulders using a scissors grip or holding them by the scruff of their neck and in an upright manner (**Fig. 2-45A**). It is important that the animal is able to sit with its back paws on a firm surface. **Golden hamsters**, **gerbils** and **mice** are grabbed by the scruff of the neck by the examiner with their free hand and held in the palm of the hand. Moreover mice are held with the small finger lying over the base of the tail. In tame gerbils, it is often enough just to hold the head and body between the fingers and thumb (**Fig. 2-45B**). In contrast to the golden hamster and mouse, gerbils go rigid in this position. Sometimes offering food to golden hamsters and degus can be a useful distraction to successfully perform an ultrasonographic examination.

2.3.3 Preparation of the patient

In contrast to the dog and cat, **rabbits** and **rodents** should never be fasted as part of the pre-examination preparation. The emptying of the **rabbit**, **guinea pig**, and **chinchilla** stomach is dependent on continual ingestion of food, therefore a period of fasting will not have the desired effect of better quality images and fasting can be dangerous as it may lead to metabolic complications and intestinal atony. **Ferrets** may also be only fasted for a maximum of 4–5 hours, due to their tendency to become hypoglycemic.

Good image quality is dependent on excellent skin coupling with the transducer. It is necessary to shave most of the small exotic mammal patients over the area being examined, prior to being sonographically examined, except for the **golden hamster**. The use of a quiet clipper is recommended to reduce patient anxiety. A frequent mistake in rabbit patient preparation for abdominal ultrasonography is leaving too much hair in the area of the cranial abdomen, whereby the examination of the liver is difficult or not possible. As a control, the costal arch should be palpated. The lateral aspect of the patient should be shaved up to the fold of the flank. If the animal is not properly shaved on its lateral abdominal areas, in species which have a voluminous appendix, renal imaging is very difficult.

A generous portion of acoustic gel should be used as a coupling medium in small rodents. To prevent hypothermia of the patient, the acoustic coupling gel should be warmed (patient's body temperature) prior to use. The use of a baby bottle warmer is very effective in warming coupling gel. For the same reason, generous use of alcohol is not recommended in small rodents as its evaporation from the abdominal skin can lead to a severe loss of body heat. Alcohol should only be used in the golden hamster to dampen the skin over the examination site.

2.3.4 Investigation protocol

The same protocol used for abdominal ultrasonographic examinations on dogs and cats can be utilized in small exotic mammals. One standard method is to initiate imaging with the urinary bladder and then adjust the total and depth-dependent amplification to the individual coupling condition of each individual patient. The investigation is performed in a counterclockwise manner through the abdomen with each organ system being systematically investigated. The imaging and documentation should be done in standard planes to enable easy comparison of follow-up examinations with the preliminary images.

2.3.5 Documentation of the results

The video printer is most frequently used to document the results of ultrasonographic examinations. Present-day ultrasound units contain all available variations of digital recording technology to preserve individual images or sequences. The ultrasonographic images can be recorded on CD-ROM or via USB on external hard drives. The optimal recording solution is a connection with the clinic's DICOM network and imaging data to a patient administration system, thereby making this information available at all times through the use of a digital index card.

Fig. 2-45: The simplest method of performing an ultrasonographic examination in the (A) degu is in the upright position with the animal sitting on its stabilized hind feet and its attention being diverted with food. Conversely, (B) gerbils remain still if they are held in the palm of a hand.

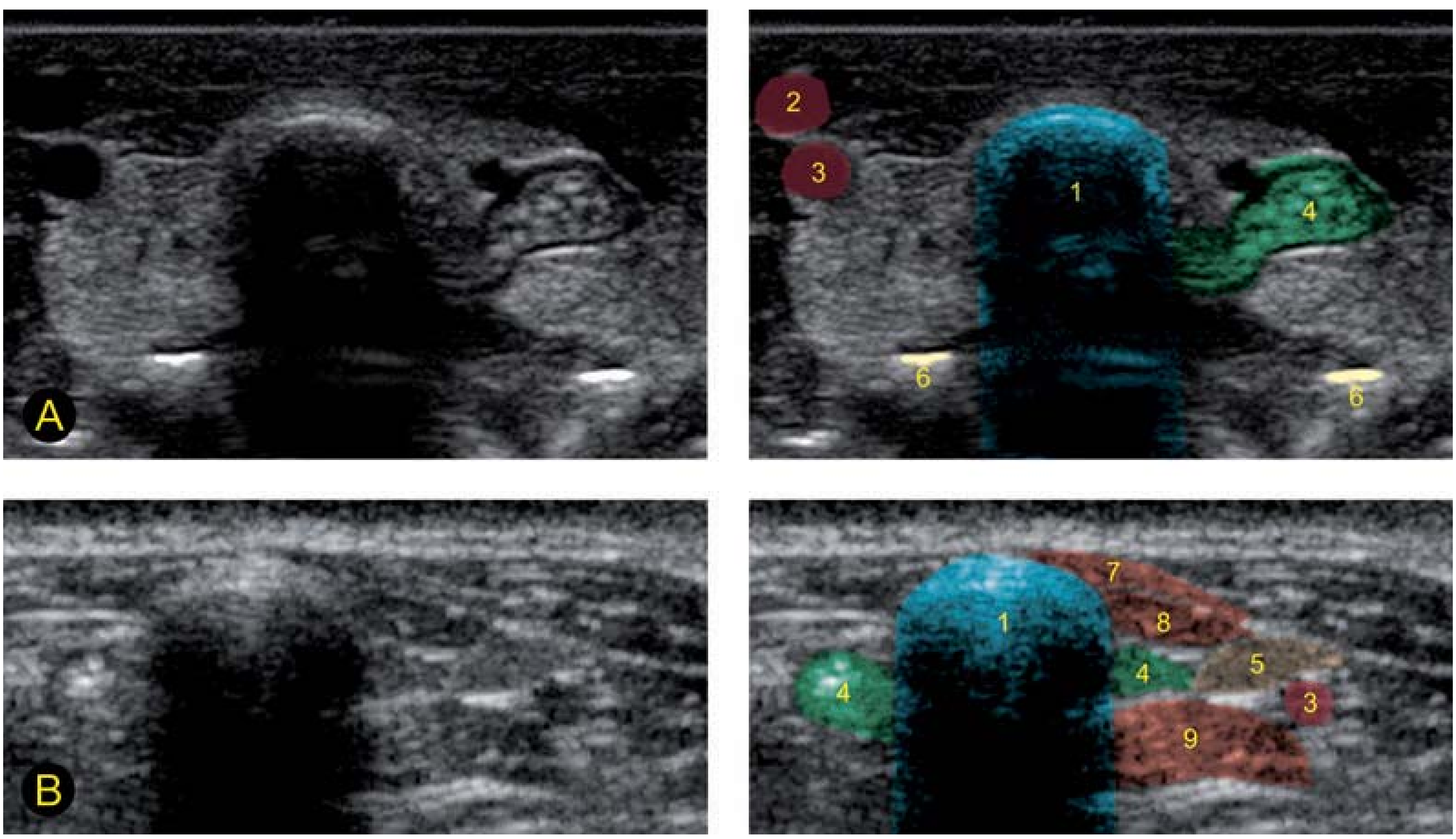

Fig. 2-46: Ultrasonographic images of the neck, transverse plane, 13 MHz.

A: PD 1.5 cm: Rabbit

B: PD 1 cm: Ferret

1: trachea
2: right jugular vein
3: right carotid artery
4: esophagus
5: left lobe of the thyroid
6: lateral processes of the cervical vertebrae
7: sternohyoideus muscle
8: sternothyreoideus muscle
9: longus collis muscle

2.4 Sonoanatomy

2.4.1 Cervical soft tissues

SVEN REESE

The ultrasonographic examination of neck tissues has become an established diagnostic tool for dog and cat patients. The small dimensions involved significantly limit the use of this technique in small exotic mammals. However, it is possible to reliably image the trachea, esophagus, and carotid artery (**Figs. 2-46A, B**) with high-resolution systems (12–15 MHz) in the **ferret, rabbit,** and **guinea pig**. In contrast, imaging of the healthy thyroid is not always possible (**Fig. 2-46B**).

2.4.2 Thorax: echocardiography

CORDULA POULSEN NAUTRUP

The air-filled lungs form a total barrier to the sonographic waves. Therefore, the ultrasonographic examination of the intrathoracic organs is only possible when they are directly in contact with the thoracic wall. In most small exotic mammals, the heart fulfills this criterion, while for the other organs there is only limited diagnostic sonographic imaging access. One can attempt to perform an ultrasonographic evaluation of the cranial mediastinum by using a microconvex probe in the cranial thoracic inlet. The ultrasonographic examination of the heart (echocardiography) has continued to develop since the first echocardiographic evaluation in the 1970s. Echocardiography is an important independent specialty area of veterinary medicine within imaging diagnostics and is becoming a useful technique with which to examine the heart of small exotic mammals.

Today, echocardiography (i.e. the ultrasonographic imaging of the heart) is an important part of every clinical cardiac examination for small exotic pet mammals. However, results from the ultrasonographic examination should never be evaluated alone but always when considering the whole clinical presentation of the patient (e.g. the anamnesis, results from auscultation, electrocardiography [ECG], radiographic investigation).

2.4.2.1 Equipment

The technical requirements for echocardiography in small exotic pet mammals are discussed in Chapter 2.3.1, especially with respect to the high **transmission frequencies** necessary for these patients. However, in some cases, good cardiac ultrasonographic images can be achieved using lower frequencies (e.g. abdominal ultrasonography).

However, if transcutaneous echocardiography is to be successful some other technical conditions, which do not play a role in abdominal ultrasonographic examinations, must be taken into consideration. It is only possible to place the transducer in the narrow intercostal spaces of small exotic mammals with mechanical sector or electronic phased-array **transducers** that have a small coupling surface. The degu, golden hamster, gerbil, and mouse all have a special status with respect to the choice of transducer as transthoracic echocardiography can be performed in these animals with small linear probes (**Figs. 2-55** and **2-59**); although the linear transducer has to be placed across the ribs to image the heart in the right parasternal short- and long-axis views. In the four species mentioned above, there are no disturbing artifacts (i.e. in the form of sound dampening) caused by the very thin bony ribs due to the fact that there is very good resolution in the near-field of a linear probe, thereby allowing small cardiac structures to be imaged in more detail than with a sector or phased-array transducer.

In addition, a **high frame rate** (number of images per second in Hertz [Hz]) is required due to the rapid heart rates in small exotic mammals. Only frame rates of more than 60 Hz (100 Hz is better) enable the evaluation and measurement of the cardiac structures with 2D echocardiography[1] at predetermine times (i.e. end-diastole, end-systole, during the point of strongest chamber contraction, or at the point of greatest atrial filling). The majority of modern ultrasound units, which can be used for echocardiography, have the required high temporal resolution in the 2D B-mode. In color Doppler[2], the frame rate dramatically drops (**Fig. 2-48A**). Effective measures for increasing the frame rate are narrowing of the sound wave field width, reduction of the penetration depth, or the choice of a lower transmission frequency. In all cases, in which the frame rate remains too low, both conventional and color-coded M-mode methods provide better results with a significantly higher temporal resolution of approximately 2000 lines per second.

1 Two-dimensional echocardiography = 2DE = two-dimensional B-mode = two-dimensional brightness mode: this provides an almost »anatomical« imaging of cardiac structures. The acoustic boundaries of the heart are shown in a sectional image using a grey scale.

2 Color Doppler = two-dimensional color-coded Doppler echocardiography = color-coded Doppler echocardiography = color-coded Doppler ultrasonography = Color Duplex ultrasonography: combination of a two-dimensional B-mode and a laminar color-coded imaging of the blood flow. The relative blood flow with respect to the transducer can be clearly identified. The velocity of the blood flow can be roughly estimated and laminar blood flow can be differentiated from turbulence. A laminar blood flow towards the transducer has a red tone, while a laminar blood flow away from the transducer is coded with a blue tone. Turbulence can be imaged in a third color, often green. Slower blood flow appears darker, while faster blood flow is shown with lighter colors. Very rapid blood flow changes color (aliasing).

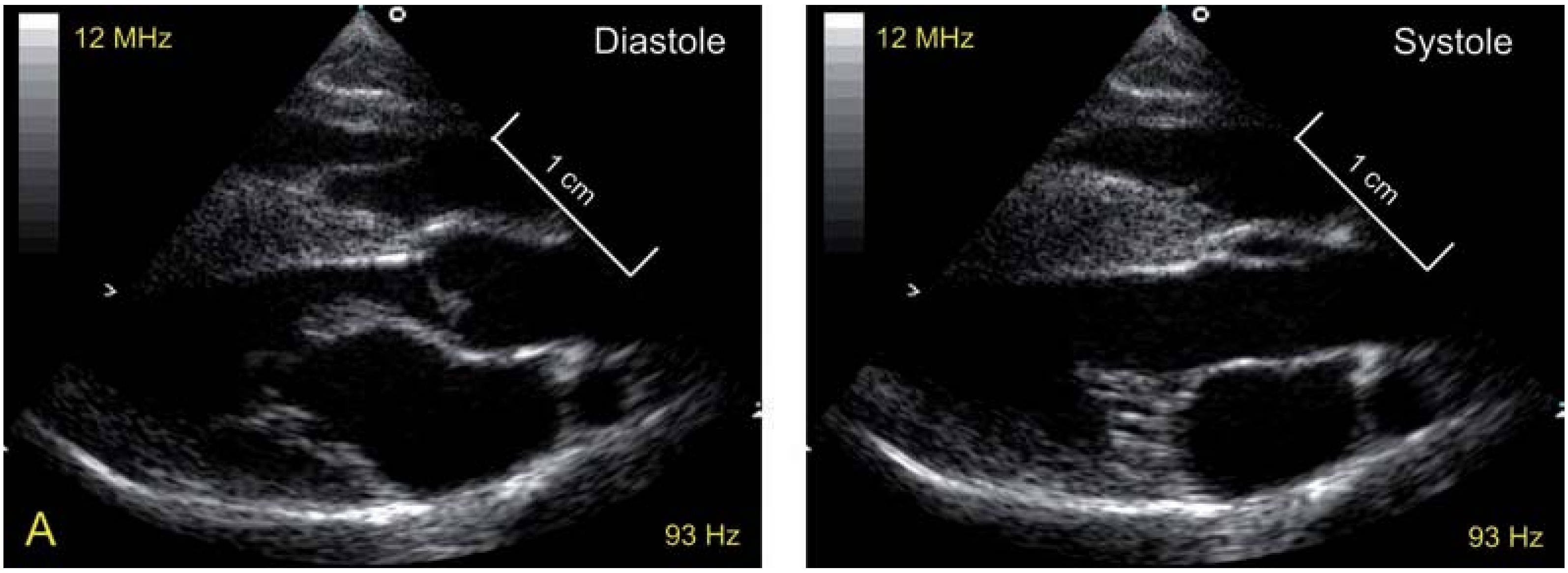

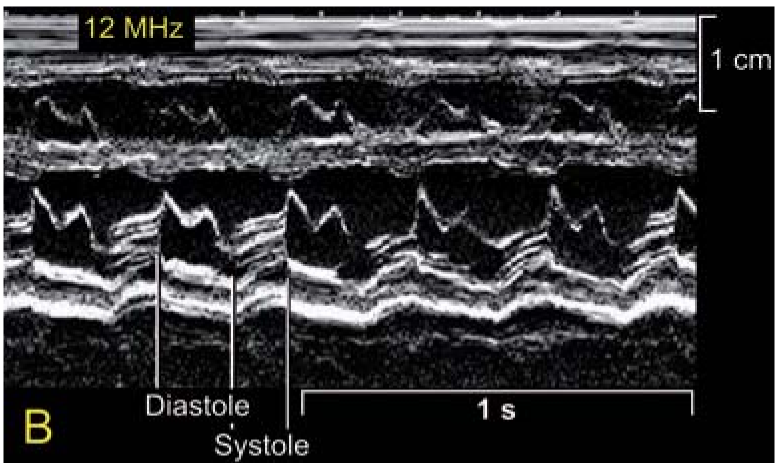

Fig. 2-47: B-mode echocardiographic images of a ferret, B-mode transmitter frequency: 12 MHz.

A: 2D echocardiography, mid-diastolic and early systolic, right parasternal long-axis view, frame rate 93 Hz.

B: M-mode echocardiography of the movements of the tricuspid valve and mitral valve.

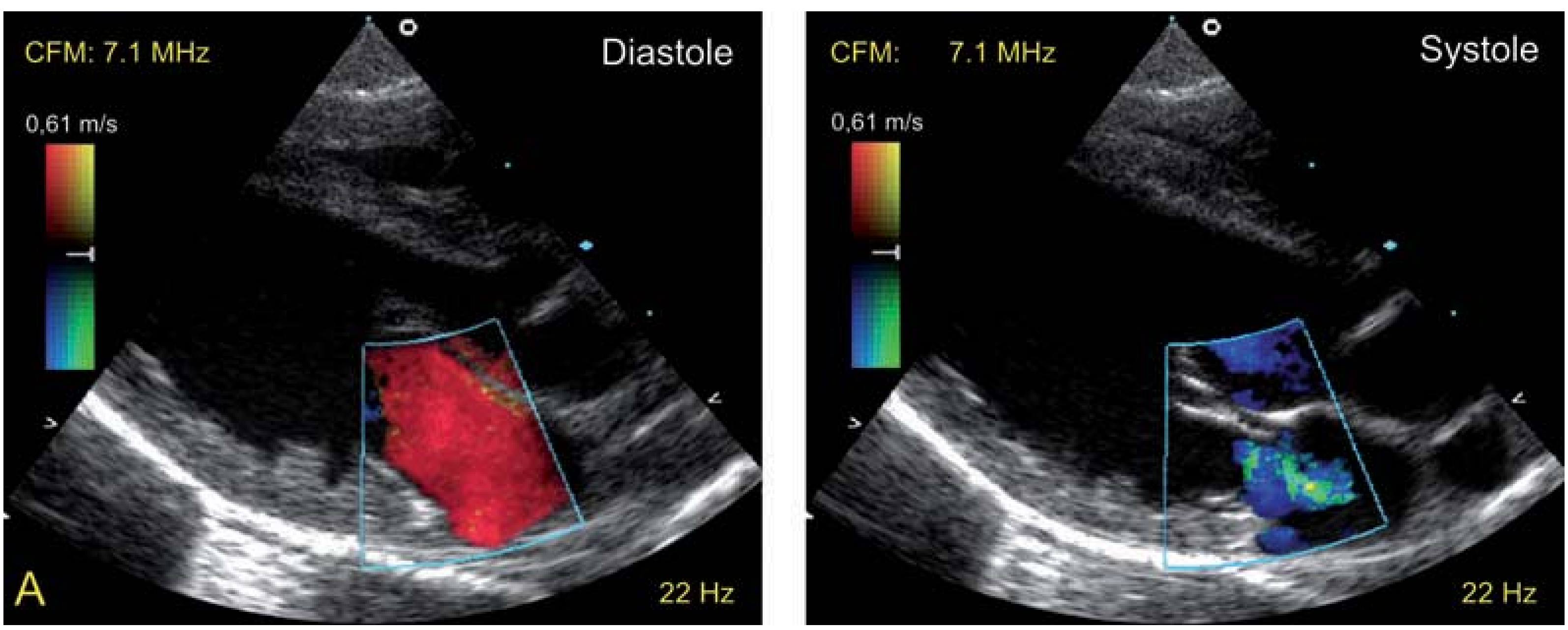

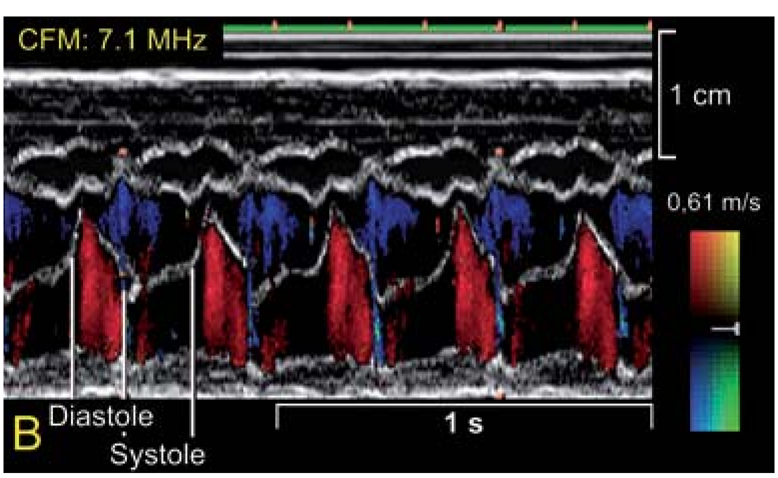

Fig. 2-48: Color-Doppler echocardiographic images of a rabbit, Color flow mode (CFM) transmitter frequency: 7.1 MHz.

A: 2D color-Doppler echocardiography, right parasternal long-axis view, early diastolic flow of blood into the left ventricle and early systolic reflux in the left atrium, frame rate 22 Hz.

B: color-coded M-mode echocardiography of blood flow through the mitral valve.

In addition to the grayscale M-mode[3], which is normally used, the color-coded M-mode method[4] is important when performing an echocardiographic examination on the commonly presented small exotic pet mammals (**Fig. 2-48B**). A further advantage of both M-mode methods is the simultaneous imaging of the different cardiac phases; therefore, the dynamics of the morphology, function, and blood flow can be better recorded, compared, and evaluated.

So that the high temporal resolution of the M-mode scans can be truly visualized, a suitable, rapid **speed of sweep (feed rate)**, with which the respective curves are recorded, should be selected (**Fig. 2-49**). This same consideration is required for recording the blood flow pattern with pulsed-wave (PW)[5] and continual-wave (CW) Doppler methods[6]. Feed rates of 100 cm/s and 200 cm/s are used in small exotic pet mammals (**Fig. 2-50**), while slower feed rates (25 cm/s or 50 cm/s) are usually used for echocardiography examinations of dogs and cats.

An ECG should be done simultaneously, as standard practice, during the echocardiographic examination to serve as an interval timer for defining the individual heart phases. All ultrasound units which are suitable for examining the heart have an ECG function. However, this type of examination is only successful on animals maintained under general anesthesia. In the majority of conscious patients, a simultaneous ECG recording cannot be performed as the electrodes greatly affect the animal's disposition, severely agitating the patient. This agitation makes the examination more difficult or even after a short period of time impossible.

3 M-Mode = motion mode = TM-Mode = time motion mode = grey scale M-mode = one-dimensional echocardiography: representation of the movement of the heart structures or of a series of changes of the structures which are lying on the sonic line. The acoustic boundaries are written as points on the y-axis; the x-axis shows the time.

4 Color-coded M-Mode: combination of an M-Mode image and the color-coded representation of the blood flow along the sonic line. The movement of the structures and the changes in the blood flow are visualized.

5 PW Doppler = pulsed wave Doppler = pulsed Doppler echocardiography: representation of slow and medium-velocity blood flows, which are measured in a predetermined area. The velocities are written on the y-axis, while the time-related changes are shown on the x-axis.

6 CW Doppler = continuous-wave Doppler = continuous-wave Doppler echocardiography: representation of the medium-velocity and rapid blood flows; however, without an exact spatial classification. The representation of the curves is the same as for PW Doppler.

2.4.2.2 Preparation and positioning

The **preparation of the animals** for an echocardiographic examination includes closely shaving a relatively large parasternal area on both the right and left thoracic wall in the locale of the heart apex beat (this is more cranial in the rabbit and guinea pig than the ferret).

The pet is then positioned in lateral recumbency on a table with a cut-out at the level of the heart or sitting on the lap of the examiner. The transducer is placed on the recumbent animal from below or on the sitting animal from the side (**Fig. 2-51A, B**). Placing the animal in the prone position in a special hanging apparatus with lateral coupling of the transducer has proven to be suitable for both the rabbit and guinea pig. Treats can be provided to increase cooperation of conscious patients (at least for a short period) during the relatively lengthy examination (**Fig. 2-51C**). Such examinations should be performed when possible, during the patient's periods of rest and not during their playtimes. Generally, echocardiography is much easier in sedated and anesthetized pets and not just for the benefit of the examiner but also because it less stressful for the patient. However, every form of anesthesia and sedation leads to changes in the heart function and hemodynamics, which must be taken into consideration when performing echocardiographic examinations and measurements. The type and extent of anesthetic and sedative influence on cardiac dynamics depends on the compound used, its dosage, and the individual patient. The comparison of one's own measurements obtained during an examination with the standard values provided in published reports (see Tables 2-4 to 2-17) is only meaningful when the conditions of the examinations are comparable. The diagnosis of congenital cardiac anomalies (e.g. ventricular septal defect, atrial septal defect, patent ductus arteriosus) is generally more successful when the patient is under general anesthesia or sedated.

2.4.2.3 Standard planes

The ultrasonographic imaging of the heart is almost always performed transcutaneously from the right parasternal, left apical, and left parasternal windows, and with certain indications (e.g. assessment of aortic stenosis) from the subcostal window. The scanning planes which are normally selected for small exotic mammals have been adapted from those provided in the literature regarding echocardiography in the dog by THOMAS et al. (1993) and the suggestions of the American Society of Echocardiography for humans (http://www.asecho.org/guidelines.php). Unusual echocardiographic scanning planes may need to be used especially when trying to locate tumors or judging tumor size.

The standard scanning planes and the resulting M-mode curves are comparable in all small exotic pet mammals and are similar to those in the dog and cat. Therefore, the echocardiograms shown in this text are mainly from healthy ferrets, rabbits, and guinea pigs, since these are the three small exotic mammal species that most frequently present with cardiac disease to a veterinary hospital.

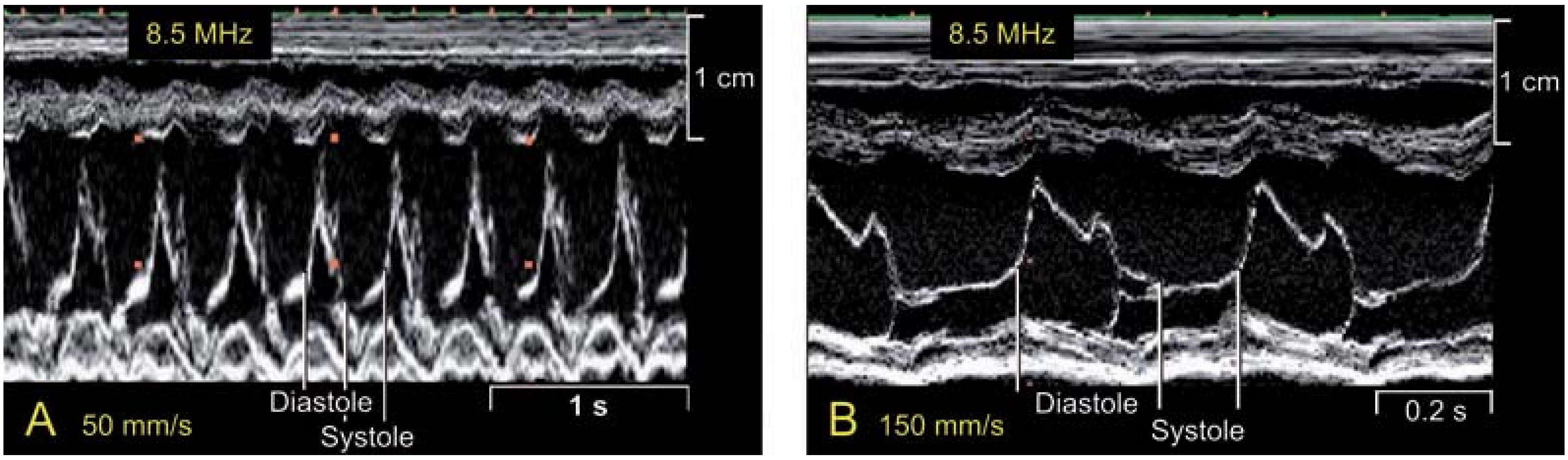

Fig. 2-49: M-mode echocardiograms of the movement of a rabbit's mitral valve, B-mode transmitter frequency: 8.5 MHz.

A: The feed rate is too slow at 50 mm/s.

B: Recommended feed rate of 150 mm/s.

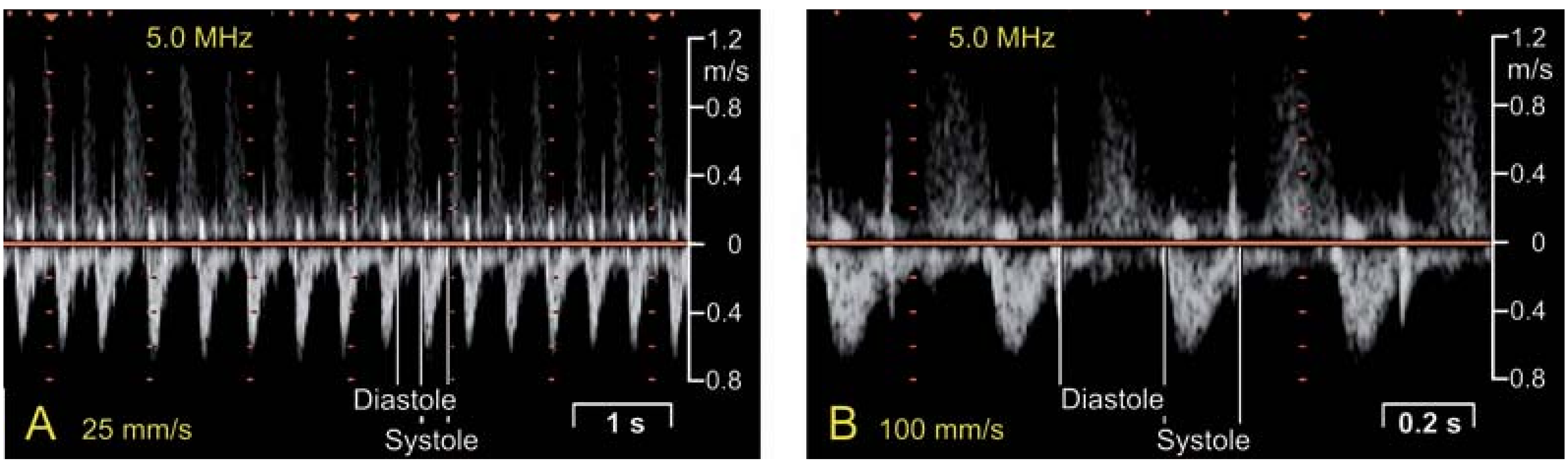

Fig. 2-50: PW-Doppler echocardiographic images of a rabbit showing normal systolic blood flow and the diastolic regurgitation through the pulmonary valve, Doppler transmitter frequency: 5 MHz.

A: The feed rate is too slow at 25 mm/s.

B: Recommended feed rate of 100 mm/s.

Fig. 2-51:

A: Positioning of a ferret on a table for an echocardiographic examination. The transducer is placed on the ventral part of the intercostal spaces.

B: Ultrasonographic examination of a ferret sitting in the lap of the person performing the procedure. A disadvantage is that the investigator cannot work the scanner alone when using this form of restraint.

C: Food will often distract nervous animals – at least for a short time.

2.4.2.4 Two-dimensional echocardiography

Right parasternal longitudinal view
(**Figs. 2-47A,B, 2-52, 2-53, 2-54, 2-55**)

The transducer is placed in the right parasternal position. The transducer orientation marker, which is shown on the right of the monitor, should point in the direction of the heart's base. The longitudinal axis of the heart lies in the scanning plane. The heart's apex is on the left of the picture, and its base is on the right. In this manner, the morphology and function of the left side of the heart can be assessed. From above, close to the transducer and from below, at a distance from the transducer, the following cardiac structures are visible:

- ☐ right ventricle (usually cannot be evaluated as the right side of the heart is too close to the transducer)
  - in-flow tract with the tricuspid valve and right atrium
- ☐ intraventricular septum, including the endocardium
- ☐ left ventricle
  - out-flow tract with the aortic valve and ascending aorta
  - in-flow tract with the mitral valve and left atrium
- ☐ left myocardium, including the endocardium
- ☐ pericardium

In dogs and cats, three different standard views in the longitudinal axis are employed: 1. just the left ventricular out-flow tract with the aortic valve and ascending aorta, 2. just the left ventricular in-flow tract with the mitral valve and the widest part of the left atrium, and 3. the simultaneous imaging of the out- and in-flow tracts with the aortic valve, part of the mitral valve, and left auricle of the left atrium. The separate imaging of the in- and out-flow tracts in small exotic pet mammals is difficult (i.e., as in human medicine, an attempt should be made to primarily simultaneously image all the parts of the left heart).

In the right parasternal longitudinal view, the evaluation of the aforementioned structures should be undertaken with respect to their morphology, such as size, size relationship of the left atrium to the aorta, echogenicity, and integrity. Also the assessment of left ventricular structure function is also performed in this standard scan, including if there is an increase in thickness of the intraventricular septum and left myocardium during systole, or an systolic narrowing or diastolic widening of the left ventricle.

Right parasternal short-axis views

The transducer remains coupled to the right parasternal window, but the transducer orientation marker after turning the transducer by approximately 90° counterclockwise is pointed in the direction of the right olecranon. Reliable, symmetrical, right parasternal short-axis views are much easier to achieve in small exotic pet mammals than the respective long-axis view, therefore in some cases the evaluation and measurement of the cardiac structures can only be performed with the following short-axis views at various levels.

1. Short-axis view at the level of the papillary muscles
(**Figs. 2-56, 2-57, 2-58, 2-59**)

- ☐ right ventricle (usually cannot be assessed as the right side of the heart is too close to the transducer)
- ☐ intraventricular septum, including endocardium
- ☐ left ventricle
- ☐ left myocardium with the papillary muscles, including endocardium
- ☐ pericardium

In this view, the wall morphology can be evaluated in addition to the systolic and diastolic sizes of the left ventricle.

2. Short-axis view at the level of the mitral valve
(**Fig. 2-60**)

- ☐ right ventricle (usually cannot be assessed as the right side of the heart is too close to the transducer)
- ☐ intraventricular septum, including endocardium
- ☐ left ventricle
  - out-flow tract
  - in-flow tract with mitral valve
- ☐ left myocardium including endocardium
- ☐ pericardium

In this plane, only the mitral valve opening is assessed. If the movement of the two mitral valve leaflets is not hampered and the left ventricle has a normal size during end-systole, then the mitral valve opens so far during early diastole that the septal cusp almost strikes against the intraventricular septum. A high frame rate is a prerequisite for the evaluation of the valve opening. Thickening of the mitral valve is barely recognizable in this plane and an inadequate systolic closure of the valve is not observed.

3. Short-axis view at the level of the aortic and pulmonary valves
(**Fig. 2-61**)

- ☐ right ventricle
  - in-flow tract with tricuspid valve and right atrium (rare as these structures usually lie in a slightly different plane)
- ☐ conus arteriosus with the pulmonary valve
- ☐ aortic valve
- ☐ left atrium (is only imaged in an acceptable manner when the right ventricular in-flow tract is not clearly observed)

In this view, the size relationship of the aorta to the pulmonary trunk at the level of their valves and the relationship of the left atrium to the aorta can be determined. The morphology of the blood vessels valves can also be evaluated when observed at this angle. This standard plane is also suitable for all Doppler examinations of the conus arteriosus, pulmonary valve, and pulmonary trunk.

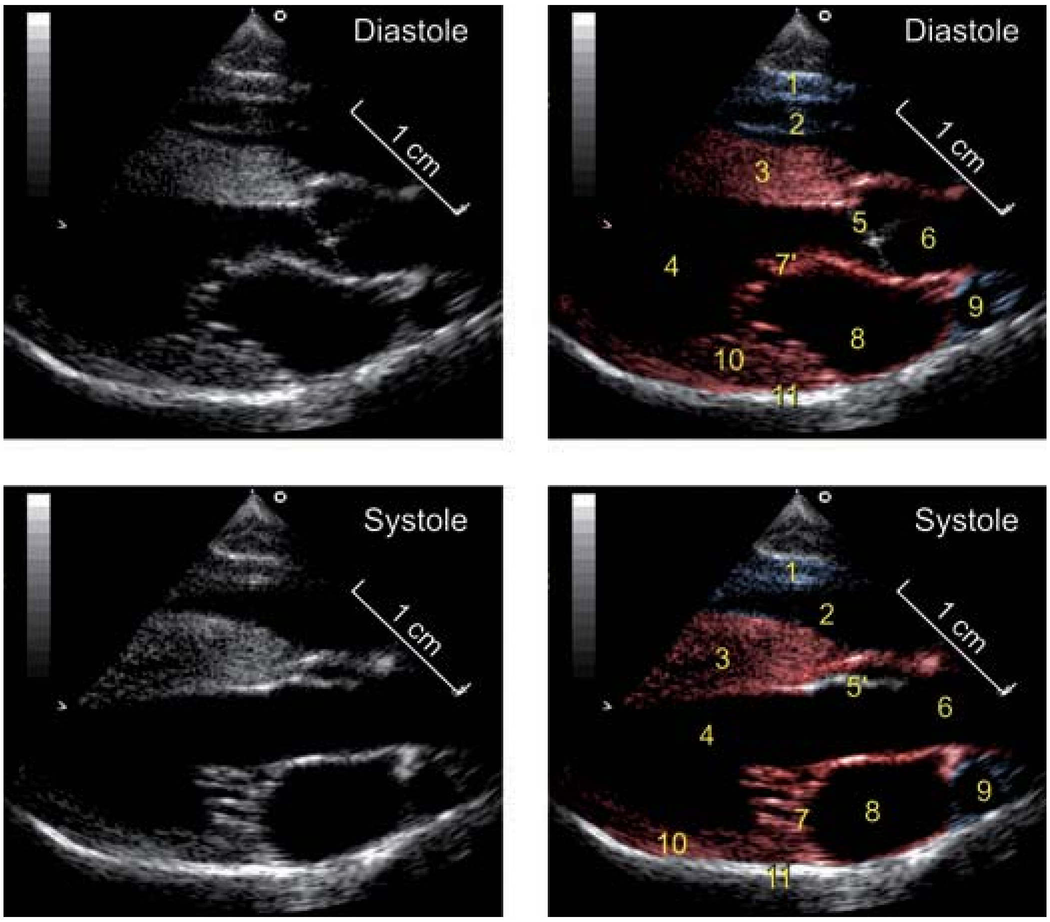

1: right myocardium
2: right ventricle
3: interventricular septum
4: left ventricle
5: closed aortic valve
5': opened aortic valve
6: ascending aorta
7: closed mitral valve with chordae tendineae
7': opened mitral valve with chordae tendineae
8: left atrium
9: right pulmonary artery
10: left myocardium
11: pericardium

Fig. 2-52: 2D echocardiographic images of a ferret, 12 MHz, end-diastolic and mid-systolic, right parasternal long-axis view, left ventricular in- and out-flow tracts.

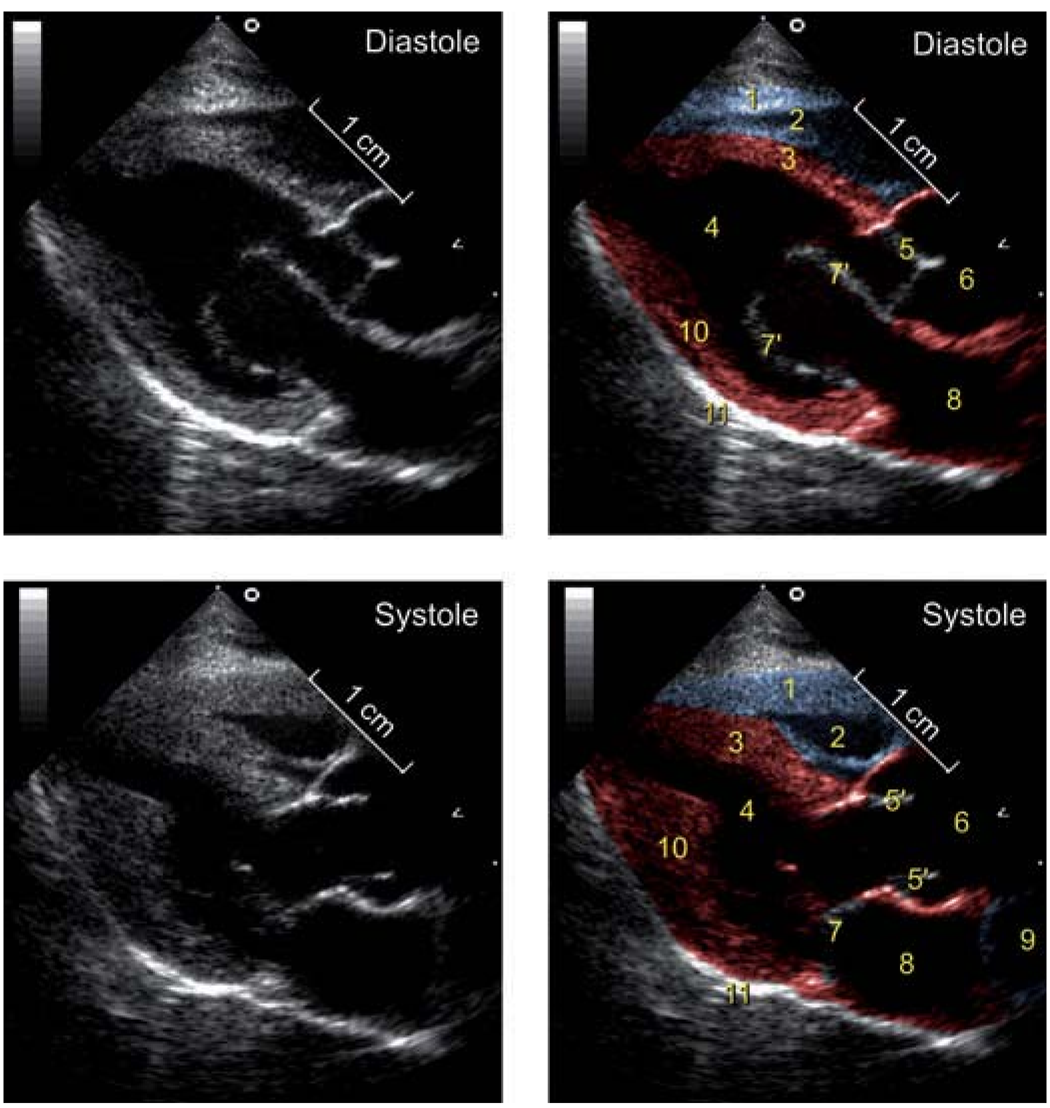

1: right myocardium
2: right ventricle
3: interventricular septum
4: left ventricle
5: closed aortic valve
5': opened aortic valve
6: ascending aorta
7: closed mitral valve
7': opened mitral valve
8: left atrium
9: right pulmonary artery
10: left myocardium
11: pericardium

Fig. 2-53: 2D echocardiographic images of a rabbit, 12 MHz, end-diastolic and end-systolic, right parasternal long-axis view, left ventricular in- and out-flow tracts. The leaflets of the mitral valve (7, 7') are long and dangling in the rabbit and are significantly different than those found in the ferret.

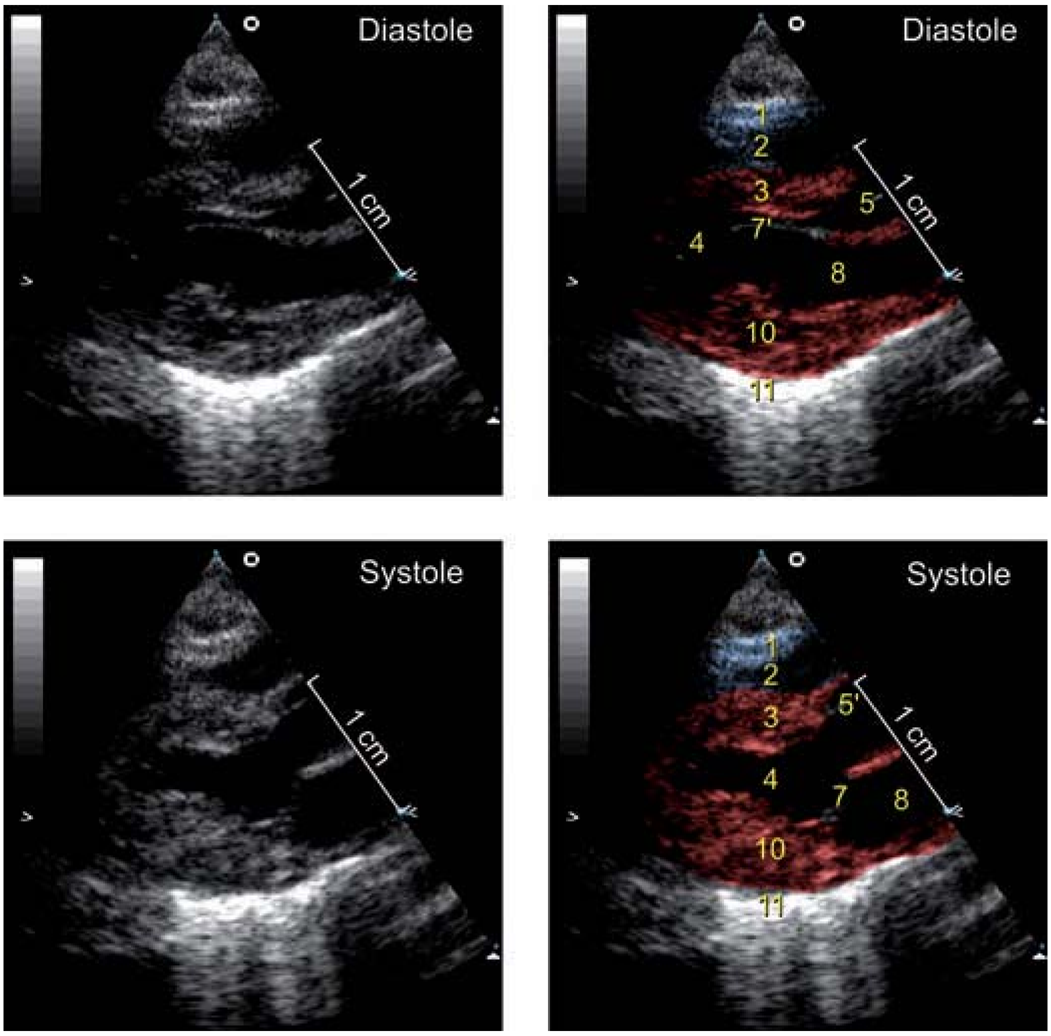

1: right myocardium
2: right ventricle
3: interventricular septum
4: left ventricle
5: closed aortic valve
5': opened aortic valve
7: closed mitral valve
7': opened mitral valve
8: left atrium
10: left myocardium
11: pericardium with attached reverberations.

Fig. 2-54: 2D echocardiographic images of a guinea pig, 12 MHz, end-diastolic and end-systolic, right parasternal long-axis view, left ventricular in- and out-flow tracts. The leaflets of the mitral valve (7, 7') are long in the guinea pig and the myocardium (1, 10) appears to be relatively thick. Often obvious reverberations in the form of so-called »comet-tail« artifacts can be found attached to the pericardium (11).

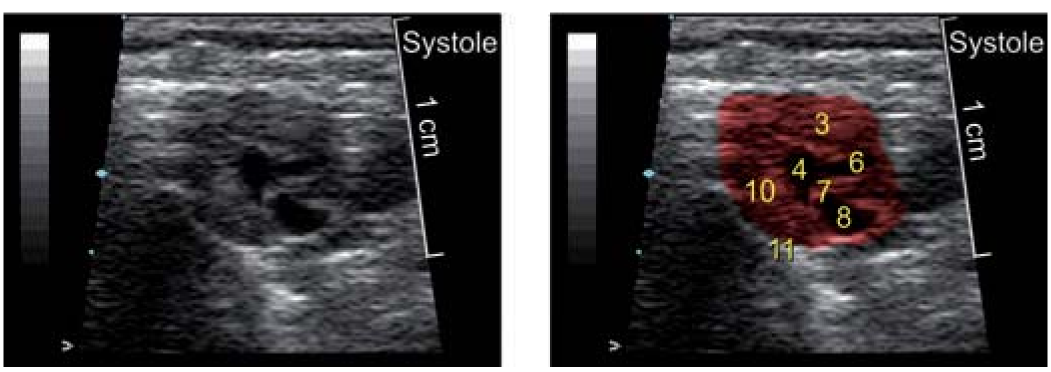

3: interventricular septum
4: left ventricle
6: ascending aorta
7: closed mitral valve
8: left atrium
10: left myocardium
11: pericardium

Fig. 2-55: 2D echocardiographic images of a gerbil using a linear array transducer, 15 MHz, end-systolic, right parasternal long-axis view, left ventricular in- and out-flow tracts. The interventricular septum (3) and left myocardium (10) appear to be relatively thick. Reverberations in the form of »comet tail« artefacts attached to the pericardium (11) are obvious. The right side of the heart is not visible.

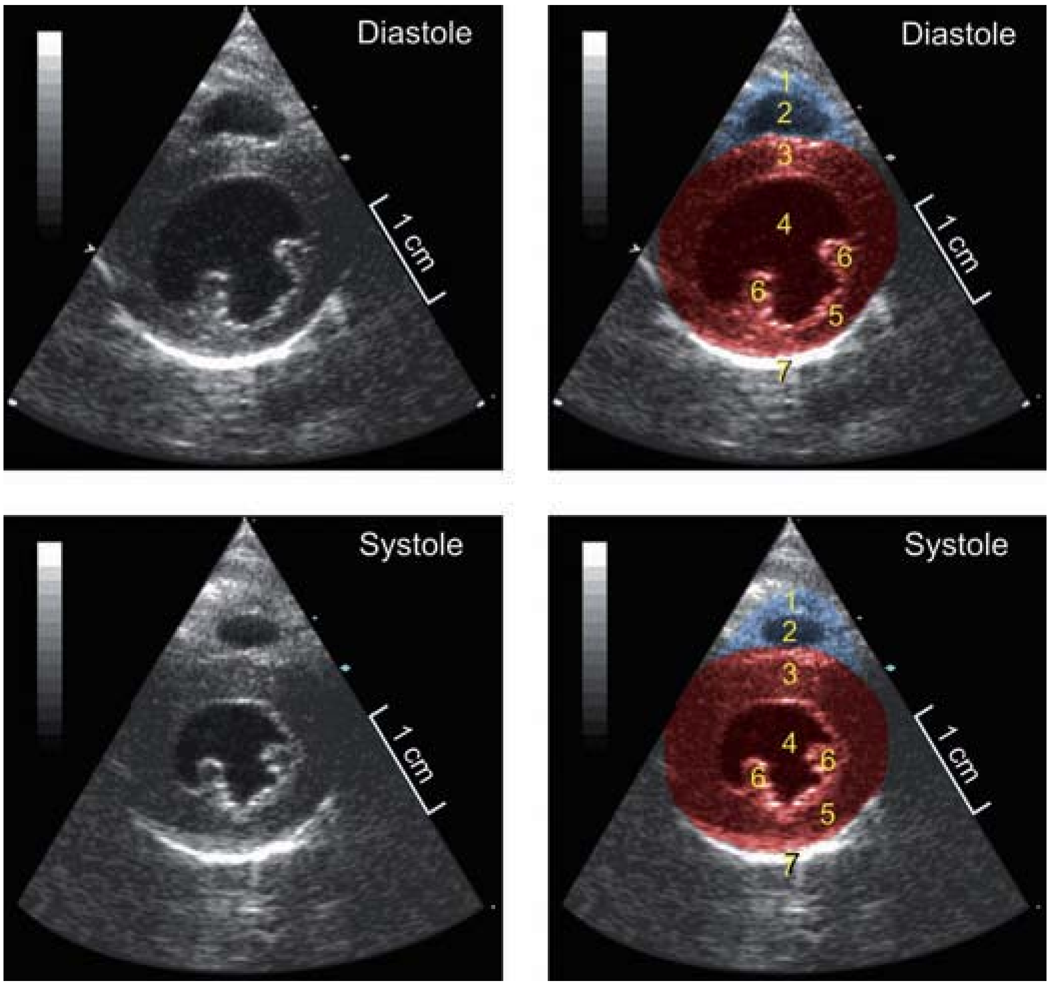

1: right myocardium
2: right ventricle
3: interventricular septum
4: left ventricle
5: left myocardium
6: papillary muscle
7: pericardium

Fig. 2-56: 2D echocardiographic images of a ferret, 12 MHz, end-diastolic and end-systolic, right parasternal short-axis view at the level of the papillary muscle.

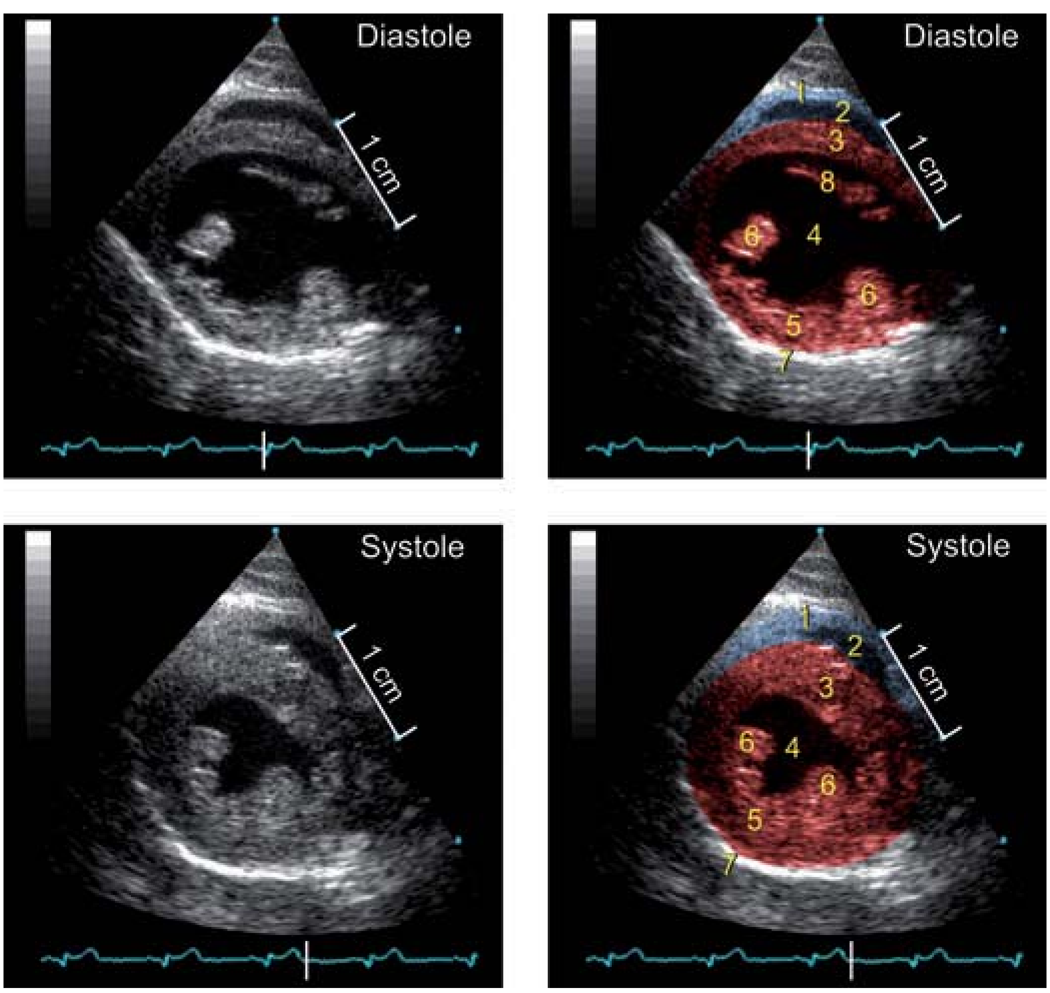

1: right myocardium
2: right ventricle
3: interventricular septum
5: left myocardium
6: papillary muscle
7: pericardium
8: chordae tendineae

Fig. 2-57: 2D echocardiographic images of a rabbit, 12 MHz, end-diastolic and end-systolic, right parasternal short-axis view at the level of the papillary muscle. The papillary muscle (6) appears thinner, especially during diastole, and projects further into the left ventricle (4) than in the ferret.

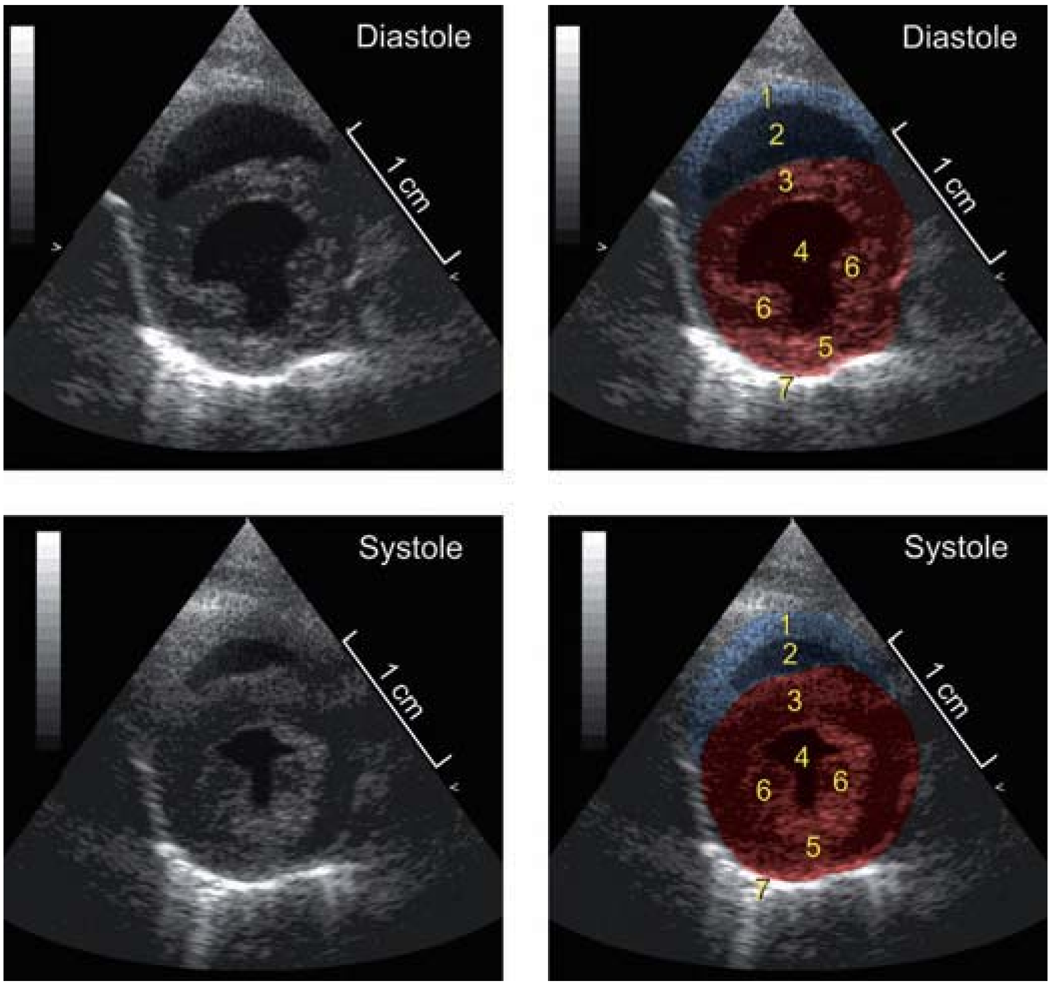

1: right myocardium
2: right ventricle
3: interventricular septum
4: left ventricle
5: left myocardium
6: papillary muscle
7: pericardium with reverberations attached to it in the form of »comet-tail« artifacts

Fig. 2-58: 2D echocardiographic images of a guinea pig, 12 MHz, end-diastolic and end-systolic, right parasternal short-axis view at the level of the papillary muscle.

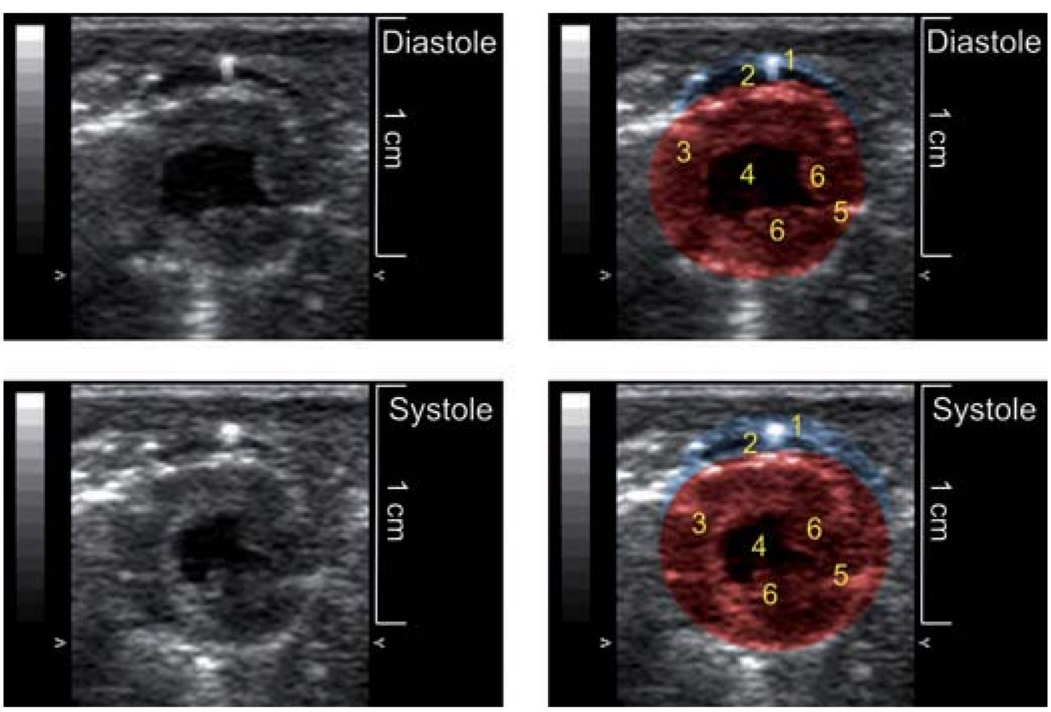

1: right myocardium
2: right ventricle
3: interventricular septum
4: left ventricle
5: left myocardium
6: papillary muscle

Fig. 2-59: 2D echocardiographic images of a degu using a linear array transducer, 15 MHz, diastolic and systolic, right parasternal short-axis view at the level of the papillary muscles.

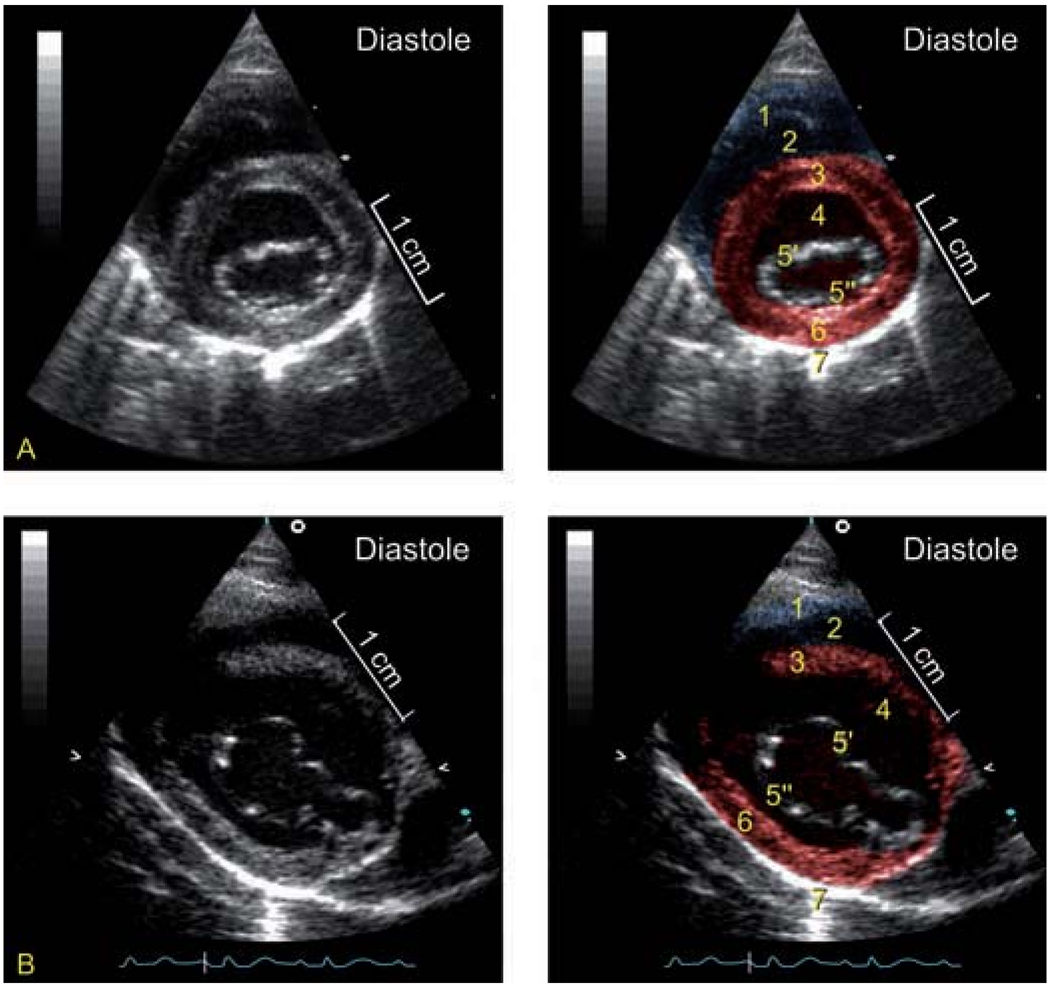

1: right myocardium
2: right ventricle
3: interventricular septum
4: left ventricle
5’: anteriomedial leaflet
5’’: posteriolateral leaflet of the mitral valve
6: left myocardium
7: pericardium

Fig. 2-60: 2D echocardiographic images, 12 MHz, mid-diastolic, right parasternal short-axis view at the level of the half-opened mitral valve, (A) ferret, (B) rabbit. With ultrasonography, the smooth leaflets of the mitral valve in the ferret (A: 5’, 5’’), are similar to those in the dog, whereas the leaflets of the rabbit mitral valve (B: 5’, 5’’) are long and »wavy«.

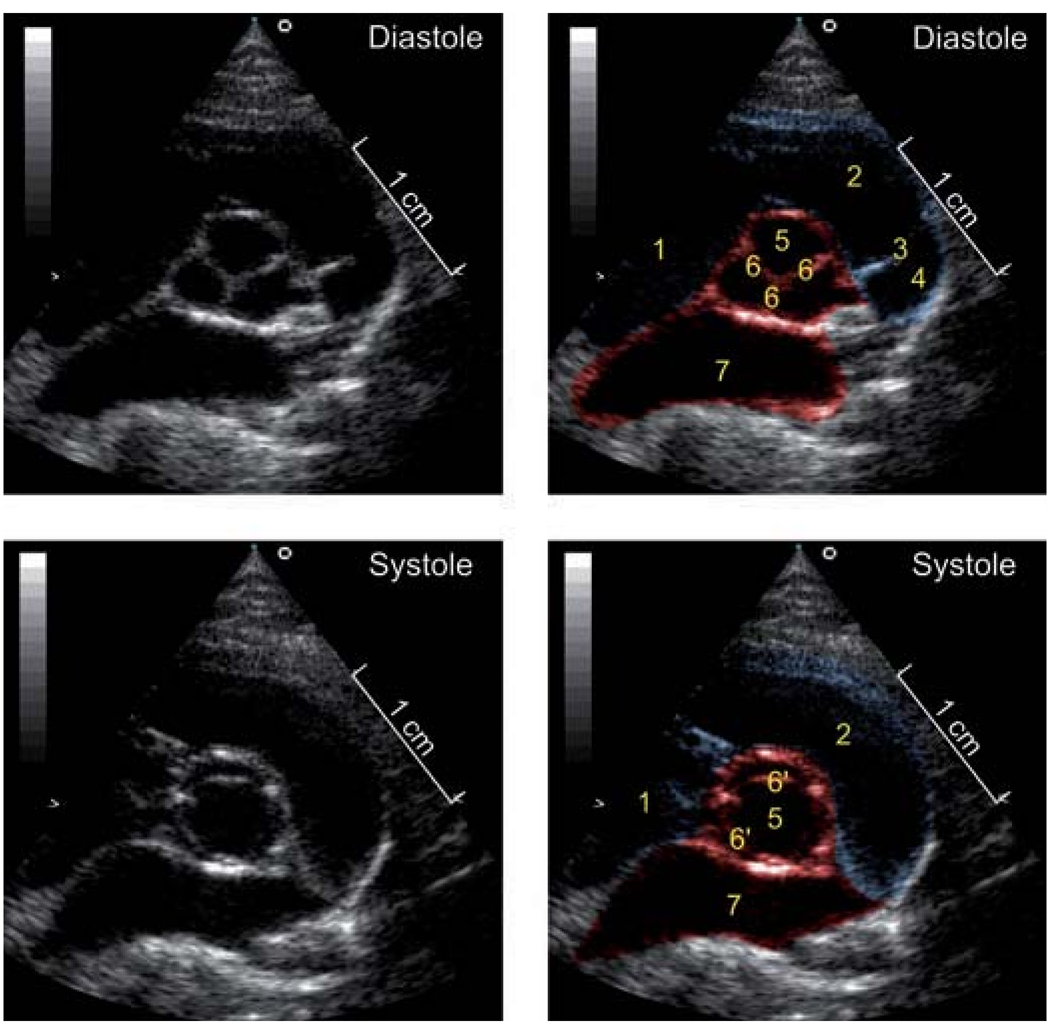

1: right atrium
2: right ventricle
3: closed pulmonary valve
4: pulmonary trunk
5: aorta
6: closed aortic valve
6’: half-opened aortic valve
7: left atrium

Fig. 2-61: 2D echocardiographic images of a ferret, 12 MHz, end-diastolic and early diastolic, right parasternal short-axis view at the level of the aortic valve and pulmonary valve.

Left apical views

The position of the transducer for the apical views is the left parasternal window, roughly at the level of the apex beat. The imaging of the heart is performed »upside-down«; i.e., in the longitudinal axis from the heart's apex (top of the picture) to the heart's base (bottom). There are five different views: four-chamber view, left ventricular and right ventricular two-chamber views, five-chamber view, and three-chamber view. Good apical ultrasonographic images of the heart are only successful on a routine basis in the ferret and rabbit, and the left apical views are part of the regular echocardiographic examination in both species. However, the desired apical standard planes cannot always be positioned in the middle of the picture and are displaced either to the right or left edge of the image. In the guinea pig, the apical views from the left can often only be achieved by using a significant amount of time. In addition, the quality and reliability of the apical images from the left are variable. These problems often discourage examinations from the left in guinea pigs or other small exotic pet mammals, apart from in ferret and rabbit patients. In such cases, Doppler assessment of blood flow has to be performed in views from the right.

1. Apical four-chamber view
(**Fig. 2-62**)

Left	Middle	Right
□ right ventricle	□ intraventricular septum	□ left ventricle
□ tricuspid valve		□ mitral valve
□ right atrium	□ intra-atrial septum	□ left atrium

After the transducer has been placed on the left parasternal window at the level of the apex beat, the transducer orientation marker is turned dorsally for the apical four-chamber view with the transducer being tipped in a somewhat cranial direction. This standard plane is suitable for assessing the size relationships of the structures of the right and left heart. In addition, this view forms the basis for Doppler investigations of the right and left ventricular in-flow tracts through the tricuspid or mitral valve, respectively. The volume of the left ventricle can also be determined in the four-chamber view (or in the two-chamber view; see 4 below) of the left chamber with the help of the monoplane slice summation method according to SIMPSON.

2. Apical five-chamber view

Left	Middle	Right
□ right ventricle	□ intraventricular septum	□ left ventricle
□ tricuspid valve	□ aortic valve	□ mitral valve
□ right atrium	□ ascending aorta	□ left atrium

In the majority of cases being examined, this view can be ignored because it either provides images with an inadequate quality or it is very time-consuming.

3. Apical right ventricular two-chamber view

- □ right ventricle
- □ tricuspid valve
- □ right atrium

4. Apical left ventricular two-chamber view

- □ left ventricle
- □ mitral valve
- □ left atrium

The apical left ventricular two-chamber view can be developed out of the four-chamber view by a slightly redirecting the scanning plane into a more caudal direction (i.e., without having to turn the probe). The right ventricle is usually just visible using this view.

All apical two-chamber views (of the right and left heart) are perfectly suitable for two- and one-dimensional color Doppler of the right and left ventricular in-flow tracts and the measurement of the respective blood flow velocities with PW and CW Doppler. Care should be taken that the course of the sonographic waves is parallel to the in-flow tract.

5. Apical three-chamber view
(**Fig. 2-63**)

Left	Right
□ left ventricle, out-flow tract	□ left ventricle, in-flow tract
□ aortic valve	□ mitral valve
□ ascending aorta	□ left atrium

This standard plane is developed from the apical four-chamber view either by slightly tilting the transducer or by turning the transducer 90° counterclockwise. In the first case, the transducer orientation marker points dorsocaudally, in the second in the caudal direction. The apical three-chamber view serves mainly for color-coded and conventional Doppler imaging of the blood flow in the left ventricular out-flow tract and the blood flow through the aortic valve into the ascending aorta. Often a parallel view of the out-flow current is achieved only when the aorta lies directly on the left edge of the ultrasonographic image.

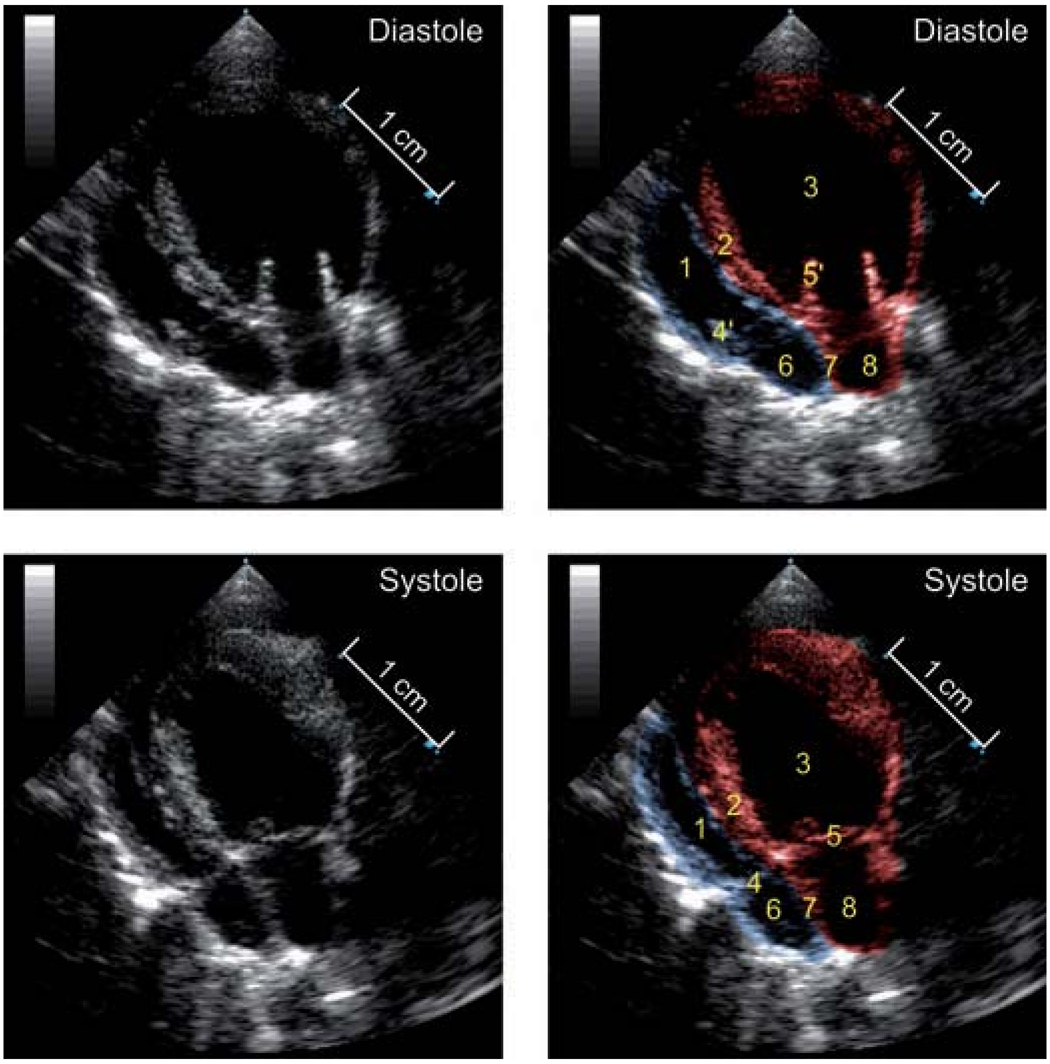

1: right ventricle
2: interventricular septum
3: left ventricle
4: closed tricuspid valve
4': opened tricuspid valve
5: closed mitral valve
5': opened mitral valve
6: right atrium
7: interatrial septum
8: left atrium

Fig. 2-62: 2D echocardiographic images of a ferret, 5 MHz, end-diastolic and mid-systolic apical four-chamber view from the left.

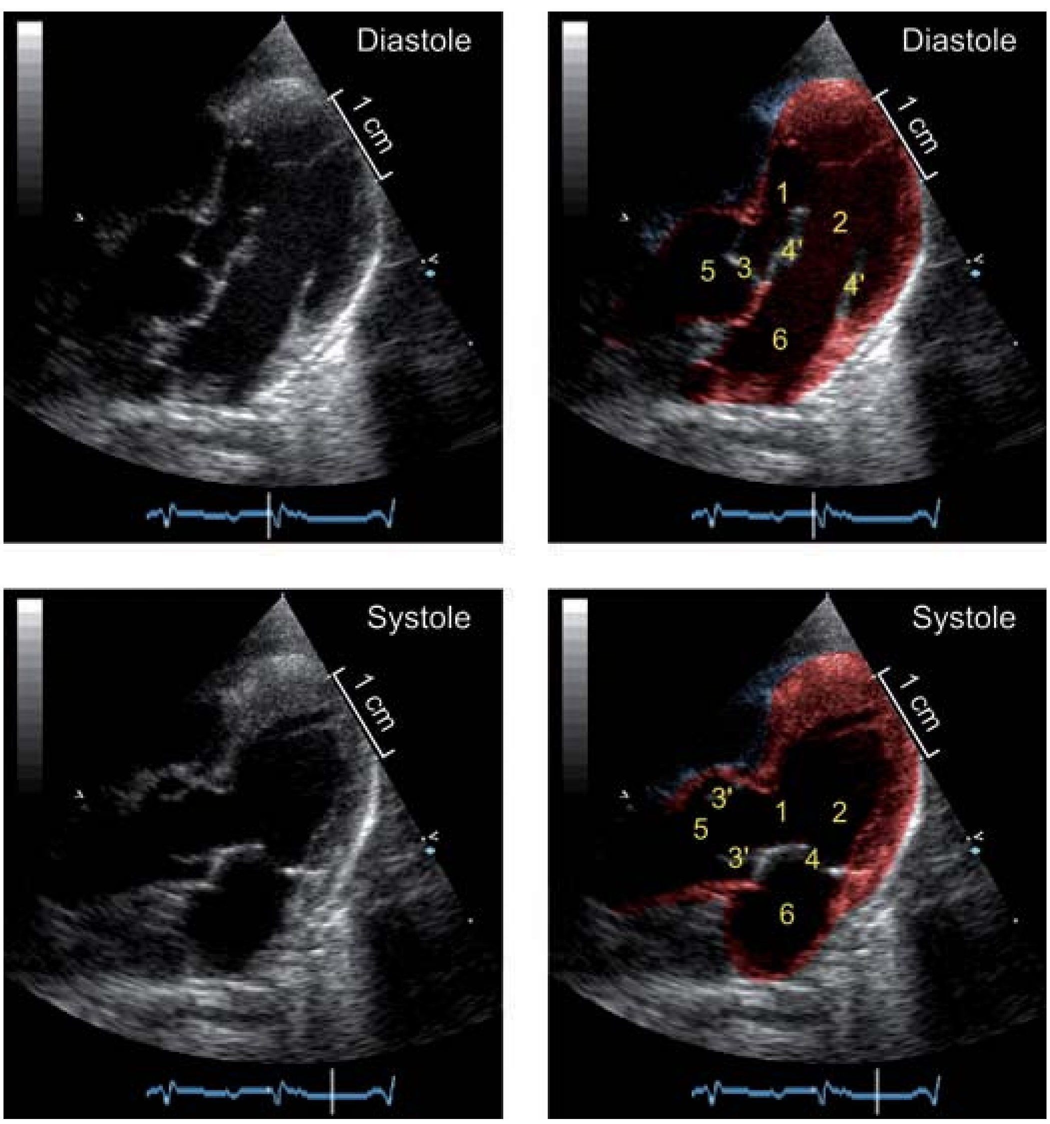

1: left ventricle, out-flow tract
2: left ventricle, in-flow tract
3: closed aortic valve
3': opened aortic valve
4: closed mitral valve
4': opened mitral valve
5: aortic sinus
6: left atrium

Fig. 2-63: 2D echocardiographic images of a rabbit, 10 MHz, end-diastolic and early systolic apical three-chamber view from the left.

Left parasternal, cranial view

For imaging the right ventricular conus arteriosus, the pulmonary valve, and the pulmonary trunk, the transducer is placed in a relatively distant cranial position on the left parasternal window. The transducer orientation marker points in the dorsal direction. The right ventricular out-flow through the pulmonary valve into the pulmonary trunk can be evaluated using color Doppler and is measured with either PW or CW Doppler in this plane. This evaluation often takes a great deal of time to achieve, even in ferret and rabbit patients. Usually, the view from the left does not need to be performed as the blood flow through the pulmonary valve can be judged more easily and quickly in the third parasternal short-axis view from the right.

Subcostal view

The transducer is placed caudal to the costal arch, directly to the right of the xiphoid cartilage (rarely to the left). The sonic cone is then directed flatly in a cranial direction. The heart is imaged from the apex through the liver and diaphragm. The blood flow in the left ventricular out-flow tract can be evaluated extremely well through the aortic valve and in the ascending aorta using this view. As a consequence, this standard plane is utilized in the dog to assess the severity of a subvalvular aortic stenosis. Although the small exotic mammals have significantly less body size and the distance between the transducer placed in the subcostal area and the heart apex is shorter than in dogs and cats, this view can only be achieved after a long search even in ferret and rabbit patients. If a gas-filled stomach lies between the transducer and heart, a diagnostic image using the subcostal view of the heart cannot be achieved. Generally, the examiner can evaluate the blood flow through the aortic valve using the apical three-chamber view.

2.4.2.5 One-dimensional echocardiography – M-mode

As described above, one-dimensional echocardiography often provides a quicker, more thorough result in the common small exotic pet mammals than 2D echocardiography due to its higher temporal resolution. However, the M-mode must be recorded directly and not calculated from 2D B-mode data (i.e., offline). In comparison to the origin of the aorta, the M-mode echocardiograms of the left ventricle, mitral valve, aorta, and left atrium are developed from the respective 2D parasternal views from the right (i.e., the sonic line is placed exactly in the 2D B-image). Originally, one-dimensional echocardiograms were produced from the right parasternal long-axis view; however, as the M-mode echocardiograms of the parasternal long- and short-axis views are comparable and provide similar measurements, it is acceptable to produce one-dimensional echocardiograms in small mammals using the easier short-axis views. Reference values in the literature are not usually separated into long- and short-axis M-mode echocardiograms.

The two minimum requirements placed on M-mode echocardiogram quality are that the M-mode line must be perpendicular to the structures being imaged and that there is a clear identification of the boundary surfaces. The white echogenic endocardium of the intraventricular septum, myocardium, and valve echoes must be clearly visible.

M-mode of the left ventricle
(**Fig. 2-64**)

This one-dimensional echocardiogram is scanned from the right parasternal long-axis view, directly cranial to the papillary muscle, or from the right parasternal short-axis view at the level of the papillary muscles. The M-mode of the left ventricle serves to assess both diastole and systole, and is used for the measurement of the intraventricular septum, left ventricle, and myocardium. The M-mode line must lie cranial to the papillary muscles in the long-axis view and be between the papillary muscles lying at 5 and 7 o'clock in the short-axis view.

M-mode of the mitral valve
(**Fig. 2-65**)

The typical M-mode echocardiogram of the mitral valve is taken either in the right parasternal long-axis view at the level of the septal cusp of the mitral valve or in the right parasternal short-axis view at the level of mitral valve. In the majority of cases, this scan shows an E-wave during early diastolic opening and an A-wave as an expression of the end-diastolic opening of the mitral valve during atrial contraction.

M-mode of the aortic valve and left atrium
(**Fig. 2-66**)

The combined imaging of the aortic valve and the left atrium is usually performed with relatively few problems using the right parasternal long-axis view in small exotic pet mammals, occasionally with less effort than in some dogs. An M-mode echocardiogram is easily performed allowing for a comparison of the end-diastolic size of the aortic base and end-systolic size of the left atrium.

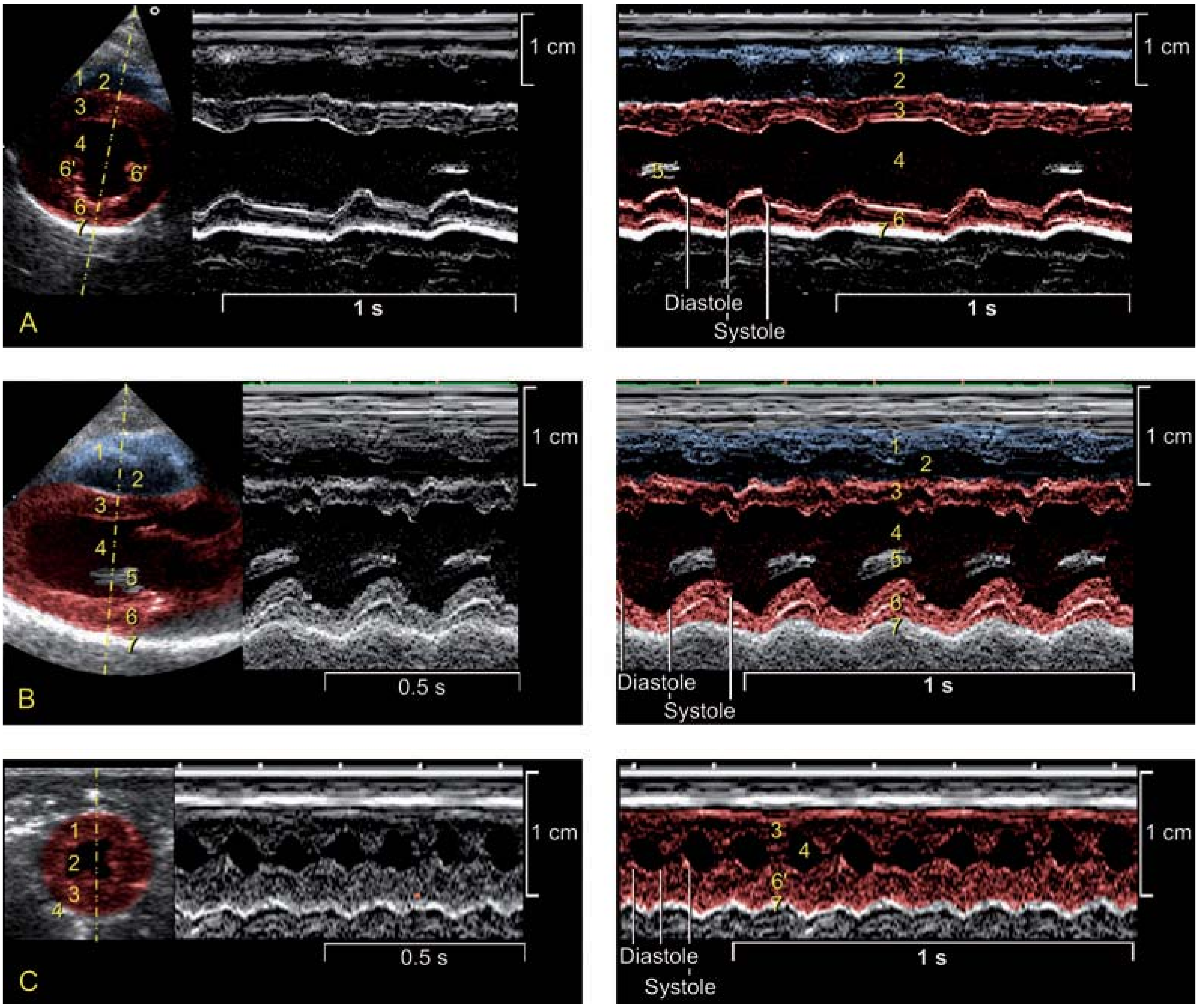

Fig. 2-64: M-mode echocardiograms of the left ventricle at the level of the papillary muscle, 12–15 MHz.

A: 12 MHz. Ferret: M-mode from the right parasternal short-axis view. The chordae tendineae (5) are rarely recognized in the M-mode.

B: 12 MHz. Rabbit: M-mode from the right parasternal long-axis view.

C: 15 MHz. Degu: M-mode produced using a linear array transducer from the right parasternal short-axis view. As the M-mode beam goes through a papillary muscle (6') when using this technique, the thickness and contractibility of the left myocardium is overestimated.

1: right myocardium
2: right ventricle
3: interventricular septum
4: left ventricle
5: chordae tendineae
6: left myocardium
6': papillary muscle
7: pericardium

dashed yellow line: M-mode line = area in which the M-mode echocardiogram was taken

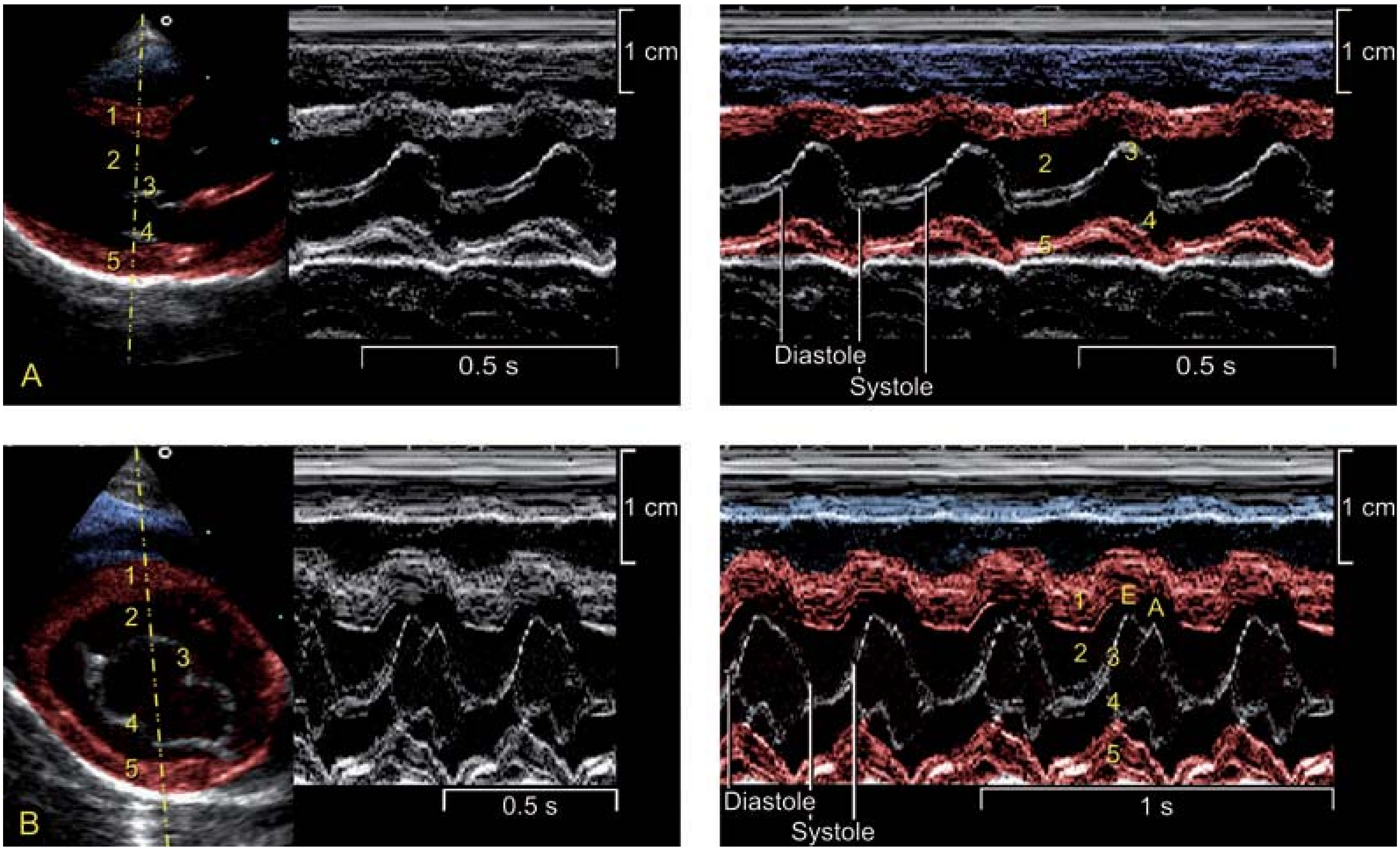

Fig. 2-65: M-mode echocardiograms of a rabbit taken at the level of the mitral valve, 12 MHz.

A: M-mode from the right parasternal long-axis view.

B: M-mode from the right parasternal short-axis view.

While in Fig. A the E and A waves have almost transposed, both waves are obviously separate in Figure B.

1: interventricular septum
2: left ventricle
3: anteriomedial leaflet of the mitral valve
4: posteriolateral leaflet of the mitral valve
5: left myocardium

E: E-wave = early diastolic opening of the mitral valve
A: A-wave = late diastolic opening of the mitral valve during atrial contraction

dashed yellow line: M-mode line = area in which the M-mode was obtained

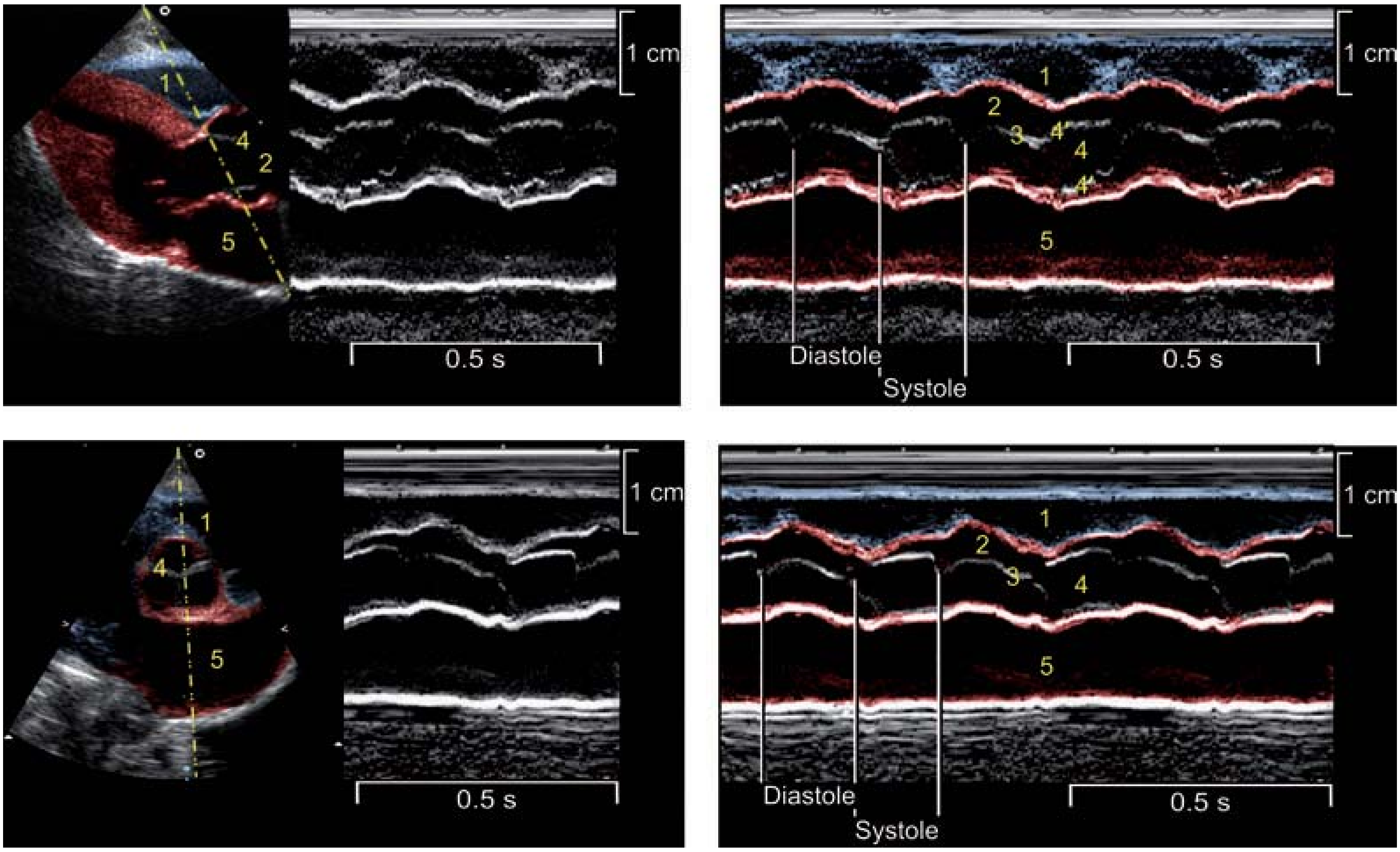

Fig. 2-66: M-mode echocardiograms of a rabbit taken at the level of the left atrium, aortic valve, and pulmonary valve.

A: 12 MHz, M-mode echocardiogram from the right parasternal long-axis view. The opened semi-lunar valves (4') of the aorta show a fluttering movement in this projection.

B: 8.5 MHz, M-mode echocardiogram from the right parasternal short-axis view.

M-mode imaging can be performed in both the ferret and rabbit from the long and short axes. In both cases, the relationship between the size of the end-systolic atrium (5) and end-diastolic diameter of the aorta (2) are comparable.

1: right ventricle
2: aortic sinus
3: closed aortic valve
4: opened aortic valve
4': semilunar valve with fluttering movement
5: left atrium

dashed yellow line: M-mode line = area in which the M-mode echocardiogram was obtained

2.4.2.6 Doppler echocardiography

The use of color-coded and conventional Doppler techniques is indispensable when evaluating cardiac hemodynamics. This imaging technology improves ones ability to diagnose, prognose, and evaluate treatment response even in small exotic mammals. It has been determined through clinical experience that one should primarily use 2D color Doppler. Moreover, with small exotic pet mammals, the color-coded M-mode is recommended. Thus, information about blood flow directions, rough estimates of blood flow velocities, and the localization of turbulence can be collected in a relatively short period of time. The next step in a color Doppler scan is recording the placement of the sonic line for the PW and CW Doppler and the respective curves for quantification of the blood flow. There is a general consensus that blood flow velocities can only be adequately determined when the direction of blood flow and the distribution of the ultrasound waves are almost parallel. An angle correction, which is frequently recommended and used for other body areas with conventional Doppler ultrasonography, should not be employed when performing a Doppler examination of the heart. Imaging of the various cardiac blood flow tracts is accomplished using predetermined standard planes (see above). Left and right ventricular in-flow tracts through the mitral or tricuspid valve are best recorded using the respective apical two-chamber view. The left ventricular out-flow, through the aortic valve, can be imaged with Doppler echocardiography using the apical left ventricular three-chamber view. Blood flow through the pulmonary valve can be documented using the parasternal short-axis view from the right at the level of the aortic and pulmonary valves.

Two-dimensional color-coded Doppler echocardiography

(**Figs. 2-67** and **2-68**)

In small exotic mammals, color-Doppler scans are frequently less aesthetic or a number of heart phases are shown simultaneously in a single image, while others are not shown at all because of the small size of their cardiac structures and rapid heart rates. Consequently, an early systolic reflux through the atrioventricular valve is often overlooked in color Doppler scans. Despite the shortcomings mentioned above, all Doppler echocardiograms should begin with 2D color Doppler.

Color-coded M-mode

(**Figs. 2-69A–D**)

The assessment of short-term blood flows is more reliable with color-coded M-mode (one-dimensional) echocardiography because its temporal resolution is much better than that of the color Doppler. The duration of normal and pathological blood flows can be determined easily and in greater detail with color-coded M-mode echocardiography. In addition, the changes in velocity of the blood flow along the M-mode line can be approximated (e.g., from the heart's apex to base and within the atrium). As a result of the information one can obtain using the aesthetic one-dimensional echocardiogram and the lack of problems associated with gathering this data, color-coded M-mode echocardiograms are highly recommended for small exotic mammals.

PW and CW Doppler echocardiography

(**Figs. 2-70A–D**)

The recording of the Doppler curves is usually achieved without difficulty in all small exotic pet mammals. PW and CW Doppler echocardiography provides excellent information in these animals because of the relatively superficial location and small area of blood flow at the locations examined. A rapid feed rate of 100 cm/s or 200 cm/s improves ones ability to evaluate the curves. In PW Doppler, the measurement volume should be adapted to the small size of the patient's heart and maintained at the lowest possible setting.

Normal, relatively slow blood flows are best determined using PW Doppler methods, while faster blood flows (e.g., stenoses) are better imaged with CW Doppler methods. Also the simultaneous recording of normal flow and regurgitation can be achieved with CW Doppler (**Fig. 2-71**). The flow pattern and blood flow velocities through the atrioventricular and other valves in small exotic mammals are the same or similar to those found in dogs and cats.

2.4.2.7 Measurements and reference values

The basic prerequisite for obtaining reliable measurements is the production of good quality one- and/or two-dimensional B-mode scans as well as conventional Doppler echocardiograms which are as artifact free as possible. If this basic prerequisite is not achievable, then the so-called »eyeball method« can be used as an alternative option. The »eyeball method« is a pure visual assessment of estimating left ventricular function and morphology. The majority of clinically significant heart anomalies can be reliably diagnosed with the aid of the sonographic methods presented here without measurements. The severity of heart anomalies should be judged based on the presence or absence of secondary anatomical and/or physiological changes. This is particularly true as echocardiography forms only part of the clinical examination of the heart.

As the majority of small exotic pet mammals have been used as animal models in human cardiology investigations, there are many, and in part different, reference values available for these species. However, extrapolating these values for use in veterinary patients is often limited because important parameters such as breed, size, age, constitution, and the conditions of the investigation are not comparable. As a consequence, all examiners should decide for themselves how reliable their own measurements are when compared to those published as reference values.

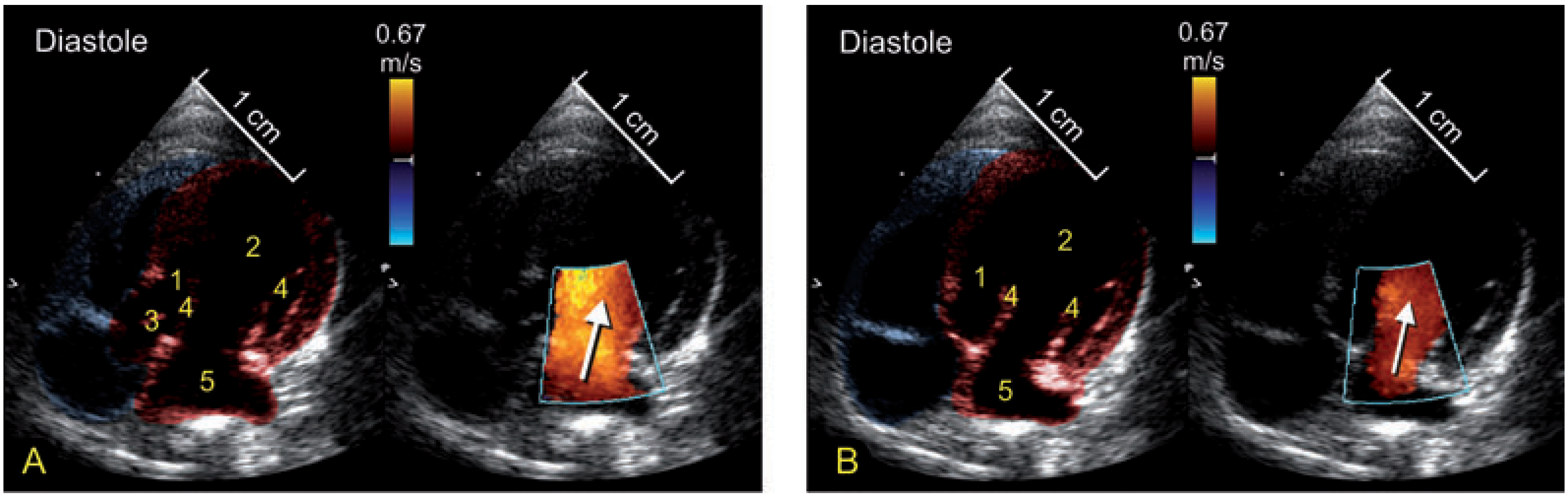

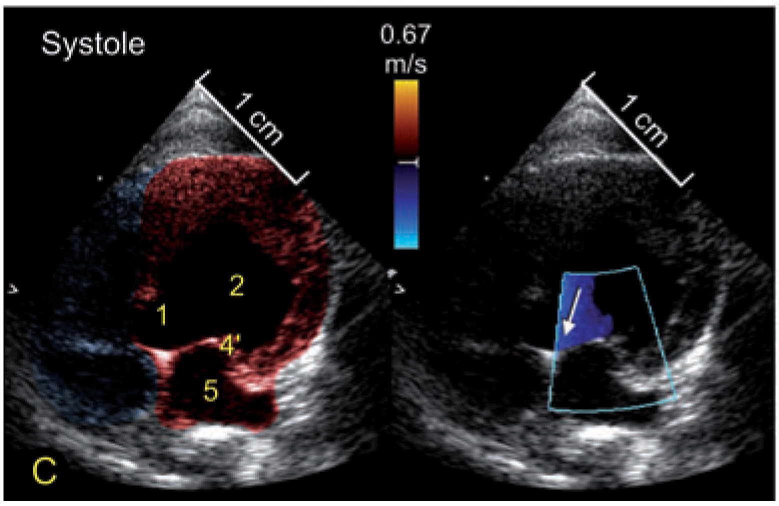

1: left ventricle, out-flow tract
2: left ventricle, in-flow tract
3: aortic valve
4: opened mitral valve
4': closed mitral valve
5: left atrium

Fig. 2-67: Color-coded Doppler echocardiographic images of a ferret showing the blood flow in the left ventricle, left apical three-chamber view.

A: Early diastolic, passive, light red-coded, broad blood flow in the left ventricle with a wide-open mitral valve.

B: Late diastolic, dark red-coded, narrow blood flow in the left ventricle during atrial contraction.

C: Hemodynamically insignificant, early diastolic blue-coded reflux in the left atrium.

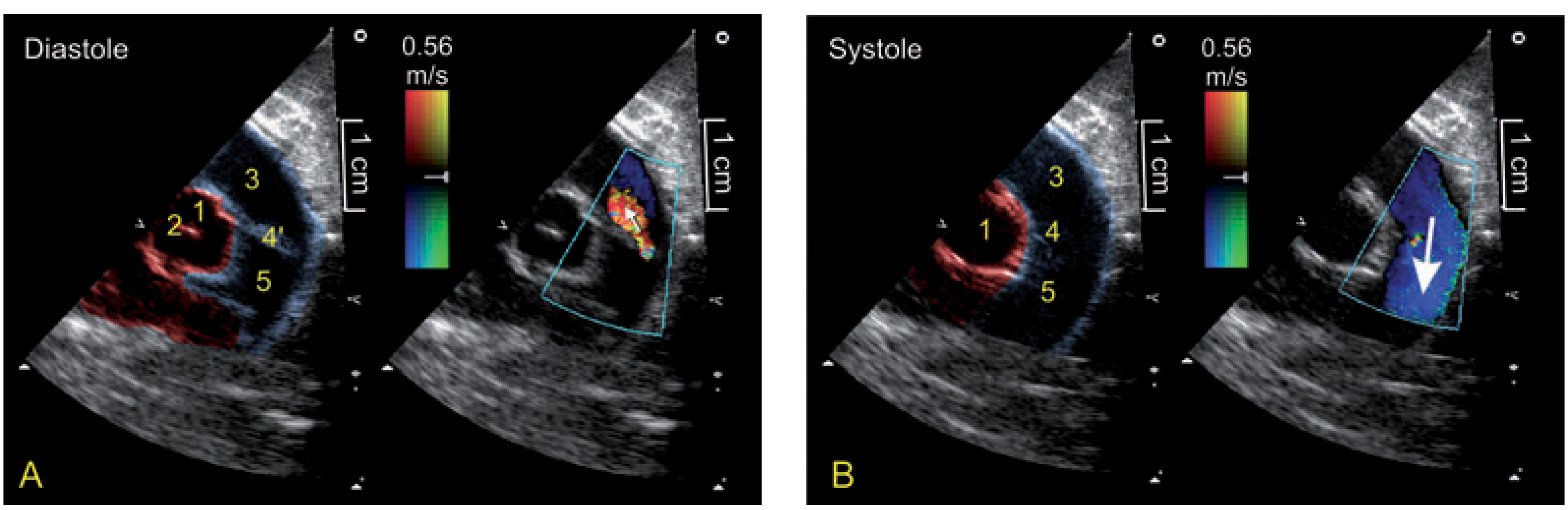

Fig. 2-68: Color-coded Doppler echocardiographic images of a rabbit showing the flow of blood from the right ventricle into the conus artery of the right ventricle and the pulmonary trunk, cranial left parasternal window.

A: Diastolic red-coded reflux through the closed pulmonary valve.

B: Systolic, normal, blue-coded blood flow in the right ventricle.

1: aorta
2: closed aortic valve, midline echo
3: right ventricle conus artery
4: opened pulmonary valve
4': closed pulmonary valve
5: pulmonary trunk

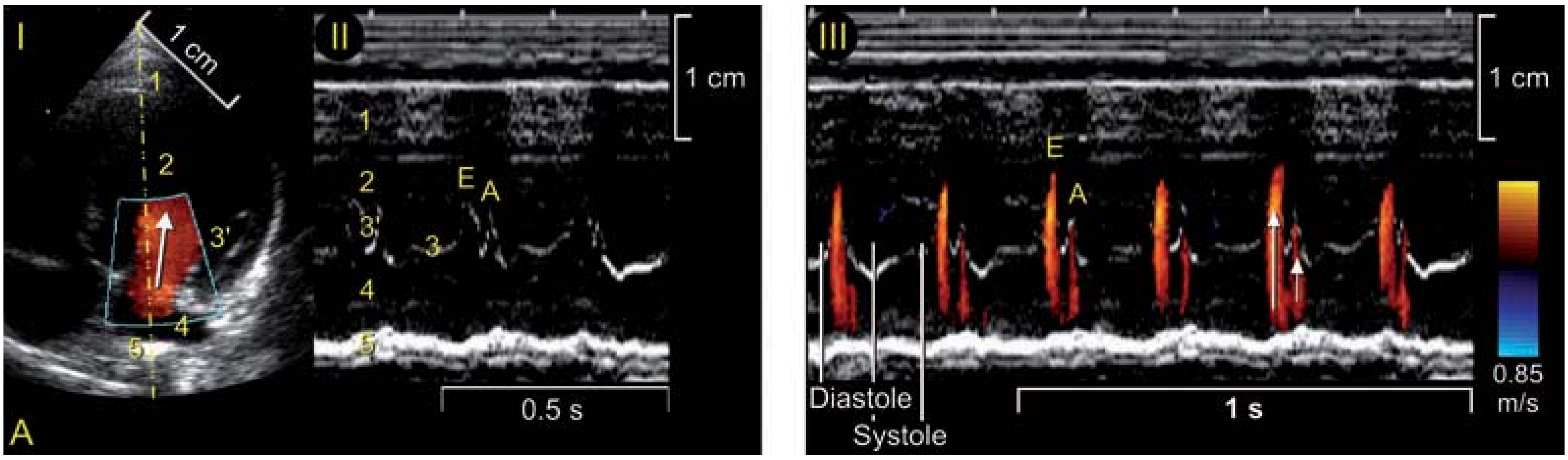

Fig. 2-69A: Color-coded M-mode echocardiograms of a ferret, apical three-chamber view from the left.

I: Color-coded 2D echocardiogram.
II: M-mode: closed and opened mitral valve.
III: Color-coded M-mode, blood flow from the left ventricle through the mitral valve.

1: myocardium, apex
2: left ventricle
3: closed mitral valve
3': opened mitral valve
4: left atrium
5: pericardium

(I) dashed yellow line: area in which the two M-mode echocardiograms were obtained.
E: E-wave = (II) early diastolic opening of the valve or (III) broad, light red-coded, early diastolic passive in-flow of blood
A: A-wave = (II) late diastolic opening of the valve or (III) narrow dark red-coded, late diastolic in-flow of blood during atrial contraction (I) dashed yellow line: area in which the two M-mode echocardiograms were obtained.

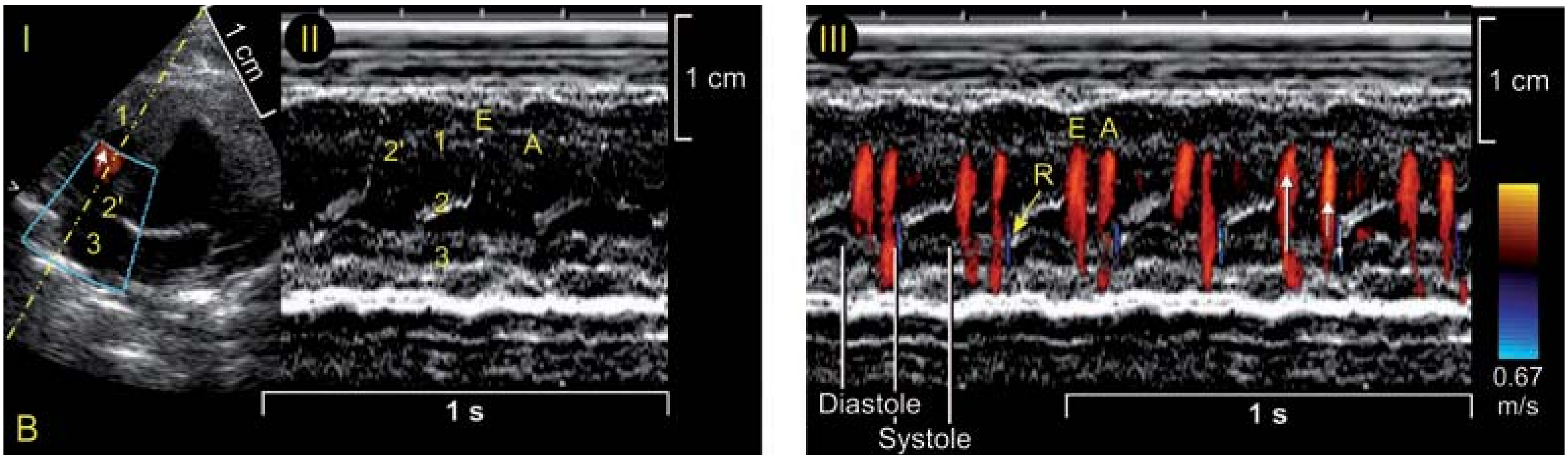

Fig. 2-69B: Color-coded M-mode echocardiograms of a ferret, apical four-chamber view from the left.

I: Color-coded 2D echocardiogram.
II: M-mode: closed and opened tricuspid valve.
III: Color-coded M-mode, blood flow from the right ventricle through the tricuspid valve.

1: right ventricle
2: closed tricuspid valve
2': opened tricuspid valve
3: right atrium

(I) dashed yellow line: area in which the two M-mode echocardiograms were obtained.
E: E-wave = (II) early diastolic opening of the valve or (III) red-coded, early diastolic passive in-flow of blood
A: A-wave = (II) late diastolic opening of the valve or (III) red-coded, late diastolic in-flow of blood during atrial contraction
R: early systolic, hemodynamically insignificant reflux.

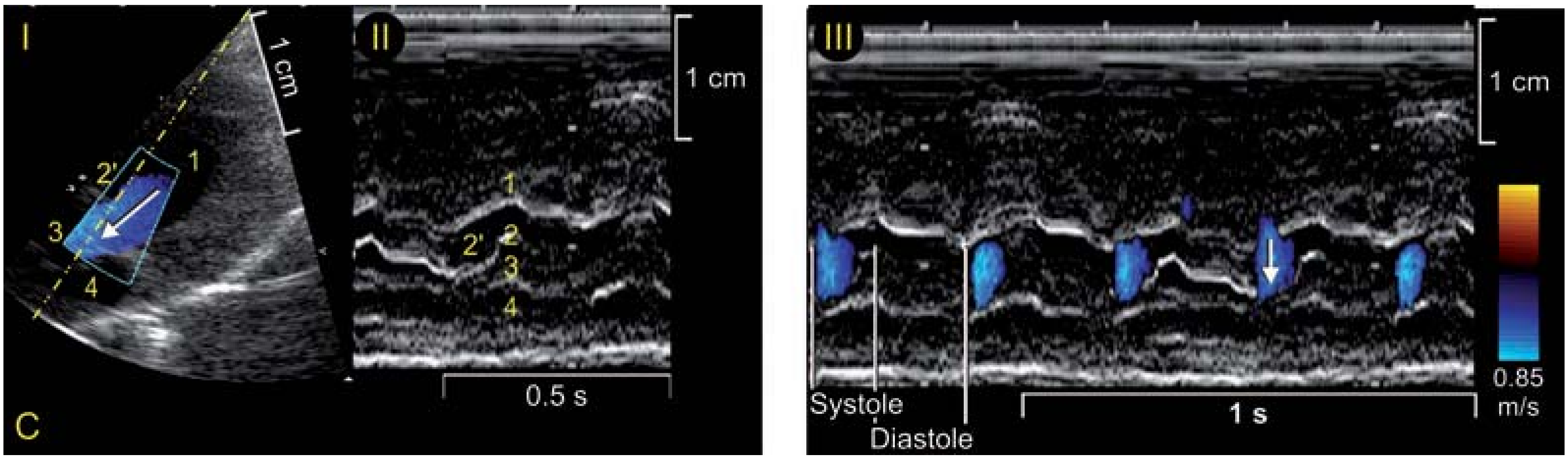

Fig. 2-69C: Color-coded M-mode echocardiograms of a ferret, apical two-chamber view from the left.

I: Color-coded 2D echocardiogram.
II: M-mode: closed and opened aortic valve.
III: Color-coded M-mode, blue-coded blood flow from the left ventricle through the aortic valve.

1: left ventricle
2: closed aortic valve
2': opened aortic valve
3: aortic sinus
4: left atrium

(I) dashed yellow line: area in which the two M-mode echocardiograms were obtained.

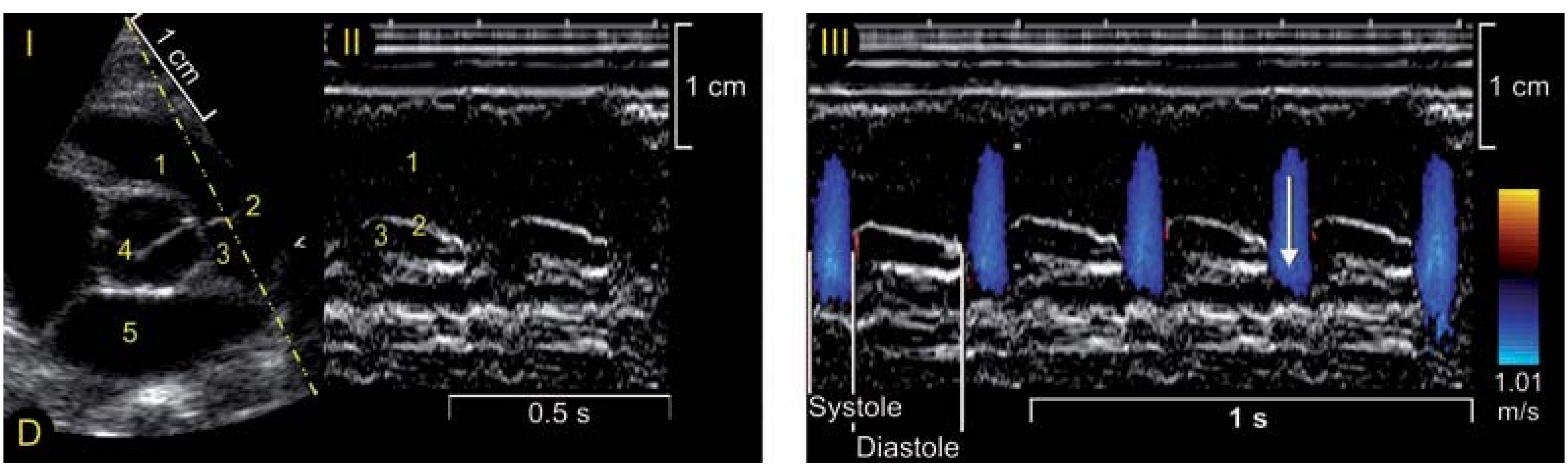

Fig. 2-69D: Color-coded M-mode echocardiograms of a ferret, right parasternal short-axis view at the level of the pulmonary valve.

I: 2D echocardiogram.
II: M-mode: closed and opened pulmonary valve.
III: Color-coded M-mode: blue-coded blood flow from the right ventricle through the pulmonary valve.

1: right ventricle, conus artery
2: closed pulmonary valve
3: pulmonary trunk
4: closed aortic valve
5: left atrium

(I) dashed yellow line: area in which the two M-mode echocardiograms were obtained

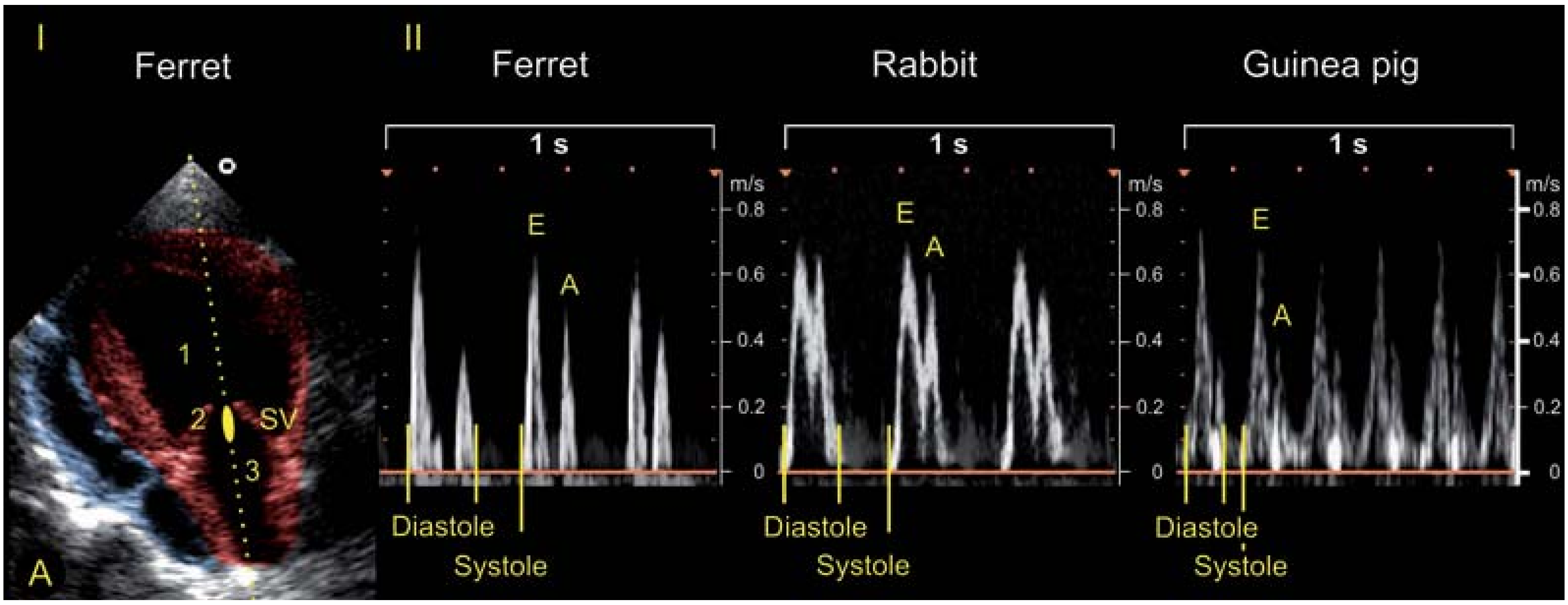

Fig. 2-70A: Image of the blood flow through the mitral valve using PW-Doppler echocardiography. The flow pattern and the rate of flow are similar in all small mammals.

I: 2D echocardiography, apical four-chamber view from the left.
II: PW-Doppler echocardiogram of the blood flow through the mitral valve. The early diastolic passive in-flow of blood (E) is usually quicker than the blood flow during atrial contraction (A).

1: left ventricle
2: half-opened mitral valve
3: left atrium

SV: yellow sample volume = area in which the PW-Doppler curves were recorded.

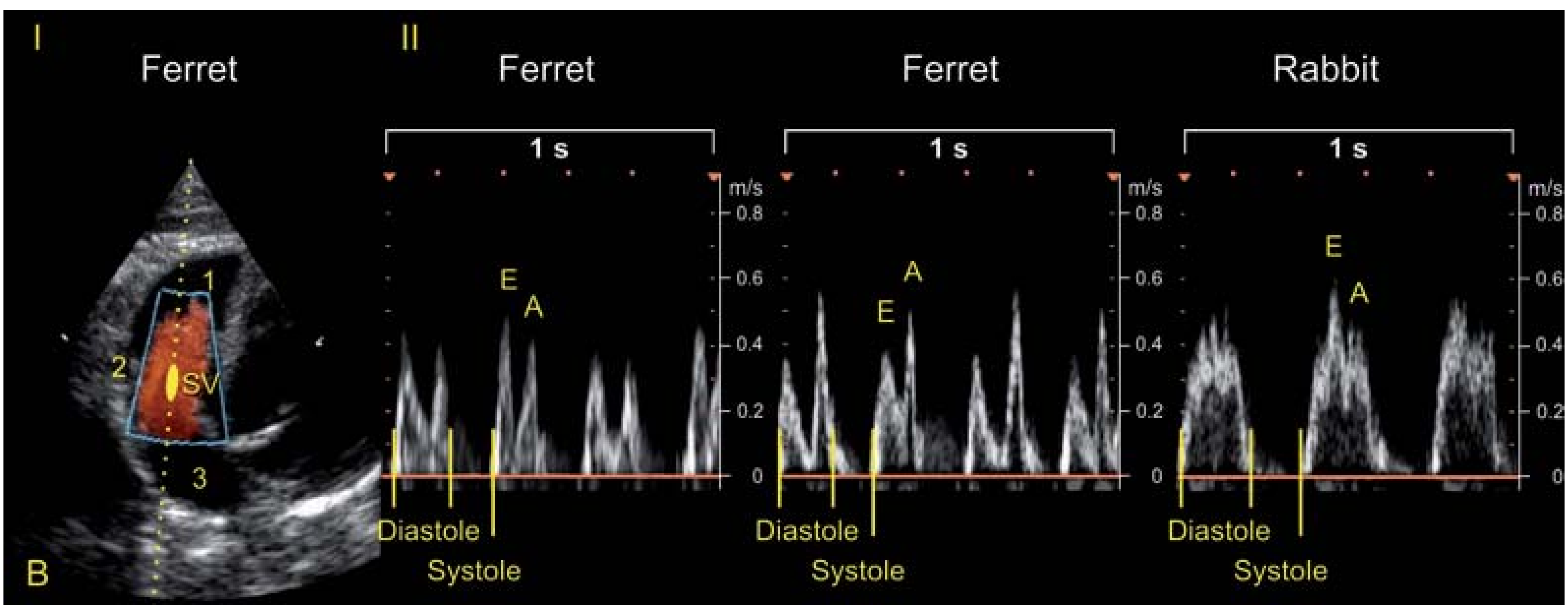

Fig. 2-70B: Image of the blood flow through the tricuspid valve using PW-Doppler echocardiography. The flow pattern and the rate of flow are similar in all small mammals.

I: Color-coded 2D Doppler echocardiography, apical two-chamber view from the left and red-coded in-flow of blood through the tricuspid valve.
II: PW-Doppler echocardiography of the blood flow through the tricuspid valve. The normal flow pattern of the in-flow of the right ventricle varies between individual animals. All three flow patterns can occur in the ferret, rabbit, and guinea pig. The speed and relation of E to A can vary even within an individual animal.

1: right ventricle
2': opened tricuspid valve
3: right atrium

SV: yellow sample volume = area in which the PW-Doppler curves were recorded

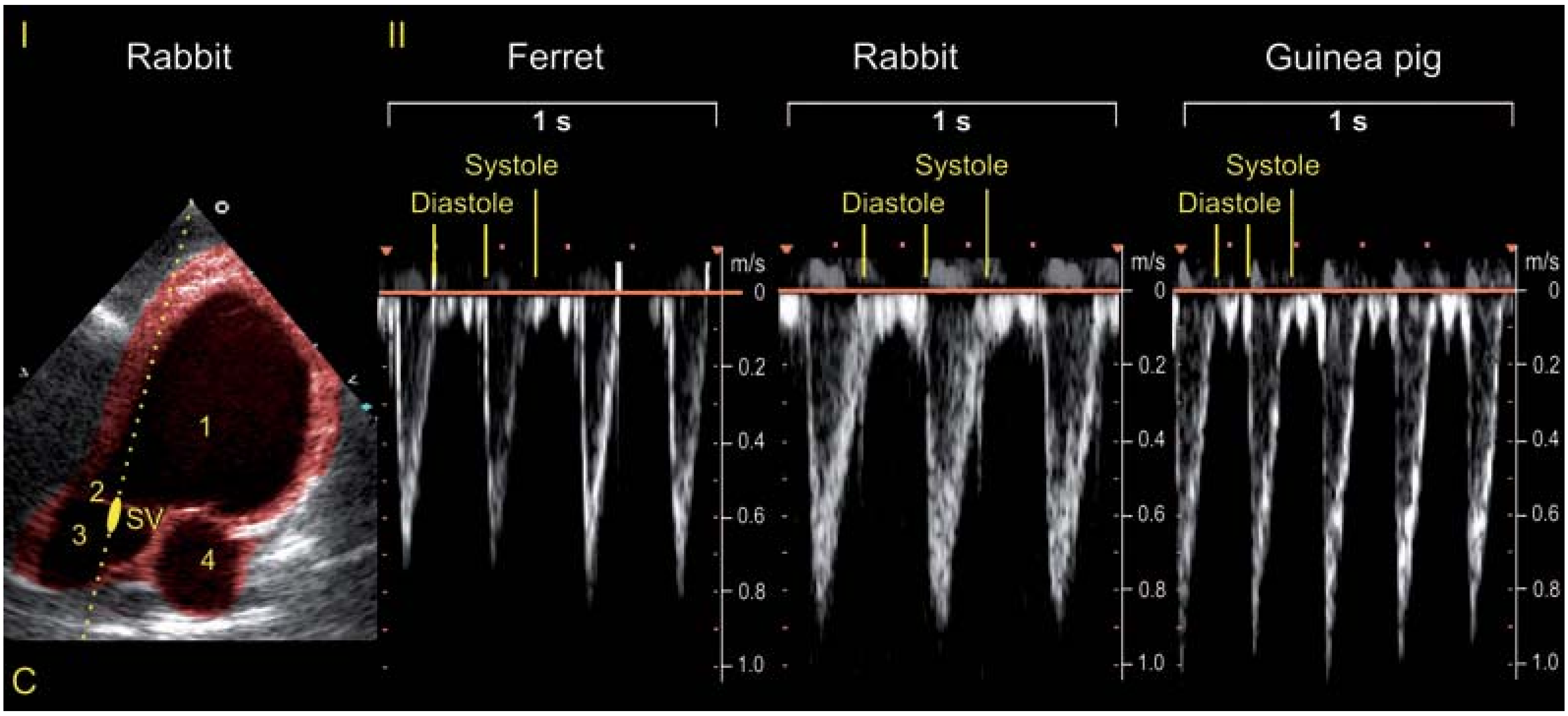

Fig. 2-70C: Image of the blood flow through the aortic valve using PW-Doppler echocardiography. The flow pattern and the rate of flow are similar in all small mammals.

I: 2D echocardiography, apical three-chamber view from the left.
II: PW-Doppler echocardiograms of the blood flow through the aortic valve. The velocity of the blood flow in the left ventricle is quicker than the normal blood flow in the right ventricle. The flow pattern looks like a right-angled triangle.

1: left ventricle
2: closed aortic valve
3: aortic sinus
4: left atrium

SV: yellow sample volume = area in which the PW-Doppler curves were recorded

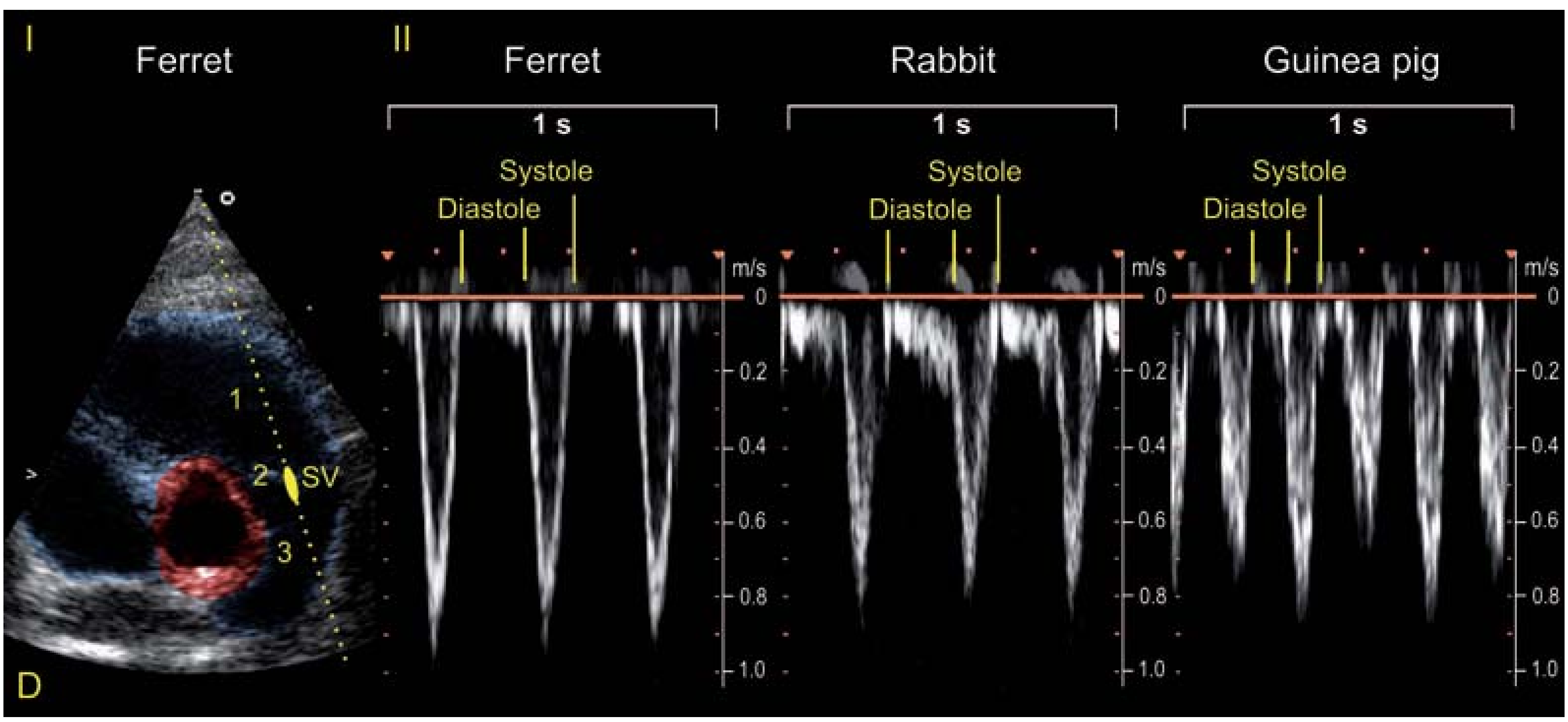

Fig. 2-70D: Image of the blood flow through the pulmonary valve using PW-Doppler echocardiography. The flow pattern and the rate of flow are similar in all small mammals.

I: 2D echocardiography, cranial left parasternal window.
II: PW-Doppler echocardiograms of the blood flow through the pulmonary valve. In comparison to normal out-flow of the left ventricle, the increase in velocity of the right ventricular out-flow is slower. The flow pattern looks like a narrow-angled isosceles triangle.

1: right ventricle, conus artery
2: closed pulmonary valve
3: pulmonary trunk

SV: yellow sample volume = area in which the PW-Doppler curves were recorded

2.4.2.8 Measurements in the M-mode and two-dimensional echocardiography

Measurements in the M-mode are normally prepared according to the Leading edge method; (i.e., the measurements of an echo are calculated from the side closest to the transducer to the leading edge of the following echo). In 2D echocardiography, the measuring cross can be placed directly on the echo (e.g., endocardium).

The morphology of the left ventricle is routinely determined according to TEICHHOLZ (**Fig. 2-72**). The percentage of systolic shortening of the left ventricle diameter (fractional shortening = FS [%]) and the ejection fraction (EF [%]) both provide evidence regarding systolic function of the left chamber.

$$FS\ [\%] = \frac{LVDd - LVDs}{LVDd} \times 100$$

$$EF\ [\%] = \frac{LVVd - LVVs}{LVVd} \times 100$$

(LVD = left ventricular diameter, LVV = left ventricular volume, d = diastolic, s = systolic)

The systolic fractional shortening is significantly influenced not only by cardiac contractility but also by the preload, afterload, and heart rate. The EF, which is calculated from the M-mode, is very inexact as the determination of volume using one-dimensional echocardiography is associated with substantial errors. For ferrets and rabbits (**Fig. 2-73A**), if not other small exotic mammals, it is more meaningful to measure and calculate the volume of the left ventricle or the EF using the monoplane summation method according to SIMPSON. This measurement is normally calculated from the left in the apical four- or two-chamber view. The distance between the intraventricular septum and the E-wave of the septal cusp of the mitral valve (EPSS = E-point to septal separation) is determined in the M-mode scan that is normally performed in the parasternal long-axis view from the right, more rarely in the short-axis view at the level of mitral valve (**Fig. 2-73B**). An enlarged EPSS indicates the presence of an end-systolic volume overloading of the left ventricle.

The measurements and evaluation of the left atrium are not uniform. The basis for determining the relationship of the left atrium to the base of the aorta is primarily the M-mode at the level of the aortic valve, recorded in the parasternal long-axis view (**Fig. 2-74A**). The diameter of the atrium and aorta can be measured in the parasternal short-axis view at the level of the aortic valve and left atrium using either 2D echocardiography (**Fig. 2-74B**) or less often, the M-mode.

2.4.2.9 Measurements using PW and CW Doppler

The maximum velocities of early diastolic in-flow (E wave) and of blood flow during atrial contraction (A wave) are separately measured and evaluated for the left and right ventricular inflow tracts through the mitral or tricuspid valves, respectively (**Fig. 2-75A**). Normally, the early diastolic blood flow is quicker than that of the late diastolic. Changes in the normal relationship between the E and A waves can be indicative of difficulties in the in-flow of blood (diastolic dysfunction) (**Fig. 2-75B**). With increases in heart rate, the use of a too slow feed rate or changes in the location of the measuring volume can lead to a fusion of these two waves, which is characterized as an EA wave. The maximum velocities of the aortic and pulmonary blood flows are also determined (**Fig. 2-75C**). The severity of an AV valve insufficiency can be assessed from the color-coded regurgitation jet (**Fig. 2-75D**).

2.4.2.10 Special measurements and investigations

In addition to the standard measurements discussed above, there many other objective methods used to assess echocardiographic images. These other assessment methods all serve to evaluate the morphology of the cardiac structures as well as determining the systolic, diastolic, and overall function or dysfunction of the heart. For most small exotic pet mammals, which are also used as animal models in human cardiac research, there exist reference values for these rare measurements and investigations in which modern echocardiographic methods are employed such as 3D echocardiography (**Fig. 2-73B**), tissue Doppler, the degree of deformation, and the rate of deformation. However, when one considers the results from other clinical cardiology diagnostic test results, the echocardiographic methods and simple measurements presented here are adequate to provide a reliable diagnosis and prognosis for initiating a suitable treatment plan in the majority of small exotic mammal case presentations.

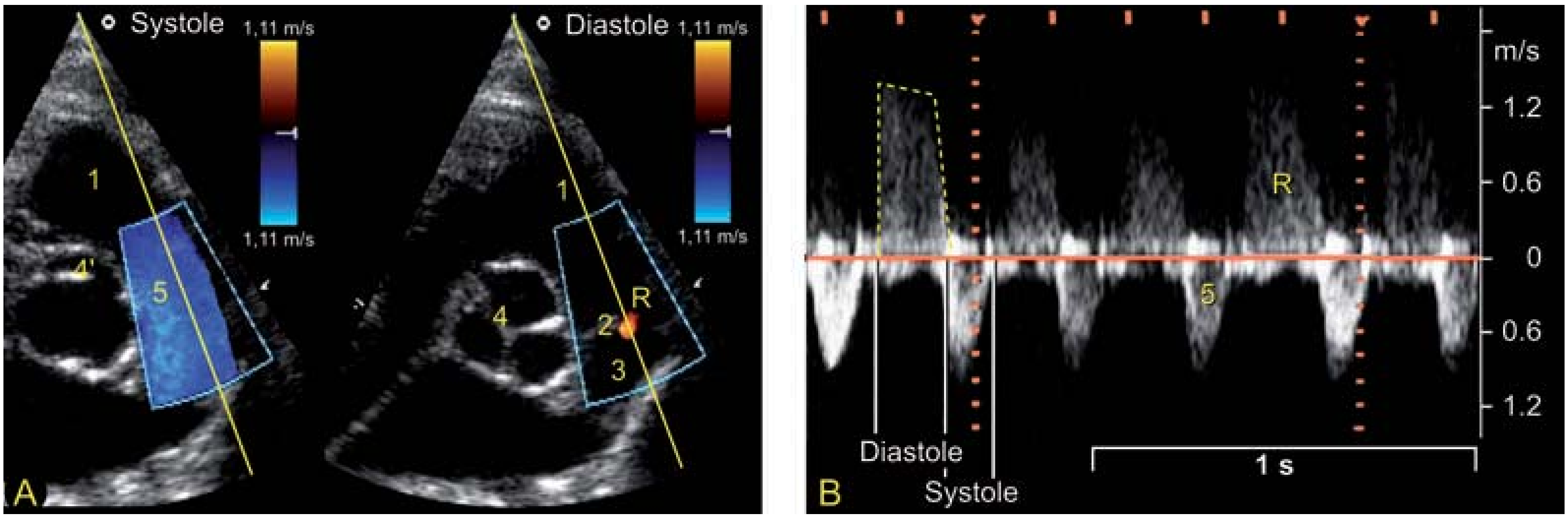

Fig. 2-71: Blood flow in the conus artery of the left ventricle in a rabbit, through the pulmonary valve and in the pulmonary trunk.

A: Color-coded 2D Doppler echocardiogram. Hemodynamically there is an insignificant small red-coded reflux through the closed pulmonary valve.

B: CW-Doppler echocardiogram. The reflux above the base line is holodiastolic and its velocity remains roughly the same throughout diastole (large pressure half time [PHT]).

The hemodynamic significance of a valve insufficiency is judged with respect to the presence of a reflux flow pattern. Valvular insufficiency is evaluated by the size of the insufficient blood flow patterns in the color Doppler images and the color-coded M-mode echocardiogram, and the absence or presence of secondary pathological changes.

1: right ventricle, conus artery
2: closed pulmonary valve
3: pulmonary trunk
4: closed aortic valve
4': opened aortic valve
5: normal systolic blood flow through the pulmonary valve

R: diastolic reflux

yellow line: total area in which the CW-Doppler scan was recorded

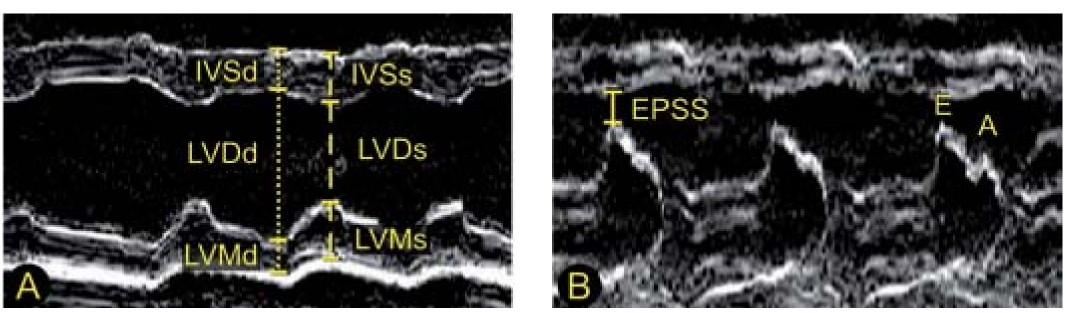

Fig. 2-72: M-mode measurement of a ferret.

A: M-mode measurements according to TEICHHOLZ for the assessment of the morphology and function of the left ventricle.

B: M-mode measurement of the EPSS (E-point to septal separation) for the assessment of the end-systolic volumes of the left ventricle.

IVSd: diastolic interventricular septal thickness
LVDd: diastolic left ventricular internal diameter
LVMd: diastolic left ventricular wall thickness
IVSs: systolic interventricular septal thickness
LVDs: systolic left ventricular wall thickness
LVMs: systolic left ventricular wall thickness
EPSS: the distance between the interventricular septum and early diastolic opening of the mitral valve
E: E-wave = early diastolic maximal opening of the anteriomedial leaflet of the mitral valve
A: A-wave = late diastolic opening of the anteriomedial leaflet of the mitral valve

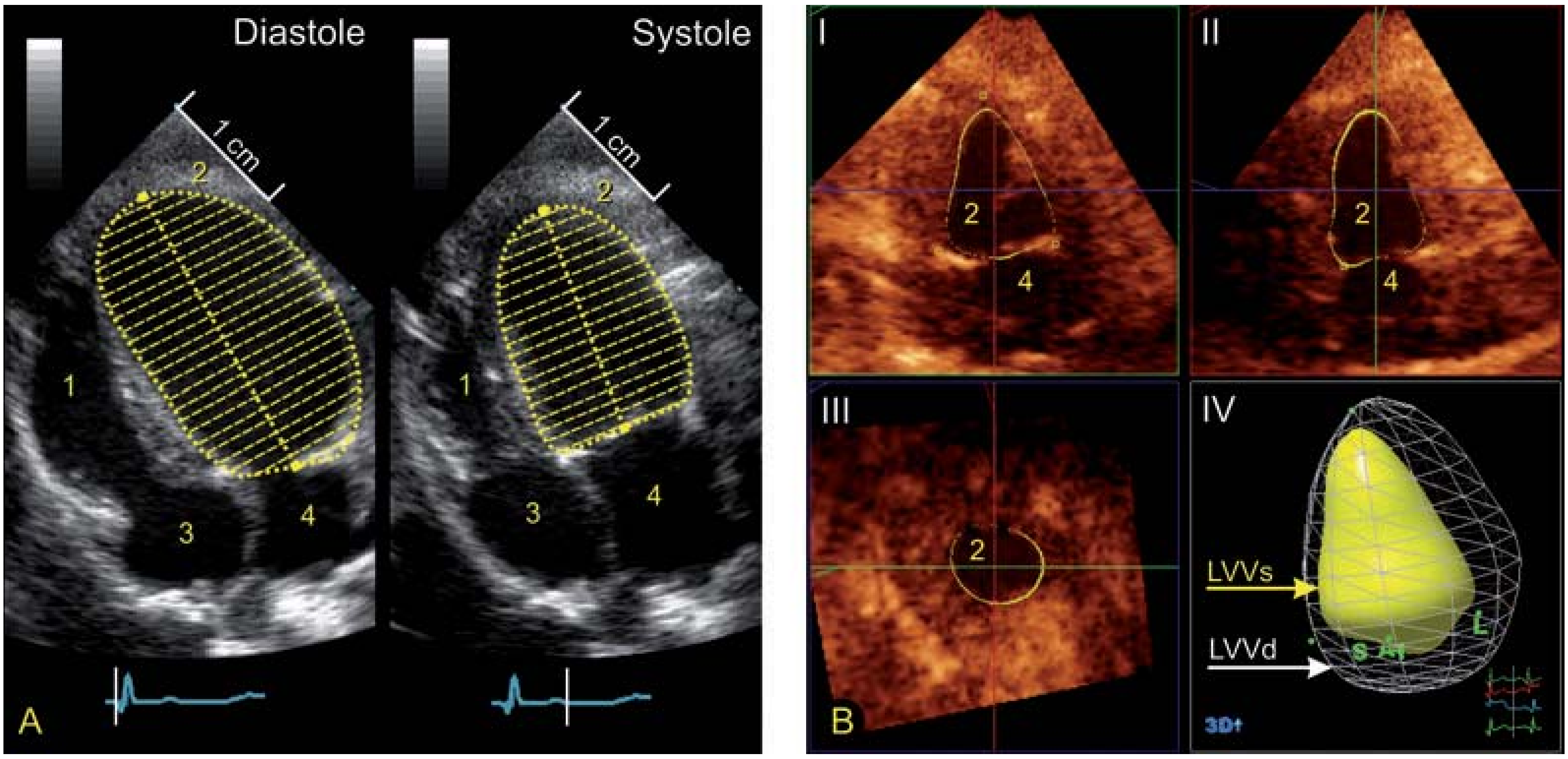

Fig. 2-73: 2D (A) and 3D (B) echocardiographic images of a rabbit for the determination of the diastolic and systolic volumes of the left ventricle as well as the ejection fraction.

A: 2D echocardiography. Volume measurement using the monoplane slice summation method according to SIMPSON. In this method, the end-diastolic (I) and the end-systolic (II) areas of the left ventricle are circumscribed (leaving out the papillary muscle) and the distance between the mitral valve and the apex of the heart are drawn in. Most ultrasonography systems automatically calculate the volume from these values.

B: 3D echocardiography. The three orthogonal images show an apical two-chamber view (I), a second orthogonal apical two-chamber view (II), and a short-axis view (III). In the image at the bottom right (IV), the left ventricular volume (LVVs = yellow cone) is compared to the diastolic volume (LVVd = white lattice).

1: right ventricle
2: left ventricle
3: right atrium
4: left atrium

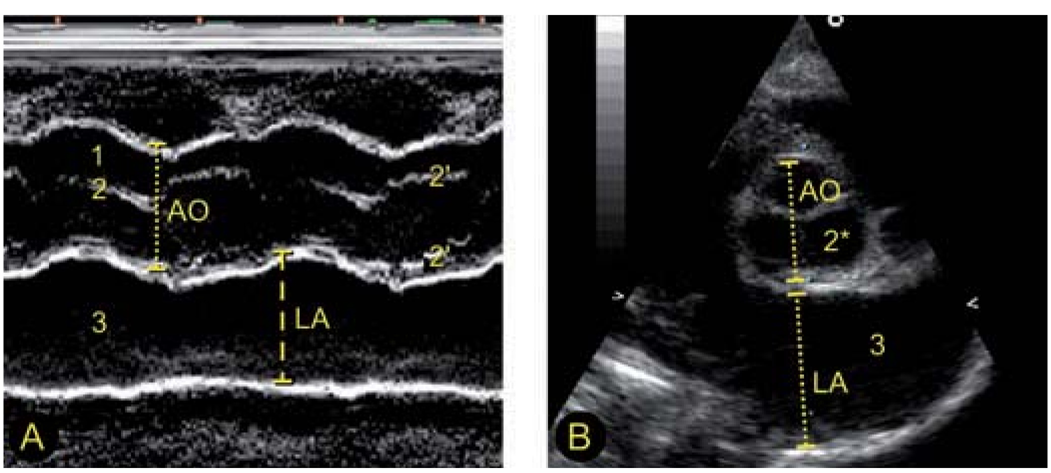

Fig. 2-74: Echocardiographic images of a rabbit.

A: M-mode echocardiogram for size determination of the left atrium in comparison to the aorta at the level of the aortic valve. Measurement of the end-diastolic thickness of the aortic sinus and the end-systolic diameter of the left atrium according to the Leading edge method.

B: 2D echocardiography, right parasternal short-axis view, measurement of the early systolic diameter of the aortic sinus along the aortic commissure (2*) close to the atrium and the early diastolic diameter of the left atrium in the extension to the aortic commissure according to the Inner edge method.

1: aortic sinus
2: closed aortic valve
2': opened aortic valve
2* aortic commissure close to the atrium
3: left atrium

AO: diameter of the aortic sinus
LA: diameter of the left atrium

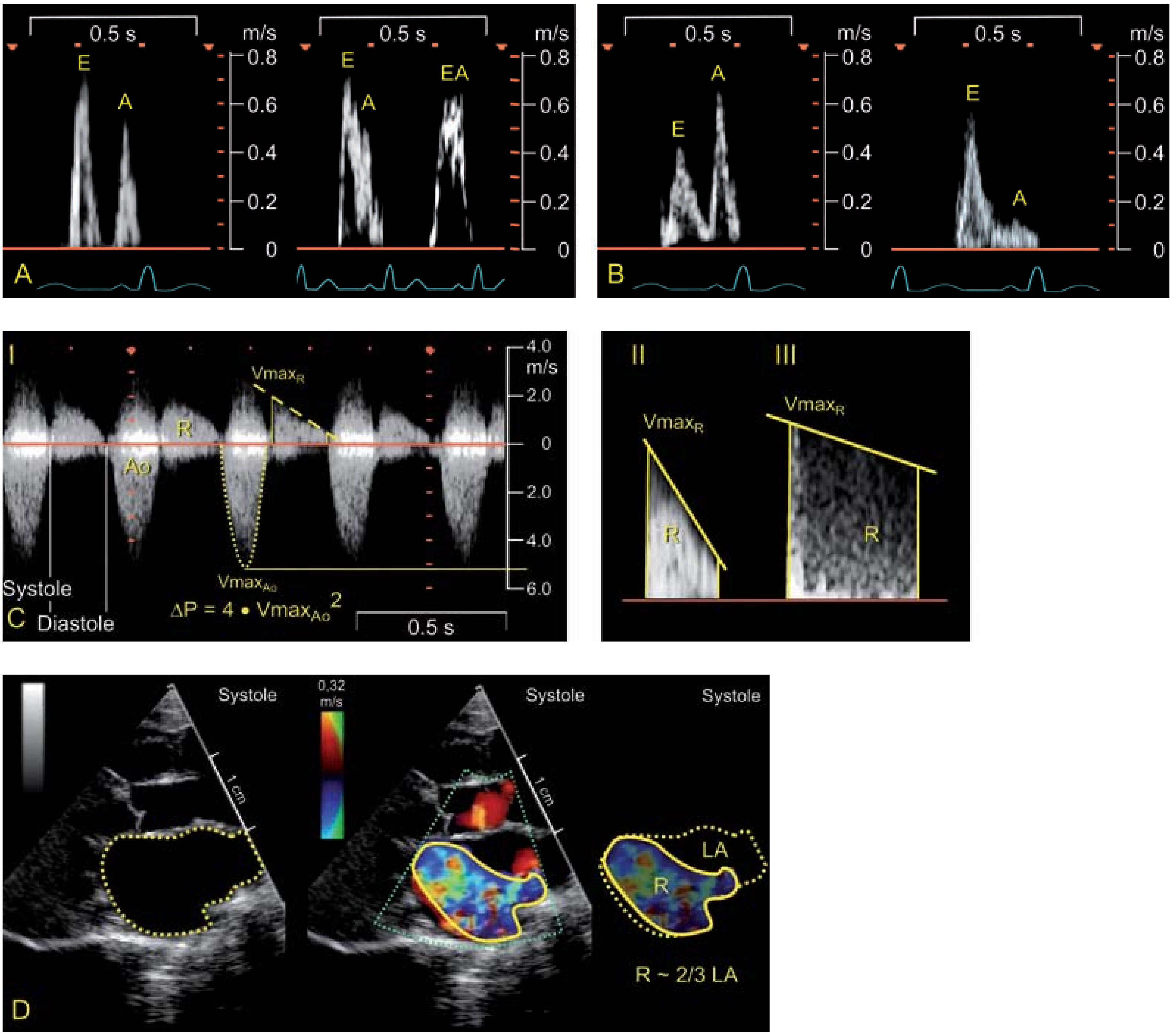

Fig. 2-75: Pulsed (A, B), continual (C), and color-coded Doppler echocardiography (D) for measuring the velocity of normal blood flow and the assessment of stenoses and insufficiencies in a ferret.

A, B: PW-Doppler echocardiogram with measurements of the early diastolic (E) and late-diastolic (A) ventricular in-flow for the determination of the E/A ratio as an indicator of a normal or impeded in-flow (B) of blood due to a diastolic dysfunction. The original ECGs have been replaced by schematic ECG curves.

C: Schematic representation of an aortic or pulmonary insufficiency for the semi-quantitative determination of the pressure half time (PHT). A small PHT indicates the presence of a severe aortic or pulmonary insufficiency.

D: Color-coded Doppler image for the determination of the size of the insufficiency jets in comparison to the visible area of the left atrium in an AV-valve insufficiency. In order to achieve reliable color-coded Doppler echocardiograms, the Nyquist limit should be adjusted with respect to the angle between the ultrasound beam and the regurgitation. As the angle is almost 90°in this case, a low maximum velocity has been chosen (0.32 m/s). Excessively high Nyquist limits lead to an underestimation of the regurgitation, while too low limits to an overestimation.

Although far from complete, Tables 2-4 to 2-17 show the reference values from a select group of the predominantly used echocardiographic measurements in various small pet mammals. Other publications contain additional measurements and calculations which are not included in these tables. Moreover, there are many accessable publications not been mentioned here because they contain only individual values or have utilized specialized echocardiographic methods.

Ferret

M-mode and two-dimensional echocardiography
See Table 2-4.

PW Doppler echocardiography
See Table 2-5.

Rabbit

M-mode and two-dimensional echocardiography
See Table 2-6.

PW and CW Doppler echocardiography
See Table 2-7.

Guinea pig

M-mode and two-dimensional echocardiography
See Table 2-8.

CW Doppler echocardiography
See Table 2-9.

Chinchilla

M-mode and two-dimensional echocardiography
See Table 2-10.

Conventional Doppler echocardiography
See Table 2-11.

Golden Hamster

M-mode and two-dimensional echocardiography
See Table 2-12.

PW Doppler echocardiography
See Table 2-13.

Mouse

M-mode and two-dimensional echocardiography
See Table 2-14.

CW Doppler echocardiography
See Table 2-15.

Rat

M-mode and two-dimensional echocardiography
See Table 2-16.

CW Doppler echocardiography
See Table 2-17.

Abbreviations for Tables 2-4 to 2-17:

2DE = 2D echocardiography
AO = aorta
A wave = atrial wave (late diastolic active filling during atrial contraction)
CW = continuous wave Doppler
d = diastolic
EA wave = fused E and A waves
EF = ejection fraction
EPSS = E-point to septal separation
E wave = early wave (early diastolic passive filling of the ventricles)
FS = systolic fractional shortening
IVS = interventricular septum thickness
LA = left atrium
LVD = left ventricular minor-axis dimension
LVM = left ventricular myocardium
LVV = left ventricular volume
n.s. = not specified
PW = pulsed wave Doppler
s = systolic
Vao = aortic valve
VM = mitral valve
Vmax = maximum speed
VP = pulmonary valve
VT = tricuspid valve

Tabelle 2-4: M-mode and two-dimensional echocardiography in the **ferret**

Author	Stepien et al. 2000	Vastenburg et al. 2004	Boonyapakorn 2004
Gender	female castrated (14) male castrated (13) male (3)	female (18) male (11)	n.s.
Age [years]	2.3 ± 1.0	2.2–4.3	adult
Body weight [g]	1117 ± 360	512–1150	n.s.
Number of animals	30	29	10
General anesthesia/sedation	ketamine and midazolam	isoflurane	none
Heart rate [beats per minute]	273 ± 31	238 ± 20	260 ± 52
Standard plane for Teichholz measurements	n.s.	right parasternal short axis	right parasternal long axis
IVS (right) [cm]	0.36 ± 0.07	0.34 ± 0.04	0.35 ± 0.13
LVD (right) [cm]	0.88 ± 0.15	0.98 ± 0.14	1.05 ± 0.24
LVM (right) [cm]	0.42 ± 0.11	0.27 ± 0.05	0.35 ± 0.12
IVS (left) [cm]	0.48 ± 0.11	0.44 ± 0.06	0.49 ± 0.16
LVD (left) [cm]	0.59 ± 0.15	0.69 ± 0.13	0.61 ± 0.14
LVM (left) [cm]	0.58 ± 0.09	0.38 ± 0.08	0.48 ± 0.11
FS [%]	33 ± 14	29.5 ± 7.9	41.4 ± 2.7
EF from the M-mode [%]	69 ± 19	–	–
Standard plane for EPSS determination	–	right parasternal short axis	–
EPSS [cm]	–	0.12 ± 0.06	–
Plane for LA measurement and assessment	right parasternal long axis (M-mode)	right parasternal short axis (M-mode)	right parasternal long axis (M-mode)
LA [cm]	0.71 ± 0.18	0.58 ± 0.09	0.74 ± 0.15
AO [cm]	0.53 ± 0.10	0.44 ± 0.06	0.56 ± 0.07
LA/AO	1.33 ± 0.27	1.3 ± 0.2	1.34 ± 0.18

Table 2-5: PW Doppler echocardiography in the **ferret**

Author	Stepien et al. 2000
Gender	female castrated (14) male castrated (13) male (3)
Age [years]	2.3 ± 1.0
Body weight [g]	1117 ± 360
Number of animals	30
General anesthesia/sedation	ketamine and midazolam
Heart rate [beats per minute]	280 ± 32
Number of animals with E waves and A waves	15 von 30
VM: Vmax E wave [m/s]	0.70 ± 0.10 (PW)
VM: Vmax A wave [m/s]	0.52 ± 0.11 (PW)
VM: E/A	1.38 ± 0.32
Vao: Vmax [m/s]	0.89 ± 0.20 (PW)
VP: Vmax [m/s]	1.10 ± 0.14 (PW)

Abbreviations: see page 214.

Table 2-6: M-mode and two-dimensional echocardiography in the **rabbit**

Author	Breithardt 2001 and Stypmann et al. 2007	Breithardt 2001 and Stypmann et al. 2007	Kattinger et al. 1999	Klawitter 2005
Gender	female (10) male (10)	female (10) male (10)	female (3) male (10)	female (15) male (6) male castrated (9)
Breed	New Zealand White	New Zealand White	various	dwarf breeds
Age [years]	n.s.	n.s.	0.8–6	1–8
Body weight [g]	2450–3350	2450–3350	1300–3500	1167–3300
Number of animals	20	20	13	30
General anesthesia/sedation	ketamine and xylazine	none	none	none
Heart rate [beats per minute]	198 ± 37	234 ± 26	190–330	238 ± 35
Standard plane for Teichholz measurements	right parasternal short axis	right parasternal long axis	right parasternal long axis	right parasternal short axis
IVS (right) [cm]	0.20 ± 0.03	0.22 ± 0.06	0.23 ± 0.04	0.24 ± 0.05
LVD (right) [cm]	1.48 ± 0.08	1.54 ± 0.11	1.25 ± 0.16	1.27 ± 0.18
LVM (right) [cm]	0.27 ± 0.05	0.27 ± 0.04	0.23 ± 0.05	0.22 ± 0.07
IVS (left) [cm]	0.34 ± 0.07	0.36 ± 0.04	0.38 ± 0.04	0.36 ± 0.08
LVD (left) [cm]	1.07 ± 0.09	1.01 ± 0.09	0.75 ± 0.15	0.81 ± 0.12
LVM (left) [cm]	0.47 ± 0.06	0.50 ± 0.05	0.41 ± 0.08	0.41 ± 0.09
FS [%]	28.5 ± 3.8	34.5 ± 497	41.2 ± 6.2	36.2 ± 5.29
EF from M-mode [%]	–	–	–	65.6 ± 9.26
Plane for LA measurement and assessment	–	–	right parasternal long axis (M-mode)	right parasternal long axis (M-mode)
LA [cm]	–	–	0.98 ± 0.11	0.62 ± 0.08
AO [cm]	–	–	0.65 ± 0.07	0.53 ± 0.07
LA/AO	–	–	1.51 ± 0.20	1.19 ± 0.12
Measurement and calculation of LVV	apical four-chamber view (single plane)	apical four-chamber view (single plane)	–	–
EF from 2DE	53 ± 9	54 ± 8	–	–

Abbreviations: see page 214.

Table 2-7: PW and CW Doppler echocardiography in the **rabbit**

Author	Breithardt 2001 and Stypmann et al. 2007	Breithardt 2001 and Stypmann et al. 2007	Kattinger et al. 1999	Klawitter 2005
Gender	female (10) male (10)	female (10) male (10)	female (3) male (10)	female (15) male (6) male castrated (9)
Breed	New Zealand White	New Zealand White	various	dwarf breeds
Age [years]	n.s.	n.s.	0.8–6	1–8
Body weight [g]	2450–3350	2450–3350	1300–3500	1167–3300
Number of animals	20	20	13	30
General anesthesia/sedation	ketamine and xylazine	none	none	none
Heart rate [beats per minute]	198 ± 37	234 ± 26	190–330	238 ± 35
Number of animals with E and A waves	11 von 20 (PW) 10 von 20 (CW)	14 von 20 (PW) 5 von 20 (CW)	–	30 von 30
VM: Vmax E wave [m/s]	0.56 ± 0.10 (PW) 0.67 ± 0.06 (CW)	0.70 ± 0.12 (PW) 0.75 ± 0.12 (CW)	–	0.86 ± 0.13 (CW)
VM: Vmax A wave [m/s]	0.39 ± 0.09 (PW) 0.40 ± 0.07 (CW)	0.52 ± 0.13 (PW) 0.53 ± 0.14 (CW)	–	0.56 ± 0.09 (CW)
Number of animals with EA waves	9 von 20 (PW) 10 von 20 (CW)	6 von 20 (PW) 15 von 20 (CW)	–	–
VM: EA wave [m/s]	0.59 ± 0.13 (PW) 0.66 ± 0.20 (CW)	0.77 ± 0.17 (PW) 0.80 ± 0.17 (CW)	–	–
VT: Vmax E wave [m/s]	0.45 ± 0.14 (PW) 0.51 ± 0.07 (CW)	0.47 ± 0.08 (PW)	–	0.80 ± 0.08 (CW)
VT: Vmax A wave [m/s]	0.22 ± 0.04 (PW) 0.29 ± 0.07 (CW)	0.29 ± 0.03 (PW)	–	0.51 ± 0.09 (CW)
VT: EA wave [m/s]	0.50 ± 0.13 (PW) 0.59 ± 0.27 (CW)	0.59 ± 0.16 (PW) 0.71 ± 0.29 (CW)	–	–
Vao: Vmax [m/s]	0.73 ± 0.17 (PW) 0.80 ± 0.16 (CW)	0.75 ± 0.20 (PW) 0.92 ± 0.15 (CW)	0.75 ± 0.08 (PW)	0.90 ± 0.15 (CW)
VP: Vmax [m/s]	0.61 ± 0.17 (PW) 0.67 ± 0.17 (CW)	0.71 ± 0.17 (PW) 0.73 ± 0.12 (CW)	0.74 ± 0.11 (PW)	0.84 ± 0.10 (CW)

Abbreviations: see page 214.

Table 2-8: M-mode and two-dimensional echocardiography in the **guinea pig**

Author	Klawitter 2005
Gender	female (27) male (39)
Breed	various
Age [years]	1–5
Body weight [g]	544–1416
Number of animals	30
General anesthesia/sedation	none
Heart rate [beats per minute]	222 ± 21
Standard plane for Teichholz measurements	right parasternal short axis
IVS (right) [cm]	0.25 ± 0.06
LVD (right) [cm]	1.09 ± 0.13
LVM (right) [cm]	0.23 ± 0.07
IVS (left) [cm]	0.32 ± 0.06
LVD (left) [cm]	0.69 ± 0.09
LVM (left) [cm]	0.43 ± 0.08
FS [%]	35.5 ± 4.43
EF from the M-mode [%]	64.5 ± 14.09
Plane for LA measurement and assessment	right parasternal long axis (M-mode)
LA [cm]	0.57 ± 0.08
AO [cm]	0.47 ± 0.07
LA/AO	1.23 ± 0.15

Abbreviations: see page 214.

Table 2-9: CW Doppler echocardiography in the **guinea pig**

Author	Klawitter 2005
Gender	female (27) male (39)
Breed	various
Age [years]	1–5
Body weight [g]	544–1416
Number of animals	30
General anesthesia/sedation	none
Heart rate [beats per minute]	280 ± 32
Number of animals with E and A waves	30 / 30
VM: Vmax E wave [m/s]	0.85 ± 0.14
VM: Vmax A wave [m/s]	0.55 ± 0.10
VT: Vmax E wave [m/s]	0.81 ± 0.08
VT: Vmax A wave [m/s]	0.57 ± 0.09
Vao: Vmax [m/s]	1.02 ± 0.12
VP: Vmax [m/s]	0.88 ± 0.08

Abbreviations: see page 214.

Table 2-10: M-mode and two-dimensional echocardiography in the **chinchilla**

Author	Linde et al. 2004	Linde et al. 2004
Gender	female (8) male (9)	female (8) male (9)
Age [years]	adult	adult
Body weight [g]	681 ± 145 (♀) 615 ± 119 (♂)	681 ± 145 (♀) 615 ± 119 (♂)
Number of animals	17	17
General anesthesia/sedation	isoflurane	none
Heart rate [beats per minute]	170 ± 22	169 ± 32
Standard plane for Teichholz measurements	n.s.	n.s.
IVS (right) [cm]	0.18 ± 0.03	0.20 ± 0.03
LVD (right) [cm]	0.64 ± 0.05	0.59 ± 0.08
LVM (right) [cm]	0.26 ± 0.02	0.24 ± 0.04
IVS (left) [cm]	–	–
LVD (left) [cm]	0.38 ± 0.05	0.29 ± 0.06
LVM (left) [cm]	–	–
FS [%]	40 ± 5	50 ± 8
EPSS [cm]	0.03 ± 0.02	0.04 ± 0.03
Plane for LA measurement and assessment	n.s.	n.s.
LA [cm]	0.49 ± 0.06	0.53 ± 0.06
AO [cm]	0.36 ± 0.05	0.41 ± 0.04
LA/AO	1.38 ± 0.20	1.28 ± 0.13

Abbreviations: see page 214.

Table 2-11: Conventional Doppler echocardiography in the **chinchilla**

Author	Linde et al. 2004	Linde et al. 2004
Gender	female (8) male (9)	female (8) male (9)
Age [years]	adult	adult
Body weight [g]	681 ± 145 (♀) 615 ± 119 (♂)	681 ± 145 (♀) 615 ± 119 (♂)
Number of animals	17	17
General anesthesia/sedation	isoflurane	none
Heart rate [beats per minute]	170 ± 22	169 ± 32
Number of animals with E and A waves	17 / 17	–
VM: Vmax E wave [m/s]	0.48 ± 0.08	–
VM: Vmax A wave [m/s]	0.29 ± 0.07	–
Number of animals with EA waves	–	17 von 17
VM: EA wave [m/s]	–	0.74 ± 0.1
Vao: Vmax [m/s]	0.46 ± 0.1	0.81 ± 0.26
VP: Vmax [m/s]	0.61 ± 0.16	0.97 ± 0.32

Abbreviations: see page 214.

Table 2-12: M-mode and two-dimensional echocardiography in the **golden hamster**

Author	Salemi et al. 2005
Gender	female
Age [weeks]	10
Body weight [g]	73–133
Number of animals	118
General anesthesia/sedation	pentobarbital
Heart rate [beats per minute]	368
Standard plane for Teichholz measurements	right parasternal short axis
IVS (right) [cm]	0.10 ± 0.01
LVD (right) [cm]	0.41 ± 0.04
LVM (right) [cm]	0.10 ± 0.01
IVS (left) [cm]	0.23 ± 0.04
FS [%]	44.7 ± 6.6

Abbreviations: see page 214.

Table 2-13: PW Doppler echocardiography in the **golden hamster**

Author	Salemi et al. 2005
Age [years]	10
Body weight [g]	73–133
Number of animals	118
General anesthesia/sedation	pentobarbital
Heart rate [beats per minute]	368
Number of animals with E and A waves	6 / 118
VM: Vmax E wave [m/s]	0.77 ± 0.13 (PW)
VM: Vmax A wave [m/s]	0.40 ± 0.12 (PW)
VM: E/A	1.92 ± 0.47

Abbreviations: see page 214.

Table 2-14: M-mode and two-dimensional echocardiography in the **mouse**

Author	**Hart et al. 2001**	**Rottmann et al. 2003**
Gender	male	female (29) male (25)
Breed	Harlan Sprague Dawley	C57BL/6
Age [weeks]	10–23	12–24.5
Body weight [g]	28–44	19.6–44.3
Number of animals	7	54
General anesthesia/sedation	ketamine and xylazine	none
Heart rate [beats per minute]	250 ± 14	683 ± 63
Standard plane for Teichholz measurements	right parasternal short axis	n.s.
IVS (right) [cm]	0.10 ± 0.03	0.09 ± 0.01
LVD (right) [cm]	0.41 ± 0.08	0.30 ± 0.03
LVM (right) [cm]	0.10 ± 0.02	0.09 ± 0.02
IVS (left) [cm]	0.17 ± 0.05	0.17 ± 0.03
LVD (left) [cm]	0.23 ± 0.05	0.12 ± 0.02
LVM (left) [cm]	0.15 ± 0.04	0.14 ± 0.03
FS [%]	45 ± 1.23	59 ± 4.7

Abbreviations: see page 214.

Table 2-15: CW Doppler echocardiography in the **mouse**

Author	**Stypmann 2007**	**Stypmann 2007**
Gender	n.s.	n.s.
Breed	CD1-mice	CD1-mice
Age [years]	adult	adult
Body weight [g]	n.s.	n.s.
Number of animals	≤ 10	≤ 10
General anesthesia/sedation	ketamine and xylazine	isoflurane
Heart rate [beats per minute]	320 ± 6	457 ± 17
Number of animals with E and A waves	n.s.	n.s.
VM: Vmax E wave [m/s]	0.65 ± 0.02 (CW)	0.73 ± 0.04 (CW)
VM: Vmax A wave [m/s]	0.26 ± 0.02 (CW)	0.41 ± 0.06 (CW)
VM: E/A	2.7 ± 0.3	1.2 ± 0.1

Abbreviations: see page 214.

Table 2-16: M-mode and two-dimensional echocardiography in the **rat**

Author	Watson et al. 2004	Stein et al. 2007	Stein et al. 2007
Gender	male	male	male
Breed	Sprague Dawley	Fischer 344	Fischer 344
Age [weeks]	13.6 ± 4.4	9–12	9–12
Body weight [g]	282 ± 47	199–220	199–220
Number of animals	44	25	25
General anesthesia/sedation	isoflurane ketamine and xylazine	isoflurane	ketamine and xylazine
Heart rate [beats per minute]	294 ± 36	363 ± 5	326 ± 4
Standard plane for Teichholz measurements	right parasternal long and short axes	right parasternal long and short axes	right parasternal long and short axes
IVS (right) [cm]	0.14 ± 0.01	–	–
LVD (right) [cm]	0.55 ± 0.08	0.67 ± 0.01	0.62 ± 0.01
LVM (right) [cm]	0.15 ± 0.01	0.14 ± 0.03	0.14 ± 0.03
IVS (left) [cm]	–	–	–
LVD (left) [cm]	0.28 ± 0.08	–	–
LVM (left) [cm]	–	–	–
FS [%]	49 ± 10	46.7 ± 0.9	47.3 ± 1
Measurement and calculation of LVV	n.s.	four-chamber view, single plane	four-chamber view, single plane
EF from 2DE	–	71.5 ± 1.5	72.1 ± 1.4

Abbreviations: see page 214.

Table 2-17: CW Doppler echocardiography in the **rat**

Author	Watson et al. 2004
Gender	male
Breed	Sprague Dawley
Age [years]	13.6 ± 4.4
Body weight [g]	282 ± 47
Number of animals	33
General anesthesia/sedation	isoflurane ketamine and xylazine
Heart rate [beats per minute]	294 ± 36
Number of animals with E and A waves	n.s.
VM: Vmax E wave [m/s]	0.73 ± 0.14 (PW)
VM: Vmax A wave [m/s]	0.47 ± 0.15 (PW)

Abbreviations: see page 214.

Further reading

AMERICAN SOCIETY OF ECHOCARDIOGRAPHY: http://www.asecho.org. Guidelines of the American Society of Echocardiography: http://www.asecho.org/guidelines.php.

BOONYAPAKORN, C. (2007): Cardiologic examinations in ferrets with and without heart disease. Dissertation Berlin.

BREITHARDT, A.-K. (2001): Echokardiographische Untersuchung gesunder Weißer-Neuseeländer-Kaninchen im wachen und narkotisierten Zustand. Diss. med. vet., München.

HART, C. Y. T., BURNETT JR., J. C., REDFIELD, M. M. (2001): Effects of avertin versus xylazine-ketamine anesthesia on cardiac function in normal mice. Am J Physiol Heart Circ Physiol **281**: 1938–1945.

KATTINGER, P., EWRINGMANN, A., WEYLAND, J., SKRODZKI, M. (1999): Kardiologische Untersuchungen beim Kaninchen. Kleintierpraxis **44**: 761–772.

KLAWITTER, A. (2005): Echokardiographische Untersuchungen im M-Mode und mit Hilfe des CW-Dopplers von herzgesunden Kaninchen und Meerschweinchen. Dissertation Hannover.

LINDE, A., SUMMERFIELD, N. J., JOHNSTON, M., MELGAREJO, T., KEFFER, A., IVEY, E. (2004): Echocardiography in the Chinchilla. J Vet Intern Med **18**: 772–774.

ROTTMAN, J. N., NI, G., KHOO, M., WANG, Z., ZHANG, W. ANDERSON, M. E., MADU, E. (2003): Temporal changes in ventricular function assessed echocardiographically in conscious and anesthetized mice. J Am Soc Echocardiography **16**: 1150–1157.

SALEMI, V. M. C., BILATE, A. M. B., RAMIRES, F. J. A., PICARD, M. H., GREGIO, D. M., KALIL, J., CUNHA NETO, E., MADY, C. (2005): Reference values from M-Mode and Doppler echocardiography for normal Syrian hamsters. European J Echocardiography **6**: 41–46.

STEIN, A. B., TIWARI, S., THOMAS, P., HUNT, G., LEVENT, C., STODDARD, M. F., TANG, X.-L., BOLLI, R., DAWN, B. (2007): Effects of anesthesia on echocardiographic assessment of left ventricular structure and function in rats. Basic Res Cardiol **102**: 28–41.

STEPIEN, R. L., BENSON, K. G., WENHOLZ, L. J. (2000): M-Mode and Doppler echocardiographic findings in normal ferrets sedated with ketamine hydrochloride and midazolam. Vet Radiol Ultrasound **41**: 452–456.

STYPMANN, J., ENGELEN, M. A., BREITHARDT, A.-K., MILBERG, P., ROTHENBURGER, M., BREITHARDT, O. A., BREITHARDT, G., ECKARDT, L., POULSEN NAUTRUP, C. (2007): Doppler echocardiography and tissue Doppler imaging in the healthy rabbit, Differences of cardiac function during awake and anaesthetised examination. Int J Cardiol **115**: 164–170.

STYPMANN, J. (2007): Doppler ultrasound in mice. Echocardiography **24**: 97–112.

THOMAS, W. P., GABER, C. E., JACOBS, G. J., KAPLAN, P. M., LOMBARD, C. W., MOISE, N. S., MOSES, B. L. (1993): Recommendations for standards in transthoracic two-dimensional echocardiography in the dog and cat. Echocardiography Committee of the Specialty of Cardiology, American College of Veterinary Internal Medicine. J Vet Intern Med **7**: 247–252.

VASTENBURG, M. H. A. C., BOROFFKA, S. A. E. B., SCHOEMAKER, N. J. (2004): Echocardiographic measurements in clinically healthy ferrets anesthetized with isoflurane. Vet Radiol Ultrasound **45**: 228–232.

WATSON, L. E., SHETH, M., DENYER, R. F., DOSTAL, D. E. (2004): Baseline echocardiographic values for adult male rats. J Am Soc Echocardiography **17**: 161–167.

2.4.3 Abdomen

Sven Reese

The following description of the sonoanatomy of the abdomen does not follow the sequence provided in the examination protocol, but is arranged according to organ system as found in the chapter on radioanatomy (Chap. 2.2.4).

2.4.3.1 Gastrointestinal tract

Stomach

The stomach is relatively easy to locate because it lies caudal to the liver. The stomach often contains food and gas which makes a complete examination of the gastric wall impossible, especially in **rabbits** and **rodents**. Under normal circumstances, only a small part of the ventral gastric wall can be imaged (**Fig. 2-76A**). The very thin gastric wall present in the rabbit, guinea pig, and chinchilla has three layers in the ultrasonographic image:

1. a echoic line of reflection on the mucosal surface
2. a hypoechoic layer formed by the mucosa and thin layer of muscle
3. an insignificant echoic line on the serosal surface of the stomach.

Rugae are never observed in rabbits, guinea pigs, chinchillas, or degus. Conversely, rugae may be present in **small rodents**. Principally in fasted **rats**, the gastric rugae may protrude radially into the lumen in the sagittal plane, which is similar to cats (**Fig. 2-76B**). The ultrasonographic image of the **ferret** stomach is comparable to that of the cat, although the stomach in a healthy ferret is never completely empty. A ferret with a totally empty stomach that has »wheel-spoke« configuration (**Fig. 2-76C**) may be indicative of inappetence due to a primary disease process (e.g., lymphoma).

Small intestines

The small intestines have only a maximum thickness of 3–5 mm, even in the larger species such as the rabbit and ferret, and so they are inconspicuous in ultrasonographic images. The five layers characteristic of canine and feline small intestines are rarely observed and even when they are, the layers are not distinct. As a rule, the intestinal wall of small exotic mammals has three layers with an inner reflection from the mucosal surface, an outer insignificant line of reflection, and a middle hypoechoic layer formed by the mucosa and the layer of muscle (**Fig. 2-77**). Only the descending duodenum can be imaged sonographically with any degree of certainty. It can be seen as an elongated section of small intestines lying against the dorsolateral part of the right abdominal wall. Mesenteric lymph nodes in healthy animals are only observed on a regular basis in ferrets. This species has very a prominent cranial mesenteric lymph node located at the root of the mesentery. It is shaped like a flat bean with a clearly indented hilus. A characteristic of this lymph node is that it has an obvious separation between its echoic medulla and hypoechoic cortex (**Fig. 2-78**). The structure of these lymph nodes will often lead sonographic

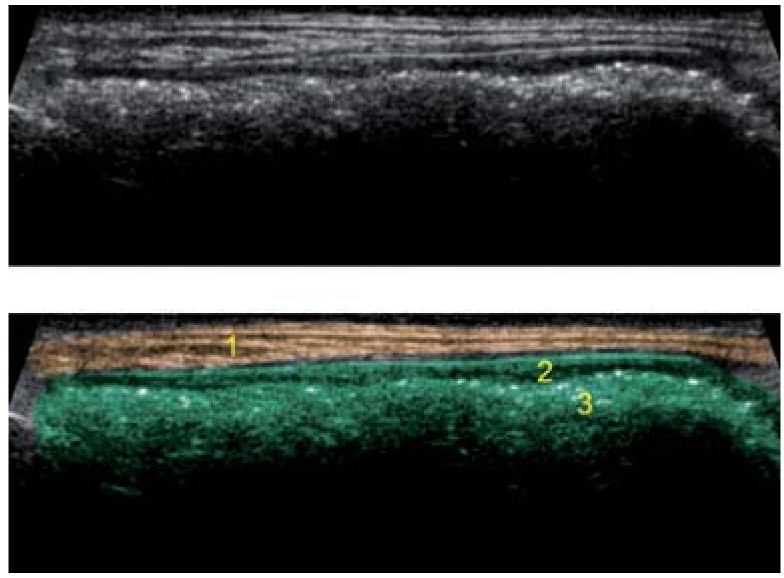

Fig. 2-76A: Ultrasonographic images of a rabbit's stomach, sagittal plane, 12 MHz, PD 1.5 cm. The wall of the stomach (2) is very thin and hypoechogenic without any individual layers. The stomach contents (3), filled with small gas bubbles, reflect the majority of the sound waves and therefore significantly hinder an ultrasonographic examination of the stomach.

1: abdominal wall
2: stomach wall
3: stomach contents

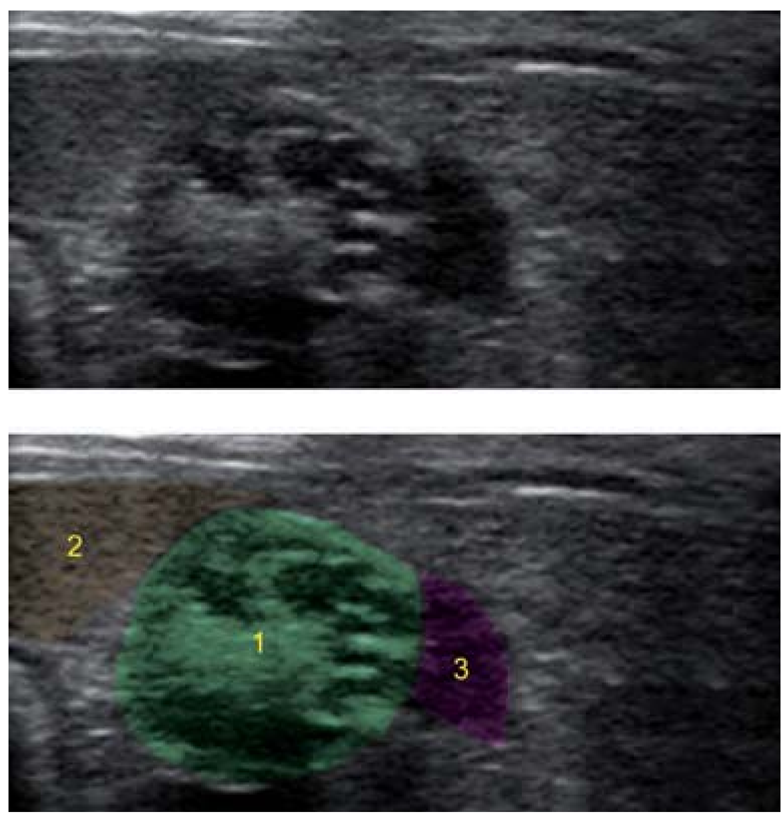

Fig. 2-76B: Ultrasonographic image of a rat's stomach, sagittal plane, 15 MHz, PD 2 cm. Radial folding of the gastric mucosa in a rat with little food in its stomach (1).

Images from Lehmann J. (2007): Abdominale Sonographie bei der Ratte (*Rattus norvegicus*). Dissertation, Munich, Germany.

1: stomach
2: liver
3: spleen

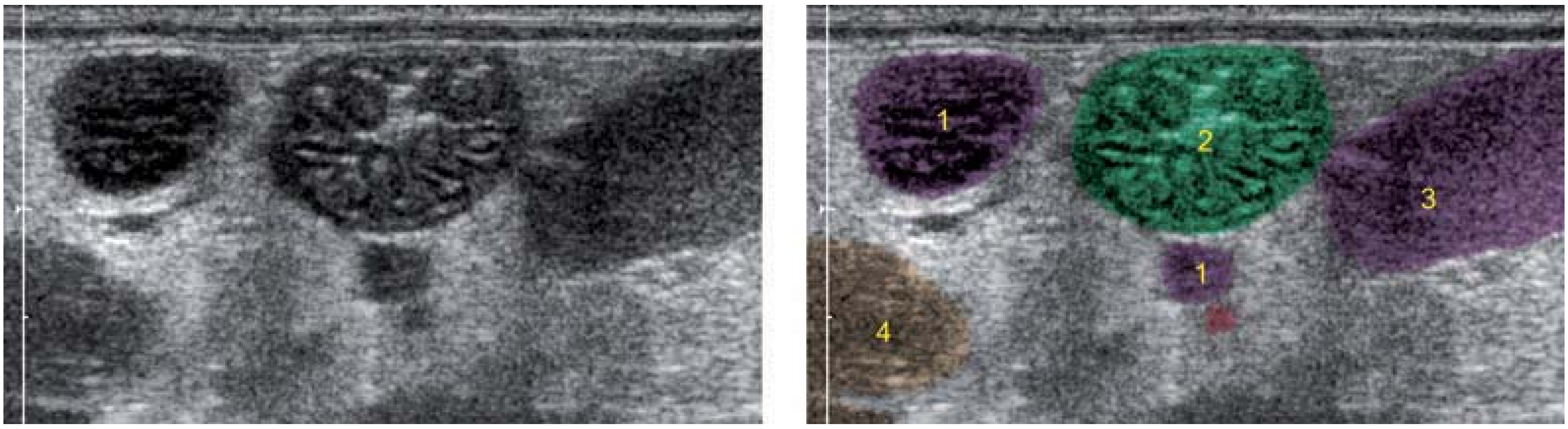

Fig. 2-76C: Ultrasonographic images of a ferret's stomach diagnosed with lymphoma, sagittal plane, 12 MHz, PD 2.5 cm. A completely empty stomach (2) with radial folds in the gastric mucosa is not normal in the ferret and is only observed in severely ill, anorexic animals.

Sonogram reproduced with kind permission from Reese, S., Frings, B. (2004): Die abdominale Ultraschalluntersuchung beim Frettchen. Tierärztl Prax **32(K)**: 182–189.

1: enlarged lymph nodes
2: stomach (empty)
3: swollen spleen
4: liver

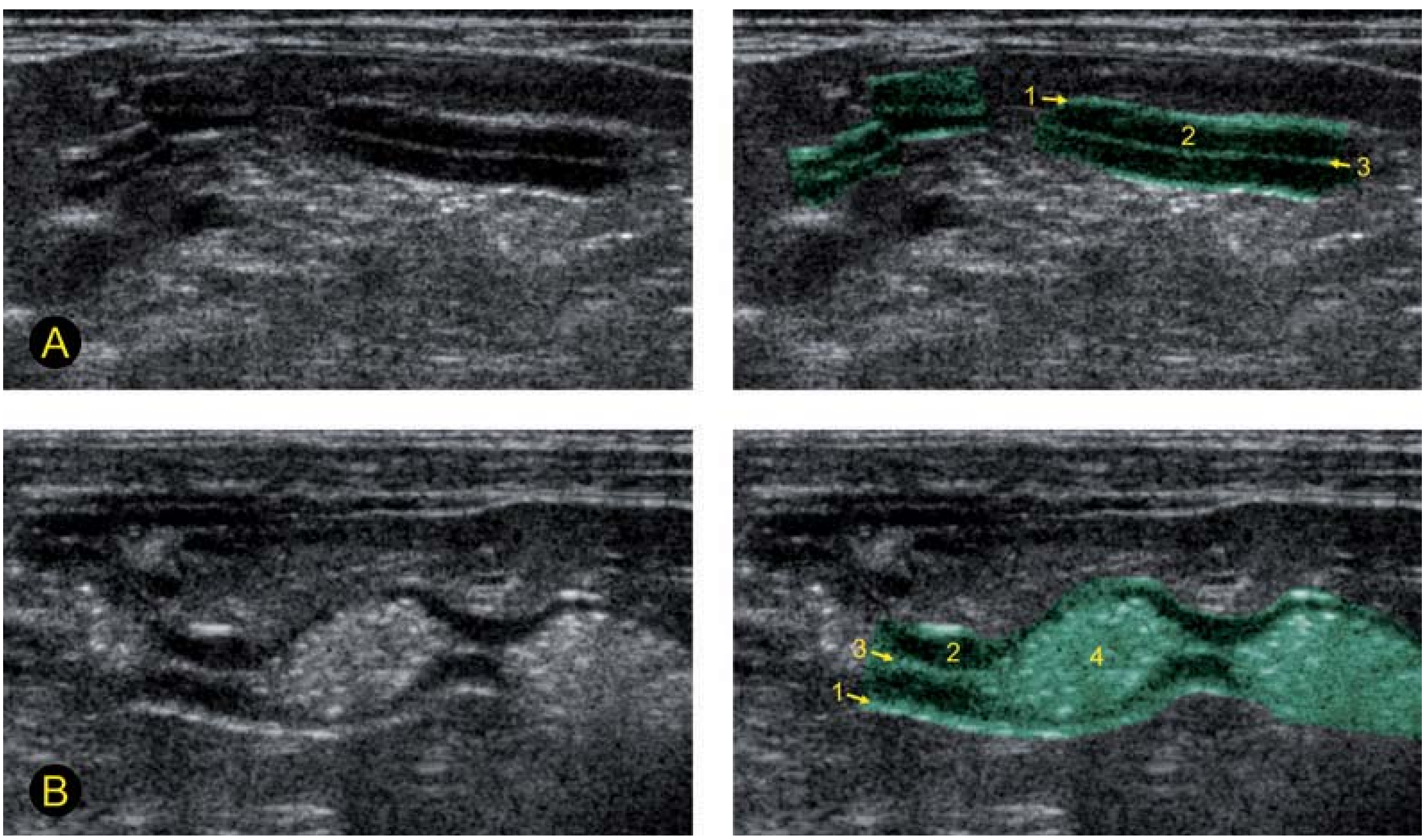

Fig. 2-77: Ultrasonographic images of a ferret's jejunum, longitudinal plane, 12 MHz, PD 1.5 cm. In areas where the small intestines are empty, the wall has three layers – an entry echo from the external surface (1), a hypoechoic main layer (2) formed by the muscular coat and the mucous tunic, and a layer due to surface reflections from the mucosa (3). The assessment of the intestinal tract should not only include the wall structure, but also (B) intestinal motility with its peristaltic waves (4).

1: jejunum: wall
2: jejunum: muscular coat and mucous tunic
3: jejunum: mucosa
4: peristaltic waves

examiners inexperienced with **ferret** anatomy to conclude that these structures are enlarged adrenal glands.

Cecum

The cecum is a large gas chamber that contains a mixture of food and gas in **rabbits** and **rodents**. Therefore, the cecum cannot be systematically examined using ultrasonography as its contents strongly reflect the ultrasound waves. Imaging the cecal wall results in a curved hyperechoic line adjacent to the transducer from which an acoustic shadow extends. **Ferrets** do not have a cecum.

Large intestines

The ultrasonographic examination of **rabbit** and **rodent** large intestines is also limited. The ascending colon, with its lumen filled with a food-gas mixture, causes similar ultrasonographic difficulties as the cecum. The remainder of the large intestines and rectum can only be imaged using ultrasonography if fecal material is present. The surface of the fecal material closest to the transducer gives rise to a hyperechoic line of reflection. Behind this hyperechoic line of reflection is an acoustic shadow. In rabbits, this phenomenon causes a typical step-like image which is enhanced by the filled rectum in the sagittal plane (**Fig. 2-79A**). The colon in the **ferret** is similar to that found in cats (**Fig. 2-79B**). Imaging the empty colon of a ferret cannot be accomplished with a great degree of confidence because of its small diameter. A typical cross-sectional image of the empty large intestines has a rosette-like appearance of the folded mucosa's surface reflections, surrounded by the hypoechoic wall.

2.4.3.2 Liver

The ultrasonographic investigation of the liver is performed systematically from left to right in the sagittal plane. One should ensure that the depth of penetration is set to completely see the diaphragmatic reflection on the ultrasonographic image. The abdominal aorta, hepatic portal vein, caudal vena cava, gallbladder (not in the **rat**), and right kidney can be used as reference points for the level at which the plane is situated – as with dogs and cats (**Figs. 2-80A** to **2-80E**). Please note that a **guinea pig's** gallbladder may be identified in a very medial position. In addition, the liver should be examined beginning with a transverse scan directly behind the costal arch, followed by a fan-like craniodorsal movement of the scanning plane. The liver has a homogeneous but relatively coarse echoic texture with a low degree of echogenicity. The echoic properties of the **ferret**, **rabbit**, **guinea pig**, and **chinchilla** liver are lower than that of the spleen. Conversely, the spleen in the smaller rodents is homogeneously hypoechic and has similar echogenic properties as the liver. Many rabbit and guinea pig patients are obese and as diagnostic evidence of these animals having hepatic fatty degeneration there are slightly increased echoic properties of the liver parenchyma. In the larger species, the branches of the portal vein are easy to image as the edges of this vein have an obvious echo. The echoless liver veins are also well visualized. To a limited degree, the liver veins can be visualized with sonographic frequencies up to 15 MHz in the **rat** and **degu**, but not at all in **golden hamsters**, **gerbils** and **mice**.

With exception of the rat, all the other small mammals discussed here have a gallbladder, which can be easily visualized using ultrasonographic techniques lying to the right of the midline. The longitudinal contour of the gallbladder is pear-shaped and the cross-sectional contour, round. Irregular forms of the gallbladder with folds are typical in the **rabbit** and these folds can mimic septation or doubling of the gallbladder (**Fig. 2-81**). Normal bile ducts cannot be imaged in any of the small exotic mammal species.

2.4.3.3 Pancreas

The pancreas has a very large surface area, particularly in the granivorous **small rodents**. However, the extreme thinness of the pancreas makes ultrasonographic imaging of this organ impossible in rabbits and rodents. Conversely, an attempt may be made to image the **ferret** pancreas by using the same reference points as recommended for dogs and cats. This may not be successful in every animal despite the examiner being experienced. The right lobe of the pancreas lies parallel to the straight descending duodenum. Usually, the pancreatic tissue is somewhat homogeneous and less echoic than the surrounding mesentery (**Fig. 2-82**). Imaging the centrally situated pancreaticoduodenal vein ensures the identification of the pancreas. However, imaging the left lobe of the pancreas, which lies between the stomach and transverse colon, is not possible with any degree of confidence.

2.4.3.4 Spleen

In all species, the spleen is connected to the greater curvature of the stomach by the gastrosplenic ligament. Consequently, the spleen can be found consistently on the left side of the body caudal to the stomach. It is tongue-shaped in all species and triangular in cross-section. Relatively speaking, the **rabbit** has smallest spleen (**Fig. 2-83A**). In many rabbits, the spleen lies close to the stomach and is covered by the jejunum, so that imaging is not always successful. Conversely, the spleen is always close to the **rodent** abdominal wall (**Fig. 2-83B**) and can easily be located using a dorsal scan going through the left kidney, even in the mouse (**Fig. 2-83C**). **Ferrets**, in relation to their body size, have the largest spleen of all the small exotic mammals. Their spleen only has a thin form with sharp edges in some animals, especially young ones. In ferrets, the spleen is frequently very large with rounded edges and may have an irregular surface even in clinically healthy animals (see Chap. 2.9.6). The cause for ferret splenomegaly remains unclear in the majority of patients, despite being subjected to a thorough physical examination. The echoic texture of the spleen is homogeneous and finely grained with a sharp delineation to surrounding tissue. With an optimal perpendicular reflection of ultrasound waves, the splenic capsule appears as an echoic line. The echogenicity of the spleen in the ferret and rabbit is greater than that of the liver. In the **guinea pig** and **chinchilla**, the spleen has a medium echogenicity, while in the small rodents it is hypoechoic. Blood vessels cannot be imaged in the spleen of rabbits and rodents in the B-mode. Conversely, the splenic veins of the **ferret** can be followed a short distance from the hilus into the splenic parenchyma.

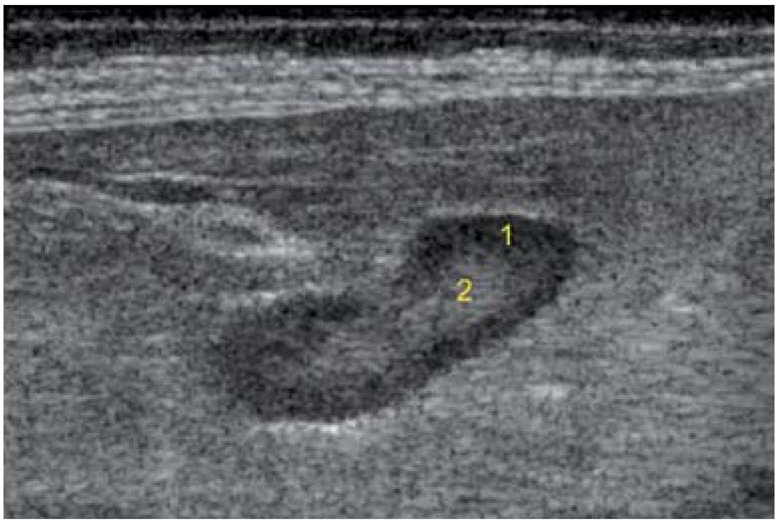

1: cortex
2: medulla

Fig. 2-78: Ultrasonographic image of a ferret's mesenteric lymph node, 12 MHz, PD 2 cm. Ferrets have prominent mesenteric lymph nodes, in which the cortex (1) and medulla (2) can be clearly differentiated.

Sonogram reproduced with kind permission from Reese, S., Frings, B. (2004): Die abdominale Ultraschalluntersuchung beim Frettchen. Tierärztl Prax **32(K)**: 182–189.

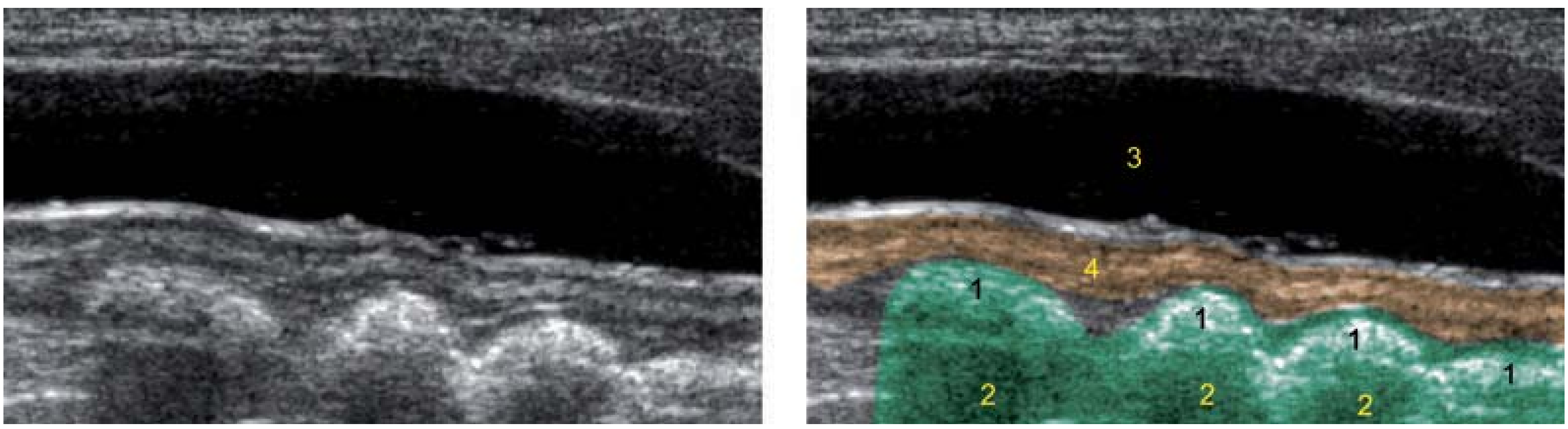

Fig. 2-79A: Ultrasonographic images of a rabbit's bladder and rectum, sagittal plane, 12 MHz, PD 2 cm. The rectum is only clearly observed sonographically when it contains sound-wave reflecting fecal pellets (1).

1: fecal pellets
2: acoustic shadow
3: urinary bladder
4: vagina

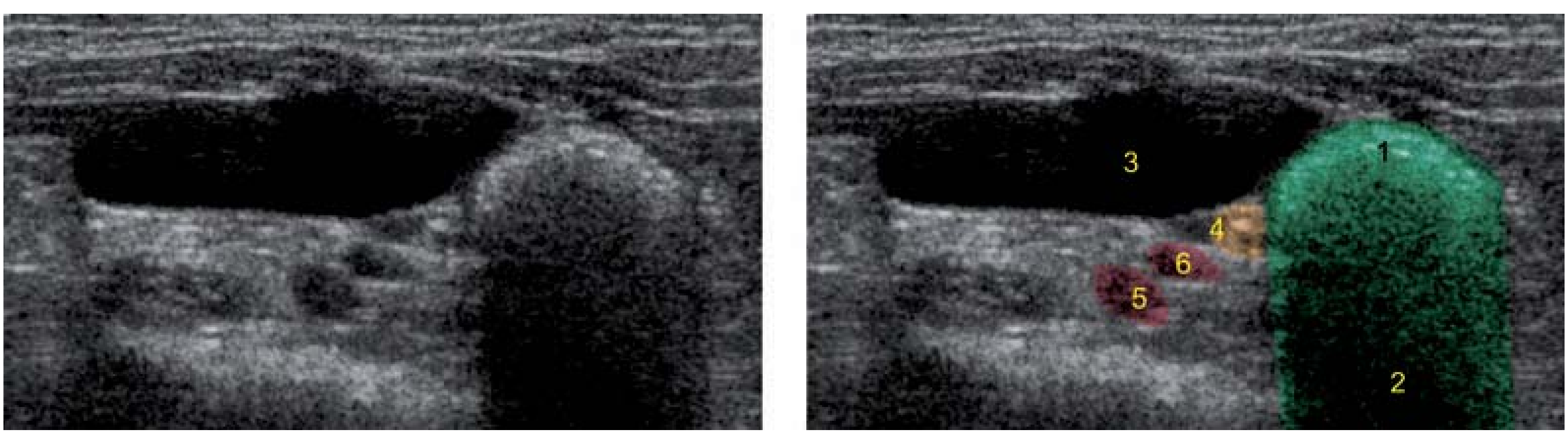

Fig. 2-79B: Ultrasonographic images of a ferret's bladder and rectum, transverse plane, 12 MHz, PD 2 cm. The filled rectum (1) has been slightly displaced to the left revealing the aorta (5) and the caudal vena cava (6).

1: rectum
2: acoustic shadow
3: bladder
4: uterus
5: aorta
6: caudal vena cava

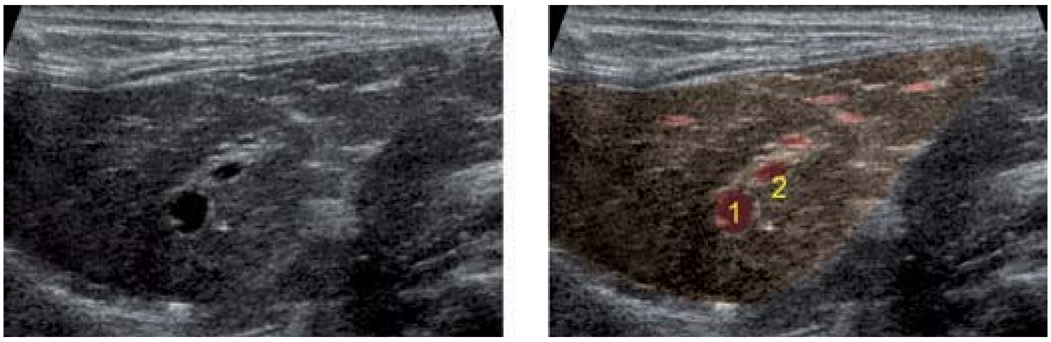

1: hepatic vein
2: portal vein

Fig. 2-80A: Ultrasonographic images of a ferret's liver, sagittal plane, 12 MHz, PD 3 cm. Left liver lobe with a section of the left main branch of the hepatic vein (1) and the portal vein (2).

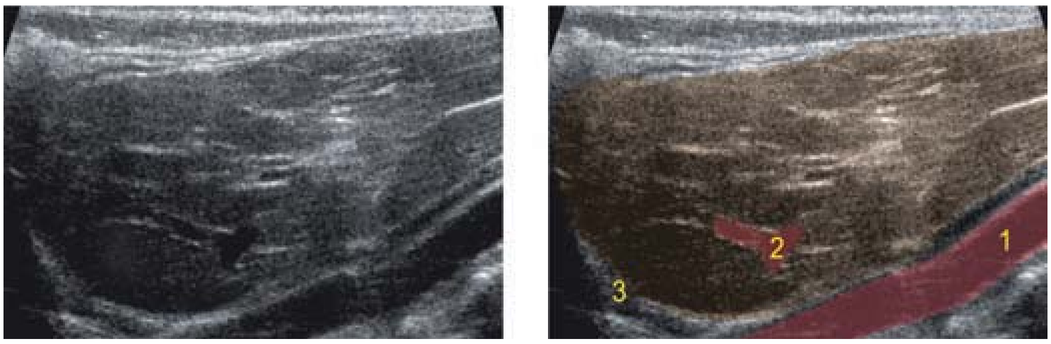

1: aorta
2: branch of the portal vein
3: diaphragmatic reflection

Fig. 2-80B: Ultrasonographic images of a ferret's liver, sagittal plane, 12 MHz, PD 3 cm. Image at the level of the aorta (1).

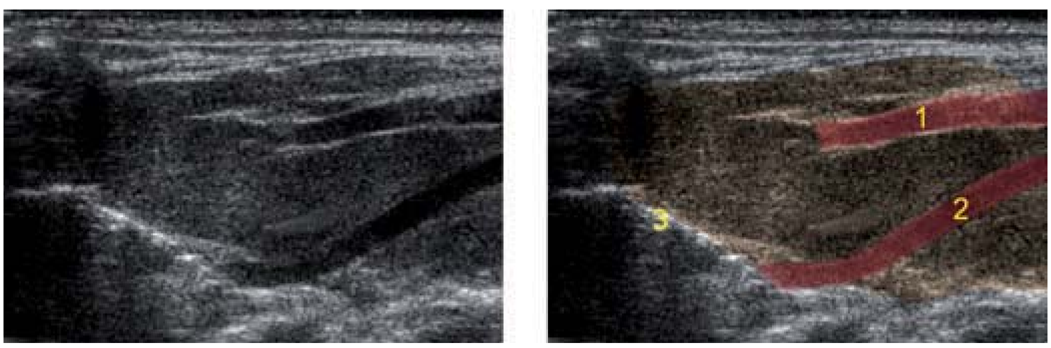

1: portal vein
2: caudal vena cava

Fig. 2-80C: Ultrasonographic images of a ferret's liver, sagittal plane, 12 MHz, PD 3 cm. Image at the level of the portal vein (1) and the caudal vena cava (2).

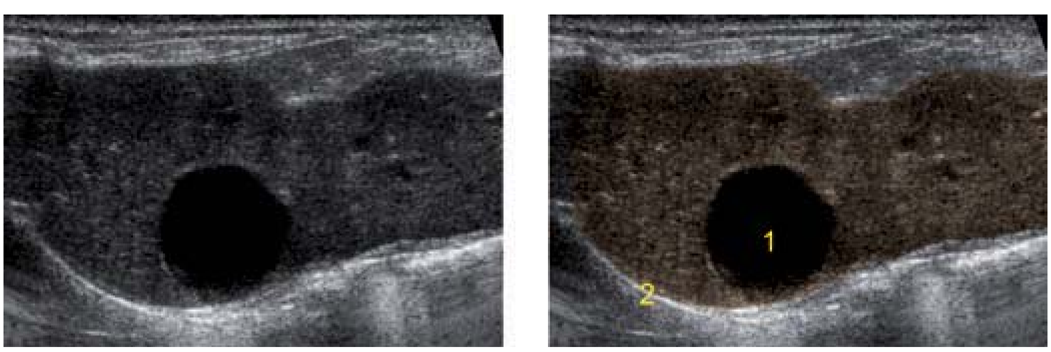

1: gallbladder
2: diaphragmatic reflection

Fig. 2-80D: Ultrasonographic images of a ferret's liver, sagittal plane, 12 MHz, PD 3 cm. Image at the level of the gallbladder (1).

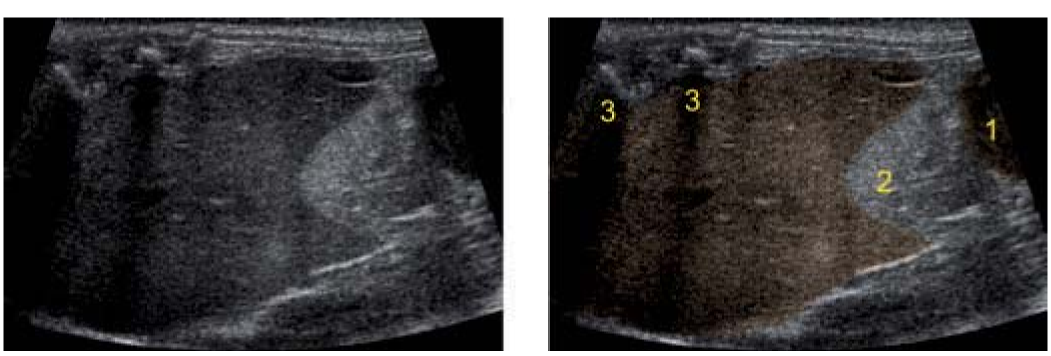

1: right kidney
2: renal impression
3: acoustic shadow behind the ribs

Fig. 2-80E: Ultrasonographic images of a ferret's liver, sagittal plane, 12 MHz, PD 3 cm. Right liver lobe with the renal impression (2).

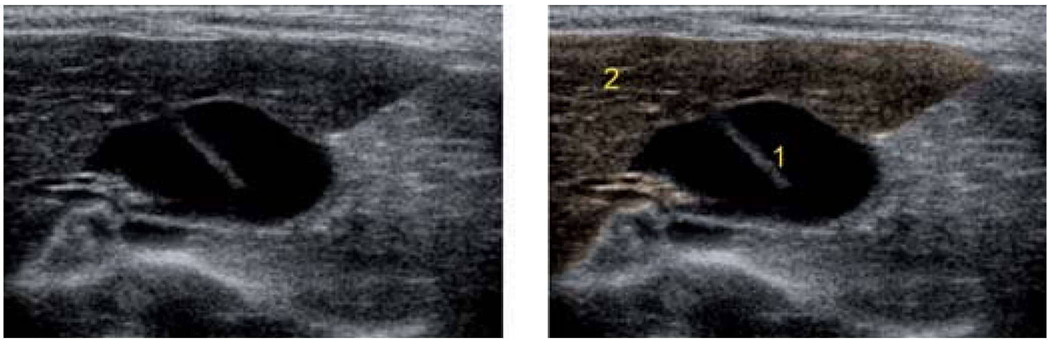

1: gallbladder, folds
2: liver

Fig. 2-81: Ultrasonographic images of a rabbit's gallbladder, 12 MHz, PD 2.5 cm. The gallbladder in the rabbit is variable in form, with folds (1) that can mimic septae.

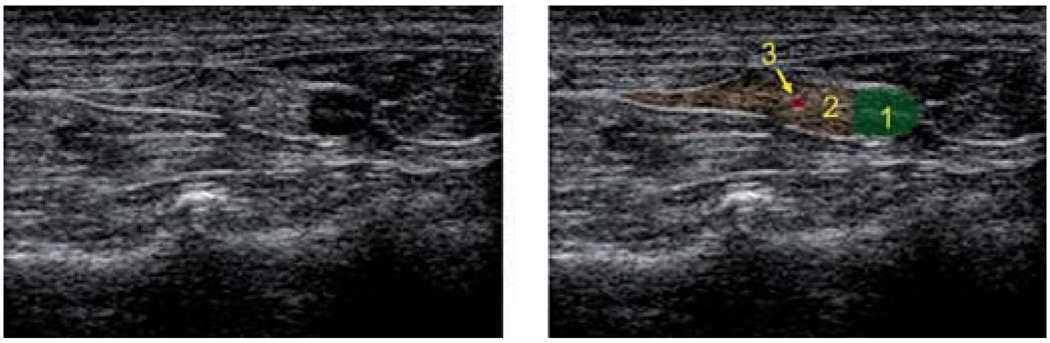

1: cranial duodenum
2: pancreas
3: pancreaticoduodenal vein

Fig. 2-82: Ultrasonographic images of a ferret's pancreas, sagittal plane, 12 MHz, PD 2 cm.

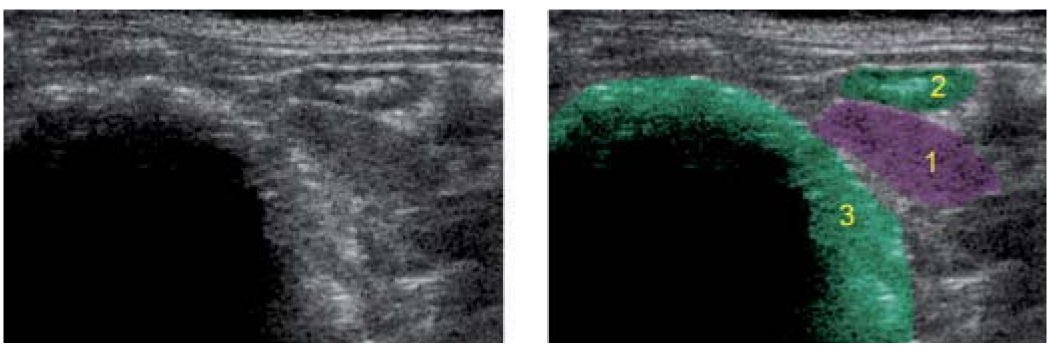

1: spleen
2: jejunum
3: stomach

Fig. 2-83A: Ultrasonographic images of a rabbit's spleen, sagittal plane, 12 MHz, PD 2 cm. The relatively small spleen (1) in the rabbit lies close to the stomach (3) and is often superimposed by the jejunum (2).

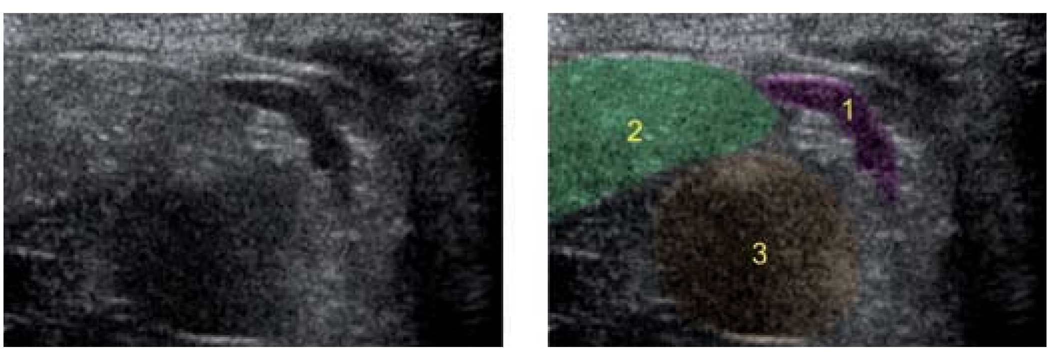

1: spleen
2: stomach
3: left kidney

Fig. 2-83B: Ultrasonographic images of a guinea pig's spleen, transverse plane, 15 MHz, PD 1.5 cm. The spleen (1) lies ventrolateral to the stomach (2) and the cranial pole of the left kidney (3). It is located very close to the abdominal wall.

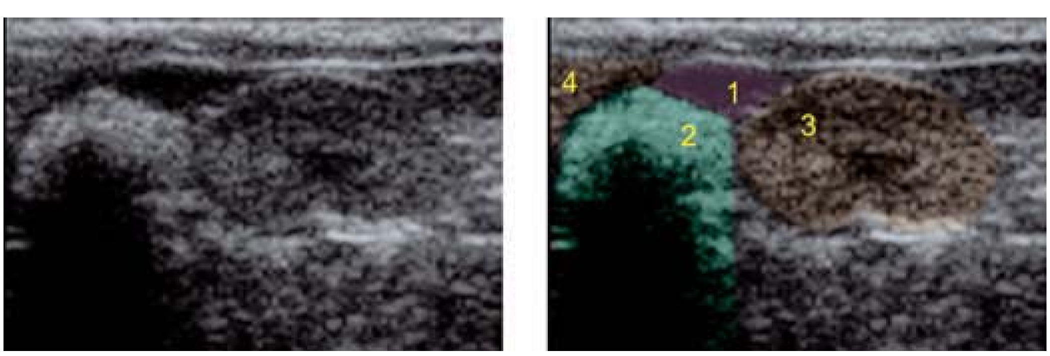

1: spleen
2: stomach
3: left kidney
4: liver

Fig. 2-83C: Ultrasonographic images of a mouse's spleen, dorsal plane, 15 MHz, PD 1.5 cm.

Sonogram courtesy of J. Mörl, Munich, Germany.

2.4.3.5 Urinary tract

Kidneys

The kidneys are smooth with a single hilus and have a similar structure to that found in dogs and cats. Kidneys are imaged in the sagittal, horizontal, and transverse planes. However, the voluminous gastrointestinal tract lies over the kidneys along the ventral aspect, especially in **rodents**, and so hampers the formation of correct sagittal planes. Thus, the kidneys can be most easily imaged from the dorsal surface in the sagittal plane. The necessity of having to shave a large area on the dorsolateral aspect of the animal means imaging of the kidneys from the dorsal body surface is rarely done.

Three zones of the kidney can be differentiated in the sagittal plane (**Fig. 2-84A**): the renal cortex with a finely grained echo texture of medium echogenicity, the hypoechoic renal medulla, and the echogenic central renal sinus (which is filled with peripelvic fat and has the renal blood vessels coursing through the tissue). The renal medulla is divided into round pseudopapillae by columns of the renal cortex and interlobar renal blood vessels. In the transverse plane, the hypoechoic pointed renal papilla is surrounded by the horseshoe-shaped renal cortex (**Fig. 2-84C**). A characteristic of the **rabbit** kidney is the obvious echoic and very wide renal sinus filled with fat (**Fig. 2-84C**). The two animal species endemic to arid climates, the **golden hamster** and **gerbil**, have a particularly long renal papilla along with the **chinchilla** and **degu**. This papilla may extend further than the hilus, projecting into the ureter (**Fig. 2-84D**). It enables the kidneys to produce highly concentrated urine. In the dorsal plane, the renal medulla has three parts in an optimal scan, including a broad, open, medial-facing hilus (**Fig. 2-84B**). In small rodents (e.g., mouse), the difference in echogenicity between the cortex and medulla is so minor that a reliable differentiation of these zones is often not possible.

In many **ferrets**, an echogenic zone of varying width, comparable to the medullary rim sign in cats, can be observed at the transition between the medulla and cortex (**Fig. 2-85**). Both in clinical examinations and diagnostic test results, these animals show no sign of renal insufficiency. Analyses of commercial ferret food has shown that this echogenic area only occurs in animals which have an excess of energy, protein, and minerals in their diet. An overview of the length, width, and height of the kidneys in the small exotic mammal species is provided in Table 2-18.

The imaging of the renal vascular tree is preferentially performed in the dorsal plane using Doppler ultrasonography (**Fig. 2-86A**). The determination of blood flow parameters using PW Doppler in unsedated small exotic mammals has only been achieved in the ferret (**Fig. 2-86B**). The resistance index for the renal artery was found to be 0.54 ± 0.04 (0.48–0.61) in nine healthy ferrets. Comparable values have also been determined for the interlobar arteries of ferrets.

Ureters

Ultrasonographic imaging of the ureters is not possible in most small exotic mammals.

Table 2-18: Length, width and height of the kidney; means in mm with range in parentheses

Species	Length	Width	Height
Chinchilla	19.8 (17.7–22.1)	10.3 (8.3–13.6)	12.7 (10.9–14.3)
Degu	13.9 (11.5–15.2)	9.7 (8.8–11.1)	11.0 (9.3–12.2)
Ferret (female)	25.1 (22.0–27.0)	11.2 (9.0–12.0)	13.0 (12.0–16.0)
Ferret (male)	29.5 (27.0–32.0)	12.6 (12.0–13.0)	14.6 (11.0–17.0)
Gerbil	11.8 (9.1–14.5)	6.3 (5.2–7.5)	7.0 (6.1–7.9)
Golden hamster	13.6 (12.0–14.0)	7.2 (6.5–7.7)	7.8 (7.0–8.1)
Guinea pig	20.3 (14.0–25.0)	13.9 (12.8–16.1)	15.0 (13.0–18.0)
Mouse	12.1 (9.7–13.6)	5.3 (4.9–5.7)	7.1 (6.2–7.5)
Rabbit, dwarf breeds (< 2 kg)	27.2 (22.0–36.0)	13.8 (10.5–17.0)	16.3 (12.0–20.0)
Rat	18.1 (15.1–20.6)	10.1 (9.1–11.7)	11.1 (10.0–12.8)

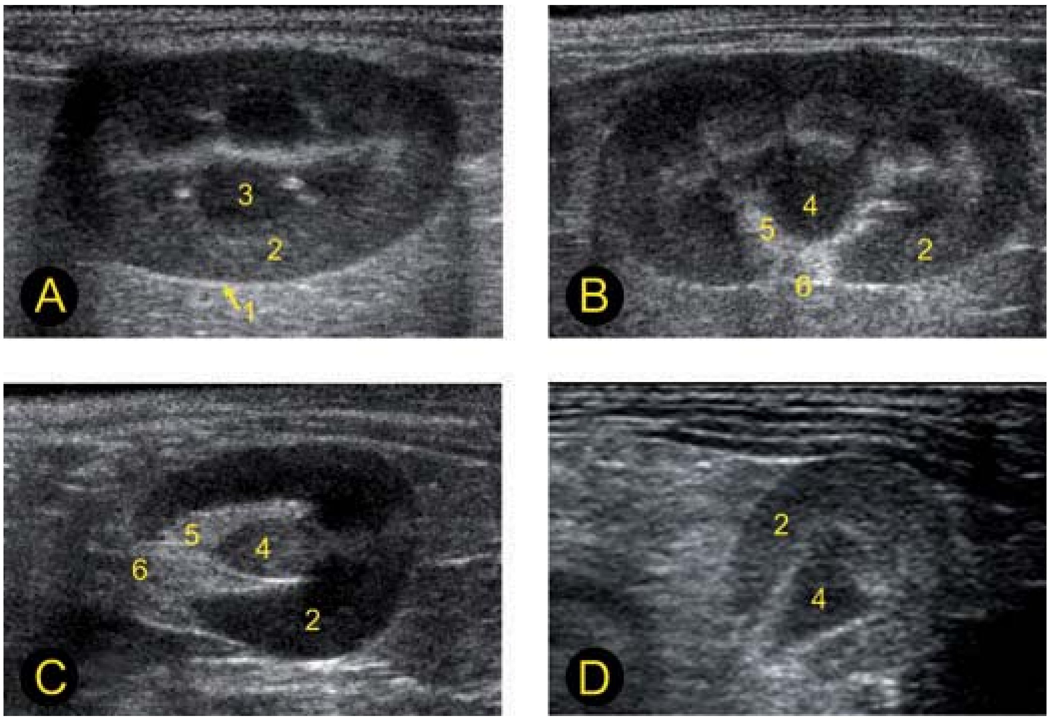

1: renal capsule
2: renal cortex
3: renal medulla
4: renal papilla
5: renal sinus
6: renal hilus

Fig. 2-84: Ultrasonographic renal images.

A–C: 12 MHz, PD 2 cm. Rabbit.

D: 15 MHz, PD 1.5 cm. Degu.

A correct assessment of the kidneys is only possible if the standard planes are used: sagittal (A), dorsal (B) and transverse (C and D).

Image D is from Gneiser, B. (2005): Abdominale Sonographie beim Degu (*Octogon degus*, Molina 1782). Dissertation, Munich, Germany.

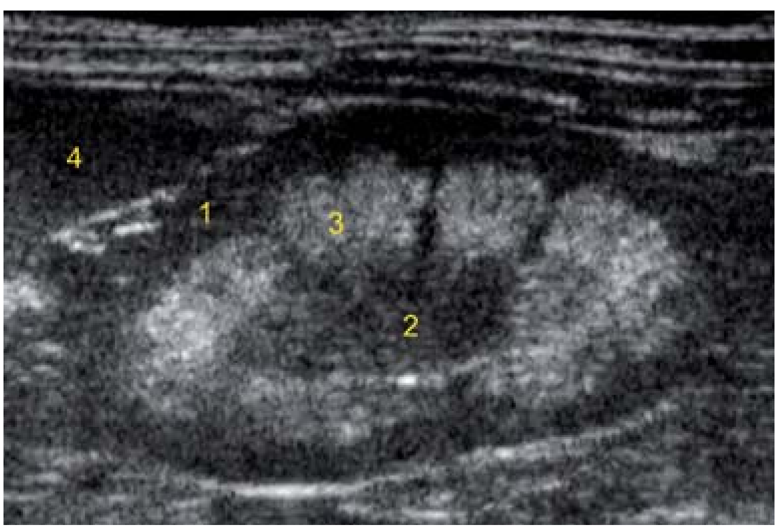

1: cortex
2: medulla
3: hyperreflective band
4: spleen

Fig. 2-85: Ultrasonographic image of a ferret's kidney, 12 MHz, PD: 2 cm. In well-nourished pet ferrets, a broad hyper-reflective band (3) can often be seen between the cortex (1) and medulla (2). This phenomenon has no clinical significance.

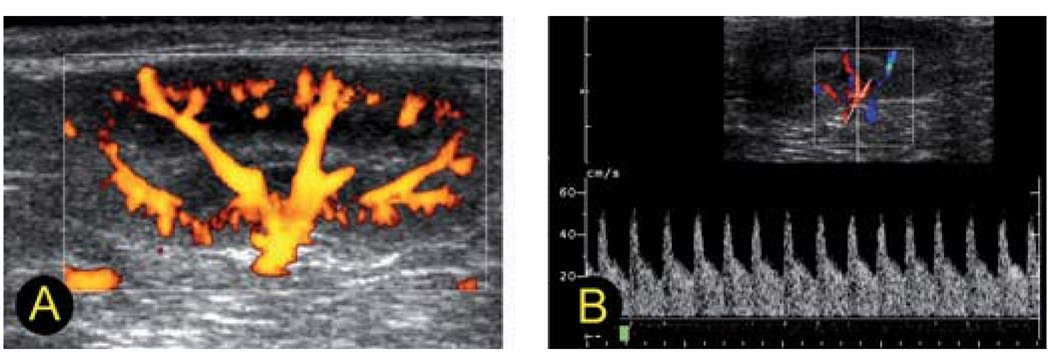

Fig. 2-86: Doppler ultrasonographic images of a ferret's kidney, dorsal plane, 12 MHz, PD: 2 cm.

A: Image of the renal vessels using power Doppler independent of flow direction (angio mode).

B: Image of the renal artery using color-Doppler and parallel to that, a PW Doppler echocardiogram.

Urinary bladder

To image the urinary bladder, the transducer is placed transversely over the body slightly in front of the pubic bone and pushed in a cranial direction until the bladder appears in the scan. For **rabbits,** it is particularly essential to use the smallest amount of pressure possible because a bladder that contains very little urine can be so compressed, it cannot be imaged. Only in the larger species (e.g., **ferret**, **rabbit**, **guinea pig**) does the wall of a full urinary bladder appear as a hypoechoic band flanked by a very thin echoic line on the inner and outer surfaces (**Fig. 2-87A**). The band narrows as it goes toward the neck of the bladder and into the urethra, which cannot be sonographically imaged. Urine is normally echo-free. However, calcium carbonate crystals can be found in the urine of many rabbits, guinea pigs, and chinchillas. Due to the rhythmic movements of the transducer these calcium carbonate crystals are disturbed and can be observed as points of echogenic reflections in the urine (**Fig. 2-87B**). Depending on the calcium concentration of the diet, the urine of even healthy rabbits, guinea pigs, and chinchillas can contain differing concentrations of calcium carbonate crystals, which can settle into a radiopaque »sludge« (**Fig. 2-155A**). The amount of sedimentation in the urinary bladder considered to be pathological or normal has not been definitely determined. In patients with »sludge«, the kidneys, ureters, and urethra should be carefully examined for the presence of pathological and/or obstructive calculi (see also Chap. 2.9.7).

Urethra

Ultrasonographic imaging of the urethra is not possible for most small exotic mammals.

2.4.3.6 Female genital tract

The ultrasonographic examination of the female genital tract is of great clinical significance and is always initiated from the caudal aspect of the body.

Vagina

The **rabbit** vagina, on the whole, is long and wide. Using the transverse plane, the rabbit vagina can be observed as a flat crosswise oval with a three-layered wall lying between the rectum and urinary bladder (**Fig. 2-88**). The vaginal wall has a strong central inner reflection, a middle hypoechoic band, and a weaker peripheral line of reflection. The vagina can also be identified lying caudal to the cervix and slightly proximal to the pelvic inlet in **guinea pigs** and in individual cases in **chinchillas**. In these species, the vagina is also observed as a hypoechoic flat crosswise oval structure, however, the wall is not differentiated into layers. In the other small exotic mammal species, the vagina lies primarily within the pelvic cavity and so is not possible to image sonographically.

Cervix

The cervix appears in the transverse plane as a round hypoechoic structure, without sharp boundaries, lying between the rectum and urinary bladder in **ferrets** and **rodents**, (**Fig. 2-89A**). In rodent species, the cervix is paired (at least in its internal structure) and cannot be sonographically imaged. However, it is possible (and relatively easy in **guinea pigs**) to show that the uterine horns arise from the cervix and diverge towards the left and right by using a slow cranial movement of the transverse transducer (**Fig. 2-87A**).

Only in the **rabbit** are both the left and right uteruses, including the two cervixes, completely separate (duplex uterus). In the transverse plane at the cranial end of the vagina, the round hypoechoic and indistinctly demarcated left and right cervixes can be clearly identified on the left and right as individual structures (**Fig. 2-89B**).

Uterine horns

The uterine horns of the **ferret** or the left and right uterus in **rabbits** and **rodents** with a duplex uterus are insignificant, hypoechoic tube-like structures which can be identified in the transverse plane lying between the urinary bladder and rectum (**Fig. 2-91**). The imaging of their course to the ovaries, in most cases, is not successful as these structures are very thin and poorly demarcated from their surroundings. Moreover, in the majority of rodent species, the uteruses course dorsolaterally over the cecum. The **rabbit** is again an exception, as its uteruses can be imaged as hypoechoic structures that normally course in a wide cranial curve dorsally over the bladder. Rabbit uteruses can be easily confused with loops of small intestines by inexperienced examiners.

Ovaries

In the majority of small exotic mammal species, the ovaries lie directly caudal to the kidney on the dorsolateral abdominal wall. The ovaries can be identified as round hypoechoic structures (**Fig. 2-90A, B**).

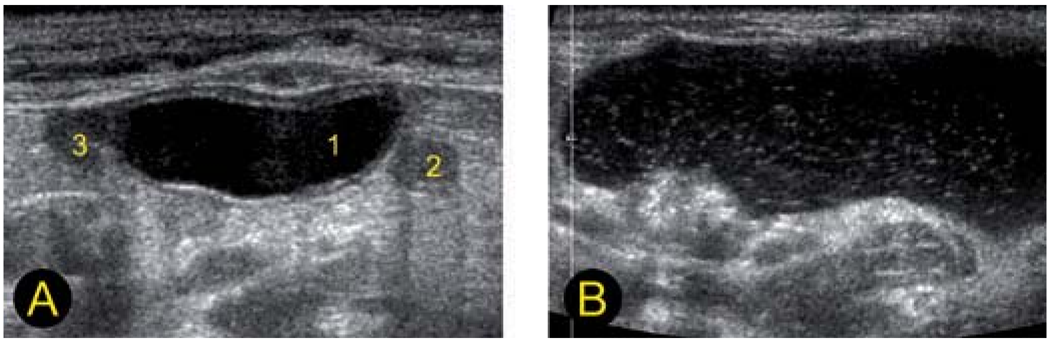

1: bladder
2: left uterine horn
3: right uterine horn

Fig. 2-87: Ultrasonographic images of urinary bladders, transverse section, 12 MHz, PD: 2.5 cm.

A: Guinea pig: The three-layered structure of the wall is clearly visible in this filled urinary bladder (1).

B: Rabbit: Well-filled urinary bladder with a small amount of urinary sludge, which after being disturbed caused the production of points of echoic reflections that can be seen here in the nonechoic urine.

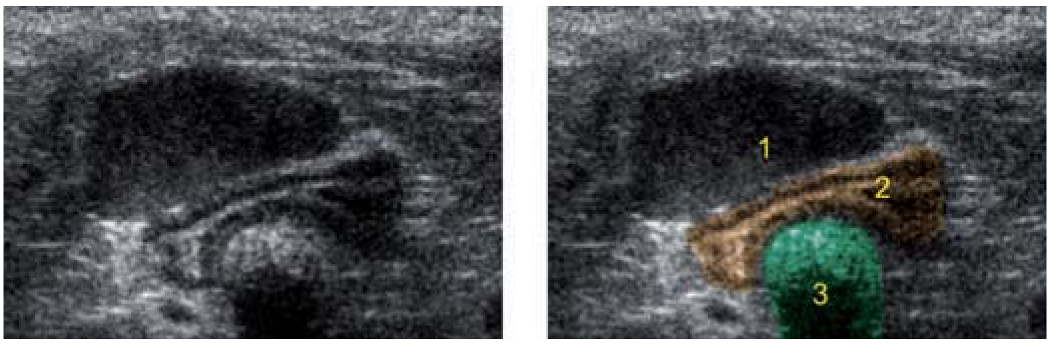

1: bladder
2: vagina
3: rectum

Fig. 2-88: Ultrasonographic images of a rabbit's vagina, transverse section, 12 MHz, PD: 2.5 cm. Rabbits have a vagina (2) that projects deep into the abdominal cavity. The vagina lies between the urinary bladder (1) and rectum (3) and can be identified by the layers that comprise the wall of this structure.

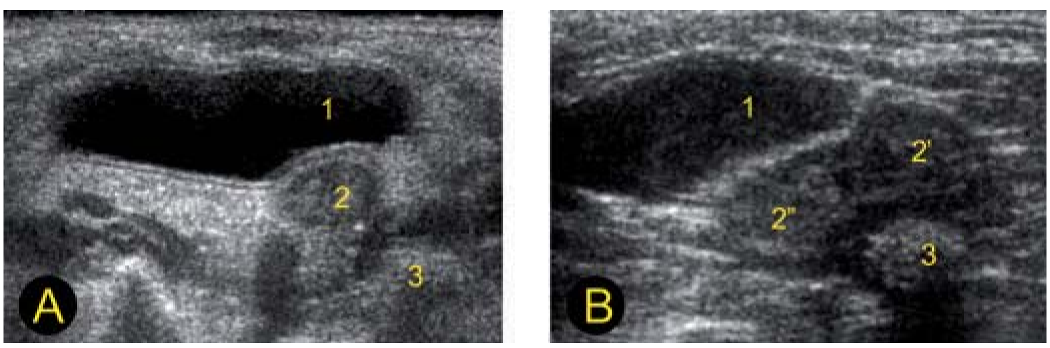

1: urinary bladder
2: cervix (single)
2': left cervix
2'': right cervix
3: rectum

Fig. 2-89: Ultrasonographic images of (A) a guinea pig's and (B) a rabbit's cervix, transverse section, 12 MHz, PD 2 cm.

The cervix (2) in the guinea pig is seen sonographically as a single organ, while the rabbit has a duplex uterus which is comprised of a left (2') and right cervix (2'').

Fig. 2-90: Ultrasonographic ovarian images.

A: 15 MHz, PD 1.5 cm. Rat.

B, C: 12 MHz, PD 1.5 cm. Rabbit.

The ovary (1) lies directly caudal to the kidney (2) in the majority of small mammal patients; however, the elongated ovary of the rabbit must be identified in the area cranial to the flank fold. The rabbit ovary has a characteristic central echogenic line (arrowheads). Corpora lutea can be directly imaged only at frequencies used for the Doppler detection of increased vascularization (C).

Images from Lehmann J. (2007): Abdominale Sonographie bei der Ratte (*Rattus norvegicus*). Dissertation, Munich, Germany.

1: ovary
2: kidney

Again, the **rabbit** is different from the other small exotic mammal species as its ovaries lie more caudal at the level of the fold of the flank on the lateral abdominal wall. The ovaries are ovoid hypoechogenic structures, which are clearly offset from their surroundings and have a mean length of 1 cm and a diameter of 4 mm × 6 mm. Usually, there is a longitudinal echoic line that runs centrally through the ovary (**Fig. 2-90B**), which should not lead the examiner to confuse the ovary with a cryptorchid testicle. Due to their small size, it is not possible to obtain reliable images of functioning ovaries using the B-mode with the ultrasound frequencies of between 10 MHz and 15 MHz (i.e. frequencies commonly used for clinical diagnostic examinations). However, it is possible to show the development of the corpus luteum in the rabbit using Doppler ultrasonography, which can be identified with color Doppler as an area of increased vascularization from the 2nd day after ovulation onward (**Fig. 2-90C**).

Pregnancy

Ultrasonography is the method of choice in the majority of small exotic mammal species for pregnancy detection (**Fig. 2-92**). One exception is the **degu**, because in this species manual handling of pregnant animals will lead to abortion even in tame animals. Another exception is the **golden hamster** as the pregnant uteruses lie dorsal to the cecum until just before parturition and therefore cannot be imaged sonographically.

On the whole, it can be assumed that the sonographic proof of pregnancy can be achieved by imaging the ampullae after implantation. Table 2-19 provides an overview of the times when transcutaneous pregnancy detection can be successfully achieved.

A placenta is imageable in the **rabbit** from the 7th day of pregnancy on. The heart beat of rabbit embryos can be detected using color Doppler from the 9th day and is recognizable in the B-mode scan from day 12. The development of the fetuses can be easily followed throughout the subsequent pregnancy. In addition to the imaging the fetuses for pregnancy detection, the clinical significance of ultrasonography is to determine if all fetuses are viable. The easiest method to check for fetal viability is detection of a heart beat.

Rodents have a discoid placenta (**Fig. 2-93A**), which is very different in its sonographic structure to that found in carnivores and should not be confused with a pathological structure. In a flat scan, a discoid placenta is shown as a large circular structure (**Fig. 2-93B**), in which the maternal endometrium interdigitates with the fetal membrane. This interweaving can be viewed on a sonogram image as alternating hypoechoic and hyperechoic lines.

Table 2-19: Times of when pregnancy can be first confirmed using ultrasonography

Species	Pregnancy confirmation (day)
Ferret	12th
Gerbil	10th
Guinea pig	10th
Mouse	7th
Rabbit	4th–6th
Rat	8th

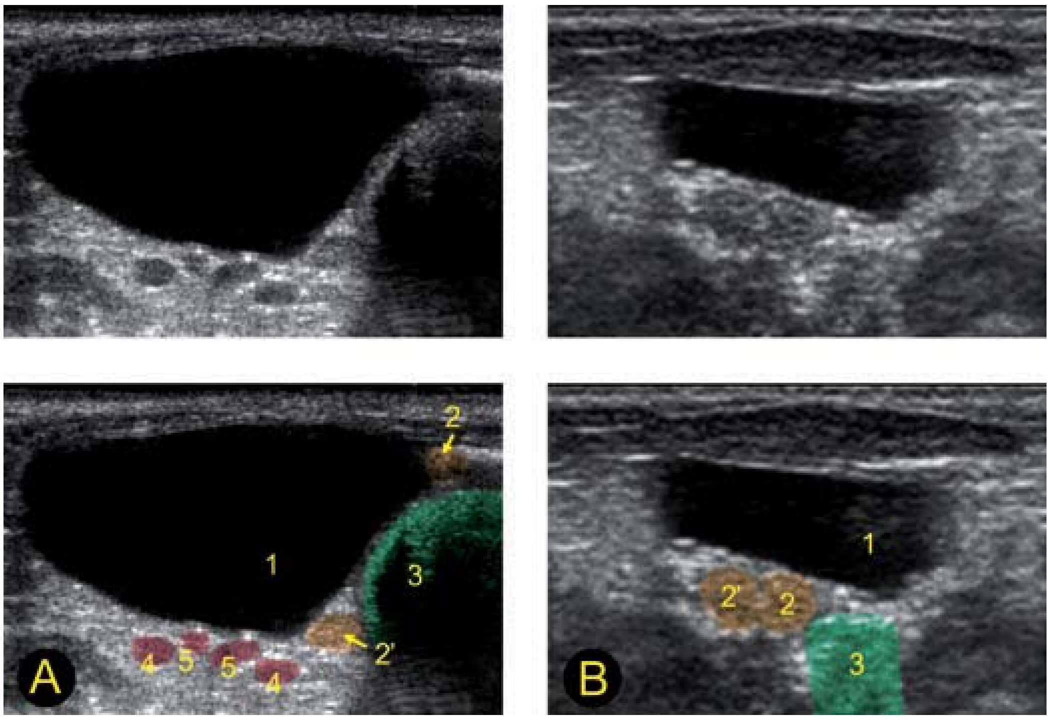

1: bladder
2: left uterine horn
2’: right uterine horn
3: rectum
4: right and left external iliac arteries
5: right and left external iliac veins

Fig. 2-91: Ultrasonographic images of uterine horns, transverse section.

A: 12 MHz, PD 2 cm. Ferret.

B: 15 MHz, PD 1 cm. Degu.

Image B is from Gneiser, B. (2005): Abdominale Sonographie beim Degu (*Octogon degus*, Molina 1782). Dissertation, Munich, Germany.

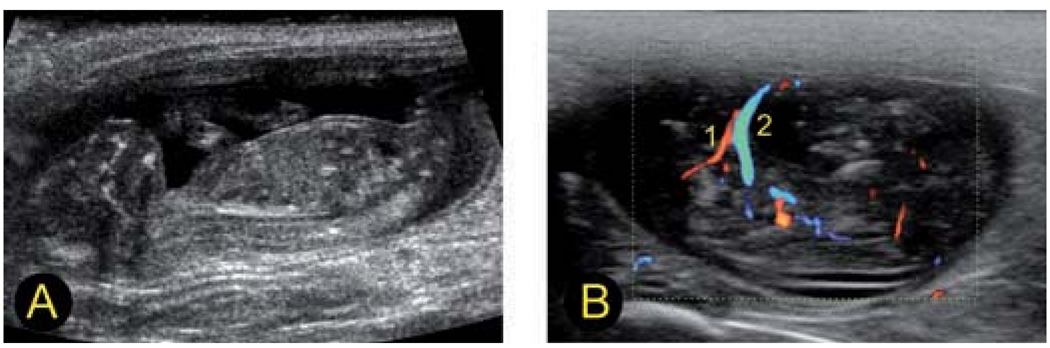

1: umbilical artery
2: umbilical vein

Fig. 2-92: Ultrasonographic images of pregnancy detection.

A: 12 MHz, PD 3 cm. Rabbit fetus: 21st day.

B: 12 MHz, PD 2 cm. Guinea pig: Color-Doppler image of the umbilical cord showing the umbilical artery (1) and umbilical vein (2).

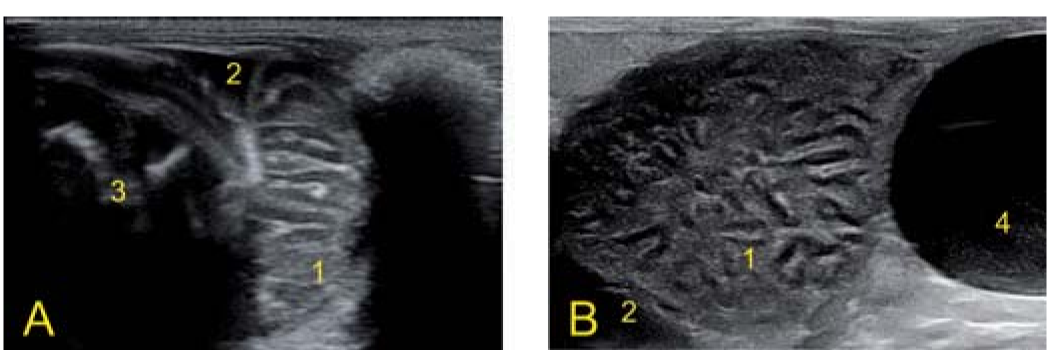

1: placenta
2: allantoic sac
3: foetus
4: urinary bladder

Fig. 2-93: Ultrasonographic images of a guinea pig’s discoid placenta, 12 MHz, PD: 2.5 cm.

A: Cross-section.

B: Flat section.

2.4.3.7 Male genital tract

Diseases of the male genital organs have much less significance than those of the female genitalia. This fact hides the danger that these organs are often given a low level of attention; therefore, pathological changes associated with disease processes (e.g., such as testicular neoplasia which has the potential to metastasize to the lungs) may be overlooked or unrecognized. For this reason, the entire male genital tract should be included as an integral part of the protocol for an abdominal ultrasonographic examination, including the extra-abdominal testicles.

Testicle

In all species of small exotic mammals, the testicles have a homogeneous, finely grained echoic texture of medium echogenicity. The mediastinum testis appears as a central hyperechoic line within the testicle (**Fig. 2-94A**). However, in the **small rodents,** the mediastinum testis is very inconspicuous and can only be imaged using an optimal scanning angle. The head and tail of the epididymis lie at the respective poles of the testicle as hypoechoic structures, whereas the very thin body of the epididymis cannot be imaged with any degree of certainty. In rodents, there is a very large fat pad cranial to the testicle which maintains the inguinal canal in an open position, thus enabling the animal to retract its testicles through the opening into the abdomen at any time. If the testicle is lying outside of the abdomen, the fat pad closes the wide inguinal canal, thereby preventing herniation of the intra-abdominal organs into Nuck's canal. The fat pad appears sonographically as a homogeneous structure but has a coarser echo texture than the testicle and does not have a mediastinum. The existence of a mediastinum is definitive proof that a testicle is present (**Fig. 2-94A**).

Accessory sex glands

The **prostate** is only well differentiated in uncastrated male **ferrets.** The prostate is an insignificant homogeneous structure of medium or low echogenicity lying caudal to the urinary bladder (**Fig. 2-95A**). While **rabbit** bucks do not have any accessory sex glands that can be imaged sonographically, **rodents** have a large **seminal vesicle** which extends far into the abdomen. Lying close and parallel to the seminal vesicle is the so-called coagulating gland, the equivalent of a prostate lobe. A sonographic differentiation between the coagulating gland and the seminal vesicle cannot be accomplished with any certainty. The very prominent seminal vesicle can be easily located, especially in male **guinea pigs**, as a tube-like hypoechoic structure lying left and right of the urinary bladder. The most reliable image of the seminal vesicle is that of a ram-horn-like structure visualized in an oblique plane through the proximal section of the urethra, directed craniolaterally along the side of the urinary bladder (**Fig. 2-95B**).

2.4.3.8 Adrenals

The location of the adrenals is very similar in all species of small exotic mammals. The left adrenal lies lateral to the aorta and cranial to the left renal vein. The right adrenal is located in a more cranial direction than the left: dorsolateral to the caudal vena cava, directly caudal to the liver and cranial to the right renal vein. Relative to the size of the animal, the adrenal glands are larger in smaller species. For this reason, it is much easier to image the adrenal glands using ultrasonography in the majority of small exotic mammal species than in dogs and cats.
In **ferrets**, the left and right adrenal glands are ovoid with a homogeneous echo texture and hypoechoic. A differentiation of the medulla and cortex is not possible even with high-resolution ultrasonography probes (**Fig. 2-96A**). The **rabbit** adrenal glands have an ovoid form with an obvious distinction between the hypoechoic cortex and the echoneutral medulla (**Fig. 2-96B**). The **chinchilla** adrenal glands are conspicuously thin and elongated in the majority of animals. Characteristic for the chinchilla adrenal is a central thin echoic strip of medulla (**Fig. 2-96C**). A peculiarity of the chinchilla adrenal glands is the right adrenal is roughly 1/3 longer and somewhat thicker than the left. In the **guinea pig** and **rat**, the adrenal glands lie close to the cranial pole of the kidneys and are hypoechoic in comparison to the renal cortex (**Fig. 2-96D**). A differentiation of the medulla and cortex is not possible. Imaging of the left adrenal is not always possible in the guinea pig and rat because when their stomach is filled, its ventral fundus extends in an extreme caudal direction. **Gerbils** have, with respect to their size, the largest adrenal glands. Ultrasonographic imaging of these glands is almost always successful when one initiates the examination by imaging the renal tissue in the dorsal plane, then visualizing the adrenals at the craniomedial pole of the kidneys.

Data about the length and diameter of the adrenal glands in various small mammalian species is shown in Table 2-20.

Table 2-20: Adrenal measurements in various species

Species	Length [mm]	Widest cross-section [mm]
Chinchilla, left adrenal	6.9 (5.2–8.7)	2.4 (2–3.1)
Chinchilla, right adrenal	9.9 (7.8–11.9)	2.7 (2.4–3.9)
Degu	5.5 ± 0.5	4.2 ± 0.5
Ferret (female)	6.2 (4.1–9.7)	2.5 (2.0–4.1)
Ferret (male)	6.5 (4.3–10.9)	2.9 (2.1–4.2)
Gerbil	5.3 ± 0.9	2.3 ± 0.4
Guinea pig	15.4 (12.6–17.7)	6.2 (4.3–8.4)
Rabbit, dwarf breeds (< 2 kg)	7.2 (6.1–9.5)	3.7 (3.0–5.2)
Rat	4.5 (4.1–6.5)	2.7 (2.5–3.7)

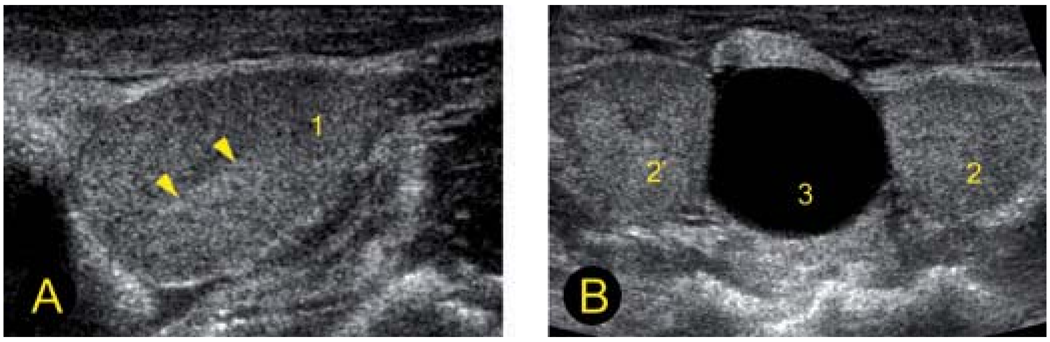

1: testicle
2: left testicular fat pad
2’: right testicular fat pad
3: bladder

Fig. 2-94: Ultrasonographic images of a chinchilla’s testicle, 12 MHz, PD 2 cm.

A: Longitudinal section of the testicle (1) with indications of the mediastinum testis (arrowheads).

B: Transverse section through the left (2) and right (2’) testicular fat pads that flank the urinary bladder (3).

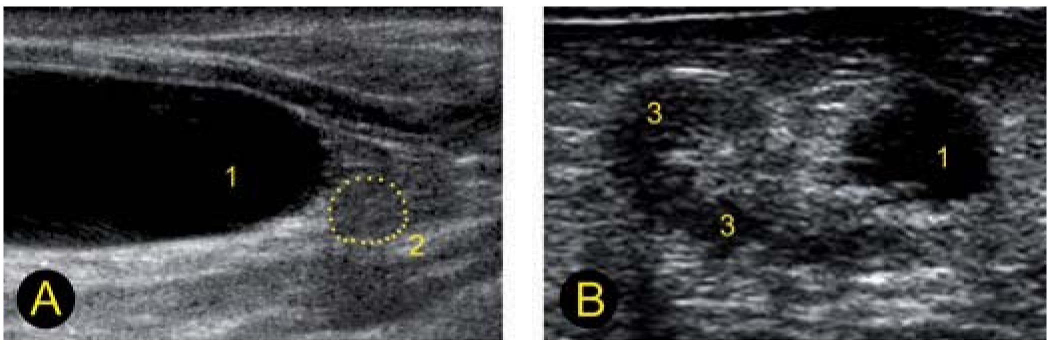

1: bladder
2: prostate
3: seminal vesicle

Fig. 2-95: Ultrasonographic images of accessory sex glands.

A: Sagittal plane, 12 MHz, PD: 2 cm. Ferret: Urinary bladder (1) and prostate (2).

B: 15 MHz, PD: 1 cm, oblique section. Gerbil: Urinary bladder (1), flanked on the right by the seminal vesicle (3).

Images from Grodtmann, E. (2007): Abdominale Sonographie der Monogolischen Rennmaus (*Meriones unguiculatus*, Milns-Edwarts 1867). Dissertation, Munich, Germany).

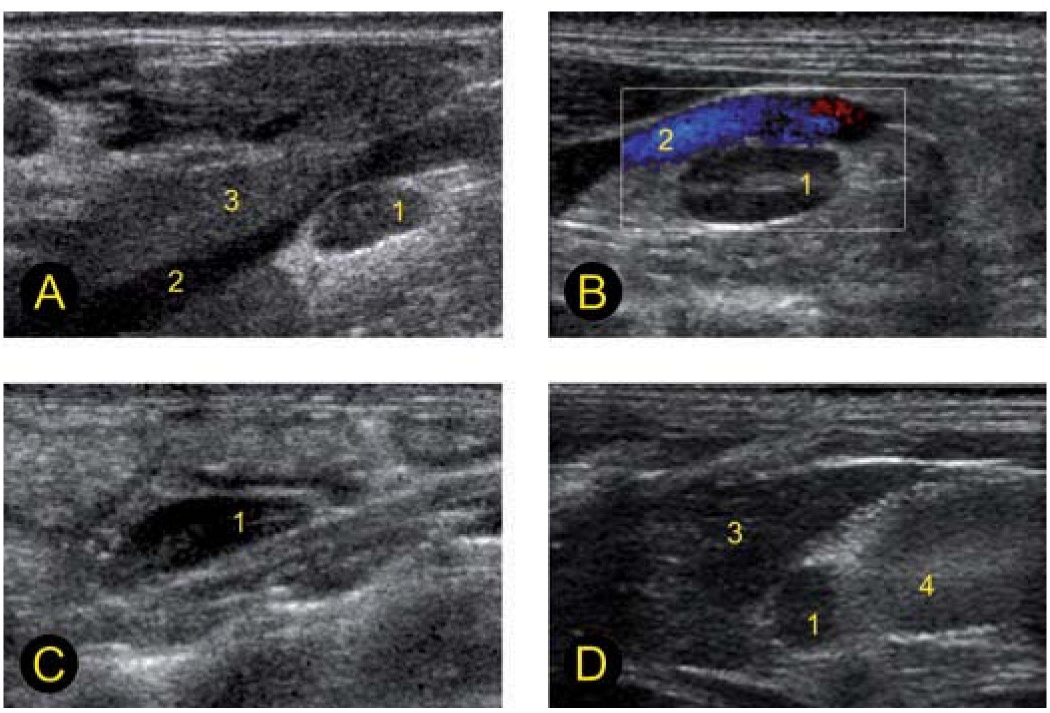

1: adrenal
2: caudal vena cava
3: liver
4: kidney

Fig. 2-96: Ultrasonographic images of adrenal glands, 12 MHz (A–C), 15 MHz (D), PD 1.5 cm.

A: Ferret: Right adrenal (1) lying dorsal to the caudal vena cava (2).

B: Rabbit: Right adrenal (1) with the caudal vena cava (2) detected using color Doppler.

C: Chinchilla: Flat triangular left adrenal.

D: Rat: Right adrenal (1) between the liver (3) and kidney (4).

Image A is from Lehmann J. (2007): Abdominale Sonographie bei der Ratte (*Rattus norvegicus*). Dissertation, Munich, Germany.

2.4.4 Miscellaneous

2.4.4.1 Eye

Ingo Hoffmann

The eye in the **rabbit** and **guinea pig** can be imaged using ultrasonography, MRI, and CT. In animals and humans, conventional radiographic techniques do not offer significant diagnostic results. The exceptions to the above statement are the identification of dental disaese associated with exophthalmos and dacryocystitis as well as lytic processes affecting the bones around the eye. Special care must be taken to prevent summation of neighboring bony structures interfering with one's ability to adequately interpret the radiographic images.

The simplest and cheapest method for imaging the eye is ophthalmosonography. The ultrasonographic investigation of the eye or »ophthalmosonography« is the oldest medical sonographic technique and was first used in humans in 1956. In veterinary medicine, ophthalmosonography was first used to examine animal eyes in the late 1960's.

Since the mean frequency of the transducer determines the resolution and depth of penetration, the use of high frequency transducers are recommended for small exotic pet mammal patients. In veterinary medicine, the examiner must decide between using mechanical sector probes which have been specifically constructed for the eye or somatic, electronically controlled probes. Mechanical sector probes usually have a poor image quality in the near field and therefore have only limited applications for use on pet eyes.

Coupling of electrical probes to the small exotic mammal's body can be difficult due to their width. To partially compensate for this problem, one can place generous amounts of acoustic coupling gel on the transducer face.

An enlargement function (zoom) should always be available as ophthalmosonography in small exotic pet mammals is limited by the size of their globe. In order to gain a satisfactory resolution of ocular structures, the transducer should have a mean frequency of at least 10 MHz.

In rabbit patients, the ophthalmosonographic examination is usually performed without difficulty. Guinea pigs will often react with defensive movements when their heads are fixed. Depending on the patient and presenting complaint, the examination can take place while the animal is under local anesthetic, sedation, or general anesthesia. Local anesthesia is usually adequate for rabbit and guinea pig ocular examinations.

Direct cornea coupling is the most frequently used coupling method, in which the transducer is placed directly on the cornea after a quantity of bubble-free gel has been applied on the eye. To improve the resolution of ocular structures lying close to the transducer, spacers (e.g., gel cushions, water-filled surgical gloves, immersion solutions) can be used.

Vertical, horizontal, or transverse coupling is acceptable for ophthalmosonographic examinations. Ideally, the plane should be written on the sonogram to identify the location of the image to expedite re-examinations when assessing specific disease conditions affecting a certain area of the eye.

The routine ophthalmosonographic examination should include measurement of the anterior ocular chamber, lens, and globe diameter (each measurement taken in an anterior to posterior direction). There are species-specific differences in these values; for example, the lens in the rabbit (18 mm) and guinea pig (4.4–5 mm up to 10 mm) is relatively large in comparison to the diameter of the globe. The anterior ocular chamber is rather flat with an anterior-posterior width of approximately 1 mm.

If at all possible, the contralateral eye should be examined for use as a comparative ocular model.

Indications for ophthalmosonography in small exotic pet mammals

- ☐ cloudy optical structures (e.g., cornea, lens)
- ☐ assessment of the structures in the eye which cannot be visualized using light ophthalmoscopy
- ☐ demarcation of intraocular space-occupying lesions
- ☐ eye measurements
- ☐ retrobulbar disease

Eyelids and nictitating membrane

The eyelids and nictitating membrane both have an average echogenic reflection.

The eyelids and nictitating membrane should never be selected as coupling sites because when used, there is a loss in image quality below these structures.

Cornea and sclera

Three distinct anatomic areas can be differentiated within the cornea during an ophthalmosonographic examination. The corneal epithelium with its basal membrane, Descemet's membrane, and the endothelium all appear as highly reflective lines. The stroma lying between these structures is a hypoechoic or an anechoic homogeneous band. The hyperechoic sclera lies directly adjacent to the cornea (**Fig. 2-97**).

Anterior and posterior ocular chambers

The anterior and posterior ocular chambers are echo-free in the healthy eye. In the anterior chamber, there are often reverberations from the hyperechoic corneal structures (**Fig. 2-97**). This phenomenon is acerbated by applying too much pressure when coupling the transducer on the cornea. In addition, too much pressure also causes the anterior chamber to appear flattened.

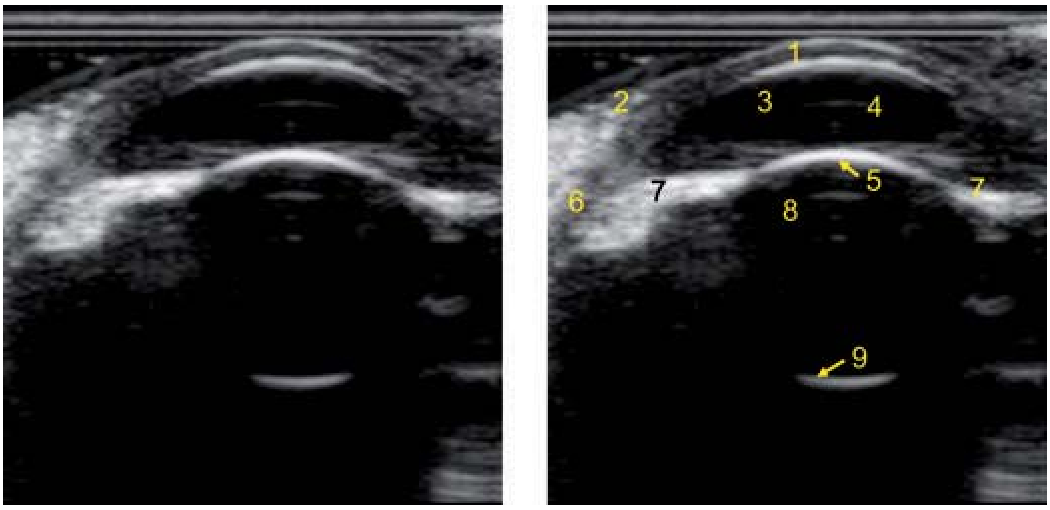

1: cornea
2: sclera
3: anterior chamber of the eye
4: reverberations from the cornea
5: anterior lens reflection
6: ciliary cleft
7: iris and ciliary body
8: reverberations from the anterior lens reflection
9: posterior lens reflection

Fig. 2-97: Ultrasonographic images of a rabbit's anterior eye, horizontal section, corneal coupling, 15 MHz, PD 1 cm.

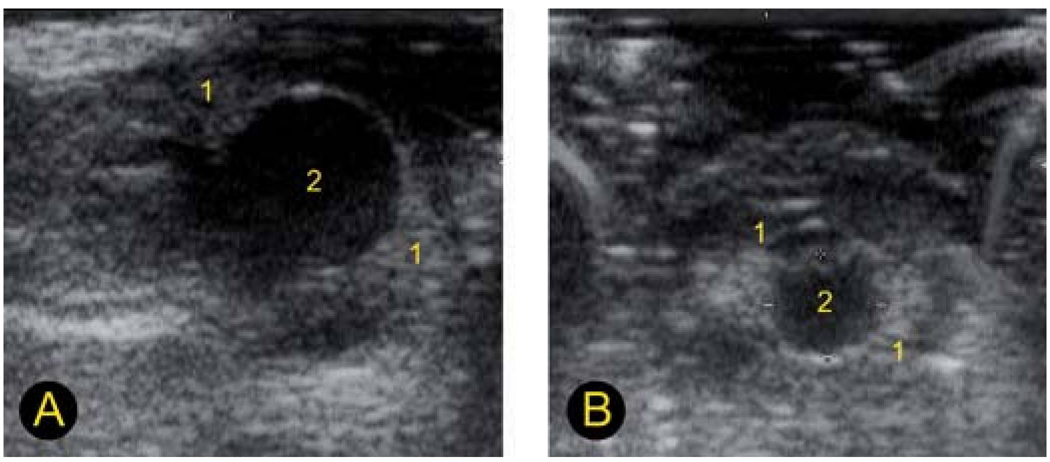

1: iris
2: wide (A) and narrow (B) pupils

Fig. 2-98: Ultrasonographic images of a rabbit's pupil, corneoscleral coupling site, transverse scanning plane, 11 MHz, PD 2 cm.

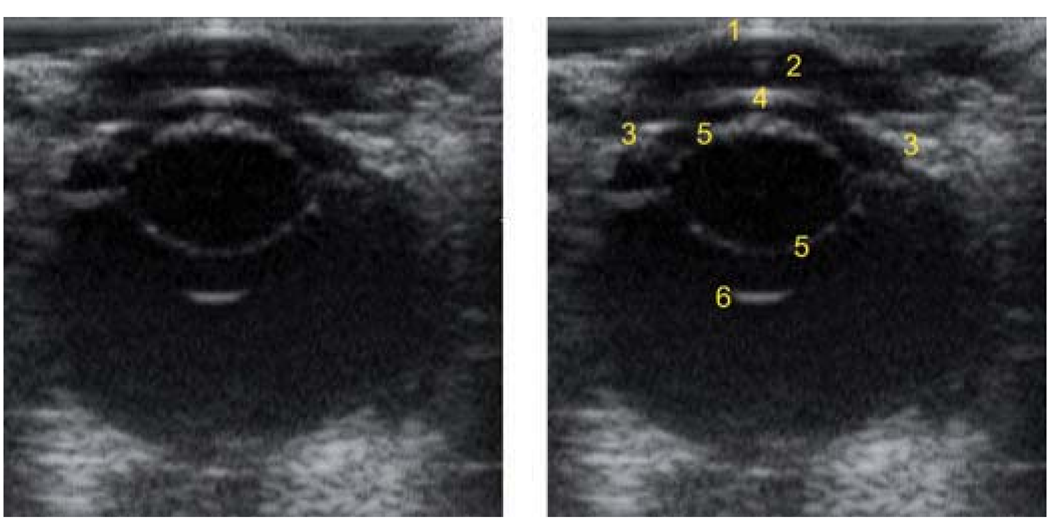

1: cornea
2: anterior chamber
3: iris
4: anterior lens reflection
5: hypoechogenic ring of a nuclear cataract
6: posterior lens reflection

Fig. 2-99: Ultrasonographic images of a rabbit's globe, corneal coupling site, 11 MHz, PD 2 cm.

Iris and ciliary body

The iris has a medium echoic, slightly nonhomogeneous structure. With both horizontal and vertical coupling, the apex of the iris lies in direct contact with a highly reflective line, the anterior lens capsule (**Fig. 2-97**). In the transverse plane, the pupil can be visualized as an anechoic circle, whose size is dependent on the iridic ring opening. The size of the pupil can therefore be measured using ultrasonography (**Fig. 2-98**).

The ciliary body is located posterior to and has a similar echogenicity as the iris (**Fig. 2-97**).

Healthy zonula fibers cannot be sonographically imaged.

The iridocorneal angle formed by the cornea, sclera, and iris (chamber angle) is echo-poor. The ciliary cleft is distinguishable from the surrounding low-middle echoic structures as a hypoechoic area (**Fig. 2-97**). The ciliary cleft can only be imaged if the scanning plane is exactly perpendicular to this structure and a high-frequency transducer is used.

Lens

The normal lens in a ultrasonographic image is depicted as two sharply drawn, hyperechoic, slightly curved lines. No image is formed for the lens »body« because the ultrasound waves do not return to the transducer (scatter) as they rebound from the other structures due to their extreme curvature. Due to the strong lens capsule, reverberations (repeat echoes) can be formed on the lens lines (**Fig. 2-97**). There is frequently a fine and irregular ring of hyperechoic structure visible in older animals resulting from nucleosclerosis (**Fig. 2-99**).

The following orientation points should be taken into consideration when performing ultrasonographic examinations of the lens: the two hyperechoic lines formed by the cornea and the lens, and the distance between these structures as well as their distance to the iris.

Vitreous body

The vitreous body should always be anechoic and the transition to the fundus should be a normal rounded form (**Fig. 2-100A**). Every so often, it is helpful to increase the gain when examining the vitreous body. Increasing the gain improves the image quality of very fine structures in this area, including those associated with clouding of the vitreum.

Retina

The retina cannot be separated sonographically from the underlying choroid and sclera. All the structures that form the fundus are hyperechoic (**Fig. 2-100A**).

Orbit

The retrobulbar anatomy which includes the eye muscles and surrounding tissues produces a mixed-echoic ultrasonographic image. The optic nerve is visible as a hypoechoic worm-like structure (**Fig. 2-100B**).

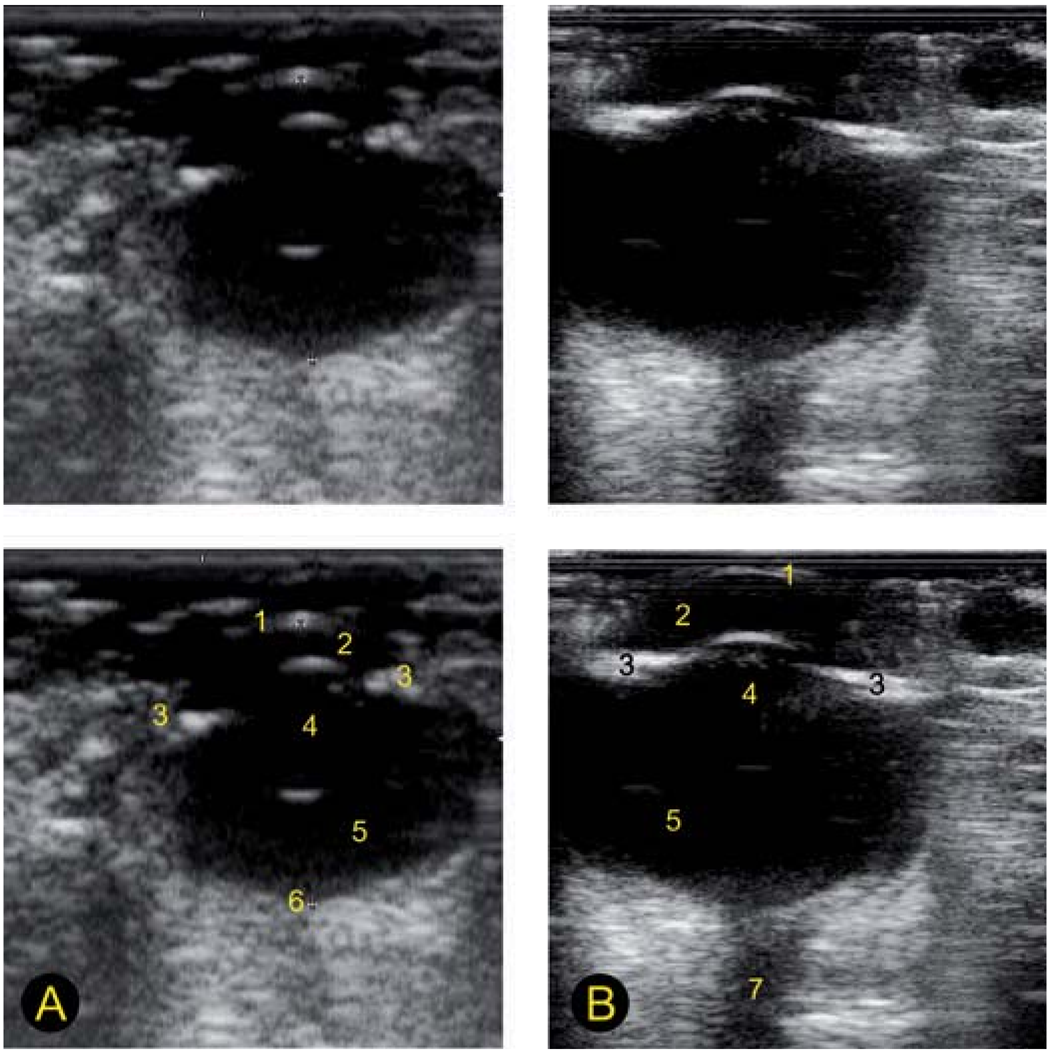

1: cornea
2: anterior chamber
3: iris and ciliary body
4: lens
5: vitreum
6: ocular fundus
7: optic nerve

Fig. 2-100: Ultrasonographic images of the globe.

A: 11 MHz, PD 2 cm, Guinea pig.

B: 15 MHz, PD: 3 cm, Rabbit.

2.5 Computed tomography (CT) and magnetic resonance imaging (MRI)

Michael Fehr

Modern developments in medical technology, especially those arising from the continued advancement of diagnostic imaging modalities (e.g., CT, MRI), have been a viable diagnostic option for some years. Although available, these imaging options were rarely used due to the high cost associated with the examination. Computed tomography and MRI quickly gained popularity within the scientific research community, veterinary teaching hospitals, and veterinary referral hospitals. Absolute immobilization of the patient using generalized anesthesia is a prerequisite for obtaining optimal images. There are reports in which CT examinations were performed on animals that were not placed under general anesthesia (e.g., using a specially formed rabbit »fixation box« with holding bars).

The most important indications for CT imaging of small exotic animal patients are dental disease (diseases of the teeth (**Figs. 2-107** and **2-175C**) and the periodontal apparatus) and other bony structures of the head (**Figs. 2-101** and **2-164B**). Computed tomographic imaging provides images of bony structures without summation. Moreover, CT images make it easier to confirm diagnoses of central nervous system (CNS) disease as well as anomalies affecting the thorax, abdomen (**Fig. 2-161D**), and pelvis (**Fig. 2-160**) of small exotic mammals.

An extremely high image resolution (up to 50 µm) is achieved by the micro-computed tomography (µCT) technique, but at this time is only available for experimental use. However, this advancement in CT technology provides an indication of what to expect regarding diagnostic imaging at the clinical level in the near future (**Figs. 2-28**, **2-31** and **2-101**).

Unfortunately, at the present time, there is a lack of published information from controlled scientific investigations relating to the clinical significance of MRI in small exotic mammals. However, the known advantages of MRI over other imaging modalities, especially for imaging soft-tissue changes (e.g., CNS disease [**Fig. 2-102**]), can be extrapolated to small exotic pet mammals. Future technological advancements of MRI will allow this diagnostic imaging modality to be commonly used for small exotic mammal patients, especially when the examination time is reduced.

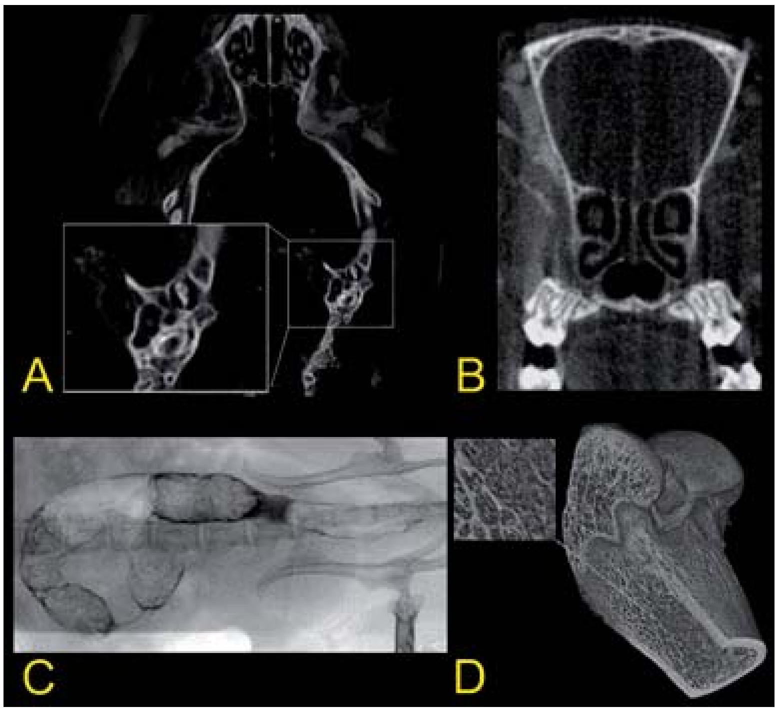

Fig. 2-101: *In-vivo* μCT investigation in the mouse, resolution 50 μm.

A: Enlargement of a transverse section of the tympanic bulla, with sections of the auditory ossicles (head of the malleus, incus).

B: Transverse section at the level of the ethmoid bone with a detailed image of the crowns and roots of the molars in the upper jaw.

C: Double-contrast image of the rectum and colon.

D: High resolution 3D image of the trabecular bone structure in the distal femur.

μCT scans courtesy of S. J. Schambach and M. A. Brockmann, Neuroradiology Department, Medical Faculty Mannheim, University of Heidelberg, Germany.

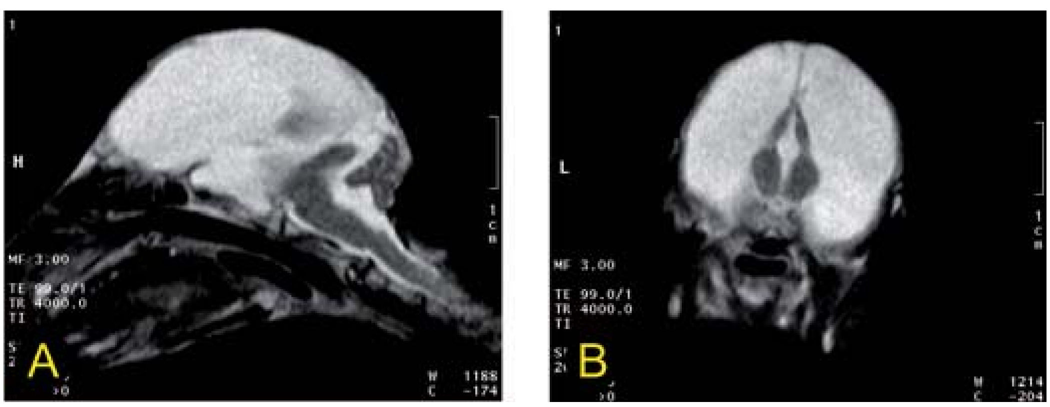

Fig. 2-102: MRI examination of a rabbit (age: 2 months), T1-weighted, brain. Severe widening of the ventricle (hydrocephalus).

A: sagittal section.

B: transverse section.

Special diagnostics, pathological findings

2.6 Skeletal system

Sven Reese, Michael Fehr

One of the commonest and most important diseases that affects the bone structure of exotic mammals is **osteodystrophy fibrosa.** The most obvious radiographic sign associated with this disease is an often dramatic decrease in bone density. This irregular demineralization will cause a patchy moth-eaten look to the affected bones, especially the long bones (e.g. humerus, femur). To compensate for the decrease in cortical stability, the compact bone will increase and become thickened. The bones of animals diagnosed with this disease are very fragile and this leads to the formation pathological fractures. Handling, positioning, and restraining such animals (e.g. for a radiographic examination) should be performed with great care due to their fragile body condition. The numerous forms of osteodystrophy fibrosa can be differentiated based on the underlying etiologic cause of the disease condition. Secondary renal osteodystrophy is a consequence of chronic renal insufficiency and occurs often in older rabbits that are infected with *Encephalitozoon cuniculi*. Nutritional deficiencies due to feeding an improper diet or selective eating by the rabbit will cause calcium/phosphorus imbalances that result in secondary osteodystrophy. At this time, satin guinea pigs are predisposed to a severe form of osteodystrophy which is believed to be associated with an underlying genetic cause (**Fig. 2-103**).

The guinea pig is the only small exotic mammal that requires nutritional supplementation of Vitamin C (15–25 mg/day). A guinea pig diagnosed with a **vitamin C deficiency** can have radiographic evidence of bone and/or joint disease in addition to the typical clinical signs associated with this disease process (e.g. gingival hemorrhages, poor wound healing, weakness, diarrhea). Radiographic abnormalities that involve the bones and joints include widening of the long bone epiphyses and the osteochondral transition zones on the ribs, and there may be an increased soft-tissue pattern affecting the joints. Affected animals are predisposed to the development of spontaneous fractures.

2.6.1 Cranium and teeth

Cranial fractures are often diagnosed after traumatic events (e.g. being dropped). Fractures of the mandible and maxilla can occur in association with loose, broken, and/or lost teeth (**Fig. 2-104**). It should be noted that a fissure-like line may be observed in the caudal region of the maxilla on radiographs of young guinea pigs; this line should not be confused with a fracture.

Tumors originating from the bones of the head are rarely diagnosed in rabbits and rodents. Occasionally, osteosarcomas are diagnosed in older rabbits and guinea pigs (**Fig. 2-105**), and are easy to misdiagnose as a jaw abscess.

The typical radiographic characteristic of **otitis media/interna** is a radiopaque shadow in the tympanic bulla of the affected side. Radiographic images should be taken in the DV projection as there is no summation of the two sides at this angle (**Fig. 2-106**). A frequent cause of **otitis media/interna** in small exotic mammals is an infection of the upper respiratory tract (e.g. rabbits/ pasteurellosis).

Temporomandibular luxations are relatively rare in small exotic mammals. Luxations involving this anatomic area may be caused by trauma or are more often the result of iatrogenic origin (e.g. mouth gag trauma). The rostrocaudal projection is recommended for radiographic assessment of the temporomandibular joint (see **Fig. 2-16C**).

The type, frequency, and clinical significance of **dental disease** are relative to the type of tooth (e.g brachyodont, elodont) and species being examined.

The **ferret**, with its secodont carnivore dentition is rarely diagnosed with dental disease in comparison to other small exotic mammals. **Tooth fractures**, loose teeth, or traumatic tooth loss, which may be associated with mandibular fractures, have all been diagnosed in ferret patients (see **Fig. 2-104**). **Periodontal disease** is frequent diagnosed in ferret patients that present to veterinary hospitals with periodontal inflammation and degradation, which may be observed as tooth root exposure and the loss of teeth. To radiographically assess the extent of dental disease, the teeth must be imaged without the diagnostic hindrance of summation. The simplest way to achieve an unobstructed image is to place a dental film in the oral cavity. Alternatively, radiographs using oblique projections should be taken with the mouth open.

The dentition of **lagomorphs** (e.g. rabbit) and **caviomorphs** (e.g. guinea pig, chinchilla, degu) are dependent on normal wear for proper development since both groups of animals have continously growing elodont incisors and molars. Pet foods are often low in fiber and have a high energy level. The lack of fiber associated with inadequate diets results in less chewing while the high energy composition of the food decreases the amount of time needed to ingest the food. These two factors combine to have a reduced abrasive effect on the teeth. In addition, there are breed/genetic associated influences which increase the likelihood of developing dental disease. The various tooth anomalies observed in these lagomorph caviomorph species can be subdivided in three categories:

- ☐ trauma
- ☐ periodontal disease
- ☐ excessive tooth growth with malocclusion

Fractures of the incisors are relatively frequent and often occur due to accidents or are of iatrogenic origin. Incisor and molar longitudinal fractures and fissures often result as an iatrogenic consequence of dental care when using dental forceps or side cutters. The diagnostic aim of radiographic examinations of tooth fractures is to determine the extent of the injury to the alveolus (e.g. fissures) and/or pulp cavity (e.g. exposure), and whether the alveolus also has fissures in it.

Periodontitis can develop when food becomes entrapped between the teeth or in the periodontal space. The development of periodontitis is unlikely when the teeth are positioned normally and there is normal wear and tear. An important predisposing factor to periodontitis is malocclusion of specific teeth or the dental arcade. In such cases, radiographs taken from a lateral position of the interdental region and the periodontium should be examined for signs of inflammation.

Improper tooth wear inevitably leads to elongation and malocclusion as well as more complex and severe dental disease. Initially, improper tooth wear induces an increase in the pressure on the occlusal surface. The back teeth of the lower jaw grow according to the surface pressure toward the tongue, while the teeth in the upper arcade grow towards the cheek. Subsequently, **buccal spurs** are formed on the upper jaw teeth (**Fig. 2-107**) and **lingual spurs** on the lower jaw teeth, which can grow until a dental **bridge** is formed over the tongue. Constantly increasing pressure on the teeth can result in **retrograde ectopic tooth growth** (**Fig. 2-108**) especially with chinchilla patients in which it is diagnosed as a severe disease. Retrograde ectopic tooth growth can occur in very young chinchillas often affecting the lower jaw with the retrograde elongation of the back teeth leading to **osteophyte** formation on the ventral edge of the mandible. Osteophytes are also formed on the upper jaw and finally the bone, and may eventually extend into the nasal cavity or orbit. Displacement of the nasolacrimal duct is often a complication associated with retrograde ectopic tooth growth. Precise radiographic positioning is required to assess the cheek teeth of rabbits for retrograde elongation. For the rabbit patient, a guide line is drawn from the rostral end of the nasal bone to the external occipital protuberance, over which the back teeth may not project (**Fig. 2-108B**). A similar guide line in the chinchilla extends from the dorsal edge of the upper incisors to the middle of the tympanic bulla (**Fig. 2-108A**).

With extreme malocclusion, the severely affected periapical germinative tissues are incapable of building tooth substance of consistent quality and therefore the teeth have a softer composition in general. Radiographically, this can be observed as reduced radiodensity of individual teeth (e.g. **hypocalcification, enamel hypoplasia**). Differences in the strength of the cheek teeth will cause irregular tooth wear thereby resulting in the formation of **stepped molars** (**Fig. 2-109**).

The pressure on elongated teeth leads to atrophy and osteolysis of the surrounding bone (**Figs. 2-110A, B**) where the increased pressure has been transmitted. This in turn allows a lateral displacement and bending of the teeth, which in chronic cases are severely malpositioned along the dental arcade (**Fig. 2-109B**). The most significant complication associated with dental malocclusion is the development of a periapical infection and subsequent formation of a tooth **root abscess**. The tooth root abscess can be mandibular (**Figs. 2-110C, D**), maxillary, or retrobulbar (see also Chap. 2.10.1.5) depending on which tooth is affected. Radiographic images must be taken in two planes in order to find the exact location and extent of the abscess(es), as well as the degree of osteolytic processes involved.

Incisor malocclusion will develop into a cranial elongation of the mandibular incisors and a caudal elongation for the maxillary incisors. The caudal elongation of the upper incisors may result in the dorsal aspect of the oral cavity being traumatized by the leading edges of these abnormally long teeth (**Fig. 2-111A**). Incisor root abscesses rarely occur relative to malocculded cheek teeth. The maxillary elongated incisor that extends caudally will irritate and damage the mandibular incisor peg teeth (**Fig. 2-111B**). Periapical inflammation and infection affecting the incisors can extend to the cheek teeth.

In the **Myomorpha** (e.g. golden hamster, gerbil, rat, mouse), only the incisors grow throughout life and rely on correct positioning and nutrition to have normal wear. An excessive elongation of the incisors in these species is rare and is often due to a nutritionally incomplete diet.

Insufficient or complete lack of wear occurs when there is no or incorrect occlusion when chewing. The most frequent causes of incisor malocclusion in myomorpha are:

- ☐ fractures of individual incisors
- ☐ brachygnathia superior (shortening of the upper jaw)
- ☐ malpositioning after a jaw fracture
- ☐ age-related loss of the incisors (gerbil).

Unrestrained growth results in upper incisors bending into the oral cavity and may cause severe injuries (e.g. to the tongue or palate). If the lower incisors are malpositioned, they will grow cranially out of the oral cavity and possibly cause labial damage. Periapical inflammation and abscesses (**Fig. 2-112**) are rarely diagnosed in Myomorpha relative to Lagomorpha or Caviomorpha.

Myomorpha seldom have disease that affect the back teeth although long-term wear will deeply reduce the crown and can result in the loss of teeth. This tooth wear is considered normal and should not be associated with clinical problems.

2.6.2 Spine, thorax

Ataxia, paresis, and paralysis (especially of the hindlimbs), are clinical presentations, for which a radiographic examination of the vertebral column/spine is warranted. Pathological conditions which can result in spinal cord or neurological compression include:

☐ luxations
☐ fractures
☐ spondylosis
☐ bone tumors
☐ abscesses

Luxations or **fractures** of the spine (**Fig. 2-113A**) often occur as the result of trauma (e.g. falls, being caught in doors, accidental kicks). Improper handling is linked with fractures and luxations of the caudal lumbar spine, especially in rabbits. A rabbit's leg muscles are so strong that in improperly restrained animal violent movements using these muscles to escape can easily cause spinal injury.

Spondylosis, narrowed intervertebral spaces, and **discospondylitis** are diagnosed in small exotic mammals, especially older rabbits (**Fig. 2-113B**). The clinical picture of patients diagnosed with any one of these diseases is often variable, ranging from a slight hindlimb weakness to complete paresis. Moreover, spondylosis is not always associated with disease signs nor is it always the cause of clinically evident neurological deficits.

Both **tumors** and/or **abscesses** may be the underlying cause of space-occupying masses. Tumors affecting the spine are relatively rare and are likely to be diagnosed in older animals. When diagnosed, spinal tumors are predominantly osteosarcomas, which during the early disease process, are difficult to radiographically differentiate from osteomyelitis. Osteolytic pathology affecting individual vertebrae can be caused by abscesses (e.g. in rabbits due to hemogenic dissemination of *Pasteurella multocida* into the vertebral canal).

Curvature of the spine is regularly diagnosed in small exotic mammals, especially rabbits, (**Fig. 2-113C**), without showing any clinical signs of disease. In the majority of small exotic mammal scoliosis cases, it is difficult to determine the underlying etiology of the disease process (e.g. congenital, poorly healed fracture, dietary osteodystrophy).

Rib fractures (**Fig. 2-113D**) are difficult to radiographically recognize and depending on location, may not be visible using standard projections. If radiographic interpretation is in question for patients that present with blunt thoracic trauma, oblique projections of the thorax should be performed.

2.6.3 Limbs

The predisposition for **fractures** involving the limb bones of small exotic mammals as a result of trauma is variable depending on the species. Rabbits and chinchillas with their long thin leg bones are particularly predisposed to fractures involving the skeletal structure of the limbs. Conversely, mice with their light body weight often survive falls from great heights with no skeletal damage. The typical causes of limb fractures in small exotic mammals, in addition to falls, are an animal's escape attempts when its paw is caught between the bars of a cage (especially small rodents) or when an animal has become entangled in the carpet due to having extremely long claws. The majority of leg bone fractures involve spiral or comminuted fractures. In rabbit patients, the femur (**Fig. 2-114A**), tibia (**Fig. 2-114B**), radius and ulna (**Fig. 2-114C**) are the leg bones most often diagnosed with fractures. Chinchillas are predisposed to tibial fractures, while the femur is the primary bone fractured in guinea pig patients. Although guinea pig olecranon fractures occur, in general it is uncommon for small exotic mammal patients to present with fractures involving bones of the forelimbs. The scapula is rarely fractured, while fractures affecting the pelvic girdle (**Fig. 2-114D**) can occur. Depending on the location, fractures are not always easy to recognize and in all cases require radiographic images obtained from two planes. In individual cases, lameness may be due to fractures of the toes. If long bone fractures are not stabilized, then **pseudoarthrosis** can occur (**Fig. 2-114E**)

Spontaneous or **pathological fractures** are rather rarely diagnosed in small exotic mammals. The most common causes of spontaneous or pathological fractures are severe osteodystrophy, bone tumors, or osteomyelitis (**Fig. 2-114F**).

An open fracture or complications of surgical fracture repair may result in the development of **osteomyelitis** (**Fig. 2-114G**). Due to the extensive tissue and bone involvement of many osteomyelitis cases determining a prognosis is often difficult. Highly invasive pododermatitis as is frequently diagnosed on the plantar surface of the hind legs of rabbits or the balls of the feet in obese guinea pigs (or more rarely in chinchillas and degus) may extend to the phalanges and develop into a severe osteomyelitis (**Fig. 2-114H**).

In addition to fractures, animals that are dropped can sustain **luxation** injuries. Luxation injuries, on average, occur less frequently than fractures. The most frequent joint luxation diagnosed in small mammals is the rabbit elbow (**Fig. 2-114I**). Although uncommon, coxofemoral luxations have been identified (**Fig. 2-114K**).

Osteosarcomas have been diagnosed in the humerus or femurs of older guinea pigs but overall **bone tumors** rarely affect the limb bones of small exotic mammals.

2.7 Cervical soft tissues

Sven Reese

A palpable space-occupying lesion in the **neck** may arise from any number of tissue origins. An ultrasonographic examination enables one to determine the topography of the lesion and possibly, in combination with fine-needle aspiration, the diagnosis. The most frequent cause of a cervical mass is thyroid neoplasia, especially in the guinea pig (**Fig. 2-115**). A guinea pig diagnosed with a thyroid tumor may develop clinical signs associated with hyperthyroidism. The differential diagnosis of a cervical mass should include enlarged lymph nodes and neoplasia of the salivary gland of the lower jaw as well as tumors of the mammary glands in the rat.

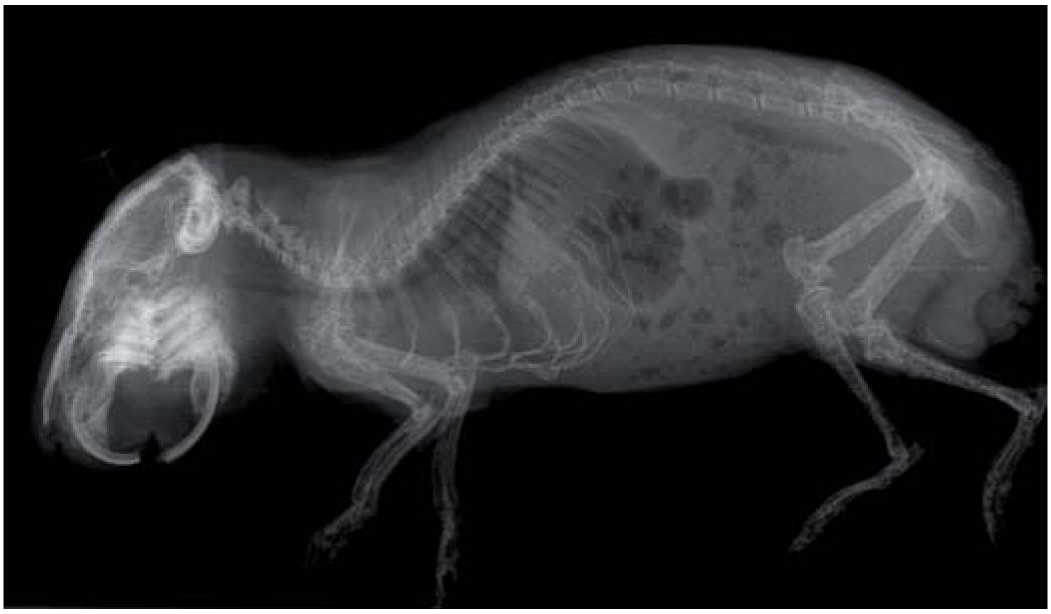

Fig. 2-103: Whole body radiographic image of a satin guinea pig with severe osteodystrophy, lateral projection. The long bones of the hindlegs, in particular, exhibit typical patterns of demineralization with a compensatory thickening of the compact bone in the femur commonly associated with osteodystrophy.

Fig. 2-104: Radiographic image of a ferret's skull, dorsoventral projection. One can observe a fissure in the intermaxillary bone (arrow) and loosening of the incisors (arrowhead) in the upper jaw.

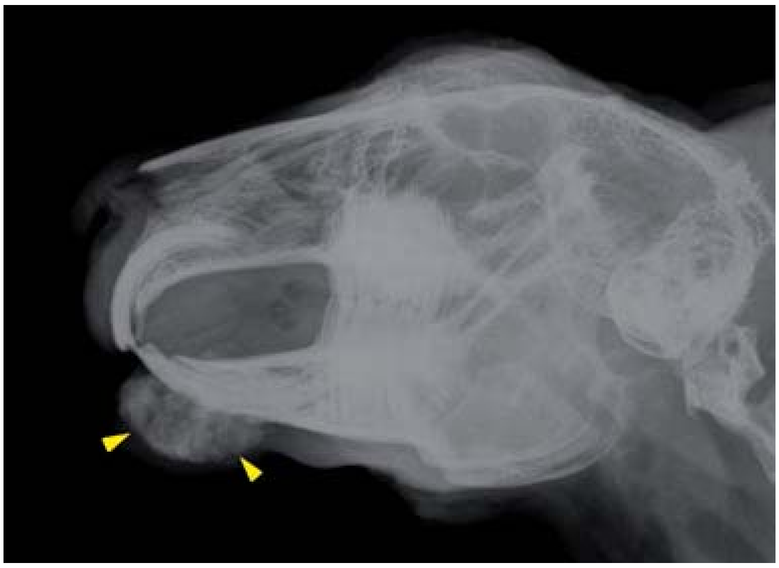

Fig. 2-105: Radiographic image of a rabbit's skull, lateral projection. Osteosarcoma in the lower jaw (arrowheads).

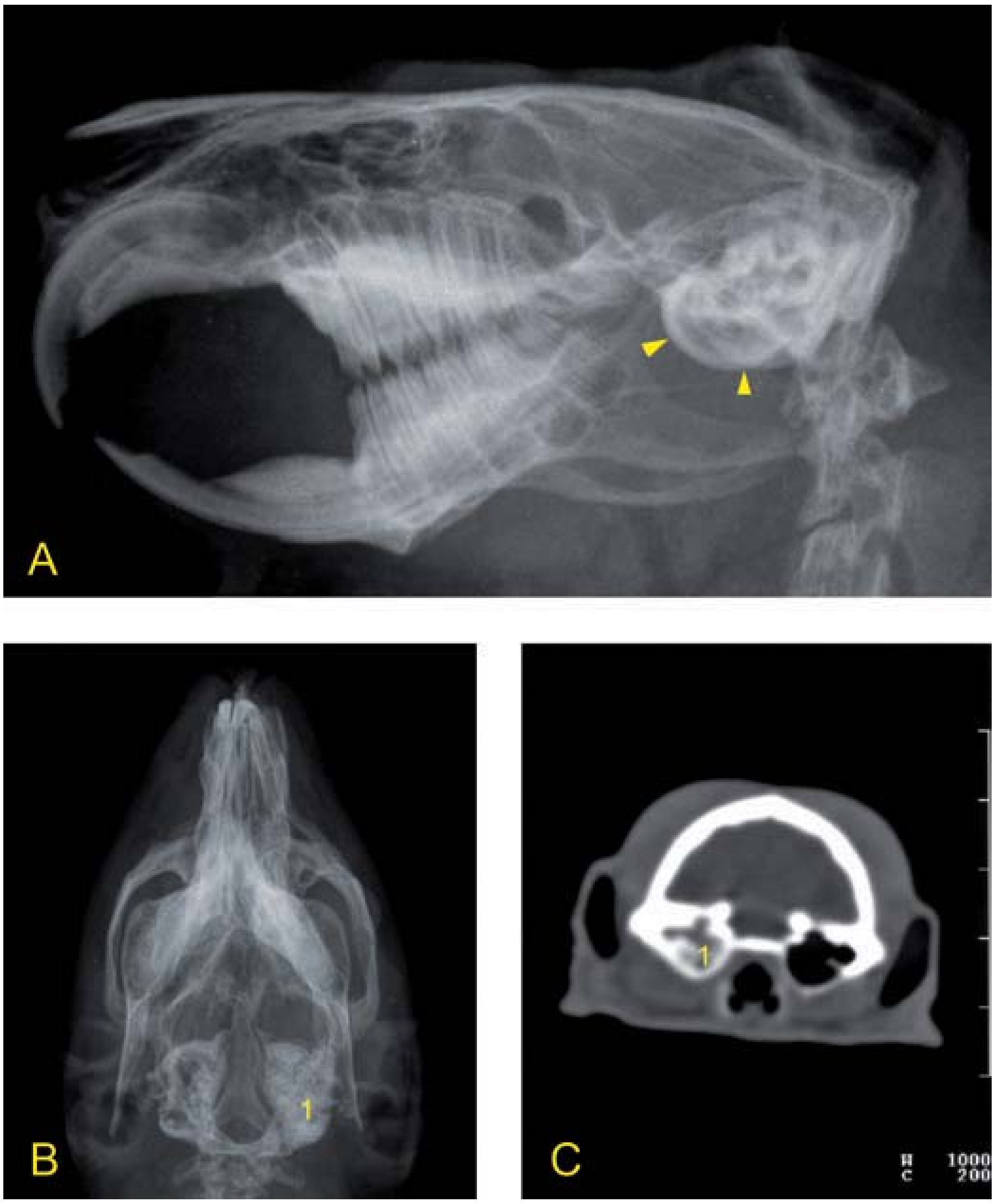

1: tympanic bulla

Fig. 2-106: Otitis media.

A, B: Radiographic images of a guinea pig's skull, (A) lateral and (B) dorsoventral projections. Shadows are present in the tympanic bulla (1, arrowheads), which can be attributed to the right side in the dorsoventral projection.

C: CT examination of a ferret, bone window, transverse section at the level of the tympanic bulla. The left tympanic bulla is highly shadowed and its wall is thicker than on the right.

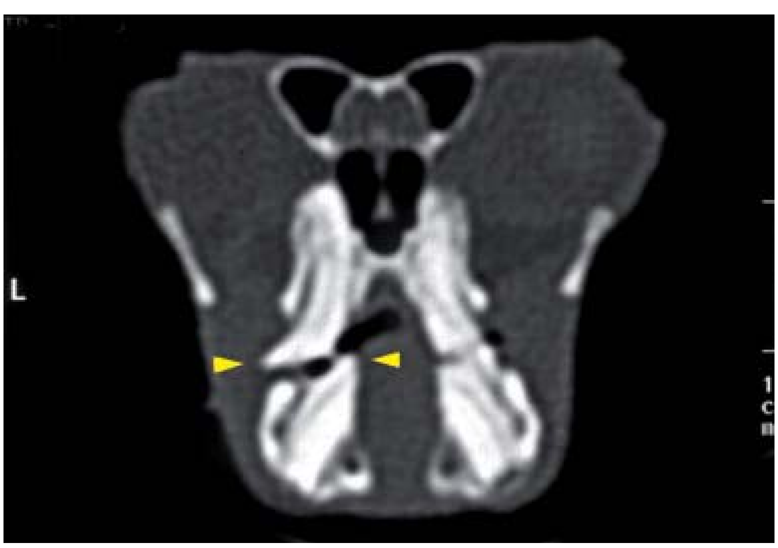

Fig. 2-107: CT examination of a chinchilla, bone window, skull, transverse section at the level of the 1st molar. Buccal spurs on M1 (arrowhead), no occlusion with the teeth of the lower back jaw, which are tipped lingually capturing the tongue (arrowhead).

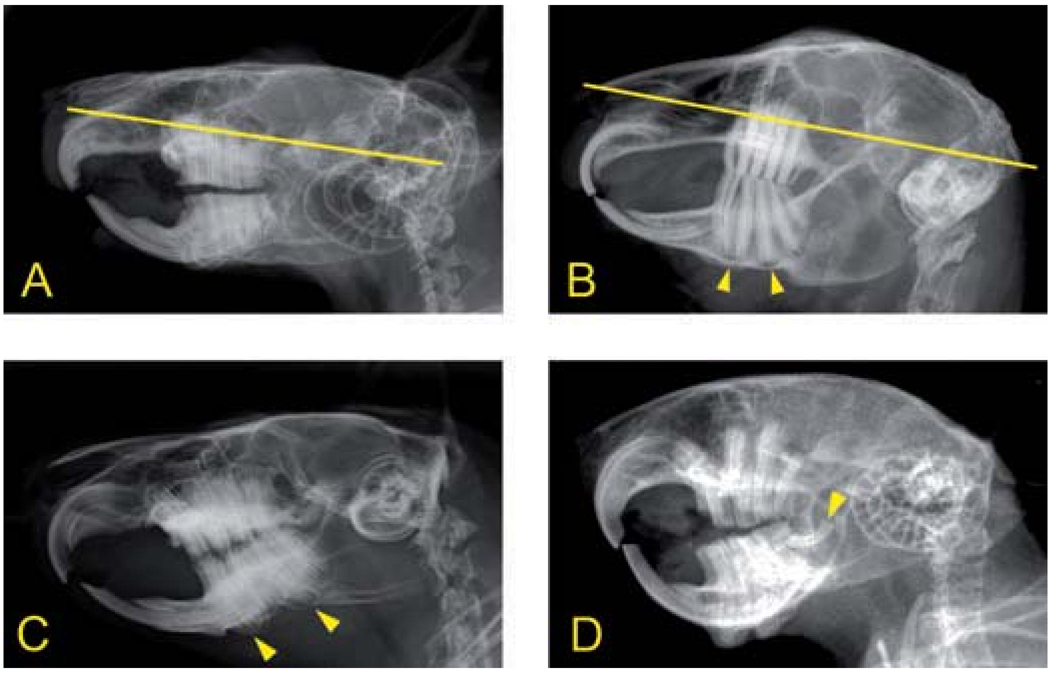

Fig. 2-108: Radiographic images of the skull, lateral projection: Retrograde ectopic tooth growth.

A: Chinchilla: Slight retrograde tooth growth. The molars in the upper jaw end apically just over the reference line.

B: Rabbit: Moderate retrograde tooth growth. The molars of the upper jaw have clearly grown above the reference line. Resolution of the compact bone under the roots of the molars has started in the lower jaw (arrowheads).

C: Guinea pig: Moderate to severe retrograde tooth growth with osteophytes on the ventral edge of the mandible (arrowheads).

D: Degu: Severe retrograde tooth growth. The molars have responded to the abnormal pressure by bending in all possible directions (arrowhead).

Radiographs A, B and C courtesy of the Veterinary Clinic Oberhaching, Munich, Germany.

Fig. 2-109: Radiographic images of the skull, lateral projection: Stepped molars. Rabbit (A), chinchilla (B). Due to the malocclusion, some teeth have hypoplastic enamel (arrowheads) and ridges have been formed on the occlusal surfaces of the molars.

Radiograph A courtesy of the Veterinary Clinic Oberhaching, Munich, Germany

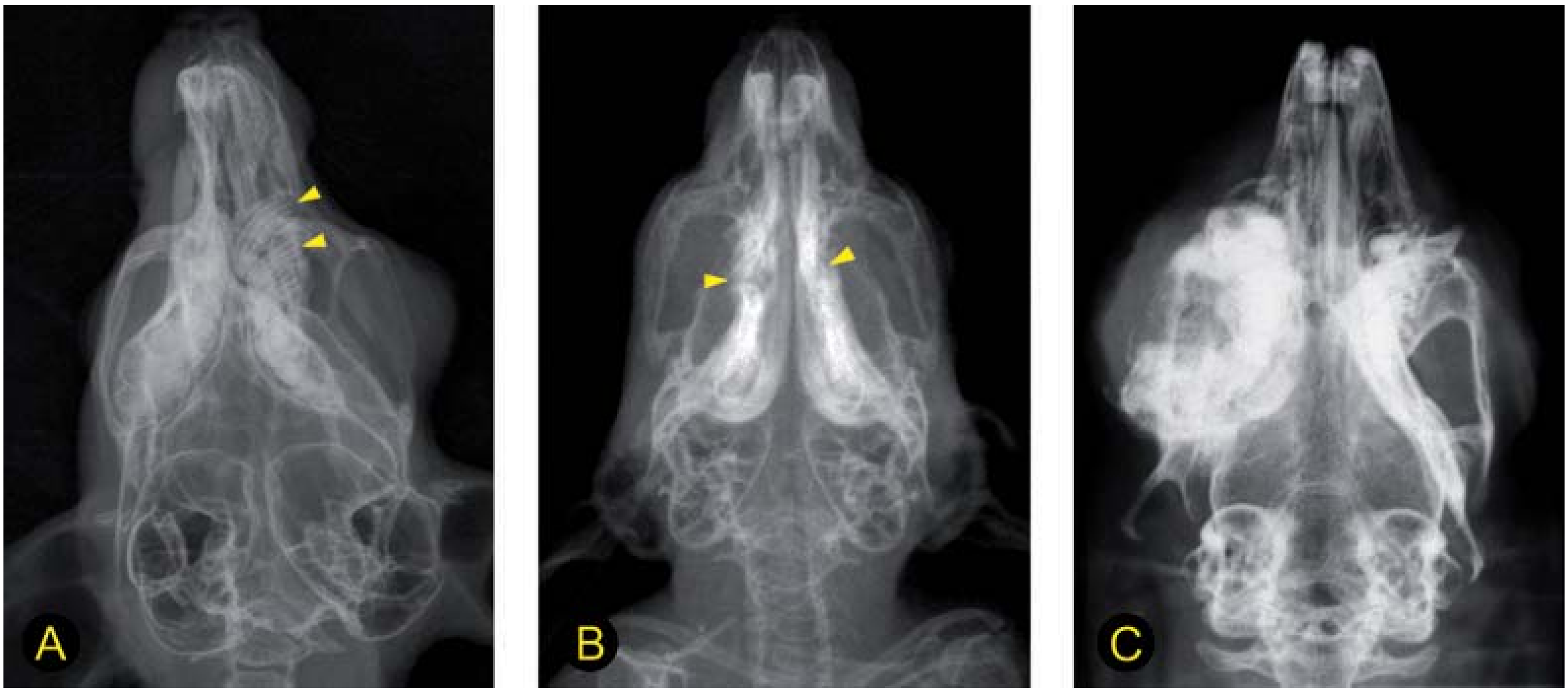

Fig. 2-110: Radiographic images of the skull of a (A, C, D) rabbit and (B) degu with osteolysis and apical tooth abscesses, dorsoventral (A–C) and lateral (D) projections. Malocclusion has led to increased pressure on the jaw bones resulting in bone atrophy (A, arrowheads) and osteolysis (B, arrowhead). (C and D) Apical tooth abscesses develop as complications of malocclusion.

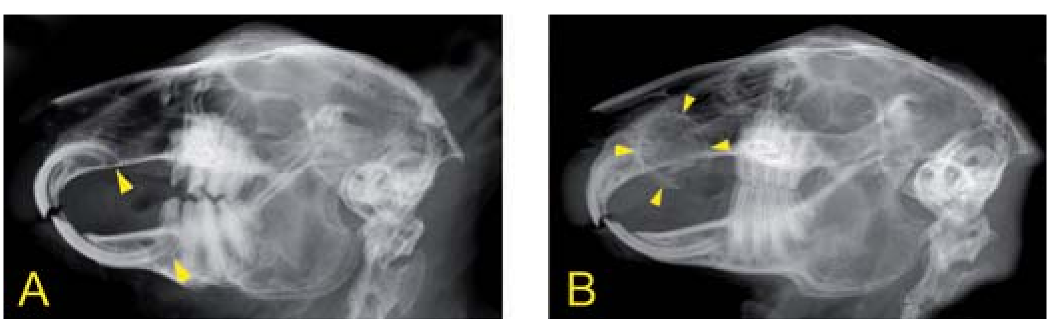

Fig. 2-111: Radiographic images of a rabbit's skull with malocclusion of the incisors, lateral projection.

A: Atrophy of the bony palate and the first molar in the lower jaw (arrowheads) under the pressure of the retrograde growth of the incisors.

B: An apical abscess (arrowheads) is a rare complication of a maloccluded incisor.

Radiographs courtesy of the Veterinary Clinic Oberhaching, Munich, Germany

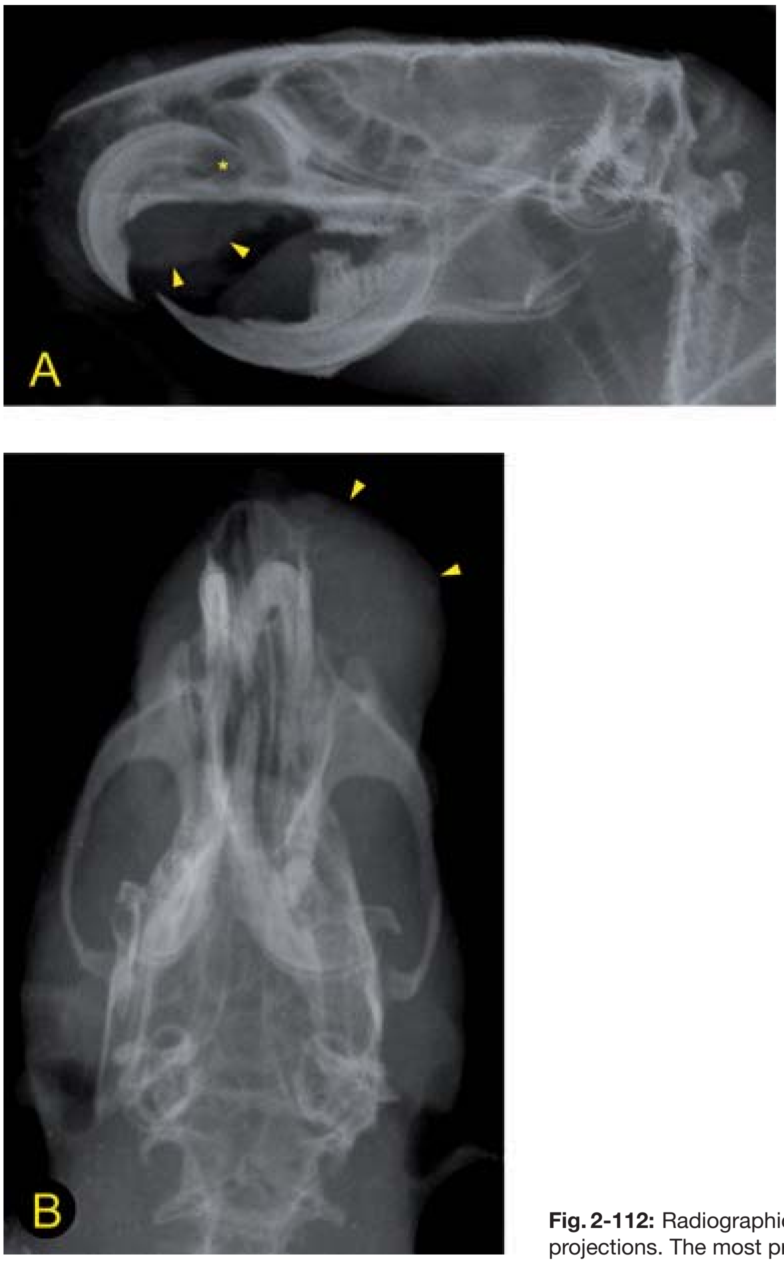

Fig. 2-112: Radiographic images of a rat's skull with an apical abscess (*), (A) lateral and (B) dorsoventral projections. The most prominent finding is a large amount of soft tissue swelling (arrowheads).

Fig. 2-113A: Radiographic image of a rabbit's spine, lateral projection. Luxated fracture between L3 and L4.

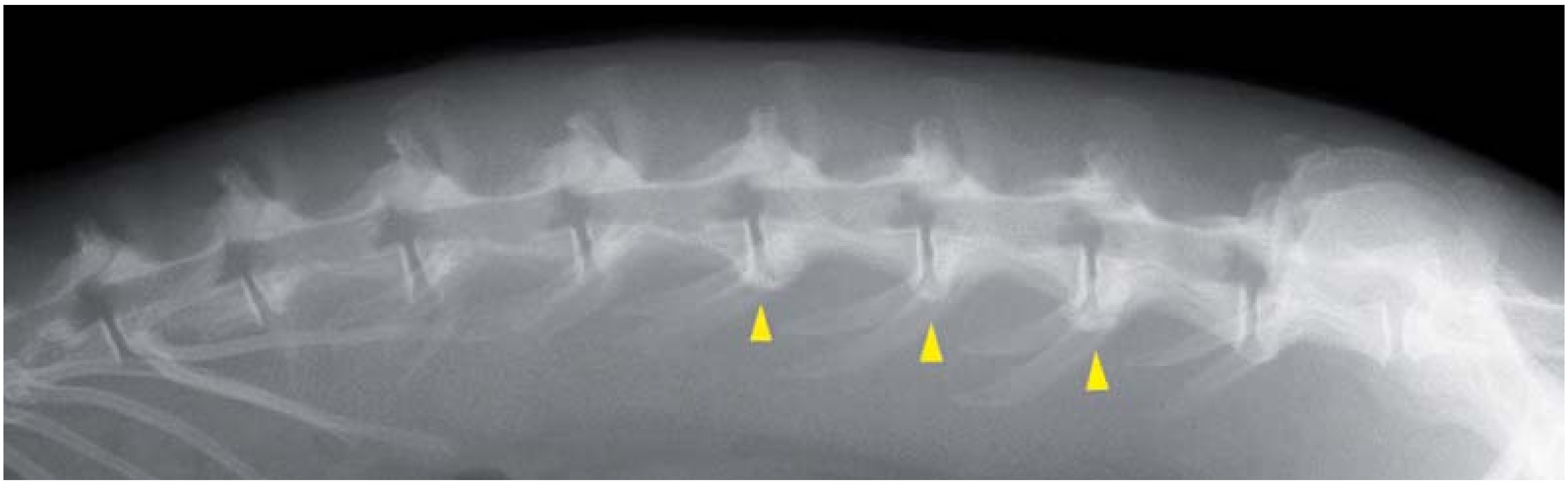

Fig. 2-113B: Radiographic image of a rabbit's spine, lateral projection. Spondylosis from L3 to L6 (arrowheads).

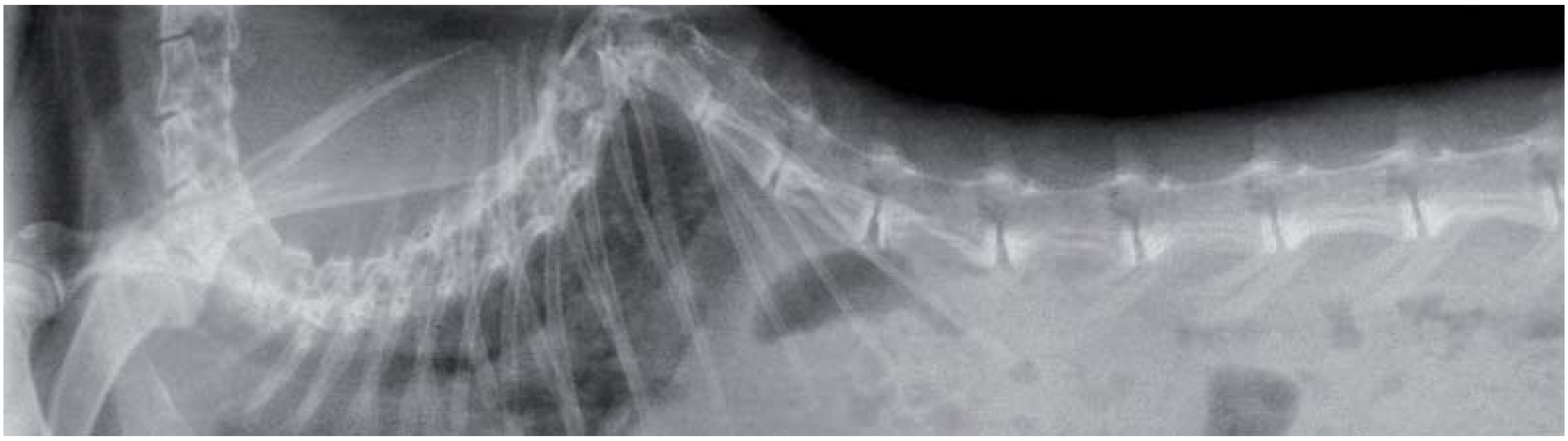

Fig. 2-113C: Radiographic image of a rabbit's spine, lateral projection. Curvature of the thoracic spine. The animal showed no neurological abnormalities.

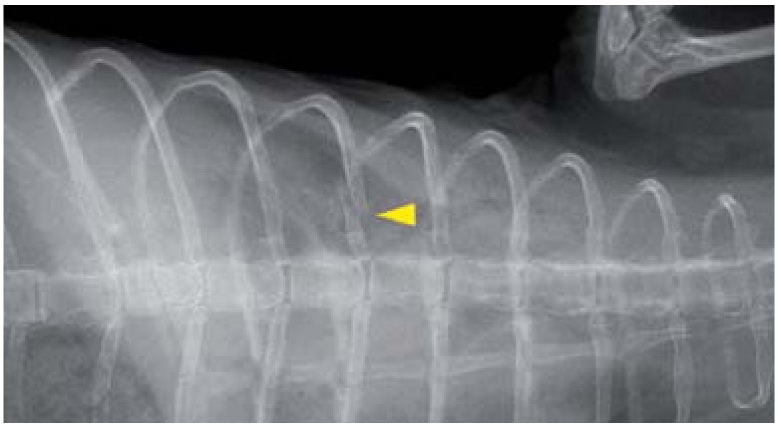

Fig. 2-113D: Radiographic image of a ferret's thorax, oblique ventrodorsal projection. Rib fracture (arrowhead).

Fig. 2-114A–C: Radiographic images of a rabbit with leg bone fractures, mediolateral projection.

A: Fracture of the femur.

B: Fracture of the tibia and fibula.

C: Fracture of the radius and ulna.

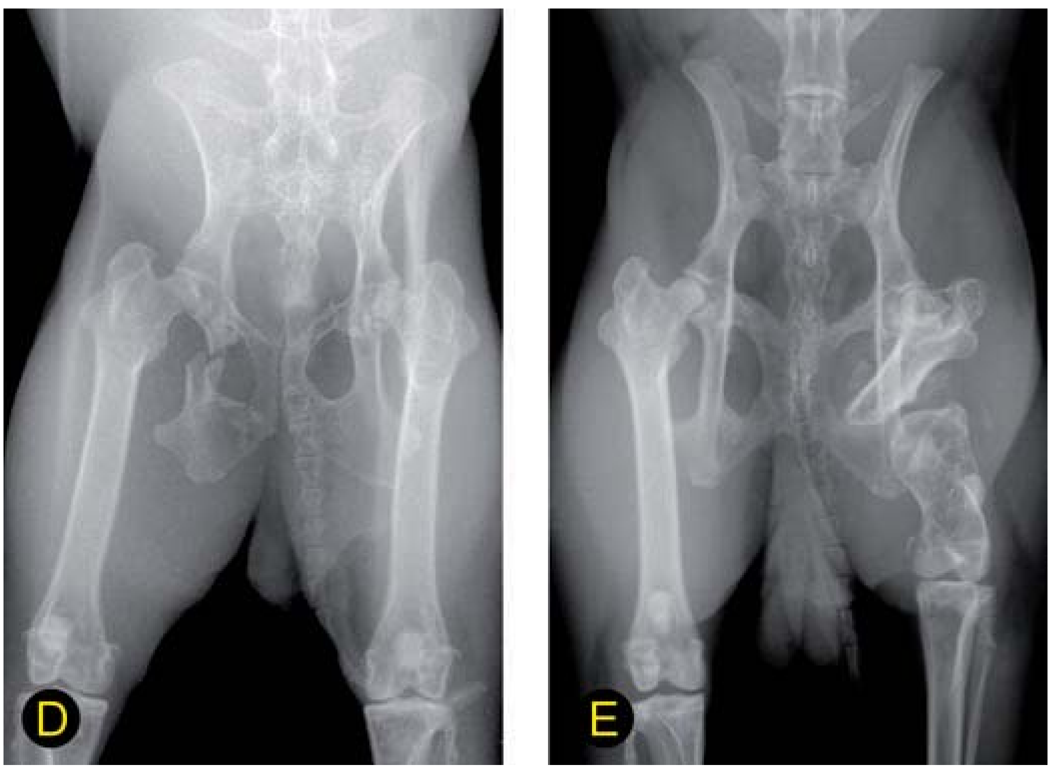

Fig. 2-114D, E: Radiographic images of the pelvis of a rabbit, ventrodorsal projection.

D: Ischial fracture.

E: Development of pseudoarthrosis after fracture of the femur.

Fig. 2-114F–H: Radiographic images of rabbits with fractures involving leg bones.

F: Mediolateral projection, pathological fracture of the humerus.

G: Osteomyelitis as complication of fracture treatment.

H: Osteomyelitis with complete destruction of the metatarsophalangeal joint on the 2nd toe.

Fig. 2-114I, K: Radiographic images of rabbits' leg joints.

I: Mediolateral projection, luxation of the elbow joint.

K: Ventrodorsal projection, luxation of the hip joint (radiograph courtesy of the Veterinary Clinic Oberhaching, Munich, Germany).

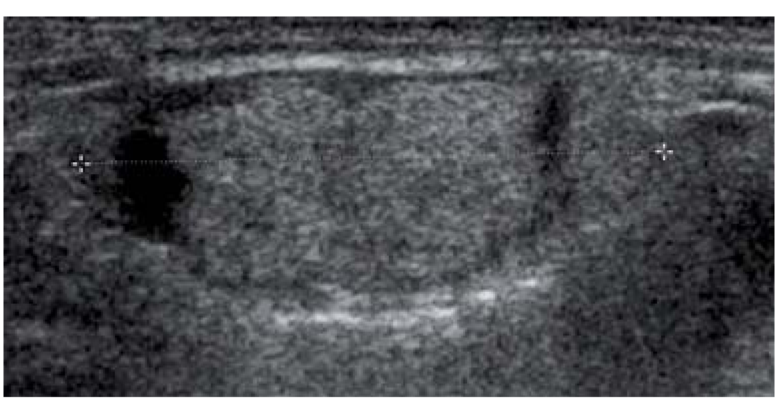

Fig. 2-115: Ultrasonographic image of a guinea pig's neck, sagittal plane, 12 MHz, PD 1.5 cm. Carcinoma of the right lobe of the thyroid (length 20.4 mm) in a hyperthyroid guinea pig.

2.8 Thorax

Sven Reese, Jutta Hein

2.8.1 Pleural cavity

The thoracic cavity is filled by the pleural cavity, which under normal conditions is a capillary gap and cannot be radiographically imaged. The diagnostic imaging characteristics change when there is increased fluid within the pleural cavity: **pleural effusion**. Typical signs of pleural effusion are displacement of the lung fields away from the thoracic wall and imaging of the interlobar fissures, which are well visualized in both the DV and VD projections (**Fig. 2-116A**). With severe pleural effusion, the contours of the heart and diaphragm are no longer recognized in the lateral projection (**Fig. 2-117**). Pleural effusion is classified by the type of fluid present with the pleural cavity (e.g. hydrothorax, pyothorax, hemothorax, chylothorax). None of the examples of pleural effusion mentioned above can be differentiated using diagnostic imaging. The recommended procedure to identify pleural effusion is an ultrasound-guided aspirate of the pleural cavity with a subsequent cytological examination of the aspirate specimen.

Pneumothorax may be defined as air that has penetrated the pleural cavity (**Fig. 2-116B**). The most common cause of pneumothorax is trauma to the thorax, whereby the presence of rib fractures may be an indication of the underlying cause of this condition (see Chap. 2.6.2).

2.8.2 Trachea

Dorsal, or even lateral, **displacement of the trachea** is an indication of a space-occupying lesion in the cranial mediastinum or cardiomegaly (**Fig. 2-117**). In small exotic mammals diagnosed with lymphoma, there is often an enlargement of the thymus or lymph nodes lying in the cranial mediastinum and above the base of the heart. Ultrasonographic imaging using a microconvex probe over the cranial thoracic inlet may be performed to diagnose the presence of a space-occupying lesion in the cranial mediastinum.

2.8.3 Esophagus

Diseases of the esophagus are rarely diagnosed in small exotic mammals. The underlying etiology is often undetermined in the majority of cases involving esophageal disease. In individual cases, a tumor over the base of the heart can lead to a narrowing of the esophagus with the subsequent formation of a precardial **megaesophagus**. Congenital megaesophagus is known to occur in the mouse. The most common clinical sign associated with megaesophagus is regurgitation of food and in rare cases, chronic vomiting. Aspiration pneumonia may occur as a complication. The presence of a megaesophagus can be confirmed by performing a contrast study through the oral administrative of a contrast agent (**Figs. 2-118A–C**; see Chap. 2.1.3.2).

2.8.4 Lungs

When radiographically assessing the lungs, the first criterion is to determine their radiodensity: is it normal, reduced, or increased? A generalized reduced radiopacity (i.e. dark lungs, virtually no blood vessel patterns) may be caused by hypovolemia and exsiccosis (i.e. due to hypovolemic pressure, forced diuresis) or in association with pulmonary emphysema.

Frequently, there is an increased radiopacity in the lung tissues. The most common forms of lung patterns associated with increased tissue radiopacity are:
- ☐ alveolar pattern
- ☐ interstitial pattern
- ☐ bronchial pattern
- ☐ vascular pattern.

An **alveolar pattern** occurs when air has been displaced out of the alveoli by fluid or exudate or the alveoli have collapsed (atelectasis) (e.g. pneumothorax). The typical radiographic characteristics of an alveolar pattern are cloudy-patchy, poorly demarcated densities in the lung parenchyma (**Fig. 2-119A**). The blood vessels and bronchial walls can be no longer visualized. The air-filled bronchi may stand out as band-like lucencies (air bronchogram, **Fig. 2-119B**). If only certain areas of the lung lobes are affected, then the unaffected lung tissue will be prominent. Common causes of a diffuse alveolar pattern disseminated over the entire lung field are:
- ☐ lung edema
- ☐ lung hemorrhages (e.g. blunt thoracic trauma)
- ☐ bronchopneumonia
- ☐ vasculitis

Interstitial patterns form when fluid, exudate, connective tissue, or tumors are distributed throughout the lung interstitium. The typical radiographic characteristics of an interstitial pattern are a diffuse density of the lung tissue with reduced contrast and poorly defined pulmonary blood vessels. In its focal form, the affected area is an obvious, delineated area of increased radiopacity (**Fig. 2-120**). If radiographs are taken in expiration or are underexposed or the animal is obese, then a false interstitial pattern may be observed. Common causes of focal interstitial patterns are:
- ☐ neoplastic metastases
- ☐ localized pneumonia
- ☐ lung abscesses
- ☐ granulomatosis (e.g. mycosis).

Common causes of a diffuse interstitial pattern are:
☐ lung edema
☐ hemorrhages
☐ fibrosis.

Bronchial patterns form when the walls of the bronchi are infiltrated by fluid (e.g. exudate, blood) or cells. The typical radiographic characteristics of a bronchial pattern are the so-called »doughnuts« (thickened bronchi in the cross-section) or rail tracks (thickened bronchi in longitudinal section; **Fig. 2-121**). Common causes of a bronchial pattern are:
☐ bronchitis (bacterial, viral, allergic)
☐ bronchiectasis
☐ neoplasia.

Vascular patterns form when the blood vessels of the lungs are congested (**Fig. 2-122**). The typical radiographic characteristics of a vascular pattern are a widening of the pulmonary arteries and/or veins. Common causes of congested pulmonary arteries are:
☐ pulmonary hypertension
☐ thrombosis, emboli
☐ dirofilariasis (ferret).

Common causes of congested pulmonary veins are:
☐ decompensated left-sided cardiac insufficiency
☐ congestive heart failure
☐ left-right shunt.

Common causes of congested pulmonary arteries and veins are:
☐ infusion (hyperperfusion)
☐ pneumonia.

Lung disease is also associated with mixed lung patterns (**Fig. 2-121**); a typical example of this is bronchopneumonia.

Bronchopneumonia and **lung abscesses** can occur in all small exotic mammalian species, though they are frequently considered as being complications of *Pasteurella multocida* infection in the rabbit or as a consequence of chronic interstitial pneumonia in the rat caused by mycoplasma.

Most **lung tumors** are metastases of uterine (rabbit) or mammary **adenocarcinomas** (see **Fig. 2-120**). In male animals, the primary tumor resulting in lung metastases can originate from the testicle.

Tumors in the thorax of small exotic mammals are often extensive when the patient is presented and in extreme cases can almost incorporate the entire thoracic cavity. In cases of significant thoracic tumor involvement, it is possible to use transthoracic ultrasonographic imaging to assess the extent of the disease condition (**Fig. 2-123**).

The majority of **thoracic effusion** and **lung edema** cases arise from cardiogenic disease in small exotic mammals.

Lung contusions with **lung hemorrhages** are particularly common in small exotic mammals that have free run of the house. The most common cause of lung contusions is closing a door on the animal, inadvertent kicks, or being stepped on. **Diaphragmatic hernias** are also associated with trauma and can be diagnosed using ultrasonography or radiography. Diaphragmatic hernias are diagnosed by observing the presence of abdominal contents (e.g. intestines, liver lobes) in the thoracic cavity.

2.8.5 Heart

Cordula Poulsen Nautrup, Susanne Schlieter, Jochen Spennes, Jan-Gerd Kresken

All acquired and congenital heart diseases diagnosed in humans, dogs and cats, and which have been described in numerous textbooks, can be also found in small exotic mammals. However, in small exotic mammals there are only a few articles on this subject, especially those relating to the radiographic and echocardiographic diagnosis of cardiac anomalies. The majority of these articles are individual ferret, rabbit, and guinea pig case studies. In addition, for decades numerous animal investigations have been performed within the framework of human medical research involving rabbits, rats, and mice. These studies, in which heart disease relevant to humans has been artificially induced by iatrogenic, interventional, or genetic means, have focused on basic research and pharmacological studies. The cardiac anomalies investigated in these studies include different forms of cardiomyopathy, changes in the valves, and ischemic heart disease (a primary human concern). Many of the induced cardiac changes were imaged using echocardiography. Myocardial ischemia is also known to occur in the rabbit due to a reduced number of collateral blood vessels and the associated decreased perfusion of cardiac tissue.

The majority of patients presented in veterinary practice suffering from cardiac disease are usually in a stage of advanced cardiac insufficiency due to acquired heart disease. The most important causes of cardiac insufficiency in small exotic mammals are **dilatative cardiomyopathy** (**DCM**)**, valvular insufficiency, myocarditis** and less commonly **hypertrophic cardiomyopathy** (**HCM**) and **pericardial or pleural effusions**. These diseases can be observed individually or in various combinations. The conditions that lead to cardiac insufficiency may be idiopathic, associated with pericardial or pleural disease, and/or tumors. Clinical signs associated with cardiac disease may be caused by a primary disease or be secondary to advanced cardiac insufficiency. Clinical cases of heart worm (**dirofilariasis**) have been described in the ferret. Cases of congenital heart disease are seldom presented, therefore **aortic and pulmonary stenoses, ventricular septal** (**VSD**) and **atrial septal** (**ASD**) **defects** are rarely diagnosed.

2.8.5.1 Radiographic findings

The most common anomaly of the heart diagnosed radiographically in small exotic mammals is **cardiomegaly**, which is frequently observed as a global enlargement of the heart silhouette. The evaluation of the heart silhouette size is mainly subjective or done using control radiographs of animals of the same breed, body weight, age, and sex. Only in the ferret are objective measurements meaningful as there are standard values available: the vertebral heart score (VHS) and the heart size in comparison to the intercostal spaces (see Chap. 2.2.3.5). However, it should be noted that generally there is a wide overlap of normal and abnormal values and exceptions (e.g. large hearts can occur in healthy animals and radiographically slim heart silhouettes can sometimes be identified in association with severe dilatative cardiomyopathy if extremely high heart rates lead to cardiac hypovolemia).

Volume overload of the ventricles and the atria, which can be recognized radiographically as cardiomegaly, can occur in advanced stages of cardiac insufficiency (e.g. idiopathic cardiomyopathy, chronic myocarditis). Similar enlargements of the heart with chronic volume overloading can also be found with primary dilatative cardiomyopathy and clinically relevant chronic atrioventricular and valvular insufficiencies. Shunts (e.g. left-right shunts in VSD and ASD) can also lead to volume overloading and may manifest themselves radiographically as cardiomegaly (**Figs. 2-124** and **2-125**).

Other causes of cardiomegaly are pericardial effusion (**Figs. 2-126A** and **2-128**) and pericardial tumors. The differentiation of these conditions, both of which lead to recognizable cardiomegaly on a radiograph, can only be done using echocardiography (**Figs. 2-126B** and **2-127**). With the latter method, the effects of a pericardial effusion on the cardiac function can be assessed. In cardiac tamponade, the atria do not fill adequately, leading to hypovolemia with severe diastolic dysfunction (**Fig. 2-126B**).

Heartworm infestation (dirofilariasis) appears radiographically in the ferret initially as an enlargement of the right heart and then as globoid cardiomegaly. Radiographic changes associated with heartworm infestation in the pulmonary arteries are not as extreme as that which occurs in the dog. Microfilaria are often observed on an echocardiogram as two short parallel echoes in the dilated right chamber and in the enlarged right atrium.

Widened pulmonary veins can be identified in small exotic mammal patients suffering from left-sided cardiac insufficiency, cardiomyopathy, and mitral valve insufficiency as a consequence of congestion and/or regurgitation. With advanced congestive left-sided cardiac insufficiency, both interstitial and alveolar lung congestion occurs (lung edema; **Fig. 2-128**). **Increased lung patterns** are caused by both heart and lung disease. The determination of heart size can be useful in the differentiation of cardiac from extracardiac disease etiologies (**Fig. 2-129**). However, the confirmation of cardiac disease can only take place with the aid of echocardiography.

An **elevated trachea** may indicate the presence of cardiac enlargement. However, this is often difficult to assess as only in the rabbit and guinea pig is there a relatively large acute angle that opens caudally between the trachea and spine. In the other small exotic mammals, the angle is much smaller (i.e. these structures run virtually parallel to each other). One peculiarity of the rabbit is that the thymus does not degenerate. The large thymus in combination with intrathoracic fat deposits may lead to radiographic shadows lying cranial to the heart, therefore making it difficult to differentiate these structures from pathological tumors.

Pleural or **thoracic effusions** are an expression of congestive right-sided cardiac insufficiency, which may occur in association with decompensated cardiomyopathy (**Fig. 2-130**) or advanced left-sided cardiac insufficiency. The typical radiographic characteristics of pleural or thoracic effusions are similar to those found in the dog and cat. Radiographic images in pleural or thoracic effusions in small exotic mammals include a fuzzy or an absent heart silhouette, lobar lung patterns, and an enlarged distance between the diaphragmatic lobe and the spine in the caudal area of the diaphragm. A radiographic and/or echocardiographic differentiation of cardiac and extra-cardiac etiologies must be undertaken when the patient is suffering from dyspnea (**Fig. 2-131**).

2.8.5.2 Echocardiographic findings

As with radiographic results, echocardiograms of the various small exotic mammalian species are similar to those in the dog and cat.

With the aid of ultrasonographic methods, the morphology of the cardiac structures, volume or pressure overloading of the heart, and/or a systolic or diastolic functional disturbance can be assessed.

Findings with M-mode and two-dimensional echocardiography

In addition to left-sided cardiac insufficiency of varying etiologies, the most frequently diagnosed heart anomaly in small exotic mammals is **dilatative cardiomyopathy (DCM)**. Due to chronic damage of the myocardium, the pumping efficiency of the heart is reduced resulting in a lower blood out-flow (systolic dysfunction). The systolic dysfunction results in a severe volume overload that leads initially to a dilatation of the left chamber, which due to the backing up of the blood and secondary insufficiency, then affects the left atrium within a short period of time (**Figs. 2-132, 2-133** and **2-136**). The consequences of the secondary insufficiency are forward heart failure with reduced cardiac performance and damage to virtually all organ systems (digestive and/or renal problems) as well as backward heart failure with lung edema (dyspnea and/or coughing), pleural effusion, and ascites. This condition can be described as congestive heart failure.

Apart from DCM, three other causes of chronic cardiac insufficiency must be considered in small exotic mammals: **idiopathic cardiomyopathy, endomyocarditis**, and/or **myocarditis**. For example, myocarditis and endocarditis can be caused in the rabbit by *Pasteurella multocida*, *coronavirus*, or *Encephalitozoon cuniculi*.

The echocardiographic changes involved in a myocardial inflammation are nonspecific and can vary between virtually unrecognizable to severe, depending on the severity of the disease.

The echocardiographic signs of endocarditis or myocarditis may include an echogenic, luminescent endocardium or the development of a nonhomogeneous echo distribution in the myocardium. However, the endocardium in all small exotic mammals frequently appears on a sonogram much brighter and more echogenic than in the dog and cat. The most apparent findings associated with advanced endocarditis or myocarditis are comparable to those observed in cases of dilatative cardiomyopathy and/or congestive heart failure.

The diseases described above lead to a systolic and diastolic volume increase within the left ventricle. This can be recognized in the M-mode by an enlargement in the diameter of the left ventricle as well as by a reduction in the thickness of the septal wall and myocardium (**Figs. 2-132** and **2-133**). Indications of a systolic dysfunction are related to a reduced systolic fractional shortening (FS) and a reduced or missing systolic increase in thickness of the myocardium. An increased distance between the septum and early diastolic maximum opening of the septal cusp of the mitral valve (EPSS = E-point to septal separation) is an indication that the left ventricle is dilated at end-systole (**Fig. 2-134**). This parameter is not only an sign of left ventricular volume overloading, but also a reduced ejection capacity. A reduced ejection fraction (EF) is best calculated in the ferret and rabbit from the volumes determined in a 2D B-scan and is a direct measurement of reduced pumping function. Volume overloading of the left atrium due to congestion and reflux is observed as a measurable enlargement of the atrium in the M-mode or 2D echocardiogram (**Figs. 2-135** and **2-136**). The echocardiographic characteristics described here form the primary basis for the ultrasonographic diagnosis of DCM in the dog.

Thickening of the myocardium is rare in small exotic mammals and may occur in association with primary **hypertrophic cardiomyopathy** (**HCM**) (**Fig. 2-137**) or secondarily to increased pressure in the ventricle (e.g. **aortic stenosis, pulmonary stenosis**). The concentric thickening of the cardiac wall leads not only to a reduction in the ventricular lumen and a lack of elasticity and stretching of the myocardium (diastolic dysfunction), but also an inadequate filling of the affected chamber. The atrium undergoes secondary dilatation due to lack of emptying and sometimes because of reflux (**Fig. 2-135**). However, in many small exotic mammals, as in some cats, the myocardium can appear subjectively thickened when in reality it is not.

Left ventricular volume overloading without reduced systolic function (i.e., with good myocardial function) is found with **valvular insufficiency**. A severe mitral valvular insufficiency leads to an enlarged end-diastolic diameter of the left ventricle, while the end-systolic ventricle size is normal or slightly reduced (**Fig. 2-138**) with an increase in the systolic FS. The thickness of the myocardium is normal or slightly hypertrophied and the left atrium is enlarged due to reflux (**Fig. 2-140**).

A severe aortic valve insufficiency can lead to end-diastolic volume overloading of the left ventricle without simultaneously causing a concurrent excessive pressure load. The morphological causes of valvular insufficiency (e.g. thickening of the valves) can be imaged using 2D echocardiography (**Fig. 2-139**).

Findings with color-coded and conventional Doppler echocardiography

While all of the changes described thus far can be recognized using M-mode and 2D echocardiography, the size of an **insufficiency jet** can be assessed using 2D color Doppler (**Figs. 2-140A, 2-141A** and **2-142A**), while color-coded M-mode is used for determining the duration of regurgitation. The duration and velocity of regurgitation can also be determined with CW Doppler (**Figs. 2-140B, 2-141B** and **2-142B**).

The size of a **shunt** is judged primarily with the aid of color-coded Doppler and the extent of a **stenosis** can be calculated with CW Doppler. Shunts and regurgitations reveal themselves by the presence of pathological blood flow and turbulence. Stenoses are recognized by an increase in velocity of the blood flow and the presence of turbulence (see **Fig. 2-75**). However, secondary changes, such as enlargement of the atrium and dilatation or hypertrophy of the ventricles, will occasionally allow one to determine pathological changes associated with the disease condition.

Difficulty in filling of the ventricles (i.e. disturbed emptying of the atria [diastolic dysfunction]), for example in **hypertrophic** or **advanced dilatative cardiomyopathy**, can only be objectively assessed using Doppler. With diastolic dysfunction, a reversal of the E and A waves of the in-flow tracts through the atrioventricular valve can occur in PW Doppler (**Fig. 2-143B**). However, ferrets, rabbits, and guinea pigs can sometimes exhibit a short-term increase in the velocity of the late diastolic ventricular in-flow (increased A wave) without any recognizable cardiac changes. In the color-coded M-mode, when there is difficulty in filling the chamber, the early diastolic, red-coded in-flow is darker than the late diastolic in-flow or the inflow takes longer than normal (**Fig. 2-143A**). In addition, with diastolic dysfunction, there is a change in the venous in-flow into the atrium.

In general, the use of ultrasonography for investigating the heart of small exotic mammals is still in the developmental stages. However, one may expect that echocardiography will reach the same diagnostic capabilities in small exotic mammals in the future as it has over the past 15 years for dogs and cats. This will be accelerated by the increasing number of small exotic mammalian patients being treated in veterinary practices, the increasing willingness of the owner to invest in the health of their pets, and the continued development and improvement of technical equipment with a concurrent reduction in price.

Further reading

BOONYAPAKORN, C. (2007): Cardiologic examinations in ferrets with and without heart disease. Dissertation, Berlin.

DUKES-MCEVAN, J., BORGARELLI, M., TIDHOLM, A., VOLLMAR, A. C., HÄGGSTRÖM, J. (2003): Guidelines for the diagnosis of canine idiopathic dilated cardiomyopathy. The ESVC Taskforce for canine dilated cardiomyopathy. J Vet Cardiol **5**: 7–19.

DZYBAN, L. A., GARROD, L. A., BESSO, J. G. (2001): Pericardial effusion and pericardiocentesis in a guinea pig (Cavia porcellus). J Am Anim Hosp Assoc **37**: 21–26.

ERDMANN, E. (ed.): Klinische Kardiologie. Krankheiten des Herzens, des Kreislaufs und der herznahen Gefäße. 7th edition, Springer Verlag, Berlin 2008.

KATTINGER, P., EWRINGMANN, A., WEYLAND, J., SKRODZKI, M. (1999): Kardiologische Untersuchungen beim Kaninchen. Kleintierpraxis, **44**: 761–772.

KÜNZEL, F., KOLM, U. S., BÖHLER, A., URL, A. (2005): Mitralklappeninsuffizienz infolge einer Papillarmuskeldysfunktion bei einem Kaninchen. Tierärztl Praxis, **33**: 423–430.

LIBBY, P., BONOW, R. O., MANN, D. L., ZIPES, D. P.: Braunwald's Heart Disease: A Textbook of cardiovascular medicine. 8th edition, Saunders Elsevier, Philadelphia 2007.

MCCALL, J. W. (1998): Dirofilariasis in the domestic ferret. Clin Tech Small Anim Pract **13**: 109–112.

SASAI, H., KATO, K., SASAKI, T., KOYAMA, S., KOTANI, T., FUKATA, T. (2000): Echocardiographic diagnosis of dirofilariasis in a ferret. J Small Anim Pract **41**, 172–174.

STEPIEN, R. L., BENSON, K. G., FORREST, L. J. (1999): Radiographic measurement of cardiac size in normal ferrets. Vet Radiol Ultrasound **40**: 606–610.

TILLEY, L. T., SMITH JR, F. W. K., OYAMA, M. A., SLEEPER, M. M.: Manual of canine and feline cardiology. 4th edition, Saunders Elsevier, St. Louis 2008.

TOBIAS, R., SKRODZKI, M., SCHNEIDER, M.: Kleintierkardiologie kompakt. Schlütersche Verlagsgesellschaft, Hannover 2008.

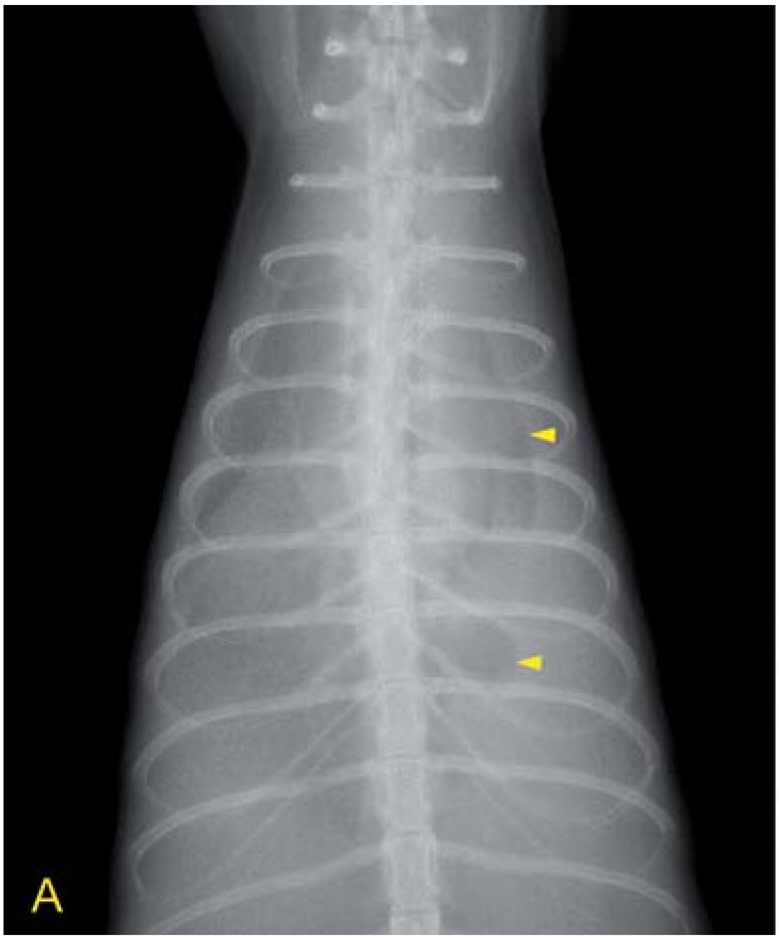

Fig. 2-116: Radiographic images of a ferret's thorax, ventrodorsal projection.

A: Severe hydrothorax with displacement of the lungs (arrowheads) from the thoracic wall.

B: Mild pneumothorax.

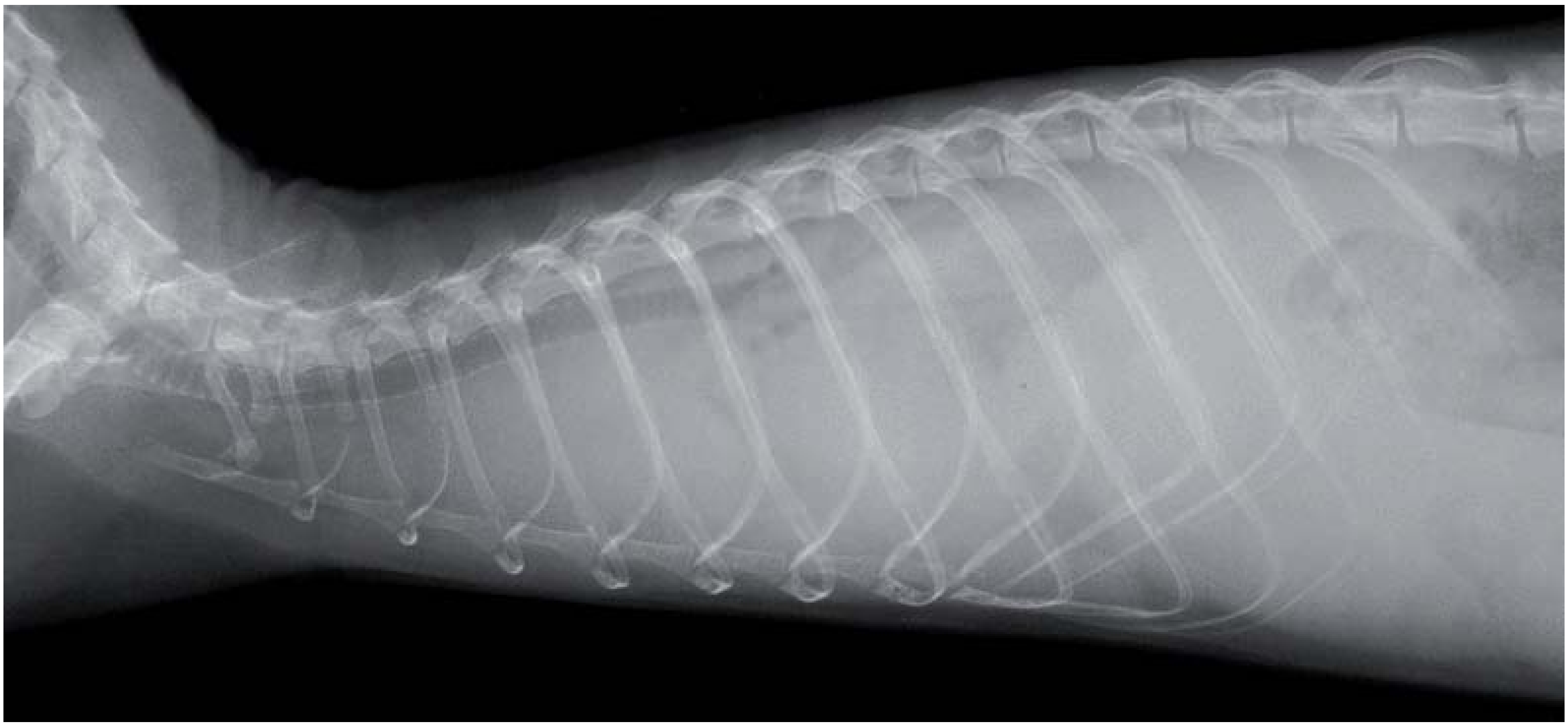

Fig. 2-117: Radiographic image of a ferret's thorax, lateral projection. The trachea has been displaced dorsally by a precardial mass. In addition, there is a severe alveolar pattern in the lungs.

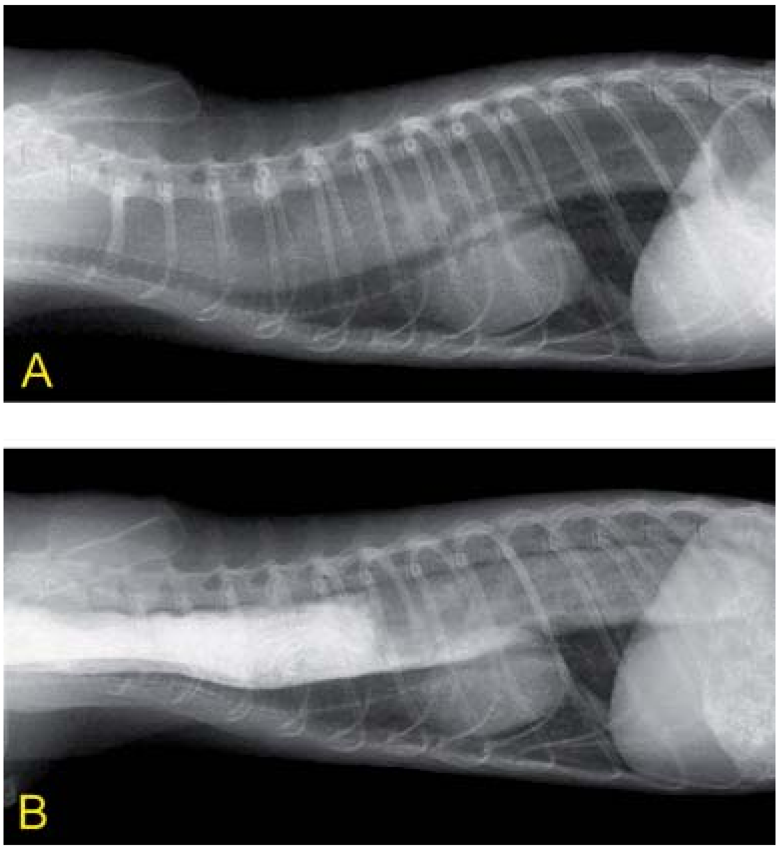

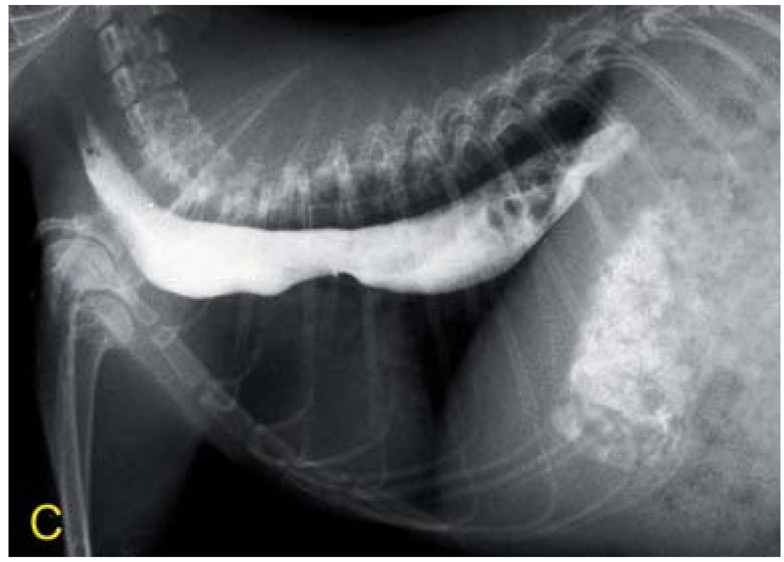

Fig. 2-118C: Radiographic image of a chinchilla's thorax, lateral projection. Image of a megaoesophagus, 15 minutes after the oral administration of a contrast agent (barium sulfate suspension).

Radiograph reproduced with kind permission from Jopp, I. P., Stengel, C., Kraft, W. (2004): Megaösophagus bei einem Chinchilla. Tierärztl Prax **32(K)**: 97 [98].

Fig. 2-118A, B: Radiographic images of a ferret's thorax, lateral projection.

A: A dorsal mass has ventrally displaced the trachea, heart, and lungs.

B: Radiograph 10 minutes after the oral administration of barium sulfate. The esophagus is severly dilated along its entire length.

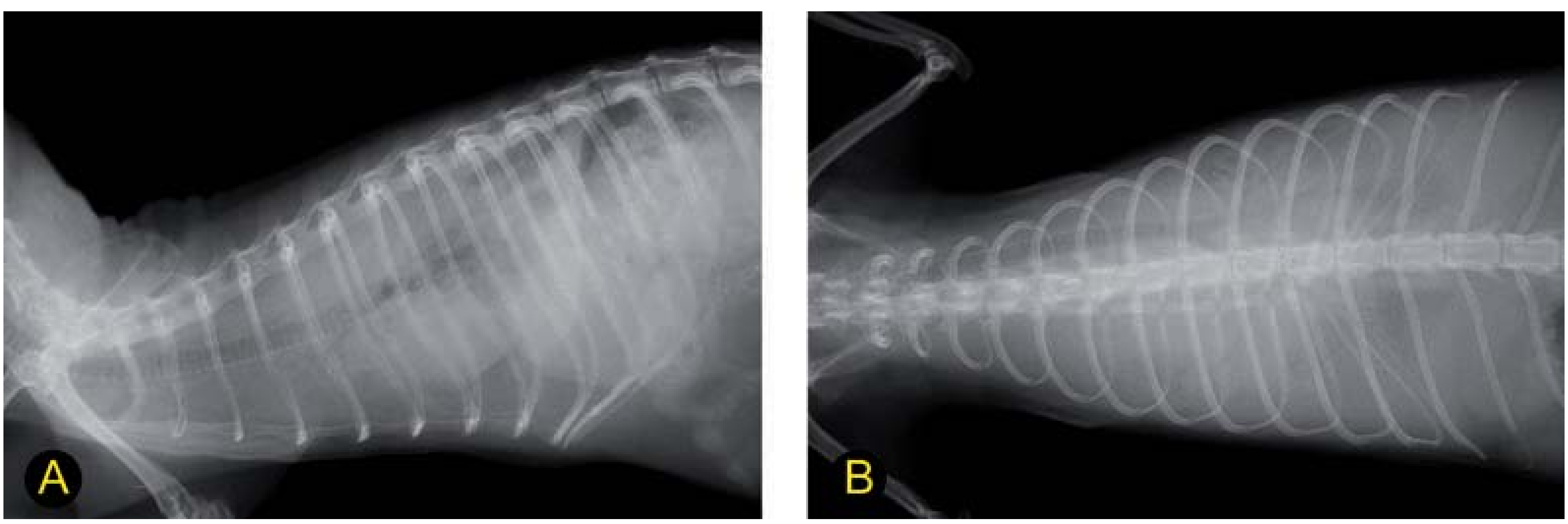

Fig. 2-119: Radiographic images of a ferret's thorax, (A) lateral and (B) ventrodorsal projections. Alveolar lung patterns with the formation of an air bronchogram can be easily identified in the ventrodorsal projection (B).

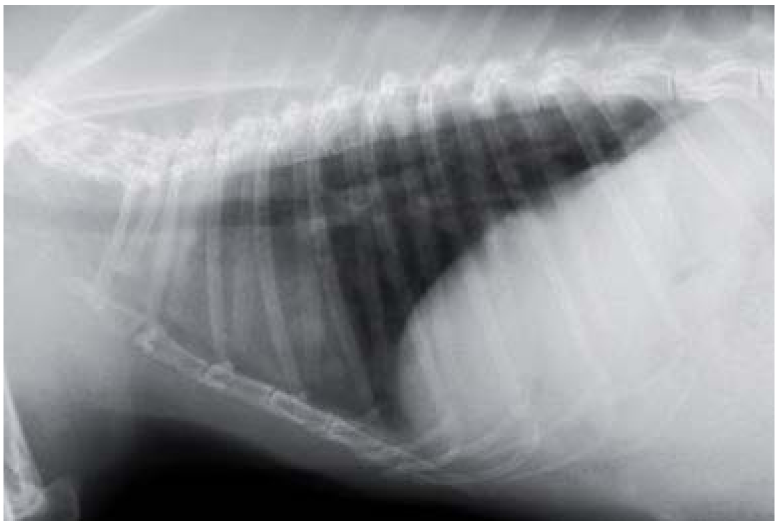

Fig. 2-120: Radiographic image of a rabbit's thorax, lateral projection. Interstitial lung pattern – multiple metastases of a mammary carcinoma.

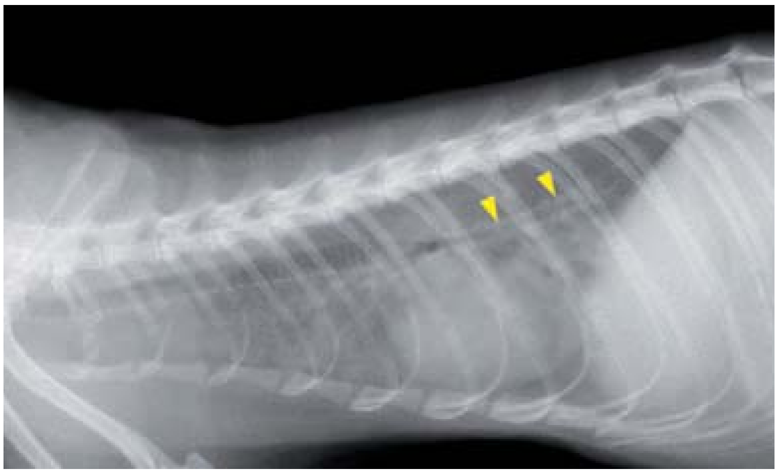

Fig. 2-121: Radiographic image of a ferret's thorax, lateral projection. Bronchial lung pattern with clearly thickened bronchial walls (arrowheads). Alveolar lung patterns are also present (cardiogenic lung edema).

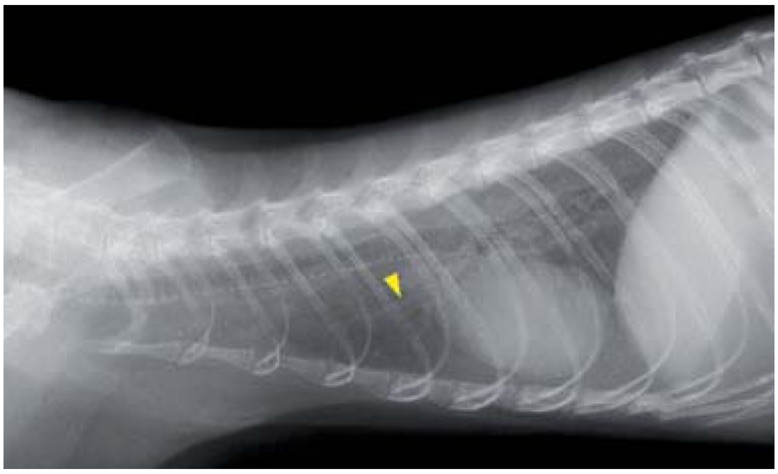

Fig. 2-122: Radiographic image of a ferret's thorax, lateral projection. Vascular lung pattern with clearly visible lung vessels (arrowhead). The heart silhouette is rounded.

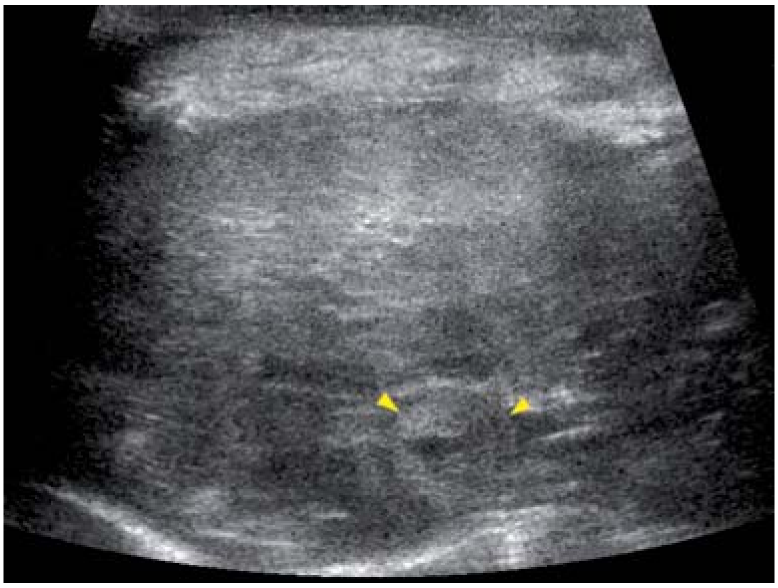

Fig. 2-123: Ultrasonographic image of a chinchilla using the right thoracic wall coupling site, horizontal scanning plane, 12 MHz, PD 4 cm. An elongated intrathoracic mass is pushing the heart (arrowheads) toward the left thoracic wall.

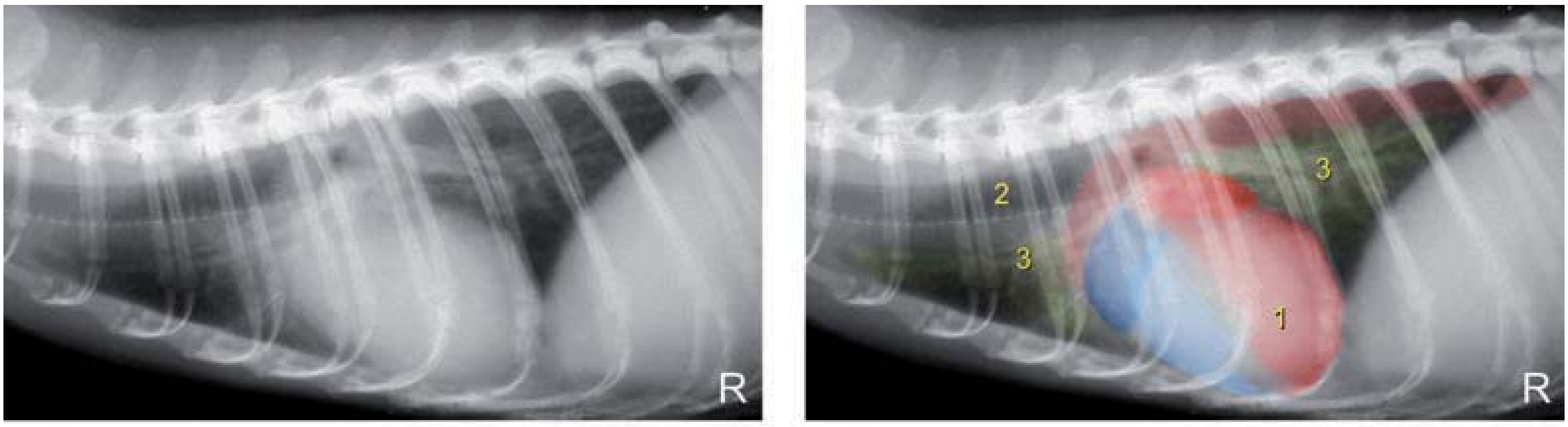

Fig. 2-124: Radiographic image of a ferret's thorax, lateral projection, right lateral recumbency. Severe cardiomegaly (1) due to dilatative cardiomyopathy. The trachea (2) is displaced dorsally. Interstitial lung pattern (3) is present as an expression of cardiogenic lung edema. (Small picture of a ferret with a healthy heart for comparison.)

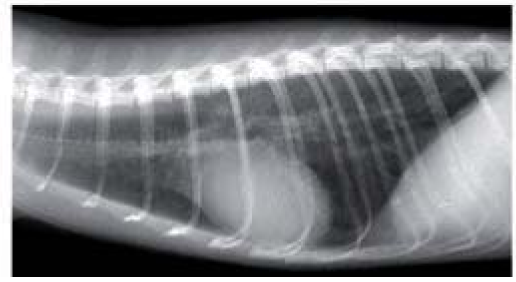

Radiograph courtesy of C. Boonyapakorn, M. Skrodzki, E. Trautvetter, Berlin, Germany.

1: heart
2: trachea
3: lung patterns

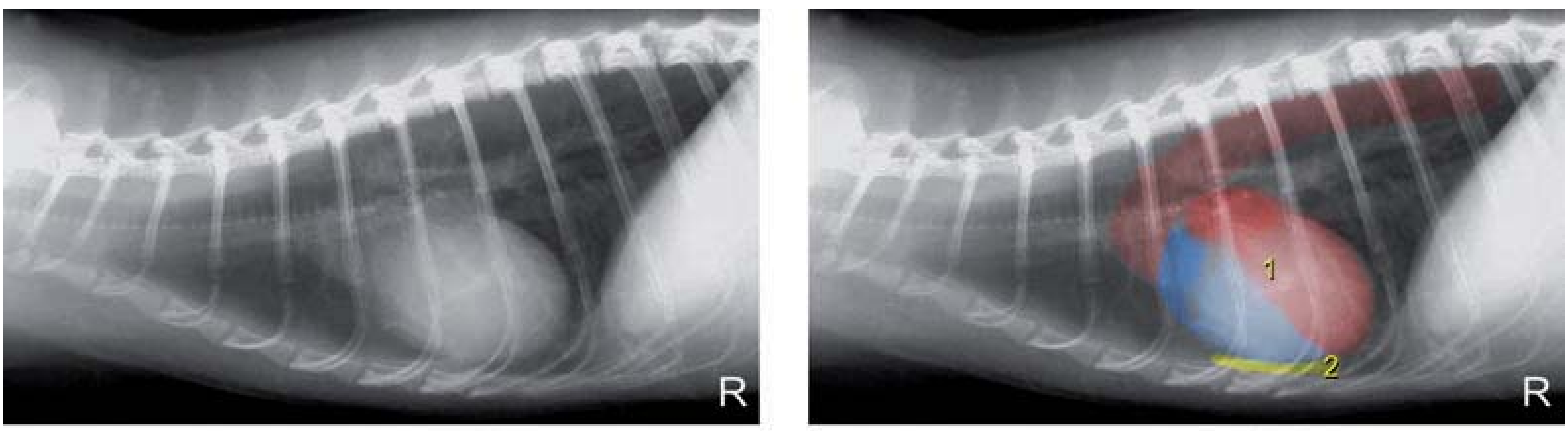

Fig. 2-125: Radiographic images of a ferret's thorax, lateral projection, right lateral recumbency. Cardiomegaly (1) due to dilatative cardiomyopathy with left-sided cardiac insufficiency. The heart is raised above the sternum (2). The trachea is displaced dorsally. (Small picture of a ferret with a healthy heart for comparison.)

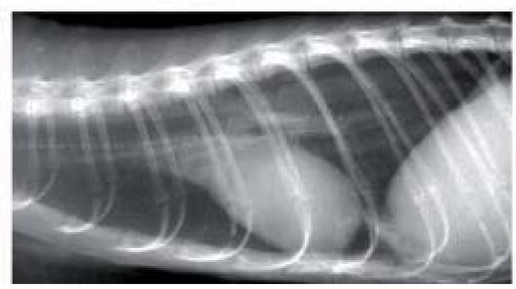

Radiograph courtesy of C. Boonyapakorn, M. Skrodzki, E. Trautvetter, Berlin, Germany.

1: heart
2: increased space between heart and sternum

Fig. 2-126: Radiographic images of a guinea pig's thorax diagnosed with pericardial effusion, (A) lateral projection with the animal in right lateral recumbency and (B) 2D echocardiography, parasternal short-axis view from the right at the level of the papillary muscle.

A: Cardiomegaly with a globally enlarged heart silhouette (7). The increased lung vessel pattern (8) and the widened caudal vena cava (9) indicate the presence of a cardiac tamponade. Due to its extremely poor health and severe dyspnea, the animal could not be adequately positioned by pulling the foreleg in a cranial direction.

B: A large amount of hypoechoic fluid in the pericardium, pseudohypertrophy of the myocardium of the left and right ventricles, and hypovolaemia are all indicators of cardiac tamponade. (Small picture of a guinea pig with a healthy heart for comparison.)

1: fluid in the pericardial sac
2: right myocardium
3: right ventricle
4: interventricular septum
5: left ventricle
6: left myocardium
7: heart silhouette
8: lung vessel pattern
9: caudal vena cava

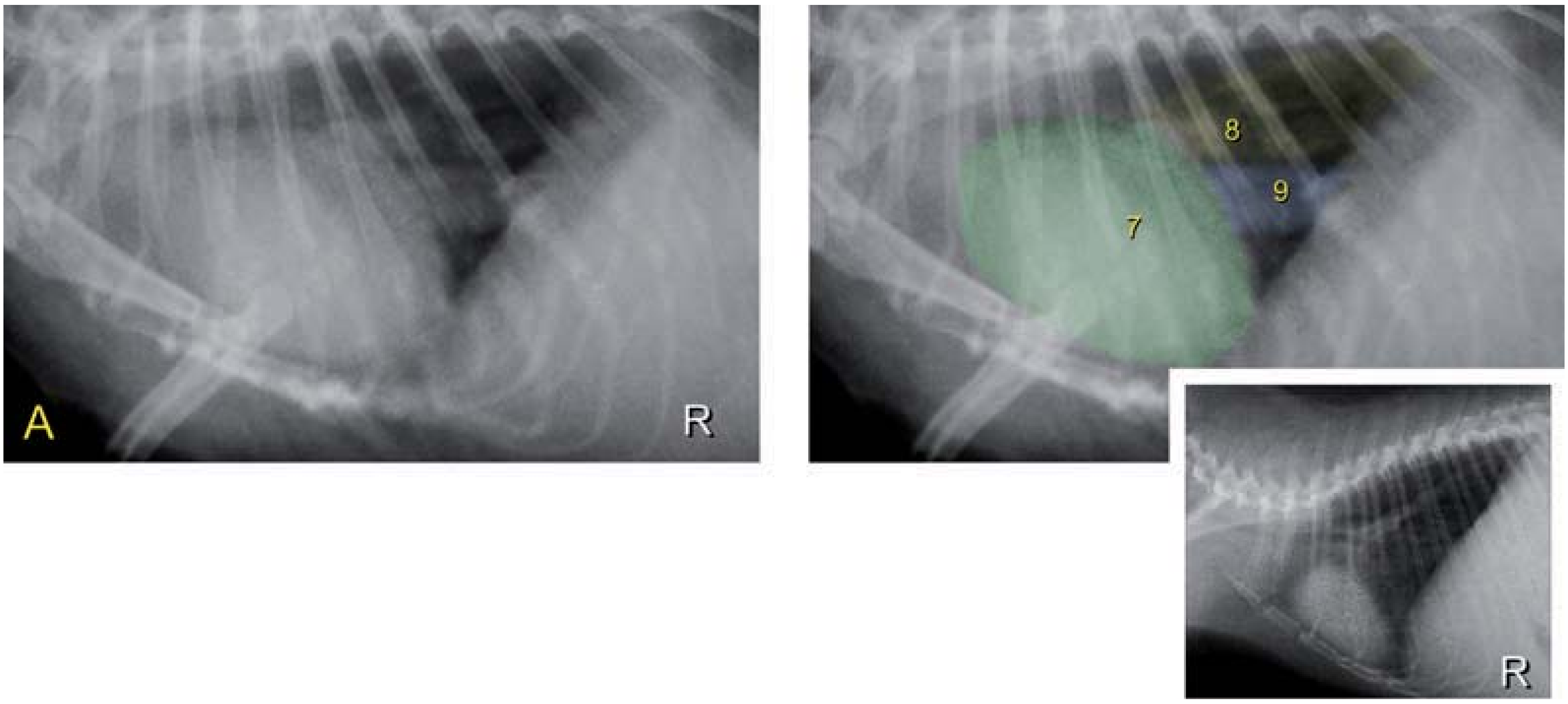
A
R
8
9
7
R

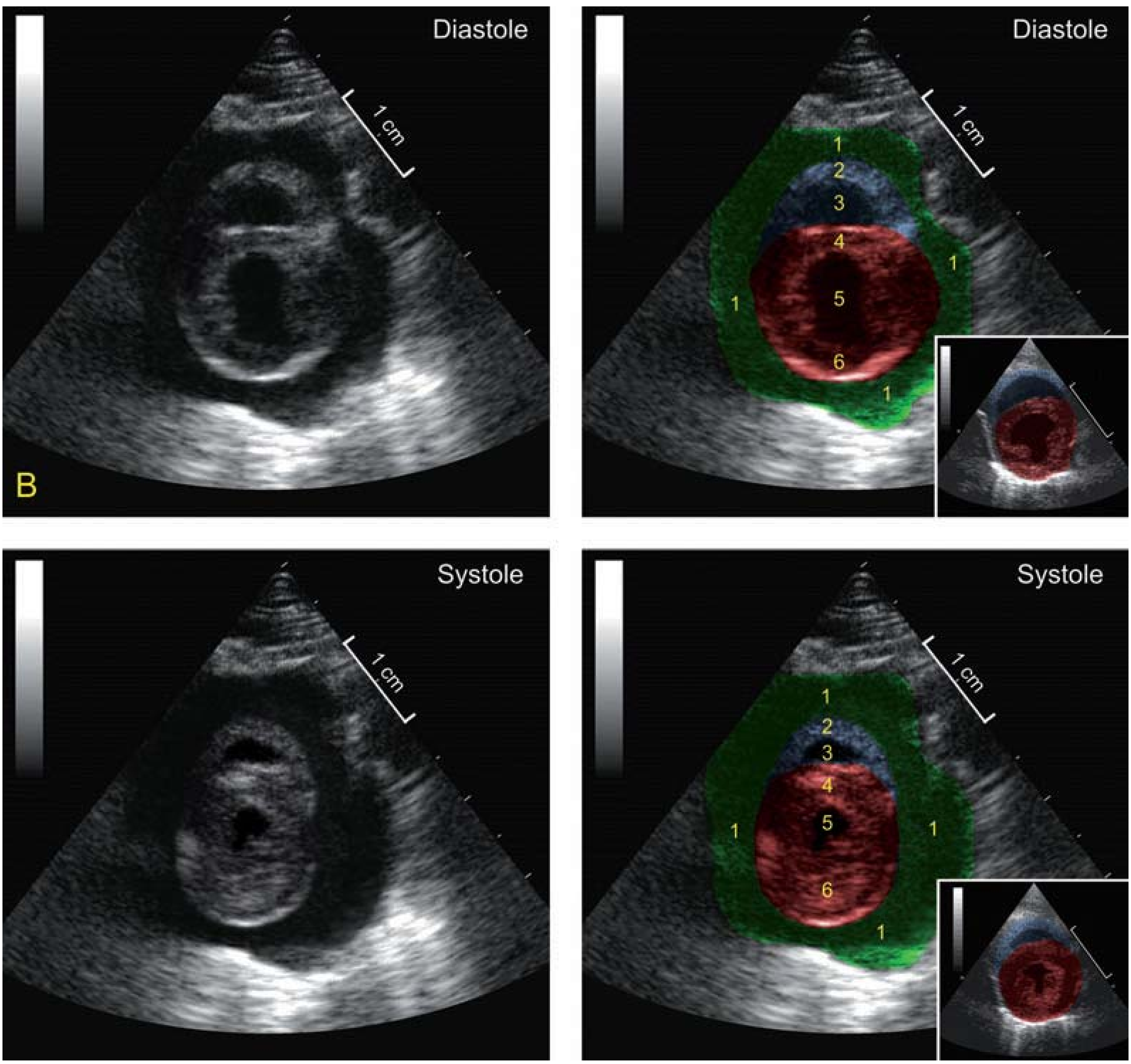
Diastole
1 cm
B
Diastole
1 cm
1
2
3
4
1
1
5
6
1
Systole
1 cm
Systole
1 cm
1
2
3
4
5
1
1
6
1

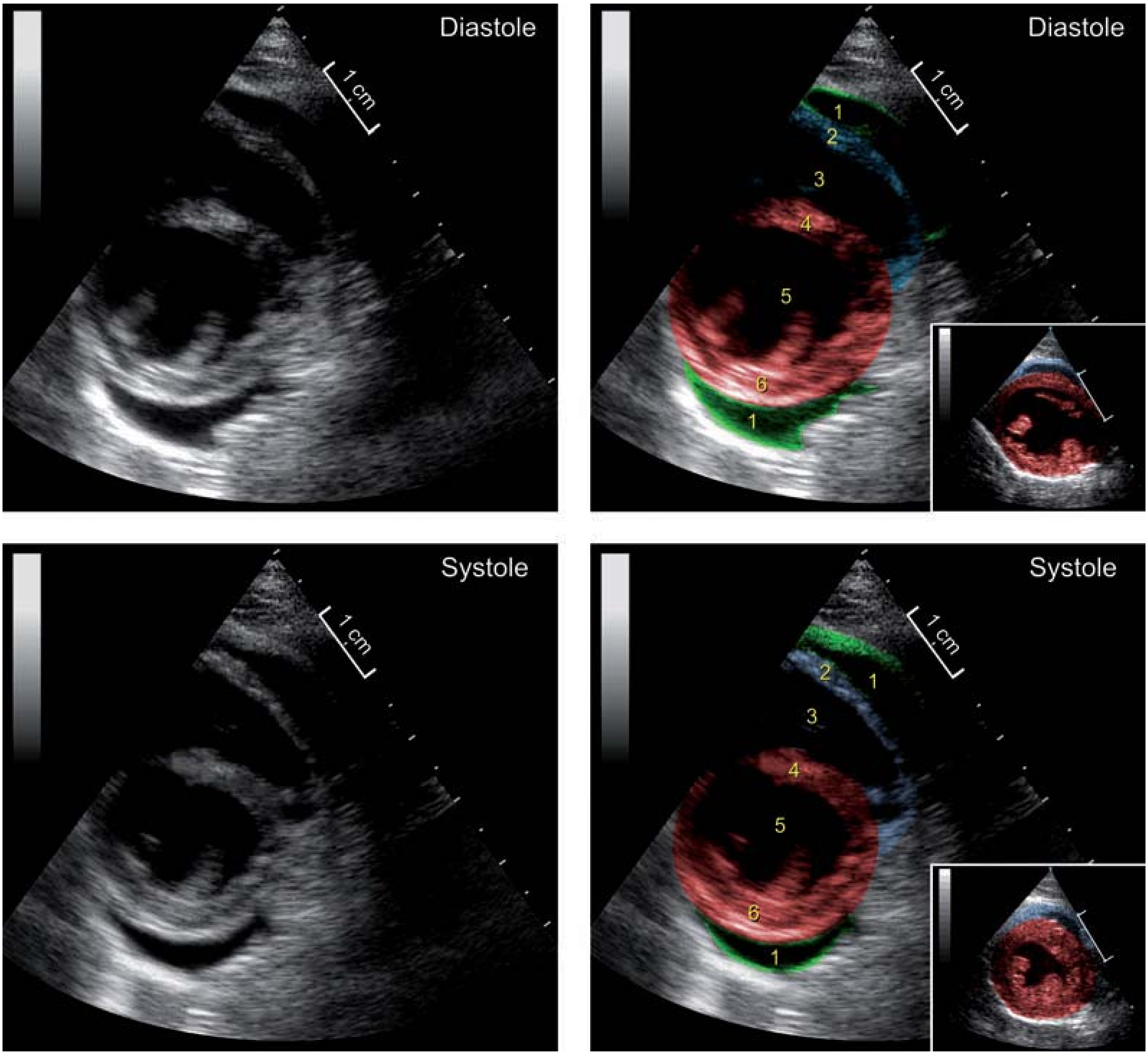

Fig. 2-127: 2D echocardiographic images of a rabbit with pericardial effusion, parasternal short-axis view from the right at the level of the papillary muscle. There is a large amount of hypoechoic fluid in the pericardium. The right and left ventricles are enlarged during both systole and diastole due to severe cardiac insufficiency resulting from a dilatative cardiomyopathy. (Small picture of a rabbit with a healthy heart for comparison.)

1: fluid in the pericardial sac
2: right myocardium
3: right ventricle
4: interventricular septum
5: left ventricle
6: left myocardium

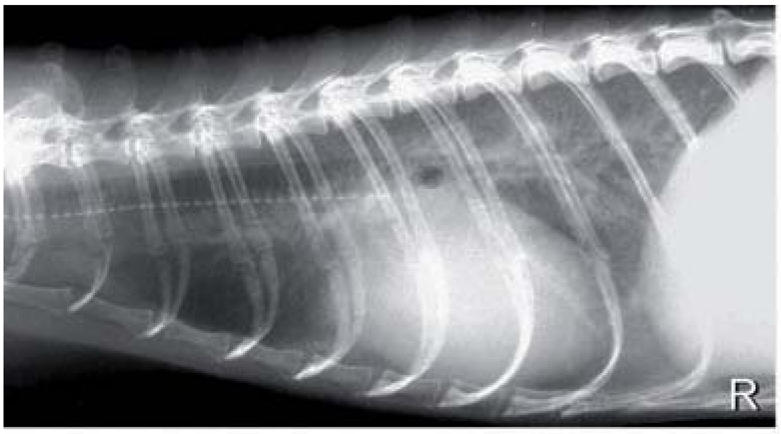

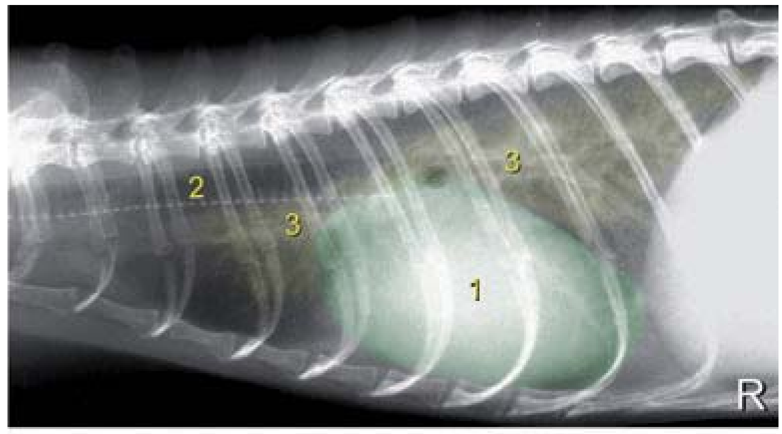

1: heart
2: trachea
3: lung pattern

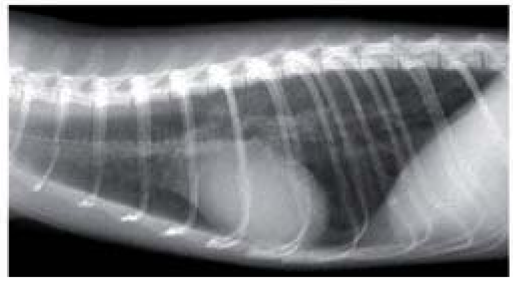

Fig. 2-128: Radiographic images of a ferret's thorax, lateral projection, right lateral recumbency. Severe cardiomegaly with pericardial effusion (1). The trachea (2) is displaced dorsally. There is interstitial to alveolar lung patterns (3) as a consequence of cardiogenic lung edema caused by congestive heart failure. A severe AV valve insufficiency was diagnosed as the underlying cause of the congestive heart failure by using echocardiography. (Small picture of a ferret with a healthy heart for comparison.)

Radiographs courtesy of C. Boonyapakorn, M. Skrodzki, E. Trautvetter, Berlin, Germany.

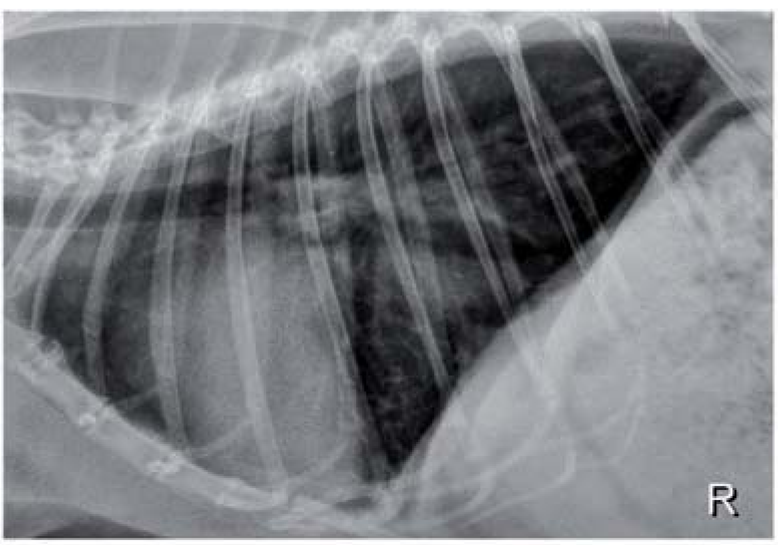

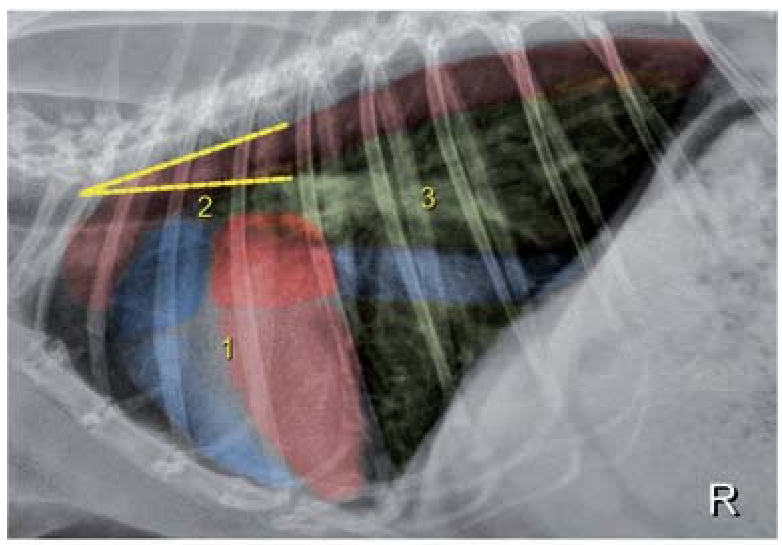

1: heart
2: trachea
3: lung pattern

Fig. 2-129: Radiographic images of a rabbit's thorax, lateral projection, right lateral recumbency. Bronchial and interstitial lung patterns (3) in a case of bronchial asthma with a normal-sized heart (1) and normal position of the trachea (2). No cardiogenic lung edema is present. (Small picture of a rabbit with healthy lungs and heart for comparison.)

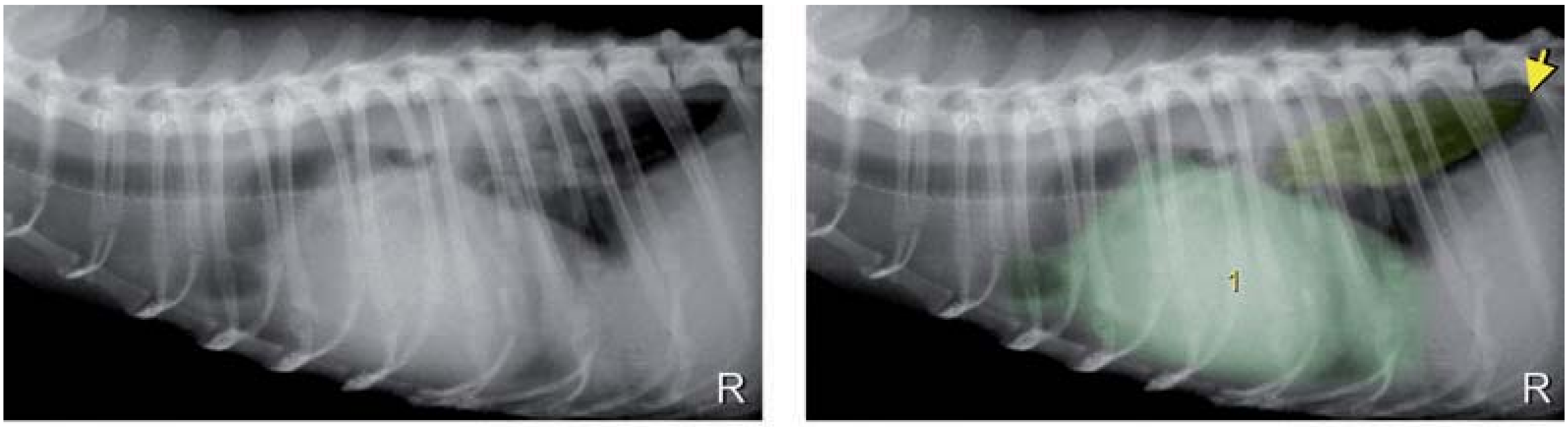

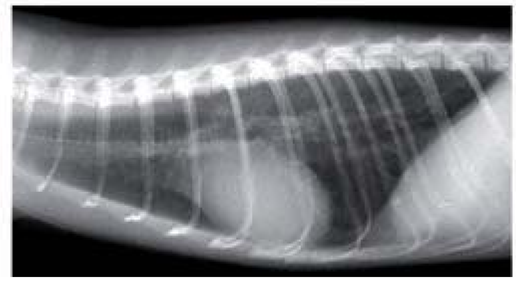

1: heart

arrowhead: candal lung lobe

Fig. 2-130: Radiographic images of a ferret's thorax, lateral projection, right lateral recumbency. Moderate pleural effusion with a rounded caudal lung lobe (arrowhead). The presence of cardiomegaly (1) indicates that the cause of these changes is cardiogenic. A severe dilatative cardiomyopathy was diagnosed using echocardiography. (Small picture of a ferret with a healthy heart for comparison.)

Radiographs courtesy of C. Boonyapakorn, M. Skrodzki, E. Trautvetter, Berlin, Germany.

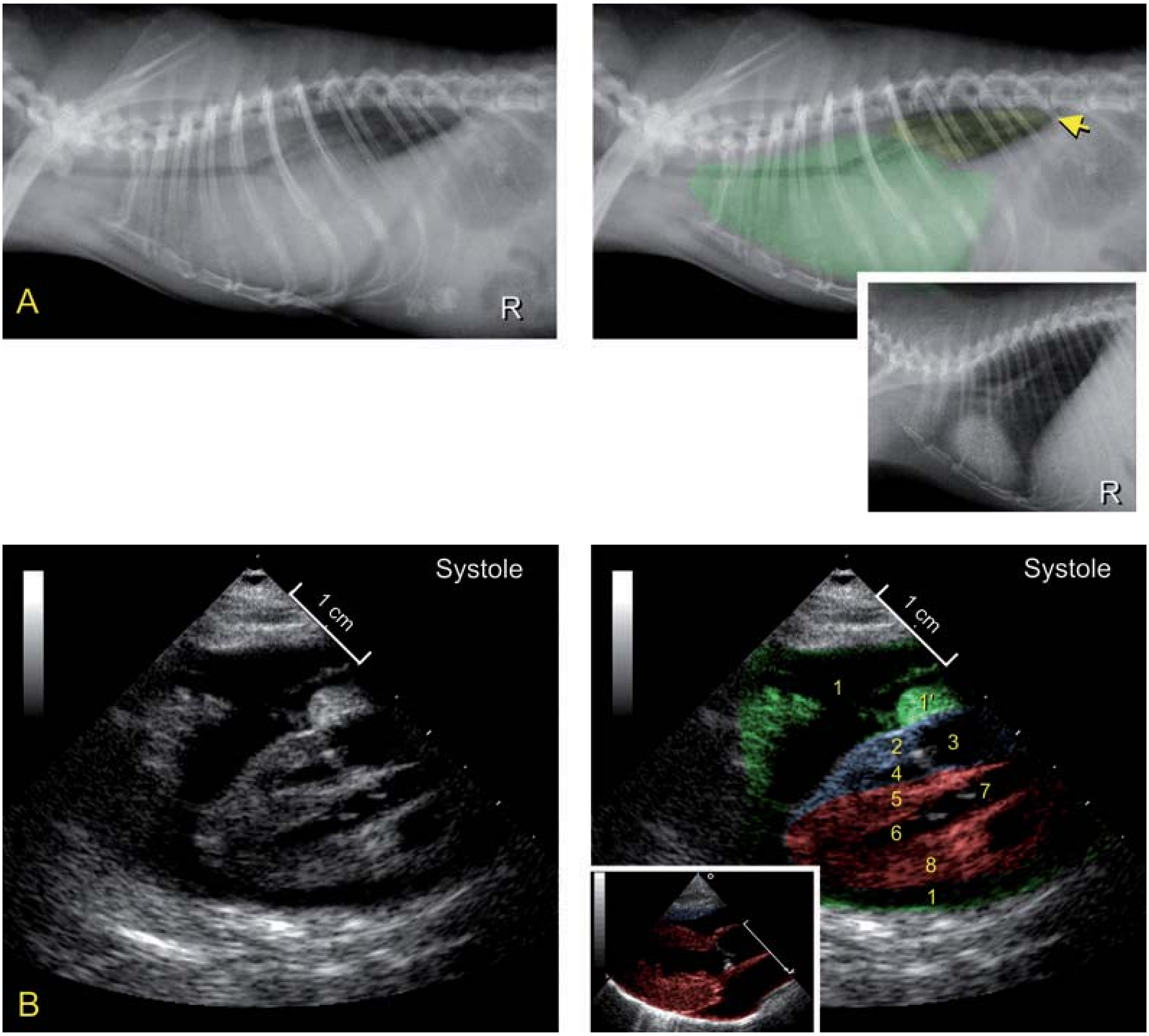

Fig. 2-131: Guinea pig diagnosed with severe pleural effusion.

A: Radiographic image of the thorax, lateral projection, right lateral recumbency.

B: 2D echocardiography, right parasternal long-axis view at the level of the left ventricular out-flow tract, same animal.

(A) Radiopaque fluid masks the heart. The caudal lung lobes (arrowhead) are rounded. (B) A roundish tumor (without tissue characterization) is present in the mediastinum. The small end-systolic left atrium indicates the presence of a tamponade. (Small picture of a guinea pig with a healthy heart for comparison.)

1: free fluid
1': tumor
2: right myocardium
3: right atrium
4: right ventricle
5: interventricular septum
6: left ventricle, out-flow tract
7: ascending aorta with end-systolic closed aortic valve
8: left myocardium

arrowhead: caudal lung lobe

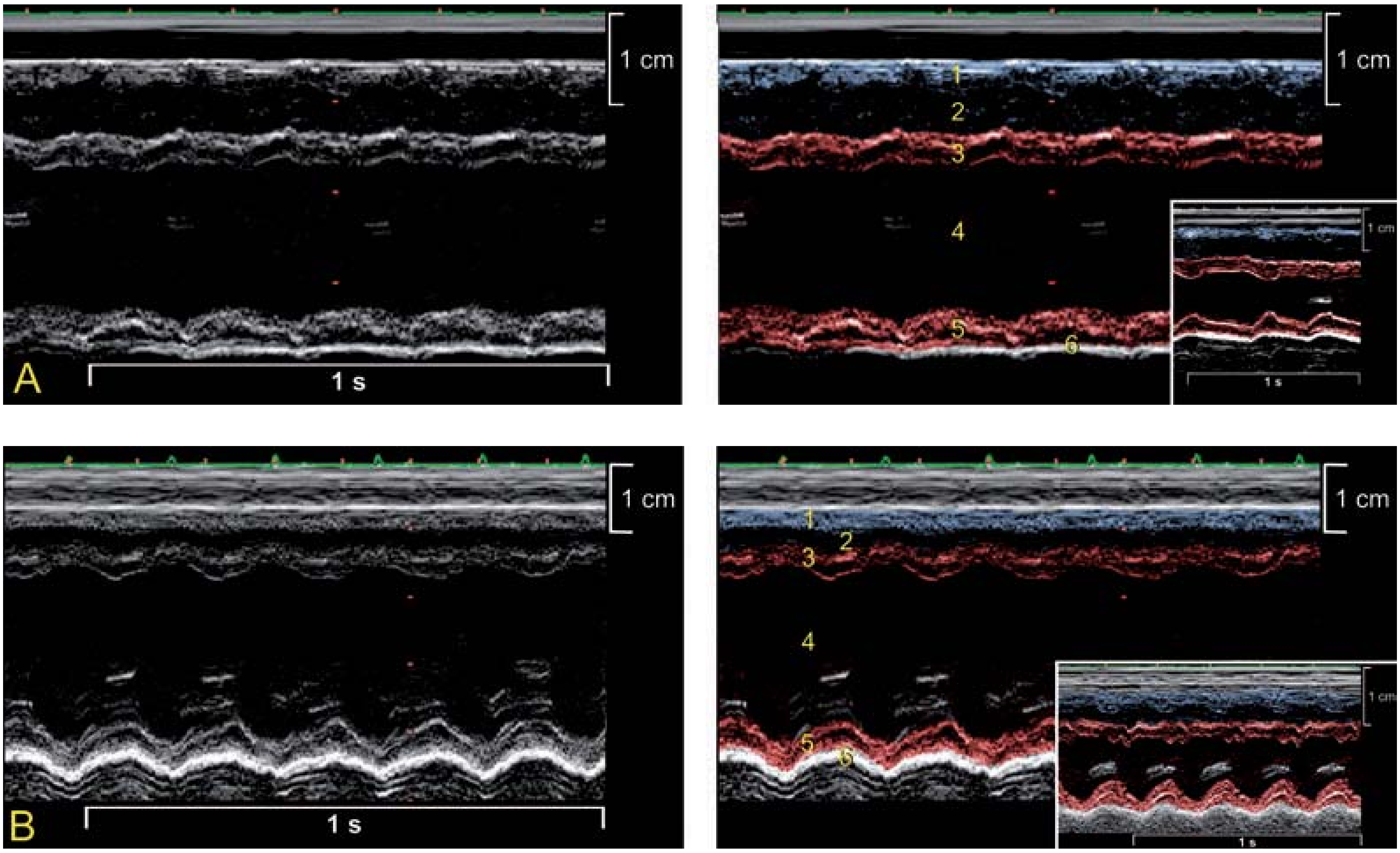

Fig. 2-132:

A: M-mode echocardiogram of a ferret from the right parasternal short-axis view at the level of the papillary muscle.

B: M-mode echocardiogram of a rabbit from the right parasternal long-axis view at the level of the chordae tendineae.

A and B: End-diastolic and end-systolic enlarged left ventricle, inadequate increase in thickness of the interventricular septum, and left myocardium during systole in a case of dilatative cardiomyopathy.

(Small pictures of a healthy heart in a ferret [A] and a rabbit [B] for comparison.)

1: right myocardium
2: right ventricle
3: interventricular septum
4: left ventricle
5: left myocardium
6: pericardium

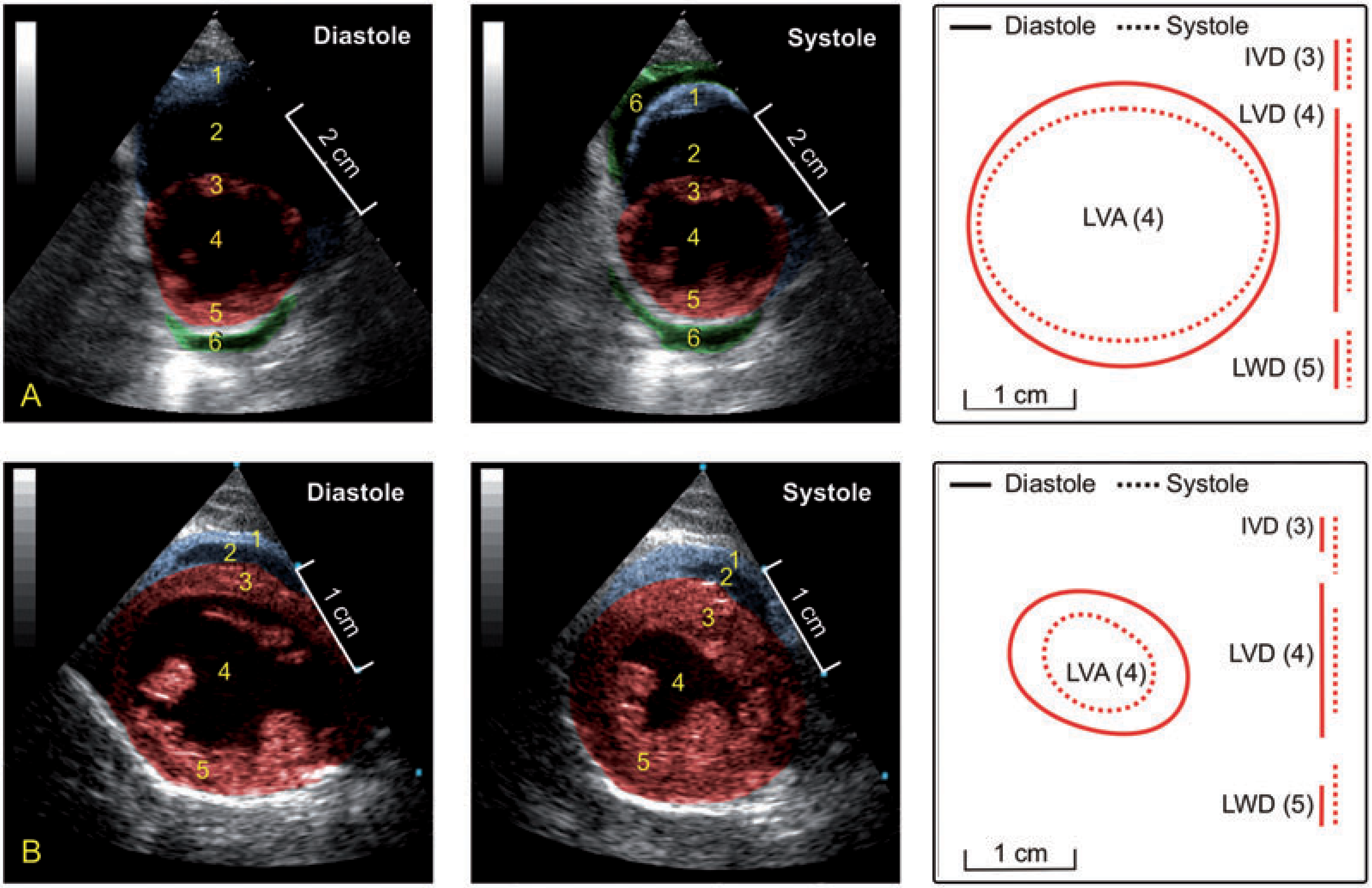

Fig. 2-133: 2D echocardiographic images of a rabbit, right parasternal short-axis view at the level of the papillary muscle.

A: End-diastolic and end-systolic severely enlarged left ventricle, inadequate systolic thickening of the interventricular septum and left myocardium as well as pericardial effusion in a case of dilatative cardiomyopathy.

B: Normal-sized, well-contracting left ventricle in a healthy heart.

The two schematic diagrams on the right with comparable scales underline the severe changes found in dilatative cardiomyopathy (A, top right) compared to a healthy heart (B, bottom right). In dilatative cardiomyopathy, the circular area (LVA) and the internal diameter (LVD) of the left ventricle are significantly increased during diastole and systole. The thickness of the interventricular septum (IVD) and the left myocardium (LWD) are generally reduced during systole.

1: right myocardium
2: right ventricle
3: interventricular septum
4: left ventricle
5: left myocardium
6: pericardial effusion

LVA: left ventricular circular area
LVD: left ventricular internal diameter
IVD: interventricular septum thickness
LWD: thickness of the left myocardium

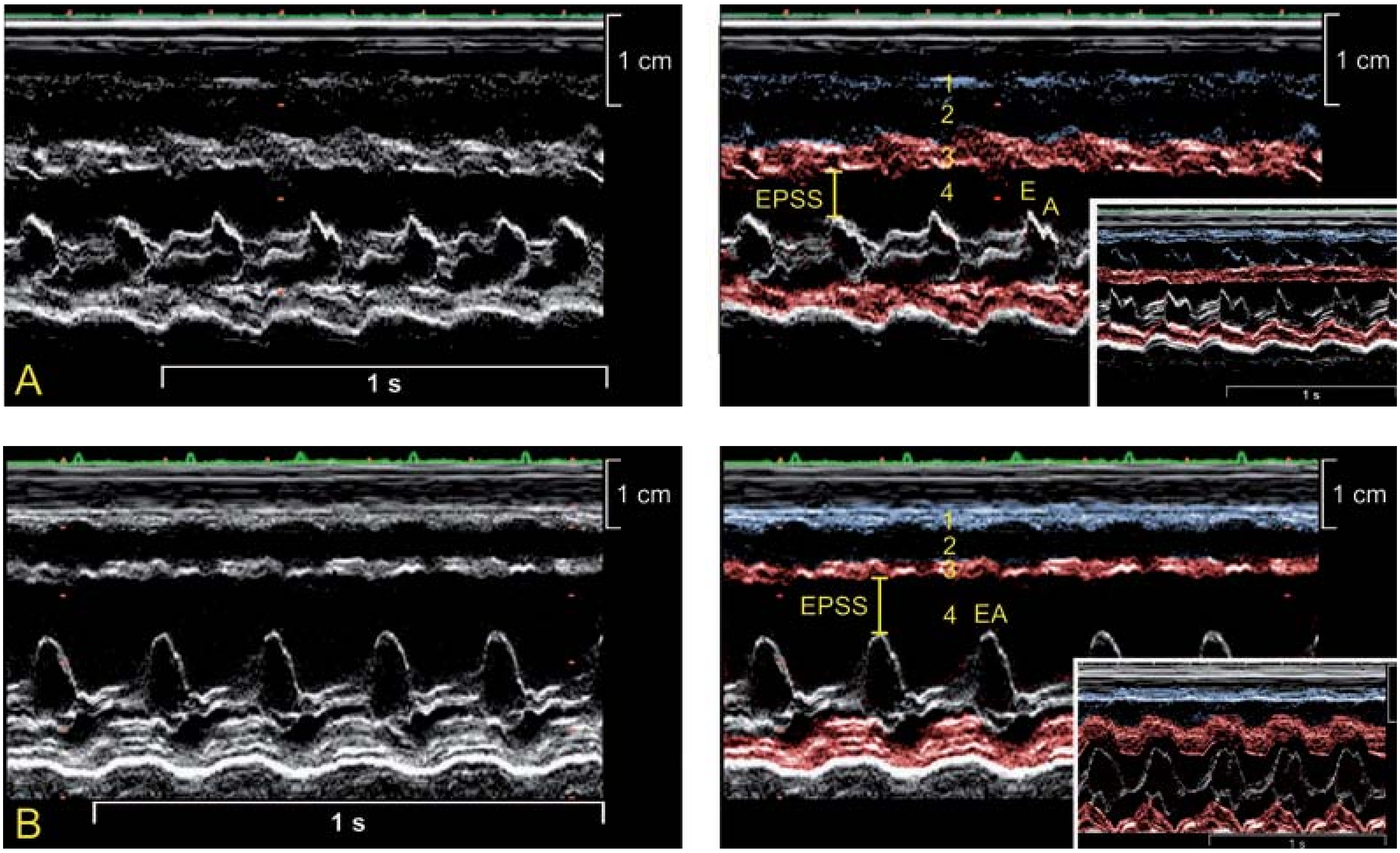

Fig. 2-134:
Dilatative cardiomyopathy with end-systolic overextended left ventricle, enlarged EPSS, and prolonged early diastolic closing of the mitral valve due to impaired early diastolic filling. The (A) initiation of and (B) complete fusion of the E and A waves is due in part to the high heart rate.

A: M-mode echocardiogram from the right parasternal long-axis view at the level of the mitral valve, Ferret.

B: M-mode echocardiogram from the right parasternal short-axis view at the level of the mitral valve, Rabbit.

(Small pictures of a healthy heart in a ferret [A] and a rabbit [B] for comparison.)

1: right myocardium
2: right ventricle
3: interventricular septum
4: left ventricle

EPSS: the distance between the interventricular septum and E-wave
E: E-wave = early diastolic maximal opening of the anteriomedial leaflet of the mitral valve
A: A wave = late diastolic opening of the anteriomedial leaflet of the mitral valve during atrial contraction
EA: EA fusion wave

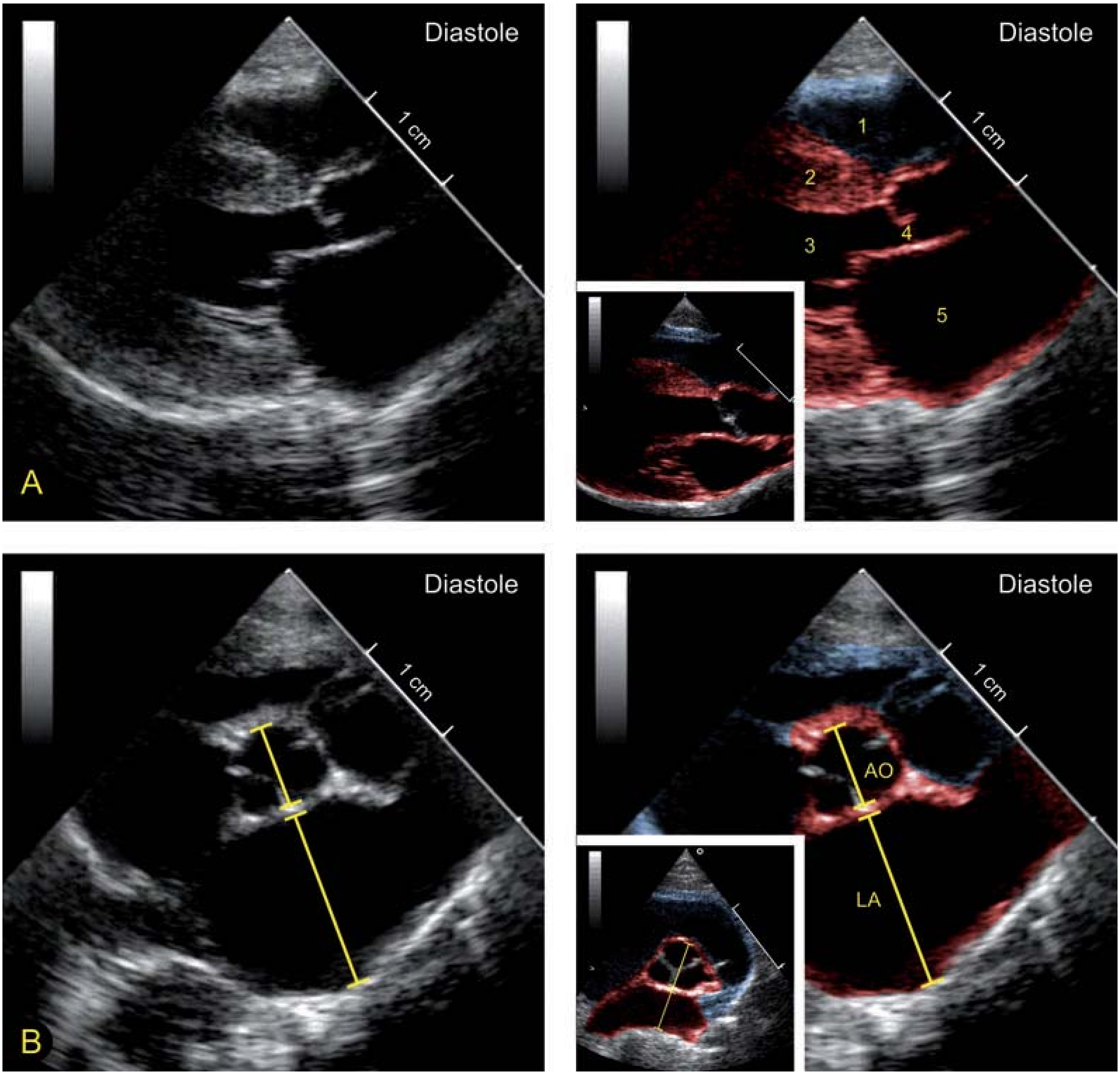

Fig. 2-135: 2D echocardiographic images of a ferret with a severely enlarged left atrium, right parasternal long-axis view of the left ventricular in- and out-flow tracts and right parasternal short-axis view at the level of the (A) aortic valve and (B) left atrium. Hypertrophic cardiomyopathy with obstruction of the out-flow tract and mitral valve insufficiency was diagnosed with the aid of additional echocardiographic examinations and color-coded and CW-Doppler scans. (Small picture of a ferret with a healthy heart for comparison.)

1: right ventricle
2: interventricular septum
3: left ventricle
4: closed aortic valve
5: left atrium

AO: diameter of the aortic sinus
LA: diameter of the left atrium

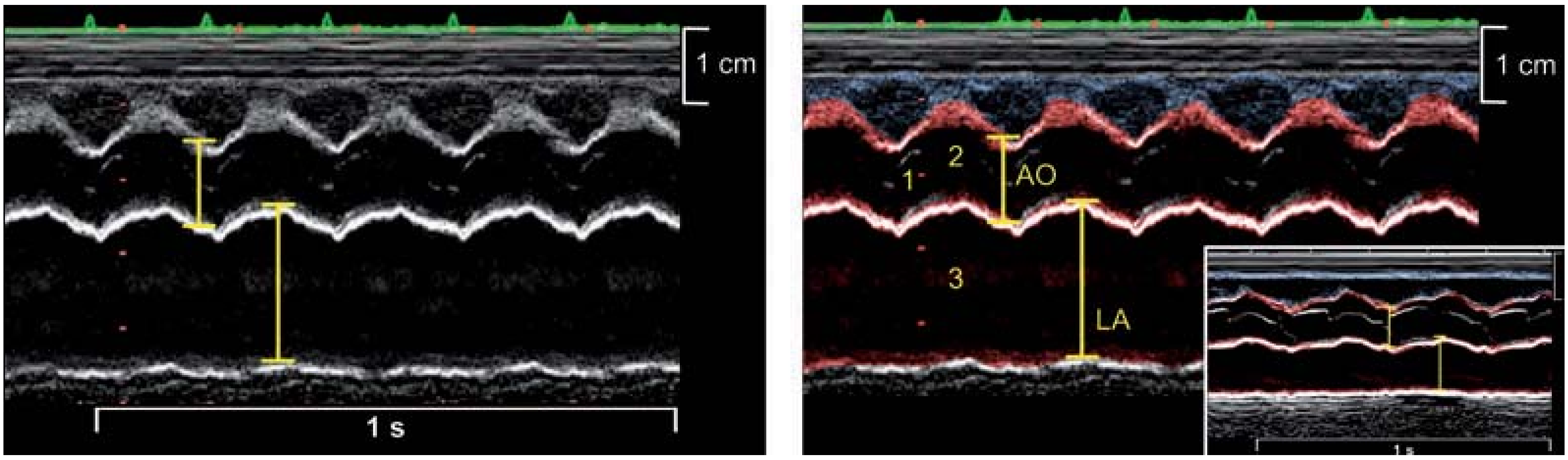

Fig. 2-136: M-mode echocardiographic images of a rabbit with an enlarged left atrium obtained from the right parasternal long-axis view at the level of the aortic valve and left atrium. A dilatative cardiomyopathy with reflux and congestion of blood in the left atrium was diagnosed with the aid of echocardiography and color-coded and CW-Doppler scans. (Small picture of a rabbit with a healthy heart for comparison.)

1: aortic sinus
2: closed aortic valve
3: left atrium

AO: diameter of the aortic sinus
LA: diameter of the left atrium

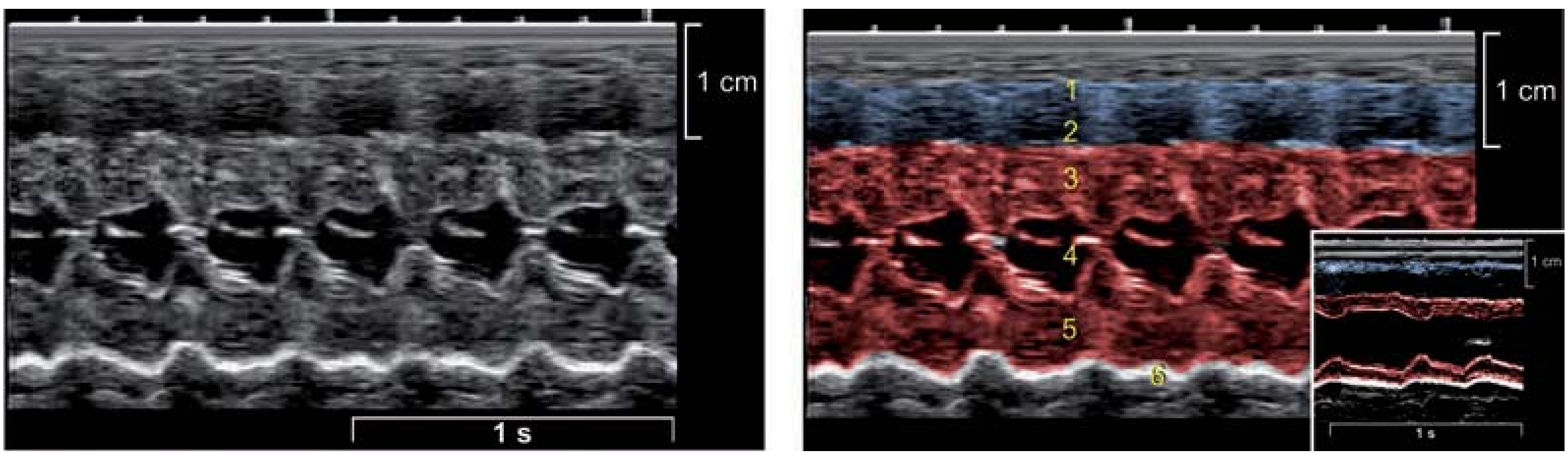

Fig. 2-137: M-mode echocardiogram of a ferret with concentric hypertrophy of the left ventricle (i.e. an obvious thickening of the interventricular septum and left myocardium in a case of hypertrophic cardiomyopathy) obtained from the right parasternal short-axis view. (Small picture of a ferret with a healthy heart for comparison.)

1: right myocardium
2: right ventricle
3: interventricular septum
4: left ventricle
5: left myocardium
6: pericardium

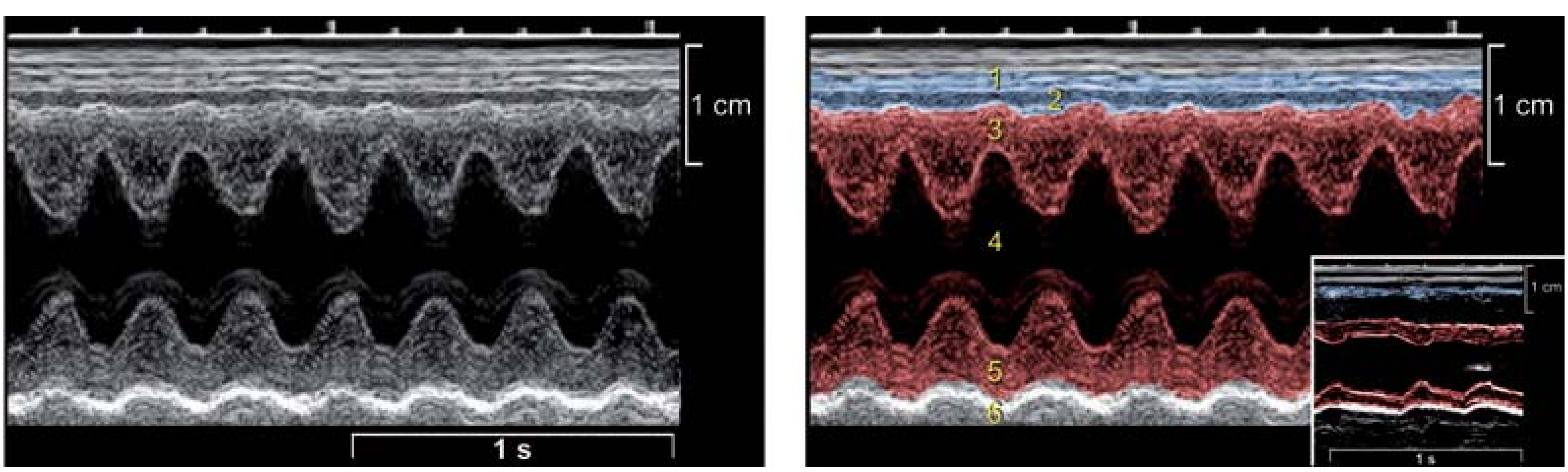

Fig. 2-138: M-mode echocardiogram of a ferret obtained from the right parasternal short-axis view. End-diastolic distended, enlarged left ventricle with very good contractility (hypercontractility) in a case of severe mitral valve insufficiency. (Small picture of a ferret with a healthy heart for comparison.)

1: right myocardium
2: right ventricle
3: interventricular septum
4: left ventricle
5: left myocardium
6: pericardium

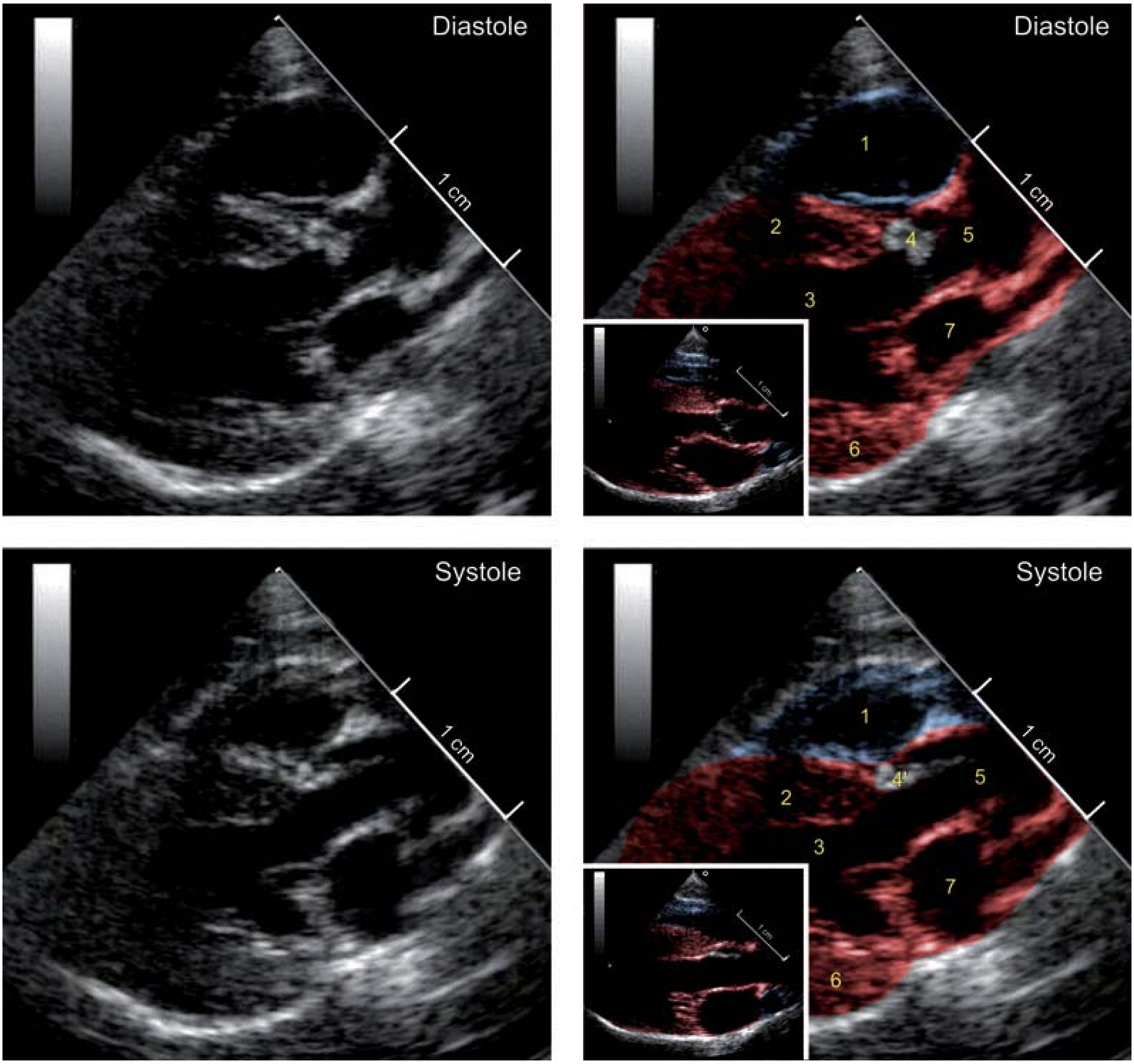

Fig. 2-139: 2D echocardiographic images of a ferret, right parasternal long-axis view of the left ventricular out-flow tract and aortic valve. Thickened septal semilunar leaflet of the aortic valve can be seen with an adequate opening of the valve. The color-coded Doppler echocardiogram clearly showed the presence of an aortic valve insufficiency. (Small picture of a ferret with a healthy heart for comparison.)

1: right ventricle
2: interventricular septum
3: left ventricle, out-flow tract
4: closed, thickened aortic valve
4': opened aortic valve
5: aortic sinus
6: left myocardium
7: left atrium

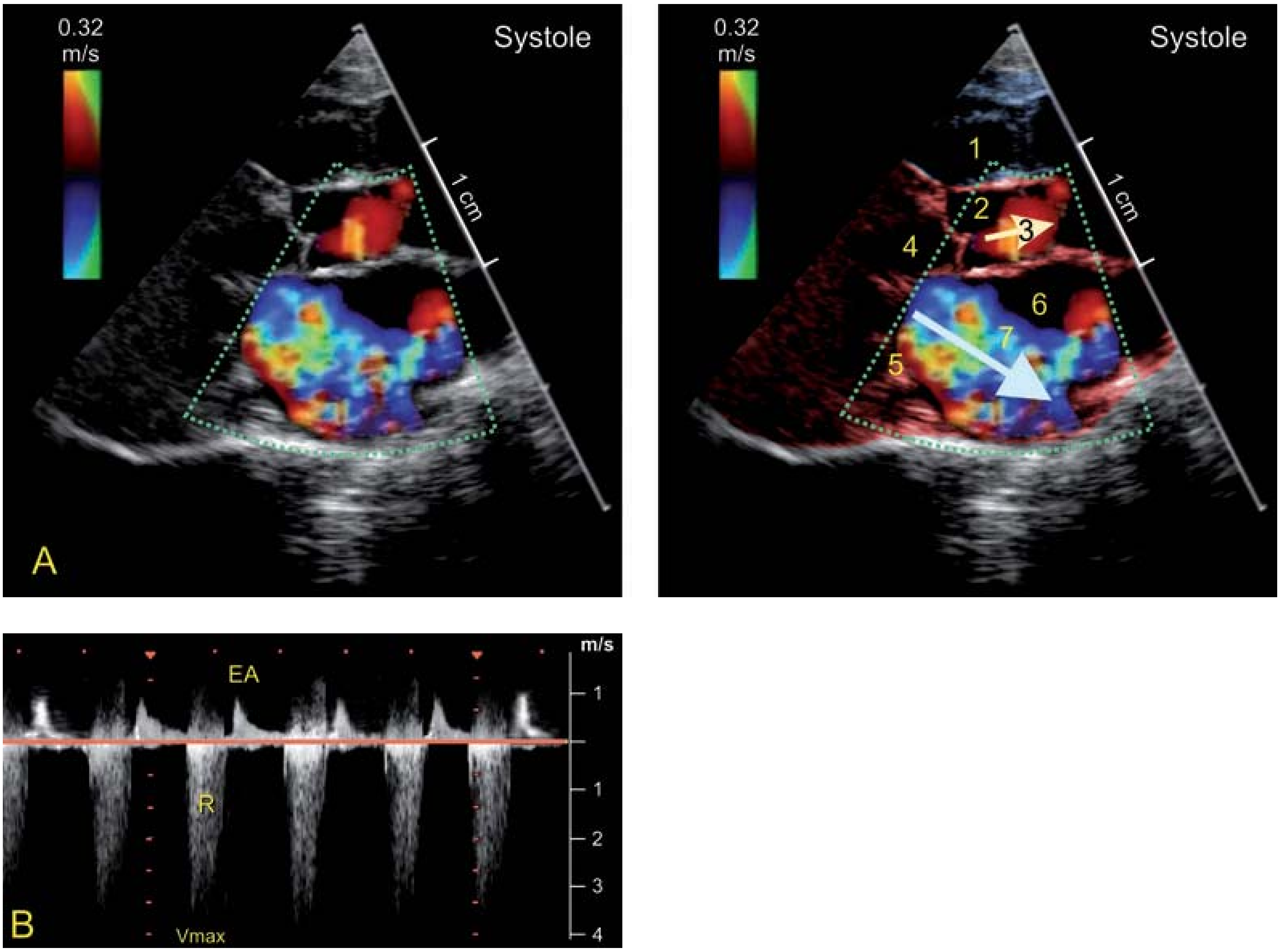

Fig. 2-140: Blood flow in mitral insufficiency of a ferret.

A: Color-coded Doppler echocardiogram of the right parasternal long-axis view: Prolonged systolic reflux in the left atrium, which includes a large part of the visible atrium.

B: CW-Doppler echocardiogram of the apical four-chamber view. Holosystolic reflux (R) with »normal« reflux velocity (V_{max}) and changed diastolic in-flow pattern (EA) due to diastolic dysfunction.

1: right ventricle
2: aortic sinus with a closed aortic valve at the end of systole
3: normal end-systolic blood flow in the aortic sinus
4: left ventricle
5: closed mitral valve
6: left atrium
7: large end-systolic reflux in the left atrium

EA: EA fusion wave, diastolic blood flow into the left ventricle
R: holosystolic regurgitation through the mitral valve
V_{max}: maximum speed of systolic regurgitation

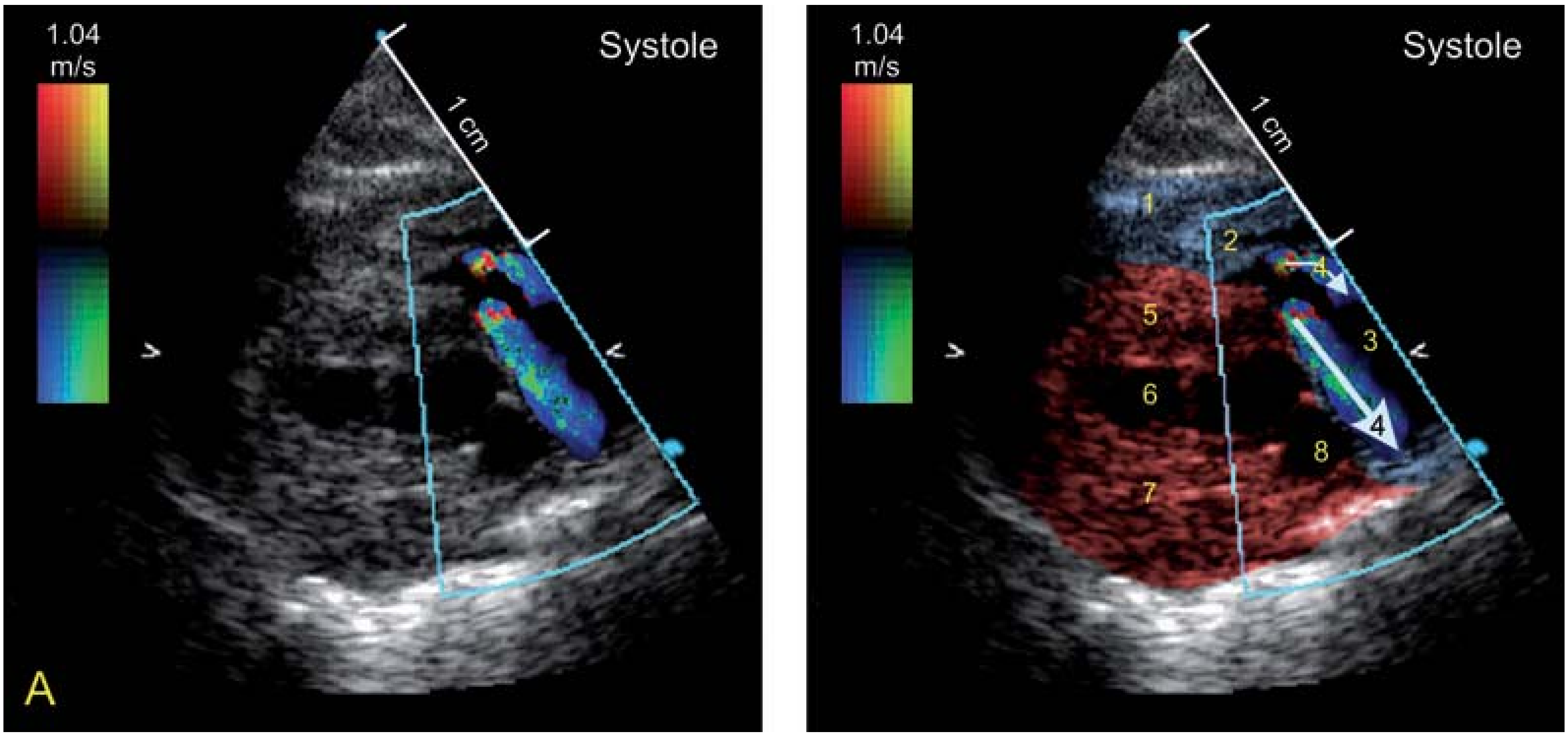

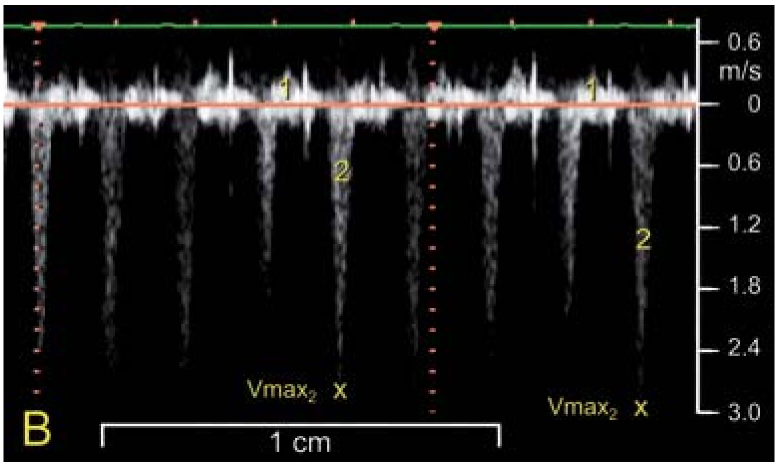

Fig. 2-141: Blood flow in tricuspid insufficiency of a guinea pig.

A: Color-coded Doppler echocardiogram of the right parasternal long-axis view. Two narrow, diverging paths of reflux are present in the right atrium.

B: CW-Doppler echocardiogram, also of the right parasternal long-axis view. There is a holosystolic, relatively rapid reflux in the right atrium. The high maximal reflux velocity (V_{max}) of ca. 3 m/s indicates the presence of increased pressure in the right ventricle, most probably due to pulmonary hypertension. This guinea pig was diagnosed with severe chronic bronchopneumonia.

1: right myocardium
2: right ventricle
3: enlarged right atrium
4: two insufficiency jets
5: interventricular septum
6: left ventricle
7: left myocardium
8: left atrium.

V_{max}: maximum speed of systolic regurgitation

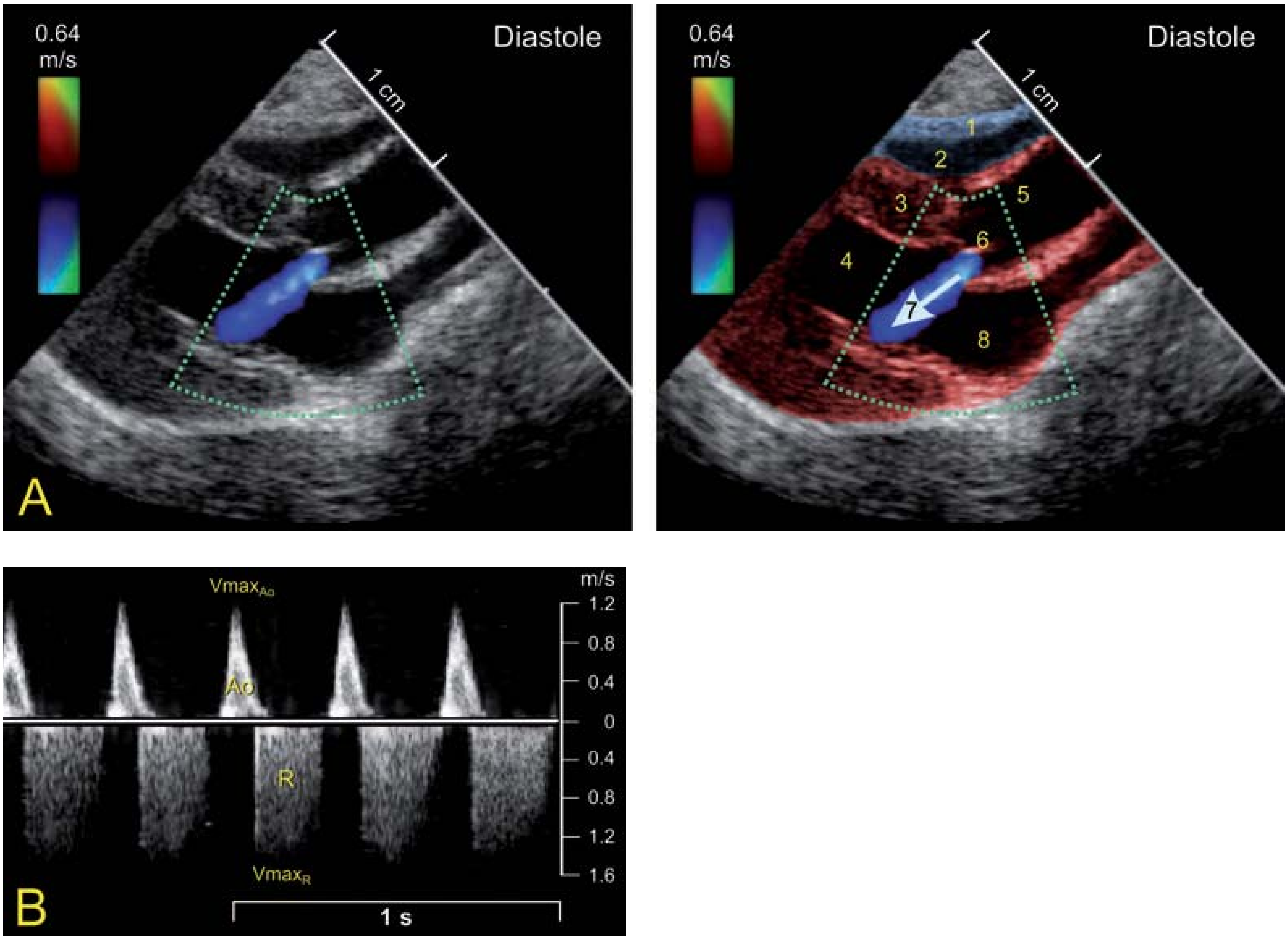

Fig. 2-142: Blood flow in aortic valve insufficiency of a ferret.

A: Color-coded Doppler echocardiogram in the right parasternal long-axis view. Long narrow reflux in the left ventricle.

B: CW-Doppler echocardiogram, also from the right parasternal long-axis view. Holodiastolic reflux (R) with an almost constant velocity (V_{maxR}), which means there is a long pressure half-life. This indicates a relatively moderate hemodynamic significance of the reflux. The systolic flow pattern (Ao) and the flow velocity (V_{maxAo}) are normal.

1: right myocardium
2: right ventricle
3: interventricular septum
4: left ventricle
5: ascending aorta
6: closed aortic valve
7: long reflux which hits the wall of the chamber
8: left atrium

Ao: blood flow in the aorta with a normal maximum flow velocity (V_{maxAo})
R: holodiastolic reflux through the aortic valve with constant flow velocity (V_{maxR}; this has almost a square-shaped flow pattern)

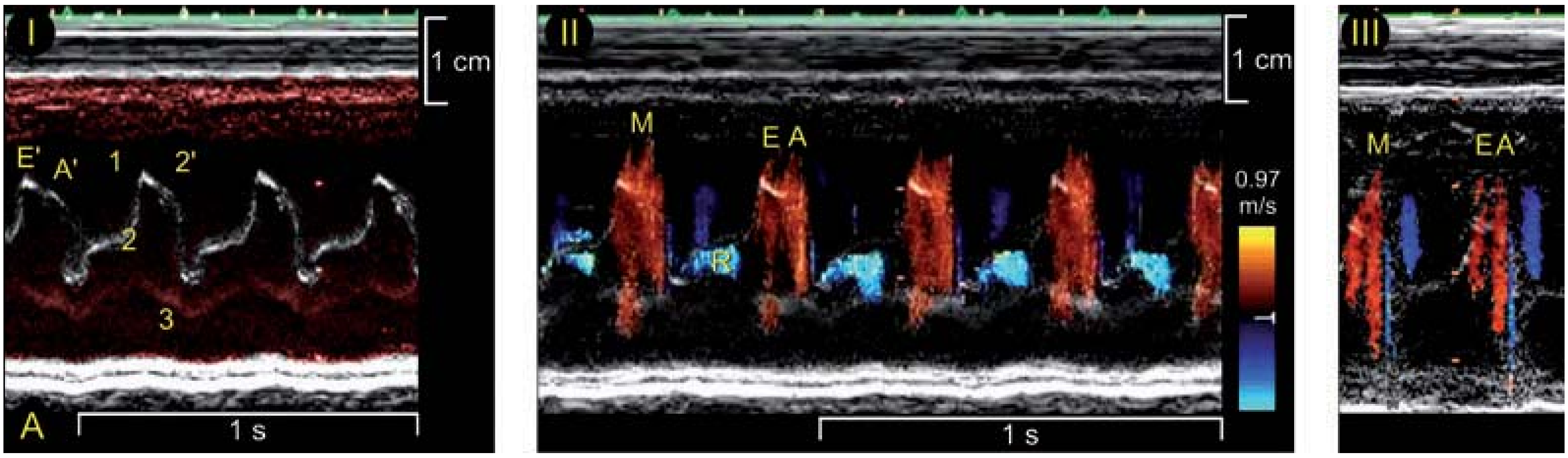

Fig. 2-143A: Blood flow in diastolic dysfunction in a rabbit due to severe dilatative cardiomyopathy with mitral insufficiency.

A: Color-coded M-mode echocardiogram from an apical four-chamber view from the left.

I: M-mode echocardiogram for orientation.
II: Color-coded M-mode echocardiogram showing impaired blood flow. The late diastolic blood flow through the mitral valve during atrial contraction is faster than the early diastolic flow, recognizable by its lighter color.
III: Color-coded M-mode echocardiogram with normal blood flow.

1: left ventricle
2: closed mitral valve
2': opened mitral valve
3: left atrium

E': early diastolic opening of the mitral valve
A': late diastolic opening of the mitral valve
M: diastolic in-flow of blood through the mitral valve
E: early diastolic in-flow
A: late diastolic in-flow
R: holosystolic reflux

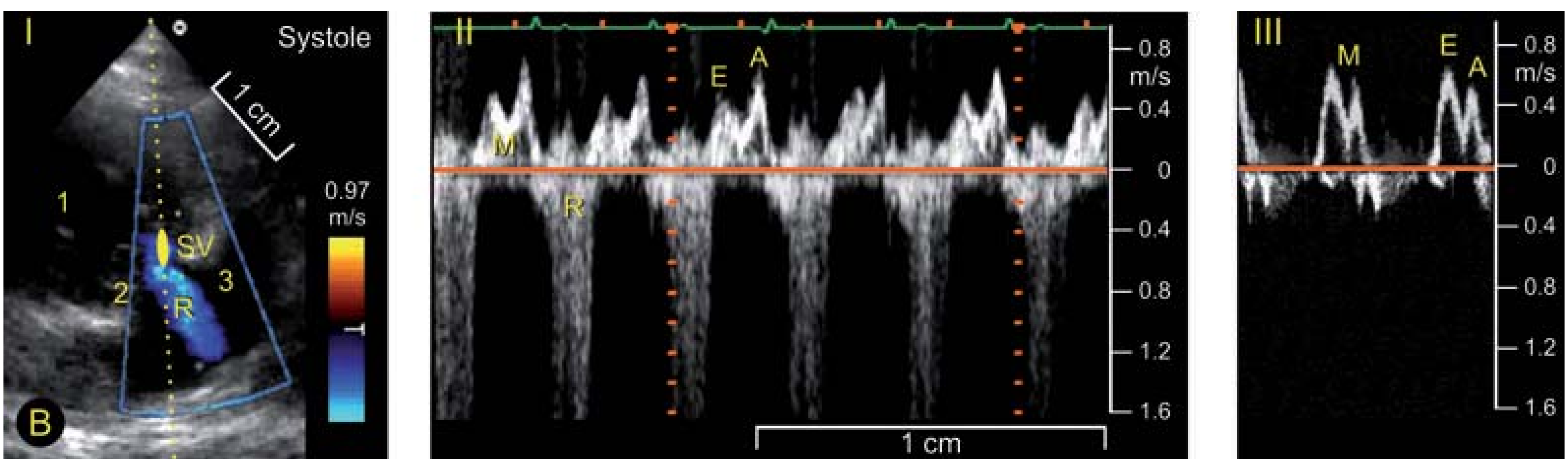

Fig. 2-143B: Blood flow in diastolic dysfunction due to a severe dilatative cardiomyopathy with mitral valve insufficiency, rabbit.

B: PW-Doppler echocardiography, also from the apical four-chamber view from the left.

I: Color-coded Doppler echocardiography for orientation.
II: PW-Doppler echocardiography with altered blood flow. The end-diastolic blood flow during atrial contraction is just as quick as or quicker than the early diastolic passive left ventricular in-flow of blood. This means that the A wave is just as high or even higher than the E wave. This phenomenon indicates the presence of an impaired diastolic in-flow of blood in the left chamber, which means that there is a diastolic dysfunction.
III: PW-Doppler echocardiography with normal blood flow.

1: left ventricle
2: closed mitral valve
3: left atrium

SV: sample volume
R: systolic reflux
M: diastolic blood flow through the mitral valve
E: early diastolic in-flow
A: late diastolic in-flow
R: systolic reflux in the left atrium

2.9 Abdomen

Sven Reese, Jutta Hein

Large volumes of fluid in the peritoneal cavity (ascites) can lead to a total loss of definition on radiographic images (**Fig. 2-144A**). When performing an ultrasonographic examination in patients with severe ascites, the organs appear to be more echogenic than normal as such fluid has a very low acoustic resistance (**Fig. 2-144B**). Small volumes of free fluid cannot be observed radiographically, although it can be distinguished using ultrasonography (**Fig. 2-144C**). Infusions are often administered subcutaneously in small exotic mammals and this fluid may collect in the subcutis of the abdominal wall (**Fig. 2-144D**) and should not be confused with ascites.

2.9.1 Stomach

Foreign bodies in the stomach (**Fig. 2-145A**) and intestines (**Fig. 2-145B**) are primarily diagnosed in ferrets, who frequently ingest such indigestible objects out of curiosity. If the foreign bodies are radiopaque, then a diagnosis is simple to determine. If the foreign bodies cannot be imaged using standard radiography, then a contrast study of the stomach should be performed (**Fig. 2-145A**) or better alternatively, a double-contrast study. Rarely can ultrasonography be used to successfully diagnose the presence of a foreign body in the stomach.

Trichobezoars and **phytobezoars** are often formed in the stomach of rabbits. The occurrence of trichobezoars and phytobezoars may be an indication of a diet that is too low in fiber, lack of water, and/or sheer boredom (e.g. fur eating, excessive licking of stall mates). Long-haired rabbit breeds tend to be more frequently affected by trichobezoars and phytobezoars than their short-haired conspecifics. Bezoars can lead to the collection of food or even a complete blockage of the stomach if they lie in front of the pylorus. In some cases, the diagnosis of a bezoar can be achieved using a standard radiographic image (**Fig. 2-146A**). If one is unable to diagnose the bezoar using standard radiographic images, then the hair mass can frequently be imaged by administering barium sulfate suspension. The contrast agent binds for a longer period of time to the bezoar than the rest of the stomach contents increasing the chances for disease diagnosis (**Fig. 2-146B**), but the quality of the image is dependent on the amount of contrast given. If too little contrast is administered, then the gastric mucosa is not adequately coated. If too much contrast agent is given, then the differentiation between the gastric wall and a bezoar is often difficult to determine. Alternatively, air can be administered via an esophageal tube into the stomach and used as a negative contrast agent (**Fig. 2-146C**). In individual cases, the diagnosis of a bezoar may require the application of a double-contrast technique (see Chap. 2.1.3.2).

With **gastric overloading**, the stomach extends widely in the ventrocaudal direction from its normal position. If the stomach is overloaded or severely tympanic (see below), it appears on lateral radiographs as a round ball and up to two-thirds of the stomach may lie outside of the thorax. The stomach may also extend to the full height of the thorax. When the stomach is overfilled, the intestines are caudally displaced. If the stomach is round and large but the intestinal tract can still be recognized behind the stomach, the degree of filling is not critical. In very obese rabbits, the gastrointestinal tract has less room in which to move when the stomach is overfilled. In such cases, it is possible that cardiovascular problems, collapse, and dyspnea may develop even when the stomach is not extremely overfilled. The stomach and intestines of guinea pigs occasionally lie next to each other reducing one's ability to delineate the boundaries of the stomach and making the degree of gastric filling hard to determine. In such cases, the use of positive contrast studies is often very helpful. In the acute stages of gastric overloading, the stomach contents will appear radiologically as a food-gas mixture (**Fig. 2-147A**). If the gastric overloading has been present for a long period of time, then its contents appear homogeneous with a soft-tissue radiodensity and in many cases, this is overlaid by a central gas bubble (»fried egg« appearance), which can be observed as a round, sharply demarcated area of somewhat lower radiodensity (**Fig. 2-147B**). Occasionally in a female guinea pig, it is difficult to determine between overloading of the stomach or a cecum with concurrent cystic ovaries on the lateral projection. A VD radiograph should ensure a reliable differentiation between these diseases. One should always confirm that there is a free passage from the stomach into the intestines by performing a contrast study by using a small amount of barium sulfate solution (**Fig. 2-147C**) before starting any therapy for gastric overloading (e.g. force feeding, administration of an oil-water solution). This is especially true if no intestines can be identified behind the stomach in the lateral projection of a rabbit patient (see Chap. 2.1.3.2)

Gastric tympany is caused mainly by abnormal digestion of food contents in the stomach. The causes of gastric tympany in the rabbit, guinea pig, chinchilla, and degu are usually related to an improper diet and nonphysiological periods of fasting. It can also result as a secondary consequence of constipation that has occurred more distal in the gastrointestinal tract. The most prominent radiographic sign of gastric tympany is the excessively dilated, rounded gas-filled stomach (**Fig. 2-147D**). In the guinea pig, occasionally the differentiation between the stomach and cecum is more difficult as these are often superimposed on each other in the lateral projection even when overfilled.

Gastric torsion is very rare in small exotic mammals, but can occur, especially in the guinea pig.

Gastritis and **ulceration** of the gastric mucosa is diagnosed quite often secondary to gastric overloading and in animals with bezoars. Diagnosis of gastritis and ulceration in rabbits and rodents cannot be achieved with absolute certainty using either radiography or ultrasonography.

2.9.2 Small intestines

Foreign bodies which have passed through the stomach may obstruct the small intestines and induce a **foreign body ileus.** This disease is diagnosed most often in ferret patients than any of the other small exotic mammals. However, obstruction of the small intestines also occurs quite often in the rabbit. In rabbits, foreign body ileus is the result of bezoars or large pieces of undigested food (e.g. pieces of carrot) passing into the intestines and causing an occlusion. Most cases of small intestinal ileus that are diagnosed in small exotic mammal medicine occur in the chinchilla. In this species, small intestinal ileus is primarily due to **invagination**, most likely a consequence of enteritis and/or hyperperistalsis. Principally, space-occupying lesions of other organs, strictures, adhesions, or tumors of the small intestines can all lead to a partial narrowing or complete occlusion of the intestines. One of the radiographic signs of an obstructive ileus is a dilatation of the intestines proximal to the ileus due to the accumulation of gas and/or fluid. A subsequent ultrasonographic examination can help determine the cause of ileus, especially in cases with invagination or tumors. The definitive diagnosis of an obstructive ileus can be achieved by performing a contrast study, which can reliably indicate the position of the intestinal blockage. Partial narrowing of the intestines can also be imaged using contrast material, although not in all cases. The prerequisite for a successful radiographic diagnosis when using a contrast study is that the amount of contrast administered is enough to completely fill the intestines.

Displacement of the small intestines is sometimes diagnosed in the rabbit and can be a sign of **volvulus**. Often there is a displacement of individual loops of small intestines over the stomach, which then dilate and can therefore be easily visualized on a radiograph. Some of these displacement conditions may spontaneously reverse themselves. Affected animals should be maintained under observation and the displacement should be surgically treated if there is no change within 24 hours.

Acute and chronic **enteritis** can occur in both the ferret and rabbit. Sonographically, some chronic enteritis cases have a diffuse hyperechoic pattern within the intestinal mucosa. Small intestinal **abscesses** occur often, particularly in the rabbit. On ultrasonography, small intestinal abscesses are observed principally as hypoechoic circular structures. Some of the intestinal abscesses may have a vague concentric echo texture (**Fig. 2-148A**), although they may also have an nonhomogeneous echogenicity (**Fig. 2-148B**).

2.9.3 Appendix and large intestines

Constipation of the appendix and large intestines in the rabbit, guinea pig, chinchilla, and degu primarily occurs due to a lack of food, a sudden change in diet, or an inadequate diet (e.g. too much energy, too little fiber in the diet, too little water). Constipation may also be associated with dental problems or lack of space in the abdomen due to large tumors (e.g. arising from the uterus) or extreme obesity. The constipated sections of the intestines which are tightly packed with relatively radiopaque food are easily visualized on radiographic images. Cranial to the area of constipation, there is a secondary development of tympany (**Fig. 2-149A**). The impacted contents of the stomach usually liquefy after about 24 hours (see Chap. 2.9.1), but with constipation the cecum becomes bloated and its contents are likely to dry out, which should be taken into consideration when determining treatment options.

Rabbits, guinea pigs, chinchillas, and degus react to a variety of diseases (e.g. dental disease, malnutrition, inappetence, gastrointestinal infections) with abnormal fermentation and **tympany** of the intestines. In addition, stress and painful conditions can induce intestinal atony, which is also associated with signs of tympany. Tympany can be severe particularly in chinchillas. In affected chinchillas, tympany can quickly develop into an acute life-threatening condition (**Figs. 2-149B, C**).

Bacterial enteritis can occur in association with a severe inflammation of the vermiform appendix, an important lymphatic defense organ in the intestinal tract of the rabbit. The normally non-imageable appendix can be observed ultrasonographically as a significantly thickened section of the intestinal tract with a conspicuously hyperechoic intestinal wall (**Figs. 2-149D, E**).

Intestinal neoplasms occur infrequently in all species of small exotic mammals. Intestinal neoplasms first become clinically evident when they interfere with intestinal function or cause ileus. The radiographic imageability of intestinal neoplasms is dependent on size, while their ultrasonographic diagnosis is only possible when the affected section of the intestine is not superimposed by other sections of the gastrointestinal tract (**Fig. 2-149F**).

2.9.4 Liver

The typical radiographic sign of **hepatomegaly** in the small exotic mammal patient is when the ventral contour of the liver extends clearly outside of the costal arch (**Fig. 2-150A**). A number of disease etiologies will result in an enlarged liver. When performing a sonogram of a patient with cardiac-related hepatomegaly, the liver veins are characteristically congested. Ascites is a common disease problem in animals diagnosed with hepatomegaly. The typical anatomical locations where a mild form of ascites can be identified are the region of the dorsal abdominal wall at the poles of the kidneys between the lobes of the liver (see **Fig. 2-144**) and craniodorsally near the apex of the urinary bladder when the patient is lying in the supine position.

Fatty liver very frequently occurs in the rabbit and guinea pig, and often results in hepatomegaly. The ultrasonographic sign of this condition is a diffuse hyperechogenicity of the liver, which even greater than that spleen (**Fig. 2-150B**). The diagnosis of hepatic lipidosis can only be confirmed with a cytological examination of a fine-needle aspirate of the liver tissue. Obtaining a definitive diagnosis of hepatic lipidosis is important since the disease condition is similar in appearance when viewing a sonogram image to the less common **steroid hepatosis** (**Fig. 2-150C**).

Bile duct coccidiosis is also a common cause of hepatomegaly in rabbits. In the healthy rabbit, widened the walls of the bile ducts are difficult to identify. In rabbit patients with bile duct coccidiosis, the walls of the bile ducts become thickened and widened and induce an alteration in the echoic texture of the liver (**Fig. 2-150D**). There may even be enlarged hepatic lymph nodes in the area of the porta hepatica associated with this disease (**Fig. 2-150E**).

In most cases, **neoplasia** of the liver does not lead to a general hepatomegaly (**Fig. 2-150F**), only to local enlargements. If the liver is enlarged, it will extend beyond the costal arch in the lateral projection and has rounded edges, which can be observed in a radiographic image of the patient. Partial enlargements are likely to be viewed in radiographic images taken of the patient in the VD or DV positions. These views are recommended to diagnose partial liver enlargements because they often induce a unilateral displacement of the stomach. Sonographically, solitary or multiple liver tumors can appear as hyperechoic, hypoechoic, or even isoechogenic enlargements (**Fig. 2-150G**). The definitive diagnosis of hepatic neoplasia can only be achieved through the use of an ultrasound-guided aspirate or biopsy of the affected area of the liver. Pseudotuberculosis should be considered a top differential diagnosis when hyperechoic round areas are identified in the liver of a rabbit. Although pseudotuberculosis is rare in pet dwarf rabbits, it is an important disease for veterinarians to be knowledgeable of because it is a zoonotic disease. A severe cystic widening of the bile ducts can, over time, occupy the whole abdomen in older hamsters and gerbils, (**Fig. 2-150H**). The cause of severe cystic widening of the bile ducts is not completely understood at this time, but is possibly a form of cholangioadenoma.

Cirrhosis of the liver as the consequence of chronic degenerative processes can lead to congestion of the hepatic portal vein (**Fig. 2-150I**). Hepatic cirrhosis is frequently associated with the formation of ascites.

2.9.5 Pancreas

Diseases of the pancreas are rarely diagnosed in small mammals. A nonspecific radiographic sign of **pancreatitis** is a diffuse area of increased radiodensity with more diffuse patterns in the right cranial abdomen. Sonographically, the pancreas is mainly hypoechoic and diffusely enlarged with acute inflammation, with the surrounding fat and mesentery being relatively hypoechoic. The ultrasonographic image also does not provide a definite diagnosis of pancreatitis in small exotic mammals. The tentative diagnosis of a **pancreatic tumor** can be achieved through a ultrasonographic examination by topographically locating the tumor. The most frequent neoplasia diagnosed in the pancreas in small exotic mammals is **insulinoma** in ferret patients (**Fig. 2-151**). Insulinomas are viewed as hypoechoic masses in the pancreatic tissue that on average, have a diameter of a few millimeters. Even when the diagnosis of an insulinoma has been confirmed by laboratory diagnostics, it is still not possible in many cases to prove their presence through a ultrasonographic examination.

2.9.6 Spleen

Splenomegaly is diagnosed primarily in ferret patients and can be definitively diagnosed using both radiographic and ultrasonographic imaging techniques (**Figs. 2-152A, B**). In the rabbit and the other small mammals, splenomegaly is not associated with any specific radiographic signs. The diagnosis of splenomegaly in these species requires an ultrasonographic examination. A significant number of ferret patients are diagnosed with splenomegaly which is not usually associated with any specific disease process; therefore, a diagnosis of splenomegaly in this species, does not have clinical relevance in most cases. The most important disease associated with splenomegaly is **lymphoma** or **lymphosarcoma**. In lymphoma or lymphosarcoma cases, splenomegaly can be associated with a change in the echoic texture of the spleen. The characteristic ultrasonographic image of lymphoma is a moth-eaten look of the spleen due to the presence of hypoechoic areas within the organ's parenchyma (**Fig. 2-152C**). In patients diagnosed with lymphoma, in addition to splenomegaly, there are many enlarged lymph nodes which when imaged during a ultrasonographic examination are surrounded by a hyperechoic area (**Fig. 2-152D**). This hyperechoic area is a typical characteristic of the mesenteric reaction which can occur as a consequence of inflammatory and neoplastic processes within the peritoneal cavity (**Fig. 2-152E**). Enlarged lymph nodes can be found with lymphoma in other species, too (**Fig. 2-152D**).

2.9.7 Urinary tract

2.9.7.1 Kidneys

Changes in the size of small exotic mammal kidneys is often poorly recognized radiographically, in contrast to deformations. Ultrasonographic examinations are clearly the recommended imaging modality for small exotic mammal kidneys. In the majority of cases, enlargement of the kidneys is due to **neoplasia** (**Fig. 2-153A**) or, in ferrets, large **cysts** (**Fig. 2-153B**). Reduction in kidney size is usually the result of **chronic interstitial nephritis**. Sonographically, renal tissue affected by chronic interstitial nephritis can be recognized by the indentation of their surface contours (**Fig. 2-153C**), a narrowing of the renal cortex (**Fig. 2-153D**), or a lost of the boundary between the cortex and medulla (**Fig. 2-153E**). A typical cause of chronic interstitial nephritis in the rabbit is an infection with *Encephalitozoon cuniculi*. **Pyelonephritis** is frequently a consequence of calculi (**nephrolithiasis; Figs. 2-153F, G**) in the renal pelvis of rabbits, guinea pigs, and chinchillas or it can be due to hydronephrosis, again caused by calculi. In severe cases, a progressive purulent-necrotic pyelonephritis can occur (**Fig. 2-153H**). Pyelonephritis may develop as a primary disease (**Fig. 2-153I**) or secondary as a reaction to hydronephrosis (**Fig. 2-153K**). Sonographically in pyelonephritis patients, there is principally a diffuse nonhomogeneous increase in hyperechoic tissue response in the renal medulla and in advanced cases, there is a reduction in the size of the renal papilla.

Small **renal cysts** occur sporadically in every species of small exotic mammals, but such renal cysts have little clinical significance. Ferret patients have a special consideration as renal cysts can be found in 50% of animals treated at veterinary hospitals. These cysts commonly lie on the corticomedullary boundary and each kidney may have up to a maximum of three cysts (**Fig. 2-153L**). **Polycystic kidneys**, in comparison, are rarely diagnosed in ferrets.

2.9.7.2 Ureter

If calculi are flushed out of the renal pelvis into the ureter and occlude this structure (preferentially just before it opens in the urinary bladder) (**Fig. 2-154A**), then there will be a back flow of urine which will then develop into a **hydroureter** and **hydronephrosis** (see **Fig. 2-153H**). Hydroureter and hydronephrosis is often diagnosed in the rabbit, guinea pig, and chinchilla. Ureter stones can be imaged using both ultrasonographic and radiographic imaging modalities (**Fig. 2-154A to C**) . It is important to always use the VD projection for the radiographic examination to ensure there is no confusion with bladder stones. It should be noted that in male animals, calculi seen radiographically as lying lateral to the urinary bladder may also be lodged in the seminal vesicle. Hydroureter of another, as yet unknown, etiology can be found as a coincidental finding time and again in the ferret. In affected animals, the ureter may be unilaterally dilated without any cause for the constriction being diagnosed during an ultrasonographic examination. What are conspicuous in these cases are the strong peristaltic waves of normal ureter function (**Fig. 2-154D**). Primarily, there is also an average degree of hydronephrosis which will develop parallel to the ureteral changes in these animals. In the five cases which have been diagnosed and treated by the authors, there were no clinical indications of renal insufficiency (neither clinically nor according to laboratory diagnostics).

2.9.7.3 Urinary bladder

Diseases of the urinary bladder occur quite rarely in ferrets and small exotic rodent patients. In comparison, bladder changes can be diagnosed quite frequently in the rabbit, guinea pig, and chinchilla. Bladder changes are correlated to the particular metabolism of the latter three species, in which the total calcium uptake from the diet is absorbed and the excess mineral has to be excreted via the kidneys. If there is an excessive amount of calcium in the food, the high concentrations of calcium carbonate in the urine crystallizes out and forms the so-called **sludge** (**Figs. 2-155A, B**). The sludge may stick together to form firm calculi that can lie in the renal pelvis, ureters, urinary bladder, or urethra as a bigger or smaller sized **urolith** (**Figs. 2-155C, D**). On a ultrasonographic examination, such uroliths have an acoustic shadow, in contrast to sludge. In many cases, chronic irritation of the bladder mucosa caused by calculi can lead to a severe **cystitis**, which is associated with polyuria and polydipsia and sometimes hematuria. In addition to a thickening of the bladder wall which can only be diagnosed in the filled bladder, the typical ultrasonographic sign of cystitis is hypervascularization of the bladder wall which can be clearly observed using Doppler (**Figs. 2-155E, F**). After successful treatment of the cystitis, this hypervascularization will no longer be evident. In severe (chronic) cases, a purulent necrotizing cystitis may develop which can result in peritonitis. The areas around the bladder then become increasingly hyperechoic (**Fig. 2-155G**) in cases of purulent necrotizing cystitis. The differentiation of this from a well-vascularized neoplasm of the bladder wall (**Fig. 2-155H**) (regularly diagnosed in the guinea pig) is not possible in every case. If a neoplastic process extends to where the ureters insert into the bladder, there may be blockage of the urine with the subsequent development of a hydroureter and hydronephrosis (see Chap. 2.9.7.2).

If a bladder stone moves into the urethra, it frequently occludes this structure just proximal to where the urethra enters into the vulva or penis. This condition can then lead to a partial or even complete displacement of the urinary tract. Animals affected by an occluded urethra usually suffer extreme pain, which in turn leads to hypomotility, intestinal dysbiosis, and tympany of the gastrointestinal tract. Intestinal dysbiosis and tympany of the gastrointestinal tract are the main reasons why an animal is presented to a veterinary hospital when suffering from cystic calculi. The diagnosis of urethral stones can only be achieved using standard radiographic imaging techniques (**Fig. 2-155I**). Every radiograph of the abdomen should include the entire pelvis with the perineum, otherwise there is the danger that a **urethral stone** (e.g., as primary cause of tympany) may be missed. If calculi are observed on a radiographic image and are located in the tip of the penis, one should determine if there is really a stone in the urethra or if there is just radiopaque dirt in the preputial sack. Collections of hardened smegma can be found in the preputial sack of male guinea pigs. The hardened smegma can cause a ring-like compression of the penis that in turn potentiates the collection of crystals in the urethra and ultimately displacement of this structure.

2.9.8 Female genital tract

With exception of the female ferret, which almost always have their ovaries and reproductive tract removed when kept as a pet, pathological changes in the female genital tract occur relatively frequently in all small mammalian species. The incidence of pathological changes in the male genitalia is much lower.

2.9.8.1 Vagina

Pathological changes in the vagina cannot be diagnosed in small exotic mammals using standard radiographic imaging. Varying quantities of pathological fluids are regularly identified in the vagina (**hydrovagina**) of female rabbits. Vaginal fluid accumulation can be imaged exceptionally well using ultrasonography (**Fig. 2-156**). One primary cause of vaginal fluid accumulation can be **incontinence** due to chronic cystitis that causes urine to remain within the vagina. However, in the majority of cases, hydrovagina is usually associated with pathological changes to uterine tissue.

2.9.8.2 Cervix

Sonographically, the cervix is easily imaged lying between the rectum and urinary bladder in almost every small exotic mammal female patient. The cervix can be observed in the transverse plane through the urinary bladder (see Chap. 2.4.3.6). In the guinea pig, the cervix is hypoechoic and oval (in cross section) with a mean width of 6.1 mm (5.2–6.8 mm) and a height of 4.6 mm (3.7–5.9 mm). Under the regular influence of estrodiol from hormonally active ovarian cysts, the diameter of the cervix increases visibly (> 8 mm diameter) (**Fig. 2-157**), therefore cervix size is a relatively good indicator in guinea pigs of whether or not ovarian cysts are producing hormones (see Chap. 2.9.8.4), even before other clinical signs of hyperestrogenism occur (e.g. bilateral symmetrical alopecia, anemia). At this point for disease confirmation, the uterus should be investigated for signs of endometrial hyperplasia.

2.9.8.3 Uterus

Pathological changes in the uterus can be found in virtually all uncastrated pet rabbits due to their reproductive cycle. Ovulation in the rabbit is induced by a tactile stimulus to the back. What is special in this species is that the rabbit almost always has follicles on their ovaries that are ready to ovulate. Roughly every two weeks, follicle atrophy occurs when there has not been an ovulation. Within the next 2–4 days, folliculogenesis reoccurs with the new follicles waiting for the next 14 days for a suitable stimulus to ovulate (induced ovulation). Ovulation in pet rabbits is induced by stroking the back which leads to the induction of a false pregnancy. The false pregnancy ceases after approximately 17 days, at which time the cycle begins again. As a consequence of this cycle, uncastrated pet female rabbits are almost always in a state of false pregnancy. The associated chronic stimulation of the endometrium and the uterine glands leads to the development of **cystic endometrial hyperplasia** (**Figs. 2-159A, B**). The hyperplastic changes of the uterine endometrium can lead to a blockage of the uterine lumen, whereby a **hydrometra** may develop proximal to the blockage (**Fig. 2-159C**). Hemorrhaging from the abnormal mucosa can result in the formation of **hemometra** (**Fig. 2-159D**). Secondary bacterial infection of the significantly altered endometrial lining of the uterus leads to the development of a **pyometra**; however, this is more commonly diagnosed in other species of small exotic mammals (e.g. golden hamster) (**Fig. 2-159E**) rather than the rabbit. Endometrial hyperplasia rarely occurs in the other species of small exotic mammals other than rabbits. The ultrasonographic proof of this condition in guinea pig patients is the presence of cystic ovaries, which overproduce hormones. An increase in the thickness of the uterine horns can also be an indication of an **endometritis** (**Fig. 2-159F**), which will need to be clarified with further gynecological examinations. Uterine hyperplasia can be visualized on radiographic images especially in obese rabbits (see **Figs. 2-154B** and **2-155A**). Occasionally calcium may become deposited in the hyperplastic uterine tissues, which are observed as radiopaque patchy areas.

In older rabbits, the incidence of endometrial neoplasia is also highly correlated to the increased incidence of hyperplastic changes. Uterine neoplasms are usually **adenocarcinomas** (**Fig. 2-159G**) that have a high rate of lung metastasis. In rare instances, uterine neoplasms have been diagnosed as **leiomyomas** or **fibrosarcomas** (**Fig. 2-159H**). The neoplastic changes cannot be reliably differentiated either with ultrasonography or radiography from endometrial hyperplasia. Generally, the neoplasms are rounder, larger, and more solid than hyperplasia. It has not been determined at this time as to whether rabbit uterine adenocarcinomas develop from endometrial hyperplasia, are caused by chronic hormonal stimulation, or whether this type of cancer is a completely independent disease process.

2.9.8.4 Ovaries

The pathological changes affecting the ovaries are predominantly **ovarian cysts; ovarian neoplasms** are much rarer. Ovarian cysts in small exotic mammals primarily occur as a geriatric disease (**Fig. 2-158A**). Ovarian cysts are especially common in the guinea pig as in this species 70–80% of all adult females develop ovarian cysts, independent of whether they have been used for breeding or not. The cysts usually occur bilaterally, have multiple chambers, and can reach considerable sizes of up to 10 cm (**Fig. 2-158B**). Although large cysts can be imaged radiographically (their presence is made more conspicuous by the displacement of the other abdominal organs), small cysts can only be diagnosed using ultrasonography (**Fig. 2-158C**). There are three different histological types of cyst:

- ☐ development from the rete ovarii (most frequent form)
- ☐ development from preovulatory follicles (10–20%)
- ☐ development from the epoophoron (rare)

It is not possible to differentiate these three forms of ovarian cysts using the currently avalible imaging modalities. The only ovarian cysts that have a clinical significance are those which have developed from preovulatory follicles and can produce steroid hormones. In approximately 5% of guinea pigs, the cystic ovaries are hormonally active and consequently cause the typical signs of hyperestrogenism (e.g. endometrial hyperplasia, infrequent bilateral symmetrical alopecia, anemia). Experience has shown that these cases almost always have ovaries with relatively small cysts.

In the uncastrated female ferret, ovarian cysts (**Fig. 2-158D**) occur when the female does not have contact with a male ferret during heat and therefore ovulation does not occur. The cystic ovaries begin autonomously to produce hormones shortly after the development of the cysts. Clinically, the affected animal shows **permanent estrous** and the long-term clinical signs of a severe **hyperestrogenism** are often associated with a lethal nonregenerative anemia.

2.9.9 Male genital tract

2.9.9.1 Testicles

There are principally three types of pathological changes which affect the testicle: 1. **testicular neoplasms**, which can be imaged using ultrasonography; 2. **orchitis**; and 3. **testicular torsion**, in which the reduced perfusion and venous congestion can be depicted using Doppler ultrasonography. Standard radiographic imaging techniques do not work well in diagnosing testicular disease.

2.9.9.2 Accessory sex glands

Pathological changes of the accessory sex glands are relatively rare in small exotic mammals. In castrated male ferrets, **prostatic hyperplasia** can develop as a consequence of hyperadrenocorticism due to an adrenal adenoma. **Prostatic cysts** have also been reported in male ferrets, which may, in individual cases, reach an excessive size (**Fig. 2-160**).

If an animal is suffering from urolithiasis, calculi move into the seminal vesicle, especially in male guinea pigs. Such calculi can induce the same clinical signs as those observed in patients diagnosed with cystitis. The presence of such calculi is identified more easily using ultrasonography than with standard radiography. Occasionally, radiographically evident calcification can be found in the accessory sex glands of the chinchilla without the presence of urolithiasis.

2.9.10 Adrenal glands

In the ultrasonographic investigation of the adrenal glands, the primary aim is to depict any changes to the size of these organs. Atrophy of the adrenal glands is very rare in small exotic mammals and is primarily observed in association with prolonged corticosteroid medication (e.g., during chemotherapy in cancer patients) (**Fig. 2-161A**).

Enlargement of the adrenal glands is differentiated into **adrenal hyperplasia**, **adrenal adenoma**, and **adrenal carcinoma**. Undoubtably, ferrets are the species affected most often by adrenal hyperplasia (**Fig. 2-161B**), adenoma (**Figs. 2-161C, D**), and carcinomas, which are rarely diagnosed (**Fig. 2-161E**). The cause of ferret adrenal disease is thought to be associated with a negative feedback from the lack of sex hormones after castration so that GnRH is continually released, leading to the production of LH and FSH. Most likely, sex-hormone-producing cells which are formed embryonically in the adrenal tissue react in the ferret to this hormonal stimulation with hyperplasia and partial differentiation to adenomas. Histologically, this nodular hyperplasia of the adrenal cortex has been found in almost all castrated male and female ferrets. Hyperplasia is very difficult to differentiate from normal adrenal tissue using ultrasonography. The adenomas begin, in contrast to cortisone-producing tumors in the dog (Cushing syndrome), to produce differing levels of sex hormones (e.g. androstenedione, oestrodiol, 17-hydroxyprogesterone, dehydroepiandrosterone sulfate). The hormones' release leads to the typical clinical signs associated with hyperadrenocorticism in the ferret patient: alopecia, swelling of the vulva, prostatic hyperplasia, and cystic endometrial hyperplasia (even of the uterine stump in hysterectomized females). If excessive amounts of estrogen are produced, then a life-threatening anemia can develop.

In all other small exotic mammalian species, neoplasia of the adrenal glands is much less common, although in rare individual cases they can also induce hyperadrenocorticism.

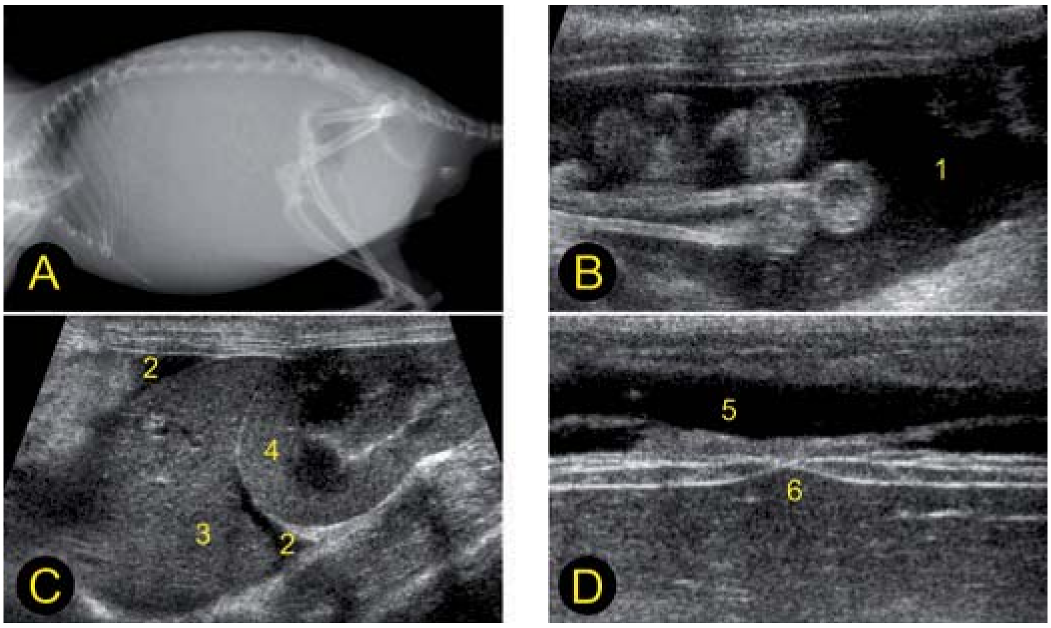

1: ascites
2: renal impression
3: liver
4: right kidney
5: subcutaneous fluid
6: linea alba

Fig. 2-144:

A: Radiographic image of a gerbil's abdomen diagnosed with severe ascites, lateral projection. (radiograph courtesy of the Veterinary Clinic Oberhaching, Munich, Germany).

B: Ultrasonographic image of a rabbit's abdomen, sagittal plane. 12 MHz, PD 3 cm. Loops of intestine are floating in severe ascites (1).

C: Ultrasonographic image of a rabbit's right liver lobe, sagittal plane, 12 MHz, PD 4 cm. Collection of fluid in the renal impression (2).

D: Ultrasonographic image of a rabbit's stomach wall, transverse section, 12 MHz, PD 1.5 cm. Subcutaneous collection of fluid.

Fig. 2-145: Radiographic images of foreign bodies in a ferret's abdomen, ventrodorsal projection.

A: 30 minutes after the administration of a contrast agent. A foreign body (long bezoar) surrounded by contrast can be seen in the stomach.

B: Multiple radiodense foreign bodies (e.g. gravel stones) are lying distally in the small intestines, colon, and rectum.

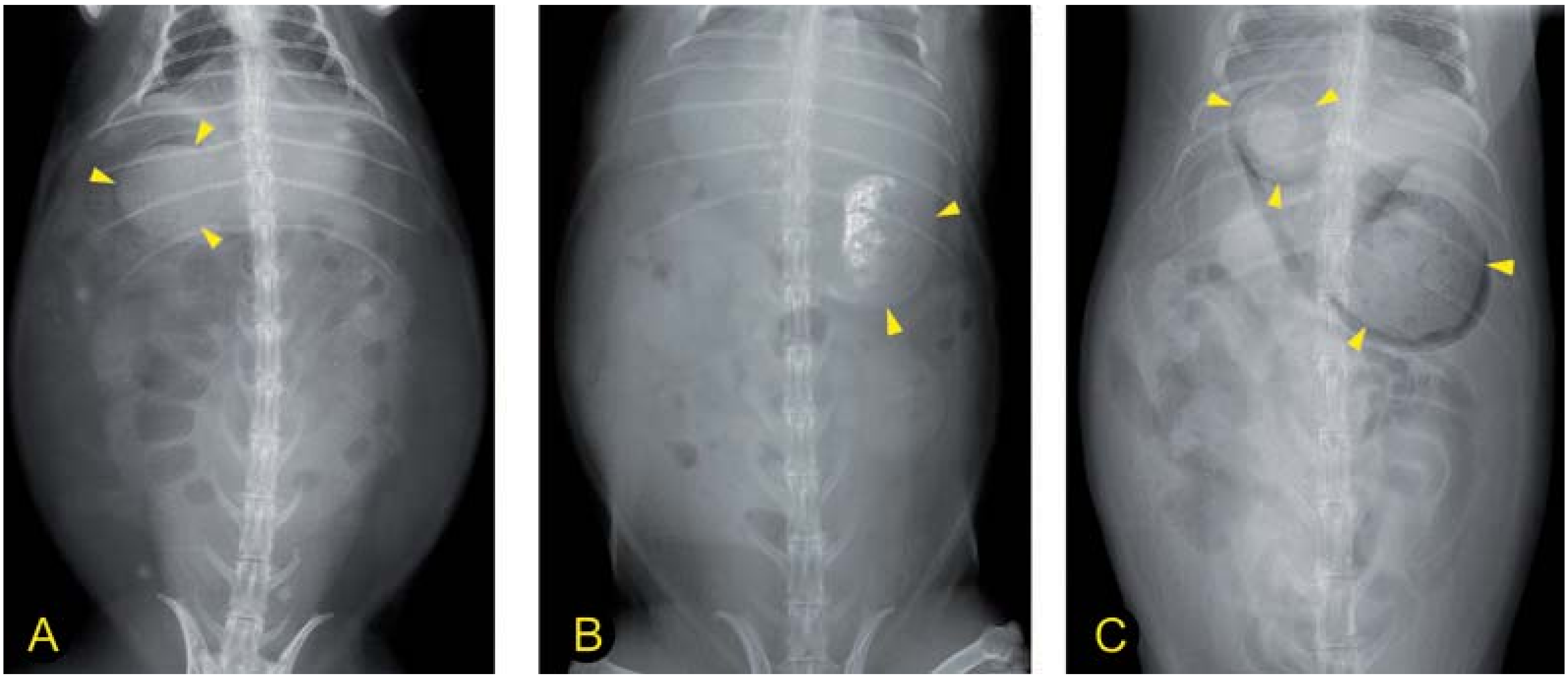

Fig. 2-146: Radiographic image of a rabbit's abdomen diagnosed with a bezoar, ventrodorsal projection.

A: Plain radiograph of a bezoar (arrowheads) lying in front of the pylorus.

B: Characterization of a bezoar (arrowheads) through contact of a positive contrast agent to its surface (barium sulfate).

C: Image of two bezoars (arrowheads) after the administration of a negative contrast agent (air).

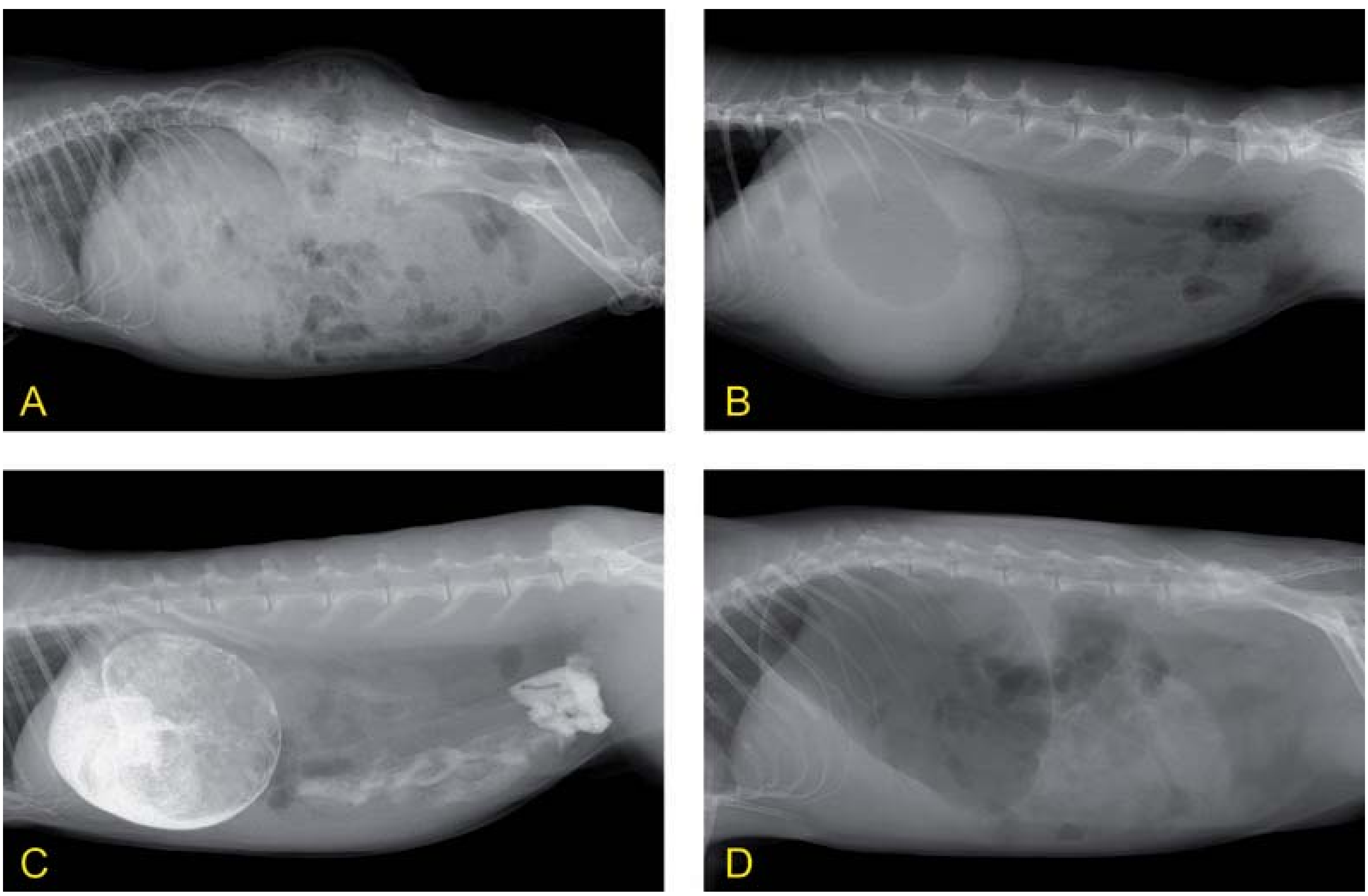

Fig. 2-147: Abdominal radiographic images, lateral projection.

A: Guinea pig with acute overfilling of the stomach.

B: Rabbit with chronic overfilling of the stomach. The stomach contents are liquefied and superimposed by a central gas bubble.

C: Rabbit after the administration of a small amount of barium sulfate to ensure that despite the overfilling of the stomach there is not an intestinal occlusion.

D: Guinea pig with gastric tympany and hepatomegaly.

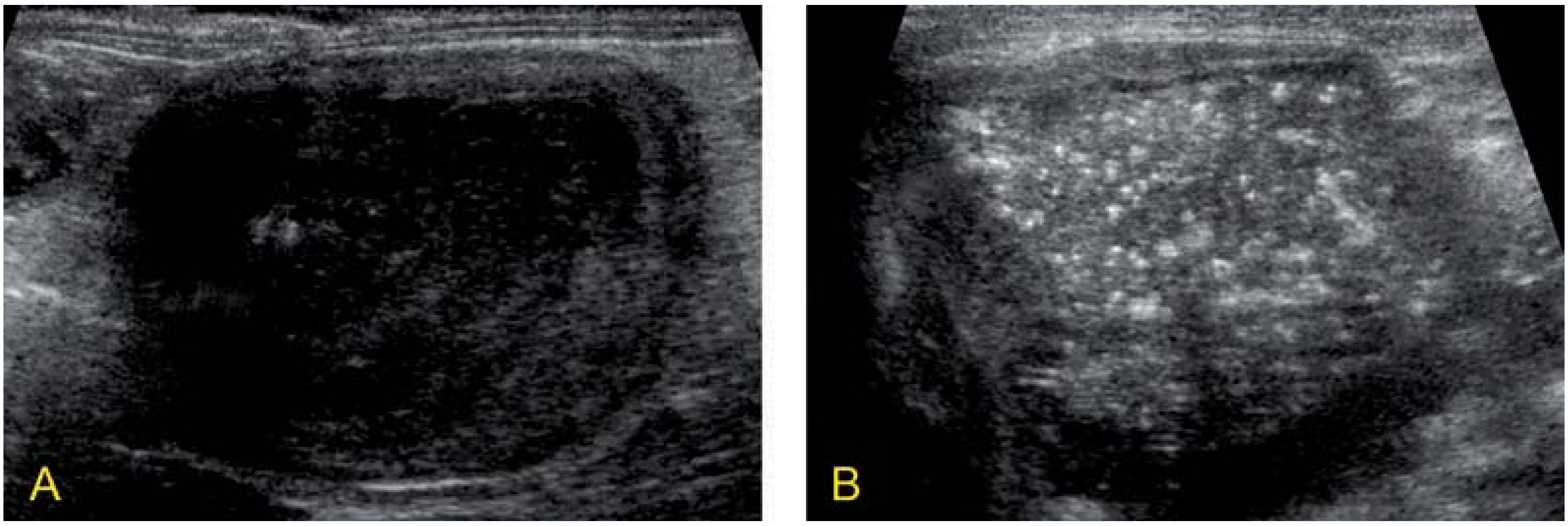

Fig. 2-148: Ultrasonographic images of a rabbit, right ventrolateral stomach wall window, 12 MHz, PD 3 cm. Two examples of intra-abdominal abscesses. Intra-abdominal abscesses are an important differential diagnosis for any increase in a rabbit patient's abdominal volume.

A: Concentric echotexture

B: Inhomogeneous echotexture

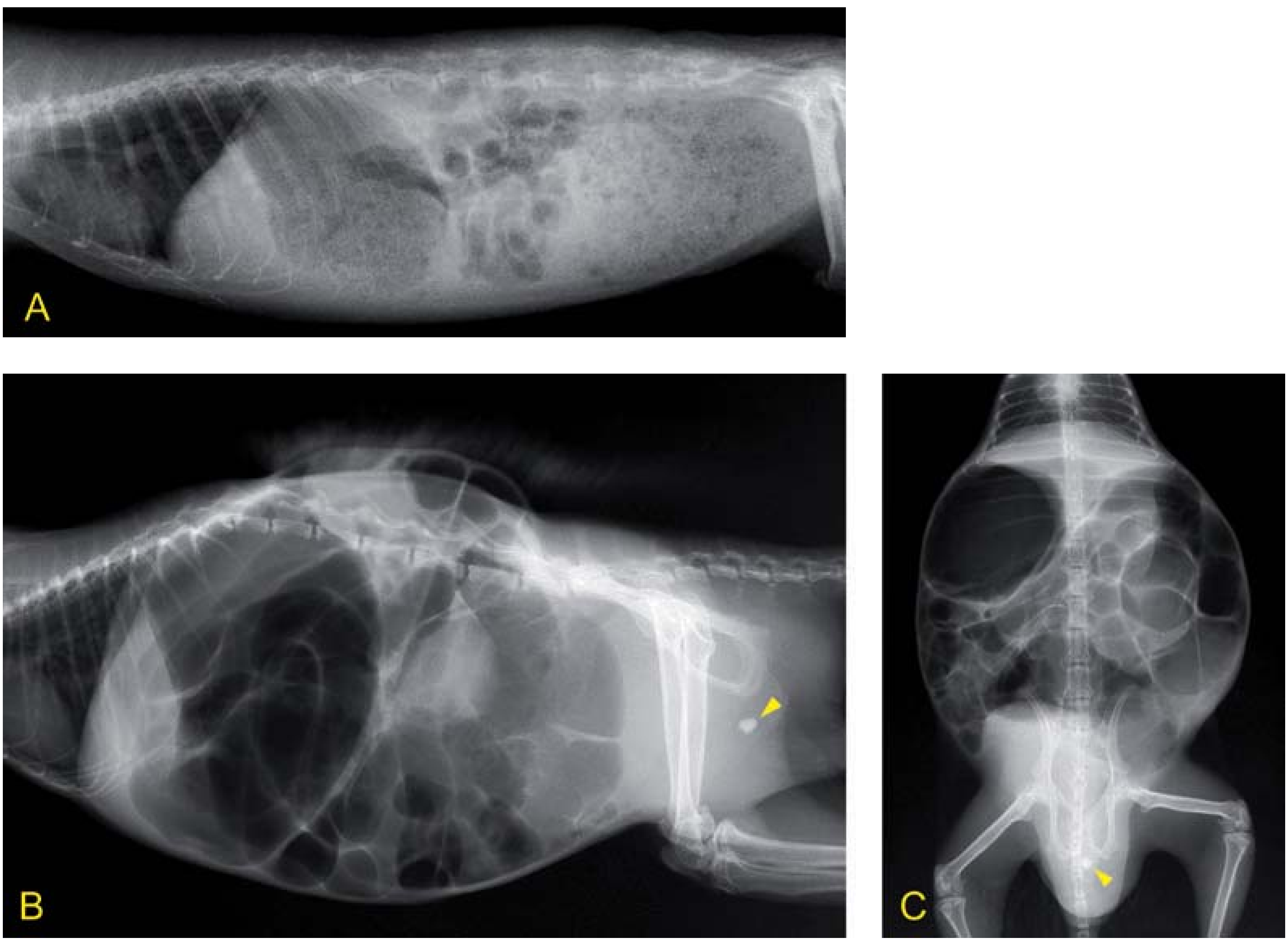

Fig. 2-149A–C:

A: Radiographic image of a guinea pig's abdomen, lateral projection. Cecal impaction with secondary tympany in the stomach and intestinal tract.

B, C: Radiographic images of a chinchilla's abdomen, (B) lateral and (C) ventrodorsal projections. Severe tympany caused by pain due to a urethral stone (arrowhead).

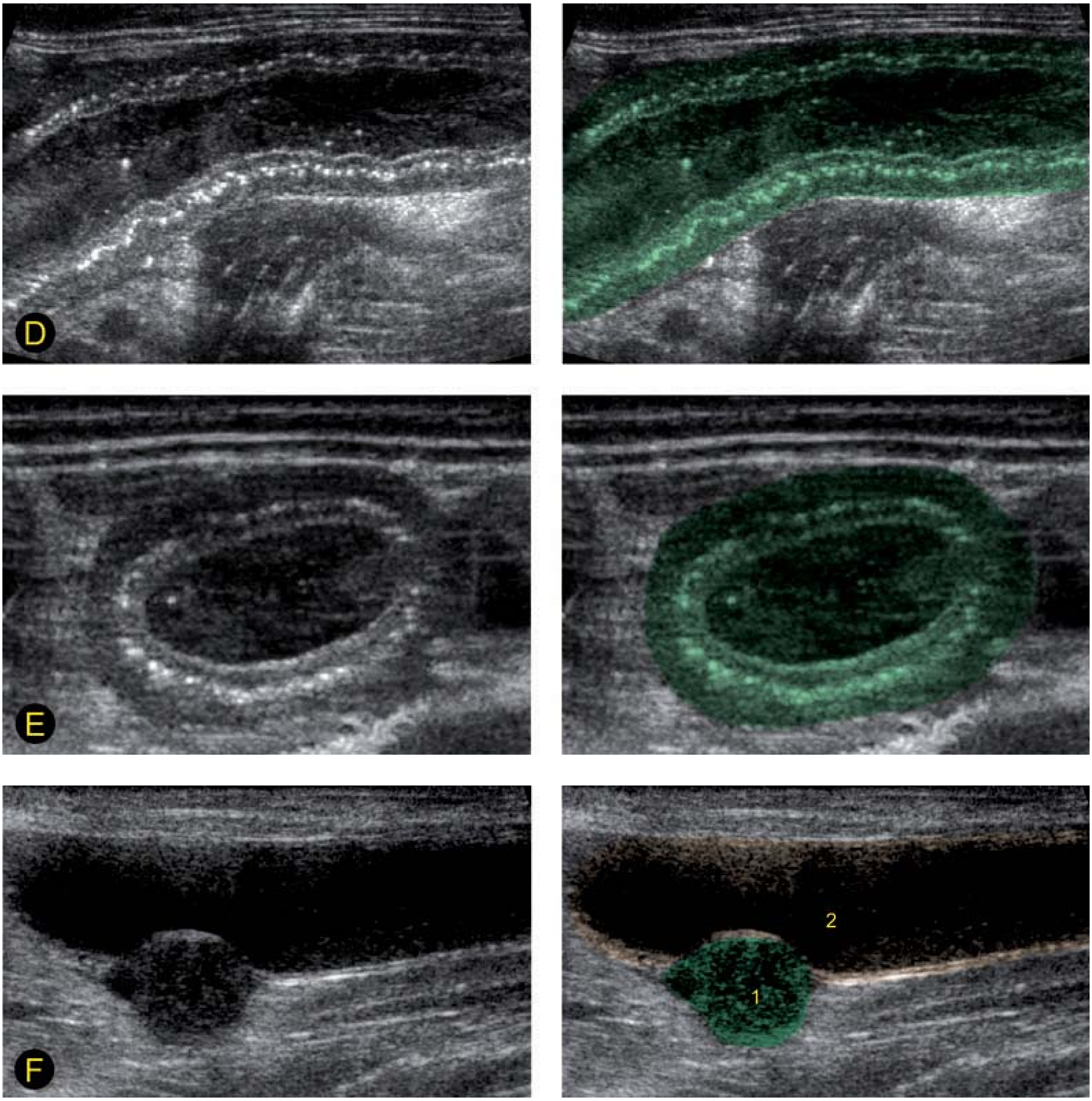

Fig. 2-149D–F:

D, E: Ultrasonographic images of a rabbit's ventral abdominal wall coupling site, 12 MHz, PD 2.5 cm. Severe appendicitis in longitudinal (D) and transverse (E) planes.

F: Ultrasonographic images of a rabbit's caudal abdomen, sagittal plane, 12 MHz, PD 2.5 cm. Tumor (1) associated with the rectum, lying dorsal to the urinary bladder (2).

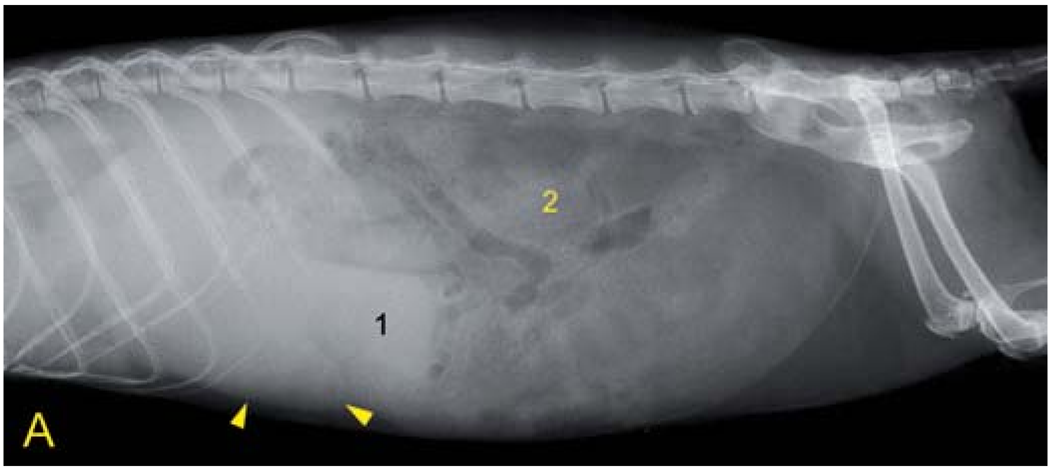

1: spleen
2: kidney

Fig. 2-150A: Radiographic image of a ferret's abdomen diagnosed with hepatomegaly, lateral projection. The liver clearly extends beyond the costal arch (arrowheads).

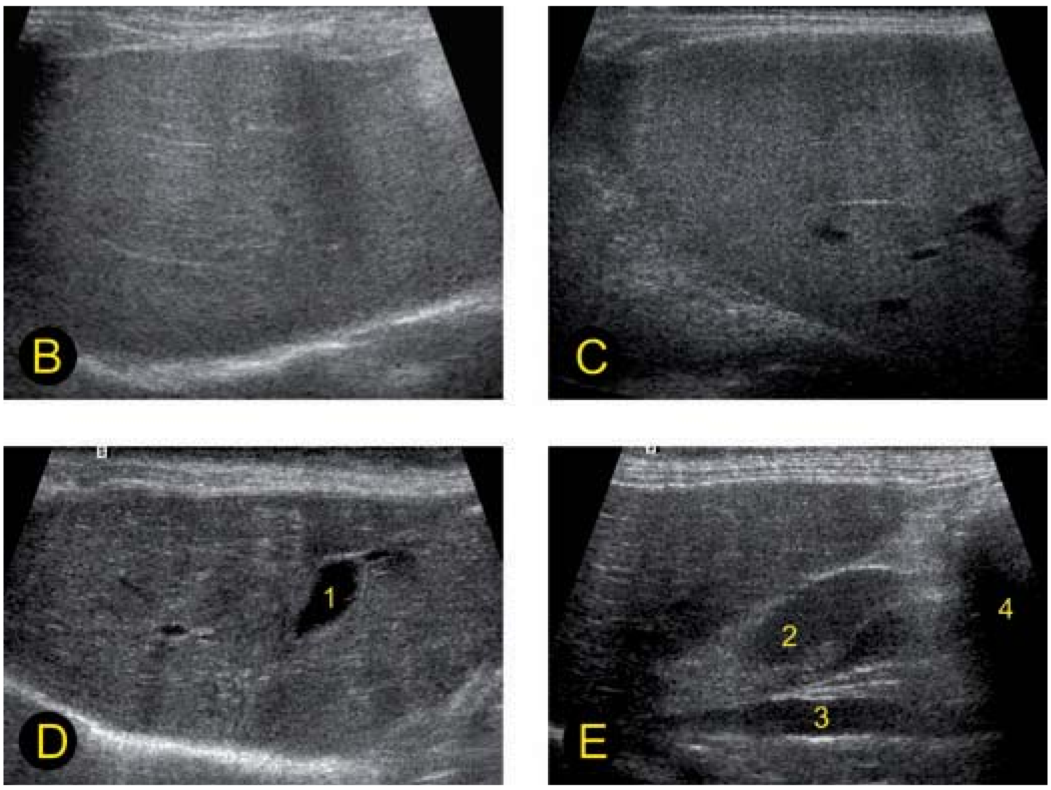

1: gallbladder
2: hepatic lymph nodes
3: hepatic portal vein
4: stomach

Fig. 2-150B–E: Ultrasonographic images of rabbits' livers, 12 MHz, PD 4 cm.

B: Severe fatty liver.

C: Steroid hepatosis as the result of a local treatment with corticosteroids.

D: Bile duct coccidiosis.

E: Enlargement of the hepatic lymph nodes (2) in a case of bile duct coccidiosis.

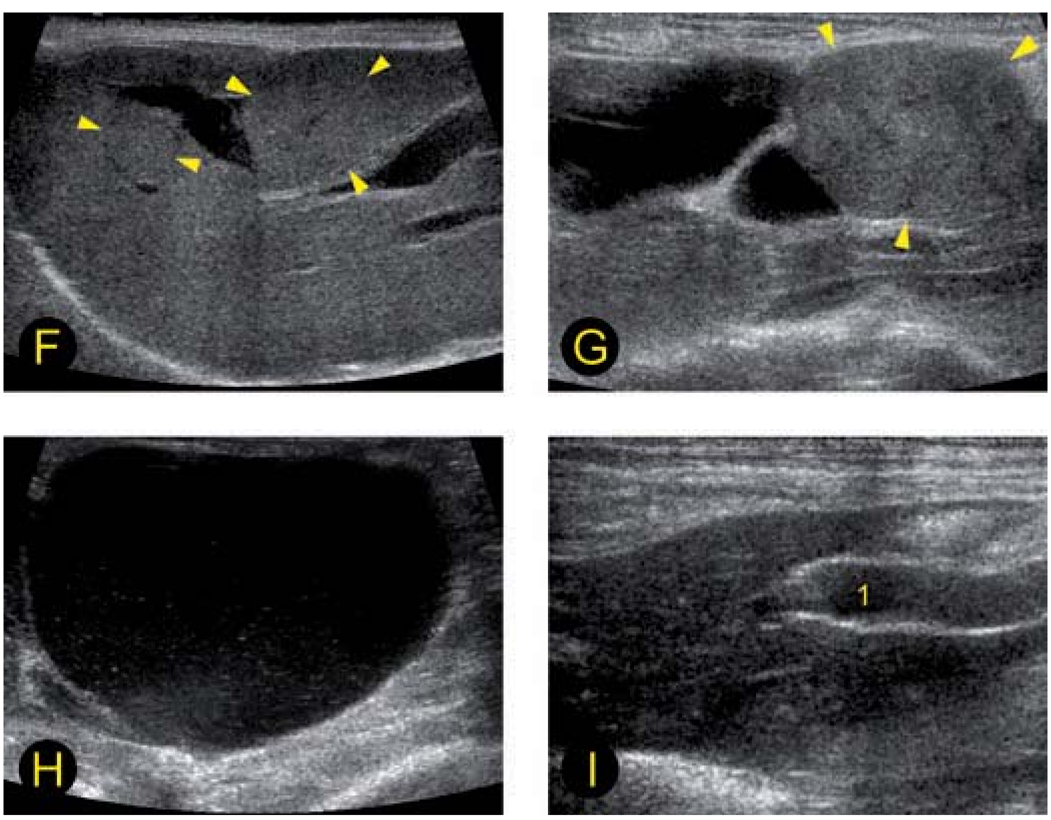

1: V. portae hepatis

Fig. 2-150F–I: Ultrasonographic liver images, 12 MHz, PD 3 cm.

F: Ferret with multicentric lymphoma and numerous isoechogenic nodes (arrowheads) in the liver.

G: Guinea pig with a single liver tumor (arrowheads).

H: Golden hamster with a highly cystic bile duct adenoma.

I: Guinea pig with liver cirrhosis and congestion of the blood in the hepatic portal vein (1).

Sonogram F reproduced with kind permission from Reese, S., Frings, B. (2004): Die abdominale Ultraschalluntersuchung beim Frettchen. Tierärztl Prax **32(K)**: 182–189.

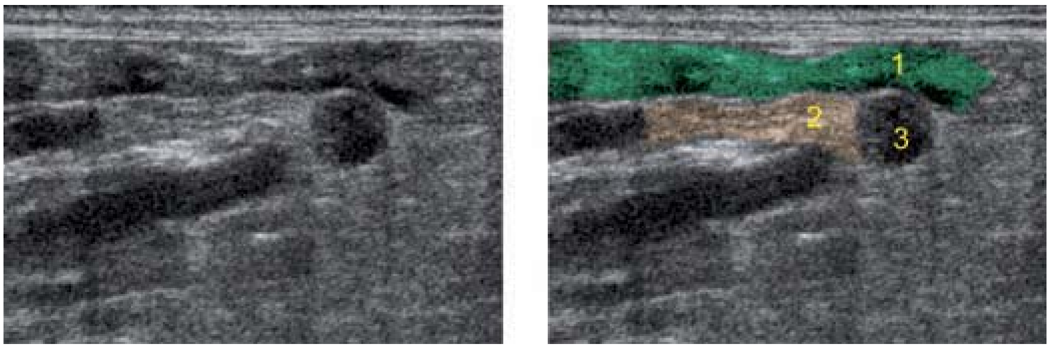

1: descending duodenum
2: pancreas
3: hypoechogenic insulinoma

Fig. 2-151: Ultrasonographic images of a ferret's pancreas diagnosed with isulinoma, 12 MHz, PD 1.5 cm. The ferret was presented in a hypoglycemic condition.

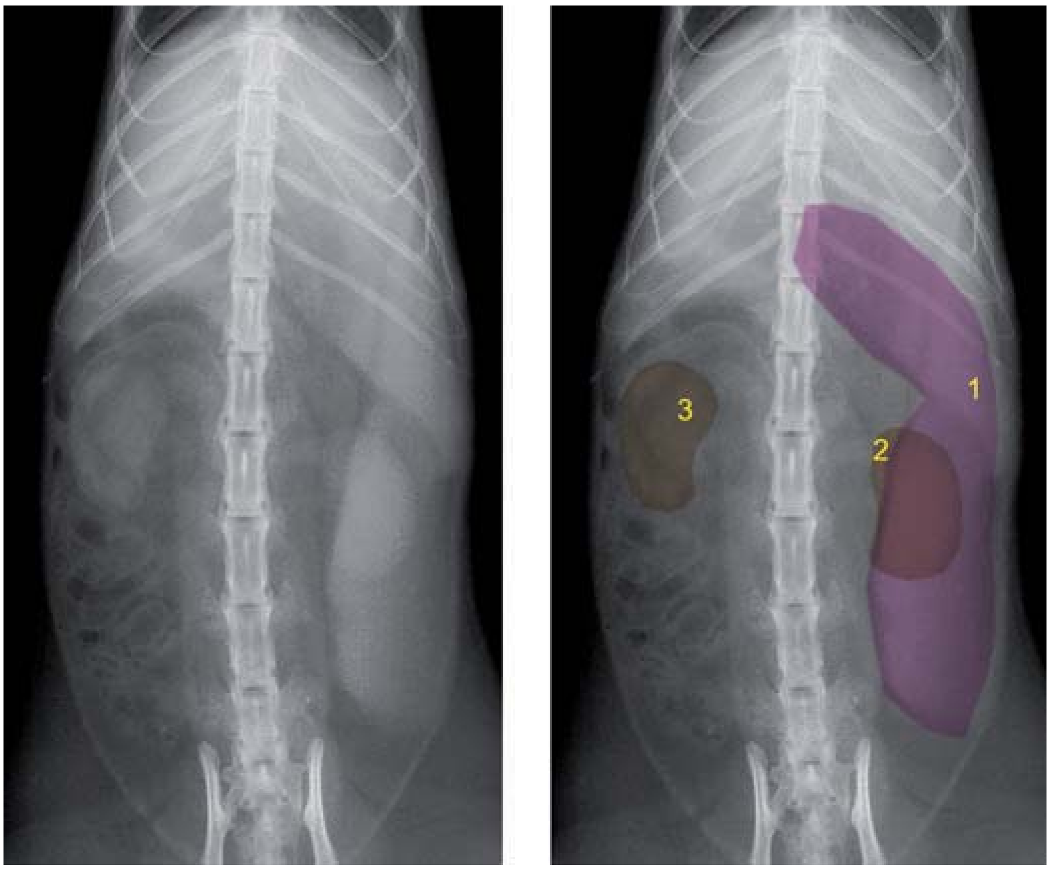

1: spleen
2: left kidney
3: right kidney

Fig. 2-152A: Radiographic images of a ferret's abdomen diagnosed with severe splenomegly (1), ventrodorsal projection.

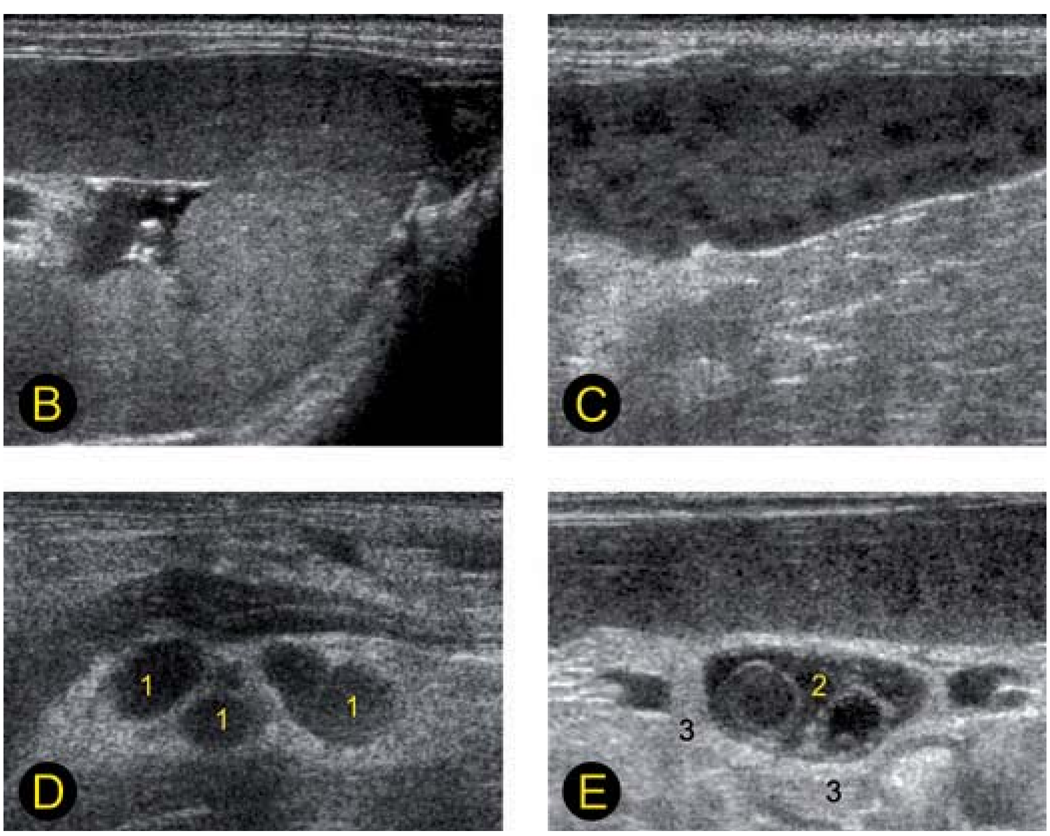

1: iliaci lymph nodes
2: lymph nodes
3: hypoechogenic (»reactive«) mesentery

Fig. 2-152B–E: Ultrasonographic images of spleens and abdominal lymph nodes, 12 MHz, PD 2.5–3 cm.

B: Ferret: Severely enlarged spleen, transverse section.

C: Ferret: Multiple hypoechogenic patches can be observed in this spleen (lymphosarcoma).

D: Guinea pig: Enlarged iliac lymph nodes (1), transverse section. Lymphoma.

E: Ferret: Hypoechogenic (»reactive«) mesentery (3) around neoplastic lymph nodes (2).

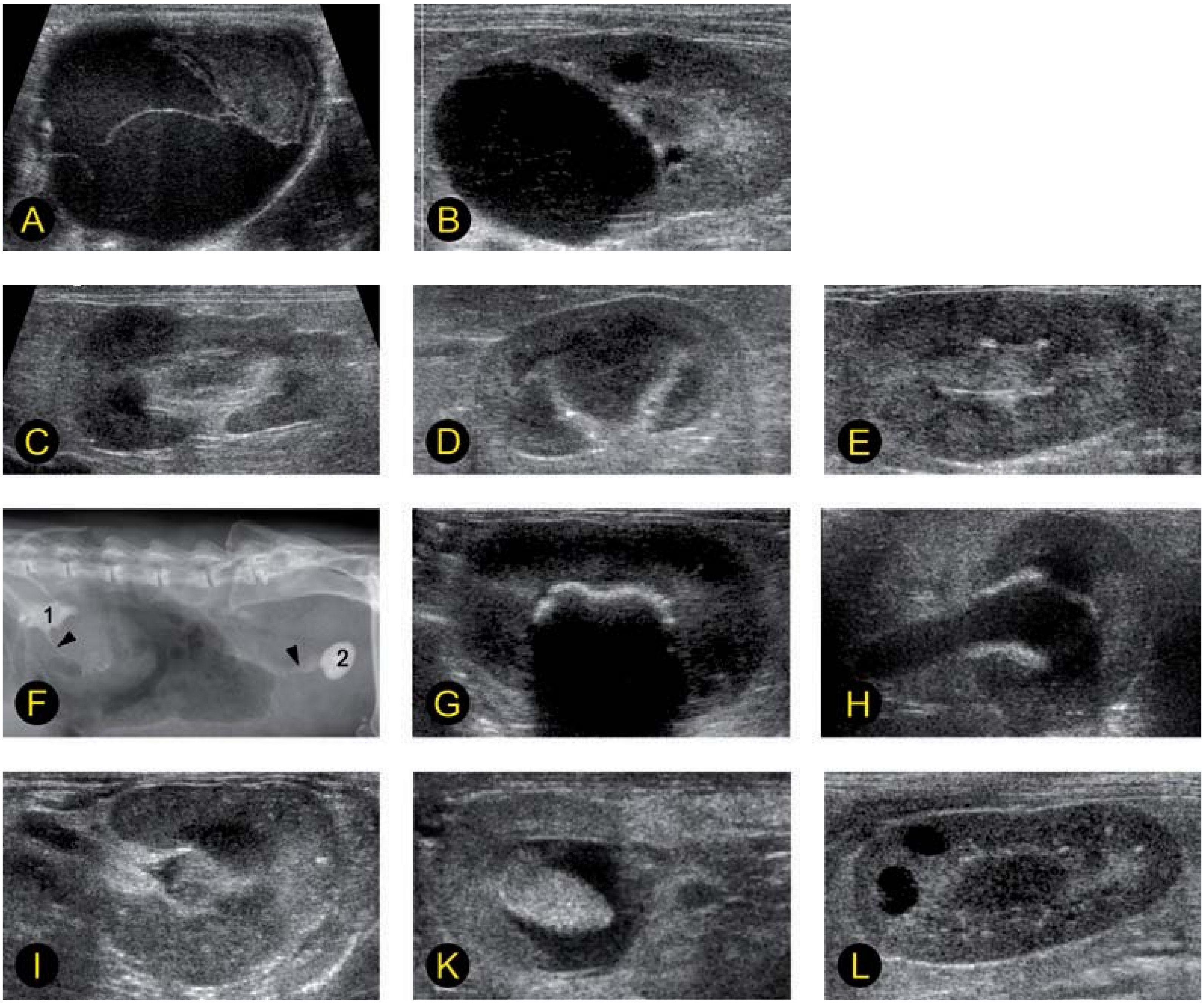

Fig. 2-153:

A: Ultrasonographic image of a rat’s kidney, 12 MHz, PD 4 cm. Hemangiosarcoma of the left kidney.

B: Ultrasonographic image of a ferret’s kidney, 12 MHz, PD 2.5 cm. An extensive renal cyst in a ferret with renal insufficiency.

C, D, E: Ultrasonographic images of a rabbit’s abdomen, 12 MHz, PD 2.5 cm. Interstitial nephritis with scarified depressions (C), degeneration of the renal cortex (D), and loss of the boundary between the medulla and cortex (E).

F: Radiographic images of a guinea pig’s abdomen, lateral projection. Severe urolithiasis with a calculus (1) of the renal pelvis (nephrolithiasis) and urinary sludge 2) as well as calculi in the ureter (arrowheads).

G: Ultrasonographic image of a guinea pig’s kidney, 12 MHz, PD 2.5 cm. The renal pelvis is filled with a kidney stone.

H: Ultrasonographic image of a guinea pig’s kidney, 12 MHz, PD 3 cm. Pyelonephritis due to the formation of calculi with hydronephrosis and necrosis of the renal papilla.

I, K: Ultrasonographic image of a rabbit’s (I) and rat’s (K) kidney, 12 MHz, PD 2 cm. Pyelonephritis with an increase in echogenicity of the renal papilla and mild (I) to severe (K) hydronephrosis.

L: Ultrasonographic image of a ferret’s kidney, 12 MHz, PD 2.5 cm. Cystic kidney.

Radiograph F courtesy of the Veterinary Clinic Oberhaching, Munich, Germany.

Sonograms B and L reproduced with kind permission from Reese, S., Frings, B. (2004): Die abdominale Ultraschalluntersuchung beim Frettchen. Tierärztl Prax **32(K)**: 182–189.

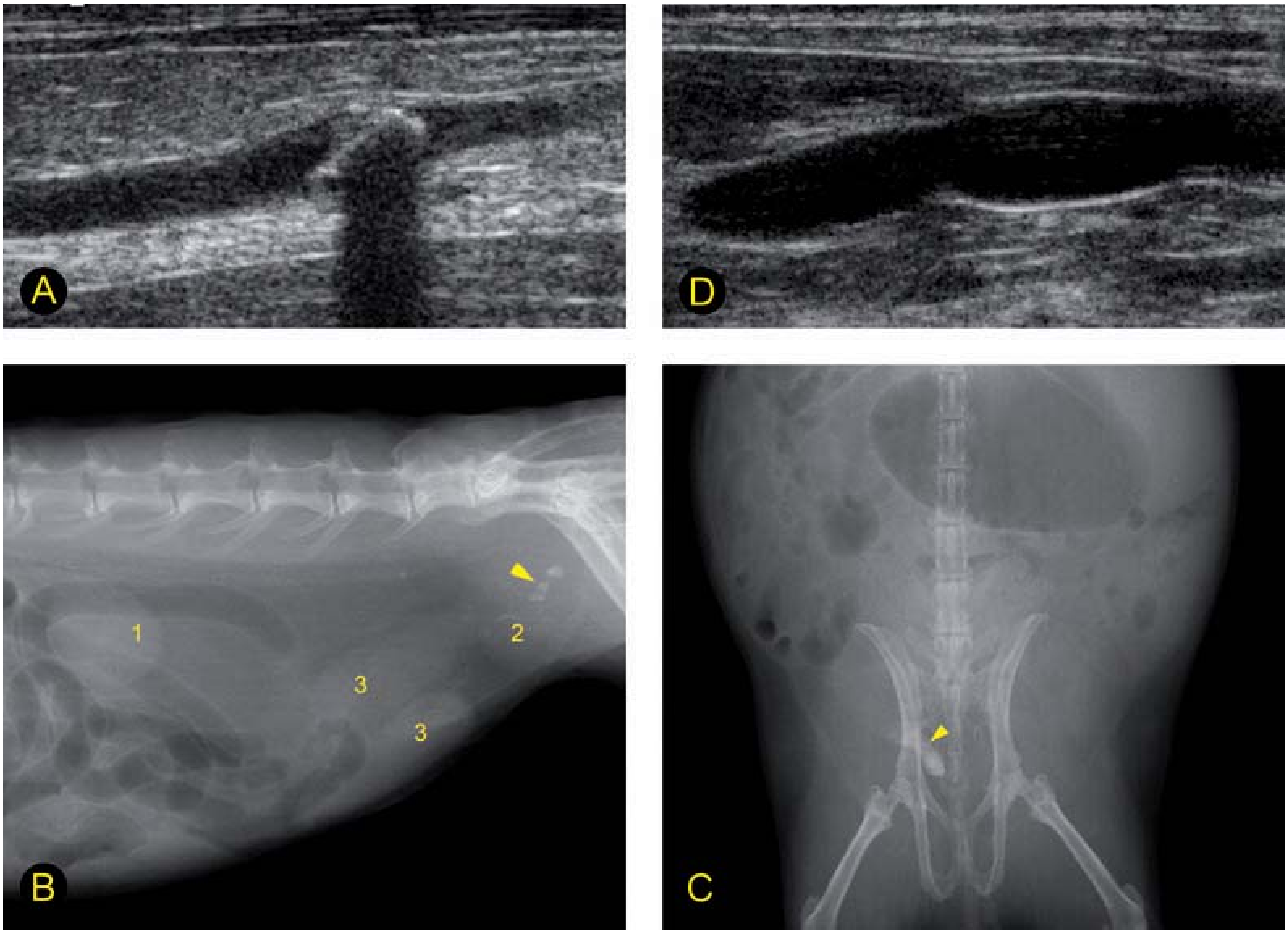

Fig. 2-154: (A and D) Ultrasonographic and (B and C) radiographic images of the ureter.

A: 12 MHz, PD 1.5 cm. Rabbit: Urethral stone.

B: Lateral projection. Rabbit: Calculi in the right ureter (arrowhead) with congestion of blood in the kidney (1), which is enlarged and rounded.

C: Ventral projection. Guinea pig: Calculi in the right ureter (arrowhead).

D: 12 MHz, PD 2 cm. Ferret: Idiopathic hydroureter showing waves of contraction.

1: kidney
2: urinary bladder
3: hyperplastic uterus

arrowheads: ureter with calculi

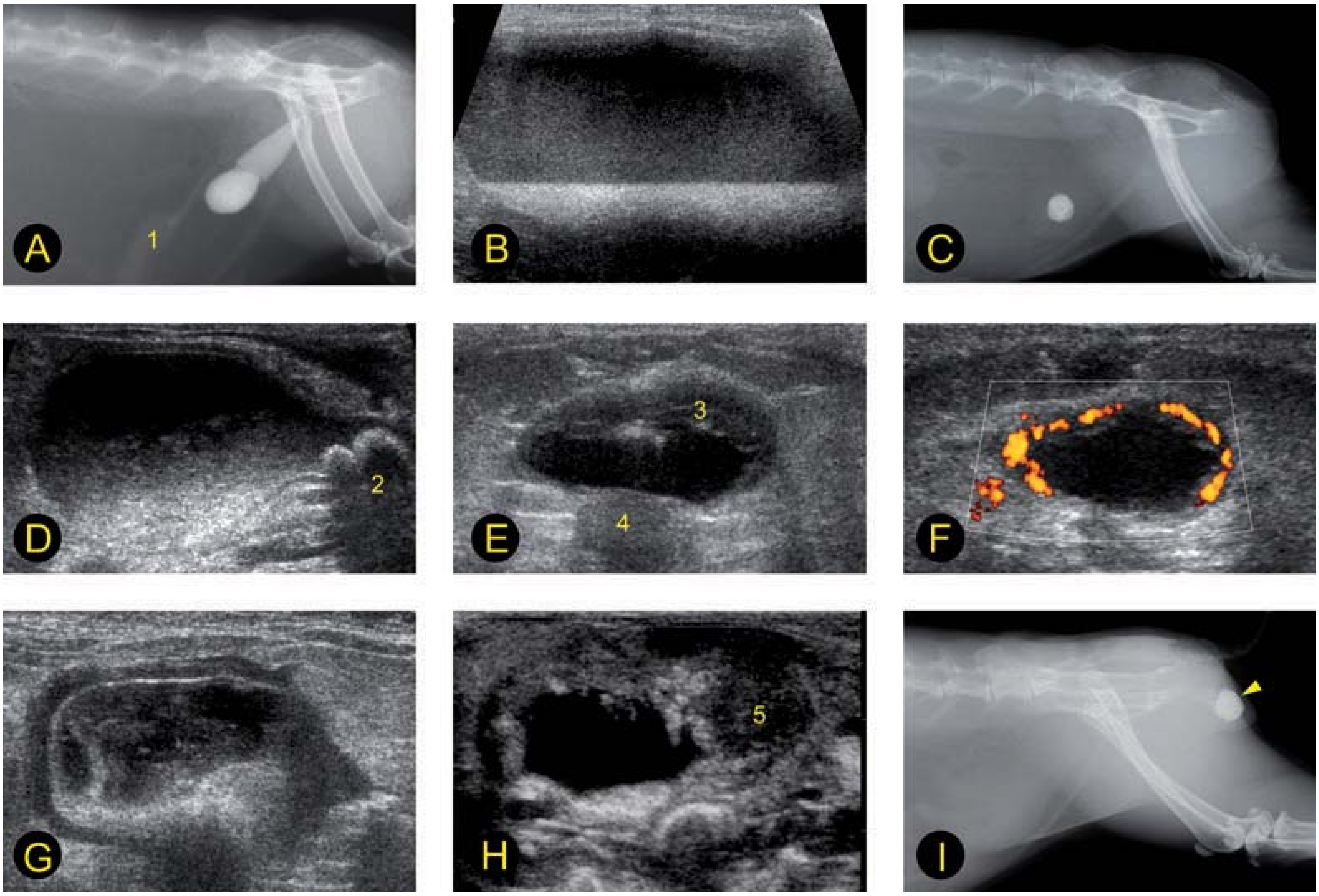

Fig. 2-155: (A, C, I) Radiographic and (B, D, E, F, G, H) ultrasonographic images of the urinary bladder.

A: Lateral projection. Rabbit: Combination of urinary sludge and stones. The hyperplastic uterus can be easily seen.

B: Transverse section, 12 MHz, PD 4 cm. Rabbit: Urinary sludge.

C: Lateral projection. Rabbit: Solitary urinary stone.

D: Sagittal section, 12 MHz, PD 3 cm. Guinea pig: Urinary stones (2) just before they pass into the urethra.

E, F: Transverse section, 12 MHz, PD 2.5 cm. Guinea pig: Severe cystitis. The ventral bladder wall is thickened (3) and hypervascular (F: diagnosis is confirmed with power Doppler).

G: Sagittal section, 12 MHz, PD 3 cm. Rabbit: Purulent necrotic cystitis with peritonitis.

H: Transverse section, 12 MHz, PD 2.5 cm. Guinea pig: Tumor of the bladder wall (5).

I: Lateral projection. Rabbit: Excessively dilated urinary bladder due to the presence of an urethral stone (arrowhead).

1: uterus
2: bladder stone
3: bladder wall
4: cervix
5: tumor of the bladder wall

arrowhead: urethral stone

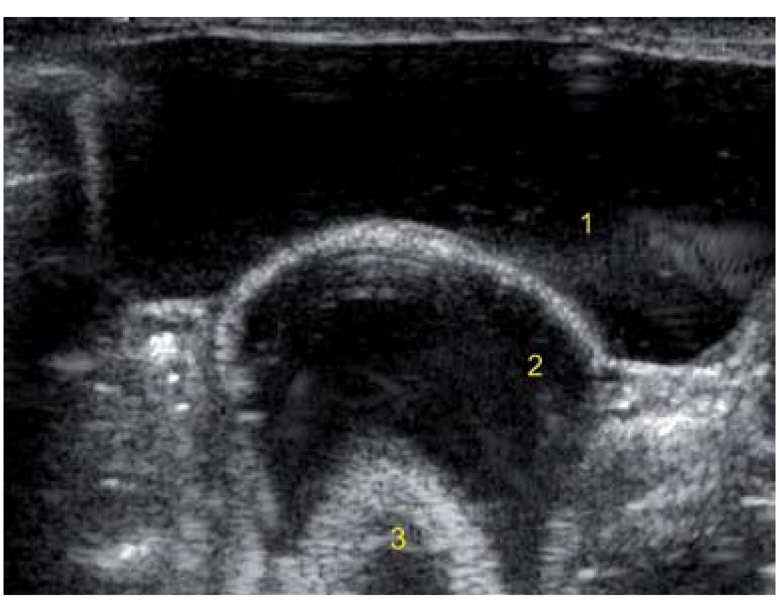

1: urinary bladder
2: vagina
3: rectum

Fig. 2-156: Ultrasonographic image of a rabbit's caudal abdomen, transverse plane, 12 MHz, PD 2.5 cm. Severe hydrovagina (2).

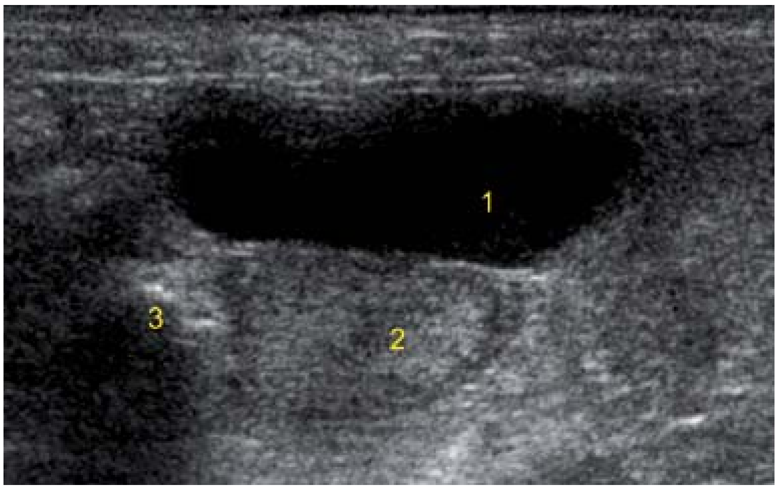

1: urinary bladder
2: cervix
3: rectum

Fig. 2-157: Ultrasonographic image of a guinea pig's caudal abdomen, transverse plane, 12 MHz, PD 2.5 cm. Thickening of the cervix (2) due to estrodiol-producing ovarian cysts.

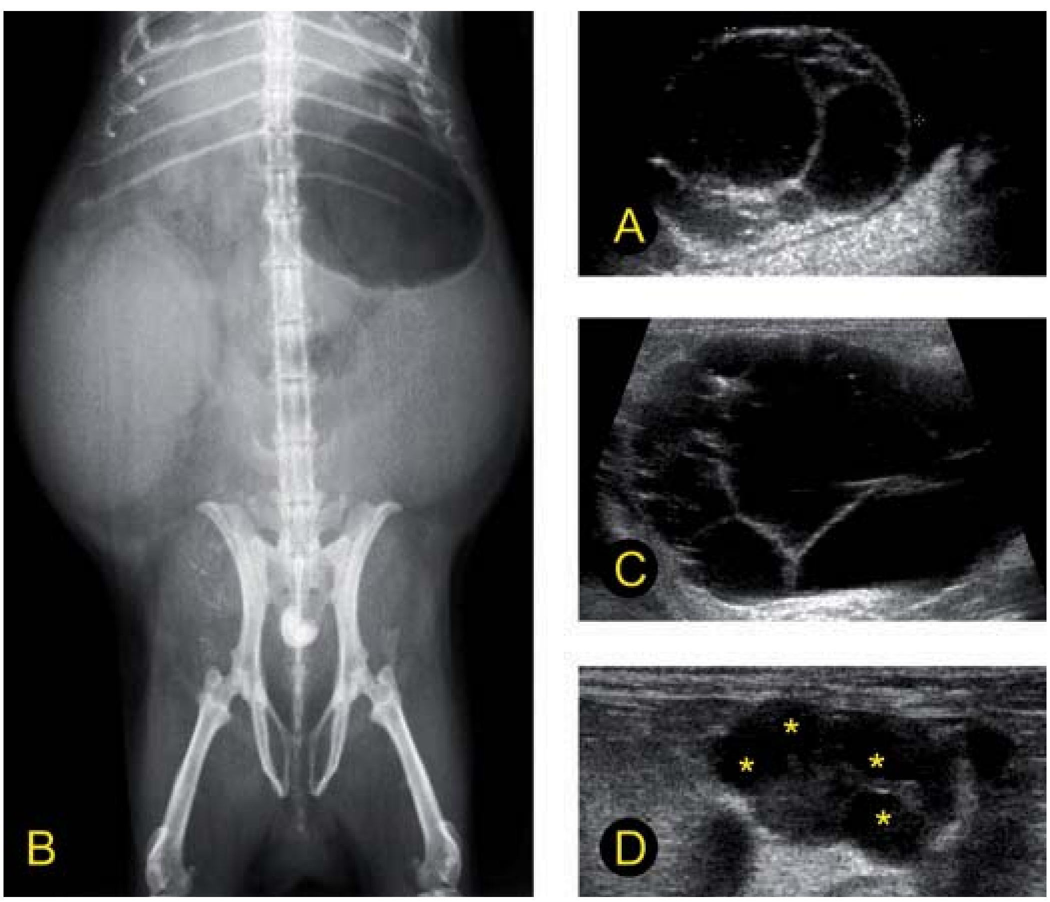

*: cysts

Fig. 2-158: (B) Radiographic and (A, C, D) ultrasonographic images of ovaries.

A: 12 MHz, PD 2.5 cm. Gerbil: Cystic left ovary, largest diameter: 18 mm.

B, C: (B) Radiography ventrodorsal projection and (C) ultrasonography 12 MHz, PD 5 cm. Guinea pig: Cystic ovaries.

D: 12 MHz, PD 2 cm. Ferret: Cystic ovaries. The ferret was presented because of permanent estrous. The ultrasonographic examination revealed the presence of numerous cysts (*) on the ovaries.

Sonogram D reproduced with kind permission from Reese, S., Frings, B. (2004): Die abdominale Ultraschalluntersuchung beim Frettchen. Tierärztl Prax **32(K)**: 182–189.

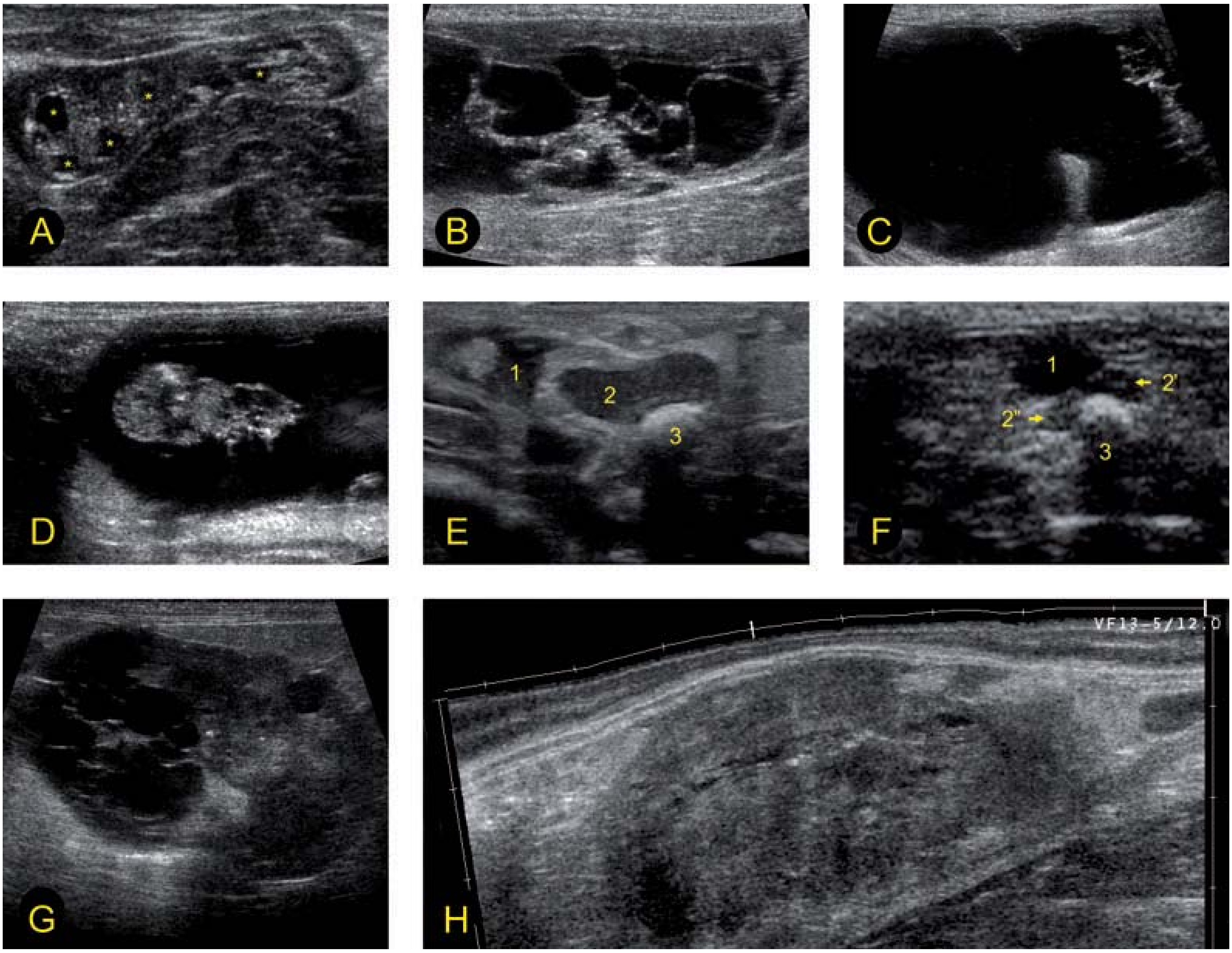

Fig. 2-159: Ultrasonographic images of the uterus, 12 MHz.

A: PD 2 cm. Rabbit: Endometrial hyperplasia with small cysts (*).

B: PD 3 cm. Rabbit: Endometrial hyperplasia with large cysts.

C: PD 4.5 cm. Rabbit: Hydrometra.

D: PD 3 cm. Rabbit: Hemometra.

E: Transverse plane, 15 MHz, PD 2 cm. Golden Hamster: (2) Pyometra.

F: Transverse plane, 15 MHz. Mouse: Endometritis.

G: PD 4.5 cm. Rabbit: Adenocarcinoma of the uterus.

H: Panoramic imaging, PD 4 cm. Rabbit: Fibrosarcoma of the uterus.

1: urinary bladder
2: uterus (pyometra)
2' and 2'': thickened left and right uterine horns
3: rectum

*: small cysts

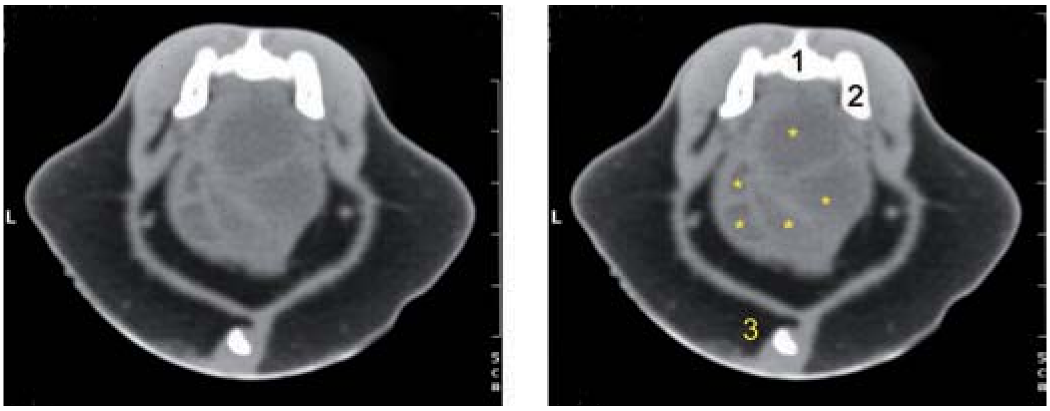

1: sacrum
2: ilium
3: penile bone

*: cysts

Fig. 2-160: CT examination of a ferret, soft tissue window, transverse section at the level of the pelvic inlet. Cystic enlargement in the pelvic inlet caused by para-urethral cysts (»prostate cysts«) (*).

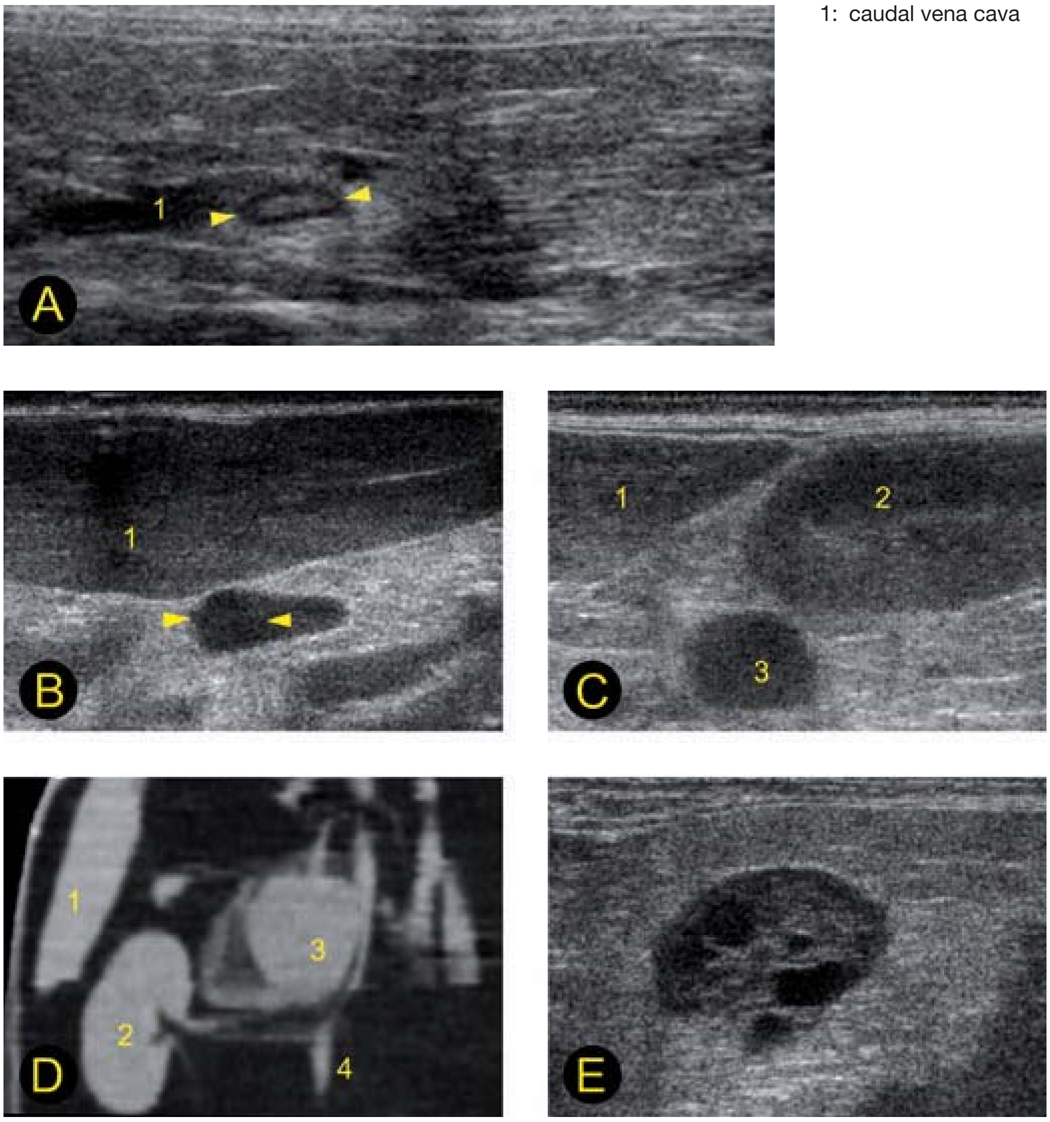

1: caudal vena cava

1: spleen
2: left kidney
3: adenoma in the left adrenal
4: abdominal aorta

Fig. 2-161:

A: Ultrasonographic image of a rabbit's adrenal gland, 12 MHz, PD 1.5 cm. The right adrenal gland (arrowheads) is located dorsally to the caudal vena cava (1). The adrenal cortex is obviously atrophied in comparison to the adrenal medulla. The animal had been subjected to several months of corticosteroid therapy.

B–E: Ultrasonography (B, C, E) and CT examination (D) of the adrenal glands. Ferret.

B: 12 MHz, PD 2 cm: Nodular hyperplasia (arrowheads) of the left adrenal.

C, D: 12 MHz, PD 2.5 cm, horizontal multiplanar reformation of the CT data: Adenoma (3) diagnosed in the left adrenal gland.

E: 12 MHz, PD 2.5 cm: Carcinoma affecting the left adrenal gland.

Sonograms reproduced with kind permission from Reese, S., Frings, B. (2004): Die abdominale Ultraschalluntersuchung beim Frettchen. Tierärztl Prax **32(K)**: 182–189. Sonogram D: M. Fehr, Hanover, Germany.

2.10 Miscellaneous

2.10.1 Eye

INGO HOFFMANN

Clouding of the cornea and lens, periorbital swelling, exophthalmos, and trauma caused by conspecifics or other animals are some of the most frequent reasons small exotic mammals are presented for an ophthalmic examination in which diagnostic imaging modalities may be used. Congenital anomalies are rarely diagnosed, while ocular neoplasms are usually present in the latter stages of development.

2.10.1.1 Cornea

Clouding of the cornea is frequently due to inflammation. With **keratitis**, there is corneal edema and an ingrowth of blood vessels. The subsequent clouding of the cornea due to keratitis can hinder the ophthalmic examination (**Fig. 2-162A**). In such cases, ultrasonography can be used to clarify whether or not there are further pathological changes within the globe itself (**Figs. 2-162B, C**).

On occasion, infectious agents that have penetrated the cornea, due to an injury, can cause a **corneal abscess** (**Fig. 2-163A**). Before conservative or surgical treatment is initiated, the ocular disease must be resolved. Often there is a secondary **uveitis** (see **Fig. 2-167C**) associated with the ocular infection, which will need to be treated, also. Especially in severe cases, the abscess may rupture into the anterior chamber (**Fig. 2-163B**).

2.10.1.2 Ciliary body

Often an animal's owner mistakenly describes clouding in the inner eye as corneal opacity. A frequent finding in guinea pig patients is osseous chorista (heterotropic or intraocular bone formation). In this uni- or bilateral anomaly, progressively differentiated bony tissue grows from the stroma of the ciliary body. This bony tissue growth is pushed over time into the anterior chamber (**Fig. 2-164A**). Due to the presence of the space-occupying lesion in the area of the iridocorneal angle, secondary glaucoma can develop with the clinical signs of ocular discharge, exophthalmos, and exposure keratitis. As a fine capillary bed forms on top of the bony tissue (**Fig. 2-164A**), spontaneous hemorrhages can occur. These hemorrhages and the increase in intraocular pressure within the affected eye can finally lead to the loss of the eye. Impressive examples of osseous chorista are shown in Figures **2-164B** and **2-165**.

2.10.1.3 Lens

Clouding of the lens is not uncommon in both rabbits (**Figs. 2-166A, B**) and guinea pigs (**Fig. 2-166C**). In rabbits, such clouding is most likely caused by vertical, intralenticular infections with *Encephalitozoon cuniculi*. Not only does clouding of the lens occur due to intralenticular infections with *Encephalitozoon cuniculi* but also tears in the lens capsule (**Fig. 2-168A**), and frequently granulomas are formed in the iris (**Figs. 2-167A, B**). The resulting lens-induced uveitis (**Fig. 2-168B**) can be reduced using steroid-containing eye drops (**Fig. 2-167B**); however, the only long-term treatment is removal of the lens using phacoemulsification. With mature cataracts (independent of their cause), a preoperative ultrasonographic examination should always be performed to determine if there are changes in the posterior chamber that would discourage such an operation (**Fig. 2-169A**).

The differential diagnosis of uveitis in the rabbit (**Fig. 2-167C**) must always include a systemic infection with *Pasteurella multocida*. In such cases, the lens is not clouded on the ultrasonographic examination (Fig. 2-168C).

Both in guinea pigs and rabbits, other causes of cataracts are diabetes mellitus and genetic abnormalities. In the guinea pig, hypovitaminosis C is also thought to induce cataract formation.

The **luxation** of a clouded lens due to chronic subclinical uveitis and its secondary clouding after the luxation can be observed both in the rabbit and guinea pig. The lens can luxate either anteriorly (**Fig. 2-169B**) or posteriorly (**Fig. 2-169C**).

2.10.1.4 Peribulbar swelling

The swellings which occur in the peribulbar region of the eye in the rabbit and guinea pig are mainly due to infection. In both species, acute prolapse of orbital fat can also occur (**Fig. 2-170A**). Prolapse of the tear gland (pea eye) has been described in the guinea pig. In addition to this, prolapse of the Harderian and orbital glands have been observed in the rabbit. These rather impressive clinical pictures (**Figs. 2-170B** and **2-173B**) of ocular prolapse can be induced by both tumors and trauma with spontaneous prolapse being a possible etiologic cause also. The removal of the prolapse should only be performed after tumor diagnosis (**Fig. 2-170C**) and unsuccessful attempts at repositioning. Care should be taken when removing the prolapsed tissue because, especially in this area, there is an extensive vascular network, which if cut, can lead to fatal hemorrhaging (can also occur with unprofessional enucleation).

Staphyloma is a very rare anterior protrusion of parts of the inner eye due to chronic inflammation of the ocular membranes. Clinically, ocular discharge and problems with lid closure are identified (**Fig. 2-171A**). The intraocular pressure can cause the weakened layers of the eye to protrude forward. In contrast to a neoplastic tumor, the externally visible tumor due to a staphyloma is not solid on a ultrasonographic image (**Fig. 2-171B**).

2.10.1.5 Exophthalmos

Exophthalmos as a consequence of a retrobulbar space-occupying lesion is a common clinical presentation of both rabbits and guinea pigs. Exophthalmos may be unilateral (**Fig. 2-172A**) or bilateral (**Fig. 2-172B**). In advanced cases, the eyelid cannot be closed causing the surface of the cornea to dry out (**Fig. 2-173A**), thereby promoting the development of secondary corneal ulcers (**Fig. 2-173B**).

Glaucoma with its sequelae (e.g. buphthalmus) (**Fig. 2-174A**) should be included in the differential diagnosis list of exophthalmos, especially in the large rabbit breeds, as should secondary glaucoma due to intraocular bone formation in guinea pigs (**Fig. 2-165**). New Zealand white rabbits can inherit glaucoma as an autosomal recessive disease and pathological intraocular pressures can be measured in affected animals within the first months of life.

The most frequent cause of exophthalmos is a retrobulbar abscess (**Fig. 2-175A**), usually as a result of one or more purulent tooth roots in the upper jaw (**Fig. 2-175B**). The extent and the causes of such abscesses can be determined using ultrasonography (**Fig. 2-175B**), CT (**Fig. 2-175C**), or MRI. Ultrasonographically, the abscesses mainly have a low or mixed echoic pattern. The roots of the teeth should always be examined radiographically.

The presence of neoplastic disease should be considered especially with bilateral exophthalmos (**Fig. 2-176A**). In the rabbit, lymphosarcoma is the most commonly diagnosed neoplastic disease associated with bilateral exophthalmos (**Figs. 2-172B** and **2-176B**). Retrobulbar tumors appear as mixed echoic or hyperechoic tissue structures in both the rabbit and guinea pig. One physiological characteristic that occurs in rabbits is temporary exophthalmos, which is mainly observed when the animals are highly stressed. Temporary exophthalmos occurs when there is a blockage of the drainage veins in the retrobulbar region of affected animals and the resulting collection of blood causes the eye to be pushed forwards. It is believed that this blockage in some animals is associated with an obstruction of the jugular veins by intrathoracic space-occupying lesions (**Fig. 2-176C**).

Retrobulbar swellings in both rabbits and guinea pigs appear mixed echogenic to hyperechogenic (**Figs. 2-176A, B**). In such cases, the roots of the teeth should be assessed radiographically to rule out the presence of a tooth-root abscess.

Other causes of exophthalmos which can be diagnosed using imaging modalities are retrobulbar hemorrhages and myositis of the conus musculature.

2.10.1.6 Trauma

Injuries to the eye are primarily caused by conspecifics, cats, or wild animals. The affected eye is reddened, often with a concurrent ocular discharge. The conjunctiva is swollen and if the cornea is affected, then this is clouded (**Fig. 2-177A**). Ultrasonographic images can show whether there is an ocular perforation even when there is severe swelling of the eyelids and conjunctiva (**Fig. 2-177B**). One must be careful when placing the transducer on the cornea that no pressure is placed on the injured tissues. If hemorrhaging has occurred in the globe, then the extent of the injury can be visualized (**Fig. 2-177C**). This information can be used to aid in decision-making with respect to whether the eye can be saved or needs to be enucleated.

2.10.1.7 Congenital eye anomalies

The number of congenital eye anomalies that have been described in the rabbit and guinea pig are low and limited to eyelid disease.

As with dogs and cats, multiple ocular changes can occur that more or less affect the sight of small exotic mammals. For example, microphakia may occur in association with a cataract (**Fig. 2-178A**).

2.10.1.8 Neoplasia within the globe

Neoplasms diagnosed within the globe have been rarely described in scientific articles. The majority of these neoplasms do not involve intraocular changes but are the ocular manifestation of systemic neoplasia. These ocular neoplasms may be misdiagnosed as uveitis due to the clinical signs of inflammation which the tumors induce. When there is inflammation without a definitive underlying etiology or where there are tumors in the eye, imaging diagnostics should be used to detrmine whether or not a neoplasm is present (**Fig. 2-178B**).

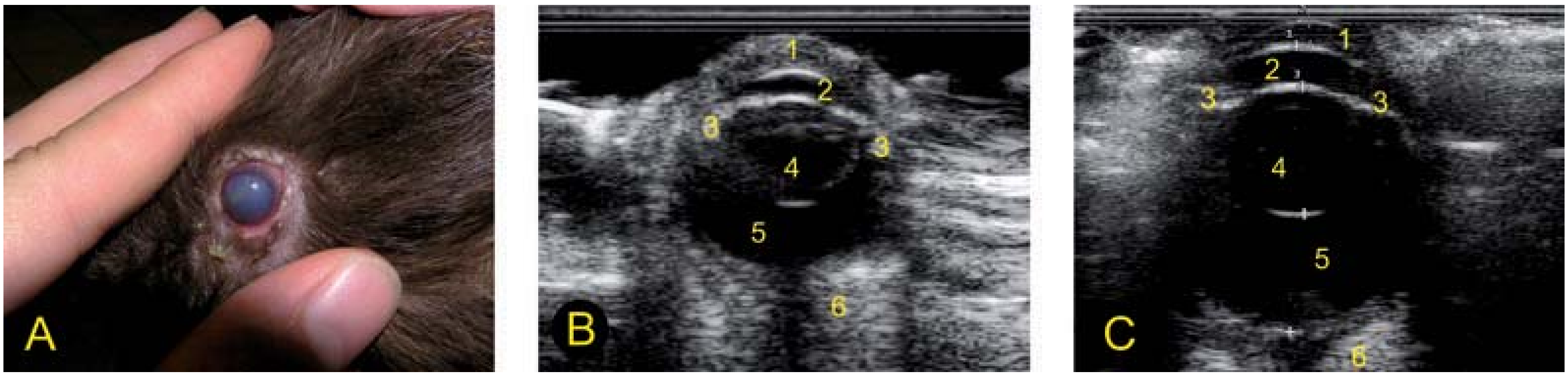

Fig. 2-162:

A: Purulent keratoconjunctivitis in a smooth-haired guinea pig.

B: Ultrasonographic image of the patient described in A using corneal coupling, 15 MHz, PD 3 cm: The hyperechogenic cornea is severely thickened. The rest of the eye is NAD according to the ultrasonographic examination.

C: Ultrasonographic examination of a lionhead rabbit using corneal coupling, 15 MHz, PD 3 cm. The cornea shows thickening that increases towards the center.

1: cornea
2: anterior chamber of the eye
3: iris and ciliary body
4: lens
5: vitreous body
6: orbit

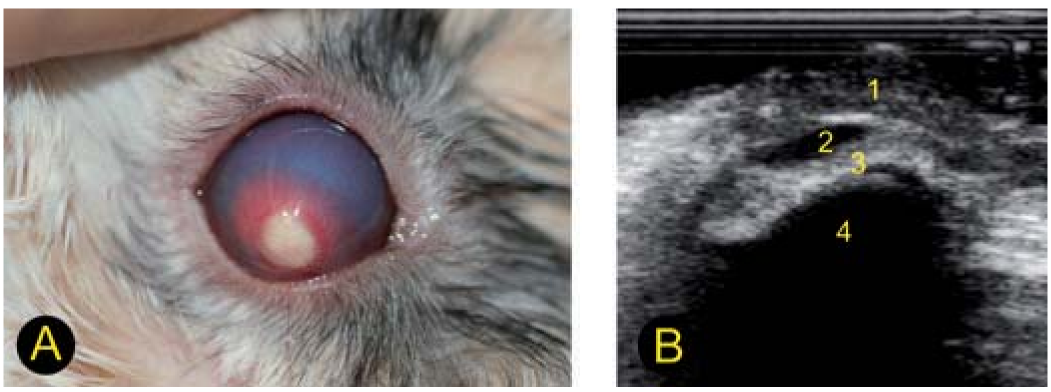

1: cornea with abscess
2: anterior chamber of the eye
3: iris
4: lens

Fig. 2-163:

A: Corneal abscess in a lionhead rabbit.

B: Ultrasonographic image of patient describe in A using corneal coupling, 15 MHz, PD 1.5 cm.

The thickened iris lies on the cloudy and thickened back of the cornea (anterior synechia). The suspicion of an abscess breaking through the corneal barrier into the eye could be confirmed intra-operatively.

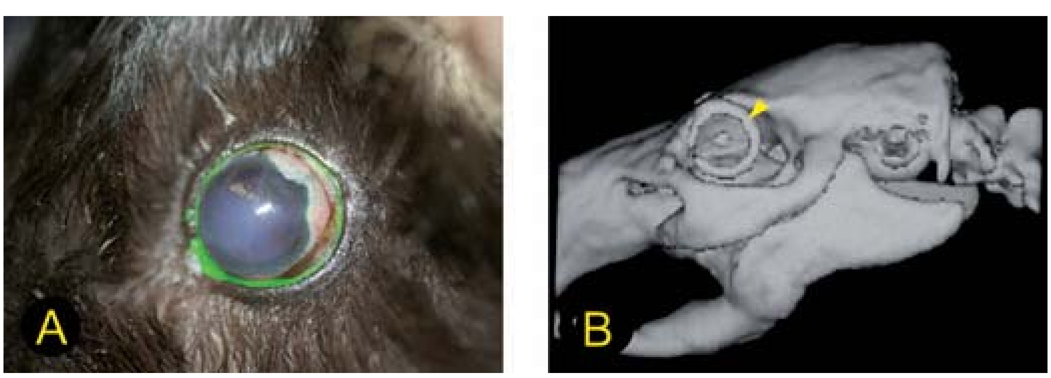

Fig. 2-164:

A: Osseous chorista in a guinea pig.

B: CT examination using 3D reconstruction of the guinea pig's skull showing the image of the ring-like bony tumor on the base of the iris (arrowhead).

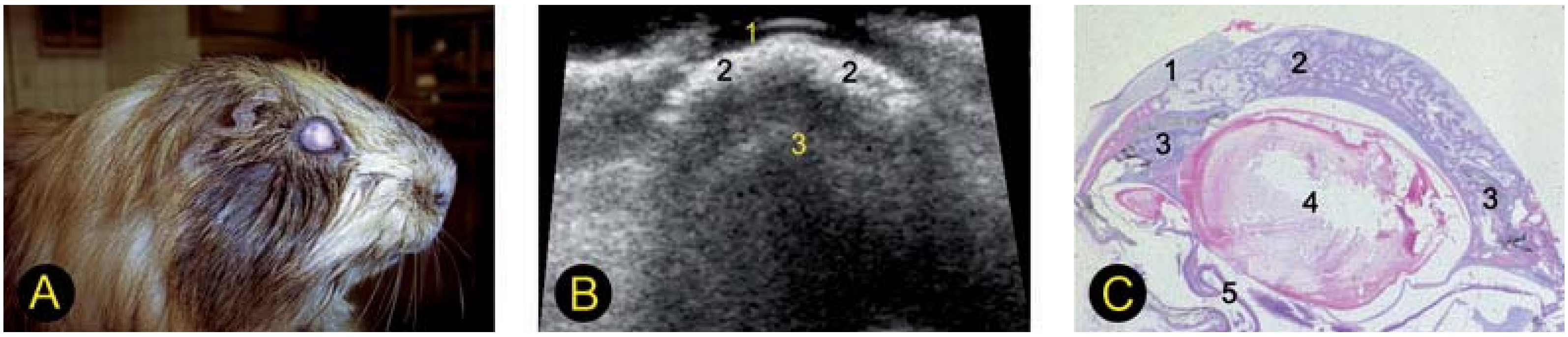

Fig. 2-165:

A: Pinky-white tumor in the right eye of a smooth-haired guinea pig. The internal ocular pressure was 40 mmHg.

B: Ultrasonographic image of the patient described in A using corneal coupling, 12 MHz, PD 1.5 cm. There is a hyperechoic change behind the cornea in the anterior ocular chamber, which has caused a complete cancellation of the echoes.

C: Histopathology to A. The anterior chamber of the eye is completely filled with trabecular bony tissue. In addition, the abnormal tissue arising from the iridocorneal angle has already completely surrounded the iris and ciliary body. Diagnosis: secondary glaucoma due to osseous chorista.

Pictures reproduced with kind permission from Hoffmann, I., Schäfer, E., Reese, S. (2004): Die sonographische Untersuchung des vorderen Augenabschnittes beim Kleintier. Tierärztl Prax **32(K)**: 241.

B:
1: cornea
2: osseous chorista
3: area of echo cancellation

C:
1: cornea
2: osseous chorista
3: iris
4: lens
5: collapsed section of the posterior eye (artefact)

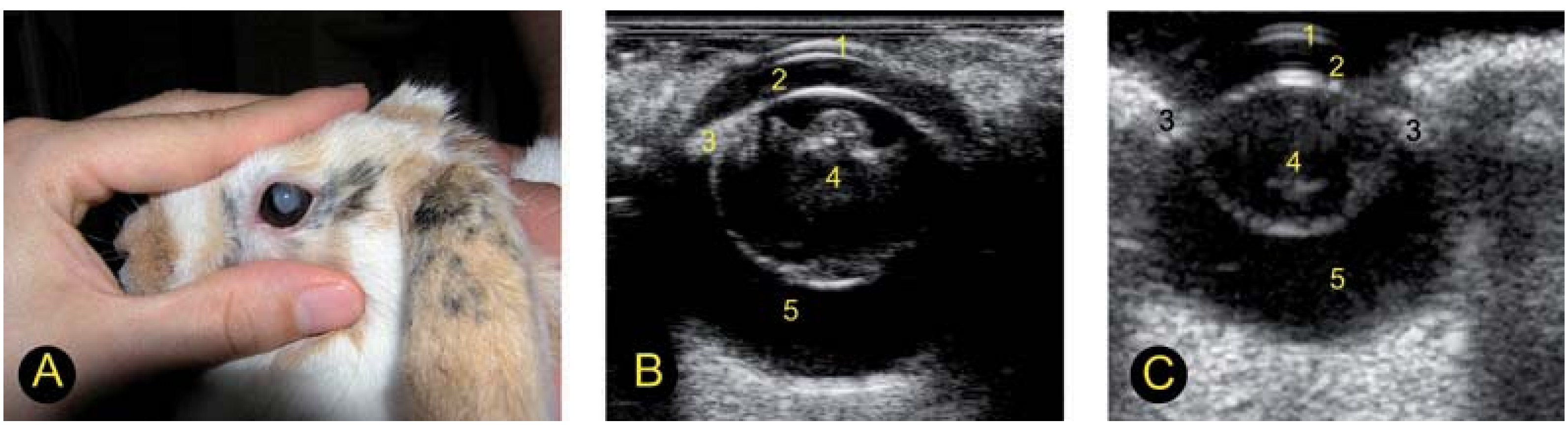

Fig. 2-166:

A: Mature cataract in a mini lop rabbit.

B: Ultrasonographic image of patient described in A using corneal coupling, 15 MHz, PD 3 cm: The lens is hyperechogenic and thickened.

C: Ultrasonographic image of a texel guinea pig using corneal coupling, 12 MHz, PD 1.5 cm. Mature cataract. The lens is hyperechogenic and thickened.

1: cornea
2: anterior chamber of the eye
3: iris and ciliary body
4: lens
5: vitreous body

Fig. 2-167:

A: Keratoconjunctivitis and uveitis in a mini lop rabbit. The view into the anterior chamber is blocked.

B: Corresponding image to A, 2 weeks after treatment with prednisolone acetate eye drops. There is an obvious reduction of the inflammation. An iridic granuloma and a cataract are now clearly visible. Diagnosis: Encephalozoonosis with ocular manifestation.

C: Uveitis with hypopyon in an Angora Rabbit.

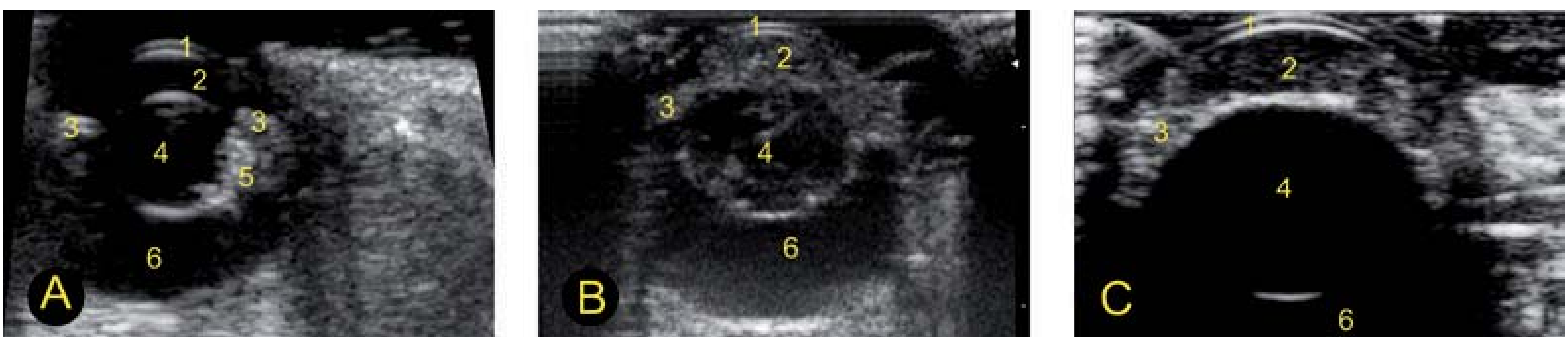

Fig. 2-168:

A: Ultrasonographic image of a dwarf rabbit using corneal coupling, 12 MHz, PD 1.5 cm. Partial hyperechogenic clouding of the lens, which extends over the hyperechogenic line of the capsule. Diagnosis: Rupture of the lens capsule with consecutive phacoclastic uveitis.

B: Ultrasonographic image of the patient described in Fig. 2-167A using corneal coupling, 11 MHz, PD 2 cm. Both the anterior chamber of the eye and the lens have hyperechogenic shadows. Diagnosis: Lens-induced uveitis.

C: Ultrasonography, corneal coupling, 15 MHz, PD 1 cm. loh rabbit: The anterior chamber of the eye has hyperechogenic shadows, so that the iris is barely delineated, the lens is sonographically normal. Diagnosis: Uveitis with hypopyon without involvement of the lens.

1: cornea
2: anterior chamber of the eye
3: iris
4: lens
5: area of cataract and capsule rupture
6: vitreous body

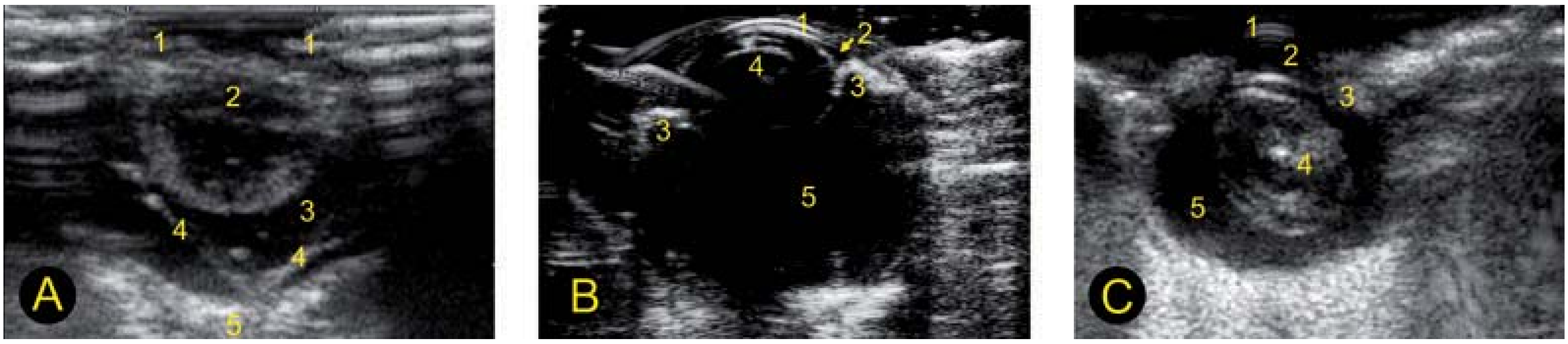

Fig. 2-169:

A: Ultrasonographic image of a mini lop rabbit with mature cataract and a negative dazzle response using corneal coupling, 11 MHz, PD 3 cm. A lily-like, hyperechogenic line originating from the area of the head of the optic nerve is evident in the ultrasonography image (retinal detachment).

B: Ultrasonographic image of a mini lop rabbit with a clouded eye using corneal coupling, 15 MHz, PD 3 cm. The hyperechogenic lens (4) is lying directly over the cornea (1). There is almost no anterior chamber (2) present in the eye. The iris (3) has been pushed laterally by the luxated lens and is curved upwards. The vitreous body (5) is echo-free. Diagnosis: Anterior luxation of the lens.

C: Ultrasonographic image of a smooth-haired guinea pig using corneal coupling, 12 MHz, PD 2 cm. The hyperechogenic lens (4) is lying in the vitreous body (5). Diagnosis: Posterior luxation of the lens, mature cataract.

A:
1: iris
2: hyperechogenic lens
3: vitreous body
4: detached retina
5: orbit

B, C:
1: cornea
2: anterior chamber
3: iris
4: lens
5: vitreous body

Fig. 2-170:

A: Prolapse of fatty orbital tissue in a Texel guinea pig.

B: Prolapse of the nictitating membrane and gland in a rabbit.

C: Ultrasonographic image of the patient described in B using corneal coupling, 15 MHz, PD 3 cm. Massive prolapse of the nictitating membrane (6) and gland tissue with congestion of the orbital vessels. The rest of the structures in the eye are inconspicuous. There is no evidence of a tumor.

1: cornea
2: anterior chamber
3: iris and ciliary body
4: lens
5: vitreous body
6: prolapsed nictitating membrane

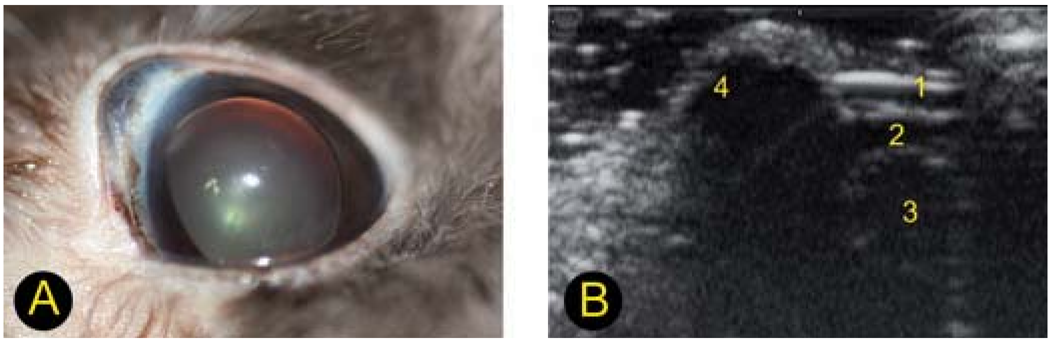

1: cornea
2: anterior chamber
3: lens
4: nonechogenic protrusion in the area of the limbus

Fig. 2-171:

A: Tumor in an 8-year-old rabbit. The owners had been aware of the tumor for some time, but noticed a significant increase in size during the previous week.

B: Ultrasonographic image of patient described in A using corneal coupling, 11 MHz, PD 1 cm. The nonechogenic protrusion in the area of the limbus led to the suspicion of a scleral staphyloma

Fig. 2-172:

A: Unilateral exophthalmus in a Texel guinea pig.

B: Bilateral exophthalmus in a dwarf rabbit (see also Fig. 2-176C).

Fig. 2-173:

A: Unilateral exophthalmus in a dwarf rabbit with corneal xerosis, purulent discharge, and severe swelling of the conjunctiva.

B: Unilateral exophthalmus in a dwarf rabbit with a fluorescein-positive corneal defect in addition to prolapse of the nictitating membrane and gland tissue (see also Fig. 2-176B).

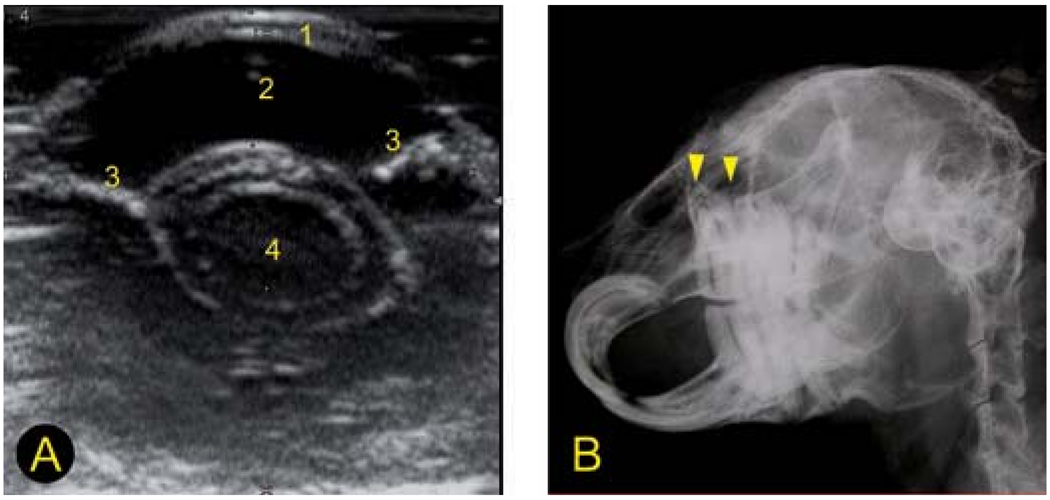

1: cornea
2: anterior chamber
3: iris
4: lens

arrowheads: bone lysis

Fig. 2-174:

A: Ultrasonographic image of a mini lop rabbit (age: 10 years) with unilateral buphthalmos and an intraocular pressure of 40 mmHg using corneal coupling, 11 MHz, PD 3 cm. The distance between the cornea (1) and lens (4) is obviously larger than normal (4.3 mm). Therefore, the anterior chamber (2) of the eye is deep. The luxated, hyperechogenic lens (4) is lying oblique to the iris (3) in the anterior cortex. The globe appears bulky and enlarged (diameter 17.9 mm) in comparison to the contralateral eye (16.4 mm). The hyperechogenic ring in the nuclear region of the lens is a nuclear cataract caused by aging.

B: Radiographic image of a rabbit, oblique lateral projection. Multiple lytic processes in the region of the tooth roots (arrowheads).

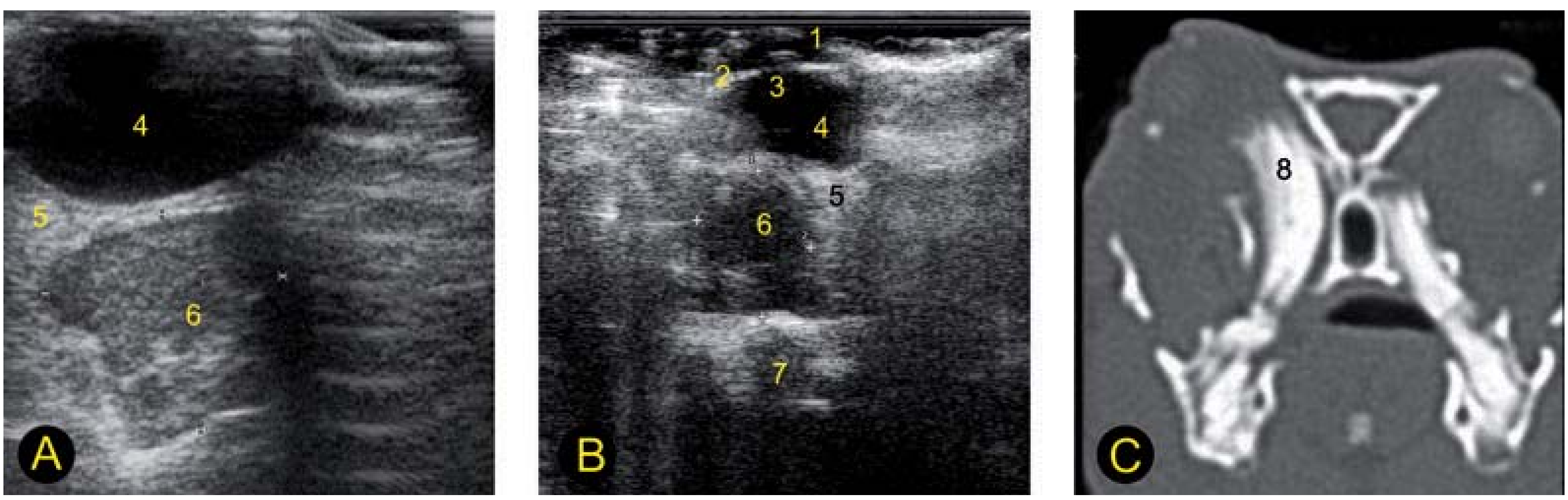

Fig. 2-175:

A: Ultrasonographic images of a mini lop rabbit with unilateral exophthalmus and similar radiological findings to Fig. 2-173B using corneal coupling, 11 MHz, PD 3 cm. Diagnosis: Retrobulbar abscess due to dental causes.

B: Ultrasonographic imaging of a guinea pig using corneal coupling, 15 MHz, PD 3 cm. Hypoechogenic tumor in the retrobulbar space, which anteriorly presses in part of the eyeball and posteriorly fuses with the acoustic shadow (7) in the area of the tooth roots.

C: CT examination of a guinea pig: An exposure keratitis due to an exophthalmus with a lagophthalmos was observed clinically in the left eye. The CT examination revealed the cause of the exophthalmus to be retrobulbar abscesses due to abnormal positioning of the teeth (8).

1: cornea
2: iris
3: lens
4: vitreous body
5: orbit
6: hypoechogenic changes
7: acoustic shadow in the area of the tooth roots
8: tooth grown retrogradely into the orbit

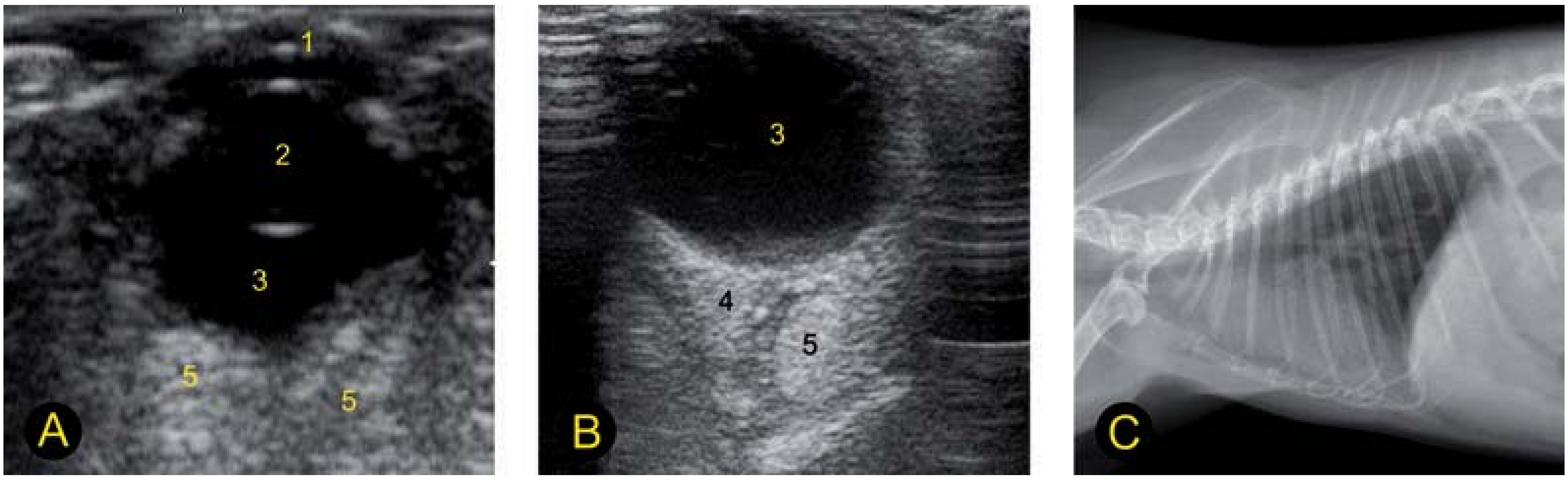

Fig. 2-176:

A: Ultrasonographic image of a guinea pig using corneal coupling, 11 MHz, PD 2 cm.

The roots of the animal's teeth exhibited no radiographic abnormalities, but the animal had cachexia and a right-sided exophthalmos. There is a hyperechogenic tumor (5) in the region of the right orbit, which is pressing on the globe. Diagnosis: retrobulbar tumor.

B: Ultrasonographic image of the dwarf rabbit described in Fig. 2-173B using corneal coupling, 11 MHz, PD 3 cm. Lymphosarcoma metastasis (5).

C: Radiographic image of the dwarf rabbit described in Fig. 2-172B, lateral projection. Precardial soft tissue shadow – suspicion of a lymphosarcoma metastasis.

1: cornea
2: lens
3: vitreous body
4: orbit
5: hyperechogenic tumor in the orbit

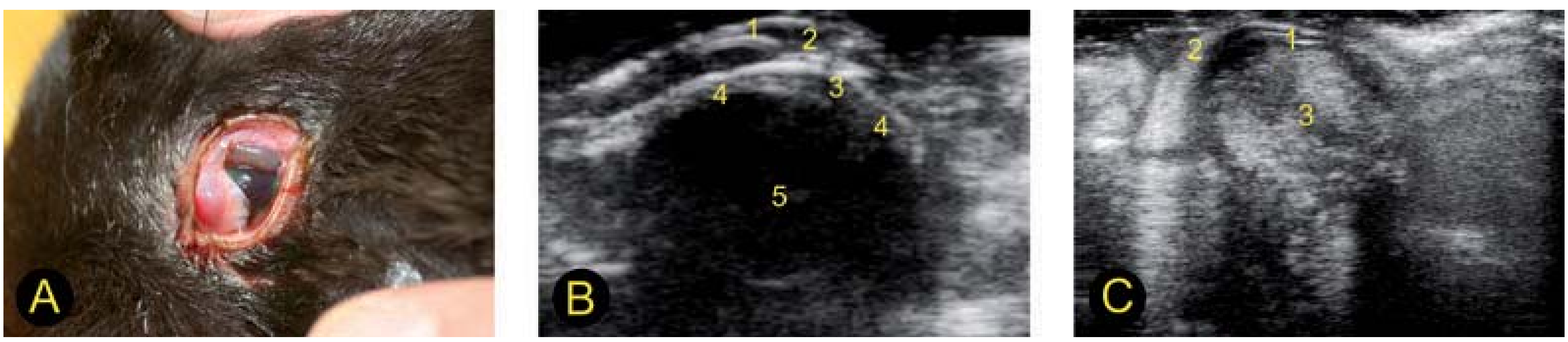

Fig. 2-177:

A: Unilateral eye injury in a dwarf rabbit after being attacked by a martin: massive conjunctival swelling and reddening, nictitating membrane prolapse, and enophthalmos. The cornea is stained dorsally with fluorescein. The interior of the eye cannot be observed as the anterior chamber is filled with a reddish mass.

B: Ultrasonographic image of a lionhead rabbit after a fight with another doe using corneal coupling, 15 MHz, PD 1.5 cm. The injured area (2) is clearly different to the healthy cornea (1). The lens capsule (3) is also affected. The anterior lens (4) is hypoechoic in comparison to the rest of the lens (5). Diagnosis: Perforating injury of the cornea also affecting the lens.

C: Ultrasonographic image of the patient described in A using corneal coupling, 15 MHz, PD 3 cm. The nictitating membrane (2) has been pushed in front of the cornea (1). The rest of the eye is filled with a hyperechogenic mass. Diagnosis: Perforating injury of the cornea with severe intraocular hemorrhage. The eye was enucleated because of a poor prognosis for recovery.

B:
1: cornea
2: corneal injury
3: lens capsule
4: anterior lens
5: lens

C:
1: cornea
2: nictitating membrane
3: intra-ocular hyperechogenic mass (hemorrhage)

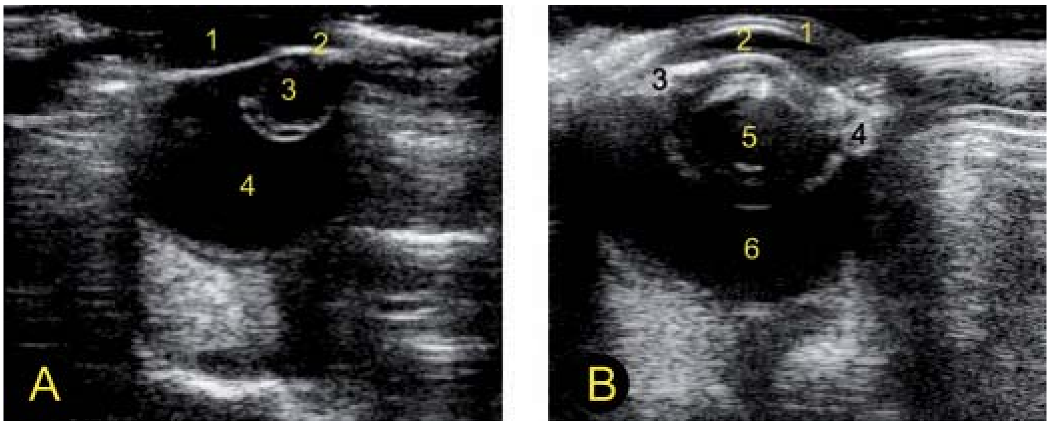

A:
1: anterior chamber of the eye
2: iris
3: shrunken and clouded lens
4: vitreous body

B:
1: cornea
2: anterior chamber of the eye
3: iris
4: thickened ciliary body
5: hyperechogenic lens
6: vitreous body

Fig. 2-178:

A: Ultrasonographic image of a dwarf rabbit with suspicion of a lens luxation using corneal coupling, 15 MHz, PD 3 cm. Diagnosis: Microphakia with a congenital cataract.

B: Ultrasonographic image of a lionhead rabbit with clouding of the lens using corneal coupling, 15 MHz, PD 3 cm. Suspicion of a ciliary body tumor (4).

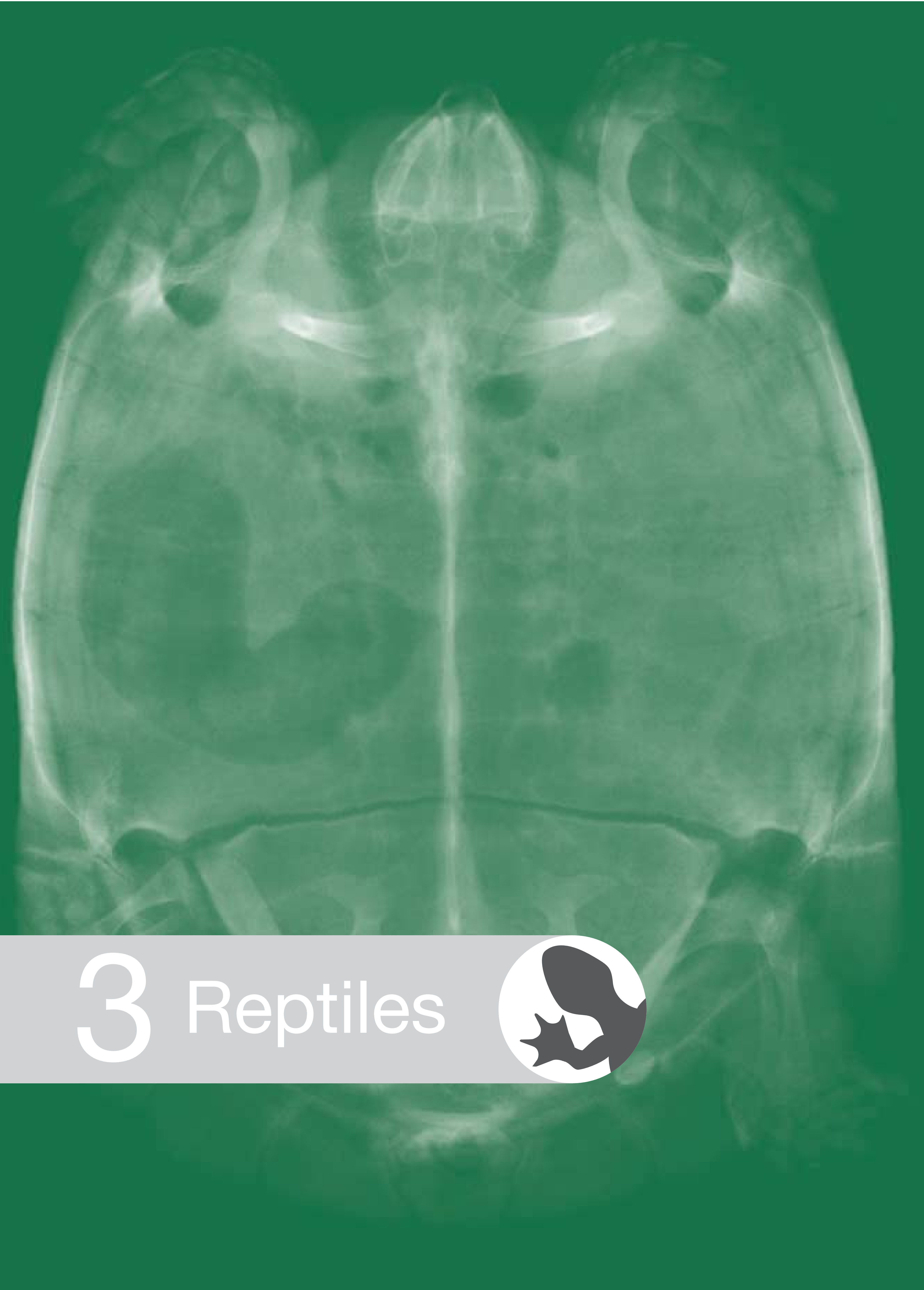

3 Reptiles

Introduction

Michael Pees

Reptile patients are treated in veterinary practice with both reptile and amphibian medical expertise continuing to advance as knowledge regarding these species is scientifically validated. Currently, there are diagnostic and therapeutic measures available that were not possible a few years ago to implement reptile and amphibian patients. These advances have led owners to expect and demand more targeted and competent diagnostic testing for their animals. Reptile patients are more difficult to assess than mammals due to their anatomical peculiarities. Both imaging and infectious diagnostic testing modalities have special significance in veterinary practice when trying to establish definitive diagnoses in reptile patients.

Radiography is commonly used as a diagnostic test to further evaluate the health of a reptile patient; however, ultrasonography is currently being performed more frequently as its availability expands within the veterinary community. Ultrasonography can be performed on these patients using standard machines and provides valuable diagnostic information. The newer imaging methods, CT and MRI are being increasingly utilized for diagnostic imaging evaluation procedures for reptile patients due to increased availability for veterinary practitioners. Computed tomography and MRI are being requested by clients on a more frequent basis. Both are excellent aids with a significant diagnostic potential for certain reptile and amphibian cases and can be utilized in cases in which the final diagnosis has yet to be determined. Recent investigative studies have established scientific information that can be used as standardized techniques in these species.

General principles

3.1 Radiographic investigation

Michael Pees

3.1.1 Equipment

The technical requirements for radiographic techniques in reptiles are similar to those needed in small animals in general. The blurring observed in avian radiographic images due to movement caused by their high respiratory rate is rarely a problem in reptiles. To enable the use of short exposure times, x-ray machines with a performance of at least 200 mA and a voltage range between 40 kV and 100 kV are recommended for reptile and amphibian patients. The size of the reptilian patient can lead to problems in very small, very large, or long animals. However, radiographic images can be obtained with standard equipment in animals between ca. 15 g to 60 kg. Radiographic images of larger chelonian species with correspondingly thick bony carapaces are rarely diagnostic.

An important requirement placed on the radiographic equipment is a movable x-ray tube so that the beam can be directed in both the vertical (the standard direction) or in the horizontal direction. The horizontal beam is indispensable for the radiographic investigation of chelonians in the lateral and craniocaudal projection (see Chap. 3.1.2.3). Horizontal projections are also recommended in both snakes and lizards. If the beam cannot be directed horizontally, then these projections are not performed in chelonian patients. In contrast, horizontal beam analysis can still be done in lizards and snakes as these species are often radiographed in lateral recumbency because the summation of organs caused by tilting these animals does not have such an adverse effect on the assessability of the radiograph as in chelonians. The film-focus distance should be about ca. 80 cm.

Films or film-screen combinations utilized in mammals are also useable in reptiles. High definition mammography films are very suitable to evaluate animals under 1000 g in weight as the detail resolution is much better than the standard film-screen combinations. A roster should not be used for reptiles with a body weight under 10 kg. For radiographs taken horizontally, a cassette holder is advantageous for attaining optimal images. The necessary positioning can be achieved with simple aids such as placing the animals on a beaker and positioning the cassette against a wall or a large object behind the animal.

When using digital radiographic systems, the same principles used in mammalian patients apply to reptile patients and may be used in a similar manner. The possibility of subsequent picture adjustment can make the diagnosis much easier, but it can also lead to misinterpretation of the radiographic images.

General anesthesia, as a rule, is not necessary for the standard projections when evaluating reptile and amphibian patients. Sedation should only be used in aggressive reptiles and those animals which cannot be manually positioned for the radiographic procedure. Sedation may also be necessary for larger snakes for correct positioning (e.g. lateral projection). The general anesthetic agent of choice for reptile patients is isoflurane as it allows better control by the veterinary anesthetist and its short duration greatly reduces anesthetic risk. An injectable anesthetic may be needed in aquatic reptile species (e.g. terrapins), as they can stop their respiration for a significant periods of time when under the influence of general anesthetic agents during diagnostic imaging protocols.

3.1.2 Positioning and projections

The different imaging positions utilized for diagnostic evaluation of reptile species varies significantly between lizards, snakes, and chelonians. The variation of positions needed to image these three groups of reptiles which are commonly treated in veterinary practice will be described in separate sections. First and foremost, protection against injuries is of special importance not only for the patient but also for the veterinary staff involved with the procedure. Lizards and snakes are usually held manually by a member of the technical staff wearing the appropriate protection against radiation exposure. Collimation of the beam, to reduce scatter radiation exposure, may prevent most of the animal from being properly imaged, especially with small patients. To ensure all of the desired anatomy is within the acquired image, a »hands off« positioning method (e.g. box) is recommended which allows for less collimation of the beam. As with mammalian species, the prerequisites for correct radiographic interpretation are proper positioning of the patient and the correct projection. An overview of the recommended positions for investigating the various organ systems of reptile species is provided in Table 3-1.

3.1.2.1 Radiography of lizards

The two standard positions for the radiographic investigation of lizards are DV and lateral. Lizards can be restrained manually, with ropes, or radiographed in radiolucent boxes. Very weak animals can also be radiographed dorsoventrally without being restrained. A radiolucent box should be used as an exception when radiographing very small or shy animals because the animal's position cannot be controlled and only the DV projection is of diagnostic quality. Moreover, in lizards with a very sensitive skin (e.g. geckos), a hands-off positioning method is preferred because sudden defensive movements can lead to skin lacerations.

Manual restraint for the DV position when investigating the body cavity of lizards is best achieved by holding the hindlegs of the animal against the tail base with one hand; the other hand should hold the forelegs together alongside the neck **(Fig. 3-1)**. In some cases, it is best to bind the legs firmly against the body. In lizards with very short limbs (e.g. caimans), this form of manual restraint can be a problem; therefore, appropriate bandage material should be used to bind the limbs. The same restraint modification is also recommended in larger lizards, which can only be held manually in position with great difficulty. If the tail needs to be radiographed, then it is usually sufficient to only fix the front end of the animal. Under no circumstances should the tail be held or tied, as many lizards are capable of autotomy (i.e. ejection of the tip of the tail).

Lizards are laid on their sides for lateral positioning. Restraint for lateral positioning is similar to that used for the DV placement. Again, the legs should be held as close to the body as possible **(Fig. 3-2)**.

A lateral projection with a horizontal beam is particularly useful when the lungs need to be examined since organ displacement into the lung field is reduced when the lizard is held in this position. However, the lateral positioning of the patient for this projection is often difficult. Usually, lizards are placed in a radiolucent box and radiographed as for chelonians to obtain a lateral projection from the radiographic beam.

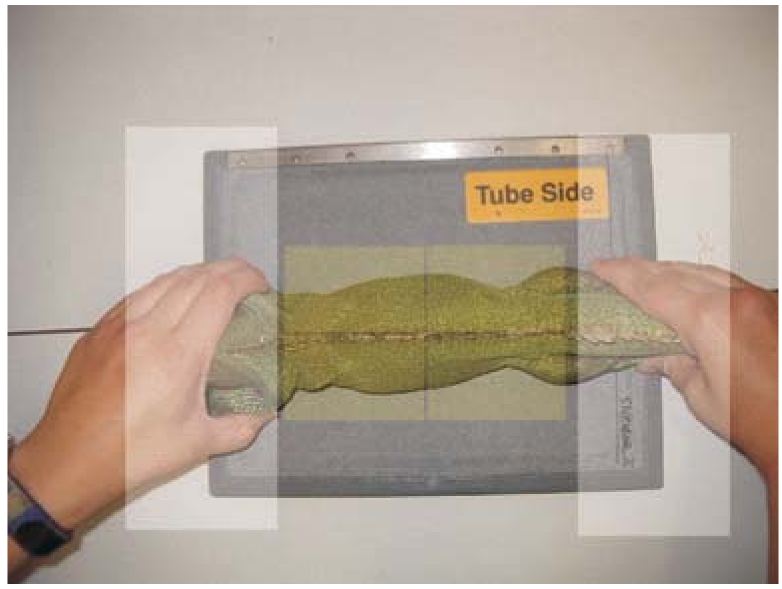

Fig. 3-1: Positioning of a Chinese water dragon (*Physignathus cocincinus*) for a dorsoventral projection. The limbs should be stretched in a cranial (forelimbs) and caudal (hindlimbs) direction and positioned near the head (forelimbs) and tail (hindlimbs). In some lizards (e.g. caimans), the positioning of their short legs is difficult. The whitish oblongs show the areas that should be shielded by using lead plates (also in Fig. 3.2).

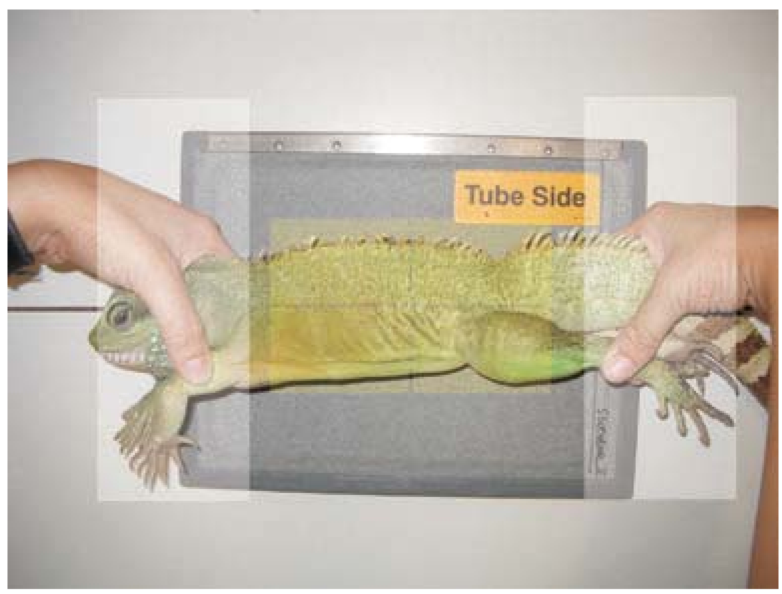

Fig. 3-2: Positioning of a Chinese water dragon (*Physignathus cocincinus*) for a lateral projection. The tuber coxae should superimpose each other in the vertical plane and the crest should be positioned as parallel to the radiographic plate as possible.

Table 3-1: Suggested projections for the examination of different organ systems (CrCa: craniocaudal, CaCr: caudocranial, L: lateral, DV: dorsoventral, DP: dorsopalmar).

	Respiratory tract	Gastrointestinal tract	Urogenital tract	Carapace, plastron	Skeleton	Limbs	Head
Chelonians	CrCa, L	L, DV	L, DV	DV, CrCa, L	L, DV	DP, poss. hanging in L	L, DV, oblique projection
Snakes	L	L, DV	L, DV	–	L, DV	–	L, DV, oblique projection
Lizards	L	L, DV	L, DV	–	L, DV	DP, CaCr	L, DV, oblique projection

To examine the limbs of a lizard patient, the affected leg should be placed against the cassette or extended using a rope. Projections of the limbs in two planes are only possible to a certain degree. To obtain a dorsopalmar projection, the patient is placed on its stomach and its leg is abducted from the body. For caudocranial projections, the leg is positioned against the body and caudally restrained before the images are taken.

For radiographic examinations of the head, occasionally oblique projections are needed in addition to the two projections mentioned above. Radiographic images taken at a 60° angle to the horizontal reveal individual structures with minimal summation. It may also be helpful to carefully hold the mouth open using two ropes which will reduce summation of the anatomic structures found in the cranial aspect of the head. Radiographs of the head should be taken when the patient is sedated or under general anesthesia for adequate positioning and to minimize the risk of injury.

As an interpretative aid for radiographic images of lizard patients, the positions of a few internal organs are shown in **Figure 3-8**.

3.1.2.2 Radiography of snakes

Snakes are usually radiographed in the DV and lateral positions. The length of these animals can be a problem when trying to obtain diagnostic radiographic images, especially with larger patients. It is possible to radiograph a snake in a radiolucent container on the cassette **(Fig. 3-3)**; however, only the less diagnostic DV projection is possible. In addition, the assessment of radiographic images of a »rolled-up« snake is difficult and is not very helpful due to the multiple summation and displacement of internal organs. Therefore, a radiographic image of a »rolled-up« or »balled-up« snake is not recommended. For larger longer animals, a segmental investigation of the relevant structures is recommended. When performing a segmental investigation of a snake, it is important to mark the individual sections on the patient with radiopaque markers or clips **(Fig. 3-4)**, thereby allowing for easy identification of anomalies to the respective region of the body in the radiographic image(s). In practice, the taping of paper clips to the snake has proved useful as they can be individually bent so that each separate section can be identified.

Often defensive movements make the positioning of snakes either difficult or even impossible. In such cases, general anesthesia of short duration to immobilize the animal is recommended. Alternatively, an acrylic plastic tube of a suitable size should be used to restrain the part of the snake to be radiographed. The radiopacity of the tube should be tested before the procedure to ensure the diagnostic quality of the radiographic image.

The tips given in Table 3-2 to localize individual organs should help the veterinarian when taking and interpreting snake radiographs. However, the position of the individual organs within the radiographic image of a snake depends significantly on the species, individual variation, and its body condition.

If at all possible, the head of a snake should be held during the radiographic procedure. Care should be taken to prevent the weight of the snake or its defensive movements from creating a tensile force that is too strong in the region of the first cervical vertebra since the spine is very sensitive in this location. The snake's head should not be held by the head itself but in a more caudal position (e.g. neck). The other hand of the person holding the snake should be used to support the animal in the cranial cervical region. A second staff member should hold the snake above and below the anatomic region which is to be radiographed, stretching it out as far as possible. Depending on the size of the animal, more people may be needed to achieve correct positioning of the patient.

The DV projection for radiographic images is usually easier to obtain as the snake remains in its natural ventrally recumbent position. A lateral projection is also recommended because there is less summation of the organs and is diagnostically more informative. These projections can be achieved with the radiographic beam aimed in either a horizontal or vertical position. Since the degree of manual positioning of the snake is limited when using a horizontal beam, sedation or general anesthesia is required when using this method to ensure adequate radiation protection of the staff.

In addition to the standard DV and lateral projections, oblique projections are taken in the region of the head as describe for lizards. Usually, the snake will have to be sedated or placed under general anesthesia to radiograph the head.

Table 3-2: Localizing individual organs in the snake.

Values for boas, in % of the body length (nose-cloaca)	
Heart	approximately 25%
Lungs	approximately 25–45%
Air sack	adjacent to the lungs, up to ca. 65%, very variable
Liver	approximately 35–60%
Stomach	approximately 50–70%
Small intestines	approximately 60–80%
Largel intestines	approximately 80%
Kidneys	left kidney cranial, right caudal, ca. 65–80%

Fig. 3-3: Positioning of a Mandarine rat snake (*Elaphe mandarina*) in a plastic vessel for a dorsoventral projection. Such radiographic images are, at best, used as overprojections because assessment of the individual internal organs is extremely difficult.

Fig. 3-4: Positioning of Mandarine rat snake (*Elaphe mandarina*) for a lateral radiograph. The different segments can be best assessed using this projection. If the radiographic plate is appropriately subdivided, a number of images can be taken on the same film. A radiodense marker (here a paper clip) is used to mark each respective section that is radiographed. The whitish oblongs show the areas which should be shielded by using lead plates.

3.1.2.3 Radiography of chelonians

The three standard projections used in chelonians are DV, lateral, and craniocaudal. Manual positioning is not recommended for these animals as it is difficult to hold the carapace and adjust the radiographic window to the body cavity. It is also not recommended to bind the legs within the shell as this causes summation making diagnostic interpretation difficult. Chelonians can be radiographed in radiolucent boxes or positioned on the cassette using adhesive tape for the DV projection **(Fig. 3-5)**. For the lateral and craniocaudal projections, it is recommended to place the animal on an upturned vessel or wooden block for immobilization **(Figs. 3-6** and **3-7)**. Placing the animal on an upturned vessel or wooden block is not only successful in calming the animal, but also encourages the majority of chelonians to hang their legs outside of their shell. In such a position, anomalies that affect either the body cavity and legs, or both can be assessed.

Due to their anatomy, turning chelonians patients to obtain radiographic images, either in the lateral or craniocaudal projection, is not at all advisable. The size of the body cavity in chelonians is dictated by the bony shell. Chelonians have a large amount of free space within the shell, allowing room for ingested food and egg production. The internal organs, including the lungs, hang freely in the chelonian body cavity; therefore, turning the animal will result in severe displacement of its internal organs with associated summation. Interpreting radiographs of a turned chelonian is virtually impossible.

Sedation or general anesthesia is always required for radiography of the head and occasionally the limbs in chelonians.

To aid in the interpretation of chelonian radiographs, the positions of some internal organs are provided in **Figure 3-9**.

Fig. 3-5: Positioining of a Hermann's tortoise (*Testudo hermanni*) with adhesive tape on the film cassette for a dorsoventral projection. Quiet animals can also be examined without fixation.

Fig. 3-6: Positioning of a Russian tortoise (*Testudo horsfieldii*) on a bucket for a lateral projection, horizontal beam. The chelonian must be positioned as close to the vertically positioned film cassette as possible for an optimal radiographic image. The center of the beam should be aimed at the lateral scutes in the middle of the animal (red cross).

Fig. 3-7: Positioning of a Russian tortoise (*Testudo horsfieldii*) on a bucket for a craniocaudal projection, horizontal beam. It is important when positioning the animal that it is as symmetrical as possible so that both sides of the lungs can be assessed against each other. The center of the beam should be aimed at the chelonian's central cervical scutes (red arrow).

1: heart
2: thyroid
3: trachea
4: liver
5: gallbladder
6: stomach
7: jejunum
8: ascending colon
9: descending colon
10: allantois

Fig. 3-8: Schematic representation of a ventral view of the internal organs of a lizard to aid in the the interpretation of radiographic images. Even in lizards, the demarcation of the organs varies greatly between species. The ventral fat bodies are not shown.

1: heart
2: thyroid
3: trachea
4: liver
5: stomach
6: jejunum
7: cecum
8: ascending colon
9: descending colon
10: allantois

Fig. 3-9: Schematic representation of the internal organs in a terrestrial chelonian to aid in the interpretation of radiographic images; ventral projection. It should be noted that position, size, and form vary considerably from species to species and between individuals.

3.1.3 Contrast studies

Contrast studies are less diagnostic in reptile species than birds. This is due to the extremely variable and often very long contrast transit times in reptiles. The transit time is dependent on the nutritional status, temperature, season, and species of patient. For example, the intestinal transit time in a healthy tortoise is more than three weeks. Conversely, turtles have a relatively quicker transit time although it is still extremely variable (see **Fig. 3-19**). In lizards, the intestinal passage for herbivorous species is much longer than in their counterpart carnivorous species: in the green iguana (*Iguana iguana*) it usually takes between two and three weeks for a normal gastrointestinal passage time, whereas only a few days are needed for the same digestive processes to occur in monitors. The intestinal transit time is particularly variable after the administration of barium sulfate. Due to the long transit time, there is a real danger that the contrast agent solidifies in the gut and its transport is delayed even further. A much quicker transit time follows the administration of non-ionic iodine-based solutions and in chelonians, diagnostic radiographs can even be obtained shortly after using this method.

The main indications for the administration of contrast agents are:

- assessment the gastrointestinal tract for patency (e.g. stenosis, foreign body, atony)
- assess the size of the gastrointestinal tract
- assess the integrity of the intestinal wall (e.g. after trauma, postoperative; use only iodine-based contrast agents)
- depiction of the size and position of other organs and structures (e.g. liver, allantois, kidney, tumors, abscesses)

The dose of barium sulfate that is often used for reptile gastrointestinal contrast studies is 20 ml/kg bwt of a ca. 35% solution administered orally using a bulb-headed gavage needle. During the time needed for the transit of the contrast suspension through the intestines, the patient should remain well hydrated and when necessary be given parenteral fluid supplementation.

When iodine-based contrast agents are used, a dose of 10 ml/kg bwt of an iodine solution (250 mg iodine/ml is recommended). The iodine solution can be administered into the patient's stomach using a bulb-headed gavage needle, as well as other methods (e.g. red rubber tube). **Figure 3-168** shows a contrast study after the intracloacal administration of an iodine-based solution.

There have been very few reports on the parenteral use of contrast agents in reptiles. The principles for parenteral use of contrast agents in reptile patients follow those used for mammals; however, finding an intravenous access in reptiles is much more difficult. **Figure 3-227** shows an example of the administration of an intravenous iodine-based contrast agent for imaging a tumor.

Double-contrast studies using a positive contrast in combination with air can be performed in both the upper and lower gastrointestinal tract. The administration of the contrast agents should be done, if possible, directly in the area to be investigated (e.g. the esophagus or stomach or retrograde into the cloaca and/or caudal intestinal tract). During retrograde instillation, it is possible to administer the contrast agent by mistake in the allantois or more rarely in a ureter or the oviduct. As a rule, the dosage of the contrast agent can be halved for double-contrast studies. By administering the same amount of air, mucosal imaging is much better when compared to simple contrast studies. The use of iodine-based contrast agents is recommended because this type of contrast agent is quickly distributed to the area being examined and has a lower risk of damaging the animal's tissues.

3.1.4 Assessment of radiographs in reptiles

The assessment of radiographs for reptile patients follows the same criteria used in mammals; however, disease abnormalities typical for reptiles should be taken into consideration (e.g. bony changes due to inadequate husbandry and nutrition). A comprehensive knowledge of the anatomy typical for reptile patients commonly treated in veterinary hospitals is a prerequisite for radiographic image assessment. Within the context of this book and in the explanation of the respective figures, only the functionally important anatomical structures will be discussed; for specific details of other structures please refer to reference texts.

The protocol for interpreting a radiographic image should follow the investigator's own personal experience and habits. Radiographic interpretation is also dictated by the information gained from the physical examination and diagnostic test results. With that said, the protocol sequence and weighting given in the following chapters serve to list the most important points when radiographing reptile patients.

3.1.4.1 Radiograph quality (exposure, contrast, positioning)

The contrast in the radiographic image of a reptile patient is often weak in comparison to other animal groups veterinarians treat (e.g. dogs, cats). The weak contrast of the image may be caused by a number of factors including the animal's thick skin or shell, which causes summation thereby leading to problems with interpretation. Furthermore, the body cavity is not divided into a thorax and abdomen in the majority of reptile species commonly radiographed. The fat is deposited in fat bodies which lie between the internal organs, making differentiation of these structures difficult. Detail recognition can also be reduced when the animals cannot be placed directly in contact with the cassette due to their positioning or anatomy. In such cases, the scattering of the x-ray beam has a negative effect on the picture quality as it passes through the body. Finally, there may be severe summation – especially in the region of the limbs – due to the animal's anatomy. Even increasing the darkness of the radiograph may not be adequate in these regions (e.g. areas around the limbs) to enhance the quality of the image.

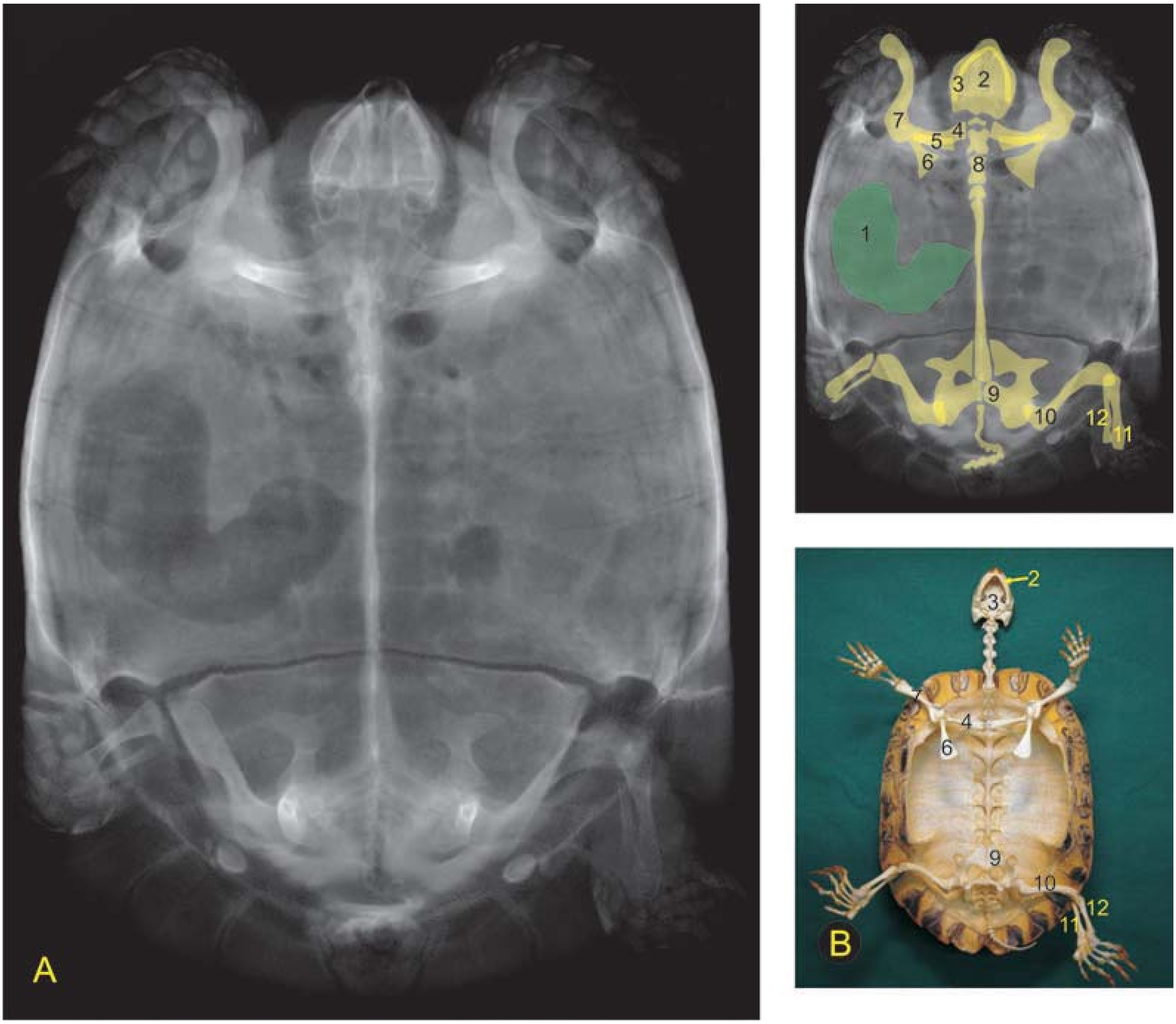

Fig. 3-10:

A: Total body radiographic image of a spur-thighed tortoise (*Testudo graeca*), dorsoventral projection.

B: Model of a aquatic chelonian skeleton for anatomical comparison.

1: stomach
2: cranium
3: mandible
4: acromion
5: scapula
6: coracoid
7: humerus
8: cervical vertebrae, number of projections as the head is retracted
9: pelvis
10: femur
11: tibia
12: fibula

3.1.4.2 Assessment of the skeleton and musculoskeletal system

The reptile skeletal system is important to assess because abnormalities due to improper husbandry and feeding are associated with arguably the most common disease diagnosed in reptiles (Metabolic Bone Disease, MBD). The overall bone density should be determined for all reptile patients. Bone density is evaluated in snakes using the ribs, in lizards the limbs and in chelonians the shell, pectoral girdle and/or pelvis. The long bones should be clearly visible and have a well defined cortex and medulla. Calcium deficiency in young animals causes disturbances in the bone metabolism leading to a thickening of the cortex, while in adults it induces a thinning and decalcification. In the shell, there is a »moth-eaten« appearance due to the presence of excessive amounts of connective tissue. Often the convex line of the carapace is no longer present as the vertebral column folds and two humps form at the location where the spine is supported by the pectoral girdle or the pelvis. The ribs and the long bones can also fold or bend.

The radiographic image of a reptile patient should also be examined for the possible presence of soft tissue calcification and osteolytic processes. The latter changes occur mainly due to infections and may involve the joints. Fusion of the spine occurs quite frequently in lizards and snakes, also as a primary result of infectious disease.

The assessing of the age of a reptile fracture can be difficult because the healing process can take a very long time. Frequently, connective tissue reactions are also involved in reptile fracture repair, which calcify at a very late stage, if at all. Complete healing of a reptile fracture may take up to 6 months.

3.1.4.3 General assessment of the internal organs

The position and size of each of the internal organs in the reptile patient being examined is dependent on the size of the surrounding organs and its nutritional status. Also large differences in the position of the internal organs can be associated with the activity of the genital tract in female animals. In addition, many lizards inflate themselves with air as part of their defensive behavior, thereby greatly enlarging the respiratory tract. In inactive chelonians, the lung field can be approximately 30–50% the height of the body cavity in the lateral projection **(Figs. 3.14** and **3-15)**. The fat bodies extend from the caudal part of the body cavity and in obese animals, these structures can cause a cranial displacement of the digestive organs. Examples of the typical organ position in clinically normal reptiles are shown in **Figures 3.8** and **3.9**.

3.1.4.4 Evaluation of the individual organ systems

The following factors should be taken into consideration when radiographically evaluating the internal organs of a reptile patient: size, homogeneity, outline, position, and if applicable, the contents.

When assessing the **gastrointestinal tract** in reptiles, one must consider that the transit time of ingesta, especially in herbivorous species, is very long. Also, in snakes the feeding intervals are much longer than in the majority of other animals that one may radiographically assess. As a consequence, the degree of ingesta filling the digestive system can have significant variation. A small amount of air in the stomach and intestinal tract should be considered a normal finding. The stomach can be identified as an anatomic structure found primarily lying on the left side of the coelom due to its air or fluid contents **(Figs. 3-10** and **3-18)**. In green iguanas (*Iguana iguana*), the fermentation region in the hindgut is often clearly identified next to the stomach, but differentiating this area from the stomach can be difficult.

The intestinal tract of reptile species is much shorter than in their mammalian counterparts. One should examine for the presence of foreign bodies (e.g. sand, stones), although these are normally present in small amounts in chelonians and lizards **(Fig. 3-15)**. However, intestinal foreign bodies can pose a problem (e.g. constipation) depending on their size and quantity.

The pancreas is routinely not visible and differentiation of the liver is difficult. The first indication of hepatomegaly is a caudal or caudodorsal displacement of the gastrointestinal tract. The exact delineation of the liver can only be observed radiographically after the administration of a contrast agent.

The inactive **genital tract** of reptile species, in most cases, cannot be identified radiographically. Even active testicles and ovaries that are normal are difficult to identify. Eggs in the oviduct may be recognized as round or oval soft-tissue structures **(Figs. 3-16, 3-22** and **3-26)**, though they may be difficult to identify, especially in the early stages of development before mineralization is complete. This is especially true in reptile species that normally produce soft-shelled eggs (Table 3-3).

Normal eggs can occupy a large amount of space in the coelomic cavity resulting in an almost complete displacement of the internal organs; in lizards, the eggs may extend to the region of the heart. Unmineralized or slightly mineralized eggs are difficult to differentiate from follicular cysts, which are the underlying cause of the so-called »pre-ovulatory« egg binding. However, such follicles can reach a size that is far larger than the normal egg **(Fig. 3-23)** and can fill most of the coelomic cavity. If there are any concerns about the identity of egg development, then the use of ultrasonography to differentiate the structures it is strongly recommended because treatment is different for egg binding and »pre-ovulatory« egg binding.

Table 3-3: Hard- or soft-shelled eggs in reptiles.

Snakes	soft
Lizards	mainly soft exceptions: crocodiles, some gecko species
Chelonians	terrestrial species, some terrapins: hard others: soft

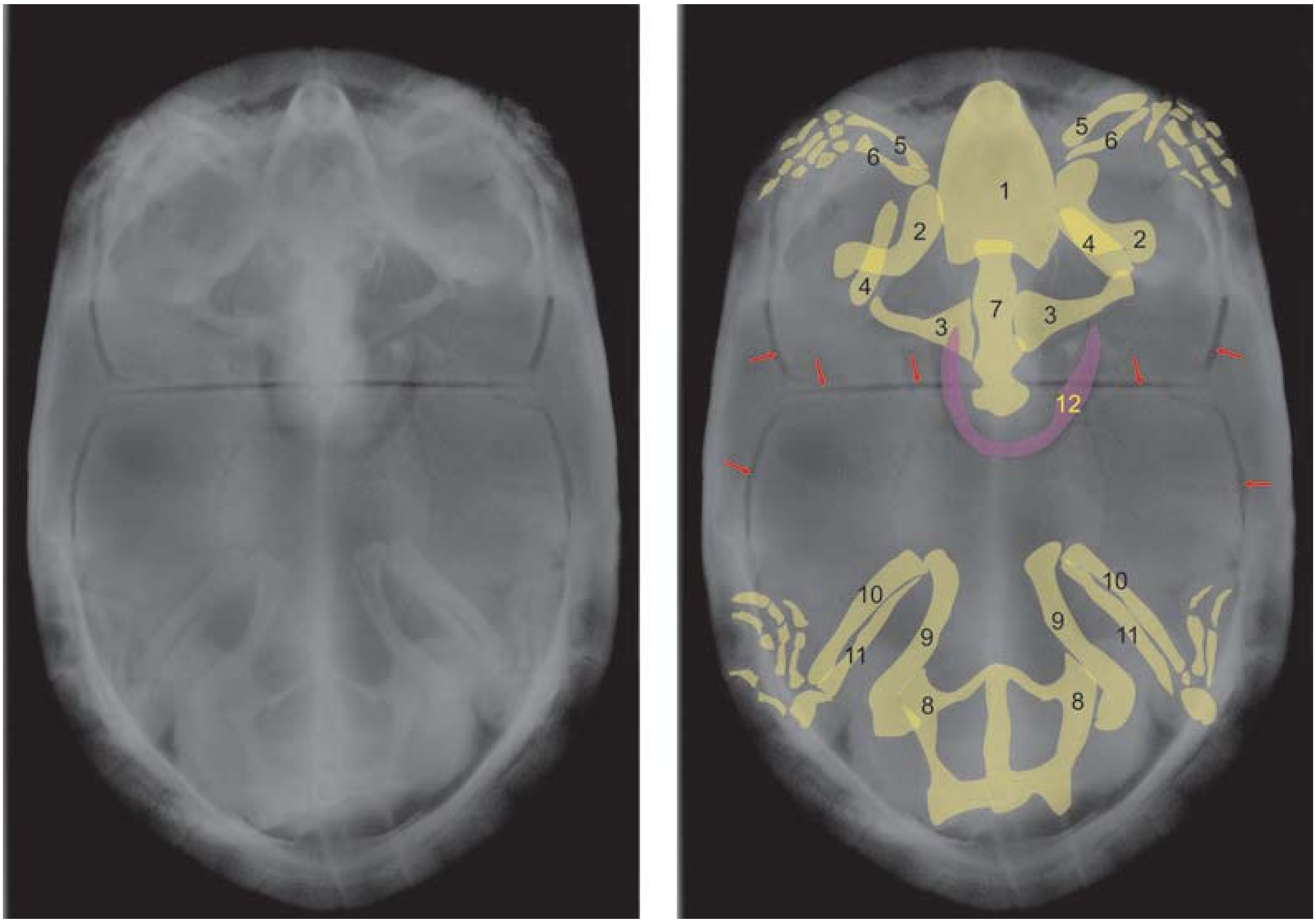

Fig. 3-11: Total body radiographic image of a terrapin (*Terrapene* sp.), dorsoventral projection. The cranial and caudal scutes can be pulled together by a movable hinge (red arrows).

1: cranium
2: humerus
3: coracoid
4: scapula
5: radius
6: ulna
7: cervical vertebrae, numerous projections
8: pelvis
9: femur
10: tibia
11: fibula
12: area of air around the retracted neck

The most remarkable radiographic findings in the **urinary tract** of reptile patients are uroliths. Uroliths occur primarily in chelonians and lizards. As the allantois can reach a large size in chelonians, uroliths are often found in the middle of the coelomic cavity. Paralysis of the allantois is, in comparison, difficult to diagnose radiographically; it is mainly associated with a craniodorsal displacement of the intestinal tract. If significantly enlarged, the craniocaudal region of the kidneys are visible in lizards. Confident radiographic identification of the kidneys is difficult in snake and chelonian species.

The assessment of the reptile **respiratory tract** includes the airways **(Figs. 3-12** to **3-14)**. The most significant diagnostic changes observed in the reptile respiratory tract are narrowing, focal or diffuse densification and, more rarely, foreign bodies. The lateral projection taken with a horizontal beam is recommended for the assessment of the respiratory tract in all reptiles. In some studies, positive-pressure ventilation under general anesthesia has been recommended in lizards and snakes to examine their lungs.

The trachea bifurcates in an extreme cranial position in chelonians and assessability to this structure depends on the position of the patient's head and neck. The lung field should be approximately 30–50% of the patient's body cavity height in chelonians when the lateral projection is viewed. In the craniocaudal projection, special attention should be paid to the symmetry of the right and left lung fields **(Fig. 3-12)**. Summation by the cranial and caudal carapace must be differentiated from other areas of the patient that are radiopaque.

When assessing lung structures, it should be noted that a reptile's lung structure is different than mammals. In snakes and the majority of lizards, the lungs are rather sac-like in their anatomical configuration, while in chelonians they have muscular trabeculae running through the tissue and are often more septated. In snakes, the lung field in the lateral or DV projection appears as an elongated tube in which the respiratory epithelium can be identified **(Figs. 3-24** and **3-25)**. The respiratory epithelium becomes thinner as it extends caudally. In the cranial region, a large blood vessel courses through the lung field in a ventral to dorsal direction. Certain reptile species (e.g., pythons) have two lungs, whereby the left lung is much smaller than the right. The air sacs are attached seamlessly to the caudal part of the lung and vary greatly in their size due to the influence of the surrounding organs.

The lung field can be also identified radiographically in lizards **(Fig. 3-21)**. Some reptile species also have air sacs. The size of the lung can vary greatly if defensive behavior takes place by the patient (e.g. inflation of the body with air). The radiographic diagnosis of anomalies in the lung tissue is usually difficult and limited to severe densification. Computed tomography offers a much better diagnostic potential than radiographs for lung field evaluation.

When assessing the **cardiovascular system**, the heart is a poorly observed structure situated in the cranial part of the coelomic cavity in chelonians and lizards. In snakes, the heart lies roughly at about 25% of the body length, and is often externally visible due to its muscular contractions. In the majority of lizard patients, the heart is relatively small and lies in an extreme cranial position **(Figs. 3-20, 3-21** and **3-30)**. In monitors, the heart lies more caudally and is much bigger. Enlargement of the heart shadow can be caused by effusions, cardiomegaly, and tumors. In snakes, the size and perfusion of the heart depends on the when the animal was fed. In general, radiographic examinations are limited in their use for diagnosing heart disease and if there is any suspicion of heart disease then ultrasonography should be performed. Atherosclerosis can occur in reptile species, especially in lizards.

Unique anatomic structures that can be radiographically identified in many gecko species are the so-called **endolymphatic sacs** or »chalk« sacs. These structures are located in the throat and can be identified in radiographic images as radiopaque structures **(Fig. 3-32)**. These calcium storage organs are not gender-specific and their size depends on the animal's calcium supply, though their presence does not mean that calcium deficiency can be ruled out.

3.1.4.5 Standard radioanatomy

Radiographic projections of clinically healthy reptiles are found in **Figures 3-10** to **3-32**. It should be noted that extreme anatomic differences can occur in healthy animals due to differences in species, age, and husbandry.

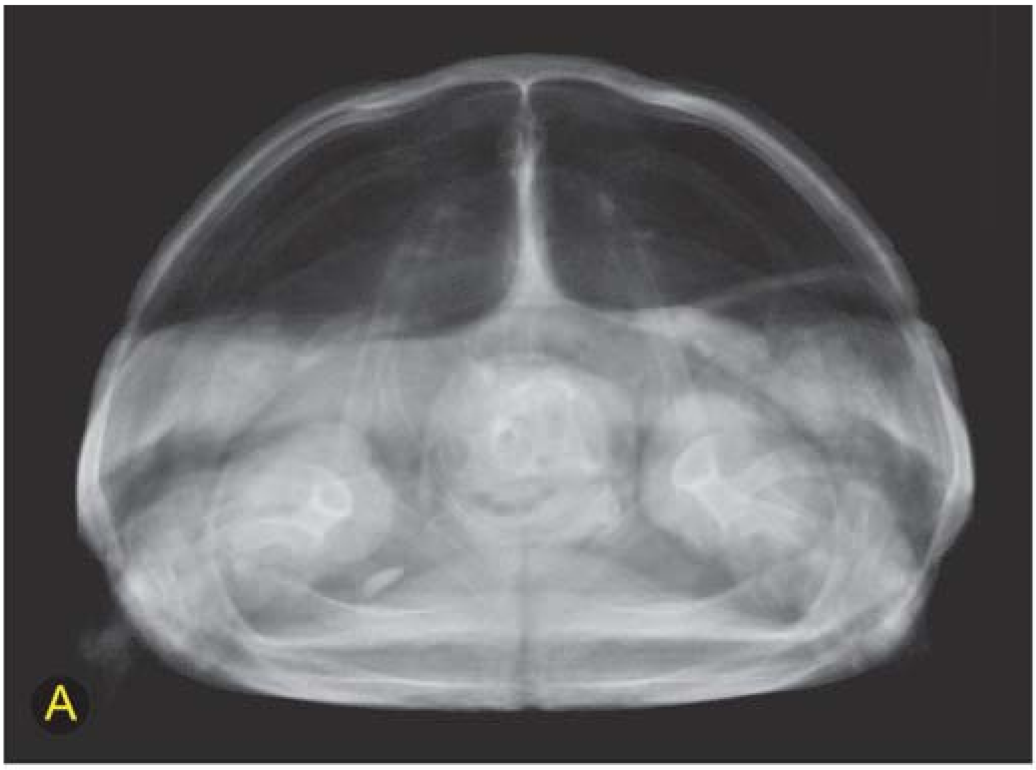

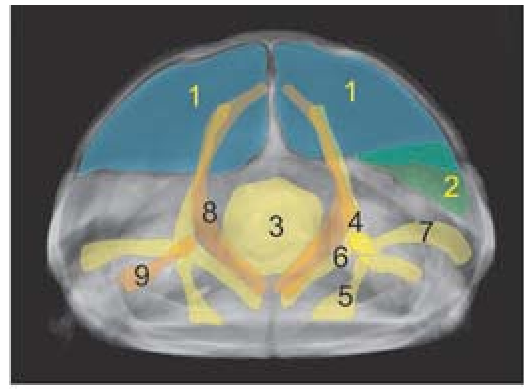

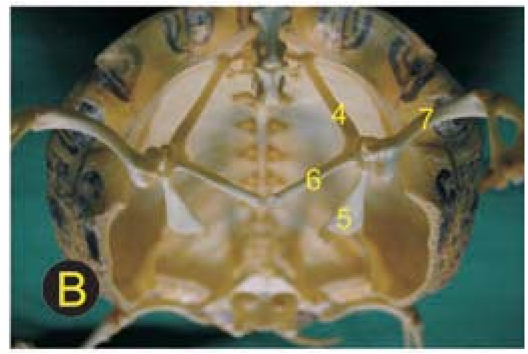

1: lung field
2: stomach
3: cranium
4: scapula
5: coracoid
6: acromial process of the scapula
7: humerus
8: pelvis
9: femur

orange: pelvic bones

Fig. 3-12:

A: Total body radiographic image of a Russian tortoise (*Testudo horsfieldii*), cranio caudal projection. In this projection, there is a great deal of summation of the bones comprising the pectoral girdle, forelegs, pelvis, and hindlegs.

B, C: Model of an aquatic chelonian skeleton for anatomic comparison, (B) pectoral girdle and (C) pelvis (ventral view).

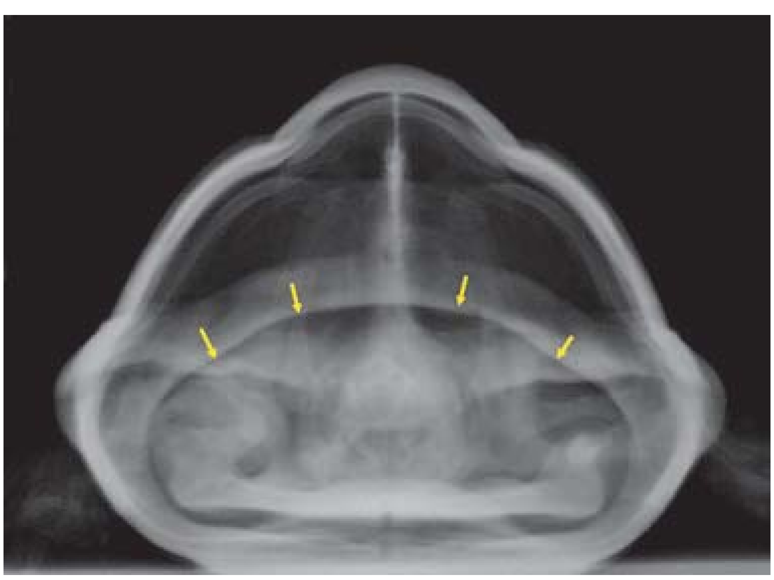

Fig. 3-13: Total body radiographic image of a spur-thighed tortoise (*Testudo graeca*), cranio caudal projection. The height of the lung field should be roughly 1/3 or 1/2 of the body cavity height. The cranial opening of the shell (arrows) is usually projected into the lung field.

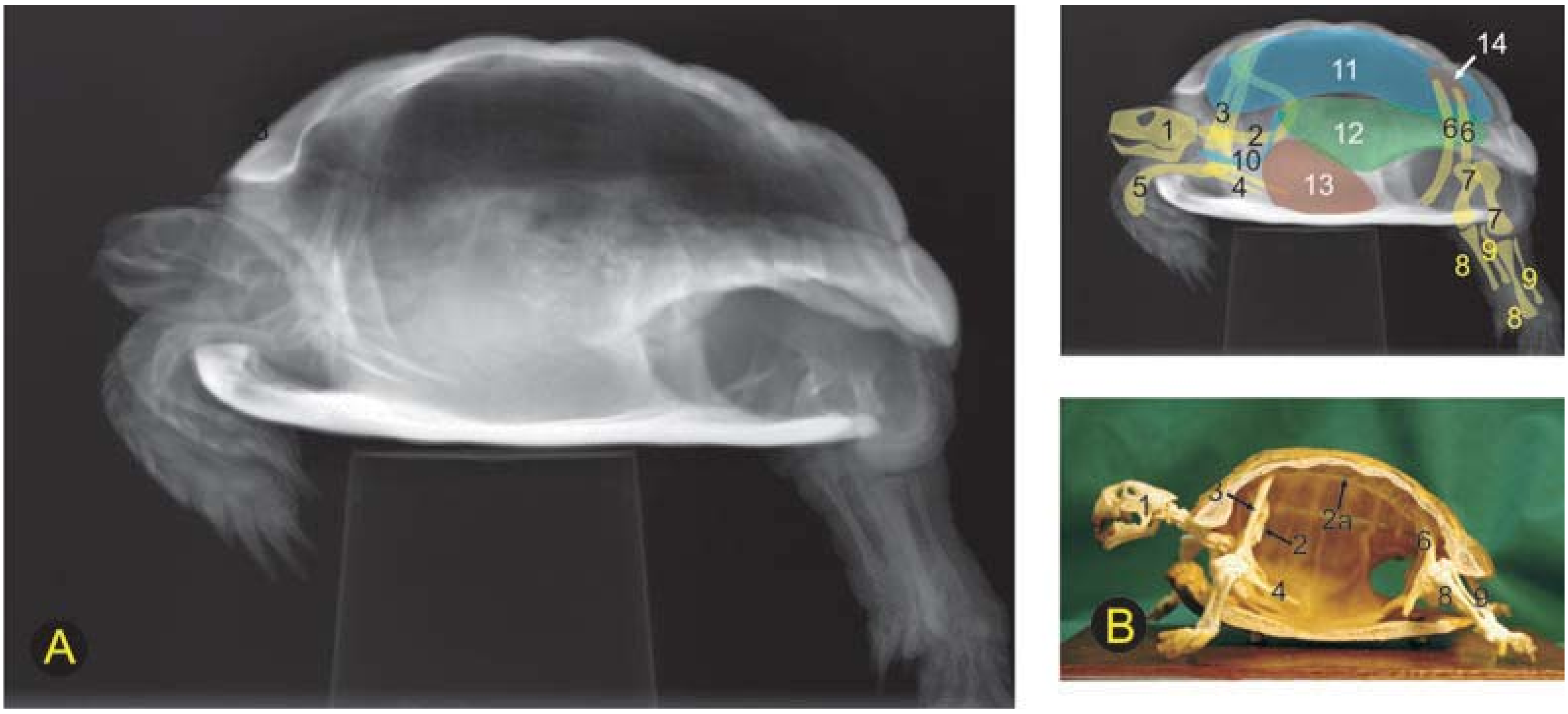

Fig. 3-14:

A: Total body radiographic image of a Russian tortoise (*Testudo horsfieldii*), lateral projection. By elevating the animal (a plastic beaker is used in this case), the limbs usually extend from under the shell making image interpretation easier.

B: Model of a terrestrial chelonian skeleton for anatomic comparison.

1: cranium and mandible
2: cervical vertebrae
2a: spine
3: scapula
4: coracoid
5: humerus
6: pelvis
7: femur
8: tibia
9: fibula
10: trachea
11: lungs
12: liver
13: gastrointestinal tract
14: kidneys

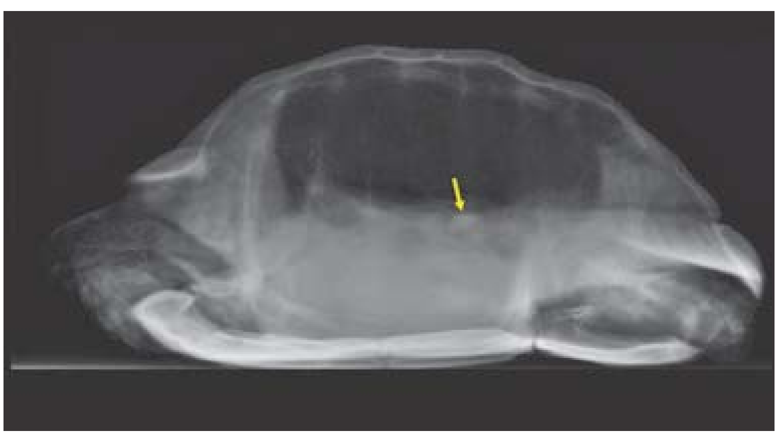

Fig. 3-15: Total body radiographic image of a Hermann's tortoise (*Testudo hermanni*), lateral projection. A small quantity of stones (arrow) in the gastrointestinal tract should be considered a normal finding. Large quantities of stones in the gastrointestinal tract may indicate a condition of malnutrition (calcium deficiency).

(Fig. 3-17:) ▶
1: cranium
2: cervical vertebrae
3: scapula
4: coracoid
5: acromion
6: humerus
7: radius and ulna
8: plastron
9: pelvis
10: femur
11: tibia and fibula

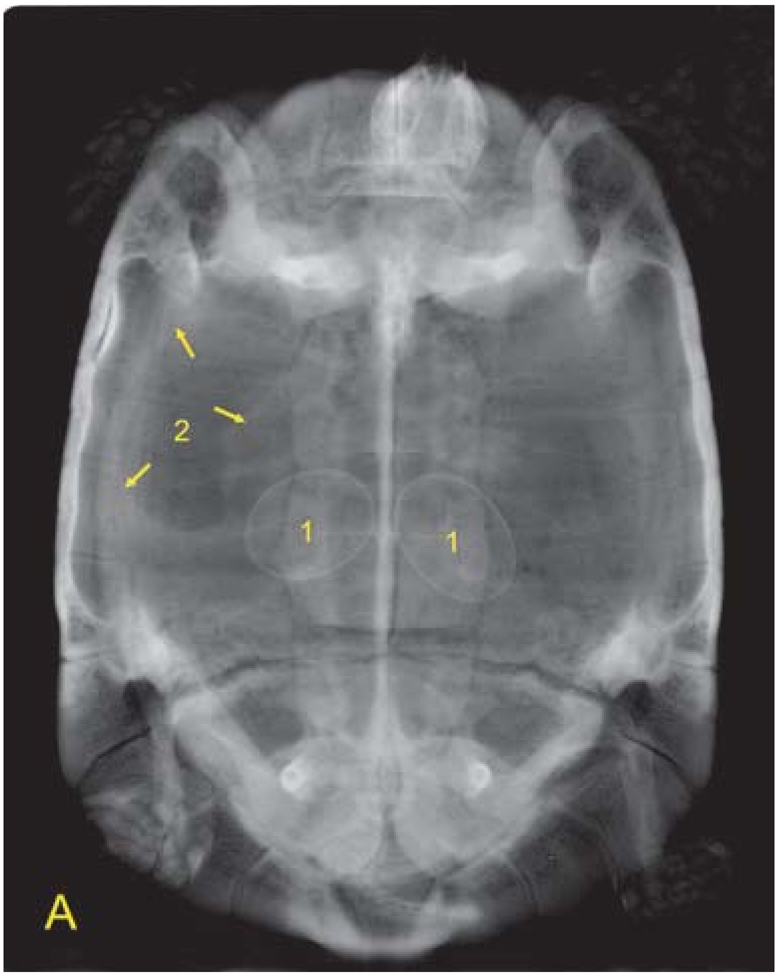

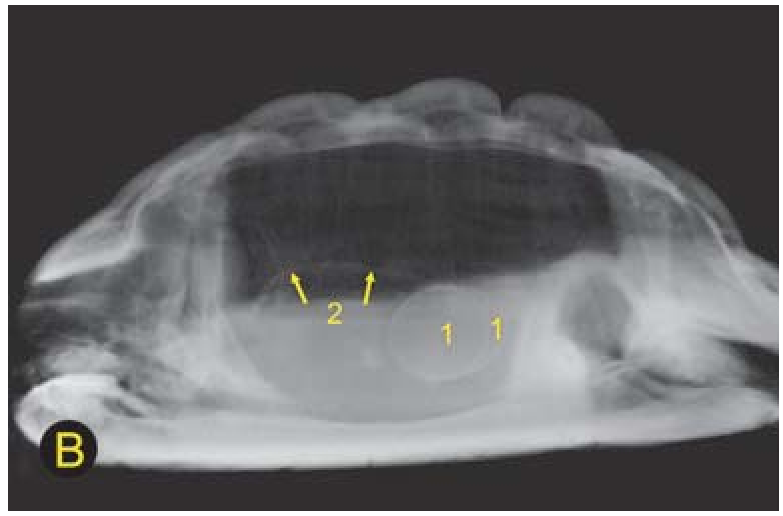

1: egg
2, arrows: stomach

Fig. 3-16: Total body radiographic images of a Hermann's tortoise (*Testudo hermanni*), (A) dorsoventral and (B) lateral projections: (1) normal egg production.

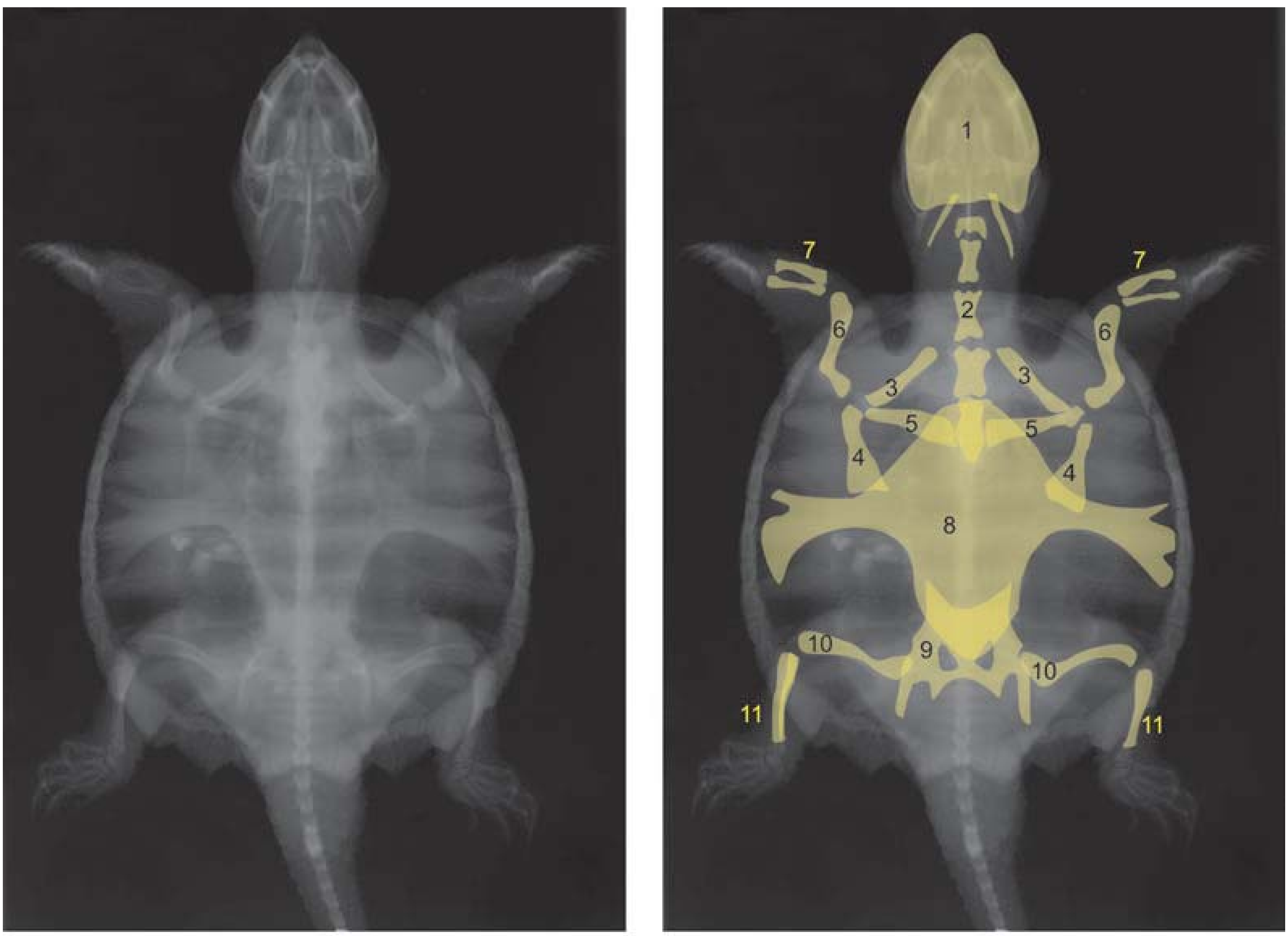

Fig. 3-17: Total body radiographic image of a common snapping turtle (*Chelydra serpentina*), dorsoventral projection. The bony structure is essentially different from than that found in terrestrial chelonians.

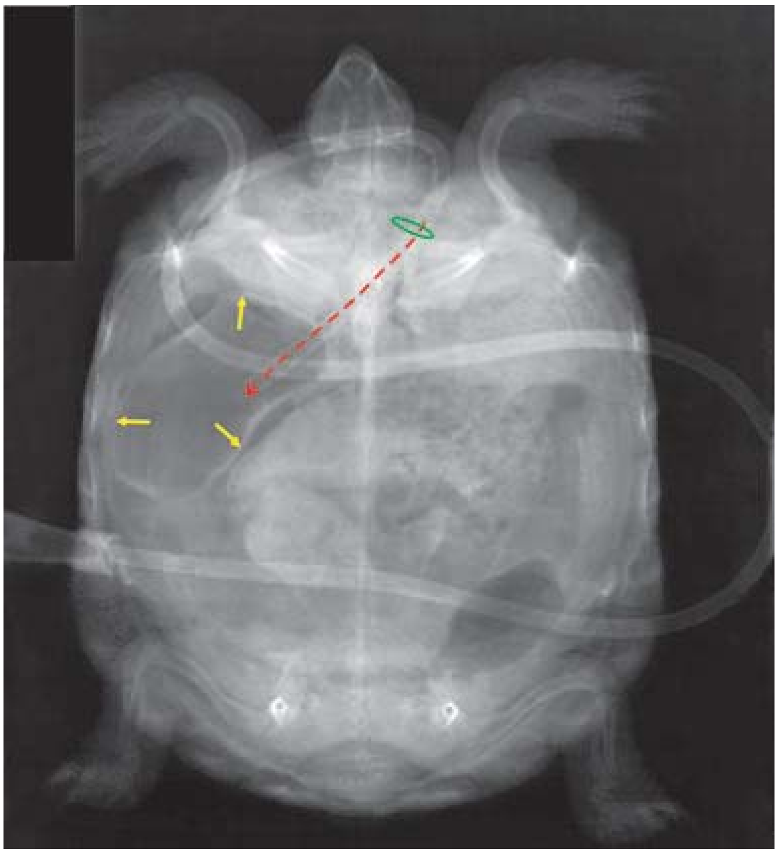

Fig. 3-18: Total body radiographic image of a Russian tortoise (*Testudo horsfieldii*): assessing the position of a permanent gastric tube (dotted red line), dorsoventral projection. The gastric tube was placed through the right side of the neck (green circle) in the esophagus and then pushed into the stomach after which it was attached to the carapace. The position of the tube in the stomach (yellow arrows) can be radiographically evaluated.

Fig. 3-19: Total body radiographic images of a red-eared slider (*Trachemys scripta elegans*) after the administration of barium sulfate (350 mg/ml, 20 ml/kg bwt in the stomach), dorsoventral projection.

A: after 2 days,

B: after 10 days,

C: after 21 days.

After passing through the jejunum (1), the food enters the proximal colon (2) and subsequently the distal colon (3). The widening in the proximal colon is the location in which foreign bodies often collect.

1: jejunum
2: proximal colon
3: distal colon

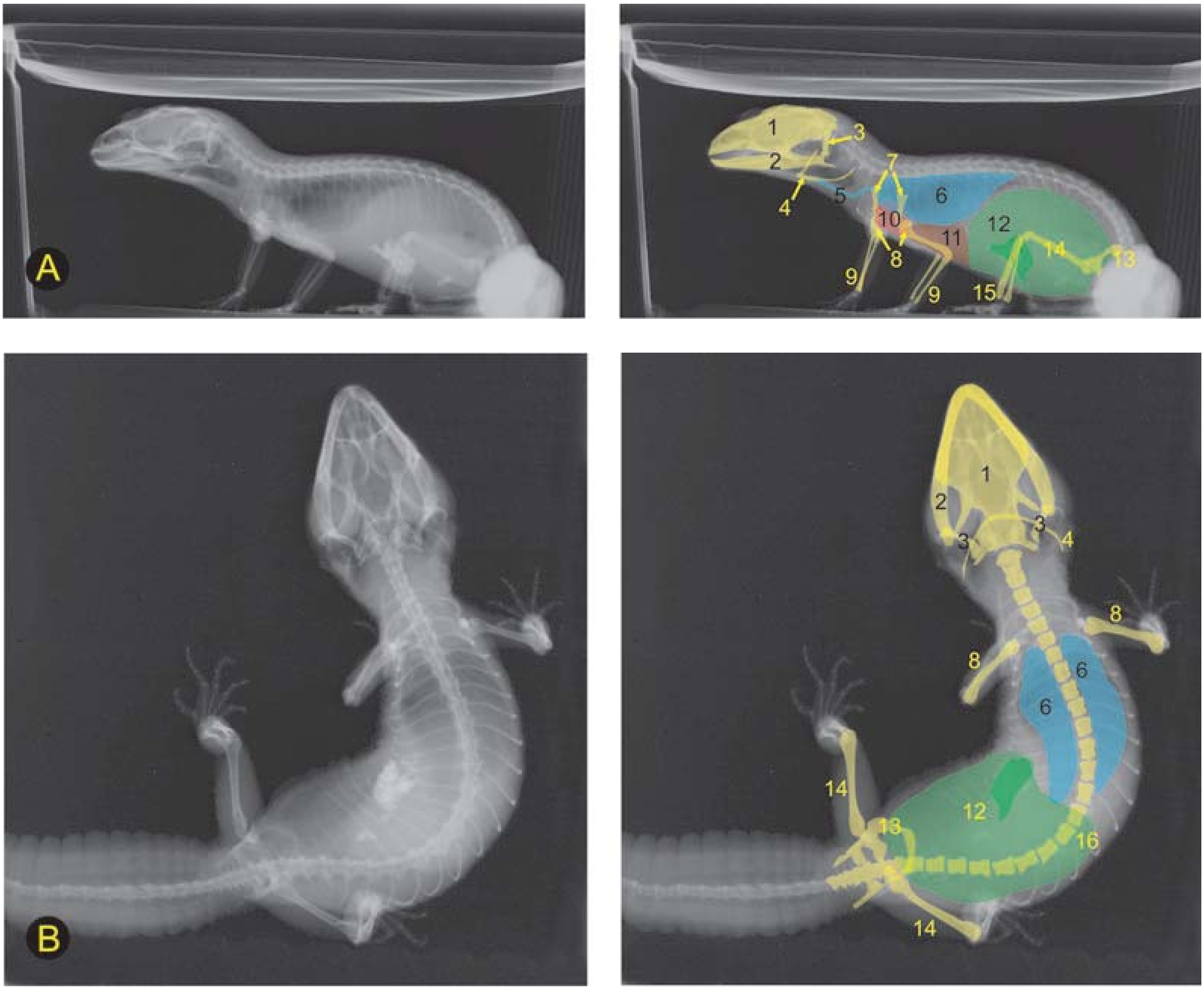

Fig. 3-20: Total bodyradiographic image of a leopard gecko (*Eublepharis macularius*) positioned in a plastic box, (A) lateral and (B) dorsoventral projections. Even the use of a radiolucent box does not allow for optimal positioning, as noted in these radiographs. However, a box or container is an acceptable method for positioning animals that are easily stressed or have sensitive skins (e.g. geckos).

1: cranium
2: mandible
3: quadrate bone
4: hyoid bone
5: trachea
6: lungs
7: scapula
8: humerus
9: radius and ulna
10: heart
11: liver
12: stomach (stones) and intestines
13: pelvis
14: femur
15: tibia, fibula
16: spine

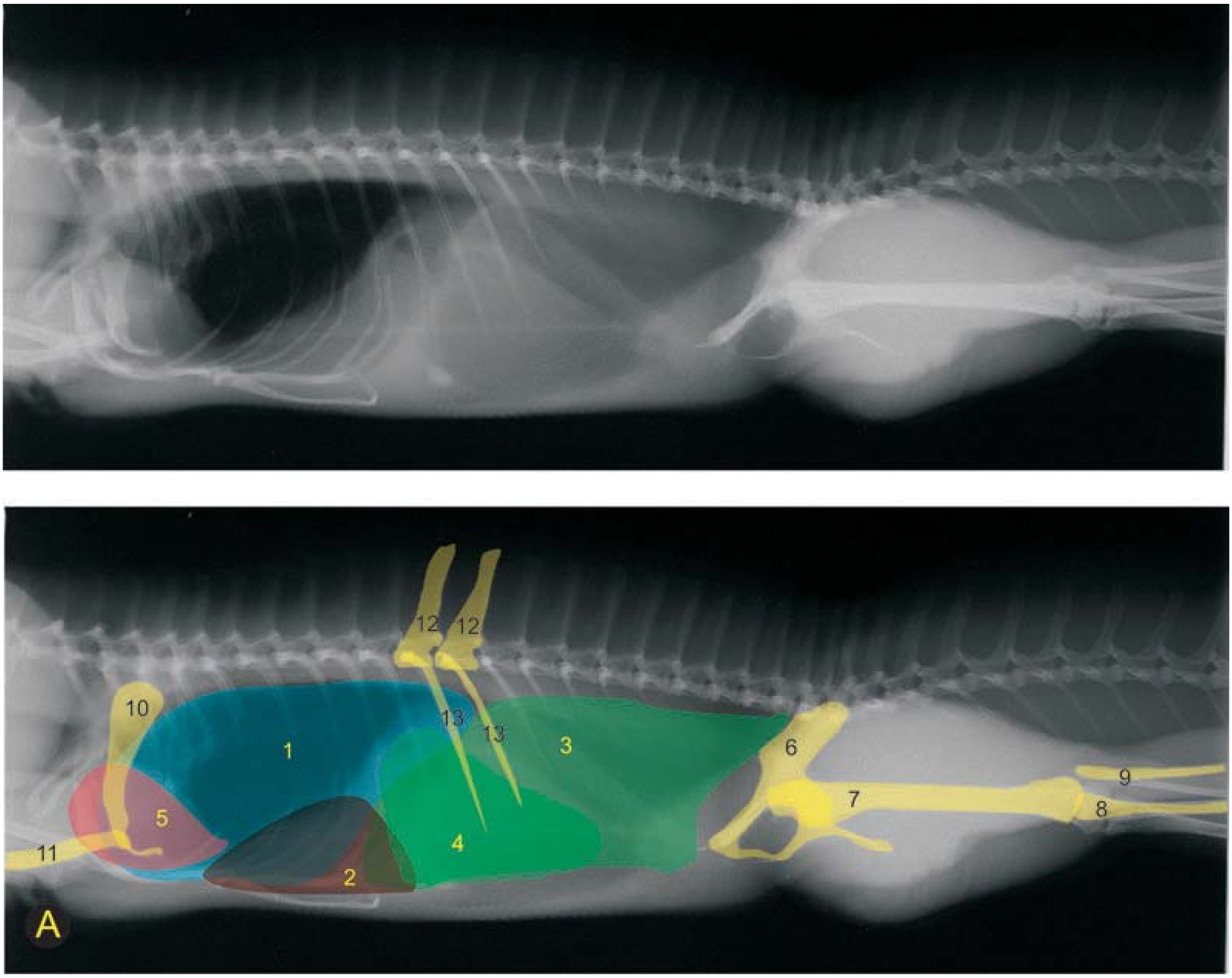

Fig. 3-21: Radiographic images of a Chinese water dragon's (*Physignathus cocincinus*) body, (A) lateral and (B) dorsoventral projections.

1: lungs
2: liver
3: intestines
4: stomach
5: heart
6: pelvis
7: femur
8: tibia
9: fibula
10: scapula
11: humerus
12: vertebrae
13: ribs

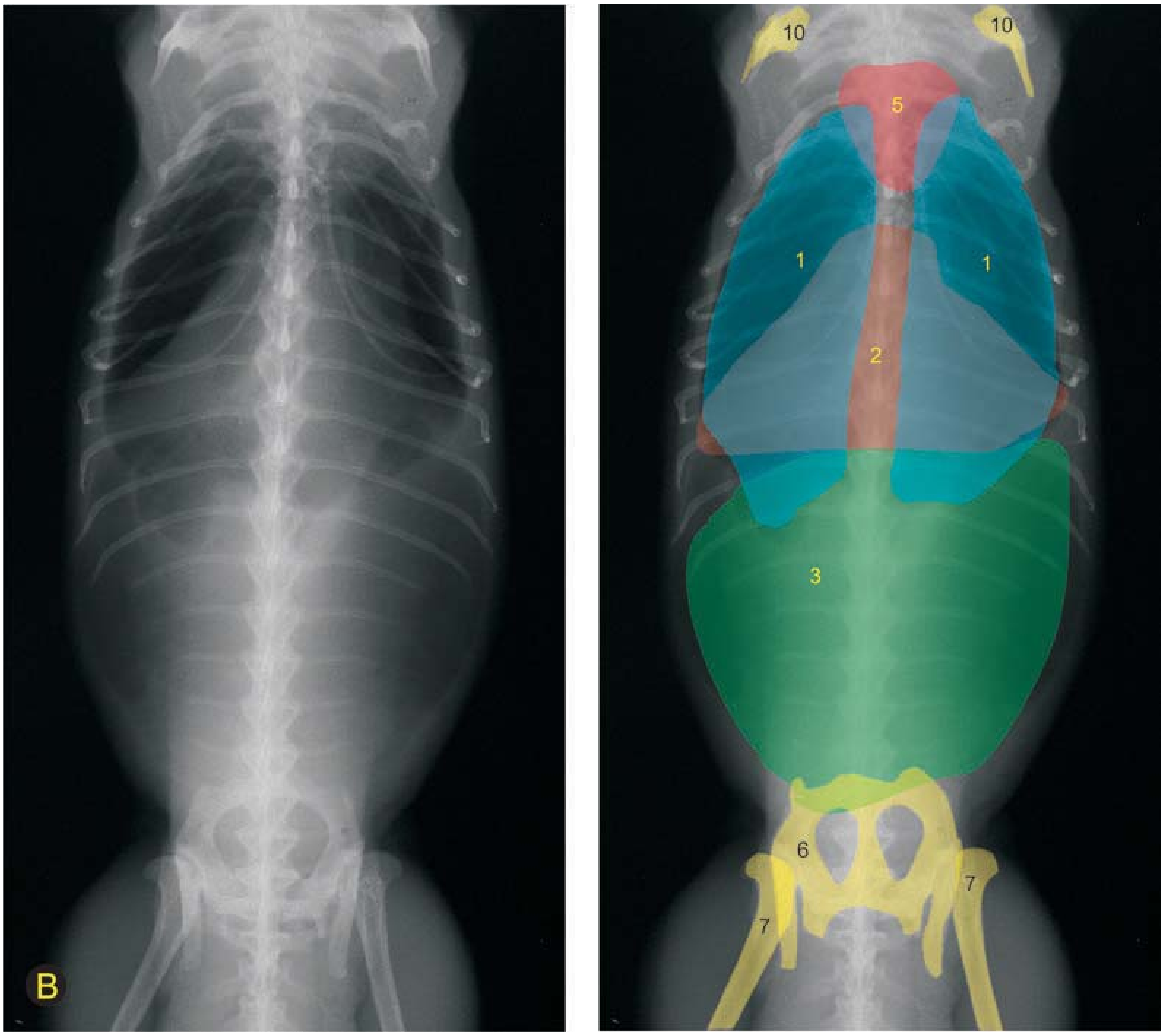
B
10
10
5
1
1
2
3
6
7
7

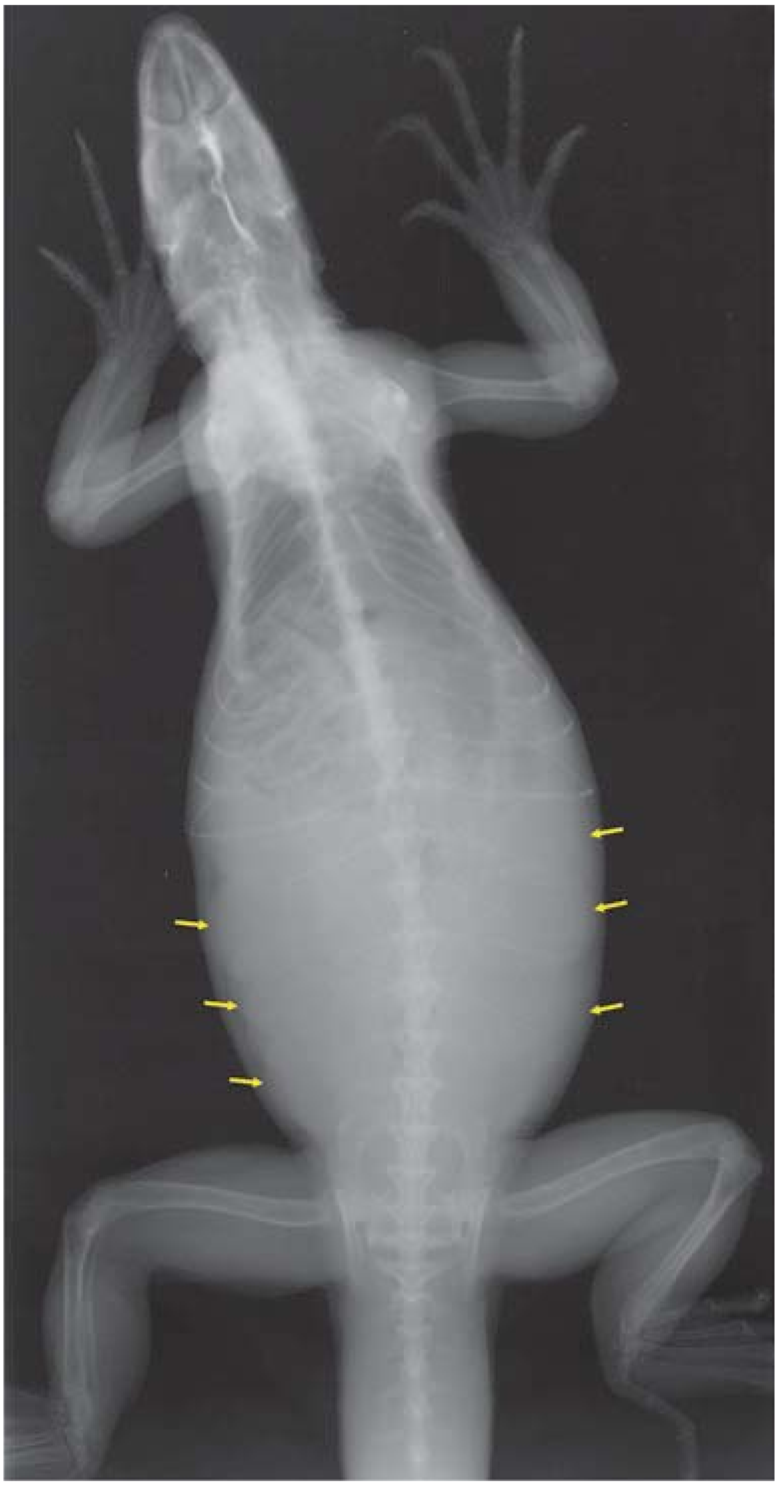

Fig. 3-22: Total body radiographic image of a green iguana (*Iguana iguana*), dorsoventral projection: normal egg production. The eggs (arrows) can fill the larger part of the body cavity. If calcification is not visible, the differentiation from follicles or ovarian cysts is often difficult and an ultrasonographic investigation should be performed to obtain a more detailed diagnosis.

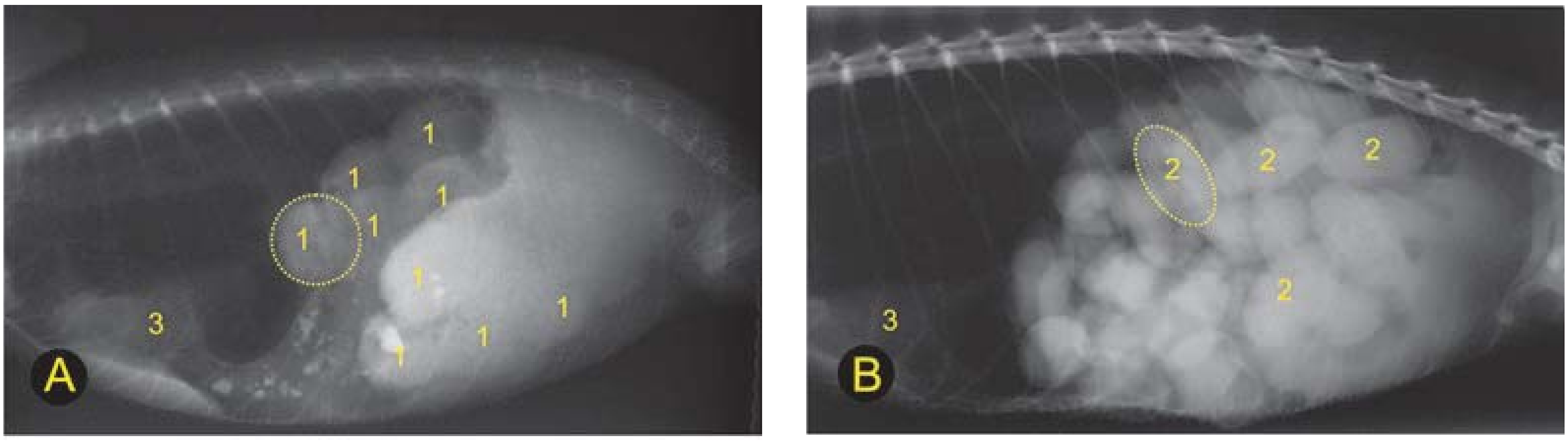

Fig. 3-23: Total body radiographic images of a veiled chameleon (*Chamaeleo calyptratus*), lateral projection.

A: Large follicles on the ovary, an abnormal finding.

B: Image of normal eggs in the body cavity. In this animal, the follicles can be differentiated because the eggs may be used for comparison.

The eggs are normal with respect to their size and shape, whereas the follicles are considered abnormal due to their exceptionally large size. In such cases, there is always concern that a preovulatory egg binding has developed.

1: follicles
2: eggs
3: liver

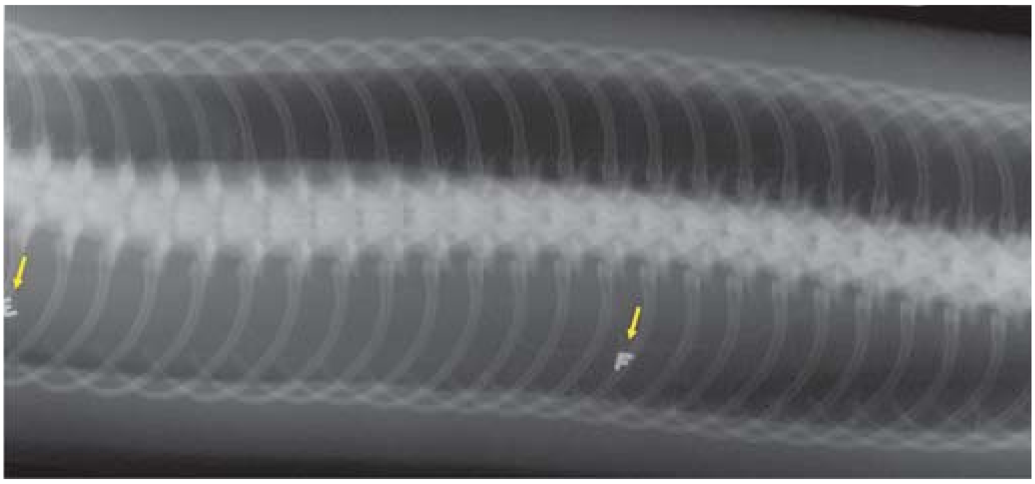

Fig. 3-24: Radiographic image of an Indian python's (*Python molurus*) body, dorsoventral projection: normal image of the lung fields. Radiodense letters (arrows) have been used to match the sections of the patient's body to the radiographic image.

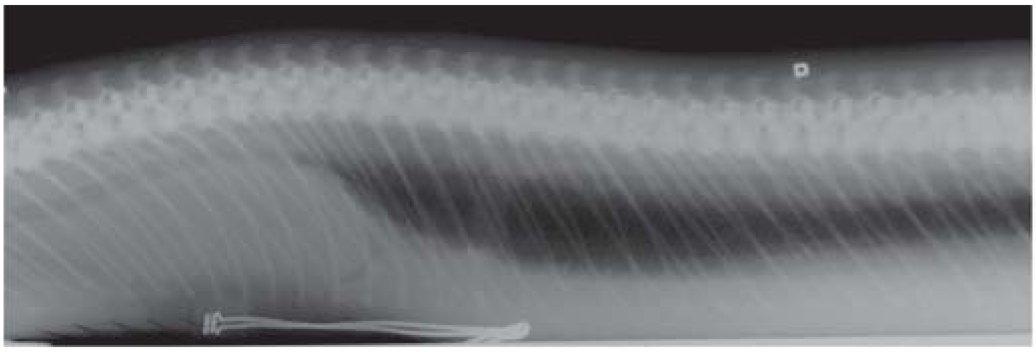

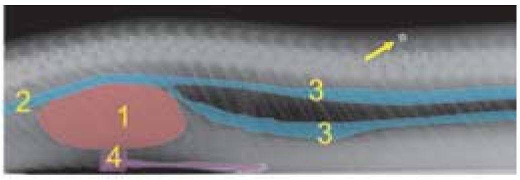

1: heart
2: trachea
3: lungs
4: ultrasonography probe

arrow: radiodense letter to match the sections of the patient's body to the radiographic image

Fig. 3-25: Radiographic image of an Indian python's (*Python molurus*) body, lateral projection: Normal representation of the lungs and the heart. A Doppler ultrasonography probe (4) has been placed in the region of the heart (1) which helps to acoustically control the animal's cardiac function while under general anesthesia. The trachea (2) merges with the lungs (3), which consist of a central lumen and a peripherally situated respiratory epithelium. The respiratory epithelium becomes thinner as it extends in a caudal direction and is no longer present in the region of the air sac.

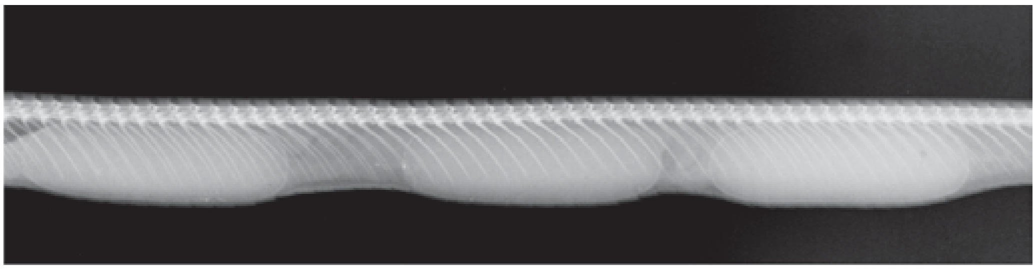

Fig. 3-26: Total body radiographic image of a corn snake (*Pantherophis guttatus*), lateral projection: Radiographic image showing three normal eggs.

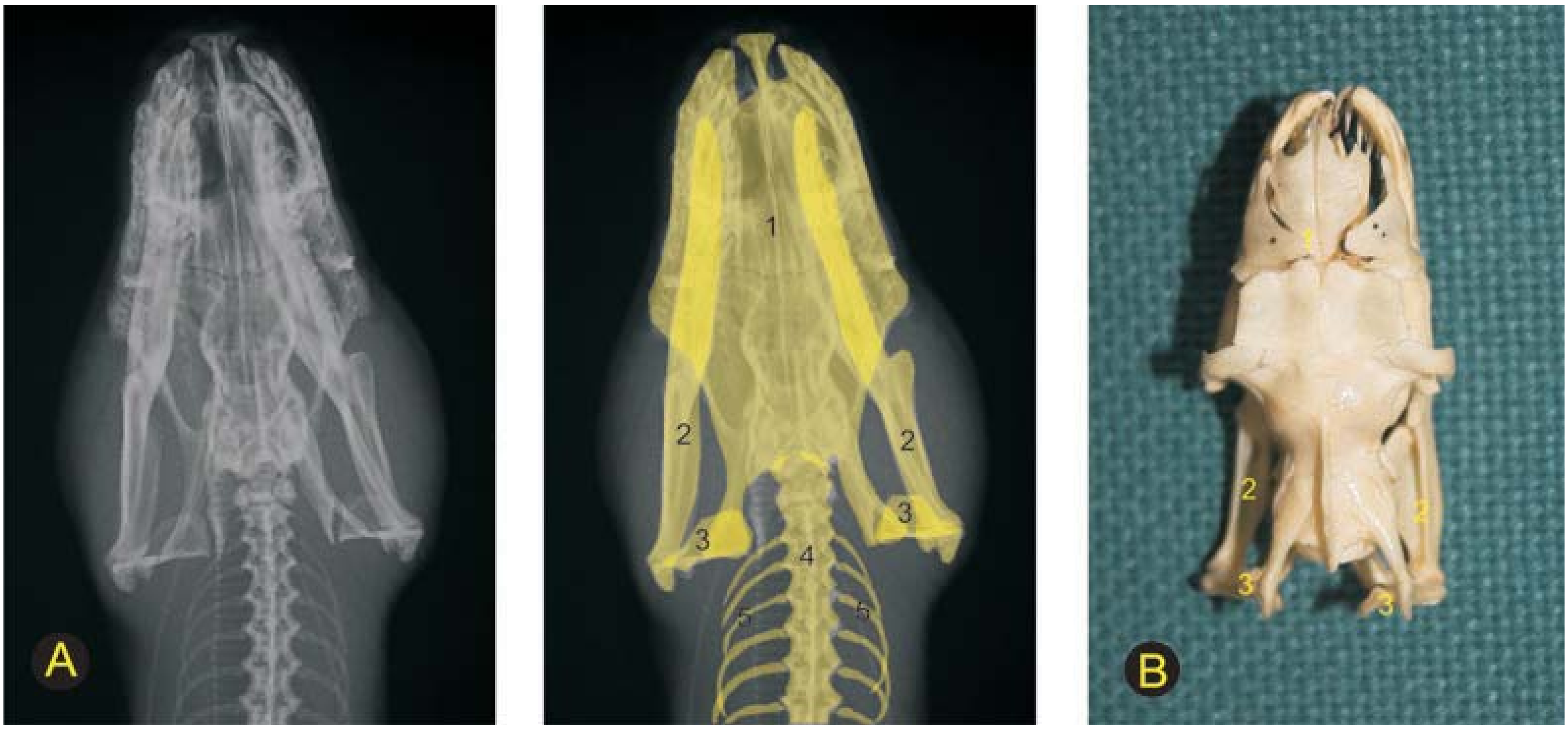

Fig. 3-27:

A: Radiographic images of a boa constrictor's (*Boa constrictor*) head, dorsoventral projection.

B: Preparation of the head of a boa constrictor for anatomic comparison.

1: cranium
2: mandible
3: quadrate bone
4: spine
5: ribs

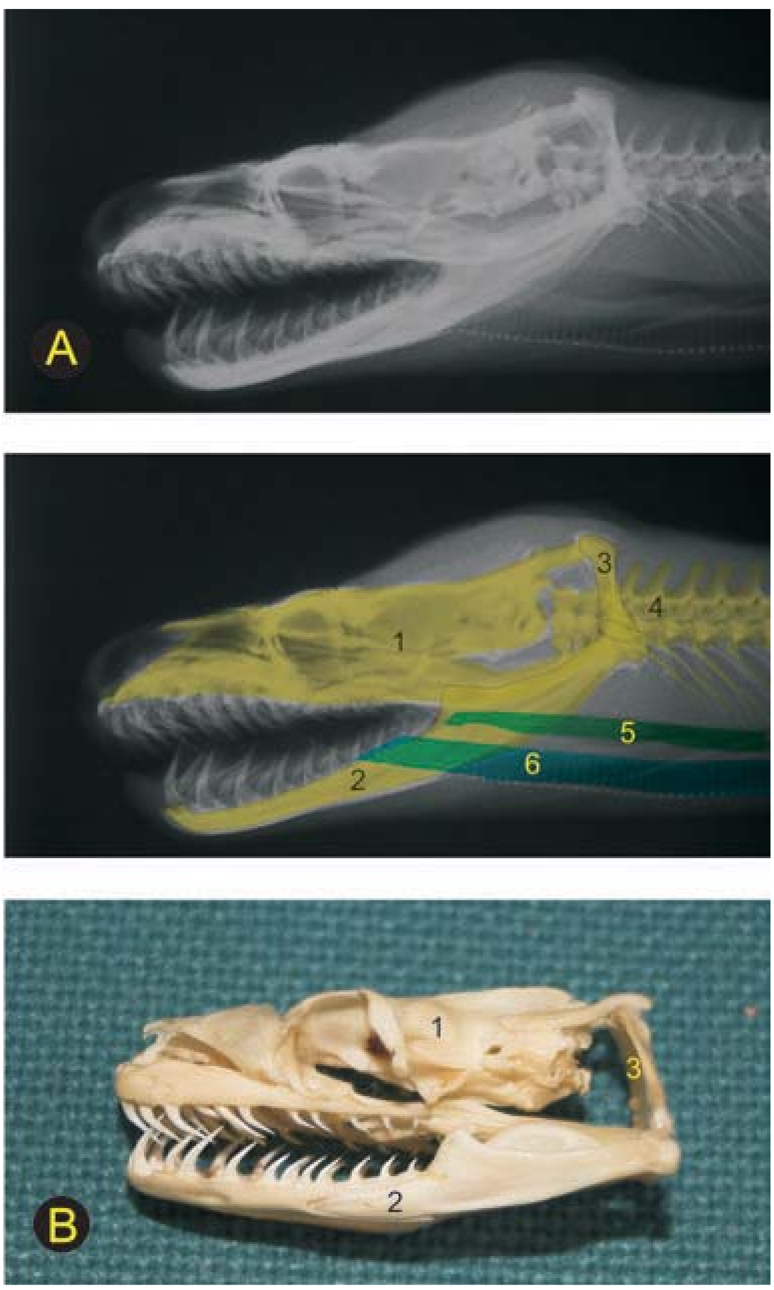

1: cranium
2: mandible
3: quadrate bone
4: spine
5: esophagus
6: trachea

Fig. 3-28:

A: Radiographic images of a boa constrictor's (*Boa constrictor*) head, lateral projection.

B: Preparation of the head of a boa constrictor for anatomic comparison.

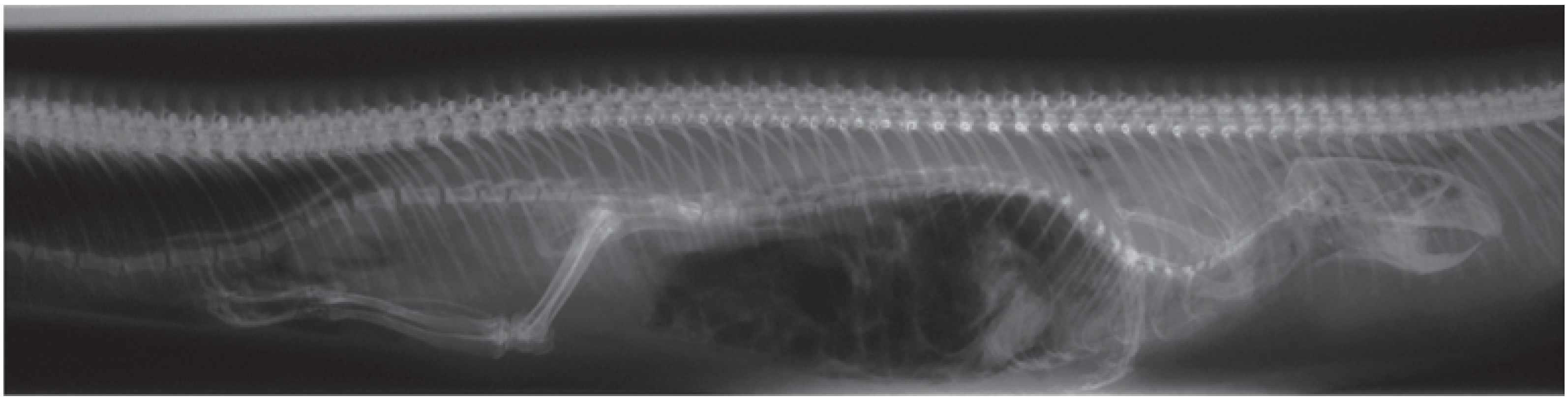

Fig. 3-29: Total body radiographic image of an Indian python (*Python molurus*), lateral projection. The body of the snake's prey (rat) can be observed in its stomach.

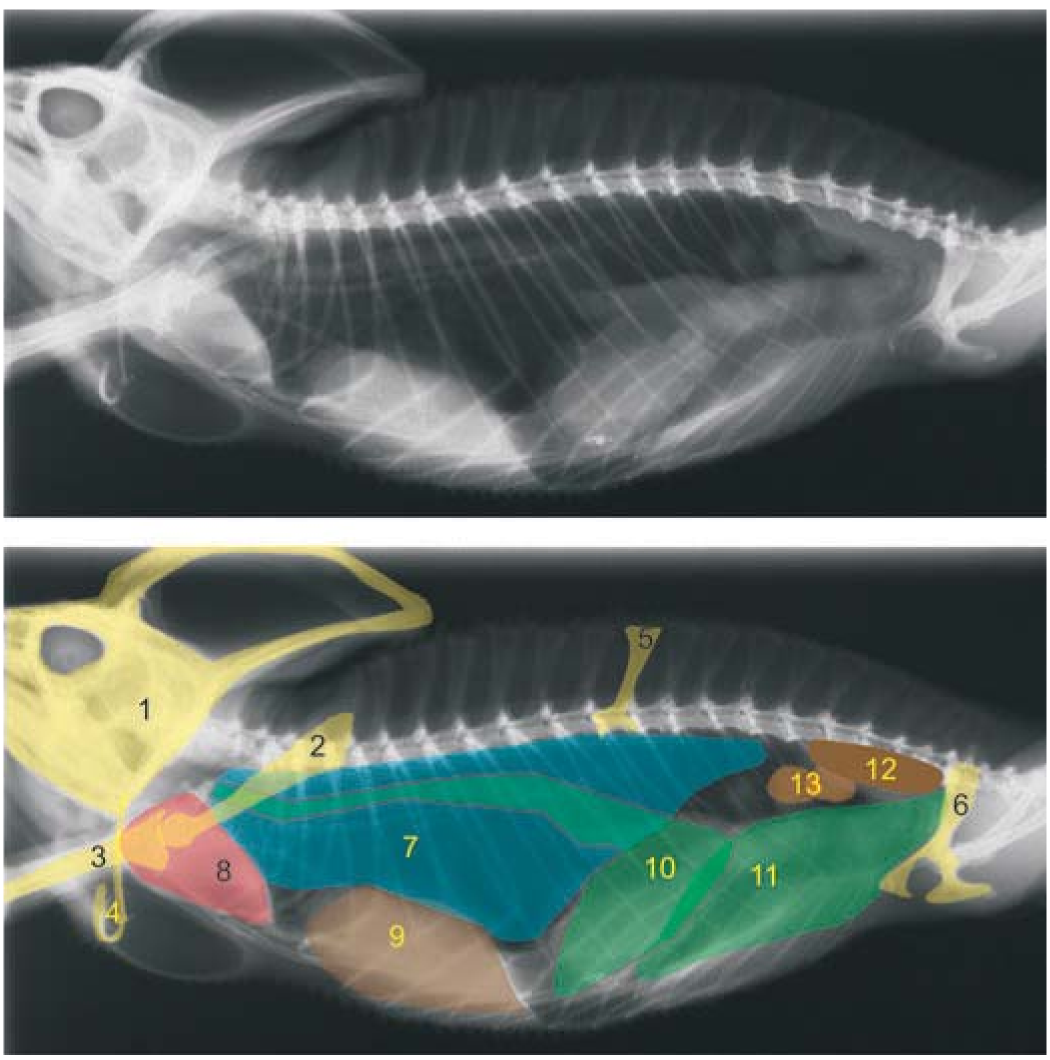

1: cranium with casque
2: scapula
3: coracoid
4: hyoid bone
5: vertebrae
6: pelvis
7: lungs
8: heart
9: liver
10: stomach
11: gastrointestinal tract
12: kidneys
13: gonads

Fig. 3-30: Total body radiographic image of a veiled chameleon (*Chamaeleo calyptratus*), lateral projection.

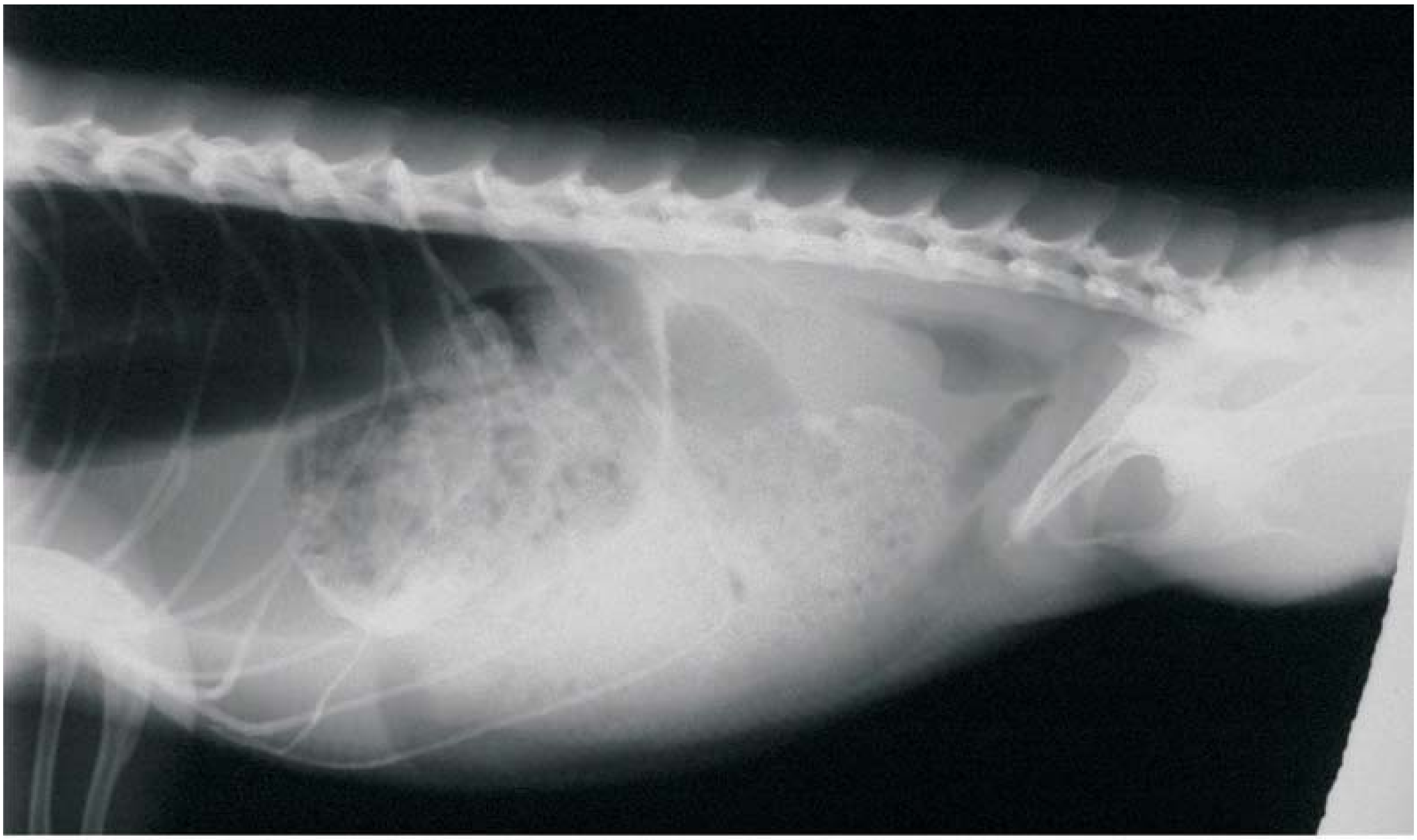

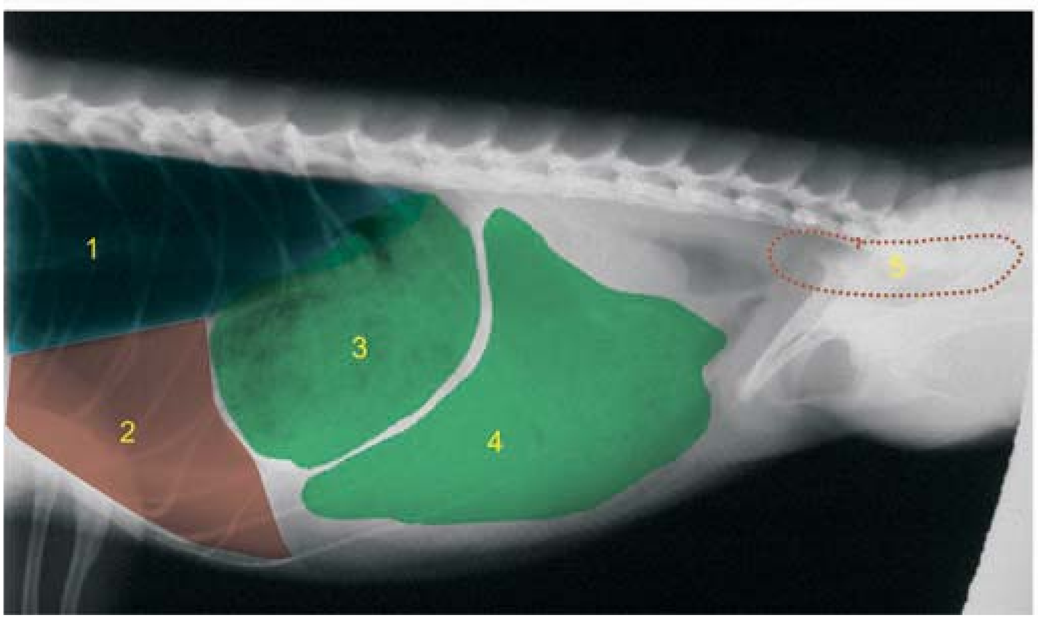

1: lungs
2: liver
3: stomach
4: intestines
5: area of the kidneys, not visible

Fig. 3-31: Radiographic image of a green iguana's (*Iguana iguana*) body, lateral projection.

1: »chalk« sacs
2: lungs
3: eggs

Fig. 3-32: Total body radiographic image of a Madagascar giant day gecko (*Phelsuma madagascariensis grandis*), dorsoventral projection, showing the endolymphatic »chalk« sacs (1), lungs (2), and eggs (3).

3.2 Ultrasonography

Michael Pees

3.2.1 Equipment

The technical development of ultrasonographic scanners has reached a point in recent years in which acceptable diagnostic capabilities are possible even when cheaper machines are used. In contrast to ultrasonographic examinations in birds, performance parameters (e.g. frame rate) play a minor role in reptile patients. Also the choice of transducer is less problematic, especially for larger lizards and snakes on which both linear and convex transducers can be used. In chelonians, the approaches for transducer placement are limited to the openings in the shell and only micro-curved transducers with a compact form can be utilized in these species. Another type of transducer that can be used to perform an ultrasonographic examination on chelonians is the so-called hockey sticks. Despite the small size of the hockey stick transducer, it can offer an excellent window **(Fig. 3-33)**. These comparatively expensive transducers, however, remain the province of specialized institutions.

The majority of ultrasonographic investigations in reptiles can be done with frequencies between 7 MHz and 12 MHz. Within this range, adequate depth of penetration of ultrasound waves through reptilian skin is achieved, while the resolution is adequate for diagnostic purposes. In larger reptile species (e.g. large chelonians, crocodiles), lower frequencies of 5 MHz or 3 MHz may be necessary to ensure a satisfactory depth of ultrasound wave penetration.

The following parameters are recommended by the author as standard equipment for performing ultrasonographic investigations in reptiles:

- ☐ a linear transducer with a frequency between 7 MHz and 10 MHz (ideal: 7–12 MHz). This type of transducer is suitable for lizards and snakes and provides a broad picture with adequate imaging in the region close to the transducer.
- ☐ a sector transducer with of a frequency of 7.5 MHz (ideal: 7–12 MHz). In addition to being used in chelonians, other reptile species can be examined with this transducer.
- ☐ the possibility of saving the digital images or sequences. The storage of pictures is not only important for follow-up (comparative) examinations but also provides the possibility of electronically forwarding the image for assessment to colleagues who are experienced in reptilian ultrasonographic diagnostics.
- ☐ a color Doppler function on the machine. The color Doppler assessment is not only important for investigation of the heart, but it also provides important information about changes in the perfusion of the organ parenchyma. With this function, it may be possible, with certain tumors, to prognose the chance for surgical success regarding removal of the mass.

Portable machines are recommended for the examination of large reptiles which cannot be easily transported or positioned. Portable ultrasonographic units are much more expensive than their stationary counterparts but have a performance that is similar.

3.2.2 Coupling sites

There is rarely a positioning problem when performing a physical examination on a reptile patient. Only in very large snakes are a number of assistants necessary to help restrain a large reptile and general anesthesia is usually not necessary except in very large and strong animals.

In reptiles with thick, calcified scales, the coupling site may be nondiagnostic and the ultrasonographic image marred by artifacts. Often there are pockets of air between the scales, which will also reduce the picture quality. Giving the patient a warm bath approximately 20–30 minutes before the investigation will cause a slight swelling of the skin thereby closing the air spaces and greatly improving image quality. Even spraying with water before ultrasonography gel is placed on the skin can be helpful. When using ultrasonography gel, a generous amount should be used to obtain the best images. The body warmth in mammals will cause liquefaction of the ultrasonography gel, but this does not occur quickly in reptiles since they are poikilothermic. Accordingly, it is sensible to use a warmed gel: an easy and cheap method is to use a baby bottle warmer to heat the gel to 35°C.

In snakes just before the shedding of the skin, the image quality is very poor as an air space has developed between the old and new skins, thereby preventing the ultrasound waves from penetrating into the body cavity. Where necessary, ultrasonographic examinations must be delayed until the snake has shed its skin. If there is bony material in the scales (osteoderms), a coupling site between the scales must be used. In such species, using a sector scanner is often preferred for performing the examination.

Small reptiles and chelonians that have a very small coupling site can also be examined in a water bath for easier coupling and because the water acts as a spacer. The majority of transducers are suitable for using in a water bath; if in doubt, ask the manufacturer. Other spacers can also be used. An example for use on the prefemoral window in smaller chelonians, is to fill the finger of a latex glove with gel (preventing the formation of air bubbles), put more gel on the outside of the gel-filled glove finger and lay it in front of the knee **(Fig. 3-34)**.

Fig. 3-33: Special transducers such as this hockey stick allow the use of sites which cannot be reached with a standard transducer. This transducer can even be placed, without difficulty, in the prefemoral window of small chelonians.

Fig. 3-34: Ultrasound coupling between the patient and the transducer can be achieved with simple techniques and allows the use of even larger transducers in the prefemoral window. As an alternative, the examination can be attempted in a water bath.

3.2.3 Approaches

3.2.3.1 Approaches in lizards

For a schematic representation of the internal organs in a lizard see **Figure 3-8** in Chapter 3.1.2.1.

There are three main approaches: the ventral approach, the renal approach from the dorsal body wall, and the heart approach from the cranial or axillary region. The ventral coupling site is the main approach to examine the majority of the organs in the body cavity.

The lizard is either positioned in dorsal recumbency or the examination is performed with the animal lying in ventral recumbency within a cavity on the examination table. The transducer is placed on the animal either along the longitudinal axis or across the animal and moved to image the organs as needed **(Fig. 3-35)**. The kidney can be examined in many species, especially the green iguana (*Iguana iguana*), from the dorsal body wall. The transducer is placed either cranial or caudal to the pelvic bones alongside the spine and positioned as needed to perform the examination **(Fig. 3-36)**. The cranial coupling site is often useful for imaging the heart. The heart can be viewed either between the bones of the pectoral girdle or the coupling site in the axilla can be used **(Fig. 3-37)**. The quality of the image depends on a number of factors, one of which being how much the animal has tried to defend itself by inflating itself with air.

3.2.3.2 Approaches in snakes

In snakes, the approach is usually along the ventral body wall in the area delineated by the ventral scales. The locations of the different organs within a snake's body cavity are shown in Table 3-2. One way to examine the patient is to position the snake on its back **(Fig. 3-38)**; however, this can cause problems in unsedated animals as they will try and defend themselves, making the investigation more difficult. This is the reason a snake should be examined using a depression in the examination table or with the animal lying between two tables pushed together. If the snake needs to be examined in dorsal recumbency, it is advantageous to have an assistant hold the region of the body to be investigated in the supine position, while the rest of the snake is in its normal ventrally recumbent position.

In snakes, both the fixation and the pressure of the transducer on the body lead to displacement of the internal organs. Also during the examination, the internal organs may be pushed so far cranially or caudally within the body cavity that the transducer will need to be repositioned. If the snake is placed in its normal ventral recumbent position, then such displacement is less of a problem. In addition, when investigating the cardiovascular system or collecting biopsy samples, the transducer coupling should be done evenly and with as little pressure as possible

Fig. 3-35: Ventral coupling site of a linear transducer in a green iguana (*Iguana iguana*). Lizards can be investigated both in ventral or dorsal recumbency.

Fig. 3-36: Dorsal coupling site in the kidney region of a savannah monitor (*Varanus exanthematicus*). The transducer is simply placed lateral to the vertebral column. In addition to the kidneys, parts of the ovaries can also be visualized using this coupling site.

Fig. 3-37: Axillary coupling site for imaging the heart in a green iguana (*Iguana iguana*). Sector transducers are more suitable for this coupling site. The image quality depends on the filling of the lungs with air. Therefore, it is advisable to wait after the initial coupling until the animal has inflated itself before initiating the examination.

Fig. 3-38: Ventral coupling site in the heart region of a boa constrictor (*Boa constrictor*). A micro-curved transducer is being used in this figure. A micro-curved transducer can lead to displacement of the internal organs if too much pressure is placed on the body wall. Snakes usually have less movement when the segment being investigated is placed in dorsal recumbency.

3.2.3.3 Approaches in chelonians

For a schematic representation of the internal organs of a chelonian see **Figure 3-9** in Chapter 3.1.2.3.

In the majority of chelonians, only the area in front of the knee (prefemoral, **Fig. 3-39**) and the sides of the neck (cervicobrachial, **Fig. 3-40**) are suitable as coupling sites, therefore very small transducers must be used on most patients. Only in soft-shell turtles (*Trionychidae*) can the internal organs be imaged through the shell. The area over the prefemoral window, in front of the knee, should be liberally filled with ultrasonography gel.

Positioning a chelonian patient for an ultrasonographic examination is usually no problem. Larger animals can be placed on a container so that their legs hang in the air. The extraction of the patient's legs, however, can still be difficult or even impossible, thereby requiring anesthesia for the examination.

It is important, especially in terrestrial chelonians, that they are not examined in a tipped position or on their backs. Their internal organs lie in a ventral position within the body cavity, while the dorsal body cavity is filled with air. Tipping the animal may lead to organ displacement, causing air to relocate between the transducer and organs. Only a very slight tipping in the direction of the transducer may be used to displace the internal organs towards the transducer. The majority of the internal organs can be imaged through the prefemoral windows located in front of the knees **(Fig. 3-39)**. The approaches on each side of the neck can be used to examine more cranial structures. The indications for each approach are listed in Table 3-4.

Table 3-4: Approaches used for the ultrasonographic imaging of the soft organs in chelonians.

prefemoral	**kidneys**	only the kidney on the respective side, bend the ultrasonic beam high dorsally
	allantois	from both sides, only identified if filled, concretions are visible when swirled by tilting the animal back and forth
	liver	from both sides, by aiming the ultrasonic beam cranio medially. The gallbladder is usually easier to visualize by using the right prefemoral window approach
	intestines	from both sides, depends on contents and length; the intestinal contractions are usually slow
	heart	only partially, lies behind the liver
	testicles	only partially, when active, cranial to the kidneys, difficult to identify
	ovaries	from both sides, when active, ovarian cysts
	oviduct	from both sides, when active
	tumors	in the caudal and central body cavity
cervicobrachial	**heart**	from both sides
	liver	from both sides
	thyroid	partly, when enlarged
	tumors	in the area of the neck and the cranial visceral cavity

Fig. 3-39: Prefemoral coupling site with a micro-curved transducer in a common musk turtle (*Sternotherus odoratus*). The hindlegs have been extended caudally and fixed. In most cases, this type of transducer can only be used in the horizontal plane on animals under 1 kg.

Fig. 3-40: Cervicobrachial coupling site with a micro-curved transducer in a common musk turtle (*Sternotherus odoratus*). In chelonians of this size, sedation is usually required for the positioning of the head and/or limbs. Low frequencies (3.5–5 MHz) are needed to examine these animals.

Fig. 3-41: Image of an ultrasonography-controlled aspiration of the allantois in an African spurred tortoise (*Geochelone sulcata*). A vacuum pump can make the procedure easier in larger animals.

3.2.4 Ultrasonographically controlled aspiration and biopsying

The imaging of the changed regions using ultrasonography is the prerequisite for well-targeted and secure sampling for diagnostic testing. In addition to diagnostic sampling, the therapeutic drainage of fluid accumulations is also an important procedure that can be accomplished using ultrasonography. The latter involves not only removing free fluid lying in the body cavity but also fluid from an overfilled allantois. In addition, therapeutic flushing can be undertaken via the access cannula as well as the administration of medications.

One important therapeutic procedure is the aspiration of an enlarged allantois under ultrasonographic control in chelonians and lizards. With adequate enlargement of this organ, the aspiration procedure is performed with relatively few complications. In chelonians, the position of the allantois should be confirmed before selecting the best approach (right or left prefemoral), as its position within the body cavity is extremely variable. In lizards, aspiration through a slightly paramedian site is usually successful. Aspiration along the midline of lizard species is not advised because of the location of the large abdominal vein. As the abdominal vein divides into two branches caudally, it is recommended to perform Doppler imaging of the area before inserting the needle for aspiration. A negative pressure aspiration system is recommended to remove large amounts of fluid, which often require a change of syringes. The aspiration procedure can be performed after proper surgical preparation of the skin using a needle of suitable size **(Fig. 3-41)**.

A liver biopsy is a useful diagnostic procedure. In addition to determining the etiology of liver pathology, it is also a valuable tool for diagnosing inclusion body disease in boas. Basically, the area of the liver selected for the biopsy should be one that is interpreted as being abnormal on the ultrasonographic image and is located a reasonable distance away from the larger blood vessels. This is especially important in snakes, where there are two large veins which course longitudinally through the liver. Aspiration of the liver, and other organs, should only be performed under a general anesthesia to minimize the risk of traumatizing the organs due to patient movement **(Fig. 3-42)**. The removal of liver cells can be accomplished with fine-needle aspiration or the same biopsy instruments used in mammalian medicine **(Fig. 3-43)**. Biopsy collection of renal tissue has been described, but due to the risk of hemorrhage only a fine-needle aspiration under ultrasonographic control should be performed on this organ.

3.2.4.1 Biopsy of the liver in snakes

(Figs. 3-43 and 3-44)

Due to the ability of the liver to change position in a snake's body cavity, biopsy collection from this organ is not without risk and the technique requires practice. It has proved useful to first examine the liver with its blood vessels in cross-section. The transducer is then turned longitudinally so the lateral liver parenchyma remains in the scan plane. Subsequently, the biopsy needle is slowly pushed between two ventral scales longitudinally toward the liver at a 45° angle. The position of the liver and the needle must be continuously monitored. The friable nature of the liver capsule makes penetration into the tissue difficult. After the removal of the tissue sample, the channel of the needle should be checked with Doppler imaging to observe for possible hemorrhaging, which must be stopped. If damage has occurred to either of the large hepatic veins, the biopsy procedure should be stopped immediately and the snake placed in the quiet environment of a critical care unit and started on fluid therapy. The surgical treatment of such a wound is difficult because it is not easy to find the iatrogenic puncture wound in the liver and by opening the body cavity the natural compression of the body wall is lost.

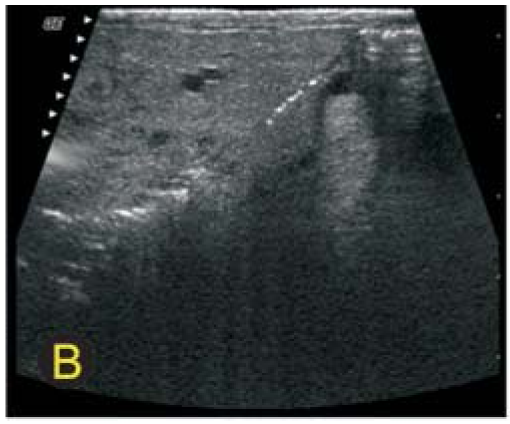

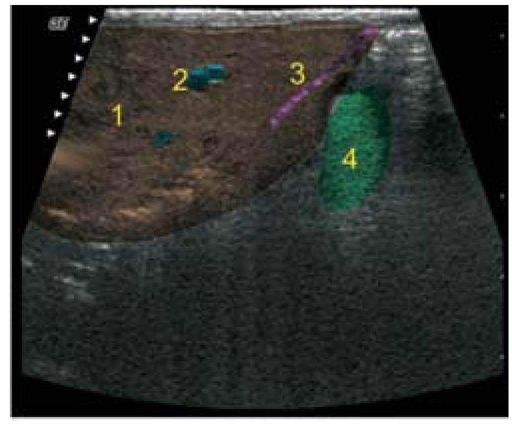

1: liver
2: blood vessels
3: biopsy needle
4: gastrointestinal tract

Fig. 3-42: Liver biopsy in a green iguana (*Iguana iguana*).

A: Photograph showing the procedure.

B: Ultrasonographic control, 12 MHz, PD 5 cm.

Fig. 3-43: (A) Liver biopsy procedure in an Indian python (*Python molurus*). (B) A standard biopsy set is used for this procedure. (C) The biopsy set should be new and unused, otherwise the insertion through the skin and liver capsule are extremely difficult. Such biopsies may be used for the histological diagnosis of Inclusion body disease.

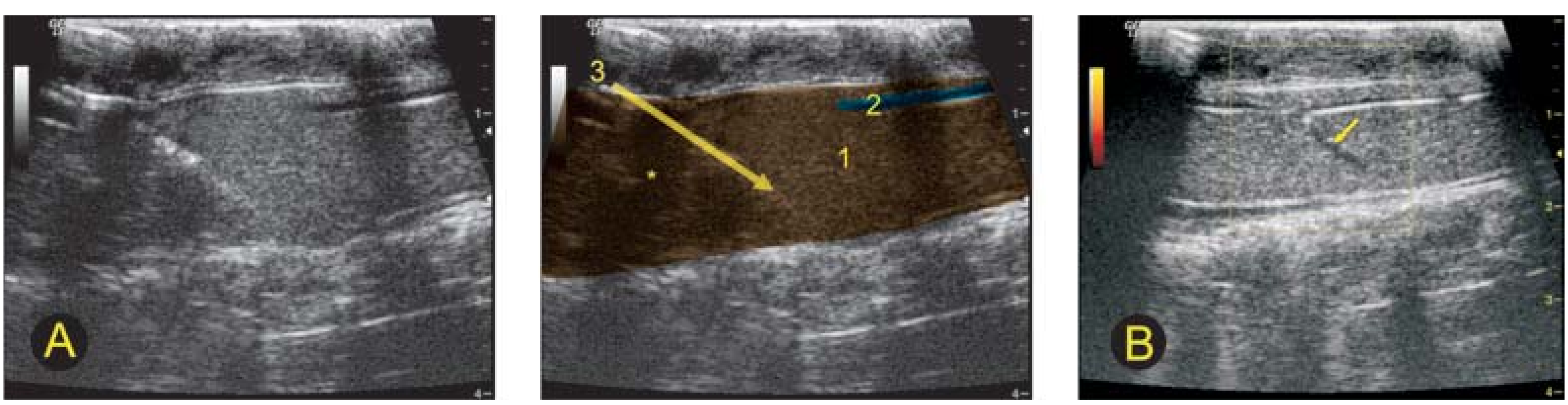

Fig. 3-44: Ultrasonographic images of an Indian python (*Python molurus*), longitudinal ventral coupling site, 12 MHz, PD 4 cm: Liver biopsy. Representation of the biopsy needle in the liver (A) and control of the needle tract (arrow) for hemorrhaging with a power Doppler (B).

1: liver
2: blood vessel
3, arrow: biopsy needle

*: acoustic shadow due to the total reflection from the surface of the needle

3.2.5 Assessment of the organs

The main indications for an ultrasonographic examination are related to the assessment of the liver, heart, urogenital tract, gastrointestinal tract, and unidentified enlargements. Often an enlarged soft-tissue shadow observed on radiographic images provides the indication for a subsequent ultrasonographic examination. It is recommended that the ultrasonographic examination of the body cavity be performed in a systematic manner, in which the organs should be evaluated in the following order.

3.2.5.1 Liver

The liver is easy to identify due to its finely granular echoic texture. In lizards and snakes, the hyperechoic fat bodies can be used for comparison when assessing the liver. In addition to the size and homogeneity of the liver, the hepatic blood vessels are also examined **(Figs. 3-45** and **3-46)**. The hepatic blood vessels are often observed as fine hypoechoic regions which can be followed coursing through the liver parenchyma. The wall of the blood vessel is not always identifiable. Snakes have two large hepatic blood vessels, which course in a cranial to caudal direction through the entire liver **(Fig. 3-47)**. The use of color Doppler imaging helps in the assessment of liver perfusion **(Fig. 3-48)**. The gallbladder can be found situated within the liver parenchyma on the right side of the body in chelonians and lizards **(Fig. 3-49)**. In the snake, the gallbladder lies caudally outside of the liver parenchyma **(Fig. 3-50)**.

Fine-needle aspiration or collection of biopsy samples can be performed in abnormal areas of liver tissue in both lizards and snakes (see Chap. 3.2.4).

Indications

- ☐ clinical signs of liver disease
- ☐ enlargement of the liver on radiographic images
- ☐ obesity, suspicion of fatty liver
- ☐ palpable tumors
- ☐ swelling of the abdomen, ascites
- ☐ biopsy collection (e.g. inclusion body disease) – diagnosis, hepatitis, neoplasia

3.2.5.2 Cardiovascular system

When assessing the heart, the different cardiac anatomy of the reptilian patient compared to that of mammals should be taken into consideration. The heart of reptile species is relatively small and consist of two atria and one ventricle (except in crocodiles) with two aortic arches being present **(Fig. 3-57)**. The ventricle has a very thick muscular wall that is internally septated **(Figs. 3-51** to **3-53)**. The thickness of this wall should not be confused with hypertrophy. The functional separation of the pulmonary and systemic blood circulations takes place in the ventricle by the arrangement of the muscles **(Fig. 3-54)**. This separation can be visualized using color Doppler imaging **(Figs. 3-55** and **3-56)**. A small amount of fluid in the pericardium is usually classified as a normal finding.

Tumors, cardiomegaly, contractility abnormalities, and fluid accumulation in the pericardium can all be diagnosed using ultrasonographic imaging. Only a small amount of data is currently available regarding the assessment of blood flow patterns and velocities **(Fig. 3-58)**. In some reptile species, the presence of a postprandial shunt of blood to the gastrointestinal tract has been established. The major blood vessels can be evaluated, whereby narrowing of the vessels and changes in the walls (e.g. calcification) can be identified.

Imaging the heart with ultrasonography is also useful for cardiac blood collection, administration of fluids or medication during emergencies, for monitoring anesthesia, and for euthanasia or to verify death. In the latter situation, it should be noted that reptilian hearts can beat for an extended period of time in a post mortem state, sometimes even for a number of days, however, there is no longer any true blood flow. This lack of blood flow can be easily verified using color Doppler imaging.

Indications

- ☐ clinical or radiographic indications of heart disease
- ☐ administration of medication (emergency)
- ☐ assessment of the circulation
- ☐ euthanasia, determining death

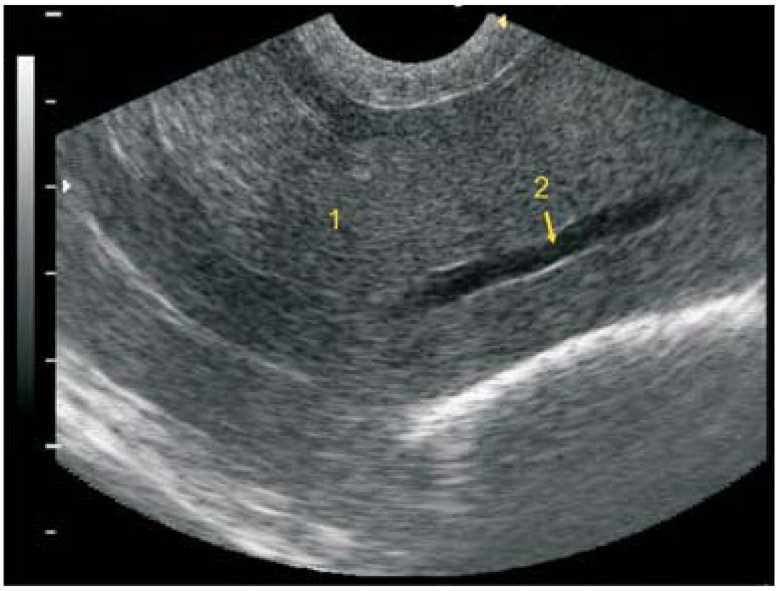

1: liver tissue
2, arrow: pointing to hepatic blood vessel

Fig. 3-45: Ultrasonographic image of a green iguana (*Iguana iguana*), transverse ventral coupling site, 7.5 MHz, PD 6 cm: The liver tissue (1) has only a few large blood vessels (2) coursing through it.

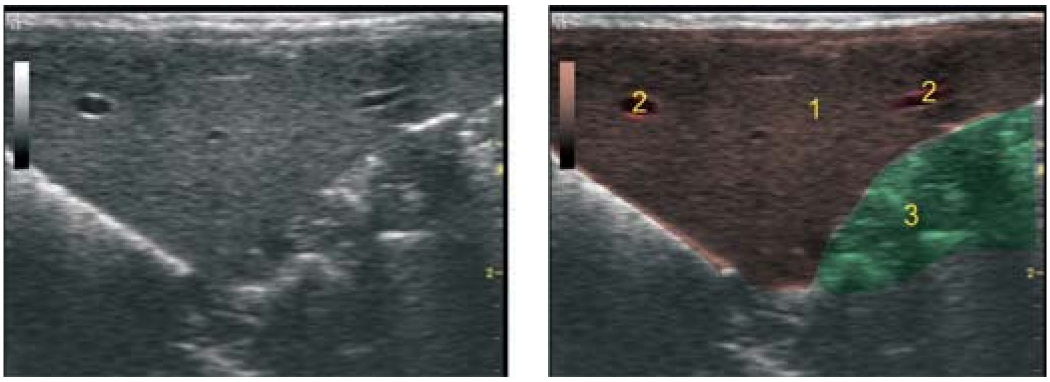

1: liver parenchyma
2: hepatic blood vessels
3: gastrointestinal tract

Fig. 3-46: Ultrasonographic images of a central bearded dragon (*Pogona vitticeps*): longitudinal ventral tranducer coupling site, 12 MHz, PD 3 cm. Hepatic blood vessels (2) are also visible in the liver tissue (1). The liver is limited cranially by the area of total reflexion from the lungs; caudally it is bounded by the gastrointestinal tract (3).

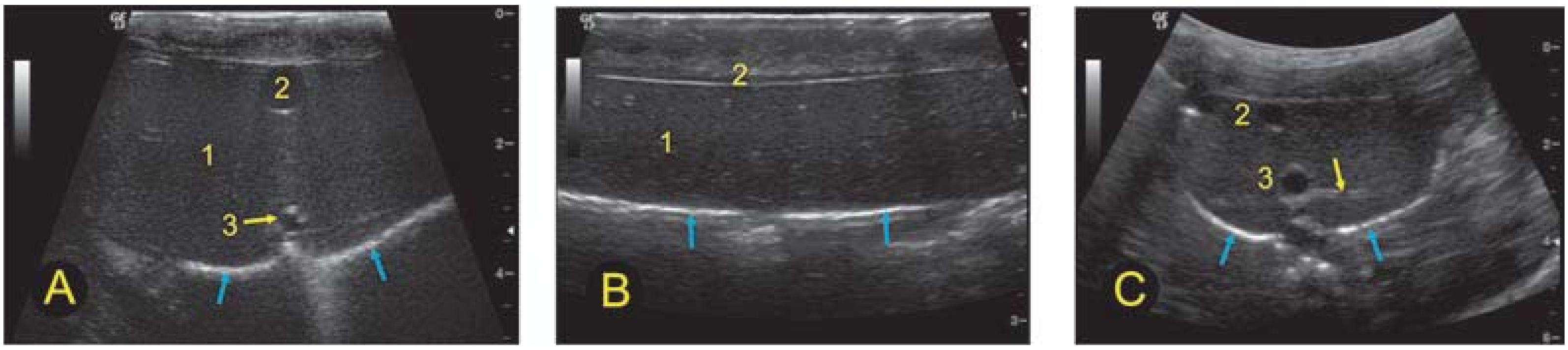

Fig. 3-47: Ultrasonographic images of snakes' livers.

A: Transverse ventral tranducer coupling site, 10 MHz, PD 6 cm. Indian python (*Python molurus*): normal liver.

B: Longitudinal ventral coupling site, 10 MHz, PD 3 cm. Boa constrictor (*Boa Constrictor*): Normal liver.

C: Transverse ventral coupling site, 4 MHz, PD 6 cm. Indian python (*Python molurus*): Normal liver.

All of these figures show no abnormalities. In the liver tissue (1) there is a ventral (2) and a dorsal (3) blood vessel. Some of the smaller blood vessels (yellow arrow) are visible. The liver is bordered by a hyperechoic capsule (blue arrows).

1: liver parenchyma
2: ventral blood vessel (hepatic vein)
3: dorsal blood vessel (hepatic portal vein)

yellow arrow: small blood vessels
blue arrows: liver capsule

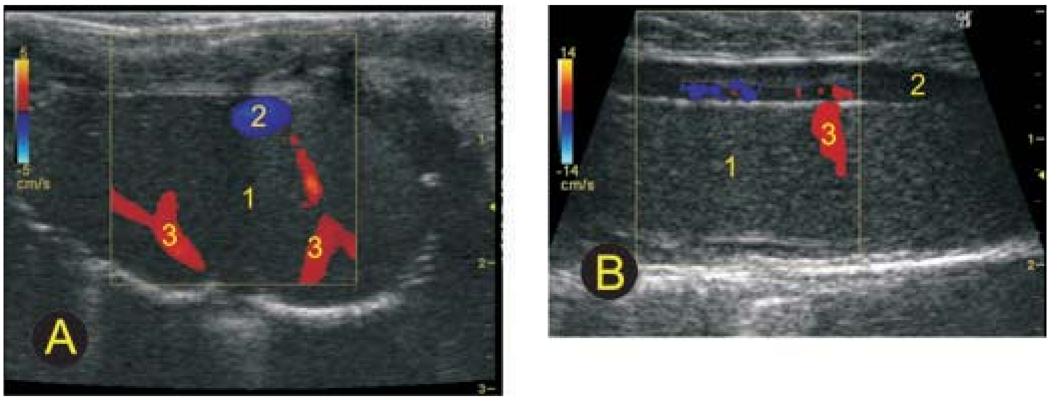

1: liver
2: V. portae hepatis
3: blood flow in hepatic vessel

Fig. 3-48: Ultrasonographic images of a royal python (*Python regius*), color Doppler, (A) transverse and (B) longitudinal ventral coupling sites, 12 MHz, PD 3 cm. Using the Doppler method, even smaller blood vessels can be imaged and their blood flow assessed.

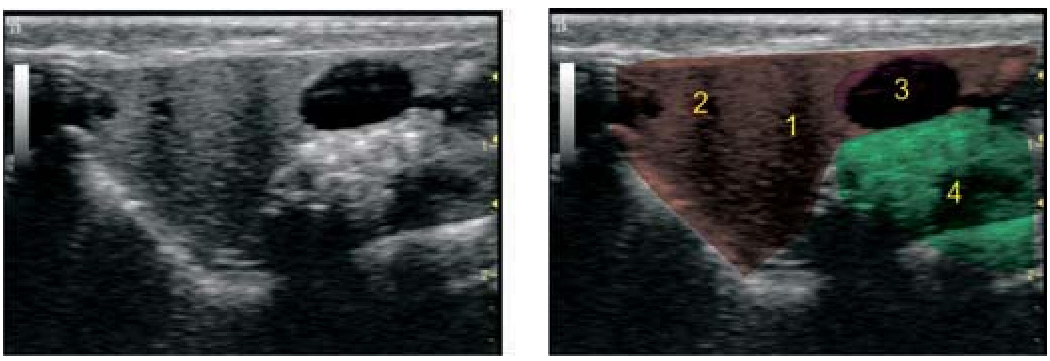

1: liver parenchyma
2: intrahepatic blood vessels
3: gallbladder
4: gastrointestinal tract

Fig. 3-49: Ultrasonographic image of a central bearded dragon (*Pogona vitticeps*), longitudinal ventral coupling site, 12 MHz, PD 3 cm. The gallbladder (3) lies within the liver parenchyma (1).

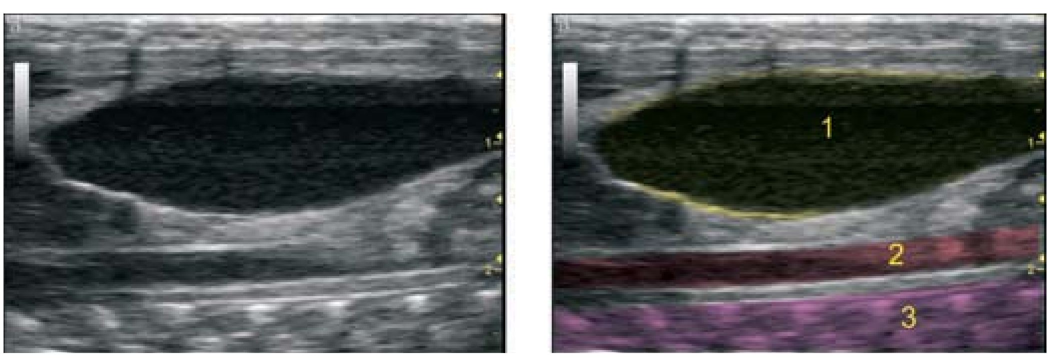

1: gallbladder
2: aorta
3: spinal musculature

Fig. 3-50: Ultrasonographic image of a corn snake (*Pantherophis guttatus*), longitudinal ventral coupling site, 12 MHz, PD 3 cm, showing the gallbladder (1) aorta (2) and spinal musculature (3).

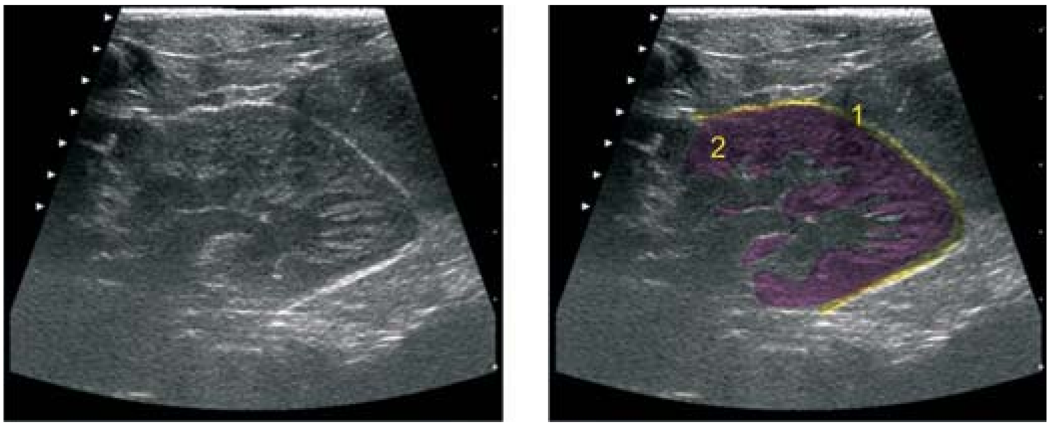

1: pericardial sac
2: cardiac musculature

Fig. 3-51: Ultrasonographic image of a green iguana (*Iguana iguana*), longitundinal axillary coupling site, 8 MHz, PD 6 cm: Heart. The sponge-like consistency of the cardiac musculature (2) and the pericardial sac (1) can be seen.

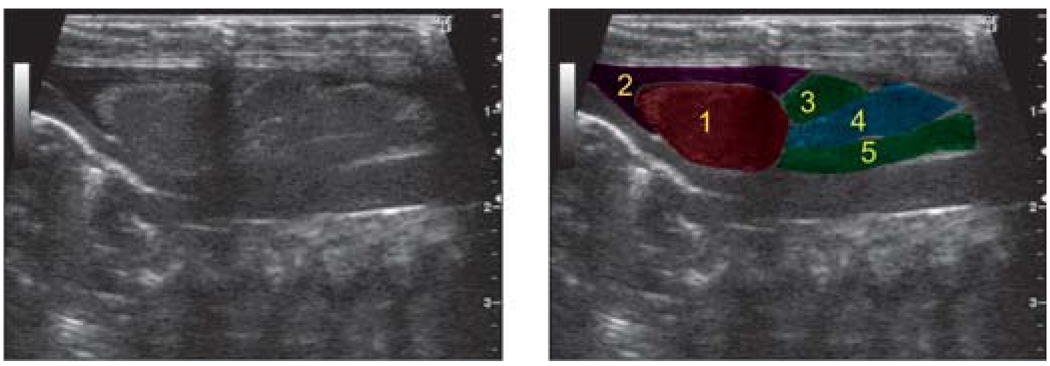

1: ventricle
2: pericardium
3: right atrium
4: pulmonary artery
5: right aortic arch

Fig. 3-52: Ultrasonographic image of a boa constrictor (*Boa constrictor*), longitudinal ventral coupling site, 12 MHz, PD 4 cm. Heart in the longitudinal plane.

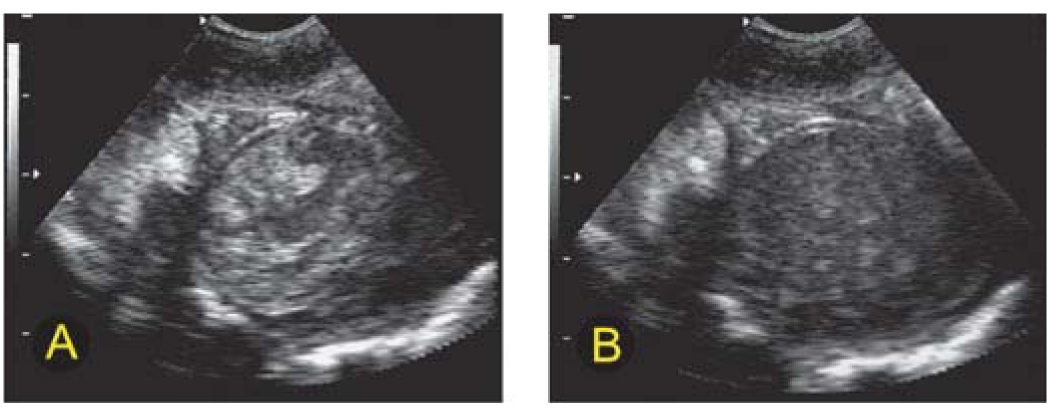

Fig. 3-53: Ultrasonographic images of a boa constrictor (*Boa Constrictor*), transverse ventral coupling site, 7.5 MHz, PD 4.5 cm. Ventricle in the transverse plane. A: systole. B: diastole.

1: muscle ridge
2: cavum pulmonale
3: cavum arteriosum/venosum

Fig. 3-54: Ultrasonographic image of an Indian python (*Python molurus*), longitudinal ventral coupling site, 10 MHz, PD 7 cm. Image of the muscle ridge (1), which separates the ventricle functionally into the cavum pulmonale (2) and the cavum arteriosum/venosum (3).

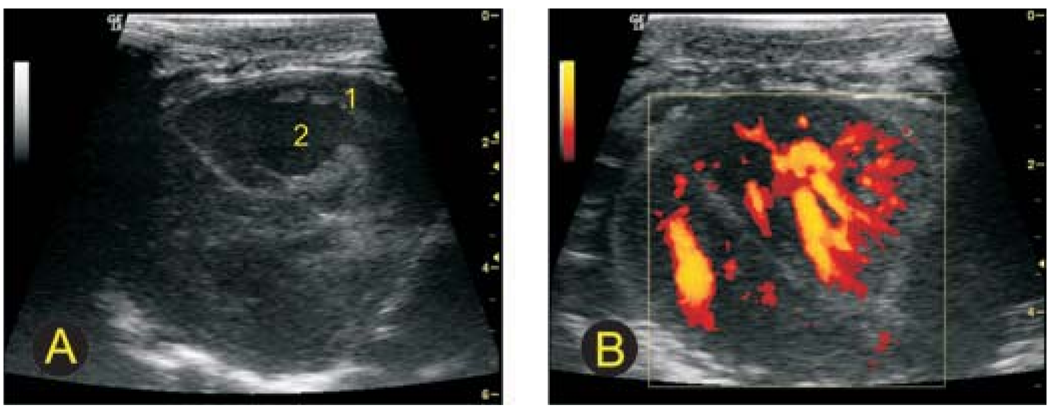

1: ventricle, myocardium
2: ventricle, lumen

Fig. 3-55: Ultrasonographic images of a reticulated python (*Python reticulatus*), transverse ventral coupling site, 10 MHz, PD (A) 6 cm and (B) 5 cm. Echocardiogram of the blood flow in the ventricle using (B) power Doppler.

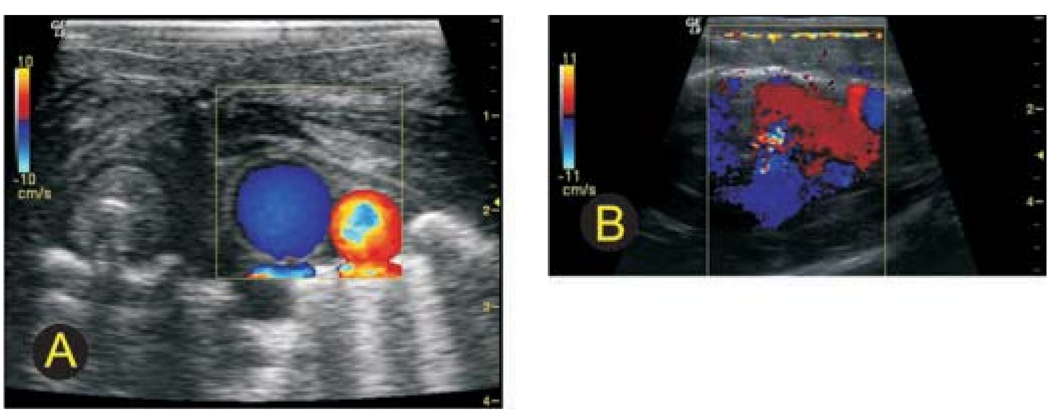

Fig. 3-56: Ultrasonographic images of an Indian python (*Python molurus*), (A) transverse and (B) longitudinal ventral coupling site, 10 MHz, PD (A) 4 cm and (B) 5 cm. Echocardiogram of the blood flow in the (A) blood vessels and (B) ventricle using color Doppler.

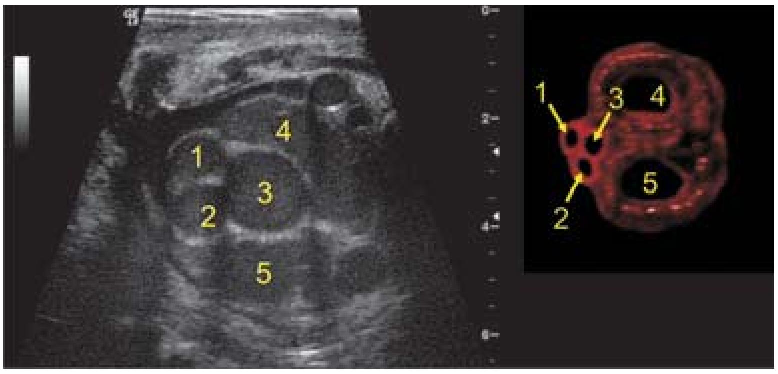

1: left aortic arch
2: right aortic arch
3: pulmonary artery
4: left atrium
5: right atrium

Fig. 3-57: Ultrasonographic images of a reticulated python (*Python reticulatus*), transverse ventral coupling site, 102 MHz, PD 6 cm. Roots of the major blood vessels. Right figure: autopsy, cross-section.

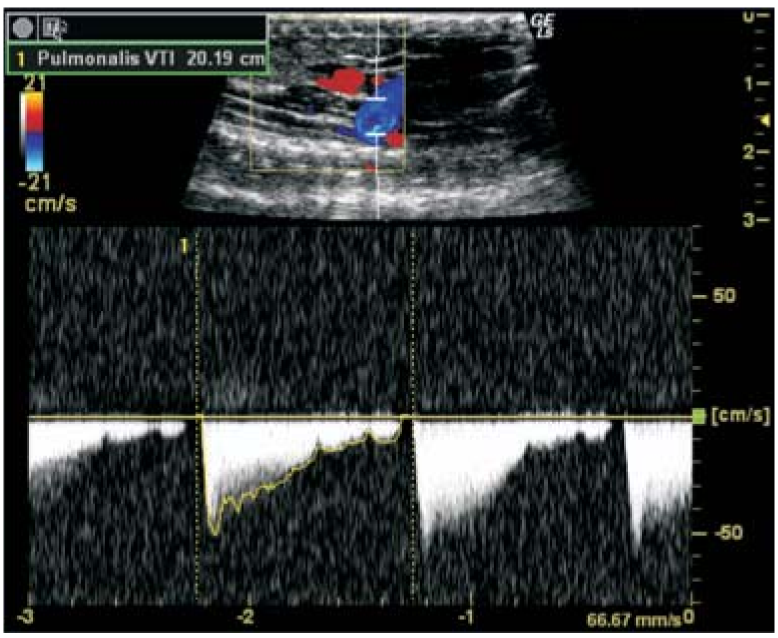

Fig. 3-58: Ultrasonographic image of a royal python (*Python regius*), longitudinal ventral coupling site, 8 MHz, PD 3 cm. Adjustment of the Doppler gate to the deflection in the pulmonary artery. Image of the blood flow and calculation of the volume-time integral (VTI).

3.2.5.3 Urinary tract

In lizards, the kidneys can be depicted from the ventral coupling site or from a site on the dorsal body wall in the region of the tail root. It is highly recommended to use color Doppler imaging to show the perfusion of the kidneys, so that the organs can be identified **(Figs. 3-59** to **3-61)**. In chelonians, the prefemoral coupling site is used for the examination of the kidneys, whereby the scanning plane is aimed dorsally. The triangular-roundish kidney can then be found cranial to the zone of total reflection from the pelvic bones and lateral to the aorta **(Fig. 3-62)**. It is difficult to image the kidney of snakes although an attempt can be made from the lateral body wall. The snake kidney is relatively thin, lobed and elongated.

Pathology of the kidneys does not only affect the size but also the echogenicity and perfusion of these organs. In cases of urate deposits or renal calcification, the kidneys often appear strongly hyperechoic. Kidney biopsies can be collected using a dorsal approach; however, there is a risk of hemorrhage.

In chelonians, the allantois appears as an anechogenic structure with a very thin wall when the prefemoral coupling site is used **(Fig. 3-63)**. In lizards, it is usually framed by the two abdominal fat bodies lying in the caudal body cavity **(Fig. 3-64)**.

Common pathological changes found in the urinary tract using ultrasonographic imaging are paralysis of the allantois and the collection of concretions. Paralysis of the allantois occurs frequently in chelonians and the sac can become extremely enlarged. Concretions and uroliths are easier to recognize when changing the animal's position during the examination due to their movement within the bladder. Furthermore, anomalies in the allantoic wall should be identified as an indication of cystitis. Ultrasonography-guided aspiration of the allantois is possible and can be performed without complications (see Chap. 3.2.4).

Indications

- ☐ control of the renal structure and function (allantois) in association with septicemia and metabolic bone disease
- ☐ clinical/biochemical indications of gout
- ☐ suspicion of uroliths
- ☐ suspicion of renal infections or insufficiency

3.2.5.4 Genital tract

Ultrasonographic imaging is of great value when examining the genital tract in female animals. Even the inactive ovary can often be identified **(Figs. 3-66** and **3-68)**. Ovarian follicles are evaluated with respect to their size and echogenicity. They initially develop as hypoechoic structures a few millimeters in size **(Figs. 3-65** to **3-67)**, and eventually grow into larger follicles with hyperechoic yolk balls before actual ovulation **(Fig. 3-70)**.

In addition to the assessment of the animal's sexual activity and the imaging of active follicles, ultrasonography can be used to image eggs. Depending on their stage of development, eggs consist of a hyperechoic shell and contents with varying degrees of structural organization **(Figs. 3-71** to **3-73)**. It is usually possible to image the egg contents when still in the oviduct because the mineralized shell contains a lot of water and the acoustic reflection is not complete. Before the shell is mineralized, the egg is often observed as a structure with a hyperechoic central »ball« of yolk surrounded by a more hypoechoic rim (the vitreous).

With the common presentation of »pre-ovulatory« egg binding, a large number of extremely enlarged follicles can be identified. In the green iguana (*Iguana iguana*), the follicles should not be much larger than 15 mm in diameter and the homogeneity and echogenicity of these follicles should be assessed. Great variability in the echogenicity often indicates the presence of a pathological process. Finally, diseases of the genital tract frequently result in effusions into the body cavity, which can also be depicted using ultrasonographic imaging.

The ability to ultrasonographically image the reptile testicle is species dependent and/or only possible in sexually active animals **(Fig. 3-69)**.

Indications

- ☐ sex determination
- ☐ determination of sexual activity or maturity
- ☐ suspicion of cystic changes in the ovary
- ☐ suspicion of disturbance in egg formation or laying
- ☐ suspicion of an infection or tumor
- ☐ swelling of the coelomic cavity

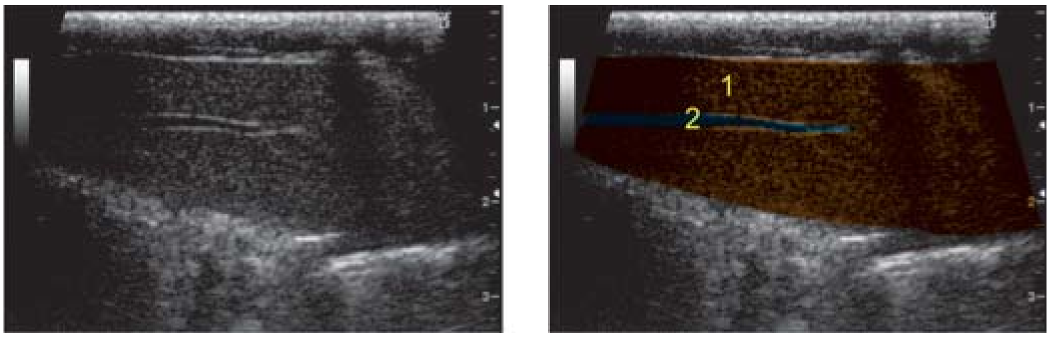

1: kidney
2: renal vein

Fig. 3-59: Ultrasonographic image of a green iguana (*Iguana iguana*), longitudinal dorsal coupling site, 7 MHz, PD 4 cm. Sonogram of the kidney (1) and the central renal blood vessel (2).

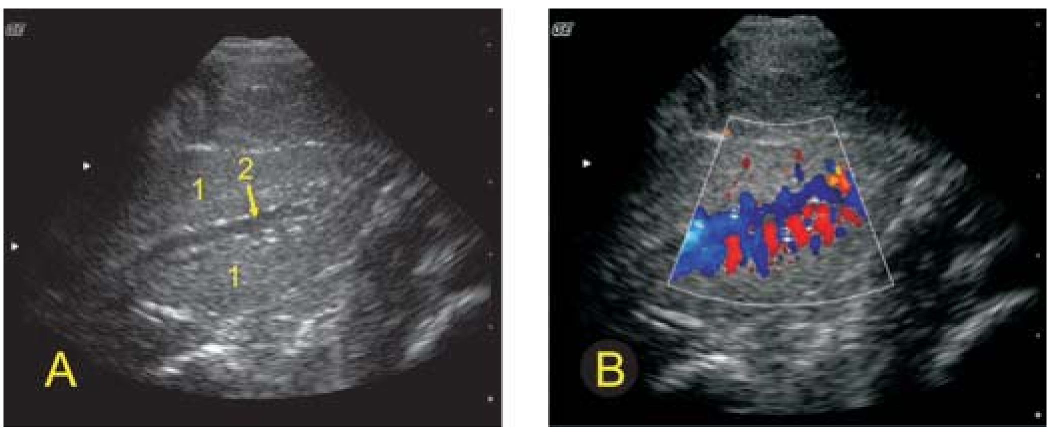

1: renal parenchyma
2: renal vein

Fig. 3-60: Ultrasonographic images of a green iguana (*Iguana iguana*), longitudinal dorsal coupling site, 8 MHz, PD 5 cm.

A: Sonogram showing the renal tissue (1) and the central blood supply (2).

B: Color-Doppler echocardiogram of the typical blood flow in the kidney.

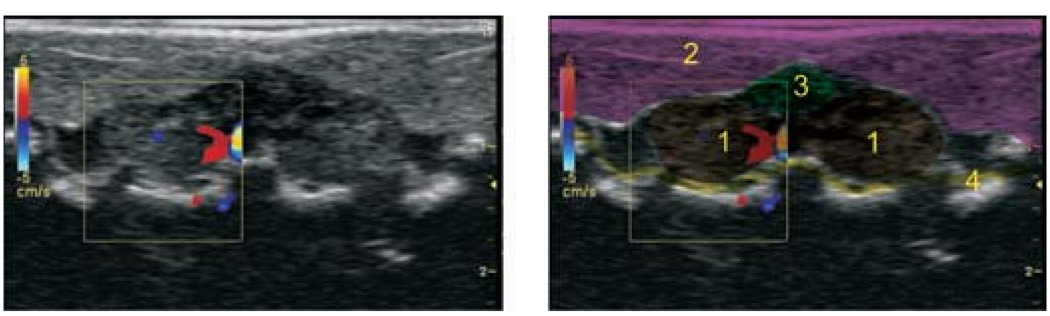

1: kidney
2: coelomic fat body
3: rectum
4: spine, body wall

Fig. 3-61: Ultrasonographic image of a central bearded dragon (*Pogona vitticeps*), color Doppler, transverse ventral coupling site, 12 MHz, PD 3 cm. Sonogram of the kidneys (1) lying under the abdominal wall and the coelemic fat bodies (2).

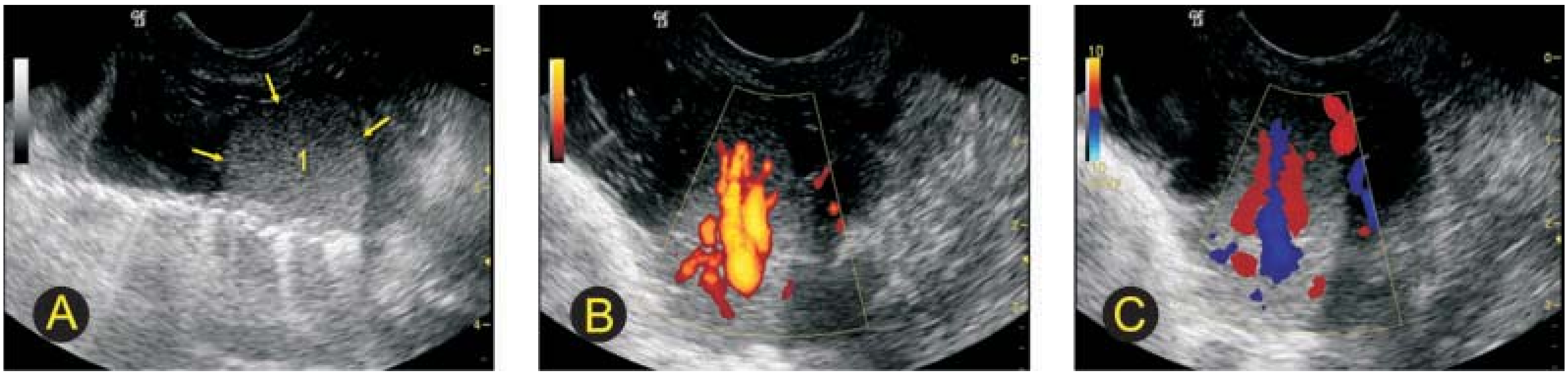

Fig. 3-62: Ultrasonographic images of a Hermann's tortoise (*Testudo hermanni*), longitudinal prefemoral coupling site, 8 MHz, PD 4 cm. Different images of the kidney – (A) plain, (B) power Doppler, and (C) color Doppler.

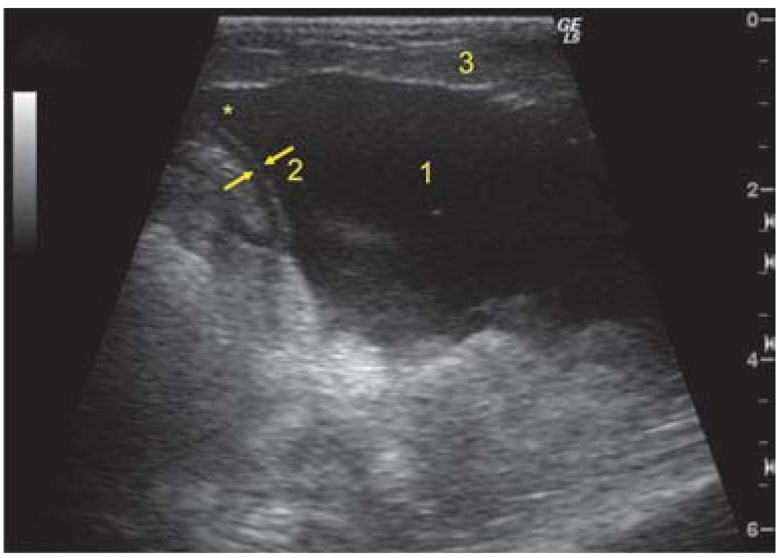

1: allantois
2, arrows: wall of the allantois
3: ventral body wall

*: exit of the allantois

Fig. 3-63: Ultrasonographic image of a green iguana (*Iguana iguana*), longitudinal ventral coupling site, 10 MHz, PD 6 cm. Image of the allantois (1) and its exit (*).

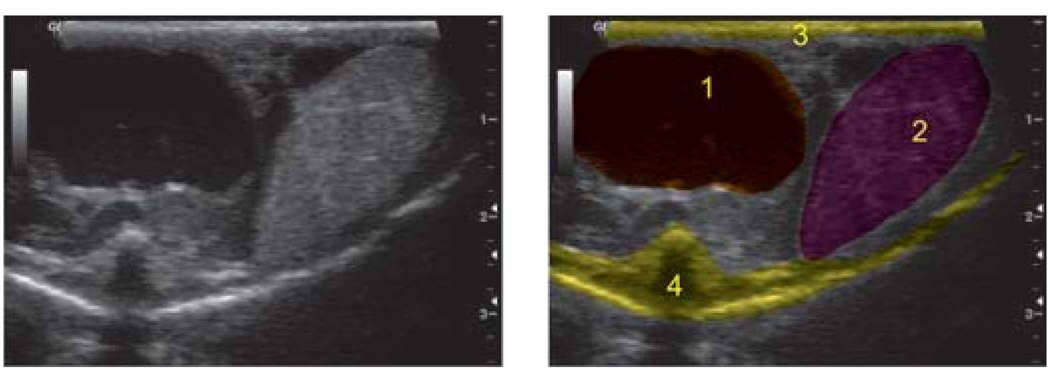

1: allantois
2: fat body
3: ventral body wall
4: dorsal body wall and spine

Fig. 3-64: Ultrasonographic image of a central bearded dragon (*Pogona vitticeps*), transverse ventral coupling site, 12 MHz, PD 4 cm. Allantois (1) and a fat body (2).

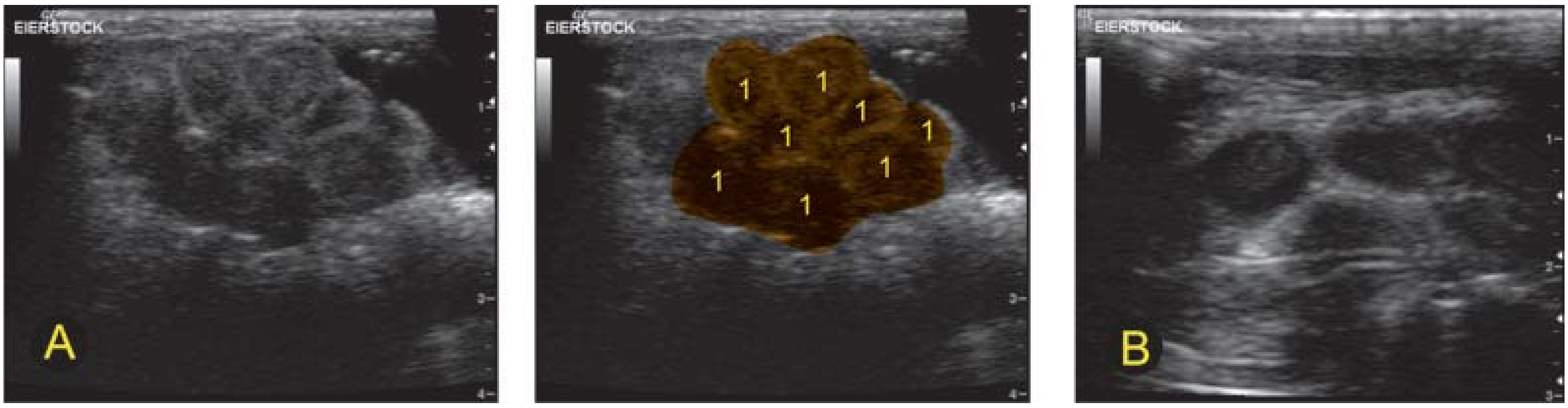

Fig. 3-65:

A: Ultrasonographic image of a green iguana (*Iguana iguana*), longitudinal ventral coupling site, 7 MHz, PD 4 cm. Ovary (1: follicle).

B: Ultrasonographic image of a reticulated python (*Python reticulatus*), longitudinal ventral coupling site, 7 MHz, PD 3 cm. Ovary.

1: follicles

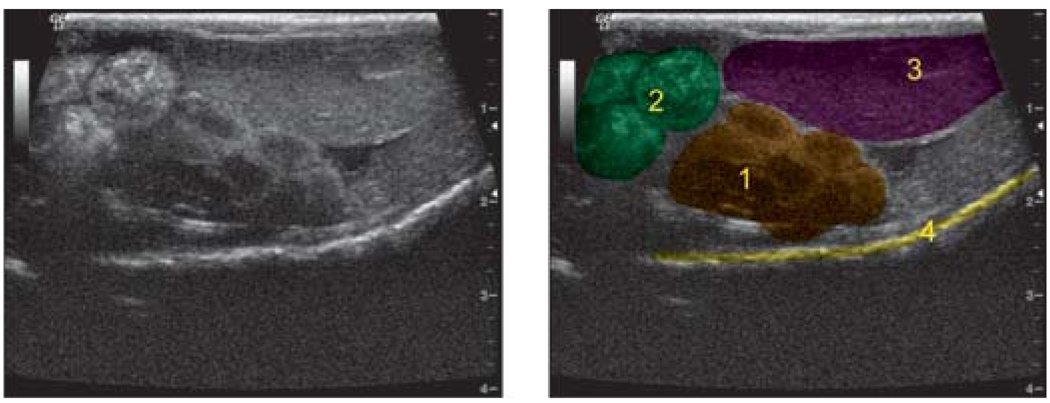

Fig. 3-66: Ultrasonographic image of a central bearded dragon (*Pogona vitticeps*), longitudinal ventral coupling site, 12 MHz, PD 4 cm. Image of the ovary.

1: ovary with follicles
2: stomach
3: liver

Fig. 3-67: Ultrasonographic image of a green iguana (*Iguana iguana*) longitudinal ventral coupling site, 7 MHz, PD 4 cm. Ovary.

1: follicle
2: spinal musculature

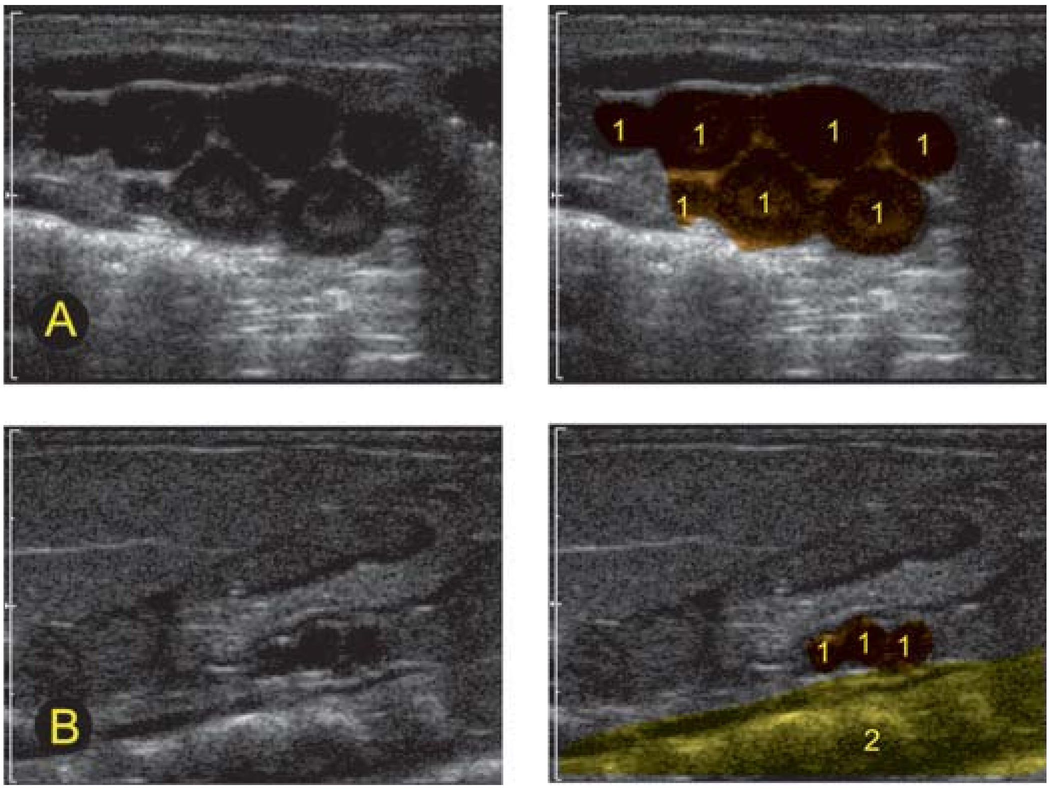

1: follicle
2: spinal musculature and spine

Fig. 3-68:

A: Ultrasonographic image of a quince monitor (*Varanus melinus*), longitudinal ventral coupling site, 12 MHz, PD 2 cm. Normal ovary.

B: Ultrasonographic image of a freckled monitor (*Varanus tristis orientalis*), longitudinal ventral coupling site, 12 MHz, PD 2 cm. Juvenile ovaries.

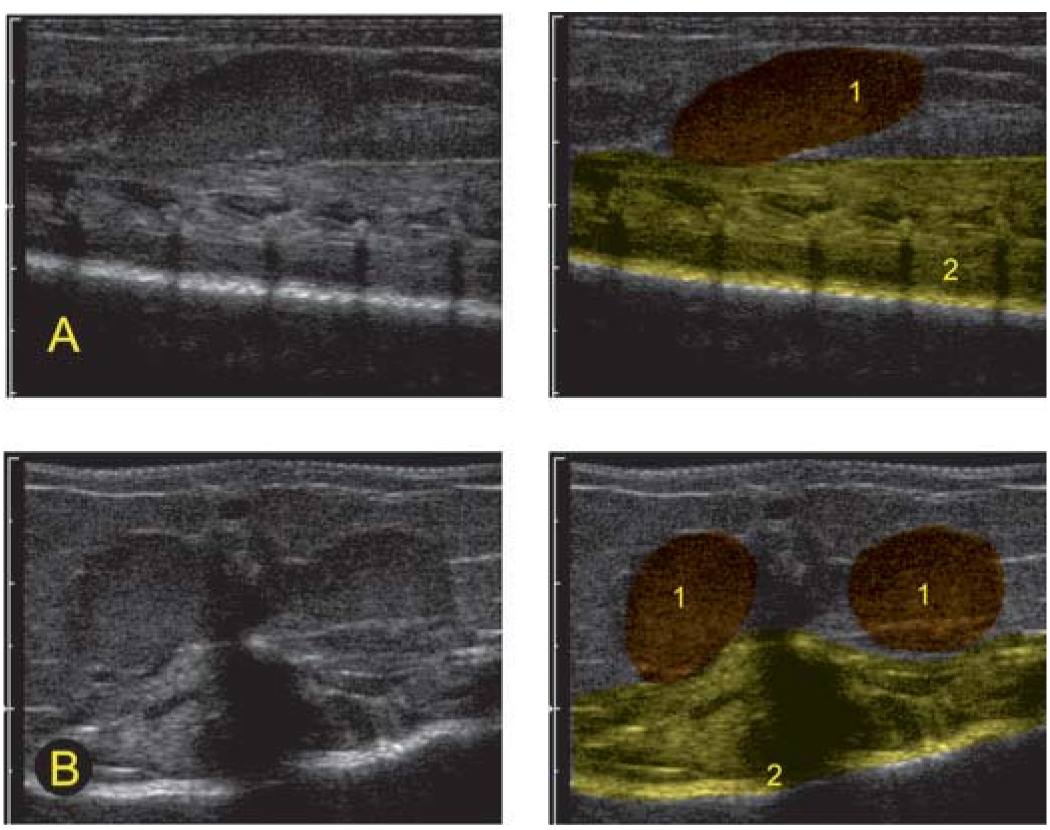

1: testicles
2: spinal musculature and spine

Fig. 3-69: Ultrasonographic images of a savannah monitor (*Varanus exanthematicus*), (A) longitudinal and (B) transverse ventral coupling sites, 12 MHz, PD 3 cm. Normal testicles (1).

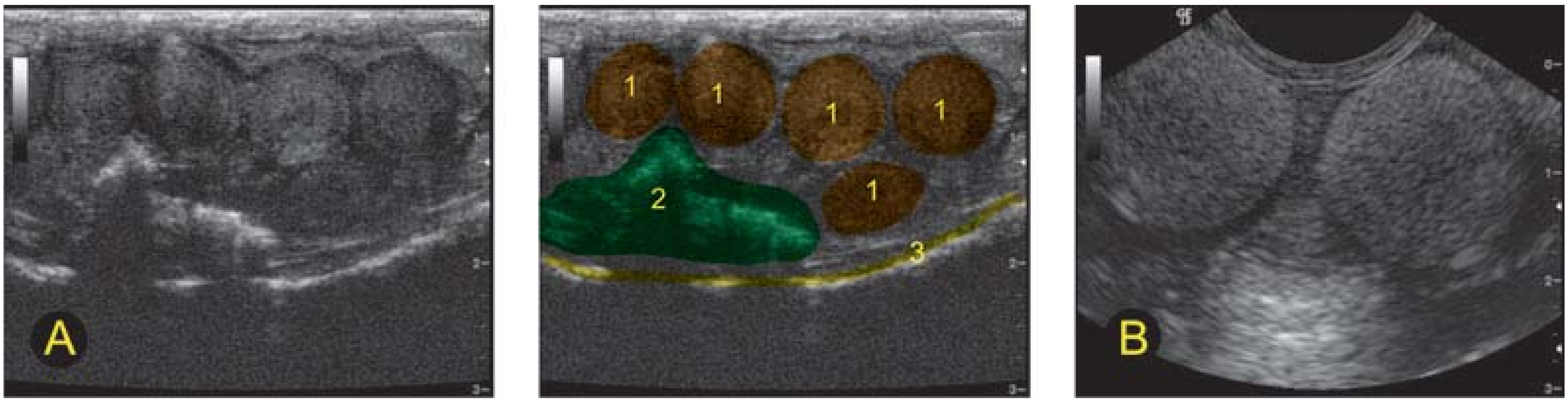

Fig. 3-70:

A: Ultrasonographic image of a central bearded dragon (*Pogona vitticeps*), transverse ventral coupling site, 12 MHz, PD 3 cm. Normal follicles (1).

B: Ultrasonographic image of a Hermann's tortoise (*Testudo hermanni*), prefemoral coupling site, 10 MHz, PD 3 cm. Normal follicles.

1: follicles
2: spine
3: dorsal body wall

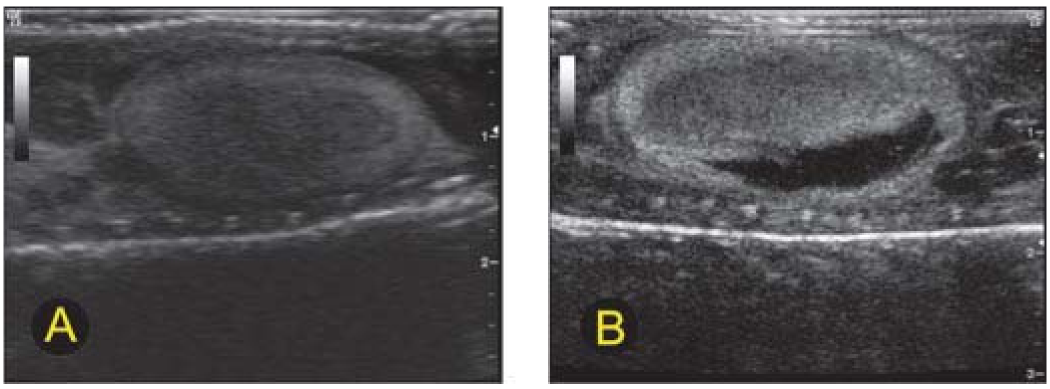

Fig. 3-71: Ultrasonographic images of a leopard gecko (*Eublepharis macularius*), longitudinal ventral coupling site, 12 MHz, PD 3 cm. Images show egg development at the (A) beginning and (B) 18 days later just before laying.

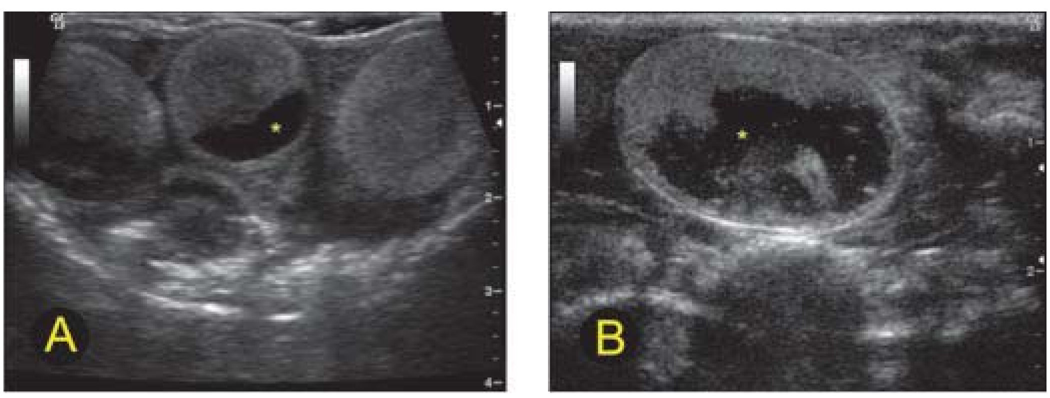

Fig. 3-72: Ultrasonographic images of a central bearded dragon (*Pogona vitticeps*). The internal stucture of the egg changes during development. It is shown as a fluid, hypoechoic area (*).

A: transverse ventral coupling site, 12 MHz, PD 3 cm.

B: longitudinal ventral coupling site, 10 MHz, PD 4 cm. Normal eggs shortly before laying.

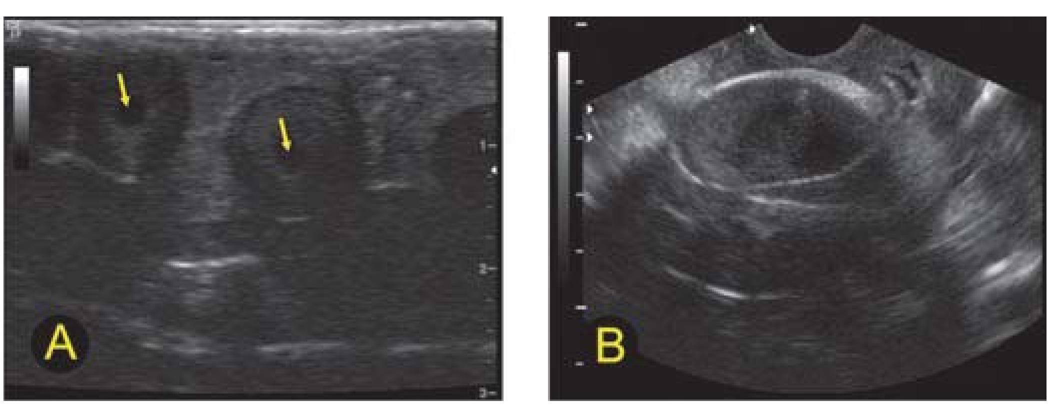

Fig. 3-73:

A: Ultrasonographic image of a central bearded dragon (*Pogona vitticeps*), transverse ventral coupling site, 12 MHz, PD 3 cm. Balls of egg yolk shortly after ovulation. The central area is usually seen as an area of low echogenicity (arrows).

B: Ultrasonographic image of a yellow-bellied slider (*Trachemys scripta scripta*), prefemoral coupling site, 7.5 MHz, PD 6 cm. Normal egg with a calcified shell just before laying. The apparently thickened shell is due to the oblique path of the ultrasound beam penetrating the shell.

3.2.5.5 Gastrointestinal tract

The ability to ultrasonographically image the reptile gastrointestinal tract is greatly dependent on the degree and type of filling within its lumen. Gaseous and stony or sandy contents hamper the imaging, while fluid contents enhance the quality.

The structure of both the stomach and the intestinal wall can be assessed **(Figs. 3-74** to **3-76)**. In lizards and chelonians, the stomach has a thin wall and lies in the left part of the body cavity. The stomach can be very large in herbivorous species and a differentiation between the stomach and the colonic fermentation area is often difficult in these animals. In snakes, when the stomach is empty, its wall is often observed to be folded **(Fig. 3-74)**, but after feeding, only the wall close to the transducer can be assessed **(Fig. 3-75)**.

The wall of the intestinal tract and contents within the lumen can also be ultrasonographically imaged **(Fig. 3-77)**. The feces are usually well formed in the region of the colon **(Fig. 3-78)**. Assessment of intestinal peristalsis is only possible with limitations, but it can provide indications of constipation.

Indications

- ☐ suspicion of obstruction, constipation, foreign bodies
- ☐ imaging of peristalsis and intestinal function
- ☐ suspicion of infection

3.2.5.6 Fat bodies

In lizards, the two intracoelomic fat bodies that extend from the caudal body cavity can be easily imaged **(Figs. 3-64** and **3-79)**. Their echogenicity is much greater than that of the liver and this echogenic disparity can be used when assessing the liver parenchyma. The size of the fat body can be used as a measure of the nutritional status of the animal – especially in obese patients. Fat bodies can also be identified in snakes, but they are not as well formed as in lizard species, instead the fat lies along the organs **(Fig. 3-78)**.

Indications

- ☐ determination of the nutritional status
- ☐ assessment of the echogenicity of the liver in the diagnosis of hepatic lipidosis (as a comparison)

3.2.5.7 Fluid

Fluid in the body cavity can be easily identified and aspirated using ultrasonographic imaging. It is important to differentiate a fluid-filled allantois or intestines from fluid lying freely in the body cavity.

3.2.5.8 Tumors

Tumor-like structures should always be investigated using the nearest coupling sites. Before aspiration, the structure's vascularity should be evaluated using color Doppler imaging.

3.2.5.9 Eye (Fig. 3-80)

INGO HOFFMANN

As in mammals, the eye of reptiles can be investigated transcorneally or through the spectacles (transspecular) in those species that have these anatomic structures. After the application of a bubble-free gel, the transducer is placed directly on the cornea or spectacle. Imminent skin sloughing can make the ultrasonographic examination in animals with spectacles more difficult or impossible due to the collection of air between the old and new layers of skin. However, the main problem when performing an ocular examination is the small size of the eyeball in reptiles. Therefore to get a satisfactory detailed image, transducers with a mean frequency of at least 12 MHz and a very good near-field resolution must be used. The contralateral eye should always be investigated and used as a comparison.

The **cornea** and the barely differentiable spectacle are characterized by two hyperechoic lines with an anechoic band lying between them. The anterior and posterior ocular chambers are echo-free in the healthy eye.

The **iris** usually has a medium echogenicity and is a slightly inhomogeneous structure. The iris is difficult to differentiate from the ciliary body, which also has a medium echogenicity.

An ultrasonographically inconspicuous **lens** is characterized by two sharply drawn hyperechoic, slightly bent lines. The **vitreous body** should always be anechoic and the transition to the **ocular fundus** should have a rounded form. Occasionally, it is useful to increase the performance (gain) of the machine when investigating the vitreous so that the finest structural changes (e.g. clouding) can be better visualized. The **papillary cone**, which projects into the vitreous body from the ocular fundus is of medium echogenicity and can only be depicted in lizards and vipers. The form of the cone varies from a rudimentary, barely elevated cushion to slim structures that extend far into the vitreous, almost touching the posterior pole of the lens.

Depending on the species, the **orbit** is more or less well defined and has a mixed echogenicity.

Indications

- ☐ non-physiological clouding of the spectacle or cornea
- ☐ clouding in the anterior chamber and of the lens
- ☐ intraocular tumors
- ☐ retinal detachment
- ☐ buphthalmos
- ☐ retrobulbar processes

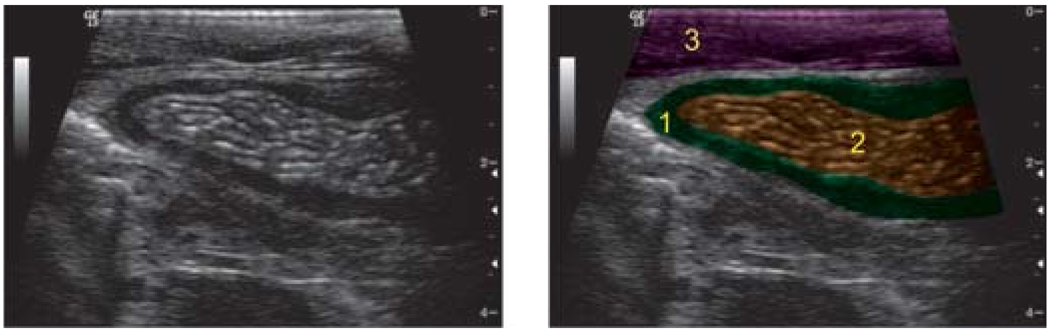

1: stomach wall
2: folded gastric mucosa
3: ventral body wall

Fig. 3-74: Ultrasonographic image of a reticulated python (*Python reticularis*), transverse ventral coupling site, 7 MHz, PD 5 cm. Empty normal stomach.

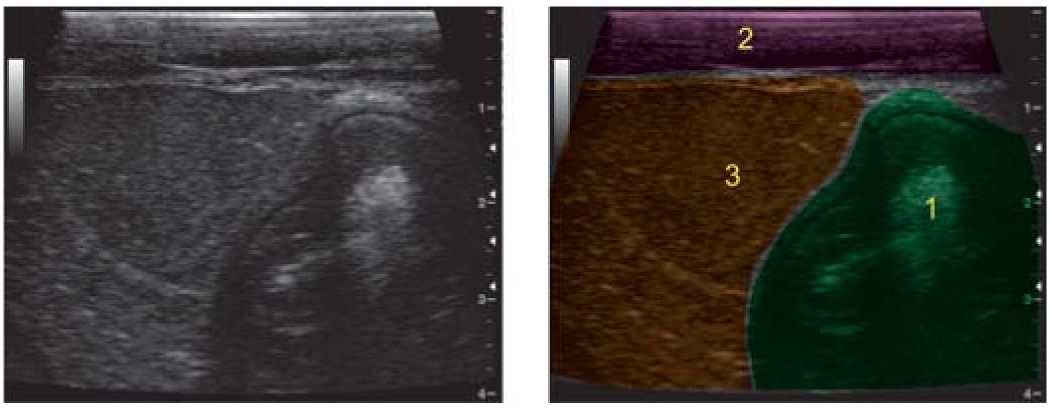

1: intestines with contents
2: ventral body wall
3: fat body

Fig. 3-75: Ultrasonographic image of a reticulated python (*Python reticularis*), transverse ventral coupling site, 10 MHz, PD 4 cm. Normal, full intestinal tract.

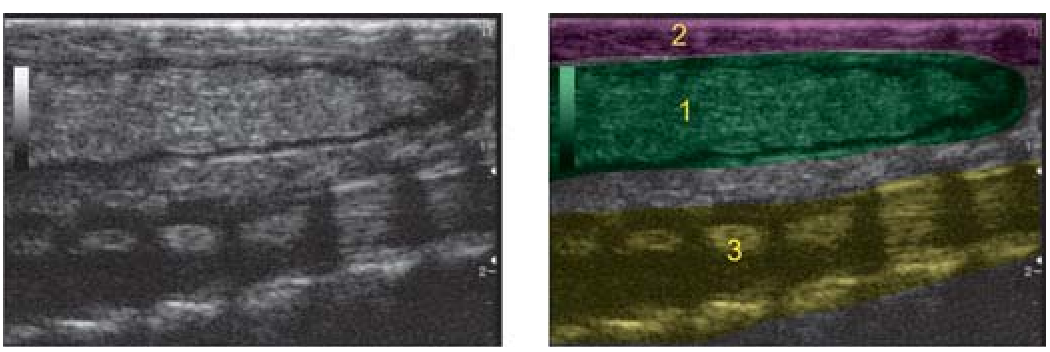

1: stomach
2: ventral body wall
3: spinal musculature and spine

Fig. 3-76: Ultrasonographic image of a corn snake (*Pantherophis guttatus*), longitudinal ventral coupling site, 12 MHz, PD 3 cm. Normal, nearly empty stomach.

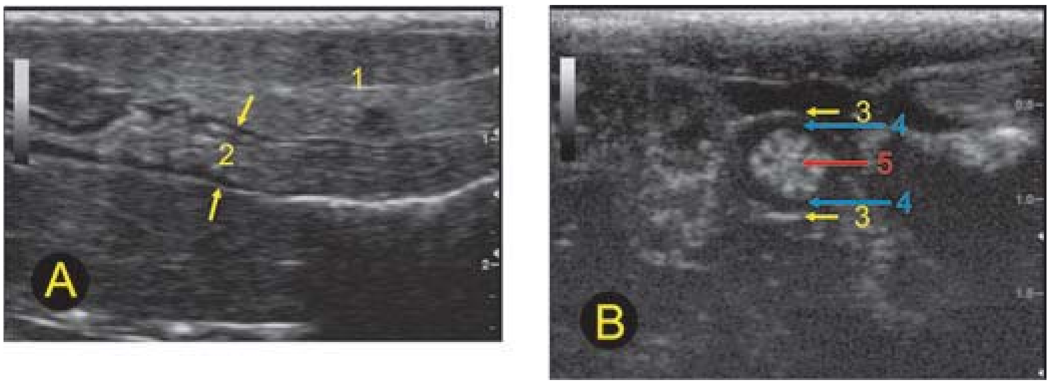

1: fat body
2: intestine with its boundary (arrows)
3: serosa
4: muscularis
5: intestinal contents

Fig. 3-77:

A: Ultrasonographic image of an emerald tree monitor (*Varanus prasinus*), longitudinal ventral coupling site, 12 MHz, PD 3 cm. Longitudinal section through normal intestines (2).

B: Ultrasonographic image of a Chinese water dragon (*Physignathus cocincinus*), transverse ventral coupling site, 12 MHz, PD 2 cm. Transverse section of the normal intestines. The intestinal wall and the intestinal contents can be clearly differentiated.

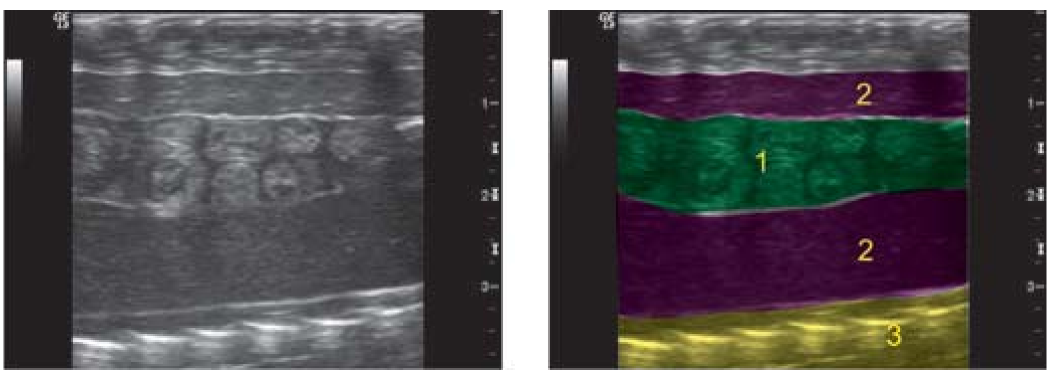

1: colon with feces
2: fat
3: spinal musculature and spine

Fig. 3-78: Ultrasonographic image of a boa constrictor (*Boa Constrictor*), longitudinal ventral coupling site, 8 MHz, PD 4 cm. Normal, full intestinal tract.

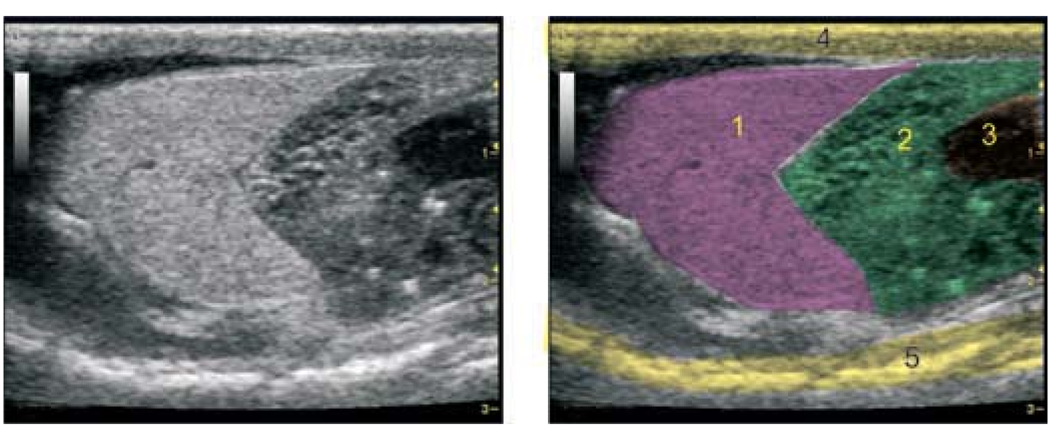

1: fat body
2: intestines
3: allantois

Fig. 3-79: Ultrasonographic image of a central bearded dragon (*Pogona vitticeps*), transverse ventral coupling site, 12 MHz, PD 3 cm. Sonogram showing one of the two intracoelomic fat bodies (1). The fat bodies have an L-form in cross-section and extend cranially to the liver on both the left and right side of the body cavity.

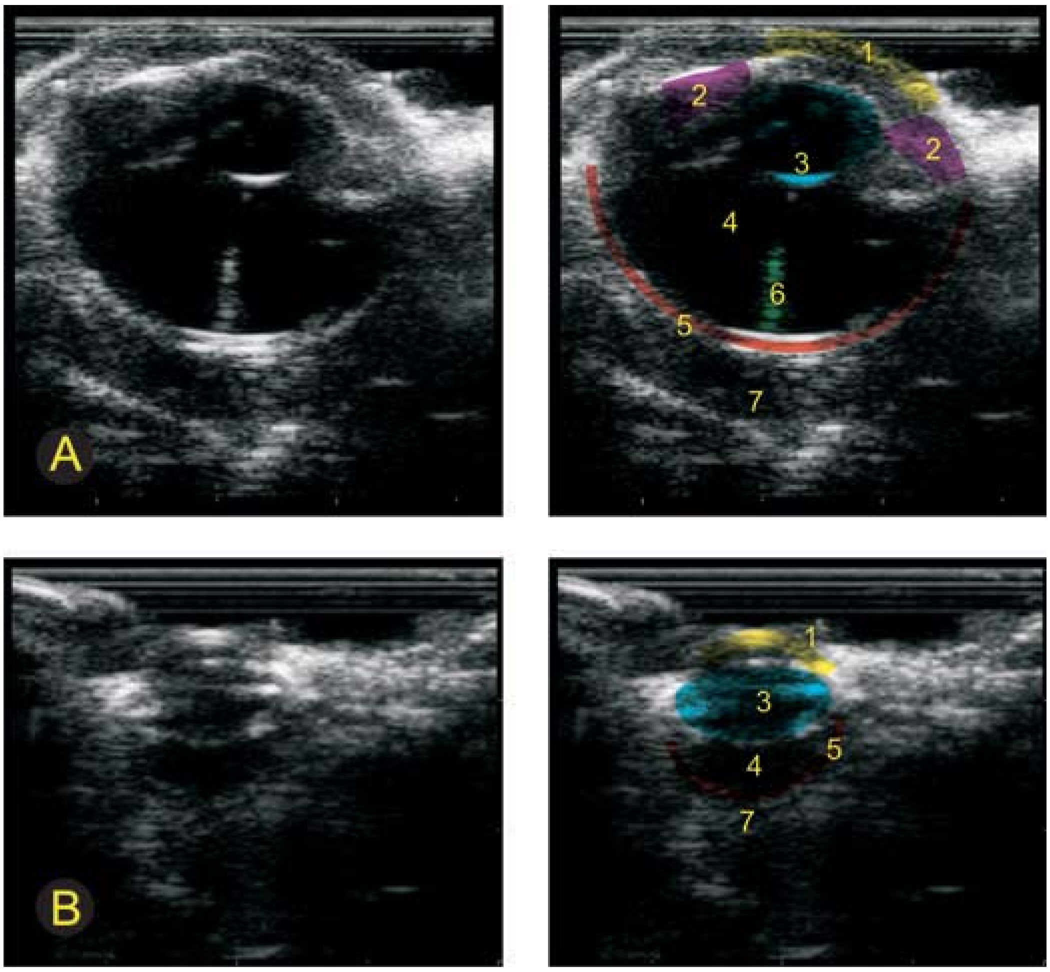

1: cornea/spectacle
2: iris
3: lens
4: vitreous body
5: background of the eye
6: papillary cone
7: orbit

Fig. 3-80:

A: Ultrasonographic image of a central bearded dragon (*Pogona vitticeps*), corneal coupling site, 15 MHz, PD 2 cm. Normal eye.

B: Ultrasonographic image of a boa constrictor (*Boa constrictor*), spectacle coupling site, 15 MHz, PD 3 cm. Normal eyes.

3.3 Computed tomography (CT)

Ingmar Kiefer, Michael Pees

3.3.1 Equipment

In a CT examination, sectional images are produced with a three-dimensional method. Using reformation and the respective reconstructions, various planes and also 3D models can be produced and assessed. The length of the investigation usually lasts for a maximum of approximately 90 seconds, which is very short in comparison to other imaging modalities such as MRI. The scanners used are usually those designed for human medicine, however, the examination parameters must be applied to the patient. Correct positioning may be difficult in very long reptiles, especially snakes. For more information about the technical details, please refer to the literature on the use of CT in mammals.

The following basic standard settings have proven to be suitable in reptiles:

Slice thickness and collimation should be adjusted to the desired examination; usually a slice thickness of 1–2 mm is adequate. Depending on the disease concern, a suitable reconstruction filter should be used which emphasizes the structures to be assessed (e.g. bone).

Other diagnostic applications of CT are the performance of virtual endoscopy and the use of contrast studies to image the vascular system. However, there is little current data about reptiles regarding these procedures.

3.3.2 Preparation, positioning, and scanning planes

To minimize motion artifacts, reptiles need to be immobilized. In chelonians, it is often adequate to bind the animal's limbs in its shell. However, anesthesia is necessary in very active chelonians, lizards, and snakes. Small, weak, and depressed lizards can be examined without any sedation by positioning them on a board or in a plexiglass cage.

For radiation protection and processing of the data, the investigation field should be limited to the respective area of interest. Chelonians, due to their compact form, are often completely scanned. Conversely, in snakes, a localization of the area to be investigated (where possible achieved by previous radiography, ultrasonography and marking) is usually needed. The examination should be done with the reptile lying in ventral recumbency to ensure that the internal organs remain in their normal position. The patients are positioned so that the images are taken cranial to caudal along the longitudinal axis of the animal, producing transverse slices **(Fig. 3-81)**. In small lizards and chelonians, where the patient can be placed across the gantry, sagittal slices along the transverse axis of the animal are recommended. This method is only used in older machines as it is not advantageous in the new generation of machines because they are capable of producing isotropic voxels. It is recommended to lay small reptiles on a foam cushion to better adjust the field of projection. Usually large snakes can only be positioned on the CT table so that the caudal part of their body is bent around and laid doubled on the table **(Fig. 3-82)**. For CT imaging of the caudal regions, the animal must be turned around so that the examination can be performed in a posteroanterior direction.

3.3.3 Assessment of the organs

The internal organs can be precisely imaged and evaluated in the CT slices. This is a significant advantage, especially in chelonians, in which the assessment of radiographic images is often not possible due to the attenuation of the beam caused by the shell and the severe summation of the internal organs arising from the compact form of these animals. The review of CT data is done using the software designed for use in mammals. The radiodensity (Hounsfield units, HU) of reptilian organs (e.g. bone, fat, parenchymal organs) is mainly that of mammals, therefore interpretation is possible using such software. The windows (and the W and L values) set in mammals for the optimal imaging of certain organs is limited for use in reptiles as the respective anatomical conditions are occasionally very different.

3.3.3.1 Skeletal system

Computed tomography is a very valuable aid for examining the skeletal system of reptiles. The assessment should always be performed in all reformations and, if need be, in 3D reconstructions. This allows for the diagnosis of metabolic bone disease (MBD) with its associated lack of mineralization, excessive osteogenesis, pathological fractures, and bending of the bones. By measuring the bone density, not only the degree of disease can be determined but also the therapeutic success of mineralization can be evaluated.

Fig. 3-81: Positioning of a green iguana (*Iguana iguana*) for a CT scan along the longitudinal axis of the animal.

Fig. 3-82: Positioning of an Indian python (*Python molurus*) for a CT scan along the longitudinal axis of the animal. Due to its length, the caudal part of the body has been positioned back onto the table. An even and symmetrical positioning of a snake patient is of great importance when interpreting the CT images.

The assessment of the bones for MBD should be done in chelonians in the region of the pectoral or pelvic girdles **(Fig. 3-83)**, lizards in the region of the long bones, and snakes, the ribs. The bone density of the cortex should be about 1000 HU. In chelonians, the thickness and structure of the shell are also used for assessing metabolic disturbances of growth or mineralization. The 3D image of the shell or skeleton of a reptile with MBD will show the obvious disease conditions (i.e. evident even to the owner) in comparison to a healthy animal **(Fig. 3-84**; pathological situation see **Fig. 3-129)**.

In complex fractures, especially in chelonian shell fractures, a 3D reconstruction can be used to clearly determine the degree of damage and the dislocation of the bone fragments. Luxations and bony changes (e.g. infections, lysis) can be observed in the region of the joints providing the examiner with opportunity to assess the severity of disease. Anomalies in the vertebrae should be examined when assessing the health of the spinal column; often osteogenesis is identified as a consequence of chronic inflammatory processes. Luxations of the vertebral bodies and narrowing of the spinal canal can be imaged using CT.

Indications

- ☐ metabolic disturbances in growth and mineralization (MBD)
- ☐ limb or shell fractures
- ☐ luxations
- ☐ infections in joints and bones
- ☐ tumors involving the musculoskeletal system

3.3.3.2 Respiratory tract

Computed tomography is the safest and most sensitive method for diagnosing lung pathology in reptiles. Due to the low respiratory rate of reptile species, the respiratory tract is rarely imaged with artifacts. Computed tomography is well suited for snakes and chelonians and is superior to traditional radiographic imaging as pathological changes can be precisely localized with respect to their distribution and size.

The snake lung is a tube-like organ with a central air canal and peripheral homogenous respiratory exchange tissue. Coursing within the pulmonary tissue is a circular blood vessel, which is also clearly visible in CT images. Apart from pythons **(Fig. 3-85)**, usually only one lung is developed **(Fig. 3-86)** in most snake species. Pneumonia may be identified as focal and/or diffuse densities within the lung parenchyma, usually affecting the ventral aspect of the organ. Commonly, the cranial section of the lung is most severely affected and may have a massive accumulation of fluid within the ventral lumen.

In chelonians and the majority of lizard species, the lung appears to have a greater degree of septation **(Figs. 3-87** to **3-89)**. In these animals, the central pulmonary vessel and airways can be easily evaluated. A density will often appear as a focal lesion and can be assessed with respect to its radiopacity. In chelonians, the size of the lungs depends to a great degree on the filling of the body cavity by the other internal organs.

Common indications for examining the upper respiratory tract include the diagnosis of obstructions (e.g. foreign bodies, tumors). When assessing the lungs, it is recommended to make objective and subjective evaluations in the *region of interest* (ROI). When investigating the lungs of an Indian python, measurements are performed on each of four ROIs along the entire length of the lung (at 0%, 25%, 50%, 75% of the length of the imageable lung tissue), whereby the ROI at each of these locations is situated in the upper, lateral and lower regions of the lung tissue **(Fig. 3-90)**. In healthy Indian pythons, no significant differences in density could be determined when evaluated at the specific measurement sites. The reference value for the density of lungs of the Indian python is given as –744.4 ± 47.1 HU (PEES et al. 2007). In addition to the diagnosis of pneumonia, CT examination of the lung tissue is also important for assessing treatment response (PEES et al. 2008).

Indications

- ☐ foreign body
- ☐ obstructive changes
- ☐ pneumonia
- ☐ tumors (abscesses, granulomas, neoplasia)
- ☐ hematomas and lung field perforation

3.3.3.3 Gastrointestinal tract and the liver

The reptile stomach is often partially air-filled and is easy to image in chelonians and lizards **(Figs. 3-91** and **3-93)**. The individual intestinal loops of reptile species can also be assessed **(Fig. 3-92)**. Computed tomography examinations are an important diagnostic tool to localize foreign bodies and tumors. The use of barium sulfate and iodine-based contrast agents in chelonians has been described and commonly used for complete assessment of the gastrointestinal tract. One advantage of CT in comparison to conventional radiographs is its ability to image certain areas of interest (e.g. boundaries, particular radiodensities) that can be enhanced by producing suitable reconstructions.

The liver, its size and structure, can also be easily visualized in reptiles using CT imaging **(Figs. 3-94** to **3-96)**. The texture of the liver and the hepatic blood vessels can be assessed as in mammals. The radiodensity of liver tissue in healthy chelonians is between 50–70 HU but it is reduced with an increase of fat deposition (GUMPENBERGER 2004). In snakes, the gallbladder is located caudal to the liver.

Indications

- ☐ constipation
- ☐ foreign body
- ☐ tumors
- ☐ liver: fatty liver, congestion, infection, abscesses, neoplasia

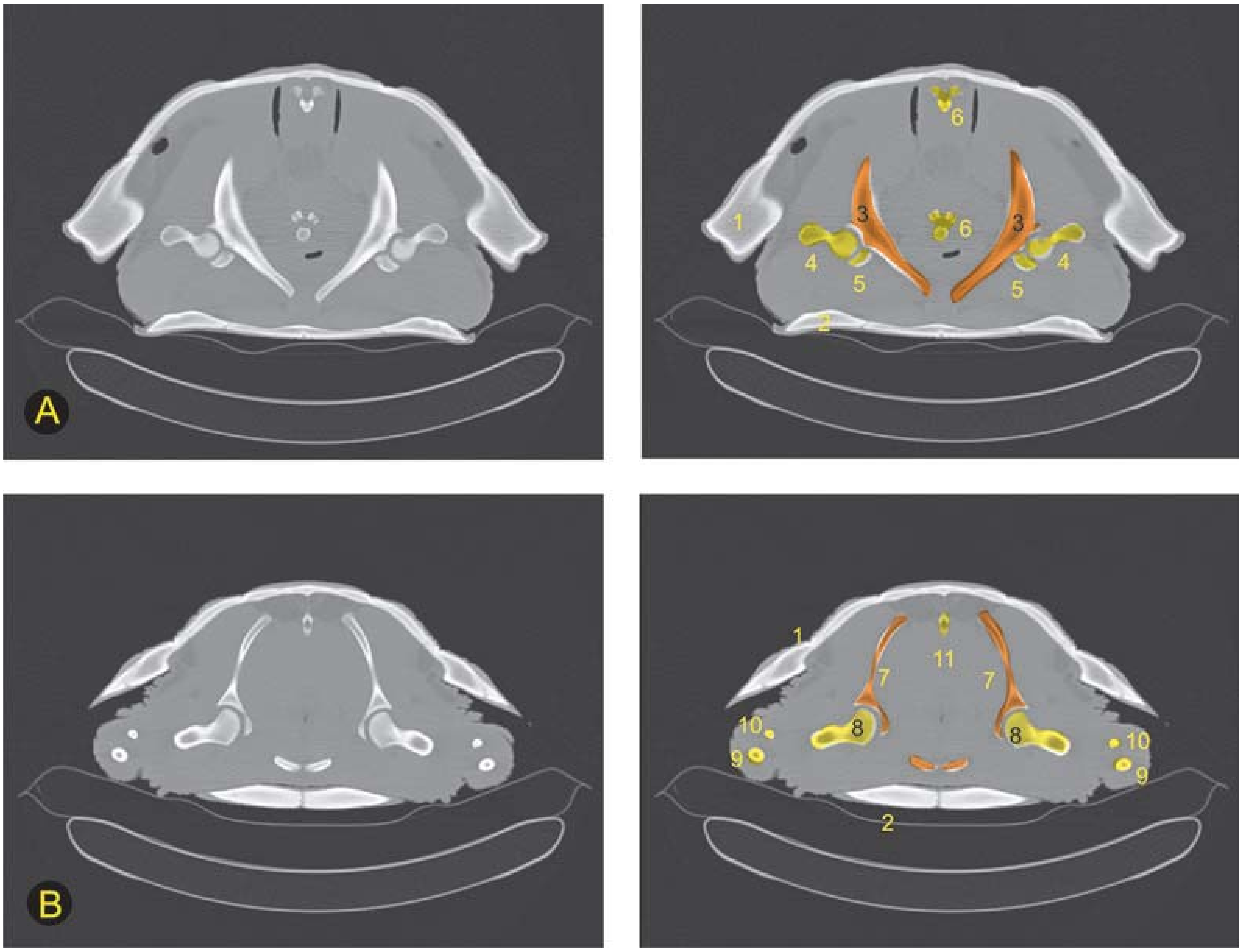

Fig. 3-83: CT images of an African spurred tortoise (*Geochelone sulcata*), body, transverse plane (140 kV, 165 mA, 2.0 mm SD, W: 2630, L: 21). (A) Pectoral and (B) pelvic girdles. The degree of calcification can be well assessed using the bones that make up these structures.

1: carapace
2: plastron
3: scapula
4: humerus
5: coracoid
6: cervical vertebrae
7: pelvis
8: femur
9: tibia
10: fibula
11: spine

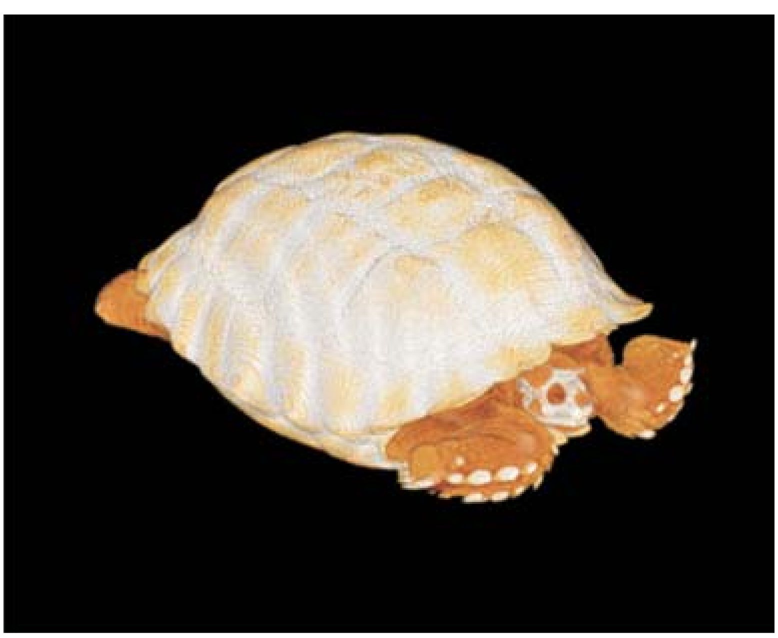

Fig. 3-84: CT image of an African spurred tortoise (*Geochelone sulcata*), body, 3D reformation. Healthy and adequately mineralized shell.

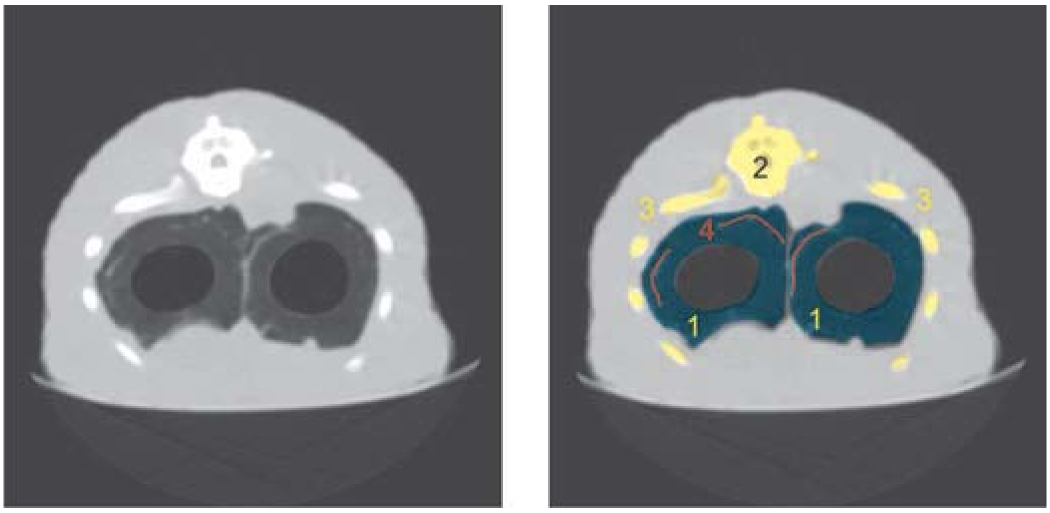

1: respiratory epithelium
2: vertebral body
3: ribs
4: circular plexus of blood vessels

Fig. 3-85: CT image of an Indian python's (*Python molurus*) lungs, transverse plane (120 kV, 204 mA, 2.0 mm SD, W: 1500, L: –600). Scan showing healthy respiratory epithelium (1) around the central airway. The circular plexus of blood vessels (4) is visible in the section. Pythons are snakes with two lungs (c.f. Fig. 3-86).

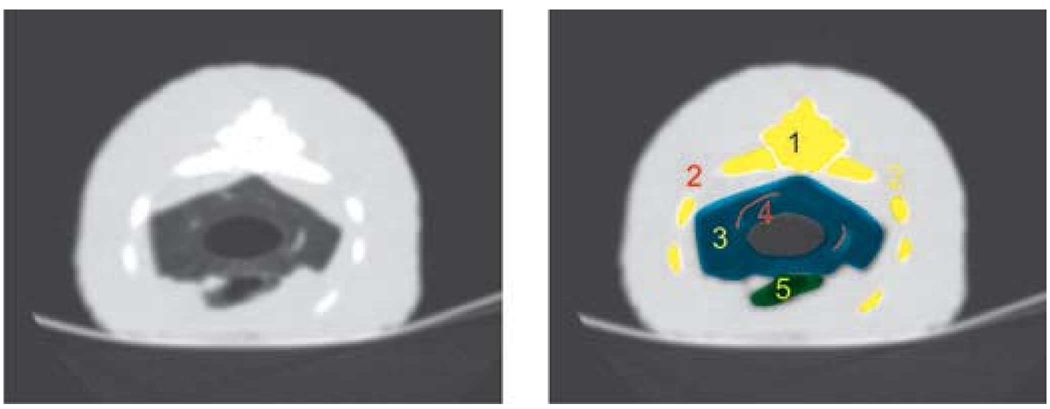

1: vertebral body
2: ribs
3: respiratory epithelium
4: circular plexus of blood vessels
5: esophagus

Fig. 3-86: CT image of a boa constrictor's (*Boa constrictor*) lung, transverse plane (120 kV, 204 mA, 2.0 mm SD, W: 1500, L: –600). Scan showing healthy respiratory epithelium (3) and the circular plexus of blood vessels (4). As in most species of snakes, only one lung is developed in this animal.

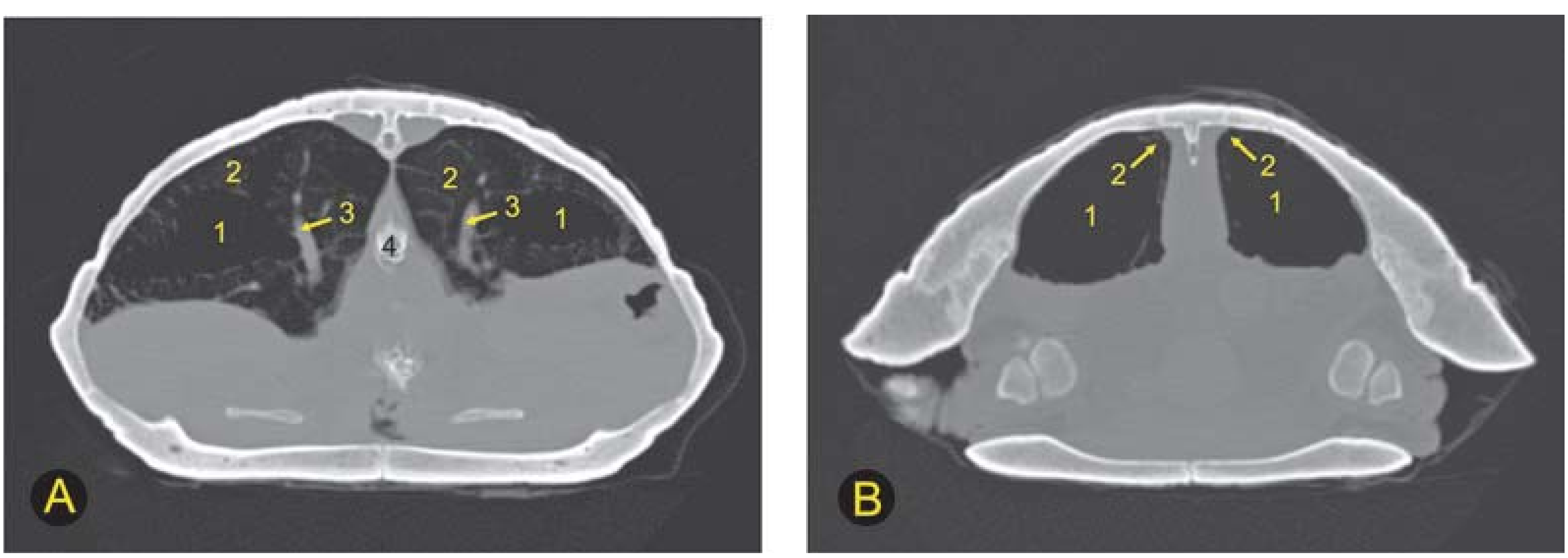

Fig. 3-87: CT images of a red-eared slider's (*Trachemys scripta elegans*) lungs, transverse plane (120 kV, 120 mA, 1.0 mm SD, W: 2642, L: 55). Scan showing normal lung tissue (2) in the cranial (A) and caudal regions (B). The lungs are septated and are aereated via a central lumen (1). In the caudal region, only a little respiratory tissue is present. The two large blood vessels are clearly visible (3).

1: lung lumen
2: lung pareuchyma
3: blood vessels

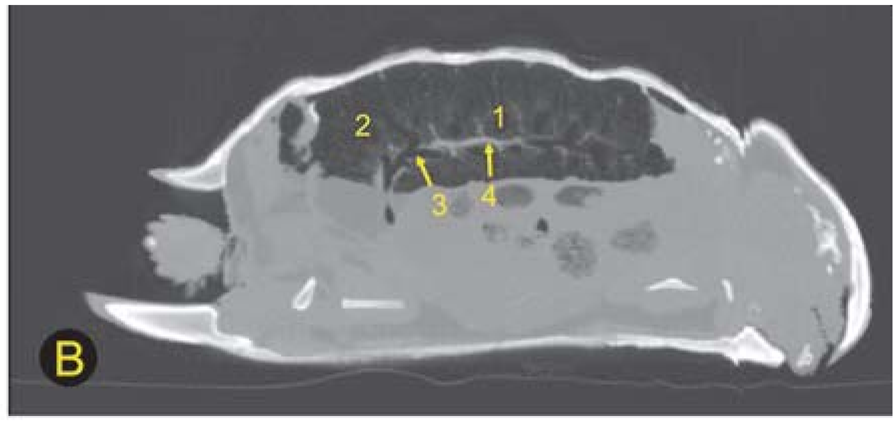

1: lung lumen
2: lung pareuchyma
3: trachea and bronchus
4: blood vessels

Fig. 3-88: CT images of an African spurred tortoise's (*Geochelone sulcata*) lungs, (A) dorsal and (B) sagittal reformation (120 kV, 240 mA, 1.0 mm SD, W: 2549, L: –153). The septations in the lungs are clearly visible as are the airways and vascular supply. The respiratory epithelium is also well developed in the caudal region in this species.

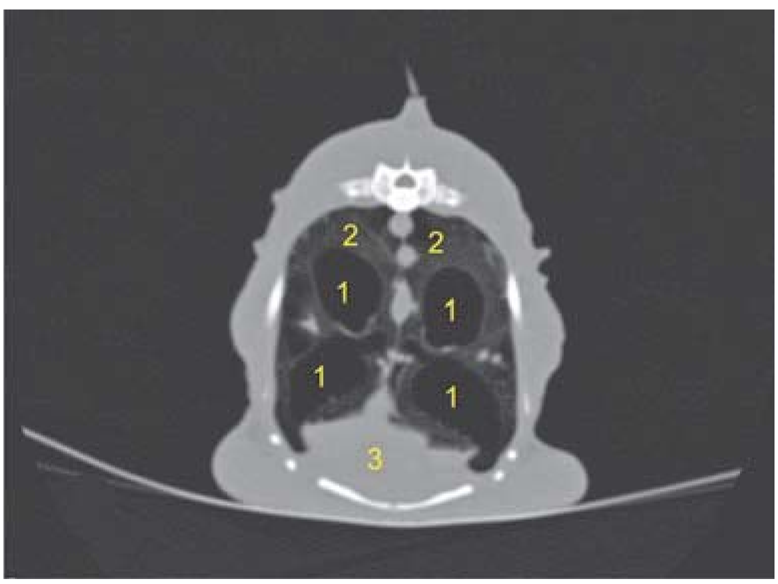

1: lung lumen
2: lung pareuchyma
3: liver

Fig. 3-89: CT images of a green iguana's (*Iguana iguana*) lungs, transverse plane (120 kV, 120 mA, 1.0 mm SD, W: 2297, L: –92). Scan showing healthy respiratory epithelium (2) around the central airway (1). Iguanas and other lizard species can fill their lungs with large amounts of air as a threatening gesture, giving the impression of hyperinflation.

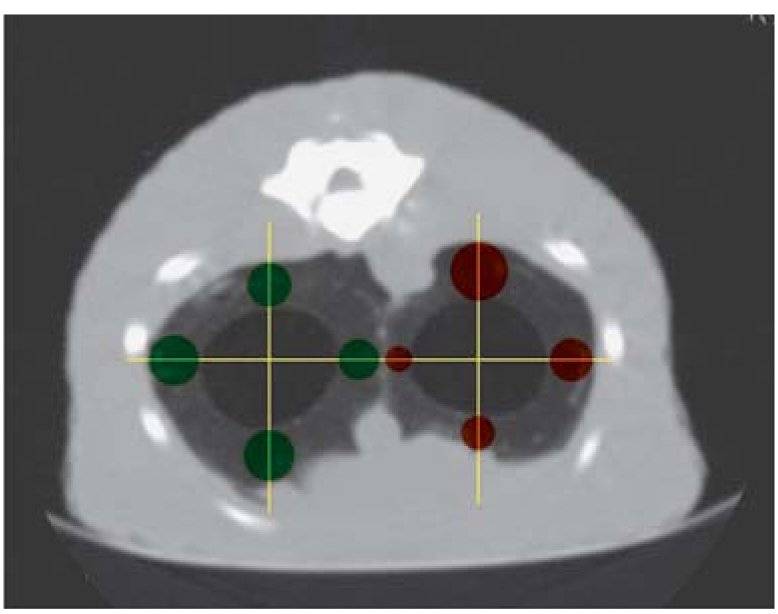

Fig. 3-90: Schematic representation of the adjustment of the ROIs for the assessment of lung density in snakes. In healthy snakes, there should be no obvious differences between the measuring fields.

1: lungs
2: blood vessels
3: stomach

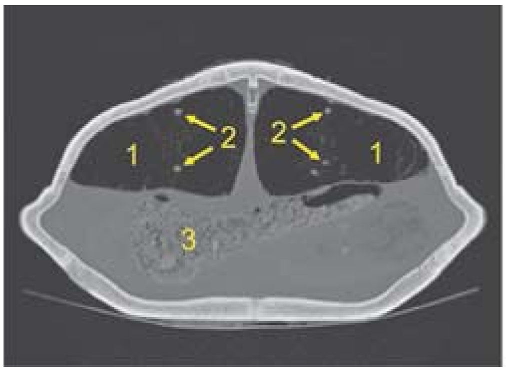

Fig. 3-91: CT image of a red-eared slider's (*Trachemys scripta elegans*) body, transverse plane (140 kV, 155 mA, 0.8 mm SD, W: 3618, L: 379). Lungs (1), blood vessels (2), and stomach (3). A moderate amount of air in the stomach is considered normal.

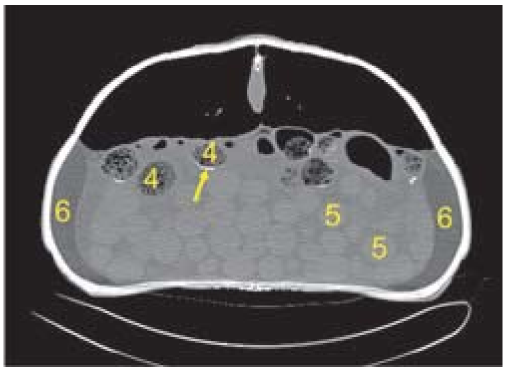

Fig. 3-92: CT image of an African spurred tortoise's (*Geochelone sulcata*) body, transverse plane (140 kV, 165 mA, 2.0 mm SD, W: 2600, L: 60). Scan showing intestinal loops (4) in cross-section and normal follicles (5). The follicles usually fill the lower part of the body cavity and the intestinal loops are displaced dorsally. A small amount of sand (arrow), lying ventrally in the intestines, is considered to be normal.

4: intestinal loops in cross-section
5: follicles
6: adipose tissue

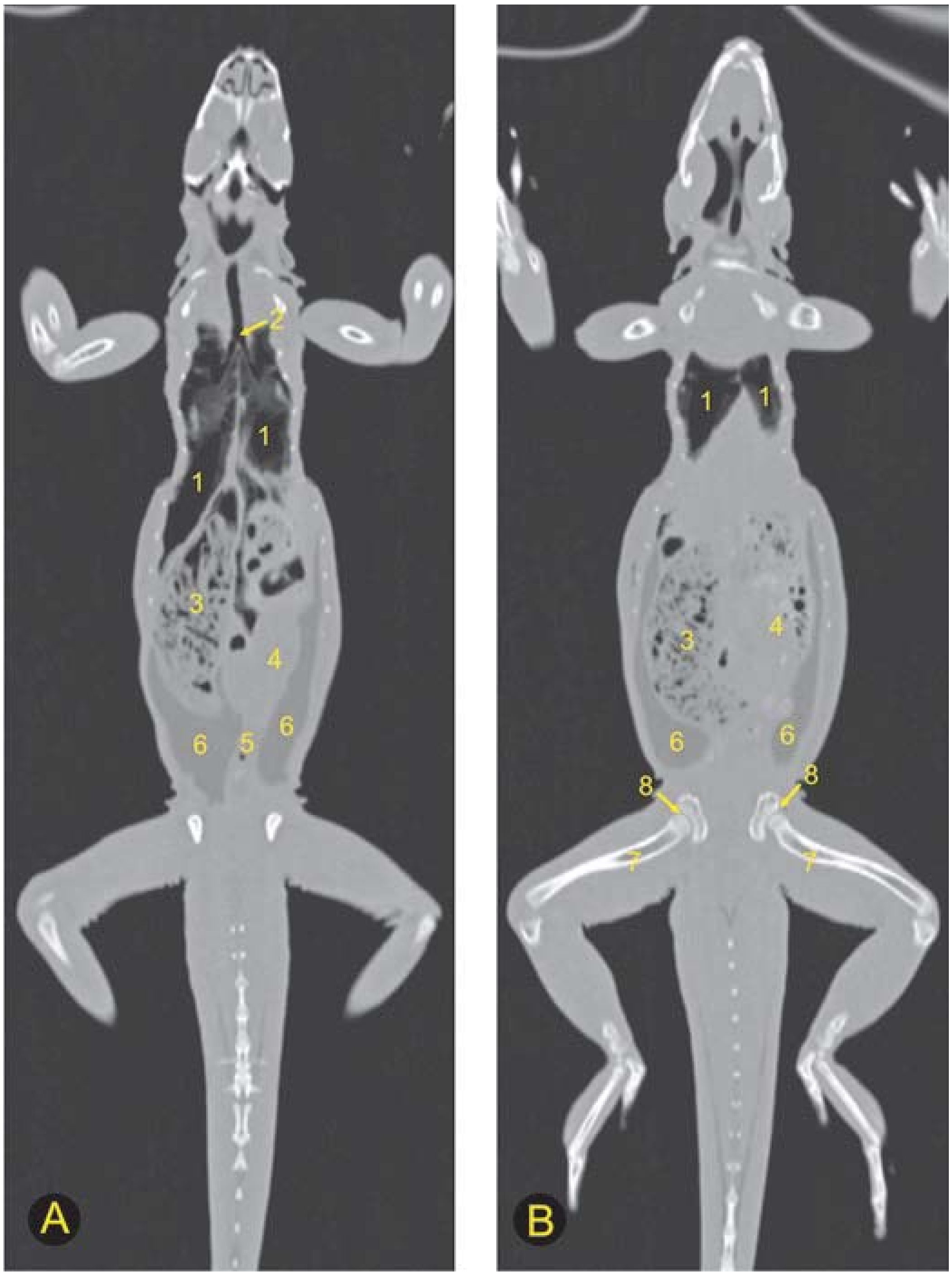

1: lungs
2: trachea
3: stomach
4: intestines
5: rectum
6: fat body
7: femur
8: hip joint

Fig. 3-93: CT images of a green iguana's (*Iguana iguana*) body, dorsal reformation (120 kV, 120 mA, 1.0 mm SD, W: 2200, L: –100). Scans showing (A) the trachea and lungs, (A, B) gastrointestinal tract, and (B) hip joint.

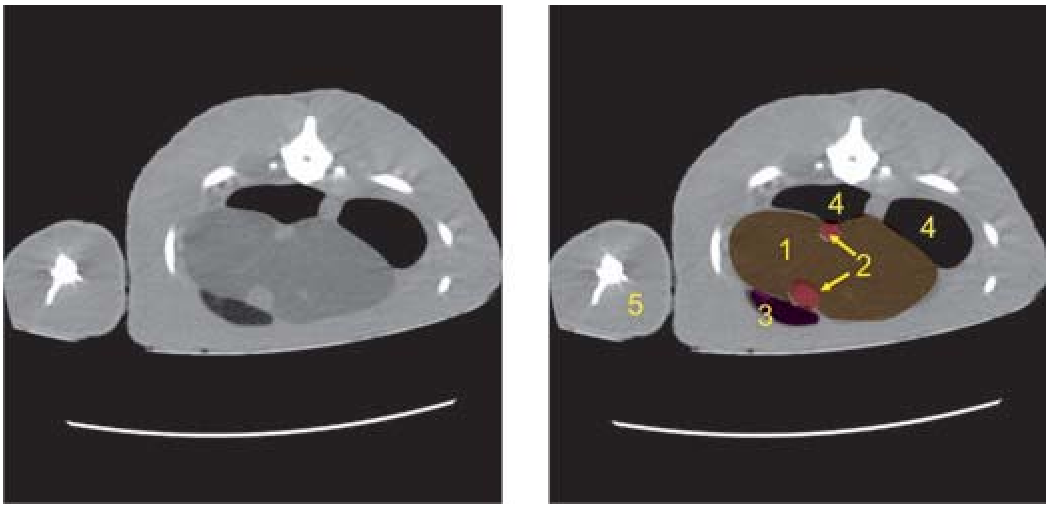

1: liver
2: large blood vessels
3: adipose tissue
4: air sacs
5: turned-over tail

Fig. 3-94: CT image of an Indian python's (*Python molurus*) liver, transverse plane (120 kV, 204 mA, 2.0 mm SD, W: 400, L: 60). Cross-sectional image of the liver (1). The two large blood vessels (2) can be viewed as they course through the liver.

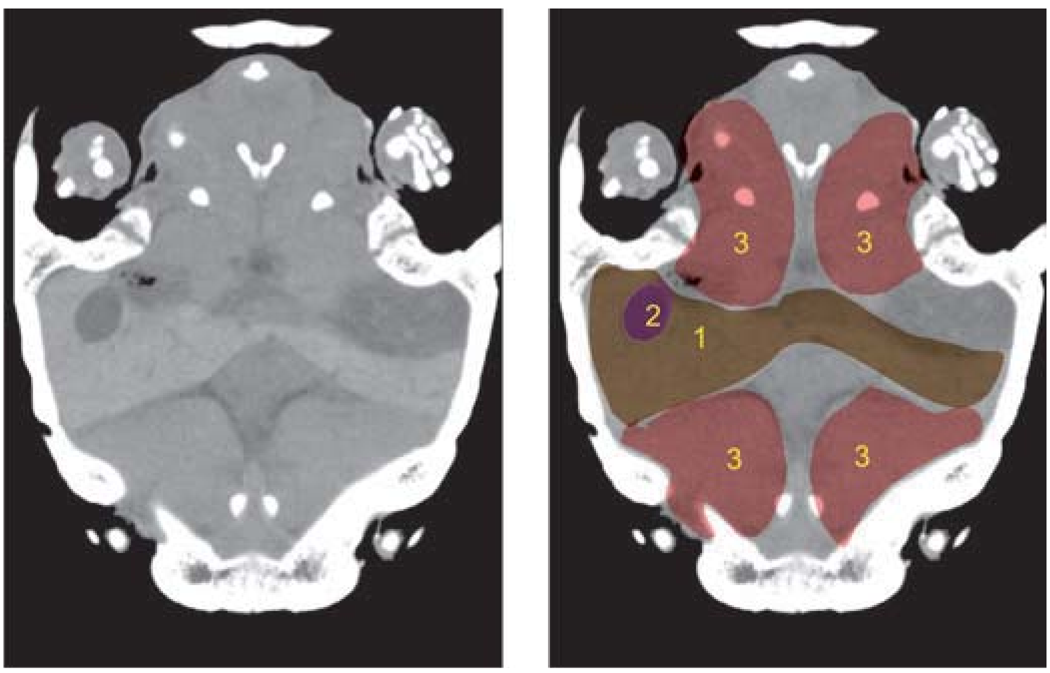

1: liver
2: gallbladder
3: limbs

Fig. 3-95: CT image of a spur-thighed tortoise's (*Testudo graeca*) body, dorsal reformation (120 kV, 151 mA, 1.0 mm SD, W: 400, L: 60). Liver (1) and gallbladder (2). The animal has retracted its head and limbs during the examination, therefore the internal organs are somewhat compressed.

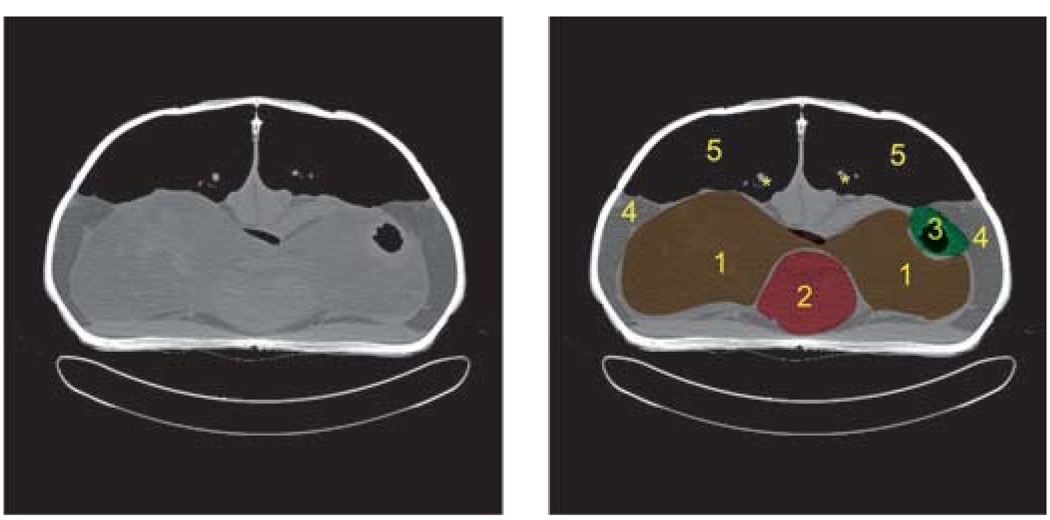

1: liver
2: heart
3: stomach
4: adipose tissue
5: lung field

*: blood vessels

Fig. 3-96: CT images of an African spurred tortoise's (*Geochelone sulcata*) body, transverse plane (140 kV, 165 mA, 2.0 mm SD, W: 903, L: 146). Liver (1).

3.3.3.4 Urogenital tract

Radiographic results in the region of the urogenital tract can be verified and optimally localized using CT and this is especially true of eggs **(Fig. 3-98)** (abnormal egg shells and egg position [e.g. in the allantois]). Bladder stones can also be visualized and their size assessed with CT imaging. Moreover one can evaluate the follicles in the body cavity and the contents of the eggs (e.g. retained, necrotic eggs).

When imaging the kidney, a dorsal reconstruction will allow comparison of both kidneys. In most cases that involve healthy reptiles, clear imaging of the kidney is not possible without the administration of an intravenous contrast agent **(Fig. 3-97)**. Conversely, enlargement and calcification (due to increased radiodensity) of the kidneys can usually be diagnosed with CT imaging.

Computed tomography of the allantois allows for the evaluation of filling, presence of urate deposits, and uroliths. The advantage of CT over ultrasonography is that the whole of the allantois can be assessed and the projection is not hampered by the limited coupling sites.

Indications

- ☐ imaging and assessment of follicles and eggs: number, size, form, contents, radiodensity
- ☐ enlargement of the kidneys and calcification
- ☐ concretions and stones in the allantois

3.3.3.5 Other organs

There are various indications for using CT for reptile patients as in mammals. The intracoelomic fat bodies found in reptiles can be easily differentiated because of their low radiodensity **(Fig. 3-99)**.

Other important diagnostic uses of CT include examination of the central nervous system after trauma and to evaluate the extent of metastatic tumors. Other tumor types can also be assessed according to their radiodensity and size. In particular, intramural abscesses can be imaged and evaluated with certainty using CT. There are a few reports regarding the examination of lizard vascular systems but the benefit of using CT for this purpose is unknown.

Further reading

GUMPENBERGER, M.: Computed tomography. In: MCARTHUR, S., WILKINSON, R., MEYER, J.: Medicine and surgery of tortoises and turtles. Blackwell, Oxford 2004, pp. 235–238.

PEES, M., KIEFER, I., LUDEWIG, E., SCHUMACHER, J., KRAUTWALD-JUNGHANNS, M.-E., OECHTERING, G. (2007): Computed tomography of the lungs of Indian pythons (*Python molurus*). Am J Vet Res **68**: 428–434.

PEES, M., KIEFER, I., OECHTERING, G., KRAUTWALD-JUNGHANNS, M.-E. (2008): The use of computed tomography for the diagnosis and treatment monitoring of bacterial-induced pneumonia in Indian pythons (*Python molurus*). Vet Rec **163**: 152–156.

1: kidneys
2: allantois
3: fat body
4: stomach
5: pelvis

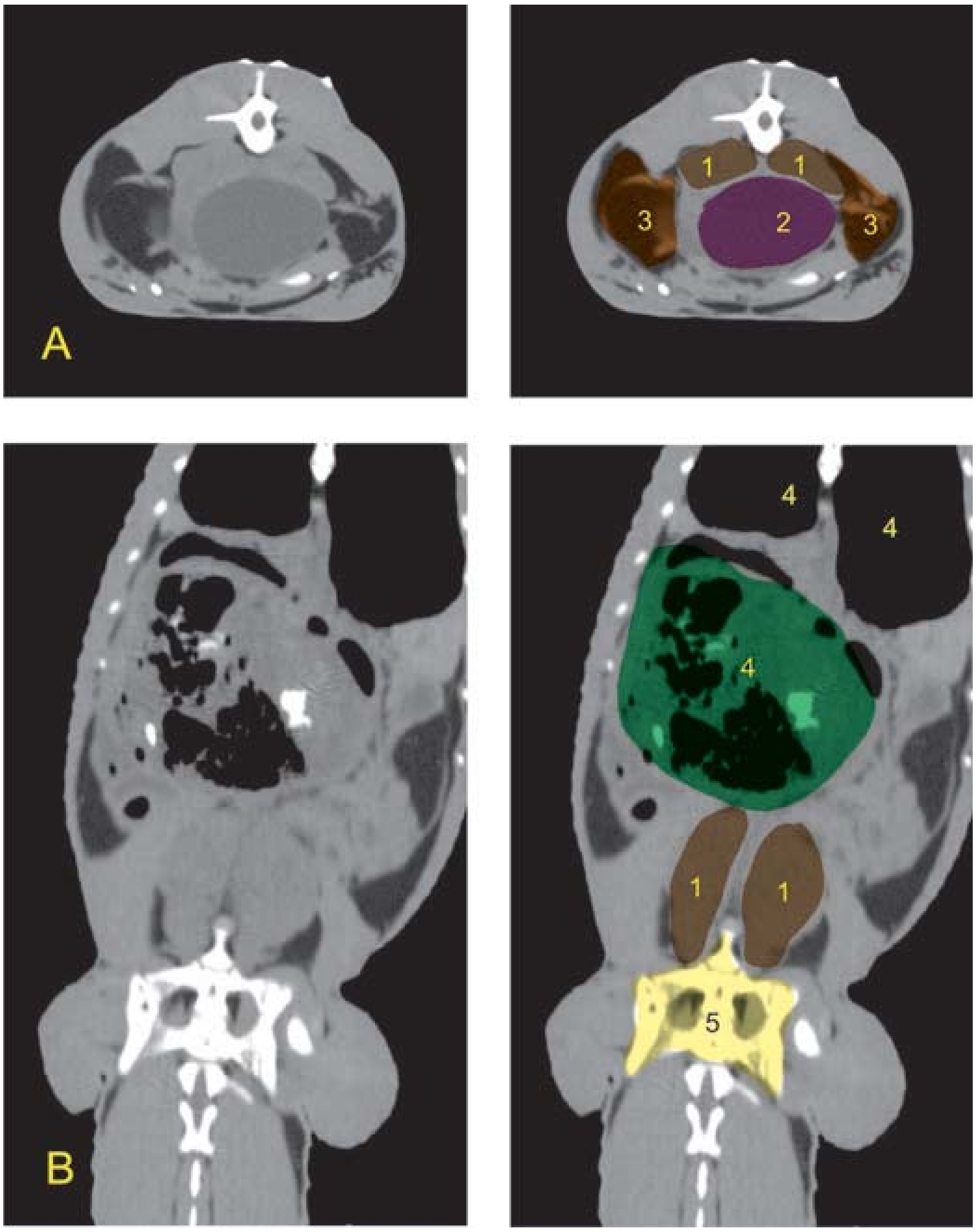

Fig. 3-97: CT images of an American alligator's (*Alligator mississippiensis*) body, (A) transverse plane and (B) dorsal reformation (120 kV, 204 mA, 2.0 mm SD, W: 400, L: 60). Scan showing the kidneys (1) and allantois (2).

1: eggs
2: fat body

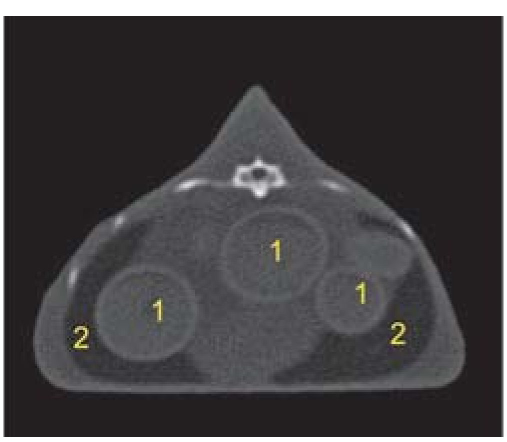

Fig. 3-98: CT image of a Chinese water dragon's (*Physignathus cocincinus*) body, transverse plane (120 kV, 120 mA, 1.0 mm SD, W: 1726, L: 570). Normal eggs (1) within the body cavity.

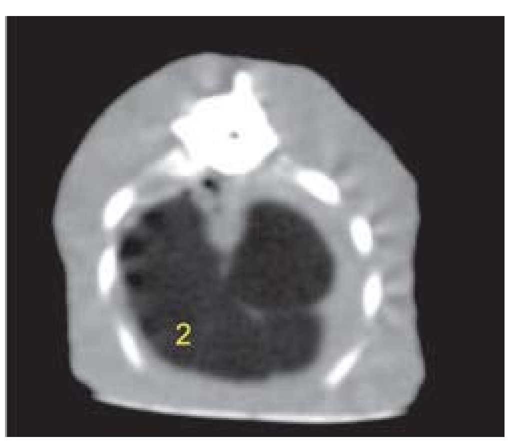

Fig. 3-99: CT image of a carpet python's (*Morelia spilota*) body, transverse plane (120 kV, 204 mA, 2.0 mm SD, W: 350, L: 40). Intracoelomic fat body (2).

3.4 Magnetic resonance imaging (MRI)

Eberhard Ludewig, Michael Pees

3.4.1 Equipment

The main advantage of MRI lies in its ability to visualize soft tissue anatomy and fluids. Magnetic resonance imaging measures the reaction of protons after they have been excited in a magnetic field and the use of different measuring techniques enable a differentiation of the various tissues for a better evaluation of the structures imaged. The most important weightings are classified as T1 and T2. The T1-weighting depicts fat as having very high signal intensity (bright), while fluids have a low signal intensity (dark). Therefore the T1-weighting is used for the assessment of structures that usually contain more fat. In contrast, in the T2-weighting, free fluid has a high signal intensity and fat has middling signal intensity (grey). In the T2-weighting, collections of fluid, such as ascites, effusions, inflammatory exudates, or even allantoic paralysis, can be assessed.

The most important part of a MRI machine is the coil with which the magnetic field is produced. Usually closed MRI systems are used for reptiles. Metallic structures (e.g. foreign bodies in the gastrointestinal tract, microchips) can disturb the magnetic field thereby negating the examination. Knowledge of MRI use on reptile species has been mainly acquired in chelonians (up to a weight of approximately 10 kg) as well as in lizards and boas up to a length of approximately 3 meters.

The potential images and which settings should be used depend to a significant extent on the desired technique and experience of the technical personnel. For specific details relating to MRI technique, please refer to the specialist literature.

3.4.2 Preparation, positioning, and scanning planes

An MRI procedure takes much longer than conventional radiography or CT examination. The length of an MRI procedure and the potential for motion significantly disturbs the measurements, reducing image quality. Therefore general anesthesia is recommended in all but very depressed animals. By anesthetizing the patient, image artifacts are reduced and the reliability of the examination is increased. A phantom (e.g. a water bottle) may be used for small reptiles, so that the coil used in the examination is occupied as much as possible. The authors have experience using quadrature knee coils, in which the animal is in a recumbent position for the examination **(Fig. 3-100)**. Flexible surface coils and head coils are also used to obtain MR images. Flexible surface coils have the advantage of a greater resolution but only have a small field of view. Therefore it is recommended in lizard patients, depending on the animal's size, that a knee coil be used for examinations of the body cavity and a surface coil for investigating individual superficial organs (e.g. kidney).

The animals are placed in ventral recumbency and positioned as needed for the desired examination. Care must be taken to ensure that the animal is positioned as symmetrically as possible for easier adjustment of the planes. The three standard scanning planes are equivalent to those used in mammals (dorsal, transversal, and sagittal).

Due to the length of snakes, it is strongly recommended that the region to be examined be predetermined using other diagnostic methods before performing the MRI. Snakes can be positioned using a plastic tube of a suitable size so that it is easier to perform the MRI examination in segments. Capsules containing either water or fat **(Fig. 3-100C)** may be used to mark the segments of interest because they produce a recognizable identification signal on the scanned images.

The proper MRI scanner settings depend on the technique being used. The authors have experience using slice thicknesses between 2 mm and 6 mm, with the field of view set between 150 mm–190 mm. Reconstruction of the slices is then performed in a matrix of 512 pixels × 512 pixels. The number of slices and the slice interval is individually set for each patient, depending on their condition and the desired results of the MRI examination. However, it is necessary to prepare the examination protocols according to species, size, and indication prior to the procedure (see Further Reading).

3.4.3 Assessment of the organs

In most cases, the ability to image different organ systems of reptile species with MRI is similar to that used in mammals. The imaging limits are primarily dependent on the size of the animals and the resolution of the scanner. Based on experience, MRI in reptiles is suitable for imaging of the respiratory tract, gastrointestinal tract, urogenital tract, liver, and kidneys as well as tumors in general.

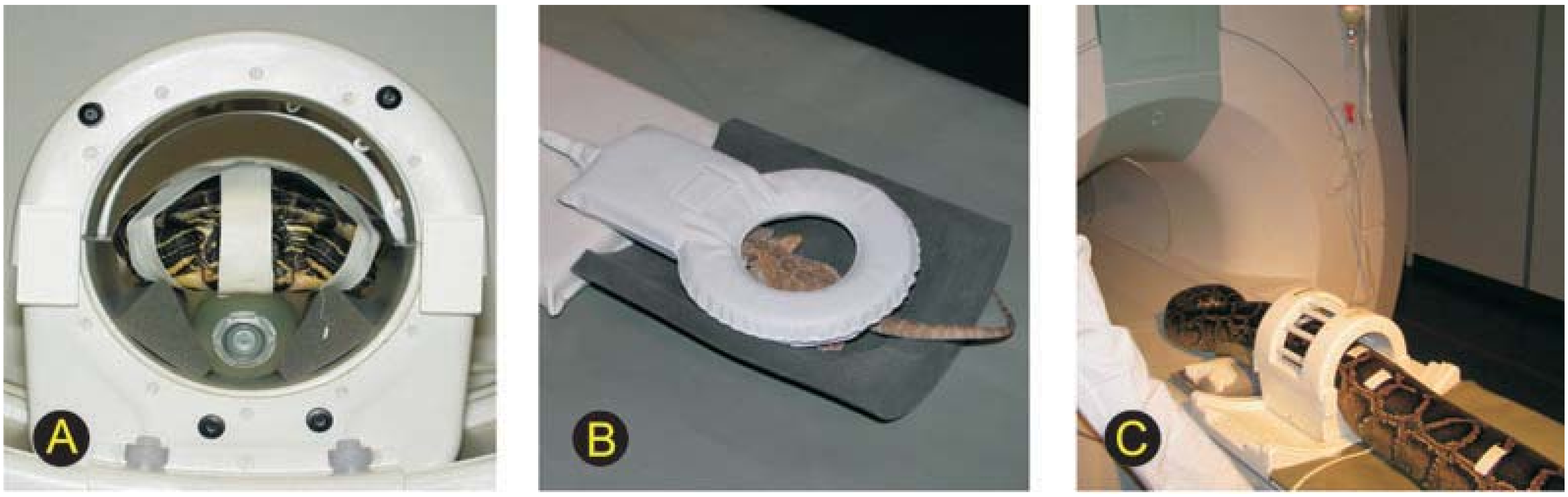

Fig. 3-100: Magnetic resonance imaging, positioning.

A: Examination of a terrestrial chelonian in a quadrature knee coil. To improve the signal quality, a water bottle has been placed as a phantom under the animal.

B: Positioning of a central bearded dragon (*Pogona vitticeps*) under a surface coil to image the the dorsum.

C: Preparation of an Indian python (*Python molurus*) for a MRI examination in a quadrature knee coil. Capsules containing fatty, signal-intensifying media are adhered to the skin, to aid in the correlation of the image slices to a particular part of the body.

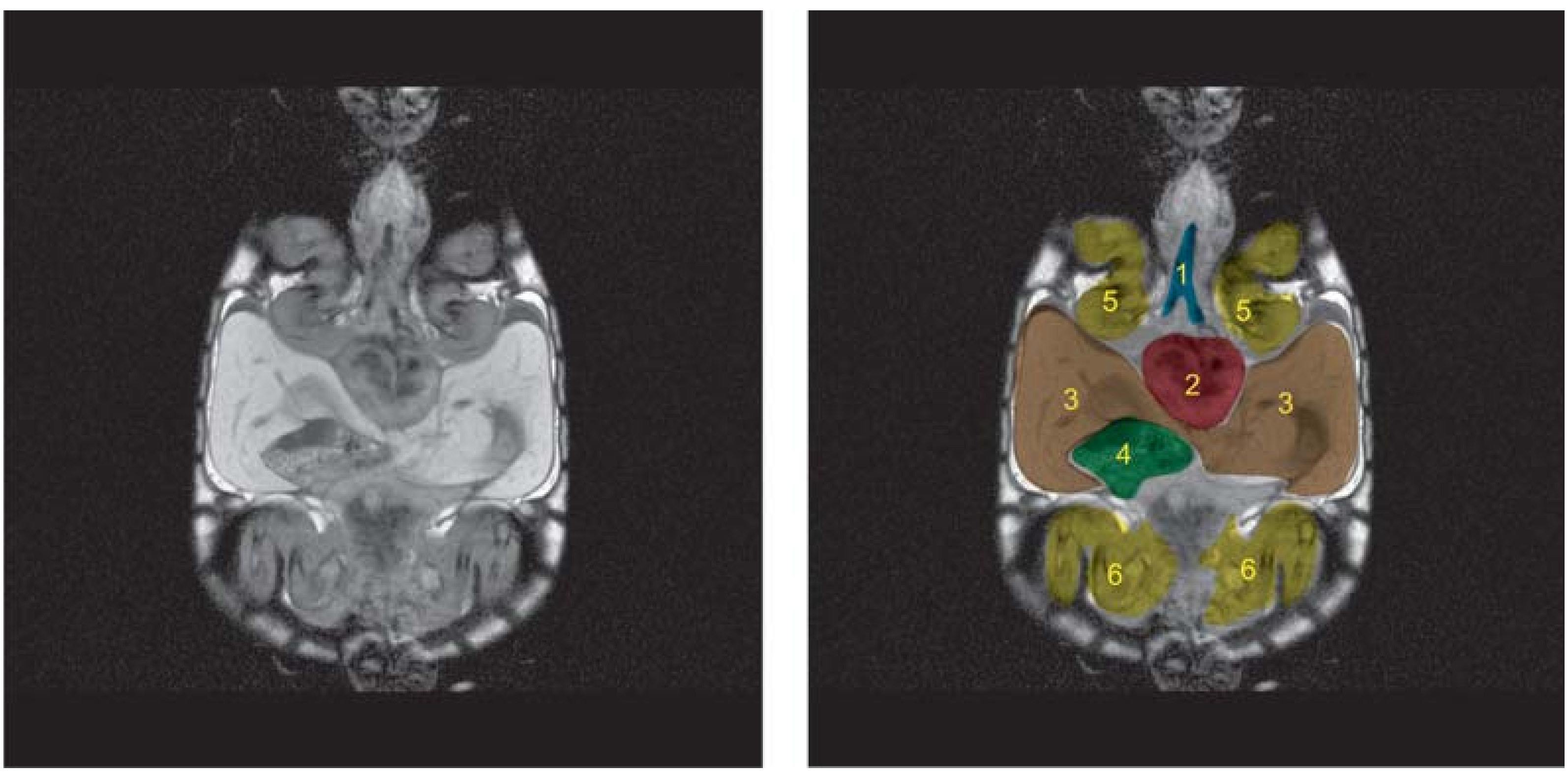

Fig. 3-101: MRI examination of a Hermann's tortoise's (*Testudo hermanni*) trunk, dorsal slice, T1-weighted. Scan showing the normal organs. The early bifurcation of the trachea (1) as seen here is typical of many chelonian species.

1: trachea
2: heart
3: liver
4: gastrointestinal tract
5: retracted forelegs
6: retracted hindlegs

3.4.3.1 Fat bodies and musculature

The fat bodies or fatty tissue have a higher signal intensity than all other organs in both T1- and T2-weightings **(Fig. 3-110)**. This tissue can be used as a comparison in the assessment of the liver parenchyma with respect to its fat content **(Fig. 3-107A)**. The internal structure of the fat bodies is reflected in their lobed configuration in cross-section.

The musculature has a middling signal intensity in both weightings, however, it has a somewhat higher signal intensity in the T1-weighting. As a consequence, the musculature can be used as a comparison for assessing internal organs. The internal structure of the muscles can be assessed using the setting for imaging connective tissue, while the T2-weighting allows the blood supply to be evaluated **(Figs. 3-102A** and **3-110B, D)**.

Indications

- ☐ general assessment and comparison of other organ systems
- ☐ trauma and tumors (musculature)
- ☐ nutritional status (musculature and fat)

3.4.3.2 Respiratory tract

The trachea and the primary bronchi can be assessed throughout their length in different planes **(Figs. 3-101** and **3-113)**. Diseases of the respiratory tract that may be observed in MR images include stenosis, obstruction, and structural anomalies. The structure and size of the lungs can be imaged and assessed. The lungs have the lowest signal intensity in both weightings. The septated chambers and densities within the lizard and chelonian lung tissue can be imaged and evaluated **(Fig. 3-104)**. The T2-weighting is especially important for assessing lizard and chelonian lungs.

Chelonians should be positioned for MR imaging of the lungs with their head and legs extended. If chelonians are not positioned in this manner, the lung fields cannot be assessed as they are compressed by the internal organs due to the presence of the limbs within the shell **(Fig. 3-102B)**.

The lung structure and the distribution of the respiratory epithelium vary greatly between reptilian species; therefore comparative pictures from the same species should be used when assessing the images. The tube-like respiratory epithelium of snakes **(Fig. 3-110)** has approximately the same intensity as the musculature. In T2-weighted images, the respiratory epithelium often has a signal-rich edge in the outer region. The respiratory epithelium can be imaged in the transitional zone between the lungs and the air sacs, whereby a number of slices are usually required.

Indications

- ☐ suspicion of narrowing of the airways
- ☐ trauma (lung hemorrhages)
- ☐ suspicion of pneumonia

3.4.3.3 Liver

The liver is more signal intensive in T1-weighted images compared to those that are T2-weighed **(Figs. 3-102, 3-103, 3-107,** and **3-110)**. In addition to its size, the homogeneity of the hepatic tissue can be assessed and its fat content compared to the fat bodies. The internal structure of the liver is primarily determined by the course of the hepatic vessels. Differentiation of the individual liver lobes is difficult. In T2-weighted images, the intrahepatic blood vessels and the gallbladder can be evaluated and appear to have a high signal intensity **(Figs.3-103** and **3-110)**.

Indications

- ☐ hepatomegaly and inhomogeneity (clinical, radiographic, ultrasonographic)
- ☐ suspicion of fatty liver

3.4.3.4 Gastrointestinal tract

The MR imaging of the gastrointestinal tract is used to assess its contents and the intestinal wall **(Figs. 3-104** and **3-107)**. The walls of the stomach and intestines can be judged with respect to their layers, although an exact differentiation of the individual layers can be difficult. To identify the stomach, it may be useful to follow the course of the esophagus into the stomach. It is not uncommon in lizards and chelonians that the MR image quality of the gastrointestinal tract is reduced by the presence of stones, which cause an extinction of the signal. The gastrointestinal transit time can be evaluated and constipation can be imaged following the oral administration of oily substances (e.g. paraffin oil).

Indications

- ☐ abnormal peristalsis
- ☐ suspicion of stenosis, tumors, or foreign bodies

3.4.3.5 Urinary tract

The kidneys can be evaluated with respect to their size and structure in both weightings. Magnetic resonance imaging is superior to both conventional radiography and CT for performing this type of investigation. In lizards, the use of a surface coil can provide better results in animals with a body weight under 1000 g.

The kidneys are triangular in chelonians **(Fig. 3-102)**, and elongated in lizards **(Fig. 3-108)**. Snakes have kidneys with a »money-roll« shape **(Fig. 3-111)**. The kidneys are often hyperintense in comparison to the musculature.

The contents of the allantois is best demonstrated in T2-weighted images and can be examined for the presence of calculi or tumors. The wall of the allantois is very thin and has the same signal intensity as the muscles. The individual slices of this organ cannot be differentiated.

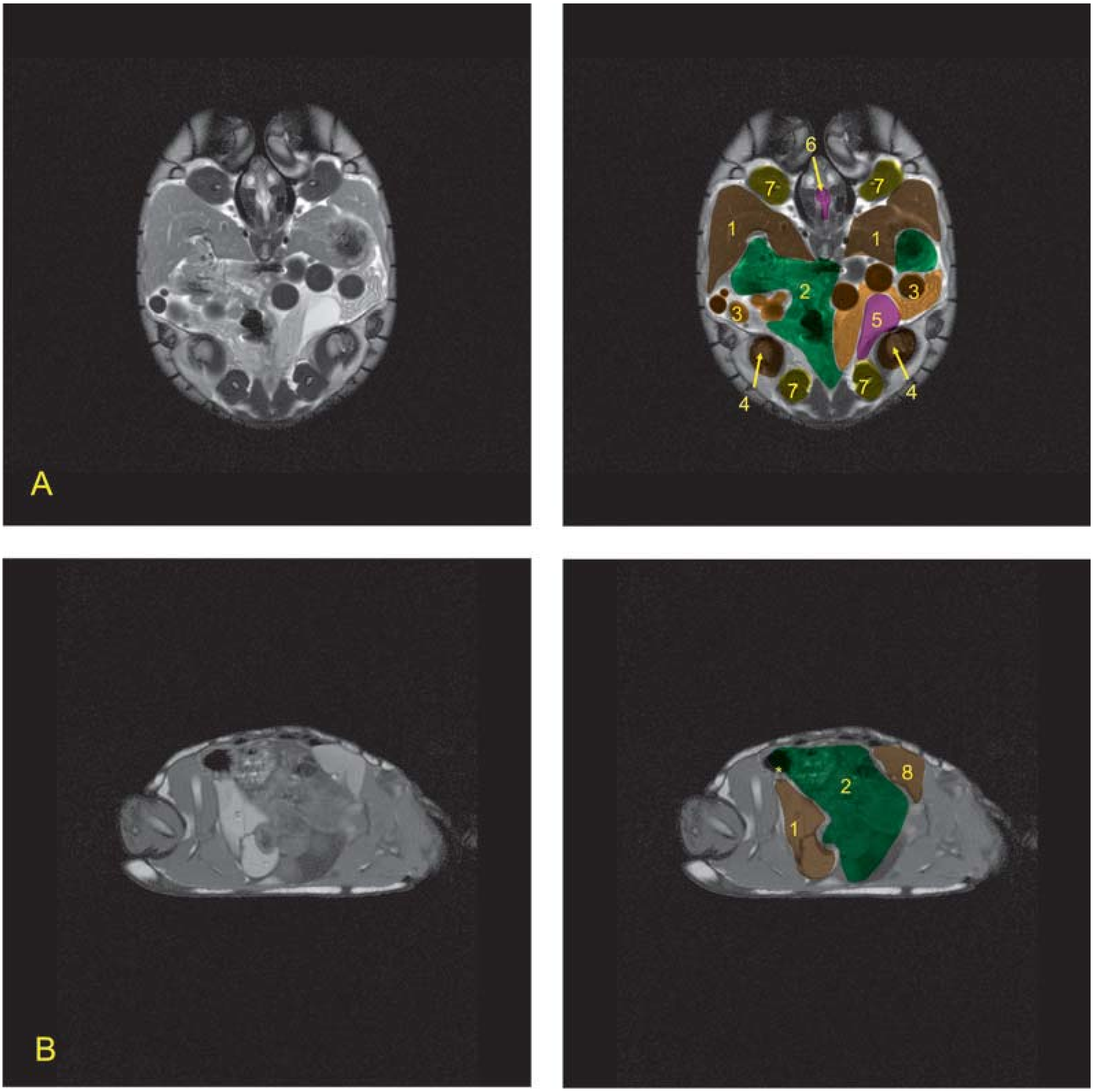

Fig. 3-102:

A: MRI examination of a Hermann's tortoise's (*Testudo hermanni*) trunk, dorsal slice, T2-weighted. Scan showing the normal organs. With this weighting, the blood vessels (1) in the liver can be assessed and the contents of the allantois (5) are shown.

B: MRI examination of a Russian tortoise (*Testudo horsfieldii*), sagittal slice, T1-weighted. As this animal has completely retracted itself inside its shell, the internal organs are compressed and displaced. The lung field is narrowed.

1: liver
2: gastrointestinal tract
3: follicle/oviduct
4: knee in cross-section
5: allantois
6: brain
7: limbs/pelvis
8: kidneys

*: gastric bubble in cross-section

Indications

- ☐ suspicion of renal insufficiency (especially lizards and chelonians)
- ☐ renal enlargement (clinical, radiographic, ultrasonographic)
- ☐ increased filling of the allantois, lack of micturition

3.4.3.6 Genital tract

The active gonads can be easily imaged using MRI and the internal structure of eggs and follicles can also be examined. The images of individual eggs can vary within a single animal **(Figs. 3-105, 3-106** and **3-109)**. During their development, the eggs may have concentric or horizontal layers, whereby the signal intensity of these layers has significant variability. With concentric layering, the egg has a signal-rich center surrounded by layers of varying intensity. Eggs with horizontal layering have three layers in T2-weighted images, whereby a signal-rich dorsal layer is followed by a layer of medium intensity and then a layer with a low signal intensity. In ovoviviparous species, the developing fetuses can be imaged; however, little information is available with respect to their assessment.

Follicles can also be assessed in both weightings **(Fig. 3-112)**. Follicles should be evaluated with respect to their size and homogeneity. As with the eggs, both a horizontal and concentric layering can be identified in the follicle images.

The testicles can be measured and differentiated as organs of medium signal intensity. The (hemi-)penis can be identified in both weightings and depending on the species, may be observed as partially folded structures.

Indications

- ☐ suspicion of ovarian tumors (neoplasia, cysts)
- ☐ disturbances in laying
- ☐ tumors in the hemipenis sac

3.4.3.7 Other Organs

As in mammals, the central nervous system, eye **(Fig. 3-113)**, and skeletal system can be examined using MR imaging. The evaluation of abnormal joint filling (abscesses, gout, tumors) is diagnostically significant. Imaging of the adrenals is not always possible in reptiles. The heart, due to the presence of motion artifacts, cannot be assessed with any great reliability; therefore other methods (e.g. ultrasonography) are more applicable for imaging this organ. The spleen is usually more signal intense in the T2-weighting, while the thymus can be better visualized in the T1-weighting. The thyroid is also more signal intense in T1-weighted images, but it is difficult to differentiate from other organs, especially in small reptiles. The assessment of structural details of the last three organs is limited due to their small size.

Further reading

EFFER, N. (2004): Zur Schnittbildanatomie der griechischen Landschildkröte (*Testudo hermanni boettgeri*) in der Magnetresonanztomographie: Physiologische und pathologische Befunde sowie transhibernale Veränderungen unter definierten Bedingungen. Dissertation, Gießen.

PREUSS, S. (2008): Die Darstellung der inneren Organe des Grünen Leguans (*Iguana iguana*) mittels Magnetresonanztomographie im Vergleich zwischen juvenilen und adulten Tieren. Dissertation, Leipzig.

STIEF, H. (2007): Zur Schnittbildanatomie von Boiden in der Magnetresonanztomographie. Dissertation, Leipzig.

STRAUB, J., JURINA, C. (2001): Magnetic resonance imaging in chelonians. Sem Avian Exot Pet Med **10**: 181–186.

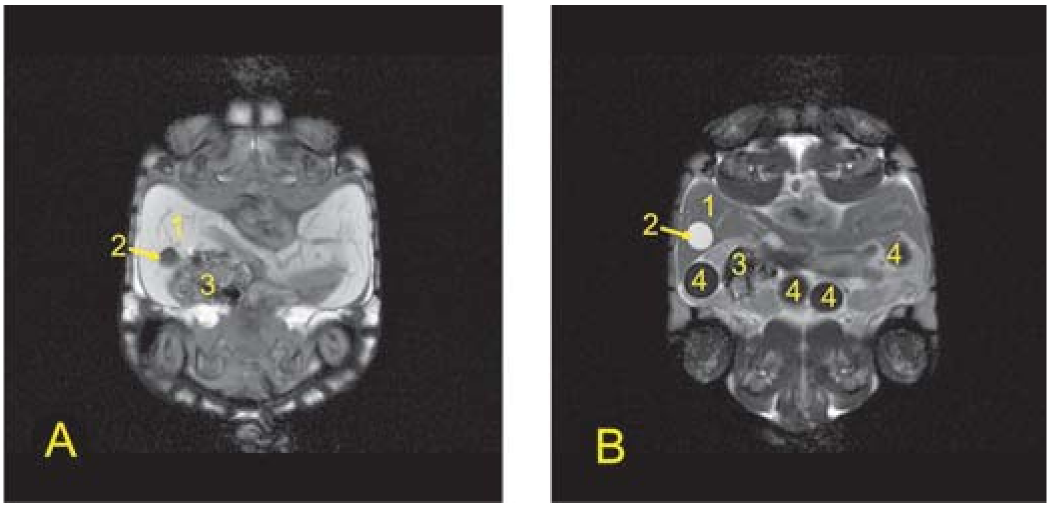

1: liver
2: gallbladder
3: stomach/intestines
4: follicle

Fig. 3-103: MRI examination of a Hermann's tortoise's (*Testudo hermanni*) trunk, dorsal slice, (A) T1-weighted, (B) T2-weighted. Due to its fat content, the liver tissue (1) can be evaluated in the T1-weighted image. The blood vessels and gallbladder (2) both have a high signal intensity in the T2-weighted image.

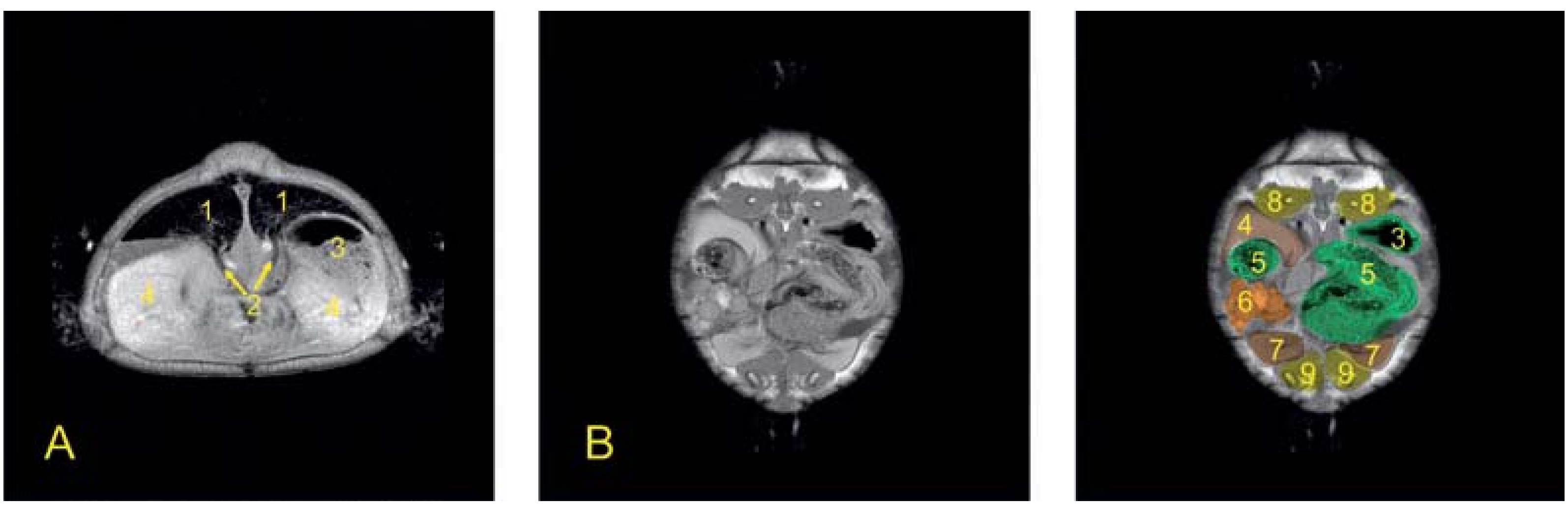

Fig. 3-104:

A: MRI examination of a Hermann's tortoise's (*Testudo hermanni*) trunk, sagittal slice, T1-weighted. Scan showing the entrance of the main bronchi (2) in the lungs (1). The lung tissues have a low signal intensity. Normally, the stomach (3) can contain a certain amount of air.

B: MRI examination of a Hermann's tortoise (*Testudo hermanni*), dorsal slice, T1-weighted. Scan showing liver (4), stomach (3), intestines (5), ovary (6) and kidneys (7). The kidneys are situated in an extreme dorsal position within the caudal body cavity.

1: lungs
2: main bronchi
3: stomach
4: liver
5: intestines
6: ovary
7: kidneys
8: forelegs
9: hindlegs

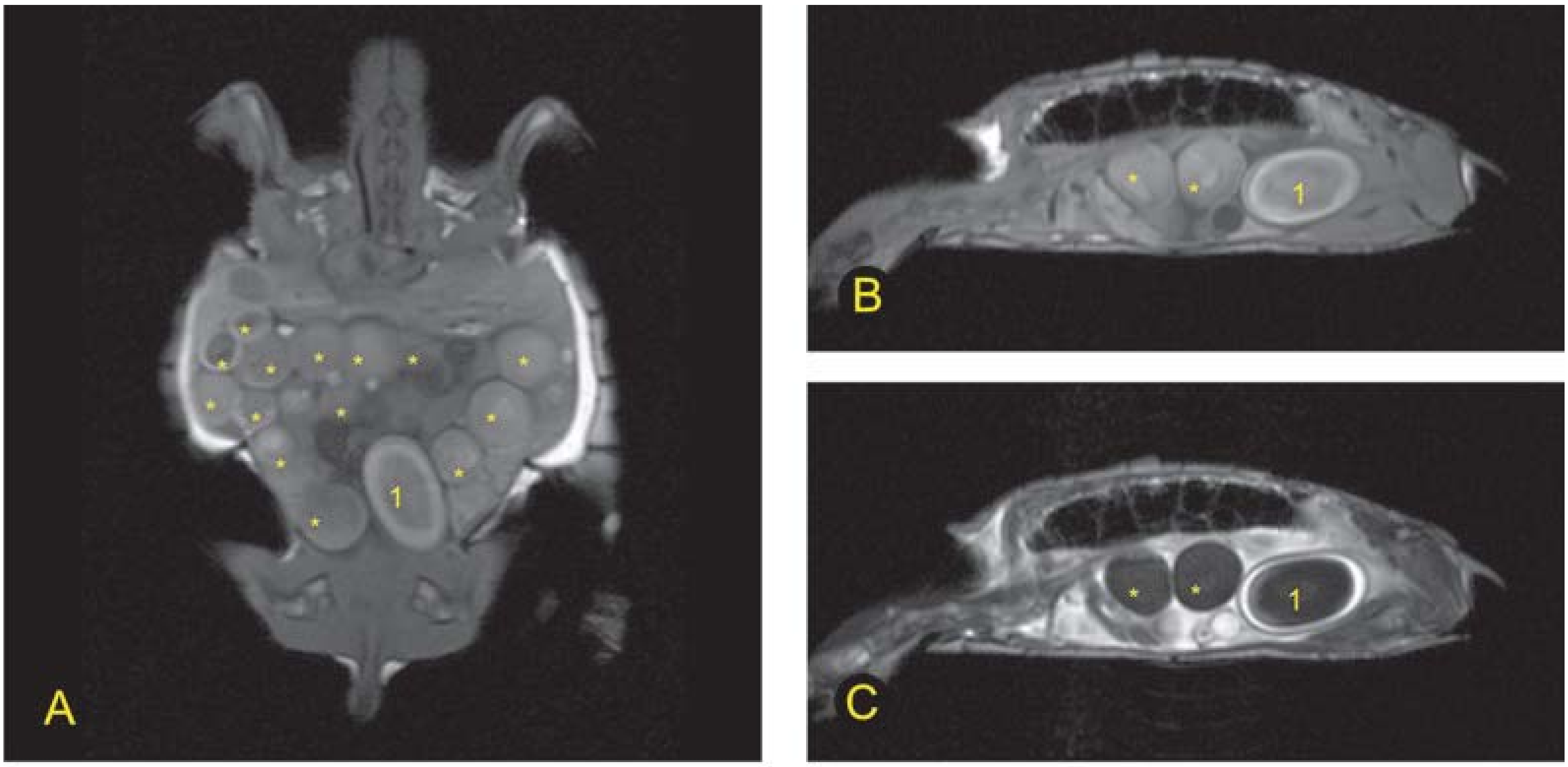

Fig. 3-105: MRI examination of a red-eared slider's (*Trachemys scripta elegans*) trunk, (A) dorsal and (B, C) sagittal slices, (A, B) T1-weighted and (C) T2-weighted. Scan showing numerous follicles (*) and an egg (1).

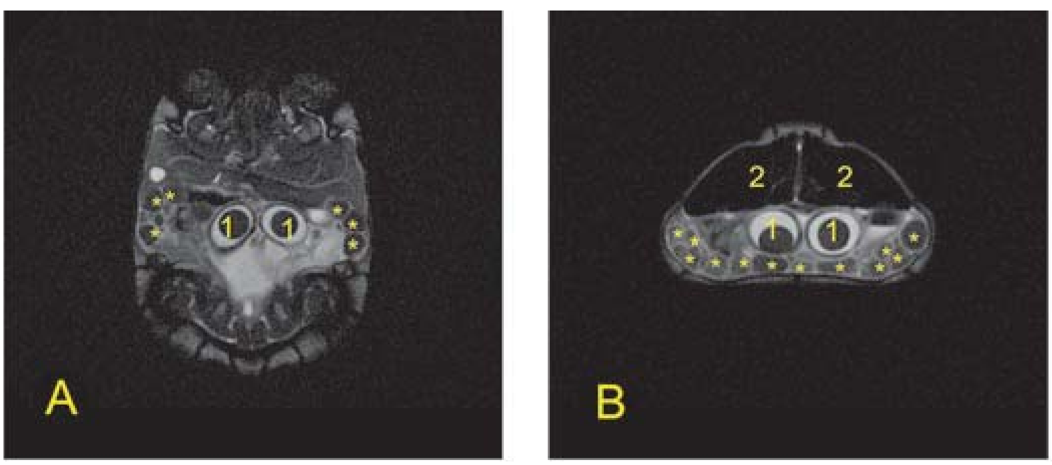

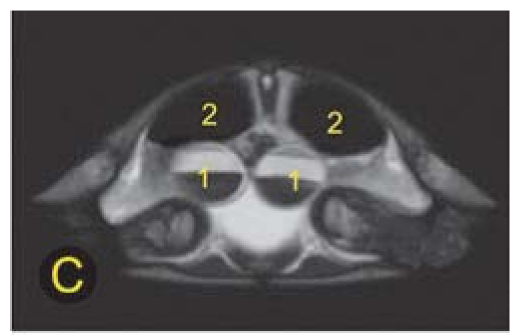

1: eggs with shells
2: lungs

*: follicles

Fig. 3-106: MRI examination of a Hermann's tortoise's (*Testudo hermanni*) trunk.

A, B: (A) dorsal and (B) transverse slices, T2-weighted. Two eggs (1) with shells and a number of follicles (*). The calcium-containing shell has a low signal intensity in the MRI image.

C: MRI examination of a yellow-bellied slider (*Trachemys scripta scripta*), transverse slice, T2-weighted. Developing eggs can also be sliced horizontally, whereby in the T2-weighted image a dorsal (fat-containing) layer of moderate signal intensity and a ventral layer with a low signal intensity can be differentiated from each other.

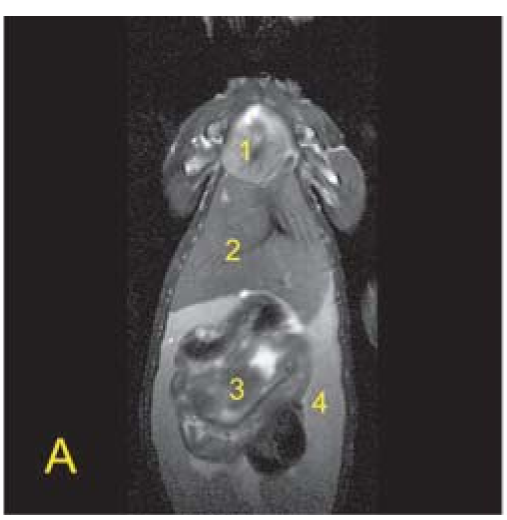

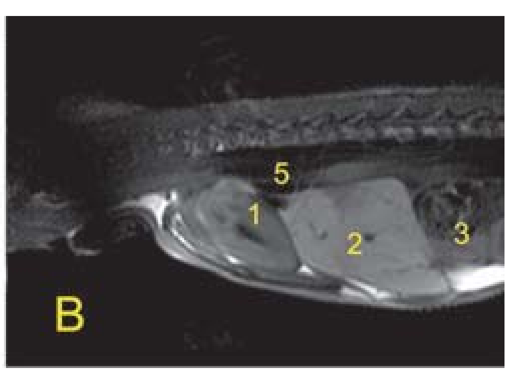

1: heart
2: liver
3: gastrointestinal tract
4: fat body
5: lungs

Fig. 3-107: MRI examination of a green iguana's (*Iguana iguana*) trunk, (A) dorsal and (B) sagittal slices, surface coil, (A)T1-weighted, (B) T2-weighted. Scan showing the heart (1), liver (2), and gastrointestinal tract (3).

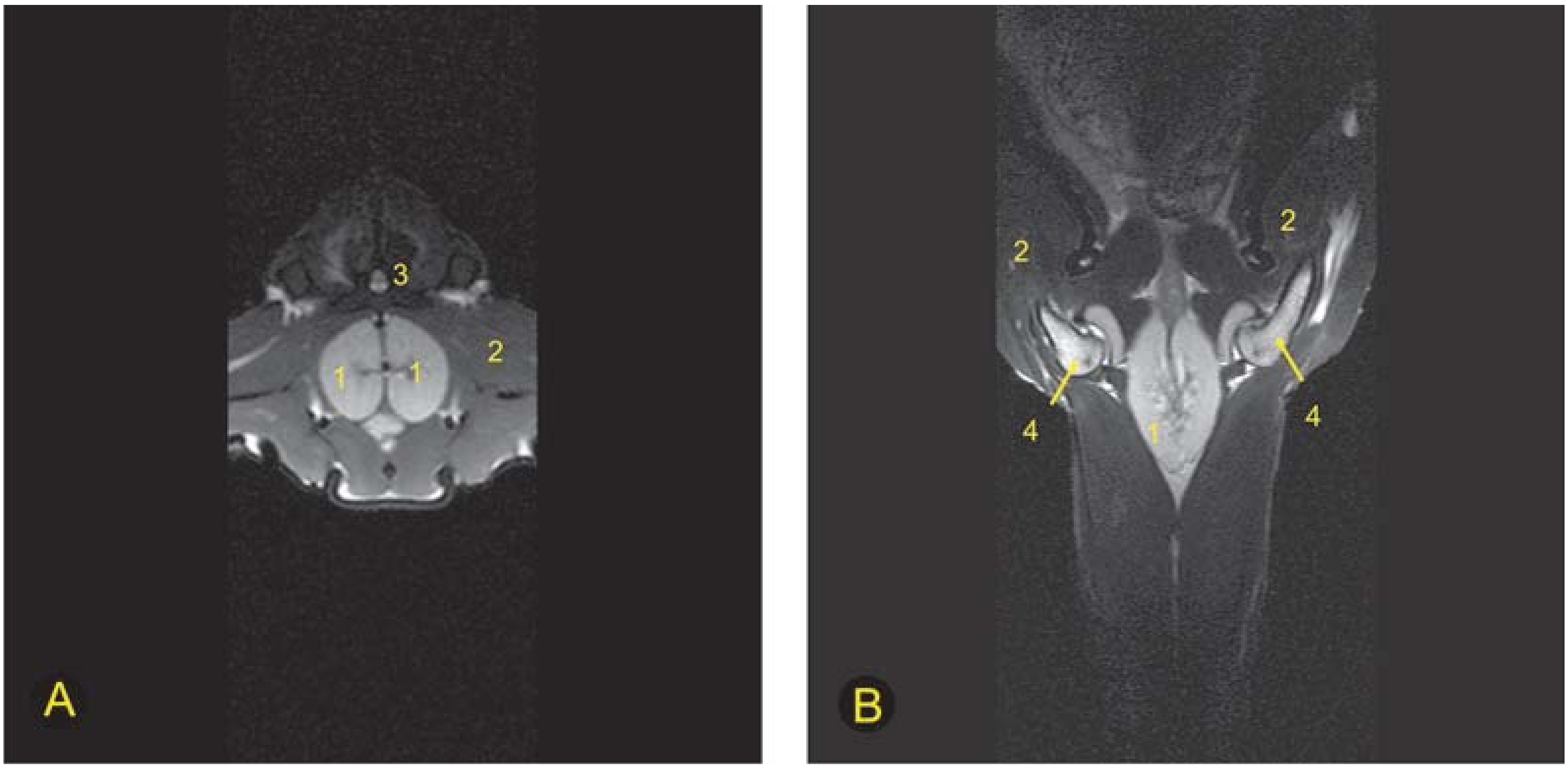

Fig. 3-108: MRI examination of a green iguana's (*Iguana iguana*) pelvic region, dorsal slice with a surface coil, T2-weighted. Normal kidneys (1). Fusing of the caudal poles of kidneys can be observed in the dorsal part of the scan.

1: kidneys
2: pelvis musculature
3: spine and spinal cord
4: femur/hip joint

1: ovary
2: liver
3: stomach
4: lungs

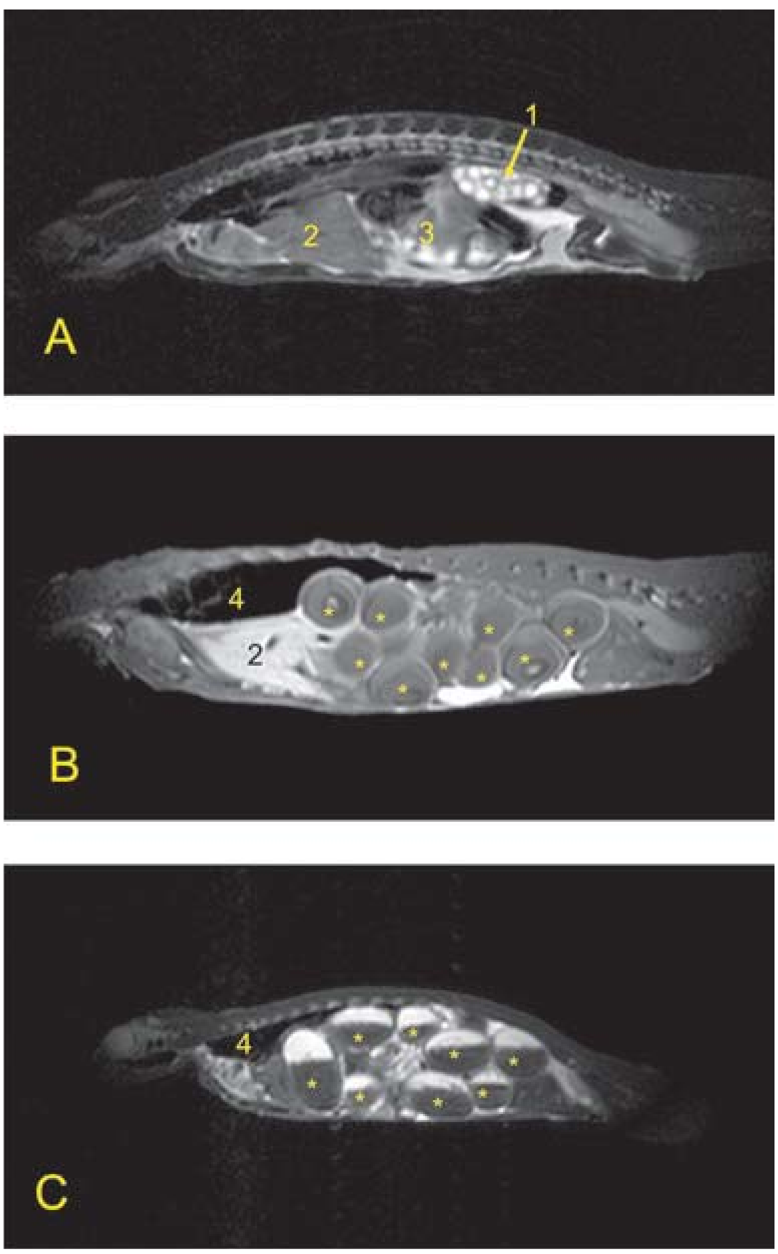

Fig. 3-109: MRI examination of a green iguana's (*Iguana iguana*) trunk, sagittal slice, (B) T1-weighted, (A, C) T2-weighted. (1) Ovaries and eggs with either concentric (B*) or horizontal layering (C*).

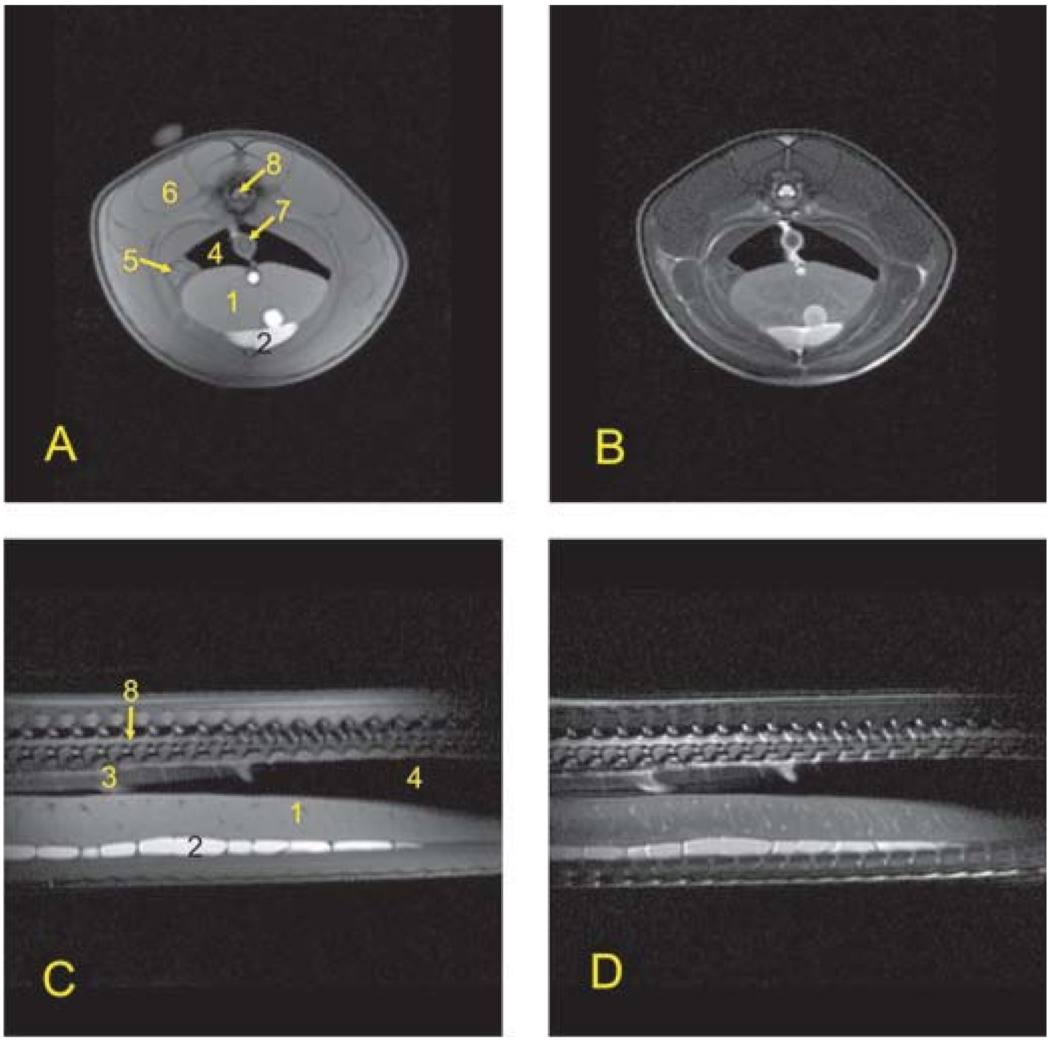

1: liver
2: fat
3: lung tissue
4: air sac
5: esophagus
6: spinal musculature
7: aorta
8: spinal cord

Fig. 3-110: MRI examination of an Indian python's (*Python molurus*) trunk, (A, B) transverse and (C, D) sagittal slices, (A, C) T1-weighted, (B, D) T2-weighted, examination at approximately 40% of the body length. (1) Normal liver. The snake liver has two large blood vessels which course longitudinally through the organ. The smaller blood vessels can be evaluated in the T2-weighted image.

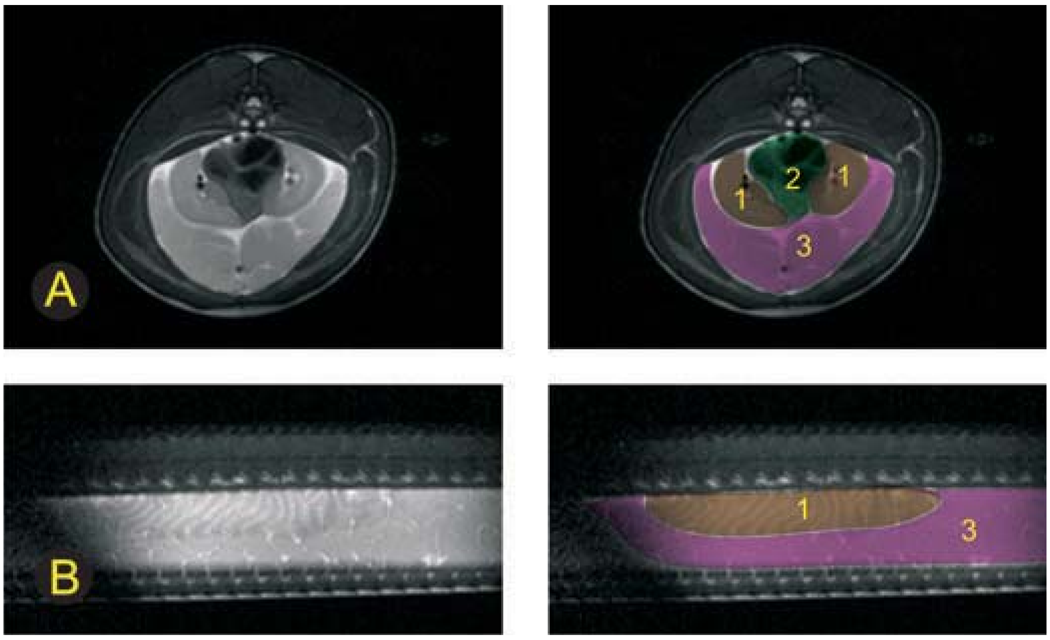

1: kidneys
2: intestines
3: adipose tissue

Fig. 3-111: MRI examination of an Indian python's (*Python molurus*) trunk, (A) transverse and (B) sagittal slices, T2-weighted, investigation at approximately 70% of the body length. The kidneys (1) lie mostly behind each other and slightly overlap. A »money-roll« type layer is visible in the sagittal slice.

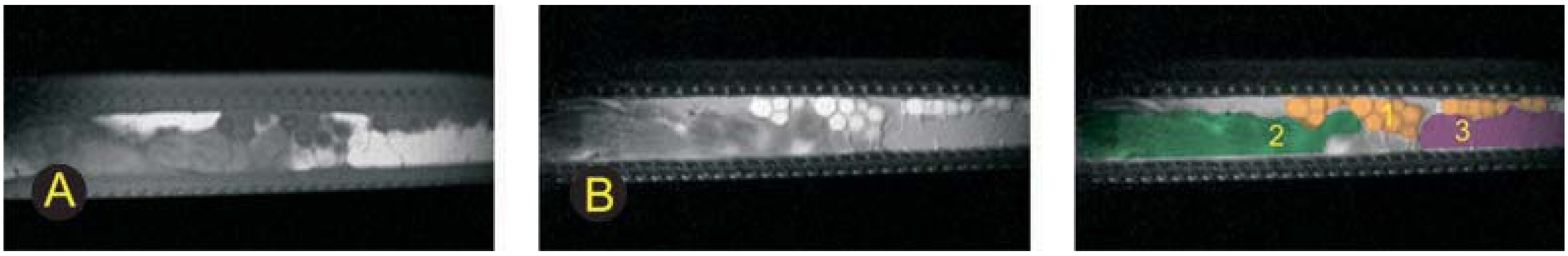

Fig. 3-112: MRI examination of an Indian python's (*Python molurus*) trunk, sagittal slice, (A) T1-weighted, (B) T2-weighted, investigation at approximately 70% of the body length. Follicles (1) on an ovary.

1: follicles
2: intestines
3: fat

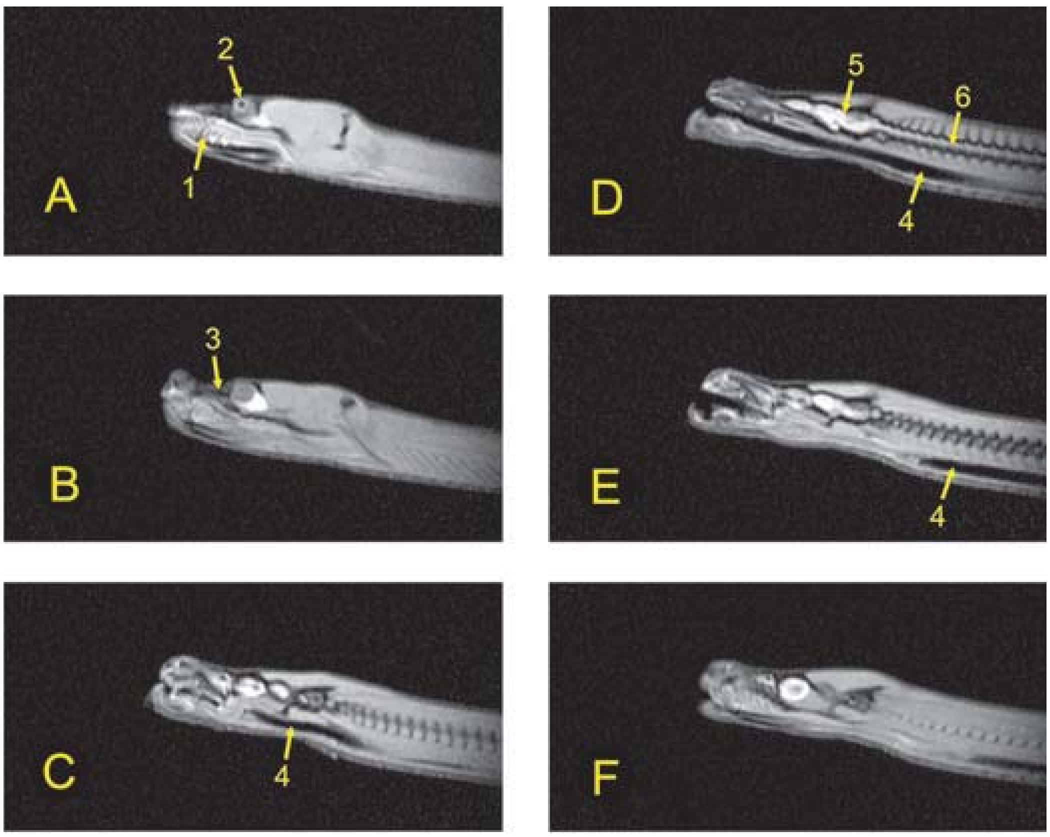

1: row of teeth/gum
2: eye
3: nasal cavity
4: trachea
5: brain
6: spinal cord

Fig. 3-113: MRI examination of an Indian python's (*Python molurus*) head, sagittal slice, T2-weighted. Depiction of sequential slices.

Special diagnostics, pathological findings

3.5 Skeletal system

Michael Pees

Abnormal presentations involving the skeletal system are among the most common indications for performing radiographic and CT examinations. The majority of pathological abnormalities identified in reptile patients are the result of inadequate husbandry and/or nutrition. In addition, pathological changes can be caused by trauma associated with falls or bites wounds. Frequently, skeletal abnormalities are diagnosed by chance when reptiles are presented to the veterinarian for other reasons. Ultrasonography does not enhance one's ability to detect disease problems when examining the skeletal system as even joint pathology can be better imaged using standard radiography. MRI can be useful in diagnosing infectious, traumatic, soft tissue trauma affecting joints, and neoplastic diseases.

3.5.1 Fractures

A general classification for reptile fractures is the underlying cause, which is differentiated into traumatic and »pathological«. Pathological fractures usually develop without significant trauma when there is severe destabilization of the bone caused by metabolic bone disease (MBD). Pathological fractures are characterized by abnormalities in the bone structure (see below).

Fractures of the **long bones** are often diagnosed in lizards (**Figs. 3-114** to **3-116**), but they also occur in chelonians. An acute fracture can be recognized radiographically by the sharp edges of the fracture fragments, similar to that found in mammals. During the course of reptile bone healing, there are many differences from the same process described for mammalian species. The reparation of the bone is much slower and is characterized by little callus formation. Instead, connective tissue forms a stabilizing matrix, which at first is not radiopaque; therefore it is not recommended to perform radiographic reexaminations to determine healing progress until after eight to twelve weeks (**Fig. 3-116**). At this time, reactions of reptile bone healing begin to show radiographically at the ends of the fracture fragments. Complete bone remodeling can take more than a year (**Fig. 3-114**). It is not uncommon for the stabilized fracture to have incomplete ossification due to calcification. One exception is the healing process associated with pathological fractures. In such cases, the remodeling of the bones is quicker because the affected bone tissue has been activated by the metabolic disturbance which may result in a distinct callus formation.

Rib fractures are identified regularly in radiographs of snake patients as a series of fractures (**Fig. 3-117**), therefore it is usually considered an incidental finding. Such rib fractures may be caused by the pressure placed on the ribs when the animal strangles its prey or other forms of trauma. Regardless of the underlying etiology of rib fractures, there are rarely clinical problems associated with this condition in snakes.

Vertebral fractures are regularly diagnosed in snakes and lizards (**Figs. 3-118** to **3-120**). One possible cause of vertebral fractures in these animals is a previous infection. Infections of the vertebra induce much stronger reactions than in other bones of the skeletal system (**Fig. 3-121**), and they often result in the fusion of the affected vertebrae (**Fig. 3-118**). The area(s) of vertebral fusion can then easily fracture after relatively mild trauma resulting in clinical signs (e.g. hindlimb paralysis). In lizards, especially young bearded dragons and iguanas, metabolic disturbances commonly damage the vertebra, therefore trauma will cause fractures to these skeletal structures (**Figs. 3-119** and **3-120**). Vertebral fractures in snakes will occur, primarily at the level of the first cervical vertebra, due to poor handling and lead to the paralysis or death of the animal. Diagnostically, in addition to standard radiography, both CT and MRI examinations are useful for determining the degree of damage to the vertebral canal (**Fig. 3-120**). The prognosis is usually poor to grave for fractures that have been caused by metabolic bone disease or an infectious process. However, depending on the location and degree of damage (sensation maintained to distal body parts, functioning gastrointestinal tract), complete regeneration may be possible.

Shell fractures in chelonians usually occur due to falls (**Fig. 3-122**) or other massive forms of trauma (e.g. after being run over with a vehicle or being bitten by a dog) (**Fig. 3-123**). Frequently, the clinical picture is dramatic, but the animals are often in good general condition.

A radiographic examination using two or three projections is necessary to diagnose the degree of shell damage. It is recommended that CT should be utilized as an imaging modality since as 3D reconstruction will aid in developing an exact diagnosis (**Fig. 3-122**). The 3D reconstruction (type and localization of the fragments) is will aid in planning and treatment implementation. An open body cavity and damage to internal organs (especially the lungs) is of particular interest when trying to determine a prognosis. To determine the extent of internal body damage associated with chelonian shell fractures, a MRI investigation will provide additional information, especially in regards to internal hemorrhage.

3.5.2 Metabolic bone disease

Under the classification of metabolic bone disease (MBD) are those conditions which cause a disturbance in the integrity and function of the bone. The most common cause of MBD in reptile species is nutritional secondary hyperparathyroidism. Nutritional secondary hyperparathyroidism is a consequence of husbandry and/or nutritional deficiencies, namely, an absolute or relative deficiency of calcium and Vitamin D in the diet and that of UVB light. Following the release of parathormone, either rickets or osteomalacia will develop. The bones that are primarily affected by MBD are those of the limbs, ribs, mouth, cranium, and vertebra. The hydroxyapatite is replaced by fibrinous connective tissue (osteodystrophy fibrosa) causing **pathological fractures** that result from bones losing their cortical strength and buckling (rubber-like) (**Fig. 3-124**). The reduced **bone density** is often evident on radiographic images (**Fig. 3-125**). As a consequence of hypertrophic osteopathy, the bone can show extensive periosteal **hyperostosis**. The cortex of the long bones may be thickened (**Fig. 3-126**) or there may be obvious pathological thinning of the cortex. In growing animals, the bones bend or may even buckle. The bones of chelonian shells become significantly thickened to compensate for the lack of stability due to inadequate calcification. The bone of the carapace becomes sponge-like, which can also be described as its radiographic appearance (**Fig. 3-127**). The vertebral column often sinks within the carapace due to the lack of stability forming two humps in the region of the pectoral girdle and pelvis due to the supported of the bones found in these two areas (**Fig. 3-128**). In addition to the skeletal abnormalities described above, there is often an indication of constipation on the radiograph which is a result of excessive ingestion of calcium-containing material (e.g. stones, sand) – an attempt by the animal to compensate for the nutritional deficiencies associated with MBD (**Fig. 3-127**).

The extent of MBD can be best identified in a CT investigation. The bones of the pectoral and pelvic girdles are best imaged using this imaging modality. In addition, the 3D reconstruction can show the lack of shell integrity (**Fig. 3-129**; compare with **Fig. 3-84**). Measurements of the density of the bones that comprise the pectoral girdle have shown that their radiodensity is severely reduced in those animals affected by MBD. In severe cases of MBD, bone densities of around 300 HU have been measured compared with the almost 1000 HU found in bones of healthy animals.

Some of the radiographic changes associated with MBD (e.g. patchiness, osteophytes, bending) remain for life despite successful therapy. The bone density can become normalized within a few months of successful treatment and elimination of underlying causative factors (e.g. nutrition, husbandry).

3.5.3 Skeletal deformities and fusion

Skeletal deformities are sometimes the result of genetic causes. Most often skeletal deformities are due to mistakes in incubation or nutritional deficiencies of the gravid female, which will affect the developing embryos within the egg(s). In such cases, the vertebral bodies are frequently affected (**Figs. 3-130** and **3-131**). However, with many cases skeletal deformities – also of the vertebral column – are a consequence of improper husbandry and diet (e.g. MBD). In addition to the long bones, the bones of the jaw and head are affected, which results in an overbite or underbite, especially in lizards.

Trauma to a lizard's tail vertebrae can lead to the induction of **regeneration.** With increasing calcification, such structures are easily visible on a radiographic image (**Fig. 3-132**).

Exostoses and bridges between the vertebral bodies can be identified as an incidental finding in both lizards and snakes (**Fig. 3-133**). Clinical complications will occur especially when fractures take place in immobile regions of the spine (see above).

3.5.4 Luxations

The relatively simple composition of reptile joints is a significant reason for a reduced incidence of **joint luxations**. When they do occur, joint luxations mainly affect the coxofemoral joint of lizard species. Occasionally trauma to the female hip areas during copulation with much larger males will result in coxofemoral joint luxation(s), especially in agamids. The radiographic examination must be performed using two projections with fine films; even with this recommended technique, the diagnosis is not always clear. If the traditional radiographic images do not lead to a definitive diagnosis, a CT examination is recommended to achieve a better evaluation of the joints (**Fig. 3-134**).

3.5.5 Bone and joint infections

Bone and joint infections occur frequently in reptiles. For example, with infections that involve the limbs, bacteria enter the body through toe and foot injuries and often result in an ascending infection of the bones and joints. A hematogenous distribution is also possible as bacteria enter the blood supply. The affected areas are usually swollen and the bone may appear lytic (**Fig. 3-135**).

A joint infection that has bone involvement is initially imaged as a soft-tissue swelling with a widened joint cavity. If an abscess forms, this can become calcified and appear as a radiopaque structure (*q.v.* **Fig. 3-225**). The differentiation between infection, neoplasia, or joint gout requires an aspiration of the joint and a microscopic examination of the aspirate material. With chronic infectious joint disease, the joints and/or bones can become severely damaged with decalcification and lysis visible on radiographic images of the affected area **(Figs. 3-135** to **3-140)**.

Infections of the vertebra occur relatively frequently in lizards and snakes. Often the bacterial organisms causing the infection can be identified. Infections of the tail primarily result from injuries to the tip of the tail. However, there can be an ascending infection from tail tip injuries to the pelvis. The bone reactions in the vertebrae are much stronger than that found in other bones. Vertebral infections can lead to bone lysis or a massive callus formation and fusion of the affected structures. The fused bone tends to appear very nonhomogeneous in radiographic images (**Fig. 3-121**). These chronic bony changes often show a progressive development ultimately leading to neurological deficits. Although the radiographic image of fused vertebra resembles Paget's disease in humans, this is another disease. A comparative disease process affecting the long bones of reptiles has not been described.

Infections of the bones and joints in the **head** are usually associated with infections of the oral cavity or, especially in turtles and terrapins, with infections in the middle ear (otitis) (**Fig. 3-141**).

3.5.6 Gout

The deposition of **urate crystals** in the joints leads to soft-tissue swelling in the immediate surrounding area. Often a number of joints, which are clinically enlarged, are affected by urate crystal deposition. In contrast to abscesses, the animals often have no desire to move themselves. If calcium is also deposited within the joints, then the changes can become radiopaque when observed on radiographs. The differentiation of joint gout requires joint aspiration to detect the urate crystals in the collected sample (*q.v.* **Fig. 3-222**).

3.5.7 Neoplasia

Primary **neoplasms of the skeletal system** are very rare in reptile patients. However, tumors from the surrounding organs can involve bone(s) or displace them which may result in osteolysis. Possible tumor types that can affect the skeletal system of reptiles include melanomas, fibromas (see **Fig. 3-226**), or fibrosarcomas.

1: acute fracture
2: partially healed fracture

Fig. 3-114: Total body radiographic image of a green iguana (*Iguana iguana*), dorsoventral projection. Fractures. Picture of an acute (1) and a partially healed (2) fracture of the long bones.

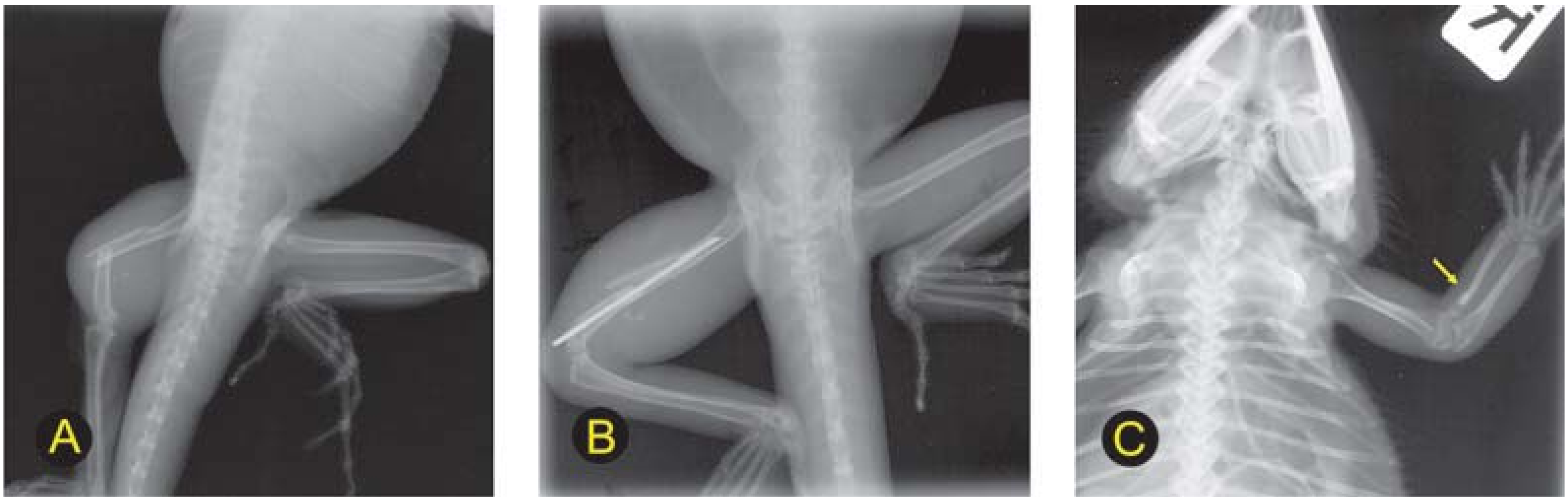

Fig. 3-115:

A, B: Radiographic images of the pelvis area of a Chinese water dragon (*Physignathus cocincinus*), dorsoventral projection. Comminuted fracture. (A) Acute stage and (B) the control radiograph after the insertion of an intramedullary pin. The prospect for osteosynthesis in reptiles is limited as the long time needed for healing often leads to infections and decalcification in the region of the implant.

C: Radiographic image of a central bearded dragon's (*Pogona vitticeps*) foreleg, dorsoventral projection. Simple fracture of the radius (arrow). Such fractures usually heal without complications if the affected limb is immobilized.

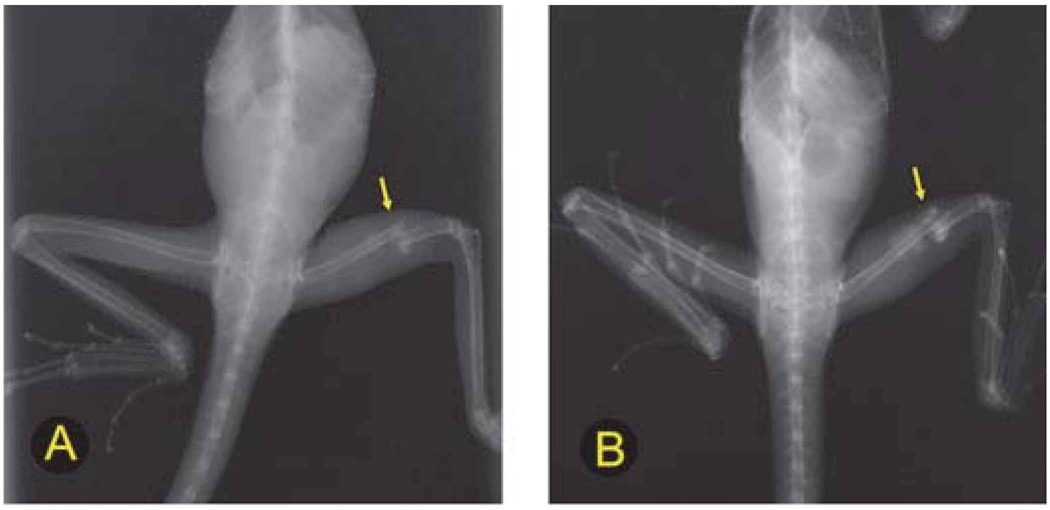

Fig. 3-116: Radiographic images of a striped basilisk's (*Basiliscus vittatus*) pelvic area, dorsoventral projection. Fracture of the femur (arrow). (A) Acute fracture and (B) the control radiograph after eight weeks. The calcification shows the healing process and the bone transformation; small splinters of bone have been integrated into the callus.

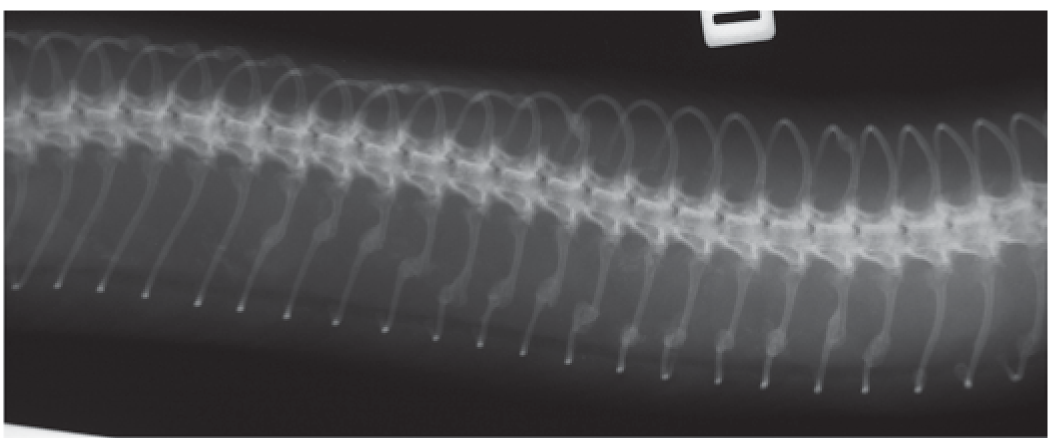

Fig. 3-117: Radiographic image of a boa constrictor's (*Boa constrictor*) middle body region, lateral projection. Old rib fractures. Rib fractures that are healed by callus formation are considered common and incidental findings in snake patients.

Fig. 3-118: Radiographic image of a green iguana's (*Iguana iguana*) pelvic area, lateral projection. Vertebral fracture (arrow) as a consequence of severe immobilization and fusion of the vertebrae. The type of vertebral fusion observed in this image is often the result of infectious processes. Due to the enormous leverage caused by the tail, fractures commonly occur between the fused vertebrae. In this case, the narrowing of the spinal canal after trauma led to signs of paralysis in the hindlimb.

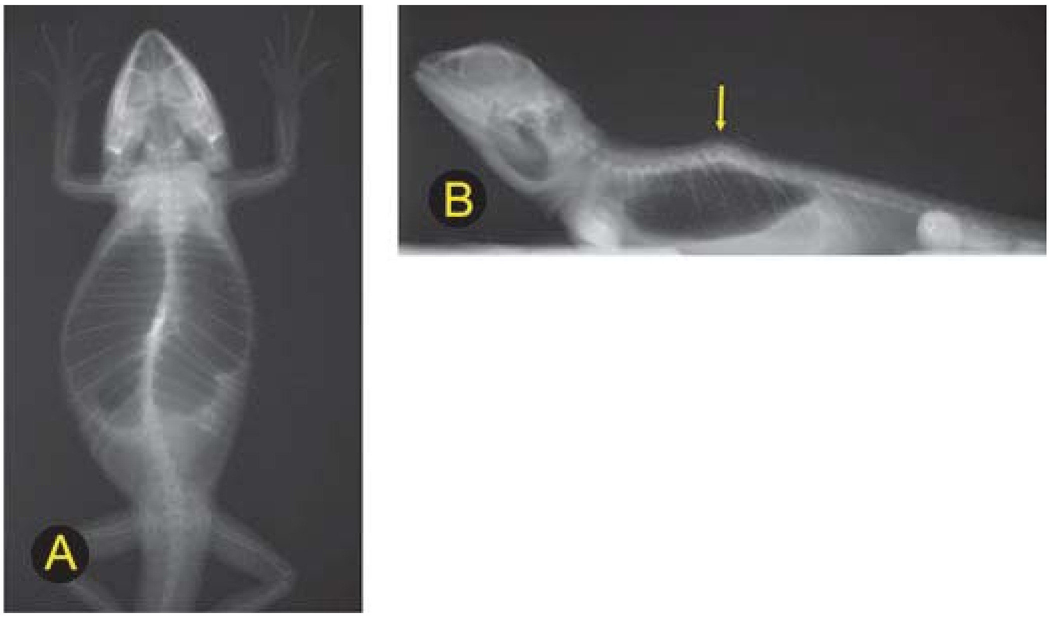

Fig. 3-119: Total body radiographic images of a central bearded dragon (*Pogona vitticeps*), (A) dorsoventral and (B) lateral projections. Fracture of the spine (arrow) after trauma (fall from the owner's hands). Young central bearded dragons, especially if subjected to the wrong diet, are predisposed to spinal fractures. The clinical signs associated with nutritional secondary hyperparathyroidism (induced bone weakness that leads to spinal fractures) consist mainly of hindlimb paralysis and problems with defecation.

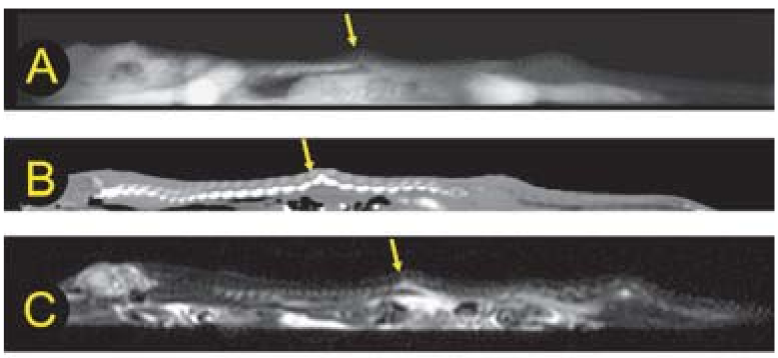

Fig. 3-120:

A: Total body radiographic image of a central bearded dragon (*Pogona vitticeps*), lateral projection. Vertebral fracture.

B: CT image of the same animal, sagittal reformation (120 kV, 200 mA, 1.0 mm SD, W: 400, L: 60).

C: MRI examination of same animal, sagittal plane, T2-weighted.

Acute fracture of the spine with displacement of the vertebrae (arrow). The CT image depicts the position of the vertebral body, while the MRI image provides additional information about the presence of hemorrhage and fluid accumulation in the affected area.

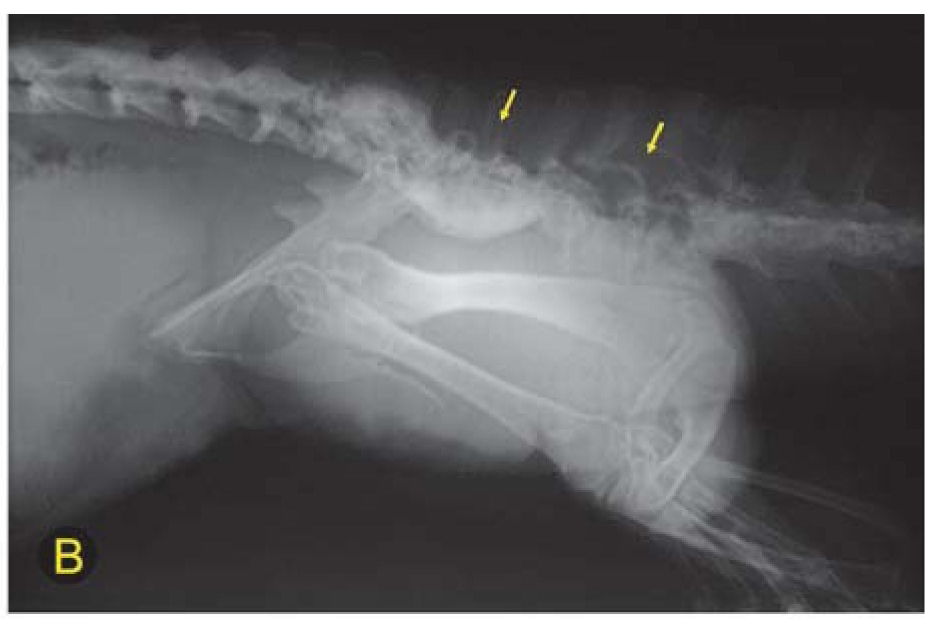

Fig. 3-121: Radiographic images of a green iguana's (*Iguana iguana*) spine, (A) dorsoventral and (B) lateral projections. Bacterial infection involving the caudal vertebral bodies. The clinical signs consisted of hindlimb paralysis. The affected vertebral bodies exhibit obvious osteolysis (arrows).

Fig. 3-122: CT image of a red-eared slider's (*Trachemys scripta elegans*) body, (A) transverse plane (120 kV, 120 mA, 1.0 mm SD, W: 1500, L: 350) and (B) 3D reconstruction (120 kV, 120 mA, 1.0 mm SD, W: 255, L: –872). Shell fracture caused by a fall from a balcony. These images help localize the individual fracture fragments. The CT image provides important assistance in deciding which therapy to use as the dislocation and fracture fragments can be precisely assessed.

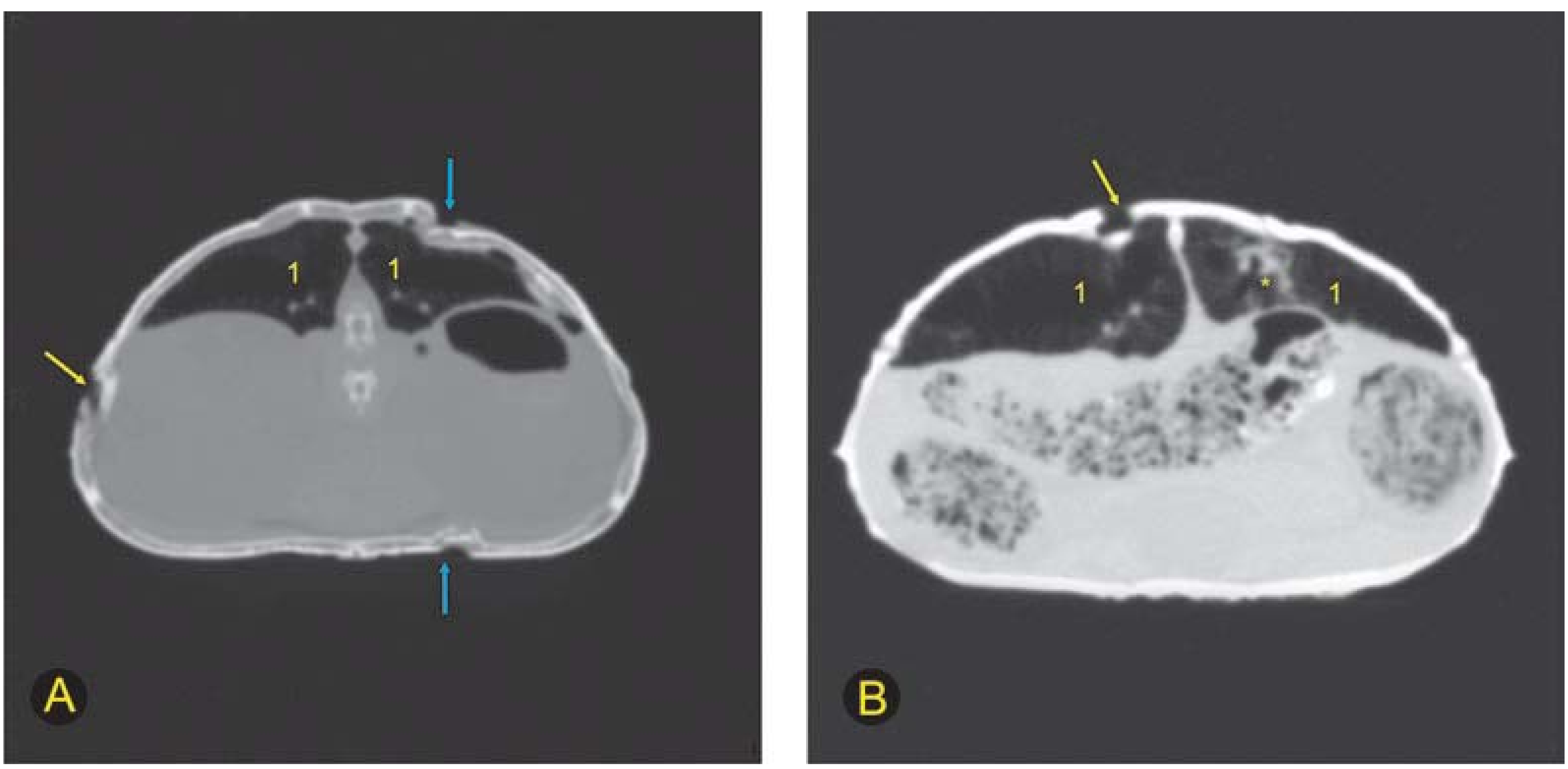

Fig. 3-123:

A: CT image of a Russian tortoise's (*Testudo horsfieldii*), body, transverse plane (140 kV, 288 mA, 1.0 mm SD, W: 2399, L: –194). Trauma due to a dog bite (arrows). The bite and counterbite are clearly observed in the image (blue arrows). The lungs (1) are not perforated.

B: CT image of a Hermann's tortoise's (*Testudo hermanni*) body (140 kV, 193 mA, 0.6 mm SD, W: 1568, L: –513). Trauma due to a dog bite (arrow). In this animal, the lungs (1) have been opened (arrow); in one lung field there is blood (*).

1: lungs

*: hemorrhage

arrows: dog bite

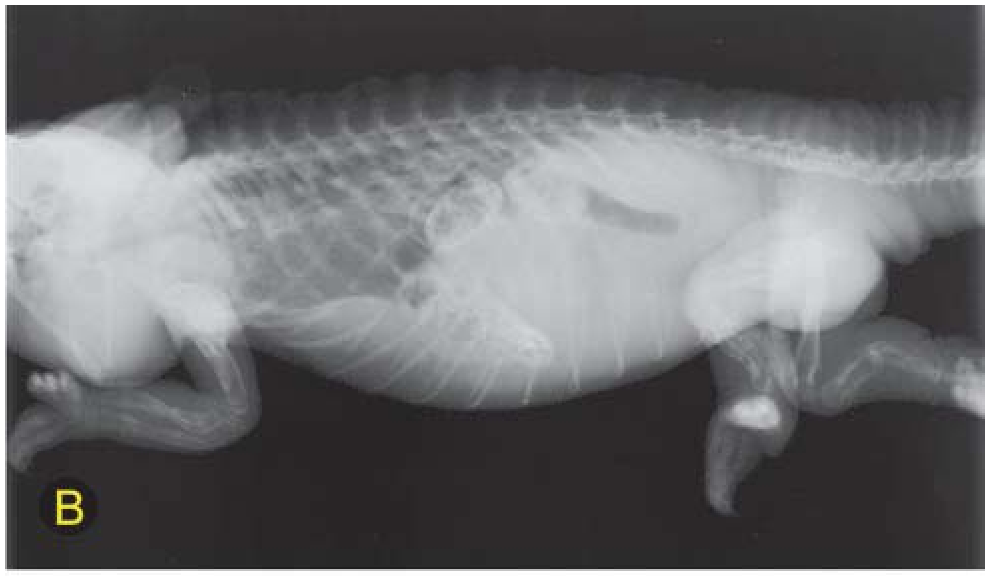

Fig. 3-124: Total body radiographic images of a veiled chameleon (*Chamaeleo calyptratus*), (A) dorsoventral and (B) lateral projections. Metabolic bone disease. Severe bone deformations including the bending of long bones as well as the presence of foreign bodies (sand) in the gastrointestinal tract are observed in these images. The abnormal skeletal signs noted in the images are typical of MBD. The shadows present in the body cavity are follicles.

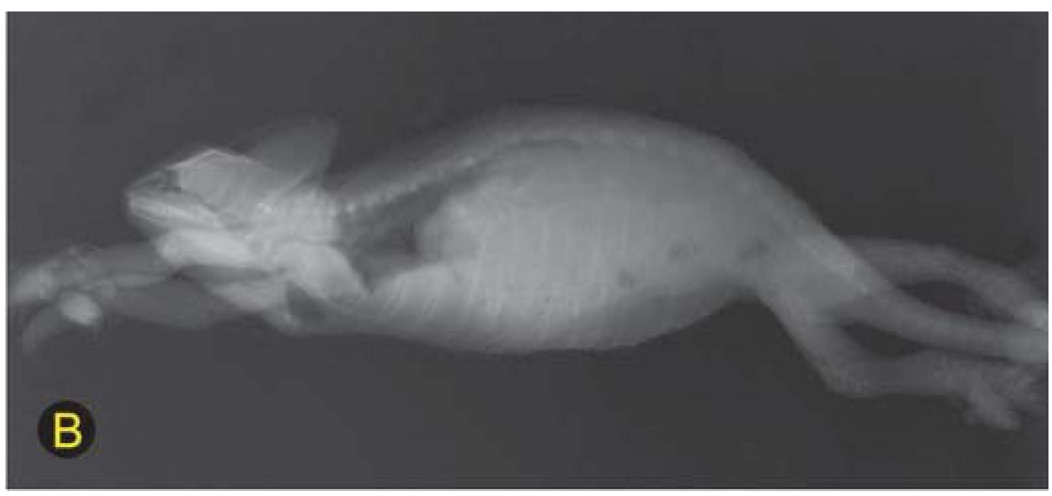

Fig. 3-125: Total body radiographic images of a veiled chameleon (*Chamaeleo calyptratus*), (A) dorsoventral and (B) lateral projections. Metabolic bone disease. The bones are inadequately mineralized and barely radioopaque. This condition is particularly evident in the hindlegs, where deformities have also developed.

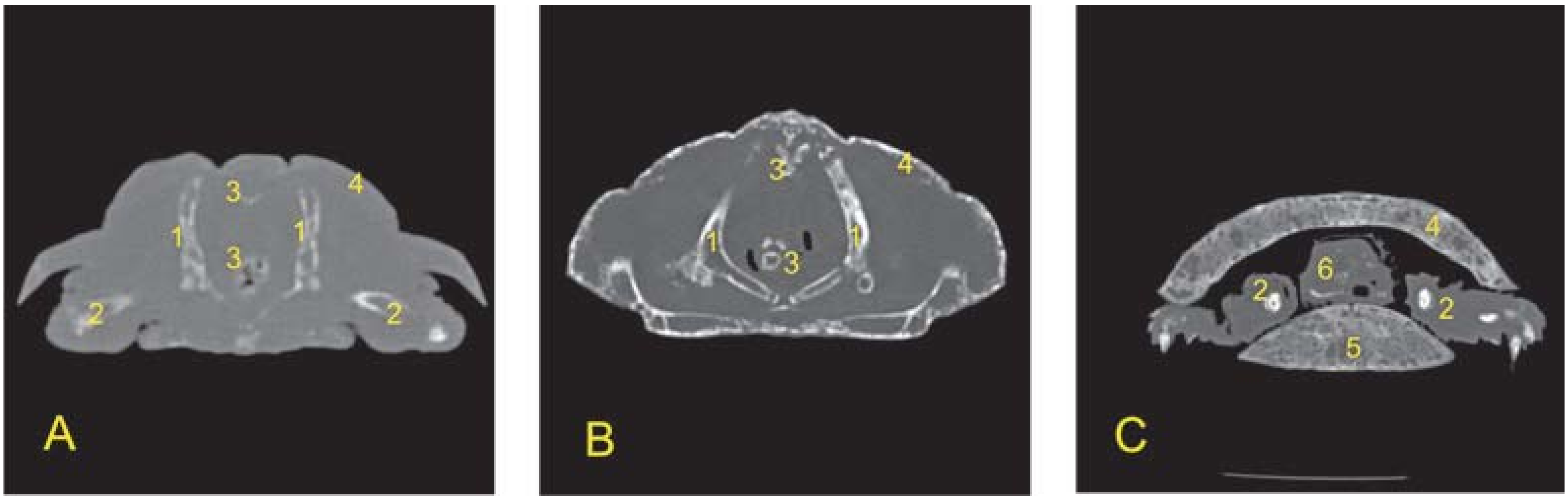

Fig. 3-126:

A: CT image of a Hermann's tortoise's (*Testudo hermanni*) pectoral girdle, transverse plane (120 kV, 120 mA, 1.0 mm SD, W: 1514, L: 184). Metabolic bone disease. The animal's shell (4) is deformed and lacks significant calcium content. The cortex of the bones comprising the pectoral girdle (1) are deformed and have irregular cortical enlargement.

B: CT image of a Hermann's tortoise's (*Testudo hermanni*) shoulder girdle, transverse plane (120 kV, 120 mA, 1.0 mm SD, W: 1500, L: 350). Metabolic bone disease. The shell also lacks significant calcification and the cortices of the bones comprising the pectoral girdle (1) have irregular cortical enlargements, too. One can adequately assess a patient's bone density by using the bone within the pectoral and/or pelvic girdles.

C: CT image of a spur-thighed tortoise's (*Testudo graeca*) body, transverse plane (120 kV, 140 mA, 1.0 mm SD, W: 1500, L: 350). Metabolic bone disease. In this animal, the plastron (5) and carapace (4) are severely enlarged therefore there the animal has difficulty retracting its (6) head.

1: pectoral girdle
2: humerus
3: cervical vertebrae
4: carapace
5: plastron
6: head

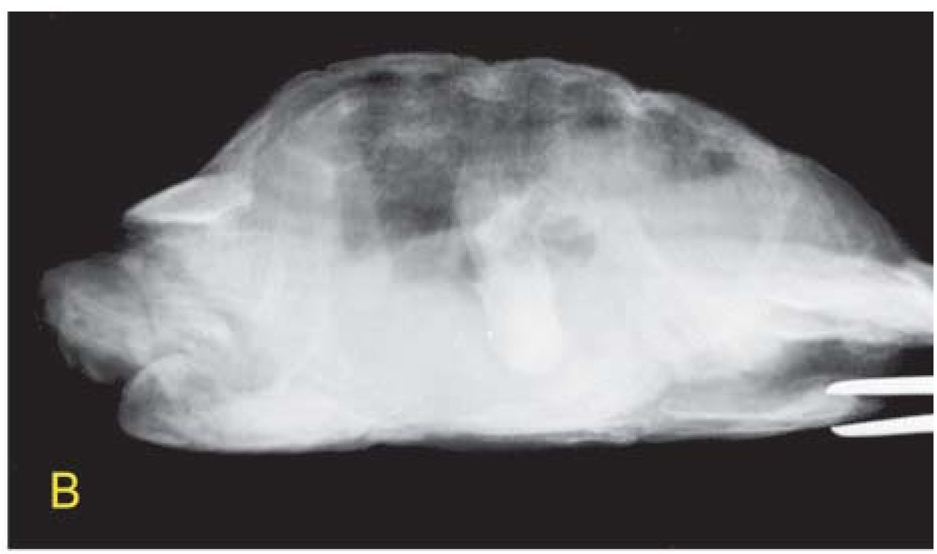

Fig. 3-127: Total body radiographic images of a spur-thighed tortoise (*Testudo graeca*), (A) dorsoventral and (B) lateral projections. Metabolic bone disease. The shell is deformed and lacks sufficient calcification. The spongy structure of the bone is readily apparent in these images. In an attempt to compensate for the mineral deficiency, the animal had ingested sand, which can be seen in the intestinal tract.

Fig. 3-128: Tortoise with severe bone deformations due to metabolic bone disease. Since the pectoral and pelvic girdles provide support to the shell, two humps have developed and the spine has sagged between them.

Fig. 3-129: Total body CT image of a spur-thighed tortoise (*Testudo graeca*), 3D reconstruction (120 kV, 83 mA, 1.0 mm SD, W: 255, L: 127). Metabolic bone bisease. Poorly calcified shell (for comparison with the image of a healthy tortoise, see Fig. 3-84).

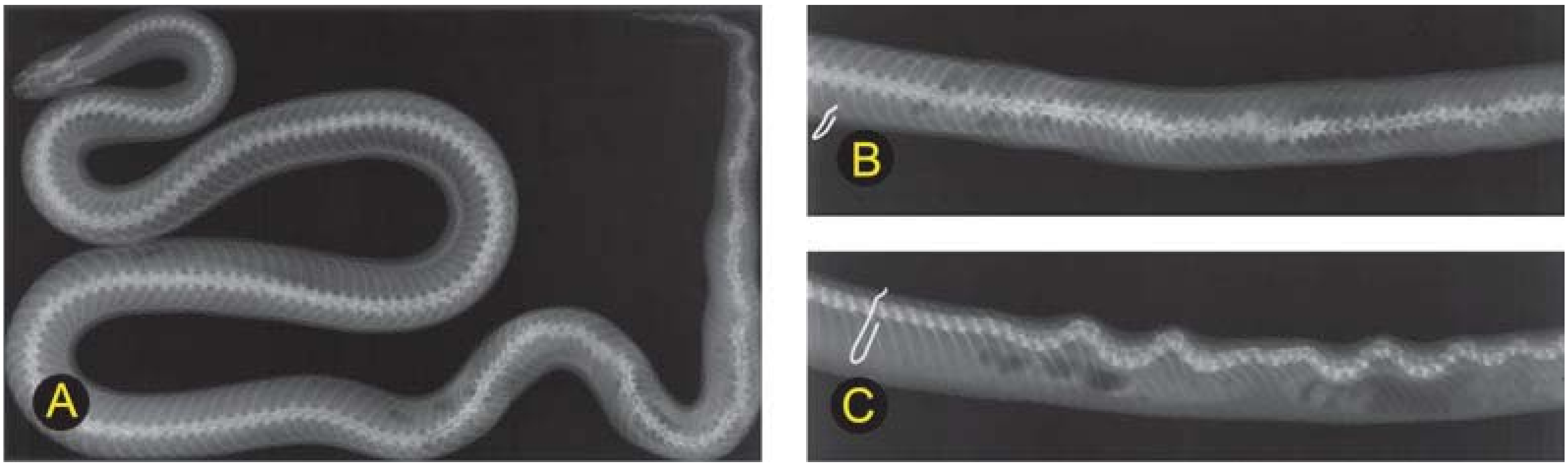

Fig. 3-130: Radiographic images of a banded water snake's (*Nerodia fasciata*) body, (A) animal placed in a box, (B) dorsoventral and (C) lateral projections. Severe deformation of the spine. The most common causes of the spinal abnormalities shown in these images are inappropriate incubation and genetic defects.

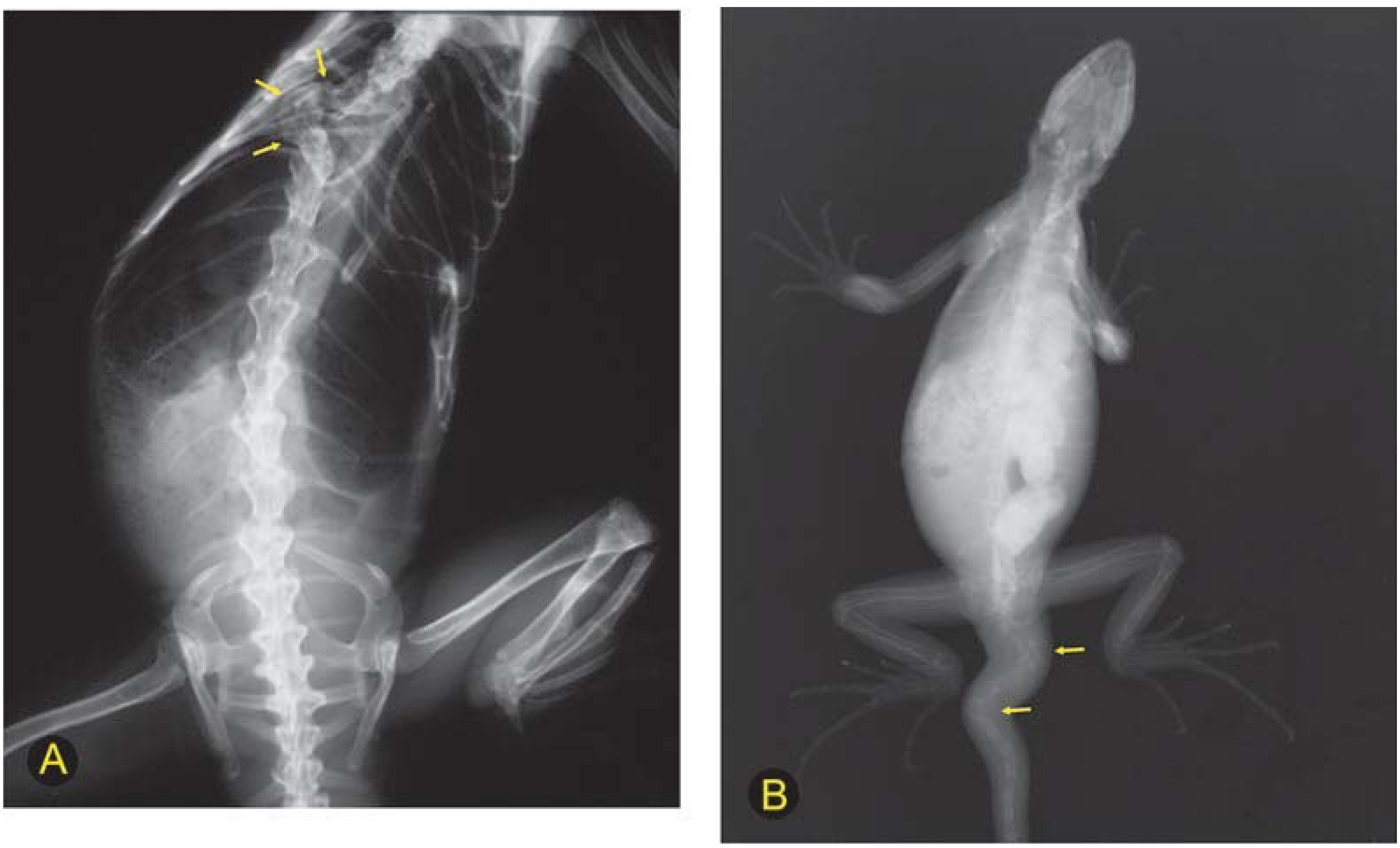

Fig. 3-131:

A: Radiographic image of a green iguana's (*Iguana iguana*) body, dorsoventral projection. Severe abnormality involving the thoracic vertebral bodies. This is an incidental finding.

B: Total body radiographic image of a green iguana (*Iguana iguana*), dorsoventral projection. Deformaties of the vertebral bodies in the tail (arrows). This animal had no overt clinical disease condition when the radiographic image was taken.

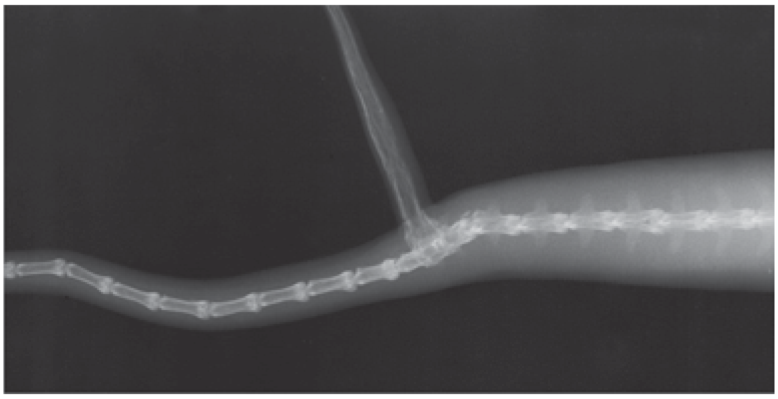

Fig. 3-132: Radiographic image of a green iguana's (*Iguana iguana*) tail, dorso-ventral projection. Regeneration of the tail after trauma.

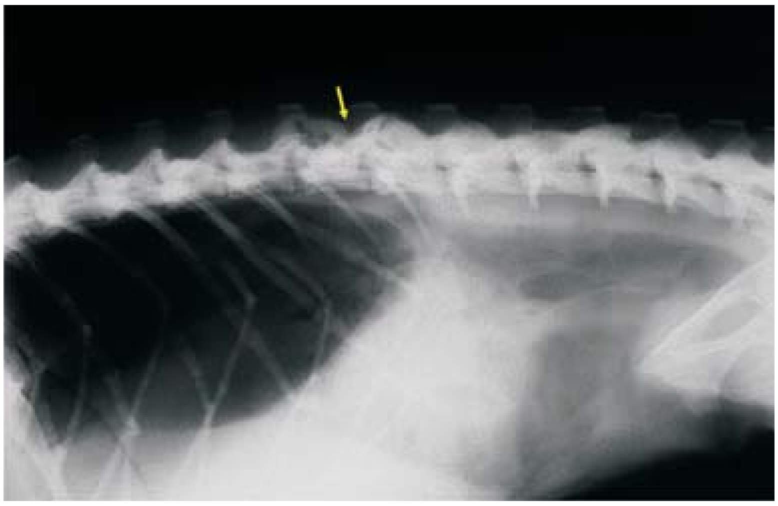

Fig. 3-133: Radiographic image of a green iguana's (*Iguana iguana*) spine, lateral projection. Bridge formation between vertebral bodies (arrow). These changes were not associated with any clinical signs of disease in this animal. With progressive ossification, fusion of the affected vertebral bodies can occur (see Fig. 3-118).

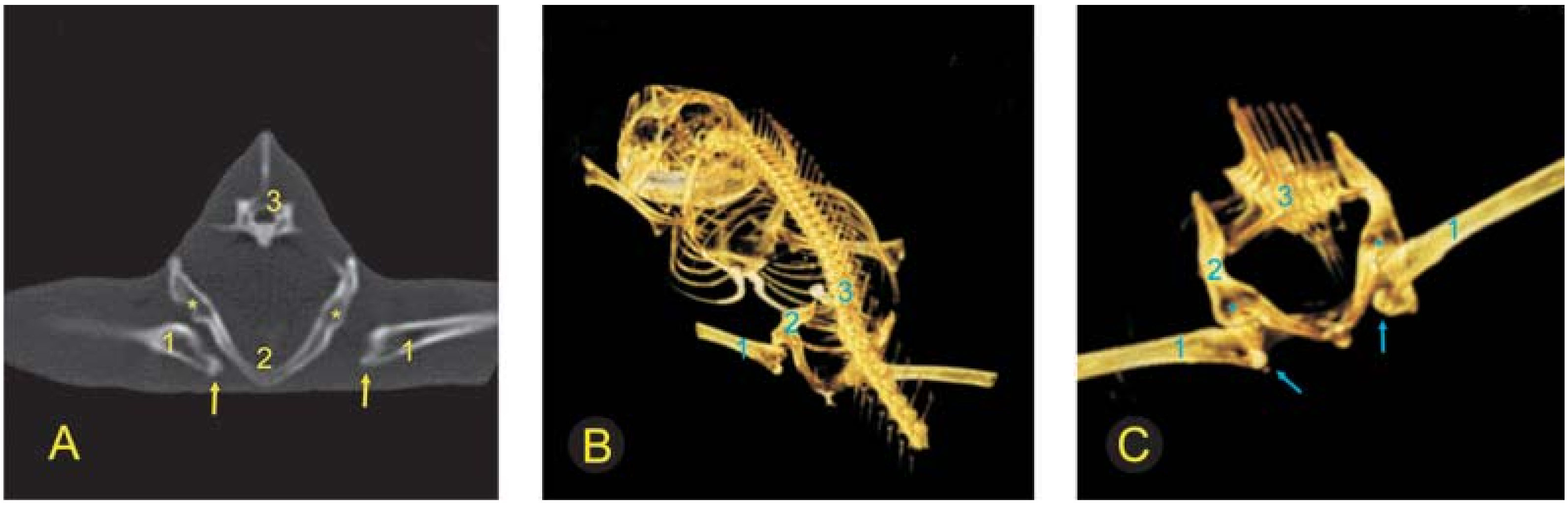

Fig. 3-134: CT images of a Chinese water dragon's (*Physignathus cocincinus*) pelvis, (A) transverse plane (120 kV, 120 mA, 1.0 mm SD, W: 1726, L: 570). (B, C) 3D reformation (120 kV, 120 mA, 1.0 mm SD, W: 255, L: 127). Bilateral luxation of the hip joints. The luxations occurred after copulation with a much larger male.

1: femur
2: pelvis
3: spine

arrow: femur head
*: acetabulum

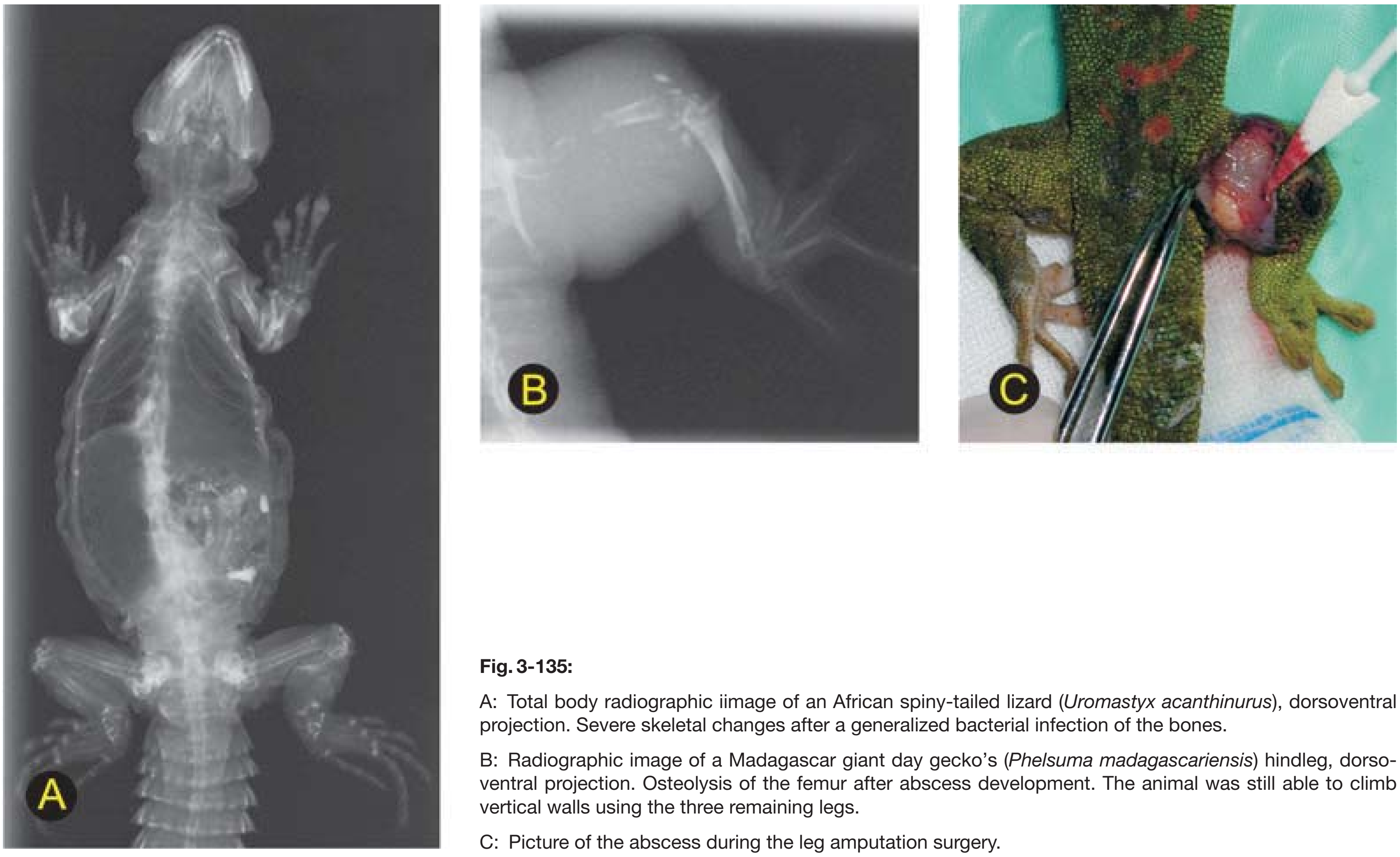

Fig. 3-135:

A: Total body radiographic iimage of an African spiny-tailed lizard (*Uromastyx acanthinurus*), dorsoventral projection. Severe skeletal changes after a generalized bacterial infection of the bones.

B: Radiographic image of a Madagascar giant day gecko's (*Phelsuma madagascariensis*) hindleg, dorsoventral projection. Osteolysis of the femur after abscess development. The animal was still able to climb vertical walls using the three remaining legs.

C: Picture of the abscess during the leg amputation surgery.

Fig. 3-136: Radiographic image of a green iguana's (*Iguana iguana*) hindleg, dorsopalmar projection. Knee swelling (arrows), bacterial Infection. A swelling of the soft tissues and a lysis of the joint can be seen in the image.

Fig. 3-137:

A, B: Radiographic images of a central bearded dragon's (*Pogona vitticeps*) foreleg, (A) dorsopalmar and (B) caudocranial projections. Lameness, bacterial infection. Osteolysis is observed in the region of the elbow joint (arrow).

C: Radiographic image of a yellow-bellied slider's (*Trachemys scripta scripta*) foreleg, dorsopalmar projection. Lameness, bacterial Infection. In this animal, the elbow joint cannot be treated, therefore a leg amputation is required.

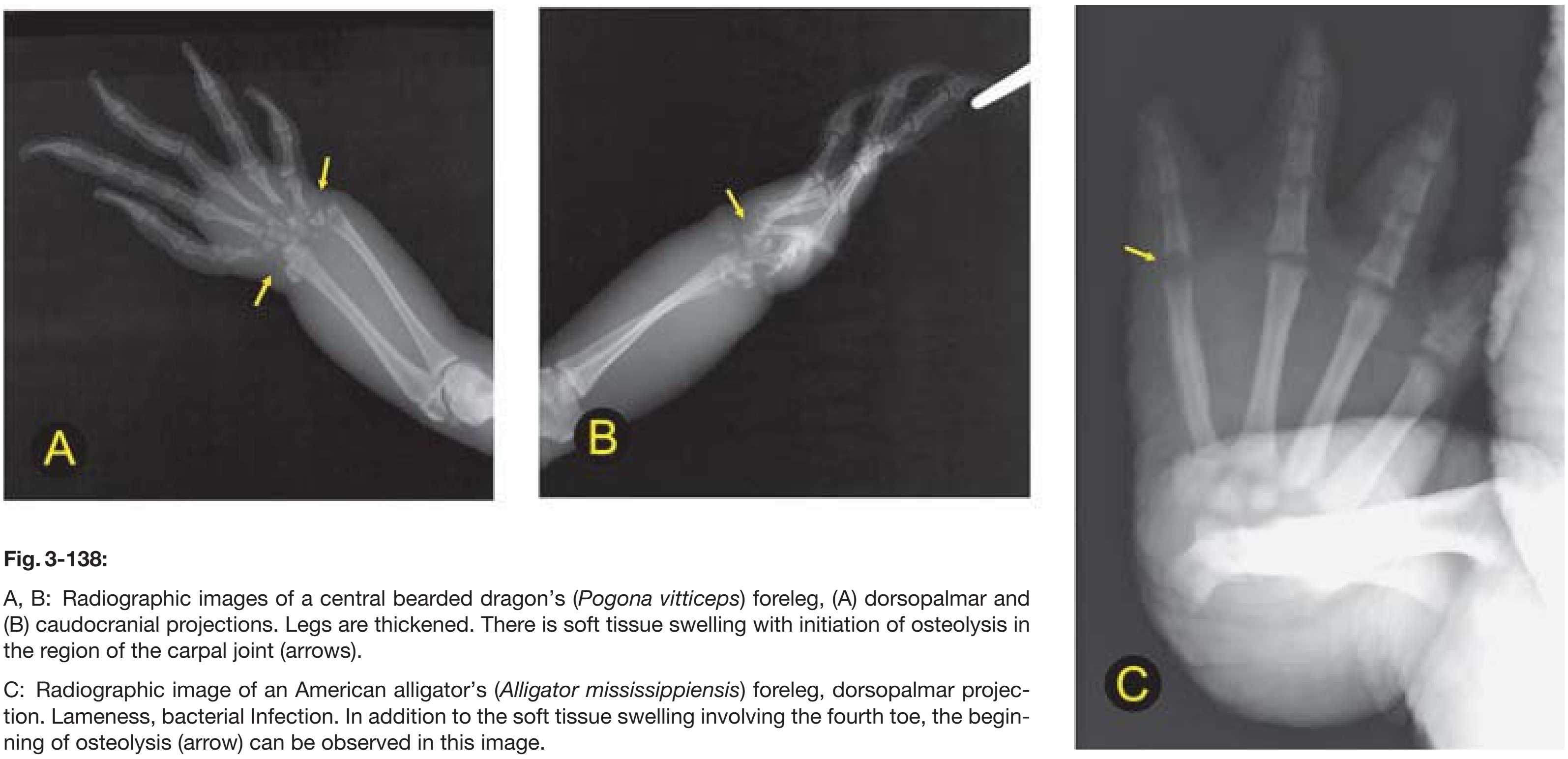

Fig. 3-138:

A, B: Radiographic images of a central bearded dragon's (*Pogona vitticeps*) foreleg, (A) dorsopalmar and (B) caudocranial projections. Legs are thickened. There is soft tissue swelling with initiation of osteolysis in the region of the carpal joint (arrows).

C: Radiographic image of an American alligator's (*Alligator mississippiensis*) foreleg, dorsopalmar projection. Lameness, bacterial Infection. In addition to the soft tissue swelling involving the fourth toe, the beginning of osteolysis (arrow) can be observed in this image.

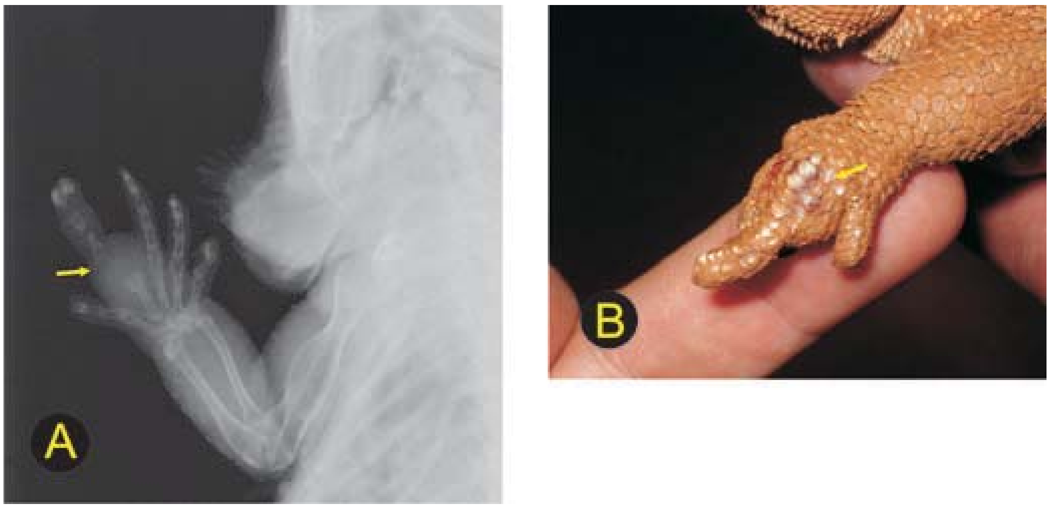

Fig. 3-139: Radiographic image of a central bearded dragon's (*Pogona vitticeps*) foreleg, (A) dorsopalmar projection. Legs, thickened, bacterial infection. The lysis of a phalanx can be clearly observed in this image (arrow). (B) With this clinical presentation, the ascending infection should be treated aggressively and an amputation of the affected bone is often the treatment of choice.

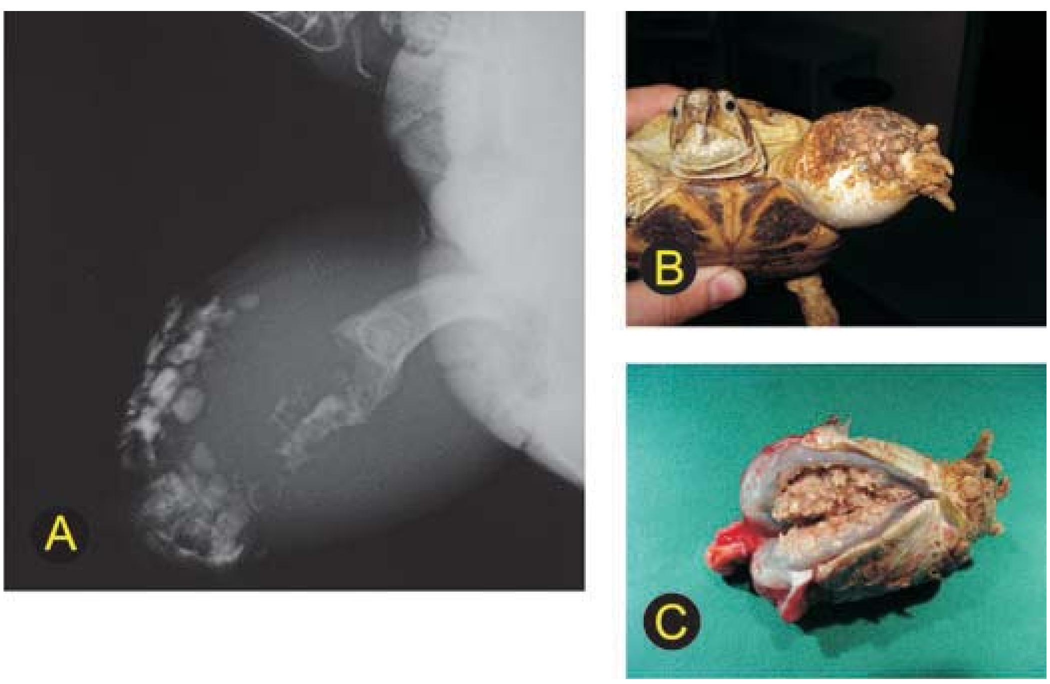

Fig. 3-140:

A: Radiographic image of a Hermann's tortoise's (*Testudo hermanni*) foreleg, dorsopalmar projection. Thickened legs: mycobacteriosis. The affected bone has completely lysed. The cytological and microbiological diagnostic tests were positive for a mycobacterium infection.

B: Clinical presentation of the affected leg.

C: Amputated leg revealing an encapsulated granuloma and subsequent incision of the mass revealing its contents.

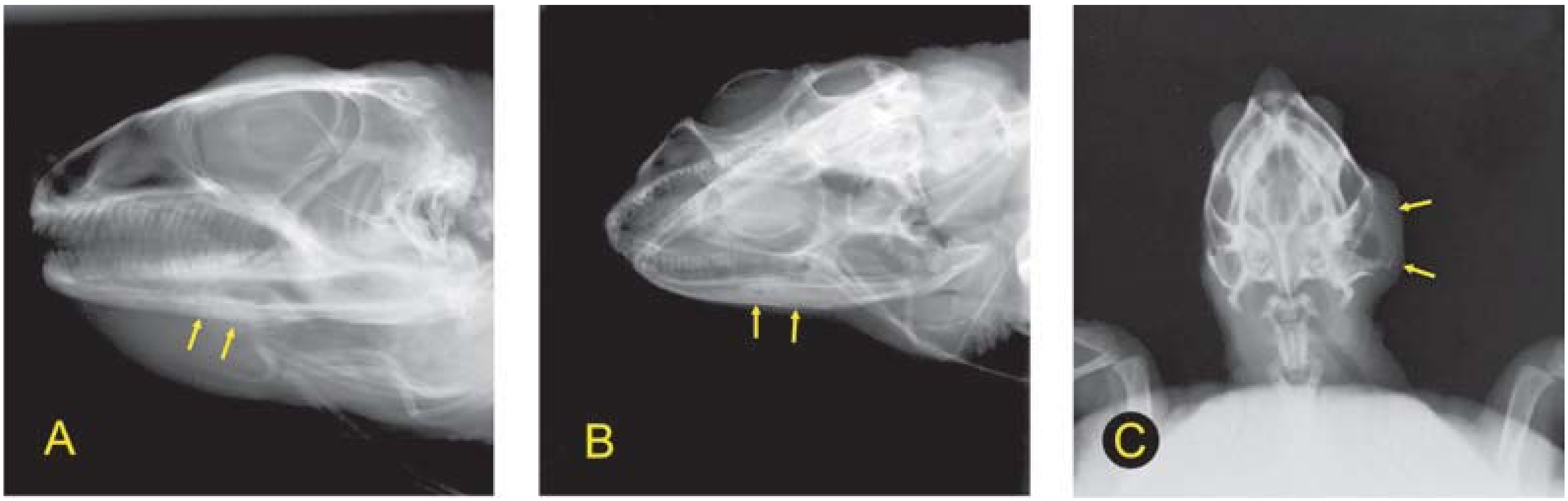

Fig. 3-141:

A, B: Radiographic images of a green iguana's (*Iguana iguana*) head, (A) lateral and (B) oblique projections. Enlargement of the mandible, osteomyelitis. Boney enlargements (arrows) are often indicative of osteomyelitis, which can be observed in both of these projections.

C: Radiographic image of a red-eared slider's (*Trachemys scripta elegans*) head, dorsoventral projection. Chronic otitis. The cranial bones in the region of the ear are thickened (arrows) and partially lytic.

3.6 Respiratory Tract

MICHAEL PEES

Within the class of reptiles, both snakes and chelonians are more susceptible to respiratory disease than lizards. The most common causes of respiratory disease in reptiles are bacterial, fungal, and viral infections as well unhygienic and unsuitable husbandry for the particular species being treated. Boas and pythons are often affected by diseases involving the respiratory tract. In land chelonians, the upper respiratory tract is usually more affected by disease processes, whereby diagnostic imaging plays a minor role. Respiratory signs frequently become first apparent in chronically diseased reptiles, consequently clinical signs that include dyspnoea are mainly indicative of severe pathology.

Although the radiographic imaging of the reptile lung has already been described, radiography is a relatively insensitive and unproductive technique for diagnosing lung infections. The reason for the difficulty of diagnosing lung disease in reptile patients is the severe summation of the lung fields by other internal body structures. A very high dose of radiation is needed in chelonian species to radiograph the animals in either a craniocaudal or lateral projection because the carapace needs to be penetrated twice. The majority of lung changes observed in reptile species with lung disease are observed as densities of soft tissue which are often inadequately differentiated. More recent imaging studies have shown that CT is a very promising modality for assessing the reptilian lung. The use of MRI is limited, especially in snakes, due to the length of time needed to perform the investigation. Ultrasonography is not useful for reptile lung examinations. The significance of imagining methods to diagnosis pneumonia in reptile species lies not only in one's ability to determine the underlying etiological cause of the disease but also by providing information about the patient's prognosis and the proper course of treatment for that particular condition.

Lung infections (pneumonia) can be best depicted radiologically in chelonians using the craniocaudal projection. In this projection, unilateral densifications in the lung tissue can be evaluated. In chelonians, there is a very proximal bifurcation of the trachea which results in a more common presentation of unilateral lung infections. With these unilateral infections, there is often a concurrent compensatory expansion of the healthy lung. This compensatory expansion of the healthy lung can occasionally be observed in the DV and craniocaudal projection (**Figs. 3-142** and **3-146**). From time to time, in the lateral projection, densities can be recognized in the lung tissue although this is mainly in concentrated foci due to the septae formed in the lungs (**Fig. 3-143**). In CT images, densities of the lung tissue are also depicted focally in the highly septated parts of the lung parenchyma (**Fig. 3-144**).

Snakes which are diagnosed with **pneumonia** have more severe changes in the ventral parts of their lungs. The affected lung tissue of snakes with pneumonia will radiograph as being nonhomogeneous and have severe densities. The radiographically evident changes are usually more prominent in the cranial part of the lungs. Generally, the lateral projection is better for diagnosis. In addition to focal densities (**Fig. 3-145**), a diffuse density of the respiratory epithelium is also observed (**Fig. 3-147**), which is especially true in snake species that rest constantly in a ventral position. Due to a green tree python's (*Morelia viridis*) usual position of being coiled around a branch, both lungs are often equally affected. The density of the affected lung tissue can be measured using CT imaging. In diseased Indian pythons (*Python molurus*), a species which is especially susceptible to lung infections, a mean radiodensity of –613.7 ± 176.4 HU has been measured (PEES et al. 2007) in comparison to mean values of –744.4 ± 47.1 HU in healthy animals (see Chap. 3.3.3.2). The increased standard deviation shows the increasing inhomogeneity of the tissue due to the presence of infectious organisms. In severe cases, large quantities of purulent secretions can collect in the central lumen of the lung. This secretion can be identified in the transverse plane lying within the lumen (**Fig. 3-144**). In addition to diagnosing pneumonia, CT can be used to monitor treatment response by the animal (PEES et al. 2008). MRI shows tissue changes resulting from inflammatory processes due to an increase in the signal intensity of the lung tissue and a stronger imaging of the blood vessels which is the result of changes in vascular perfusion (**Fig. 3-148**). However, detailed knowledge about the use of MRI for diagnosing pneumonia in snakes is not available.

Another indication for imaging the reptile lungs is to assess the lung damage of reptile patients caused by various types of **trauma**. Chelonian lung tissue is particularly affected by trauma which is commonly caused by falls and bite injuries. The dyspnoea identified in animals after falls (i.e. usually from balconies, terraces or the vivarium/terrarium) or bites can be examined using either CT or MRI imaging, enabling one to determine the extent of tissue damage and hemorrhaging (**Fig. 3-149**). Such changes are also often associated with damage to the shell (see Chap. 3.5.1). Imaging the injured animal to determine lung integrity after perforating bite wounds is important when establishing a treatment protocol (**Figs. 3-123** and **3-150**). If the lung integrity has been compromised (e.g. perforation due to a bite wound), then antimicrobial therapy is highly recommended for that animal.

Further reading

PEES, M., KIEFER, I., LUDEWIG, E., SCHUMACHER, J., KRAUTWALD-JUNGHANNS, M.-E., OECHTERING, G. (2007): Computed tomography of the lungs of Indian pythons (*Python molurus*). American J Vet Res **68**: 428–434.

PEES, M., KIEFER, I., OECHTERING, G., KRAUTWALD-JUNGHANNS, M.-E. (2008): The use of computed tomography for the diagnosis and treatment monitoring of bacterial-induced pneumonia in Indian pythons (*Python molurus*). Vet Rec, in press.

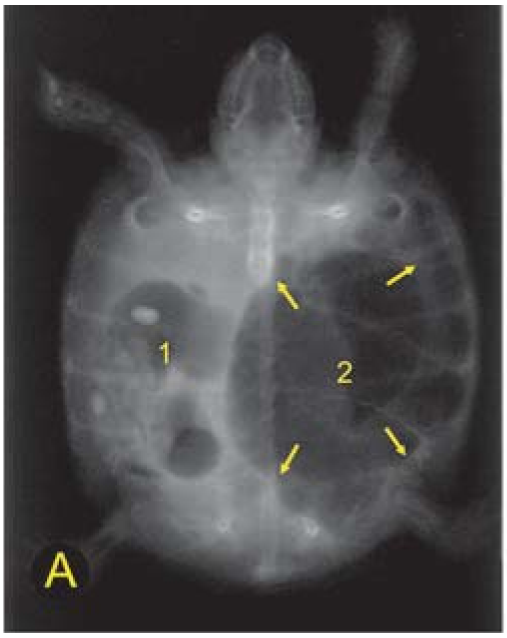

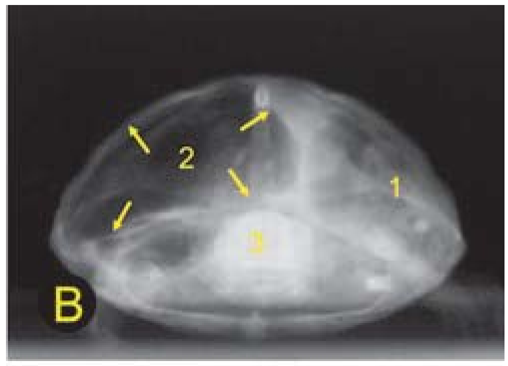

1: left lung
2, arrows: right lung
3: head

Fig. 3-142: Total body radiographic images of a Hermann's tortoise (*Testudo hermanni*), (A) dorsoventral and (B) craniocaudal projections. Pneumonia. The stomach, which is filled with stones, overlies the left lung (1) which is severely consolidated and reduced in size in the dorsoventral projection; conversely, the right lung (2) is severely expanded.

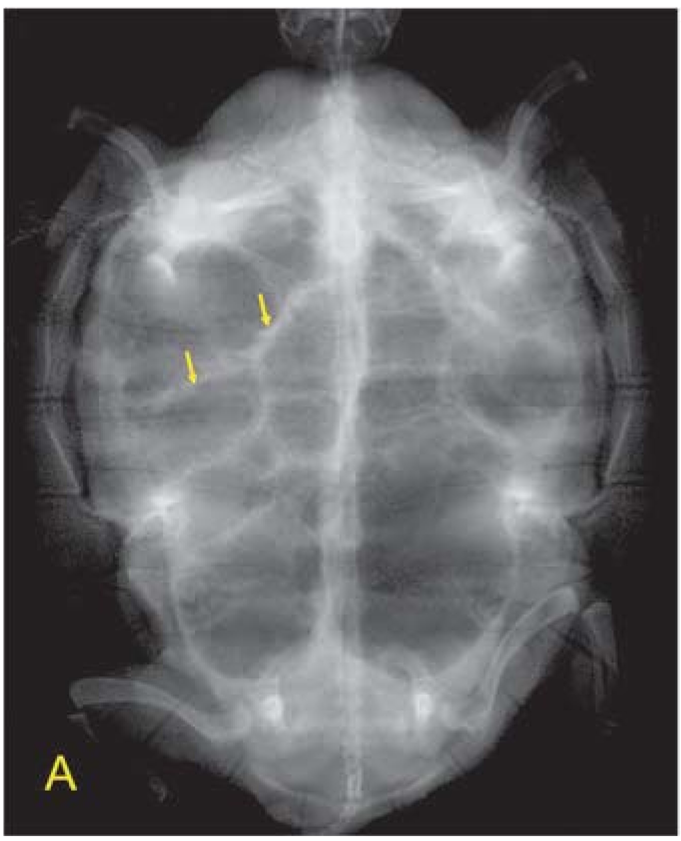

Fig. 3-143: Total body radiographic images of a red-eared slider (*Trachemys scripta elegans*), (A) dorsoventral and (B) lateral projections. Pneumonia. In the lateral projections radiodense tissue (*) can be observed. These areas of radiodensity (arrows) are also visible in the dorsoventral projection; however, the differentiation of consolidated areas of the lung (pneumonia) from the shell is difficult.

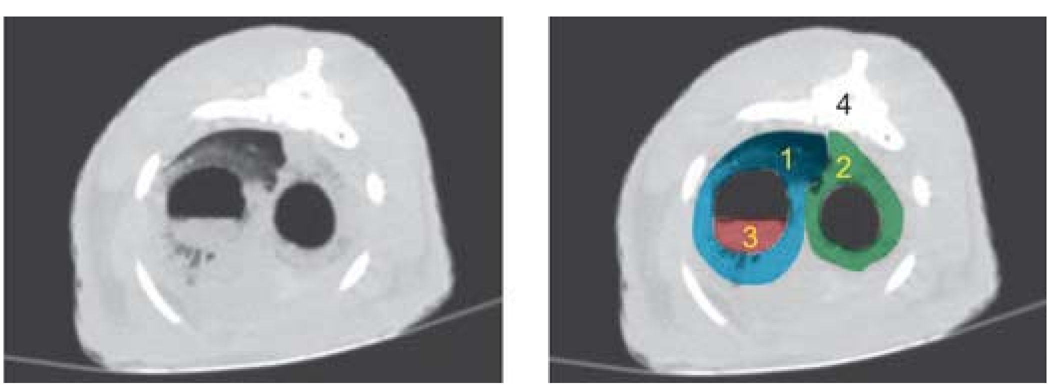

1: right lung
2: left lung
3: purulent exudate
4: vertebrae

Fig. 3-144: CT image of an Indian python's (*Python molurus*) body, transverse plane (120 kV, 204 mA, 2.0 mm SD, W: 1500, L: –600). Severe pneumonia. The radiodensity of the left lung epithelium (2) is severely increased. The right lung (1) also has a radiodense and nonhomogeneous epithelium. In the lumen of the right lung is a purulent exudate (3).

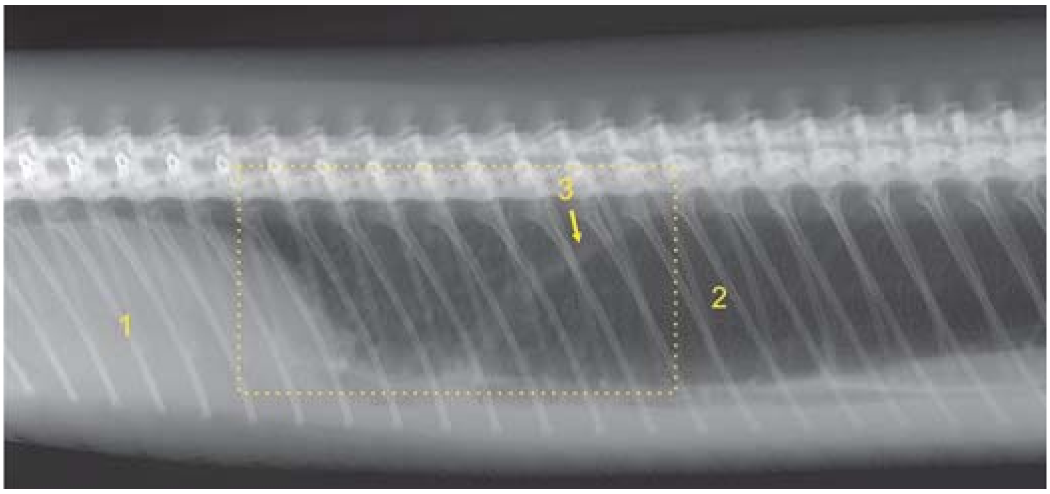

1: heart
2: lung lumen
3: blood vessel

Fig. 3-145: Radiographic image of an Indian python's (*Python molurus*) body, lateral projection. Pneumonia. There are multifocal shadows within the cranial part of the lung epithelium (square).

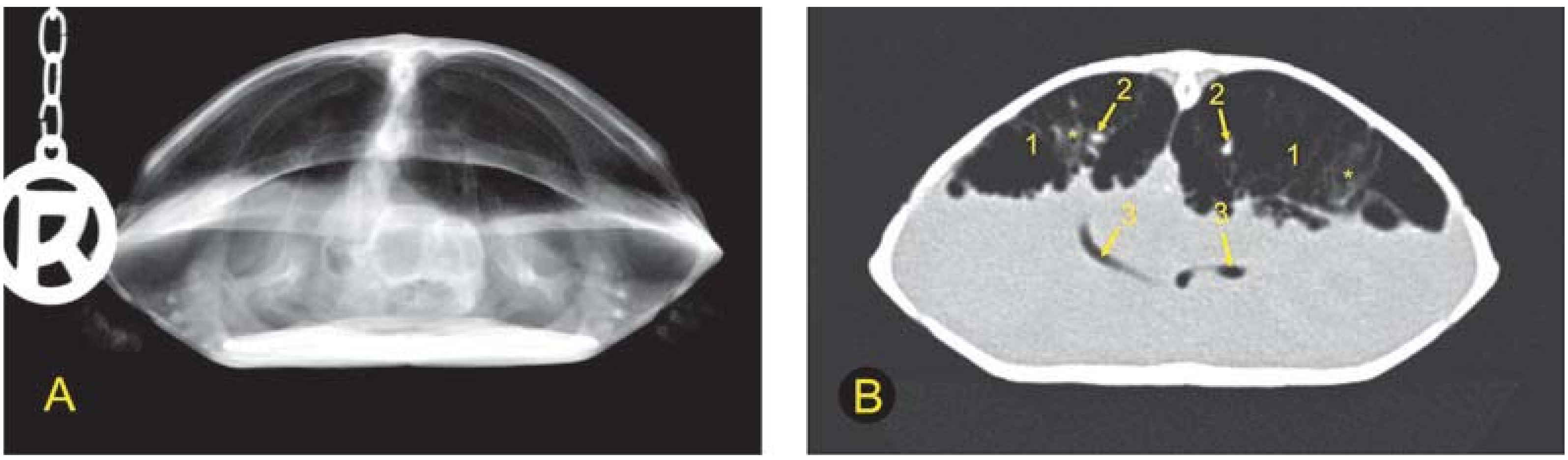

Fig. 3-146:

A: Total body radiographic image of a yellow-bellied slider (*Trachemys scripta scripta*), craniocaudal projection: Pneumonia. The lung fields in this projection are inconspicuous.

B: CT image of the same animal, transverse plane (120 kV, 83 mA, 0.8 mm SD, W: 1332, L: –361). Radiodense areas (*) are visible in both lung fields (1).

1: lungs
2: lung blood vessels
3: trachea after the bifurcation

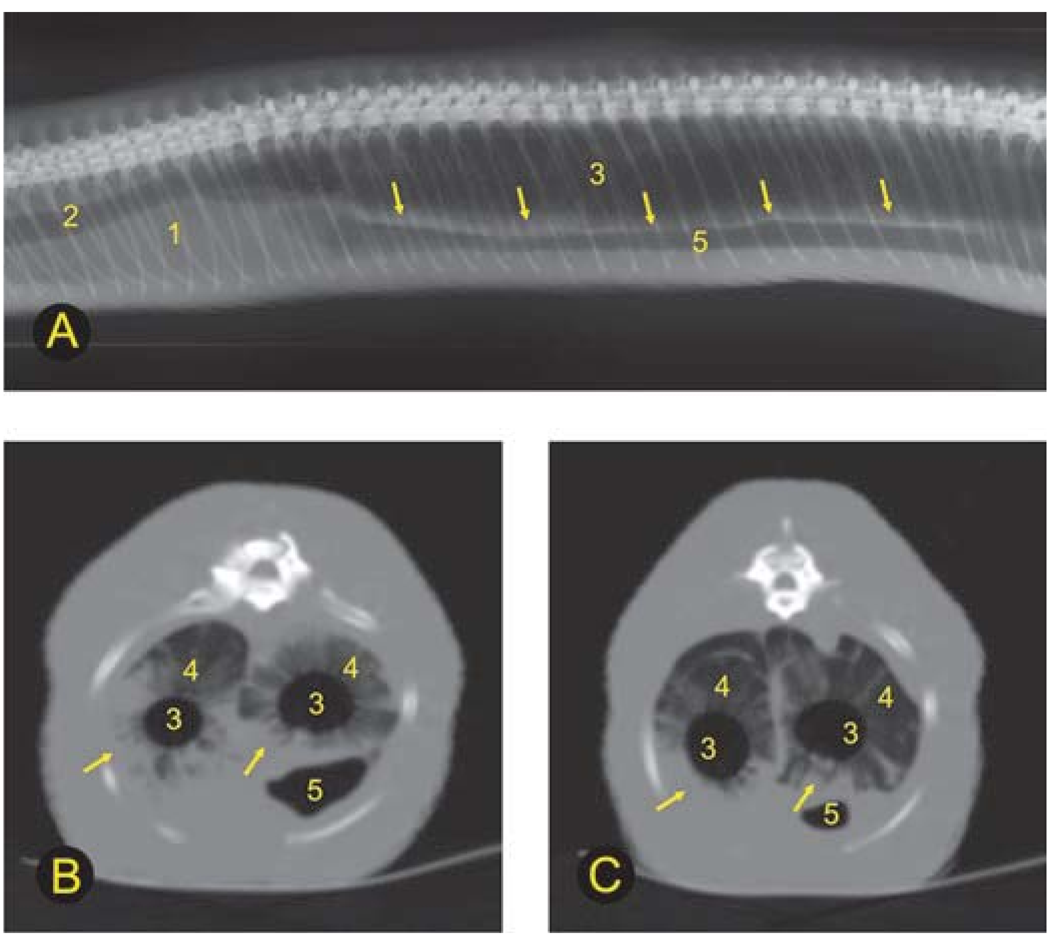

1: heart
2: trachea
3: lung lumen
4: lung epithelium
5: esophagus

Fig. 3-147:

A: Radiographic image of an Indian python's (*Python molurus*) body segment, lateral projection. Pneumonia. The ventral respiratory epithelium is thickened (arrows) and is clearly offset against the lung lumen (3).

B, C: CT images of the same animal's body, transverse plane (120 kV, 204 mA, 2.0 mm SD, W: 2605, L: 176). The ventral areas of radiodensity (arrows) and overall inhomogenicity of the lung epithelium (4) around the central lumen (3) can be seen.

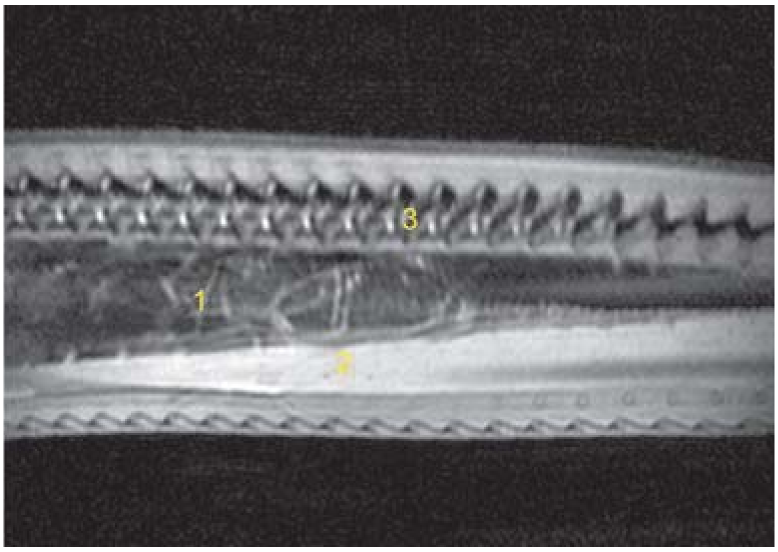

1: lung tissue
2: fat tissue
3: spine

Fig. 3-148: MRI examination of an Indian python's (*Python molurus*), body, sagittal plane, T1-weighted. Pneumonia. The lung tissue (1) is shown in the region of the respiratory epithelium and appears to have a higher signal intensity then normal (for comparison: lung tissue in Fig. 3-110C).

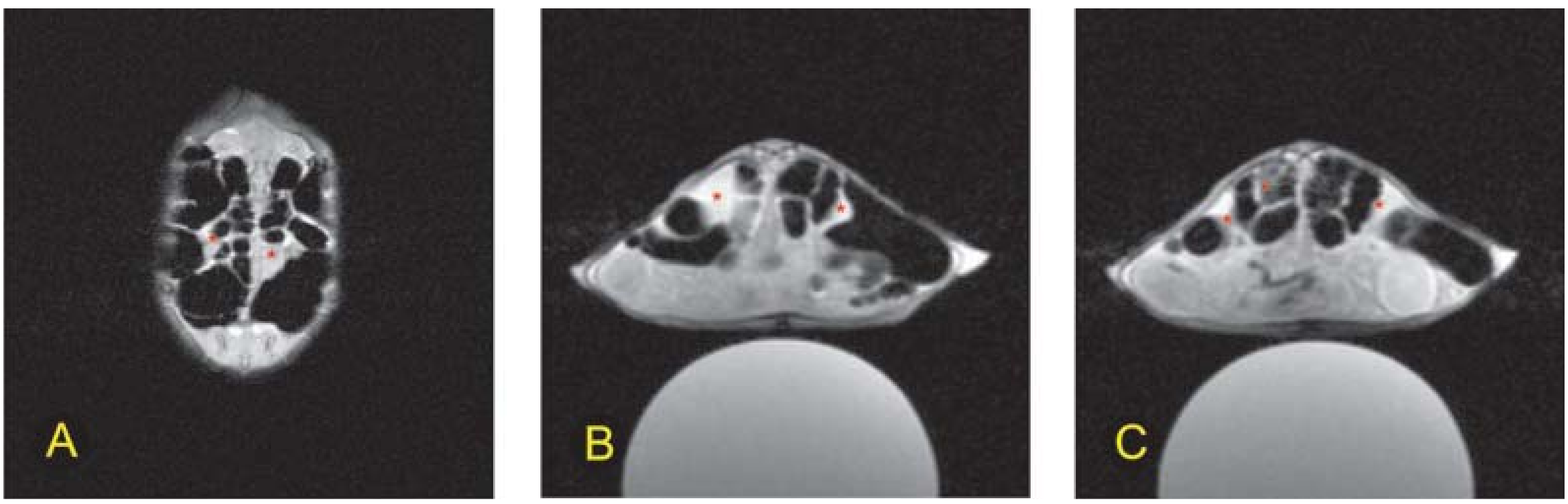

Fig. 3-149: MRI examination of a yellow-bellied slider (*Trachemys scripta scripta*), body, (A) dorsal and (B, C) transverse planes, T1-weighted, with a (B, C) phantom. Free fall trauma. Hemorrhages (*) can be identified within the lung tissue.

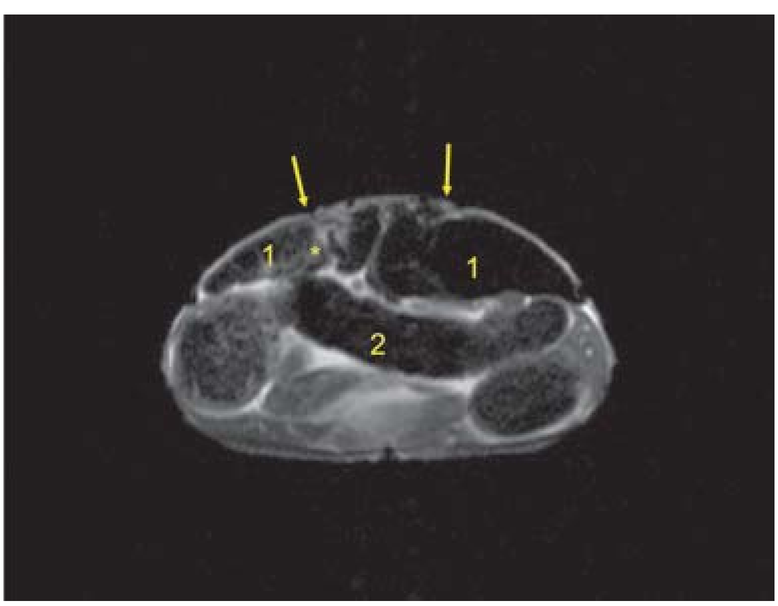

1: lungs
2: intestines

*: hemorrhage

Fig. 3-150: MRI examination of a Hermann's tortoise's (*Testudo hermanni*) body, transverse plane, T2-weighted. Dog bite. Both sides of the lungs (1) have been dorsally exposed (arrows), and there is evidence of hemorrhaging (*) into the lung tissue.

3.7 Gastrointestinal tract

MICHAEL PEES

Disturbances of the gastrointestinal tract are a frequent problem in reptiles. The causes of gastrointestinal abnormalities include infectious disease, malnutrition (see metabolic bone disease), and husbandry problems. The radiographic examination of the gastrointestinal tract provides the most important evidence regarding disturbances in emptying or of the presence of a foreign body. Ultrasonography, and where possible MRI and CT, can be used to help determine the type and cause of the disturbance.

3.7.1 Excessive emptying of the gastrointestinal tract

An almost complete emptying of the gastrointestinal tract due to the feeding intervals is normal and also necessary for snakes. The gastrointestinal tract in herbivorous lizards and chelonians should always have some content within it. One exception is during hibernation, in which the inanition during the preparation phase serves to empty the gut. Otherwise, the lack of intestinal contents should be considered an indication of chronic anorexia. In the anorexic chelonian, the lung field takes up more than half of the body cavity's height (**Fig. 3-151**).

3.7.2 Foreign bodies

Foreign bodies in the gastrointestinal tract are the most common radiographic findings in reptiles. The cause of this allotrophagia is partly due to malnutrition – the animals try to compensate for their nutritional insufficiencies by ingesting sand and stones. A certain amount of sand and small stones is considered normal in terrestrial chelonians. The ingestion of stones for the digestion of food in the gizzard is also normal in some species of lizards, such as alligators (**Fig. 3-152**). Problems arise when the quantity of stones is too high (**Figs. 3-153** and **3-154**) or unsuitable foreign bodies are ingested (**Figs. 3-152** and **3-155** to **3-158**). The ingested foreign bodies usually come from the terrarium or from the surrounding environment. Sand (**Figs. 3-154A, B**), metal objects (**Figs. 3-157** and **3-158**), and toys (**Fig. 3-152**) are regularly found in the gastrointestinal tract of reptiles. Radiolucent material such as wood, ear plugs, or fibrous material (**Fig. 3-156**) can lead to intestinal blockage of reptile patients. The actual cause of the intestinal blockage can only be determined by using other diagnostic methods (e.g. ultrasonography, endoscopy, exploratory laparotomy).

Another cause of intestinal blockage is the feeding of egg shells as a calcium supplement. Apart from this practice being hygienically questionable, another objection to feeding this material is the animal's inability to digest this material (**Fig. 3-155**). Intestinal blockage often occurs when the shells are ground down to a paste which then solidifies within the gastrointestinal tract as fluid is resorbed in the intestines. Iodine-based contrast studies are very helpful in diagnosing foreign body ingestion by reptile patients.

3.7.3 Disturbances in emptying

Along with other causes, ingestion of foreign bodies (see above) is the most important factor affecting gastrointestinal tract emptying (e.g. **constipation**). A lack of fluid can lead to an increased solidification of the ingesta, thereby rendering transportation and excretion of ingested material impossible (**Fig. 3-159**). In addition to using traditional radiographic techniques to examine the dilated gastrointestinal tract, a lack of gastrointestinal peristalsis and increased quantity of ingesta can be imaged using ultrasonography (**Fig. 3-160**). One should also consider that in some cases, a radiographic examination of the gastrointestinal tract will not provide an answer to the underlying cause of constipation, especially if the gastrointestinal tract is not overfilled due to the animal being fasted. In addition to contrast studies, MRI can provide information concerning the consistency of the intestinal contents (**Fig. 3-161**).

Narrowing of the intestinal tract can be caused by inflammatory changes, mechanical displacement (**Fig. 3-162**), and space-occupying lesions within the intestinal wall. The latter conditions include intramural abscesses (**Fig. 3-163**), which are frequently diagnosed in lizard species. Most likely, gastrointestinal intramural abscesses form as the result of microlesions within the intestinal wall. In chronic cases, these abscesses can reach such excessive sizes that they hinder peristalsis and cause narrowing of the intestinal lumen. Such abscesses are diagnosed often in snakes. Ultrasonography is a very helpful imaging modality for the diagnosis of intestinal abscesses. Administering water as a contrast agent (**Fig. 3-164**) can aid in differentiating the intestinal contents from the wall.

Atony is diagnosed in conjunction with septicemia and other severe general disease processes that may affect the body. There is a lack of peristalsis and emptying of the gut with gastrointestinal atony, mainly followed by bloating of the intestinal lumen (see below).

3.7.4 Infections

Clinical signs associated with gastrointestinal tract infections are often nonspecific. Bloat and thickening of the intestinal tract wall can be imaged using radiography. The presence of yeasts or anerobic bacteria within the gastrointestinal tract must be determined since they may be the underlying etiology causing the clinical signs mentioned above (**Figs. 3-165** and **3-166**). Bacterial and parasite infections will often lead to fluid accumulation within the intestinal lumen and increased peristaltic movement (**Fig. 3-167**), which can be ultrasonographically imaged. Another clinical presentation, especially with parasite (flagellate) infections, is the prolapse of cloacal tissue. Imaging the prolapsed cloaca is a method to control the veterinarian's ability to correctly replace the exposed tissue (**Fig. 3-168**).

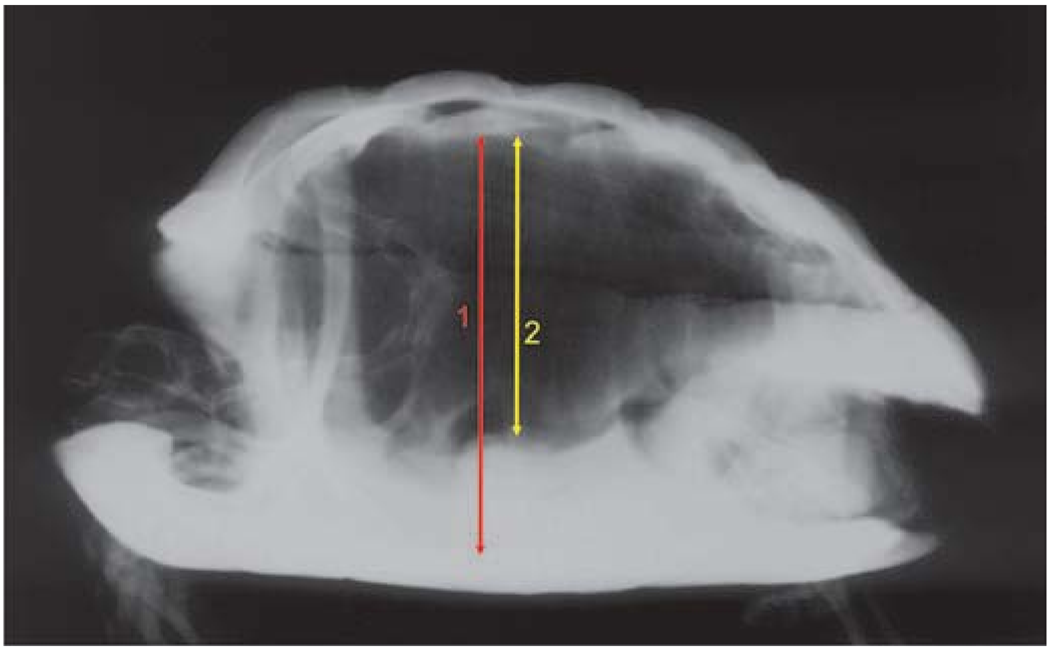

1: body cavity height
2: lung height

Fig. 3-151: Total body radiographic image of a Hermann's tortoise (*Testudo hermanni*), lateral projection. Inappetence lasting several weeks. The intestinal tract contains very little ingested material. The relationship of the lung height (2) and the body cavity height (1) has been changed to the advantage of the lungs.

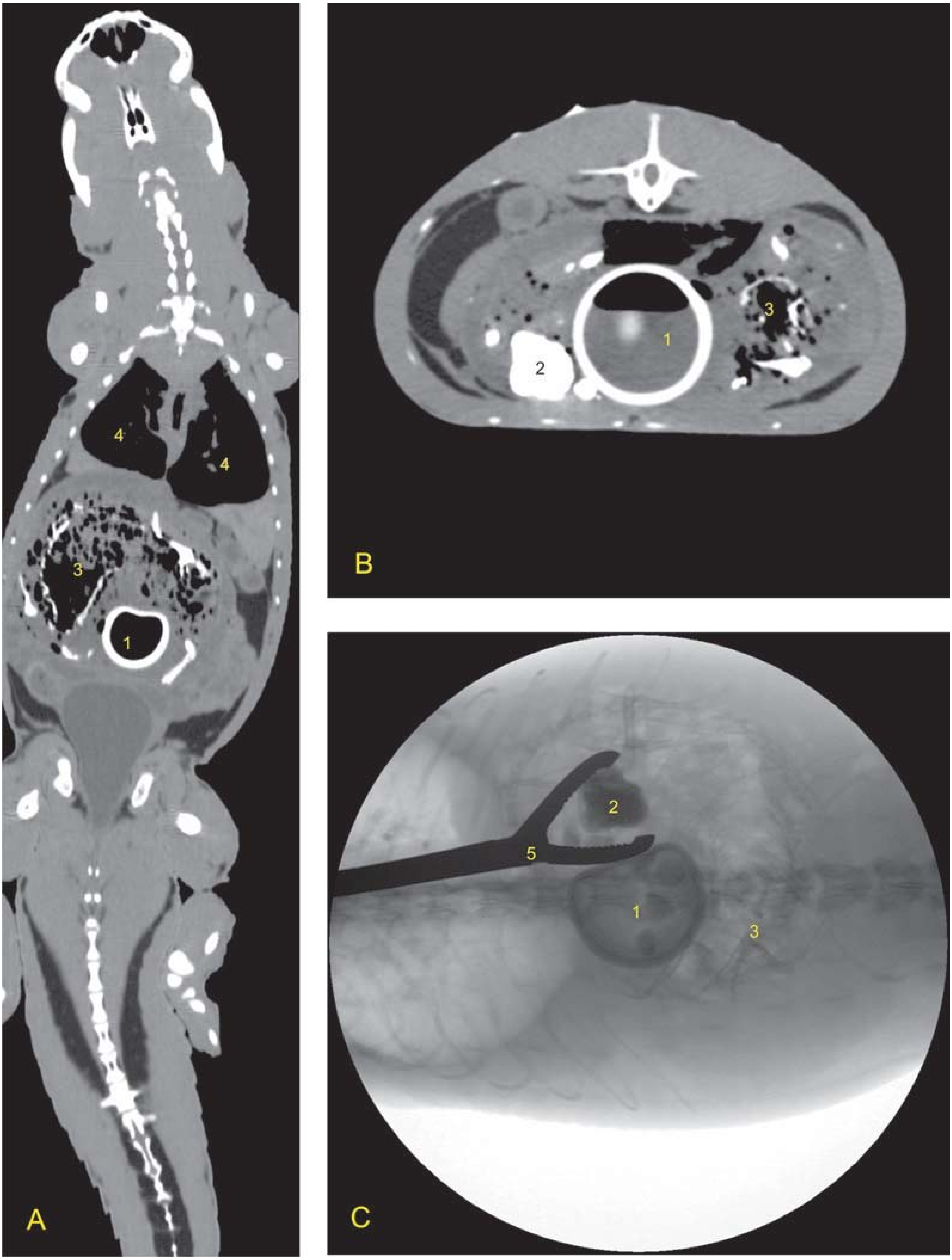

Fig. 3-152: CT images of an American alligator's (*Alligator mississippiensis*) body, (A) dorsal reformation and (B) transverse plane (120 kV, 204 mA, 2.0 mm SD, W: 400, L: 60). Foreign body. Within the image one can observe the stomach (3) contents that contain a stone (2) and a rubber ball (1). Foreign bodies are a frequent disease problem in alligators, although the presence of smaller stones in the stomach is considered normal. (C) The ball was removed with foreign body forceps (5) under radiographic guidance.

1: foreign body (rubber ball)
2: stone
3: stomach contents
4: lung
5: foreign body forceps

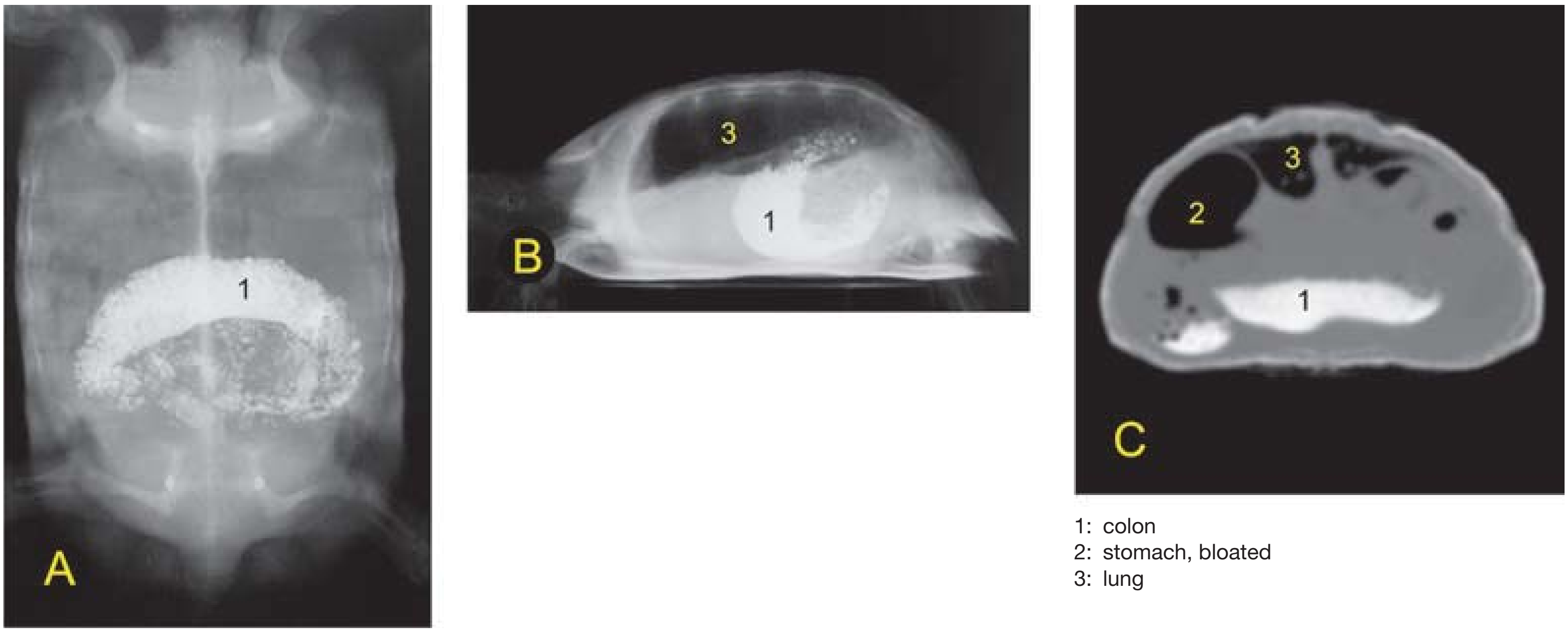

1: colon
2: stomach, bloated
3: lung

Fig. 3-153:

A, B: Total body radiographic images of a Hermann's tortoise (*Testudo hermanni*), (A) dorsoventral and (B) lateral projections. Stone constipation. The colon (1) is severely filled with radiopaque stones.

C: CT image of a Hermann's tortoise's (*Testudo hermanni*) body, transverse plane (140 kV, 200 mA, 1.0 mm SD, W: 2439, L: 369). Stone constipation. The colon (1) is filled with stones that have become deposited ventrally.

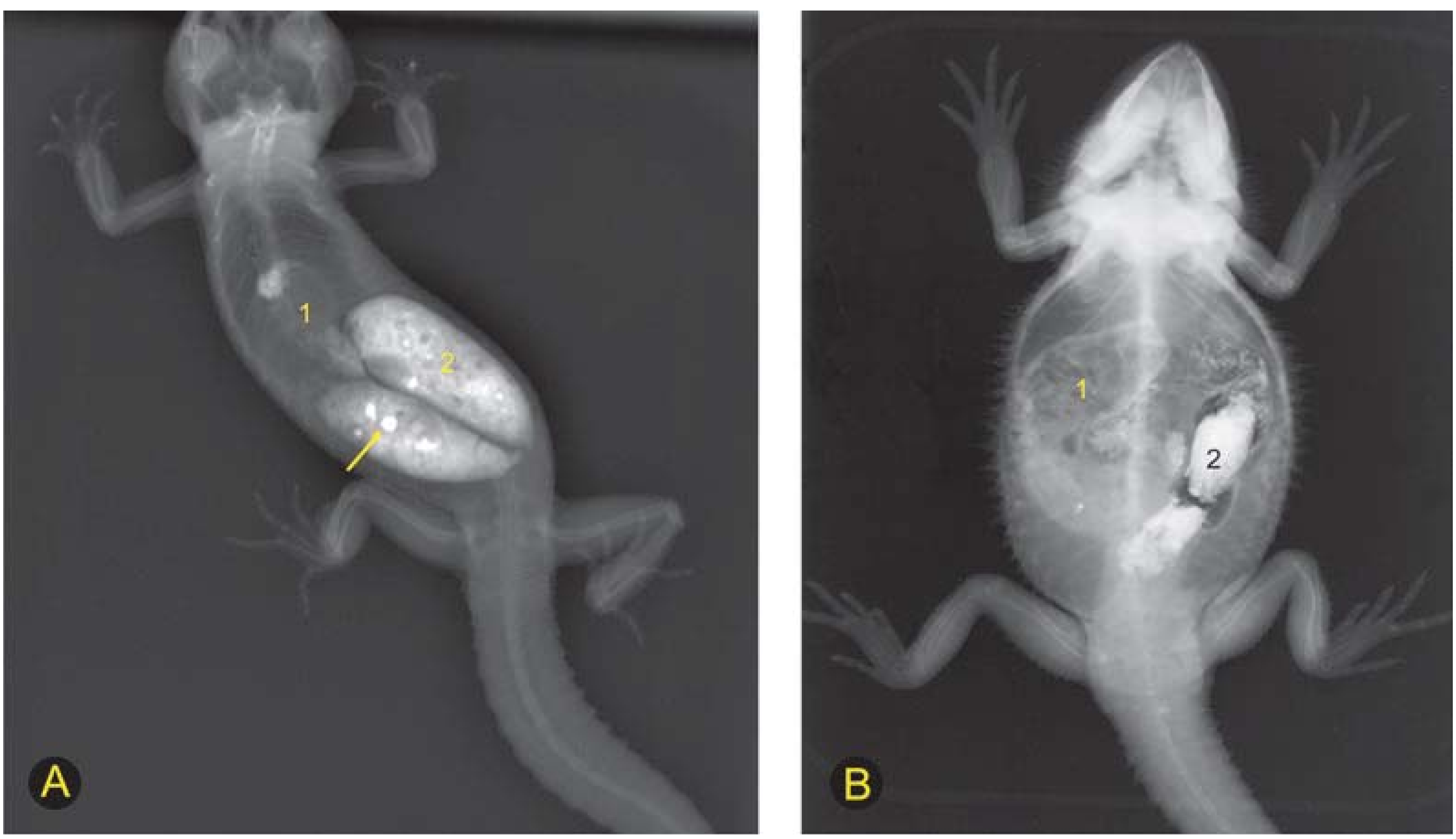

Fig. 3-154: Total body radiographic images, dorsoventral projections.

A: Leopard gecko (*Eublepharis macularius*). Sand constipation.

B: Central bearded dragon (*Pogona vitticeps*). Sand constipation.

As a consequence of a calcium-poor diet, both animals have ingested large amounts of sand which has concentrated in the colon (2). The leopard gecko has also ingested other radiopaque particles (arrow).

1: stomach, with more sand in the cranial region
2: colon: sand constipation

arrow: radiopaque particles

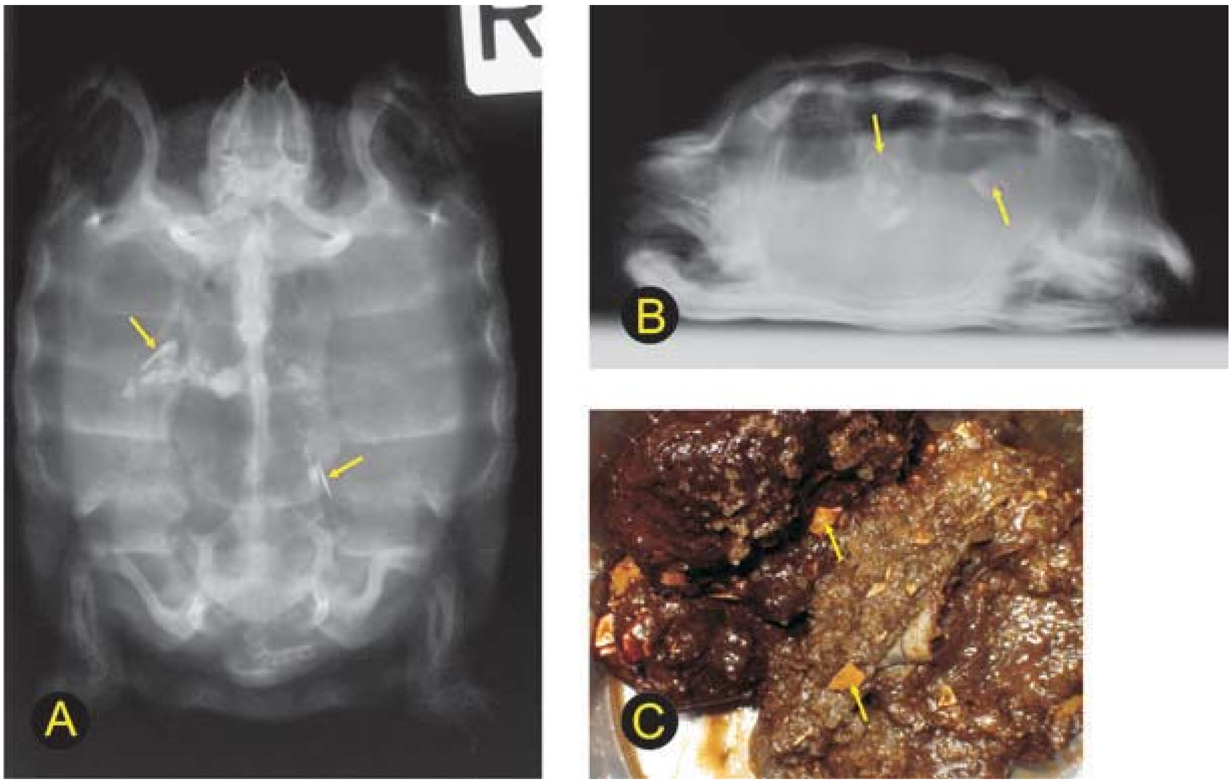

Fig. 3-155:

A, B: Total body radiographic images of a Hermann's tortoise (*Testudo hermanni*), (A) dorsoventral and (B) lateral projections. Constipation. Egg shell fragments (arrows) are in the intestines.

C: Egg shell fragments are also present in the animal's feces (arrows). Feeding of egg shells should be discouraged as it is neither nutritionally nor hygienically appropriate.

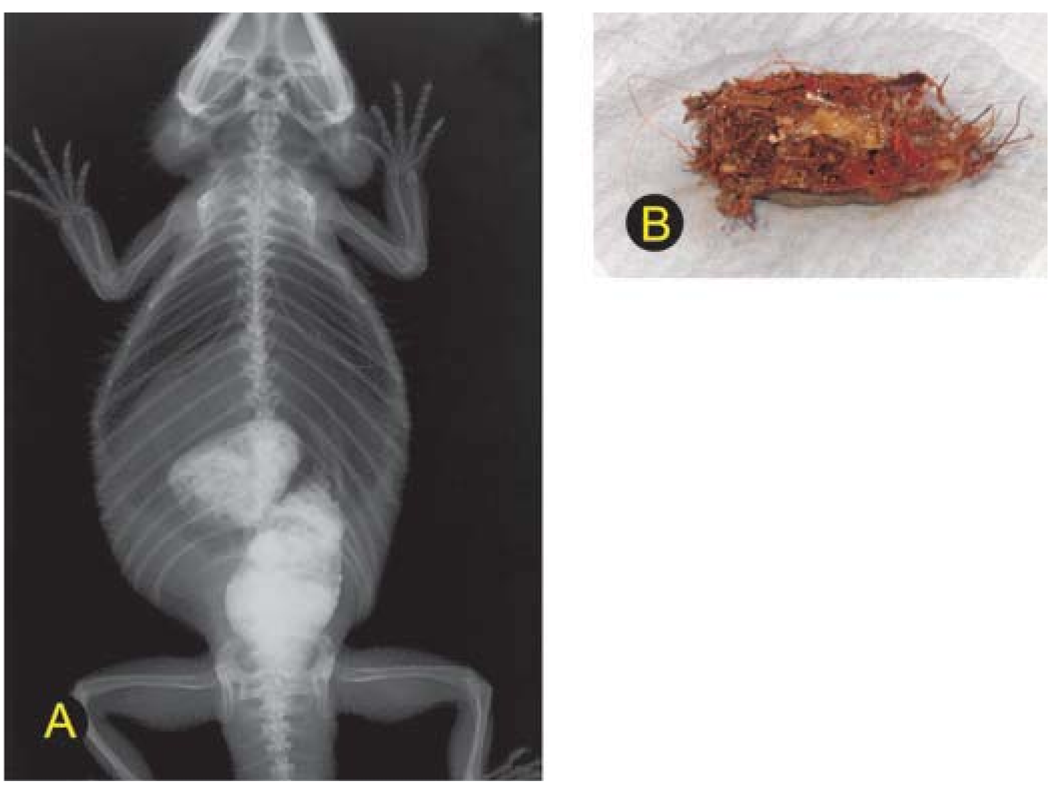

Fig. 3-156:

A: Total body radiographic image of a central bearded dragon (*Pogona vitticeps*), dorsoventral projection. Constipation. The colon and cloaca are filled with large amounts of sand, which could not be removed by flushing.

B: A highly interwoven sand-copra mixture was removed endoscopically. Central bearded dragons often ingest large foreign bodies relative to their own body size.

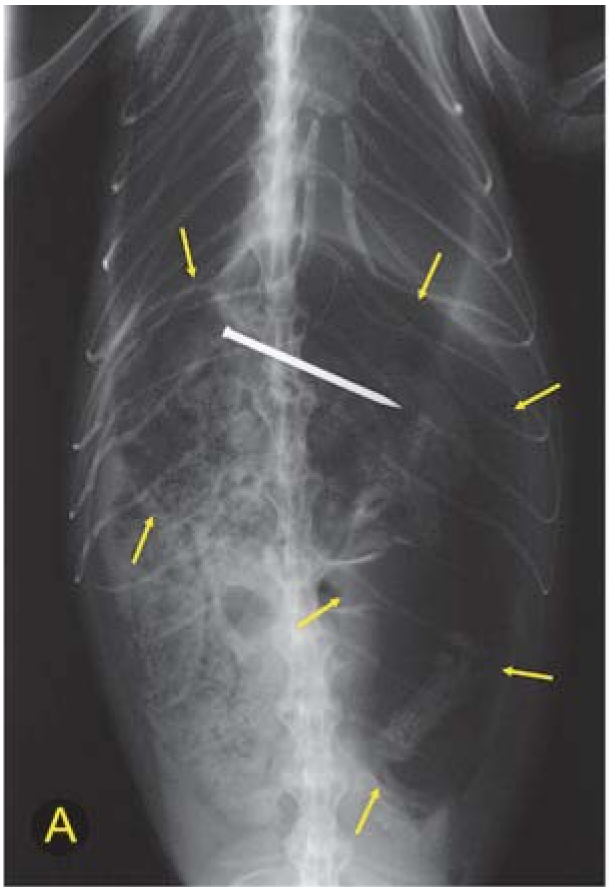

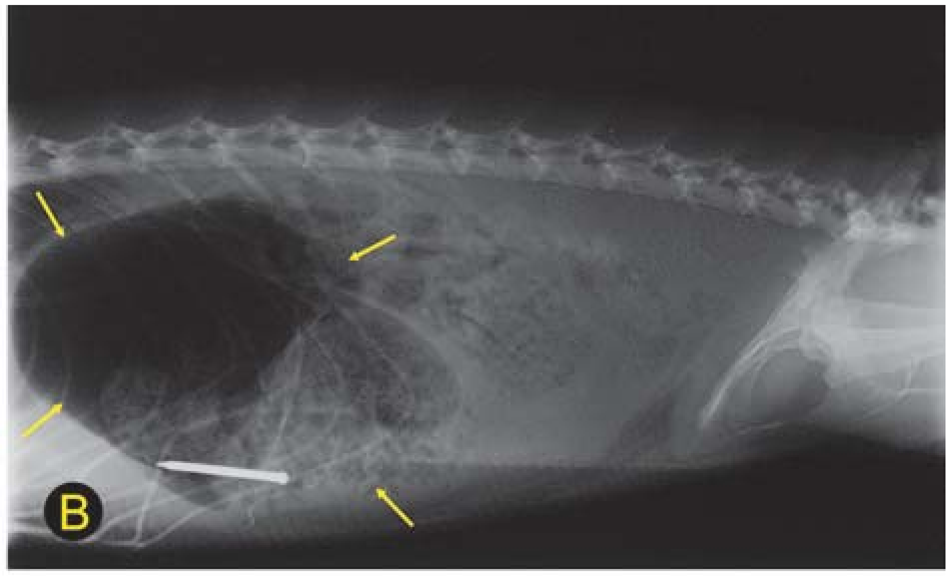

Fig. 3-157: Radiographic images of a green iguana's (*Iguana iguana*) trunk, (A) dorsoventral and (B) lateral projections. Foreign body. There is a nail in the animal's intestinal tract, which has penetrated the intestinal wall (surgical finding). The colon (arrows) is distended. In this case, there was complete blockage of the intestinal tract prior to surgery.

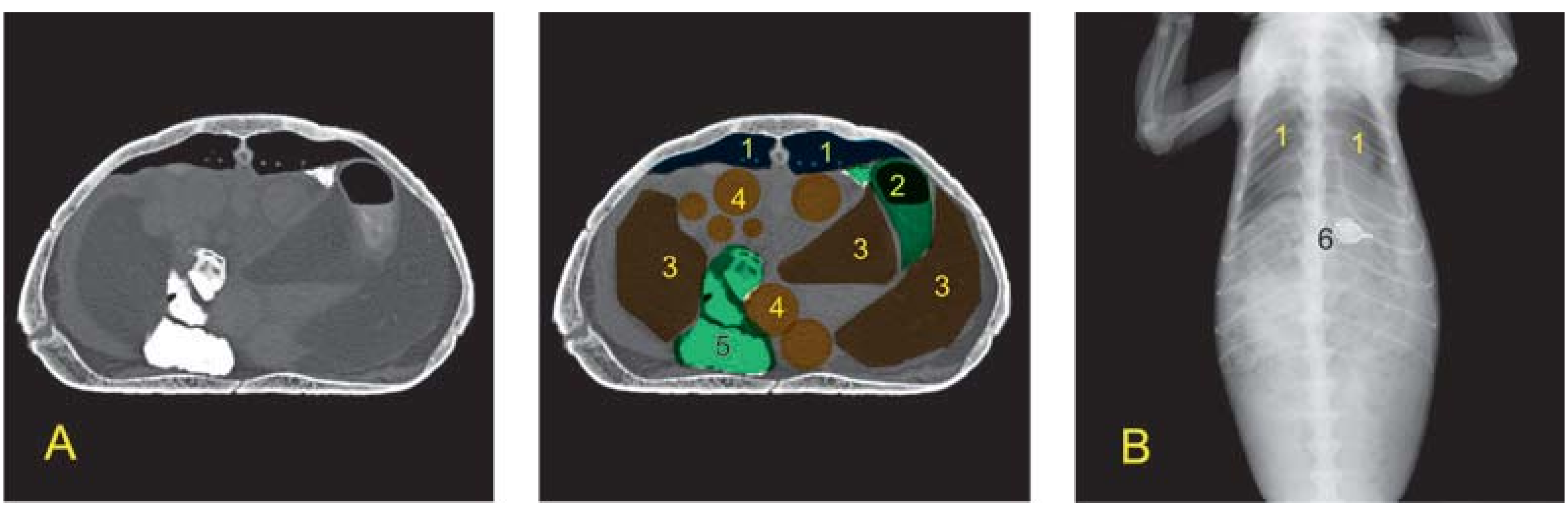

Fig. 3-158:

A: CT images of a Hermann's tortoise's (*Testudo hermanni*) trunk, transverse plane (120 kV, 120 mA, 1.0 mm SD, W: 1500, L: 350). Foreign body. Radiodense particle (5: piece of lead) in the intestines. The liver (3) is severely enlarged and congested

B: Radiographic image of a green iguana's (*Iguana iguana*) trunk, dorsoventral projection. Foreign body. The radiodense foreign body (6) in the stomach is an ear ring.

1: lung
2: stomach
3: liver
4: follicle
5: piece of lead
6: foreign body

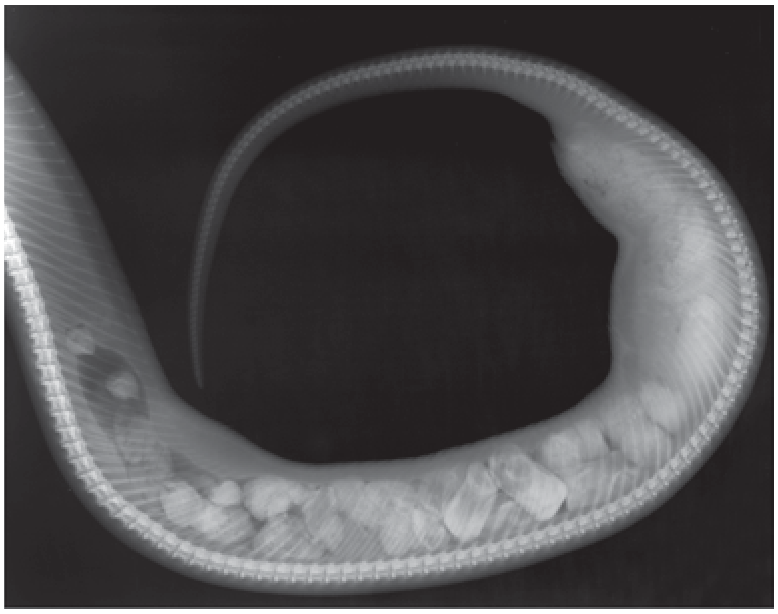

Fig. 3-159: Radiographic image of an Indian python's (*Python molurus*) body, oblique projection. Constipation in the colon. The ingesta is compacted, hardened and relatively radiopaque. The concentrated ingesta within the gastrointestinal tract is observed in a region cranial to the cloaca.

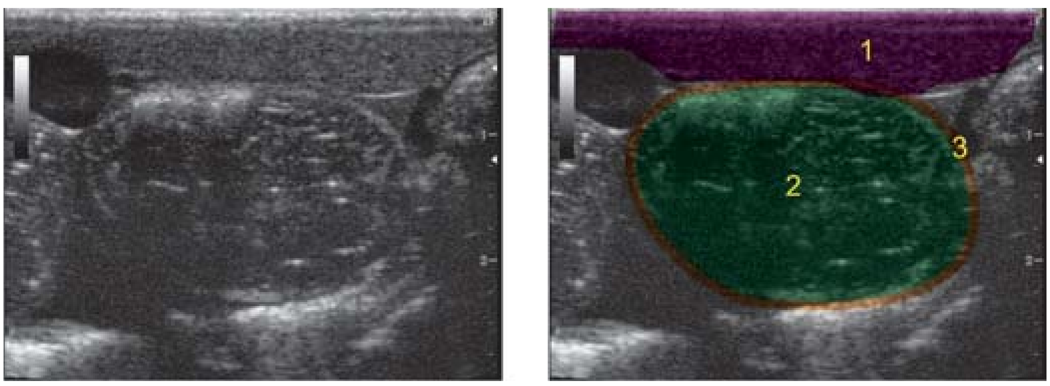

1: abdominal wall/fat body
2: ingesta
3: intestinal wall

Fig. 3-160: Ultrasonographic image of a central bearded dragon (*Pogona vitticeps*), ventral coupling site, oblique, 12 MHz, PD 3 cm. Constipation. Increased concentration of ingesta (2) in the intestines; peristalsis was no longer evident.

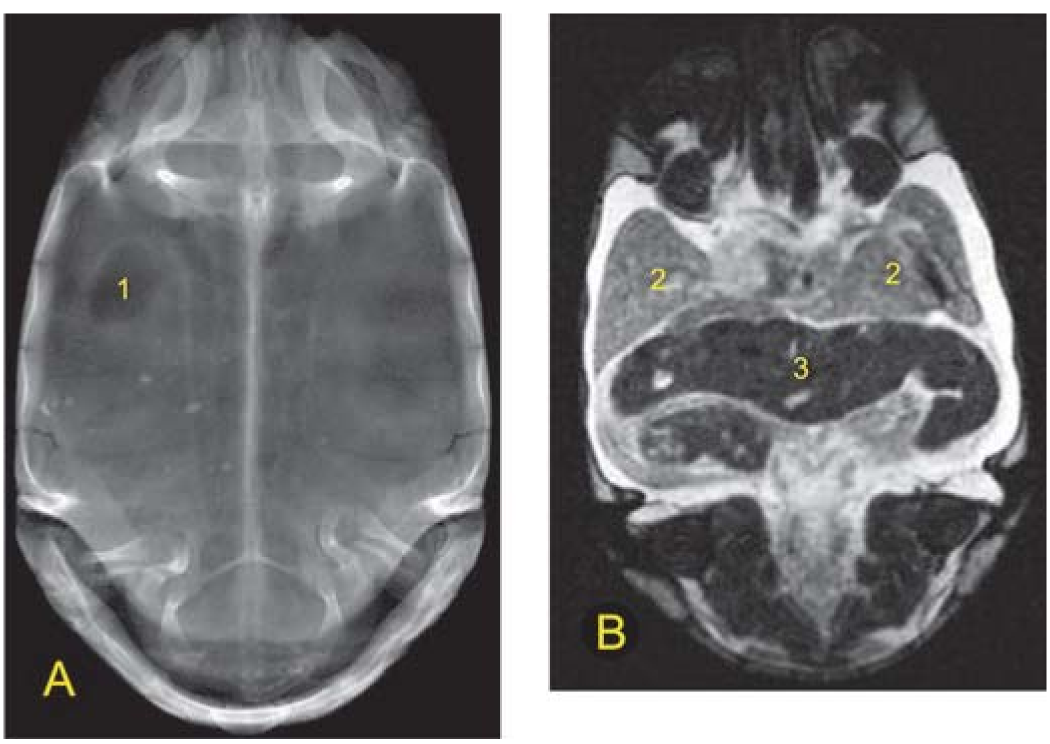

1: stomach
2: liver
3: intestines

Fig. 3-161:

A: Total body radiographic image of a spur-thighed tortoise's (*Testudo graeca*) body, dorsoventral projection. Constipation. The radiograph reveals a small amount of stones within the intestinal tract.

B: Total body MRI examination of the same animal, dorsal plane, T1-weighted. The intestines and their contents can be assessed in this image. There is a compaction without the presence of radiopaque particles.

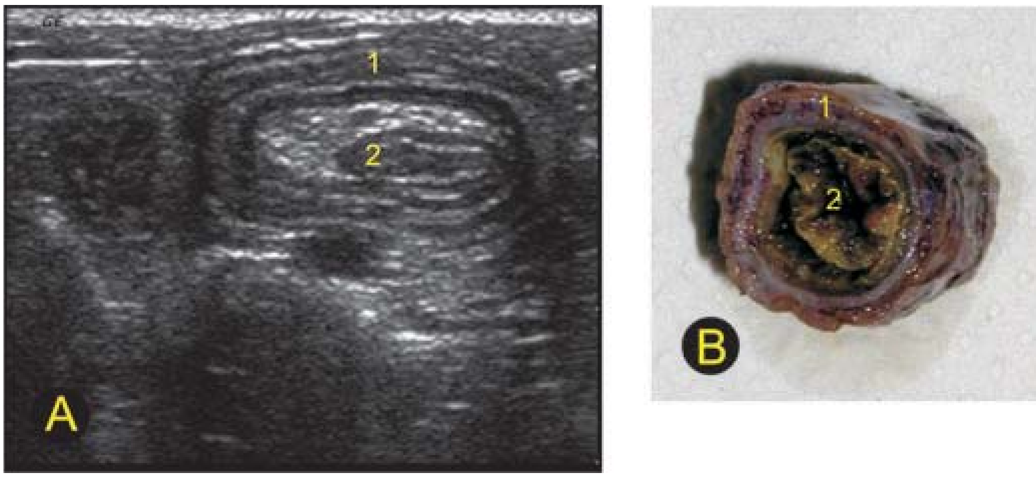

1: invagination: outer section of the intestine
2: invagination: inner section of the intestine

Fig. 3-162:

A: Ultrasonographic images of a green iguana (*Iguana iguana*), ventral coupling site, longitudinal, 12 MHz, PD 3.0 cm. Invagination of a section of the intestines (2 in 1). The inner section was necrotic and had to be surgically removed.

B: Results after resection.

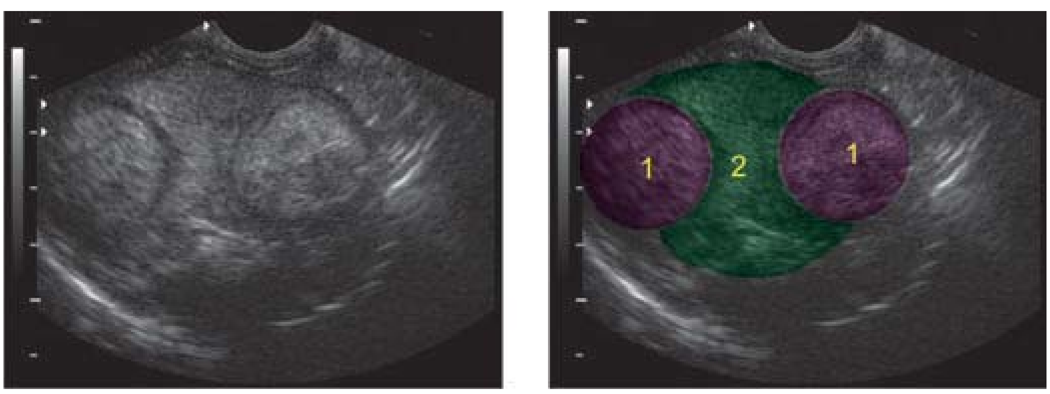

1: abscess
2: ingesta

Fig. 3-163: Ultrasonographic image of a Madagascar ground boa (*Acrantophis madagascariensis*) in the region of the intestines, ventral coupling site, oblique, 7.5 MHz, PD 6.0 cm. Abscessation. Numerous intramural abscesses (1) are present throughout the intestines and hinder the passage of the ingesta (2).

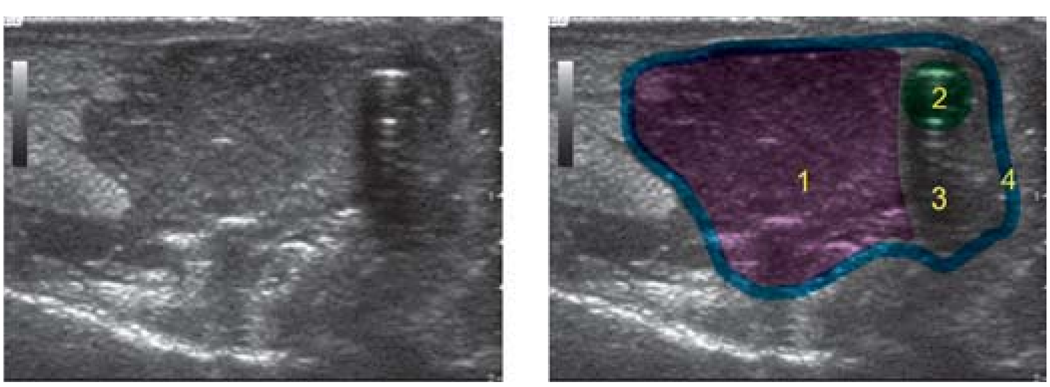

1: abscess
2: gastric tube
3: fluid
4: esophageal wall

Fig. 3-164: Ultrasonographic image of a corn snake (*Pantherophis guttatus*) in the region of the esophagus after the instillation of water through a gastric tube, ventral coupling site, oblique, 12 MHz, PD 2.0 cm. Abscess in the intestinal wall. The observed increase in intestinal thickness (1) could be correlated to the intestinal wall (4) after the administration of fluid. The gastric tube (2) is shown in cross-section by the reflections from its boundary layers.

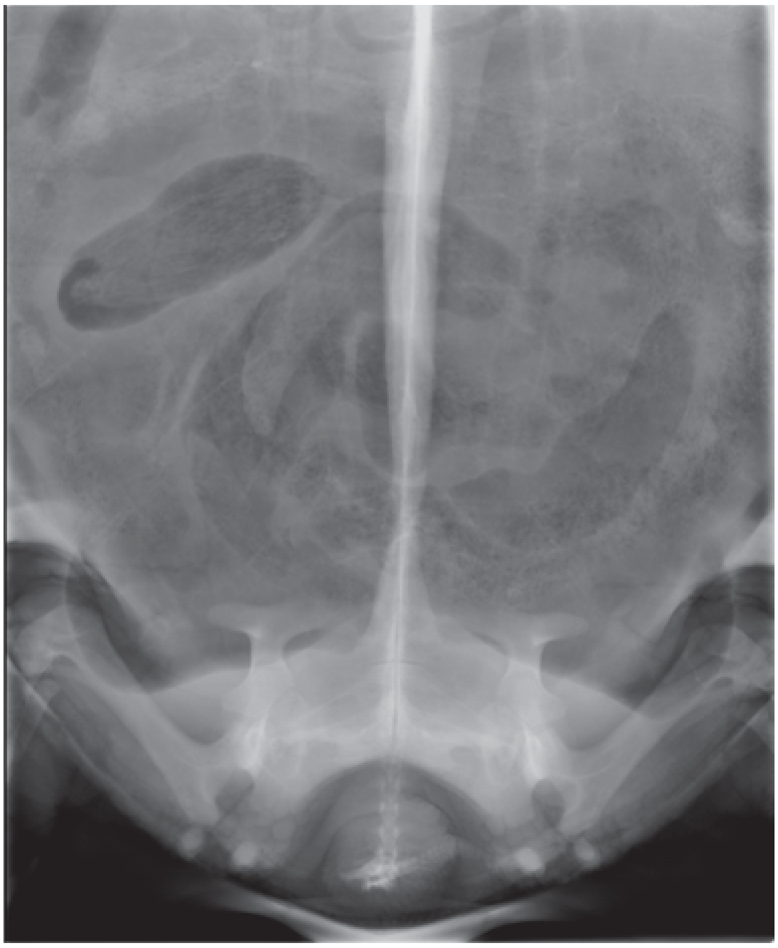

Fig. 3-165: Radiographic image of an African spurred tortoise's (*Geochelone sulcata*) caudal trunk, dorsoventral projection. Yeast infection. The bloating of the intestinal loops can be easily seen. The intestinal loops are also partly visible due to the ingesta present in the lumen which acts as a negative contrast material.

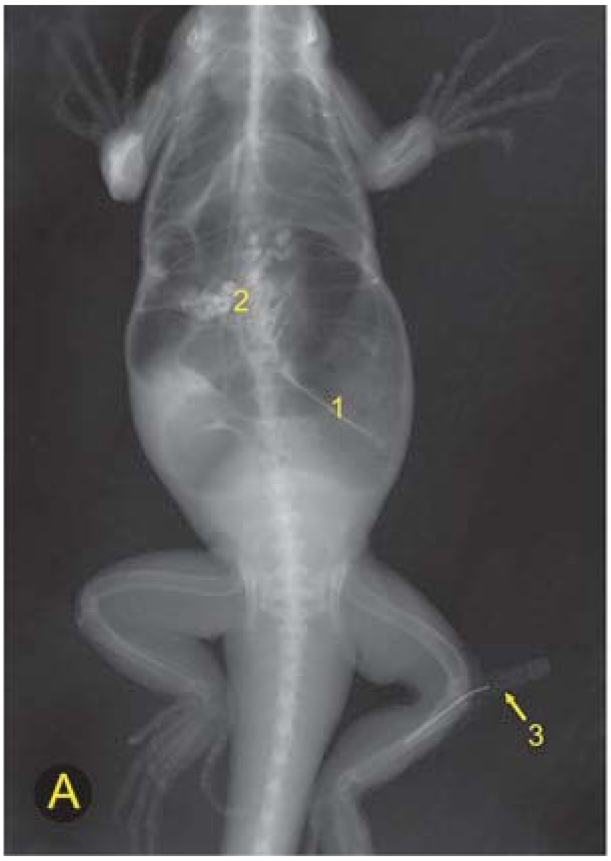

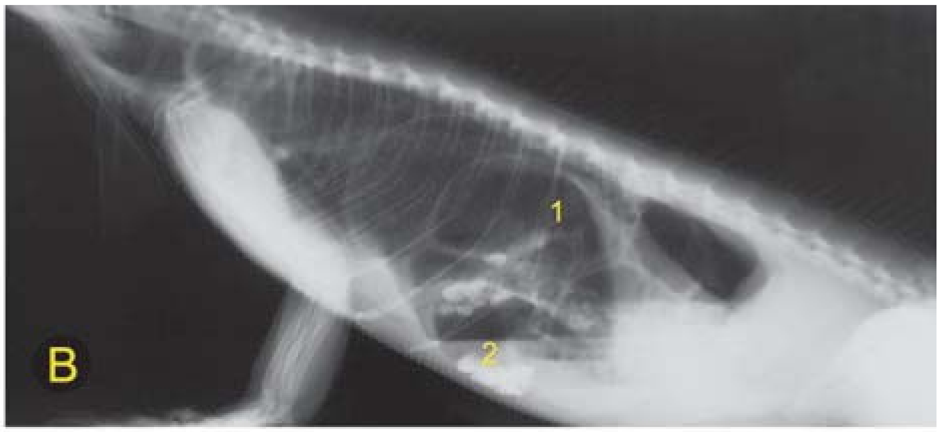

1: colon
2: stones in the stomach
3: intraosseous catheter in the tibia for fluid administration

Fig. 3-166: Radiographic images of a green iguana's (*Iguana iguana*), body, (A) dorsoventral and (B) lateral projections. Enteritis. Severe bloating of the colon (1) and stones in the stomach (2).

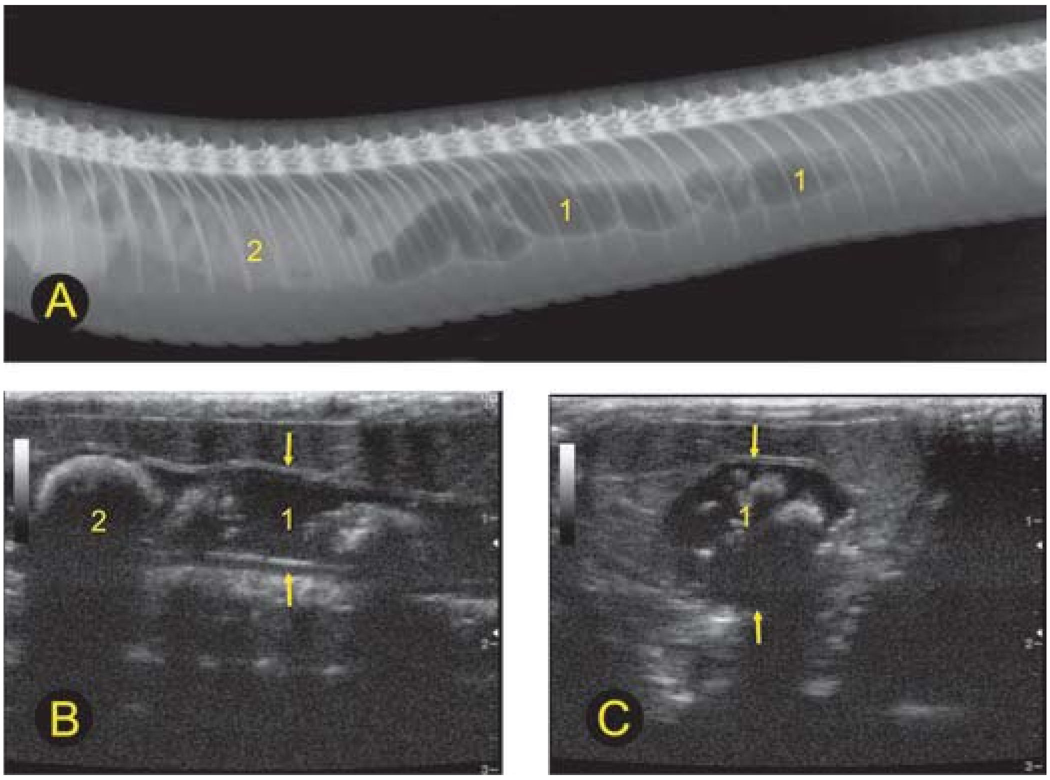

1: bloat within the intestinal tract
2: solid ingesta

arrows: intestinal boundary

Fig. 3-167:

A: Radiographic image of a green tree python's (*Morelia viridis*) caudal section of the body, lateral projection. Enteritis. The radiographic image shows both solid (2) and fluid matter associated with a bloat condition (1) within the intestinal tract.

B, C: Ultrasonographic image of the same animal, ventral coupling site, (B) longitudinal and (C) oblique planes, 12 MHz, PD 3.0 cm. Increased fluid content and (1) increased peristalsis were diagnosed as the result of a flagellate infection.

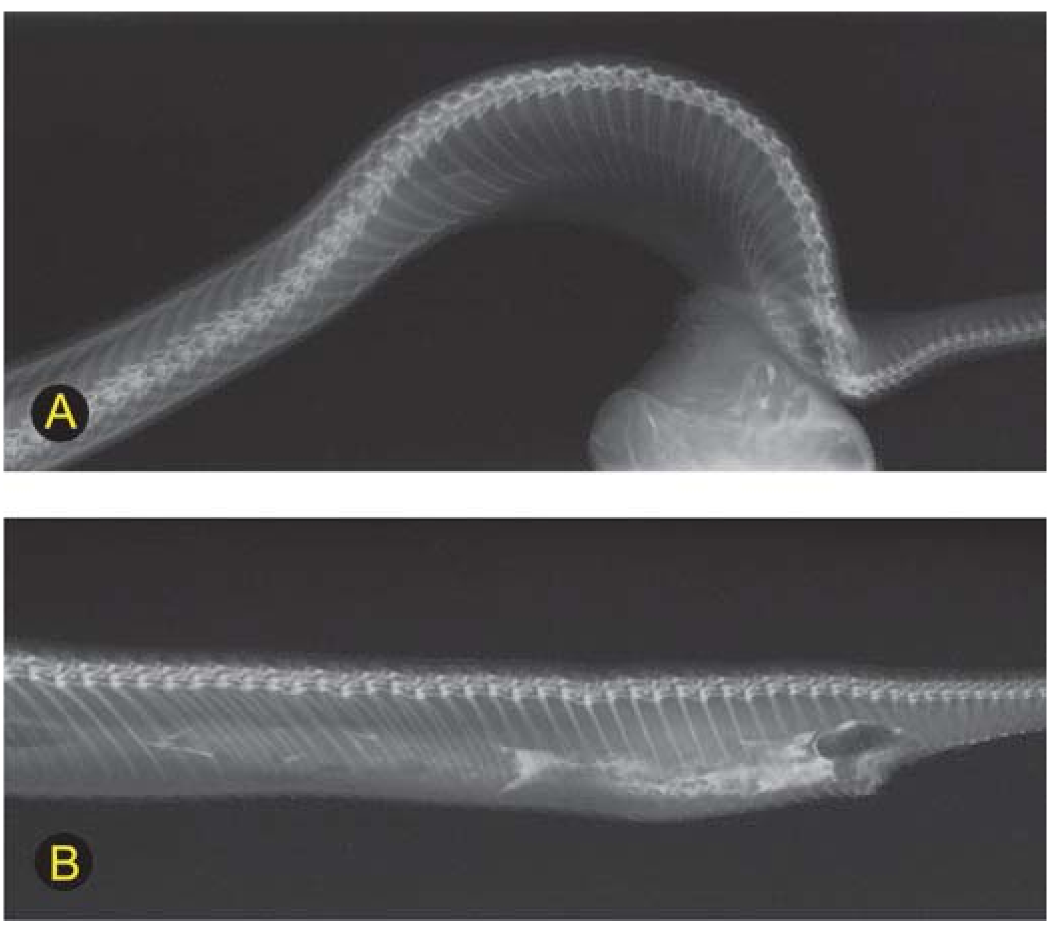

Fig. 3-168: Radiographic images of a green tree python (*Morelia viridis*), caudal section of the body, (A) oblique projection before repositioning and (B) lateral projection after repositioning and the administration of an iodine-based contrast medium (Iomeprol 300 mg/ml, 10 ml/kg bwt) in the cloaca. Enteritis, flagellate infection. (A) Prolapse of tissue out of the cloaca. (B) After the tissue was repositioned, the contrast medium was applied to assess the integrity and position of the intestinal tract in the snake.

3.8 Liver

Michael Pees, Veit Kostka

The liver is adversely affected by many systemic diseases. However, even with the high incidence of hepatic pathology associated with systemic disease, the corresponding clinical and diagnostic abnormalities are often overlooked. To diagnose liver disease, a combined work-up using imaging modalities and other diagnostic testing methods (e.g. blood biochemistry, biopsy, bile acid) is needed to properly evaluate hepatic function. In contrast to the other classes of animals, radiography plays a subordinate role when trying to assess liver disease in reptile species because it is difficult to differentiate the liver from the fat body and neighboring organs. Moreover, the anatomy of the liver of many reptile patients is different between species, making it hard to evaluate on radiographic images. Space-occupying lesions within the body cavity are difficult to associate with hepatic origins using standard radiography (**Fig. 3-169**); ultrasonographic imaging is far more sensitive for such cases.

One of the most common ultrasonographic findings is **hepatic lipidosis**. There are areas of increased echogenicity disseminated throughout the liver tissue and it is not uncommon that individual blood vessels are enlarged. In extreme cases, the edge of the liver is rounded, so confirming the increased organ size (**Fig. 3-170**). The echogenicity of the fat bodies can be used for assessing the echogenicity of lizard hepatic tissue. The liver and fat body can be imaged together especially when the transducer is place transversely to the body's longitudinal axis. It is often not possible to differentiate the liver and fat body from each other when the patient is suffering from hepatic lipidosis (**Fig. 3-171**). Due to the enlargement of both organs in obese animals, the liver and fat body are often in close proximity to each other. Hepatic lipidosis also plays an important role in chelonians. Although it is not possible to compare the liver with a fat body, increased echogenicity of hepatic tissue can still be identified in chelonian patients with hepatic lipidosis. In addition to ultrasonography, MRI can also be used to image fat deposits in the liver tissue (**Fig. 3-172**).

Occasionally **space occupying masses** are identified in liver tissue. These tissue masses include neoplasms (**Fig. 3-173B**), granulomas (**Fig. 3-174**), and abscesses (**Fig. 3-175**) and are definitively diagnosed by submitting a biopsy sample of the affected area. Color-Doppler imaging aids in the ultrasonographic assessment of the mass and also in performing an ultrasonographic-guided biopsy (see Chap. 3.2.4).

The **nonhomogenicity** of liver tissue can be best assessed using ultrasonography (**Fig. 3-173A**). The inconsistent echoic imaging of hepatic tissue is often the result of an inflammatory process and/or focal necrosis. Necrotic areas will appear as hypoechoic regions. The differentiation of hepatic tissue from blood vessels is accomplished using color Doppler (**Fig. 3-176**).

In snakes, liver disease will cause **pathological changes to the walls of blood vessel walls** or in the tissue surrounding blood vessels. Hyperechoic areas within a snake's hepatic tissue may be a consequence of fibrotic and inflammatory processes (**Figs. 3-177** and **3-178**). However, such changes can also be identified in older animals or as the consequence of chronic disease processes.

With chelonian species, **septicemia** may result in a significantly enlarged liver. The enlarged liver can be imaged ultrasonographically, but due to limited coupling sites a complete assessment of the liver can never be achieved. Dilated hepatic blood vessels are mainly associated with septicemic disease (**Fig. 3-179**) and can be assessed using CT (**Fig. 3-180**) and MRI.

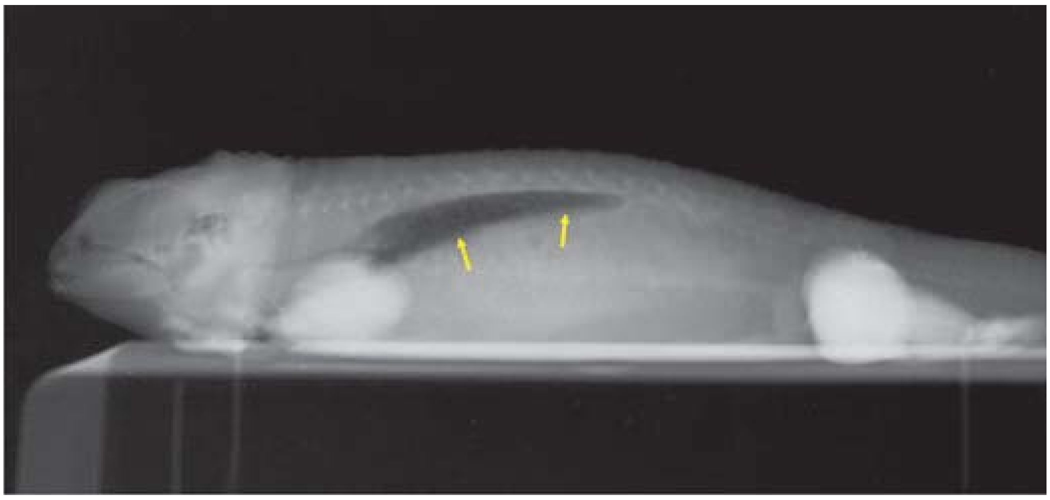

Fig. 3-169: Radiographic image of a central bearded dragon's (*Pogona vitticeps*) body, lateral projection. Swollen liver. In the majority of reptiles, the liver is barely differentiable from the surrounding tissues. The hepatomegaly (arrows) in this case is indicated by a reduction in the size of the lung field. In cases where there is any doubt, a contrast investigation is advisable.

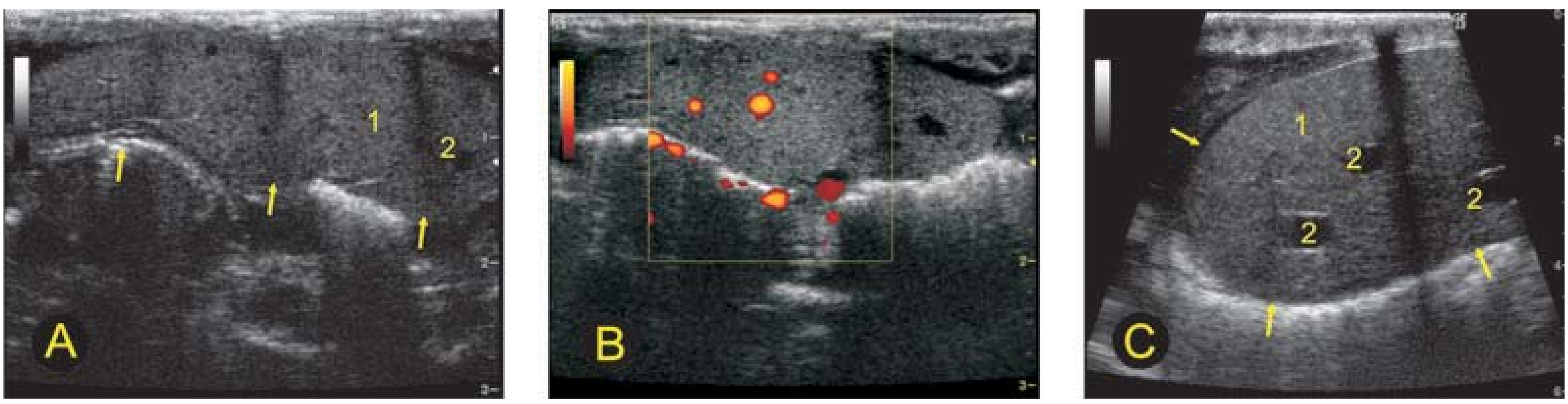

Fig. 3-170:

A, B: Ultrasonographic image of a central bearded dragon (*Pogona vitticeps*), ventral coupling site, longitudinal, 12 MHz, PD 3 cm, (B) power Doppler: Fatty liver. The liver is obviously hypoechoic. The blood vessels (2) are well defined and the edge of the liver is rounded (arrows).

C: Ultrasonographic image of a Savannah monitor (*Varanus exanthematicus*), ventral coupling site, longitudinal, 7 MHz, PD 6 cm. Fatty liver. The edge of the liver (arrows) is well defined and rounded. The echogenicity of the tissue is increased and the blood vessels (2) are enlarged.

1: hepatic tissue
2: blood vessels

arrows: boundaries
box in B: Doppler field

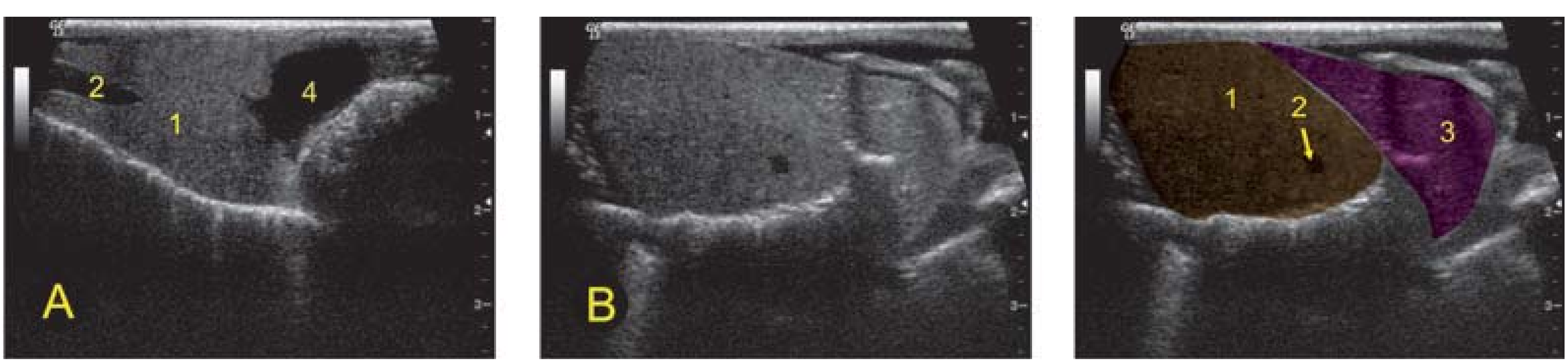

Fig. 3-171: Ultrasonographic images of a central bearded dragon (*Pogona vitticeps*), ventral coupling site, (A) longitudinal and (B) oblique planes, 12 MHz, PD 4 cm. Fatty liver. The hepatic tissue (1) is hyperechoic and the blood vessels (2) are enlarged. In the oblique coupling site, the hepatic tissue (1) and fat body (3, in the typical L-shaped cross-section found in lizards) are lying next to each other. The tissue of these structures is barely dicernable as their echogenicity is very similar.

1: hepatic tissue
2: blood vessels
3: fat body
4: gallbaldder

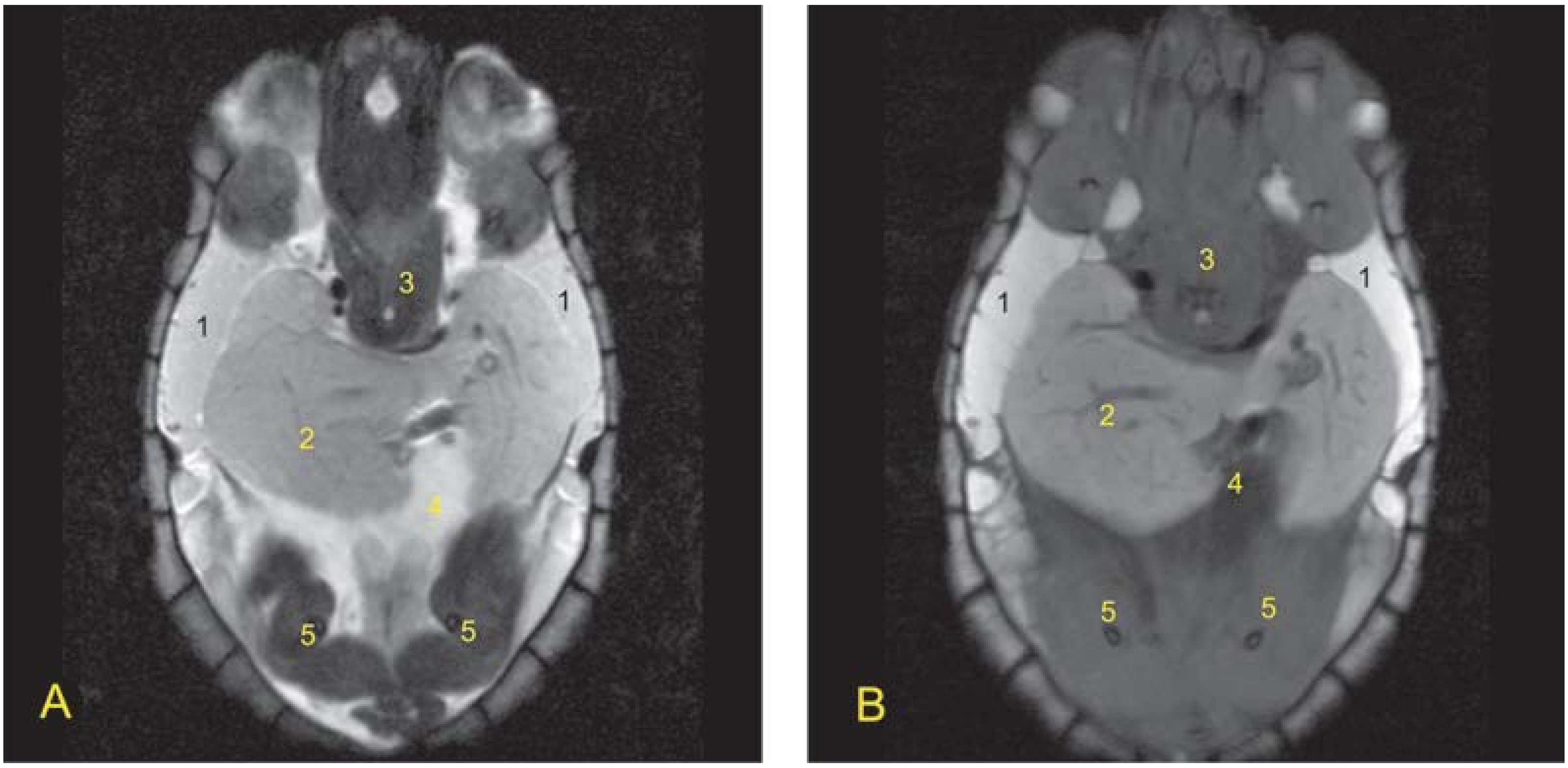

Fig. 3-172: MRI examination of a keeled box turtle (*Pyxidea mouhotii*), body, dorsal plane, (A) T1-weighted and (B) T2-weighted. Obesity and fatty liver degeneration. The liver (2) has a relatively high signal intensity in the T1-weighted image because of its fat content. In general, there is a lot of fat deposited in the body cavity (1) and around the gastrointestinal tract (4).

1: body cavity
2: liver
3: cervical vertebrae
4: gastrointestinal tract
5: hindlegs

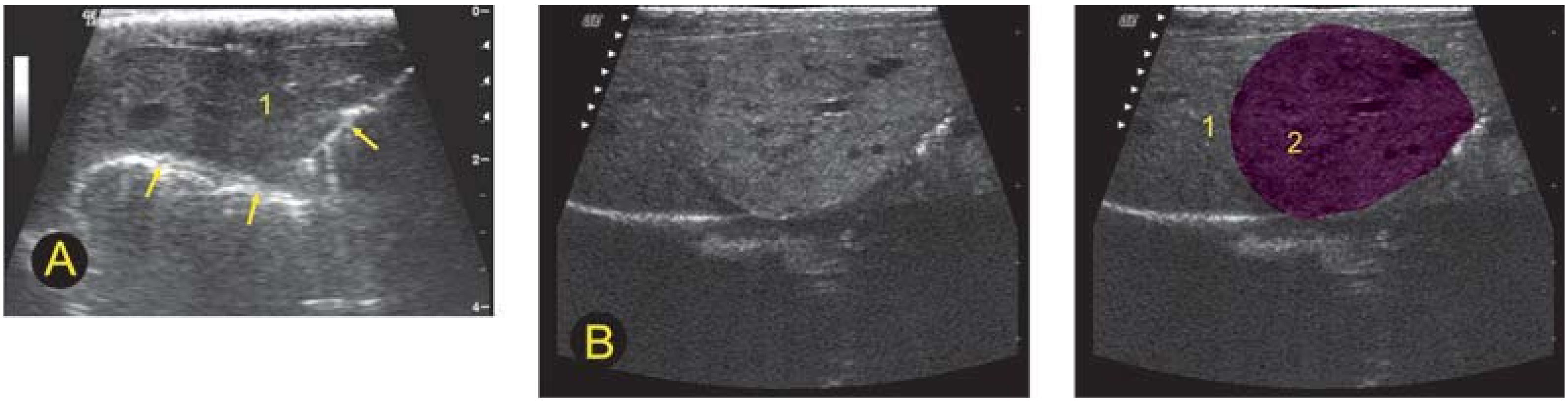

Fig. 3-173:

A: Ultrasonographic image of a green iguana (*Iguana iguana*), ventral coupling site, longitudinal, 7 MHz, PD 5 cm. Liver necrosis. The hepatic tissues show a high degree of nonhomogenicity (1, arrows).

B: Ultrasonographic image of a Savannah monitor (*Varanus exanthematicus*), ventral coupling site, longitudinal, 12 MHz, PD 5 cm. Adenocarcinoma in the liver. A tumor (2) can be seen lying in hepatic tissue (1). The diagnosis of adenocarcinoma was achieved through biopsy collection and the resulting histopathology.

1: hepatic tissue
2: tumor

arrows: nonhomogenicity of hepatic tissue

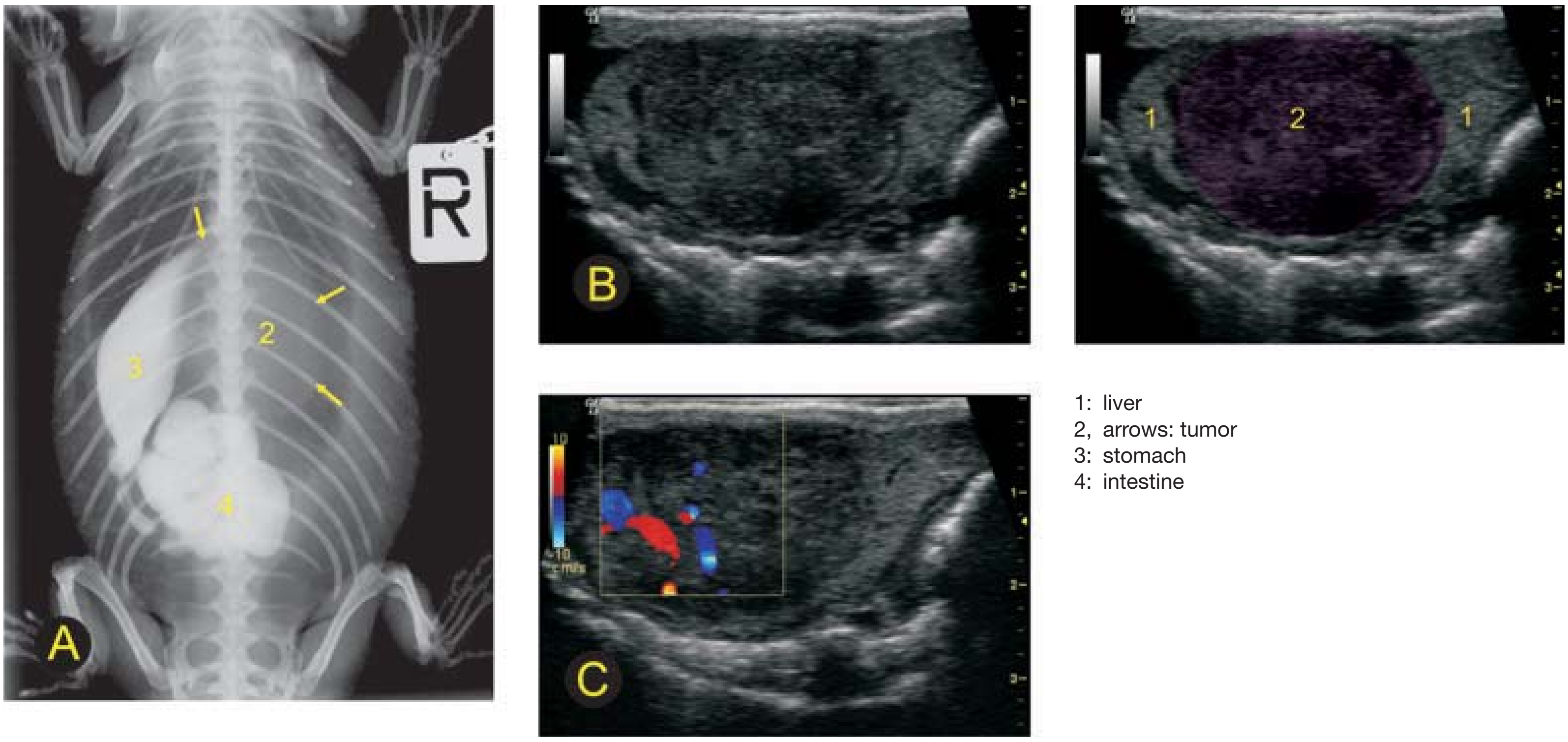

1: liver
2, arrows: tumor
3: stomach
4: intestine

Fig. 3-174:

A: Radiographic image of a central bearded dragon's (*Pogona vitticeps*) body, 2 hours after the oral administration of an iodine-based contrast medium (Solutrast®), dorsoventral projection. Hepatic tumor in the liver, mycobacteriosis. The tumor (arrows) is offset from the stomach by the contrast medium, however, no other conclusions can be reached.

B, C: Ultrasonographic image of the same animal, ventral coupling site, longitudinal, 12 MHz, PD 4 cm, color Doppler (C). The tumor (2) obviously lies within the liver (1). The color-Doppler image shows in part the perfusion of the tumor. A tissue biopsy sample revealed an active granulomatous process in the presence of mycobacteria.

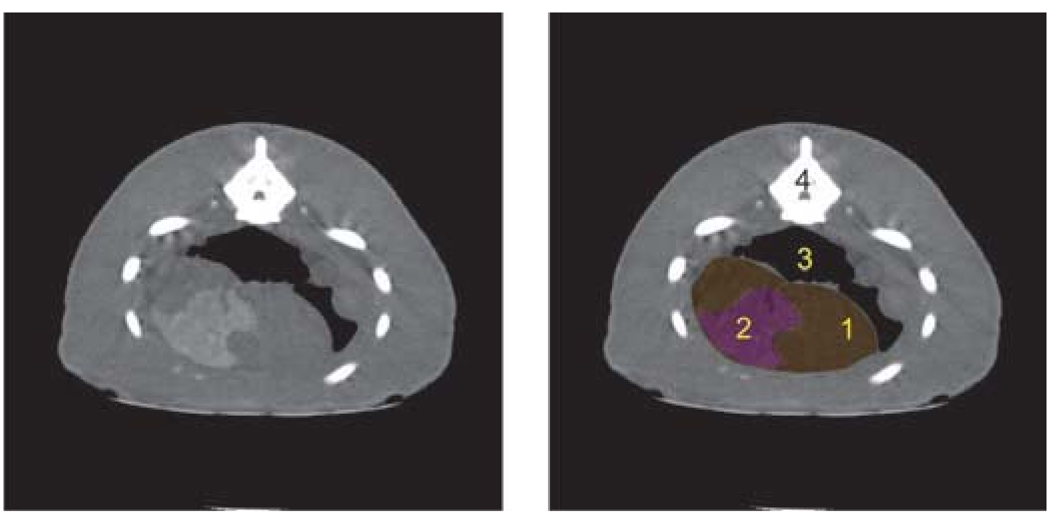

1: liver
2: abscess
3: air sac
4: spine

Fig. 3-175: CT image of a reticulated python's (*Python reticulatus*) body, transverse plane (120 kV, 204 mA, 2.0 mm SD, W: 258 L: 75). Abscess in the liver. The abscess (2) can be seen as a radiopaque entity in the hepatic tissue (1).

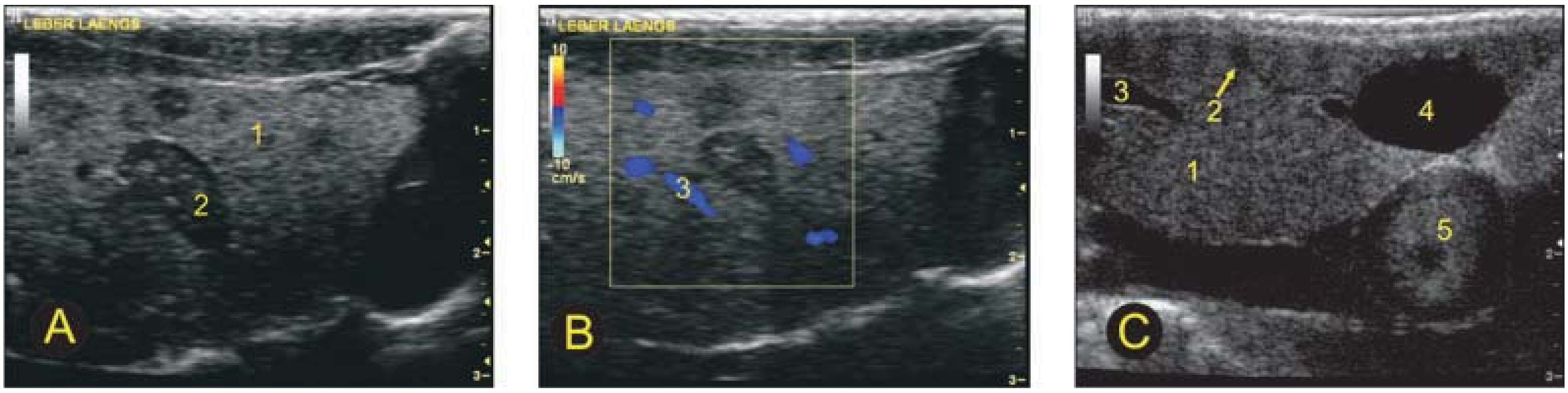

Fig. 3-176:

A: Ultrasonographic image of an emerald tree monitor (*Varanus prasinus*), ventral coupling site, oblique, 12 MHz, PD 3 cm, (B) color Doppler. Liver necrosis. The hypoechoic necrotic areas (2) in the hepatic tissue (1) can be easily differentiated from the blood vessels (3) using color Doppler.

C: Ultrasonographic images of a Central Bearded Dragon (*Pogona vitticeps*), ventral coupling site, longitudinal, 10 MHz, PD 3 cm. Focal liver necrosis (2), etiology unclear.

1: hepatic tissue
2: liver necrosis
3: vessel
4: gallbaldder
5: follicle

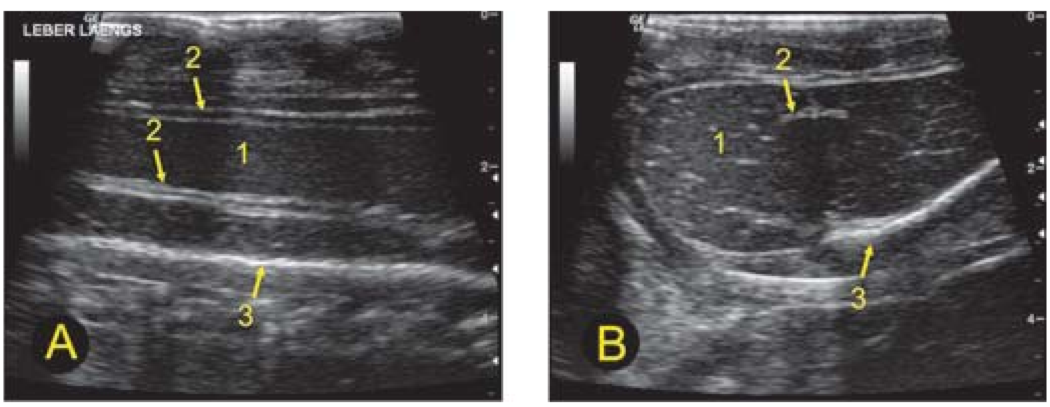

Fig. 3-177: Ultrasonographic image of a reticulated python (*Python reticulatus*), ventral coupling site, (A) longitudinal and (B) oblique, 7 MHz, PD 5 cm. Bacterial hepatitis. The hepatic tissue (1) is very nonhomogeneous. The blood vessels have a clearly hyperechoic zone in their walls (2).

1: hepatic tissue
2: blood vessels
3: dorsal liver capsule

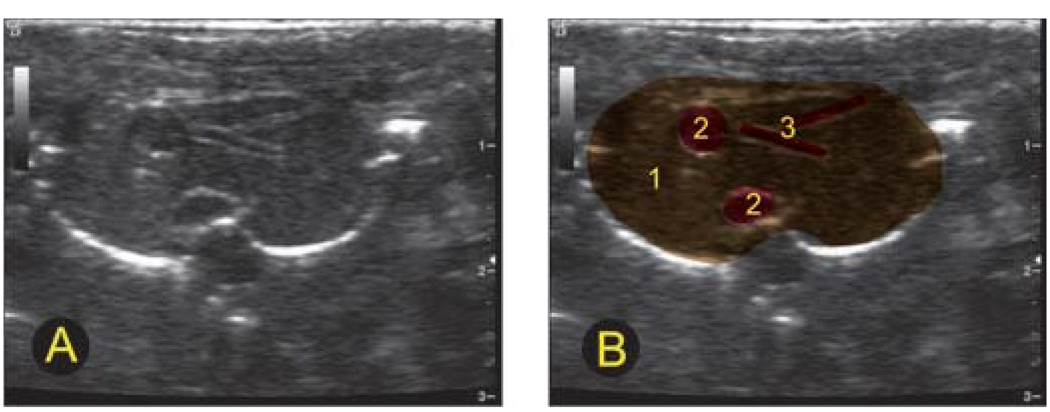

Fig. 3-178: Ultrasonographic image of an Indian python (*Python molurus*), ventral coupling site, oblique, 7 MHz, PD 3 cm. Inclusion body disease, hepatitis. The blood vessels here are also easy to recognize because they are hyperechoic.

1: hepatic tissue
2: main blood vessels
3: smaller blood vessels

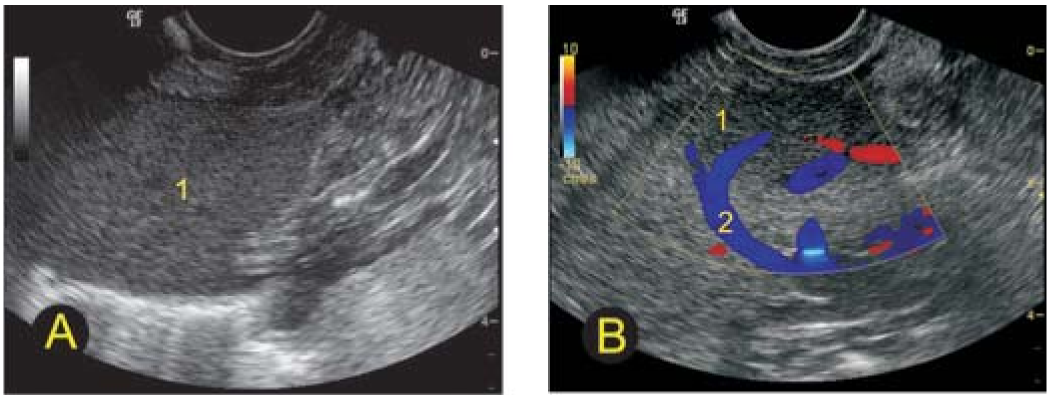

1: hepatic tissue
2: hepatic blood vessels

Fig. 3-179:

A: Ultrasonographic image of a yellow-bellied slider (*Trachemys scripta scripta*), prefemoral coupling site, 10 MHz, PD 5 cm, (B) Color Doppler. Septicemia and hepatitis. The liver (1) is significantly enlarged and can barely be delineated from the rest of the body. The hepatic blood vessels (2) are distended and clearly visible.

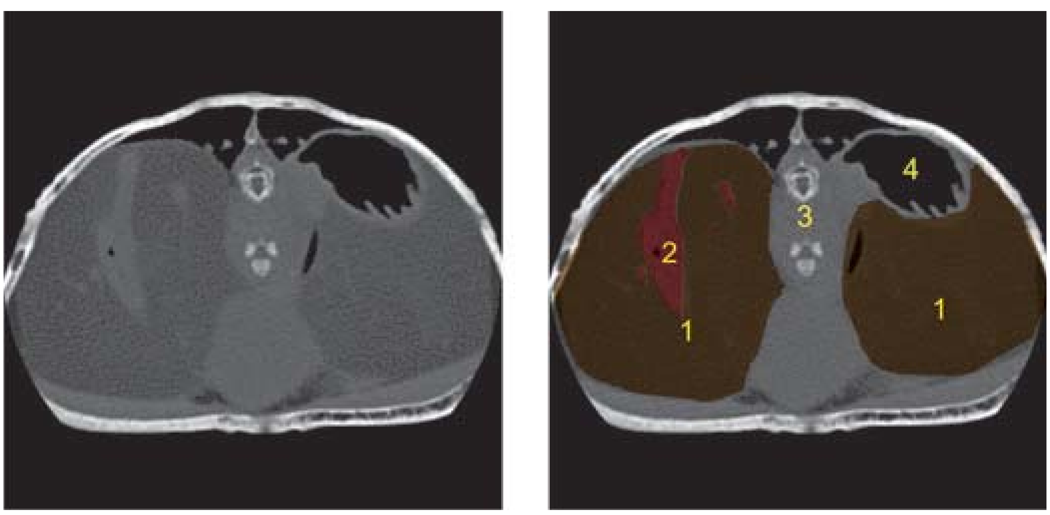

1: liver
2: intrahepatic blood vessels
3: cervical vertebrae
4: stomach

Fig. 3-180: CT image of a Russian tortoise's (*Testudo horsfieldii*) body, transverse plane (120 kV, 120 mA, 1.0 mm SD, W: 1174, L: 329). Septicemia and hepatitis. The liver (1) is severely enlarged. The intrahepatic blood vessels (2) are distended.

3.9 Urinary tract

Michael Pees, Maria-Elisabeth Krautwald-Junghanns

Mistakes regarding husbandry and nutrition, and infectious disease are important underlying factors relating to the development of renal and allantoic disease. Radiography often plays a subordinate role in the diagnosis of urinary tract disease with the exception of radiopaque uroliths. Ultrasonography provides the best diagnostic information when evaluating renal tissue, although with certain case presentations CT and especially MRI will significantly contribute to the disease assessment.

The allantois does not develop in snakes, crocodiles, and some lizards. However, urinary calculi and uroliths (bladder stones) can form within the urinary tract and induce corresponding clinical signs associated with that disease process.

3.9.1 Kidneys

The majority of kidney diseases are associated with renomegaly, often allowing the veterinarian an opportunity to palpate these organs during the clinical examination. However, radiography rarely provides diagnostic images because the kidney is poorly differentiated from the surrounding organs. One exception is the chameleon, in which the kidneys, if enlarged, can be imaged in caudodorsal coelomic cavity due to the lateral flattening of the body (**Figs. 3-181** and **3-182**). This is particularly useful in chameleons that have a gastrointestinal tract that contains little to no ingesta (**Fig. 3-182**).

In general, ultrasonography has a special significance in the assessment of reptile renal tissue. The **enlarged kidneys** are well visualized in lizards and chelonians, whereas in snakes it is often more difficult to evaluate this organ due to its lobed and elongated anatomy. In most cases, both kidneys must be examined and assessed. This is of particular importance for chelonian species because with this group of animals, the approach must be changed from one prefemoral window to the other. Important indications on the sonogram are the size of the kidneys, their echogenicity and perfusion (**Figs. 3-183** and **3-184**). The larger the image of the kidney, the easier it is to differentiate and obtain measurements. The **echogenicity** of renal tissue in reptile cases with **urate deposits (gout)** is either diffusely (**Fig. 3-184**) or focally (**Fig. 3-183C**) increased. With concurrent measurements, the central renal blood flow can be imaged; however, the parenchyma of the kidneys will appear to be barely perfused (**Figs. 3-183B** and **3-184B**). As inflammatory changes within the kidney can have a similar appearance, a blood biochemistry investigation is needed to confirm the diagnosis of gout. For the radiographic imaging of **joint gout,** please see Chapter 3.11.3 and **Figure 3-222**.

The kidneys and their pathological changes can be imaged with MRI. The renal size and structure can be judged in the various planes of MRI imaging and often is very useful in supplementing the results of an ultrasonography investigation (**Fig. 3-185**).

3.9.2 Allantois

Diseases of the allantois are often associated with renal disease; therefore conspicuous changes frequently occur in both organs. A common disease is **paralysis of the allantois**, in which the allantois becomes so enlarged that the organ incorporates a significant part of the body cavity. In such cases, standard radiography is not reliable as the images only show a general diffuse shadowing within the body cavity. After the administration of a contrast agent within the gastrointestinal tract, the intestines can be observed »swimming« on top of the allantois (**Figs. 3-186**, **3-189** and **3-190**). The size and the contents of the allantois should be assessed during the ultrasonography examination. In addition to increases in size of the allantois, calculi are often ultrasonographically observed. During the ultrasonographic examination an enhanced evaluation of the allantois **calculi** occur when the patient's position is changed as the suspended particles are displaced by gravity (**Fig. 3-187**). Conversely, solid uroliths (see below) within the allantois are not easy to identify compared to those found in the urinary bladder. In a few case presentations, allantois inflammation may be observed as thickening of the organ's wall (**Fig. 3-188**). Enlargement of the allantois can also be imaged and assessed with CT (**Fig. 3-189**) and MRI (**Figs. 3-185** and **3-190**).

Allantoic stones (syn.: **bladder stones**) can be imaged radiographically if they are calcified and therefore radiopaque (**Fig. 3-191**). Green iguanas (*Iguana iguana*) are predisposed to developing such stones, though they are also found in other species. If the stones have a low degree of calcification, they can be difficult to identify in chelonians due to their radiodense shells (**Fig. 3-192**). With chelonian species and particularly for reptile cases in which the patient has stones with low concentrations of calcium, CT is a very useful diagnostic imaging modality. Computed tomography also shows the internal structure of the uroliths (**Fig. 3-193**) which is very important when determining treatment options (surgical removal vs. endoscopic fragmentation and flushing out, **Fig. 3-192**).

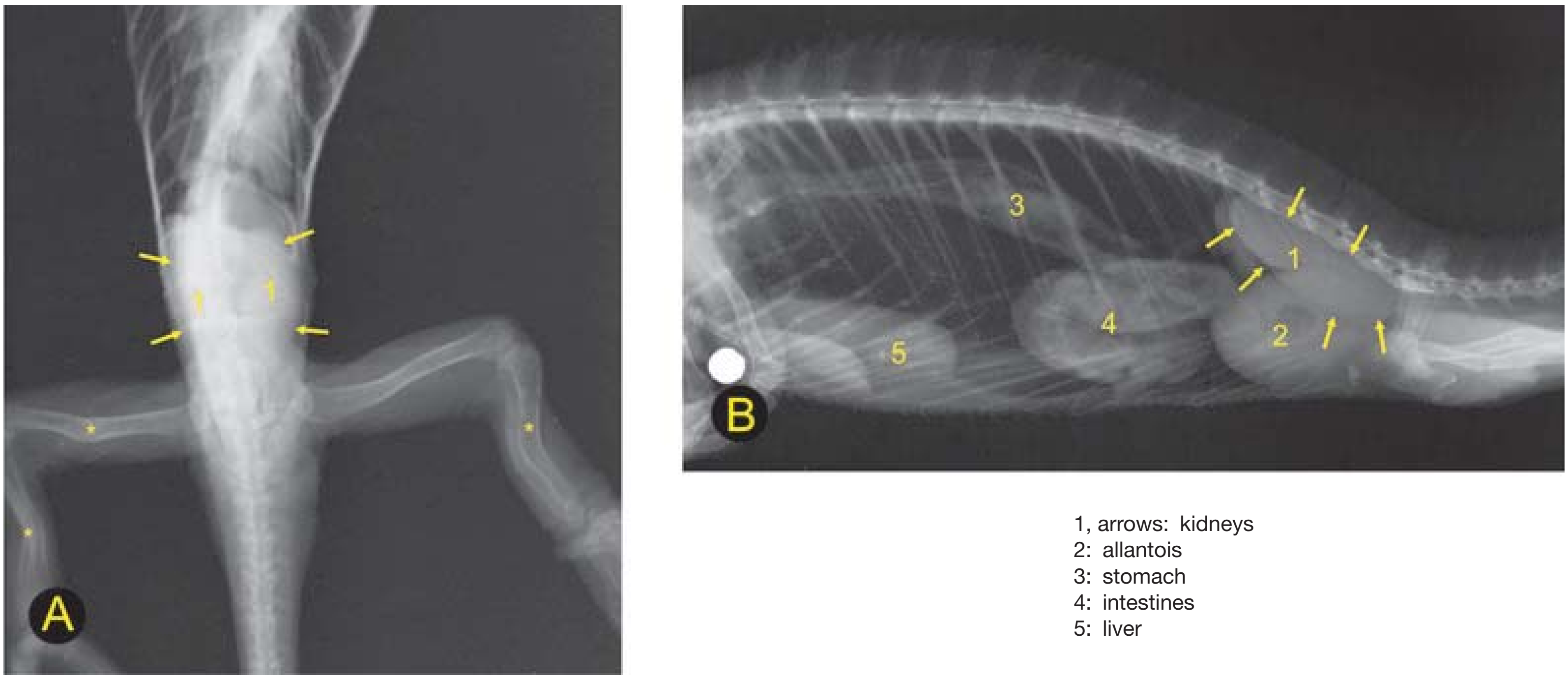

1, arrows: kidneys
2: allantois
3: stomach
4: intestines
5: liver

Fig. 3-181: Radiographic image of a veiled chameleon's (*Chamaeleo calyptratus*) body, (A) ventrodorsal and (B) lateral projections. Renomegly. The kidneys (1) can be easily identified in the caudodorsal body cavity.

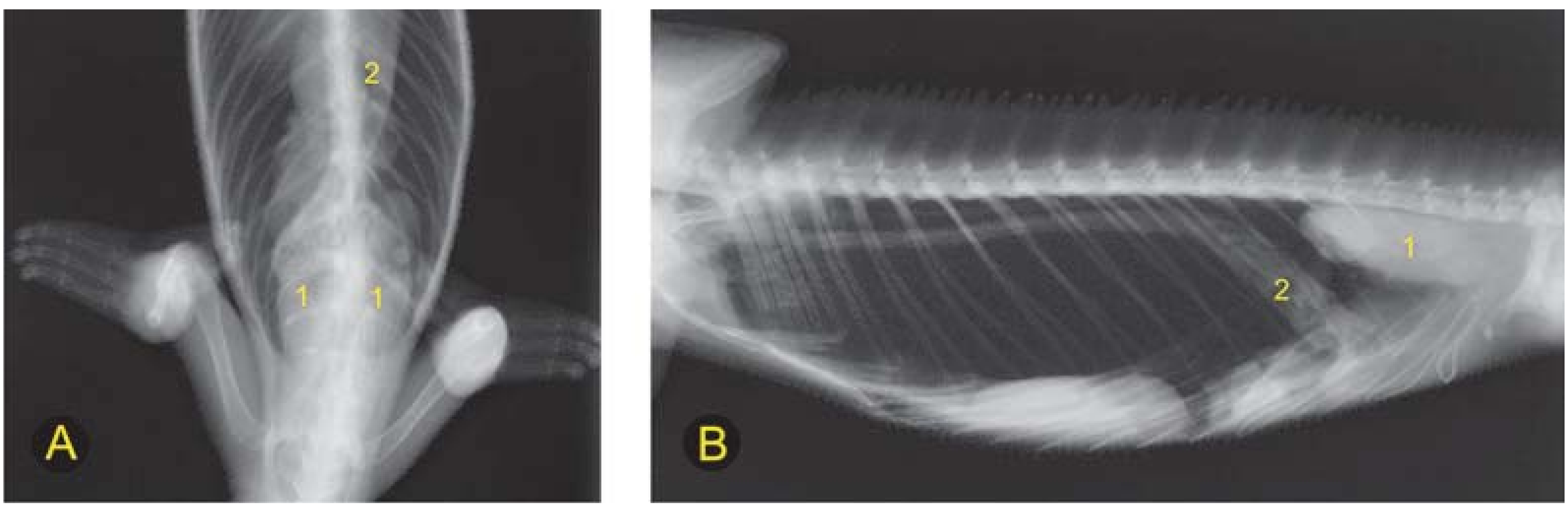

Fig. 3-182: Radiographic image of a Madagasgar giant chameleon's (*Furcifer oustaleti*) body, (A) ventrodorsal and (B) lateral projections. Gout. The kidneys (1) are severely swollen and were palpable in the clinical examination. The gastrointestinal tract (2) is mainly empty as a consequence of the animal's anorexic condition.

1: kidneys
2: gastrointestinal tract

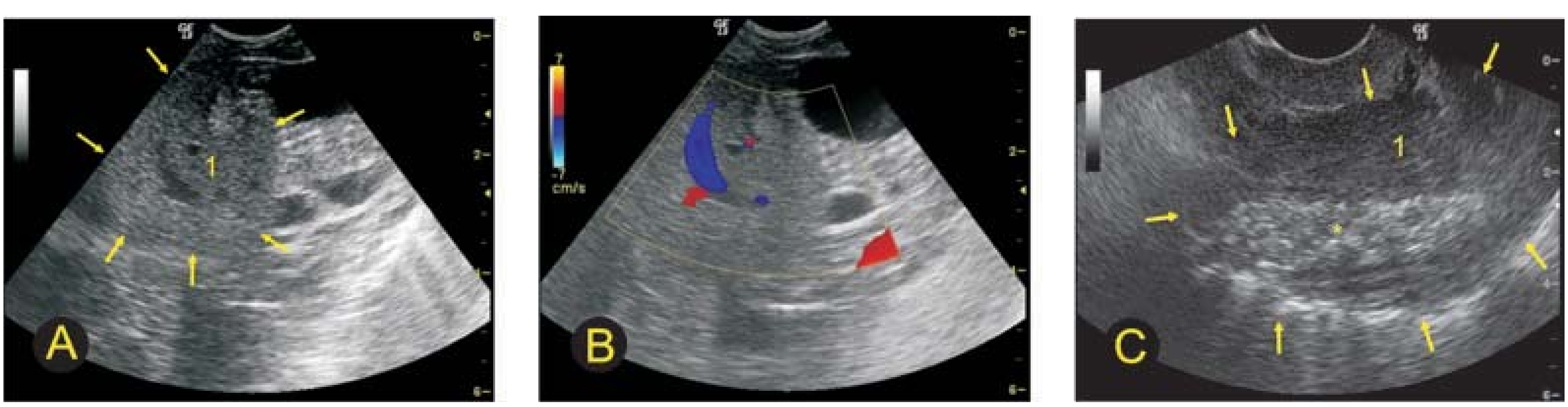

Fig. 3-183:

A, B: Ultrasonographic images of a yellow-bellied slider (*Trachemys scripta scripta*), prefemoral coupling site, longitudinal, 10 MHz, PD 6 cm, color Doppler (B). Renal failure. The kidneys (1) are severely swollen. Perfusion can only be shown in the central region.

C: Ultrasonographic image of a Hermann's tortoise (*Testudo hermanni*), prefemoral coupling site, longitudinal, 10 MHz, PD 6 cm. Gout. The central region (*) of the kidney (1) is clearly more echogenic due to the presence of urate deposits. The kidneys are significantly enlarged.

1: kidneys

arrows: circumference of the kidney
*: strongly echogenic central region of the kidney

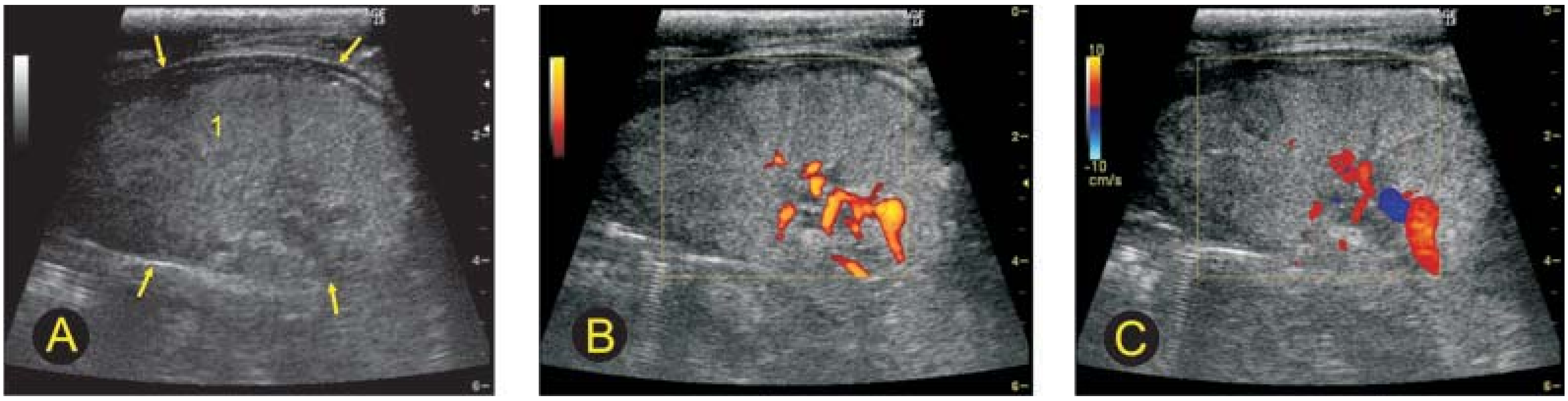

Fig. 3-184: Ultrasonographic images of an African spurred tortoise (*Geochelone sulcata*), (A) prefemoral coupling site, longitudinal, 12 MHz, PD 3 cm, (B) power Doppler, (C) color Doppler. Gout. The kidneys (1) are enlarged and difficult to demarcate from the surrounding tissues. The renal tissue is hyperechoic. Blood flow is only found in the center of the renal tissue, even with the highly sensitive power Doppler.

1, arrows: kidneys

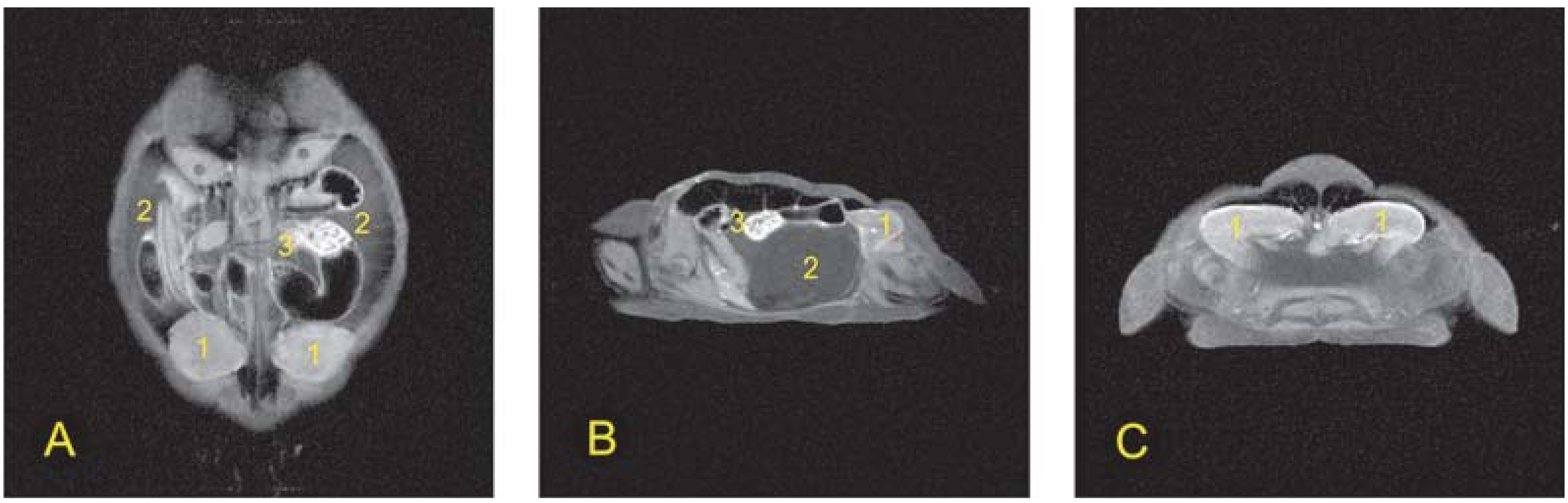

Fig. 3-185: MRI examination of a spur-thighed tortoise's (*Testudo graeca*) body, (A) dorsal, (B) sagittal and (C) transverse planes, T1-weighted. Renal failure and allantoic paralysis. The kidneys (1) have a high signal intensity and are obviously enlarged. The kidneys have been affected by toxic fatty degeneration. The allantois (2) fills a greater part of the body cavity.

1: kidneys
2: allantois
3: intestines

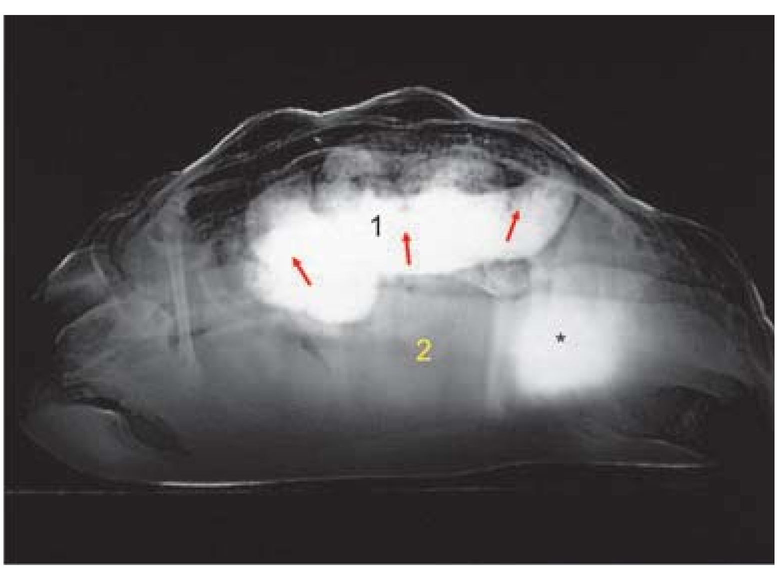

1: gastrointestinal tract
2: allantois

arrows: dorsally displaced gastrointestinal tract
*: allantois and hindleg are superimposed so there is a reduction in the strength of the beam in this area

Fig. 3-186: Total body radiographic image of a Hermann's tortoise (*Testudo hermanni*), lateral projection, 24 h after the oral administration of barium sulfate (350 mg/ml, 20 ml/kg bwt in the stomach). Allantoic paralysis. The gastrointestinal tract (1) has been displaced dorsally due to the excessively filled allantois (2).

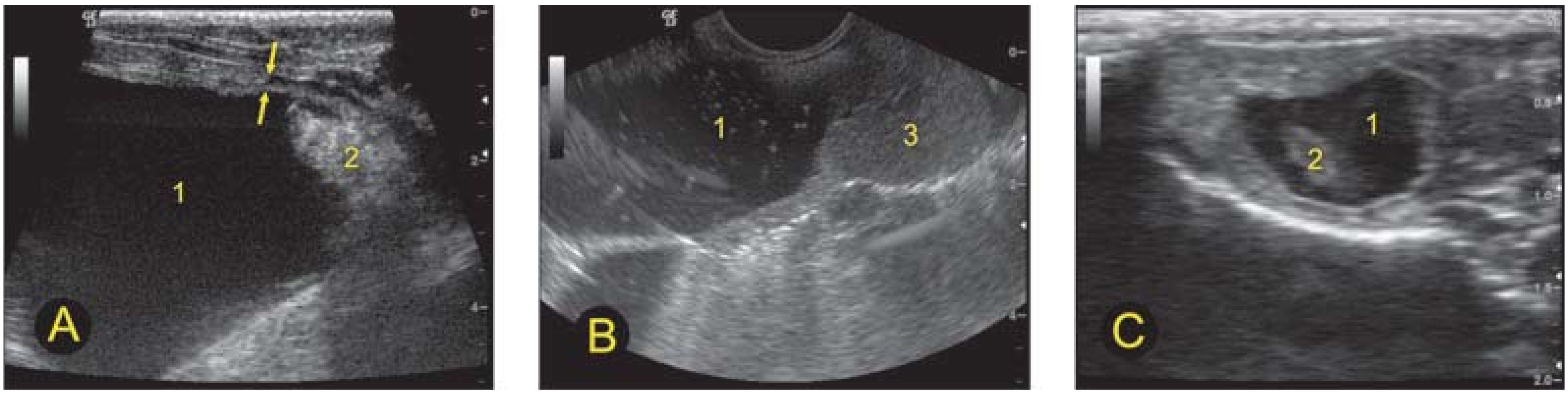

Fig. 3-187:

A: Ultrasonographic image of a green iguana (*Iguana iguana*), ventral coupling site, longitudinal, 7 MHz, PD 5 cm. Allantoic paralysis and calculus formation. The allantois (1) is greatly enlarged and has a thickened wall (arrows). The echogenic calculi (2) always sank to the lowest level when the patient was repositioned; therefore these structures could be assessed.

B: Ultrasonographic image of a marginated tortoise (*Testudo marginata*), prefemoral coupling site, longitudinal, 10 MHz, PD 5 cm. Allantoic paralysis and enlargement of the kidneys.

C: Ultrasonographic image of a frilled neck lizard (*Chlamydosaurus kingii*), ventral coupling site, longitudinal, 12 MHz, PD 2 cm. Allantoic paralysis (1) and calculus formation. The calculi (2) appear to be relatively solid and could be precursors of uroliths.

1: allantois
2: echogenic calculi
3: kidney

arrows: allantois, thickened wall

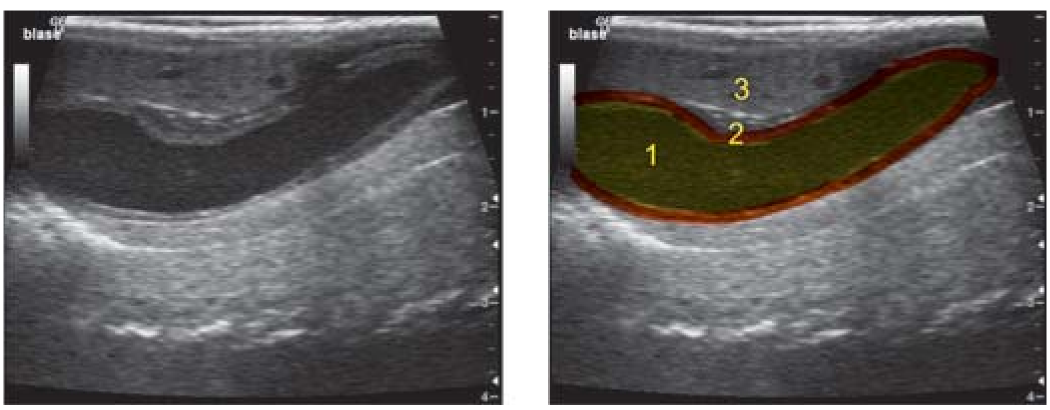

Fig. 3-188: Ultrasonographic image of a central bearded dragon (*Pogona vitticeps*), ventral coupling site, longitudinal, 12 MHz, PD 4 cm. Inflammation of the allantois. The wall (2) of the allantois (1) is clearly thickened.

1: allantois
2: allantois, wall
3: fat body

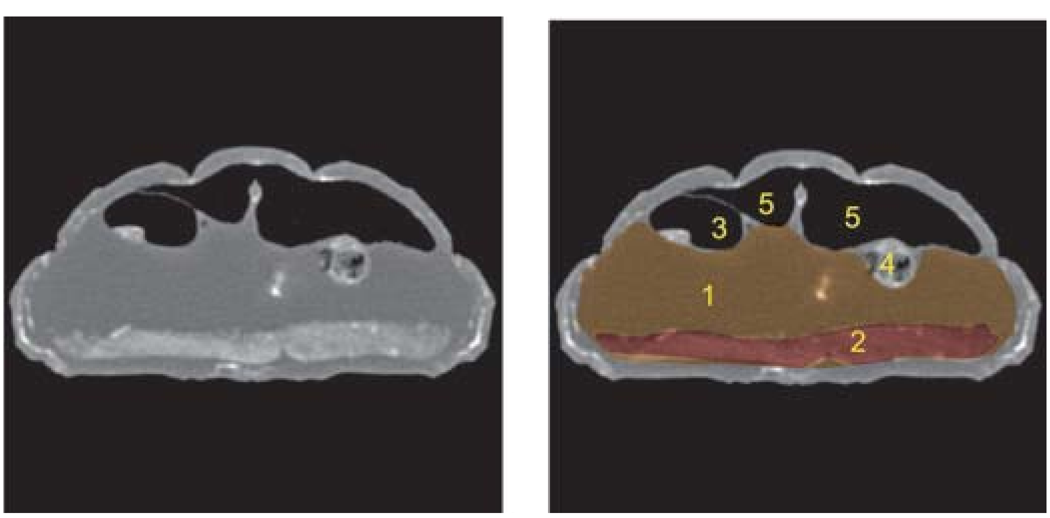

Fig. 3-189: CT image of a spur-thighed tortoise's (*Testudo graeca*) body, transverse plane (120 kV, 120 mA, 1.0 mm SD, W: 1117, L: 30). Allantoic paralysis. The allantois (1) fills the ventral body cavity and contains many calculi (2). The stomach (3) and the intestines (4) are »swimming« on top of the allantois. The shell of this animal is obviously poorly calcified (metabolic bone disease), a problem which is often associated with allantoic paralysis.

1: allantois
2: calculi
3: stomach
4: intestines
5: lung

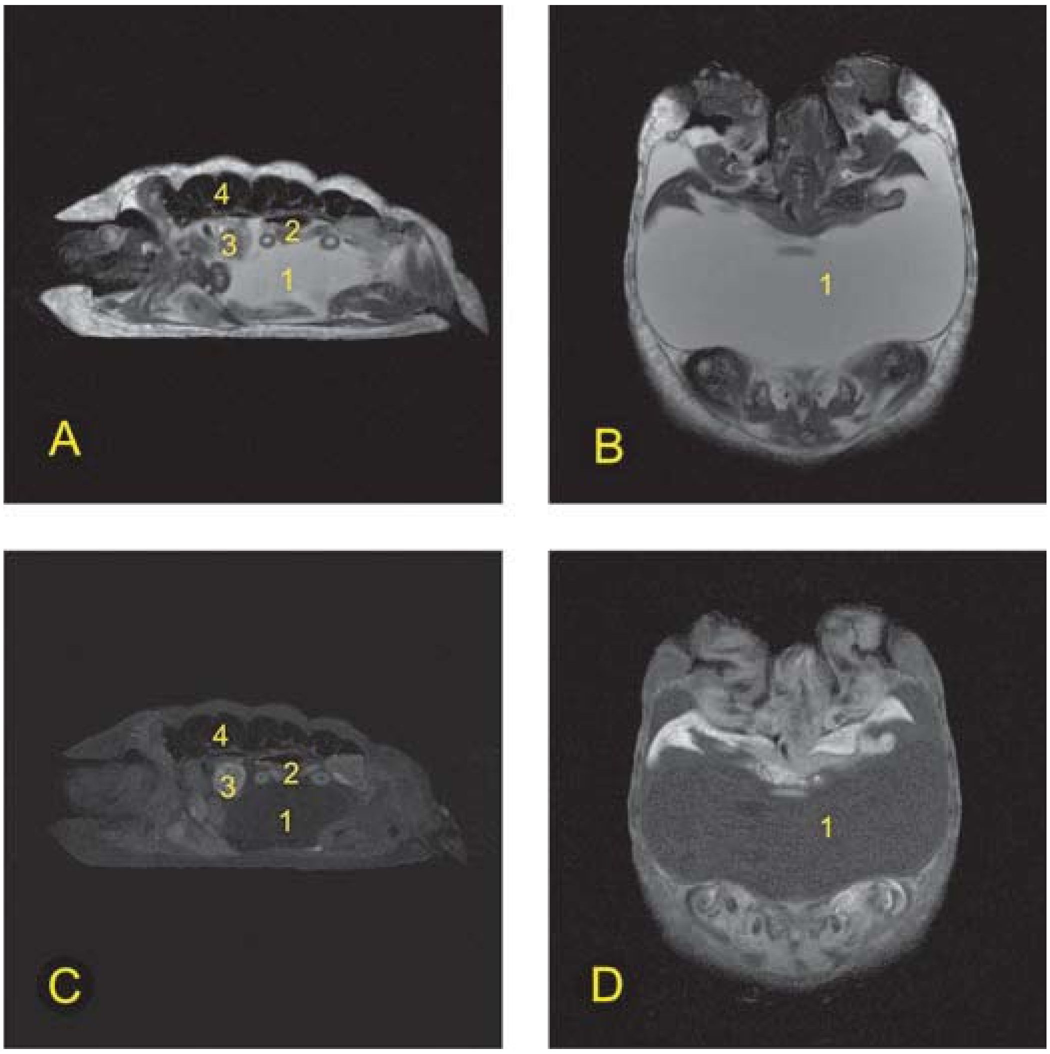

1: allantois
2: stomach
3: intestines
4: lung

Fig. 3-190: MRI examination of a spur-thighed tortoise's (*Testudo graeca*) body, (A, C) sagittal and (B, D) dorsal planes, (A, B) T2-weighted, (C, D) T1-weighted. Allantoic paralysis.

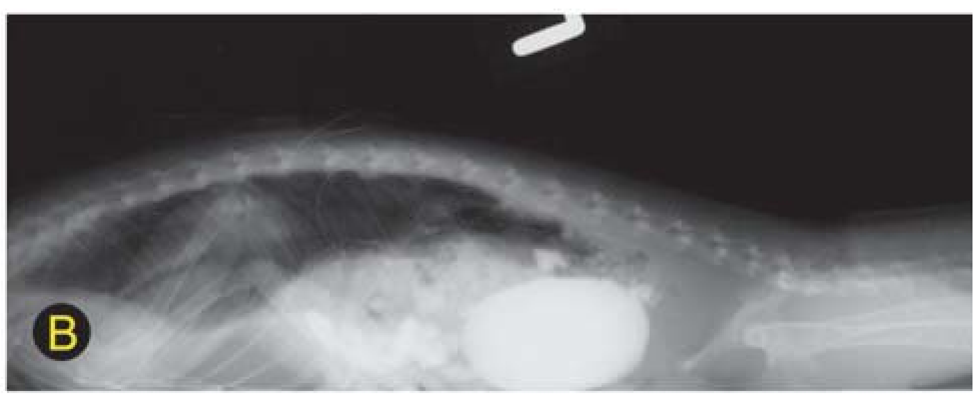

Fig. 3-191: Radiographic images of a green iguana's (*Iguana iguana*) body, dorsoventral and lateral projections. Bladder stone. Due to its position, the bladder stone has caused a displacement of the intestinal tract in the pelvis area. This can lead to problems with defecation.

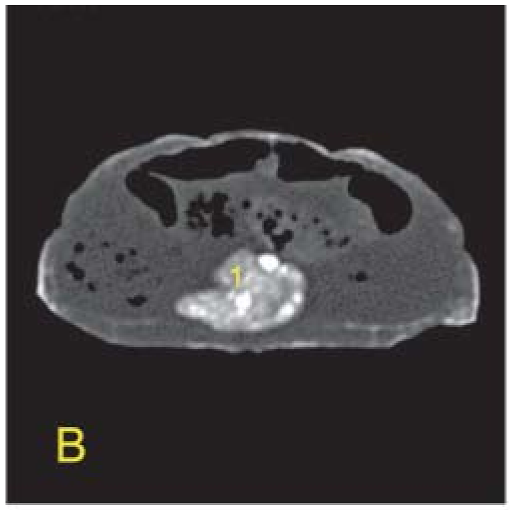

1: bladder stone

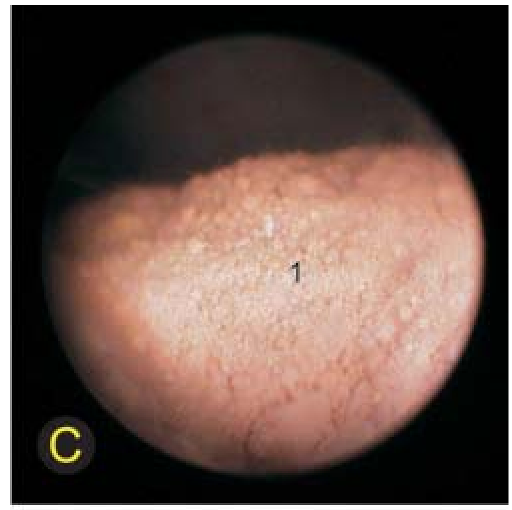

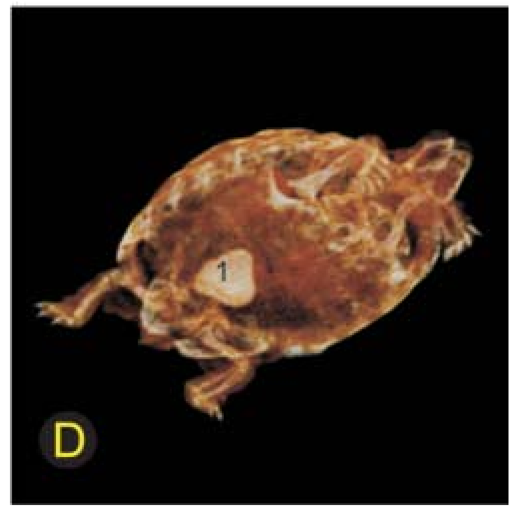

Fig. 3-192:

A: Total body radiographic image of a spur-thighed tortoise (*Testudo graeca*), dorsoventral projection. Bladder stone. Apart from an inadequate calcification of the animal's shell, no other abnormalities can be observed in the radiographic image.

B, D: CT images of the same animal's body, (B) transverse plane and (D) 3D reconstruction (120 kV, 1670 mA, 0.8 mm SD, W: 783, L: 263). The bladder stone appears to be very nonhomogeneous and brittle in this image.

C: Endoscopic view of the stone before it was removed by fragmentation and lavage.

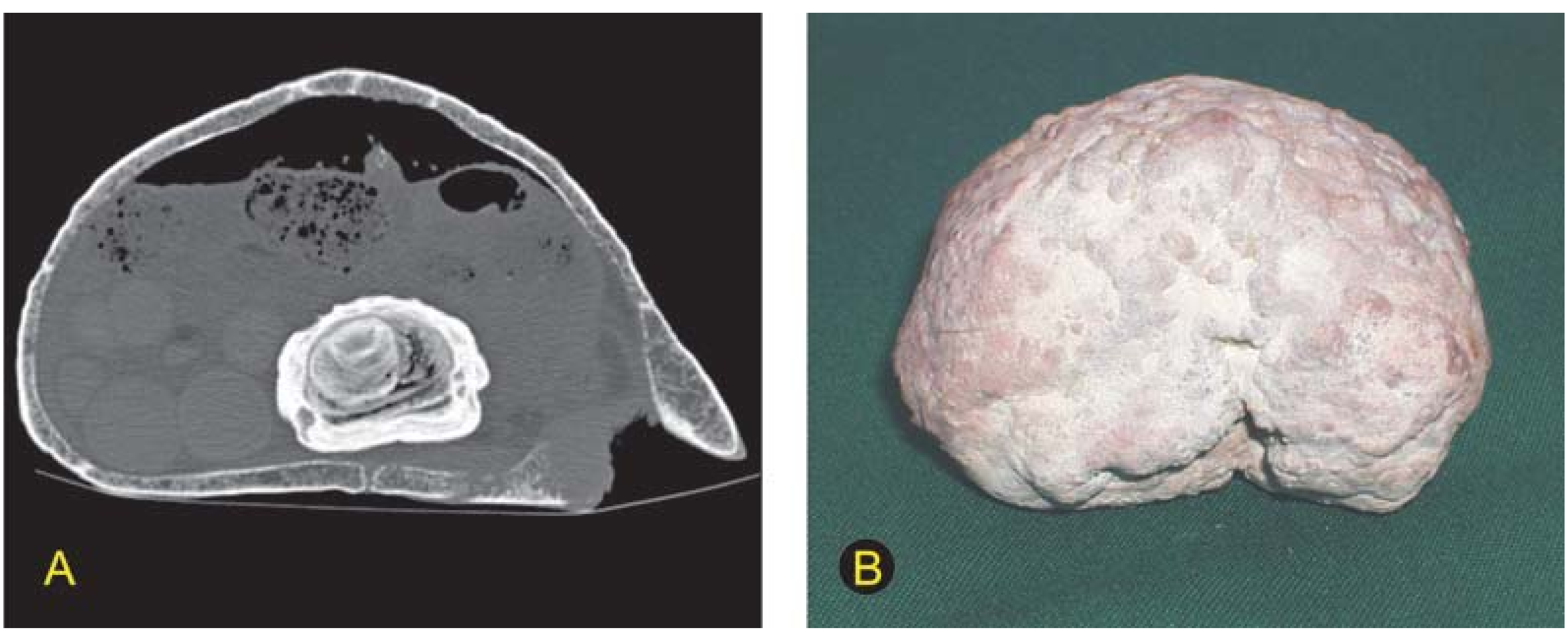

Fig. 3-193:

A: CT image of a Hermann's tortoise's (*Testudo hermanni*) body, transverse plane (120 kV, 120 mA, 1.0 mm SD, W: 1359, L: 294). Bladder stone. The internal structure of the bladder stone can be seen in the CT image. The cause of this disease condition was an egg that had been deposited in the bladder.

B: The bladder stone after surgical removal.

3.10 Genital tract

Ingmar Kiefer, Michael Pees

Improper husbandry is the primary cause of pathological changes to the female genital tract, thereby resulting in many reptiles being presented to hospitals. Due to the anatomical structure of the reptile urogenital tract, clinical examination is limited. Indications of disease include a tense abdomen or in lizards and snakes, a palpable space-occupying lesion within the body cavity. Eggs can be externally palpated in lizards and snakes, and possibly in some chelonian patients. However, specific disease information regarding urogenital abnormalities is difficult and further investigations are usually necessary to achieve a definitive diagnosis and particulary imaging modalities have a special importance for diagnosing pathological changes that affect the genital tract. While standard radiography techniques are especially effective when imaging eggs or assessing the egg shell, ultrasonography can provide additional information about egg contents and the position of the egg (e.g. allantois). In addition, ultrasonography is the method of choice for the differentiation of preovulatory and postovulatory changes of egg formation within the genital tract of reptiles.

Although the testicle can be imaged (especially in the active state), pathological changes in these reproductive structures are rarely diagnosed and described.

3.10.1 Ovary

With **preovulatory egg binding**, the follicle remains on the ovary and there is no formation of an egg nor does ovulation occur, causing the follicle to significantly increases in size. Sometimes these large preovulatory follicles can be differentiated on a radiograph as soft-tissue structures (**Fig. 3-194**). The differentiation from eggs undergoing development is difficult particularly in those species that have soft-shelled eggs (see Chap. 3.1.4.4). Basically, the follicles tend to be more rounded as opposed to the oval shape of eggs (**Fig. 3-195**). However, depending on the positioning of the animal, deformation of the follicles can also occur giving the oval appearance of an egg. If peritonitis is a complicating factor, then radiographic differentiation of the follicle is often no longer possible. As a consequence, ultrasonography is the method of choice for the diagnosis of preovulatory egg binding. On a sonogram, the follicles can be clearly differentiated from each other as roundish structures of medium echogenicity (**Figs. 3-194, 3-196** and **3-197**). The size of the individual follicles can be enormous with preovulatory egg diameters of 2.5–3 cm being diagnosed in the green iguanas (*Iguana iguana*) (**Fig. 3-197**). Fluid accumulation in the body cavity is frequently identified with preovulatory egg binding (**Figs. 3-196** and **3-197**), whereby the fluid's corpuscular contents indicates the presence of inflammatory changes and/or a compromised follicle. With chronic presentations of preovulatory egg binding, the follicles can become so irregular in composition that they vary greatly in echogenicity and size (**Figs. 3-196** and **3-197**). These preovulatory follicles have an altered structure and construction, which can identified using CT (**Fig. 3-196**). Such changes should be given an unfavorable prognosis as the abnormalities indicate a greatly advanced stage of disease.

Space-occupying lesions involving the testicle or neoplastic changes of ovarian tissue of reptiles are rare. By using contrast, the reproductive organs can be differentiated from the surrounding intestines. A definite identification with ultrasonography is difficult as both the testicles and ovarian tissue have a variable echogenicity and therefore differentiation from surrounding soft tissue structures is problematic.

3.10.2 Oviduct and eggs

While the inactive oviduct cannot be imaged with non-invasive diagnostic imaging modalities, changes in the active oviduct are often clearly visible and associated with massive space-occupying lesions. Since the wall of reptile oviducts is often extremely thin, it can only be observed, even in the active organ, ultrasonographically when inflammatory changes have resulted in thickening of the structure. For a discussion of imaging the normal stages of egg maturation in the oviduct see Chapter 3.2.5.4.

Egg binding is classified as the inability of the reptiles to move the egg, or in viviparous animals the living progeny, out of the oviduct. In contrast to the bird, this condition can be chronic, lasting for several months until clinical signs of disease become apparent. A radiographic investigation often provides the first indications of chronic egg binding, whereby egg assessment is of particular importance. Attention should be paid to the number of eggs and to their size. Lizard species often produce a large number of eggs. By producing a large number of eggs, an energy deficiency can occur in young and weak animals, which results in an inability to lay the eggs (**Fig. 3-198**). The position of the egg should also be assessed because constipation (e.g. sand) can adversely affect egg laying (**Figs. 3-199** and **3-200**).

The typical pathological changes associated with reptile eggs are listed in Table 3-5.

The calcification of the egg can be most reliably judged with standard radiography (**Fig. 3-201A**) and CT. Attention should also be paid to the presence of changes in the skeletal system and shell to see if there are any indications of a generalized calcium deficiency (Metabolic Bone Disease, see Chap. 3.5.2).

Although irregular mineralization may be detected, ultrasonography is not a recommended method to examine the egg shell of reptile species for abnormalities (**Fig. 3-201B**). Ultrasonography is better suited for assessing egg contents, which in some cases allows the veterinarian to determine if the egg(s) are living or dead. Nonviable eggs will view as having liquefied contents (**Fig. 3-204**) or an increasingly dense center solid that develops into the production of so-called »wax« eggs (**Figs. 3-205** to **3-207**). The assessment of reptile egg contents is easier when CT (**Figs. 3-206** and **3-207C, D**) and MRI imaging modalities are used.

Changes in the oviduct wall are usually associated with a chronic infectious process. On occasion, there is an accumulation of fluid within the oviduct lumen (**Fig. 3-208**), which causes the wall of this structure to appear significantly thickened. Reptile patients that develop severe chronic infectious salpingitis, calcium deposits may form within the wall of the oviduct and are viewed as radiodense structures in the CT image (**Figs. 3-207C, D**). Such thickening of the oviduvt wall can also bo imaged using ultrasonography (**Fig. 3-207B**).

Laying of eggs in the allantois is a abnormal condition that occurs in chelonians and rarely in lizards. The normal movement of the egg from the oviduct through and out of the cloaca does not occur. Instead, the egg follows an improper pathway and is pressed into the allantois, where it remains. The cause of the allantois positioning of the egg(s) includes a displacement of the cloaca (e.g. by another egg) or the administration of oxytocin to stimulate egg laying. The clinical signs occur only after the egg has been lying in the allantois for a long time. As a consequence, the egg shell will show radiographic signs of decomposition (**Fig. 3-209**) or completely disappear. Eggs in this condition can only be imaged using ultrasonography or MRI (**Fig. 3-210**). With most cases of egg binding, ultrasonography should be used to evaluate the position of the egg(s) within the oviduct or if their location is in the allantois (**Fig. 3-209**).

Table 3-5: Pathological findings frequently found in eggs when imaged radiographically.

Changes	Possible causes
irregular or generally insufficient calcification of the egg **(Fig. 3-201)**	always an indication of a disturbance in the calcium metabolism (metabolic bone disease) or an infection in the oviduct
egg too large / too many eggs (especially in chameleons)	more often in young animals provided a diet with an excessive energy content and premature sexual maturity; in turtles with metabolic bone disease due to which a stricture in the area of the cloaca has developed
variable egg size **(Fig. 3-202A)**	infections, egg remains too long in the oviduct, ovulation in the visceral cavity
asymmetrical eggs **(Fig. 3-208B)**	retained, necrotic eggs (N.B.: physiological egg form in some species, e.g. some geckos)
broken egg shells **(Figs. 3-202B** and **3-203)**	trauma, manipulation, inadequate calcification (see above.)
signs of dissolution of the egg shell **(Fig. 3-209A)**	infections, egg remains too long in the oviduct, ovulation in the visceral cavity, egg deposited in the allantois

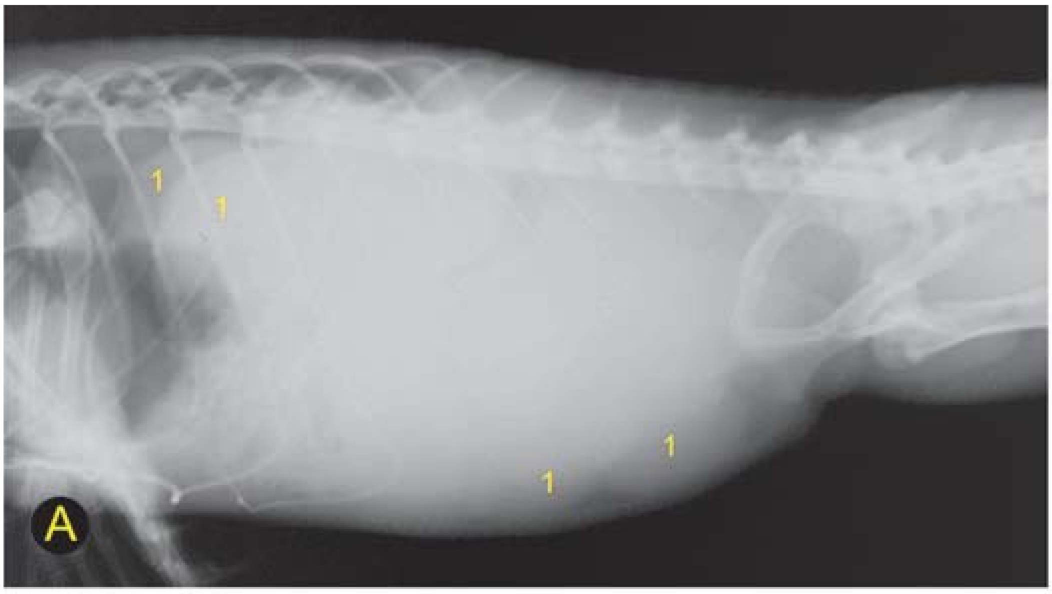

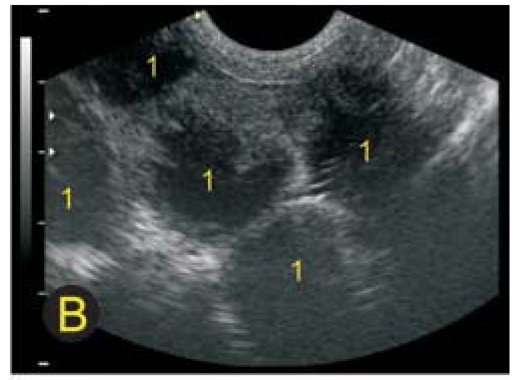

1: follicles
2: intestines

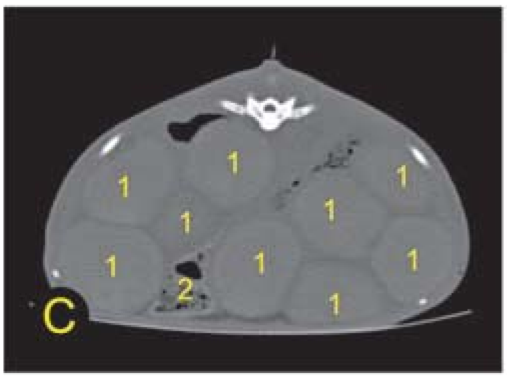

Fig. 3-194:

A: Radiographic image of a green iguana's (*Iguana iguana*) body, lateral projection. Preovulatory egg binding. The body cavity is almost completely filled with abnormal preovulatory follicles (1). These follicles are difficult to see and to differentiate from eggs.

B: Ultrasonographic image of the same animal, ventral coupling site, oblique, 7.5 MHz, PD 6 cm. Image showing numerous enlarged follicles (1, diameter ca. 2 cm) on the ovary.

C: CT image of the same animal's body, transverse plane (120 kV, 120 mA, 1.0 mm SD, W: 1423, L: 253). Image of follicles (1), which virtually fill the whole body cavity and have almost completely displaced the (2) intestines.

D: The two ovaries of the iguana patient after removal.

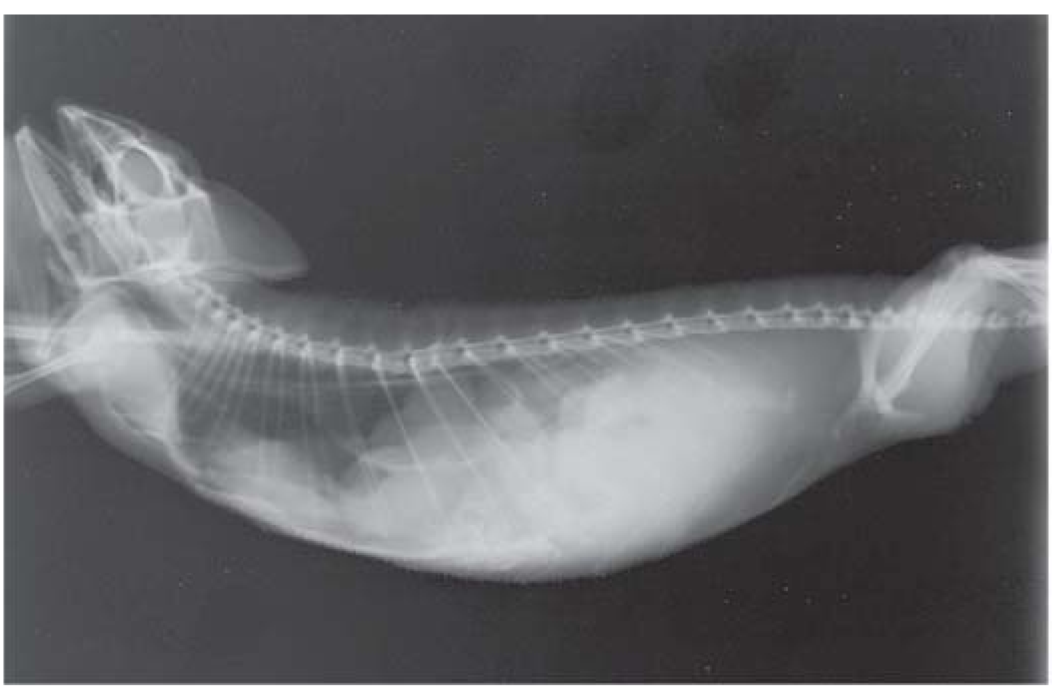

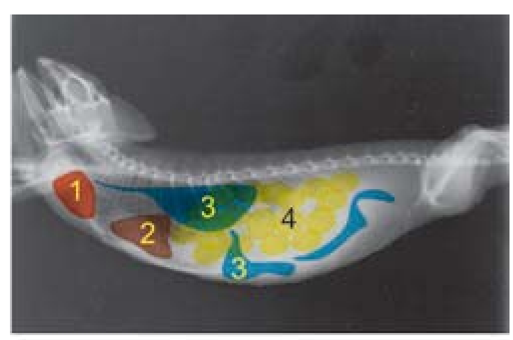

1: heart
2: liver
3: gastrointestinal tract
4: follicles

Fig. 3-195: Total body radiographic image of a veiled chameleon (*Chamaeleo calyptratus*), lateral projection. Preovulatory egg binding. The follicles (4) take up a major part of the body cavity and have, both cranially and ventrally, displaced the gastrointestinal tract (3). Such a displacement can become more problematic resulting in the animal's inability to climb.

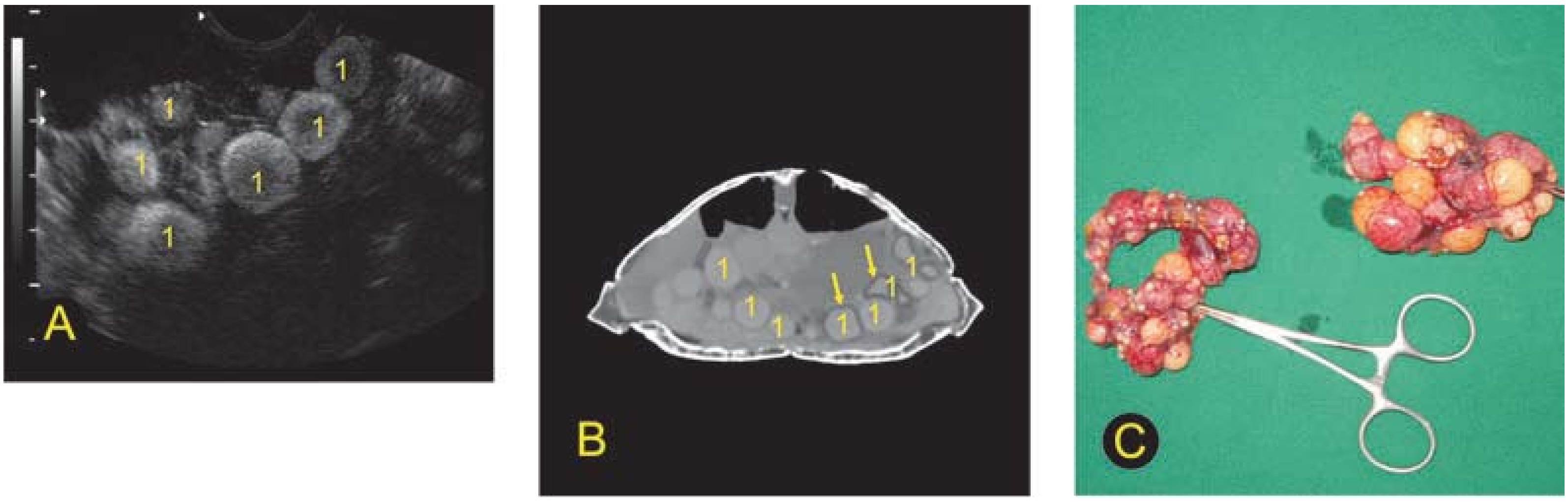

1, arrows: follicles

Fig. 3-196:

A: Ultrasonographic image of a yellow-bellied slider (*Trachemys scripta scripta*), prefemoral coupling site. Preovulatory egg binding. The follicles (1) are of various sizes and have varying degrees of echogenicity. There is an increased amount of fluid within the body cavity.

B: CT image of the same animal's body, transverse plane (120 kV, 360 mA, 2.0 mm SD, W: 400, L: 60). The follicles (1) are very heterogeneous and some are clearly changed on the edges (arrows).

C: The ovaries of the slider after surgical removal.

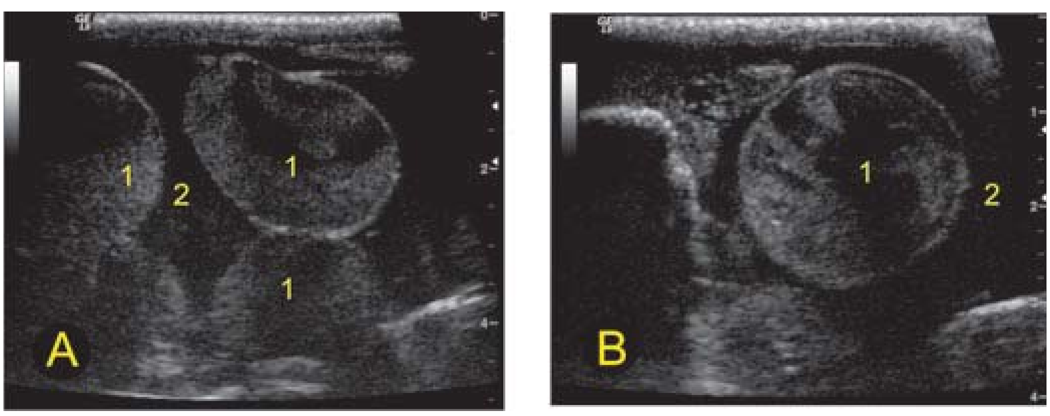

1: follicles
2: fluid

Fig. 3-197: Ultrasonographic image of a green iguana (*Iguana iguana*), ventral coupling site, oblique, 7 MHz, PD (A) 5 cm and (B) 4 cm. Preovulatory egg binding. The follicles (1) are enlarged, inhomogeneous, and severely altered. There is fluid lying free in the abdominal cavity (2).

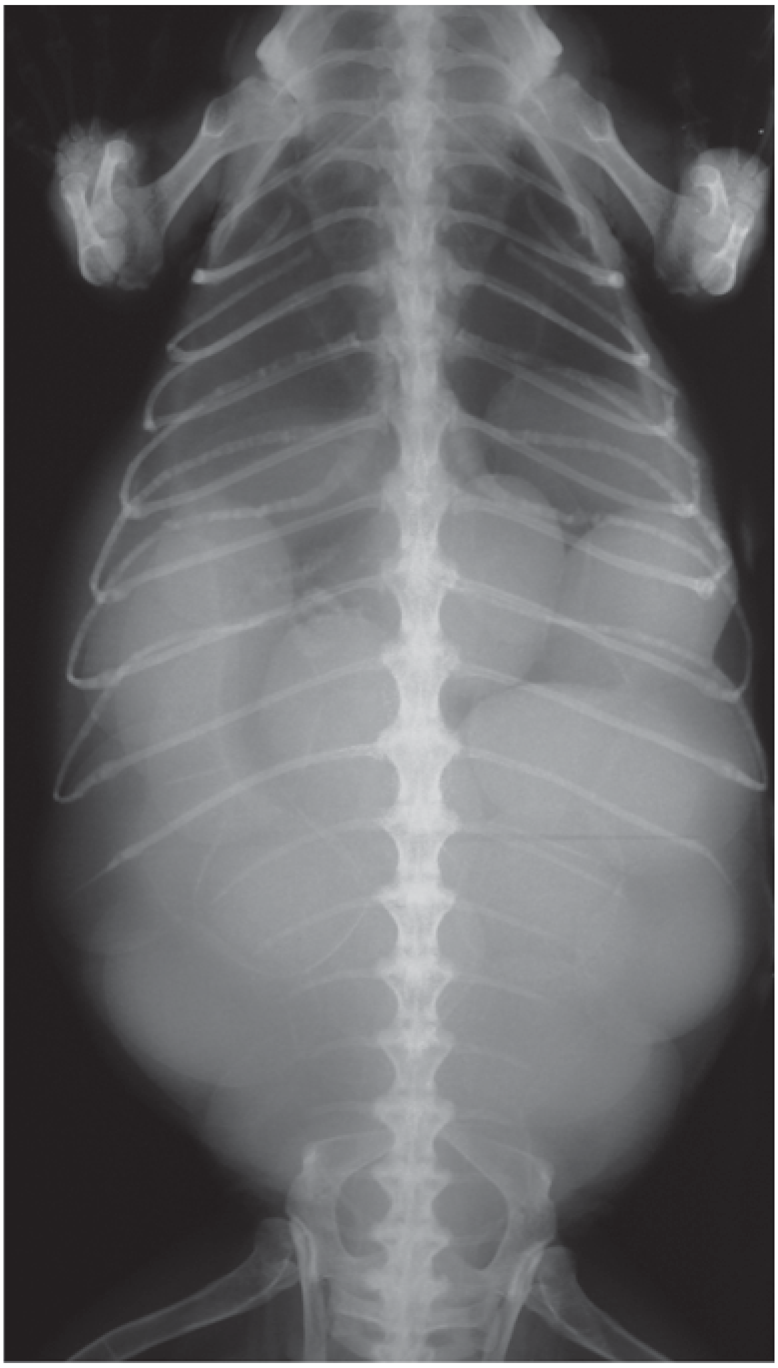

Fig. 3-198: Radiographic image of a green iguana's (*Iguana iguana*) body, dorsoventral projection. The body cavity is severely filled with eggs. Although the eggs appear to be normal, and the degree of body cavity filling can be classed as normal too, egg binding occurs often in such animals due to exhaustion.

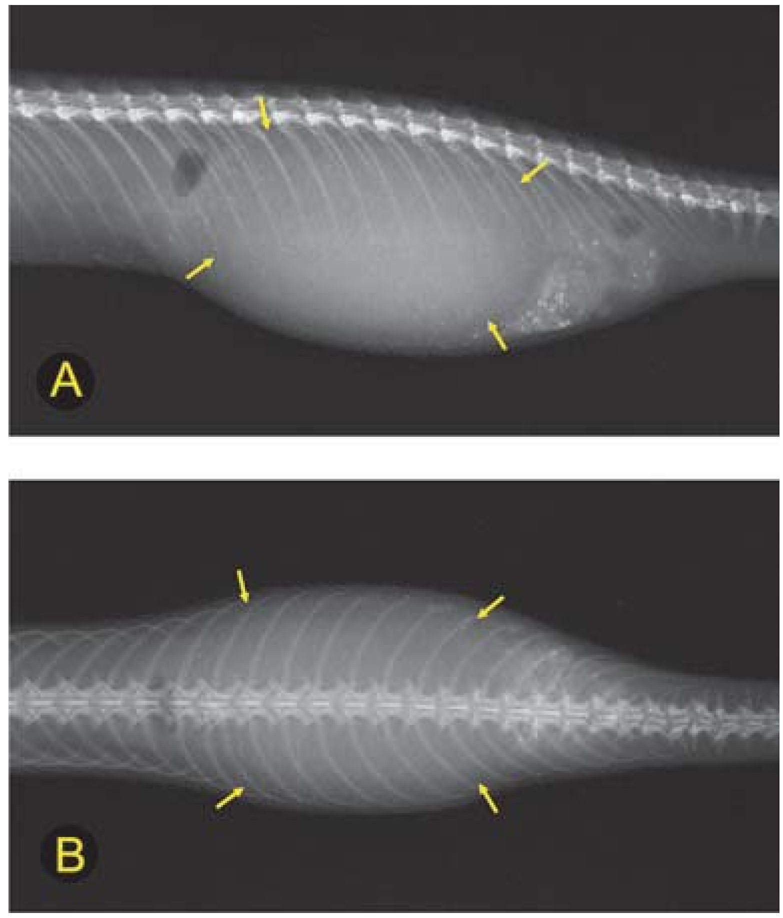

Fig. 3-200: Radiographic images of a corn snake (*Pantherophis guttatus*) showing the region of the cloaca, (A) lateral and (B) dorsoventral projections. Egg binding due to the collection of feces in the cloaca. Hardened feces cause a dispacement of the cloaca and hinder the passage of the egg (arrows). Such fecal concretions are also found in the caudal region of the intestinal tract after attempts of removing them manually with massage. The feces, intestinal tract, and oviduct are pushed caudally with manual message into the caudal body cavity when trying to remove fecal concretions (fecoliths).

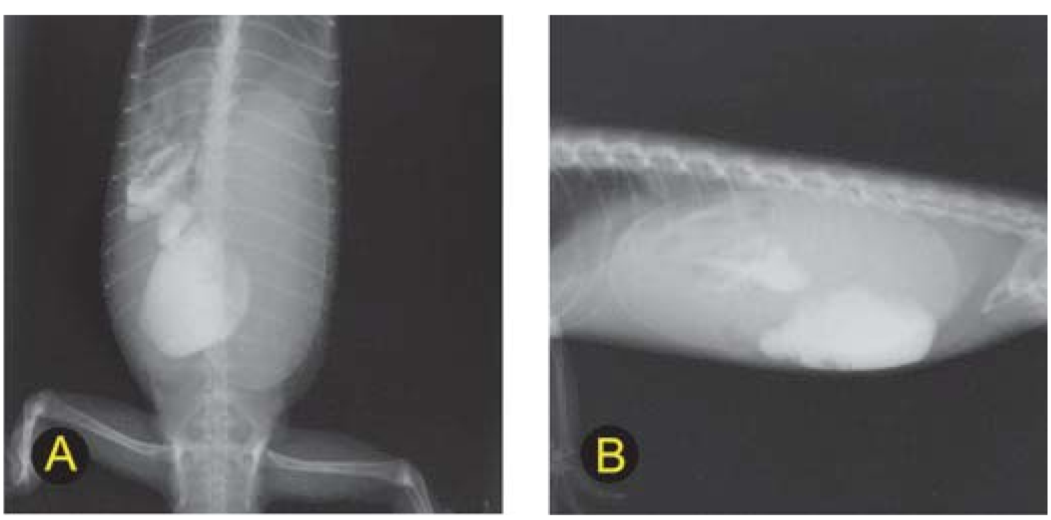

Fig. 3-199: Radiographic images of a leopard gecko's (*Eublepharis macularius*) body, (A) dorsoventral and (B) lateral projections. Sand impaction and egg binding. The filling of the gastrointestinal tract with foreign bodies frequently leads to disturbances in egg laying. A calcium deficiency can exacerbate such a problem. In this animal, only one egg has been formed (normally there are two) and the egg is too large to be laid.

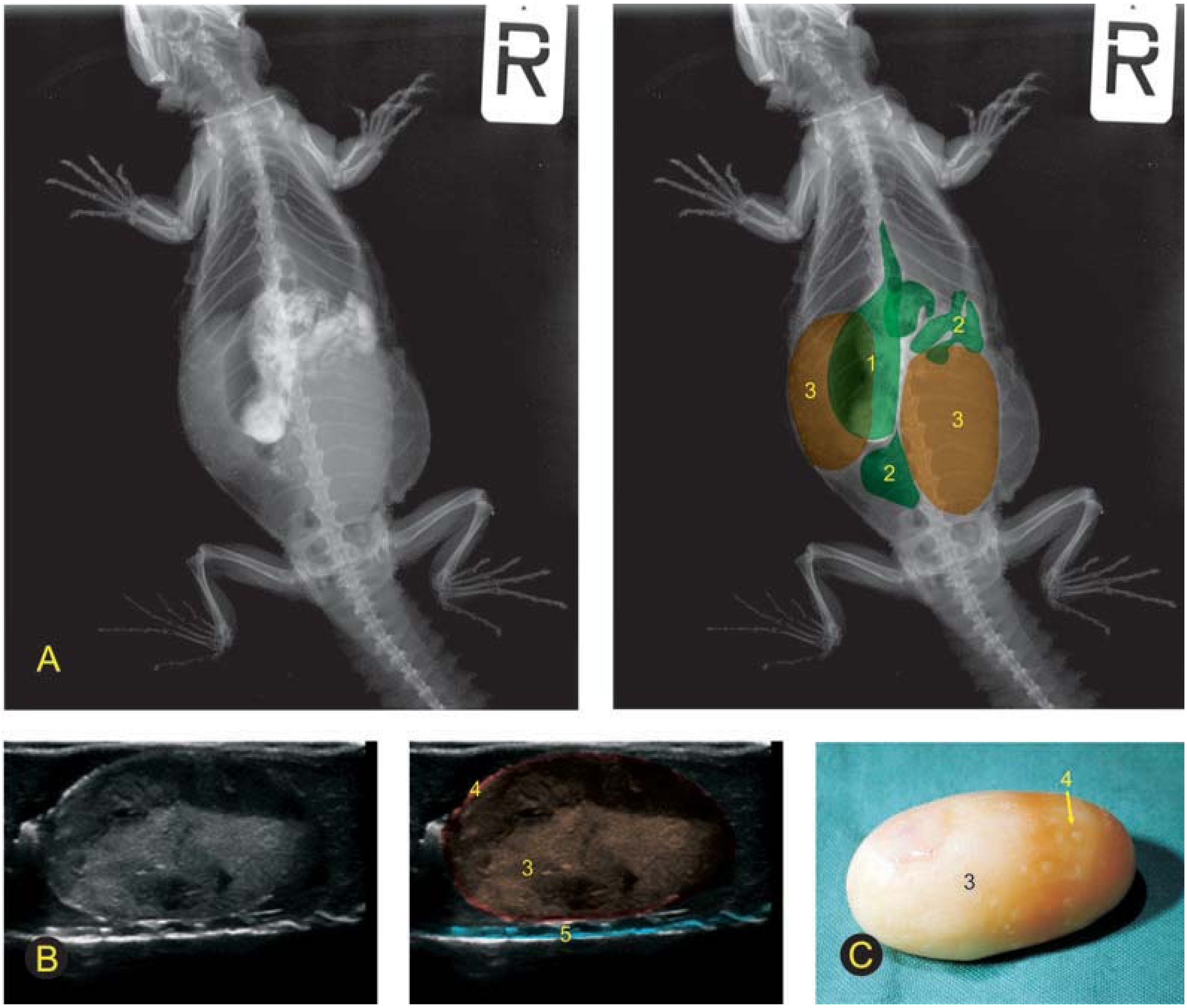

Fig. 3-201:

A: Radiographic image of a Saharan spiny-tailed lizard's (*Uromastyx geyri*) body, dorsoventral projection, 2 h after the oral administration of an iodine-based contrast medium (Iomeprol, 300 mg/ml, 10 ml/kg bwt in the stomach). Egg binding. The stomach (1) and intestines (2) have been displaced by two unevenly calcified eggs (3).

B: Ultrasonographic image of the same animal, ventral coupling site, longitudinal, 14 MHz, PD 2.0 cm. Only patchy calcification of the shell (4) can also been seen ultrasonographically.

C: Surgically removed egg. The uneven calcification (4) is also grossly evident on the surgically removed egg.

1: stomach
2: intestines
3: egg
4: egg shell
5: skin of the back

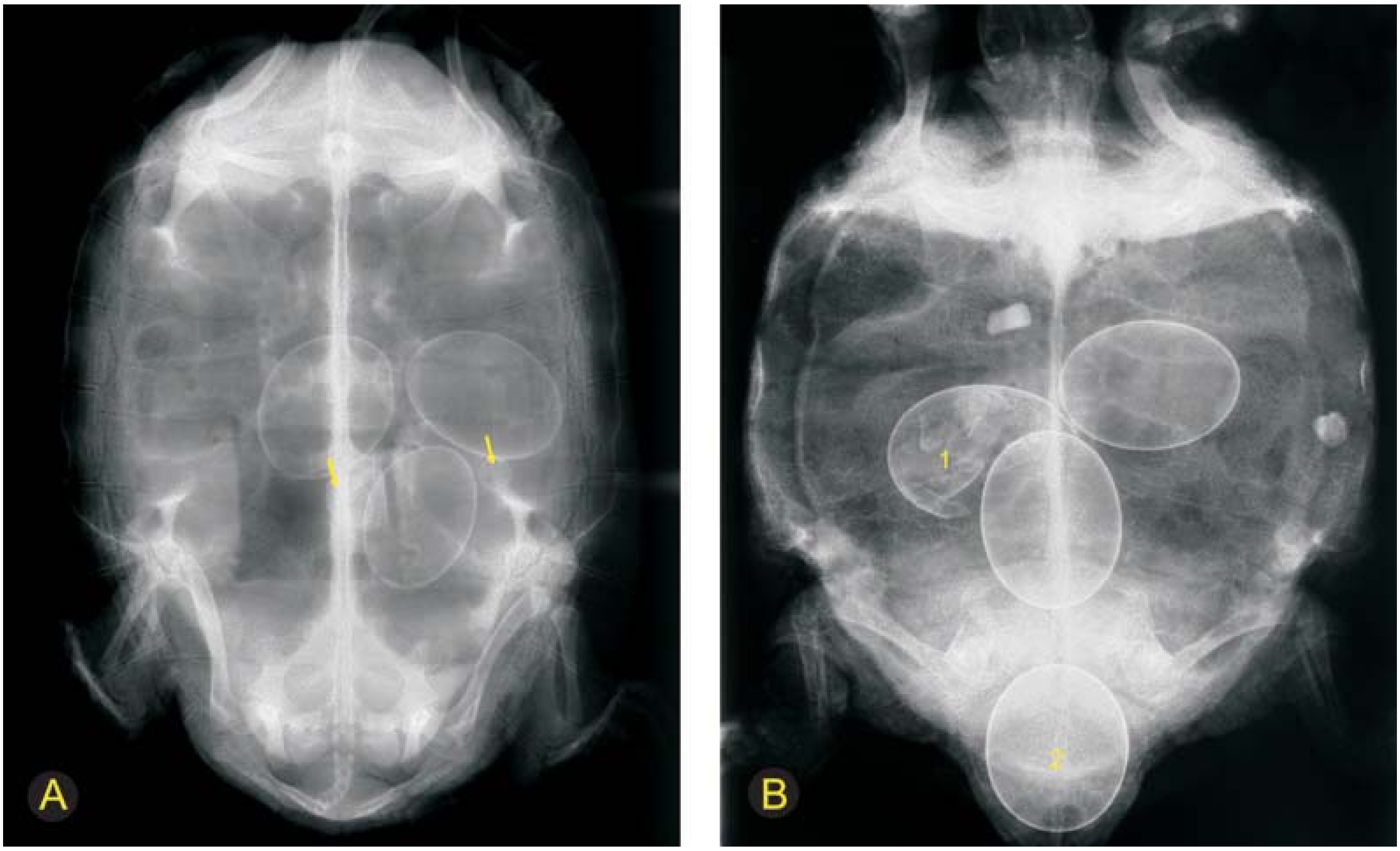

Fig. 3-202:

A: Total body radiographic image of a red-eared slider (*Trachemys scripta elegans*), dorsoventral projection. Egg binding. In addition to three normal appearing eggs, there are two smaller calcified eggs (arrows). Such disturbances in egg formation are often the result of an infectious cause and can lead to problems in laying.

B: Total body radiographic image of a marginated tortoise (*Testudo marginata*), dorsoventral projection. Interrupted egg laying. Both an abnormal and a collapsed egg (1) are lying in the oviduct. The other eggs are inconspicuous and one egg (2) is in the cloaca. As the seepage of egg contents often leads to infections and adhesions within the oviduct, it is unlikely that a natural egg laying is possible by this animal.

1: collapsed egg
2: egg in the cloaca

arrow: small calcified eggs

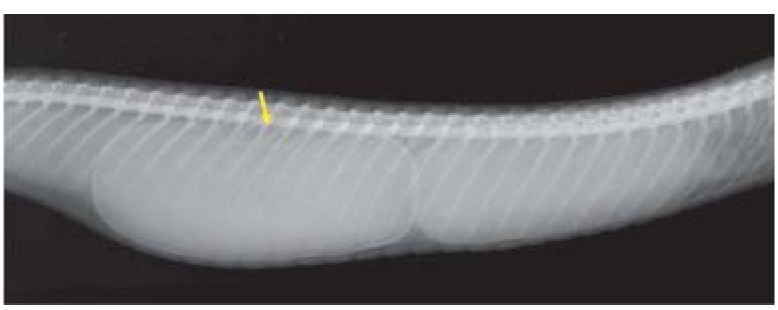

Fig. 3-203: Radiographic image of a Japanese rat snake's (*Elaphe climacophora*) body, lateral projection. Egg binding due to a defective egg. The calcium shell of the front egg is no longer fully intact (arrow). In such cases, the egg usually requires surgical removal.

1: solid and fluid contents
2: shell

Fig. 3-204: Ultrasonographic image of an Indian python (*Python molurus*), ventral coupling site, longitudinal, 10 MHz, PD 6.0 cm. Dead egg. The contents of this egg are nonhomogenous.

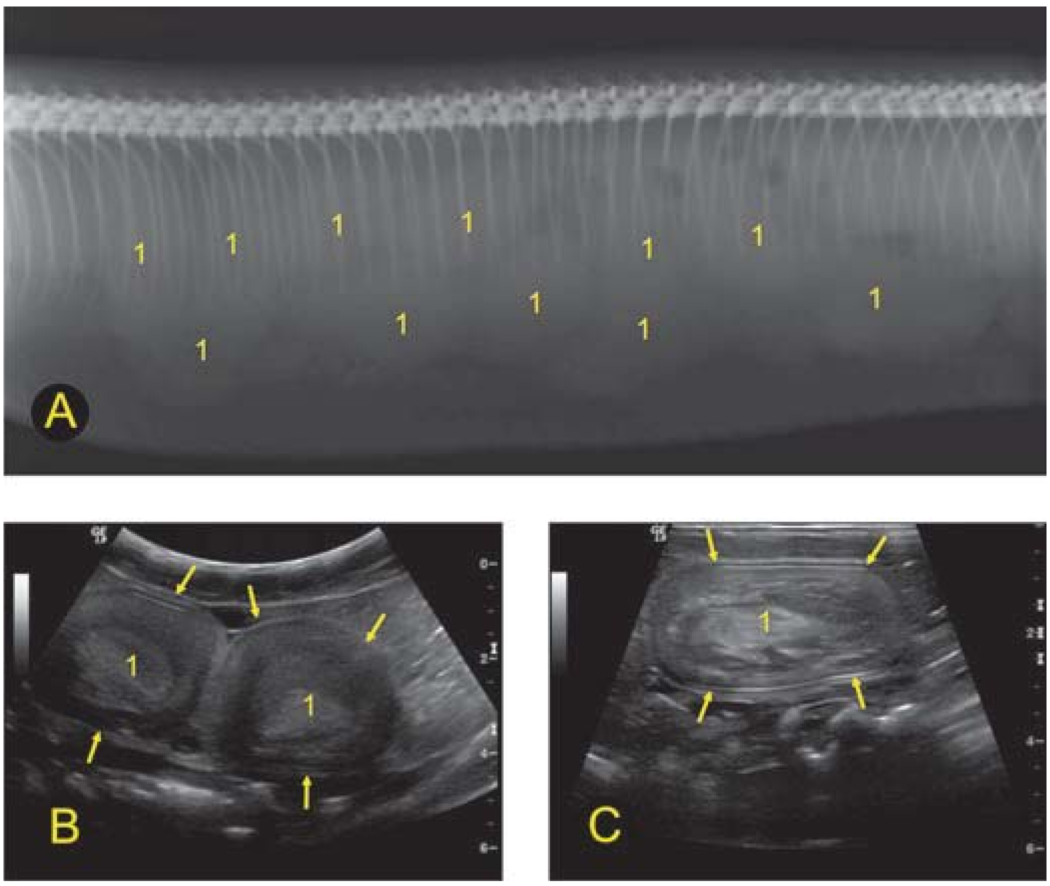

1: eggs

arrows: shell

Fig. 3-205:

A: Radiographic image of an Indian python's (*Python molurus*) body, lateral projection. Egg binding, retained eggs. The eggs (1) are barely discernable from one another, though they appear homogenous and uniform in shape.

B, C: Ultrasonographic image of the same animal, 8 MHz, PD 6 cm. The eggs and their contents can be assessed much better using this imaging modality. The eggs (1) are dead. Their contents are nonhomogeneous and have a hyperechoic central area (arrows: egg shell).

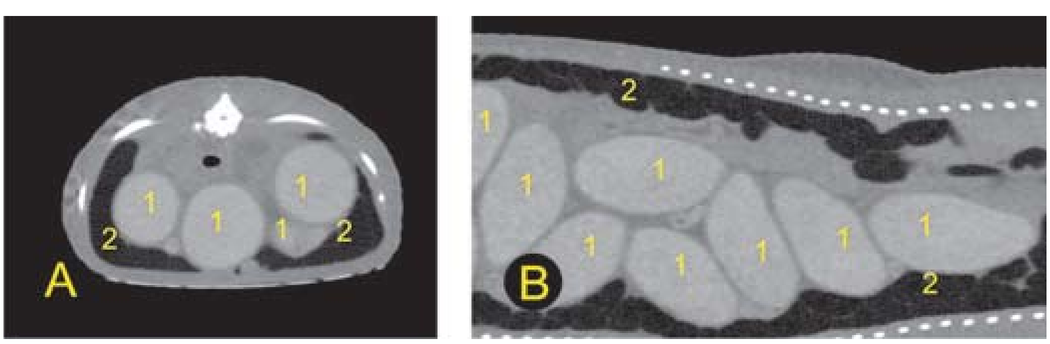

1: dead eggs
2: fat tissue

Fig. 3-206: CT image of an Indian python (*Python molurus*) body, (A) transverse plane and (B) coronary reformation (140 kV, 120 mA, 2.0 mm SD, W: 350, L: 50). Wax egg. The dead eggs (1) have an increased radiodensity and internally appear to be very homogenous.

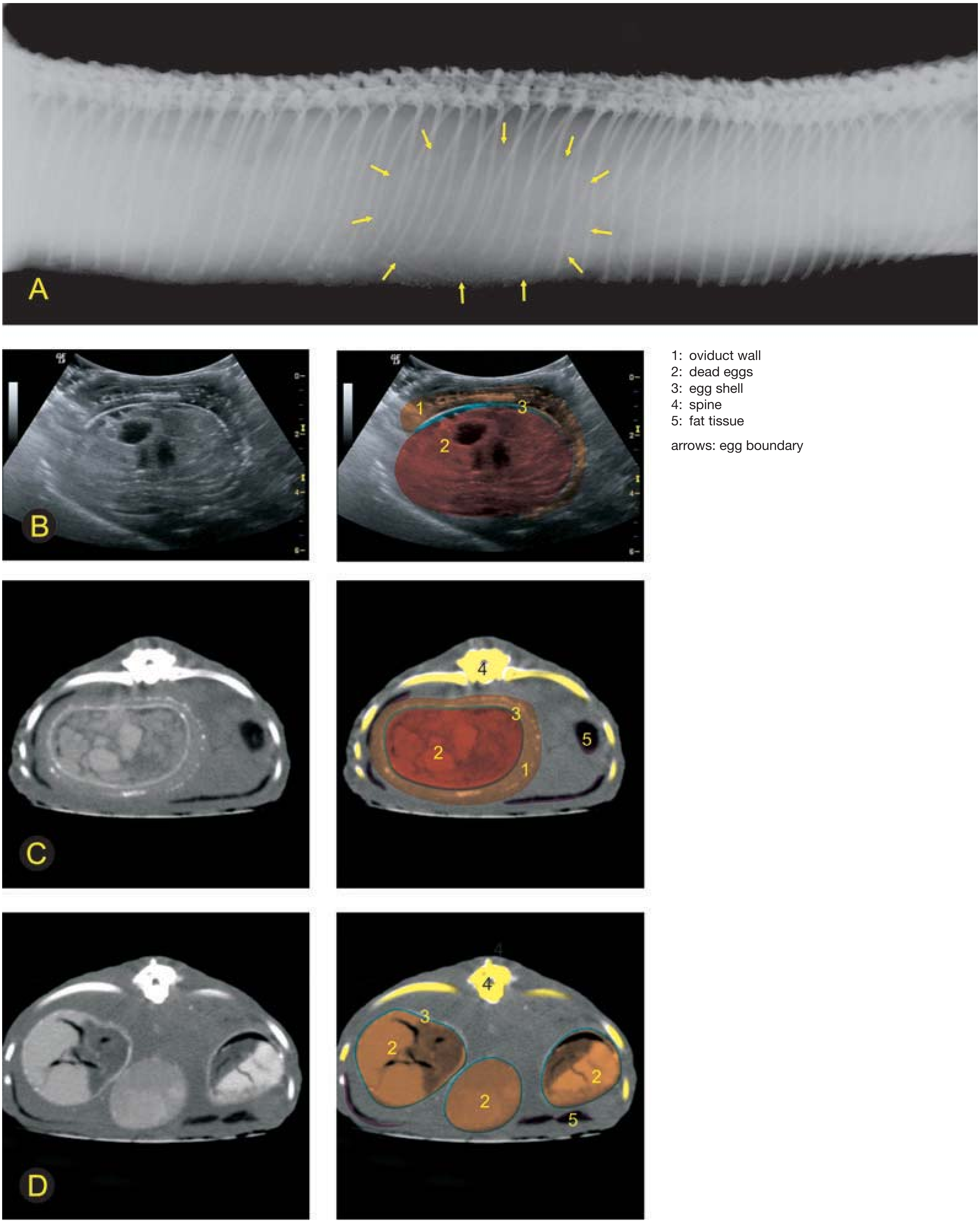

Fig. 3-207:

A: Radiographic image of an Indian python's (*Python molurus*) body, lateral projection. Dead eggs and oviduct infection. The eggs are barely evident in the radiograph.

B: Ultrasonographic image of the same animal, ventral coupling site, longitudinal, 10 MHz, PD 6 cm. The dead eggs (2) with their inhomogeneous contents can be observed lying in a thickened oviduct wall (1), which in places is hyperechoic (because it is calcified).

C, D: CT image of the same animal's body, transverse plane (120 kV, 204 mA, 2.0 mm SD, W: 359, L: 110). The dead eggs (2) with their shells (3) are clearly imaged. The oviduct wall (1) is severely thickened.

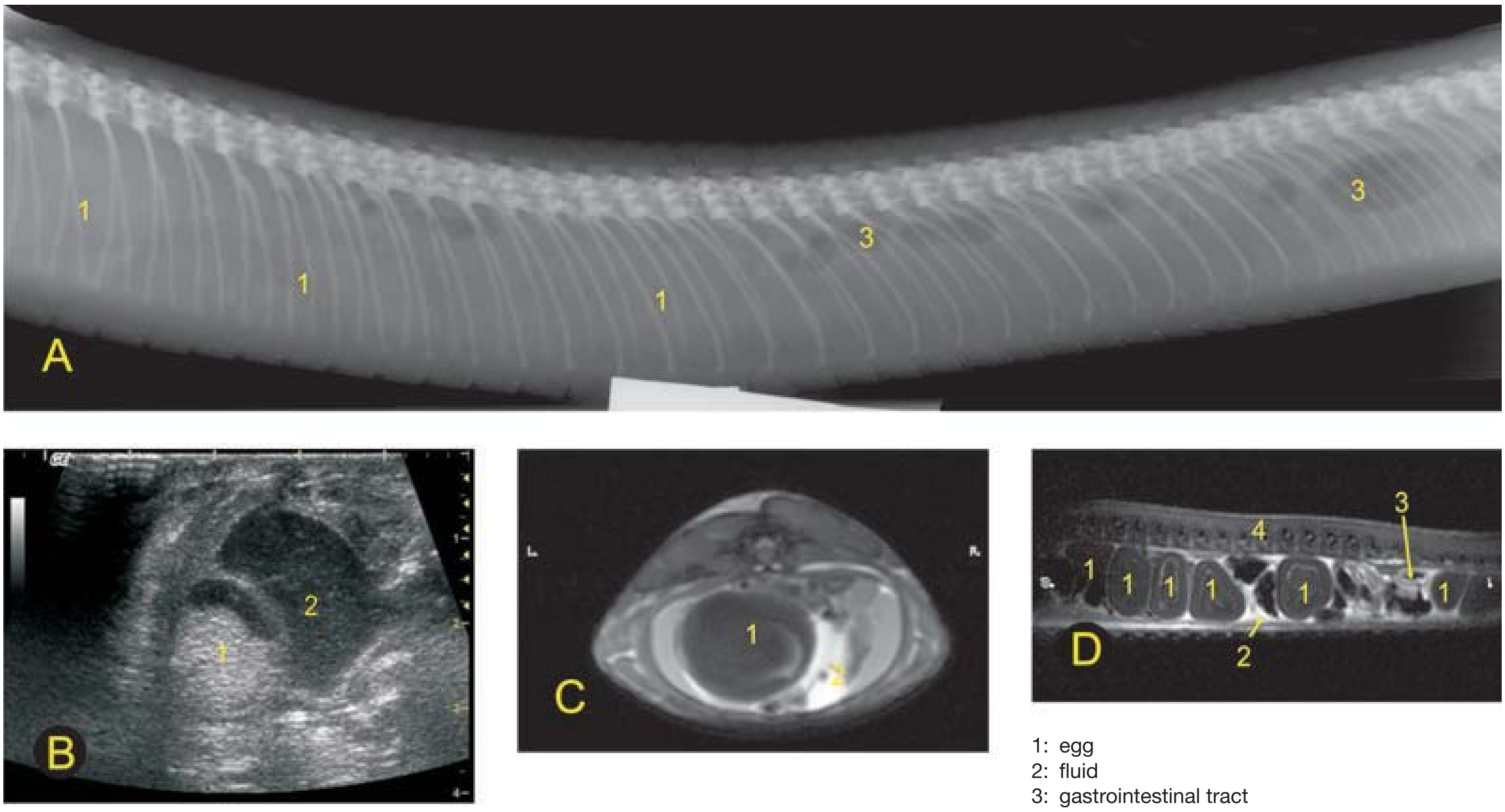

1: egg
2: fluid
3: gastrointestinal tract
4: spinal musculature

Fig. 3-208:

A: Radiographic image of a rainbow boa's (*Epicrates cenchris*) body, lateral projection. Dead and abnormal eggs after a bacterial infection (viviparous species). The abnormal contents (1) can be seen on the radiograph as shadows. The intestinal loops (3) are bloated.

B: Ultrasonographic image of the same animal, ventral coupling site, oblique, 10 MHz, PD 4.0 cm. Fluid (2) can be seen in the oviduct. The egg (1) is asymmetrical and the contents are hyperechoic.

C, D: MRI examination of the same animal, T2-weighted, (C) transverse and (D) sagittal planes. The MRI image also shows the changes in the oviduct with fluid accumulation (2) between the abnormal eggs.

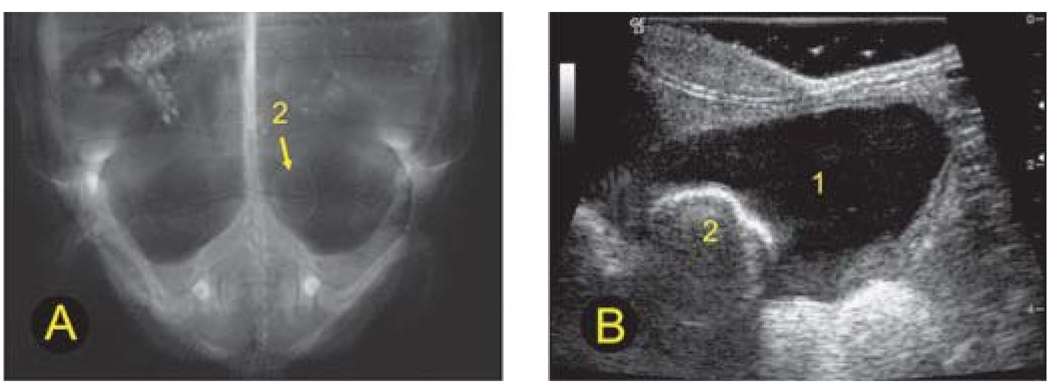

1: allantois
2: egg

Fig. 3-209:

A: Radiographic image of a yellow-bellied slider's (*Trachemys scripta scripta*) caudal body, dorsoventral projection. An egg has been laid in the allantois. Only a relatively small egg (2) can be observed in the radiograph and the shell is beginning to show evidence of degeneration.

B: Ultrasonographic image of the same animal, prefemoral coupling site, longitudinal, 7 MHz, PD 5 cm. The egg (2) has been identified lying in the allantois (1).

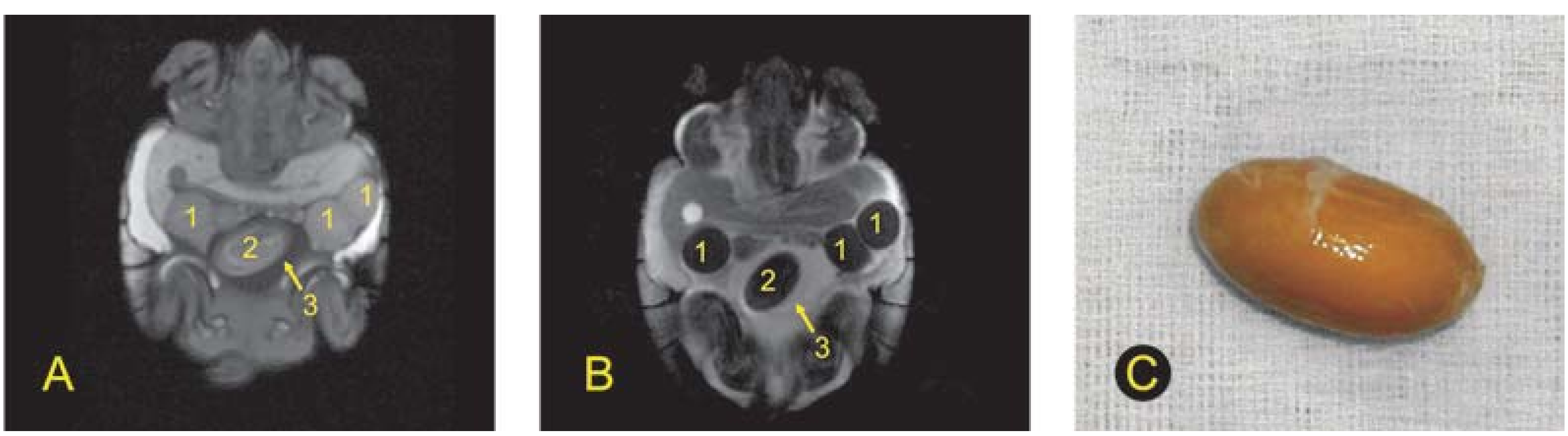

Fig. 3-210:

A, B: MRI examination of a red-eared slider's (*Trachemys scripta elegans*) body, dorsal plane, (A) T1-weighted and (B) T2-weighted images. An egg has been laid in the allantois. In both weightings, eggs (2) can be observed lying in the oviduct (1) and the allantois (3).

C: Egg removed from the allantois.

1: eggs in the oviduct
2: egg in allantois
3: allantois

3.11 Other organ systems, space-occupying lesions

Ingo Hoffmann, Michael Pees

3.11.1 Heart

Scientific reports detailing reptile heart pathology are rare, especially when antemortem diagnostic testing was used to detect the disease condition. If a reptile patient is malnourished, its heart can be significantly smaller than that of a properly fed animal. Occasionally, pericardial **fluid accumulation** has been identified. When there is a circulatory disturbance affecting the liver or body cavity (**Fig. 3-211**) a larger volume of pericardial fluid is observed than that associated with healthy animals. With some reptile patients, **cardiomegaly** can be diagnosed both radiographically and through external physical examination, but determining the underlying cause of the cardiac disease condition is difficult (**Fig. 3-212**).

Radiologically, alterations other than cardiac changes are more commonly determined in lizards: in particular, arteriosclerotic changes in the walls of the great vessels. The most commonly affected species is the green iguana (*Iguana iguana*). The clinical signs are often sudden cramp-like spasms. As a consequence of the calcification, a sclerotic aortic wall can be imaged ultrasonographically due to its hyperechogenicity and the blood flow measured (**Fig. 3-213**). Even though there are no reference values for the assessment of aortic blood flow, the success of treatment can be controlled using ultrasonography.

3.11.2 Eye

Ultrasonography will provide the best diagnostic images of a reptile patient's eye. At this time neither MRI nor CT have any significant ophthalmic diagnostic value for reptile species. Due to slight differences in the radiopacity of the internal ocular structures, in most cases, traditional radiography can only provide inadequate diagnostic images. One exception is the presence of lytic processes affecting the bony tissues around the eye. A common problem that complicates radiographic image interpretation of the lytic processes is summation of neighboring bony structures.

The most common causes of reptile ocular disease includes congenital abnormalities, infectious disease, malnutrition, improper husbandry, degenerative processes, neoplasia, and trauma. Ultrasonography is often less diagnostic and difficult to perform in reptiles than mammals because of the globe's small size in many reptile species.

Congenital abnormalities affecting the reptile eye are frequently caused by improper incubation temperatures. In addition to other congenital abnormalities, microphthalmia and unilateral anophthalmia have been reported (**Fig. 3-214A**). Ultrasonography can be used to determine whether the animal has an anophthalmia or a microphthalmia (**Fig. 3-214B**), although a diagnosis of this nature is rarely of clinical relevance.

An ultrasonographic examination in combination with a clinical ophthalmological assessment of patients with congenital ocular abnormalities may reveal other anomalies present affecting the eye that cannot be diagnosed using standard ophthalmoscopic techniques (**Fig. 3-215**).

Ocular infections can develop through the introduction of infectious agents into or behind the eye (e.g., prey bite injury, foreign body) or by hematogenous dissemination. Prey bite wounds and/or foreign bodies are mainly associated with acute blepharospasm and enophthalmos (**Fig. 3-216**). During an ultrasonographic examination of a patient's eye that presents with ocular prey bite wounds and/or foreign body exposure, hyperechoic areas are apparent in the normally anechoic ocular chambers and/or vitreous body, or there are hypoechogenic regions within the orbit (**Figs. 3-216A** and **3-217B**). Parasites can also infect the eye and in some cases may overcome the protective ocular barriers (**Fig. 3-217A**).

As with mammals, **abscesses** affecting the retrobulbar space (orbit) have been observed in reptiles. During an ultrasonographic examination, the abscesses appear as mixed echoic or anechoic areas. Clinically, exophthalmos is often diagnosed in traumatized reptile patients. With ultrasonography, it is possible to differentiate mixed echoic abscesses from anechoic cysts (**Fig. 3-218A**).

The underlying causes of **lens opacities** (**cataract**) in reptiles are as variable as those recognized for mammals. Both nutritional and traumatic cataracts have been described in reptile species. Cataracts and intraocular hemorrhages have been documented in chelonians after brumation. Generally, the lens contents are anechoic, and normally lie within the sharply demarcated hyperechoic lines of the lens. Cataracts are viewed ultrasonographically as hyperechoic areas between the hyperechoic lines of the lens (**Fig. 3-218B**). A preoperative ultrasonography investigation is recommended for reptiles in which lens removal is being considered due to severe lens opacities. As with mammals, retinal detachments in reptile patients can also be imaged with ultrasonography. An ultrasonographic image of a reptile retinal detachment will show a hyperechogenic structure protruding from the wall of the globe into the vitreous. If there is a complete retinal detachment a lily-like structure will be visible (**Fig. 3-219**).

Generally, **ocular neoplasms** are diagnosed less in reptiles than in mammals of similar size. Ultrasonography can be helpful in differentiating between cystic and solid neoplasms (**Fig. 3-220**).

Injuries of the eye occur with improper husbandry conditions (e.g., overcrowding) or frequently when feeding live prey. Infections initiated by prey bite injuries may ultimately result in the enucleation of the affected eye (**Fig. 3-216**).

Intraocular hemorrhage caused by blunt trauma will appear as hyperechoic areas within the globe and may be confused with local inflammatory reactions (**Fig. 3-221**).

3.11.3 Space-occupying lesions

Space-occupying lesions are common in reptiles, although their origin to a specific organ system is often difficult to determine. Therefore in this chapter, those space-occupying lesions which cannot be classified to one of the organs discussed above will be discussed. This particularly involves abscesses and tumors. More information about this presentation is given in Chapters 3.5 and 3.7.

Space-occupying lesions associated with the joints are often due to **urate deposits (gout)**, especially in chelonians. The radiographic differentiation of urate deposits from abscesses is usually not possible due to calcium deposition within the affected areas of both disease processes, appearing radiopaque. Aspiration or surgical incision of the lesion is necessary for determining a definitive diagnosis of an enlarged radiopaque joint (**Fig. 3-222**).

Abscesses are very common in reptiles and become massive space-occupying lesions. Space-occupying lesions in the cloacal region are often the consequence of prolapsed tissues (see Chap. 3.7.4 and **Fig. 3-168**), but this is also an area for abscess development (**Fig. 3-223**). Contrast studies are necessary to assess the significance of abscess's effect on the intestinal tract by the increase in diameter of the lesion. In many cases, space-occupying lesions cannot often be really reached by an external investigation or they may occur multifocally within the body cavity. In such cases, ultrasonography is recommended, though both CT and MRI offer excellent possibilities for the imaging and assessment of the number and location of space-occupying lesions. Abscesses frequently appear relatively radiodense in CT scans (**Fig. 3-224**) and are often the result of chronic inflammation. Occasionally, abscesses can be imaged using standard radiography. However, changes in radiodensity observed with inflammatory processes are not limited to abscesses, but are also associated with chronic **pododermatitis** (**Fig. 3-225**).

Neoplasms are relatively rare in reptiles. In addition to those neoplasms which are linked with specific organ cell types (see corresponding chapters), both neoplastic disease of the connective tissue and lymphatic system can also occur. Although connective tissue and lymphatic system neoplasms cannot be associated with a particular organ, they can form massive space-occupying lesions and induce the clinical signs associated with disease. The clinical disease signs of these generalized neoplasms usually are the body's response to the infiltrative growth of the mass, the resulting damage to the affected organs (**Figs. 3-226** and **3-227**) and subsequent compression of other organs. Organ compression from neoplastic masses is particularly problematic in snakes due to their narrow body width.

Endolymphatic sacs are atypical anatomic structures found in the caudal pharynx of some lizard species (e.g. *Anolis* spp.). Occasionally, depending on the size and species of lizard, these endolymphatic sacs can be externally examined. The endolymphatic sacs can respond to disease processes by swelling and becoming inflamed. When radiographically imaged, the endolymphatic sacs appear radiopaque (**Fig. 3-228**).

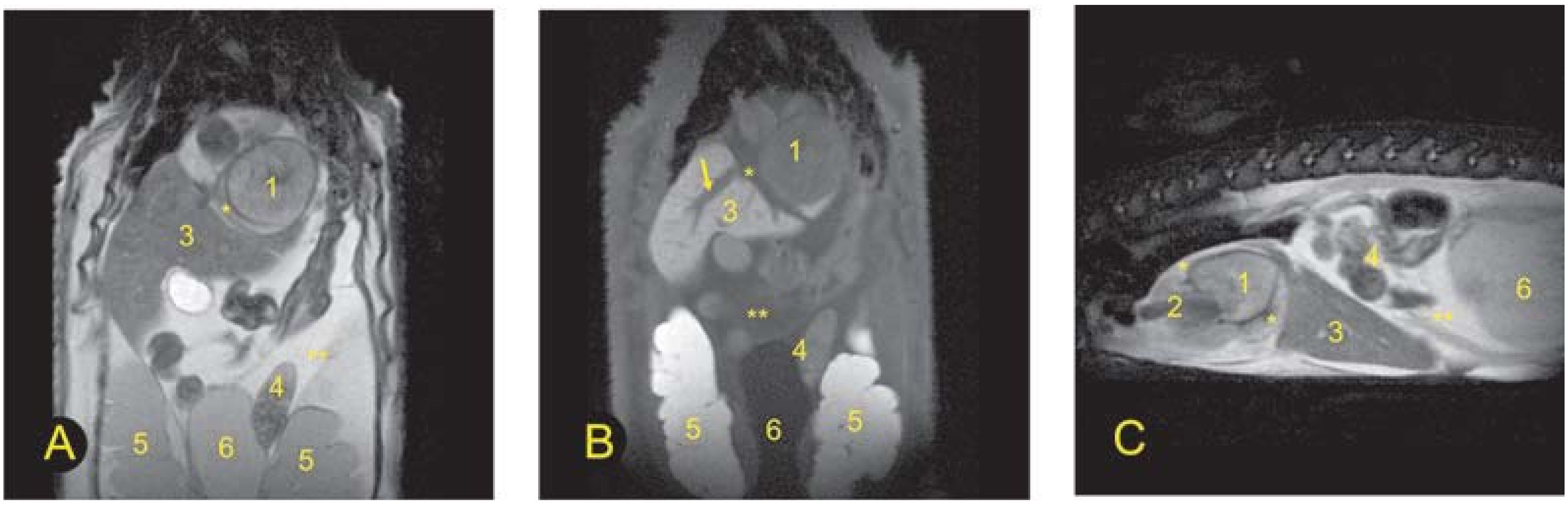

Fig. 3-211: MRI examination of a Savannah Monitor (*Varanus exanthematicus*), (A, B) sagittal and (C) dorsal planes, (A, C) T2-weighted and (B T1-weighted) images. Pericardial effusion and congestion of the hepatic blood vessels. The ventricle (1) is surrounded by an obvious layer of fluid (*). The liver (3) contains congested blood vessels (arrow). Free fluid (**) can also be seen in the body cavity. The allantois (6) is distended. The fat bodies (5) are clearly identified.

1: ventricle
2: atria
3: liver
4: intestines
5: fat bodies
6: allantois

*: fluid surrounding the heart chamber
**: free fluid in the body cavity

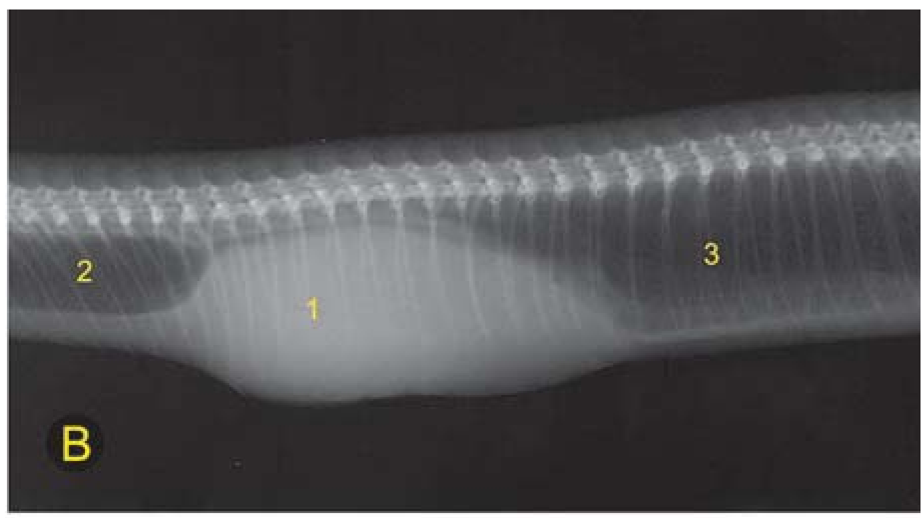

1: heart
2: esophagus
3: trachea

Fig. 3-212: Radiographic image of a bull snake's (*Pituophis catenifer sayi*) heart region, (A) dorsoventral and (B) lateral projections. Cardiomegaly of uncertain etiology.

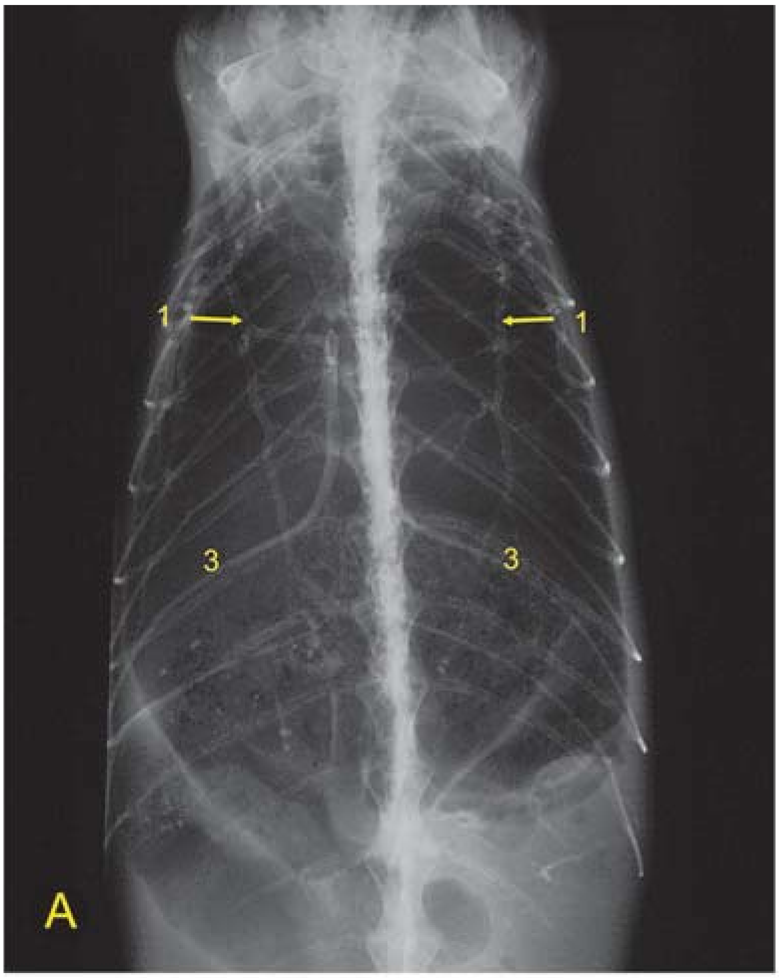

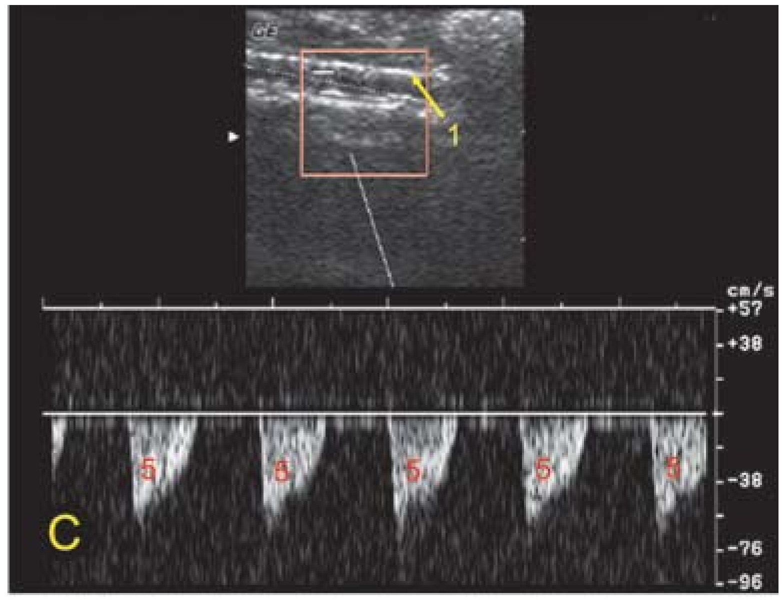

1: blood vessels
2: primary bronchi
3: lungs
4: stomach

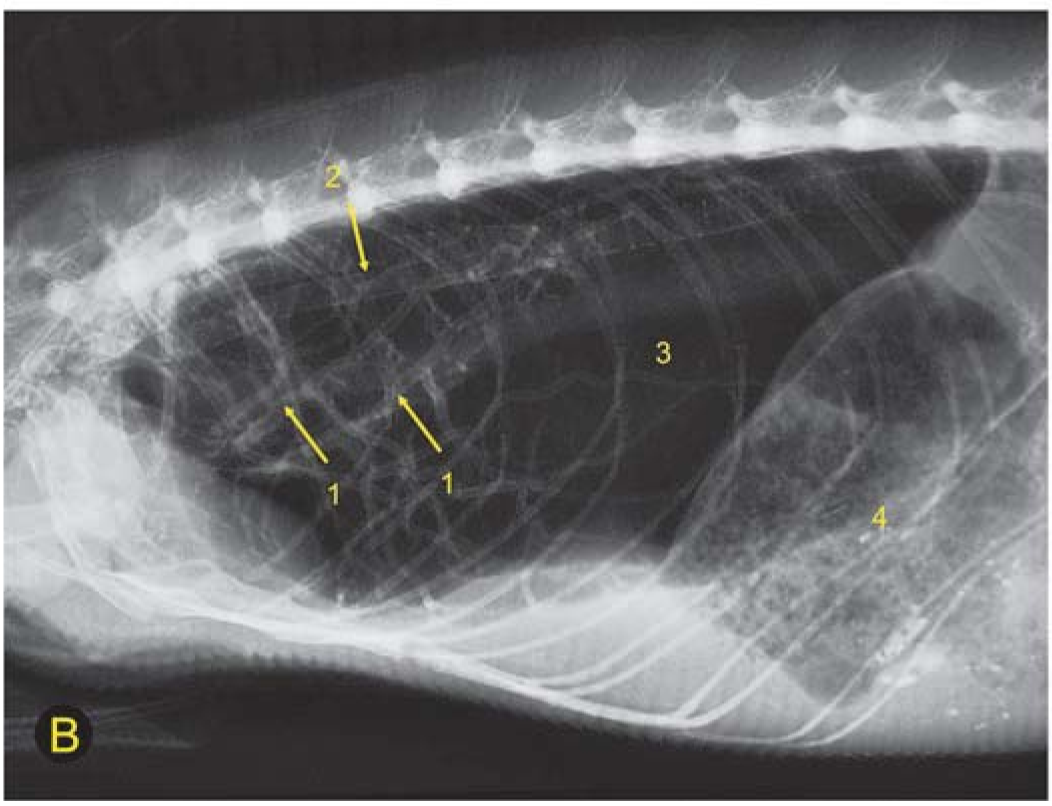

Fig. 3-213:

A, B: Radiographic images of a green iguana's (*Iguana iguana*), trunk, (A) dorsoventral and (B) lateral projections. Arteriosclerosis. The course of the radiodense blood vessels (1) can be easily traced. The primary bronchi (2) have increased calcification and are visible. Clinically, these changes were associated with sudden seizures.

C: Ultrasonographic image of the same animal, lateral coupling site, longitudinal, 7 MHz, PD 2 cm, PW-Doppler method. The hyperechogenic vessel wall (1) is visible in this image. The extraction of the Doppler signal depicts the blood flow in the vessel.

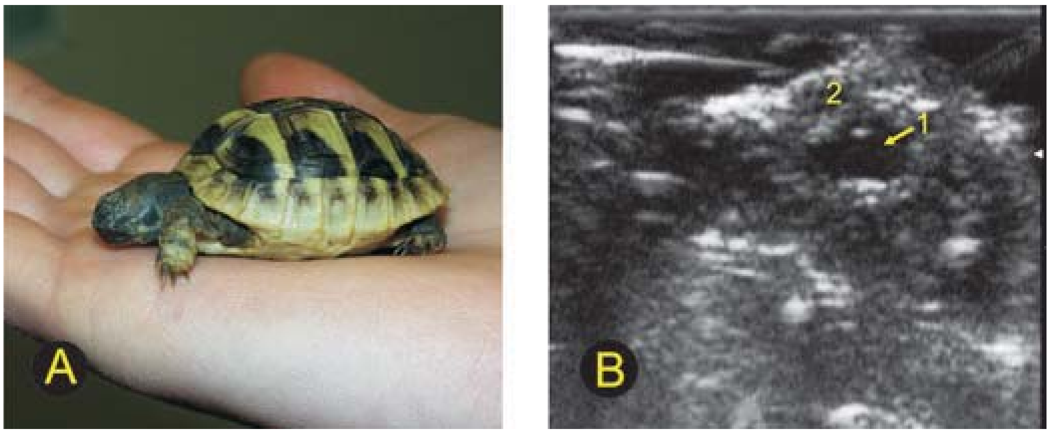

Fig. 3-214:

A: Anophthalmia in a juvenile Hermann's Tortoise (*Testudo hermanni*).

B: Ultrasonographic image of a Hermann's Tortoise (*Testudo hermanni*), corneal coupling site, 11 MHz, PD 2 cm. Microphthalmus. The abnormally small and deformed eye (1) is lying deep in the orbit and is covered by the eyelid (2).

1: eye
2: eyelid

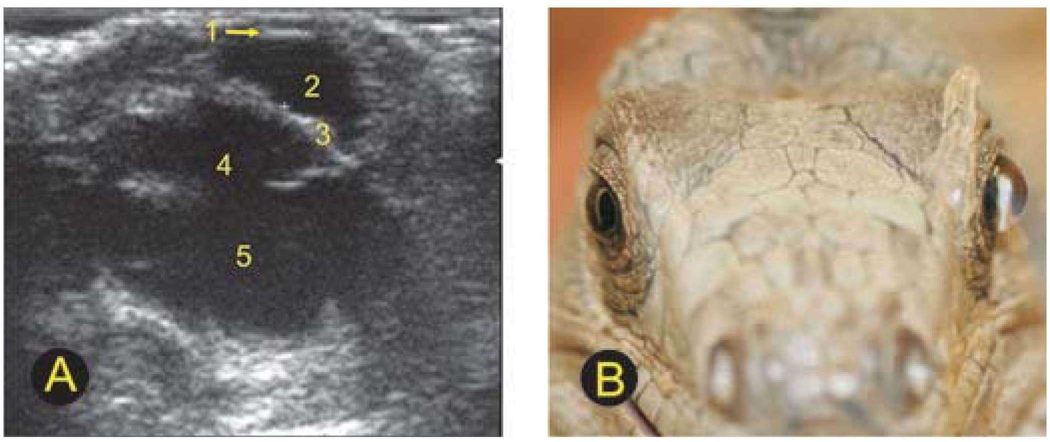

Fig. 3-215:

A: Ultrasonographic image of a green iguana (*Iguana iguana*), corneal coupling site, 11 MHz, PD 2 cm. Megalocornea. The anterior eye chamber (2) is significantly enlarged.

B: Photograph showing the clinical presentation of this animal.

1: cornea
2: anterior eye chamber
3: iris
4: lens
5: vitreous body

Fig. 3-216:

A: Ultrasonographic image of a flap-necked chameleon (*Chamaeleo dilepsis*), transpalpebral coupling site, 11 MHz, PD 2 cm. Blepharospasm and enophthalmos. The eye itself could no longer be examined with a light. The vitreous body hab hyperachogenic shadows (4) and lines (3) in it, indicating the possible presence of retinal detachment.

B: Photograph showing the clinical presentation of this animal.

C: Macroscopic photograph of the eye of this animal (removed surgically). Histological diagnosis: panophthalmitis due to a bite from a prey animal causing perforation of the eye with prolapse of the iris (6), retina (7), vitreous body (4) and fundus (5).

1: corneal region,
2: lens
3: hyperechogenic lines in the vitreous body
4: hyperechogenic shadowy vitreous body
5: fundus
6: prolapse of the iris
7: retina

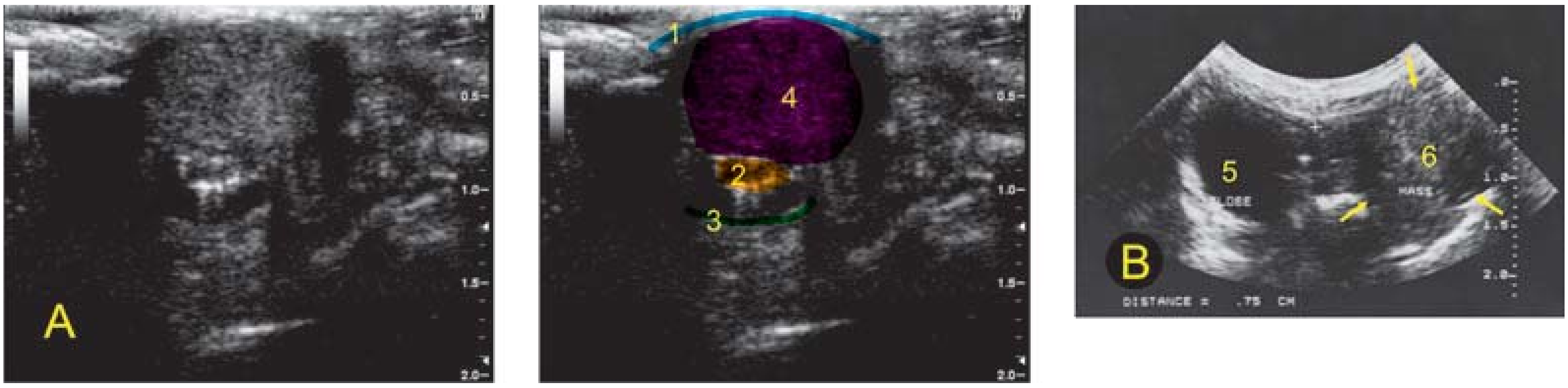

Fig. 3-217:

A: Ultrasonographic image of an Indian python (*Python molurus*), spectacle coupling site, 12 MHz, PD 2 cm. Subspectacle abscess. Flagellates were found between the spectacle and the cornea. The eye itself is barely recognizable.

B: Ultrasonographic image of a green iguana (*Iguana iguana*), spectacle coupling site, 10 MHz, PD 2 cm. Abscess in the orbit. The abscess (6) appears to be hyperechoic in comparison to the eye (5).

1: spectacle
2: cornea/lens
3: ocular fundus
4: abscess
5: eye
6, arrows: abscess

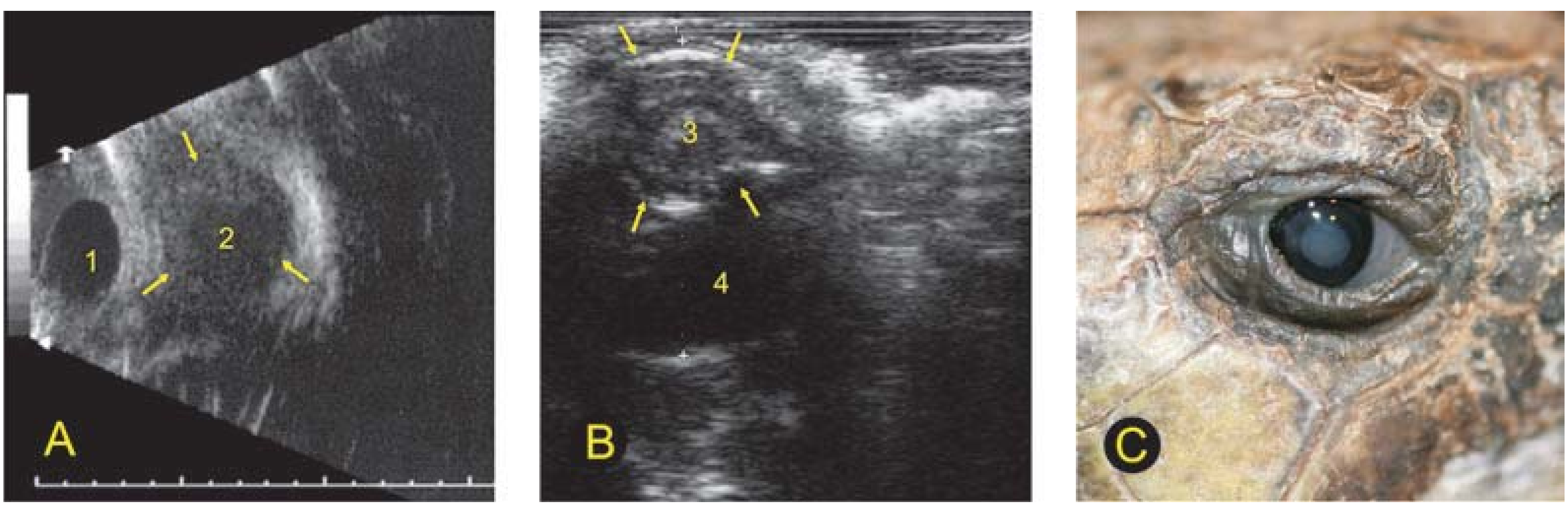

Fig. 3-218:

A: Ultrasonographic image of a red-eared slider (*Trachemys scripta elegans*), corneal coupling site, 10 MHz, PD 2 cm. Retrobulbal cyst. A large hypoechogenic structure is situated behind the eye (1). Fine-needle aspiration revealed the structure to be a cyst (2).

B: Ultrasonographic image of a central bearded dragon (*Pogona vitticeps*), corneal coupling site, 15 MHz, PD 3 cm. Mature cataract. The (3) lens is significantly swollen and hyperechoic.

C: Photograph showing the clinical presentation of a mature cataract in a Hermann's tortoise (*Testudo hermanni*) that occurred after brumation.

1: eye
2, arrows: cyst
3, arrows: lens
4: vitreous body

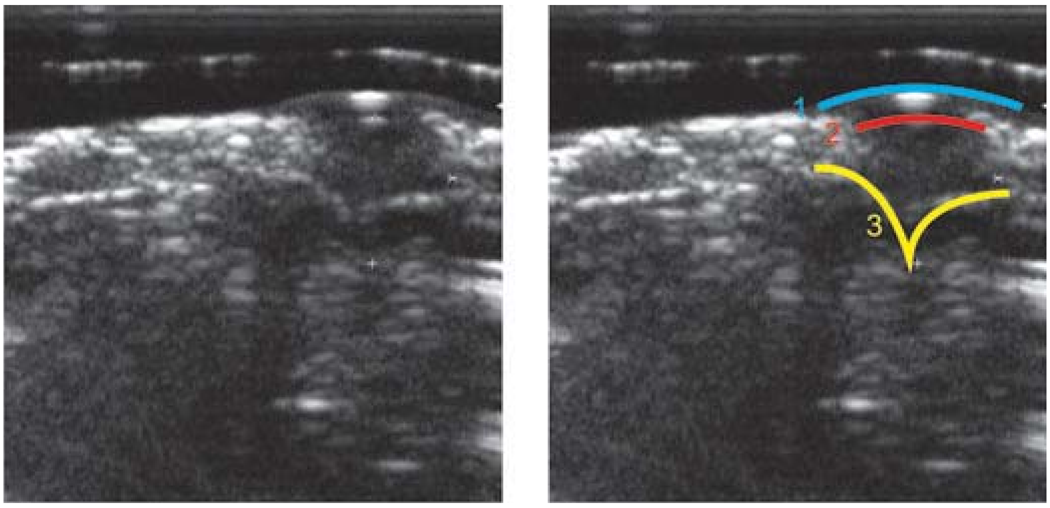

1: spectacle
2: cornea
3: detached retina

Fig. 3-219: Ultrasonographic image of a boa constrictor (*Boa constrictor*), spectacle coupling site, 11 MHz, PD 2 cm. Retinal detachment. The typical lily-like hyperechoic form of the detached retina (3) projects into the vitreous body.

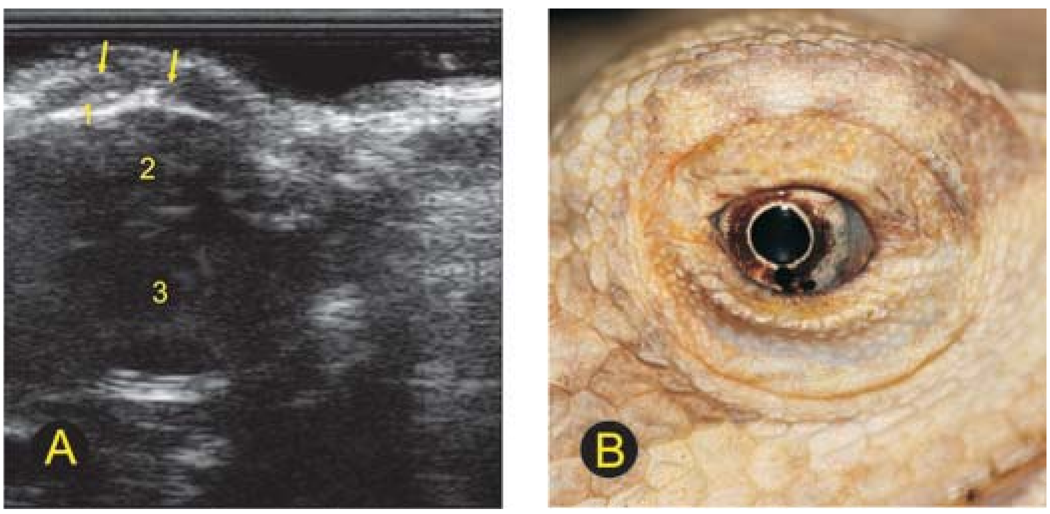

1: iris
2: lens
3: vitreous body

arrows: iris cyst

Fig. 3-220:

A: Ultrasonographic image of a central bearded dragon (*Pogona vitticeps*), corneal coupling site, 15 MHz, PD 3 cm. Iris cysts. In the anterior chamber of the eye, there are structures with a hyperechoic edge and anechoic contents (arrows – iris cyst).

B: Photograph showing the clinical presentation of this animal with brown tumors in the anterior chamber.

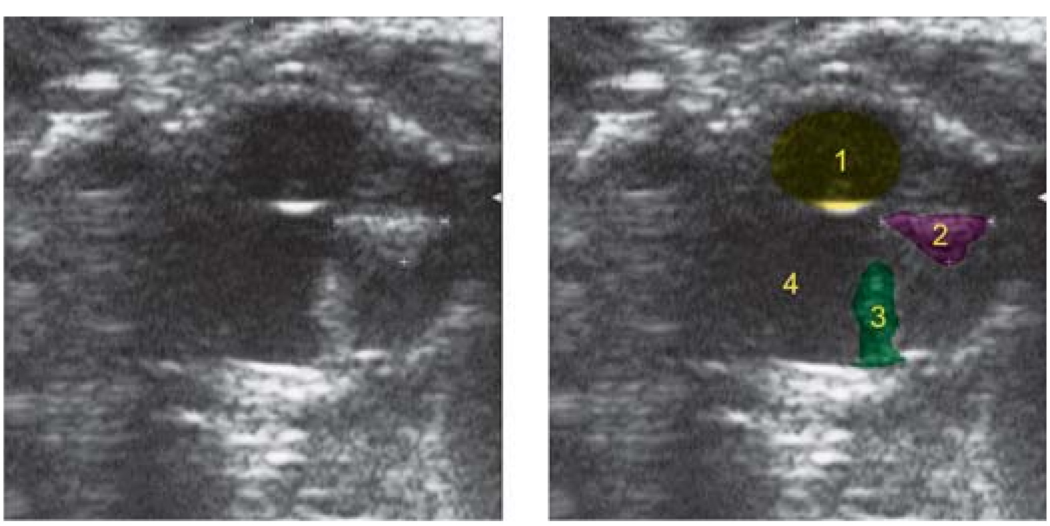

1: lens
2: hemorrhage
3: papillary cone
4: vitreous body

Fig. 3-221: Ultrasonographic image of a frilled neck lizard (*Chlamydosaurus kingii*), corneal coupling site, 11 MHz, PD 2 cm. Hemorrhage in the vitreous body. The hemorrhage (2) within the vitreous body (4) most likely came from the papillary cone (3) and was caused by a traumatic incident.

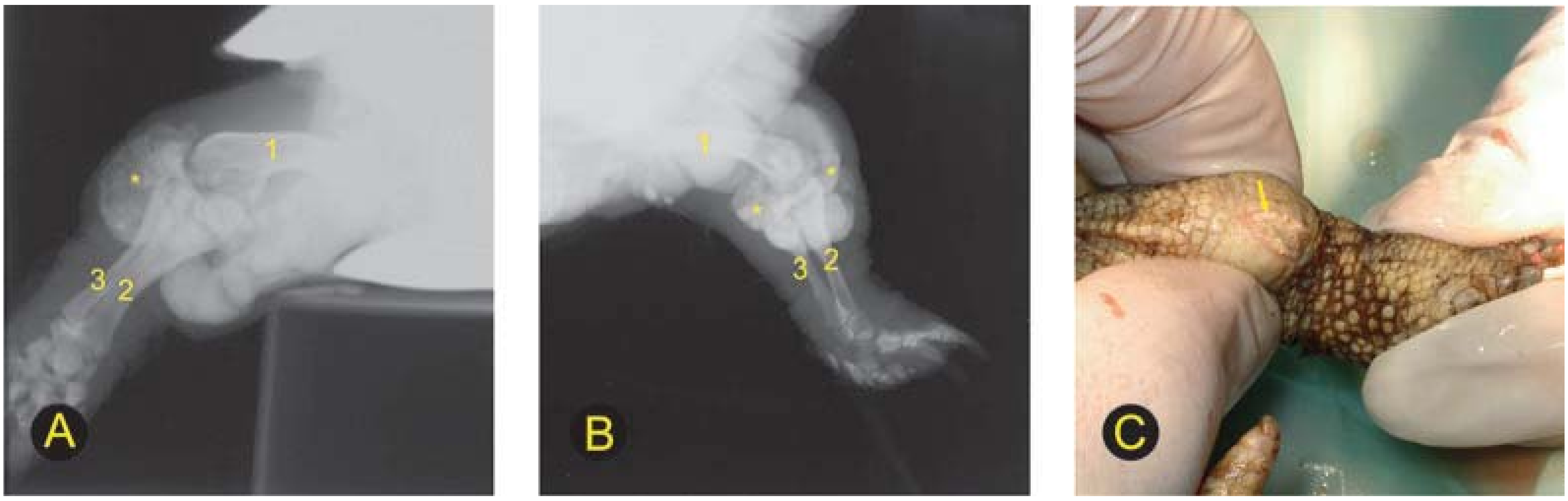

Fig. 3-222:

A, B: Radiographic images of a Hermann’s tortoise’s (*Testudo hermanni*) hindleg, (A) dorsopalmar and (B) lateral projections. Gout. The urate deposits (*) in the joint can be seen as radiodense calculi due to the large number present and secondary calcification.

C: Surgical site, same animal. Urates are typically found as a white, friable mass (arrow). Microscopic examination enables the material to be differentiated from that found in an abscess.

1: femur
2: tibia
3: fibula

*: urate deposits in the joint

arrow: urate deposit

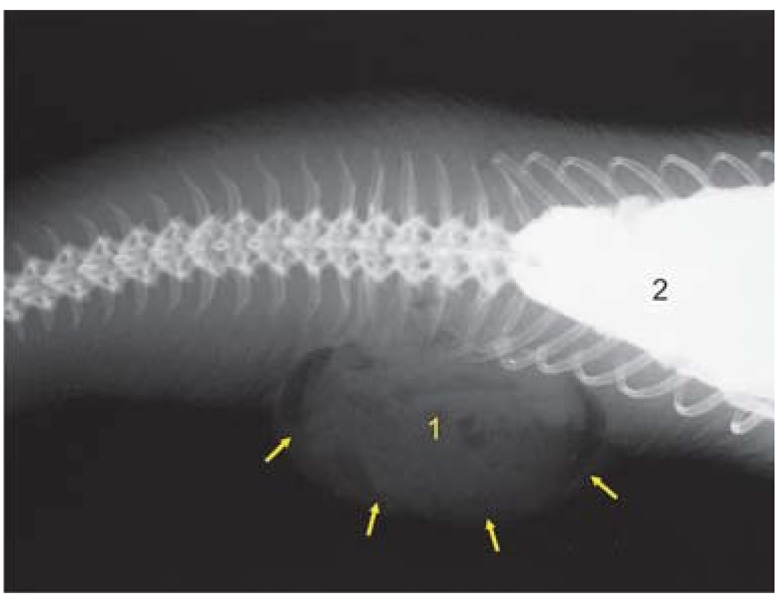

1, arrows: abscess
2: contrast medium

Fig. 3-223: Radiographic image of a boa constrictor’s (*Boa constrictor*) cloacal region, dorsoventral projection, 1 hour after the intracloacal administration of a iodine-based contrast medium. Pericloacal abscess. The contrast medium (2) enabled the abscess (1) to be differentiated from the gastrointestinal tract.

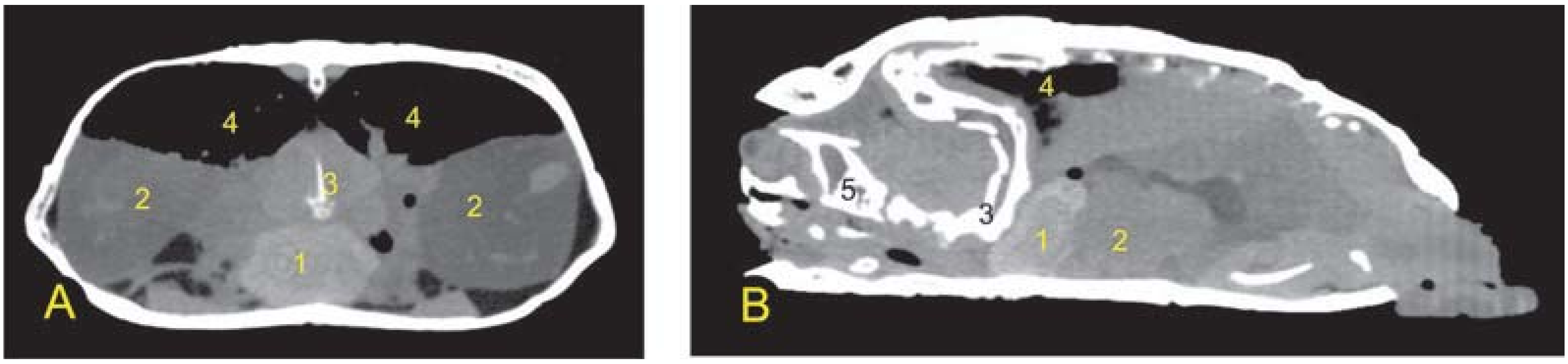

Fig. 3-224: CT image of a red-eared slider (*Trachemys scripta elegans*), (A) transverse plane and (B) sagittal reconstruction (120 kV, 204 mA, 1.0 mmSD, W: 400, L: 60). Abscess. Being calcified, the abscess (1) on the animal's neck was relatively radiodense. The liver (2) is enlarged. The blood vessels are congested (septicemia).

1: abscess
2: liver
3: cervical vertebrae
4: lungs
5: cranium

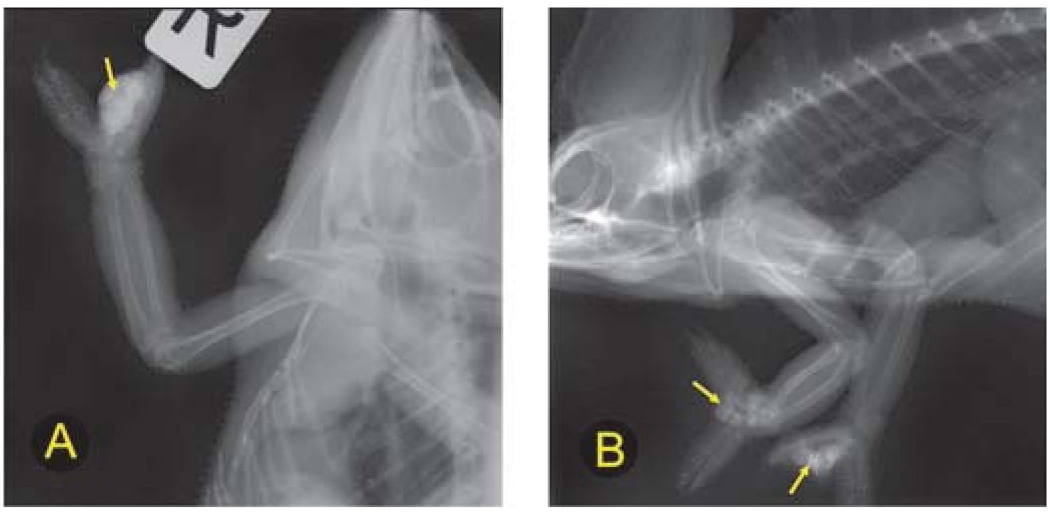

Fig. 3-225: Radiographic images of a veiled chameleon's (*Chamaeleo calyptratus*) foreleg, (A) dorsopalmar and (B) lateral projections. Pododermatitis. Radiodense calcification (arrows) has occurred subsequent to a chronic inflammation involving the plantar surface of the animal's feet.

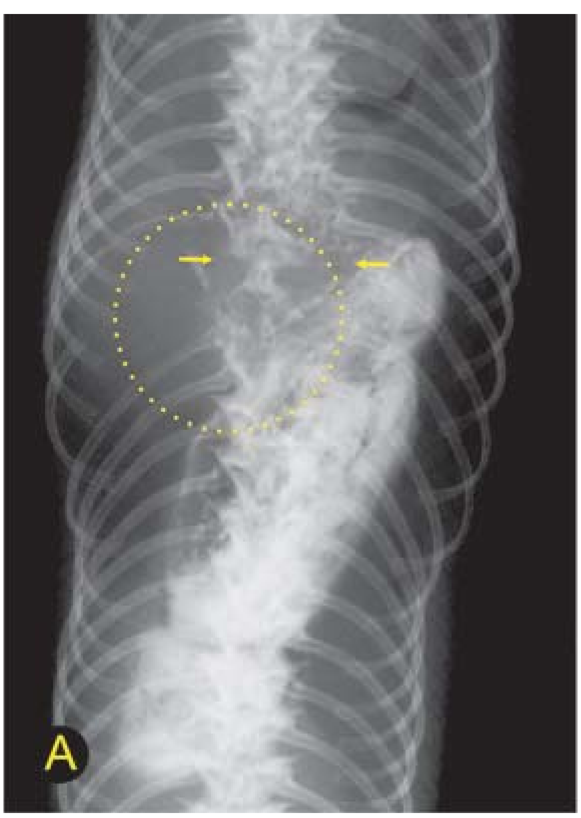

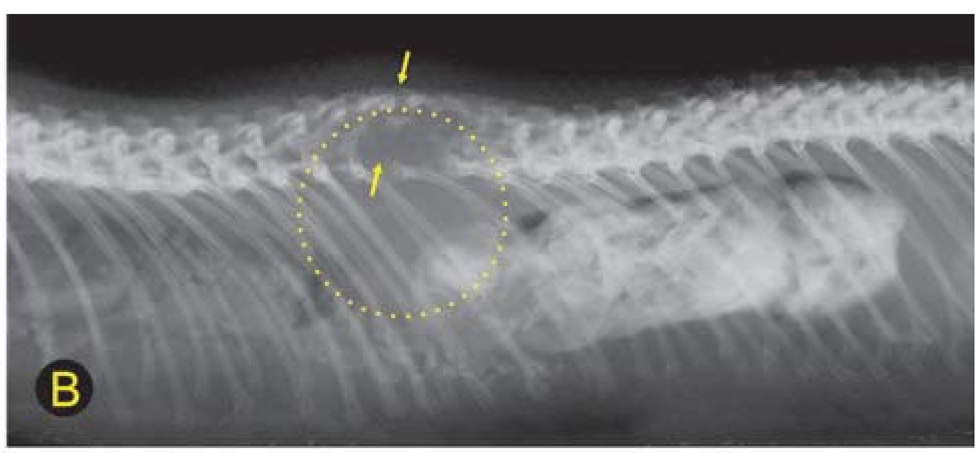

Fig. 3-226: Radiographic images of a boa constrictor's (*Boa constrictor*) trunk, (A) dorsoventral and (B) lateral projections. A fibroma has grown into the spine. The massive neoplasm (circle) has induced clinical signs of paralysis by damaging the spine (arrows).

1, arrows: tumor
2: spine

Fig. 3-227:

A, B: Ultrasonographic images of a green anaconda (*Eunectes murinus*), ventral coupling site, oblique, 14 MHz, PD 5 cm, (B) power Doppler. Lymphosarcoma. The tumor (1) is well defined and has a vascular supply. The echogenicity is characteristic for a tumor. The neoplasm (1) is well demarcated, whereby the perfusion in the center of the tumor is lower than in its periphery.

C: CT image of the same animal, transverse plane, after the intravenous administration of Iomeprol (300 mg/ml, 5 ml/kg bwt IV), (120 kV, 204 mA, 2.0 mm SD, W: 267, L: 115). The neoplasm (1) is also well demarcated in the contrast CT image.

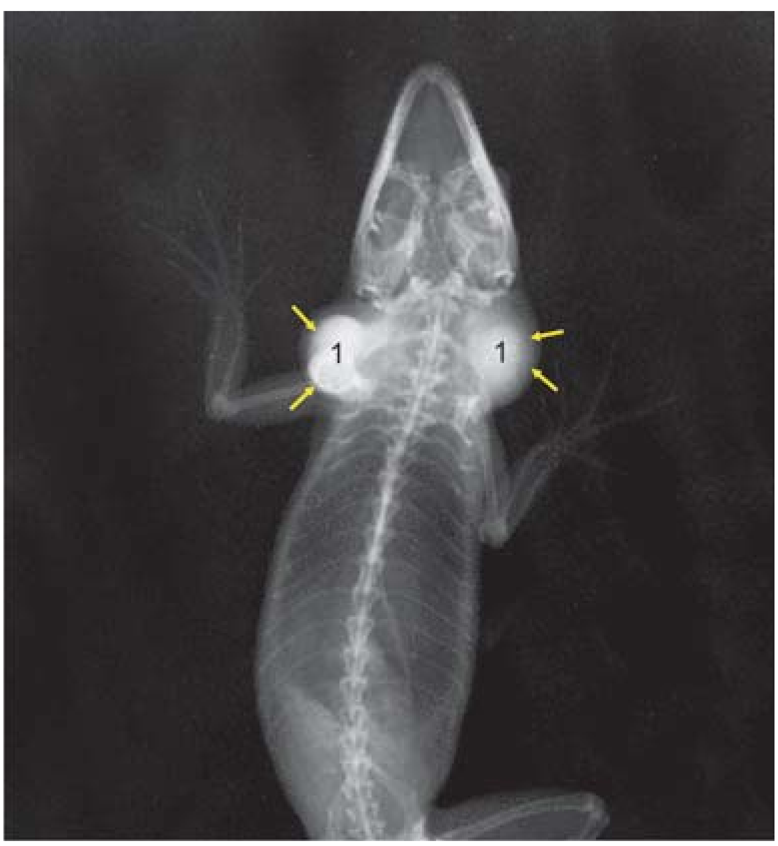

1, arrows: .endolymphatic sacs

Fig. 3-228: Radiographic image of a Carolina anole’s (*Anolis carolinensis*) body, dorsoventral projection. Abscessation of the endolymphatic sac. The endolymphatic sacs (1). On both sides of the body are enlarged and poorly differentiated (arrows)

Photograph credits

Chapter 1

Enders, Frank (Freiberg, Germany): 1-66, 1-67

Gumpenberger, Michaela (Vienna, Austria): 1-206 to 1-209

Hermann, Thomas (Schalbach-Elm, Germany): 1-95, 1-96

Department of Small Animal Medicine, Leipzig, Germany: 1-41, 1-56B, 1-63, 1-76, 1-82 to 1-91, 1-114, 1-139, 1-140

Tully, Thomas (Baton Rouge, USA): 1-17, 1-20, 1-30, 1-36, 1-94, 1-97, 1-102, 1-105, 1-111, 1-116, 1-152, 1-153

All other photographs: Clinic for Birds and Reptiles, Leipzig, Germany

Chapter 2

Boonyapakorn, Chavalit, Skrodzki, Marianne, Trautvetter, Eberhardt (Berlin, Germany): 2-29, 2-34, 2-35, 2-124, 2-125, 2-128, 2-130A, 2-130B

Fehr, Michael (Hanover, Germany): 2-14, 2-102A, 2-102B, 2-103, 2-105, 2-106A, 2-106B, 2-106C, 2-107, 2-108D, 2-109B, 2-110A, 2-110B, 2-112A, 2-112B, 2-113A, 2-114C, 2-114D, 2-114E, 2-114F, »-114H, 2-114I, 2-160, 2-161D

Gneiser, Barbara (Munich, Germany): 2-84D, 2-91B

Grodtmann, Elina (Munich, Germany): 2-95B

Hein, Jutta (Munich, Germany): 2-1B

Hoffmann, Ingo (Nuremberg, Germany): 2-97, 2-98A, 2-98B, 2-99, 2-100A, 2-100B, 2-162A, 2-162B, 2-162C, 2-163A, 2-163B, 2-164A, 2-165A, 2-165B, 2-166A, 2-166B, 2-166C, 2-167A, 2-167B, 2-167C, 2-168A, 2-168B, 2-168C, 2-169A, 2-169B, 2-169C, 2-170A, 2-170B, 2-170C, 2-171A, 2-171B, 2-172A, 2-172B, 2-173A, 2-173B, 2-174A, 2-174B, 2-175A, 2-175B, 2-176A, 2-176B, 2-176C, 2-177A, 2-177B, 2-177C, 2-178A, 2-178B

Jopp, Ilka (Leipzig, Germany): 2-8, 2-118C

Kresken, Jan-Gerd, Spennes, Jochen (Duisberg, Germany): 2-36, 2-126C, 2-126B

Lehmann, Julia (Munich, Germany): 2-76B, 2-90A, 2-96D

Mörl, Jessica (Munich, Germany): 2-83C

Poulsen Nautrup, Cordula (Munich, Germany): 2-7, 2-13A, 2-13B, 2-47, 2-48A 2-48B, 2-49A, 2-49B, 2-50A, 2-50B, 2-52 to 2-59, 2-60A, 2-60B, 2-61, 2-62, 2-63, 2-64A, 2-64B, 2-64C, 2-65A, 2-65B, 2-66A, 2-66B, 2-67, 2-68A, 2-68B, 2-69A, 2-69B, 2-69C, 2-69D, 2-70A, 2-70B, 2-70C, 2-70D, 2-71A, 2-71B, 2-72A, 2-72B, 2-73A, 2-73B, 2-74A, 2-74B, 2-75A, 2-75B, 2-75C, 2-75D, 2-129, 2-132A, 2-132B, 2-133 (illustrations), 2-134A, 2-134B, 2-136, 2-138, 2-142A, 2-142B, 2-143A, 2-143B

Reese, Sven (Munich, Germany): 2-1A, 2-3, 2-4A, 2-4B, 2-5A, 2-5B, 2-6A, 2-6B, 2-16A, 2-16B, 2-16C, 2-17B, 2-25A, 2-25B, 2-44A, 2-44B, 2-45, 2-46, 2-51A, 2-51B, 2-51C, 2-76A, 2-76C, 2-77, 2-78, 2-79, 2-80A, 2-80B, 2-80C, 2-80D, 2-80E, 2-81, 2-82, 2-83A, 2-83B, 2-84A, 2-84B, 2-84C, 2-85, 2-86A, 2-86B, 2-87A, 2-87B, 2-88, 2-89A, 2-89B, 2-90B, 2-90C, 2-91A, 2-92A, 2-92B, 2-93A, 2-93B, 2-94A, 2-94B, 2-95A, 2-96A, 2-96B, 2-96C, 2-115, 2-123, 2-144B, 2-144C, 2-144D, 2-148A, 2-148B, 2-149D; 2-149E, 2-149F, 2-150B, 2-150C, 2-150D, 2-150E, 2-150F, 2-150G, 2-150H, 2-150I, 2-151, 2-152B, 2-152C, 2-152D, 2-152E, 2-153A, 2-153B, 2-153C, 2-153D, 2-153E, 2-153G, 2-153H, 2-153I, 2-153K, 2-153L, 2-154A, 2-154D, 2-155B, 2-155D, 2-155E, 2-155F, 2-155G, 2-155H, 2-156, 2-157, 2-158A, 2-158C, 2-158D, 2-159A, 2-159C, 2-159D, 2-159E, 2-159F, 2-159G, 2-159H, 2-161A, 2-161B, 2-161C, 2-161E, 2-165C

Schambach, Sebastian J., Brockmann, Marc A. (Mannheim, Germany): 2-28, 2-31, 2-101A, 2-101B, 2-101C, 2-101D

Schlieter, Susanne (Freiburg im Breisgau, Germany): 2-127, 2-131A, 2-131B, 2-133A, 2-133B, 2-135A, 2-135B, 2-137, 2-139, 2-140A, 2-140B, 2-141A, 2-141B

Small Animal Medical Clinic, Munich, Germany: 2-2, 2-9, 2-11A, 2-11B, 2-11C, 2-11D, 2-12, 2-19A, 2-19B, 2-20, 2-23B, 2-24B, 2-24C, 2-27, 2-30, 2-32, 2-33, 2-37, 2-38C, 2-39B, 2-40, 2-110C, 2-110D, 2-113C, 2-118A, 2-118B, 2-145A, 2-146B, 2-146C, 2-147A, 2-147B, 2-147C, 2-147D, 2-149A, 2-150A, 2-152A, 2-154B, 2-154C, 2-155A, 2-155C, 2-155I, 2-158B

Tully, Thomas (Baton Rouge, USA): 2-10, 2-15, 2-17A, 2-18, 2-21, 2-22, 2-23A, 2-26, 2-38A, 2-38B, 2-39A, 2-41, 2-42, 2-104, 2-113B, 2-113D, 2-114A, 2-114B, 2-114G, 2-116A, 2-116B, 2-117, 2-119A, 2-119B, 2-120, 2-121, 2-122, 2-145B, 2-146A, 2-149B, 2-149C

Veterinary Clinic Oberhaching (Oberhaching, Germany): 2-19A, 2-24A, 2-43A, 2-43B, 2-108A, 2-108B, 2-108C, 2-109A, 2-111A, 2-111B, 2-114K, 2-144A, 2-153F

Wagner, Felix (Hanover, Germany): 2-164B, 2-175C

Chapter 3

Allgöwer, Ingrid (Berlin, Germany): 3-218A

Hoffmann, Ingo (Nuremberg, Germany): 3-80, 3-214 to 3-216, 3-217C, 3-218 to 3-221

Kostka, Veit (Hamburg, Germany): 3-18, 3-23A, 3-127, 3-128, 3-132, 3-143, 3-169, 3-181, 3-191, 3-199, 3-203, 3-212, 3-228

Pees, Kathrin (Leipzig, Germany): 3-3, 3-9

Reese, Sven (Munich, Germany): 3-68, 3-69

Department of Small Animal Medicine, Leipzig, Germany: 3-42B, 3-60, 3-83 to 3-99, 3-105, 3-106C, 3-120B, 3-120C, 3-122, 3-123, 3-126, 3-129, 3-134, 3-144, 3-146B, 3-147B, 3-14C, 3-148 to 3-150, 3-152C, 3-153, 3-158A, 3-161B, 3-162A, 3-164, 3-172, 3-173B, 3-175, 3-180, 3-185, 3-189, 3-190, 3-192B, 3-192D, 3-193A, 3-194C, 3-196B, 3-204, 3-20B, 3-206, 3-207B, 3-207C, 3-207D, 3-208B, 3-208C, 3-208D, 3-210A, 3-211, 3-213C, 3-224, 3-227

Tully, Thomas (Baton Rouge, USA): 3-17, 3-22, 3-24, 3-25, 3-114, 3-166

All other photographs: Clinic for Birds and Reptiles, Leipzig, Germany

Subject Index

Birds

Small Mammals

Reptiles